Universität Rostock Traditio et Innovatio

Catalysis LIKAT Leibniz-Institut für Katalyse e.V.

Investigations on Carbon Dioxide Reduction and CO_2 Reductive Coupling Facilitated by Fe and Cu Complexes

Untersuchungen zur Reduktion von Kohlenstoffdioxid und zur reduktiven CO_2 Kupplung ermöglicht durch Fe und Cu Komplexe

Dissertation
zur Erlangung des akademischen Grades
Doctor rerum naturalium **(Dr. rer. nat.)**
der Mathematisch-Naturwissenschaftlichen Fakultät
Universität Rostock

vorgelegt von
Maximilian Marx, M.Sc.
geboren in Itzehoe
am 29. September 1992

2020

https://doi.org/10.18453/rosdok_id00003573

Gutachter:
Prof. Dr. Dr. h.c. mult. Matthias Beller, Leibniz-Institut für Katalyse e.V., Universität Rostock
Prof. Dr. Troels Skrydstrup, Interdisciplinary Nanoscience Center, Department of Chemistry, Aarhus University

Jahr der Einreichung: 2020
Jahr der Verteidigung: 2021

Declaration of the doctoral candidate according to § 4 (1) letters g and h of the doctoral degree regulations of the Faculty of Mathematics and Natural Sciences of the University of Rostock

1. The opportunity for this PhD project was not communicated to me commercially. In particular, I have not engaged any organisation that for money seeks supervisors for the drawing up of dissertations or that performs entirely or partially on my behalf the duties incumbent upon me regarding the examinations.

2. I hereby declare under oath that I have completed the work submitted here independently and have composed it without outside assistance. Furthermore, I have not used anything other than the resources and sources stated and where I have taken sections from these works in terms of content or text, I have identified this appropriately.

Rostock, _____ _____

(Place, Date) (Maximilian Marx)

Acknowledgements

First, I would like to thank Prof. Dr. Dr. h.c. mult. Matthias Beller for giving me the opportunity to work in his group and under his supervision. The enjoyable discussions, your suggestions and innovative ideas helped me to evaluate new possibilities. I am very grateful for enabling me to pursue own ideas and highly appreciate your kind and open-minded guidance. Your enthusiasm, broad knowledge not only in the field of chemistry, fundamental curiosity for any scientific discovery and ability to motivate everyone you are working with is exceedingly inspiring. Especially with respect to your tight schedule, I would like to thank you for making time for all our meetings as well as for proofreading this thesis.

I would also like to thank Dr. Helfried Neumann for accepting me as part of the group *"Transition-metal catalyzed synthesis of fine chemicals"*. Your expertise in synthetic procedures and more than helpful suggestions significantly contributed to this work. I am grateful for the enjoyable discussion and likewise would like to thank you for proofreading this thesis.

I would like to thank all participants of our "Friday seminars", namely Dr. Anastasiya Agapova, Fabio Delolo, Johannes Fessler, Yan-Jun Guo, Dr. Yannick Hermans, Hilario Huerta, David Leonard, Dr. Alexander Léval, Dr. Xiang Li, Dr. Fabrizio Monda, Dr. Pavel Ryabchuk, Dr. Rui Sang, Jacob Schneidewind, and Dr. Wei Zhou for all the interesting presentations, inspiring discussions and helping suggestions.

I would especially like to thank Dr. Anastasiya Agapova, Dr. Alexander Léval, Dr. Elisabetta Alberico, Hilario Huerta, Dr. Xiang Li, Elisabeth Oberem, Dr. Patrick Piehl, Jacob Schneidewind, and Dr. Wei Zhou for all the help and guidance you provided to tackle many of the problems I faced. I am thankful to Dr. Alexander Léval for also proofreading major parts of this thesis and to Dr. Paola A. Forero-Cortés for proofreading the section addressing CO_2 reduction in ILs.

Also, I would like to thank Dr. Anastasiya Agapova, Vishwas Chandrashekhar, Dr. Paola A. Forero-Cortés, Dr. Yannick Hermans, Anja Kammer, Sara Kopf, Dr. Alexander Léval, Dr. Jagadeesh Rajenahally, Dr. Thomas Schareina, Jacob Schneidewind, Dr. Christoph Steinlechner and Dr. Wei Zhou for the enjoyable atmosphere in lab and office.

For delightful cooperations and interesting discussions I would like to thank Dr. Henrik Junge, Dr. Paola A. Forero-Cortés, Prof. Dr. Andrew W. Maverick, Dr. Andrea Mele, and Prof. Dr. Philippe Schollhammer.

For their support with and maintenance of laboratory equipment, I would like to thank Anja Kammer, Sandra Leiminger, Matthias Auer, and Andreas Hutter. Fast mass spectrometric and NMR spectroscopic measurements by the analytical department of the LIKAT are gratefully acknowledged. I would specifically like to thank Dr. Anke Spannenberg for measuring and solving all the X-ray structures of this work and for helping with revision of the crystallography sections of this thesis. Also, I am grateful to Dr. Holm Frauendorf for discussions and help with the HR-MS analysis of oxalate.

Prof. Dr. Karl Anker Jørgensen and all members of the Jørgensen group deserve my gratitude for accepting me as a visiting PhD student and introducing me to cutting-edge organocatalysis and the “Scandinavian lifestyle”.

I am grateful to the Stiftung Stipendienfonds der Chemischen Industrie which enabled me to pursue this work by granting me a Kekulé fellowship. Furthermore, I am grateful to the European Union for funding of my research stay in the group of Prof. Dr. Karl Anker Jørgensen as part of the Erasmus+ program.

For making the time in Rostock significantly more joyful, I would like to especially thank Alexander Léval, Anastasiya Agapova, Jacob Schneidewind, Patrick Piehl, Elisabeth Oberem, Wei Zhou, and Xiang Li.

Finally, I would like to thank my family for continuous support over the past eight years of my academic education, and I am exceedingly grateful to my parents.

To my parents.

"The first principle is that you must not fool yourself–
and you are the easiest person to fool. So you have to be very careful about that.
After you've not fooled yourself, it's easy not to fool other scientists."
Richard P. Feynman

Abstract

This dissertation deals with the chemical reduction of carbon dioxide into C_1 and C_2 compounds following two different approaches to achieve these transformations of interest. The major objective of this thesis is to contribute to future developments in the fields of photocatalytic CO_2 reduction and CO_2 reductive coupling.

In the first part of this thesis, photocatalytic CO_2 reduction into C_1 compounds, namely CO and formic acid, was investigated. Initially, an established photocatalytic protocol based on an Fe cyclopentadienone reduction catalyst in combination with a Cu photosensitizer was transferred from conventional organic solvents into ionic liquids. While the overall activity is reduced compared to traditional solvents, the results highlight the possibility of utilizing ionic liquids as the solvent for described photocatalytic CO_2 reduction systems.

Next, [FeFe] hydrogenase mimics were evaluated as potential CO_2 reduction catalysts in combination with the same $[Cu(N\text{^}N)(P\text{^}P)]^+$ photosensitizer. Interestingly, poor reproducibility was observed, which was partially caused by ligand substitution of the [FeFe] complex with the bidentate ligands of the Cu PS. The results showcase the importance of assessing reproducibility for novel photocatalytic transformations and common guidelines on how to evaluate and address reproducibility in these reactions were established.

In the second part of this thesis, CO_2 reductive coupling reactions enabled by Fe and Cu complexes were investigated. The investigations were initiated based on literature procedures with the aim of establishing key parameters that would guide further systematic improvements for this peculiar reaction.

In-depth investigations on a protocol employing 1,4,7-triazacyclononane-derived ligands and Cu as the active metal center remained unsuccessful in identifying oxalate in yields described in the literature. For this, various novel mono- and dinuclear Cu complexes bearing *NNN*- and PNP-type ligands were prepared and numerous reaction parameters and additives investigated. While the formation of oxalate traces was detected by a combination of analytical methods (FTIR, NMR, CE), these results highlight the sophisticated analysis of CO_2 reduction products when studying its reductive coupling.

A dinuclear Cu-based system that was described to produce oxalate from atmospheric CO_2 after *in situ* formation of the active Cu^I complex with ascorbate was investigated. Here, the oxidative degradation of ascorbate was identified as the true origin of oxalate.

Likewise, investigations on the CO_2 reductive coupling starting from an α-ketocarboxylate complex suggested an oxidative degradation pathway as the source of oxalate. Moreover, tris(pyrazolyl)borate-ligated Cu complexes were found to facilitate oxidative decarboxylation, while simple Cu^{2+} enabled oxidative degradation of the α-ketocarboxylate into oxalate.

The presented results establish the importance of careful analysis of the obtained CO_2 reduction products and consideration of alternative reaction pathways, such as oxidative degradation reactions, that might result in false positives. Moreover, these investigations will serve as an expedient guideline for future investigations on CO_2 reductive coupling.

Abbreviations

9CNA	9-cyanoanthracene
18-c-6	1,4,7,10,13,16-hexaoxacyclooctadecane (18-crown-6)
Å	Ångström
Ar	aryl
ATR	attenuated total reflection
bcp	2,9-dimethyl-4,7-diphenyl-1,10-phenanthroline (bathocuproine)
BDC	benzene-1,4-dicarboxylate
bdt	benzene-1,2-dithiolate
BIH	1,3-dimethyl-2-phenylbenzo[*d*]imidazol
$bmim^+$	1-butyl-3-methylimidazolium
$bmpyrr^+$	1-butyl-1-methylpyrrolidinium
BNAH	1-benzyl-1,4-dihydropyridine-3-carboxamide
bpdt	1,1'-biphenyl-2,2'-dithiolate
bpy	2,2'-bipyridine
br	broad
Bu	butyl
CCS	carbon capture and storage
CCR	carbon capture and recycling
CE	capillary electrophoresis
CF	carbon fiber
Cl-bdt	1,4-dichlorobenzene-2,3-dithiolate
cod	1,5-cyclooctadiene
Cy	cyclohexyl
cyclam	1,4,8,11-tetraazacyclotetradecane
δ	chemical shift
d	days
d	doublet
DCC	dicyclohexylcarbodiimide
DCM	dichloromethane
DEC	diethyl carbonate
DFT	density functional theory
dien	diethylenetriamine
diglyme	diethylene glycol dimethyl ether
Dipp	2,6-di-*iso*-propylphenyl
DMA	*N,N*-dimethylacetamide
dmb	4,4'-dimethyl-2,2'-bipyridine
DMC	dimethyl carbonate
DMF	*N,N*-dimethylformamide
DMI	1,3-dimethylimidazolidinone
dmp	2,9-dimethyl-1,10-phenanthroline
DMSO	dimethyl sulfoxide
dpa	di-(2-picolyl)amine
DPEPhos	bis[(2-diphenylphosphino)-phenyl] ether
DSR	disordered structure refinement
E^{00}	standard redox potential
EA	electron acceptor
ED	electron donor
e.g.	*exempli gratia*
EI	electron ionization
$emim^+$	1-ethyl-3-methylimidazolium
equiv.	equivalents
ESI	electrospray ionization
Et	ethyl
et al.	*et alii*
η	overpotential
Fc	ferrocene
Fc^+	ferrocenium cation
FTIR	Fourier-transform infrared
ΔG	Gibbs free energy
g	gram
GCE	glassy carbon electrode
GDP	gross domestic product
$Giso^-$	$(DippN)_2CNCy_2^-$
h	hour
hept	heptet

HIHD	historical index of human development
hmim	1-hexyl-3-methylimidazolium
HOMO	highest occupied molecular orbital
HR-MS	high resolution mass spectrometry
i.a.	*inter alia*
i.e.	*id est*
IL	ionic liquid
^{i}Pr	*iso*-propyl
IR	infrared
J	coupling constant
KC_8	potassium graphite
KHMDS	potassium bis(trimethylsilyl)amide
λ	wavelength
L	unspecified monodentate ligand
L	liter
LED	light-emitting diode
LUMO	lowest unoccupied molecular orbital
M	mol/L
M	unspecified metal center
m	meta
m	multiplet
Me	methyl
Mes	2,4,6-trimethylphenyl (mesityl)
min	minute
MOF	metal organic framework
MS	mass spectrometry
MS	molecular sieves
^{m}ter	*meta*-terphenyl
m-xpt	1,3-bis((4-(2-pyridyl)-1*H*-1,2,3-triazolyl)methyl)benzene
m/*z*	mass-to-charge ratio
ν	frequency
$\tilde{\nu}$	wavenumber
^{n}Bu	*n*-butyl
NHC	*N*-heterocyclic carbene
n.d.	not determined
NHE	normal hydrogen electrode
NMP	1-methylpyrrolidin-2-one
NMR	nuclear magnetic resonance
N^N	bidentate diimine-type ligand
NPC	nitrogen doped porous carbon
NTf_2^-	bis(trifluoromethanesulfonyl)imide
oe	oil equivalent
OERS	one electron reduced species
$^-$OTf	trifluoromethanesulfonate
ox	oxidant
p	*para*
pdt	1,3-propanedithiolate
Ph	phenyl
piq	1-phenylisoquinoline
POP	2,8-dimethyl-10-phenoxaphosphano
POP-xantphos	4,5-bis(2,8-dimethyl-10-phenoxaphosphano)-9,9-dimethylxanthene
P^P	bidentate bisphosphine ligand
ppb	parts per billion
ppm	parts per million
PPN^+	bis(triphenylphosphoranylidene)ammonium
ppy	2-phenylpyridine
Pr	propyl
proc.	procedure
PS	photosensitizer
PTFE	polytetrafluoroethylene
pyr	pyrazole
q	quartet
qpy	2,2':6',2":6",2"'-quaterpyridine
quant.	quantitative

quint	quintet
R	unspecified organic residue
RHE	reversible hydrogen electrode
RNA	ribonucleic acid
r.t.	room temperature
RuBisCO	ribulose-1,5-bisphosphate-carboxylase-oxygenase
s	second
s	singlet
SAPO	silicoaluminophosphate
sat.	saturated
SC-XRD	single crystal X-ray diffraction
$scCO_2$	supercritical carbon dioxide
SCE	saturated calomel electrode
sext	sextet
SED	sacrificial electron donor
SHE	standard hydrogen electrode
solv	solvent
syngas	synthesis gas (CO/H_2 mixture)
Θ	angle of incidence (X-ray)
t	ton
t	triplet
T	temperature
tacn	1,4,7-triazacyclononane
$tbmp^+$	tributylmethylphosphonium
^{t}Bu	*tert*-butyl
TEOA	tris(2-hydroxyethyl)amine
Tf	trifluoromethanesulfonyl
TFE	trifluoroethanol
THF	tetrahydrofuran
thixantphos	4,5-bis(2,8-dimethyl-10-phenoxaphosphano)-2,7-dimethylphenoxathiin
TLC	thin layer chromatography
TMS	trimethylsilyl
tmtaa	4,11-dihydro-5,7,12,14-tetramethyldibenzo[*b*,*i*][1,4,8,11]-tetraazacyclotetradecine
TON	turnover number
TOF	turnover frequency
$Tp^{R,R}$	tris(pyrazolyl)borate (R,R = 3,5-substituents on pyrazole)
TP	*para*-terphenyl
TPP	tetraphenylporphyrin
Ts	4-toluenesulfonyl
USD	United States dollar
UV/Vis	ultraviolet-visible absorption spectroscopy
WGSR	water-gas shift reaction
wt%	mass fraction (% by weight)
X^-	unspecified anion
xantphos	4,5-bis(diphenylphosphino)-9,9-dimethylxanthene
ZSM-5	Zeolite Socony Mobil-5

Table of Contents

1 Introduction

Fossil fuels, namely coal, gas, and oil, have powered industrialization and played a key-role in the unprecedented economic growth within the last 60 years (Figure 1).[1–3] This economic growth has been accompanied by an enhancement of the globally averaged quality of life, which can partially be quantified using the *Historical Index of Human Development* (HIHD), in terms of an increased global life expectancy[4] and higher levels of education for the general public.[5] At the same time, global population increased from 3 billion in 1960 up to an estimated number of 7.79 billion in 2020.[6]

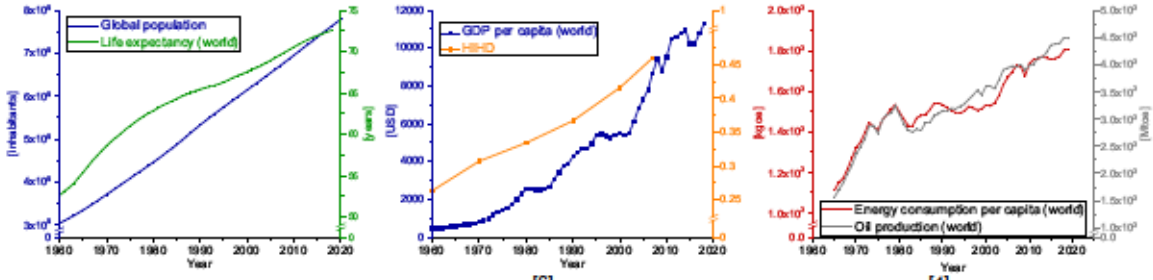

Figure 1: Annual data of global population,[6] world life expectancy (at birth),[4] Historical Index of Human Development (HIHD),[5] world oil production (including naphtha obtained from natural gas production and natural gas liquids),[7] world energy consumption per capita[7] and world GDP per capita[2] from 1960 until 2020 (unless data points are not reported in the literature).

All of these rapid developments sharply increasing after the Second World War, which are nowadays coined the *"Great Acceleration"*, have been accompanied by an increasing demand in energy[7] that is likely going to rise at least for the next 10 years.[1,8] Nowadays, fossil fuels still contribute the majority of globally employed energy resources with 27% coal, 24% gas, and 33% oil, respectively (Figure 2, data from 2019), despite a noticeable shift towards more sustainable energy sources.[7,8]

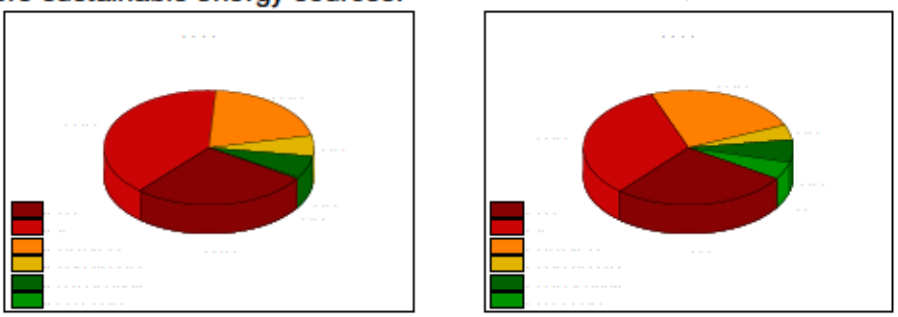

Figure 2: Comparison of the global energy consumption by fuel divided into coal, oil, natural gas, nuclear energy, hydroelectricity and renewables (mainly biofuels, biomass, geothermal, solar, wind) for the years 1990 and 2019.[7]

With respect to the expected increase in energy demand over the next 20 years based on currently declared energy policies,[8] rise in global population over at least the next 30 years,[9] and the anticipated growing demand in food supply,[10–12] the transition from fossil fuels to more environmentally benign energy sources will arguably pose a major challenge.[13,14] Furthermore, all improvements and progress achieved by exploitation of fossil fuels in the past and present might come at a cost that could substantially impact the future of humanity.[1,3,12–14]

The main reason for their impact on mankind's future is the inevitable formation of greenhouse gases, such as carbon dioxide, methane, and to some extent nitrous oxide resulting from fossil fuel production and exploitation.[1,3,13,14] Historical data indicates a significant increase of their atmospheric concentration since mid of the 19th century with a substantial ascent during the *"Great Acceleration"* (Figure 3).[1,14] Likewise, global CO_2 emissions originating from fossil fuel utilization, cement production, and flaring of natural gas, vastly increased over the same timeframe (Figure 4).[1,14,29]

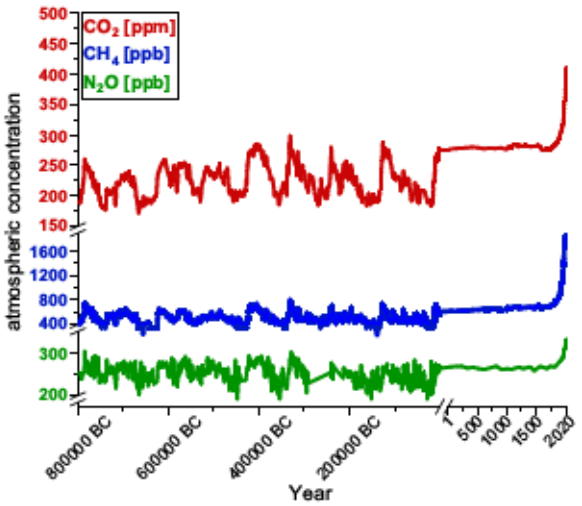

Figure 3: Atmospheric CO_2, CH_4, and N_2O concentrations from approx. 800000 BC until 2019. Atmospheric concentrations compiled and processed by the United States Environmental Protection Agency (796562 BC-1955 [CO_2],[15] 797446 BC-1980 [CH_4],[16] 796475 BC-2000 [N_2O][17] - based on data from *EPICA Dome C* and *Vostok Station*,[18–20] *Law Dome*,[21,22] *Siple Station*,[23] *Cape Grim*,[24] and Antarctica[25]) were combined with data from the *Global Monitoring Laboratory/National Oceanic and Atmospheric Administration* (1959-2019 [CO_2],[26] 1984-2019 [CH_4],[27] 2001-2019 [N_2O][28]). Note that for N_2O, no datapoints in between 291028 and 240650 BC are included in the utilized datasets resulting in a straight line that does not hamper the overall information of this figure. The development over the past 2019 years is highlighted by segmentation of the x-axis.

Various parameters indicate a correlation between the increasing atmospheric greenhouse gas concentrations and changes in the global climate.[1,12–14] In between 1880 and 2012, the global surface temperature (average) has increased by 0.65-1.06 °C.[14] This has been accompanied by a decline in ice mass of glaciers, decreased icecaps in Antarctica and Greenland (in between 1992 and 2011) and reduced amounts of sea-ice in the Artic (1979 to 2012).[14] Consequently, a notable increase of the global sea level (mean) by 0.17-0.21 m was detected during the timeframe 1901 to 2010.[14] While natural sinks for greenhouse gases, such as CO_2 uptake by the ocean, have mitigated their atmospheric concentrations over a certain time window, it appears plausible that *climate change* is caused by utilization of fossil fuels since the beginning of industrialization during the 18th century and especially since the *Great Acceleration*.[1,3,13,14,30]

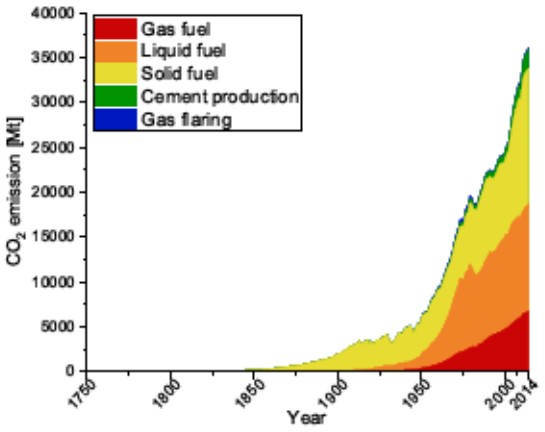

Figure 4: Global CO_2 emission data separated into different origins of CO_2 (solid, liquid, and gas fuels, production of cement, and flaring of natural gas) from 1751-2014.[29]

In fact, climate change in combination with an observable decline in biodiversity, humanities impact on the global hydrological cycle due to i.a. alteration of river course by dams, and interference with element cycles (phosphorus, nitrogen, and sulphur) resulted in the proposal to register the time frame starting from 1800 entitled *Anthropocene* as a new geological epoch.[1]

Climate change is associated with major impacts on humanity for the upcoming decades.[1,12,14] Global average temperatures as well as the sea level are expected to rise and weather extremes, such as heat waves and floods, are proposed to become more common.[1,12–14] Food insecurity and drinking water shortage are predicted results of these changes in climate.[12,14] These alarming predictions are demanding actions to alleviate the consequences of greenhouse gas emissions and required steps were agreed upon by 197 countries in the 2016 Paris agreement which targets a maximum increase in global temperature of 2 °C (relative to pre-industrial temperature), with an intended boundary of 1.5 °C.[14,31,32] Reducing greenhouse gas emission *via* a reduced application of fossil fuels and enhanced utilization of renewable energy sources is one of the major approaches to achieve this goal.[3,13,14,31] A recent report indicates that an inverse U-shaped relation between income (in terms of real GDP per capita) and the share of fossil fuels in the overall energy consumption of countries might exist (with oil/natural gas producing countries in the Middle East being the exception).[31] This would implicate a decrease in fossil fuel utilization in case developing countries achieve a higher GDP per capita as their economic situation enables them to pursue a more sustainable energy production and appears to be in accordance with the increasing share of renewables in the overall global energy consumption (Figure 2).[7,8,31] While this might be encouraging with respect to the desired decreasing application of fossil fuels in the near future, further strategies to reduce greenhouse gas concentrations in the atmosphere and to limit temperature increase will be required.[1,3,14,30] Despite geo-engineering strategies for cooling the earth that might pose unsuspected implications, carbon dioxide capture and storage (CCS) is a major strategy to reduce atmospheric CO_2 emissions and thereby extenuate global warming.[1,3,14,30,33,34]

CCS might reduce energy production related CO_2 emissions by up to 20% by segregation and purification of CO_2 directly from the source of its emission, such as fossil fuel power plants.[30] This separation of CO_2 can be achieved by utilization of amines or ammonia which are capable of CO_2 uptake directly from the waste gas and release CO_2 upon heating.[3,30,33] The major advantage of this postcombustion CO_2 capture lies in its compatibility with existing power plants.[3,30,33] However, energy-demanding release of CO_2, degradation of the amine, possible formation of harmful byproducts during CO_2 release and comparatively space demanding equipment are inherent drawbacks of this technology.[3,30,33] Precombustion CO_2 capture, on the other hand, removes CO_2 prior to energy production *via* steam reforming or gasification of coal resulting in CO/H_2 mixtures (syngas) with CO being further converted in the water-gas shift reaction (WGSR) to produce H_2 as the final fuel and highly concen-

trated CO_2 as by-product (Figure 5).[3,30,33] This is a major advantage of this technology, as it allows for the production of not only electricity, but also hydrogen as a promising energy carrier.[3,30] While the fundamental method for CO_2 enrichment is known to be operative even on large scale, costly construction remains a major downside of precombustion capture.[30,33] So-called oxyfuel combustion constitutes another approach for CO_2 segregation.[3,30,33] Here, the fossil fuel is combusted in an oxygen atmosphere containing recycled waste gas for controlling the temperature of the process yielding a mixture of CO_2 and H_2O as the main components of the flue gas.[3,30,33] Even though CO_2 purification is comparatively simple for this approach, expensive cryogenic O_2 isolation and the required high-temperature resistant materials are its main disadvantages.[3,30,33] After separation of CO_2 from the waste gas of major emission sites, transportation through pipes to the geological storage sites and injection into former natural gas and oil fields or saline aquifers complete the CCS method.[3,30] Specifically, segregation of CO_2 is an energy demanding process consuming up to 40% of the energy produced from its origin (the initial fossil fuel combustion).[3,30,33] However, a 10-20% energy requirement for the extraction has been estimated based on contemporary developments.[30] Despite the costs associated with CCS, its application might be inevitable in case global warming should *"likely"* be confined to $\leq$2 °C.[14,30,33] However, potential threats, such as abrupt liberation of stored CO_2 due to geological incidents, gradual leaking, high costs at low profit and protracted processing time might render CCS ineffective as an answer for the removal of surplus CO_2.[3,35]

An alternative approach contrasting CCS is recycling of CO_2 after capture (CCR).[3,35] Here, CO_2 is converted into valuable feedstock or fuels, with methanol considered as a prime product.[3,35,36] A number of intrinsic properties justify the privileged rank of methanol as future fuel and feedstock candidate: 1) processes for the preparation of ethylene, propylene and hydrocarbons starting from MeOH exist; 2) MeOH can directly be burned as a fuel in commonly employed internal combustion engines; 3) direct methanol fuel cells enable electricity production without combustion; 4) readily accessible dimethyl ether can largely act as a surrogate for diesel, natural gas liquids and liquefied petroleum gas; 5) MeOH can act as potential liquid hydrogen carrier with a comparatively high gravimetric hydrogen density (12.6 wt%).[3,35,37–40] However, CCR still relies on capturing CO_2 either from its source of emission or directly from the atmosphere.[3,35] Several methods for separation of CO_2 from gas mixtures exist that rely on its distinct physical and chemical properties (Figure 5).[3,30,33–35,41] CO_2 permeable membranes allow for separation of CO_2, but require comparatively high CO_2 concentrations in the gas mixture.[3] Energy-demanding cryogenic separation of CO_2 has been investigated for postcombustion capture, but is generally perceived as being incompatible with large-scale application.[3,30] Absorption of CO_2, also utilized in postcombustion capture, is the most widespread technique for its separation.[3,33] Simple alkanolamines, among others mono- and diethanolamine, frequently utilized for selective fixation of CO_2 *via* formation of bicarbonates and carbamates, enable CO_2 capture on a large scale from flue gas despite

their disadvantages that were described earlier.[3,33,35] More recently, ionic liquids have been suggested as an alternative to amines for the capture of CO_2.[33] Adsorption in porous solids, such as activated carbon, silica or zeolites, is another strategy.[3] However, low selectivity for CO_2 capture over other gases and significant temperature-dependence of the adsorption capacity are major drawbacks.[3] Metal-organic frameworks (MOFs) show promising properties for CO_2 capture,[42–45] but further improvements for their application at lower pressures are required.[3] Another strategy relies on the modification of solids to enable chemical fixation of CO_2.[3] This has been achieved utilizing (poly)amine-functionalized solids, (poly)amines on solid supports or directly with solid (poly)amines.[3,35] Simple hydroxides, such as $Ca(OH)_2$ or NaOH, are known to form the corresponding carbonates ($CaCO_3$ and Na_2CO_3) with CO_2 even from the atmosphere.[3,34,41] However, extensive contact with high quantities of air is required for full conversion and regeneration of the absorbents remains an energy-demanding process.[3,34,41] Due to less strong binding of CO_2 in bicarbonates, CO_2 fixation by the corresponding alkali or alkaline earth metal carbonates (e.g. $CaCO_3$, Na_2CO_3 or K_2CO_3), despite proceeding slowly, facilitates more feasible CO_2 recovery.[3] In addition, ionic resins capable of capturing CO_2 from dry air and undergoing desorption upon contact with moisture have been reported.[3,41] Despite major progress, direct CO_2 capture from the atmosphere at a concentration of approximately 400 ppm[26] requires further improvements to become economically feasible as current estimations propose a price of 80-200 USD per ton of CO_2.[3,35,41] Nevertheless, direct CO_2 capture from the atmosphere would not only decouple the location of CO_2 emission from that of its capture, a major advantage if CO_2 capture is to be deployed in the transportation sector, but also enable CO_2 isolation and valorization all over the world.[3,34,35,41]

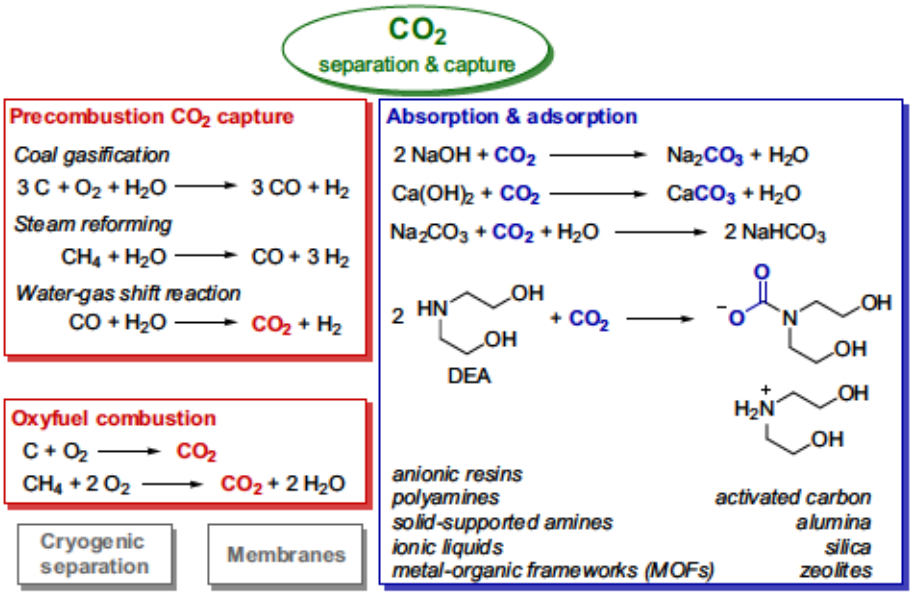

Figure 5: Possible strategies for CO_2 capture from its emission site or the atmosphere *via*, among others, oxyfuel combustion, precombustion capture, and absorption.[3,30,33–35,41]

1.1 Carbon Dioxide Valorization

Various strategies for the valorization of CO_2 are in place today and numerous transformations into fuels and chemicals as well as its technological application in water treatment, conservation of cereal and food, and as a solvent in the form of supercritical CO_2 ($scCO_2$), currently deployed for manufacture of decaffeinated coffee, have already been achieved at least on a laboratory scale.[3,35,36,46–48] Nevertheless, a vast number of challenges remain for the utilization of CO_2, especially with respect to commercial production of fuels starting from CO_2.[3,35,36,46–48] Some of these challenges result from the nature of CO_2 itself impacting the energy profile of its transformations.[35,36,46–48]

Carbon dioxide, a linear gaseous (ambient temperature and pressure) molecule, is the final product of combustion of carbon-based compounds, in combination with H_2O, resulting from its low standard formation Gibbs free energy of $\Delta G_f^\circ = -396$ kJ/mol.[35,36,48] This stability impacts its valorization as changes in the oxidation state of the C^{+4} will directly impact the overall energy requirement and frequently increase with decreasing oxidation state of the C atom in the final product.[35,36] Furthermore, conversion of CO_2 gas is often accompanied by an unfavorable change in reaction entropy resulting in additional energy requirements for the transformation.[35] Its comparatively high ionization potential (13.78 eV) prohibits strong interactions with Lewis or Brønsted acids.[48] However, localization of the lowest unoccupied molecular orbital (LUMO) on the C and the highest occupied molecular orbital (HOMO) on the O atoms (Figure 6) in combination with the considerable electronegativity difference between O (3.50) and C (2.50),[49] resulting in a partial positive charge of the C and a partial negative charge of the O, render the C atom prone to nucleophilic attack while electrophiles can interact with the O atoms.[46–48]

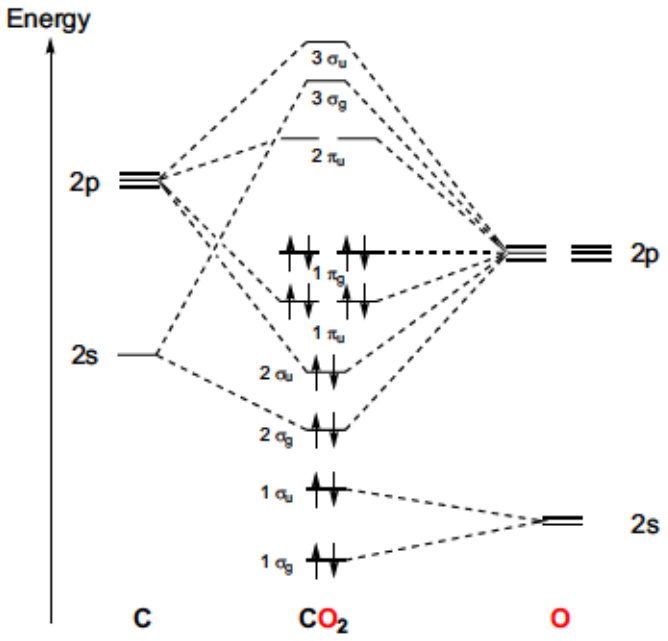

Figure 6: Molecular orbital diagram (qualitative) of CO_2.[47]

In a similar fashion, one CO_2 molecule can interact with a metal center forming CO_2 coordinated complexes in which C-, O-, κ^2-O_2C-, η^2-OCO-coordination as well as coordination *via* one of the CO bonds are conceivable (Figure 7).[46,47,50] In addition, two molecules of CO_2 can coordinate to one metal center either *via* twofold C- or O-coordination, coordination across one C=O bond or in an alternating fashion where one C- and one O-atom of different CO_2 molecules are coordinated.[50] Finally, two metal centers can coordinate to

one or two CO_2 molecules as depicted in Figure 7.[50] Of particular interest are structures **13**, **15**, and **20** where two CO_2 molecules are coordinated to one or two metal centers in such a way that allows for their coupling to form the mono- or dinuclear oxalato complexes **14**/**16** and **21**, respectively.[50] Finally, the formation of chains and rings containing more than two metal centers is possible, as displayed in structure **24**.[50] However, for its conversion, bending of the linear CO_2 constitutes a general prerequisite, a step with a significant energy requirement.[47,48] Strong electrophiles or nucleophiles are required to enable this structural modification in case no dual activation *via* joint electrophilic and nucleophilic interactions is feasible.[48] Efficient catalysts help to overcome these obstacles associated with CO_2 valorization.[35,36,46–48,50] Thus, the development of catalysts that facilitate activation of CO_2 and permit its conversion into a variety of products represents a major area of research within the field of catalysis.[35,36,46–48,50]

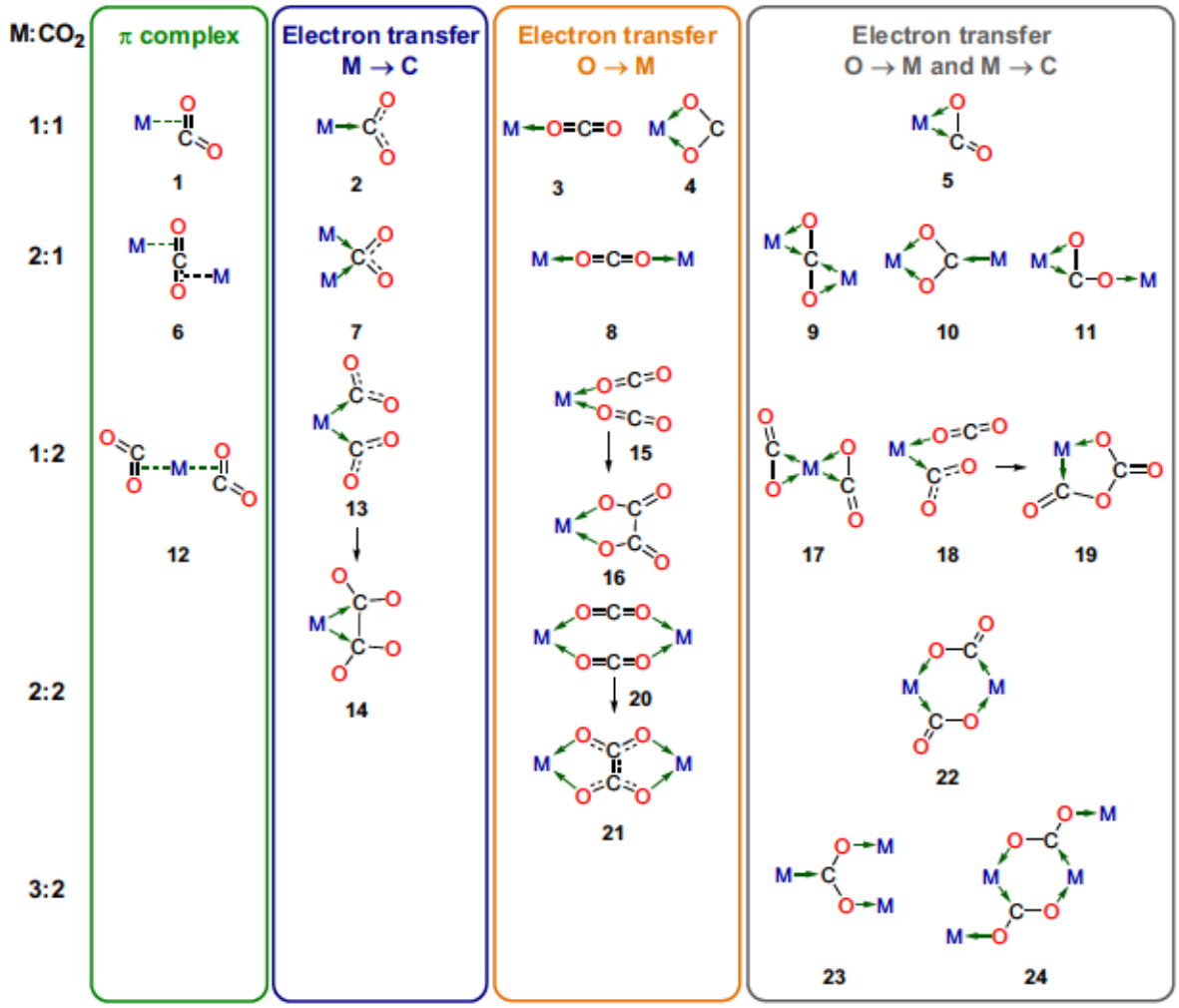

Figure 7: Possible coordination modes of CO_2 in metal complexes with varying CO_2:M composition.[50]

1.1.1 Conversion of CO_2 into Chemicals without CO_2 Reduction

With a scale of 155 Mt/year, urea production is currently one of the largest industrial processes utilizing CO_2.[35] Due to its importance as a fertilizer, the global production capacity of urea is expected to increase over the upcoming decades at a 5-7% rate per year.[35] The production is based on two steps (Scheme 1).[35,51] First, exothermic reaction of CO_2 and NH_3 results in the formation of ammonium carbamate.[35,51] Dehydration of the ammonium carbamate in the second step yields urea.[35,51] In the future, further increase of urea production based on its potential application in the fabrication of polymers or in synthetic chemistry has been envisioned.[35] However, hydrogen required for the formation of NH_3 *via* the *Haber-Bosch* process is still mainly produced using fossil fuels, a strategy that ultimately needs to be replaced by H_2 production from water to render CO_2 conversion with the use of hydrogen sustainable.[3,35,52]

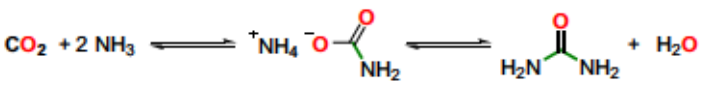

Scheme 1: Industrial synthesis of urea.[35,51]

Inorganic carbonates, $CaCO_3$ ensued by Na_2CO_3 as the major products, that were previously discussed as potential products of CO_2 capture from gas mixture or the atmosphere,[3,34,41] are currently produced on a scale of approximately 200 Mt per year (in 2014).[35] While they are nowadays mostly employed for the production of pulp and plastics, especially $CaCO_3$ and $MgCO_3$ have widely been discussed for storing CO_2.[35] However, this would require faster carbonate formation, but could ultimately facilitate the replacement of concrete as a construction material offering a tremendous market potential (32000 Mt per year).[35]

Organic carbonates can be subdivided into acyclic, cyclic, and polymeric carbonates and different production processes and applications exist for these three classes of compounds (Figure 8).[35,46,53–56] Acyclic carbonates are traditionally synthesized *via* direct reaction of phosgene with alcohols.[35,53,54] The high toxicity of phosgene, however, encourages the quest for an alternative production process, ideally based on CO_2 or readily available urea.[35,53,54] Catalysts for the preparation of mainly diethyl (DEC) and dimethyl carbonate (DMC) using CO_2 and the primary alcohol are mainly based on Sn and group five alkoxides or heterogeneous Ce, Zr, and Ti oxides.[35,53,54] Dehydrating agents, such as DCC (dicyclohexylcarbodiimide), facilitate the direct reaction of alcohols with CO_2 to the desired carbonates under mild conditions.[35,53] Stoichiometric formation of the corresponding dicyclohexylurea is a major disadvantage of this reaction, but recycling through dehydration with especially group 4/5 metal halides is possible.[35,53] Nevertheless, large amounts of waste generated in this process render it unsuitable for large scale application.[35,53] Direct reaction of urea and the alcohol for the production of acyclic alkyl carbonates is another feasible approach and a number of catalysts based on homogeneous Sn compounds, ionic liquids, and metal oxides, such as MgO, CaO, and ZrO_2, have been reported to catalyze this process.[35] Cyclic carbonates can readily be accessed *via* catalyzed reaction of epoxides

with CO_2.[35,46,54–56] This reaction is frequently conducted in $scCO_2$ which acts as reagent and solvent.[35,54] Numerous metal-based, mostly Al, Zn, Mg or Co complexes, and metal-free, such as phosphonium- or ammonium-salts, homogeneous and heterogeneous catalysts have been investigated for the formation of cyclic carbonates, such as propylene carbonate and ethylene carbonate.[35,46,54–56] In addition, the reaction of aziridines with CO_2 for the formation of oxazolidinones has been described in the literature.[46,57] Besides, direct conversion of olefins in an oxidative carboxylation has been studied, but limited examples based on O_2 as the ultimate oxidant have been described in the literature.[35,54] Finally, catalyzed reaction of diols with CO_2 is of interest since the formation of acyclic carbonates can be achieved by transesterification from cyclic carbonates frequently utilized in the production of DMC.[35,53,54] Propylene carbonate can be prepared *via* this route starting from 1,2-propanediol and CO_2 in the presence of a catalyst, such as MgO or $Zn(OAc)_2$.[35,54]

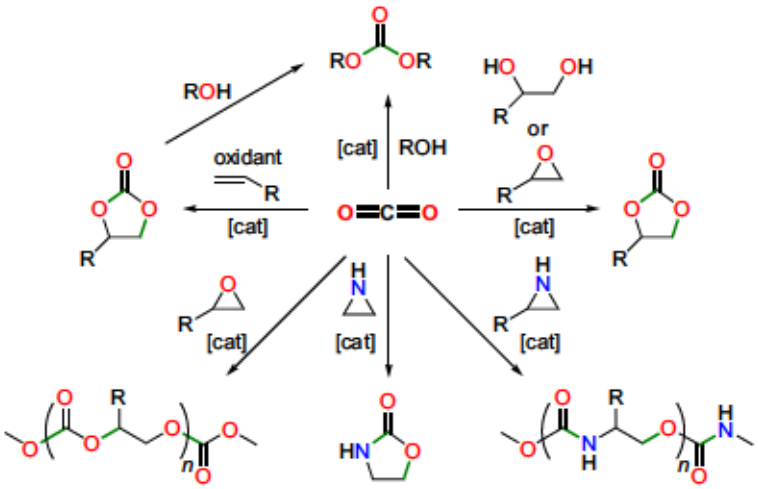

Figure 8: Possible applications of CO_2 in the synthesis of cyclic, acyclic, and polymeric carbonates and carbamates.[35,46,53–59]

Polycarbonates which are applied in various relevant industrial sectors, such as construction, packaging, automotive, or electronics, have experienced an increasing demand (more than 4 Mt in 2012) over the last decades and are nowadays industrially manufactured *via* copolymerization of epoxides with CO_2.[35,46,54,56] Catalysts that ensure alternating incorporation of the epoxide and CO_2 are mainly based on homogeneous Zn and Al complexes, albeit other metals, e.g. highly active salen-coordinated Cr(II) and Co(III), have been reported.[35,46,55,56] Variation of the substituents on the starting epoxides offers a multitude of properties of the resulting polymer.[35,56] Again, aziridines instead of epoxides have successfully been utilized for the direct preparation of polyurethanes starting from CO_2.[35,46,58,59]

1.1.2 CO_2 as a C_1 Building Block

One of the first industrial applications for CO_2 as a C_1 building block was the synthesis of salicylic acid starting from sodium phenoxide in the *Kolbe-Schmitt* reaction (Scheme 2).[35,46,60,61] In 2014, approximately 20000 tons of acetylsalicylic acid (*Aspirin*), one of the WHO essential

non-opioid analgesics,[62] were produced from thus prepared salicylic acid.[35]

A traditional approach for carboxylation reactions using CO_2 is based on high-energy starting materials, such as organolithium or -magnesium compounds.[35,46,63,64] Not surprisingly, various catalytic protocols for incorporation of CO_2 as a carboxylic acid, ester or lactone moiety, have been reported in the past that do not require sensitive organometallic starting materials (Figure 9).[35,46,63–65] One of these strategies relies on the utilization of organoboron compounds which are considerably less reactive than Grignard or organolithium reagents, and thus offer an easier handling and enhanced functional group tolerance.[46,63,64] C-C bond formation utilizing organoboron starting materials has been described with Rh[64] and Ag catalysts, but homogeneous Cu complexes proved to be especially active at low catalyst loadings and under comparatively mild conditions.[46,65–67] Alkenes and alkynes have also been utilized for this carboxylation approach from which the organoboron starting materials can be prepared *via* preformation with simple boranes.[65,68] In addition, the direct carboxylation of aryl, vinyl and benzylic halides has been achieved using Pd, Ni, or Cu complexes in combination with a reductant, such as Zn, organozinc compounds or Mn.[46,65,69] Activated C-H bonds offer the possibility of direct catalytic carboxylation with CO_2, a concept that has been reported for terminal alkynes and activated sp^2-C-H bonds in (hetero)arenes utilizing (among others) Cu, Ag, and Au catalysts.[35,46,63,65] Furthermore, direct catalytic carboxylation of alkenes and internal alkynes has been achieved using catalysts based on Ni, Pd, and Cu.[35,46,50,63,65,70] Initial reports based on Ni for this reaction were relying on stoichiometric reaction of the metal complex with alkenes or alkynes in combination with CO_2 resulting in oxidative cyclometallation yielding the metallacycles.[46,50] Catalytic versions of this transformation have also been described yielding e.g. pyrone derivatives in a Ni-catalyzed [2+2+2] cycloaddition of a diyne.[46,70] While the oxidative cyclometallation strategy is limited to expanded π bonds (di-, tri-, polyenes/-ynes), hydrocarboxylation with CO_2 in combination with a reducing agent is applicable to simple alkenes/alkynes.[46,65] However, all of these carboxylation procedures, despite not demanding the utilization of reactive starting materials, still yield (over)stoichiometric quantities of metal salts as waste resulting from the reducing agents, organometallic reagents utilized for transmetalation onto the catalyst, or metal compounds utilized as a base for activation of the electrophile.[35,46,63,65] Ideally, carboxylation with CO_2 would proceed either *via* hydrocarboxylation with H_2 or by C-H carboxylation without the necessity of any stoichiometric reagent required for C-H bond activation.[36,46,63]

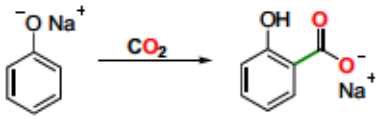

Scheme 2: *Kolbe-Schmitt* reaction yielding sodium salicylate *via* carboxylation of sodium phenoxide.[35,46,61]

Besides the application of amines for CO_2 capture, as discussed previously, their interaction with CO_2 can also enable further functionalization.[35,46,71–73] One possibility is the preparation of formamides, e.g. with NHCs as organocatalysts in combination with a mild silane or polysiloxane reductant.[46,71] Further reduction of formamides and ureas from CO_2 is pos-

sible and even the catalytic direct methylation of anilines and amines with CO_2 has been reported.[46,72,73]

Finally, CO_2 has been investigated as a substitute for CO in carbonylation reactions of alkenes based on the concept of *in situ* formation of CO *via* reduction of CO_2 under the reaction conditions.[36,46,74,75] Following this method, the direct hydroformylation followed by hydrogenation, yielding alcohols as main products has been described.[46,74] Interestingly, Ru-catalyzed alkoxycarbonylation of alkenes yielding the carboxylic acid esters has been achieved in the presence of ionic liquids relying on *"hydrogen borrowing"* from the alcohol for the *in situ* formation of CO or to a minor extent alkyl formates.[36,46,75] While significant progress in the utilization of CO_2 for the production of bulk and specialty chemicals has already been achieved, further improvements with respect to selectivity of the transformations, general reaction conditions, and specifically by-product formation as a result of essential reagents are highly desirable.[46]

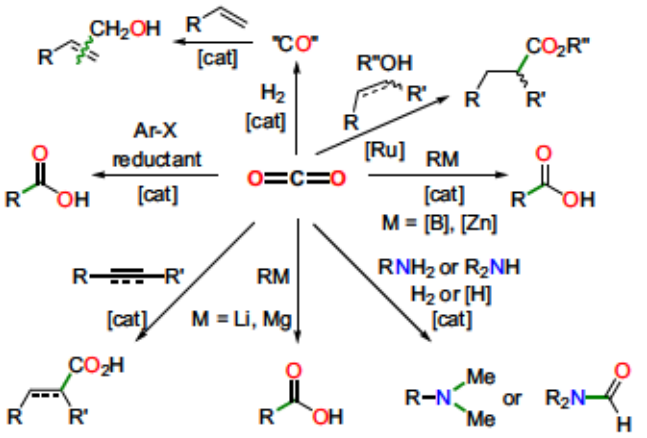

Figure 9: Selected examples of CO_2 as a C_1 building block in carboxylation, methylation, and formylation reactions and as a CO surrogate.[35,36,46,63–69,71–75]

1.2 CO_2 Reduction to C_1 Compounds

CO_2 reduction, especially to valuable C_1 compounds, namely formic acid, CO, formaldehyde, methanol, and methane, constitutes another possibility for the valorization of carbon dioxide.[35,36,47,48,52,76–81] Various catalytic protocols for CO_2 reductions relying on different forms of energy, such as electro- and photochemical as well as thermal reduction reactions utilizing e.g. hydrogen have been successfully developed over the past decades.[35,36,47,48,52,76–81] The ever-increasing interest in such transformations is not least a consequence of the potential application of these products as fuels or hydrogen storage materials.[35,36,47,52,76–81] Ideally, such CO_2 reduction reactions are ultimately combined with water oxidation and based on sunlight as energy resource in analogy to nature's photosynthesis - a strategy commonly referred to as *artificial photosynthesis*.[52,76–78,80,82,83]

1.2.1 Hydrogenation of CO_2 to C_1 Compounds

Formic acid, with a hydrogen content of 4.4 wt%, has been proposed as a liquid material for hydrogen storage and several transition metal complexes as well as heterogeneous materials with activity in its dehydrogenation have been reported.[35,52,84–91] The reverse reaction, CO_2 hydrogenation to formic acid, has likewise been subject to extensive investigation.[35,48,52] The

overall formation of liquid HCO_2H starting from gaseous H_2 and CO_2 is thermodynamically unfavorable (ΔG°_{298K} = 32.8 kJ/mol) due to the negative reaction entropy.[52] However, addition of bases or utilization of a solvent can alter the energetics and thereby favor the desired reaction pathway.[52] Hence, hydrogenation of CO_2 to HCO_2H is already exergonic when conducted in aqueous solution (ΔG°_{298K} = −4.0 kJ/mol) and becomes even more feasible when bases, such as ammonia, are added (ΔG°_{298K} = −9.5 kJ/mol).[52] Numerous homogeneous metal complexes have been reported for the hydrogenation of CO_2 to formates since the initial study by Inoue and co-workers, but some of the most active catalysts nowadays are still based on precious Ru and Ir.[35,48,52] One example for an outstanding catalytic activity was reported by Nozaki and co-workers.[92] A PNP-ligated Ir trihydride complex (**25**) enabled a total TON of 3500000 at 120 °C under 60 bar CO_2/H_2 in aqueous KOH solution containing THF (50:1, *v*:*v*) (Scheme 3).[35,48,52,92] A more sustainable concept for the continuous hydrogenation of CO_2 in a flow reactor was proposed by Leitner and co-workers and is based on combining a stationary ionic liquid phase with a mobile $scCO_2$ phase.[93] Using a Ru complex based on a sulfonylated phosphine ligand in an imidazolium-based ionic liquid, a TOF of >295 h^{-1} at a total TON of 1968 was achieved under 100 bar CO_2/H_2 (1:1) at 50 °C (Scheme 3).[36,52,93] Continuous extraction of the HCO_2H into $scCO_2$ was successfully achieved despite it being the bottleneck of this method.[36,52,93]

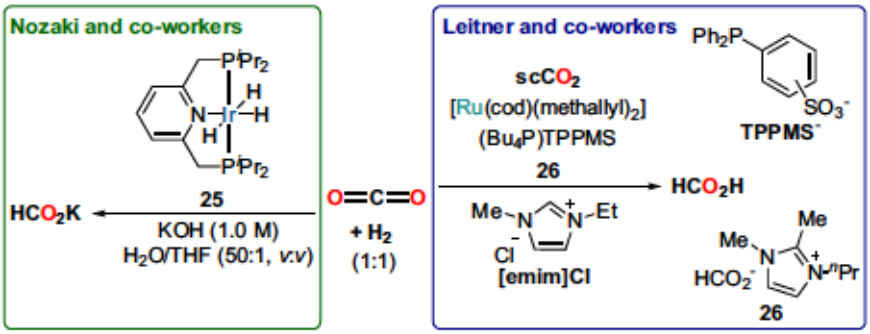

Scheme 3: CO_2 hydrogenation to formic acid catalyzed by PNP-ligated Ir complex **25** or [Ru] in an ionic liquid media.[36,52,92,93]

In contrast to formic acid hydrogenation, the direct production of MeOH from gaseous CO_2 and H_2 is an exergonic reaction when liquid H_2O is formed as the by-product (ΔG°_{298K} = −9.5 kJ/mol).[52] Hence, the production of MeOH starting from CO_2 has been known for nearly one century.[3] Nowadays, most of the industrially produced MeOH is formed from CO/H_2 mixtures using heterogeneous Cu/ZnO catalysts that contain Al_2O_3 (60/30/10 wt%).[3,36,48,94] Interestingly, mechanistic investigations indicated that MeOH is for the most part formed from hydrogenation of CO_2 present in the syngas mixtures or formed *via* WGSR from CO and H_2O.[3,36,48,94] This is evident not only from isotopic labeling studies, but also from the observation that dry and CO_2-free syngas depicted nearly no MeOH formation under otherwise identical reaction conditions.[3,48,94] Despite the process relying on syngas, the industrial-scale production of MeOH (4000 t/y) using CO_2 captured from the exhaust of a geother-

mal power plant in combination with hydrogen from water electrolysis has been established in Iceland in *"The George Olah Renewable Methanol Plant"* by *Carbon Recycling International*.[3,36,95] Meanwhile, homogeneously catalyzed direct hydrogenation of CO_2 to MeOH remains a challenging transformation.[52] However, the Leitner group was able to accomplish the direct formation of MeOH starting from CO_2/H_2 (1/3) at 80 bar (pressure re-adjusted twice) and 140 °C using a triphos-coordinated Ru complex in combination with bis(trifluoromethane)sulfonimide in THF yielding a TON of 603 (48 h) (Scheme 4).[36,52,96] More recently, Beller and co-workers reported a similar method for CO_2 hydrogenation using Co triphos complexes in the presence of EtOH instead of a precious Ru-based catalyst (Scheme 4).[97,98] By careful optimization of the reaction conditions, a TON of 70 was achieved at 90 °C under 90 bar CO_2/H_2 (2:7) using $Co(NTf_2)_2$/triphos as the catalyst in THF/EtOH.[98]

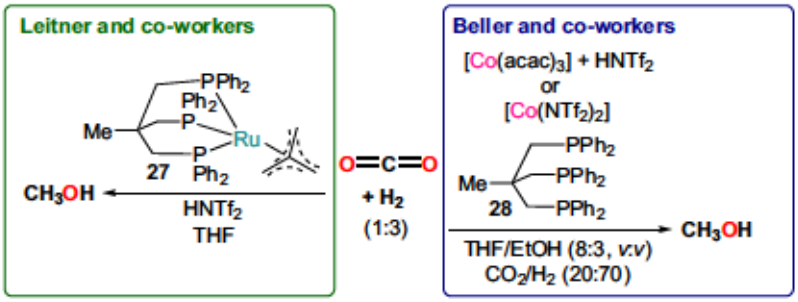

Scheme 4: Formation of MeOH *via* hydrogenation of CO_2 catalyzed by Ru and Co triphos complexes as reported by the Leitner and the Beller group.[36,52,96–98]

1.2.2 Electrochemical CO_2 Reduction to C_1 Compounds

Apart from H_2 as reducing agent for the valorization of CO_2, electricity, i.e. electrons as the ultimate reductant, arguably offers great potential for future applications.[35,47,81] While electricity production using fossil fuels for the sake of converting CO_2 into C_1 building blocks would be an unsustainable approach, application of excess electricity generated from fossil fuels or utilizing low-C electric energy renders the general methodology valuable.[35] Moreover, electrochemical CO_2 reduction into fuels would establish a convenient technology for the storage of electrical energy, as batteries are restricted by their low volumetric energy density.[35] However, direct electrochemical CO_2 reduction to form $CO_2^{\bullet-}$ is thermodynamically challenging, obvious from the significantly negative standard redox potential (E^{00} = −1.90 V *vs.* NHE), result-

Table 1: Standard redox potentials for selected CO_2 reduction reactions in aqueous solutions.[47]

Reaction	E^{00} [V *vs.* SHE]
$CO_2(aq) + e^- \rightleftarrows CO_2^{\bullet-}$	−1.90[a]
$CO_2(g) + 2H^+ + 2e^- \rightleftarrows HCO_2H(l)$	−0.25
$CO_2(g) + 2H^+ + 2e^- \rightleftarrows CO(g) + H_2O(l)$	−0.11
$CO_2(g) + 4H^+ + 4e^- \rightleftarrows H_2CO(l) + H_2O(l)$	−0.07
$CO_2(g) + 6H^+ + 6e^- \rightleftarrows MeOH(l) + H_2O(l)$	+0.02
$CO_2(g) + 8H^+ + 8e^- \rightleftarrows CH_4(g) + 2H_2O(l)$	+0.17
$2CO_2(g) + 2H^+ + 2e^- \rightleftarrows H_2C_2O_4(aq)$	−0.50
$2CO_2(g) + 2e^- \rightleftarrows C_2O_4^{2-}(aq)$	−0.59
$2CO_2(g) + 12H^+ + 12e^- \rightleftarrows EtOH(l) + 3H_2O(l)$	+0.08

[a]Potential reported *vs.* NHE.

ing from the associated geometry change.[47,52,81] With respect to thermodynamics, proton-coupled multi-electron reductions are more feasible (Table 1), but these reactions generally require catalysts.[47,52,79,81] It is noteworthy that these reactions not only require a proton source, but display a significant pH dependence of the electrode potentials when conducted in aqueous solution due to varying proton availability.[47,81] Moreover, unfavorable reaction kinetics of these processes render the applied electric potentials more negative than thermodynamically needed, with the difference between applied and theoretical potential to obtain a certain reaction rate defined as the overpotential η.[47,81] Product selectivity constitutes another major challenge in electrochemical CO_2 reduction, as perceived from the relatively close proximity of the redox potentials for different reduction reactions enabling a multitude of potential reaction pathways.[47,79] Both, higher selectivity and reduced overpotentials, can be accomplished with the help of suitable catalysts for the CO_2 reduction reaction.[47,79,81]
Single electron reduction of CO_2 at a low potential on an inert electrode, such as lead or mercury, results mainly in coupling of the CO_2 radical anion to form oxalate.[47,79,81,99–102] In case the CO_2 interacts with the electrode material, the energy barrier for its reduction might be reduced enabling lower η values for the electron transfer onto the chemisorbed CO_2 and the subsequent reaction.[47] Furthermore, the product selectivity can be affected by this interaction.[47] While inert electrodes function *via* outer-sphere electron transfer to CO_2, the latter reduce CO_2 in an inner-sphere process and can thus be designated as electrocatalyst.[47] Suitable metals that interact with CO_2 in such a way are Au, Ag, and Cu.[47] While the former mainly yield CO as CO_2 reduction product, the latter is known to produce formaldehyde, methanol and even hydrocarbons, when the electrochemical CO_2 reduction is conducted in aqueous media.[3,47,81,103–106] Homogeneous electrocatalysts allow for readily adjustable properties by varying the metal, the ligand, or its substituents in case of metal-free catalysts.[47,81] As for the heterogeneous electrocatalysts, homogeneous electrocatalysts can function *via* either outer-sphere or inner-sphere reduction.[47,81] In the former case, the reduced electrocatalyst transfers an electron to the CO_2 generating the $CO_2^{\bullet-}$ that undergoes further transformations.[47,81] In this process, termed redox catalysis, the homogeneous nature of the catalyst enables beneficial CO_2 reduction in solution away from the electrode surface, albeit the energy required for the electron transfer is unaltered compared to an inert electrode.[47,81] Moreover, outer-sphere electrocatalysts are prone to react with CO_2 resulting in the formation of carboxylated products.[47,81] In contrast, homogeneous catalysts enabling inner-sphere electron transfer will bind to the CO_2 molecule prior to its reduction and further conversion.[47,81] In this case, coordination of CO_2 can facilitate bending of the molecule, thus omitting the requirement of geometry change as part of the reduction step.[47] In general, the energy barrier for inner-sphere reduction of CO_2 is reduced compared to the outer-sphere process.[47,81] For both strategies, the electron transfer should proceed first from the electrode to the catalyst and subsequently *via* the reduced catalyst to CO_2.[47,81] Hence, the redox potential of the catalyst is the potential required for CO_2 reduction which implies that this is

generally more positive than that of the direct uncatalyzed CO_2 reduction reaction.[47]
Over the past decades, numerous homogeneous catalysts based on various metals, such as Mn, Fe, Co, Ni, Cu, or Ru, have been reported for electrochemical reduction of CO_2.[47,76,78,79,81,107,108] A recent report by Robert and co-workers highlights the flexibility of homogeneous catalysts with respect to tunable product selectivities.[107] Electrolysis of Co complex **29** coordinated by a pentadentate macrocyclic ligand in DMF (containing 0.1 M $^n Bu_4NPF_6$) at −1.5 V *vs.* SCE selectively yielded CO (82% Faradaic yield) in 1 h (Scheme 5).[47,107] In contrast, the analogous Fe complex **30** produced formic acid with a high selectivity (75-80% Faradaic efficiency) when electrolyzed at −1.25 V *vs.* SCE in DMF for 3 h.[47,107] The distinct product selectivity was likewise obtained in the photochemical CO_2 reduction utilizing these complexes.[107]

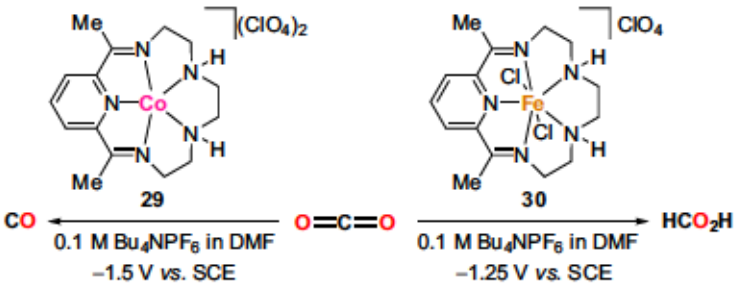

Scheme 5: Electrocatalytic CO_2 reduction to CO and formate catalyzed by macrocycle-ligated Co and Fe complexes reported by Lau, Robert, and co-workers.[47,107]

While homogeneous electrocatalysts for more than two-electron reduction of CO_2 remain scarce, specifically those based on non-precious metals, Koper and co-workers reported the formation of small quantities of CH_4 and traces of MeOH when conducting CO_2 reduction in aqueous electrolyte at low pH using a porphyrin-ligated Co complex that was immobilized on a pyrolytic graphite electrode.[47,79,108] However, the major CO_2 reduction product was CO, with a Faradaic efficiency of up to approx. 60% accompanied by H_2 evolution.[47,108]
Besides competing formation of hydrogen in the presence of protons, long-term catalyst stability remains a major challenge in the development of electrochemical CO_2 reduction protocols, albeit significant progress has been achieved in the past decades to tackle these problems.[3,47,52,79,81,107]

1.2.3 Photochemical CO_2 Reduction to C_1 Compounds

Direct utilization of light for the reduction of CO_2 into energetically enriched materials is another research area of increasing interest, due to its inherent advantage of possibly employing sunlight as the ultimate environmentally benign energy resource.[35,76–80,82] However, most CO_2 reduction catalysts have to be combined with another light absorbing compound, frequently a semiconductor or homogeneous photosensitizer, to enable the energetic conversion of light.[35,48,52,76–80,82] Illumination of the photosensitizer (PS) will result in its excitation giving rise to PS* which has significantly altered redox potentials and can thus undergo

two potential follow-up reactions.[76,77,79,80,82,109] The first possible reaction is so-called oxidative quenching where an electron is transferred from PS* onto an electron acceptor (e.g. the reduction catalyst) yielding the single-reduced acceptor molecule and the oxidized $PS^{\bullet+}$ (Scheme 10).[76,77,79,82,109] The most common reaction pathway in photocatalytic CO_2 reduction is reductive quenching, a process in which PS* is reduced by an electron donor (ED) to $PS^{\bullet-}$ accompanied by formation of $ED^{\bullet+}$.[52,76,77,79,80,82] For the photocatalytic CO_2 reduction process, a sufficiently long lifetime of the excited PS* is required to facilitate the reductive quenching process and an excitation should ideally be possible in the visible light region without overlapping with the absorption wavelength of the electron donor or the CO_2 reduction catalyst.[76,77] Furthermore, the redox potentials of the PS in the ground and excited state have to be compatible with the oxidation potential of the ED and the reduction potential of the CO_2 reduction catalyst.[52,77,79,82,109] The $PS^{\bullet-}$ subsequently transfers the electron onto the reduction catalyst which in many cases has to be capable of storing the electrons transferred from the PS due to the thermodynamically favored multi-electron reduction reactions of CO_2, in contrast to electrochemical CO_2 reduction where more than one electron can be transferred to the catalyst in a short timeframe.[52,77,79,80,82]

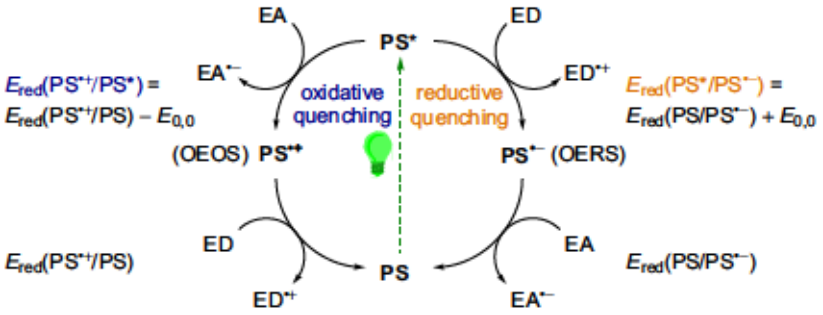

Figure 10: Fundamental reactions of a photosensitizer consisting of reductive and oxidative quenching by an electron donor or acceptor after excitation and the altered redox potentials of these processes ($E_{0,0}$ constitutes the energy difference between ground and lowest excited state), respectively.[77,80,109]

Importantly, the oxidation product of the electron donor should be short-lived to circumvent oxidation of $PS^{\bullet-}$ by reverse electron transfer.[77,82] While the ideal electron donor would be water, resulting in the formation of O_2 as the oxidation product,[35] the combination of water oxidation and CO_2 reduction in a single photocatalytic protocol remains challenging, hence sacrificial electron donors (SEDs), such as tertiary amines, alcohols or NADH models, are commonly employed for investigations on homogeneous photocatalytic CO_2 reduction.[52,76–80,82]

Photocatalytic CO_2 reduction to a mixture of C_1 products consisting of mainly HCO_2H, formaldehyde, and methanol with traces of methane, were first observed by Inoue *et al.* utilizing various semiconductors, such as SiC, TiO_2, or CdS, in aqueous solution.[77,110] Only a few years later, Lehn and Ziessel accomplished the first homogeneous photocatalytic CO_2 reduction based on well-known $[Ru(bpy)_3]^{2+}$ as photosensitizer and $CoCl_2$ as the CO_2 re-

duction catalyst.[76,111] At this point, the best selectivity for CO_2 reduction of ca. 24:1 CO/H_2 was achieved using triethanolamine (TEOA) as sacrificial electron donor by illuminating (Xe lamp, >400 nm) the reaction for 22 h in a MeCN/TEOA/H_2O mixture (3:1:1, *v*:*v*:*v*).[111] It is noteworthy to mention that the addition of 2,2'-bipyridine decreased the observed CO/H_2 selectivity by enhancing proton reduction.[111] However, substituting 2,2'-bipyridine by 2,9-dimethylphenanthroline (dmp) facilitated a significant increase in catalytic activity and 19 mL H_2 together with 8 mL CO were produced by illuminating $CoCl_2 \cdot 6H_2O$, dmp and $[Ru(bpy)_2]^{2+}$ in CO_2 containing DMF/TEOA (5:1) over 15 h.[112]

As part of the same work, $[Re(bpy)(CO)_3X]$ (X = Cl, Br) complexes were identified as suitable CO_2 reduction catalysts that also served as photosensitizers.[76–78,80,112] These Re^{I} complexes showed a significantly improved CO selectivity and no concurrent H_2 formation was observed under optimized conditions, where illumination of $[Re(bpy)(CO)_3Cl]$ in DMF/TEOA (5:1) at >400 nm (250 W) over 4 h in the presence of Et_4NCl yielded CO with a TON of 48 (Scheme 6).[112] Isotopic labeling with $^{13}CO_2$ ensured the origin of CO being photocatalytic CO_2 reduction.[112,113] The addition of a Cl^- source proved to be crucial for the long-term stability of the catalytic system due to the formation of a catalytically less active Re formate complex ($[Re(bpy)(CO)_3(OOCH)]$) when no stabilizing Cl^- was present.[80,112,113]

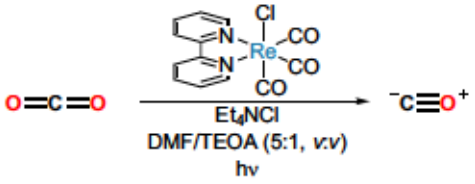

Scheme 6: Re catalyzed CO_2 reduction to CO in DMF/TEOA (5:1, *v*:*v*) utilizing visible light in the presence of Et_4NCl.[112,113]

In an attempt to further optimize the photocatalytic capability, both of the required functions have been combined by molecularly linking the photosensitizer and the reduction catalyst through a bridging ligand giving rise to a class of so-called supramolecular catalysts.[52,76–78,80] The desired enhancement of catalytic activity for these supramolecular complexes was envisaged based on elimination of the diffusion limited electron transfer in the bicatalytic system, which requires a collision of the isolated PS and the CO_2 reducing complex.[52,77] This strategy has already been pursued by Kimura and co-workers in the 1990s by combining Ru-based photosensitizers with well-known $[Ni(cyclam)]^{2+}$ *via* a methylene linker on one of the diimine (N^N) ligands.[77,80,114,115] The initial dyad **31** (Figure 11) based on a cyclam-substituted 2,2'-bipyridine containing a methylene-bridge in the 6-position of bpy depicted poor stability resulting in decomposition of the

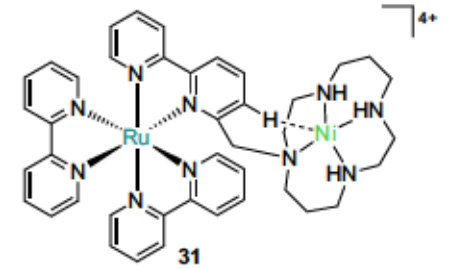

31

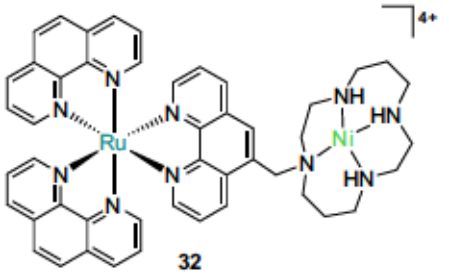

32

Figure 11: Dyads consisting of a $[Ni(cyclam)]^{2+}$ and a Ru PS moiety developed by Kimura and co-workers.[114,115]

complex upon illumination.[114,115] Refinement of the supramolecular catalyst to reduce the steric crowding imposed by the linker *via* application of a 5-substituted phenanthroline-based bridging ligand gave the Ru-Ni-based complex **32**.[115] Complex **32** acted as an active catalyst for photocatalytic CO_2 reduction upon irradiation (Xe lamp, 500 W) of an aqueous CO_2 solution containing ascorbate (1.0 M) as the SED at 25 °C yielding 3.51 μL CO in a 2.5:1 CO/H_2 mixture over 44 h.[115] While the overall activity remained comparatively low, the dyad proved to be more stable and selective than the combination of the mononuclear complexes $[Ru(phen)_3]^{2+}$ and $[Ni(cyclam)]^{2+}$ which produced 1.29 μL of CO and depicted a CO/H_2 selectivity of 0.57:1 under identical conditions.[80,115]

Various supramolecular complexes for the photocatalytic CO_2 reduction combining diverse metals with the help of a plethora of bridging ligands have been reported since these pioneering examples.[77,78,80] One revolutionary system enabling high TONs for CO_2 reduction to CO utilizing visible light was achieved by combining Re^I complexes that mainly absorb UV light with a Ru-based PS.[52,76–78,80,116] Ishitani and co-workers prepared different of these Ru-Re complexes bridged by bipyridine and phenanthroline analogues, evaluated their electro- and photochemical properties, and validated their applicability in photocatalytic CO_2 reduction.[116] The most active complexes, tetranuclear **33** and dinuclear **34**, yielded CO with high TONs of 170 and 240, respectively, upon illumination at ≥500 nm for 16 h in DMF/TEOA (5:1, *v*:*v*) containing BNAH (0.1 M) as the SED (Scheme 7).[116] This indicated a significant improvement compared to the analogous $[Re(dmb)(CO)_3Cl]/[Ru(dmb)_3]^{2+}$ (dmb = 4,4'-dimethylbipyridine) combination which produced CO with a TON of 100 over 16 h.[116]

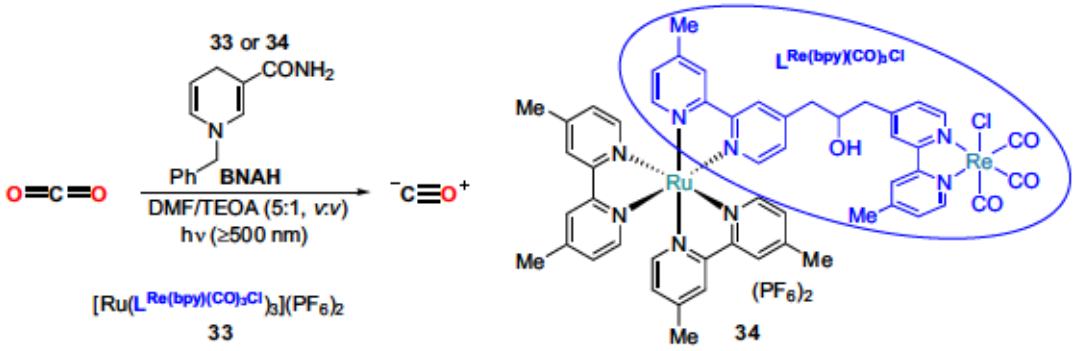

Scheme 7: Supramolecular complex combining a Ru PS with a Re reduction catalyst reported by Ishitani and co-workers for the photocatalytic reduction of CO_2 to CO.[116]

A major disadvantage of the systems based on Re and Ru as the CO_2 reduction catalysts is the comparatively low abundance of these metals, hence earth-abundant first-row transition metal catalysts would be favorable in the long run.[47,76,78,79] An early example for this approach was reported by Tinnemans and co-workers and is based on tetraazacycle-ligated Co complexes.[80,117] Besides their activity in electrocatalytic CO_2 reduction, high TONs of up to 100 for CO/H_2 (0.29/1) at a decent CO selectivity were obtained upon irradiation of complex **35** and $[Ru(bpy)_3]^{2+}$ for 18 h with daylight lamps in CO_2 saturated H_2O containing ascorbic acid/ascorbate as the SED (Scheme 8).[117] The selectivity toward CO_2 reduction

was not only dependent on the ligand employed and complex **36** produced nearly no CO with a CO/H_2 ratio of <0.01, but also on the [Co] catalyst concentration.[117] Interestingly, structurally related complex **29** enabled CO_2 reduction to CO (~97% selectivity) with a TON of 270 when irradiated with $[Ir(ppy)_3]$ and NEt_3 as SED in MeCN for 22 h.[107]

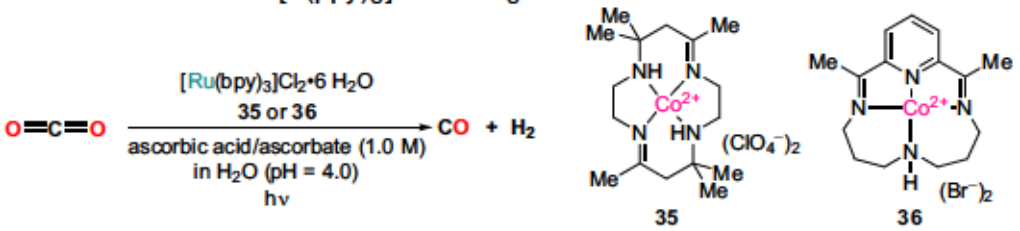

Scheme 8: Tetraazacycle-ligated Co complexes and their application in photocatalytic CO_2 reduction in combination with $[Ru(bpy)_3]^{2+}$ and ascorbic acid.[117]

Analogous Ni complexes, such as $[Ni(cyclam)]^{2+}$, were likewise investigated in combination with $[Ru(bpy)_3]^{2+}$ and ascorbic acid in water and depicted a high selectivity for the reduction of CO_2 to CO as well.[118] However, the quantum yield remained rather low with only 6.0×10^{-4} for CO using a 1000 W lamp at 440 nm.[118]

Iron porphyrins, such as [Fe(TPP)Cl] (TPP = tetraphenylporphyrin), were also capable of reducing CO_2 to CO even in the absence of an additional photosensitizer.[119] Irradiation of [Fe(TPP)Cl] (10^{-5} M) in DMF containing NEt_3 (5%) using a Xe lamp (300 W) enabled CO_2 reduction with a TON up to 70 (Scheme 9), albeit a decrease in catalytic activity was observed over time due to decomposition of the porphyrin ligand.[119] Interestingly, combining the Fe porphyrin with an organic photosensitizer (*p*-terphenyl - TP) enabled significantly higher activity for CO production with a near sixfold increase in CO yield accompanied by considerable H_2 quantities.[121]

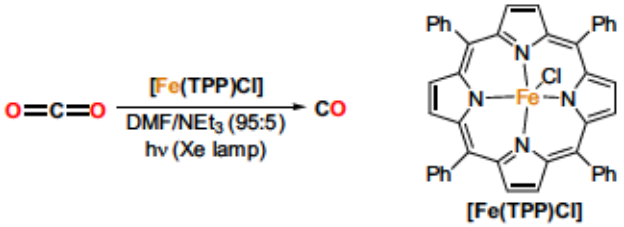

Scheme 9: Fe porphyrins as CO_2 reduction catalysts in DMF containing NEt_3 (5%) as reported by Neta and coworkers.[119]

Modification of the porphyrin ligand by introduction of 2,6-dihydroxophenyl substituents and combination of the derived Fe complex with $[Ir(ppy)_3]$ (ppy = 2-phenylpyridine) as the PS was recently reported by Bonin *et al.* to increase CO selectivity and catalytic activ-

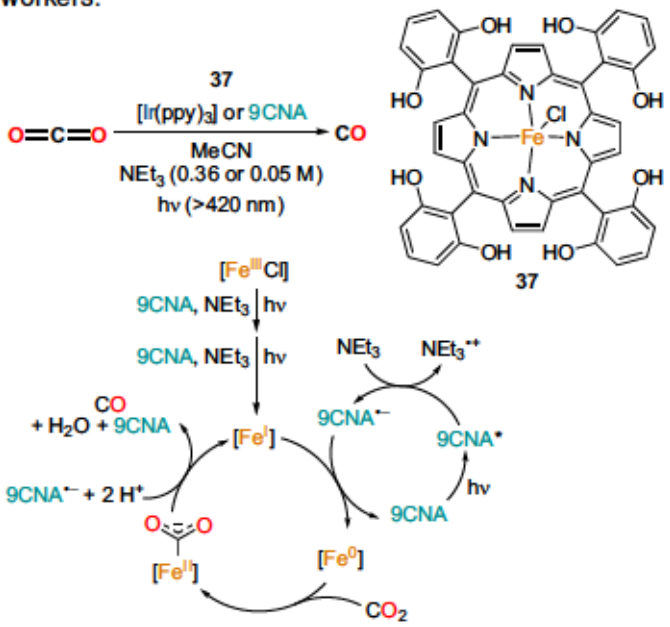

Scheme 10: Photocatalytic CO_2 reduction catalyzed by substituted Fe porphyrin **37** with $[Ir(ppy)_3]$ or 9CNA and the proposed reaction mechanism.[120]

ity.[120] Reaction with CO_2 for 55 h with NEt_3 (0.36 M) as SED in MeCN containing $[Ir(ppy)_3]$ and complex **37** using visible light (>420 nm) resulted in the formation of CO with a TON of 140 and a CO/H_2 selectivity of 93% (Scheme 10).[120] Most importantly, replacement of the Ir Ps by 9-cyanoanthracene (9CNA) not only enhanced the CO selectivity even further to 100%, but still gave rise to a CO TON of ~60 in less than 50 h at a lower NEt_3 concentration (0.05 M).[120] A possible reaction mechanism was proposed and comprised reductive quenching of excited 9CNA* by NEt_3 as indicated by fluorescence quenching experiments followed by multiple reduction steps of **37** to the Fe^0 complex.[120] Reaction with CO_2 to an H-bond stabilized intermediate, enabled by the OH substituents on the porphyrin backbone,[77] follow-up reduction, and C-O bond cleavage yield the observed CO.[120]

Non-macrocyclic Fe complexes were likewise reported for the photocatalytic CO_2 reduction to CO and one particularly useful ligand was found to be 2,2':6',2":6",2"'-quaterpyridine (qpy) as reported by the groups of Chen, Lau and Robert.[122] In combination with $[Ru(bpy)_3]^{2+}$ and 1,3-dimethyl-2-phenylbenzimidazol (BIH) as the SED in a MeCN/TEOA mixture (4:1), $[Fe(qpy)(H_2O)_2]^{2+}$ (**38**) formed CO with a TON of 1879 and a selectivity of 97% within 3 h of irradiation with a blue LED (Scheme 11).[122] Minor quantities of H_2 (TON=15) and formate (TON=48) were formed as by-products which increased upon lowering the catalyst concentration to 0.005 mM to 118 and 534 for H_2/HCO_2^-.[122] However, at this reduced catalyst loading an impressive TON for CO of 3844 within 45 min was obtained.[122] In addition to the Fe complex, $[Co(qpy)(H_2O)_2]^{2+}$ (**39**) and $[Cu(qpy)]^{2+}$ (**40**) were utilized applying the same photocatalytic CO_2 reduction protocol.[122,123] For the Co complex, a TON of 2660 for CO at 98% selectivity was obtained utilizing a 5 μM catalyst concentration and 80 min reaction time.[122] For the analogous Cu complex, a CO TON of 2425 was observed upon irradiation with visible light (>420 nm) in MeCN containing 15% TEOA and 0.1 M BIH.[123] However, a lower CO selectivity of 80% was observed due to considerable quantities of H_2 (TON=623) and traces of formate (TON=8) which were simultaneously formed.[123]

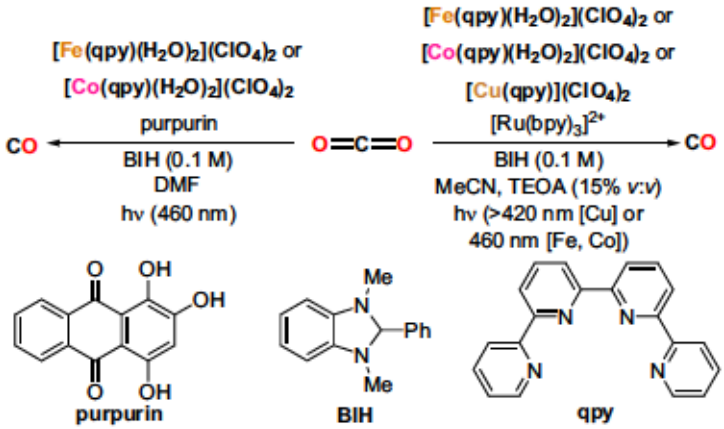

Scheme 11: Co, Fe, and Cu quaterpyridine complexes as catalysts for the CO_2 reduction to CO/formate/H_2 utilizing visible light and BIH as SED.[122,123]

The CO_2 reduction activity could be significantly increased by addition of water and at a 3% H_2O and 1 μM **40** concentration, a CO TON of 12400 within 3 h was achieved accompanied

by an enhancement of the CO selectivity to 97%.[123] The observed effect was rationalized by a stabilizing influence of water during CO_2 coordination by hydrogen bonding/protonation as well as potential facilitation of the required C-O bond scission.[123] At high H_2O concentrations, proton reduction competes with CO_2 reduction, thus formation of H_2 was found to increase at higher [H_2O].[123] For the Fe and Co complexes **38** and **39**, a protocol in the absence of precious metals by combination with purpurin as the PS was reported.[122] CO production was accomplished with TONs of 1365 (**38**) and 790 (**39**) with high to ideal selectivity of 100% and 95% upon irradiation of the complexes (5 μM) for 12 h in DMF containing BIH (0.1 M) and 0.02 mM purpurin.[122]

While molecular Cu complexes are seldom utilized for photocatalytic CO_2 reduction,[123] they have frequently been applied as photosensitizers for various photoredox transformations.[124–139] Heteroleptic Cu^I complexes of the general structure $[Cu(N^{\wedge}N)(P^{\wedge}P)]^+$ bearing a bisphosphine and a diimine ligand depicted promising electro- and photochemical properties, such as sufficient excited state lifetimes of >10 μs,[130] and were thus utilized in photocatalytic proton reduction[128,129] or organic photoredox catalysis[136,138,139].[124–127,137] Not surprisingly, their area of application was recently broadened to photocatalytic CO_2 reduction by Ishitani and co-workers, enabling another noble metal free system for the photocatalytic formation of CO.[130–135] Different mono- and dinuclear $[Cu(N^{\wedge}N)(P^{\wedge}P)]^+$ complexes were prepared and evaluated in combination with $[Fe(dmp)_2(NCS)_2]$ in MeCN/TEOA (5:1, *v*:*v*) utilizing BIH as the sacrificial reductant.[130] Dinuclear Cu PS **41** depicted the highest activity arguably due to the stability of **41** itself and its one electron reduced species (OERS).[130] Irradiating a CO_2 saturated MeCN/TEOA solution of **41** (0.25 mM) and $[Fe(dmp)_2(NCS)_2]$ (50 μM) containing BIH (10 mM) at 436 nm for 5 h gave CO and H_2 (Scheme 12) in high quantum yields of 6.7% and 2.8% corresponding to TONs of 95 (CO) and 56 (H_2), respectively.[130] Higher BIH concentrations (50 mM) enabled even higher TONs of 273 (CO) and 75 (H_2) equivalent to a CO selectivity of 78%.[130]

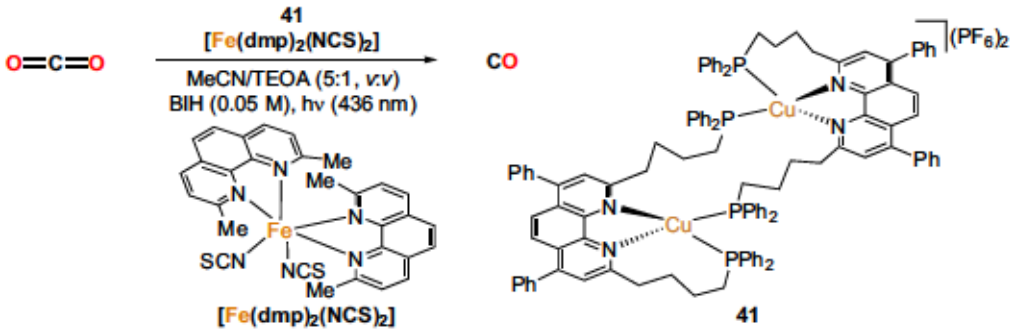

Scheme 12: Dinuclear heteroleptic Cu PS **41** and its application in the photocatalytic CO_2 reduction with $[Fe(dmp)_2(NCS)_2]$ and BIH.[130]

A similar CO_2 reduction protocol based on the combination of mononuclear heteroleptic Cu photosensitizers with cyclopentadienone-ligated Fe complexes, previously utilized in electrochemical[140] and photocatalytic CO_2 reduction together with an Ir PS,[141] was recently described.[131] The optimum combination was achieved with [Cu(bcp)(xantphos)]PF_6

(bcp = 2,9-dimethyl-4,7-diphenyl-1,10-phenanthroline) and complex **43** in a *N*-methylpyrrolidone (NMP)/TEOA mixture (5:1, *v*:*v*) using BIH (0.1 M) as the SED and visible light (400-700 nm, 1.50 W) resulting in CO/H_2 formation with a total TON of 432 and a CO selectivity of 99% (Scheme 13).[131] Interestingly, the Cu PS could be formed *in situ* analogously to a previous procedure for Fe catalyzed proton reduction[129] and an improved performance for CO formation (TON=487) at retained selectivity was obtained when a mixture of $[Cu(MeCN)_4)]PF_6$, xantphos and bathocuproine in a 1:3:1 ratio was employed instead of the pre-formed complex.[131] The steric impact of the substituents in 2,9-positions of the diimine ligand was further investigated using this *in situ* system, as steric bulk in these positions can impact the possibility of solvent coordination in the flattened excited state of the Cu PS that might result in exciplex quenching and reduce the excited state lifetime.[124,126,127,131,142] However, an increased steric bulk imposed by substitution of Me groups in bathocuproine with ^{i}Pr, ^{i}Bu or ^{n}Hex led to a decreased CO production as did the substitution of xantphos by DPEPhos.[131] Increased steric bulk on the Fe catalyst by replacement of a Me from the $SiMe_3$ substituent with ^{i}Pr resulted in a nearly 50% decrease in catalytic activity.[131] In addition, introduction of an oxygen-bridge into the cylopentadienone ligand (**45**) decreased the TON for CO formation to 80, a trend that had already been observed in combination with an Ir PS,[141] indicating the importance of the electronic and steric properties of the cyclopentadienone ligand.[131] Albeit deactivation was observed after 5 h reaction time, a high quantum yield for CO formation of 13.3% after 2 h (415 nm) was achieved.[131]

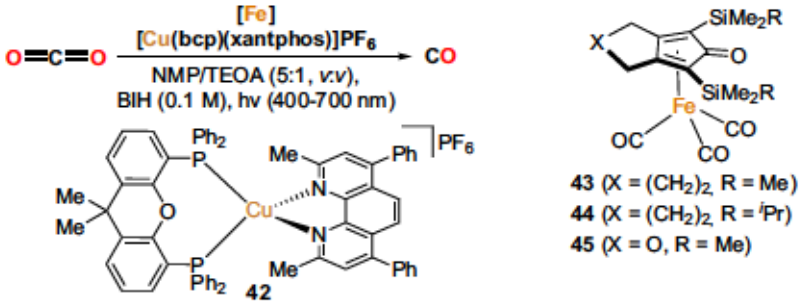

Scheme 13: *Knölker*-type complex **43**[143] and $[Cu(bcp)(xantphos)]PF_6$ in the photocatalytic CO_2 reduction to CO.[131]

The same photosensitizer **42** was recently combined with another tetraazacycle-derived Fe catalyst **46** for the photochemical transformation of CO_2 into CO (Scheme 14).[132] **46** facilitated CO formation in 84% selectivity over 8 h with a TON of 565 during illumination with visible light (>400 nm, 179 mW·cm^{-2}) in the presence of $[Cu(bcp)(xantphos)]^+$ in DMF/TEOA (4:1, *v*:*v*) utilizing BIH as the sacrificial reductant.[132] Additional xantphos (2 equiv. based on [Cu]) was required to achieve this TON which is not

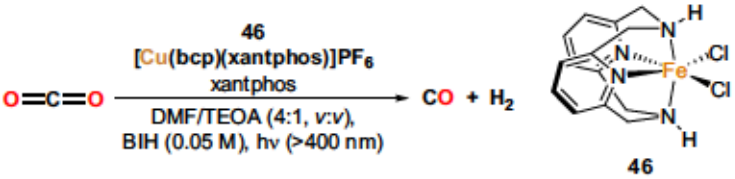

Scheme 14: Iron catalyzed CO_2 reduction to CO/H_2 based on $[Cu(bcp)(xantphos)]^+$ and BIH in DMF/TEOA (4:1).[132]

surprising as the $[Cu(N^{\wedge}N)(P^{\wedge}P)]^+$ complexes are known to form the inactive corresponding homoleptic $[Cu(N^{\wedge}N)_2]^+$ complex in a ligand-exchange equilibrium.[124,127–129,131,132,142,144,145] $[Mn(N^{\wedge}N)(CO)_3X]$ complexes, inspired by their heavier Re analogues, have likewise been utilized for the photocatalytic reduction of CO_2 to formate and CO.[77,79,133,134,146,147] Initially, $[Mn(bpy)(CO)_3Br]$ was combined with $[Ru(dmp)_3]^{2+}$ as the PS and produced HCOOH/CO/H_2 with respective TONs of 149/12/14 upon irradiation with 480 nm light in a DMF/TEOA mixture over 12 h in the presence of BNAH.[146] When the photosensitizer was replaced by the dinuclear Cu PS **41** and BIH was utilized as the sacrificial reductant, the same Mn catalyst yielded a HCOOH/CO/H_2 mixture with 157/50/4 TONs in *N,N*-dimethylacetamide (DMA)/TEOA (4:1, *v*:*v*) over 2 h (λ = 436 nm) (Scheme 15).[133] The product selectivity was drastically altered when substituents were introduced into the bipyridine ligand and the 4,4'-dimethoxy analogue **48** produced mainly CO (CO/HCOOH/H_2 TONs of 150/65/11) under unaltered conditions.[133] Moreover, introducing a mesityl substituent in the 6,6'-positions of the ligand further enhanced the CO selectivity and CO/HCOOH/H_2 were formed with TONs of 208/5/3.[133] The system based on Mn and Cu, unlike that based on Fe cyclopentadienone complexes,[131] depicted superior long-term stability.[133] In fact, irradiation of **47** for 24 h with an increased BIH concentration (0.1 M) efficiently reduced CO_2 to CO with a TON of 1004 (TONs for H_2 and HCOOH were 68 and 310).[133] At this point, most of the employed BIH had already been consumed while only 2% deactivation of the Cu PS occurred after the first 12 h of the reaction, highlighting its excellent stability.[133]

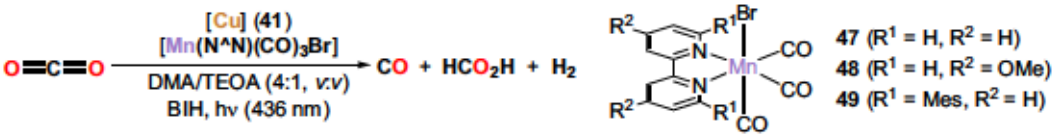

Scheme 15: First Mn/Cu photocatalytic system for the reduction of CO_2 to CO/HCO_2H/H_2 mixtures with the help of BIH as SED.[133]

Even higher selectivity for the formation of CO over H_2 production was reported utilizing the $[Cu(bcp)(xantphos)]PF_6$ photosensitizer in combination with a slightly modified Mn complex **50** in which 2-(4,4-dimethyl-2-oxazolinyl)pyridine instead of bipyridine is coordinated to Mn.[134,147] Under optimized conditions at 415 nm (70 mW) applying the *in situ* formation protocol for the Cu PS starting from $[Cu(MeCN)_4]PF_6$, bathocuproine, and xantphos in a 1:1:3 ratio and with 10 nmol of catalyst **50** in MeCN/TEOA (5:1, *v*:*v*), a CO TON of 913 and 94% selectivity over H_2 formation (TON=57) was observed after 5 h using BIH as the SED (Scheme 16).[134,147] Albeit decomposition of the Mn complex due to CO dissociation occurred during irradiation and photocatalytic activity essentially stopped after 5 h reaction time, addition of $[Cu(MeCN)_4]PF_6$ after these 5 h enabled further

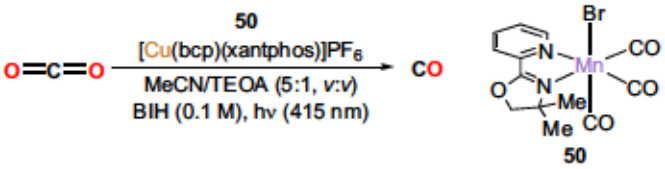

Scheme 16: Mn^I complex **50** reported for photocatalytic CO_2 reduction to CO in high selectivity when combined with $[Cu(bcp)(xantphos)]PF_6$, BIH and TEOA.[134]

conversion of CO_2 for another 5 h, yielding a total TON of 1543 for CO with 96% selectivity.[134,147] **50** was also an efficient electrocatalyst for the reduction of CO_2 to CO yielding a TON of 32 with >99% Faradaic efficiency upon controlled potential electrolysis at −1.2 V *vs.* NHE in MeCN containing 1 M trifluoroethanol (TFE) and Bu_4NBF_4 (0.1 M) as the electrolyte.[134] While photocatalytic CO_2 reduction with the help of homogeneous complexes mainly resulted in the formation of CO and formate, in many cases accompanied by H_2 production, the multi-electron reduction to CH_4 was recently implemented by Bonin, Robert and co-workers.[148] Visible light (>420 nm) illumination of a MeCN solution of cationic Fe porphyrin **51** (0.2 mM) in the presence of NEt_3 (50 mM) and TFE (0.1 M) applying $[Ir(ppy)_3]$ as the PS gave CH_4 with a TON of 66 in addition to CO (TON=240) as the major product and H_2 (TON=73) after 47 h (Scheme 17).[148] Extended illumination for 102 h in the absence of TFE gave an even higher CH_4 TON of 79 (TON(CO)=367, TON(H_2)=26).[148]

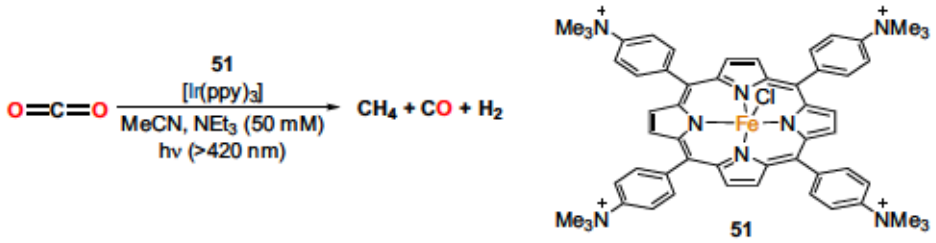

Scheme 17: Photocatalytic CO_2 reduction to methane, CO, and H_2 catalyzed by Fe porphyrin **51** and $[Ir(ppy)_3]$.[148]

Since CH_4 formation required a certain concentration of CO in the reaction mixture, indicating the initial formation of CO followed by its conversion to methane, experiments were conducted starting from CO instead of CO_2.[148] Indeed, illumination under CO atmosphere under otherwise unaltered conditions for 102 h yielded CH_4 with a TON of 159 in 83% selectivity which is twice that obtained with CO_2.[148] Interestingly, unsubstituted [Fe(TPP)Cl] produced no methane and substitution of $[Ir(ppy)_3]$ by $[Ru(bpy)_3]^{2+}$ likewise gave only CO and H_2 as the observable products.[148] These experiments highlight the importance of the required combination of a sufficiently strong reducing PS with a CO_2 reduction catalyst that is capable of stabilizing the reduction intermediates.[148]

Recently, an outstanding improvement of the TON for CH_4 production was reported by Jurss, Delcamp and co-workers.[149] Three different Ni complexes based on macrocyclic bis-pyridine-dicarbene ligands (**52**, **53**) or the non-cyclic congener (**54**) were combined with $[Ir(ppy)_3]$ (0.1 mM) and BIH (10 mM) in MeCN containing 5% NEt_3 and illuminated using a 150 W solar simulator for 72 h (Scheme 18).[149] Under these conditions, **54** produced CH_4 with a TON of 4000 as a by-product with CO/H_2 (TONs of 108000/278000) as the main products, while **52** and **53** showed no methane formation despite an impressive TON for CO of 310000 obtained with **52** at 90% selectivity.[149] However, addition of 2% of H_2O facilitated CH_4 production for both macrocyclic complexes with a high catalytic activity of 19000 and 5000 for **52** and **53**, respectively, whereas **54** produced H_2 in 90% selectivity after addition of water, with no detectable methane formation.[149] **52** proved to be the most

selective CO_2 reduction catalyst under these conditions providing $CO/CH_4/H_2$ with TONs of 175000/19000/29000 compared to **53** (8000/5000/34000).[149] It is noteworthy that low catalyst concentrations of 2 nM were utilized to achieve these turnover numbers.[149] Both, CO and H_2 were found to be crucial for CH_4 formation with complex **52** and isotopic labeling with $^{13}CO/D_2$ (1:1) produced $^{13}CD_4$ as well as $^{13}CD_2H_2$ indicating a mechanism in which H_2 and D_2 are entirely incorporated in the formed methane as no other isotopic distributions were observed.[149]

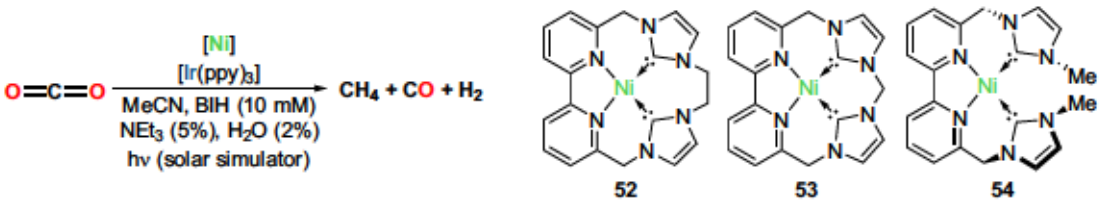

Scheme 18: Photocatalytic CO_2 reduction to $CH_4/CO/H_2$ catalyzed by bis-pyridine-dicarbene-ligated Ni complexes as reported by Jurss, Delcamp and co-workers.[149]

1.3 CO_2 Reduction to C_2 Compounds

In nature, CO_2 is utilized as the building block to construct complex organic molecules containing more than one C atom, such as carbohydrates or carboxylic acids.[35,36,48,150] The most important of the underlying processes for their construction is arguably photosynthesis due to its pivotal role in the development of life on earth and its unrivaled scale of approximately 260 billion tons of converted CO_2 per year.[35,48] The CO_2 conversion step as part of the photosynthesis is catalyzed by ribulose-1,5-bisphosphate-carboxylase-oxygenase (RuBisCO) which is one of the most abundant enzymes on the planet contributing up to 50% of the proteins in leaves.[35,48,150] Interestingly, RuBisCO lacks high selectivity, thus oxidation of ribulose-1,5-bisphosphate is competing with its desired transformation into a C_6 sugar intermediate that yields two 3-phosphoglycerate molecules *via* subsequent C-C bond scission.[35,48,150] Furthermore, the TOF for CO_2 conversion mediated by RuBisCO is utterly slow with only one turnover per second, hence an enhanced CO_2 conversion efficiency of 5-10% could supposedly counterbalance the rising CO_2 concentration in the atmosphere by its fixation as biomass.[35,48,150] The importance of the catalyzed transformation of CO_2 into higher carbon compounds, evident from the natural abundance of RuBisCO, inspired researchers not only to modify the natural protein to enable higher activity and selectivity, but also to attempt similar CO_2 conversion reactions into $C_{\geq 2}$ compounds, ideally relying on sunlight as the energy resource.[35,48,150] Nowadays, catalytic CO_2 reduction into $C_{\geq 2}$ compounds as well as stoichiometric conversion mediated by metal complexes constitute one of the major research areas toward potential CO_2 utilization.[35,48,100,104–106,151–195]

1.3.1 Photochemical CO_2 Reduction to $C_{\geq 2}$ Compounds

The conversion of CO_2 into $C_{\geq 2}$ compounds with the help of catalysts using light as the energy source has already been reported in the 1990s.[151] CH_4 was the major product of

photocatalytic CO_2 reduction and only minor amounts of C_2H_4 were formed using TiO_2 in water under ca. 28 bar CO_2 in combination with a Xe lamp.[151] However, illumination of a 5 wt% Cu on TiO_2 catalyst under identical conditions yielded ethylene as the major product accompanied by traces of ethane and methane.[151] Since then, major improvements in terms of selectivity and catalytic activity have been achieved as outlined by a recent report by Li *et al.*.[152] A MOF (MIL-125) based on TiO_2 and benzene-1,4-dicarboxylate (BDC) with a general formula of $Ti_8O_8(OH)_4(BDC)_6$ was utilized in combination with 1% Cu and 0.02% Co as a dopant to yield ethane (267.60 μmol) as the major product accompanied by CH_4 (169.79 μmol), C_3H_8 (10.07 μmol) and CO (150.58 μmol) under 10 bar of CO_2 within 3 h of illumination (Xe lamp).[152] Recently, a metal-free approach for the direct photocatalytic conversion of CO_2 into valuable C_2 compounds was described by Cao, Yu and co-workers.[153] Polymeric carbon nitride as the CO_2 reduction catalyst was immobilized on hydrophobic carbon fiber (CF) as the supporting material.[153] When the resulting material was illuminated with a Xe lamp (300 W, equipped with a 100 mW cm^{-2} filter) in the presence of CO_2, a mixture of H_2, CO, CH_4, and C_2H_4 was formed with a CO_2 conversion of 415.50 μmol h^{-1} m^{-2} and a C_2 selectivity of ca. 28% (of the CO_2 reduction products).[153] To reach this high conversion, the unfunctionalized part of the CF support had to remain outside of the solution to ensure efficient transport of CO_2 from the gas phase *via* the hydrophobic support to the active catalyst in a "*gas-liquid-solid*" reaction system.[153]

1.3.2 CO_2 Hydrogenation to $C_{\geq 2}$ Compounds

One well-established strategy to achieve formation of C_2 or even higher carbon compounds directly from CO_2 is hydrogenation.[154–157] A major challenge in the hydrogenation to multicarbon compounds is the kinetically unfavorable C-C bond forming step.[154,156,157] Nevertheless, C-C bond formation has been achieved by simple combination of CO_2 and hydrogen with different homogeneous and heterogeneous catalysts.[154–160] Gao *et al.* recently reported a strategy for the formation of mixtures consisting of C_2-$C_{\geq 5}$ compounds based on the combination of an indium oxide (In_2O_3) with a zeolite (HZSM-5).[157] Initial investigations indicated that In_2O_3 was capable of hydrogenating CO_2 to MeOH and the zeolite enabled further conversion of thus formed MeOH into various hydrocarbons with a $C_{\geq 5}$ selectivity of 71.4% at 340 °C under a pressure of 30 bar $H_2/CO_2/N_2$ (73:24:3).[157] Albeit no catalyst deactivation was observed over 150 h and despite the excellent catalytic ability for the formation of $C_{\geq 2}$ compounds, the CO_2 conversion remained at 13.1% and the major product was CO (~40%).[157] The formation of C_2-C_4 compounds has been investigated as well and combination of a zeolite (SAPO-34), which is known for catalyzing the conversion of MeOH into olefins, and a mixed indium zirconium oxide was found to be suitable for catalyzing this transformation.[154] At 400 °C and a pressure of 30 bar $CO_2/H_2/N_2$ (24:73:3) a selectivity of 76.4% for C_2-C_4 olefins and 16.5% for C_2-C_4 alkanes for the non-CO reduction products was obtained at 35.5% CO_2 conversion using a 2/1 In-Zr oxide/SAPO-34 catalyst.[154]

Interestingly, even aromatic compounds, such as xylenes, can be obtained from direct hydrogenation of CO_2 when a combination of HZSM-5 zeolite and a mixed zinc-aluminum oxide ($ZnAlO_x$) is utilized as the catalyst.[156] In long-term experiments using this $ZnAlO_x$/HZSM-5 catalyst at 320 °C under a constant H_2/CO_2/Ar (30 bar, 3:1:0.2) stream, a CO_2 conversion of ~6% was observed, with CO (~50-60% selectivity) being the main product and aromatic compounds constituting the major non-CO CO_2 reduction product (66-72% selectivity without CO).[156] Higher selectivities for the formation of a C_2 compound by hydrogenation of CO_2 were recently accomplished in the preparation of EtOH.[155] Cobalt nanoparticles supported by aluminum oxide ($CoAlO_x$) catalyzed EtOH formation with a selectivity of 92.1% at 140 °C under 40 bar H_2/CO_2 (3:1).[155] Neither CO nor hydrocarbons were observed and MeOH and higher alcohols were the only by-products emphasizing the high selectivity of these catalysts.[155] Despite the inherent advantage of heterogeneous catalysts for industrial applications, such as stability and separability,[47,196] and the outstanding catalytic activity achieved in the field,[154–157] the limited selectivity for desired multicarbon products obtained by CO_2 reduction and the comparatively high reaction temperatures for the formation of hydrocarbons are challenges that require further improvements.[158,159]

Qian and co-workers attempted to tackle these problems by employing a homogeneous catalyst based on Ru and Rh in combination with LiI as a promoter.[158] At 200 °C under 80 bar CO_2/H_2 (1:1) using $Ru_3(CO)_{12}$ and $Rh_2(CO)_4Cl_2$ in a 28.2/51.5 ratio (based on the metal) together with LiI in 1,3-dimethylimidazolidinone (DMI) a selectivity for the formation of higher alcohols with $C_{\geq 2}$ of 96.4% was obtained with EtOH being the main product (47% selectivity).[158] Isotopic labeling experiments with ^{13}C-MeOH and $^{13}C_2$-EtOH added to the reaction mixture were conducted and proved both, conversion of MeOH into EtOH and EtOH into higher alcohols, thus showcasing their roles as reaction intermediates.[158] Later, the same group improved the catalytic activity of homogeneous CO_2 hydrogenation to alcohols by replacing Rh with Co and LiI by a combination of LiBr and PPNCl (bis(triphenylphosphoranylidene)ammonium chloride).[159] While the selectivity for higher alcohols $C_{\geq 2}$ marginally decreased to 90.8% using $Ru_3(CO)_{12}/Co_4(CO)_{12}$ in a 2:1 ratio (based on the metal) combined with LiBr and PPNCl in DMI at 200 °C and 90 bar CO_2/H_2 (1:2), the space time yield in mmol of C per liter and hour increased from 12.86 C mmol L^{-1} h^{-1} (for Ru/Rh/LiI) to 33.7 C mmol L^{-1} h^{-1} for the Ru/Co/LiBr/PPNCl system (after 12 h).[158,159]

Recently, Liu and co-workers described the application of a homogeneous Pd/Fe catalyst system for the formation of C_2-C_4 hydrocarbons *via* CO_2 hydrogenation.[160] $Pd(P^tBu_3)_2$, $FeCl_2$, and xantphos enabled hydrogenation of CO_2 at 180 °C under 90 bar CO_2/H_2 (1:2) in the ionic liquid [bmim]PF_6 with a C_2-C_4 selectivity above 98% (Scheme 19).[160] Traces of CH_4 (1%) and CO (0.7%) were detected as by-products of the reaction.[160] Under these reaction conditions, recycling of the IL and the catalyst system

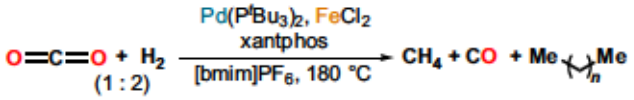

Scheme 19: Hydrogenation of CO_2 to C_2-C_4 compounds catalyzed by a Pd/Fe system reported by Liu and co-workers.[160]

was possible for five consecutive runs without significant changes in product yield and selectivity.[160] This recent report elegantly indicates the future potential of homogeneous catalysts for the direct conversion of CO_2 into multicarbon compounds.[160]

1.3.3 Electrochemical CO_2 Reduction to C_2 Compounds

As discussed in section 1.2.2, inert electrodes reduce CO_2 mainly to yield the reductive coupling product oxalate.[47,79,81,99–102] The strongly negative potential of −1.90 V *vs.* NHE for this direct reduction renders the application of suitable catalysts for this transformation desirable.[47,81,100,161] Another problem associated with direct reduction of CO_2 at inert electrodes is the obtained product selectivity.[81,99,102,197,198] Mixtures of oxalate and CO with varying constitution in between 89/10 up to 1.4/82 (Faradaic yield) were obtained when CO_2 was electrolyzed in anhydrous DMF (containing 0.2 M Bu_4NClO_4) using a Hg electrode depending on the CO_2 concentration and the temperature.[81,99] In addition, formate is produced in case the electrolysis is conducted in the presence of water, further altering the product distribution.[81,99,102,197,198] Formation of these products has been studied and revealed the competing processes which the $CO_2^{\bullet-}$ can undergo (Scheme 20).[81,99,102,197,198] Besides reductive coupling of two $CO_2^{\bullet-}$ radical anions, reaction with a proton source, such as water, can result in the formation of formate.[81,99,102,198] Furthermore, reaction with an additional CO_2 molecule to form an O-bridged adduct followed by a second reduction step might yield carbonate and CO *via* so-called reductive disproportionation.[47,81,99,102,197] It is noteworthy that reductive disproportionation and coupling do not require protons and are thus frequently conducted in aprotic media.[47,99–102,197,198]

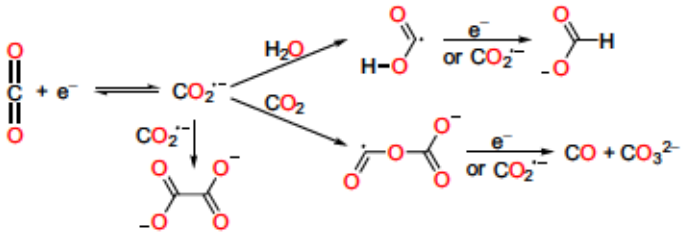

Scheme 20: Possible reaction pathways of electrochemically formed $CO_2^{\bullet-}$ toward the formation of CO/CO_3^{2-}, HCO_2^-, and $C_2O_4^{2-}$.[81,99,102,197,198]

The unique property of Cu electrodes to enable the construction of C-C bonds and facilitate the formation of hydrocarbons upon electrolytic CO_2 reduction has already been observed in the 1980s by Hori and co-workers.[103–106] In early attempts, electrolysis of CO_2 in a 0.1 M aqueous KCl solution at −1.44 V *vs.* NHE yielded a mixture of different products with a total 99.8% Faradaic efficiency that consisted of (efficiencies for each product given in brackets) H_2 (5.9%), CO (2.5%), HCO_2^- (6.6%), CH_4 (11.5%), C_2H_4 (47.8%), EtOH (21.9%), and even ^{n}PrOH (3.6%) which is produced *via* 18 electron reduction.[105] Investigations on the mechanism indicated formation of surface bound CO that undergoes further reactions to yield the CO_2 reduction products.[105,106,199] Higher selectivities for C_2H_4 have recently been reported by Roldán Cuenya and co-workers.[162] By treating Cu foils with an oxygen plasma (20 W, 2 min), which resulted in the formation of Cu oxides on the surface of the material,

they obtained an active catalyst for CO_2 reduction that depicted a high selectivity of 60% for ethylene formation at –0.9 V *vs.* RHE in 0.1 M aqueous $KHCO_3$ solution after 60 min.[162] Interestingly, selectivity towards EtOH and C_3H_7OH can also be increased with modified Cu-based electrocatalysts.[163] Kim and co-workers described a strategy to enhance the CO concentration on the surface of the catalyst by combining a Cu nanoparticle catalyst capable of CO reduction to hydrocarbons and alcohols with nitrogen-doped porous carbon.[163] *N*-Doped porous carbon (NPC) prepared from porous carbon and polypyrrols contains pyridinic nitrogen species which are known to catalyze CO_2 to CO reduction.[163] The best catalyst yielded EtOH/C_3H_7OH in 64.6% and 8.7% Faradaic efficiency, respectively, while only minor quantities of CO (7.1%), H_2 (14.8%), and C_2H_4 (3.6%) were observed as by-products upon electrolysis at –1.05 V *vs.* RHE in 0.2 M $KHCO_3$.[163]

One prominent example for catalytic electrochemical CO_2 reduction to oxalate with the help of homogeneous catalysts was already reported in 1984 and is based on benzonitrile as catalyst.[200] Later, various alkyl and phenyl benzoates were employed for this transformation and Faradaic yields for oxalate in between 74-99% were achieved upon electrolysis in 0.1 M $^nBu_4NClO_4$ in dry DMF depending on temperature and CO_2 concentration.[100] Interestingly, the reaction does not proceed *via* a simple outer-sphere electron transfer as for redox catalysis, but through nucleophilic attack of the organic radical anion to the C of CO_2 followed by homolytic bond scission yielding the $CO_2^{\bullet-}$ (Scheme 21).[47,100] The major bottleneck for the utilization of aromatic nitriles or esters in oxalate formation is the low potential of the reaction (around –2.2 V *vs.* SCE) which is comparable to that reported for the direct CO_2 reduction on a Hg electrode (–2.21 V *vs.* SCE)[197] in DMF.[81,100]

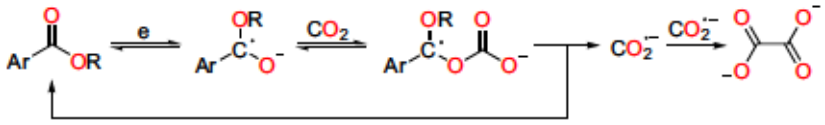

Scheme 21: Proposed mechanism for the electrocatalytic conversion of CO_2 into oxalate with the help of aromatic esters (and aromatic nitriles proceeding analogously).[47,100]

Metal complexes have been reported to catalyze the electrochemical CO_2 reduction to oxalate as well.[47,161,164–169,201,202] Formation of oxalate can be observed as a side reaction with metal catalysts, as reported by Pun *et al.*, utilizing chelated salen-inspired Fe complexes that reached a maximum Faradaic efficiency for $C_2O_4^{2-}$ of 13.4%.[201] However, catalysts enabling higher selectivities for electrocatalytic $C_2O_4^{2-}$ formation have been developed over the past decades.[161,164–169] In 1985, Becker and co-workers reported Ag and Pd porphyrin complexes that were found to selectively reduce CO_2 to oxalate at –1.50 to –1.65 V *vs.* Ag wire (+0.15 V *vs.* SCE).[161] Another example for an active electrocatalyst for the formation of oxalate is a dinuclear Rh sulfur cluster (**55**) reported by Tanaka and co-workers.[164] While electrolysis at –1.50 V *vs.* SCE in MeCN containing Bu_4NBF_4 (0.1 M) resulted in the formation of formate with a Faradaic efficiency of 60%, oxalate formation with 60% efficiency was observed when the electrolyte was exchanged for $LiBF_4$ (Scheme 22).[164]

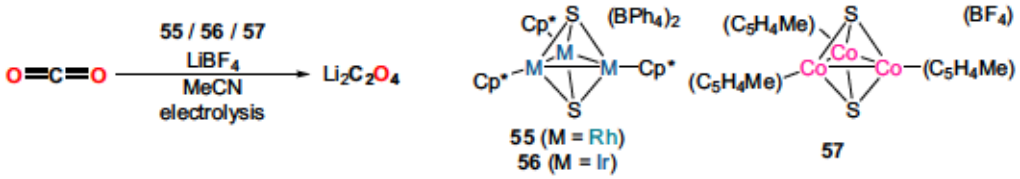

Scheme 22: Co, Rh, and Ir sulfur cluster applied in the electrocatalytic transformation of CO_2 into $Li_2C_2O_4$.[164,165]

Further investigations by the same group found analogous Ir (**56**) and Co (**57**) complexes which showed likewise activity in catalyzing electrochemical CO_2 reductive coupling.[165] Ir complex **56** yielded $Li_2C_2O_4$ and $(Me_4N)_2C_2O_4$ in 60% selectivity when a MeCN solution containing $LiBF_4$ or Me_4NBF_4 as the electrolyte was electrolyzed at –1.30 V *vs.* Ag/AgCl.[165] Importantly, no carbonate or CO was observed as a product of the electrochemical CO_2 reduction with **56**.[165] The Co congener **57** proved to be active for oxalate formation in the presence of $LiBF_4$ (2.5 M) at an even less negative potential of –0.70 V *vs.* Ag/AgCl and with a Faradaic efficiency of 80% in MeCN.[165] Mechanistic investigations for Ir complex **56** revealed complex **58**$^+$ which was formed upon reaction of *in situ* prepared $[Ir_3(C_5Me_5)_3(\mu_3\text{-}S)_2]^0$ with CO_2 in MeCN (Scheme 23).[166] Similar to **56**, **58**$^+$ was an active catalyst for CO_2 reductive coupling and enabled $(Me_4N)_2C_2O_4$ formation in 64% Faradaic efficiency upon electrolysis at –1.60 V (Ag/AgCl) in MeCN.[166] *In situ* IR spectroscopy enabled the identification of two IR bands (1680 and 1600 cm^{-1}) assigned to CO_2-coordinated intermediates as well as observation of the oxalate band (1633 cm^{-1}).[166] Based on these observations, a mechanism for the formation of oxalate starting from complex **56** was proposed (Scheme 23).[166] After formation of **58**$^+$ accompanied by the first formation of oxalate from CO_2, CO_2 is activated reversibly to yield an adduct ($[(\mathbf{58})(CO_2)]^+$).[166] Reduction of this adduct, which arguably results in Ir-Ir bond cleavage, enables electrophilic attack of another CO_2 yielding the unstable intermediate $[(\mathbf{58})(CO_2)_2]^-$ that regenerates complex **58**$^+$ upon oxalate release.[166]

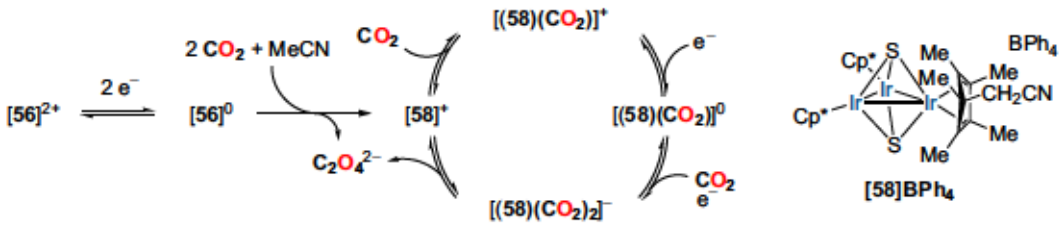

Scheme 23: Ir complex **58**$^+$ formed during the electrochemical reduction of CO_2 and the proposed mechanism for the Ir-catalyzed formation of oxalate.[166]

In addition to metal-sulfide clusters, chelated mono- and dinuclear Ru complexes (**59** and **60**) were found to catalyze formation of oxalate in MeCN with a selectivity of 64% and 70 % at –1.65 and –1.55 V *vs.* Ag/AgCl, respectively (Scheme 24).[167] Interestingly, the selectivity shifted entirely to formate production upon addition of water, providing HCO_2^- in 89% and 90% selectivity.[167]

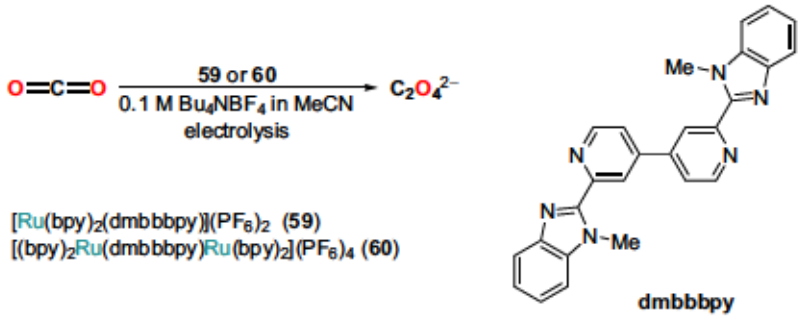

Scheme 24: Mono- and dinuclear Ru complexes reported by Tanaka for the electrocatalytic production of oxalate.[167]

Significantly higher Faradaic yields for the formation of oxalate from CO_2 were reported by Jäger and co-workers using macrocyclic Ni complexes (Figure 12).[168] In contrast to earlier reports based on macrocyclic Ni complexes, such as the well-known [Ni(cyclam)], which produce CO as the major product resulting from electrocatalytic CO_2 reduction,[203,204] the most active catalyst **61** favored formation of oxalate.[168] A remarkable 98% Faradaic efficiency for the formation of oxalate at a turnover frequency of 55 h^{-1} was obtained within the first 130 cycles of electrolysis in MeCN (+0.25 M Bu_4NClO_4).[168] Furthermore, stability of the catalyst for up to 750 turnovers was achieved, albeit with a slightly reduced oxalate selectivity of 90% (Faradaic yield) due to CO formation (5%).[168] Mechanistic investigations indicated a mechanism similar to that of aromatic esters and nitriles.[168] Despite the mechanistic analogy and the observation that ester or ketone substituents on the ligand are required for high catalytic activity, reduction of the Ni complex yields an anion in which the unpaired electron is mainly located on the Ni.[168] Albeit formidable catalytic activity was accomplished, reduction potentials remained unfavorable, with a standard potential of –2.176 V *vs.* SCE for **61**.[168]

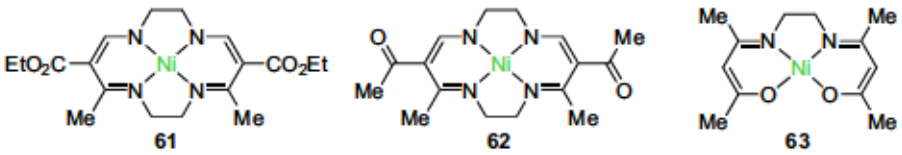

Figure 12: Tetraazacycle-ligated Ni complexes reported by Jäger and co-workers for the selective electrochemical reduction of CO_2 into $C_2O_4^{2-}$ [168] and acyclic **63** employed for the electrocatalytic CO_2 reduction yielding $(Bu_4N)_2C_2O_4$ [202].

More recently, another Ni complex which is coordinated by a Schiff base ligand (**63**) has been reported to yield $(Bu_4N)_2C_2O_4$, identified by NMR and IR spectroscopy, upon electrolysis at –2.0 V (*vs.* Fc/Fc^+) in CD_3CN in the presence of Bu_4NPF_6 over 10 min.[202]

1.3.4 CO_2 Reduction to Oxalate Mediated by Homogeneous Metal Complexes

Apart from catalytic approaches for conversion of CO_2 into C_2 compounds, several metal complexes have been reported to mediate the conversion of CO_2 into oxalate resulting mainly in the formation of oxalate-coordinated complexes or coordination polymers in the presence or even absence of chemical reducing agents. One recent example for the fixation of CO_2 in the form of oxalate within coordination polymers has been described by the Banerjee group.[170] $CuCl_2$ and bpy were treated with $AgClO_4$ in MeOH prior to reaction of the resulting Cu complex with CO_2 in benzonitrile yielding a Cu oxalate coordination polymer of general formula $[Cu(bpy)(\mu\text{-}C_2O_4)]_n$ (Scheme 25).[170] CO_2 reductive coupling facilitated by benzonitrile in combination with electron storage in the aromatic ligand of the Cu complex was suggested as the origin of oxalate.[170]

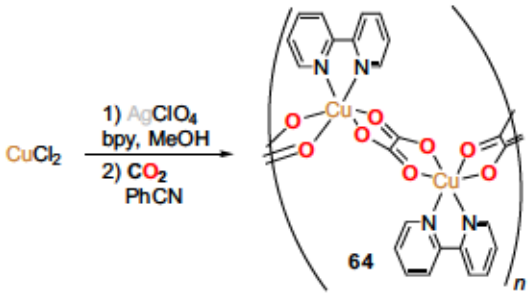

Scheme 25: Copper oxalate coordination polymer reported by Banerjee and co-workers.[170]

The *in situ* formation of oxalate coordination polymers[205–212] or defined complexes[212–219] in the presence of carbohydrates,[219] alcohols[206] or carboxylic acid derivatives[207–218] has been observed in various cases for different metals.[220] Often, aerial[205,206,216,217,219] or hydrothermal conditions[207,208,210–215,218] were utilized and heat or prolonged reaction times were required to form the oxalate complexes.[220] Oxalate compounds based on e.g. U,[208,211] Cu,[206,207,213,216–219] Zn,[209] and even mixed or co-crystallized oxalate-containing compounds based on Cu and U,[208,211,214] Cu and V,[215], Cu and Cr/Mo,[205] or lanthanide complexes based on, among others, Nd[212,220] or Tb[210,212] have been obtained in this way. Multiple reaction pathways have been proposed for the formation of the observed oxalate, such as reductive coupling of CO_2,[205,217] decarboxylation of the carboxylic acid followed by reductive coupling,[207,208,210,213] and oxidation or oxidative degradation of alcohols,[206] carbohydrates or organic acids[211,216,218,219].[220] However, only in few cases control experiments were conducted to narrow down the true origin of the observed oxalate.[205,206,208,210,220] One particularly insightful report was presented by the groups of Cahill and Nakahara.[220] In contrast to most of the aforementioned examples, the species present in solution in addition to the crystalline solid obtained after completion of the reaction were investigated.[220] The reaction of $Nd(NO_3)_3 \cdot 6H_2O$ with 2,3-pyrazinedicarboxylic acid under hydrothermal conditions (120 °C) resulted in the formation of oxalate previously assumed to proceed *via* decarboxylation of the dicarboxylic acid, evidenced by observation of the monocarboxylic acid,[212] and subsequent reductive coupling of CO_2 was proposed for an analogous Th compound.[220] However, NMR spectroscopy enabled the time-dependent quantification of mono- and dicarboxylic acid and following their concentration over the reaction time indicated a non-proportional relationship between these two species, thus suggesting a more sophisticated reaction than simple de-

carboxylation and reductive coupling.[220] Compounds obtained *via* ring-opening, such as glycolic and 2-hydroxymalonic acid, were observed by NMR spectroscopy and a reduced proportion of the oxalate complex was obtained when the reaction was conducted in partially degassed solvent.[220] These observations in combination with the oxidative reaction environment substantiate the proposed oxidative degradation pathway for oxalate formation (Scheme 26).[220] This work indicates the importance of in-depth investigations for confirmation of the true origin of *in situ* formed oxalate, specifically in cases where oxidative reaction conditions or hydrolyzable C-N bonds are present.[220]

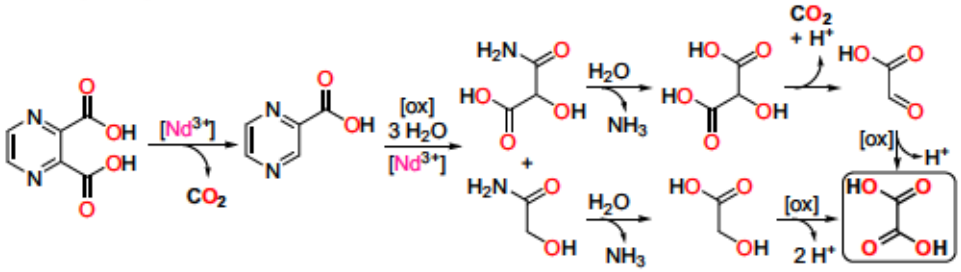

Scheme 26: Plausible pathway for the formation of oxalate under hydrothermal conditions *via* decarboxylation of pyrazine dicarboxylic acid and subsequent ring opening followed by degradation under oxidative conditions in the presence of Nd^{3+}.[220]

The reductive coupling of gaseous CO_2 by homogeneous complexes is a well-known phenomenon which has been observed by Fröhlich and Schreer as early as 1983.[171] Due to their interest in the carboxylation of Ti alkyl complexes in benzene at 10 °C yielding carboxylic acids after acid hydrolysis, they isolated a dinuclear μ-C_2O_4 titanium cyclopentadienyl complex **67** (Scheme 27).[171] This first literature precedent paved the way for CO_2 reductive coupling mediated by homogeneous metal complexes enabled by simultaneous oxidation of the metal center in the absence of additional reductant or energy input in terms of light or electricity.[171]

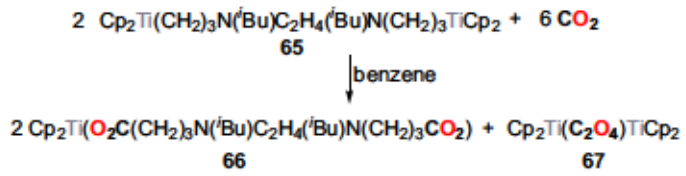

Scheme 27: First example for the reductive coupling of CO_2 into oxalate mediated by a homogeneous Ti alkyl complex reported by Fröhlich and Schreer.[171]

Mechanistic investigations to identify the possibility of the involvement of dimetalloxycarbenes as intermediates for oxalate formation were undertaken for a Ti complex ligated by ^{t}Bu(3,5-$Me_2C_6H_3$)N ligands (Scheme 28).[172] A dinuclear bridged formate complex **70** stabilized against CO elimination by the interaction of two Ti centers in combination with a weakly-coordinating anion $B(C_6F_5)_4^-$ was prepared as the starting material for this investigation.[172] Deprotonation of this formate complex resulted in the formation of the desired dimetalloxycarbene **71** stabilized *via* C-Ti coordination in a fluctuating manner between both Ti centers above –55 °C.[172] DFT calculations suggested a minor energy difference of 10.5 kJ mol^{-1}

between this κ^2C,O:κ^1O'-coordinated compound and the actual dimetalloxycarbene, but the former was identified by crystallographic as well as NMR spectroscopic analysis, indicating a considerably shorter lifetime of the latter.[172] Nevertheless, treatment of the novel complex with CO_2 resulted in the expected formation of the oxalate-bridged Ti complex **72**.[172] Theoretical investigation of the mechanism revealed the direct nucleophilic attack of this dimetalloxycarbene intermediate onto a second non-activated CO_2 molecule as the energetically favorable reaction path further underpinning the intermediate's carbene properties.[172]

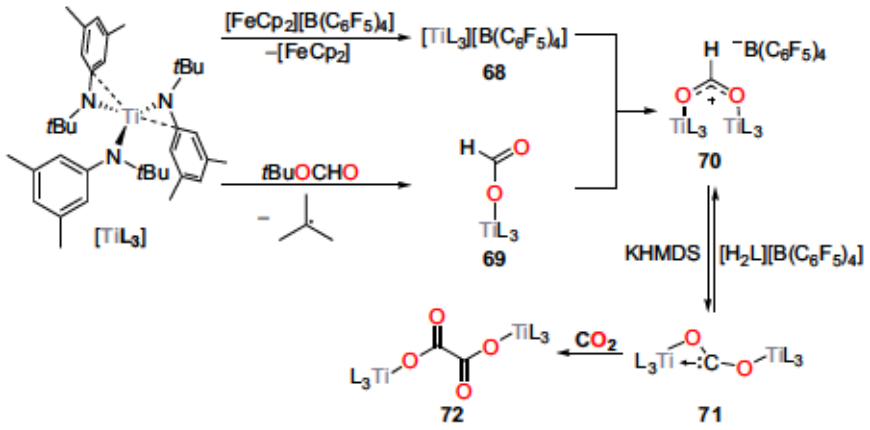

Scheme 28: Mechanistic pathway for the formation of oxalate starting from a dinuclear formate-bridged Ti complex and proceeding *via* a dimetalloxycarbene intermediate **71** as the key species.[172]

Besides Ti, Sc has been identified to enable similar chemistry once reduced to the rather unusual oxidation state Sc^{II} with K or Cs in combination with 18-crown-6 (18-c-6) (Scheme 29).[173] Reaction of Sc^{2+} complex [K(18-c-6)][Sc(N(SiMe$_3$)$_2$)$_3$] with CO_2 in Et_2O yielded a CO_2^- coordination polymer [K(18-c-6)(μ-OCO-κ^1O:κ^1O')Sc(N(SiMe$_3$)$_2$)$_3$]$_n$ bridged *via* an interaction between K and a methyl group of one N(SiMe$_3$)$_2$ ligand as well as the CO_2^-.[173] Additionally, the dinuclear oxalate-bridged Sc^{III} complex **74** was isolated in which the $C_2O_4^{2-}$ coordination occurs in a κ^1 fashion.[173]

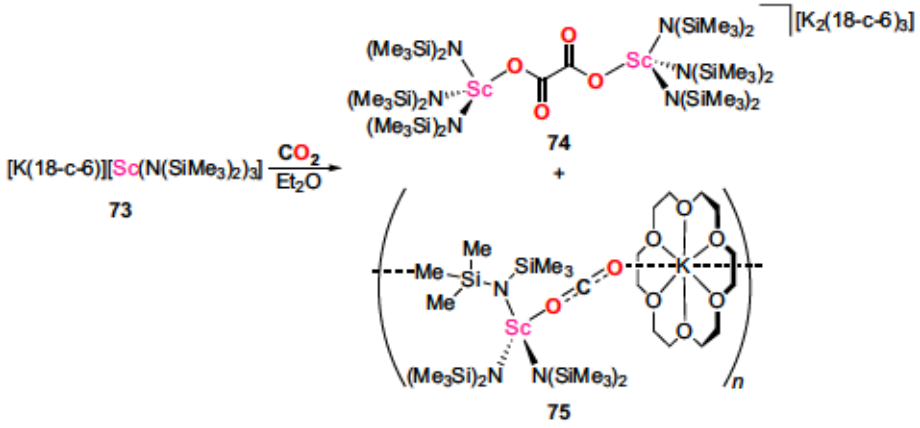

Scheme 29: Formation of oxalate-bridged Sc complex **74** *via* reductive coupling of CO_2.[173]

One particularly active class of metals for the conversion of CO_2 into oxalate are lanthanides and actinides. Interestingly, lanthanides can be precipitated as the corresponding oxalates, a method that can be utilized for their separation or analysis.[221] Lanthanum itself, as well as praseodymium, were identified as suitable promoters for the conversion of CO_2 into oxalate in the presence of small quantities of HNO_3 and precursors initially intended for the construction of a macrocyclic ligand upon contact with the atmosphere for prolonged times (1 month).[174] The formation of the resulting oxalate coordination polymers of the general formula $([Ln_2(C_2O_4)_3(H_2O)_6]\cdot 3H_2O\cdot 0.5HNO_3)_n$ (Ln = La, Pr) was significantly accelerated by mixing the ligand precursors with the lanthanide nitrates under a CO_2 atmosphere (balloon) for 20 min in alcoholic solvent (Scheme 30).[174]

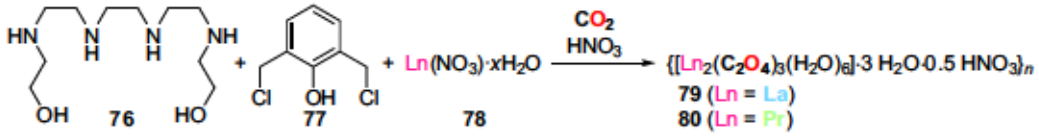

Scheme 30: Formation of oxalate-containing La and Pr coordination polymers by treatment of the precursors with CO_2 as reported by Kahwa and co-workers.[174]

Ytterbium has likewise been reported to form an oxalate complex upon reaction of tetraphenylporphyrin with $[Yb(N(SiMe_3)_2)_3]\cdot x[LiCl(THF)_3]$ in boiling diglyme (diethylene glycol dimethyl ether) and subsequent work up in air (Scheme 31).[222] Albeit no conclusive statement has been made on the exact origin of thus formed oxalate, treatment of the reaction mixture obtained under nitrogen atmosphere with CO_2 indicated the formation of the same oxalate complex according to mass spectrometric analysis.[222]

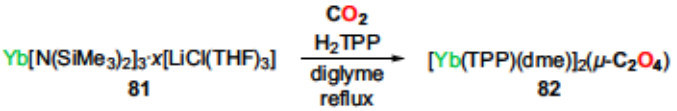

Scheme 31: CO_2 treatment of *in situ* formed Yb tetraphenylporphyrin giving rise to a novel oxalate-bridged dinuclear Yb complex.[222]

A straightforward determination of the origin of oxalate is possible for the Sm oxalate complex reported by Evans and co-workers.[175] CO_2 treatment of $[Sm(C_5Me_5)_2(THF)_2]$ in THF at room temperature resulted in oxalato-bridged complex **85** in 92% yield within 6 min (Scheme 32).[175] A strong solvent dependence of this reaction was observed and complex product mixtures were obtained when the reaction

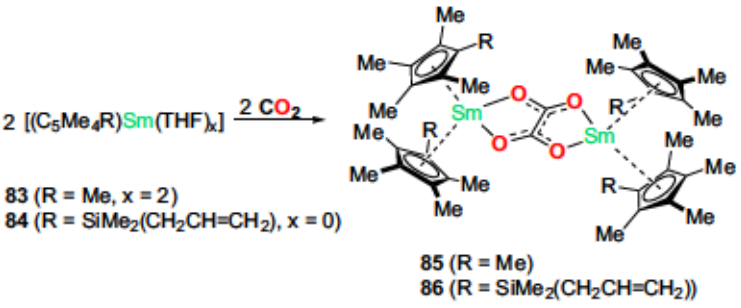

Scheme 32: Reductive CO_2 coupling mediated by cyclopentadienyl-coordinated Sm complexes reported by Evans and co-workers.[175,176]

was conducted in hexanes or toluene even at −78 °C. The capability of **83** to couple CO_2 was explained with its strong reducing ability indicated by its reaction with stilbene (E^0 = −2.22 V *vs.* SCE).[175] Further modifications of the ligand, such as replacement of a methyl group by an allyldimethylsilyl substituent, did not impact the reactivity towards CO_2.[176] Hence, the oxalato-bridged congener **86** was obtained in 95% yield after reaction with CO_2 for 2 min in hexanes.[176]

Moreover, changing the metal indicated a significant difference in the complexes ability to mediate CO_2 reductive coupling.[177] CO_2 treatment of Lu complex **87** in benzene/THF (25:1) enabled once again the isolation of an analogous oxalato complex **88** (Scheme 33), while the analogous La complex yielded a mixture of products.[177]

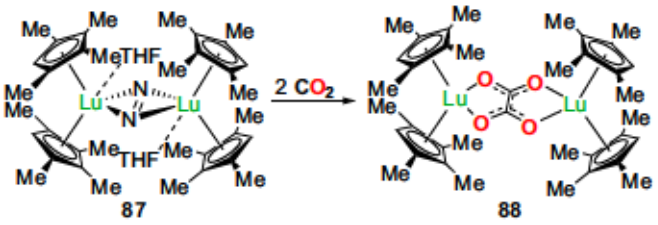

Scheme 33: Conversion of N_2-bridged Lu complex **87** into the oxalate complex **88** by CO_2 reductive coupling.[177]

The influences of metal, solvent, and coordination sphere have further been investigated by Mazzanti and co-workers.[178,179] Initially, they observed the formation of CO_3^{2-}, CO, and $C_2O_4^{2-}$ upon reaction of the ytterbium siloxide complex [Yb(OSi(O^{t}Bu)$_3$)$_4$K$_2$] (**89**) with CO_2 in toluene and subsequent treatment with D_2O in a total oxalate/carbonate yield of 95% (Scheme 34).[178] Yb is oxidized in this transformation to the corresponding Yb^{III} complex **90**, which encouraged attempts on a catalytic CO_2 reduction by converting **90** back into **89** *via* treatment with KC_8.[178] This procedure allowed for a total of five consecutive CO_2 reduction runs prior to significant decrease of the **89** concentration in the sample.[178]

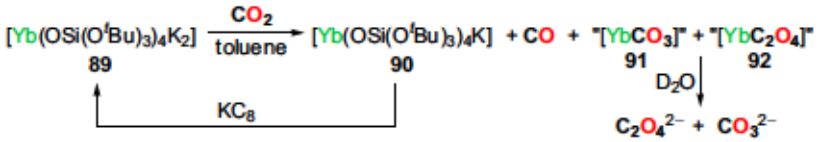

Scheme 34: Simultaneous CO_2 reductive coupling and reductive disproportionation facilitated by Yb complex **89** developed by the Mazzanti group.[178]

The analogous Sm complex was found to also yield a mixture of CO_3^{2-}, CO, and $C_2O_4^{2-}$ when reacted with CO_2 in toluene-d_8, albeit with a higher percentage of oxalate formation compared to Yb.[179] Hence, Mazzanti and co-workers investigated the influence of the solvent, metal (Yb or Sm), and ligand properties on the $CO_3^{2-}/C_2O_4^{2-}$ ratio.[179] The dinuclear complexes [Yb$_2$(OSi(O^{t}Bu)$_3$)$_4$] and [Sm$_2$(OSi(O^{t}Bu)$_3$)$_4$] were prepared and compared to the mononuclear dianionic complexes **89** and [Sm(OSi(O^{t}Bu)$_3$)$_4$K$_2$].[179] Reaction of the former complexes with CO_2 in cyclohexane-d_{12} allowed for isolation of two crystalline tetranuclear complexes, namely the carbonate complex [Sm$_4$(OSi(O^{t}Bu)$_3$)$_8$(μ_3-CO$_3$-κ^4-O,O',O")$_2$] (**93**) and oxalato complex [Yb$_4$(OSi(O^{t}Bu)$_3$)$_8$(C$_2$O$_4$)] (**94**).[179] Despite the obtained crystal structures, Yb complexes yielded in general lower quantities of oxalate compared to Sm.[179] Furthermore, the solvent played a significant role and while polar THF enabled higher quantities

of carbonate formation, nonpolar solvents, such as toluene-d_8 and cyclohexane-d_{12}, favored the reductive coupling over reductive disproportionation.[179] The best oxalate/carbonate ratio was obtained with [Sm(OSi(O^{t}Bu)$_3$)$_4$K$_2$] (**95**) in either toluene-d_8 or cyclohexane-d_{12} with a yield of 92% and an oxalate/carbonate ratio of 1:0.8.[179] DFT calculations were conducted to supplement the experimental data.[179] The results of both, experiment and theory, indicate a preferable formation of oxalate when CO_2 reacts with dimeric lanthanide species, which are primarily existing in non-polar solvents.[179] However, two dimers might interact, as in the formation of **93** and **94**, which supposedly results in the observed formation of carbonate as a by-product.[179]

Besides CO_2 reductive coupling to oxalate, carboxylation of a guanidato-type ligand (Giso = (DippN)$_2$CNCy$_2$) was observed for a Sm^{II} complex.[180] Here, after initial formation of the oxalate complex, the thermodynamically favorable product is formed *via* *N*-carboxylation resulting in the [(Giso)(κ^2-O,O'-GisoCO$_2$)Sm(μ-C$_2$O$_4$)Sm(Giso)$_2$] product.[180]

An early example for an actinide system facilitating CO_2 reductive coupling to oxalate was reported by Cloke, Maron, and co-workers in 2014 and is based on uranium.[181,223] Reaction of U complexes ligated by a disubstituted 1,4-bis(trimethylsilyl)cyclooctatetraenyl and different cyclopentadienyl ligands with CO_2 in toluene-d_8 resulted in the formation of oxalate-bridged dinuclear uranium complexes in addition to the bridged oxide or bridged dinuclear carbonate complexes (Scheme 35).[181] The ratio was strongly dependent on the substituent on the cyclopentadienyl ligand as well as on the reaction conditions.[181] Thus, running the reaction in scCO_2 resulted mainly in formation of the carbonate complexes and only minor amounts of CO_2 reductive coupling were observed (5% instead of 40% for **97**).[181] In addition, increasing steric demand favored reductive disproportionation and only the carbonate complex was observed for the ^{t}Bu substituted cyclopentadienyl U complex **98**.[181] DFT calculations suggested a kinetically favorable reductive disproportionation mechanism despite the oxalate complex being the thermodynamically stable product and precipitating from the reaction mixture thereby shifting the equilibrium.[181]

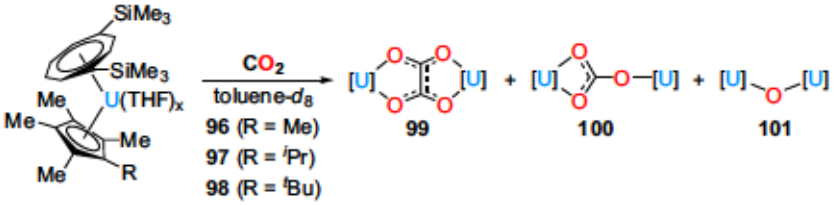

Scheme 35: Uranium-mediated CO_2 reductive coupling and reductive disproportionation yielding the derived carbonato-, oxalato- and oxo-bridged dinuclear complexes.[181]

Similar observations were made when complex **102** based on Cp* and a bisphenol ligand was reacted with CO_2, providing the dinuclear carbonate complex **104** upon reaction in scCO_2, while the oxalate complex **103** was obtained *via* reaction in toluene-d_8 (Scheme 36).[182] Interestingly, the oxalate-bridged complex **103** was found to be the kinetic product in this case based on the higher ratio of **103** *vs.* **104** obtained when the reaction was conducted

at –78 °C for 2 d (70:30) while **104** was favored upon fast warming to ambient temperature (17:83).[182]

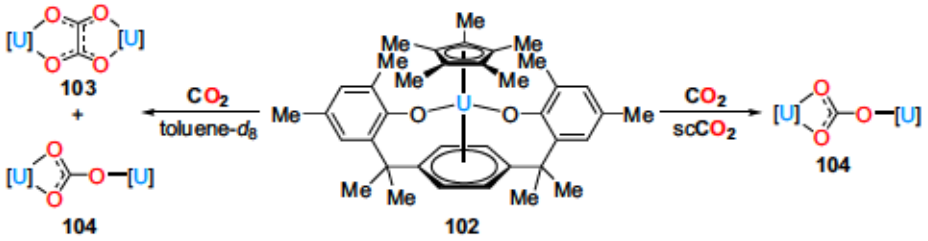

Scheme 36: Bisphenol-ligated U complex **102** reported by Cloke and co-workers for the CO_2 reduction to oxalate.[182]

A hexadentate triazacyclononane-derivative has likewise been utilized as a ligand for U to facilitate activation of CO_2.[183,223] Reaction of complex **105** with CO_2 in the presence of KC_8 in THF yielded oxalate-bridged complex **106** and after extraction with D_2O a mixture of K_2CO_3 and $K_2C_2O_4$ was identified by NMR spectroscopy (Scheme 37).[183] Since the carbonate complex was the kinetically preferred product, as indicated by DFT calculations, strong reductant KC_8 was required to enable the formation of oxalate.[183] In contrast, SO_2 treatment of **105** enabled formation of the analogous dithionite complex in good yield *via* reductive coupling of SO_2, indicating a lower activation energy than for the CO_2 coupling consistent with DFT calculations which was ascribed to the bent nature of SO_2.[183]

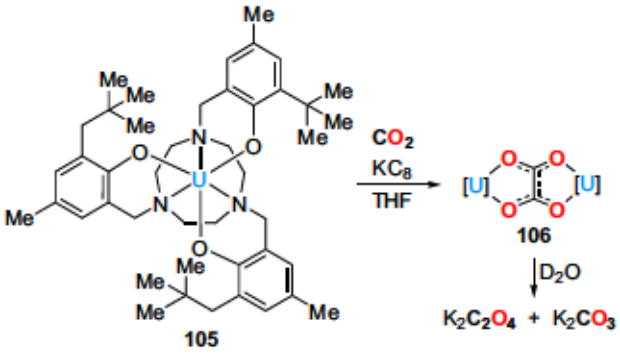

Scheme 37: CO_2 reduction to oxalate and carbonate in the presence of KC_8 mediated by a triazacyclononane-ligated U complex **105**.[183]

Aside from uranium, a thorium complex has recently been found to mediate CO_2 reductive coupling by Maron, Mills, and co-workers.[184,223] Reaction of tris-cyclopentadienyl-ligated complex **107** with CO_2 at –78 °C to r.t. in toluene resulted in the μ-C_2O_4 complex **108** (Scheme 38).[184] Here, not only reductive coupling of CO_2 occurred, but simultaneous carboxylation of and proton/silyl migration on the cyclopentadienyl-type ligand were observed.[184] While the latter reactivity can proceed in lanthanide and actinide compounds, DFT calculations suggested the formation of a dimetalloxycarbene as the key intermediate, reacting with another

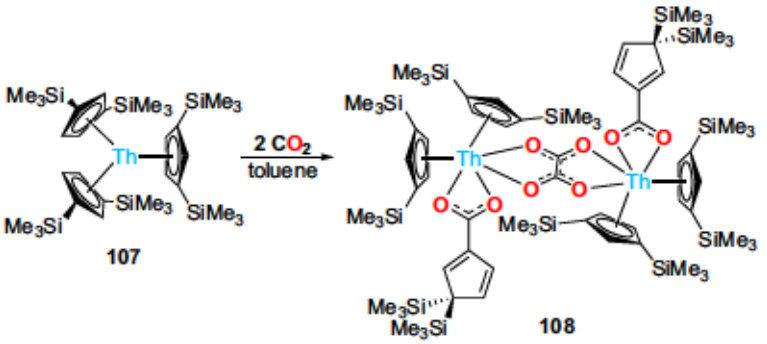

Scheme 38: Th-mediated CO_2 reductive coupling observed by Maron, Mills, and co-workers.[184]

unactivated CO_2 molecule to form the oxalate-bridged dimer.[184] This reactivity is adversative to those predicted for aforementioned uranium complexes while resembling the mechanism proposed for a Ti complex[172] showcasing the unique behavior of this Th complex.[184]
Apart from oxophilic lanthanides and actinides, the reductive coupling of CO_2 has been observed as a minor fraction in the reaction of CO_2 with Mg^I complex **109**, albeit the carbonate complex was the main product of this transformation (Scheme 39).[185,224] Calculations on the mechanism indicated the attack of a second activated CO_2 molecule onto a CO_2-bridged intermediate as the likely reaction pathway which possessed a higher energetic barrier than the formation of the respective carbonate complex.[224]

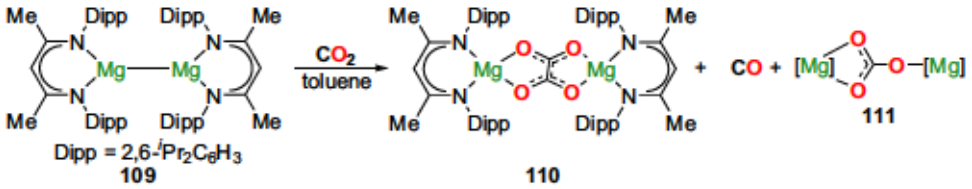

Scheme 39: Formation of oxalate observed as a side reaction in the reductive disproportionation of CO_2 with β-ketiminate-ligated Mg^I complexes.[185,224]

In light of their broad applicability and catalytic activity, the possibility of utilizing first row transition metals, such as Fe, Ni, or Cu, for the reductive coupling of CO_2 does not come as a surprise. Interestingly, even the well-known Aresta's complex $[Ni(PCy_3)_2(CO_2)]$ (**112**), the first structurally characterized CO_2 coordination complex,[225] was capable of coupling the coordinated CO_2 to oxalate in THF upon addition of AgOTf at –23 °C yielding $Ag_2C_2O_4$ as the isolated product identified by NMR spectroscopy.[186] The reaction was supposed to proceed *via* activation of the coordinated CO_2 by Ag^+ followed by $AgCOO^\bullet$ radical formation resulting from homolytic Ni-C bond cleavage and subsequent dimerization of these radical intermediates (Scheme 40).[186]

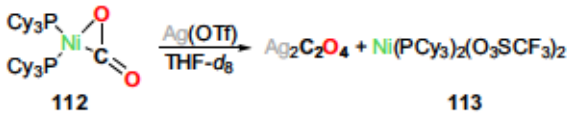

Scheme 40: Aresta's complex enabling reductive coupling of coordinated CO_2 into $Ag_2C_2O_4$.[186]

A closed cycle for the formation of potassium oxalate from CO_2 mediated by a homogeneous dinuclear Ni β-diketiminate complex has been described as well.[187] Reaction of the N_2-bridged complex **114** with CO_2 in hexane over 60 h provided complex **115** in 20% yield, accompanied by the formation of a Ni^I carbonyl complex **116** (Scheme 41), presumably formed *via* reductive disproportionation of CO_2.[187] Subsequent treatment of oxalate complex **115** with KC_8 under a N_2 atmosphere

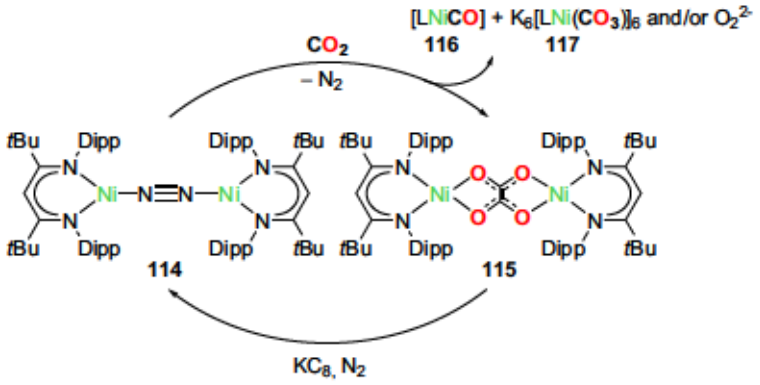

Scheme 41: Stepwise CO_2 reductive coupling to potassium oxalate mediated by a Ni(bisketiminate) complex.[187]

enabled re-isolation of the starting complex **114**, thereby closing the stepwise cycle for CO_2 reduction to oxalate.[187]

The analogous conversion of CO_2 into sodium oxalate was observed by the Floriani group utilizing a macrocyclic Fe^I complex [Fe(tmtaa)Na(THF)$_3$] (**119**) prepared by reaction of [Fe(tmtaa)] with Na (Scheme 42).[188]

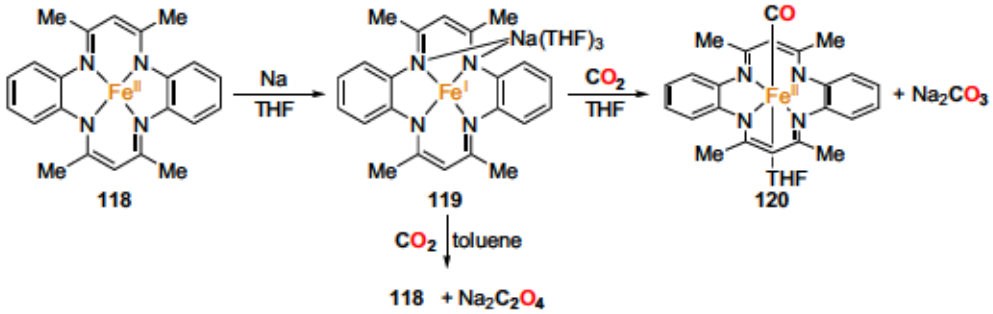

Scheme 42: Solvent dependence of the CO_2 reduction by [Fe(tmtaa)Na(THF)$_3$] yielding either carbonate and **120** or oxalate in THF or toluene, respectively.[188]

The CO_2 reduction step itself displayed a significant solvent dependence: CO_2 treatment of **119** in THF gave rise to the carbonyl complex [Fe(tmtaa)CO(THF)] in combination with sodium carbonate *via* reductive disproportionation.[188] Contrasting this reactivity, [Fe(tmtaa)] accompanied by $Na_2C_2O_4$ were obtained upon reaction in toluene under similar conditions.[188] Since no oxalate complex has been observed in this transformation, the resulting $Na_2C_2O_4$ was solely identified by titration with $KMnO_4$.[188]

In-depth analyses of factors controlling the CO_2 reductive coupling were reported by Peters and co-workers based on a triphosphine-based Fe system.[189,190] After identifying the formation of an oxalate-bridged Fe complex **123** as a by-product of the reductive cleavage of CO_2 to yield the μ-CO,μ-O complex **122** (Scheme 43), variation of the ligand substitution pattern and the solvent were conducted.[189,190] When the PCy_3 derivative **121** was reacted with CO_2 in methylcyclohexane (MeCy), the reductive cleavage was observed as the only reaction, while oxalate formation was observed in THF, 2-methyltetrahydrofuran (2-MeTHF) or 2,5-dimethyltetrahydrofuran (2,5-Me_2THF) with varying **123**/**122** ratios.[190] Here, the less sterically demanding, and therefore more coordinating, solvents generally enabled higher percentages of CO_2 reductive coupling with the **123**/**122** ratio being 13:1 (THF), 7:1 (2-MeTHF), and 1:4 (2,5-Me_2THF) employing 2 equiv. of CO_2, respectively.[190] Interestingly, analogous complexes of type [Fe(PhBP$_3^R$)(PR$'_3$)] bearing differently substituted

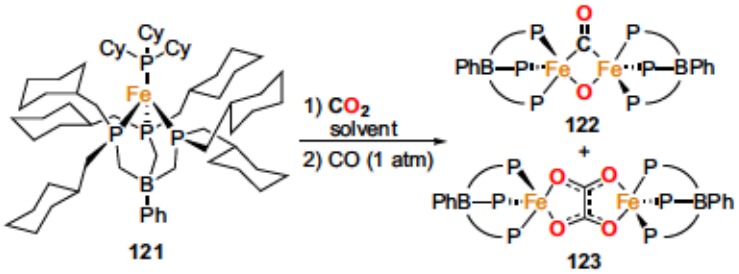

Scheme 43: CO_2 deoxygenation and reductive coupling facilitated by triphosphine-ligated Fe complexes reported by the Peters group.[189,190]

[$PhBP^R_3$] (R = CH_2Cy, Ph, ^iPr, ^{m}ter) ligands showed no direct reactivity towards CO_2 (1 atm) for R=^{i}Pr (R′=Me) and R=Ph (R′=Ph).[190] Hence, *in situ* reduction of the chlorido complexes [Fe($PhBP^R_3$)Cl] with Na/Hg conducted under CO_2 in THF at 0 °C was investigated in these cases.[190] Oxalate formation was only observed for the CH_2Cy-based ligand, while the bridged oxide [Fe($PhBP^R_3$)(μ-O)] in addition to the dicarbonyl complex [Fe($PhBP^R_3$)($CO)_2$] were obtained for R=^{i}Pr.[190] Corresponding analogues in combination with the single-reduced [$Na(THF)_5$][Fe($PhBP^R_3$)($CO)_2$] salt were identified as the products for R=Ph, whereas no reaction occurred for the complex derived from the R=^{m}ter substituted ligand.[190] These results served to rule out electronic ligand properties as the major influence on product selectivity, since the [Fe($PhBP^R_3$)Cl] complexes with R = ^{i}Pr and CH_2Cy possess similar reduction potentials and their dicarbonyl congeners [Fe($PhBP^R_3$)($CO)_2$] display similar CO stretching frequencies.[190] Steric parameters, on the other hand, clearly impact the product selectivity, with the least sterically demanding ligand enabling high selectivity for the formation of oxalate in a sufficiently coordinating solvent, such as THF.[190] Both of these factors are proposed to enable stabilization of a potential 19-electron [Fe($PhBP^R_3$)(η^1-OCO)($solv)_2$] intermediate that could undergo C-C bond formation as suggested by DFT calculations.[190]

Ligand non-innocence in a dinuclear dinitrosyl iron complex bearing a simple 3-methylpyrazole (^{Me}pyr) ligand was recently observed to enable direct conversion of CO_2 into CaC_2O_4.[191] The first step of this reaction cycle is the activation of CO_2 by dinuclear $\{Fe(NO)_2\}^{10}$ complex **125**, prepared *via* KC_8 reduction of the $\{Fe(NO)_2\}^9$-type [Fe_2(μ-^{Me}pyr)$_2$($NO)_4$] in the presence of 18-crown-6, to yield mononuclear **126** (Scheme 44).[191] Activation of CO_2 occurred on the ligand resulting in the construction of a chelating carbamate in **126** which, however, remains in the $\{Fe(NO)_2\}^{10}$ configuration.[191] Cleavage of the carbamate under release of CO_2 can be achieved by oxidation with $[FeCp_2]^+$ yielding **124**.[191] More interesting is the reaction observed upon treatment of **126** with $Ca(OTf)_2$ which also produces **124**, but is accompanied by reductive coupling of CO_2 to form insoluble CaC_2O_4 in ca. 75% yield identified by IR and ^{13}C NMR spectroscopy after protonation with DCl.[191] This stepwise CO_2 reductive coupling has been repeated for three closed reaction cycles starting from **124** with essentially unaltered oxalate yield.[191] Kinetic data in combination with DFT calculations suggested CO_2 reduction by the $\{Fe(NO)_2\}^{10}$ fragment upon coordination of Ca^{2+} to the carbamate resulting in heterolytic

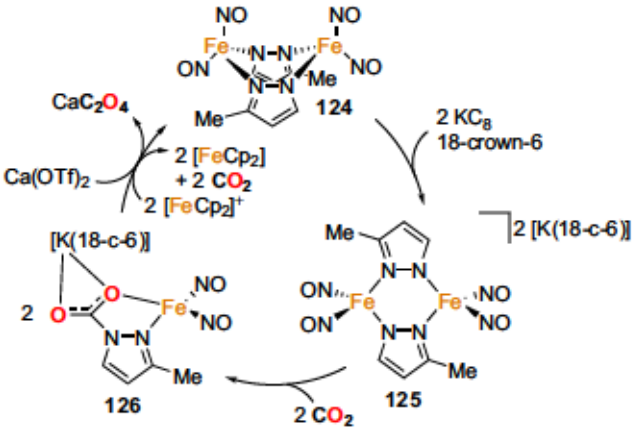

Scheme 44: Iron nitrosyl complex **124** enabled the stepwise catalytic conversion of CO_2 into CaC_2O_4 utilizing KC_8 as the reducing agent.[191]

C-N bond cleavage and formation of oxalate possibly through a Fe-coordinated $CO_2^{\bullet-}$ intermediate.[191]

As for the electrochemical reduction of CO_2 to C_2 products, Cu complexes are among the most frequently utilized compounds for the molecular conversion of CO_2 into oxalate. The first example of this kind was reported by the Peacock group and is based on an allyl-substituted 1,4,7-triazacyclononane ligand.[192] Crystalline dinuclear oxalate complex **128** was first unsuspectedly isolated upon oxidation of an *in situ* formed Cu^I complex starting from CuI, 1,4,7-tacn derivative **127**, and $NaBPh_4$ in air/exhaled air (Scheme 45).[192] Further attempts revealed the possibility of synthesizing complex **128** by CO_2 bubbling through a solution of the Cu^I complex in the presence of H_2O traces or by direct reaction with $CsHCO_3$ in MeOH. The complex is antiferromagnetically coupled, a common feature of oxalato-bridged Cu complexes,[226] and displays a distinct C-O vibration at 1660 cm^{-1}.[192]

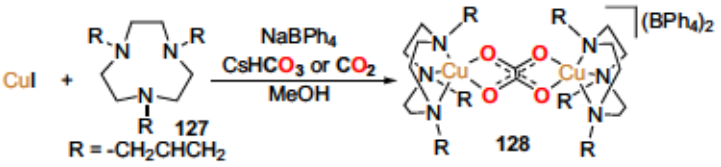

Scheme 45: Formation of triazacyclononane-coordinated copper oxalato complex **128** *via* reaction with CO_2 or $CsHCO_3$ reported by Peacock and co-workers.[192]

A more sophisticated reaction was observed by Fujisawa and co-workers when reacting a tris(pyrazolato)borohydride-coordinated Cu α-ketocarboxyl complex with air yielding the $C_2O_4^{2-}$-bridged Cu complex **130** (Scheme 46).[193] The presence of O_2 was crucial for the reaction and oxalate formation starting from Cu^{II} complex **129** was only observable in pure O_2, air or in a CO_2/O_2 mixture.[193] Decomposition of the α-ketocarboxylate in the presence of O_2 to form $CO_2^{\bullet-}$ was proposed as the likely cause for this observation.[193] This is also underlined by the reaction of the derived peroxido-bridged copper complex with sodium 3-methyl-2-oxobutyrate producing the oxalate complex **130**.[193] CO_2 incorporation into the final oxalate was proven by reaction of **129** with a $^{13}CO_2/O_2$ mixture in toluene resulting in an isotopic shift of the oxalate vibration of 49 cm^{-1} to 1607 cm^{-1}.[193] Finally, reaction of *in situ* formed [Cu(Tp^{iPr,iPr})] with bicarbonate in various solvents (MeOH, acetone, DCM) produced a product with an IR vibration in the 1650 cm^{-1} region, supposedly oxalate complex **130**, albeit isolation of this complex has not been achieved for this specific reaction.[193]

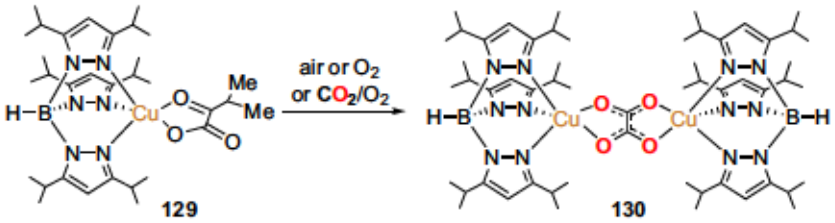

Scheme 46: Scorpionate-derived Cu α-ketocarboxylate complex **129** and its conversion into an oxalato complex by reaction with O_2 or CO_2/O_2.[193]

An outstanding example for CO_2 reductive coupling facilitated by a homogeneous Cu complex was reported by Bouwman and co-workers and is based on a disulfide-bridged dipi-

colylamine derivative as the ligand.[169] Cu^I complex **132**, prepared from the ligand and $[Cu(MeCN)_4]BF_4$ or $Cu(acac)_2$, HBF_4 and the corresponding thiol in MeCN, captured CO_2 from the air in form of reductively coupled $C_2O_4^{2-}$ yielding a tetranuclear Cu complex **134** (Scheme 47).[169] Reaction with $^{13}CO_2$ and ESI-MS of the product provided evidence for reductive coupling being the origin of the observed oxalate.[169] Treating the oxalate complex with $LiClO_4$ enabled removal of oxalate alongside formation of a dinuclear Cu^{II} complex **131**.[169] Having identified the possibility of $C_2O_4^{2-}$ removal after reductive coupling, bulk electrolysis of complex **134** in MeCN constantly purged with CO_2 containing $LiClO_4$ over 7 h at a very mild potential of only −0.03 V *vs.* NHE enabled the formation of 12 molecules of oxalate per utilized molecule of **134**, thus achieving a TON of 3 per Cu center.[169] Considering the mild overpotential, the electrochemical formation of oxalate with the help of this protocol, supposedly proceeding *via* generation of a Cu-coordinated $CO_2^{\bullet-}$ intermediate followed by reductive coupling and subsequent precipitation as $Li_2C_2O_4$ (Scheme 47), provides a promising catalytic route towards C_2 products.[169] However, Stack and co-workers found an equilibrium between the starting Cu(I) complex and a derived Cu(II) bis-thiolate and were unable to identify the formation of oxalate despite various attempts.[227]

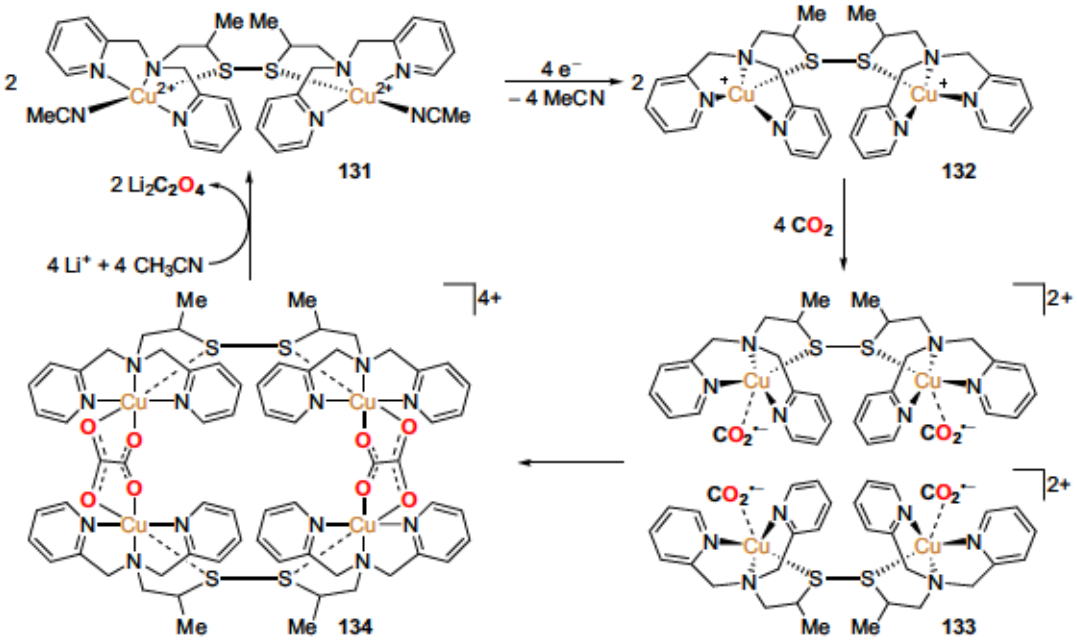

Scheme 47: Electrocatalytic cycle for the reduction of CO_2 into $Li_2C_2O_4$ at mild overpotential catalyzed by a dinuclear Cu complex reported by the Bouwman group.[169]

Another CO_2 reductive coupling protocol relying on a mild chemical reductant was accomplished by Maverick and co-workers.[194] Starting from dinuclear pentacoordinate Cu^{II} complexes of type $[Cu_2(m\text{-xpt})_2X_2](PF_6)_2$ (**135** & **136**) *in situ* reduction with sodium ascorbate in DMF followed by crystallization in air yielded oxalate complex **137** (Scheme 48).[194] Due to a distinct color change during the CO_2 induced oxidation, the reaction with pure CO_2 was followed by UV/Vis spectroscopy over 128 h and indicated an almost complete conversion.[194]

Isotopic labeling was achieved upon reaction with $^{13}CO_2$ and an isotopic shift of the C-O vibration of 19 cm^{-1} was reported.[194] The high yield obtained for the reaction with CO_2 from air (96%) when starting from nitrate complex **135** reveals the tremendous selectivity for CO_2 reduction over O_2 activation by the *in situ* formed Cu^I complex.[194] Moreover, treatment of the oxalate complex with dilute HCl or HNO_3 resulted in the isolation of oxalic acid and formation of Cu^{II} chlorido and aqua (for HNO_3) complexes, respectively, thereby essentially closing the stepwise CO_2 reductive coupling cycle.[194]

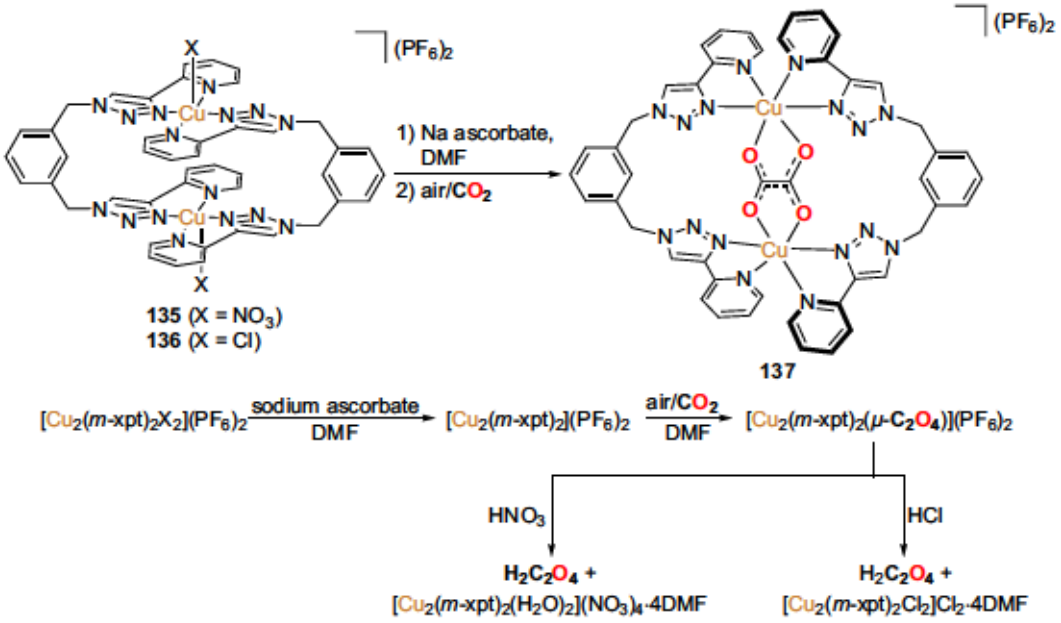

Scheme 48: CO_2 conversion into oxalic acid by *in situ* reduction of dinuclear Cu complexes with sodium ascorbate and subsequent acid treatment of the resulting oxalato complex described by Maverick and co-workers.[194]

More recently, direct conversion of CO_2 to $K_2C_2O_4$ was achieved using homogeneous trinuclear Cu complexes in combination with strong chemical reductants.[195] Chalcogen (S, Se) complexes **138** and **139** were reduced with [K(18-c-6)][$C_{10}H_8$] or $KC_{10}H_8$ to give the corresponding anionic $[Cu_3(E)(\mathbf{142})]^-$ complexes in which the $[K(THF)_3]^+$ fragment is coordinated to one of the ligand's ketiminate units, similar to the [$Na(THF)_3$Fe(tmtaa)] complex[188] reported by the Floriani group.[195] Reaction of these complexes with CO_2 at –80 °C in THF resulted in the formation of $K_2C_2O_4$ evident from IR and ^{13}C NMR spectroscopy in combination with isotopic labeling using $^{13}CO_2$ and the starting $[Cu_3(E)(\mathbf{142})]$ complexes were recovered.[195] Interestingly, a distinct cation dependence was observed and reactions relying on alkali metal cations (Na, K) proceeded at considerably lower reaction temperatures than those with Bu_4N^+, PPN^+ or Ph_4P^+.[195] Catalytic approaches utilizing an excess of reductant with respect to the complex were conducted with KC_8, $CuCp^*_2$ and $FeCp(C_6Me_6)$, but required the addition of KPF_6 in the latter two cases to enable oxalate formation.[195] In case the Se-bridged complex **139** was utilized, the $K_2C_2O_4$ yield was above 95% and a TON of 24 was reached (54% for **138**).[195] Stopped-flow experiments were conducted to obtain kinetic

data for the reaction which revealed an unequivocally faster reaction for **139** compared to **138** in addition to a distinct solvent dependency of the reaction with higher rates observed in DMF as opposed to THF.[195] Moreover, the dependence on the CO_2 concentration was found inconsistent with reductive coupling of non-coordinated $CO_2^{\bullet-}$ (second or inverse first order in $[CO_2]$).[195] Based on these result, the proposed mechanism consists of formation of an anionic CO_2-coordinated intermediate $[Cu_3(\mathbf{142})(CO_2)]^-$ *via* the arguably rate-limiting electron transfer assisted by the cation after initial reduction and subsequent dimerization with another $[Cu_3(\mathbf{142})]$ or electron transfer from another reduced $[Cu_3(\mathbf{142})]^-$ complex.[195] In the former case, attack of the resulting bridging CO_2 moiety onto another CO_2 would result in formation of oxalate and close the catalytic cycle.[195] Interestingly, no oxalate- or CO_2 bound intermediates or products were observed.[195] This illustrates one challenging factor in the development of CO_2 reductive coupling catalysts, as the resulting oxalate might inhibit or slow-down the homogeneous catalyst for further turnovers by coordination.[195] In contrast, strong reductants are required in cases where product inhibition or oxalate coordination has not been observed, as is the case for the systems described by Murray and Floriani[188].[195]

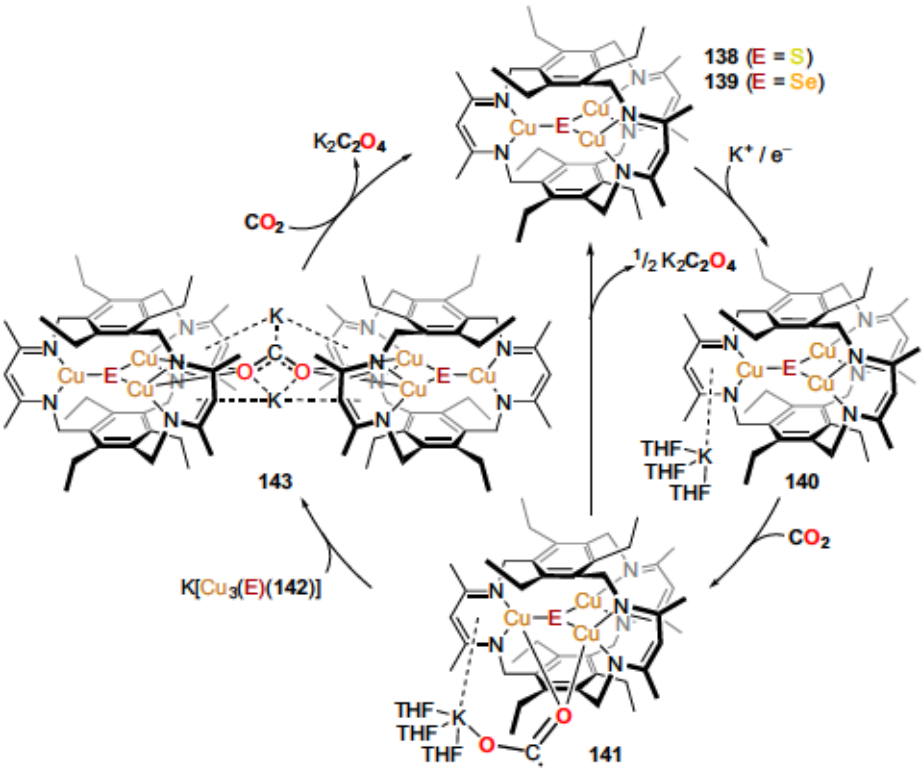

Scheme 49: Proposed mechanism for the catalytic conversion of CO_2 into $K_2C_2O_4$ facilitated by trinuclear Cu chalcogen complexes in combination with strong reductants, such as KC_8.[195]

2 Results and Discussion

2.1 Photocatalytic CO_2 Reduction

2.1.1 Photocatalytic CO_2 Reduction in Ionic Liquid Media

The results presented within this section have previously been reported elsewhere.[228]

Photocatalytic reduction of CO_2 into C_1 compounds, namely CO, formate, MeOH, or formaldehyde, constitutes a major research area within the field of CO_2 utilization and significant advances have been reported over the past decades, especially with respect to the formation of formic acid and CO, as discussed in section 1.2.3.[35,76–80] Especially in recent years, the development of photocatalytic protocols relying entirely on earth-abundant base metals has increased and systems based on Cu photosensitizers in combination with Mn[133,134,147], Co[229] and Fe[130–132] or organic dyes combined with Fe[120,122] and Co[122] reduction catalysts were found to actively catalyze CO_2 conversion.[79] Despite their requirement for sacrificial reductants, thereby generating stoichiometric quantities of waste, the utilization of base metals constitutes a major step towards environmentally benign photocatalysis for the valorization of CO_2.[78,120,122,130–134,147] However, these protocols require the application of classical organic solvents, resulting in additional waste formation in the absence of solvent reusability and potential loss into the atmosphere due to non-negligible vapor pressure.[33,230] Besides employment of water as environmentally friendly solvent, recently achieved with the help of homogeneous cobalt porphyrin complexes in combination with a water-soluble heteroleptic [Cu(N^N)(P^P)]-type photosensitizer,[229] ionic liquids (ILs) offer great potential due to their intrinsic properties, namely low volatility and intriguing electronic properties resulting from their ionic nature.[33,230–236] Ionic liquids are usually consisting of an organic cation and a corresponding anion and possess a melting point below 100 °C, albeit those liquid at room temperature are frequently utilized.[33,231–235] Their constitution offers a myriad of potential designs and fine-tuning of their properties for the specific transformation of interest by combination of different cation-anion pairs.[33,231–237] Moreover, ionic liquids have proven not only satisfactory solubility of CO_2, especially at high pressure,[230] but are capable of its capture from the atmosphere or gas mixtures and its activation for further reactions.[33,231–236,238,239] However, despite major developments in the utilization of ILs for CO_2 conversion in electrochemical and thermal processes into, among others, organic carbonates, CO, formic acid, or urea, the application of ionic liquids as solvent in photocatalytic CO_2 reduction remains underdeveloped.[231,233,236–239] Nevertheless, photo- and photoelectrocatalytic CO_2 reduction into CO or HCO_2H utilizing organic conjugated polymers,[236] Pt nanoparticles in combination with indium phosphide that was passivated with TiO_2,[239] or $WO_3/BiVO_4$[238] have recently been described.

An early example for the utilization of homogeneous transition metal catalysts in ILs for photocatalytic activation of CO_2 was reported by Grills and co-workers (Figure 13).[232] Illumination of a solution of [Re(bpy)(CO)$_3$Cl] and TEOA in 1-buty-1-methylpyrollidinium tetracyanoborate

([bmpyrr]$B(CN)_4$) under atmospheric or high (134 bar) CO_2 pressure, the latter resulting in a biphasic liquid CO_2/IL system, using ~400 nm light for 3 h yielded CO in TONs of 0.7 and 5 (high pressure), respectively.[232]

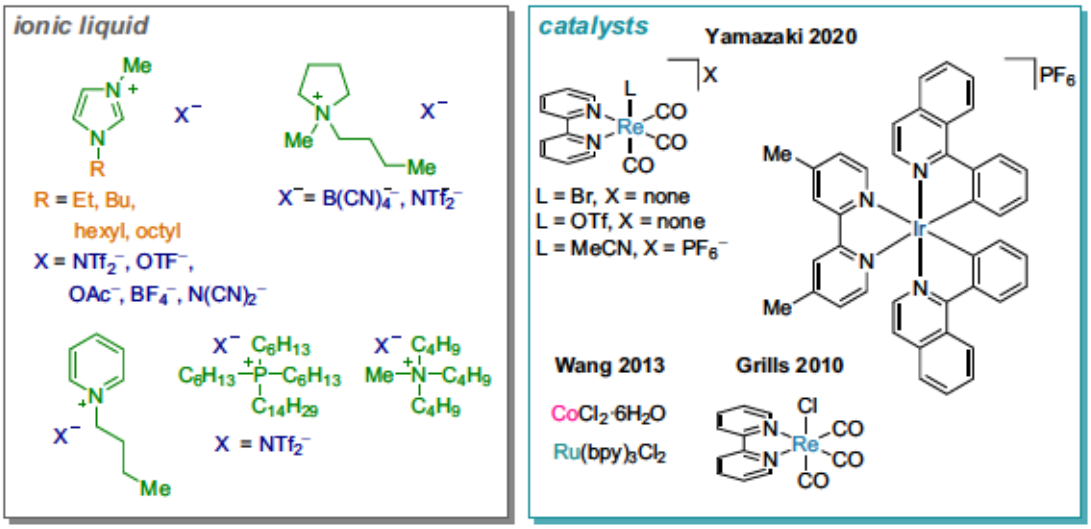

Figure 13: Previously reported photocatalytic systems for CO_2 reduction in ionic liquids with the help of homogeneous catalysts, displaying the utilized ILs as well as the employed photosensitizers and reduction catalysts.[232,233,237]

The influence of anions and varying substituents in imidazolium-based ILs was investigated by Wang and co-workers utilizing $[Ru(bpy)_3]Cl_2$ as the photosensitizer with $CoCl_2{\cdot}6H_2O$ as electron mediating reagent and TEOA as sacrificial reductant (Figure 13).[233] Initially, irradiating a mixture containing these reagents (1 µmol [Co]) in H_2O/[emim]BF_4 (emim = 1-ethyl-3-methylimidazolium) for 2 h with visible light at 30 °C produced 35.1 µmol of a CO/H_2 mixture with 88% CO selectivity.[233] Variation of the anion indicated an increasing photocatalytic activity in the order $OAc^- < N(CN)_2^- < OTf^- < NTf_2^-$, an effect rationalized by the enhanced interaction of the NTf_2^--based ILs with CO_2 resulting from the ion size in combination with the CF_3-substituents, and the reduced viscosity of the triflimide-based IL.[233] Thus, 34.7 µmol of CO and 10.9 µmol H_2 were obtained with [emim]NTf_2 under unaltered conditions using >420 nm light.[233] Significantly higher CO selectivities were observed in [hmim]BF_4 (hmim = 1-hexyl-3-methylimidazolium), giving rise to 13.1 µmol CO and 0.5 µmol H_2, corresponding to a 96.3% selectivity.[233] However, the overall reactivity was significantly reduced compared to the ethyl-substituted congener.[233] This tendency was even more pronounced for the octyl-substituted imidazolium IL (7.1 µmol of total product), which is caused by an increased steric demand of the cation and an enhanced viscosity of the derived IL.[233]

A detailed evaluation of the photocatalytic process in ionic liquids with the help of $[Re(bpy)(CO)_3L]X$ (L = Br^-, OTf^-, X = none; L = MeCN, X = PF_6^-) complexes in combination with an Ir-based PS ($[Ir(piq)_2(dmb)]PF_6$; dmb = 4,4'-dimethylbipyridine, piq = 1-phenylisoquinoline) and BIH as the sacrificial reductant was recently conducted by the Yamazaki group (Figure 13).[237] Initially, photo- and electrochemical properties of the Ir PS and the Re

complexes in various ionic liquids were measured.[237] For the ILs investigated, absorption and emission maxima of the Ir complex, its excited state lifetimes and the reductive quenching of the Ir PS by BIH were comparable to frequently employed DMA, an ammonium-based IL being the exception with a quenching fraction of only 80%.[237] However, significantly decreased quenching rates were observed, being one to two orders in magnitude smaller than those in DMA, which was mostly attributed to the higher viscosity of ILs.[237] Nonetheless, quenching was sufficient to provide the possibility of photocatalytic CO_2 reduction and a reaction with [Re(bpy)(CO)$_3$Br] (0.05 mM) combined with the Ir PS (0.5 M) and BIH (0.1 M) yielded CO with a TON of 230 in [emim]OTf compared to 77 for DMA.[237] Replacement of the bromide by MeCN further improved the catalytic properties, resulting in a CO TON of 540 over 4 h in the same IL.[237] While this particular IL turned out to be the most suitable for photocatalytic CO_2 reduction at this concentration, a few general characteristics with respect to an optimum combination of anion and cation were made.[237] In highly viscous ILs, the diffusion of the Re catalyst decreases resulting in a diminished possibility of reaction with the Ir PS and CO_2.[237] Moreover, pyridinium- or phosphonium-based ILs or ILs containing BF_4^- anions were insufficient for photocatalytic applications, due to either absorption in the utilized light range (pyridinium) or diminished photosensitizing properties (phosphonium and BF_4^-).[237] Interestingly, OTf^- and NTf_2^--based ILs proved to be advantageous for photocatalytic applications, albeit in the latter case the corresponding cation played a major role, with a pyrrolidinium- or ammonium-derived cation showing low photocatalytic ability.[237] For the most efficient class of ILs, those based on imidazolium cations, a strong influence of the chain length of the *N*-substituents was observed, and decreased turnover numbers were observed upon exchange of ethyl- for butyl- or hexyl-substituents in the triflate-based ILs.[237] This was attributed to different limiting steps in the photocatalysis, with the photosensitizing process being limiting in [emim]OTf and the CO_2 reduction by [Re] being rate-determining in [bmim]OTf or [hmim]OTf.[237]

In parallel to the study reported by Yamazaki and co-workers,[237] the possibility of straightforward transfer of an existing CO_2 reduction protocol entirely utilizing base metal catalysts into ionic liquid media was investigated. For this purpose, a photocatalytic system developed by Beller and co-workers based on a Cu PS and a Fe reduction catalyst[131] in combination with different classes of ILs was explored. The main objective of this feasibility study was to derive a general concept that would facilitate further development of photocatalytic small molecule activation in non-volatile ILs, thereby eventually enabling recycling of the solvent in the long run.

Inspired by the literature, a novel heteroleptic Cu PS **144** was prepared which featured a bis(phenoxaphosphano)-substituted xantphos analogue in addition to the established bathocuproine ligand.[l] A similar bisphosphine constructed from a thixantphos backbone[240] was

[l] Preparation and characterization of **144** and evaluation of its photo- and electrochemical properties was conducted by Dr. P. A. Forero-Cortés and F. Brunner under guidance of Prof. E. C. Constable, Prof. C. E. Housecroft, and Prof. P. C. J. Kamer. Detailed procedures are reported in the ESI of the initial report.[228]

previously utilized in an analogous Cu PS and depicted the highest activity for the investigated water reduction with $[Fe_3(CO)_{12}]$.[126] Hence, an evaluation of the performance of its novel analogue by direct comparison with [Cu(bcp)(xantphos)]PF_6 (**42**) appeared worthwhile. The photophysical properties of **42** were comparable to those of the novel Cu complex **144**, with a broad metal-to-ligand charge-transfer band at approx. 395 nm in both cases and emission maxima at 539 nm (**42**) and 555 nm (**144**) in CH_2Cl_2 solution, respectively. Despite a slightly increased excited-state lifetime of 9.42 µs (±15%) for **144** in degassed CH_2Cl_2 compared to **42** (7.24 µs±15%), electrochemical properties and geometries in the solid state, assessed by single crystal X-ray diffraction, resembled each other.

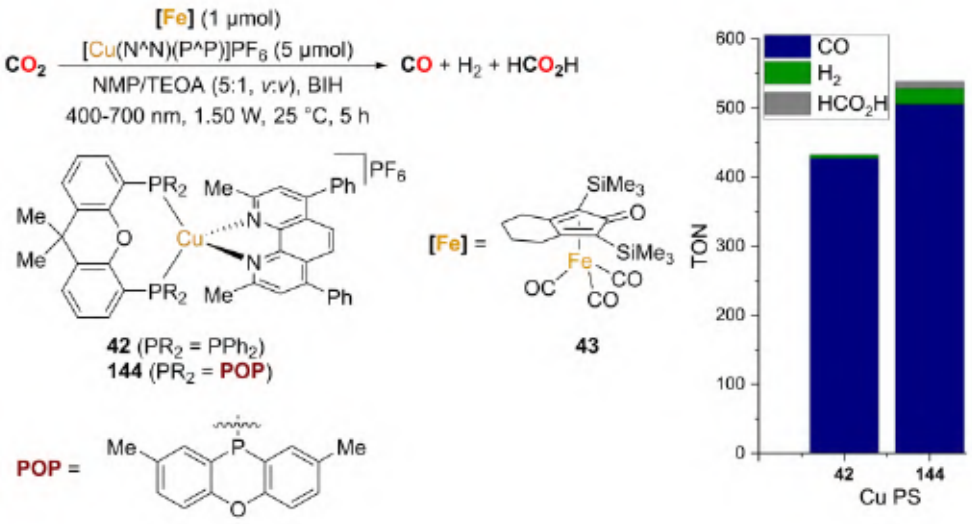

Figure 14: Photocatalytic CO_2 reduction with Knölker-type[143] Fe complex **43** and heteroleptic Cu photosensitizers **42** or **144** in NMP/TEOA (5:1, *v*:*v*) utilizing BIH and visible light (400-700 nm, 1.50 W) at 25 °C for 5 h.

To evaluate whether the photocatalytic properties of **144** would follow the same trend as its inherent characteristics, CO_2 reduction in combination with cyclopentadienone-ligated Fe carbonyl complex **43** previously developed by the Beller group[131] was chosen as the benchmark reaction. The main reason for this selection is the utilization of base metal catalysts at reasonable catalyst loadings (1 µmol [Fe]) producing CO in high selectivity (99%) and with a high TON of 427 over 5 h.[131] Moreover, complex **43** had previously been utilized for CO_2 reduction in combination with an Ir-based PS[141] or in an electrocatalytic approach[140] and the mechanism, specifically for the electrochemical CO_2 reduction, has been extensively investigated.[241] Interestingly, the ability of the ligand to act as a proton reservoir upon protonation of the oxygen was found to play a key-role in the photocatalytic reaction pathway.[141] Here, a Fe-H intermediate with O-protonated ligand was identified as an active intermediate,[141] thereby contrasting the electrochemical pathway where no Fe-H is formed and in which initial dimerization after reduction is favored over O-protonation at low proton concentration.[140,241]

In an initial experiment,[II] novel Cu PS **144** and Fe catalyst **43** were illuminated in NMP/TEOA (5:1, *v*:*v*) using visible light (400-700 nm, 1.50 W) and BIH as the sacrificial reductant for 5 h (Figure 14). Under these conditions, CO was formed with a TON of 505 (average of two reactions), accompanied by H_2 (TON=23), which is slightly higher than the activity observed with isolated **42**.[131] Moreover, HCO_2H with a TON of 10 was observed resulting in a CO selectivity of ≥93% for novel **144**, slightly lower than that obtained with **42**, albeit the formation of formate is not commented upon in the original report.[131]

Next, the two Cu PS / **43** combinations were evaluated in four different ionic liquids (Table 2), representing three commonly applied classes, namely pyrrolidinium-, imidazolium- and phosphonium-based ionic liquids.[33,234,237]

Table 2: Photocatalytic CO_2 reduction with *Knölker*-type complex **43** in combination with Cu PS **42** or **144**.[228]

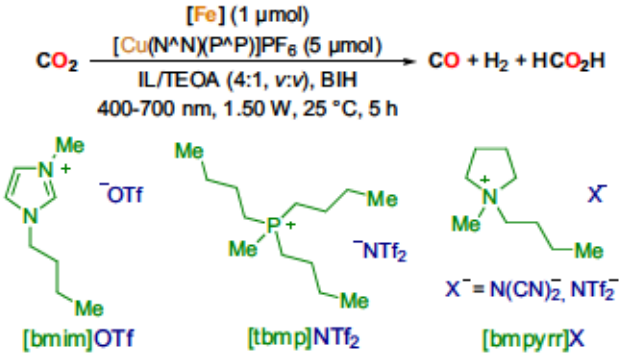

Entry	Cu PS	IL mixture	TON (CO)	TON (H_2)	TON (HCO_2H)	Sel. (CO) [%]
1	**144**	[bmim]OTf/TEOA (4:1, *v*:*v*)	171	171	6	49
2[a]	**42**	[bmim]OTf/TEOA (4:1, *v*:*v*)	60	124	11	30
3[b]	**42**	[tbmp]NTf_2/TEOA (4:1, *v*:*v*)	60	274	9	17
4	**144**	[bmpyrr]$N(CN)_2$/TEOA (4:1, *v*:*v*)	29	≤3	≤3	≥82
5	**42**	[bmpyrr]$N(CN)_2$/TEOA (4:1, *v*:*v*)	77	≤3	≤3	≥92
6[b]	**42**	[bmpyrr]NTf_2/TEOA (4:1, *v*:*v*)	60	338	5	15
7[b,c]	**42**	[bmpyrr]$N(CN)_2$/TEOA (4:1, *v*:*v*)	1	≤3	≤3	≥14
8[d]	**42**	[bmpyrr]$N(CN)_2$/TEOA (4:1, *v*:*v*)	79	≤3	≤3	≥92

Detailed experimental procedures and single experimental results are presented in the appendix, section 4.3 or the ESI. Reaction conditions: **43** (1 µmol), Cu PS **42** or **144** (5 µmol) and BIH (150 mg) were irradiated with visible light (400-700 nm, 1.50 W) for 5 h at 25 °C in CO_2 saturated IL/TEOA (7.5 mL, 4:1, *v*:*v*) mixtures under a constant CO_2 atmosphere (1 atm). Reactions at least performed in duplicate unless stated (averages are presented). [a]Result of a single experiment. [b]Biphasic due to a lack of miscibility between TEOA and IL. [c] *In situ* formation starting from $[Cu(MeCN)_4]PF_6$ (5.0 µmol), bathocuproine (5.1 µmol) and xantphos (15 µmol) was attempted. [d]Total reaction time of 23 h. After 5.5 h, **42** (5.0 µmol) in [bmpyrr]$N(CN)_2$ (1 mL) was added.

In the imidazolium-based IL ([bmim]OTf) a CO/H_2 mixture of equal constitution with a TON of 171 for either product was obtained with **144** in a 4:1 (*v*:*v*) [bmim]OTf/TEOA mixture under otherwise unaltered photocatalytic conditions compared to NMP, which is a surprising drop in CO selectivity to 49% (Table 2, entry 1). This became even more apparent when **42** was

[II] Photocatalytic experiments within section 2.1.1 were designed and conducted jointly with Dr. P. A. Forero-Cortés.

utilized, resulting in a $CO/H_2/HCO_2H$ mixture with TONs of 60, 124, and 11, respectively (Table 2, entry 2), contrasting the excellent selectivities obtained in the same IL for the Ir/Re system developed by the Yamazaki group.[237] Favored proton reduction was likewise observed in the phosphonium-based IL [tbmp]NTf_2 (tbmp = tributylmethylphosphonium), yielding a $CO/H_2/HCO_2H$ mixture with a total TON of 343 and a poor CO selectivity of 17% with **42** as the photosensitizer (Table 2, entry 3). Higher selectivity for the desired CO_2 reduction to CO was observed when the reaction was conducted in pyrrolidinium-based IL [bmpyrr]$N(CN)_2$ for either Cu PS (Table 2, entries 4 and 5). Interestingly, literature-known **42** proved to be significantly more active compared to novel **144** under these conditions, providing CO with a TON of 77 and a selectivity $\geq$92%, while the latter gave CO in $\geq$82% selectivity with a TON of 29. Given the similar properties of both complexes, the nature of this significant difference is currently unknown, and thus requires further investigations. Interestingly, exchanging the dicyanamide anion for triflimide, previously reported to be beneficial in certain cases,[233,237] drastically altered the selectivity of the photocatalytic reaction to favor H_2 formation (Table 2, entry 6). The obtained TONs for CO (60), H_2 (338) and HCO_2H (5), corresponding to a 15% CO selectivity, are in discordance with the results obtained for the dicyanamide analogue, which was reported to provide insufficient applicability in photocatalytic CO_2 reduction for [emim] ILs.[233] Coordination of the dicyanamide, well-known for Re^{I} carbonyl or Fe^{II} complexes,[242,243] as a beneficial influence contributing to the enhanced selectivity cannot be entirely excluded. However, despite a major shift in selectivity, the TON for CO formation is only slightly diminished in [bmpyrr]NTf_2, thus a beneficial influence of the dicyanamide for the formation of CO is not expected while suppression of the H_2 formation cannot be foreclosed. Another possible factor for the observed altered selectivity might be the biphasic reaction medium obtained when triflimide-derived ILs are utilized, as these were not miscible with TEOA.

To fully mimic the protocol for CO_2 reduction transferred from NMP into ILs, the possibility of *in situ* formation of Cu PS **42** in the most promising IL [bmpyrr]$N(CN)_2$ was evaluated (Table 2, entry 7). Yet, the *in situ* formation starting from $[Cu(MeCN)_4]PF_6$, xantphos, and bathocuproine in a 1/3/1 ratio, remained unsuccessful, arguably due to the increased viscosity compared to NMP and reduced solubility of the starting materials, a drawback of ILs also encountered by Yamazaki and co-workers.[237] Finally, deactivation of the catalyst was confirmed by addition of a second equivalent of Cu PS **42** after 5.5 h of reaction time (Table 2, entry 8). Deactivation after 5 h has previously been described for this photocatalytic system[131] and presents one of the main challenges for future improvements of photocatalytic CO_2 reduction with these kind of Fe and Cu complexes.[135] Incorporation of the catalysts into MOFs might provide a feasible strategy to achieve the requested enhancement of stability, as recently presented by Lin and co-workers.[135]

Control experiments conducted with Cu PS **144** confirmed the necessity of all components to facilitate photocatalytic CO_2 reduction in [bmpyrr]$N(CN)_2$ (Table S 2). Moreover, the origin

of CO being CO_2 was assessed under high-purity conditions using a blank experiment under He atmosphere for direct comparison.[III]

In conclusion, a novel heteroleptic Cu PS was prepared and characterized, revealing similar electrochemical and photophysical properties to [Cu(bcp)(xantphos)]PF_6 and displaying similar catalytic properties in the photocatalytic CO_2 reduction in NMP. Moreover, the CO_2 reduction protocol entirely relying on non-precious metal catalysts was successfully transferred into ionic liquids, with significant differences in the photocatalytic activity and product selectivity observed depending on the respective IL class and the corresponding anion. These results complement previous and parallel investigations and indicate the feasibility of transfer of the methodology developed in traditional solvents into ionic liquids.[233,237] Furthermore, recycling of the solvent might eventually be enabled by this strategy, albeit extraction after photocatalytic experiments remained unsuccessful in this first precedent.

A remaining limitation is catalyst stability, but incorporation into MOFs might prove as vital approach to tackle this challenge.[135] Furthermore, albeit TONs and selectivities herein are higher than for early examples utilizing homogeneous complexes,[232,233] they cannot compete with those obtained in traditional amide solvents or activities obtained with precious metal complexes in ILs.[131,237] Nevertheless, the low number of ILs investigated, and the tremendous dependence of the photocatalytic activity on anion and cation,[233,237] will eventually enable higher activities upon evaluation of a larger library of potential solvents. Finally, the conceptual study presented herein[228] will hopefully encourage researchers to investigate transfer of established and sufficiently understood photocatalytic protocols from traditional solvents into ionic liquids.

[III] High-purity measurements were conducted by Dr. N. G. Moustakas under supervision of Prof. J. Strunk.

2.1.2 [FeFe] Hydrogenase Mimics in the Photocatalytic Reduction of CO_2

The results presented within this section have previously been reported elsewhere.[244]

Following the interest in photocatalytic CO_2 reduction to CO with the help of base metal complexes, the idea to utilize biomimetic complexes based on Fe as CO_2 reduction catalysts appeared intriguing. For this, dinuclear iron dithiolate complexes were evaluated under photocatalytic conditions. These [FeFe] complexes resemble the active site of the [FeFe] hydrogenases, enzymes that efficiently catalyze the interconversion of protons/electrons and dihydrogen with formidable TOFs as high as 10^4 s^{-1} for the production of H_2.[245–248] Besides the azadithiolate bridge linking both Fe centers, the dinuclear active sites contain CO and CN^- ligands which are uncommon in naturally occurring enzymes.[245–248] In view of the high catalytic efficiency and the peculiar, comparatively simple structure of the dinuclear active site, a vast interest in synthetic procedures for the preparation of analogous butterfly-like $[Fe_2S_2]$ complexes and their follow-up reactivity is not surprising.[83,245–270] Moreover, these [FeFe] hydrogenase mimics have frequently been utilized in the electro- and photocatalytic generation of hydrogen in combination with different proton sources and under varying conditions and are among the most active homogeneous Fe catalysts for water reduction.[83,145,246,248,250–260] Interestingly, their application has not been expanded to CO_2 reduction, until recently.[271]

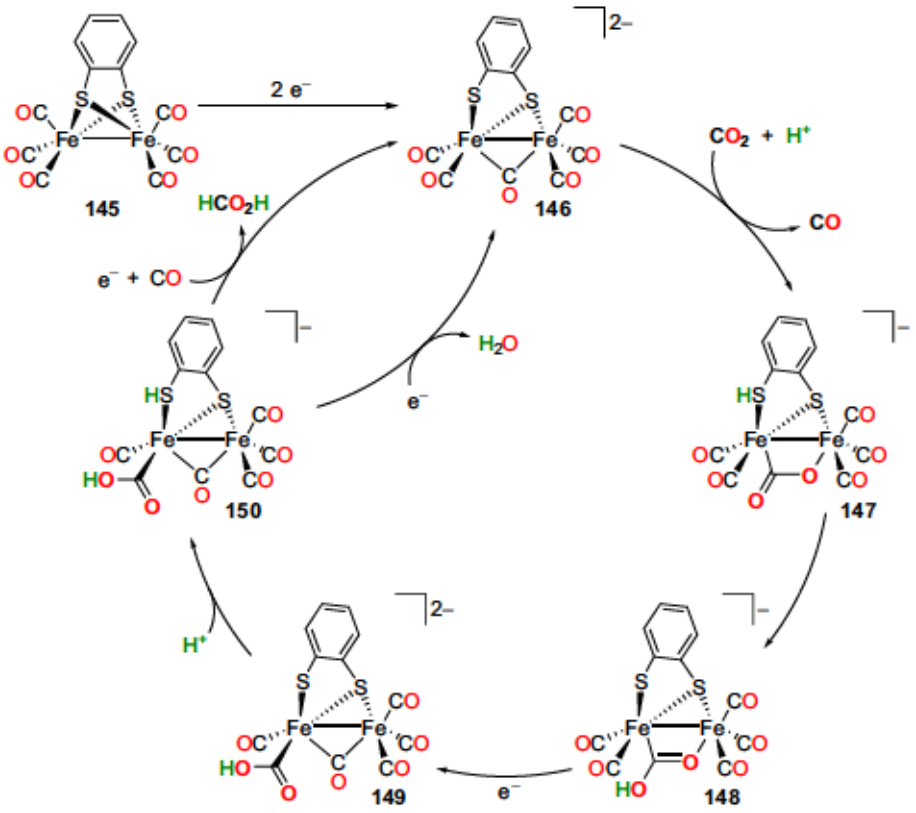

Scheme 50: Proposed catalytic cycle for the electrochemical reduction of CO_2 into CO and formic acid catalyzed by [FeFe] complex **145**.[271]

Wang and co-workers employed $[Fe_2(\mu\text{-bdt})(CO)_6]$ (**145**, bdt = benzene-1,2-dithiolate) and

its congener [$Fe_2(\mu$-edt)$(CO)_6$] (edt = ethane-1,2-dithiolate) under electrocatalytic conditions for the formation of formate, CO, and H_2.[271] Protic conditions were required for CO_2 reduction and HCO_2H/CO/H_2 were produced with TONs of 35/4/3 upon controlled potential electrolysis at −2.35 V *vs.* Fc/Fc^+ for 2 h with **145** in MeOH/MeCN.[271] TOFs as high as 195 s^{-1} were obtained for complex **145**, which proved to be significantly more active than [$Fe_2(\mu$-edt)$(CO)_6$].[271] Furthermore, water was successfully utilized instead of MeOH and total Faradaic efficiencies of 86% or 88% and selectivities for CO_2 reduction of 92% or 94-95% were obtained in 0.1 M MeOH/MeCN or 0.1 M H_2O/MeCN, respectively, with formic acid as the major product in both cases.[271] Kinetic measurements indicated a first order dependence of the reaction on [**145**] and [CO_2].[271] Moreover, electrochemical investigations combined with DFT calculations were conducted to provide a plausible reaction mechanism (Scheme 50).[271] Two-electron reduction of **145** generates a dianionic species featuring a non-bridging thiolate unit, which undergoes CO loss accompanied by protonation and electrophilic CO_2 addition.[271] Subsequent proton shift onto the Fe-coordinated OCO unit, follow-up reduction and another protonation of the κ^1-S substituent yields the pivotal intermediate **150**.[271] This intermediate undergoes either release of formic acid and subsequent coordination of CO upon further reduction or reduction followed by water release in the CO-producing pathway.[271]

In parallel to these inspiring results, the application of **145** with the help of photocatalysis was evaluated.[244] Initial experiments with **145** (0.1 μmol) utilizing BIH as the sacrificial reductant in combination with *in situ* formed [Cu(bcp)(xantphos)]PF_6, starting from a mixture of [$Cu(MeCN)_4$]PF_6 (1 μmol), bathocuproine (1 μmol), and xantphos (3 μmol), were conducted in NMP/TEOA (5:1, *v*:*v*), a combination successfully employed for other Fe catalysts[131]. Irradiation of this mixture with violet-blue light (415 nm, 1.00 W) for 3 h resulted in a 1.8/1.5/1 mixture of CO/H_2/HCO_2 at a total TON of 614 (Table 3, entry 1), thus yielding CO as the major product contrasting the electrochemical reaction[271].[IV] However, detection of formic acid is in good agreement with the results reported by Wang and co-workers,[271] albeit a poor reproducibility for these specific TONs was obtained, which was at this point assigned to partial uncatalyzed CO_2 reduction by BIH.[272] While the *in situ* prepared Cu PS gave results similar to those obtained with the preformed complex in earlier studies,[129,131] a distinct difference in selectivity and activity in combination with complex **145** (Table 3, entry 2) was detected. In fact, illumination of **145** and Cu PS **42** under unaltered conditions yielded CO/H_2/HCO_2H (1/7/3) with a total TON of 865 accompanied by a significant drop in reproducibility for the formed H_2 quantities (623 *vs.* 476 for two reactions).

The plain difference between the preformed and the *in situ* Cu PS is the absence of excess bisphosphine, thus causing formation of increased fractions of catalytically inactive $[Cu(bcp)_2]^+$.[129,131,132] While this might explain the diminished catalytic activity for CO_2 re-

[IV] Detailed single experiment results are presented in the appendix, section 4.4.6, and the supplementary material (DOI: 10.1002/cctc.201901686) of the original publication.[244]

duction with the molecular Cu PS, the significantly different ratio of $CO/HCO_2H/H_2$ might suggest a more sophisticated role of the ligands of the *in situ* Cu PS. To minimize the formation of the homoleptic $[Cu(N^{\wedge}N)_2]^+$ complex and shift the equilibrium towards the heteroleptic $[Cu(N^{\wedge}N)(P^{\wedge}P)]^+$,[124,127–129,131,132,142,144,145] the [Cu]/bcp/xantphos ratio was evaluated. Besides optimization of the catalytic activity, an enhanced reproducibility of the results of this photocatalytic approach was desired. However, changing to 1/10/3, 1/1/10, 1/1/6, or 1/3/3 [Cu]/bcp/xantphos ratios did not result in the desired enhancement of reproducibility (Table S 4). The highest catalytic activity, despite insufficient reproducibility, was observed for a 1/2/5 [Cu]/bcp/xantphos ratio, yielding a 1.7/1.1/1 $CO/H_2/HCO_2H$ mixture with a total TON of 756 (Table 3, entry 3).

Table 3: Initial photocatalytic CO_2 reduction experiments utilizing **145** as the catalyst in combination with Cu PS **42**.[244]

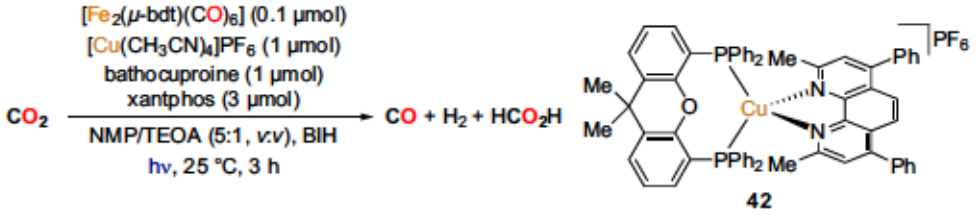

42

Entry	[Cu]/bcp/xantphos [μmol]	λ [nm]	Radiant flux [W]	Total TON	$CO/H_2/HCO_2H$
1[a]	1/1/3	415	1.00	614	1.8/1.5/1
2[b]	1/0/0	415	1.00	865	1/6.8/2.9
3[c]	1/2/5	415	1.00	756	1.7/1.1/1
4[d]	1/2/5	400-500	1.50	880	2.1/1.1/1

Detailed experimental procedures and single experimental results are presented in the appendix, section 4.4.6 or the ESI. Reaction conditions: **145** (0.1 μmol), $[Cu(MeCN)_4]PF_6$ (x μmol), xantphos (x μmol), bathocuproine (x μmol), and BIH (120 mg) were irradiated with visible light for 3 h at 25 °C in CO_2 saturated NMP/TEOA (5:1, *v:v*) under a CO_2 atmosphere (1 atm). [a]The presented result is the average of 7 reactions. [b]Preformed molecular [Cu(bcp)(xantphos)]PF_6 (1.0 μmol) was utilized as the photosensitizer. The presented result is the average of 2 reactions. [c]The presented result is the average of 5 reactions. [d]The presented result is the average of 3 reactions.

Variation of the wavelength of illumination or its radiant flux, likewise, did not facilitate the required reproducibility when utilizing 415 nm at 0.50 W or 1.50 W or blue light with a wider 400-500 nm range at 0.50 W or 1.00 W (Table S 5). Initially, a reproducibility within 10% margin for the formation of CO (TON = 411, 439, 460) was observed when 400-500 nm light was employed at 1.50 W radiant flux and a 2/1/1 $CO/H_2/HCO_2H$ mixture was obtained with a total TON of 880 (Table 3, entry 4). Yet, the same reaction resulted in significantly altered results upon attempted reproduction six months after these initial experiments.

Impurities, even in minor quantities, are well-known to impact the reproducibility of catalytic transformations.[273] Hence, replacement of the utilized reagents, the solvent, and the catalyst batch were undertaken. However, these measures failed to restore the initially observed catalytic activity in a reproducible manner and indicated an unpredictable outcome assessed by 59 experiments (Figure 15 and Table S 6). Five-fold enhancement of the catalyst loading, likewise, did not establish consistent reaction outcomes (Table S 7), precluding the low catalyst loading (0.1 μmol) as the sole reason for the poor reproducibility.

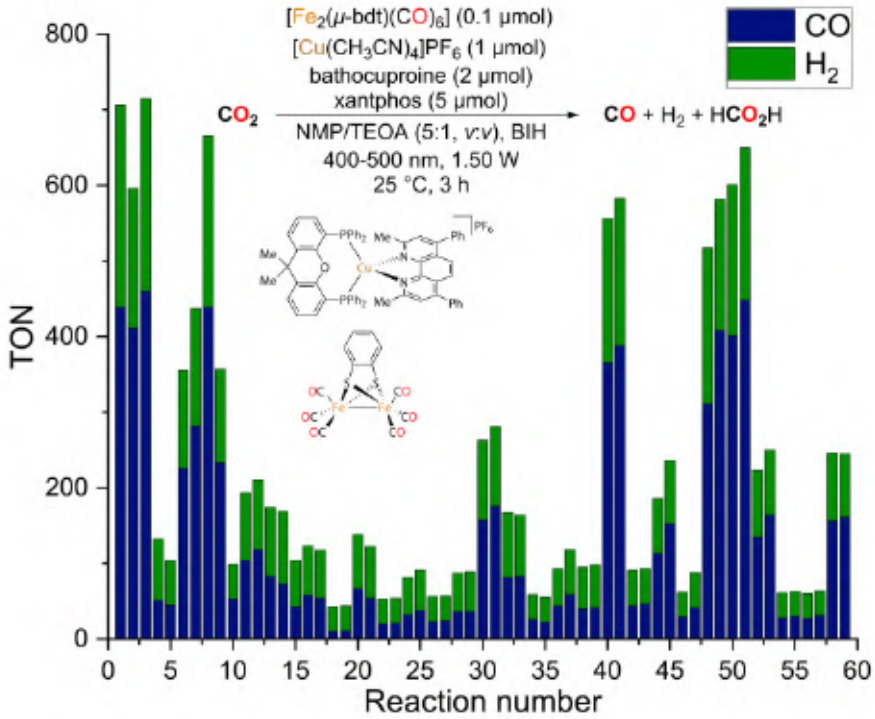

Figure 15: Single experimental results for reactions conducted with catalyst **145**, *in situ* prepared [Cu(bcp)(xantphos)]PF_6 and BIH in NMP/TEOA (5:1, *v*:*v*) utilizing blue light (400-500 nm, 1.50 W) at 25 °C for 3 h (TONs for HCO_2H are omitted, as these have not been determined for all reactions; detailed HCO_2H TONs are given in Table S 6).

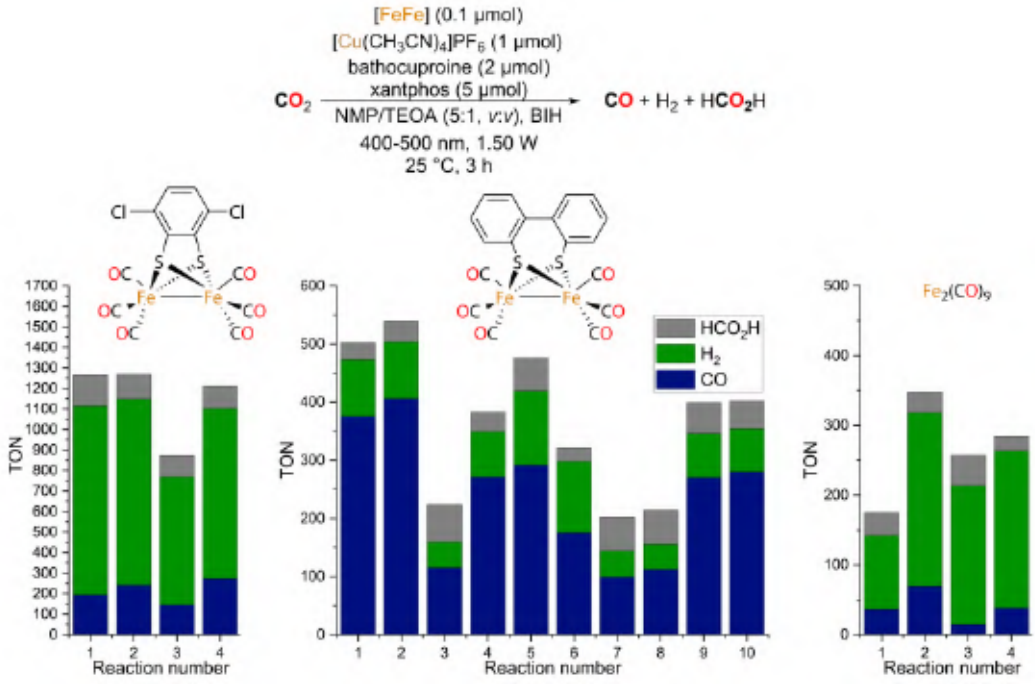

Figure 16: Single experimental results for reactions conducted with [Fe_2(μ-Cl-bdt)$(CO)_6$], [Fe_2[μ-bpdt)$(CO)_6$], or [$Fe_2(CO)_9$] in combination with *in situ* prepared [Cu(bcp)(xantphos)]PF_6 and BIH in NMP/TEOA (5:1, *v*:*v*) utilizing blue light (400-500 nm, 1.50 W) at 25 °C for 3 h.

Other [FeFe] complexes were subsequently investigated to identify whether these suffer from analogous reproducibility issues. Photocatalytic reactions with [Fe_2(μ-Cl-bdt)$(CO)_6$] (Cl-bdt = 1,4-dichlorobenzene-2,3-dithiolate), [Fe_2(μ-bpdt)$(CO)_6$] (bpdt = 1,1'-biphenyl-2,2'-dithiolate), and [$Fe_2(CO)_9$] were conducted utilizing 400-500 nm (1.50 W) for 3 h in NMP/TEOA (5:1, *v*:*v*) in the presence of BIH (120 mg). A tendency for [Fe_2(μ-bpdt)$(CO)_6$] favoring CO_2 reduction over H_2 formation, contrasting [Fe_2(μ-Cl-bdt)$(CO)_6$] and [$Fe_2(CO)_9$], can be observed (Figure 16 and Table S 8). However, in all cases poor to mediocre reproducibility was observed, thus, confirming the problem encountered with complex **145**.

Despite the insufficient consistency of the photocatalytic reactions, a significant difference between the preformed Cu PS **42** and its *in situ* version complemented by a pronounced influence of the [Cu]/bcp/xantphos ratio was observed early on. Due to the renowned property of [FeFe] complexes, such as **145**, to undergo CO substitution by bidentate nitrogen- or phosphorus-based ligands,[247,253–257,259,261,263–269] these observations suggested reaction of the [FeFe] complexes with either bidentate ligand of the Cu PS. Such a reaction might even account for the observed lack of reproducibility, as it would sophisticate the existing equilibrium between homo- and heteroleptic Cu complexes.

Consequently, **145** was illuminated (415 nm, 1.00 W) in the presence of equimolar quantities of xantphos or bathocuproine (Scheme 51). Indeed, the resulting CO-substitution products **151** and **152** were obtained in 64% and 76% yield, respectively.

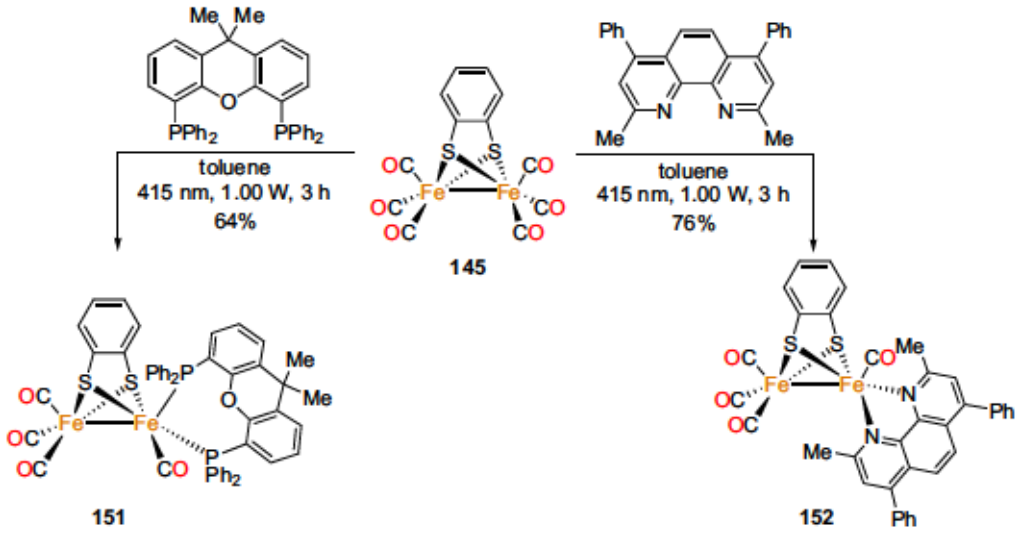

Scheme 51: Preparation of complexes **151** and **152** by irradiation (415 nm, 1.00 W) of a toluene solution of **145** in the presence of xantphos or bathocuproine, respectively.

In both complexes, the C-O vibrations are shifted to lower wavenumbers (**151**: $\tilde{\nu}$ = 2021, 1971 (shoulder), 1947, 1883 cm^{-1}; **152**: $\tilde{\nu}$ = 2008, 1948 (shoulder), 1929, 1886 cm^{-1}) compared to **145** ($\tilde{\nu}$ = 2080, 2044, 2004 cm^{-1})[262] highlighting the electron-donating properties of both ligands, which appear to be of comparable strength.

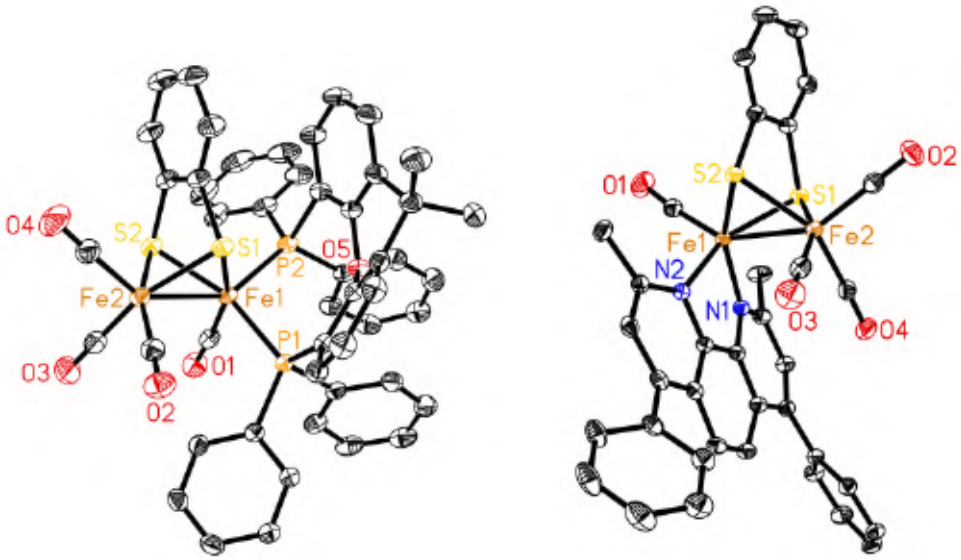

Figure 17: Molecular structures of complexes **151** and **152** (thermal ellipsoid displayed at 50% probability, H atoms and solvent molecules (**151**) are omitted for clarity). Selected bond lengths [Å] and angles [°] for **151**: Fe-C(O), 1.744(3), 1.784(3), 1.788(3), 1.801(3); Fe-S, 2.2512(7), 2.2597(8), 2.2747(8), 2.2950(7); P-Fe-Fe, 104.05(2), 145.46(2); P-Fe-S, 92.99(3), 99.82(3), 100.30(3), 158.75(3); S-Fe-S, 79.67(3), 79.93(3). Selected bond lengths [Å] and angles [°] for **152**: Fe-C(O), 1.7620(15), 1.7763(15), 1.7771(15), 1.8086(15); Fe-S, 2.2442(4), 2.2517(4), 2.2726(4), 2.2769(4); N-Fe-S, 92.04(3), 93.38(3), 152.68(3), 153.61(3); S-Fe-S, 79.467(14), 80.607(14).

Single-crystal X-ray diffraction conducted with crystals obtained by slow diffusion of hexane into CH_2Cl_2 solutions at 7 °C permitted unambiguous elucidation of the coordination geometry (Figure 17). The dithiolate moiety remained intact in both complexes and the chelating xantphos or bathocuproine is coordinated in a κ^2-mode to a single Fe center. Previously reported analogous [FeFe] complexes are in good accordance with this observation.[253–256,259,263–268] A major difference is the coordination mode of the introduced chelating ligands. While xantphos coordinates in an apical-basal fashion, bathocuproine is ligated in a basal-basal mode. The latter geometry is matching literature-known N^N-ligated congeners,[254,255,265] while for bisphosphine complexes both, apical-basal and basal-basal, coordination modes have been described.[253,256,259,263,264,266–268] A broad singlet at 58.9 ppm is observed in the $^{31}P\{^1H\}$ NMR of **151**, highlighting equivalence of both P atoms in solution, hence suggesting a fast equilibration between the apical-basal and basal-basal coordination, as observed for related complexes[264]. Fe-Fe (2.5709(5) Å for **151** and 2.5397(3) Å for **152**) as well as Fe-S distances (2.2442(4)-2.2950(7) Å) remain in a similar range and indicate a minor disturbance of the symmetry of the $[Fe_2S_2]$ core in both cases. Moreover, Fe-P distances (2.2635(7)/2.2689(8) Å) and especially the P-Fe-P angle (101.11(3)°) are increased compared to similar apical-basal dppe-containing[256,268] and even bidentate carborane-derived [FeFe] complexes[264]. This is likely caused by the increased bite angle of xantphos (111.7°) compared to dppe (84.4°),[v] a result of the rigidity of the xanthene-derived backbone.[240,274]

[v] Presented bite angles are calculated natural bond angles reported in the literature.[240,274]

In contrast, Fe-N distances in **152** (1.9808(11) and 1.9925(11) Å) and the N-Fe-N angle (81.56(5)°) are very close to those observed for its congener [Fe_2(μ-pdt)(phen)$(CO)_4$] (**153**; N-Fe: 1.9864(15), 1.9931(15) Å; N-Fe-N: 81.71(7)°; pdt = 1,3-propanedithiolate)[265], despite smaller N-Fe-Fe angles (98.17(3), 98.51(3)° in [**152**]; 104.89(5), 105.33(4)° in [**153**][265]) resulting in an increased tilt of the bidentate bathocuproine ligand with respect to the Fe-Fe axis. Successful CO displacement with the help of UV light irradiation in analogous [FeFe] complexes has widely been utilized.[253,257,259,266] However, visible light with a maximum intensity at a wavelength of 415 nm appears to be sufficient in specific cases, as indicated by the results presented herein and in previous literature studies.[275,276]

After isolation and characterization of these novel disubstituted [FeFe] hydrogenase mimics, their behavior in the photocatalytic reduction of CO_2 was evaluated. For a direct comparison, CO_2 saturated reaction mixtures containing **151** or **152**, BIH, and Cu PS **42** were irradiated with 415 nm light (1.00 W) for 3 h in 5:1 NMP/TEOA (Figure 18 a)). In both cases, the results appeared to be more consistent than those obtained with **145** and **42** and a total TON of 510 with a $CO/H_2/HCO_2H$ ratio of 1/32/15 was observed for **151** (average of 2 reactions), while **152** produced a 1/7/1 $CO/H_2/HCO_2H$ mixture with a total TON of 530 (average of 4 reactions). However, within the four experiments for **152** and the isolated Cu PS **42**, a significant deviance between the highest (CO: 76; H_2: 450) and lowest (CO: 44; H_2: 367) observed TONs indicated once again an insufficient reproducibility.

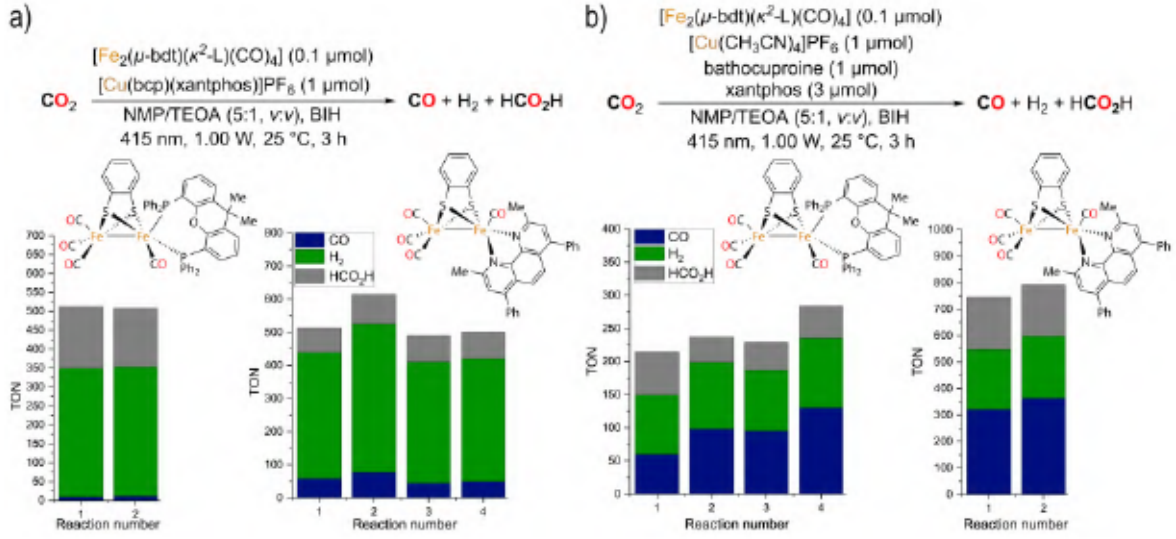

Figure 18: Single experimental results for photocatalytic CO_2 reduction reactions conducted with **151** or **152** and BIH in NMP/TEOA (5:1, *v*:*v*) utilizing violet-blue light (415 nm, 1.00 W) at 25 °C for 3 h and in combination with a) [Cu(bcp)(xantphos)]PF_6 or b) *in situ* prepared [Cu(bcp)(xantphos)]PF_6, starting from [$Cu(MeCN)_4$]PF_6, bathocuproine, and xantphos (1/1/3).

This was even more pronounced upon changing from the isolated to the *in situ* Cu PS, utilizing a 1/1/3 [Cu]/bathocuproine/xantphos ratio (Figure 18, b)). Overall, higher CO formation was observed under these conditions for both novel [FeFe] complexes. **151** was significantly less active in the CO_2 reduction yielding $CO/H_2/HCO_2H$ in a 2/2/1 mixture with a total TON

of 241, compared to **152** which produced a 1.7/1.2/1 $CO/H_2/HCO_2H$ product mixture with a total TON of 769. These results, especially upon comparison with **145** (Table 3, entry 1), suggest a preferential role of **152** for the generation of an active CO_2 reduction catalyst, an observation reminiscent of the enhanced photocatalytic CO_2 reduction with $[Fe_3(CO)_{12}]$ in the presence 2,2'-bipyridine.[277] Nevertheless, the obvious inconsistency of the absolute results, especially when taking the previous results into account, precludes a final statement on this possibility. This again underscores the complexity of this system and highlights that the reproducibility is not entirely determined by the utilized [FeFe] pre-catalyst.

The results obtained for the photocatalytic CO_2 reduction with the utilized [FeFe] complexes clearly highlight the necessity of careful evaluation of the reproducibility of catalytic transformations. Reaction yields, specifically for synthetic transformations, and their consistency at lower catalyst loadings are a good parameter to assess whether a reduced concentration of catalyst remains feasible for the reaction of interest. However, in photocatalytic transformations, such as the photocatalytic CO_2 reduction reported herein, the yield with respect to converted CO_2 is not commonly measured and would be far from complete, as indicated by GC analysis of the headspace. In contrast, TONs and TOFs are routinely stated and utilized for comparison of the catalytic activity, a process that certainly encourages further development and facilitates innovative discoveries. Yet, the possibility of enhancing these activity parameters by lowering the catalyst concentration for the sake of outperforming earlier protocols, unfortunately, renders this process ambivalent in case reproducibility is not carefully evaluated. Moreover, protocols relying on these low catalyst concentrations are most commonly not advanced to larger scales and might therefore prove less applicable in the long run.

In case of the [FeFe] catalyzed CO_2 reduction utilizing visible light, a competing ligand exchange with the constituents of the Cu PS, indicated by the formation novel complexes **151** and **152** resulting from photolytic CO replacement, sophisticated the reaction system. Consequently, the isolated photosensitizer was combined with the starting [FeFe] complex **145** and the novel [FeFe] derivatives, but did not provide sufficient results, indicating that well-defined materials or complexes do not naturally warrant reproducibility. In addition, fluctuations in the light source and the liquid-gas reaction medium for CO_2 conversion further increase the predisposition for challenging reproducibility. Despite these obstacles, statements of single experimental results and their deviance or the number of independently performed reactions remain rather uncommon in the field of photocatalytic CO_2 reduction. Moreover, in a recent survey regarding reproducibility in various scientific fields, 90% out of 1576 participants see a *"slight"* or *"significant crisis of reproducibility"* and more than 80% of those working in the field of chemistry (106 participants) have been unable to reproduce the results obtained by others in the past.[278]

Since reproducibility is an inevitable prerequisite for scientific progress, the outcome of herein presented investigations on photocatalytic CO_2 reduction was utilized to showcase essential

guidelines on how to assess the consistency of such catalytic results. Furthermore, recommendations for the scientific community investigating novel catalysts or methods, especially in the area of photocatalysis for the activation of small molecules, such as water or CO_2, were derived:
1. At least two independent reactions (i.e. not the identical catalyst solution and not on the same date) should ideally be conducted. 2. The total number of these independent reactions should be reported when evaluating a novel catalysis protocol, particularly when single experimental results are reported. 3. Reproducibility at significantly reduced catalyst loadings for the sake of higher TONs should be carefully evaluated and only pursued when repeatable results are obtained under these conditions. Single experimental results should ideally be stated as a verification of consistent outcomes in this case. Finally, reactions at two different catalyst concentrations should ideally be conducted to validate reproducibility.
Higher reproducibility for novel catalytic protocols, such as the photocatalytic reduction of CO_2, will hopefully be accomplished by adapting these simple standards. Increased reproducibility will alleviate the process of establishing benchmark reactions for a better comparison between catalytic systems which will ultimately benefit future development in cutting-edge research areas, such as water splitting or CO_2 reduction.

2.2 Investigations on CO_2 Reductive Coupling to Oxalate

Over the past decades, significant improvements in the direct conversion of CO_2 into $C_{\geq 2}$ compounds with the help of (transition) metal catalysts have been achieved and understanding of the underlying reaction mechanisms, specifically evaluated for the stoichiometric formation of C_2 compounds, such as oxalate, has been enhanced (see section 1.3). In an attempt to mimic nature's ability to construct complex organic molecules from CO_2 and the possibility of direct production of fuels containing more than one C atom, the formation of higher carbon compounds *via* CO_2 reduction holds tremendous potential for future applications,[48,169] provided that industrially viable protocols will be developed. This certainly requires the identification and construction of suitable catalysts that enable C-C bond formation from CO_2 in high selectivity and under mild conditions. To achieve these goals, a fundamental understanding of the guiding reactivity patterns and possibilities for tuning the selectivity of the CO_2 reduction into higher carbon compounds will arguably be inevitable. Since C-C bond formation is the key step in the CO_2 to $C_{\geq 2}$ reduction, further investigations on this particular reaction are relevant for optimizing the overall reactivity.

The plainest C-C bond forming step starting from CO_2 represents its reductive coupling to the two-electron reduction product oxalate (or oxalic acid).[192,195] Thus, CO_2 reductive coupling constitutes an ideal transformation to gain expedient insight into the C-C bond formation. Furthermore, dimethyl oxalate is a product of industrial interest as it can be converted into ethylene glycol or methyl glycolate.[169,190,279–281] Despite the identification of catalysts enabling the formation of $CO_2^{\bullet-}$ or analogous intermediates and allowing for its reductive coupling to oxalate in high selectivity,[100,170,175,190,193] novel reactivities, such as dimetalloxycarbenes that undergo nucleophilic attack onto another CO_2 molecule,[172,179,184] have been identified as important intermediates in the reductive coupling of carbon dioxide.[166,181,183,191,195,282] Furthermore, the influence of electronic and steric properties of ancillary ligands and possible solvent effects have been evaluated as parameters to tune CO_2 reduction toward the desired C-C bond formation.[175–177,179,181–183,188,190,195] However, reactivity patterns, specifically influence of solvents, but even thermodynamics of the reaction, appear to vary significantly from one system to another. While non-coordinating solvents seem to improve CO_2 reductive coupling in certain cases,[179,188] the coordination of solvents during the C-C bond forming process was found to be mandatory for other protocols[175,190]. In addition, oxalate appeared to be the thermodynamically favored CO_2 reduction product in multiple examples,[172,179–181,183,224,282] but was identified as the kinetic product in a recent report[182]. Moreover, the presence of protic solvents or water had to be avoided to achieve oxalate formation in various cases,[47,99,102,167,191,198] but in few cases,[174,193] especially when bicarbonate was identified as the reactive form of CO_2,[192] the presence of protons or water facilitated oxalate formation. Also, oxalate formation was commonly observed under hydrothermal conditions[207,208,210–215,218] and even in the presence of oxidants,[169,193,205,206,216,217,219] such as O_2 from the atmosphere.[220]

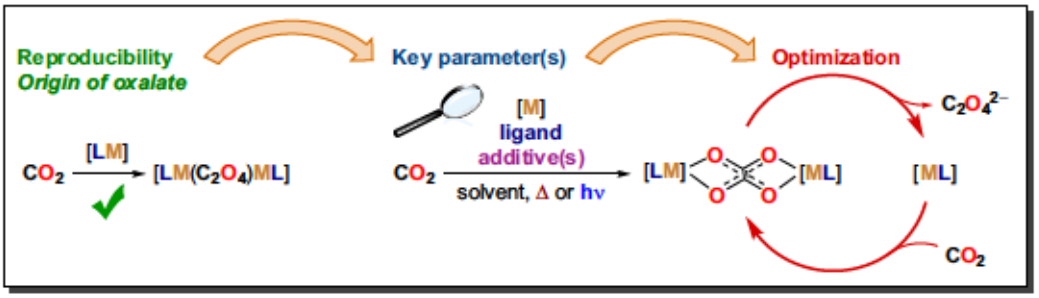

Figure 19: Approach for further improvements in the field of CO_2 reductive coupling followed within this work: After assessing reproducibility and the origin of oxalate, evaluation of key parameters will eventually establish advanced insight into the C-C bond formation and facilitate optimization of this transformation.

All these observations indicate the complexity of the seemingly simple formation of the small oxalate molecule from carbon dioxide. While differences in solvent influence, thermodynamics and sensitivity to reaction conditions might merely be a result of the specificity of each of the reported protocols, a generally applicable design principle for prospective catalysts would substantially ameliorate the foundation for future developments in this field. Hence, the aim of this work is to gain further insights into the formation of oxalate starting from CO_2 in combination with environmentally benign first-row transition metal Fe and Cu complexes. To achieve this goal, initial investigations based on complexes previously reported for the CO_2 reductive coupling should be undertaken. This strategy rests upon the fact that, in contrast to the plethora of CO_2 reduction protocols yielding C_1 products, such as CO, HCO_2H, and MeOH (see section 1.2), the selective formation of oxalate with the help of first-row transition metals is rather rare.[179,181,182,187,190,192,195] Moreover, the reproducibility of reported CO_2 reductive coupling systems proved challenging,[227] while the pathway for the formation of oxalate turned out to be oxidative degradation rather than initially presumed reductive coupling in a recent study.[220] However, knowledge on the true nature of the formed oxalate is of indisputable importance when pursuing optimization of the desired CO_2 reductive coupling and reproducibility of the literature precedent an outright necessity for benchmarking any novel protocol. Hence, an initial reproducibility assessment for the literature examples of interest should be performed and the true origin of oxalate formation being CO_2 reductive coupling should be established (Figure 19). Following these prerequisite trials, further modifications of the electronic and steric properties of ancillary ligands and the derived complexes should be conducted. Moreover, alterations of general reaction conditions should be evaluated and the key parameters impacting the outcome of the CO_2 reductive coupling reactions should be elucidated. By following this strategy, the major challenges associated with this transformation should presumably become evident. Furthermore, guiding principles for studying CO_2 reductive coupling and analyzing the true origin of the observed products should be derived and will hopefully contribute to prospective improvements in this cutting-edge research area.

2.2.1 Investigations on CO_2 Reductive Coupling with Disulfide-derived Cu Complexes

The Cu-based catalyst ligated by a bis(pyridyl)amine disulfide reported by Bouwman and coworkers is one of the important examples reported for the conversion of CO_2 into oxalate.[169] The electrocatalytic reaction, proceeding *via* a tetranuclear oxalate complex (Scheme 47), was conducted at an exceptionally mild potential of –0.03 V *vs.* NHE indicating outstanding catalytic properties of the Cu complex considering the –1.90 V (–1.97 V in DMF)[47,52,81] required in the absence of a catalyst.[169]

The mechanism of this CO_2 reductive coupling has recently been investigated with the help of computational methods.[282] The results of these DFT calculations suggest reduction of one CO_2 molecule by two Cu centers to form a $Cu_2(CO_2^{\bullet-})$ intermediate in which the radical character of the intermediate is delocalized between metal centers and the CO_2, a feature enabled by a small singlet-triplet gap (2.1 kcal/mol) of the Cu^I_2-CO_2 precursor intermediate (Scheme 52).[282] A second reduction and attack of the resulting nucleophilic CO_2 onto another CO_2 yields the observed oxalate-bridged complex.[282] The capability of the catalyst to switch between open- and closed-shell was found crucial, as the Cu^I catalyst was calculated in a closed-shell structure, while the C-C bond formation occurred *via* open-shell transition states resulting finally in open-shell products.[282] Furthermore, two Cu complexes were required and the formation of oxalate by a single dinuclear complex or with a single Cu center was energetically unfavorable.[282] Finally, comparison to a reductive disproportionation pathway was performed and found to be thermodynamically unfeasible while oxalate formation was even kinetically preferred.[282] Interestingly, the cationic charge of the Cu catalyst appeared crucial for the observed oxalate formation as π-backdonation could stabilize a potential CO complex intermediate during the reductive disproportionation pathway.[282] Furthermore, energy barriers for both competing reactions were found to decrease with increasing electron density on the complex rendering the reductive disproportionation the preferred pathway for electron-rich complexes.[282] Similar observations were made for metals with increased singlet/triplet energy barriers, such as the Ag/Au analogues of the catalyst, rendering CO_2 reductive coupling unfavorable.[282] Surprisingly, despite the mechanistic insight and the encouraging catalytic properties of the

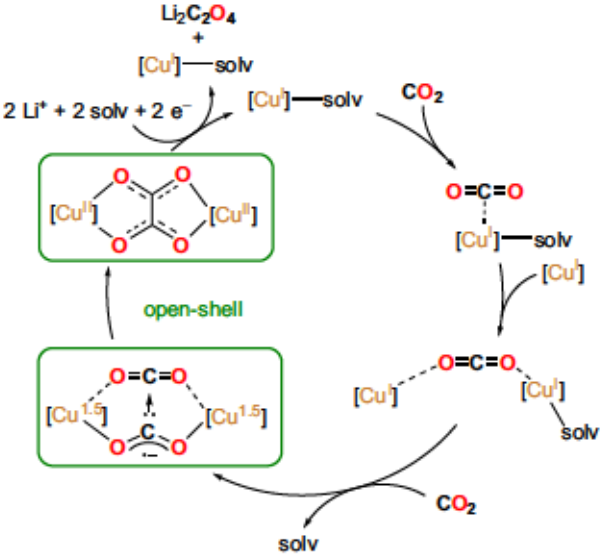

Scheme 52: Calculated schematic mechanism for the formation of the Cu oxalate *via* reductive activation of CO_2 (open-shell species are marked by green boxes).[282]

reported system with its striking overpotential of –0.03 V *vs.* NHE,[169] no further improvements of the initial system have been reported. Moreover, analogous disulfide ligands bearing different backbones and substituents and their derived Cu complexes have been reported and the essential reactivities resulting in the formation of the Cu^{I} disulfide complexes have been investigated.[227,283] Yet, no analogous system facilitating the CO_2 reductive coupling has, to the best of our knowledge, been described. However, Stack and co-workers reported reproducibility problems as part of a study revealing the interconversion possibilities between the Cu^{I} disulfide originally described by the Bouwman group[169] and a thiolate-bridged Cu^{II} complex (Scheme 53).[227] In addition, Thomas *et al.* declare that formation of oxalate was not observed despite elaborate attempts.[227] These difficulties with respect to the reproducibility of oxalate formation and the absence of any follow-up work on this protocol for CO_2 reductive coupling prompted evaluation of the system to clarify whether the originally reported oxalate formation would be reproducible in another laboratory. In addition, identification of starting points for further modifications of the system that could enable even higher catalytic activity would be highly desirable.

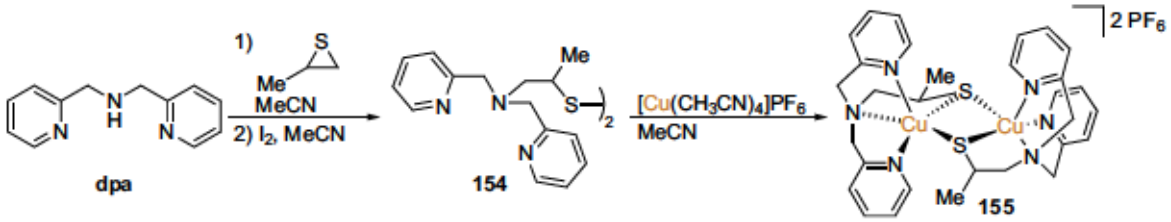

Scheme 53: Synthesis of the required disulfide ligand **154** by addition and oxidation followed by reaction with $[Cu(MeCN)_4]PF_6$ yielding Cu^{II} complex **155**.[227]

Investigations were initiated by preparation of the required ligand, as reported in the initial publications,[169,227] *via* reaction of nucleophilic dipicolylamine with propylene sulfide and subsequent oxidation to the disulfide (Scheme 53). Aerial oxidation, as reported by Bouwman and co-workers,[169] proved to be challenging and stirring the reaction mixture obtained after heating propylene sulfide and dipicolylamine in dry acetonitrile (13 h) in air (18 h) did not provide the desired disulfide (Figure S 96). Hence, the synthesis reported by Stack and co-workers[227] was followed and oxidation with I_2 after nucleophilic addition to the thiirane enabled isolation of the ligand as a mixture of isomers, as previously described.[227] With the ligand in hand, complex formation with $[Cu(MeCN)_4]PF_6$ was conducted, as significantly different reactivities were described in the literature.[169,227] While in the initial report by Angamuthu *et al.* a yellow solution of the corresponding Cu^{I} complex was obtained upon addition of $[Cu(MeCN)_4]BF_4$ to a solution of the disulfide ligand in acetonitrile,[169] Stack and co-workers observed partial oxidation of the Cu precursor to form the bis-thiolate Cu^{II} complex accompanied by a distinct color change to dark green.[227] The resulting Cu^{II} bis-thiolate was reported to exist in an equilibrium with the corresponding Cu^{I} disulfide, with strongly coordinating solvents stabilizing the Cu^{I} form.[227] Hence, the reaction of $[Cu(MeCN)_4]PF_6$ with the respective ligand in MeCN under argon was performed. This resulted in an instant

color change from yellow/orange for the disulfide ligand in acetonitrile, to dark green (see Figure S 2). It is noteworthy that, even though the PF_6^- instead of the BF_4^- salt was utilized, the Stack group described no significant influence of the counterion on the formation of the dithiolate, assessed by evaluation five different anions.[227] In addition to the distinct color change, the ^{1}H NMR spectra of the resulting product was recorded (Figure 20). As evident from the range of chemical shifts up to 37 ppm, the product obtained is partially paramagnetic, indicating the presence of a Cu^{II} species. Moreover, the chemical shifts are in accordance with those reported by Stack and co-workers.[227] Interestingly, evaporation of a dark green acetonitrile solution of **154** and $[Cu(MeCN)_4]PF_6$ in air over 5 days yielded a green solid, which displayed IR bands at 1656 cm^{-1} and 1612 cm^{-1} (Figure S 246), close to those observed for the initially reported oxalate complex (1611 cm^{-1}).[169] The ^{1}H NMR spectrum of this green solid suggested the presence of paramagnetic Cu^{II} species other than **155** (Figure S 98). Extraction of the product with aqueous NaOH solution[193] and subsequent NMR spectroscopic analysis indicated the presence of formate, which might potentially form *via* CO_2 reduction. However, no signal hinted at the presence of oxalate.

Due to at least partial oxidation of the Cu metal centers by the ligand, further reaction with CO_2 would require oxidation of the bridging thiolate. Interestingly, protonation of the ligand was reported to quantitatively convert the Cu^{II} complex back into a dinuclear Cu^{I} complex.[227] This reaction is accompanied by oxidation of the ligand to form the disulfide and protonation of one of the pyridine moieties (Scheme 54).[227] Following these results reported by Stack and co-workers, protonation of the complex **155** with HOTf in acetonitrile was conducted, resulting in a distinct color change from dark green to light orange/yellow indicating the formation of the desired Cu^{I} species.[227]

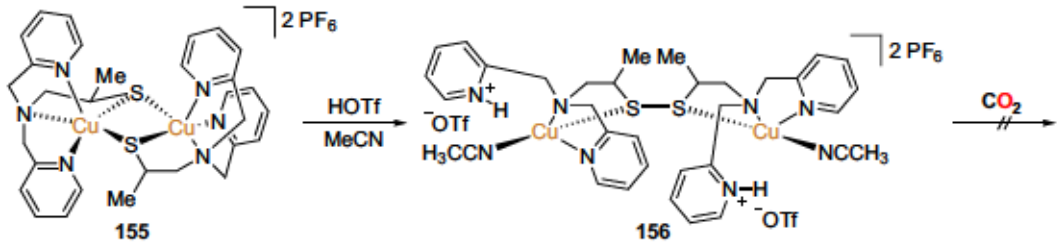

Scheme 54: Protonation of **155** with HOTf to form the Cu^{I} complex **156**, as reported by Stack and co-workers,[227] and subsequent attempted reaction with CO_2.

Due to the copper(I) nature of this complex and the original isolation of the oxalate complex starting from the thiol ligand, $Cu(acac)_2$, and HBF_4,[169] protonation of the ligand to stabilize the active Cu^{I} complex might be a prerequisite for its follow-up reaction with CO_2. Hence, *in situ* formed complex **156** was treated with CO_2 by bubbling, but no change in color over the course of 10 min was observed. Furthermore, the ^{1}H NMR spectrum after this CO_2 treatment displayed no evidence for any reaction with CO_2 and was thus in accordance with that previously reported for complex **156**[227] (Figure 20).

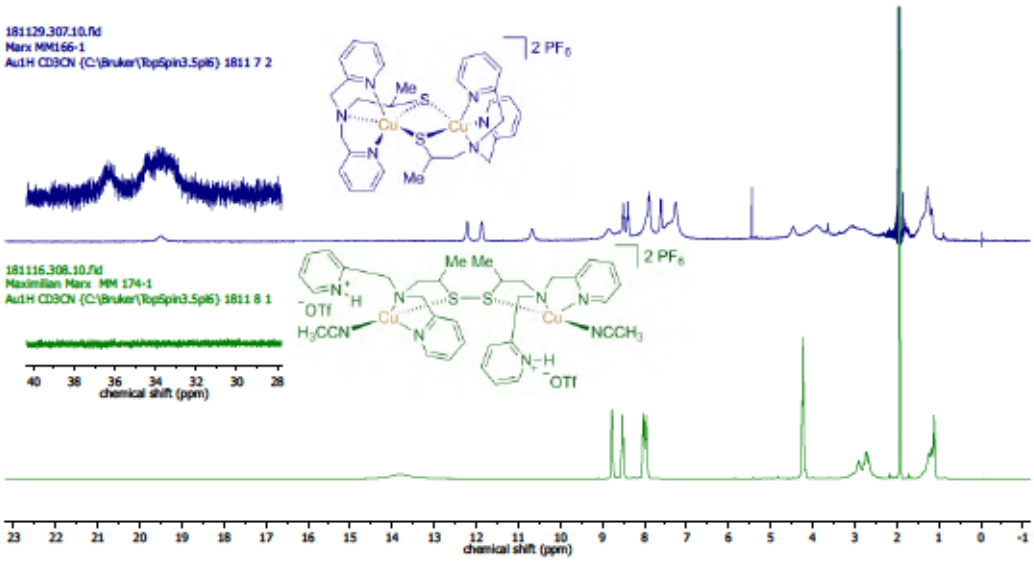

Figure 20: ^{1}H NMR spectra (300 MHz, CD_3CN) of the dark green product obtained by reaction of ligand **154** with $[Cu(MeCN)_4]PF_6$ indicating the formation of Cu^{II} complex **155**[227] (blue) and after protonation and subsequent CO_2 treatment yielding **156**[227] (green).

These experimental results are in good agreement with those reported by Stack and co-workers.[227] Therefore, the described oxalate formation by reaction with CO_2 from the atmosphere cannot be rationalized. This initial evaluation of a literature protocol for CO_2 reductive coupling clearly showcases the importance of assessing reproducibility prior to further modifications of these literature systems, as failed attempts to improve the desired CO_2 reductive coupling reactivity could readily be misleading when the original reaction is not proceeding as described.

2.2.2 Investigating CO_2 Reductive Coupling Facilitated by a Macrocyclic Fe Complex

After the initial study on the reductive coupling protocol reported by Bouwman and co-workers,[169] the [Fe(tmtaa)] complex reported by the Floriani group was envisaged as a promising candidate for an active CO_2 reductive coupling catalyst.[188] This air-sensitive[284] Fe^{II} complex was reported to react with sodium in THF to form an iron(I) complex in which the resulting Na^+ ion is coordinated to the bisketiminate-type moiety of the tmtaa ligand (Scheme 42).[188] Here, utilization of a strong reductant (ca. –3 V *vs.* Fc/Fc^+ for Na in THF[285]) seemed more reasonable for facilitating formation of oxalate from CO_2. A solvent dependence for the consecutive CO_2 treatment was reported with reductive disproportionation being observed in THF while oxalate formation was observed in toluene.[188] However, no further investigations on the mechanism of the reaction were reported and sodium oxalate was only identified by titration with $KMnO_4$.[188] Consequently, collecting additional evidence for the formation of oxalate and gaining further experimental data on the reaction to ideally modify the system to allow for an improved reaction, ideally employing a less strong reductant, was captivating.
Hence, the free H_2tmtaa ligand was prepared following a combination of modified literature procedures (Scheme 55).[286,287] Notably, the synthesis presented herein does not require pressurized HCl gas and formation of gaseous HCl by treatment of dried NaCl with concentrated H_2SO_4 was sufficient for the removal of Ni.[VI] The desired complex was then prepared following the procedure utilized by the Floriani group,[188] which was slightly modified to avoid overnight stirring at –20 °C.

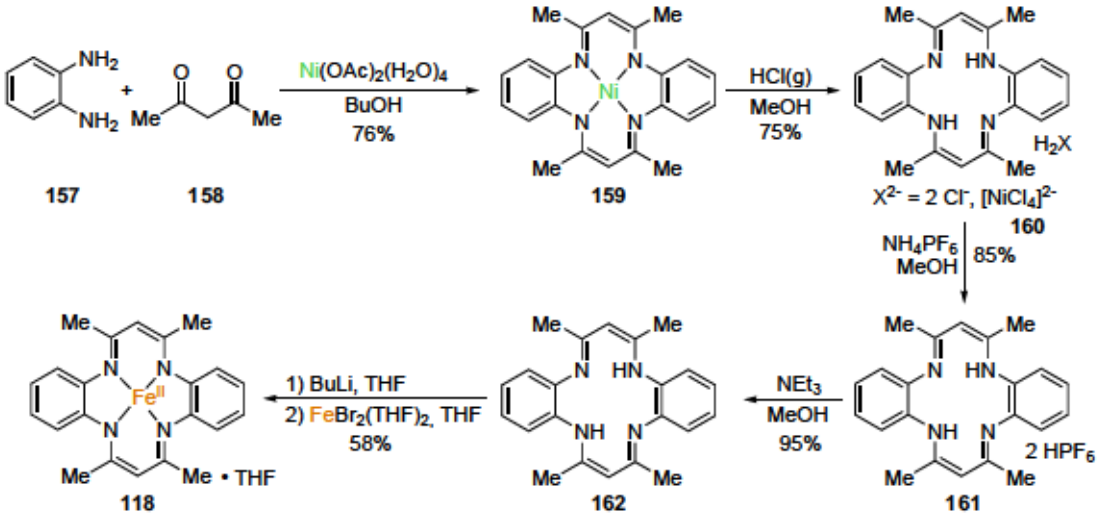

Scheme 55: Synthesis of [Fe(tmtaa)]·THF *via* a combination of different literature procedures.[188,286,287]

With the complex in hand, investigations were focused on the CO_2 reduction reaction. For this purpose, [Fe(tmtaa)] was reacted with Na analogously to the initial report[188] and the

VI Hochloch *et al.* likewise reported that HCl generated from concentrated H_2SO_4 and aqueous HCl can be utilized, albeit a 25% drop in yield was observed.[287] As described in the literature,[287] subsequent anion exchange was required for further application of the resulting H_2tmtaa salt.

resulting black/dark brown residue was subsequently treated with CO_2 by bubbling it through the toluene solution at −30 °C (Scheme 56; detailed results are given in Table S 12).

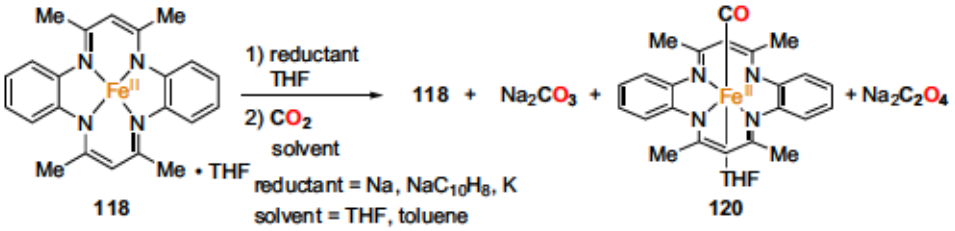

Scheme 56: CO_2 reduction with [Fe(tmtaa)] *via* reduction with Na, $NaC_{10}H_8$, or K and subsequent CO_2 treatment.

However, extraction of the remaining solid obtained by removal of all volatiles *in vacuo* with water and further analysis by NMR spectroscopy (Figure 21) and capillary electrophoresis (Figure S 338) indicated the absence of oxalate.

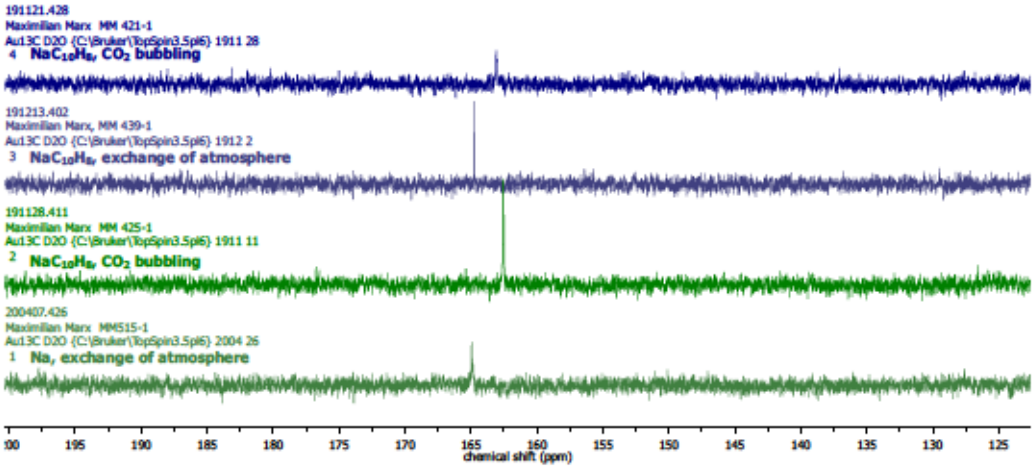

Figure 21: $^{13}C\{^1H\}$ NMR spectra (D_2O) of the aqueous extract after CO_2 treatment of [Fe(tmtaa)(THF)] reacted with Na or $NaC_{10}H_8$, respectively.

In contrast, a peak at 162.5 ppm in the ^{13}C NMR, which apparently showed minor variations in its chemical shift when compared to similar experiments, was observed. Basification of one sample with aqueous NaOH resulted in its shift to 168 ppm indicating a pH dependency of the signal and ultimately coinciding with that of CO_3^{2-} in basic solution (see Table S 12). As treatment with CO_2 *via* bubbling utilizing a needle reaching into the reaction mixture is potentially prone to the undesired introduction of traces of air, replacement of the Ar atmosphere by CO_2 after removal of the volatiles *in vacuo* and prior to addition of the solvent utilized for the reaction was conducted. The outcome of the reaction, however, remained unaltered. Due to the poor solubility of alkali metals in THF or toluene, a reductant soluble in organic solvents was envisaged to potentially improve the formation of the reactive Fe^I species. Hence, treatment of the purple [Fe(tmtaa)] with $NaC_{10}H_8$ was conducted and resulted in a color change to dark brown/black. Subsequent treatment with CO_2 resulted in the

formation of a dark purple solution/suspension. The color change to purple/violet upon treatment with CO_2 in toluene indicating the formation of [Fe(tmtaa)] was already observed by the Floriani group, while a red color for the analogous reaction in THF indicated formation of the CO complex **120**.[188] However, subsequent extraction of the $NaC_{10}H_8$ reaction product into water once again indicated the formation of carbonate by NMR spectroscopic analysis, whereas no evidence for the formation of oxalate was obtained (Figure 21 and Table S 12). Recently, a cation influence on the formation of oxalate based on a similar complex in which the alkali metal ion is coordinated to the bisketiminate-type ligand of the reduced complex (Scheme 49) was reported and potassium ions enhanced the catalytic properties of the system for CO_2 reduction.[195] Hence, replacement of Na by the more reactive K might enable not only faster reduction of the Fe^{II} complex, but could perhaps facilitate the desired formation of $K_2C_2O_4$. Thus, [Fe(tmtaa)] was treated with K in THF, resulting in a black solid after removal of the volatiles *in vacuo*. Subsequent treatment with CO_2 in dry toluene at –30 °C (to r.t.) gave rise to a red/purple suspension. Interestingly, analysis of the product obtained by removal of the volatiles after continuous stirring under CO_2 for 3 days indicated the formation of the CO complex [Fe(tmtaa)(CO)(X)] identified by the distinct C-O vibration at 1912 cm^{-1} (Figu

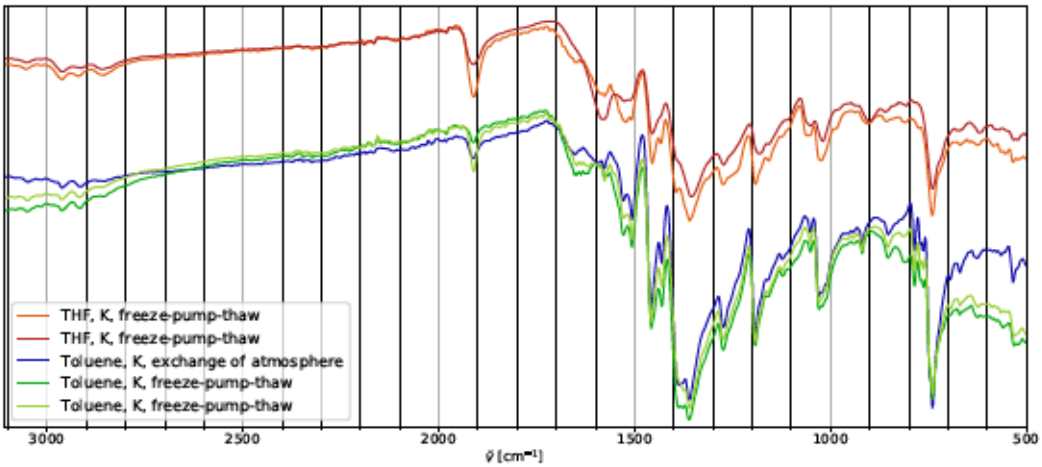

Figure 22: FTIR spectra obtained after reduction of [Fe(tmtaa)] with K in THF followed by CO_2 treatment in THF or toluene (as indicated) *via* freeze-pump-thaw exchange of the atmosphere or by replacement of the atmosphere after reduction and removal of the THF *in vacuo*.

The formation of CO following the reductive disproportionation pathway obviously requires the concomitant formation of carbonate and indeed a signal at 163.1 ppm in the ^{13}C NMR spectrum (Figure 23) was observed after extraction of the product with H_2O.[VII] To ensure no possibly undesirable reaction of the solid Fe complex with CO_2, thereby prohibiting the reported impact of the solvent on the reaction outcome, and circumvent the introduction of CO_2 gas by bubbling, a freeze-pump-thaw procedure recently described for CO_2 reductive

[VII] Note that the pH of the NMR sample for one reaction with K in toluene and THF, respectively, was adjusted with 1 M NaOH solution, resulting in a shift of the ^{13}C signal to 168 ppm, verifying that these signals indeed correspond to carbonate.

coupling[195] was adapted. Applying this procedure, similar results with the iron carbonyl complex identified by IR spectroscopy and carbonate identified by NMR spectroscopy after aqueous work-up were obtained. All reactions with K as the reductant conducted in toluene were moreover analyzed by capillary electrophoresis after extraction with water. However, neither of the samples contained detectable amounts of oxalate (Figure 24), thus the formation of oxalate in quantities corresponding to more than 0.1% yield based on the Fe complex can be precluded. Since formation of the Fe carbonyl complex was observed for reactions in toluene, analysis of the gaseous headspace of the reaction to possibly identify significant quantities of CO was conducted. However, gas chromatographic analysis identified no detectable amounts of CO_2 reduction products, namely CO and CH_4. This indicates that complexation of the formed CO seems to proceed nearly quantitatively, provided that no follow-up reaction of the formed CO occurs.

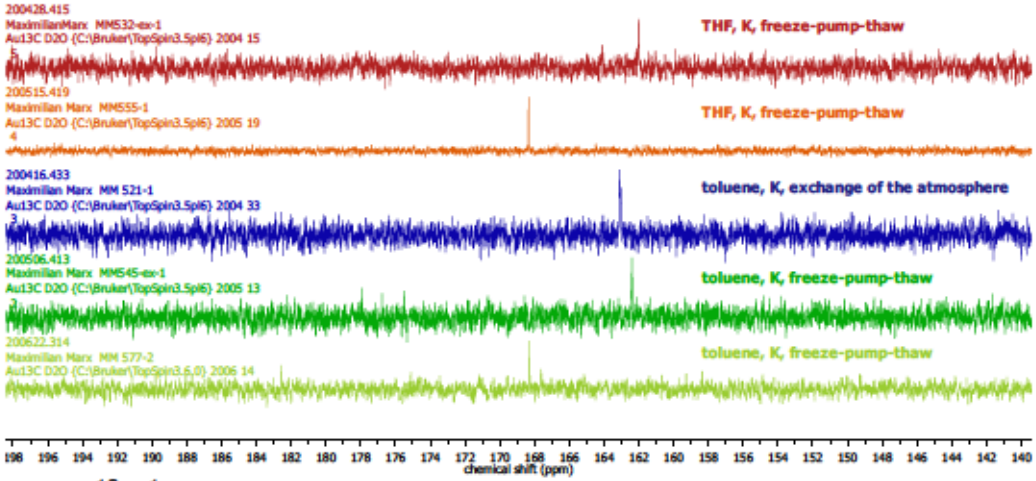

Figure 23: $^{13}C\{^1H\}$ NMR spectra (D_2O) of the aqueous extract after [Fe(tmtaa)] was treated with K followed by CO.

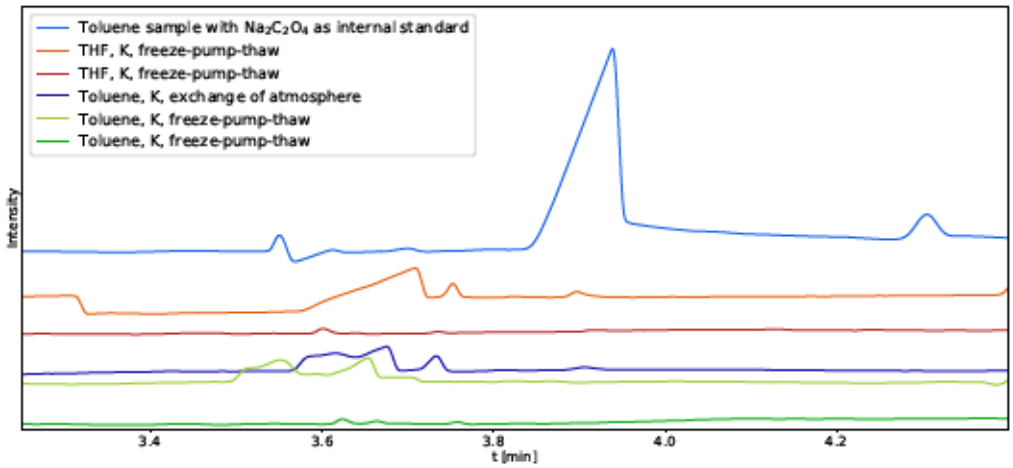

Figure 24: Capillary electropherograms of the aqueous extract after **118** was treated with K followed by CO_2.

Due to the significant solvent effect initially described by Floriani and co-workers,[188] the

reaction in THF was investigated next, to see if a different reactivity depending on the utilized solvent could be identified. Exchanging the atmosphere from argon to CO_2 applying the freeze-pump-thaw procedure resulted in a color change from dark brown to dark red, as reported[188]. IR spectroscopic analysis after overnight reaction with CO_2 clearly indicated the formation of the expected CO complex (Figure 22). The CO band appeared to be more intense when the reaction was conducted in THF instead of toluene, which might indeed indicate a higher percentage of CO_2 reduction to CO. Again, NMR spectroscopic analysis of the aqueous extract proved the accompanying formation of CO_3^{2-} while capillary electrophoresis (Figure 23 and 24) found no evidence for the formation of oxalate (i.e. <0.1% based on [Fe][VIII]). To identify the major products in solution after reduction with potassium and subsequent CO_2 treatment, the obtained solid product was analyzed by NMR spectroscopy in pyridine-d_5. For the reaction in toluene, the major signals correspond to those of the starting [Fe(tmtaa)] (Figure 25). Despite the absence of detectable quantities of oxalate, this is well in accordance with the initial literature report.[188] In contrast, the spectrum obtained for the THF reaction product appeared significantly broadened, arguably due to the presence of a paramagnetic Fe species, and signals at –13 and –22 ppm further corroborate this observation. The major signals, albeit being significantly broadened, are nevertheless located at the chemical shift of the starting material [Fe(tmtaa)]. The derived carbonyl complex [Fe(tmtaa)(CO)(THF)] was reported to feature similar ^{1}H NMR signals to [Fe(tmtaa)] with the major difference being the shift of the two CH protons on the bisketiminate bridge which are located at 3.48 ppm for [Fe(tmtaa)] and shifted downfield to 4.14 ppm for **120**.[188] While no signal in the 4-5 ppm range was observed for the THF reaction product, possibly indicating the presence of [Fe(tmtaa)] as the main species similar to the reaction in toluene, the paramagnetic broadening prohibits a conclusive statement based exclusively on the NMR spectroscopic analysis.

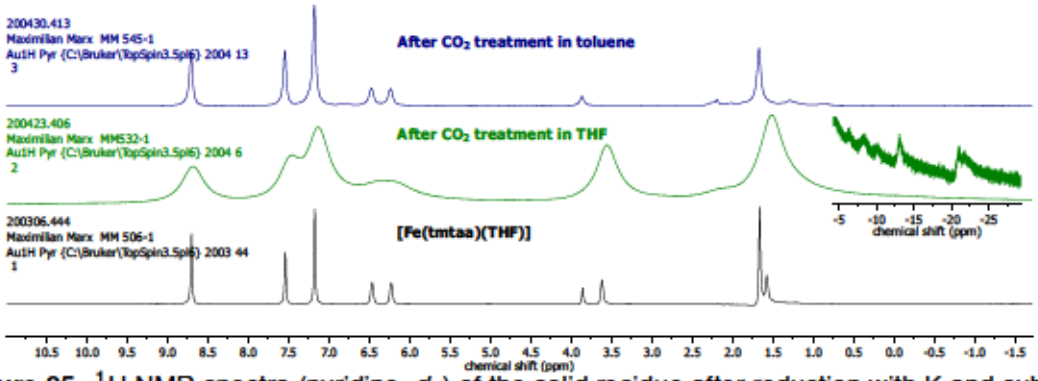

Figure 25: ^{1}H NMR spectra (pyridine–d_5) of the solid residue after reduction with K and subsequent CO_2 treatment in either toluene or THF and the spectrum of [Fe(tmtaa)] for comparison.

Utilizing [Fe(tmtaa)] and different alkali metal reductants, the described CO_2 reduction to CO and carbonate *via* reductive disproportionation was confirmed as presented herein. Interestingly, while CO_2 reduction to CO might potentially give rise to higher yields in THF, likewise

[VIII] Due to different sample dilution, the detection limit is <0.5% in one case (see Table S 12).

reactivity was observed in toluene, contrasting previously reported results[188]. Furthermore, the presence of [Fe(tmtaa)] after reaction with K and subsequent treatment with CO_2 was identified. As the conversion to the carbonyl complex remained incomplete in toluene and THF, the latter result being in accordance with the literature,[188] there are two major remaining possibilities for the presence of [Fe(tmtaa)]. The first possibility would be another reduction reaction yielding either a CO_2 reduction product, which appears unlikely, as the reaction with alkali metals should effectively enable aprotic conditions by removal of trace water in the supposedly dry solvents, and both CO_2 reduction products that could be formed under aprotic conditions, namely CO and oxalate, were sought after with the help of various analytical methods. It is noteworthy that traces of H_2 were detected by GC analysis of the headspace of a CO_2 treatment in toluene after reduction with K. Arguably, the observed H_2 results from proton reduction of water traces in the solvent, despite it being continuously stored under Ar over activated molecular sieves. However, it cannot be stated whether the proton reduction is a result of the reaction of H_2O with K or the Fe^I complex. In addition, no evidence for another CO_2 reduction product was obtained in either reaction. Assuming that there is no competing reduction reaction occurring, the incomplete conversion of [Fe(tmtaa)] into the active Fe^I complex seems to be a plausible explanation for the experimental results. This might originate from the poor solubility of Na or K and their comparatively small surface area. Nonetheless, reduction with soluble sodium naphthalenide was attempted and likewise remained unsuccessful in achieving observable conversion of CO_2 into oxalate. Therefore, it can be concluded that no formation of oxalate from CO_2 utilizing [Fe(tmtaa)] in combination with strong reductants was observed, but partial conversion of CO_2 into CO regardless of the utilized solvent was confirmed. These results substantially differ from those reported in the literature.[188] The Floriani group reported identification of oxalate after extraction with H_2O and filtration with activated charcoal by titration of the slightly brown sample solution with $KMnO_4$.[188] While oxalate is indeed utilized for standardizing $KMnO_4$ solutions,[288] it is certainly capable of oxidizing potential impurities such as Fe^{2+} [289] or various organic compounds, containing C=C bonds, and even toluene resulting in benzoic acid.[290] In fact, organic compounds in the aqueous extract after the CO_2 treatment were observed by ^1H NMR spectroscopy. While no additional filtration with activated charcoal was performed, the presence of oxidizable impurities in the aqueous extract is a plausible explanation for a false positive oxalate identification by $KMnO_4$. Thus, the findings presented herein suggest that the previous report might have resulted from a false positive identification of oxalate by redox titration with $KMnO_4$. Again, this outcome highlights the importance of in-depth investigations by multiple analytical methods for a consistent elucidation of the formed products when studying CO_2 reductive coupling. Moreover, the results showcase that even strong reducing agents, such as alkaline metals,[285] do not warrant the formation of oxalate.

2.2.3 1,4,7-Triazacyclononane-derived Cu Complexes in the Reductive CO_2 Coupling

Molecular conversion of CO_2 into oxalate described by Peacock and co-workers utilizes a Cu complex ligated by 1,4,7-allyl-1,4,7-triazacyclononane in the presence of $NaBPh_4$ (Scheme 45).[192] The reduction of CO_2 starting from the Cu^I complex solely relies on concomitant oxidation of the metal center to Cu^{II} resulting in the formation of the oxalate-bridged Cu^{II} dimer.[192] The intriguing feature of this system for CO_2 reductive coupling is the capability of producing this oxalato dimer **128** without the apparent requirement of additional reductant and *via* reaction with either CO_2, even from exhaled air, or $CsHCO_3$.[192] However, the mechanism of this specific CO_2 reductive coupling protocol has not yet been investigated, to the best of our knowledge. Interestingly, despite the multitude of 1,4,7-triazacyclononane derivatives and their corresponding Cu complexes reported in the literature,[226,291–322] the ligand utilized by the Peacock group[192] appears to be unique in facilitating CO_2 reductive coupling. One possible explanation for this distinct reactivity is the effective shielding of the Cu centers imposed by the allyl substituents prohibiting coordination of another ligand.[192] Nevertheless, enhancement of the oxalate yield by ligand modification, pre-formation of dinuclear complexes or the transfer of the protocol to related nitrogen-based tridentate cyclic or acyclic ligands has not been accomplished. This inspired investigations to gain further insight into the underlying mechanism of the transformation, evaluate the possible electronic and steric influences of ligand congeners, and possibly even enable a stepwise catalytic approach by removal of oxalate from the dinuclear Cu complex and reduction back to Cu^I. However, due to previous experience regarding literature-known CO_2 reductive coupling protocols, confirmation of the reproducibility of this report was considered a mandatory requirement. Therefore, evaluation of the oxalate formation, further alterations of reaction conditions, modifications of the employed ligand, and possibly reduction of the oxidized complex to close the stepwise CO_2 reductive coupling cycle are the main objectives of this section.

For preparation of the required 1,4,7-triazacyclononane (1,4,7-tacn) derivative, tosylation of ethylene glycol and bis(2-aminoethyl)amine (dien) was conducted following literature procedures (Scheme 57).[323] Subsequent cyclization *via* condensation of the diamide, obtained by reaction with sodium ethoxide, with the tosylated diol (**164**)[324] and deprotection of the tosyl groups with concentrated sulfuric acid at elevated temperature gave the tris(hydrochloride) salt of 1,4,7-tacn (**167**) upon precipitation with HCl.[325] Deprotonation of the tris(hydrochloride) with KOH and subsequent allylation with allyl bromide in toluene gave the desired ligand **127** in decent yield.[326]

With the ligand in hand, isolation and characterization of the derived Cu^I complex was attempted, as no structural or general analytical data was available in the literature, to the best of our knowledge. Following the procedure utilized by Peacock for synthesizing solutions of [Cu(**127**)X] (X = BPh_4, I),[192] **127**, $NaBPh_4$, and CuI were mixed in deoxygenated MeOH. Extraction of the off-white solid residue obtained after removal of the volatiles *in vacuo* with THF yielded [Cu(**127**)X] (X = BPh_4, I) as indicated by NMR spectroscopic analysis.

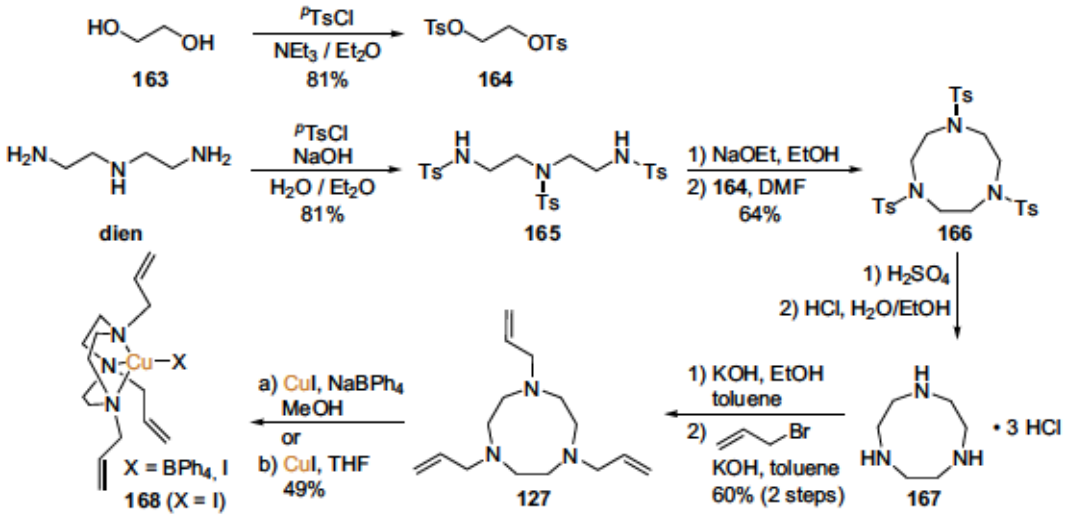

Scheme 57: Synthesis of ligand **127** utilized by Peacock and co-workers following a combination of literature procedures[323–326] and subsequent formation of the derived Cu^{I} complex **168**.

Crystals suitable for X-ray crystallographic analysis were obtained by slow diffusion of hexane into a THF solution of this mixture, albeit crystals with identical unit cell were likewise obtained from 1,2-dichlorobenzene/hexane at –32 °C.[IX] Interestingly, the crystalline material consisted of the iodo complex **168** (Figure 26) and no crystalline BPh_4^- analogue was observed. Hence, exchange of the iodide by sodium tetraphenylborate remains incomplete when conducted in MeOH. Extensive disorder of the molecular structure precludes a discussion of bond lengths and angles. Nevertheless, the overall coordination geometry displays an almost tetrahedral environment created by the three nitrogen-donors and the iodide. **127** was further characterized by NMR and FTIR spectroscopy in addition to mass spectrometry, albeit only the $[Cu(\mathbf{127})]^+$ fragment was detectable by HR-MS (see Appendix, section 4.7.6).

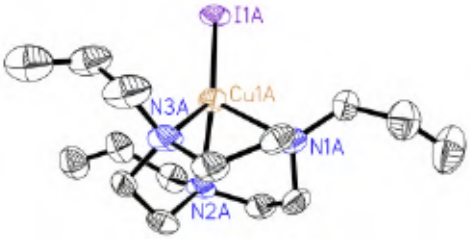

Figure 26: Molecular structure of **168** (thermal ellipsoids are presented at 50% probability level, the minor orientation of the molecule and hydrogen atoms are omitted for clarity).

Reaction of CO_2 with *in situ* formed [Cu(**127**)X] was reported to proceed with a distinct color change from slightly yellow to blue/green and eventually result in the formation of oxalate complex **128** (Scheme 45).[192] Hence, an initial reaction of the *in situ* formed Cu^{I} complex with CO_2 was conducted by bubbling CO_2 through the reaction mixture for 11 h. This experiment, indeed, displayed the expected color change to blue/green, but was accompanied by precipitation of a yellow solid. The remaining solid residue obtained after removal of the solvent featured a vibration at 1628 cm^{-1}, clearly distinct from that reported by Peacock and co-workers (1660 cm^{-1})[192]. Moreover, isolation of the oxalate complex by attempted recrys-

[IX] Crystallization by slow diffusion of hexane into a 1,2-dichlorobenzene solution was conducted with **168** prepared in the absence of $NaBPh_4$.

tallization from $MeNO_2$[192] remained unsuccessful.

A color change from slightly yellow to blue/green during CO_2 bubbling was observed within the first two hours (as reported[192]), thus saturation of the solution with CO_2 over two hours and subsequent stirring of the reaction mixture under an Ar atmosphere presumably containing residual CO_2 to achieve completion of the CO_2 reduction was conducted. Interestingly, despite the initial color change and precipitation of a yellow solid, decolorization back to slightly yellow occurred during overnight stirring without CO_2 bubbling. This observation was unexpected as it suggested the formation of a Cu^{II} compound that converts back into a colorless/slightly yellow Cu^{I} complex once CO_2 bubbling is stopped. One plausible explanation for this observation could be reduction of an initially formed Cu^{II} species by $NaBPh_4$, which has previously been reported to facilitate reduction of a Cu^{II} complex at 20 °C within one day.[327] The role of tetraphenylborate as a potential reductant is also suggested by the absence of decolorization within 19 h when $NaBPh_4$ was replaced by $NaPF_6$ under similar conditions (Table 5, entry 7). However, elucidation of the exact nature of this Cu^{II} species required further investigations.

Consequently, NMR spectroscopic analysis of the yellow precipitate formed during CO_2 bubbling in the presence of $NaBPh_4$ was conducted. The signals in the $^1H/^{13}C$ NMR spectra indicate formation of a complex of the general formula [Cu(**127**)X]. However, signals in both spectra are considerably shifted compared to complex **168** and hence might correspond to a complex in which the iodo ligand has successfully been substituted, e.g. by reaction with sodium tetraphenylborate (Figure S 120). Crystals formed upon slow evaporation of the NMR solution and its contact with air. These were of sufficient quality for single crystal X-ray diffraction, which revealed the formation of μ-hydroxo complex $[(\mathbf{127})Cu(\mu\text{-}OH)_2Cu(\mathbf{127})](BPh_4)_2$[X] (Figure 27). **169** arguably forms in the presence of small quantities of O_2 and water and indicates the possibility of trace oxygen induced oxidation during CO_2 bubbling experiments causing the observed color change. Analogous hydroxo-bridged dinuclear Cu complexes ligated by triazacyclononane-derivatives are well-known in the literature[299,303,305] and commonly formed *via* decomposition of $[(L)Cu(\mu\text{-}O)_2Cu(L)]$ complexes[299] or by aerial oxidation of the $[Cu^{I}(L)I]$ complex[303,305]. In fact, the similar μ-OH complex $[(\mathbf{127})Cu(\mu\text{-}OH)Cu(\mathbf{127})](BPh_4)_2$ was the original product of interest for Peacock and co-workers.[192]

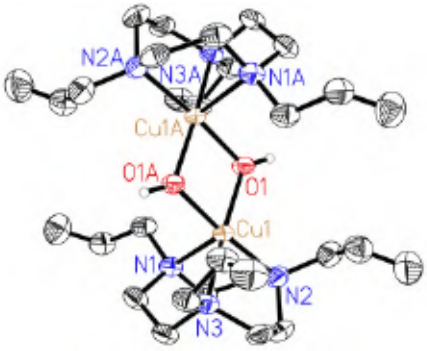

Figure 27: Molecular structure of **169** (thermal ellipsoids are presented at 50% probability level and solvent molecules, the counterion and carbon-bound hydrogen atoms are omitted for clarity).

The color change and subsequent decolorization by CO_2 bubbling followed by stirring un-

[X] Note that due to the distinct blue color indicating a Cu^{2+} compound and the observation of two anions, an analogous aqua-bridged complex can be excluded.

der constant Ar atmosphere turned out to be repeatable for the same reaction mixture and a maximum of six cycles (Figure S 3) was performed with a CuI/ligand/$NaBPh_4$ ratio of 1.7/1.0/1.3.[XI] Formation of the yellow precipitate, which was removed by filtration and analyzed by NMR spectroscopy (Figure S 121), was likewise observed. The recorded spectra displayed only minor differences compared to the NMR spectra of the previously analyzed precipitate, which were attributed to the utilized THF-d_8/D_2O mixture.
In these cases, where *in situ* formed [Cu(**127**)X] was treated with CO_2 by multiple bubbling steps, an IR vibration at ~1630 cm^{-1} was observed for the product (Figure 28), contradicting the reported 1660 cm^{-1} [192]. However, identification of oxalate by ATR-FTIR spectroscopy can be challenging, as multiple C-O vibrations of different species can be found in the area between 1550 and 1700 cm^{-1}. IR spectra of selected compounds, namely $NaHCO_3$, Na_2CO_3, HCO_2Na, $Na_2C_2O_4$, and CuC_2O_4 are presented in Figure 28 and compared to the IR spectra obtained after CO_2 bubbling experiments discussed previously. The close proximity of their C-O vibrations clearly indicates the necessity of employing another analytical meth

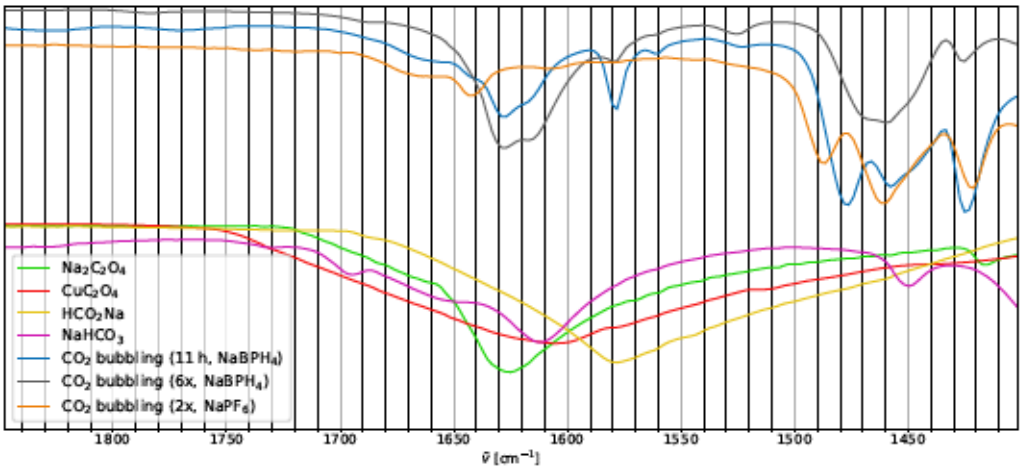

Figure 28: FTIR spectra of $Na_2C_2O_4$, CuC_2O_4, HCO_2Na, $NaHCO_3$, and the crude products obtained after bubbling CO_2 through solutions of CuI, **127** and $NaBPh_4$ or $NaPF_6$ (Table 5, entries 1, 3 and 7) in the 1850-1400 cm^{-1} area.

Thus, independent synthesis of the desired product [(**127**)Cu(μ-C_2O_4)Cu(**127**)]X_2, not only for a more precise comparison of the expected C-O vibration frequency, but also to explore the possibility of $C_2O_4^{2-}$ removal from the complex and its subsequent analysis by spectroscopic and/or separation techniques, such as capillary electrophoresis, was explored.
For this purpose, the dinitrate **170** was synthesized by straightforward reaction of ligand **127** with copper nitrate trihydrate in ethanol (Scheme 58). Reaction of complex **170**, formed *in situ* from copper nitrate trihydrate and ligand **127** in EtOH, with an equimolar amount of sodium

[XI] This ratio was chosen as it corresponds to the masses reported in the experimental part by Farrugia *et al.*, rather than the stated 1/1/1 molar ratio.[192] Exchanging the reported masses for CuI and the ligand results in the correct 1/1/1 ratio, hence reactions were mainly carried out utilizing the logical 1/1/1 stoichiometry (detailed ratios and results are presented in Tables S 13-18).

oxalate yielded the mononuclear oxalato complex **171** in low yield (Scheme 58). Crystals of these complexes were obtained by slow evaporation of an acetone solution (**170**) or from $MeNO_2$ at –32 °C (**171**) and subjected to single crystal X-ray diffraction (Figure 29).

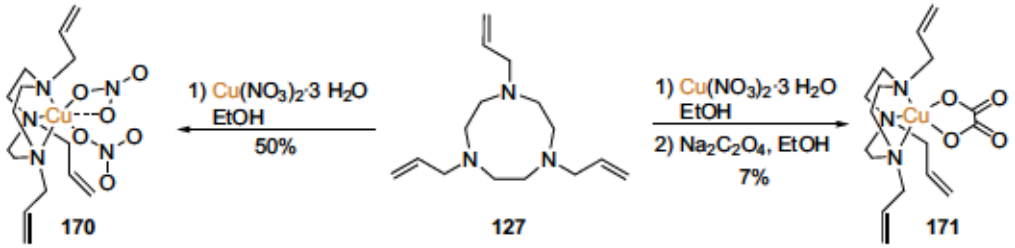

Scheme 58: Synthesis of the Cu complexes **170** and **171** by reaction of **127** with $Cu(NO_3)_2 \cdot 3H_2O$ and $Na_2C_2O_4$.

Cu adopts a square-pyramidal coordination geometry in complex **171** with one nitrogen donor located in the apical position and the oxalate ligand and the remaining nitrogen atoms in the base plane. N-Cu-N angles of 83.77(5)° [84.77(5)°][XII] or 84.87(5)° [84.87(5)°] between apical and basal nitrogen atoms and O-Cu-N^{apical} angles of 100.24(5)° [99.69(5)°] and 105.26(5)° [105.25(5)°] indicate a distortion from the ideal pyramidal structure, arguably caused by the restricted flexibility of the triazacyclononane backbone. In contrast, a 0.07 Å mean deviation from the best plane defined by Cu1, N1, N2, O1, and O2 indicates a nearly planar base. Despite being mononuclear, bond angles and lengths are similar to those reported in dinuclear 1,4,7-triazacyclononane-ligated copper oxalate complexes,[226] further underpinned by Cu-O distances of 1.9446(11) Å [1.9409(11) Å] and 1.9575(11) Å [1.9588(11) Å]. Cu-N distances of 2.0455(12) Å [2.0302(13) Å], 2.0554(12) Å [2.0619(13) Å], and 2.2314(13) Å [2.2273(13) Å], with the longer distance observed between the metal center and the apical nitrogen, add to this picture.

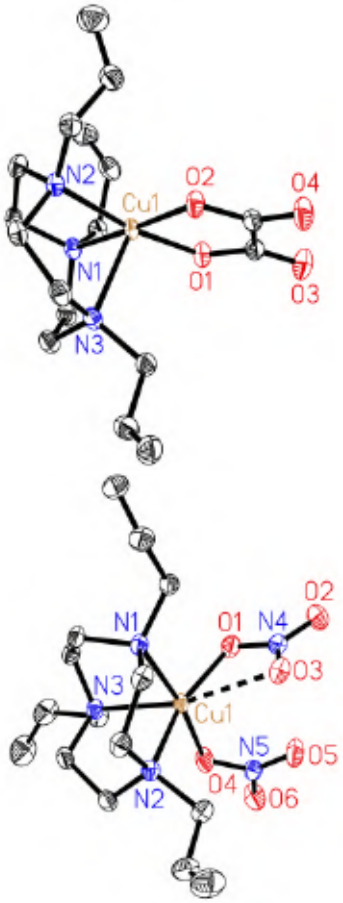

Figure 29: Molecular structures of **170** and **171** (thermal ellipsoids set to 50% probability level, hydrogen atoms, solvent (H_2O) and the second molecule of the asymmetric unit (**171**) are omitted for clarity).

Cu-N (2.0356(11), 2.0774(11), 2.2516(11) Å) and Cu-O (1.9751(10), 2.0201(10) Å) distances in **170** are similar to those observed in **171**, despite the replacement of the oxalate by two nitrate anions. Likewise, N-Cu-N angles of 84.22(4)°, 84.07(4)°, and 86.05(5)° are observed. However, the geometry is significantly disturbed by the interaction between the Cu center and another O atom of one nitrate ligand, displaying a Cu-O distance of

[XII] Values for the second molecule of the asymmetric unit are given in square brackets throughout this work.

2.5424(11) Å, which is significantly longer than both Cu-O bonds, but shorter than the sum of their van der Waals radii[328]. The disturbed geometry manifests e.g. in O-Cu-N^{equatorial} angles of 161.01(4)° and 170.09(4)°, respectively.

The desired binuclear oxalato complex was finally obtained as the tetrafluoroborate salt **172** by reaction of ligand **127** with copper tetrafluoroborate hexahydrate and subsequent treatment with 0.5 equivalents of sodium oxalate in MeOH/H_2O (Scheme 59), resulting in the formation of blue needles of **172**.

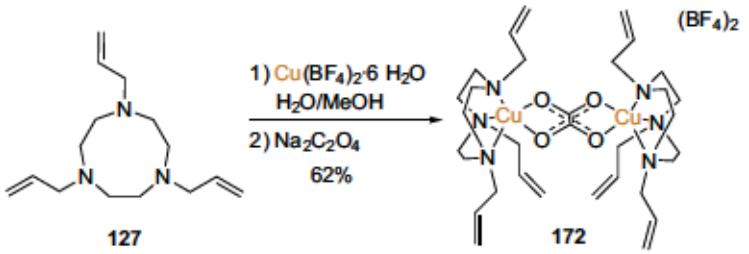

Scheme 59: Preparation of μ-oxalato complex **172** starting from $Na_2C_2O_4$, $Cu(BF_4)_2{\cdot}6H_2O$, and **127** *via* a modified procedure describing the synthesis of similar Cu oxalato complexes[226].

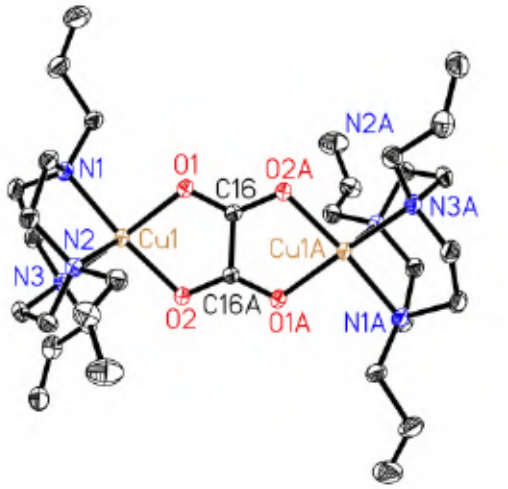

Figure 30: Molecular structure of complex **172** (thermal ellipsoids are presented at 50% probability level, anions and hydrogen atoms are omitted for clarity).

Table 4: Selected bond angles and distances for complex **172** and its congener **128**[192].

	172	**128**[192]
Cu-O [Å]	1.9796(14)	1.982(3)
	1.9902(15)	1.995(3)
Cu-N [Å]	2.0303(17)	2.008(4)
	2.0392(18)	2.016(4)
	2.2193(18)	2.162(5)
N-Cu-N [°]	84.95(7)	85.27(17)
	85.59(7)	87.1(2)
	86.67(7)	87.19(16)
O-Cu-N [°]	92.46(7)	93.71(14)
	95.76(6)	95.23(14)
	101.35(6)	96.99(16)
	101.89(6)	108.6(2)
	172.29(7)	164.24(18)
	173.56(7)	177.60(15)
O-Cu-O [°]	84.30(6)	83.31(11)

Slow evaporation of a methanol solution of **172** at 5 °C provided crystals of suitable quality for X-ray crystallographic analysis (Figure 30). Table 4 summarizes important bond lengths and angles for **172** and those observed for the BPh_4^- congener **128**[192].

Comparison of the bond lengths and angles of **172** and **128** indicates a similar coordination geometry for both dinuclear Cu μ-oxalato complexes, which is to be expected as their only difference is the non-coordinating anion. Cu-Cu distance (5.20 Å in **128** and 5.167 Å in **172**) are reminiscent of this behavior.[XIII] An observable difference are the shorter Cu-N bonds in **128** compared to **172**, especially for the apical nitrogen (Table 4). The major disparity

[XIII] C-O-Cu-N torsion angles (for **128**) and Cu-Cu distances were determined using the Mercury 2020.1 (Build 280197) software provided by the CCDC.[329]

relies in the O-Cu-N angles of both complexes with the most pronounced discrepancy of 172.29(7)/173.56(7)° *vs.* 164.24(18)/177.60(15)°[192] between the oxalate oxygens, copper, and the opposite basal nitrogen for **172** and **128**, respectively. These differences are resulting from the marginally different coordination geometry quantifiable e.g. by the C-O-Cu-N torsion between the oxalate C-O, Cu, and the apical nitrogen. While the absolute values of these torsions are nearly identical for **172** (109.97(14)/–109.54(14)°), they clearly diverge for **128** (90.79/–103.77°),[192] indicating a twist of the triazacyclononane ligand with respect to the O-Cu-O plane.

172 revealed a strong C-O stretching vibration at 1651 cm^{-1} in the FTIR spectrum (Figure 31), which is similar to that reported for **128** (1660 cm^{-1})[192]. In contrast, **171** depicted two vibrations in the same region, located at 1668 and 1650 cm^{-1}, respectively, that are a result of the inequivalent C-O bonds. Furthermore, even the ligand **127** and the derived CuI complex **168** display weak C=C vibrations at 1641 and 1640 cm^{-1}. While these possess comparatively moderate intensity, their location further corroborates the necessity of additional analytical methods for the determination of potentially formed oxalate

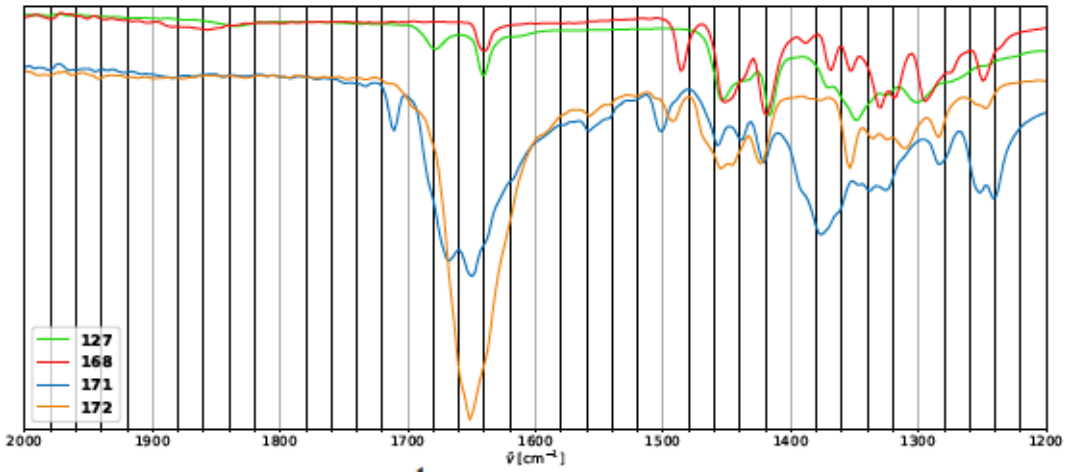

Figure 31: Section (2000-1200 cm^{-1}) of the FTIR spectra of complexes **168**, **171**, **172**, and ligand **127**.

Thus, removal of oxalate by treatment of complex **172** with NaOH in a biphasic H_2O/toluene mixture (Scheme 60) following a protocol previously utilized for the removal of oxalate from dinuclear copper complexes[193] was attempted. Subsequent analysis by capillary electrophoresis clearly indicated successful removal and detection of $C_2O_4^{2-}$ with an approximate yield of 48% determined by CE (average of two experiments conducted on 24 µmol scale utilizing the CE calibration as described in

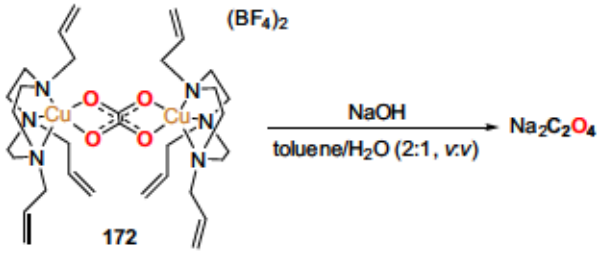

Scheme 60: Treatment of complex **172** with NaOH in H_2O/toluene for the subsequent detection of $Na_2C_2O_4$.

section 4.15.1). Identification of the oxalate by ^{13}C NMR spectroscopy proved to be more challenging, as the oxalate signal at 173 ppm was barely detected for one of the two experiments (Figure 32) and displayed a low intensity, indicating the detection limit of this method (for the 24 μmol scale). Due to inconsistent chemical shifts reported for the ^{13}C NMR signal of oxalate ranging from 160 ppm[166] over 173-174 ppm[178,179,183] up to 178-180 ppm[179,202], ^{13}C NMR spectra of $Na_2C_2O_4$, $K_2C_2O_4$, $H_2C_2O_4$, HCO_2Na, $NaHCO_3$, and Na_2CO_3 were recorded (Figure 32) to enable a concise signal assignment.

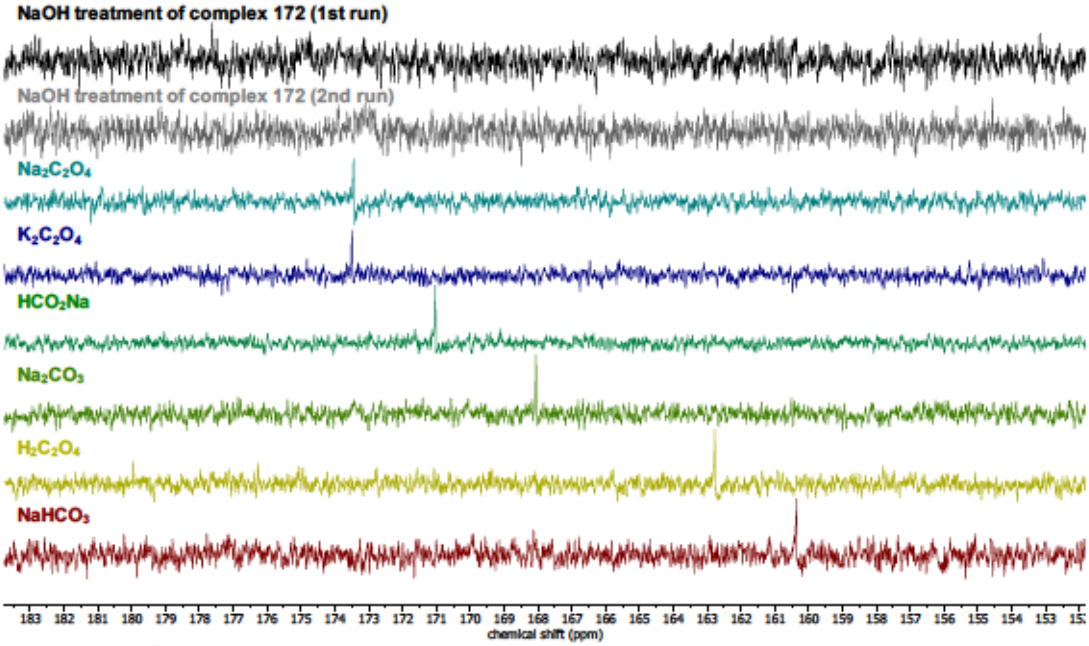

Figure 32: $^{13}C\{^1H\}$ NMR spectra (183-153 ppm, D_2O) for compounds frequently encountered when investigating CO_2 reduction/reductive coupling, namely $Na_2C_2O_4$, $K_2C_2O_4$, $H_2C_2O_4$, HCO_2Na, Na_2CO_3, and $NaHCO_3$ and the spectra obtained for NaOH treatment of **172** (24 μmol scale).

By coupling FTIR spectroscopy of the crude product, which would be obtained after treating the *in situ* prepared Cu complex with CO_2 in the presence of additives, with subsequent removal of potentially formed oxalate according to this procedure and finally analysis by NMR spectroscopy and CE should enable a more precise analysis of the reaction outcome. Following this protocol, the CO_2 bubbling experiments resulting in the distinct color changes were analyzed, but no oxalate in yields close to those reported (21%[192]) was detected by NMR spectroscopy or capillary electrophoresis ($\leq$2% in these cases, see Table 5, entries 1-7). However, traces of formate were observed by NMR spectroscopy when $NaPF_6$ was utilized instead of $NaBPh_4$ (Table 5, entry 7), indicating at least partial reduction of CO_2. Furthermore, the presence of carbonate was observed in all cases which is a result of CO_2 saturation of non-dry methanol and subsequent base treatment during the work-up.

Table 5: Results for the attempted CO_2 reductive coupling by CO_2 bubbling utilizing CuI, **127**, and $NaBPh_4$ or $NaPF_6$.

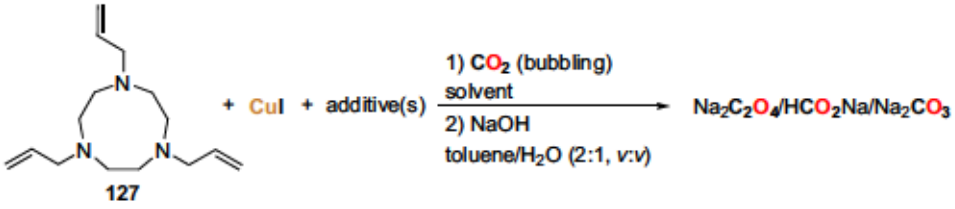

127

Entry	Additive	CuI/127/Add. [equiv.]	Solv.	*t* [h]	FTIR $\tilde{\nu}$ [cm^{-1}][a]	^{13}C NMR ($C_2O_4^{2-}$/ HCO_2^-/CO_3^{2-})[b]	CE ($C_2O_4^{2-}$) approx. yield [%][c]
1	$NaBPh_4$	1/1/1	MeOH	11	1628	n.d.	n.d.
2	$NaBPh_4$	1.7/1/1.5	MeOH	6 (3×)	1628	x/x/✓	n.d.
3	$NaBPh_4$	1.7/1/1.3	MeOH	14 (6×)	1628, 1617	x/x/✓	<0.5
4	$NaBPh_4$	1/1/1	MeOH	12.5	1617	x/x/✓	2
5	$NaBPh_4$	1/1/1	MeOH	5 (3×)	1639, 1609	x/x/✓	1
6	$NaBPh_4$	1/1/1	MeOH	4 (2×)	1623	x/x/✓	2
7	$NaPF_6$	1.7/1/1.5	MeOH	6 (2×)	1642	x/✓/✓	<0.5
8	$NaBPh_4$	1.7/1/1.3	MeOH/THF (3.8:1)	6 (2×)	1628	x/x/✓	<0.5

Detailed experimental procedures and results are presented in Table S 13. Total reaction times are stated for experiments in which multiple CO_2 bubbling steps and intermittent stirring under Ar atmosphere was performed (the number of CO_2 bubbling repetitions is given in brackets). [a]Vibrations between 1700-1600 cm^{-1} are reported. [b]n.d. = not determined; x = not observed. [c]Note that approximate oxalate yields determined by CE are stated for signals coinciding with the signal of internal standard (Na_2C_2

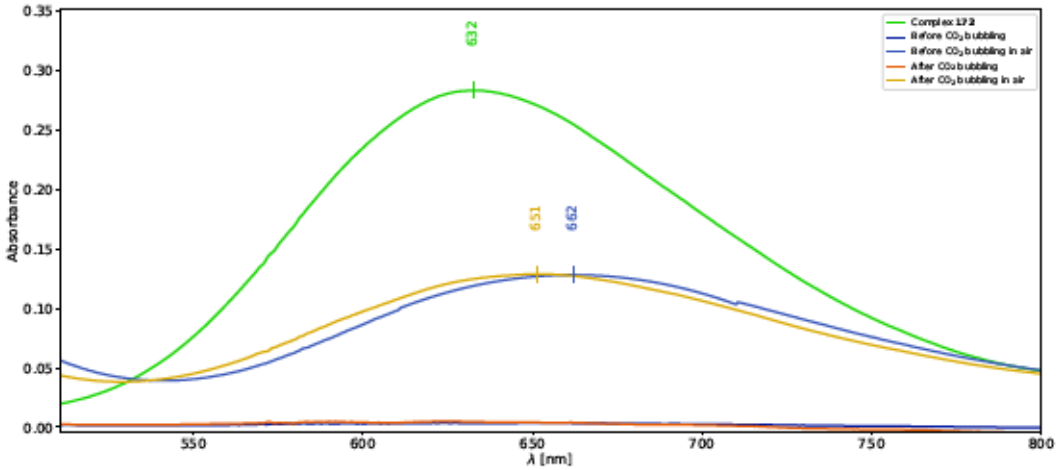

Figure 33: UV/Vis spectrum (500-800 nm) of **172** (1.7 mM in MeOH) and a mixture of **127**, CuI and $NaBPh_4$ in MeOH (Table 5, entry 5) before (2.3 mM) and after (ca. 2.1 mM) CO_2 bubbling (3 h) and the same samples in air (plots were partially smoothed using a Savitzky-Golay filter in OriginPro[330] to remove an artifact produced by the spectrometer; original data in Figure S 433).

To evaluate whether formation of the oxalate complex could be observed based on the color change, typical CO_2 bubbling experiments (Table 5, entries 5 and 6) were analyzed by UV/Vis spectroscopy and compared to **172** (Figure 33, further data in the appendix, section 4.17.1). **172** displays an absorption at 632 nm associated with d→d transitions and in good

accordance with similar 1,4,7-tacn-ligated oxalate complexes.[226] While CO_2 bubbling did not result in detectable formation of a Cu^{II} species in the 500-800 nm region, subsequent exposure of the sample to air caused oxidation resulting in broad bands with maxima at 662 nm before and 651 nm after CO_2 treatment. While both are not identical to the isolated oxalate complex, Cu^{II} species arising from aerial oxidation, such as a μ-hydroxo complex, have been described to feature similar absorptions.[331] Attempts to identify whether the same product could be obtained by reaction with O_2 were hampered by precipitation of a green solid (Table 9, entry 4, see Figure S 435).

Next, additives and different reaction parameters which might impact the reactivity towards CO_2 reductive coupling were evaluated. Precipitation of a Cu^{I} complex during CO_2 bubbling when conducting the reaction in MeOH was observed while decent solubility of this precipitate was obtained in THF. Therefore, the CO_2 treatment by bubbling was conducted in a mixture of MeOH and THF (Table 5, entry 8). Indeed, addition of THF prevented precipitation during the CO_2 bubbling. Moreover, decolorization was not observed over the course of 48 h under Ar/CO_2, contrasting the results in pure methanol. Despite the distinct color change to blue, no evidence for the formation of a CO_2 reduction product was found.

Table 6: Results for the treatment of *in situ* formed **127**-ligated Cu complexes with solid bicarbonates.

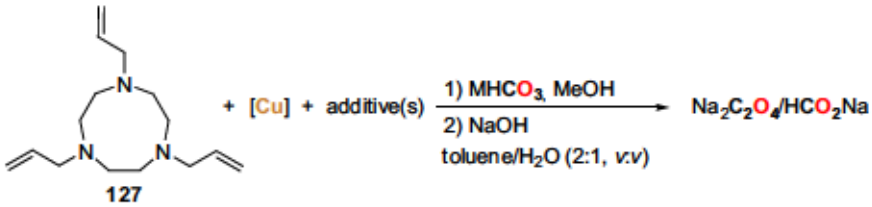

Entry	$MHCO_3$	[Cu] [µmol]	Additive	*t* [h]	FTIR $\tilde{\nu}$ [cm^{-1}][a,b]	^{13}C NMR ($C_2O_4^{2-}$/ HCO_2^-)[b]	CE ($C_2O_4^{2-}$) approx. yield [%][c]
1[d]	$CsHCO_3$	CuI	$NaBPh_4$	48	n.d.	n.d.	n.d.
2[e]	$CsHCO_3$	CuI	$NaBPh_4$	16	1628, 1617	x/x	<1
3[f]	$CsHCO_3$	CuI	$NaBPh_4$	117	1628, 1617	x/x	<1
4[g]	$CsHCO_3$	CuI	$NaBPh_4$	71	1629	x/✓	n.d.
5[h]	$CsHCO_3$	CuI	$NaPF_6$	168	1640	x/x	<0.5
6[e]	$CsHCO_3$	CuI	-	16.5	1661, 1644	x/x	11[j]
7[i]	$NaHCO_3$	CuI	$NaBPh_4$	210	1625	x/x	<1
8[f]	$CsHCO_3$	$[Cu(MeCN)_4]PF_6$	-	118	1659	x/x	<0.5
9[f]	$NaHCO_3$	$[Cu(MeCN)_4]PF_6$	-	118	1629	x/x	<1

Detailed experimental procedures and results are presented in Table S 14. 1/1/1 combinations of [Cu]/**127**/additive were utilized in degassed methanol unless stated otherwise. The bicarbonate was utilized in excess (1.05-2.05 equiv.). [a]Vibrations between 1700-1600 cm^{-1} are reported. [b]n.d. = not determined; x = not observed. [c]Note that approximate oxalate yields determined by CE are stated for signals coinciding with the signal of internal standard ($Na_2C_2O_4$) added to the samples after a first CE measurement. [d]Column chromatography, extraction of the green solid with $MeNO_2$ followed by recrystallization from hot $MeNO_2$ gave rise to **173**. [e]Analyzed by NMR spectroscopy prior to NaOH treatment. [f]GC analysis of the headspace was performed. [g]H_2O (6 %vol) was added after 6.5 h. [h][Cu]/**127**/$NaPF_6$ ratio of 1/1/1.3. [i][Cu]/**127**/$NaBPh_4$ ratio of 1.7/1/1.3. [j]Overlapping with an underlying signal.

Peacock and co-workers observed higher isolated yields (53%) of oxalato-complex **128** when $CsHCO_3$ was utilized instead of CO_2 for the reaction with **127**, CuI, and $NaBPh_4$.[192] This observation suggests HCO_3^- as the active form of CO_2 converted into oxalate *via* reductive coupling.[192] Hence, a 1/1/1 mixture of CuI/**127**/$NaBPh_4$ in non-dry MeOH was treated with $CsHCO_3$ (Table 6, entry 1). After stirring for 48 h under Ar, a white precipitate and a slightly greenish color were observed, contrasting the distinct blue color observable within 1-2 h reported in the literature[192]. The initial report describes isolation of the desired complex **128** by column chromatographic separation on silica with a polar eluent mixture (7:1:2 MeOH/$MeNO_2$/2 M NH_4Cl).[192] Hence, purification of the obtained crude product utilizing the same method was attempted. However, the blue band, presumably corresponding to the desired complex **128**, turned green on silica during purification. Recrystallization of the resulting green fraction enabled elucidation of the structure of complex [Cu(**127**)Cl_2] (**173**) by elemental and X-ray crystallographic analysis (Figure 34). **173** likely formed by substitution with NH_4Cl from the eluent *via* protonation of either a potential bicarbonate or hydroxo complex, such as **169**. In addition, **173** can be prepared by targeted synthesis from $CuCl_2$ and **127** in MeOH and subsequent recrystallization from nitromethane in 34% yield (Scheme 61).

The coordination geometry of **173** resembles that of complex **171**. Cu-N distances of 2.0990(16) Å, 2.1135(15) Å, and 2.2357(15) Å indicate only slightly elongated Cu-N bonds for both basal nitrogens compared to both **170** and **171**, while the Cu-N distance for the apical nitrogen is in between those of its congeners. N-Cu-N angles of 83.23(6), 83.46(6), 84.37(6)° are again conforming those of **171**. Moreover, a mean deviation of 0.11 Å from the best plane defined by Cu1, Cl1, Cl2, N2, and N3 indicates a slight deviation from planarity of the base. When treatment of CuI, $NaBPh_4$, and **127** with $CsHCO_3$ was repeated under similar conditions for 16 h or 117 h instead of 48 h, yielding slightly blue suspensions, no oxalate was detectable by NMR spectroscopy or CE (Table 6, entries 2 and 3). Interestingly, formation of sodium formate was observed upon addition of small quantities of water, identified by NMR spectroscopy (Table 6, entry 4). Again, substitution of $NaBPh_4$ with $NaPF_6$ was conducted (Table 6, entry 5), but remained unsuccessful. Exchanging $CsHCO_3$ for $NaHCO_3$ (Table 6, entry 7) did likewise not enable the identification of oxalate despite a 210 h reaction time. Incomplete substitution of the iodide ligand during the *in situ* formation of the reactive com-

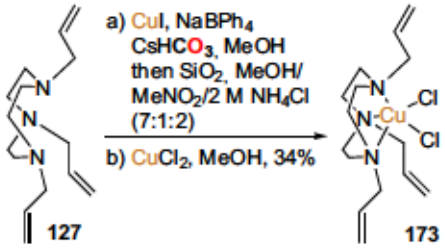

Scheme 61: Reaction pathway for the initial isolation of **173** and targeted synthesis by reaction of **127** with $CuCl_2$.

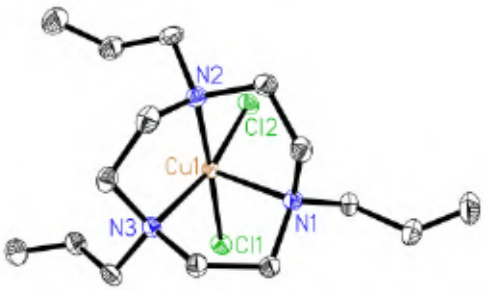

Figure 34: Molecular structure of complex **173** (thermal ellipsoids are presented at 50% probability level and hydrogen atoms are omitted for clarity).

plex from ligand **127**, CuI, and $NaBPh_4$ was observed early on, but a free coordination site might constitute a prerequisite for the reduction of CO_2. Consequently, experiments with $[Cu(MeCN)_4]PF_6$ in combination with $CsHCO_3$ and $NaHCO_3$ were conducted (Table 6, entries 8, 9). In these cases, substitution of the acetonitrile ligands by **127** would result in a cationic complex which might even be beneficial for the desired CO_2 reductive coupling[282]. Still, the desired reactivity was not observed in both cases over the course of 118 h. To exclude the formation of gaseous CO_2 reduction products, such as CO, their absence was confirmed by GC analysis of the headspace above the solution for selected examples (Table 6, entries 3, 8, 9). Without addition of $NaBPh_4$, an enhanced solubility in MeOH was observed, giving rise to a slightly blue solution after stirring with $CsHCO_3$ for 16.5 h (Table 6, entry 6). Surprisingly, in the absence of any additive, a peak in the electropherogram that could correspond to the oxalate dianion and would integrate to a yield of 11% was observed. However, non-ideal separation causing overlapping with a broadened underlying signal (Figure S 357) renders the approximate yield unreliable. A distinct IR vibration at 1661 cm^{-1} (Figure S 264) coinciding with the literature value[192] was identified and could indeed indicate the formation of oxalate, even though a similar band was observed for another reaction in the absence of $NaBPh_4$ (Table 6, entry 8). The plausibility of this result is further questioned by NMR spectroscopic analysis of the solid residues of analogous reactions in the presence and absence of $NaBPh_4$ prior to NaOH treatment (Table 6, entries 2 and 6). The NMR spectra in CD_3OD depict no significant broadening, and thus indicate the presence of mainly Cu^I species in both cases (Figure 35).

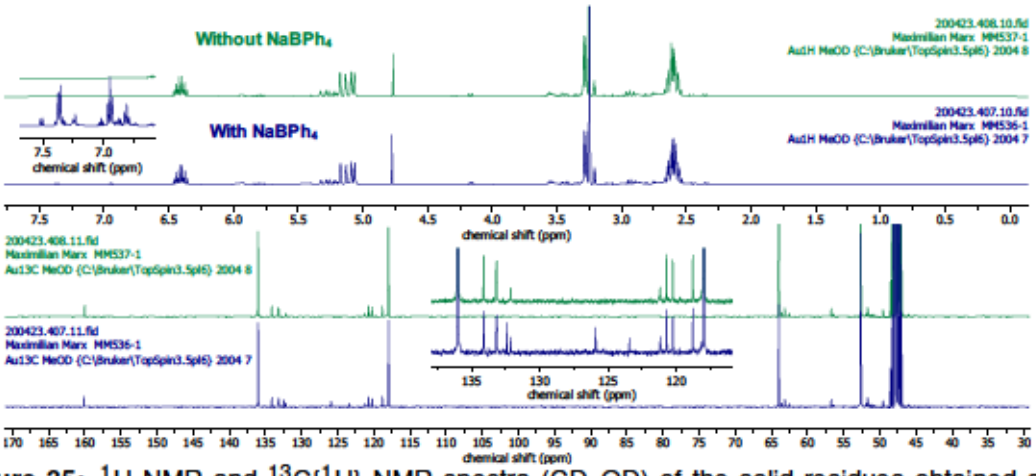

Figure 35: ^1H NMR and $^{13}C\{^1H\}$ NMR spectra (CD_3OD) of the solid residues obtained after stirring CuI, **127**, and $CsHCO_3$ under Ar in the presence and absence of $NaBPh_4$ corresponding to entries 2 & 6 in Table 6.

In both cases, a major species of the general formular [Cu(**127**)X] is observed and could possibly correspond to a bicarbonate complex indicated by the 160 ppm signal in the ^{13}C NMR, albeit the signal could likewise be a result of dissolved $CsHCO_3$. Both, the ^1H and ^{13}C NMR spectra in the presence and absence of $NaBPh_4$ are nearly identical and only minor signals indicating the presence of the BPh_4^- anion can be found in the aromatic region for

both nuclei. This similarity of the observed species and the significant difference observed by CE after NaOH treatment can be explained as follows: 1) the underlying signal in the electropherogram in the absence of $NaBPh_4$ compromises the analysis and integration; 2) one of the minor species detected by NMR spectroscopy in the presence of $NaBPh_4$, $NaBPh_4$ itself or a non-observable paramagnetic compound hampers the reductive coupling reaction, which would contrast the initial results by Peacock and co-workers[192]; or 3) in the presence of $NaBPh_4$, formation of a colorless precipitate was observed which was filtered off prior to NMR spectroscopic analysis and NaOH treatment. While the precipitate was colorless (i.e. white), the oxalate complex **172** was found to be soluble in MeOH, no precipitation was reported by the Peacock group, and no oxalate was observed for 5 d reaction time (Table 6, entry 3) under otherwise unaltered conditions, inadvertent removal of the reductive coupling product due to this filtration cannot be entirely excluded.

Apart from these experimental results possibly indicating the formation of oxalate in quantities significantly lower than those reported by Peacock and co-workers,[192] no clear evidence for CO_2 reductive coupling was found utilizing the reported reaction conditions. To evaluate whether the CO_2 reductive coupling could still be achieved with the help of this literature protocol,[192] the impact of different reaction parameters, such as temperature, solvent, and illumination on the outcome of the CO_2 treatment (Table 7) was assessed. For these experiments, a constant CO_2 atmosphere was employed to minimize the risk of potential oxidative side reactions resulting from trace oxygen, as air is more readily introduced using a needle for CO_2 bubbling. Moreover, CO_2 was chosen over solid bicarbonates as the fundamental interest was the possibility of converting gaseous CO_2 into the solid oxalate dianion or its base metal complexes.

To enable a direct comparison to the results obtained under CO_2 bubbling conditions or with $CsHCO_3$, experiments with a 1/1/1 CuI/**127**/$NaBPh_4$ mixture in MeOH for 24 or 118 h, but under a constant CO_2 atmosphere, were conducted (Table 7, entries 1 and 2). Again, neither reaction yielded oxalate in quantities corresponding to more than 1% yield (by CE) and neither oxalate nor formate were detected by NMR spectroscopy. Carbonate was observed for both reactions by NMR spectroscopy, but no CO could be detected by GC analysis of the headspace indicating that it likely results from dissolved CO_2 in non-dry MeOH. To allow for sufficient contact with gaseous CO_2 under constant CO_2 atmosphere, most of the CO_2 treatments reported in the following paragraphs were conducted over five days. Addition of THF as a co-solvent (Table 7, entries 3 and 4) or replacement of MeOH by THF (Table 7, entries 5 and 6) did not result in an improved reactivity and again no CO_2 reduction products were observed even for extended CO_2 treatment over more than 26 d (Table 7, entry 6). Less coordinating solvents were observed to favor CO_2 reductive coupling in certain cases,[179,188] hence CO_2 treatment in toluene was evaluated (Table 7, entry 7). This modification again remained unsuccessful in providing detectable quantities of oxalate. To exclude a potential impact of varying ambient temperatures or a possible influence of the temperature on the

reactivity towards CO_2, slightly elevated temperatures of 40 °C (Table 7, entry 8) and 35 °C (entry 9 - with a CuI/**127**/$NaBPh_4$ ratio of 1.7/1/1.3) were studied. In the latter case, a small signal corresponding to formate in addition to that of carbonate was observed in the ^{13}C NMR spectrum, yet no oxalate was detected by CE. When the treatment was conducted at 40 °C, a signal possibly belonging to oxalate with an integral amounting to a 3% yield was observed by CE. Finally, alteration of the reactivity by illumination of the reaction mixture using visible light (400-700 nm, 0.09 W) over 18 h (Table 7, entry 10) was attempted. However, no oxalate was formed according to CE and NMR analysis.

Table 7: CO_2 treatment (constant atmosphere) of CuI, $NaBPh_4$, and **127** under varying reaction conditions.

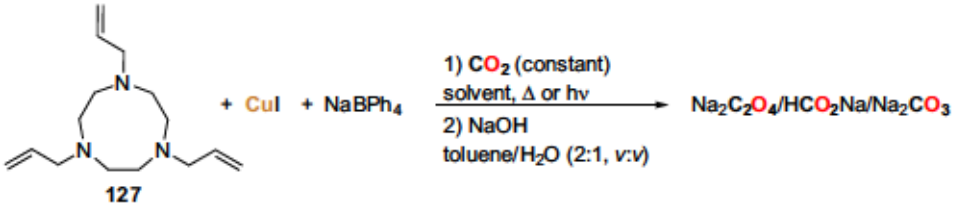

127

Entry	CuI/127/$NaBPh_4$ [equiv.]	Solv.	*t* [h]	FTIR $\tilde{\nu}$ [cm^{-1}][a]	^{13}C NMR ($C_2O_4^{2-}$/HCO_2^-/CO_3^{2-})[b]	CE ($C_2O_4^{2-}$) approx. yield [%][c]
1[d]	1/1/1	MeOH	24	1620	x/x/✓	<1
2[d]	1/1/1	MeOH	118	1641	x/x/✓	<0.5
3[d]	1/1/1	MeOH/THF (9/1)	118	1641	x/x/✓	<0.5
4[e]	1.7/1/1.3	MeOH/THF (3/1)	354	1629	x/x/✓	n.d.
5[d]	1/1/1	THF	120	1641, 1621, 1609	x/x/x[j]	<0.5
6[f]	1/1/1.4	THF	644	1654, 1644, 1620, 1601	x/x/x[j]	1
7	1/1/1	toluene	121	1638, 1620	x/x/✓	<1
8[d,g]	1/1/1	MeOH	114	1643	x/x/✓	3
9[h]	1.7/1/1.3	MeOH	165	1641, 1628	x/✓/✓	<0.5
10[i]	1/1/1	MeOH	18	1635, 1622, 1608	x/x/✓	<0.5

Detailed experimental procedures and results are presented in Table S 15. CuI/**127**/$NaBPh_4$ mixtures were utilized in degassed solvents as indicated and unless stated otherwise. [a]Vibrations between 1700-1600 cm^{-1} are reported. [b]x = not observed [c]Note that approximate oxalate yields determined by CE are stated for signals coinciding with the signal of internal standard ($Na_2C_2O_4$) added to the samples after a first CE measurement. [d]GC analysis of the headspace was performed. [e]Filtered after 30 min under Ar. CO_2 was bubbled through the solution for 30 min, the reaction mixture sealed under CO_2 atmosphere and stirred for 186 h. Dry THF (3 mL) was then added and stirring continued for 7 d under CO_2. CO_2 was bubbled through the solution for 5.5 h. [f]CO_2 bubbling for 26 min after stirring under CO_2 for 27 d. [g]Reaction conducted at 40 °C. [h]Reaction conducted at 35 °C. [i]Reaction illuminated at 400-700 nm (0.09 W). [j]Possibly residual paramagnetic Cu^{2+}, hence ^{13}C NMR signals might not be observable.

After fruitless identification of parameters that significantly alter the observed reactivity of complex **168** or its BPh_4^- analogue towards CO_2, the impact of different additives was stud-

ied (Table 8).

Table 8: CO_2 treatment (constant atmosphere) of CuI, **127**, and different additives in MeOH.

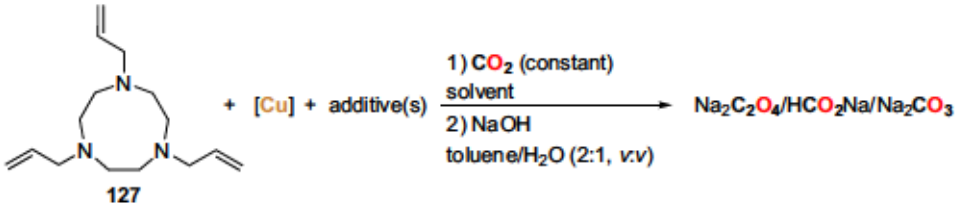

127

Entry	Additive	[Cu]/127/Add. [equiv.]	*t* [h]	FTIR $\tilde{\nu}$ [cm^{-1}][a,b]	^{13}C NMR ($C_2O_4^{2-}$/ HCO_2^-/CO_3^{2-})[b]	CE ($C_2O_4^{2-}$) approx. yield [%][c]
1[d]	KPF_6	1/1/1	119	1643	x/x/x[h]	<0.5
2[e]	$AgBPh_4$	1/1/1	115	1665, 1641, 1611	x/✓/✓[i]	2
3[d,f]	-	1/1/-	119	1639	x/x/x[h]	<1
4[f]	-	1/1/-	166	1639	x/x/x[h]	<1
5[f]	$NaBPh_4$	1/1/1.3	119	1631	x/x/x	<1
6[f]	NaO_2CH	1/1/3	114	1618	x/✓/x	1
7[f]	$Mg(OTf)_2$	1/1/2	117	1649	x/x/✓	<0.5
8[f]	$LiBF_4$	1/1/1.2	162	1638	x/x/x	<1
9[f]	$LiBF_4$, NaO_2CH	1/1/2.2/3	113	1624	x/✓/x	<0.5
10[f]	Na_2SO_3	1/1/2.5	116	1637	x/x/✓	n.d.[k]
11[g]	$NaBPh_4$, $NaC_{10}H_8$	1/1/1/1	116	x	x/x/x[h]	5
12[g]	$NaBPh_4$, $NaC_{10}H_8$	1/1/1/1.1	118	1618	x/x/✓	7
13[g]	$NaC_{10}H_8$	-/-/1	116	x	✓[i]/x/✓	6

Detailed experimental procedures and results are presented in Table S 16. [Cu]/**127**/additive mixtures as indicated were treated with CO_2 in degassed methanol unless stated otherwise. [a]Vibrations between 1700-1600 cm^{-1} are reported. [b]x = not observed. [c]Note that approximate oxalate yields determined by CE are stated for signals coinciding with the signal of internal standard ($Na_2C_2O_4$) added to the samples after a first CE measurement. [d]GC analysis of the headspace was performed. [e]Dehalogenation with $AgBPh_4$ in dry THF followed by filtration and solvent exchange to MeOH. [f]$[Cu(MeCN)_4]PF_6$ instead of CuI was utilized. [g]Reaction conducted in dry THF. $NaC_{10}H_8$ freshly prepared from Na and $C_{10}H_8$. [h]Possibly residual paramagnetic Cu^{2+}, hence ^{13}C NMR signals might not be observable. [i]Poor signal-to-noise ratio. [j]Possibly oxalate, albeit with poor signal-to-noise ratio (see Figure S 156 for comparison with internal standard). [k]Due to overlapping of the SO_3^{2-} and a potential $C_2O_4^{2-}$ signal, oxalate identification was not possible by CE.

Substituting $NaBPh_4$ by $NaPF_6$ remained unsuccessful when applied in the CO_2 bubbling protocol or in combination with $CsHCO_3$. Likewise, PF_6^- as the anion under constant CO_2 atmosphere in combination with K^+ as the cation gave no detectable quantities of oxalate (Table 8, entry 1). To ensure an increased substitution of I^- by BPh_4^-, *in situ* formed **168** was dehalogenated with $AgBPh_4$ [332] in THF (Table 8, entry 2). The resulting yellow foam, after filtration and removal of the volatiles *in vacuo*, was then treated with CO_2 in MeOH. In this case, formate was detected as CO_2 reduction product and a small peak possibly corresponding to oxalate was observed by CE (2%). Since this result might indicate that the absence of halides could be beneficial for the reductive coupling, further additives were evaluated in combination with $[Cu(MeCN)_4]PF_6$. Stirring of $[Cu(MeCN)_4]PF_6$ and **127** in the absence of any additive under constant CO_2 atmosphere in MeOH provided no evidence for a CO_2 reduction reaction by CE and GC analysis of the headspace (Table 8, entries 3

and 4). To evaluate the impact of $NaBPh_4$, it was combined with $[Cu(MeCN)_4]PF_6$ and the allylated 1,4,7-tacn ligand without success (Table 8, entry 5). Formate could be a key intermediate in the conversion of CO_2, as indicated by the recent conversion of a bridged Ti formate complex into a dimetalloxycarbene intermediate and its subsequent reaction to the oxalato complex with CO_2[172] and the thermal conversion of alkali metal formates into their oxalates in the presence of base[333]. Consequently, sodium formate was explored as a potential additive (Table 8, entry 6), but did not facilitate an increase in the reactivity of interest. Lewis acid activation of CO_2 is another possibility to enhance its reactivity for subsequent conversion (Section 1.1), thus $Mg(OTf)_2$ and $LiBF_4$ were examined (Table 8, entries 7 and 8). However, neither Lewis acid appeared to improve the outcome of the CO_2 treatment even if both, sodium formate and $LiBF_4$, were added (Table 8, entry 9). Finally, combination of the *in situ* prepared Cu complex with different reductants was studied. Combination of $[Cu(MeCN)_4]PF_6$, **127** and Na_2SO_3, which has been utilized for the reduction of Cu^{II} to Cu^{I},[334] did not result in formation of oxalate quantities detectable by NMR spectroscopy (Table 8, entry 10 - CE analysis was impeded by overlapping of the SO_3^{2-} signal with that of possibly formed oxalate). Ultimately, sodium naphthalenide was chosen as a strong reductant (Table 8, entries 11-13), analogous to the recent report by Murray and co-workers[195]. Indeed, CE analysis after NaOH treatment indicated an enhanced formation of the desired oxalate in 4-7% yield (see Table S 16 for detailed results). ^{13}C NMR spectroscopy did not indicate the formation of $C_2O_4^{2-}$, but it should be noted that the detection limit for reactions at this scale (and for most of those reported in this section - detailed reaction scales are given in Section 4.7 in the appendix), assessed by NaOH treatment of 24 μmol of complex **172** (Figure 32), corresponds to a yield of approximately 20-40% (depending on the NaOH treatment efficiency). Since $NaC_{10}H_8$ is theoretically capable of facilitating $CO_2^{\bullet-}$ formation, due to its strong reducing potential of ca. –3 V in THF,[285] the reaction of $NaC_{10}H_8$ with CO_2 was conducted as a blank experiment. As expected, the formation of an analogous signal in the CE is observed which corresponds to similar quantities of 6-7% (Table 8, entry 13). Interestingly, in this case a minor signal with poor signal-to-noise ratio potentially corresponding to oxalate was found in the ^{13}C NMR spectrum (see Figure S 123). Moreover, signals in the 170-190 ppm range of the ^{13}C NMR spectra were observed for multiple reactions with major peaks being located at 182 and 177 ppm. These presumably correspond to carboxylic acid derivatives of naphthalene, such as 1,4-dihydronaphthalene-1,4-dicarboxylic acid and 1,2-dihydronaphthalene-1,2-dicarboxylic acid, which are well-known to form in the reaction of $NaC_{10}H_8$ with CO_2.[335,336] Analogous signals were observed when reactions were conducted in the presence of CuI, **127** and $NaBPh_4$, indicating that the *in situ* formed Cu complex does neither impact the reaction of $NaC_{10}H_8$ with CO_2 nor act as a catalyst in the presence of this strong reductant. Moreover, shorter reactions times of one day resulted in a decrease in the potential oxalate peak, corresponding to 1% and 2% yield in the presence and absence of [Cu], respectively (Table S 16).

Formation of oxalate complex **128** was originally discovered during aerial oxidation of the *in situ* prepared **127**-derived Cu^{I} complex.[192] Therefore, similar reactions were conducted to assess the possibility of formation of oxalate in air either from atmospheric CO_2 or possibly *via* an unsuspected oxidative process. Exposure of CuI, **127**, and $NaBPh_4$ in MeOH to first exhaled air and subsequently to the atmosphere for 7 or even 41 days did not result in the isolation of sodium oxalate through NaOH treatment in >1% yield (Table 9, entries 1 and 2). However, for the shorter exposure time, an IR signal at 1653 cm^{-1} and a peak indicating the formation of formate in the NMR spectrum was observed. Oxidation of ethanol to oxalate catalyzed by Cu has recently been suggested to explain the observed formation of pyrazole and hydroxymethylpyrazole containing copper oxalate coordination polymers.[206] Accordingly, a 4:1 mixture of ethanol and methanol was utilized for air exposure of the *in situ* prepared **127**-based Cu complex (Table 9, entry 3). Still, no distinct increase in the oxalate yield, proceeding through either CO_2 reductive coupling or EtOH oxidation, was noticed. To further preclude a potential oxidative pathway resulting in the formation of oxalate, CuI, $NaBPh_4$, and ligand **127** in MeOH were reacted with pure O_2 (Table 9, entry 4). The absence of $C_2O_4^{2-}$ and HCO_2^{-} indicates that both are unlikely formed *via* an oxidative pathway. Interestingly, omitting $NaBPh_4$ in the reaction, as for the treatment with $CsHCO_3$ (Table 6, entry 6), resulted in considerable formation of oxalate in 7% yield after 8 days in air (Table 9, entry 5), provided that the CE signal corresponds to the oxalate dianion. Again, integration might be compromised which presumably impacts the calculated yield due to broadening and overlapping with another signal (Figure S 391). An IR band at 1654 cm^{-1} and ^{13}C NMR signals corresponding to formate and carbonate were observed.

Table 9: Exposure of CuI, **127**, and additives in MeOH to air.

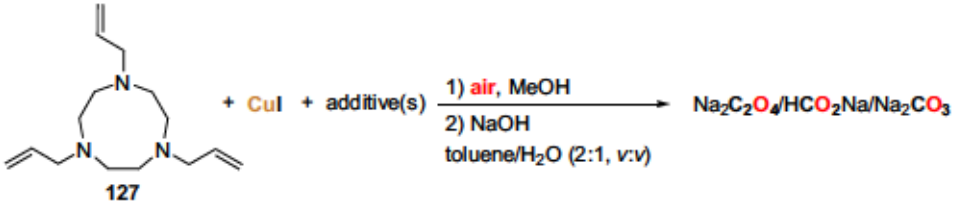

127

Entry	Additive	CuI/127/Add. [equiv.]	*t* [d]	FTIR $\tilde{\nu}$ [cm^{-1}][a]	^{13}C NMR ($C_2O_4^{2-}$/HCO_2^{-}/CO_3^{2-})[b]	CE ($C_2O_4^{2-}$) approx. yield [%][c]
1	$NaBPh_4$	1/1/1	41	1638, 1619	x/x/✓	1
2[d]	$NaBPh_4$	1/1/1	7	1653, 1638, 1618	x/✓/✓	<1
3[e]	$NaBPh_4$	1/1/1	1	1645	x/x/✓	1
4[f]	$NaBPh_4$	1/1/1	3	1619	x/x/x	<0.5
5	-	1/1/-	8	1654	x[g]/✓/✓	7[h]

Detailed experimental procedures and results are presented in Table S 17. CuI/**127**/additive were utilized in degassed methanol unless stated otherwise and after preformation exposed to air. [a]Vibrations between 1700-1600 cm^{-1} are reported. [b]x = not observed. [c]Note that approximate oxalate yields determined by CE are stated for signals coinciding with the signal of internal standard ($Na_2C_2O_4$) added to the samples after a first CE measurement. [d]Extracted and partially re-crystallized from $MeNO_2$ before NaOH treatment. [e]A mixture of MeOH and EtOH (1:4) was utilized. [f]Treatment with pure O_2 (balloon) for 90 min and subsequent stirring under O_2/Ar. UV/Vis samples were taken as stated in Table S 17. GC analysis of the headspace was conducted. [g]At 173.0 ppm, a signal might be observable, but the signal-to-noise ratio does not allow for a conclusive assignment (Figure S 122). [h]Broadening and apparent overlapping with another signal compromise integration.

Since reactions with the initially described 1,4,7-tacn derivative failed to produce oxalate in quantities presented in the literature,[192] the procedure of CO_2 treatment under constant atmosphere followed by removal of possibly formed oxalate *via* NaOH treatment was employed to examine other tridentate donor ligands (Table 10). Consequently, two 1,4,7-triazacyclononane derivatives, namely the *N*, *N*, *N*-tribenzyl- (**174**) and the 1,4,7-tris(1-propyl)- (**175**) derivatives were prepared by alkylation of 1,4,7-tacn with benzylbromide or 1-bromopropane in the presence of KOH in 61% and 38% yield, respectively (Scheme 62).

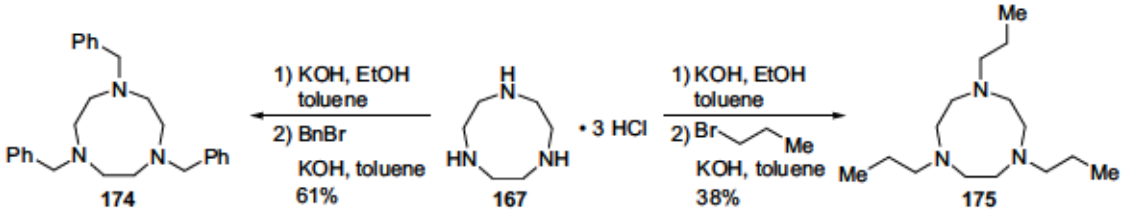

Scheme 62: Preparation of 1,4,7-triazacyclononane derivatives **174** and **175**.

Treating solutions of CuI, $NaBPh_4$ and either ligand in MeOH with CO_2 over five days did not result in an observable enhancement of the reactivity and <1% oxalate yield (by CE), no oxalate in the NMR spectra and no CO in the headspace of the reaction mixture were detected (Table 10, entries 1 and 2). For less donating 1,4,7-tris(4-toluenesulfonyl)-substituted congener **166**, disturbance of the baseline of the electropherogram precludes a conclusive statement on the oxalate yield (integral would correspond to 3%, Table 10, entry 3). Non-cyclic tridentate dipicolylamine (dpa) was likewise evaluated and a similar quantity (2%) of presumably $C_2O_4^{2-}$ was detected by CE (Table 10, entry 4). Interestingly, application of simple diethylenetriamine (dien) resulted in the formation of a blue/grey suspension and gave rise to a signal in the electropherogram corresponding to 28% oxalate yield (Table 10, entry 5). However, the absence of appropriate signals in the ^{13}C NMR spectrum and only a broad signal (major peak at 1578 cm^{-1}) in the distinct 1600-1700 cm^{-1} region prompted aggregation of further evidence. A twofold increase in the scale resulted in a slightly decreased integral equivalent to a 10% yield (Table 10, entry 6). Moreover, stirring CuI, $NaBPh_4$ and dien under Ar resulted in an analogous color change to provide a blue suspension and a matching integral of the CE signal corresponding to 26% oxalate yield (Table 10, entry 7). While the exact nature of this signal has not been elucidated, the latter result clearly demonstrates that it is not resulting from a presumable CO_2 reduction reaction. Indeed, the occurrence of a signal with (nearly) identical retention time as $C_2O_4^{2-}$ indicates the importance of combining CE analysis under the employed conditions with additional analytical methods (e.g. IR/NMR spectroscopy) for the unequivocal identification of oxalate.

Due to the absence of evidently improved CO_2 reductive coupling reactivity with the selected tridentate nitrogen donor ligands, a change towards phosphine ligands was pursued. Specifically, PNP-based pincer ligands, frequently applied in various catalytic processes largely due to their non-innocent properties, were envisaged as suitable candidates.[37–40,84–86,92,279,337–356]

Table 10: CO_2 treatment (constant atmosphere) of CuI, $NaBPh_4$, and different ligands in MeOH.

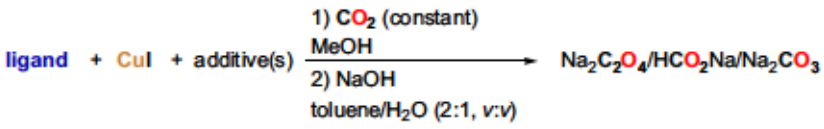

Entry	L	CuI/L/$NaBPh_4$ [equiv.]	*t* [h]	FTIR $\tilde{\nu}$ [cm^{-1}][a,b]	^{13}C NMR ($C_2O_4^{2-}$/ HCO_2^-/CO_3^{2-})[b]	CE ($C_2O_4^{2-}$) approx. yield [%][c]
1[d]	**174**	1/1/1	120	1629	x/x/✓	0.5
2[d]	**175**	1/1/1	120	1656, 1633	x/x/✓	<0.5
3[d]	**166**	1/1/1	119	1629	x/x/✓	3[h]
4[d]	**dpa**	1/1/1	120	1619, 1600	x/x/x[g]	2
5[d]	**dien**	1/1/1	119	1648 (br)	x/x/✓[g]	-[i]
6	**dien**	1/1/1	119	1655 (br)	x/x/✓	-[i]
7[e]	**dien**	1/1/1	120	x	x/x/x	-[i]
8[d,f]	**176**	1/-/1	119	x	x/x/x	<0.5
9[d,f]	**177**	1/-/1	118	x	x/x/x	<1
10[d,f]	**178**	1/-/1	120	x	x/x/x	<0.5
11[d,f]	**179**	1/-/1	120	1631	x/x/✓	<0.5
12[d]	**184**	1/0.5/1	118	1630	x/x/✓	29[j]
13[d]	**184**	1/1/1	114	1628, 1618	x/x/✓	5[j,k]

Detailed experimental procedures and results are presented in Table S 18. CuI/ligand/additive mixtures as indicated were treated with CO_2 in degassed methanol unless stated otherwise. [a]Vibrations between 1700-1600 cm^{-1} are reported. [b]x = not observed. [c]Note that approximate oxalate yields determined by CE are stated for signals coinciding with the signal of internal standard ($Na_2C_2O_4$) added to the samples after a first CE measurement. [d]GC analysis of the headspace was performed. [e]Conducted under Ar. [f]Isolated [Cu] employed instead of CuI+ligand. [g]Possibly residual paramagnetic Cu^{2+}, hence ^{13}C NMR signals might not be observable. [h]Integration hampered by disturbance of the baseline. [i]Blank experiment (Table 10, entry 7) highlights the signal cannot correspond to oxalate formed in the reaction (theoretical yields corresponding to the integral are given in Table S 18). [j]Further investigations for confirmation of the yield required. [k]Overlapping with another signal.

Furthermore, only few PNP-ligated Cu complexes have been reported in the literature[357–374] and even less have been applied in catalytic transformations.[352–356]

Hence, four simple ^{H}PNP-ligated Cu complexes of type [(^{H}PNP^{R})CuBr] were prepared in medium to good yields from the respective ^{H}PNP ligand and [(Me_2S)CuBr] in THF (Scheme 63). CuCl complexes[356] of the *iso*-propyl- and *tert*-butyl-substituted PNP ligands as well as **176**[370] had been described, while the phenyl- and cyclohexyl-substituted analogues have not previously been reported, to the best of our knowledge. All complexes feature a singlet in the $^{31}P\{^1H\}$ spectrum indicating the equivalence of both phosphorous atoms located at 3.1 ppm (**176**), 13.8 ppm (**177**), –5.1 ppm

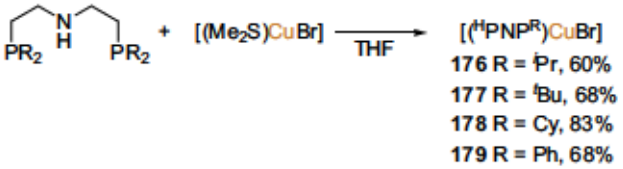

Scheme 63: Preparation of ^{H}PNP^{R}-ligated (R = ^{i}Pr, ^{t}Bu, Cy, Ph) Cu complexes starting from (Me_2S)CuBr.

(**178**), and –15.7 ppm (**179**). However, broadening of the signals indicates (partial) ligand exchange, presumably resulting in ligand-bridged complexes as previously reported.[361,374] Solid state structures (Figure 36) were assessed by X-ray diffraction with crystals obtained from THF/hexane at 5 °C (**176**)[XIV] and –32 °C (**177** and **178**) or from 1,2-dichlorobenzene/hexane at ambient temperature (**179**).

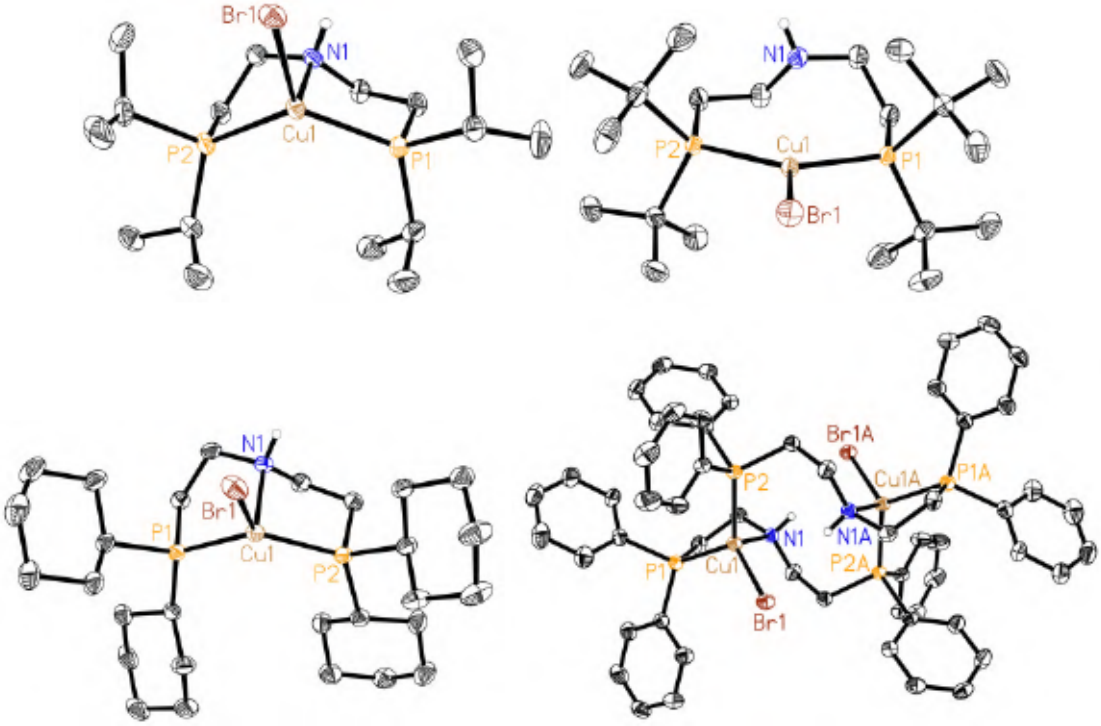

Figure 36: Molecular structures of **176**, **177**, **178** and **179** (thermal ellipsoid at 50% probability, non *N*-bound H atoms and co-crystallized solvent molecules (**178** and **179**) are omitted for clarity). Selected bond lengths [Å] and angles [°] for **176**: Cu-P, 2.2501(4), 2.2509(4); Cu-Br, 2.4468(3); Cu-N, 2.2401(13); P-Cu-P, 129.181(16); P-Cu-Br, 112.098(13), 118.165(14); Br-Cu-N, 106.20(3). Selected bond lengths [Å] and angles [°] for **177**: Cu-P, 2.2566(4), 2.2609(4); Cu-Br, 2.4200(2); P-Cu-P, 133.637(14); P-Cu-Br, 107.339(15), 119.974(16). Selected bond lengths [Å] and angles [°] for **178**: Cu-P, 2.2546(5), 2.2588(5); Cu-Br, 2.4552(3); Cu-N, 2.2231(16); P-Cu-P, 128.78(2); P-Cu-Br, 111.010(16), 119.620(17); Br-Cu-N, 107.11(4). Selected bond lengths [Å] and angles [°] for **179**: Cu-P, 2.2608(5), 2.2638(5); Cu-Br, 2.4679(3); Cu-N, 2.2100(16); P-Cu-P, 118.85(2); P-Cu-Br, 112.339(11), 113.960(11); Br-Cu-N, 117.67(4).

Complexes **176**, **177**, and **178** were identified as mononuclear structures, **179** forms ligand-bridged dimers in accordance with similar phenyl-substituted PNP-derived Cu complexes[361]. Furthermore, for **177** bearing sterically-demanding *tert*-butyl groups, coordination of the *N*-donor was not observed, mirroring the behavior observed for the analogous pyridine-derived PNP ligand.[366] Cu-P (2.2501(4)-2.2638(5) Å) and Cu-Br (2.4200(2)-2.4679(3) Å) bond distances displayed no significant discrepancies and are mostly in ranges reported for similar PNP-ligated CuBr complexes.[354,365,366,373] Cu-N distances for complexes **176**, **178**, and **179** were equally comparable (2.2100(16)-2.2401(13) Å). The major difference between the

[XIV] A different crystal structure of **176** ($P\bar{1}$) had previously been described.[370]

structure of **176** obtained from THF/hexane (this work) and that obtained from toluene relies in the crystal system, the former being monoclinic ($P2_1/c$) and the latter triclinic ($P\bar{1}$)[370]. Moreover, the reported Cu-N distances (2.2562(15) [2.2744(15)] Å)[370] are slightly longer than those observed herein. Overall, the structures of **176** and **178** were largely akin, with P-Cu-P angles of 129.181(16)° (**176**) and 128.78(2)° (**178**). The dinuclear structure of **179** as well as the tridentate coordination sphere of **177** resulted in altered coordination geometries which manifested in discernable differences in the bond angles, for instance P-Cu-P angles of 133.637(14)° (**177**) and 118.85(2)° (**179**).

After complete characterization, the reactivity of these pincer-ligated Cu complexes was evaluated. Unfortunately, literature-known **176**[370] and novel **177**, **178**, and **179**, did not provide CO_2 reduction products detectable by NMR spectroscopy, CE, IR spectroscopy and GC analysis of the reaction headspace upon treatment with CO_2 (Table 10, entries 8-11).

As mononuclear Cu complexes demonstrated no activity in CO_2 reductive coupling in yields comparable to those initially reported,[192] a dinuclear Cu complex was envisaged to possibly render enhanced activity due to close proximity of two metal centers. A suitable candidate for these investigations was developed by Chin and co-workers, namely 1,8-bis((1,4,7-triazonanyl)methyl)naphthalene (**183**).[297] The derived Cu^{II} complex was originally employed in phosphate diester cleavage of ribonucleic acid (RNA).[297] Later, the same group, in cooperation with Kim and co-workers, reported coordination of oxalate to form an oxalato-bridged Cu^{II} complex.[316] Interestingly, titration of Eosin-Y with the starting $CuCl_2$ complex resulted in quenching of the Eosin-Y fluorescence *via* interaction with the complex.[316] Addition of dicarboxylates, specifically oxalate, restored the fluorescence of Eosin-Y.[316] The respectable 4- to 200-fold selectivity for oxalate- over malonate- or glutarate-coordination, respectively, underpins the preferable coordination of the former for this specific ligand.[316]

Hence, preparation of a ligand combining the favorable coordination environment for a desired [Cu-(μ-C_2O_4)-Cu] product, provided by **183**,[316] with the presumable shielding of the Cu metal centers by allyl-substituents hampering coordination of an additional ligand[192] was pursued. Consequently, the *N*-allyl-substituted congener of **183** was prepared in four consecutive steps starting from **167** (Scheme 64). After formation of 1,4,7-triazacyclononane,[325] reaction with *N,N*-dimethylformamide dimethyl acetal in MeCN provided 1,4,7-triazatricyclo-[5.2.1.$0^{4,10}$]decane.[296] Subsequent substitution with 1,8-bis(bromomethyl)naphthalene and hydrolysis of the resulting ammonium salt, following modified literature procedures,[296,297] provided **183**. Finally, allylation with allyl bromide and KOH in toluene yielded **184**, which was characterized by NMR and IR spectroscopy as well as HR-MS, in mediocre yield (13%) over three steps starting from **182**. Reaction of this novel ligand with CuI in THF gave the dinuclear Cu^{I} complex **185** in 24% yield after crystallization and subsequent re-precipitation from THF. Crystals of suitable quality for single crystal X-ray diffraction were obtained by recrystallization of **185** from boiling THF.

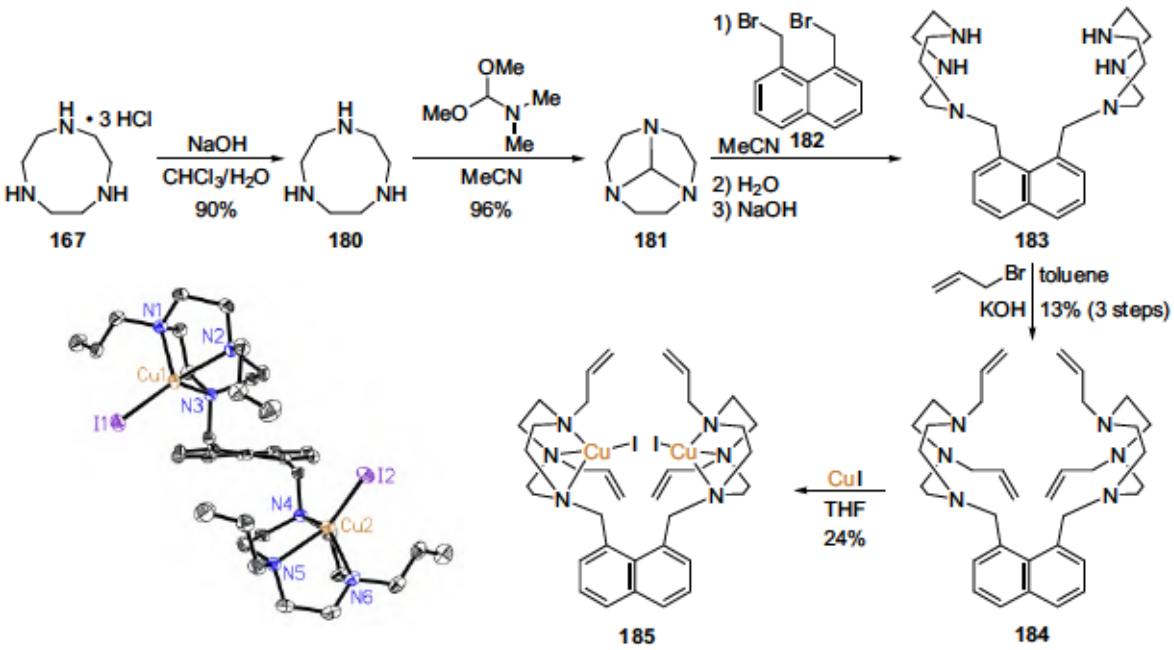

Scheme 64: Synthesis of novel 1,4,7-triazacyclononane-derivative **184** *via* allylation of **183**[297,316] and subsequent formation of its CuI complex **185**. One orientation of the molecular structure of **185** (hydrogen atoms omitted and thermal ellipsoids at 50%) is displayed on the left.

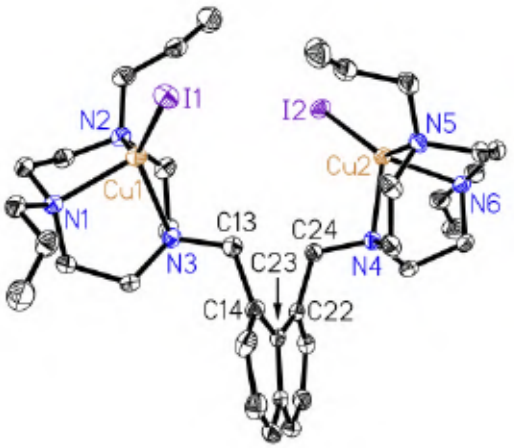

Figure 37: Molecular structure of **185** (thermal ellipsoid presented at 50% probability, H atoms are omitted for clarity).

Table 11: Selected bond angles and distances for complex **185**.

	Cu1	Cu2
Cu-N [Å]	2.153(3)	2.142(3)
	2.150(3)	2.157(3)
	2.225(3)	2.202(3)
Cu-I [Å]	2.4610(5)	2.4495(5)
N-Cu-N [°]	85.08(11)	85.13(12)
	82.59(10)	82.55(11)
	82.76(10)	83.43(11)
N-Cu-I [°]	135.69(8)	134.10(8)
	121.57(8)	128.29(8)
	131.32(7)	126.07(7)

The coordination geometries for both Cu metal centers are similar (Figure 37) and bond lengths and angles (Table 11) are in good agreement with each other, except for minor differences in the N-Cu-I angles. Both [Cu(*NNN*)I]-moieties are rotated with respect to the naphthalene backbone and the Cu-I units point into almost opposite directions (Scheme 64), arguably to minimize steric repulsion induced by Cu-I coordination in addition to the allyl substituents. The strain imposed on the rigid ligand backbone by introduction of iodo-ligands on the Cu centers and allyl-substituents on the 1,4,7-tacn scaffolds causes the observed deviance of planarity for the aromatic naphthalene frame. Comparison to the previously described $C_2O_4^{2-}$-bridged complex [Cu_2(**183**)(μ-C_2O_4)Cl(H_2O)]$^+$ (**186**), in which both metal

centers adopt an octahedral geometry,[316] highlights the induced steric crowding in **185**. Furthermore, the significantly increased deviation from planarity for the C13-C24 moiety compared to **186** becomes apparent from C13-C14-C23-C22 and C24-C22-C23-C14 torsion angles of 17.2(5)° and 18.7(5)° in **185** compared to 5.8(5)° and 7.4(4)° in **186**[316].
Since novel ligand **184** proved to be capable of forming the derived dinuclear Cu^{I} complex **185**, the reactivity of this complex toward CO_2 was assessed. For this purpose, CuI, $NaBPh_4$, and ligand **184** were treated with CO_2 in MeOH for five days and subsequently analyzed after NaOH treatment (Table 10, entry 12). Carbonate was detected by NMR spectroscopy in combination with a vibration at 1630 cm^{-1} in the IR spectrum. Surprisingly, a signal matching the retention time of oxalate was observed in the CE with an integral corresponding to 29% yield. This astonishing result, in view of the difficult reproducibility of the initially published oxalate formation,[192] might possibly indicate the supposed beneficial impact of two reactive Cu centers confined within a single complex. This confinement was envisaged to result in an ideal geometry for oxalate coordination, given the analogous literature precedent illustrating the privileged coordination of oxalate.[316] It is noteworthy that for the employed reaction scale (31 μmol of **184**) and assuming a 29% oxalate yield, a ^{13}C NMR signal is unlikely to be observed (as discussed previously). Moreover, when a 1/1/1 mixture of ligand **184** and $NaBPh_4$ was reacted under essentially unaltered conditions (Table 10, entry 13), a more intense vibration at 1628 cm^{-1} was observed in the IR spectrum, but the potential oxalate yield dropped to approx. 5%, albeit integration was complicated by an underlying signal. Based on the steric strain in dinuclear Cu complex **185**, a 1/1 ratio of Cu and **184** is assumed to result in the formation of mononuclear complexes similar to **168**. Thus, the outcome of the CO_2 treatment might perhaps indicate that a **184**-derived dinuclear Cu complex indeed facilitates CO_2 reductive coupling more effectively than mononuclear congeners. However, overlapping of potential signals with that of oxalate or other compounds resembling its retention time, as in the case of **dien** (Table 10, entry 7), cannot be excluded. Moreover, IR vibrations at approx. 1630 cm^{-1} were observed for numerous experiments conducted with various ligands (Table 10) or **127** in combination with solid bicarbonates that showed no sign of oxalate formation. Consequently, additional experimental evidence for the unambiguous identification of potentially formed oxalate is indispensable and part of on-going investigations.
In conclusion, reproduction of the results reported by Peacock and co-workers, namely CO_2 reductive coupling providing oxalate in 21% or 53% starting from CO_2 or $CsHCO_3$, respectively,[192] has not been accomplished. By preparing the BF_4^- analogue of the original oxalato dimer and establishing the possibility of removal of oxalate with aqueous NaOH,[193] an approach for reaction analysis by NMR and IR spectroscopy combined with CE was designed. Various parameters, such as solvent, temperature, illumination, various additives and ligands were evaluated in combination with solid bicarbonates, constant CO_2 atmosphere or CO_2 bubbling, and exposure to the atmosphere or O_2. In some cases, specifically in the absence of originally added $NaBPh_4$[192] and in the presence of strong reductant $NaC_{10}H_8$,

CE signals corresponding to oxalate yields of up to approx. 11% were observed, albeit additional evidence for the presence of oxalate is desirable as integrals and the signals themselves were found to be biased by hitherto unknown by-products or impurities. Complex **168** has, to the best of our knowledge, not been isolated and characterized prior to this work. Moreover, three novel aliphatic PNP-ligated CuBr complexes were prepared and fully characterized as part of these studies. Furthermore, a novel *N*-allylated bis(1,4,7-tacn) ligand bearing a naphthalene backbone was prepared and its derived CuI complex isolated. This novel ligand might indeed display promising parameters allowing for CO_2 reductive coupling, yet additional experimental data and further analysis of the CO_2 treatment products is required for a conclusive statement. All in all, the results showcase the prerequisite of careful analysis by a combination of different spectroscopic and/or separation techniques of the obtained products when investigating CO_2 reductive coupling. In fact, striking similarities in the FTIR spectra for C-O stretching frequencies of different carbonate/oxalate/formate species (Figures 28 and 31) clearly highlight this circumstance. In the original report, elemental analysis, IR spectroscopy and single crystal X-ray diffraction were utilized to analyze the reaction products and the initially crystallized oxalato-complex **128**, in addition to its magnetic properties. As traces of oxalate might indeed be formed in various reactions described herein, indicated by corresponding signals in the CE analysis, formation of **128** in sufficient quantities to form small crystals suitable for SC-XRD cannot be entirely precluded. However, the presented investigations pose a question on the reported yields for the reaction of interest, and thus render this protocol unsuitable as a starting point for mechanistic investigations and directed design of a revised system.

2.2.4 The Origin of Oxalate in CO_2 Reductive Coupling with Sodium Ascorbate

The results presented within this section have previously been reported elsewhere.[375]

CO_2 reductive coupling, especially when conducted with mild reducing agents, remains a challenging transformation, as indicated in previous sections. Hence, the report by Maverick and co-workers suggesting the formation of oxalate with the help of a dinuclear Cu^I complex and sodium ascorbate as mild reductant (E^{OX}=0.46 V *vs.* SCE)[82] comes as a surprise.[194] Dinuclear Cu^{II} complexes (**135** and **136**) were prepared as precursors employing a multidentate ligand based on a *meta*-xylene backbone functionalized with a 4-(2-pyridyl)-1,2,3-triazolyl substituent (Scheme 48).[194] These were subsequently reduced by sodium ascorbate to form the respective Cu^I complex which proved to be suitable for incorporation of oxalate, presumably formed *via* CO_2 reductive coupling, as a bridging ligand between both metal centers.[194] The constraint geometry of the precursor was even reported to effectively mediate C-C bond formation with atmospheric CO_2 yielding the oxalate complex **137** in up to 96% when starting from **135**.[194] As for the previous reports, no follow-up investigation was reported over the past years, to the best of our knowledge. Therefore, further investigations on the mechanism of this transformation and the origin of oxalate with the aim of constructive improvement of the system by potentially enabling a catalytic transformation, after reported removal of the oxalate,[194] are the major objectives for this section.

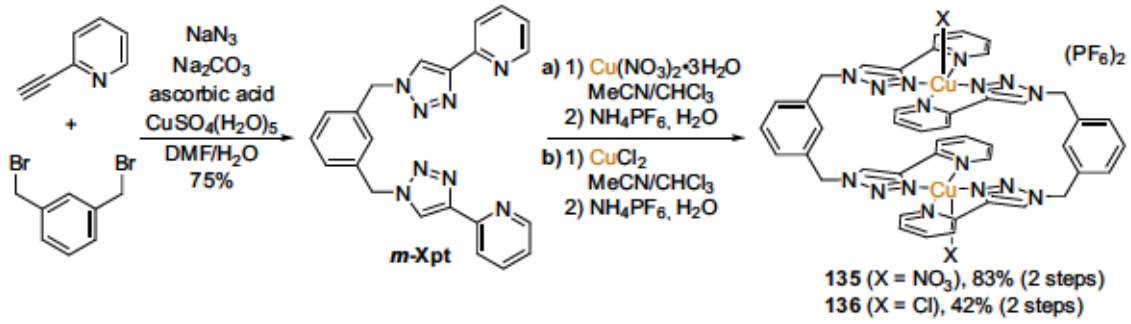

Scheme 65: Synthesis of *m*-xpt and subsequent formation of derived Cu^{II} complexes **135** and **136** following the reported route.[194,376,377]

Investigations were initiated with preparation of the required Cu^{II} complexes **135** and **136** following literature protocols (Scheme 65).[194,376,377] Subsequently, an initial attempt for the formation of oxalate was conducted according to the literature[194] by *in situ* reduction of **135** with sodium ascorbate in DMF and subsequent slow evaporation of the yellow Cu^I solution in air over two weeks (Scheme 66). Fortunately, the resulting green crystalline product was indeed identified as the desired oxalate complex by elemental analysis, single-crystal X-ray diffraction (determination of the unit cell revealed identical cell parameters to those reported[194]) and FTIR spectroscopy (Figure 39). A similar blue/green solid was obtained when starting from **136** and leaving the *in situ* prepared Cu^I solution evaporate in air over 11 d, verifying the possibility of oxalate formation under these conditions.

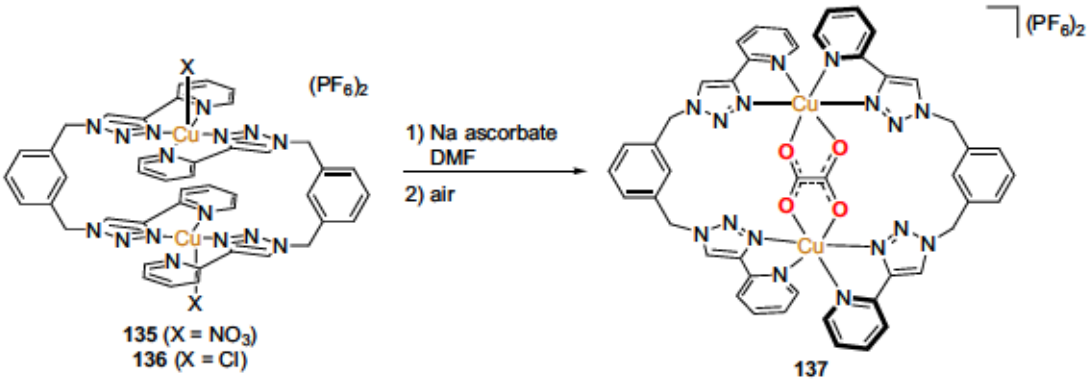

Scheme 66: *In situ* reduction of **136** or **135** with sodium ascorbate and subsequent evaporation in air yielding the oxalate complex **137**, as reported.[194]

This encouraging result heralded the start for further evaluating potential refinements of the system. The applicability of the oxalate formation by prolonged contact with air was slightly diminished by the time required for crystallization of the product. Consequently, an attempt to enhance the kinetics of the reaction was pursued. In the initial publication, treatment of the *in situ* formed Cu^{I} dimer **187** with pure CO_2 resulted in almost full conversion within 128 h.[194] Accordingly, an analogous reaction was conducted by *in situ* formation of $[Cu_2(m\text{-xpt})_2](PF_6)_2$ starting from **135** and sodium ascorbate and subsequent stirring under a CO_2 atmosphere (Scheme 67). Interestingly, no color change of the yellow solution was observed over a period of six days (Figure S 4). In addition, the UV/Vis spectrum of the reaction mixture provided no evidence for the formation of a Cu^{II} species (Figure 38). Yet, addition of air into the UV/Vis sample and the main reaction mixture caused a comparatively rapid change in color, which was traced by UV/Vis spectroscopy over 189 h. It is noteworthy that the resulting time-dependent UV/Vis spectra are in good agreement with those reported in the initial report.[194]

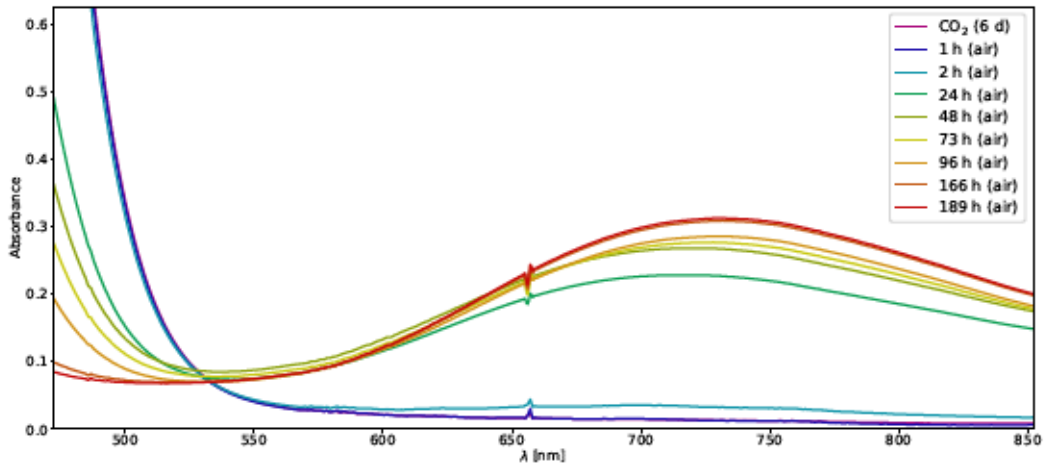

Figure 38: UV/Vis spectra of solutions of *in situ* formed **187** starting from **135** and sodium ascorbate in DMF (3.1 mM) after stirring under CO_2 (6 d) and subsequent oxidation by air over 189 h.

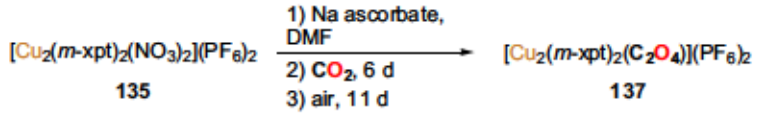

Scheme 67: *In situ* reduction of **135** and subsequent treatment with CO_2 for 6 d resulting in no reaction and follow-up reaction with air to yield **137**.

Subsequent FTIR spectroscopic analysis of the resulting product revealed the expected oxalate complex **137** (Figure 39). Surprisingly, the formation of oxalate in this specific case appeared to involve air while no reaction proceeded in the presence of only CO_2. Naturally, this encouraged a closer look at the experimental evidence originally provided for the CO_2 reductive coupling pathway. Apart from the crystallographic analysis of the resulting oxalate complex and the UV/Vis spectroscopic time profile of the reaction, ^{13}C-labeling of the resulting oxalate was reported to proceed by straightforward utilization of $^{13}CO_2$.[194] In this case, an isotopic shift of the presumable C-O vibration was observed from 1670 cm^{-1} to 1651 cm^{-1}, thus resulting in $\Delta\tilde{\nu}(^{12}C/^{13}C)$=19 cm^{-1}.[194] Compared to an isotopic shift reported for a similar Cu oxalate complex, this difference seemed rather small.[193] Moreover, simple estimation[378] with the assumption of identical force constants for ^{12}C and ^{13}C predicted a shift of approximately 37 cm^{-1}. In addition, the IR spectroscopic analysis is, yet again, sophisticated by the comparatively close proximity of the presumable C-O vibration at ~1670 cm^{-1} and possibly C=C vibrations in the starting material **135** or even the Cu^{I} complex **187** (Figure 39), which was prepared following the literature by reaction of **135** with sodium ascorbate and subsequent precipitation by vapor diffusion of Et_2O into the DMF solution.[194] Most importantly, **187** synthesized *via* this procedure[194] depicted a similar IR band at ~1661 cm^{-1}, nearly identical to that of the oxalate complex **137**. **187** still contained DMF, evident from the NMR spectroscopic analysis (Figure S 81) and a direct comparison with the FTIR spectrum of DMF revealed that this band in fact coincides with the C-O vibration of DMF. Likewise, the crystallized oxalate complex was reported to contain DMF,[XV] hence the proposed isotopic shift could presumably result from varying DMF content in the analyzed samples and misinterpretation of the compiled IR data.

In summary, these observations hinted at an oxidative pathway for oxalate formation in sharp contrast to the described[194] CO_2 reductive coupling. Apparently, sodium ascorbate represents an obvious source for the observed oxalate, as ascorbic acid oxidation by Cu is well-known.[216,379–383] As a matter of fact, degradation of vitamin C by Cu-based boilers was identified as one plausible cause contributing to *sea scurvy*, due to faster decomposition compared to boilers built from iron.[384] Moreover, oxalate has frequently been observed as a product of the oxidative decomposition of ascorbic acid/ascorbate in the presence of strong oxidations, such as NaIO[385] or $NaIO_4$[386], in the presence of Cd,[387] Pt,[388] Pd,[388] Gd,[389,390] Co,[389] Fe,[391,392] and even with simple oxygen[385,393,394]. In addition, Chakravorty and co-workers described a bpy-ligated dinuclear Cu^{II} complex capable of catalytic oxidation

[XV] Two molecules of DMF were reported to co-crystallize in the literature,[194] while elemental analysis presented herein suggest only one molecule of DMF.

of ascorbic acid into oxalic acid with O_2 as the terminal oxidant and obtained the solid state struc

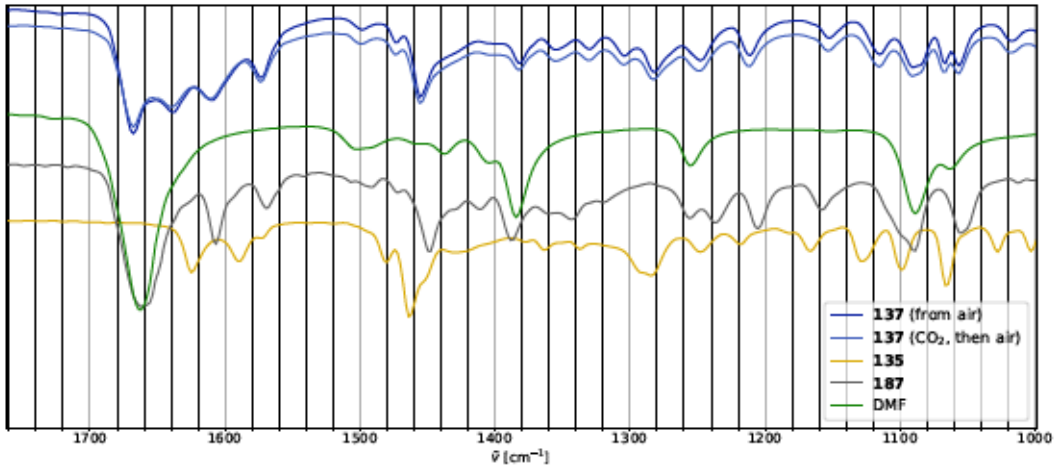

Figure 39: FTIR spectra of the product formed upon air exposure after stirring under CO_2 atmosphere and isolated **137** prepared *via* evaporation of *in situ* formed **187** in air. IR spectra of **135**, **187** and DMF are displayed for comparison.

Evaluation of this hypothesis was pursued by reaction of *in situ* generated **187**, again starting from sodium ascorbate and **135**, with gaseous O_2 under exclusion of CO_2 and air (Scheme 68). Oxidation of **187** proceeded rapidly, and a distinct color change of the yellow solution to green was observed (Figure S 6). Oxygen treatment was continued for a five-day period, the solvent removed and the yellow/green solid subjected to FTIR analysis (Figure 40). Fortunately, thus obtained product displayed an IR spectrum in good agreement with that of the oxalate complex **137**. It is noteworthy that essentially identical products were obtained upon prolonged reaction with O_2 (7 d).

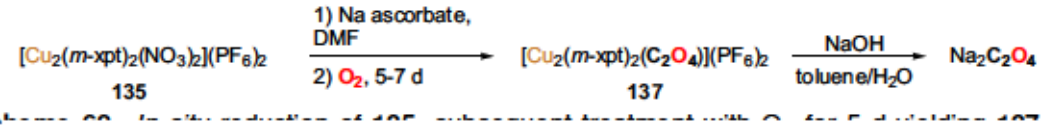

Sc[illegible] *In situ* reduction of **135**, subsequent treatment with O_2 for 5 d, yielding **137** and sul

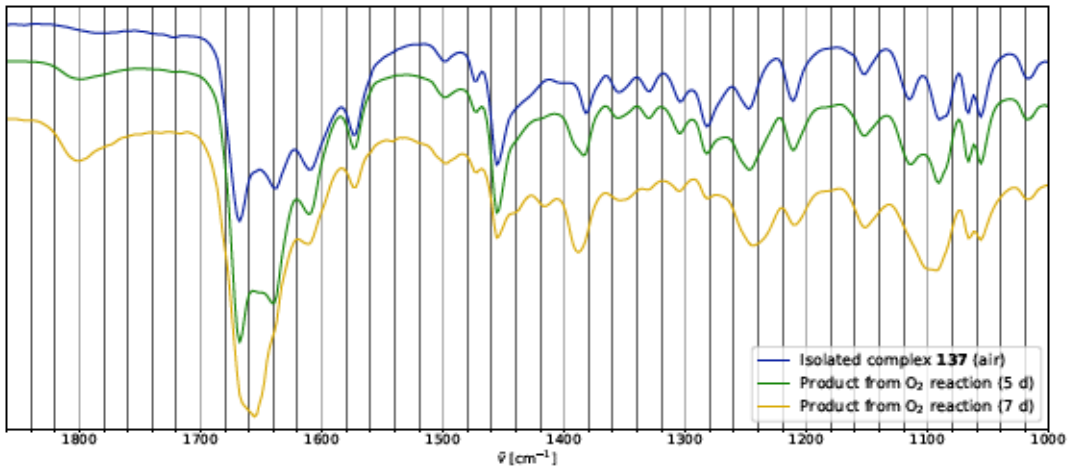

Figure 40: FTIR spectra of **137** and the products obtained after reaction of *in situ* formed **187**, starting from sodium ascorbate and **135**, with O_2.

The matching IR spectra of the O_2 product and the previously isolated oxalate complex in combination with the observations discussed earlier clearly supported the validity of the proposed oxidative degradation pathway. However, the initial report already indicated the complicated assignment solely based on FTIR spectroscopy.

Thus, additional experimental evidence for oxalate formation in the absence of CO_2 was collected by detection of isolated $C_2O_4^{2-}$. In the original publication, treatment of **137** with dilute HCl or HNO_3 is reported to yield oxalic acid.[194] However, repetition of this experiment failed and only DMF was observed in the ^{13}C NMR spectrum. As discussed in section 2.2.3, NaOH treatment[193] should facilitate isolation of $Na_2C_2O_4$. To verify the suitability of this procedure with **137**, synthesis of the complex by insertion of $C_2O_4^{2-}$ into the starting material **135** was performed, as described in the literature.[194] Treatment of thus prepared **137** with NaOH and subsequent analysis of the aqueous layer by NMR spectroscopy indeed revealed the possibility of $C_2O_4^{2-}$ extraction (Figures 41 and S 176). Accordingly, the same procedure was applied to the product obtained from slow evaporation in air and again testified the formation of oxalate (Figure S 178). In addition, a signal corresponding to formate was observed in both the ^1H and the ^{13}C NMR spectra, likely resulting from base hydrolysis of co-crystallized DMF.[395]

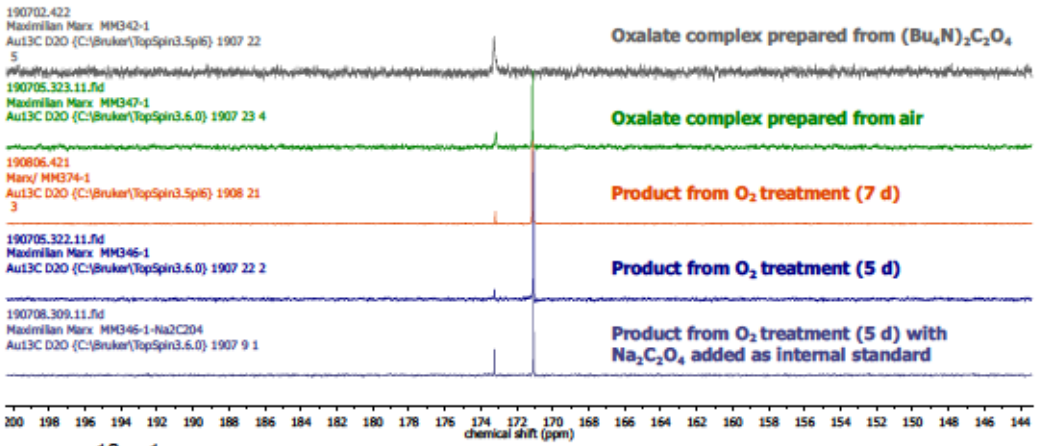

Figure 41: $^{13}C\{^1H\}$ NMR spectra of the aqueous layers obtained upon NaOH treatment of **137** prepared from **135** and: a) $(Bu_4N)_2C_2O_4$; b) air and Na ascorbate; c) O_2 and Na ascorbate (7 d); d) O_2 and Na ascorbate (5 d) ($Na_2C_2O_2$ was added to the sample as an internal standard).

Finally, NaOH treatment in degassed solutions under an Ar atmosphere of the product obtained from the reaction with O_2 also gave rise to the corresponding oxalate signal in the ^{13}C NMR spectrum (Figure 41), validated by addition of $Na_2C_2O_4$ as internal standard to the same NMR solution. This additional identification of oxalate unequivocally verifies the oxidative degradation of ascorbate as its true origin.

Further evidence proving the initially incorrect assignment of the IR band were obtained by preparation of the ^{13}C labeled oxalate complex with $(Bu_4N)_2{}^{13}C_2O_4$ which showed an isotopic shift of 39 cm^{-1}.[XVI] This value was not only closer to that expected from literature

[XVI] Preparation of ^{13}C labeled **137**, its analysis by HR-MS and IR spectroscopy as well as DFT calculations were conducted by F. Khamespanah and Prof. Dr. A. W. Maverick.

precedent,[193] but also found in accordance with DFT calculation-based estimations. Furthermore, no CO_2 incorporation into the oxalate complex was observed by HR-MS when a mixture of $^{13}CO_2$ and O_2 was reacted with *in situ* prepared **187** utilized.[XVII] Finally, in the absence of ascorbate, **187** was found to react with CO_2 and O_2 to yield a trinuclear carbonato complex of the formula $[Cu_3(m\text{-xpt})_3(\mu_3\text{-}CO_3)](BF_4)_4$ (**188**).[XVIII]

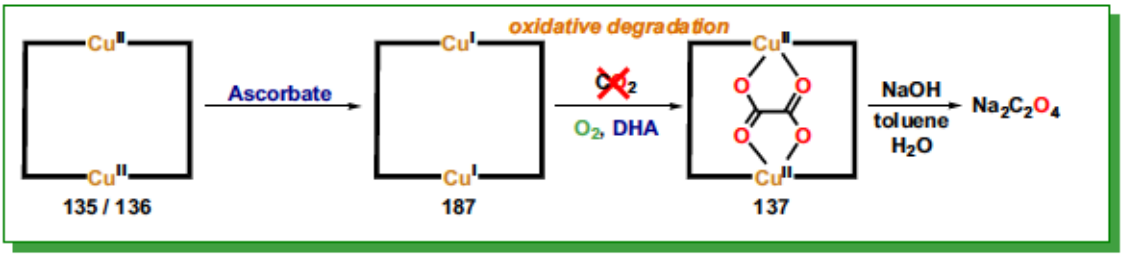

Scheme 69: Updated scheme comprising the reactivity of *m*-xpt-ligated Cu complexes in the presence of ascorbic acid and O_2 based on the experimental results reported herein and elsewhere.[375]

In conclusion, the reported CO_2 reductive coupling reactivity with dinuclear Cu^{II} complexes and sodium ascorbate as mild reductant[194] was investigated and revealed a reaction pathway entirely contrasting that initially assumed. Oxygen was found to be a prerequisite for the formation of oxalate and no reaction was observed in the sole presence of CO_2. Moreover, sophisticated IR spectroscopic identification of the product again indicated the necessity of additional analytical techniques for analysis of potential CO_2 reductive coupling reactions. The true origin of observed oxalate was identified to be oxidative degradation of sodium ascorbate, utilized for reduction of the Cu^{II} starting materials. Experimental evidence for the oxidative degradation pathway was obtained by reaction with O_2 under strict exclusion of air or CO_2 and subsequent analysis by FTIR spectroscopy and ^{13}C NMR after extraction of $Na_2C_2O_4$ by NaOH treatment of the oxidation product. Further evidence was provided by Maverick and co-workers by isotopic-labeling experiments precluding incorporation of CO_2 into the resulting oxalate. Based on these results, the initially reported reactivity of *m*-xpt-ligated Cu complexes required significant revision (Scheme 69). After *in situ* formation of **187**, reaction with dehydroascorbic acid (DHA) and O_2 accounts for the formation of oxalate complex **137** which allows for $C_2O_4^{2-}$ isolation by NaOH treatment. Moreover, **187** undergoes oxidation in the presence of O_2 and CO_2 (or air) to form the trinuclear carbonate **188**, provided no ascorbate or DHA is present. While the results presented herein preclude further improvements of this protocol for enhanced CO_2 reductive coupling, they unequivocally highlight the importance of considering reaction pathways apart from the coveted reactivity to explain the observed product; especially when studying challenging transformations.

[XVII] Reaction with $^{13}CO_2/O_2$ was conducted by F. Khamespanah and Prof. Dr. A. W. Maverick.

[XVIII] $[Cu_3(m\text{-xpt})_3(\mu\text{-}CO_3)](BF_4)_4$ was prepared and analyzed by F. Khamespanah, Dr. U. R. Pokharel, Dr. F. R. Fronczek and Prof. Dr. A. W. Maverick.

2.2.5 CO_2 Reductive Coupling Based on Cu and α-Ketocarboxylates

Fujisawa and co-workers reported a sophisticated system for the formation of a dinuclear Cu oxalate complex that was obtained starting from a Cu^{II} α-ketocarboxylate complex bearing a scorpionate-type ligand (Figure 46).[193] Formation of oxalate was observed upon treatment with air, O_2 or CO_2/O_2 (1:1), whereas pure CO_2 did not facilitate this transformation.[193] Nevertheless, incorporation of CO_2 into product oxalate was confirmed by isotopic labeling with $^{13}CO_2$.[193] Moreover, reaction of the tris(pyrazolyl)borate ligand and CuCl with Et_4NHCO_3 reportedly yielded the same oxalate complex, identified by a change in color to light blue in combination with an IR signal at 1650 cm^{-1}.[193] Interestingly, the reactivity of the described α-ketocarboxylate contrasts the well-known decarboxylation reactivity commonly observed for similar Cu or Fe α-ketocarboxylates.[396–400] Besides, the initial presence of Cu^{I} or Fe^{II} centers constitutes a prerequisite for their oxidative decarboxylation chemistry by activation of O_2,[396–400] while formation of oxalate was possible starting from the Cu^{II} α-ketocarboxylate complex.[193] This peculiar reactivity was attributed to the distinct properties of the specific α-ketocarboxylate allowing for the formation of a $CO_2^{\bullet-}$ intermediate which undergoes oxalate formation.[193] However, in light of identification of oxidative degradation of sodium ascorbate resulting in the formation of oxalate previously assumed to result from CO_2 coupling,[194] further evaluation of the origin of oxalate for this protocol appeared advisable. Especially the uncommon requirement for O_2 in a reductive transformation and the possibility of a C2-C3 bond scission observed for certain Co[401] and Fe[396,402] complexes resulting in oxalate formation prompted additional in-depth investigations.

Investigations were initiated by preparation of the tris(pyrazolyl)borate ($Tp^{iPr,iPr}$) ligand **190** *via* a modification of literature protocols (Scheme 70).[331,403] For preparation of the α-ketocarboxylate complex, an alternative pathway *via* the CuBr complex of **190** instead of the CuCl congener utilized by the Fujisawa group[193] was pursued.[404] Interestingly, upon recrystallization of the red solid formed from $CuBr_2$ and **190** in acetone,[404] a mixture of dark-red crystals of the complex of interest **191** and colorless crystals of an unforeseen Cu^{I} complex **192** were obtained and identified by single crystal X-ray diffraction (Figure 42). The origin of the latter complex is unknown and might arise from residual 3,5-di-*iso*-propylpyrazole in the employed ligand. However, the re-

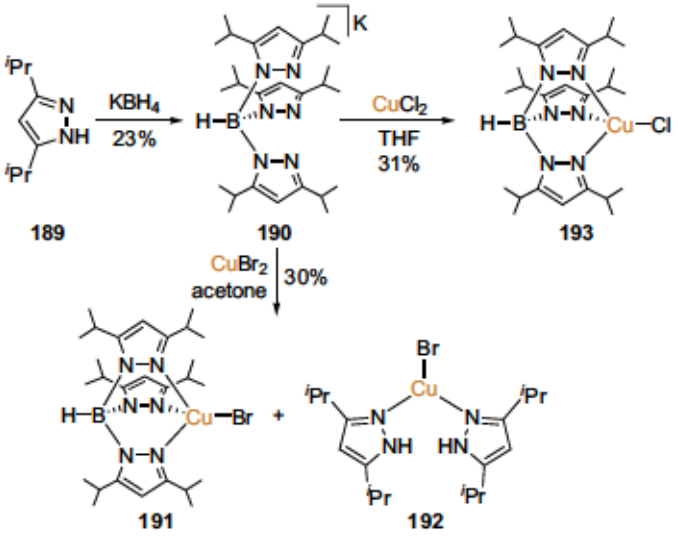

Scheme 70: Synthesis of Tp ligand **190** and its conversion into derived Cu^{II} halide complexes **193** and **191**, the latter being accompanied by formation of **192**.

quirement of Cu^{II} reduction and the well-known capability of $Tp^{R,R}$ ligands to decompose into the free pyrazole,[405] suggest its formation *via* degradation of the ligand and simultaneous reduction of $CuBr_2$. In contrast to the result obtained with $CuBr_2$, reaction of **190** with $CuCl_2$ resulted in formation of **193**.[404]

Cu adopts a distorted tetrahedral geometry in complex **191** with N-Cu-N angles of 90.91(8)°, 92.63(8)°, and 93.00(8)°, respectively, as well as N-Cu-Br angles of 117.18(6), 123.04(6), and 130.57(6)°. Cu-N distances of 1.948(2) Å, 1.950(2) Å, and 2.085(2) Å are comparable to those observed in its Cl congener **193** (1.980(13)/1.985(11) Å).[404] Complex **192** had previously been synthesized by reaction of the respective pyrazole with CuBr and indicated interesting luminescence properties upon excitation at 277 nm.[406] In **192**, Cu adopts a trigonal coordination geometry with N-Cu-Br angles of 107.81(4)° and 108.85(4)° and a N-Cu-N angle of 141.81(5)°, as expected due to the higher steric demand of sterically encumbered 3,5-di-*iso*-propylpyrazole. Cu-N (1.9371(12)/1.9380(12) Å) and Cu-Br (2.5165(3) Å) distances are slightly shorter than those observed for its phenyl- (Cu-N: 1.9432(18)/1.9608(19) Å; Cu-Br: 2.5328(5) Å) and *tert*-butyl (Cu-N: 1.961(4)/1.969(4) Å; Cu-Br: 2.561(4) Å) analogues.[406] Interestingly, a comparatively short Cu-Cu distance of 2.9343(4) Å for each pair of molecules was observed. However, this Cu-Cu distance is longer than the sum of the van der Waals radii, thus, no d^{10}-d^{10} interaction is assumed.[XIX]

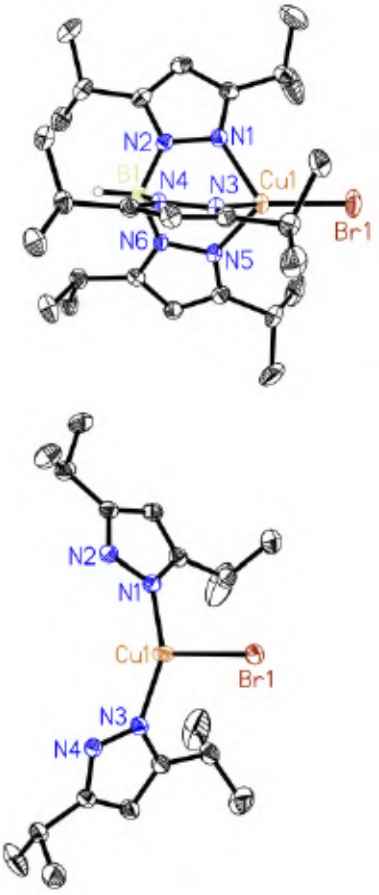

Figure 42: Molecular structures of complexes **191** and **192** (thermal ellipsoid at 50% probability, H atoms are omitted for clarity).

Due to the observed formation of **191**/**192** mixtures, the prerequisite α-ketocarboxylate complex **129** was obtained following the literature route by reaction of sodium 3-methyl-2-oxobutyrate (**194**) with **193** and subsequent recrystallization (Scheme 71).[193] To gain insight into the origin of oxalate formation, the analogous $^{13}C_5$ complex **196** was prepared *via* the same protocol starting from sodium $^{13}C_5$-3-methyl-2-oxobutyrate (**195**). Successful isolation of the $^{13}C_5$-labeled complex was confirmed by ESI HR-MS analysis of both complexes (**129** and **196**). Moreover, labeling of the α-ketocarboxylate ligand caused the expected isotopic shift of the C-O stretching frequencies (Figure 43) from 1687/1666 cm^{-1} in **129** to 1644/1625 cm^{-1} in **196** ($\Delta\tilde{\nu}(^{12}C/^{13}C) \approx 42$ cm^{-1}).

XIX The observed Cu-Cu distance is shorter than that in analogous complexes bearing diphenyl- and di-*tert*-butyl-substituted pyrazole ligands (>4 Å),[406] but significantly longer than Cu-Cu distances in tetranuclear pyrazole-coordinated [Cu(*NNN*)I] pincer complexes (2.6127(8) Å) or metallic copper (2.556 Å).[407]

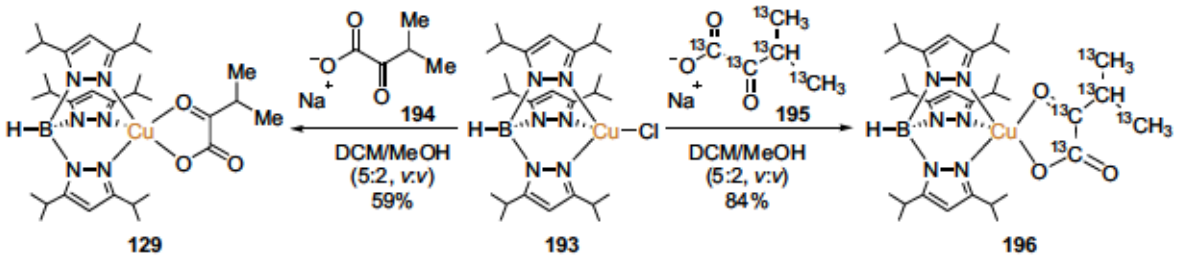

Scheme 71: Synthesis of α-ketocarboxylate complex **129**[193] and its $^{13}C_5$ analogue **196**.

With these complexes in hand, the straightforward exposure to air in DCM solution was explored, as this was reported to yield the oxalato-bridged dimer **130** resulting in a distinct shift of the C-O stretching frequency to ca. 1655 cm^{-1}.[193] Exposure of a CH_2Cl_2 solution of **129**, layered with heptane, to air for 18 h (Scheme 72) indeed resulted in the formation of a green-blue solid displaying the described C-O vibration at 1654 cm^{-1} in addition to another broad vibration at 1602 cm^{-1} not observed in the literature[193] (Figure 43). Nevertheless, the IR spectrum suggested formation of the expected oxalate complex **130** as the major product in addition to presumably full conversion of starting **129**, indicated by the absence of the 1687/1666 cm^{-1} signal.

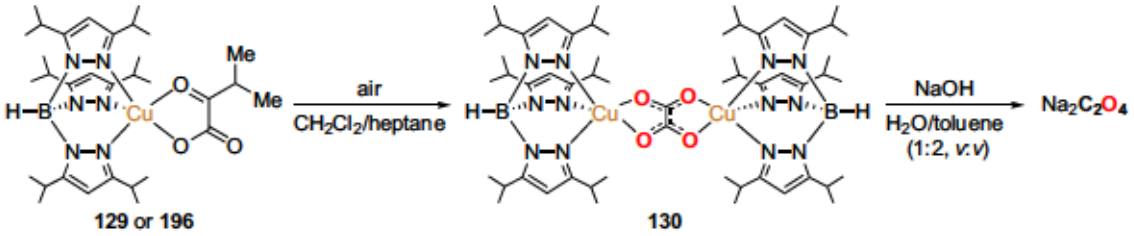

Scheme 72: Reaction of complex **129** or its ^{13}C-labeled analogue **196** with air in DCM/heptane an

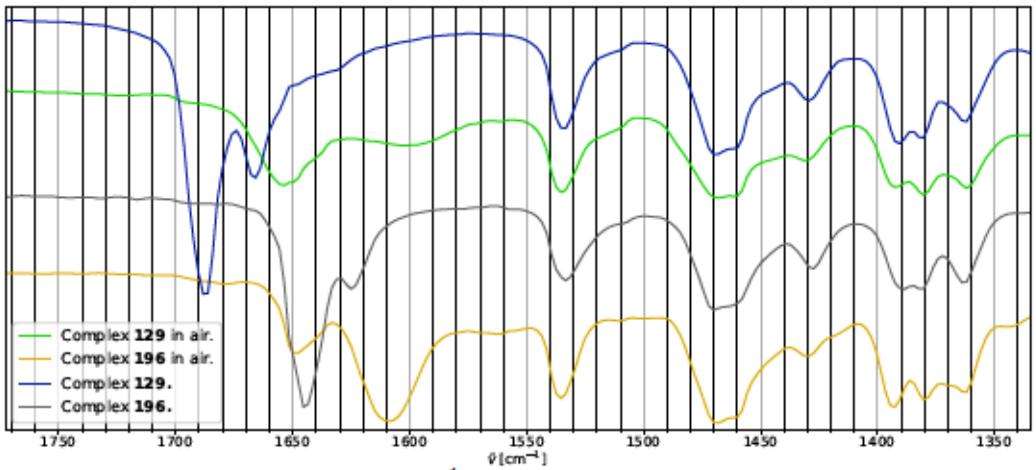

Figure 43: FTIR spectra (1750-1350 cm^{-1}) of **129** and **196** and the products obtained from air exposure of these in DCM/heptane.

Likewise, prolonged contact of a heptane-layered dichloromethane solution of **196** with air under identical conditions resulted in an analogous shift of the C-O vibration from 1644 cm^{-1}

and 1625 cm^{-1} to 1609 cm^{-1}, hence in agreement with the initially reported absolute $\Delta\tilde{\nu}$ of 40 cm^{-1} and the C-O vibration at 1607 cm^{-1} reported for the product obtained with $^{13}CO/O_2$[193]. Moreover, a significantly broadened signal at 1562 cm^{-1} and a signal at 1649 cm^{-1} were detected. While the former likely resembles an analogous species to that observed at 1602 cm^{-1} for the non-^{13}C-labeled starting material, given the 40 cm^{-1} red-shift, the latter could correspond to two separate species: a) non-converted starting material **196** with its C-O signal at 1644 cm^{-1}; or b) the ^{12}C-containing oxalate complex **130** resulting from incorporation of CO_2 from the atmosphere, as proposed in the initial publication[193].

For further identification of oxalate, treatment with NaOH in a H_2O/toluene mixture was conducted according to the literature procedure[193] and the resulting aqueous extract analyzed by NMR spectroscopy and capillary electrophoresis. In both cases, the formation of oxalate was confirmed by CE and oxalate yields of 6% and 21%[XX] were detected for reactions starting from **129** and **196**, respectively (CE diagrams can be found in section 4.15.4 in the appendix). Moreover, the oxalate signal was observed by NMR spectroscopy (Figure 44) in the case of **196**, indicating at least partial incorporation of the ^{13}C-labeled α-ketocarboxylate into the product with respect to the small reaction scale (9 µmol). Furthermore, signals corresponding to carbonate and formate were observed by NMR spectroscopy, suggesting the formation of by-products in the conversion of the α-ketocarboxylic acid. Most importantly, intense signals corresponding to 2-hydroxy-2-methylpropanoic acid (184.1 ppm (d), 73.7 ppm (dt), 26.4 ppm (d))[408] and less intense signals corresponding to 2-methylpropanoic acid (187.9 ppm (d), 36.9 ppm (dt), 19.3 ppm (d))[409] were observed in the ^{13}C NMR spectrum of the aqueous extract.[XXI]

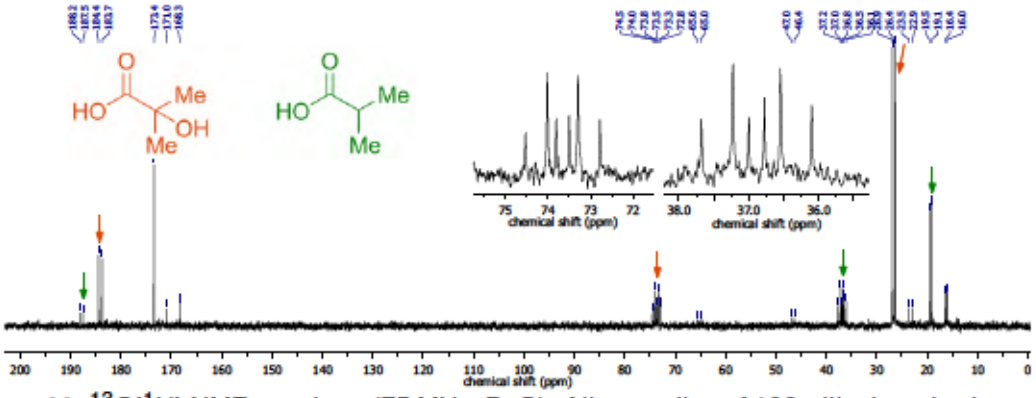

Figure 44: $^{13}C\{^1H\}$ NMR spectrum (75 MHz, D_2O) of the reaction of **196** with air and subsequent NaOH treatment.

The presence of both carboxylic acids indicates substantial decarboxylation of the α-ketocarboxylate, in agreement with the common reactivity of analogous Tp-ligated α-ketocarboxylate complexes and the proposed formation of a $CO_2^{\bullet-}$ species.[193,396,397] In addition, the formation of [Cu(Tp^{iPr,iPr})($O_2CC(CH_3)_2(OH)$)] was observed by Fujisawa and co-workers when

[XX] Yields are stated assuming a bimolecular mechanism and not taking into account the efficiency of oxalate removal as the procedure was initially reported for this system.[193]

[XXI] Literature ^{13}C NMR spectra were reported for the carboxylic acids in $CDCl_3$.[408,409]

dry air was utilized,[XXII] while [Cu(Tp^{iPr,iPr})($O_2CH(CH_3)_2$] was independently prepared.[193] Neither of these complexes were found capable of forming oxalate complex **130**.[193]
Despite the detection of oxalate by CE and NMR, the low oxalate yield assessed by CE in comparison with the literature (89% of **130**[193]) was unexpected given the considerable amounts of 2-methylpropanoic acid derivatives detected by NMR spectroscopy. Moreover, the IR stretching frequency observed at 1649 cm^{-1} for the reaction of **196** could correspond to residual starting material which would indicate non-effective CO_2 incorporation from the atmosphere. For gaining additional insight into the oxalate formation, the treatment of **129** and **196** with a CO_2/O_2 mixture (approx. 1:1) was conducted, as reported by the Fujisawa group[193] (Scheme 73). Due to the enhanced CO_2 concentration compared to the approximate 411 ppm in the atmosphere,[26] an increased incorporation of CO_2 into oxalate would be expected and should hence be readily detectable by IR spectroscopic analysis.

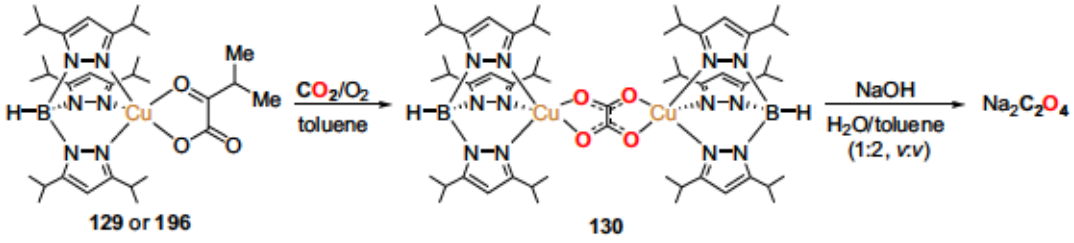

Scheme 73: Reaction of complex **129** or its ^{13}C-labeled analogue **196** with CO_2/O_2 (~1:1) in toluene and subsequent removal of oxalate with NaOH.

Again, stirring a solution of **129** in toluene under a CO_2/O_2 atmosphere for 42 h resulted in the described change in the FTIR spectrum giving rise to a new vibration at 1659 cm^{-1}, presumably corresponding to the respective oxalate complex,[193] in addition to the broad vibration at 1600 cm^{-1} (Figure 45). Thus, for **129** the obtained IR spectra for exposure to CO_2

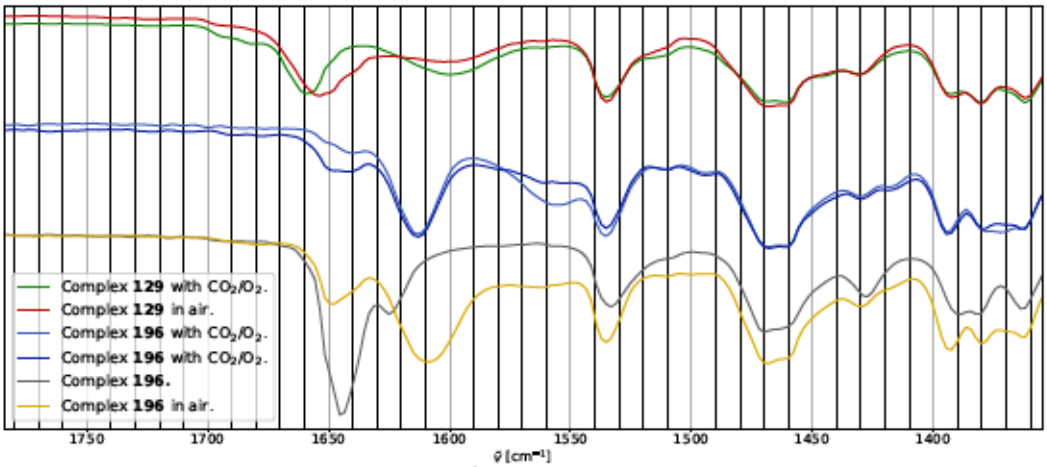

Figure 45: FTIR spectra (1750-1350 cm^{-1}) of the products obtained by CO_2/O_2 treatment of **129** and **196** in toluene, the products obtained from air exposure of these in CH_2Cl_2, and **196** for comparison.

[XXII] No comment regarding dry air can be found in the supplementary material.[193]

The same trend was observed for **196** where the distinct C-O vibration was shifted upon reaction with CO_2/O_2 for 67 h to 1613 cm^{-1}. Moreover, a broad signal at 1555 cm^{-1} (1561 cm^{-1} for an identical reaction) was observed, again likely resembling the 1600 cm^{-1} species in the reaction of **129**. In addition, the vibration at ~1640 cm^{-1} was observed as for the air exposure of **196**. Interestingly, the intensity of this band compared to the air exposure was not significantly increased and is nearly identical to that of the starting material ($\Delta\tilde{\nu}$ =~4 cm^{-1}) with an increased shift compared to the product obtained from **129** ($\Delta\tilde{\nu}$ =~15 cm^{-1}). These results might indicate inefficient incorporation of CO_2 into the oxalate product even in the presence of enhanced CO_2 concentration, albeit broadening of the signal at ~1640 cm^{-1} renders a conclusive statement on its origin, either residual **196** or ^{12}C-incorporated oxalate complex **130**, impossible. More elucidative were the ^{13}C NMR spectra of the aqueous layer obtained after NaOH treatment which again indicated the formation of 2-hydroxy-2-methylpropanoic acid as the major product accompanied by 2-methylpropanoic acid, carbonate, and the desired oxalate for the reaction of **196** (Figure S 201 and S 203), while only the CH_3 signals of these carboxylic acids were observed for **129** due to the low concentration (Figure S 199). Furthermore, the corresponding oxalate yields assessed by CE were 6% for **129** and 1-2% for **196**, thus significantly lower than reported.[193]

Additional evidence for the inefficacious incorporation of CO_2 into the observed oxalate was gained from HR-MS analysis of the aqueous extracts obtained after NaOH treatment.[XXIII] For the reactions under CO_2/O_2 starting from complex **196**, $Na^{13}C_2O_4^-$ was detected with low intensity while no oxalate ions with mixed isotopic constitution were observed utilizing this method (Figure 46). Similar observations were made for the reaction of **196** with air. Moreover, 2-hydroxy-2-methylpropanoic acid was identified for reactions of **129** or **196** with air or CO_2/O_2. It is noteworthy that traces of $Na^{12}C_2O_4^-$ were found for the reaction of **196** with air. Nevertheless, the absence of $Na^{12}C^{13}CO_4^-$ suggests an inefficient incorporation of gaseous CO_2.

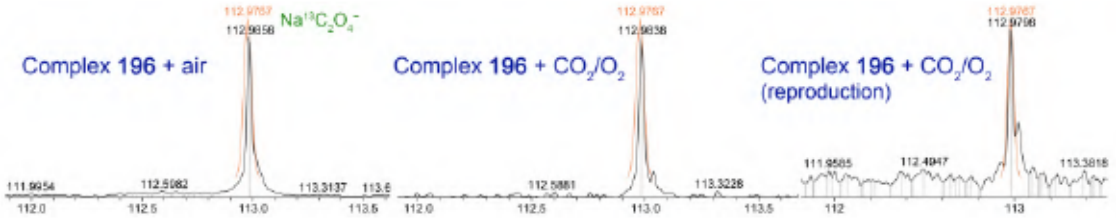

Figure 46: HR-MS (ESI) of the aqueous solution of the reaction of **196** with air or CO_2/O_2 and subsequent NaOH treatment (simulated exact *m/z* values are presented in orange).

In the initial publication, the necessity of traces of H_2O was suggested to constitute a prerequisite and the formation of the $[Cu(Tp^{iPr,iPr})(O_2CC(CH_3)_2(OH))]$ was reported to proceed in the absence of these traces.[193] However, the reported experimental procedures for the preparation of $[Cu(Tp^{iPr,iPr})(O_2CC(CH_3)_2(OH))]$ and desired complex **130** are surprisingly identical.[193] Moreover, it is clearly indicated that the employed solvents were either pur-

[XXIII] HR-MS analysis of the aqueous solutions was conducted by Dr. H. Frauendorf (University of Göttingen).

chased anhydrous (octane) or dried over common drying reagents (heptane and toluene over Na/benzophenone ketyl and DCM over P_4O_{10}).[193] Thus, the nature of the reported H_2O prerequisite[193] is not entirely explicable. Another complication of the analysis emerges from comparison of the FTIR data of complex **130** and [Cu(Tp^{iPr,iPr})($O_2CC(CH_3)_2(OH)$)], as their distinct C-O vibrations appear to be virtually identical with 1656 cm^{-1} for the latter and 1653 cm^{-1} for **130**.[193] It is important to note that formation of **130** was reported to proceed even upon treatment of [Cu(Tp^{iPr,iPr})] with Et_4NHCO_3 in various solvents[XXIV].[193] However, the formation of oxalate was only confirmed by IR spectroscopy which displayed *"a strong characteristic band around 1650 cm^{-1}"*,[193] an experimental evidence which was previously shown to be potentially misleading in case different compounds containing C=O bonds could be formed (see e.g. Figure 28).

Based on the contradictory information with respect to the necessity of possible traces of H_2O and the observations reported herein, which were not indicating a noticeable incorporation of CO_2 into the oxalate product, apart from the inconclusive band at ~1640 cm^{-1}, another plausible reaction mechanism was investigated. While decarboxylation was unambiguously observed upon exposure of **129** or **196** to air or O_2/CO_2, the low oxalate yields obtained for these reactions might indicate that oxalate formation is not coupled with decarboxylation, albeit decomposition *via* C-C bond scission of the α-ketocarboxylate was proposed to yield the active $CO_2^{\bullet-}$ intermediate.[193] The necessity of the α-keto-functionality was proven by the absence of oxalate formation when the analogous 2-methylpropionate complex was treated with CO_2/O_2 or O_2.[193] However, the analogous complex [Cu(Tp^{iPr,iPr})($O_2CC(O)Ph$)], likewise, did not yield oxalate,[193] in accordance with similar Cu^{II} complexes being air-stable,[410] while decarboxylation was observed for its Fe^{II} congener[397] and related Co^{II}[401] or Cu^{I}[398,400] complexes. This might be a result of the electronic properties of [Cu(Tp^{iPr,iPr})($O_2CC(O)Ph$)] which prohibit oxidative decomposition of the α-ketocarboxylate.[193] However, it might also indicate that oxidative C-C bond cleavage toward oxalate proceeds between the C2 and C3 of the 2-methyl-2-oxobutyrate, while decarboxylation (i.e. C1-C2 bond cleavage) yields the observed (2-hydroxo)-2-methylpropionic acid.[396,401,402] In this case, no CO_2 incorporation would be expected, as the O_2C-C(O) moiety of the α-ketocarboxylate would directly form the required oxalate structure upon oxidation with O_2. Moreover, this pathway would explain the absence of oxalate production for the phenyl-substituted α-ketocarboxylate, as the prerequisite C-C bond cleavage might proceed *via* an energetically unfavorable phenyl radical intermediate.[411] Interestingly, the C2-C3 bond scission pathway has been observed previously and resulted in the formation of well-defined dinuclear oxalate Fe or Co complexes, the latter even characterized by single crystal X-ray diffraction.[396,401] Moreover, the Fe containing enzyme Dke1 (acetylacetone cleaving enzyme) was found to catalyze an identical C2-C3 bond cleavage in *p*-hydroxyphenylpyruvate yielding oxalate and the corresponding *p*-hydroxybenz-

[XXIV] The experimental details for the described reaction of [Cu(Tp^{iPr,iPr})] with Et_4NHCO_3 are not reported in the Supplementary material[193] and can, consequently, not be discussed in more detail.

aldehyde.[402] This unprecedented reaction was initially proposed to proceed *via* attack of O_2 onto the coordinated enolized carboxylate.[396,401] On the contrary, mechanistic investigations for the Dke1-mediated reaction suggest a more favorable iron oxo-epoxide intermediate which undergoes ring-opening to form a C3-centered radical.[402] Either of these mechanistic pathways explains the lack of oxalate formation for benzoylformate reported by the Takisawa group.[193] In addition, the low oxalate yield obtained by reaction of the tris(pyrazolyl)borate-ligated complexes **129** or **196** with CO_2/O_2 or air suggest a comparatively low activity in the desired oxalate formation.

To evaluate these hypotheses, direct reactions of the sodium 3-methyl-2-oxobutyrates with $Cu(BF_4)_2{\cdot}6H_2O$ were chosen as the model reaction (Scheme 74), as simple Cu^{II} salts might result from decomposition of the $Tp^{iPr,iPr}$-derived complexes. Additionally, copper ions are well-known for catalyzing the oxidation of organic molecules, such as ascorbic acid, with molecular O_2.[380]

Air exposure of an equimolar mixture of $Cu(BF_4)_2{\cdot}6H_2O$ and sodium 3-methyl-2-oxobutyrate in DCM, containing 10 %vol MeOH to enhance the solubility, layered with heptane for 4 d (or 3 d) indeed resulted in a shift of one the C-O vibrations from 1630 cm^{-1} to 1607 cm^{-1} (or 1610 cm^{-1}) while the second distinct vibration at ca. 1707 cm^{-1} remained essentially unaltered, possibly indicating incomplete conversion (Figure 47). Likewise, reaction with air over 3 d (or 2 d) starting from the $^{13}C_5$-labelled sodium salt caused a shift of one of the C-O vibrations from 1588 cm^{-1} to 1563-1564 cm^{-1}. In addition, a significantly broadened signal at approx. 1625 cm^{-1} was observed.

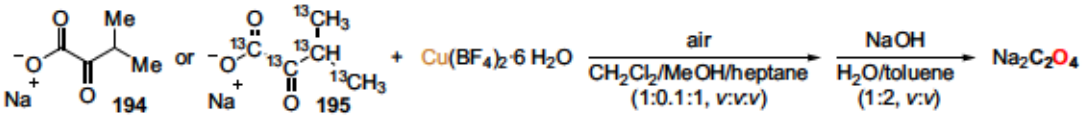

Scheme 74: Exposure of suspensions of the sodium α-ketocarboxylates and $Cu(BF_4)_2{\cdot}6H_2O$ in DC

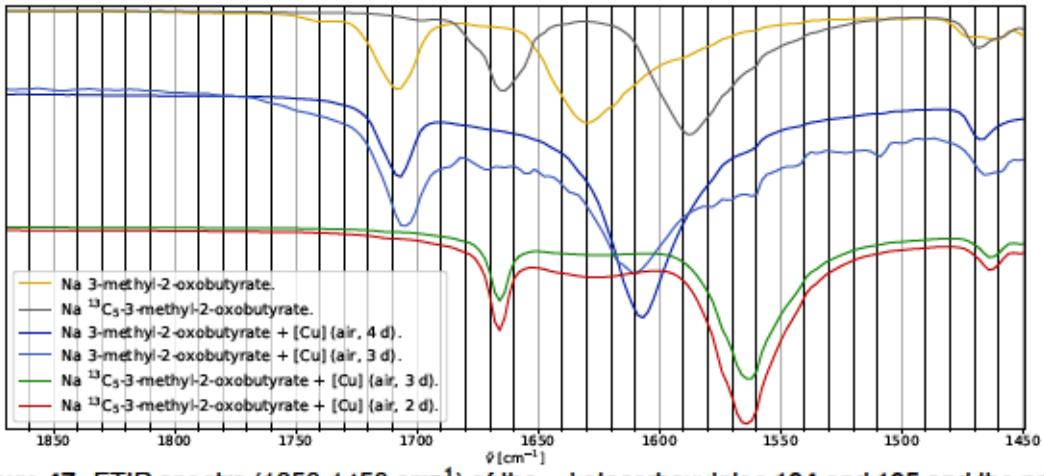

Figure 47: FTIR spectra (1850-1450 cm^{-1}) of the α-ketocarboxylates **194** and **195** and the products obtained by exposure of these in the presence of $Cu(BF_4)_2{\cdot}6H_2O$ in DCM/MeOH/heptane (1:0.1:1, *v*:*v*:*v*) to air.

Thus, the obtained FTIR spectra presage an oxidative decomposition of the α-ketocarboxylic acid in the presence of Cu^{2+}. Indeed, the ^{13}C NMR spectra obtained from unlabeled **194** display a signal corresponding to $C_2O_4^{2-}$ (Figure 48), hinting at an enhanced oxalate yield, despite the increased reaction scale. CE analysis substantiated this assumption with an oxalate yield of 36% or 47% for the 4 d and 3 d air exposure, respectively. It is noteworthy that, in contrast to the yields presented earlier in this section, a mononuclear mechanism for the formation of $C_2O_4^{2-}$ was assumed, thus one molecule of α-ketocarboxylate would result in one molecule of oxalate. Similar yields, namely 55% (3 d) and 42% (2 d) were obtained for the reaction with ^{13}C-labeled **195**, thus verifying the more effective formation of oxalate in the absence of the scorpionate ligand. The corresponding oxalate signal, in addition to small signals for formate and carbonate, is clearly noticeable as the major species in the ^{13}C NMR spectra for reactions with **195**. Additionally, signals belonging to the previously observed decarboxylation products were detected, albeit in significantly lower quantities. Surprisingly, two sets of signals, which were assigned to sodium acetate (181.5 ppm (d, $J_{^{13}C-^{13}C}$ = 52 Hz), 23.3 ppm (d, $J_{^{13}C-^{13}C}$ = 52 Hz))[412] and sodium 3-hydroxybutyrate (180.5 ppm (dd, $J_{^{13}C-^{13}C}$ = 51, 3 Hz), 65.6 ppm (t, $J_{^{13}C-^{13}C}$ = 38 Hz), 46.5 ppm (dd, $J_{^{13}C-^{13}C}$ = 51, 37 Hz), 21.7 ppm (dd, $J_{^{13}C-^{13}C}$ = 39, 2 Hz)),[413,414] were additionally observed in minor quantities. Even though these products displayed significantly smaller intensities than $C_2O_4^{2-}$, they indicate a more sophisticated oxidative degradation of the α-ketocarboxylate and potential follow-up reactions in the presence of Cu^{2+}, as formation of these by-products seems to increase with prolonged reaction time. Nevertheless, the clearly enhanced formation of oxalate in the absence of the $Tp^{iPr,iPr}$ ligand constitutes a first evidence for the proposed pathway of its formation *via* oxidative degradation facilitated by Cu^{2+}.

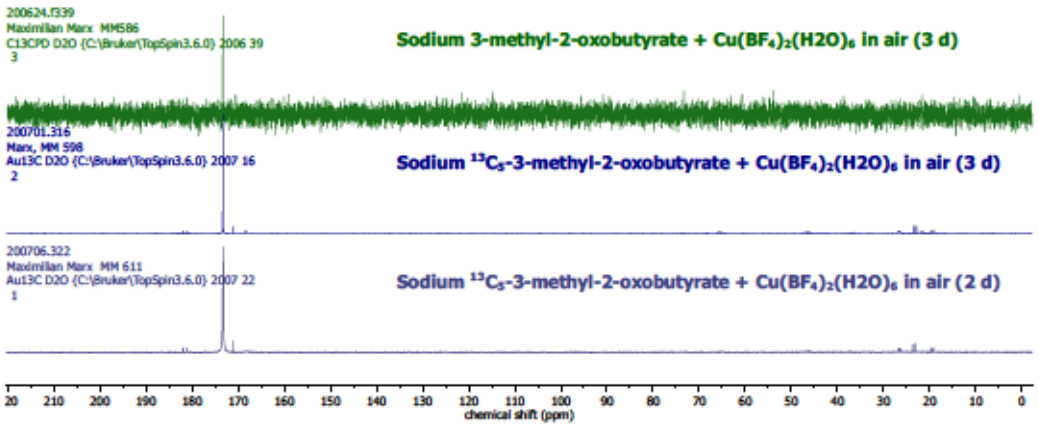

Figure 48: $^{13}C\{^1H\}$ NMR spectra (75 MHz, D_2O) of the reaction of **194** and **195** and $Cu(BF_4)_2{\cdot}6H_2O$ with air and subsequent NaOH treatment.

It is noteworthy that electron-rich methyl 4-methoxyphenylpyruvate decomposed into methyl oxalate by simple purging with O_2 at pH 7.5 over 48 h at 0 °C.[415] Thus, to confirm the beneficial impact of Cu on the formation of oxalate, specifically in the absence of the ligand, a blank reaction by simple exposure of sodium 3-methyl-2-oxobutyrate under analogous conditions to air was performed. After evaporation of the solvents over 2 d, the IR spectrum displayed

no sign of conversion of the starting material and likewise no oxalate signal was observed in the NMR spectrum after NaOH treatment (Figure S 327 and S 195). The oxalate yield determined by CE accounted for 4%, highlighting the beneficial influence of [Cu].

Additional mechanistic insight was obtained by HR-MS (ESI) analysis of the product solutions.[XXV] Oxalate as well as its dimer were successfully detected as their sodium salts and as expected, the $Na^{12}C_2O_4^-$ (*m/z*=110.9700) and $Na_3{}^{12}C_4O_8^-$ (*m/z*=244.9292) were detected for the reaction starting from unlabeled **194** (Figure 49). Likewise, their ^{13}C labeled analogues $Na^{13}C_2O_4^-$ (*m/z*=112.9782) and $Na_3{}^{13}C_4O_8^-$ (*m/z*=248.9433) were observed for the reaction of **195** and no species with mixed isotopic constitution was found. This further showcases the proposed origin of oxalate being oxidative degradation of the α-ketocarboxylate facilitated by Cu^{2+} without CO_2 incorporation from the atmosphere taking place.

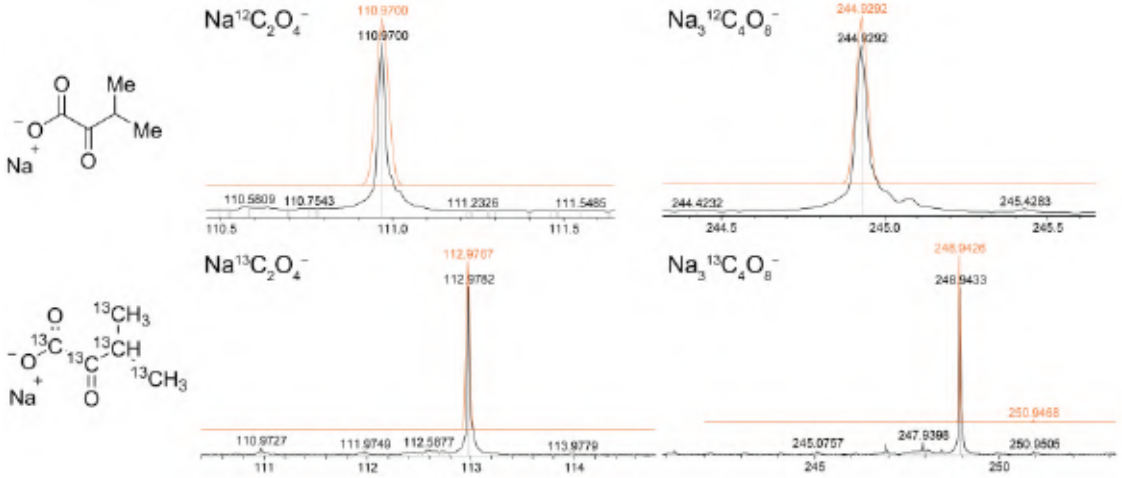

Figure 49: HR-MS (ESI) of the aqueous solution of the reaction of **194** and **195** and $Cu(BF_4)_2{\cdot}6H_2O$ with air and subsequent NaOH treatment (simulated exact *m/z* values are presented in orange).

Naturally, the oxidative C-C bond scission between the 2C and 3C giving rise to the observed oxalate should simultaneously yield a C_3-compound, most likely acetone resembling the aldehydes observed in the literature,[396,401,402] which was not detected in these experiments, possibly due its volatility. Hence, reaction of **195** with CO_2/O_2 in the presence of $Cu(BF_4)_2{\cdot}6H_2O$ was conducted in CD_2Cl_2 or C_6D_6, containing 10 %vol CD_3OD for an enhanced solubility, in a sealed Schlenk tube (Scheme 75). Under these conditions, direct analysis of the solutions precludes evaporation of a conceivable C_3 decomposition product.

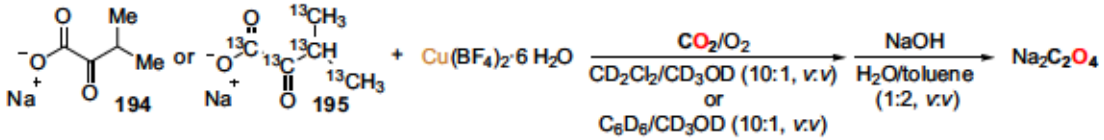

Scheme 75: Treatment of a suspension of **195** and $Cu(BF_4)_2{\cdot}6H_2O$ in CD_2Cl_2/CD_3OD or C_6D_6/CD_3OD with CO_2/O_2 and subsequent NaOH treatment.

[XXV] HR-MS analysis of the aqueous solutions was conducted by Dr. H. Frauendorf (University of Göttingen).

Fortunately, stirring an equimolar mixture of **195** and the Cu^{2+} salt in either solvent for 4 d under a CO_2/O_2 atmosphere indeed resulted in the appearance of two new signals at 208.7 ppm (t, $J_{^{13}C-^{13}C}$= 40 Hz) and 31.1 ppm (d, $J_{^{13}C-^{13}C}$= 40 Hz) in CD_2Cl_2 or 206.3 ppm (t, $J_{^{13}C-^{13}C}$= 40 Hz) and 30.1 ppm (d, $J_{^{13}C-^{13}C}$= 40 Hz) in C_6D_6, respectively (Figure 50). These signals can be assigned to entirely ^{13}C-labeled acetone,[412] hence underscoring the suggested oxidative C2-C3 bond cleavage[396,401,402]. Additionally, residual CO_2 was observed at ca. 125 ppm. It is noteworthy that neither the starting material, nor resulting anionic products, e.g. oxalate, are detected arguably due to their insolubility in C_6D_6 or CD_2Cl_2.

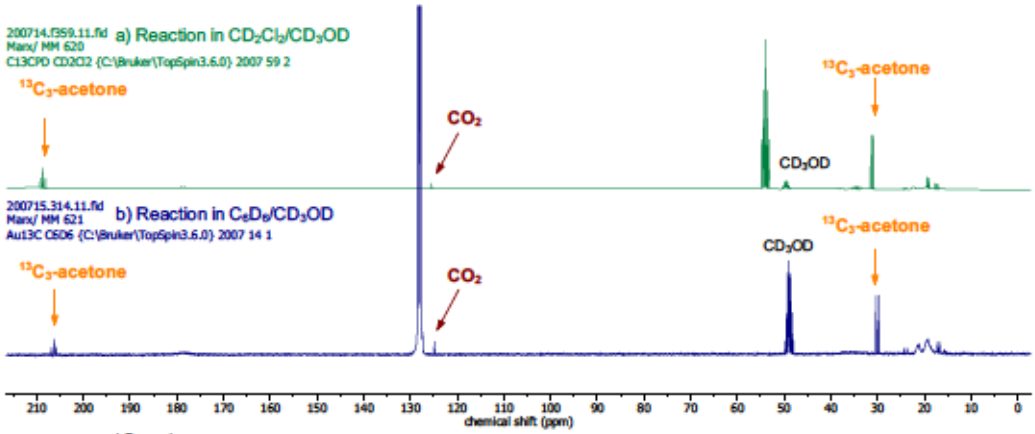

Figure 50: $^{13}C\{^1H\}$ NMR spectra (75 MHz, CD_2Cl_2 or C_6D_6) of the reaction of **195** and $Cu(BF_4)_2{\cdot}6H_2O$ with CO_2/O_2.

IR spectroscopic analysis of the solid obtained after drying *in vacuo* further confirmed the resemblance of the obtained product to that obtained by air exposure of **195** in the presence of Cu^{2+}, with the major C-O vibration located at ~1560 cm^{-1} (Figure 51). However, the product obtained from the CD_2Cl_2 reaction displayed significant broadening of all signals, possibly due to the presence of water indicated by a broad signal from ca. 3700-2800 cm^{-1} (Figu

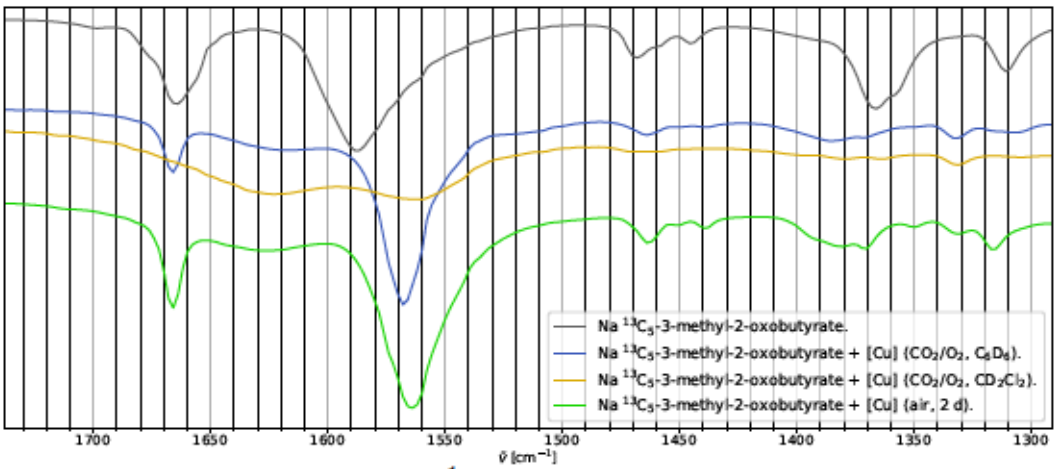

Figure 51: FTIR spectra (1700-1300 cm^{-1}) of **195** and the products obtained from its exposure to air or CO_2/O_2 in the presence of $Cu(BF_4)_2{\cdot}6H_2O$ in DCM/MeOH/heptane (air) or CD_2Cl_2/CD_3OD and C_6D_6/CD_3OD (CO_2/O_2).

Capillary electrophoresis after NaOH treatment of the solid residues revealed the formation of oxalate in 17% and 31% yield for the reactions in CD_2Cl_2 and C_6D_6, respectively. The lower yield for the reaction in dichloromethane-d_2 was surprising given the higher intensity of the acetone signals in the initial ^{13}C NMR spectrum and might thus indicate at least partial formation of oxalate or the observed acetone *via* another pathway than C2-C3 bond cleavage or further oxidative decomposition during the NaOH treatment. The clearly higher quantities of 2-methylpropionate observed in the ^{13}C NMR spectrum of the CD_2Cl_2 reaction after NaOH treatment compared to that in C_6D_6 (Figure S 181) substantiate this suggestion. A plausible explanation for these observations would be the formation of 2-methylpropionic acid *via* initial oxidative decarboxylation, followed by a second oxidative decarboxylation yielding acetone. In this case, the acetone quantity would not correlate with the oxalate yield. However, it should be noted that determined yields for these reactions are easily decreased by partial sample loss during transfer of the NMR solutions,[XXVI] especially pronounced for the reaction in CD_2Cl_2 as the solid did not settle entirely, and FTIR analysis of the solid residues after solvent removal. Nevertheless, it appears that decarboxylation competes with formation of oxalate. Hence, while the observed quantities of acetone cannot conclusively be aligned with the pathway toward oxalate formation, oxidative C1-C2 scission clearly does not provide the desired product.

To evaluate whether the oxidative degradation of α-ketocarboxylates is specific to 3-methyl-2-oxobutyrate, as suggested by Fujisawa and co-workers,[193] a suspension of sodium pyruvate and an equimolar amount of $Cu(BF_4)_2{\cdot}6H_2O$ in DCM/MeOH (10:1, *v*:*v*) layered with heptane was exposed to air and left to evaporate. The ^{13}C NMR spectrum after NaOH treatment revealed signals at 181.6 ppm, 23.4 ppm and 173.2 ppm, respectively. However, despite a slight shift in the methyl signal of pyruvate to higher field, the peak at 173.2 ppm likely corresponds to non-converted sodium pyruvate rather than oxalate. In addition, CE analysis supported oxalate formation in 5% yield (Figure S 415) which is not significantly higher than the blank reaction conducted with **194**. The negligible yield is in good accordance with the reaction pathway suggested herein, as an oxidative C2-C3 bond cleavage in pyruvate should be energetically less favorable than in 3-methyl-2-oxobutyrate, as a possibly formed $^{\bullet}CH_3$ species[402] as well as enolization of pyruvate[396,401] would pose an increased energetic barrier.

In conclusion, the intriguing CO_2 coupling reactivity of tris(pyrazolyl)borate-coordinated Cu α-ketocarboxylate complexes yielding oxalate in the presence of O_2[193] was explored and the mechanism of this transformation investigated. CO_2 incorporation was reported to proceed starting from complex **129** under a $^{13}CO_2/O_2$ atmosphere, resulting in a distinctly ($\Delta\tilde{\nu}$=49 cm^{-1}) shifted IR vibration.[193] It should be noted that a dinuclear carbonato-complex [($Tp^{iPr,iPr}$)Cu(μ-CO_3)Cu($Tp^{iPr,iPr}$)] was reported in the same publication which displayed a

[XXVI] Note that partial loss of the NMR sample cannot be avoided when employing J. Young NMR tubes connected *via* adapter to a Schlenk line.

similar C-O vibration (1595 cm^{-1}) to that of the presumably ^{13}C-containing oxalate complex.[193] Yet, the initial investigators suggested the formation of a $CO_2^{\bullet-}$ intermediate as a result of O_2 initiated degradation of the α-ketocarboxylate which reportedly required specific electronic features to proceed.[193] To reveal the origin of oxalate and thereby gain further insight into the reaction pathway, the $^{13}C_5$-labeled complex **196** was prepared and its reactivity compared to reported **129**. For the reaction of **196** with air or CO_2/O_2, a similar shift of the IR vibration was observed indicating formation of the analogous ^{13}C-labeled product. In addition, an IR vibration possibly corresponding to a ^{13}C-^{12}C mixed product was identified, albeit the IR band also coincides with starting material, thus precluding a conclusive statement. However, oxalate yields determined by capillary electrophoresis turned out to be significantly lower (at least fourfold) than those reported in the literature[193]. In addition, no oxalate with mixed isotopic constitution was detected by HR-MS, while the $^{13}C_2$-oxalate was identified for reactions of **196** with air or CO_2/O_2 suggesting the absence of CO_2 incorporation from the atmosphere. Moreover, oxidative decarboxylation products, namely 2-hydroxy-2-methylpropionate and 2-methylpropionate, were identified as the major products by ^{13}C NMR spectroscopy under these conditions. Even though the formation of the former had already been observed by the Fujisawa group,[193] their quantities suggested a different mechanism for the formation of oxalate. To assess a potential oxidative C2-C3 bond cleavage pathway,[396,401,402] reactions in the absence of the ligand starting from the sodium α-ketocarboxylates and simple $Cu(BF_4)_2{\cdot}6H_2O$ were explored. In this case, significantly higher oxalate yields were identified by capillary electrophoresis and ^{13}C NMR spectroscopy, thus supporting the proposed oxidative degradation mechanism. This was further highlighted by HR-MS analysis of the obtained oxalate which indicated no incorporation of ^{12}C from a potential C-C coupling with CO_2 from the atmosphere. Finally, NMR spectroscopic analysis of the reaction of $^{13}C_5$-labeled sodium 3-methyl-2-oxobutyrate with CO_2/O_2 in deuterated solvents revealed the formation of $^{13}C_3$-labeled acetone, possibly resulting from the proposed oxidative C2-C3 bond cleavage.[396,401,402] However, acetone quantities appeared to correlate also with the amount of 2-methylpropionate, presumably formed *via* oxidative decarboxylation, thus, another oxidative process might be responsible for the formation of oxalate.

Based on these observations, the following conclusions for the formation of oxalate starting from 3-methyl-2-oxobutyrate can be drawn (Scheme 76). $Tp^{iPr,iPr}$-ligated complexes **129** or its congener **196** efficiently decarboxylate the coordinated α-ketocarboxylate in the presence of O_2, resulting in the formation of 2-hydroxy-2-methylpropionate and 2-methylpropionate.

In contrast, simple Cu^{2+} facilitates the oxidative degradation, possibly *via* C2-C3 bond scission[396,401,402] yielding acetone and oxalate, which apparently undergo side or subsequent reactions, as indicated by the presence of 3-hydroxybutyrate, formate, and acetate after prolonged air exposure. Moreover, another plausible origin for the observed acetone might be twofold oxidative decarboxylation facilitated by copper. Hence, the true pathway for the formation of oxalate through oxidative degradation of the α-ketocarboxylate remains speculative

and requires further investigations. Likewise, examples for the C2-C3 bond scission are capable of O_2 activation accompanied by oxidation of the metal.[396,401,402] Naturally, this would suggest Cu^I as the active species, but additional evidence is necessary for an in-depth understanding of the process. However, the experimental results presented herein clearly indicate a competing relation between oxidative decarboxylation of the α-ketocarboxylate and the oxidative degradation yielding oxalate without incorporation of atmospheric CO_2. Whether the observed formation of oxalate in low yields starting from **129** or **196** arises from initial decomposition of the complexes, possibly during or after decarboxylation, or whether these complexes possess a diminished ability to facilitate the formation of oxalate by an analogous oxidative decomposition cannot be stated based on the results presented herein. Nevertheless, it can be concluded that simple Cu^{2+} ions are substantially more active in the formation of oxalate starting from α-ketocarboxylates and O_2. This reactivity partially resembles the oxidative C-C bond cleavage of tricarbonyl compounds by simple Fe^{3+} ions[392] and might potentially play a role in the oxidative degradation of cellulose into oxalate by CuO at elevated temperatures[416]. Albeit this reactivity of Cu^{2+} ions has not been reported, to the best of our knowledge, possible applications of this methodology appear to be restricted by the proposed mechanism, requiring stabilizing substituents in the 3-position to enable enol or radical formation.[396,401,402] Finally, it can be concluded that the desired C-C bond formation initially reported has again not been observed and an alternative oxidative pathway turned out to account for the observed oxalate.

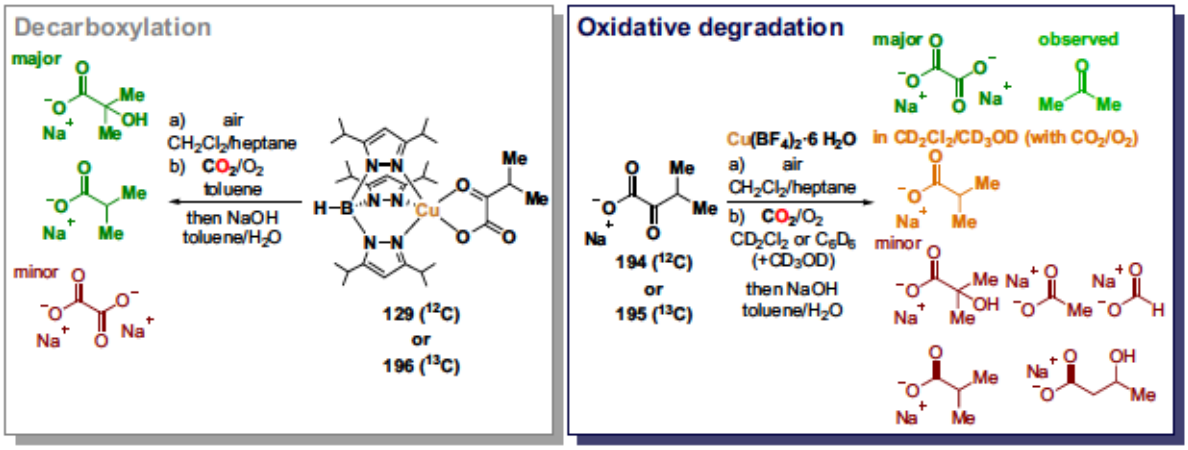

Scheme 76: Observed major and minor products for the reactions of complex **129** (and **196**) or sodium 3-methyl-2-oxobutyrate and $Cu(BF_4)_2{\cdot}6H_2O$ with air or CO_2/O_2 as reported herein.

3 Summary and Outlook

The reduction of the notorious greenhouse gas CO_2 into value-added chemicals with the help of first-row transition metal complexes based on Fe and Cu has been investigated following two fundamentally different approaches.

3.1 Photocatalytic CO_2 Reduction

First, the direct photocatalytic reduction of CO_2 into CO, accompanied by formic acid and competing hydrogen formation was investigated.

In a first approach, a system based on heteroleptic $[Cu(N^N)(P^P)]^+$ photosensitizers in combination with a cyclopentadienone-ligated Fe carbonyl complex[131] for the production of mainly CO (Figure 52) was transferred from a traditional solvent into ionic liquids.[228] Four different classes of ionic liquids were investigated and a pyrrolidinium-based IL with a dicyanamide was found to facilitate CO formation in high selectivity. Interestingly, the product distribution varied distinctly depending on the deployed solvent composition. Despite the call for further improvements of the catalytic performance, the general strategy of transferring a CO_2 reduction protocol consisting of base metal complexes from a traditional solvent into ionic liquids was demonstrated. This straightforward switch to essentially non-volatile ionic liquids will hopefully contribute to future improvements of CO_2 reduction in ILs and eventually enable solvent recycling in photocatalytic CO_2 reduction.

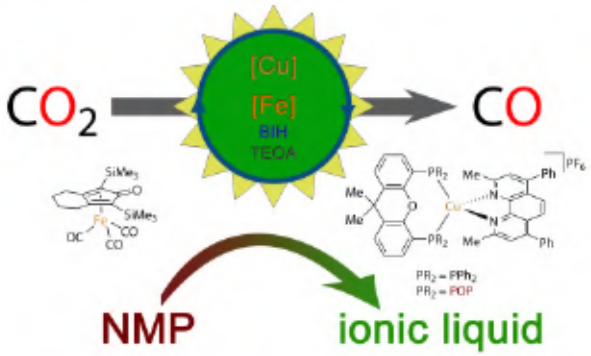

Figure 52: Schematic summary of the photocatalytic CO_2 reduction to CO in ionic liquids with a Fe-based catalyst and heteroleptic Cu photosensitizers.[228]

[FeFe] hydrogenase mimics were evaluated as potential CO_2 reduction catalyst in another approach to generate CO and formic acid in combination with the same heteroleptic Cu PS.[244] Besides initial activity, a poor reproducibility for the photocatalytic CO_2 reduction with biomimetic $[Fe_2S_2]$-based complexes was observed (Figure 53). This poor reproducibility was identified to be independent of the [FeFe] complex or the catalyst loading. Further investi-

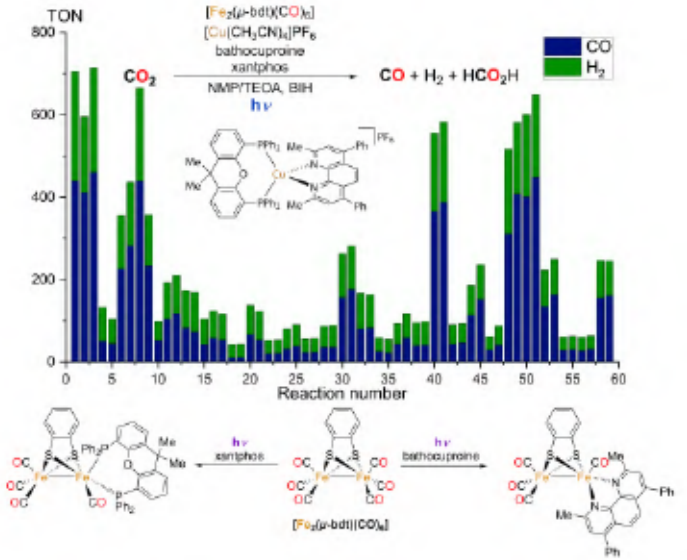

Figure 53: Irreproducibility of the photocatalytic CO_2 reduction and novel [FeFe] complexes reported herein.[244]

gations of the system identified a sophisticated equilibrium between the ligands of the $[Cu(N^N)(P^P)]^+$ and the [FeFe] complex and two novel bidentate donor-ligated [FeFe] complexes were prepared and characterized. Investigation of their catalytic properties still revealed insufficient reproducibility. These results clearly showcase the importance of reproducibility assessment in the development of novel catalytic protocols and highlight that well-defined precatalysts cannot *per se* warrant reproducibility. Suggestions for researchers specialized in the development of catalytic transformations on how to assess and address reproducibility of novel catalytic processes were derived from these findings. These guiding principles will ideally facilitate an increase in readily reproducible literature precedents and thereby help to tackle an on-going challenge in the field of photocatalytic CO_2 reduction, namely the catalyst benchmarking separated from experimental requirements[79]. Both, benchmarking and enhanced reproducibility, will certainly support future improvements in the field of photocatalytic CO_2 reduction.

3.2 Investigations on CO_2 Reductive Coupling

CO_2 reductive coupling, albeit appearing trivial in terms of coupling two $CO_2^{\bullet-}$ fragments, remains a challenging transformation. The major objective of this work was to identify common patterns that guide the reactivity of interest and will facilitate further improvements toward increased reductive coupling selectivity and activity. For this, an in-depth mechanistic understanding of the C-C bond formation was targeted based on existing systems known to form oxalate upon treatment with air or CO_2. This approach was chosen due to the small number of reports on CO_2 reductive coupling compared to the overwhelming number of catalysts reported for C_1 product formation. Moreover, validation of the reactivity of interest and CO_2 as the origin of oxalate was considered as the mandatory first step.

Initial investigations on dinuclear Cu complexes in combination with a disulfide-based ligand remained unsuccessful and ligand oxidation by Cu was observed hampering the reactivity towards CO_2.

Fe complex **118** was evaluated, as it was described to display a distinct solvent dependence for the CO_2 reduction step.[188] In contrast to the literature, no significant solvent effect was observed and reductive disproportionation of CO_2 into carbonate and the corresponding iron carbonyl complex was observed as the only CO_2 reduction reaction with different reductants and independent of the solvent (Scheme 77). A plausible explanation for this difference is

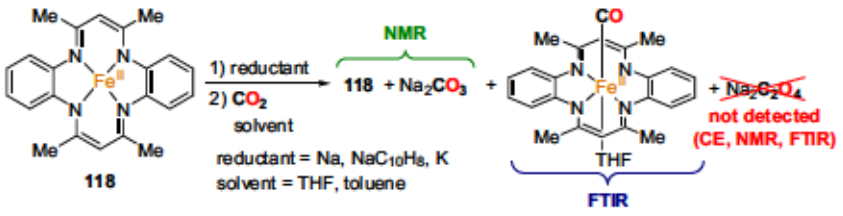

Scheme 77: Observed reactivity of [Fe(tmtaa)] in combination with alkali metal-based reductants toward CO_2 contrasting the described[188] $Na_2C_2O_4$ formation.

based on the utilized analytical methods: While the initial report identified oxalate by titration with $KMnO_4$,[188] a combination of FTIR and NMR spectroscopy as well as capillary electrophoresis was employed herein.

A Cu complex bearing a 1,4,7-triazacyclononane-derived ligand was reported to not only form an oxalate-bridged dimer from air, but also yield the same complex upon reaction with CO_2 or $CsHCO_3$.[192] Reproduction attempts failed and only a dinuclear μ-OH complex was identified upon air contact of the reaction mixture. Analysis of the reaction outcome by FTIR spectroscopy proved to be challenging due to the similarity of various CO_2 species. Hence, the oxalate complex was independently prepared and removal of the oxalate enabled the establishment of a convenient procedure to analyze the reaction outcome by coupling of the incipient FTIR analysis with NMR spectroscopy and capillary electrophoresis (Figure 54). However, the formation of oxalate in quantities and under the conditions stated in the literature remained elusive in view of the evaluated parameters, such as solvent, temperature, illumination, additives, Cu precursor, and the CO_2 source (air, solid bicarbonates, CO_2 under constant atmosphere or bubbling). Different tridentate ligands, including 1,4,7-triazacyclononane-derivatives, were evaluated, but did not improve the $C_2O_4^{2-}$ yield.

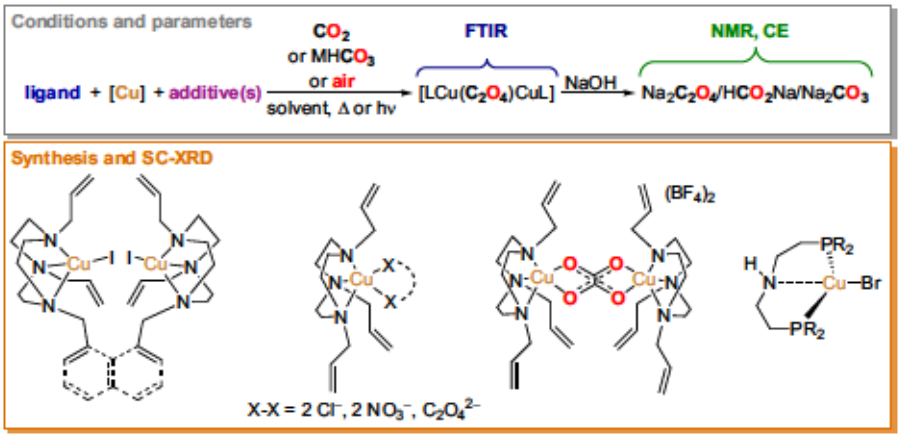

Figure 54: Schematic summary of attempted alterations to facilitate CO_2 reductive coupling with tridentate ligand-derived Cu complexes utilizing a combination of analytical techniques benchmarked with the independently synthesized oxalate complex and novel Cu complexes described herein.

In addition, three novel [(^{H}PNP)CuBr] complexes were prepared, characterized and evaluated in this transformation. No oxalate formation was detected with these novel complexes, but further investigations on their reactivity might be worthwhile. Finally, a dinuclear Cu complex based on a novel *N*-allylated bis(1,4,7-tacn)naphthalene ligand was prepared. With the help of this ligand, a CE signal potentially corresponding to oxalate in competitive yield was observed. However, the limitation of the developed analysis protocol became apparent in cases where signals overlapping with that of oxalate preclude determination of its yield solely based on CE analysis. Therefore, further elucidation of the nature of this signal is mandatory. While the formation of oxalate in small quantities cannot entirely be precluded based on the results obtained as part of this work, the initially reported yields[192] appear questionable.

Investigation on a Cu-based system for the CO_2 reductive coupling with sodium ascorbate as mild reductant[194] revealed another hurdle when studying this transformation. Contrasting the initial report, the presence of air was found to pose a prerequisite for the formation of the oxalate dimer.[375] Further experiments with O_2 in the absence of CO_2 validated the oxidative degradation of sodium ascorbate as the true origin of the observed oxalate (Scheme 78).

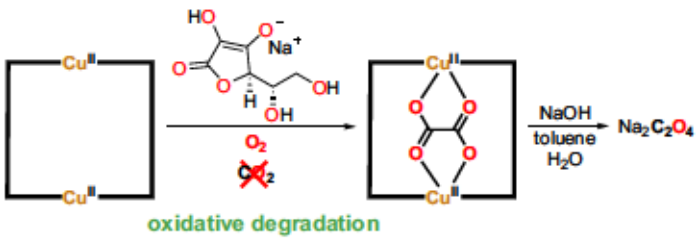

Scheme 78: Oxidative degradation identified as the true origin of oxalate for a proposed CO_2 reductive coupling protocol.[375]

Finally, a copper 3-methyl-2-oxobutyrate complex was described to form oxalate upon reaction with air, O_2 or CO_2/O_2.[193] As reported herein the described Cu complex and its $^{13}C_5$-labeled analogue mainly facilitated oxidative decarboxylation yielding pyruvic acid derivatives upon contact with air or CO_2/O_2 (Scheme 79). On the other hand, a simple Cu^{2+} salt was found to efficiently facilitate conversion of the sodium α-ketocarboxylate into oxalate upon prolonged air contact in the absence of additional ligands. No incorporation of CO_2 from the atmosphere was found by HR-MS analysis utilizing the $^{13}C_5$-labeled α-ketocarboxylate or its derived copper complex suggesting an oxidative degradation pathway and precluding a potential CO_2 reductive coupling. Acetone was detected by NMR spectroscopic analysis when reactions were conducted with CO_2/O_2, but the quantity of formed acetone did not correspond to the oxalate yield, thereby indicating a more complex reaction pathway than the well-known C2-C3 bond cleavage[396,401,402].

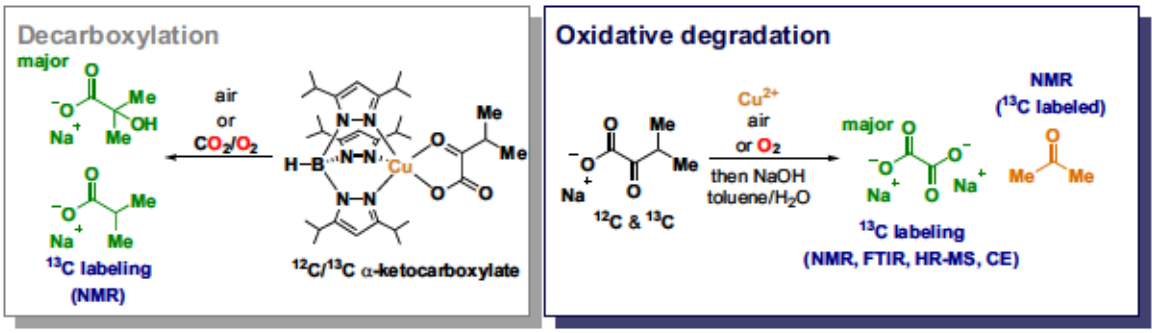

Scheme 79: Decarboxylation reactivity observed for Tp^{iPr,iPr}-ligated Cu α-ketocarboxylates ($^{12}C/^{13}C$) and contrasting oxidative degradation to oxalate in the presence of simple Cu^{2+}.

In conclusion, investigations on Fe and Cu complexes previously reported to enable CO_2 reductive coupling showcase not only the difficulty of the C-C bond formation in general, but highlight important general considerations for investigations on this transformation. First, the necessity to employ more than one (e.g. FTIR) analytical method for a correct assignment of the obtained CO_2 reduction product was demonstrated. In addition to FTIR, NMR spectroscopy after removal of bound oxalate proved to be a viable technique. Moreover, a

separation based technique, such as capillary electrophoresis, allowed for additional experimental evidence. Nevertheless, especially for low scale reactions, these techniques can suffer from false positives and care should be taken during interpretation of the obtained data. The latter aspect was clearly highlighted for two literature systems. Here, oxidative degradation of potential reducing agents or substrates resulted in the formation of oxalate. However, applying the principles derived from the investigations presented herein, that is combination of multiple analytical techniques, careful contemplation of reaction parameters, such as oxidative conditions in a reductive transformation, and open-minded consideration of possible reaction pathways, will hopefully facilitate future developments in the field of CO_2 reductive coupling.

While the investigations presented herein were unsuccessful in providing additional understanding of the C-C bond formation from CO_2 or establishing enhanced reactivity in this transformation, a few promising starting points and strategies can be suggested (Figure 55).

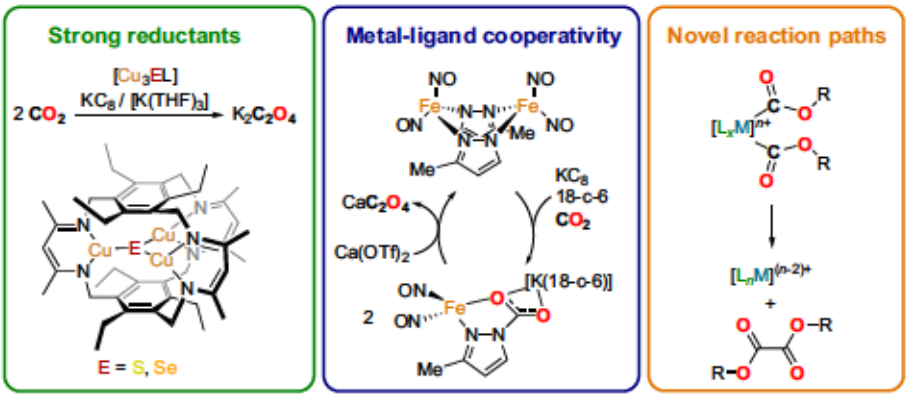

Figure 55: Possible starting points for future developments towards efficient CO_2 reductive coupling: 1) Utilization of strong reductants in combination with multinuclear complexes;[195] 2) Metal-ligand cooperativity for the activation of CO_2;[191] 3) Reductive elimination from bis(hydroxycarbonyl) (R=H) or bis(alkoxycarbonyl) (R=CR'$_3$) complexes (or oxidative coupling of CO)[281,417–420].

The combination of trinuclear Cu complexes with intriguing electronic properties and strong reductants reported by Murray and co-workers facilitated the catalytic formation of $K_2C_2O_4$ (Scheme 49).[195] While the yield and selectivity towards oxalate over formate have not yet been reached in preliminary investigations in our hands, the formation of oxalate was indeed suggested by CE (Appendix, section 4.10). Further modification of the electronic and steric parameters of these trinuclear complexes might be of interest for future investigations. In addition, metal-ligand cooperativity was beautifully demonstrated by Liaw, Lu, and co-workers to enable CO_2 reductive coupling after activation as a carbamate by the pyrazole ligand (Scheme 44).[191] This strategy might indeed provide a valuable starting point, not only for CO_2 reductive coupling itself, but also for its combination with CO_2 capture from the atmosphere. Finally, the formation of oxalate(s) *via* reductive elimination starting from bis(hydroxycarbonyl) or bis(alkoxycarbonyl) complexes appears to be another approach. While mononuclear dihydroxycarbonyl complexes are, to the best of our knowledge,

not structurally reported, their alkoxy-analogues are well-known. In fact, complexes of this type based on e.g. Fe,[421–427]XXVII Co,[428,429] Mo,[430] Ru,[431–436] Rh,[281] Pd,[417–419,437,438] Os,[439] and Pt[440] have been reported, but only those based on Rh[281], Pd,[417–419] and those presumed for Ni,[420] have been described to undergo reductive elimination to form dialkyl oxalates. The major challenge, apart from the reductive elimination step, would arguably constitute their formation starting from CO_2. Eventually, combination of a CO_2 to CO reduction step, subsequent formation of the dialkoxy-carbonyl complex and terminal reductive elimination might circumvent this obstacle.

In conclusion, further investigations on the simplest, yet challenging, C-C bond formation from CO_2 are highly desirable and will not only provide an expanded understanding of the chemistry of carbon dioxide, but eventually contribute to the development of processes enabling its utilization.

XXVII It is noteworthy that Fe(alkoxycarbonyl)(alkyloxalyl) complexes ([Fe(CO_2R)($COCO_2$R)($CO)_4$]) were found to yield alkyl oxalates *via* reductive elimination.[422]

References

[1] W. Steffen, J. Grinevald, P. Crutzen, J. McNeill, *Phil. Trans. A* **2011**, *369*, 842–867.

[2] The World Bank, *World Development Indicators, GDP per capita*, **2020**, data.worldbank.org/indicator/NY.GDP.PCAP.CD (accessed 20.06.2020).

[3] G. A. Olah, G. K. S. Prakash, A. Goeppert, *J. Am. Chem. Soc.* **2011**, *133*, 12881–12898.

[4] The World Bank, *World Development Indicators, Life expectancy at birth*, **2020**, data.worldbank.org/indicator/SP.DYN.LE00.IN (accessed 14.06.2020).

[5] L. Prados de la Escosura, *Rev. Income Wealth* **2015**, *61*, 220–247.

[6] United Nations, Department of Economic and Social Affairs, Population Division, *World Population Prospects* **2019**, *Online Edition (Rev. 1)*, population.un.org/wpp/ (accessed 13.06.2020).

[7] bp, *Statistical Review of World Energy*, **2020**, www.bp.com/en/global/corporate/energy-economics/statistical-review-of-world-energy.html (accessed 20.06.2020).

[8] International Energy Agency, *World Energy Outlook* **2019**, 38-41.

[9] United Nations, Department of Economic and Social Affairs, Population Division, *World Population Prospects* **2019**, Volume II: Demographic Profiles (ST/ESA/SER.A/427), population.un.org/wpp/ (accessed 13.06.2020).

[10] D. Tilman, C. Balzer, J. Hill, B. L. Befort, *PNAS* **2011**, *108*, 20260–20264.

[11] B. L. Bodirsky, S. Rolinski, A. Biewald, I. Weindl, A. Popp, H. Lotze-Campen, *PLOS ONE* **2015**, *10*, e0139201.

[12] T. Wheeler, J. von Braun, *Science* **2013**, *341*, 508–513.

[13] J. Chow, R. J. Kopp, P. R. Portney, *Science* **2003**, *302*, 1528–1531.

[14] IPCC, *Climate Change 2014: Synthesis Report. Contribution of Working Groups I, II, and III to the Fifth Assessment Report of the Intergovernmental Panel on Climate Change* [Core Writing Team, R. K. Pachauri and L. A. Meyer (eds.)] **2014**.

[15] EPA, *EPA's Climate Change Indicators: Global Atmospheric Concentrations of Carbon Dioxide Over Time* **2016**, https://www.epa.gov/climate-indicators/climate-change-indicators-atmospheric-concentrations-greenhouse-gases (accessed 05.07.2020).

[16] EPA, *EPA's Climate Change Indicators: Global Atmospheric Concentrations of Methane Over Time* **2016**, https://www.epa.gov/climate-indicators/climate-change-indicators-atmospheric-concentrations-greenhouse-gases (accessed 05.07.2020).

[17] EPA, *EPA's Climate Change Indicators: Global Atmospheric Concentrations of Nitrous Oxide Over Time* **2016**, https://www.epa.gov/climate-indicators/climate-change-indicators-atmospheric-concentrations-greenhouse-gases (accessed 05.07.2020).

[18] D. Lüthi, M. Le Floch, B. Bereiter, T. Blunier, J. M. Barnola, U. Siegenthaler, D. Raynaud, J. Jouzel, H. Fischer, K. Kawamura, T. F. Stocker, *Nature **2008**, 453, 379-382* (dataset: edc-co2-2008), www.ncdc.noaa.gov/paleo-search/study/6091 (accessed 05.07.2020).

[19] L. Loulergue, A. Schilt, R. Spahni, V. Masson-Delmotte, T. Blunier, B. Lemieux, J.-M. Barnola, D. Raynaud, T. F. Stocker, J. Chappellaz, *Nature **2008**, 453, 383-386* (dataset: edc-ch4-2008), https://www.ncdc.noaa.gov/paleo-search/study/6093 (accessed 05.07.2020).

[20] A. Schilt, M. Baumgartner, T. Blunier, J. Schwander, R. Spahni, H. Fischer, T. F. Stocker, *Quat. Sci. Rev. **2010**, 29, 182-192* (dataset: edc-n2o-2010-800k), https://www.ncdc.noaa.gov/

paleo-search/study/8615 (accessed 05.07.2020).

[21] D. M. Etheridge, L. P. Steele, R. L. Langenfelds, R. J. Francey, J.-M. Barnola, V. I. Morgan, Historical CO_2 record from the Law Dome DE08, DE08-2, and DSS ice cores, **1998**, https://cdiac.ess-dive.lbl.gov/trends/co2/lawdome.html (accessed 05.07.2020).

[22] D. M. Etheridge, L. P. Steele, R. J. Francey, R. L. Langenfelds, Historical CH_4 Records from Antarctic and Greenland Ice Cores, Antarctic Firn Data, and Archived Air Samples From Cape Grim, Tasmania, **2002**, https://cdiac.ess-dive.lbl.gov/ftp/trends/atm_meth/EthCH498A.txt (accessed 05.07.2020).

[23] A. Neftel, H. Friedli, E. Moor, H. Lotscher, H. Oeschger, U. Siegenthaler, B. Stauffer, Historical CO_2 Record from the Siple Station Ice Core, **1994**, https://cdiac.ess-dive.lbl.gov/trends/co2/siple.html (accessed 05.07.2020).

[24] Advanced Global Atmospheric Gases Experiment, Monthly mean N_2O concentrations for Cape Grim, Australia, **2015**, Current data can be accessed at https://www.csiro.au/en/Research/OandA/Areas/Assessing-our-climate/Latest-greenhouse-gas-data (accessed 05.07.2020).

[25] M. Battle, M. Bender, T. Sowers, P. P. Tans, J. H. Butler, J. W. Elkins, J. T. Ellis, T. Conway, N. Zhang, P. Lang, A. D. Clarket, *Nature **1996**, 383, 231-235*.

[26] P. Tans, R. Keeling, NOAA/GML, Scripps Institution of Oceanography, *Mauna Loa CO_2 annual mean data* **2019**, ftp://aftp.cmdl.noaa.gov/products/trends/co2/co2_annmean_mlo.txt (accessed 05.07.2020).

[27] E. Dlugokencky, NOAA/GML, *Globally averaged marine surface CH_4 annual mean data* **2019**, ftp://aftp.cmdl.noaa.gov/products/trends/ch4/ch4_annmean_gl.txt (accessed 05.07.2020).

[28] E. Dlugokencky, NOAA/GML, *Globally averaged marine surface N_2O annual mean data* **2019**, ftp://aftp.cmdl.noaa.gov/products/trends/n2o/n2o_annmean_gl.txt (accessed 05.07.2020).

[29] T. A. Boden, G. Marland, R. J. Anders, *Global, Regional, and National Fossil-Fuel CO_2 Emissions 1751-2014* **2017**, https://cdiac.ess-dive.lbl.gov/ftp/ndp030/global.1751_2014.ems (accessed 06.07.2020).

[30] R. S. Haszeldine, *Science* **2009**, *325*, 1647–1652.

[31] A. Kibria, S. B. Akhundjanov, R. Oladi, *Int. Rev. Econ. Finance* **2019**, *59*, 253–264.

[32] United Nations Framework Convention on Climate Change, *Paris Agreement* **2016**, https://unfccc.int/files/essential_background/convention/application/pdf/english_paris_agreement.pdf (accessed 28.06.2020).

[33] M. Ramdin, T. W. de Loos, T. J. Vlugt, *Ind. Eng. Chem. Res.* **2012**, *51*, 8149–8177.

[34] F. Zeman, *Environ. Sci. Technol.* **2007**, *41*, 7558–7563.

[35] M. Aresta, A. Dibenedetto, A. Angelini, *Chem. Rev.* **2014**, *114*, 1709–1742.

[36] J. Klankermayer, W. Leitner, *Phil. Trans. A* **2016**, *374*, 20150315.

[37] M. Nielsen, E. Alberico, W. Baumann, H.-J. Drexler, H. Junge, S. Gladiali, M. Beller, *Nature* **2013**, *495*, 85–89.

[38] E. Alberico, P. Sponholz, C. Cordes, M. Nielsen, H.-J. Drexler, W. Baumann, H. Junge, M. Beller, *Angew. Chem. Int. Ed.* **2013**, *52*, 14162–14166.

[39] E. Alberico, A. J. J. Lennox, L. K. Vogt, H. Jiao, W. Baumann, H.-J. Drexler, M. Nielsen, A. Spannenberg, M. P. Checinski, H. Junge, M. Beller, *J. Am. Chem. Soc.* **2016**, *138*, 14890–14904.

[40] M. Andérez-Fernández, L. K. Vogt, S. Fischer, W. Zhou, H. Jiao, M. Garbe, S. Elangovan, K. Junge, H. Junge, R. Ludwig, M. Beller, *Angew. Chem. Int. Ed.* **2017**, *56*, 559–562.

[41] K. S. Lackner, *Eur. J. Phys. Spec. Top.* **2009**, *176*, 93–106.

[42] A. R. Millward, O. M. Yaghi, *J. Am. Chem. Soc.* **2005**, *127*, 17998–17999.
[43] R. Banerjee, A. Phan, B. Wang, C. Knobler, H. Furukawa, M. O'Keeffe, O. M. Yaghi, *Science* **2008**, *319*, 939.
[44] H. Furukawa, N. Ko, Y. B. Go, N. Aratani, S. B. Choi, E. Choi, A. Ö. Yazaydin, R. Q. Snurr, M. O'Keeffe, J. Kim, O. M. Yaghi, *Science* **2010**, *329*, 424.
[45] D. Alezi, Y. Belmabkhout, M. Suyetin, P. M. Bhatt, Ł. J. Weseliński, V. Solovyeva, K. Adil, I. Spanopoulos, P. N. Trikalitis, A.-H. Emwas, M. Eddaoudi, *J. Am. Chem. Soc.* **2015**, *137*, 13308–13318.
[46] Q. Liu, L. Wu, R. Jackstell, M. Beller, *Nat. Commun.* **2015**, *6*, 5933.
[47] R. Francke, B. Schille, M. Roemelt, *Chem. Rev.* **2018**, *118*, 4631–4701.
[48] A. M. Appel, J. E. Bercaw, A. B. Bocarsly, H. Dobbek, D. L. DuBois, M. Dupuis, J. G. Ferry, E. Fujita, R. Hille, P. J. A. Kenis, C. A. Kerfeld, R. H. Morris, C. H. F. Peden, A. R. Portis, S. W. Ragsdale, T. B. Rauchfuss, J. N. H. Reek, L. C. Seefeldt, R. K. Thauer, G. L. Waldrop, *Chem. Rev.* **2013**, *113*, 6621–6658.
[49] E. J. Little, M. M. Jones, *J. Chem. Ed.* **1960**, *37*, 231.
[50] A. Behr, *Angew. Chem. Int. Ed.* **1988**, *27*, 661–678.
[51] J. Meessen, *Chem. Ing. Tech.* **2014**, *86*, 2180–2189.
[52] W.-H. Wang, Y. Himeda, J. T. Muckerman, G. F. Manbeck, E. Fujita, *Chem. Rev.* **2015**, *115*, 12936–12973.
[53] M. Honda, M. Tamura, Y. Nakagawa, K. Tomishige, *Catal. Sci. Technol.* **2014**, *4*, 2830–2845.
[54] M. North, R. Pasquale, C. Young, *Green Chem.* **2010**, *12*, 1514–1539.
[55] G. W. Coates, D. R. Moore, *Angew. Chem. Int. Ed.* **2004**, *43*, 6618–6639.
[56] D. J. Darensbourg, *Chem. Rev.* **2007**, *107*, 2388–2410.
[57] Z.-Z. Yang, Y.-N. Li, Y.-Y. Wei, L.-N. He, *Green Chem.* **2011**, *13*, 2351–2353.
[58] O. Ihata, Y. Kayaki, T. Ikariya, *Angew. Chem. Int. Ed.* **2004**, *43*, 717–719.
[59] O. Ihata, Y. Kayaki, T. Ikariya, *Macromolecules* **2005**, *38*, 6429–6434.
[60] H. Kolbe, *Liebigs Ann. Chem.* **1860**, *113*, 125–127.
[61] R. Schmitt, *J. Prakt. Chem.* **1885**, *31*, 397–411.
[62] World Health Organization, *Model List of Essential Medicines*, **2019**, 21st List, Geneva, https://apps.who.int/iris/bitstream/handle/10665/325771/WHO-MVP-EMP-IAU-2019.06-eng.pdf?ua=1 (accessed 11.07.2020).
[63] J. Hong, M. Li, J. Zhang, B. Sun, F. Mo, *ChemSusChem* **2019**, *12*, 6–39.
[64] K. Ukai, M. Aoki, J. Takaya, N. Iwasawa, *J. Am. Chem. Soc.* **2006**, *128*, 8706–8707.
[65] H.-R. Li, L.-N. He, *Organometallics* **2020**, *39*, 1461–1475.
[66] J. Takaya, S. Tadami, K. Ukai, N. Iwasawa, *Org. Lett.* **2008**, *10*, 2697–2700.
[67] P. J. Riss, S. Lu, S. Telu, F. I. Aigbirhio, V. W. Pike, *Angew. Chem. Int. Ed.* **2012**, *51*, 2698–2702.
[68] M. Juhl, S. L. R. Laursen, Y. Huang, D. U. Nielsen, K. Daasbjerg, T. Skrydstrup, *ACS Catal.* **2017**, *7*, 1392–1396.
[69] H. Tran-Vu, O. Daugulis, *ACS Catal.* **2013**, *3*, 2417–2420.
[70] J. Louie, J. E. Gibby, M. V. Farnworth, T. N. Tekavec, *J. Am. Chem. Soc.* **2002**, *124*, 15188–15189.
[71] O. Jacquet, C. Das Neves Gomes, M. Ephritikhine, T. Cantat, *J. Am. Chem. Soc.* **2012**, *134*, 2934–2937.
[72] Y. Li, X. Fang, K. Junge, M. Beller, *Angew. Chem. Int. Ed.* **2013**, *52*, 9568–9571.

[73] K. Beydoun, T. Vom Stein, J. Klankermayer, W. Leitner, *Angew. Chem. Int. Ed.* **2013**, *52*, 9554–9557.
[74] Q. Liu, L. Wu, I. Fleischer, D. Selent, R. Franke, R. Jackstell, M. Beller, *Chem. Eur. J.* **2014**, *20*, 6888–6894.
[75] L. Wu, Q. Liu, I. Fleischer, R. Jackstell, M. Beller, *Nat. Commun.* **2014**, *5*, 3091.
[76] S. Berardi, S. Drouet, L. Francas, C. Gimbert-Surinach, M. Guttentag, C. Richmond, T. Stoll, A. Llobet, *Chem. Soc. Rev.* **2014**, *43*, 7501–7519.
[77] Y. Yamazaki, H. Takeda, O. Ishitani, *J. Photochem. Photobiol. C* **2015**, *25*, 106–137.
[78] C. D. Windle, R. N. Perutz, *Coord. Chem. Rev.* **2012**, *256*, 2562–2570.
[79] H. Takeda, C. Cometto, O. Ishitani, M. Robert, *ACS Catal.* **2017**, *7*, 70–88.
[80] A. J. Morris, G. J. Meyer, E. Fujita, *Acc. Chem. Res.* **2009**, *42*, 1983–1994.
[81] C. Costentin, M. Robert, J.-M. Savéant, *Chem. Soc. Rev.* **2013**, *42*, 2423–2436.
[82] Y. Pellegrin, F. Odobel, *C. R. Chimie* **2017**, *20*, 283–295.
[83] F. Wang, W.-G. Wang, H.-Y. Wang, G. Si, C.-H. Tung, L.-Z. Wu, *ACS Catal.* **2012**, *2*, 407–416.
[84] A. Agapova, E. Alberico, A. Kammer, H. Junge, M. Beller, *ChemCatChem* **2019**, *11*, 1910–1914.
[85] A. Agapova, H. Junge, M. Beller, *Chem. Eur. J.* **2019**, *25*, 9345–9349.
[86] W. Zhou, Z. Wei, A. Spannenberg, H. Jiao, K. Junge, H. Junge, M. Beller, *Chem. Eur. J.* **2019**, *25*, 8459–8464.
[87] X. Zhou, Y. Huang, C. Liu, J. Liao, T. Lu, W. Xing, *ChemSusChem* **2010**, *3*, 1379–1382.
[88] X. Gu, Z.-H. Lu, H.-L. Jiang, T. Akita, Q. Xu, *J. Am. Chem. Soc.* **2011**, *133*, 11822–11825.
[89] C. Tang, A.-E. Surkus, F. Chen, M.-M. Pohl, G. Agostini, M. Schneider, H. Junge, M. Beller, *Angew. Chem. Int. Ed.* **2017**, *56*, 16616–16620.
[90] X. Li, A.-E. Surkus, J. Rabeah, M. Anwar, S. Dastigir, H. Junge, A. Brückner, M. Beller, *Angew. Chem. Int. Ed.* **2020**, *59*, 15849–15854.
[91] A. Léval, A. Agapova, C. Steinlechner, E. Alberico, H. Junge, M. Beller, *Green Chem.* **2020**, *22*, 913–920.
[92] R. Tanaka, M. Yamashita, K. Nozaki, *J. Am. Chem. Soc.* **2009**, *131*, 14168–14169.
[93] S. Wesselbaum, U. Hintermair, W. Leitner, *Angew. Chem. Int. Ed.* **2012**, *51*, 8585–8588.
[94] G. C. Chinchen, P. J. Denny, D. G. Parker, M. S. Spencer, D. A. Whan, *Appl. Catal.* **1987**, *30*, 333–338.
[95] Carbon Recycling International, *The George Olah Renewable Methanol Plant*, Svartsengi, https://static1.squarespace.com/static/56926c502399a318016c5ed8/t/5daefd1f358b762b8348189d/1571749152527/GO+Plant-+Profile.pdf (accessed 16.07.2020).
[96] S. Wesselbaum, V. Moha, M. Meuresch, S. Brosinski, K. M. Thenert, J. Kothe, T. Vom Stein, U. Englert, M. Hölscher, J. Klankermayer, W. Leitner, *Chem. Sci.* **2015**, *6*, 693–704.
[97] J. Schneidewind, R. Adam, W. Baumann, R. Jackstell, M. Beller, *Angew. Chem. Int. Ed.* **2017**, *56*, 1890–1893.
[98] F. K. Scharnagl, M. F. Hertrich, G. Neitzel, R. Jackstell, M. Beller, *Adv. Synth. Catal.* **2019**, *361*, 374–379.
[99] A. Gennaro, A. A. Isse, M.-G. Severin, E. Vianello, I. Bhugun, J.-M. Saveant, *J. Chem. Soc., Faraday Trans.* **1996**, *92*, 3963–3968.
[100] A. Gennaro, A. A. Isse, J.-M. Savéant, M.-G. Severin, E. Vianello, *J. Am. Chem. Soc.* **1996**, *118*, 7190–7196.

[101] D. A. Tyssee, J. H. Wagenknecht, M. M. Baizer, J. L. Chruma, *Tetrahedron Lett.* **1972**, *13*, 4809–4812.
[102] C. Amatore, J. M. Saveant, *J. Am. Chem. Soc.* **1981**, *103*, 5021–5023.
[103] Y. Hori, K. Kikuchi, S. Suzuki, *Chem. Lett.* **1985**, *14*, 1695–1698.
[104] Y. Hori, K. Kikuchi, A. Murata, S. Suzuki, *Chem. Lett.* **1986**, *15*, 897–898.
[105] Y. Hori, A. Murata, R. Takahashi, S. Suzuki, *J. Chem. Soc., Chem. Commun.* **1988**, 17–19.
[106] Y. Zheng, A. Vasileff, X. Zhou, Y. Jiao, M. Jaroniec, S.-Z. Qiao, *J. Am. Chem. Soc.* **2019**, *141*, 7646–7659.
[107] L. Chen, Z. Guo, X.-G. Wei, C. Gallenkamp, J. Bonin, E. Anxolabéhère-Mallart, K.-C. Lau, T.-C. Lau, M. Robert, *J. Am. Chem. Soc.* **2015**, *137*, 10918–10921.
[108] J. Shen, R. Kortlever, R. Kas, Y. Y. Birdja, O. Diaz-Morales, Y. Kwon, I. Ledezma-Yanez, K. J. P. Schouten, G. Mul, M. T. M. Koper, *Nat. Commun.* **2015**, *6*, 8177.
[109] J. W. Tucker, C. R. J. Stephenson, *J. Org. Chem.* **2012**, *77*, 1617–1622.
[110] T. Inoue, A. Fujishima, S. Konishi, K. Honda, *Nature* **1979**, *277*, 637–638.
[111] J.-M. Lehn, R. Ziessel, *PNAS* **1982**, *79*, 701–704.
[112] J. Hawecker, J.-M. Lehn, R. Ziessel, *J. Chem. Soc., Chem. Commun.* **1983**, 536–538.
[113] J. Hawecker, J.-M. Lehn, R. Ziessel, *Helv. Chim. Acta* **1986**, *69*, 1990–2012.
[114] E. Kimura, S. Wada, M. Shionoya, T. Takahashi, Y. Litaka, *J. Chem. Soc., Chem. Commun.* **1990**, 397–398.
[115] E. Kimura, X. Bu, M. Shionoya, S. Wada, S. Maruyama, *Inorg. Chem.* **1992**, *31*, 4542–4546.
[116] B. Gholamkhass, H. Mametsuka, K. Koike, T. Tanabe, M. Furue, O. Ishitani, *Inorg. Chem.* **2005**, *44*, 2326–2336.
[117] A. H. A. Tinnemans, T. P. M. Koster, D. H. M. W. Thewissen, A. Mackor, *Recl. Trav. Chim. Pays–Bas* **1984**, *103*, 288–295.
[118] C. A. Craig, L. O. Spreer, J. W. Otvos, M. Calvin, *J. Phys. Chem.* **1990**, *94*, 7957–7960.
[119] J. Grodkowski, D. Behar, P. Neta, P. Hambright, *J. Phys. Chem. A* **1997**, *101*, 248–254.
[120] J. Bonin, M. Robert, M. Routier, *J. Am. Chem. Soc.* **2014**, *136*, 16768–16771.
[121] T. Dhanasekaran, J. Grodkowski, P. Neta, P. Hambright, E. Fujita, *J. Phys. Chem. A* **1999**, *103*, 7742–7748.
[122] Z. Guo, S. Cheng, C. Cometto, E. Anxolabéhère-Mallart, S.-M. Ng, C.-C. Ko, G. Liu, L. Chen, M. Robert, T.-C. Lau, *J. Am. Chem. Soc.* **2016**, *138*, 9413–9416.
[123] Z. Guo, F. Yu, Y. Yang, C.-F. Leung, S.-M. Ng, C.-C. Ko, C. Cometto, T.-C. Lau, M. Robert, *ChemSusChem* **2017**, *10*, 4009–4013.
[124] Y. Zhang, M. Schulz, M. Wächtler, M. Karnahl, B. Dietzek, *Coord. Chem. Rev.* **2018**, *356*, 127–146.
[125] A. Hossain, A. Bhattacharyya, O. Reiser, *Science* **2019**, *364*, eaav9713.
[126] S.-P. Luo, E. Mejía, A. Friedrich, A. Pazidis, H. Junge, A.-E. Surkus, R. Jackstell, S. Denurra, S. Gladiali, S. Lochbrunner, M. Beller, *Angew. Chem. Int. Ed.* **2013**, *52*, 419–423.
[127] E. Mejía, S.-P. Luo, M. Karnahl, A. Friedrich, S. Tschierlei, A.-E. Surkus, H. Junge, S. Gladiali, S. Lochbrunner, M. Beller, *Chem. Eur. J.* **2013**, *19*, 15972–15978.
[128] S. Fischer, D. Hollmann, S. Tschierlei, M. Karnahl, N. Rockstroh, E. Barsch, P. Schwarzbach, S.-P. Luo, H. Junge, M. Beller, S. Lochbrunner, R. Ludwig, A. Brückner, *ACS Catal.* **2014**, *4*, 1845–1849.
[129] A. J. J. Lennox, S. Fischer, M. Jurrat, S.-P. Luo, N. Rockstroh, H. Junge, R. Ludwig, M. Beller,

Chem. Eur. J. **2016**, *22*, 1233–1238.
[130] H. Takeda, K. Ohashi, A. Sekine, O. Ishitani, *J. Am. Chem. Soc.* **2016**, *138*, 4354–4357.
[131] A. Rosas-Hernandez, C. Steinlechner, H. Junge, M. Beller, *Green Chem.* **2017**, *19*, 2356–2360.
[132] Y. Sakaguchi, A. Call, M. Cibian, K. Yamauchi, K. Sakai, *Chem. Commun.* **2019**, *55*, 8552–8555.
[133] H. Takeda, H. Kamiyama, K. Okamoto, M. Irimajiri, T. Mizutani, K. Koike, A. Sekine, O. Ishitani, *J. Am. Chem. Soc.* **2018**, *140*, 17241–17254.
[134] C. Steinlechner, A. F. Roesel, E. Oberem, A. Päpcke, N. Rockstroh, F. Gloaguen, S. Lochbrunner, R. Ludwig, A. Spannenberg, H. Junge, R. Francke, M. Beller, *ACS Catal.* **2019**, *9*, 2091–2100.
[135] X. Feng, Y. Pi, Y. Song, C. Brzezinski, Z. Xu, Z. Li, W. Lin, *J. Am. Chem. Soc.* **2020**, *142*, 690–695.
[136] C. Wang, M. Guo, R. Qi, Q. Shang, Q. Liu, S. Wang, L. Zhao, R. Wang, Z. Xu, *Angew. Chem. Int. Ed.* **2018**, *57*, 15841–15846.
[137] C. Minozzi, A. Caron, J.-C. Grenier-Petel, J. Santandrea, S. K. Collins, *Angew. Chem. Int. Ed.* **2018**, *57*, 5477–5481.
[138] X.-L. Lyu, S.-S. Huang, H.-J. Song, Y.-X. Liu, Q.-M. Wang, *Org. Lett.* **2019**, *21*, 5728–5732.
[139] A. Caron, É. Morin, S. K. Collins, *ACS Catal.* **2019**, *9*, 9458–9464.
[140] A. Rosas-Hernández, H. Junge, M. Beller, M. Roemelt, R. Francke, *Catal. Sci. Technol.* **2017**, *7*, 459–465.
[141] A. Rosas-Hernández, P. G. Alsabeh, E. Barsch, H. Junge, R. Ludwig, M. Beller, *Chem. Commun.* **2016**, *52*, 8393–8396.
[142] S.-M. Kuang, D. G. Cuttell, D. R. McMillin, P. E. Fanwick, R. A. Walton, *Inorg. Chem.* **2002**, *41*, 3313–3322.
[143] H.-J. Knölker, J. Heber, C. H. Mahler, *Synlett* **1992**, *1992*, 1002–1004.
[144] A. Kaeser, M. Mohankumar, J. Mohanraj, F. Monti, M. Holler, J.-J. Cid, O. Moudam, I. Nierengarten, L. Karmazin-Brelot, C. Duhayon, B. Delavaux-Nicot, N. Armaroli, J.-F. Nierengarten, *Inorg. Chem.* **2013**, *52*, 12140–12151.
[145] H. Junge, N. Rockstroh, S. Fischer, A. Brückner, R. Ludwig, S. Lochbrunner, O. Kühn, M. Beller, *Inorganics* **2017**, *5*, 14.
[146] H. Takeda, H. Koizumi, K. Okamoto, O. Ishitani, *Chem. Commun.* **2014**, *50*, 1491–1493.
[147] C. Steinlechner, A. F. Roesel, E. Oberem, A. Päpcke, N. Rockstroh, F. Gloaguen, S. Lochbrunner, R. Ludwig, A. Spannenberg, H. Junge, R. Francke, M. Beller, *ACS Catal.* **2020**, *10*, 578–579.
[148] H. Rao, L. C. Schmidt, J. Bonin, M. Robert, *Nature* **2017**, *548*, 74–77.
[149] H. Shirley, X. Su, H. Sanjanwala, K. Talukdar, J. W. Jurss, J. H. Delcamp, *J. Am. Chem. Soc.* **2019**, *141*, 6617–6622.
[150] R. J. Spreitzer, M. E. Salvucci, *Annu. Rev. Plant Biol.* **2002**, *53*, 449–475.
[151] K. Adachi, K. Ohta, T. Mizuno, *Solar Energy* **1994**, *53*, 187–190.
[152] N. Li, B. Wang, Y. Si, F. Xue, J. Zhou, Y. Lu, M. Liu, *ACS Catal.* **2019**, *9*, 5590–5602.
[153] Y. Xia, K. Xiao, B. Cheng, J. Yu, L. Jiang, M. Antonietti, S. Cao, *ChemSusChem* **2020**, *13*, 1730–1734.
[154] P. Gao, S. Dang, S. Li, X. Bu, Z. Liu, M. Qiu, C. Yang, H. Wang, L. Zhong, Y. Han, Q. Liu, W. Wei, Y. Sun, *ACS Catal.* **2018**, *8*, 571–578.

[155] L. Wang, L. Wang, J. Zhang, X. Liu, H. Wang, W. Zhang, Q. Yang, J. Ma, X. Dong, S. J. Yoo, J.-G. Kim, X. Meng, F.-S. Xiao, *Angew. Chem. Int. Ed.* **2018**, *57*, 6104–6108.
[156] Y. Ni, Z. Chen, Y. Fu, Y. Liu, W. Zhu, Z. Liu, *Nat. Commun.* **2018**, *9*, 3457.
[157] P. Gao, S. Li, X. Bu, S. Dang, Z. Liu, H. Wang, L. Zhong, M. Qiu, C. Yang, J. Cai, W. Wei, Y. Sun, *Nat. Chem.* **2017**, *9*, 1019–1024.
[158] Q. Qian, M. Cui, Z. He, C. Wu, Q. Zhu, Z. Zhang, J. Ma, G. Yang, J. Zhang, B. Han, *Chem. Sci.* **2015**, *6*, 5685–5689.
[159] M. Cui, Q. Qian, Z. He, Z. Zhang, J. Ma, T. Wu, G. Yang, B. Han, *Chem. Sci.* **2016**, *7*, 5200–5205.
[160] H. Wang, Y. Zhao, Y. Wu, R. Li, H. Zhang, B. Yu, F. Zhang, J. Xiang, Z. Wang, Z. Liu, *ChemSusChem* **2019**, *12*, 4390–4394.
[161] J. Y. Becker, B. Vainas, R. Eger, L. Kaufman, *J. Chem. Soc., Chem. Commun.* **1985**, 1471–1472.
[162] H. Mistry, A. S. Varela, C. S. Bonifacio, I. Zegkinoglou, I. Sinev, Y.-W. Choi, K. Kisslinger, E. A. Stach, J. C. Yang, P. Strasser, B. Roldan Cuenya, *Nat. Commun.* **2016**, *7*, 12123.
[163] H. Han, Y. Noh, Y. Kim, S. Park, W. Yoon, D. Jang, S. M. Choi, W. B. Kim, *Green Chem.* **2020**, *22*, 71–84.
[164] Y. Kushi, H. Nagao, T. Nishioka, K. Isobe, K. Tanaka, *Chem. Lett.* **1994**, *23*, 2175–2178.
[165] Y. Kushi, H. Nagao, T. Nishioka, K. Isobe, K. Tanaka, *J. Chem. Soc., Chem. Commun.* **1995**, 1223–1224.
[166] K. Tanaka, Y. Kushi, K. Tsuge, K. Toyohara, T. Nishioka, K. Isobe, *Inorg. Chem.* **1998**, *37*, 120–126.
[167] M. M. Ali, H. Sato, T. Mizukawa, K. Tsuge, M.-a. Haga, K. Tanaka, *Chem. Commun.* **1998**, 249–250.
[168] M. Rudolph, S. Dautz, E.-G. Jäger, *J. Am. Chem. Soc.* **2000**, *122*, 10821–10830.
[169] R. Angamuthu, P. Byers, M. Lutz, A. L. Spek, E. Bouwman, *Science* **2010**, *327*, 313–315.
[170] P. Ghosh, A. Roychowdhury, M. Corbella, A. Bhaumik, P. Mitra, S. M. Mobin, A. Mukherjee, S. Basu, P. Banerjee, *Dalton Trans.* **2014**, *43*, 13500–13508.
[171] H.-O. Fröhlich, H. Schreer, *Z. Chem.* **1983**, *23*, 348–349.
[172] A. Paparo, J. S. Silvia, C. E. Kefalidis, T. P. Spaniol, L. Maron, J. Okuda, C. C. Cummins, *Angew. Chem. Int. Ed.* **2015**, *54*, 9115–9119.
[173] D. H. Woen, G. P. Chen, J. W. Ziller, T. J. Boyle, F. Furche, W. J. Evans, *Angew. Chem. Int. Ed.* **2017**, *56*, 2050–2053.
[174] D. M. Y. Barrett Adams, I. A. Kahwa, J. T. Mague, *New J. Chem.* **1998**, *22*, 919–921.
[175] W. J. Evans, C. A. Seibel, J. W. Ziller, *Inorg. Chem.* **1998**, *37*, 770–776.
[176] W. J. Evans, J. M. Perotti, J. C. Brady, J. W. Ziller, *J. Am. Chem. Soc.* **2003**, *125*, 5204–5212.
[177] W. J. Evans, S. E. Lorenz, J. W. Ziller, *Inorg. Chem.* **2009**, *48*, 2001–2009.
[178] J. Andrez, J. Pécaut, P.-A. Bayle, M. Mazzanti, *Angew. Chem. Int. Ed.* **2014**, *53*, 10448–10452.
[179] A. R. Willauer, D. Toniolo, F. Fadaei-Tirani, Y. Yang, M. Laurent, M. Mazzanti, *Dalton Trans.* **2019**, *48*, 6100–6110.
[180] L. Castro, D. P. Mills, C. Jones, L. Maron, *Eur. J. Inorg. Chem.* **2016**, *2016*, 792–796.
[181] N. Tsoureas, L. Castro, A. F. R. Kilpatrick, F. G. N. Cloke, L. Maron, *Chem. Sci.* **2014**, *5*, 3777–3788.
[182] C. J. Inman, A. S. P. Frey, A. F. R. Kilpatrick, F. G. N. Cloke, S. M. Roe, *Organometallics* **2017**,

36, 4539–4545.
[183] A.-C. Schmidt, F. W. Heinemann, C. E. Kefalidis, L. Maron, P. W. Roesky, K. Meyer, *Chem. Eur. J.* **2014**, *20*, 13501–13506.
[184] A. Formanuik, F. Ortu, C. J. Inman, A. Kerridge, L. Castro, L. Maron, D. P. Mills, *Chem. Eur. J.* **2016**, *22*, 17976–17979.
[185] R. Lalrempuia, A. Stasch, C. Jones, *Chem. Sci.* **2013**, *4*, 4383–4388.
[186] M. Aresta, R. Gobetto, E. Quaranta, I. Tommasi, *Inorg. Chem.* **1992**, *31*, 4286–4290.
[187] B. Horn, C. Limberg, C. Herwig, B. Braun, *Chem. Commun.* **2013**, *49*, 10923–10925.
[188] A. Klose, J. Hesschenbrouck, E. Solari, M. Latronico, C. Floriani, N. Re, A. Chiesi-Villa, C. Rizzoli, *J. Organomet. Chem.* **1999**, *591*, 45–62.
[189] C. C. Lu, C. T. Saouma, M. W. Day, J. C. Peters, *J. Am. Chem. Soc.* **2007**, *129*, 4–5.
[190] C. T. Saouma, C. C. Lu, M. W. Day, J. C. Peters, *Chem. Sci.* **2013**, *4*, 4042–4051.
[191] Y.-T. Tseng, W.-M. Ching, W.-F. Liaw, T.-T. Lu, *Angew. Chem. Int. Ed.* **2020**, *59*, 11819–11823.
[192] L. J. Farrugia, S. Lopinski, P. A. Lovatt, R. D. Peacock, *Inorg. Chem.* **2001**, *40*, 558–559.
[193] H. Takisawa, Y. Morishima, S. Soma, R. K. Szilagyi, K. Fujisawa, *Inorg. Chem.* **2014**, *53*, 8191–8193.
[194] U. R. Pokharel, F. R. Fronczek, A. W. Maverick, *Nat. Commun.* **2014**, *5*, 5883.
[195] B. J. Cook, G. N. Di Francesco, K. A. Abboud, L. J. Murray, *J. Am. Chem. Soc.* **2018**, *140*, 5696–5700.
[196] J. F. Hartwig, *Organotransition metal chemistry: From bonding to catalysis*, University Science Books, **2010**, 546–547.
[197] E. Lamy, L. Nadjo, J. M. Saveant, *J. Electroanal. Chem.* **1977**, *78*, 403–407.
[198] U. Kaiser, E. Heitz, *Ber. Bunsenges. Phys. Chem.* **1973**, *77*, 818–823.
[199] Y. Hori, A. Murata, R. Takahashi, S. Suzuki, *J. Am. Chem. Soc.* **1987**, *109*, 5022–5023.
[200] G. Filardo, S. Gambino, G. Silvestri, A. Gennaro, E. Vianello, *J. Electroanal. Chem.* **1984**, *177*, 303–309.
[201] S.-N. Pun, W.-H. Chung, K.-M. Lam, P. Guo, P.-H. Chan, K.-Y. Wong, C.-M. Che, T.-Y. Chen, S.-M. Peng, *J. Chem. Soc., Dalton Trans.* **2002**, 575–583.
[202] M. Y. Udugala-Ganehenege, N. M. Dissanayake, Y. Liu, A. M. Bond, J. Zhang, *Transit. Metal Chem.* **2014**, *39*, 819–830.
[203] B. J. Fisher, R. Eisenberg, *J. Am. Chem. Soc.* **1980**, *102*, 7361–7363.
[204] M. Beley, J.-P. Collin, R. Ruppert, J.-P. Sauvage, *J. Chem. Soc., Chem. Commun.* **1984**, 1315–1316.
[205] K. Pavani, M. Singh, A. Ramanan, *Austr. J. Chem.* **2011**, *64*, 68–76.
[206] A. M. López Marzo, M. Guerrero, T. Calvet, M. Font-Bardia, E. Pellicer, M. D. Baró, J. Pons, J. Sort, *RSC Adv.* **2015**, *5*, 32369–32375.
[207] A.-H. Yang, Y.-P. Quan, L.-h. Zhao, J.-Z. Cui, H.-L. Gao, F.-L. Lu, W. Shi, P. Cheng, *J. Coord. Chem.* **2009**, *62*, 3306–3313.
[208] M. Frisch, C. L. Cahill, *J. Solid State Chem.* **2007**, *180*, 2597–2602.
[209] S. K. Ghosh, G. Savitha, P. K. Bharadwaj, *Inorg. Chem.* **2004**, *43*, 5495–5497.
[210] D. Min, S. W. Lee, *Inorg. Chem. Commun.* **2002**, *5*, 978–983.
[211] P. Thuéry, J. Harrowfield, *Eur. J. Inorg. Chem.* **2018**, *2018*, 1016–1027.
[212] P. C. R. Soares-Santos, L. Cunha-Silva, F. A. A. Paz, R. A. S. Ferreira, J. Rocha, L. D. Carlos, H. I. S. Nogueira, *Inorg. Chem.* **2010**, *49*, 3428–3440.

[213] G.-X. Liu, K. Zhu, H. Chen, R.-Y. Huang, X.-M. Ren, *Z. Anorg. Allg. Chem.* **2009**, *635*, 156–164.
[214] P. Thuéry, *Cryst. Growth Des.* **2014**, *14*, 2665–2676.
[215] P. DeBurgomaster, J. Zubieta, *Inorg. Chim. Acta* **2010**, *363*, 2912–2919.
[216] A. M. Thomas, G. C. Mandal, S. K. Tiwary, R. K. Rath, A. R. Chakravarty, *J. Chem. Soc., Dalton Trans.* **2000**, 1395–1396.
[217] R. T. Stibrany, H. J. Schugar, J. A. Potenza, *Acta Cryst. E* **2005**, *61*, m1904–m1906.
[218] M. Mangoli, M. Tabatabaee, S. Jame-Bozorgi, M. Ramazani, M. Kučeráková, *Inorg. Nano-Met. Chem.* **2020**, *50*, 1353–1357.
[219] M. Kato, A. K. Sah, T. Tanase, M. Mikuriya, *Inorg. Chem.* **2006**, *45*, 6646–6660.
[220] K. E. Knope, H. Kimura, Y. Yasaka, M. Nakahara, M. B. Andrews, C. L. Cahill, *Inorg. Chem.* **2012**, *51*, 3883–3890.
[221] S. A. Cotton, *Lanthanide and actinide chemistry*, Inorganic chemistry, Wiley, Chichester and Hoboken, **2006**, 6, 38.
[222] W.-K. Wong, L.-L. Zhang, F. Xue, T. C. W. Mak, *J. Chem. Soc., Dalton Trans.* **2000**, 2245–2246.
[223] P. L. Arnold, Z. R. Turner, *Nat. Rev. Chem.* **2017**, *1*, 0002.
[224] C. E. Kefalidis, A. Stasch, C. Jones, L. Maron, *Chem. Commun.* **2014**, *50*, 12318–12321.
[225] M. Aresta, C. F. Nobile, V. G. Albano, E. Forni, M. Manassero, *J. Chem. Soc., Chem. Commun.* **1975**, 636–637.
[226] M. J. Belousoff, B. Graham, B. Moubaraki, K. S. Murray, L. Spiccia, *Eur. J. Inorg. Chem.* **2006**, *2006*, 4872–4878.
[227] A. M. Thomas, B.-L. Lin, E. C. Wasinger, T. D. P. Stack, *J. Am. Chem. Soc.* **2013**, *135*, 18912–18919.
[228] P. A. Forero-Cortés, M. Marx, N. G. Moustakas, F. Brunner, C. E. Housecroft, E. C. Constable, H. Junge, M. Beller, J. Strunk, *Green Chem.* **2020**, *22*, 4541–4549.
[229] X. Zhang, M. Cibian, A. Call, K. Yamauchi, K. Sakai, *ACS Catal.* **2019**, *9*, 11263–11273.
[230] L. A. Blanchard, D. Hancu, E. J. Beckman, J. F. Brennecke, *Nature* **1999**, *399*, 28–29.
[231] Y. Chen, T. Mu, *Green Chem.* **2019**, *21*, 2544–2574.
[232] D. C. Grills, E. Fujita, *J. Phys. Chem. Lett.* **2010**, *1*, 2709–2718.
[233] J. Lin, Z. Ding, Y. Hou, X. Wang, *Sci. Rep.* **2013**, *3*, 1056.
[234] M. Ramdin, T. J. H. Vlugt, T. W. de Loos, *J. Chem. Eng. Data* **2012**, *57*, 2275–2280.
[235] M. Klähn, A. Seduraman, *J. Phys. Chem. B* **2015**, *119*, 10066–10078.
[236] Y. Chen, G. Ji, S. Guo, B. Yu, Y. Zhao, Y. Wu, H. Zhang, Z. Liu, B. Han, Z. Liu, *Green Chem.* **2017**, *19*, 5777–5781.
[237] Y. Asai, H. Katsuragi, K. Kita, T. Tsubomura, Y. Yamazaki, *Dalton Trans.* **2020**, *49*, 4277–4292.
[238] W. Lu, B. Jia, B. Cui, Y. Zhang, K. Yao, Y. Zhao, J. Wang, *Angew. Chem. Int. Ed.* **2017**, *56*, 11851–11854.
[239] G. Zeng, J. Qiu, B. Hou, H. Shi, Y. Lin, M. Hettick, A. Javey, S. B. Cronin, *Chem. Eur. J.* **2015**, *21*, 13502–13507.
[240] M. Kranenburg, Y. E. M. van der Burgt, P. C. J. Kamer, P. W. N. M. van Leeuwen, K. Goubitz, J. Fraanje, *Organometallics* **1995**, *14*, 3081–3089.
[241] E. Oberem, A. F. Roesel, A. Rosas-Hernández, T. Kull, S. Fischer, A. Spannenberg, H. Junge, M. Beller, R. Ludwig, M. Roemelt, R. Francke, *Organometallics* **2019**, *38*, 1236–1247.
[242] W. J. Dressick, J. R. Deschamps, R. H. Schmehl, K. P. Martinez, S. A. Trammell, E. Goldberg, D. Andrew Knight, *Inorg. Chem. Commun.* **2017**, *83*, 55–58.

[243] O. G. Shakirova, L. G. Lavrenova, N. V. Kuratieva, A. S. Bogomyakov, L. A. Sheludyakova, A. P. Mosalkova, Y. V. Grigoriev, *J. Struct. Chem.* **2017**, *58*, 919–925.
[244] M. Marx, A. Mele, A. Spannenberg, C. Steinlechner, H. Junge, P. Schollhammer, M. Beller, *ChemCatChem* **2020**, *12*, 1603–1608.
[245] M. Frey, *ChemBioChem* **2002**, *3*, 153–160.
[246] W. Lubitz, H. Ogata, O. Rüdiger, E. Reijerse, *Chem. Rev.* **2014**, *114*, 4081–4148.
[247] J.-F. Capon, F. Gloaguen, F. Y. Pétillon, P. Schollhammer, J. Talarmin, *Eur. J. Inorg. Chem.* **2008**, *2008*, 4671–4681.
[248] S. Tschierlei, S. Ott, R. Lomoth, *Energy Environ. Sci.* **2011**, *4*, 2340–2352.
[249] Y. Li, T. B. Rauchfuss, *Chem. Rev.* **2016**, *116*, 7043–7077.
[250] L.-C. Song, *Acc. Chem. Res.* **2005**, *38*, 21–28.
[251] G. A. N. Felton, C. A. Mebi, B. J. Petro, A. K. Vannucci, D. H. Evans, R. S. Glass, D. L. Lichtenberger, *J. Organomet. Chem.* **2009**, *694*, 2681–2699.
[252] J.-F. Capon, F. Gloaguen, P. Schollhammer, J. Talarmin, *J. Electroanal. Chem.* **2004**, *566*, 241–247.
[253] P.-H. Zhao, Z.-Y. Ma, M.-Y. Hu, J. He, Y.-Z. Wang, X.-B. Jing, H.-Y. Chen, Z. Wang, Y.-L. Li, *Organometallics* **2018**, *37*, 1280–1290.
[254] S. Roy, T. L. Groy, A. K. Jones, *Dalton Trans.* **2013**, *42*, 3843–3853.
[255] S. Roy, J. A. Laureanti, T. L. Groy, A. K. Jones, *Eur. J. Inorg. Chem.* **2017**, *2017*, 2942–2950.
[256] L.-C. Song, W. Gao, X. Luo, Z.-X. Wang, X.-J. Sun, H.-B. Song, *Organometallics* **2012**, *31*, 3324–3332.
[257] M. E. Carroll, B. E. Barton, T. B. Rauchfuss, P. J. Carroll, *J. Am. Chem. Soc.* **2012**, *134*, 18843–18852.
[258] L. Schwartz, P. S. Singh, L. Eriksson, R. Lomoth, S. Ott, *C. R. Chimie* **2008**, *11*, 875–889.
[259] P.-H. Zhao, M.-Y. Hu, J.-R. Li, Z.-Y. Ma, Y.-Z. Wang, J. He, Y.-L. Li, X.-F. Liu, *Organometallics* **2019**, *38*, 385–394.
[260] S. Bruña, I. Cuadrado, E. Delgado, C. J. Gómez-García, D. Hernández, E. Hernández, R. Llusar, A. Martín, N. Menéndez, V. Polo, F. Zamora, *Dalton Trans.* **2014**, *43*, 13187–13195.
[261] B. R. Garrett, A. Awad, M. He, K. A. Click, C. B. Durr, J. C. Gallucci, C. M. Hadad, Y. Wu, *Polyhedron* **2016**, *103*, 21–27.
[262] J. Zhao, Z. Wei, X. Zeng, X. Liu, *Dalton Trans.* **2012**, *41*, 11125–11133.
[263] M. Cheng, M. Wang, D. Zheng, L. Sun, *Dalton Trans.* **2016**, *45*, 17687–17696.
[264] M. Karnahl, S. Tschierlei, O. F. Erdem, S. Pullen, M.-P. Santoni, E. J. Reijerse, W. Lubitz, S. Ott, *Dalton Trans.* **2012**, *41*, 12468–12477.
[265] P.-Y. Orain, J.-F. Capon, N. Kervarec, F. Gloaguen, F. Pétillon, R. Pichon, P. Schollhammer, J. Talarmin, *Dalton Trans.* **2007**, 3754–3756.
[266] W. Wang, T. B. Rauchfuss, C. E. Moore, A. L. Rheingold, L. De Gioia, G. Zampella, *Chem. Eur. J.* **2013**, *19*, 15476–15479.
[267] S. Ezzaher, J.-F. Capon, F. Gloaguen, F. Y. Pétillon, P. Schollhammer, J. Talarmin, R. Pichon, N. Kervarec, *Inorg. Chem.* **2007**, *46*, 3426–3428.
[268] S. Ezzaher, J.-F. Capon, F. Gloaguen, F. Y. Pétillon, P. Schollhammer, J. Talarmin, *Inorg. Chem.* **2007**, *46*, 9863–9872.
[269] S. Munery, J.-F. Capon, L. De Gioia, C. Elleouet, C. Greco, F. Y. Pétillon, P. Schollhammer, J. Talarmin, G. Zampella, *Chem. Eur. J.* **2013**, *19*, 15458–15461.

[270] P. S. Singh, H. C. Rudbeck, P. Huang, S. Ezzaher, L. Eriksson, M. Stein, S. Ott, R. Lomoth, *Inorg. Chem.* **2009**, *48*, 10883–10885.
[271] M. Cheng, Y. Yu, X. Zhou, Y. Luo, M. Wang, *ACS Catal.* **2019**, *9*, 768–774.
[272] C.-H. Lim, S. Ilic, A. Alherz, B. T. Worrell, S. S. Bacon, J. T. Hynes, K. D. Glusac, C. B. Musgrave, *J. Am. Chem. Soc.* **2019**, *141*, 272–280.
[273] C. Lübbe, A. Dumrath, H. Neumann, M. Schäffer, R. Zimmermann, M. Beller, R. Kadyrov, *ChemCatChem* **2014**, *6*, 684–688.
[274] P. Dierkes, P. W. N. M. van Leeuwen, *J. Chem. Soc., Dalton Trans.* **1999**, 1519–1530.
[275] J. L. Bingaman, C. L. Kohnhorst, G. A. van Meter, B. A. McElroy, E. A. Rakowski, B. W. Caplins, T. A. Gutowski, C. J. Stromberg, C. E. Webster, E. J. Heilweil, *J. Phys. Chem.* **2012**, *116*, 7261–7271.
[276] B. W. Caplins, J. P. Lomont, S. C. Nguyen, C. B. Harris, *J. Phys. Chem.* **2014**, *118*, 11529–11540.
[277] P. G. Alsabeh, A. Rosas-Hernández, E. Barsch, H. Junge, R. Ludwig, M. Beller, *Catal. Sci. Technol.* **2016**, *6*, 3623–3630.
[278] M. Baker, *Nature* **2016**, *533*, 452–454.
[279] K. Dong, S. Elangovan, R. Sang, A. Spannenberg, R. Jackstell, K. Junge, Y. Li, M. Beller, *Nat. Commun.* **2016**, *7*, 12075.
[280] B.-Y. Yu, I.-L. Chien, *Chem. Eng. Res. Des.* **2017**, *121*, 173–190.
[281] P. L. Burk, D. van Engen, K. S. Campo, *Organometallics* **1984**, *3*, 493–495.
[282] J. Lan, T. Liao, T. Zhang, L. W. Chung, *Inorg. Chem.* **2017**, *56*, 6809–6819.
[283] E. C. M. Ording-Wenker, M. A. Siegler, E. Bouwman, *Inorg. Chim. Acta* **2015**, *428*, 193–202.
[284] V. L. Goedken, Y.-A. Park, *J. Chem. Soc., Chem. Commun.* **1975**, 214–215.
[285] N. G. Connelly, W. E. Geiger, *Chem. Rev.* **1996**, *96*, 877–910.
[286] J. H. Niewahner, K. A. Walters, A. Wagner, *J. Chem. Ed.* **2007**, *84*, 477–479.
[287] S. Hohloch, M. E. Garner, C. H. Booth, W. W. Lukens, C. A. Gould, D. J. Lussier, L. Maron, J. Arnold, *Angew. Chem. Int. Ed.* **2018**, *57*, 16136–16140.
[288] R. S. McBride, *J. Am. Chem. Soc.* **1912**, *34*, 393–416.
[289] W. R. Knocke, J. E. van Benschoten, M. J. Kearney, A. W. Soborski, D. A. Reckhow, *J. Am. Water Works Ass.* **1991**, *83*, 80–87.
[290] N. Singh, D. G. Lee, *Org. Proc. Res. Dev.* **2001**, *5*, 599–603.
[291] B. A. Sayer, J. P. Michael, R. D. Hancock, *Inorg. Chim. Acta* **1983**, *77*, L63–L64.
[292] K. Wieghardt, U. Bossek, M. Guttmann, J. Weiss, *Z. Naturforsch. B* **1983**, *38b*, 81–89.
[293] M. J. van der Merwe, J. C. A. Boeyens, R. D. Hancock, *Inorg. Chem.* **1985**, *24*, 1208–1213.
[294] K. Wieghardt, E. Schoeffmann, B. Nuber, J. Weiss, *Inorg. Chem.* **1986**, *25*, 4877–4883.
[295] G. A. McLachlan, G. D. Fallon, R. L. Martin, L. Spiccia, *Inorg. Chem.* **1995**, *34*, 254–261.
[296] X. Zhang, W.-Y. Hsieh, T. N. Margulis, L. J. Zompa, *Inorg. Chem.* **1995**, *34*, 2883–2888.
[297] M. J. Young, J. Chin, *J. Am. Chem. Soc.* **1995**, *117*, 10577–10578.
[298] S. Mahapatra, J. A. Halfen, E. C. Wilkinson, G. Pan, C. J. Cramer, L. Que Jr., W. B. Tolman, *J. Am. Chem. Soc.* **1995**, *117*, 8865–8866.
[299] S. Mahapatra, J. A. Halfen, E. C. Wilkinson, G. Pan, X. Wang, V. G. Young, C. J. Cramer, L. Que Jr., W. B. Tolman, *J. Am. Chem. Soc.* **1996**, *118*, 11555–11574.
[300] S. Mahapatra, V. G. Young, S. Kaderli, A. D. Zuberbühler, W. B. Tolman, *Angew. Chem. Int. Ed.* **1997**, *36*, 130–133.

[301] R. P. Houser, J. A. Halfen, V. G. Young, N. J. Blackburn, W. B. Tolman, *J. Am. Chem. Soc.* **1995**, *117*, 10745–10746.
[302] R. P. Houser, V. G. Young, W. B. Tolman, *J. Am. Chem. Soc.* **1996**, *118*, 2101–2102.
[303] L. J. Farrugia, P. A. Lovatt, R. D. Peacock, *Inorg. Chim. Acta* **1996**, *246*, 343–348.
[304] J. A. Halfen, V. G. Young, W. B. Tolman, *J. Am. Chem. Soc.* **1996**, *118*, 10920–10921.
[305] L. J. Farrugia, P. A. Lovatt, R. D. Peacock, *J. Chem. Soc., Dalton Trans.* **1997**, 911–912.
[306] R. Haidar, M. Ipek, B. DasGupta, M. Yousaf, L. J. Zompa, *Inorg. Chem.* **1997**, *36*, 3125–3132.
[307] J. L. Schneider, J. A. Halfen, V. G. Young, W. B. Tolman, *New J. Chem.* **1998**, *22*, 459–466.
[308] D. Ellis, L. J. Farrugia, R. D. Peacock, *Polyhedron* **1999**, *18*, 1229–1234.
[309] M. Enomoto, T. Aida, *J. Am. Chem. Soc.* **1999**, *121*, 874–875.
[310] A. J. Blake, J. P. Danks, W.-S. Li, V. Lippolis, M. Schröder, *J. Chem. Soc., Dalton Trans.* **2000**, 3034–3040.
[311] M. Di Vaira, F. Mani, P. Stoppioni, *Inorg. Chim. Acta* **2000**, *303*, 61–69.
[312] A. C. Benniston, D. Ellis, L. J. Farrugia, R. Kennedy, R. D. Peacock, S. Walker, *Polyhedron* **2002**, *21*, 333–342.
[313] S. Pulacchini, K. F. Sibbons, K. Shastri, M. Motevalli, M. Watkinson, H. Wan, A. Whiting, A. P. Lightfoot, *Dalton Trans.* **2003**, 2043–2052.
[314] L. Tei, A. J. Blake, V. Lippolis, C. Wilson, M. Schröder, *Dalton Trans.* **2003**, 304–310.
[315] D. Dussalt, S. Friedle, L. J. Zompa, *Inorg. Chim. Acta* **2004**, *357*, 1478–1486.
[316] L. Tang, J. Park, H.-J. Kim, Y. Kim, S. J. Kim, J. Chin, K. M. Kim, *J. Am. Chem. Soc.* **2008**, *130*, 12606–12607.
[317] J. Ackermann, S. Buchler, F. Meyer, *C. R. Chimie* **2007**, *10*, 421–432.
[318] K. E. Dalle, T. Gruene, S. Dechert, S. Demeshko, F. Meyer, *J. Am. Chem. Soc.* **2014**, *136*, 7428–7434.
[319] M. Le Fur, M. Beyler, N. Le Poul, L. M. P. Lima, Y. Le Mest, R. Delgado, C. Platas-Iglesias, V. Patinec, R. Tripier, *Dalton Trans.* **2016**, *45*, 7406–7420.
[320] S. T. Li, B. Braun-Cula, S. Hoof, M. Dürr, I. Ivanović-Burmazović, C. Limberg, *Eur. J. Inorg. Chem.* **2016**, *2016*, 4017–4027.
[321] S. T. Li, B. Braun-Cula, S. Hoof, C. Limberg, *Dalton Trans.* **2018**, *47*, 544–560.
[322] A. Guillou, L. M. P. Lima, M. Roger, D. Esteban-Gómez, R. Delgado, C. Platas-Iglesias, V. Patinec, R. Tripier, *Eur. J. Inorg. Chem.* **2017**, *2017*, 2435–2443.
[323] A. Buttafava, L. Fabbrizzi, A. Perotti, A. Poggi, G. Poli, B. Seghi, *Inorg. Chem.* **1986**, *25*, 1456–1461.
[324] D. W. White, B. A. Karcher, R. A. Jacobson, J. G. Verkade, *J. Am. Chem. Soc.* **1979**, *101*, 4921–4925.
[325] C. A. Barta, S. R. Bayly, P. W. Read, B. O. Patrick, R. C. Thompson, C. Orvig, *Inorg. Chem.* **2008**, *47*, 2280–2293.
[326] M. V. Baker, D. H. Brown, B. W. Skelton, A. H. White, *Austr. J. Chem.* **2002**, *55*, 655–660.
[327] M. G. B. Drew, C. Cairns, S. G. McFall, S. M. Nelson, *J. Chem. Soc., Dalton Trans.* **1980**, 2020–2027.
[328] S. S. Batsanov, *Inorg. Mater.* **2001**, *37*, 871–885.
[329] C. F. Macrae, I. Sovago, S. J. Cottrell, P. T. A. Galek, P. McCabe, E. Pidcock, M. Platings, G. P. Shields, J. S. Stevens, M. Towler, P. A. Wood, *J. Appl. Cryst.* **2020**, *53*, 226–235.
[330] OriginLab Corporation, *OriginPro*, Version 2020, Northampton, MA, USA.

[331] N. Kitajima, K. Fujisawa, C. Fujimoto, Y. Morooka, S. Hashimoto, T. Kitagawa, K. Toriumi, K. Tatsumi, A. Nakamura, *J. Am. Chem. Soc.* **1992**, *114*, 1277–1291.
[332] R. F. Jordan, S. F. Echols, *Inorg. Chem.* **1987**, *26*, 383–386.
[333] P. S. Lakkaraju, M. Askerka, H. Beyer, C. T. Ryan, T. Dobbins, C. Bennett, J. J. Kaczur, V. S. Batista, *ChemCatChem* **2016**, *8*, 3453–3457.
[334] Y.-X. Li, S.-S. Li, D.-M. Xue, X.-Q. Liu, M.-M. Jin, L.-B. Sun, *J. Mater. Chem. A* **2018**, *6*, 8930–8939.
[335] J. F. Walker, N. D. Scott, *J. Am. Chem. Soc.* **1938**, *60*, 951–955.
[336] D. E. Paul, D. Lipkin, S. I. Weissman, *J. Am. Chem. Soc.* **1956**, *78*, 116–120.
[337] E. Ben-Ari, G. Leitus, L. J. W. Shimon, D. Milstein, *J. Am. Chem. Soc.* **2006**, *128*, 15390–15391.
[338] A. Mukherjee, D. Milstein, *ACS Catal.* **2018**, *8*, 11435–11469.
[339] E. Peris, R. H. Crabtree, *Chem. Soc. Rev.* **2018**, *47*, 1959–1968.
[340] S. Chakraborty, H. Dai, P. Bhattacharya, N. T. Fairweather, M. S. Gibson, J. A. Krause, H. Guan, *J. Am. Chem. Soc.* **2014**, *136*, 7869–7872.
[341] S. Elangovan, C. Topf, S. Fischer, H. Jiao, A. Spannenberg, W. Baumann, R. Ludwig, K. Junge, M. Beller, *J. Am. Chem. Soc.* **2016**, *138*, 8809–8814.
[342] I. Klopsch, M. Kinauer, M. Finger, C. Würtele, S. Schneider, *Angew. Chem. Int. Ed.* **2016**, *55*, 4786–4789.
[343] P. O. Lagaditis, B. Schluschaß, S. Demeshko, C. Würtele, S. Schneider, *Inorg. Chem.* **2016**, *55*, 4529–4536.
[344] P. Piehl, M. Peña-López, A. Frey, H. Neumann, M. Beller, *Chem. Commun.* **2017**, *53*, 3265–3268.
[345] F. Schneck, M. Finger, M. Tromp, S. Schneider, *Chem. Eur. J.* **2017**, *23*, 33–37.
[346] F. Schneck, J. Ahrens, M. Finger, A. C. Stückl, C. Würtele, D. Schwarzer, S. Schneider, *Nat. Commun.* **2018**, *9*, 1161.
[347] M. Garbe, K. Junge, S. Walker, Z. Wei, H. Jiao, A. Spannenberg, S. Bachmann, M. Scalone, M. Beller, *Angew. Chem. Int. Ed.* **2017**, *56*, 11237–11241.
[348] K. Junge, B. Wendt, A. Cingolani, A. Spannenberg, Z. Wei, H. Jiao, M. Beller, *Chem. Eur. J.* **2018**, *24*, 1046–1052.
[349] T. Leischner, A. Spannenberg, K. Junge, M. Beller, *Organometallics* **2018**, *37*, 4402–4408.
[350] P. Ryabchuk, K. Stier, K. Junge, M. P. Checinski, M. Beller, *J. Am. Chem. Soc.* **2019**, *141*, 16923–16929.
[351] P. Piehl, R. Amuso, E. Alberico, H. Junge, B. Gabriele, H. Neumann, M. Beller, *Chem. Eur. J.* **2020**, *26*, 6050–6055.
[352] J. M. Ahn, J. C. Peters, G. C. Fu, *J. Am. Chem. Soc.* **2017**, *139*, 18101–18106.
[353] S. Y. de Boer, Y. Gloaguen, M. Lutz, J. I. van der Vlugt, *Inorg. Chim. Acta* **2012**, *380*, 336–342.
[354] M. Mastalir, E. Pittenauer, B. Stöger, G. Allmaier, K. Kirchner, *Org. Lett.* **2017**, *19*, 2178–2181.
[355] L. M. Kumar, R. M. Ansari, B. R. Bhat, *Appl. Organomet. Chem.* **2018**, *32*, e4054.
[356] K. Abdur-Rashid, T. Graham, C.-W. Tsang, X. Chen, R. Guo, W. Jia, D. Amoroso, C. Sui-Seng, *Kanata Chemical Technologies Inc.* ,WO2008141439A1, *The generation of hydrogen from ammonia borane through catalytic hydrolysis*, **2008**.
[357] M. M. T. Khan, P. Paul, K. Venkatasubramanian, S. Purohit, *Inorg. Chim. Acta* **1991**, *183*, 229–237.
[358] M. M. T. Khan, P. Paul, K. Venkatasubramanian, S. Purohit, *J. Chem. Soc., Dalton Trans.* **1991**,

3405–3412.
[359] S. B. Harkins, J. C. Peters, *J. Am. Chem. Soc.* **2005**, *127*, 2030–2031.
[360] S. B. Harkins, N. P. Mankad, A. J. M. Miller, R. K. Szilagyi, J. C. Peters, *J. Am. Chem. Soc.* **2008**, *130*, 3478–3485.
[361] Z. Pan, M. T. Gamer, P. W. Roesky, *Z. Anorg. Allg. Chem.* **2006**, *632*, 744–748.
[362] E. Deschamps, B. Deschamps, J. Laure Dormieux, L. Ricard, N. Mezailles, P. Le Floch, *Dalton Trans.* **2006**, 594–602.
[363] A. Hayashi, M. Okazaki, F. Ozawa, R. Tanaka, *Organometallics* **2007**, *26*, 5246–5249.
[364] C. Ganesamoorthy, M. S. Balakrishna, P. P. George, J. T. Mague, *Inorg. Chem.* **2007**, *46*, 848–858.
[365] C. Müller, E. A. Pidko, M. Lutz, A. L. Spek, D. Vogt, *Chem. Eur. J.* **2008**, *14*, 8803–8807.
[366] J. I. van der Vlugt, E. A. Pidko, D. Vogt, M. Lutz, A. L. Spek, A. Meetsma, *Inorg. Chem.* **2008**, *47*, 4442–4444.
[367] J. I. van der Vlugt, E. A. Pidko, D. Vogt, M. Lutz, A. L. Spek, *Inorg. Chem.* **2009**, *48*, 7513–7515.
[368] J. I. van der Vlugt, E. A. Pidko, R. C. Bauer, Y. Gloaguen, M. K. Rong, M. Lutz, *Chem. Eur. J.* **2011**, *17*, 3850–3854.
[369] J. C. Deaton, S. C. Switalski, D. Y. Kondakov, R. H. Young, T. D. Pawlik, D. J. Giesen, S. B. Harkins, A. J. M. Miller, S. F. Mickenberg, J. C. Peters, *J. Am. Chem. Soc.* **2010**, *132*, 9499–9508.
[370] S. S. Rozenel, J. B. Kerr, J. Arnold, *Dalton Trans.* **2011**, *40*, 10397–10405.
[371] V. Peruzzo, C. Pretzsch, F. Tisato, M. Porchia, F. Refosco, C. Marzano, V. Gandin, E. Schiller, M. Walther, H.-J. Pietzsch, *Inorg. Chim. Acta* **2012**, *387*, 163–172.
[372] S. Kumar, G. Mani, D. Dutta, S. Mishra, *Inorg. Chem.* **2014**, *53*, 700–709.
[373] G. K. Rao, S. I. Gorelsky, I. Korobkov, D. Richeson, *Dalton Trans.* **2015**, *44*, 19153–19162.
[374] P. Arce, C. Vera, D. Escudero, J. Guerrero, A. Lappin, A. Oliver, D. H. Jara, G. Ferraudi, L. Lemus, *Dalton Trans.* **2017**, *46*, 13432–13445.
[375] F. Khamespanah, M. Marx, D. B. Crochet, U. R. Pokharel, F. R. Fronczek, A. W. Maverick, M. Beller, *Nat. Commun.* **2021**, *accepted manuscript*, DOI: 10.1038/s41467–021–21817–w.
[376] U. R. Pokharel, F. R. Fronczek, A. W. Maverick, *Dalton Trans.* **2013**, *42*, 14064–14067.
[377] J. D. Crowley, P. H. Bandeen, *Dalton Trans.* **2010**, *39*, 612–623.
[378] P. W. Atkins, J. de Paula, *Physical chemistry*, 8th ed., W.H. Freeman, New York, **2006**, 452–454.
[379] J. Xu, R. B. Jordan, *Inorg. Chem.* **1990**, *29*, 2933–2936.
[380] M. B. Davies, *Polyhedron* **1992**, *11*, 285–321.
[381] Y. Yano, S. Takano, Y. Kato, W. Tagaki, *J. Chem. Soc., Perkin Trans. 2* **1979**, 1227–1229.
[382] M. Scarpa, F. Vianello, L. Signor, L. Zennaro, A. Rigo, *Inorg. Chem.* **1996**, *35*, 5201–5206.
[383] E. Atrián-Blasco, M. del Barrio, P. Faller, C. Hureau, *Anal. Chem.* **2018**, *90*, 5909–5915.
[384] E. Jones, R. E. Hughes, *Med. Hist.* **1976**, *20*, 80–81.
[385] R. W. Herbert, E. L. Hirst, E. G. V. Percival, R. J. W. Reynolds, F. Smith, *J. Chem. Soc.* **1933**, 1270–1290.
[386] R. J. Harkrader, L. M. Plunkett, B. M. Tolbert, *Anal. Biochem.* **1976**, *72*, 310–314.
[387] P. Orioli, B. Bruni, M. Di Vaira, L. Messori, F. Piccioli, *Inorg. Chem.* **2002**, *41*, 4312–4314.
[388] M. J. Arendse, G. K. Anderson, N. P. Rath, *Polyhedron* **2001**, *20*, 2495–2503.
[389] C. Ünaleroğlu, B. Zümreoğlu-Karan, Y. Zencir, T. Hökelek, *Polyhedron* **1997**, *16*, 2155–2161.

[390] D. Magda, N. Gerasimchuk, P. Lecane, R. A. Miller, J. E. Biaglow, J. L. Sessler, *Chem. Commun.* **2002**, 2730–2731.
[391] G. de Ruiter, J. S. Costa, K. Lappalainen, O. Roubeau, P. Gamez, J. Reedijk, *Inorg. Chem. Commun.* **2008**, *11*, 787–790.
[392] J. Mecinović, R. B. Hamed, C. J. Schofield, *Angew. Chem. Int. Ed.* **2009**, *48*, 2796–2800.
[393] D. B. Shin, M. S. Feather, *J. Carbohydr. Chem.* **1990**, *9*, 461–469.
[394] T. Kurata, N. Miyake, Y. Otsuka, *Biosci. Biotechnol. Biochem.* **1996**, *60*, 1212–1214.
[395] E. Buncel, E. A. Symons, *J. Chem. Soc. D* **1970**, 164–165.
[396] T. K. Paine, H. Zheng, L. Que, *Inorg. Chem.* **2005**, *44*, 474–476.
[397] A. Mukherjee, M. A. Cranswick, M. Chakrabarti, T. K. Paine, K. Fujisawa, E. Münck, L. Que, *Inorg. Chem.* **2010**, *49*, 3618–3628.
[398] S. Hong, S. M. Huber, L. Gagliardi, C. C. Cramer, W. B. Tolman, *J. Am. Chem. Soc.* **2007**, *129*, 14190–14192.
[399] S. M. Huber, M. Z. Ertem, F. Aquilante, L. Gagliardi, W. B. Tolman, C. J. Cramer, *Chem. Eur. J.* **2009**, *15*, 4886–4895.
[400] A. K. Gupta, W. B. Tolman, *Inorg. Chem.* **2010**, *49*, 3531–3539.
[401] B. Chakraborty, P. Halder, P. R. Banerjee, T. K. Paine, *Eur. J. Inorg. Chem.* **2012**, *2012*, 5843–5853.
[402] A. R. Diebold, G. D. Straganz, E. I. Solomon, *J. Am. Chem. Soc.* **2011**, *133*, 15979–15991.
[403] T. Tietz, C. Limberg, R. Stößer, B. Ziemer, *Chem. Eur. J.* **2011**, *17*, 10010–10020.
[404] N. Kitajima, K. Fujisawa, Y. Morooka, *J. Am. Chem. Soc.* **1990**, *112*, 3210–3212.
[405] Z. R. Bell, G. R. Motson, J. C. Jeffery, J. A. McCleverty, M. D. Ward, *Polyhedron* **2001**, *20*, 2045–2053.
[406] F. Wu, H. Tong, K. Wang, X. Zhang, J. Zhang, W.-K. Wong, X. Zhu, *J. Coord. Chem.* **2016**, *69*, 926–933.
[407] O. Jana, G. Mani, *New J. Chem.* **2017**, *41*, 9361–9370.
[408] National Institute of Advanced Industrial Science and Technology, *SDBSWeb, 2-hydroxy-2-methylpropionic acid* , SDBS No. 1483, https://sdbs.db.aist.go.jp/sdbs/cgi-bin/landingpage?sdbsno=1483 (accessed 07.07.2020).
[409] National Institute of Advanced Industrial Science and Technology, *SDBSWeb, isobutyric acid* , SDBS No. 1224, https://sdbs.db.aist.go.jp/sdbs/cgi-bin/landingpage?sdbsno=1224 (accessed 07.07.2020).
[410] H. Zheng, L. Que, *Inorg. Chim. Acta* **1997**, *263*, 301–307.
[411] J. Clayden, N. Greeves, S. Warren, P. Wothers, *Organic chemistry*, 1st reprinted ed., Oxford University Press, Oxford, **2001**, 1026–1028.
[412] H. E. Gottlieb, V. Kotlyar, A. Nudelman, *J. Org. Chem.* **1997**, *62*, 7512–7515.
[413] Bio-Rad Laboratories, *3-hydroxybutanoic acid, sodium salt*, Spectrum ID: NC_11282, viewed on scifinder.cas.org (CAS: 150-83-4) (accessed 20.09.2020).
[414] T. Zweifel, J.-V. Naubron, H. Grützmacher, *Angew. Chem. Int. Ed.* **2009**, *48*, 559–563.
[415] C. W. Jefford, W. Knöpfel, P. A. Cadby, *Tetrahedron Lett.* **1978**, *19*, 3585–3588.
[416] Z. Jiang, Z. Zhang, J. Song, Q. Meng, H. Zhou, Z. He, B. Han, *ACS Sust. Chem. Eng.* **2016**, *4*, 305–311.
[417] F. Rivetti, U. Romano, *J. Organomet. Chem.* **1978**, *154*, 323–326.
[418] F. Rivetti, U. Romano, *J. Organomet. Chem.* **1979**, *174*, 221–226.

[419] F. Ragaini, *Dalton Trans.* **2009**, 6251–6266.
[420] H. Hoberg, F. J. Fañanás, H. J. Riegel, *J. Organomet. Chem.* **1983**, *254*, 267–271.
[421] J.-Y. Salaün, G. Le Gall, P. Laurent, H. Des Abbayes, *J. Organomet. Chem.* **1992**, *441*, 99–108.
[422] P. Laurent, J.-Y. Salaün, G. Le Gall, M. Sellin, H. Des Abbayes, *J. Organomet. Chem.* **1994**, *466*, 175–183.
[423] M. Sellin, D. Luart, J.-Y. Salaün, P. Laurent, L. Toupet, H. Des Abbayes, *Organometallics* **1996**, *15*, 521–526.
[424] M. Sellin, D. Luart, J.-Y. Salaün, P. Laurent, H. Des Abbayes, *J. Organomet. Chem.* **1998**, *562*, 183–189.
[425] D. Luart, N. Le Gall, J.-Y. Salaün, L. Toupet, H. Des Abbayes, *Inorg. Chim. Acta* **1999**, *291*, 166–177.
[426] N. Le Gall, D. Luart, J.-Y. Salaün, H. Des Abbayes, L. Toupet, *J. Organomet. Chem.* **2001**, *617-618*, 483–494.
[427] N. Le Gall, D. Luart, J.-Y. Salaün, J. Talarmin, H. Des Abbayes, L. Toupet, N. Menendez, F. Varret, *Organometallics* **2002**, *21*, 1775–1781.
[428] H. Werner, L. Hofmann, R. Zolk, *Chem. Ber.* **1987**, *120*, 379–385.
[429] G. Fachinetti, T. Funaioli, D. Masi, C. Mealli, *J. Organomet. Chem.* **1991**, *417*, C32–C35.
[430] S. Jali, H. B. Friedrich, M. D. Bala, *Inorg. Chim. Acta* **2012**, *383*, 52–59.
[431] J. D. Gargulak, M. D. Noirot, W. L. Gladfelter, *J. Am. Chem. Soc.* **1991**, *113*, 1054–1055.
[432] J. D. Gargulak, A. J. Berry, M. D. Noirot, W. L. Gladfelter, *J. Am. Chem. Soc.* **1992**, *114*, 8933–8945.
[433] J. D. Gargulak, W. L. Gladfelter, *J. Am. Chem. Soc.* **1994**, *116*, 3792–3800.
[434] J. D. Gargulak, W. L. Gladfelter, *Organometallics* **1994**, *13*, 698–705.
[435] J. D. Gargulak, W. L. Gladfelter, *Inorg. Chem.* **1994**, *33*, 253–257.
[436] E. W. Evans, M. B. Howlader, M. T. Atlay, *Inorg. Chim. Acta* **1995**, *230*, 193–197.
[437] R. Santi, A. M. Romano, R. Garrone, R. Millini, *J. Organomet. Chem.* **1998**, *566*, 37–43.
[438] J. Liu, B. T. Heaton, J. A. Iggo, R. Whyman, *Angew. Chem. Int. Ed.* **2004**, *43*, 90–94.
[439] J. Arnold, G. Wilkinson, B. Hussain, M. B. Hursthouse, *Polyhedron* **1989**, *8*, 597–602.
[440] G. Vasapollo, L. Toniolo, G. Cavinato, F. Bigoli, M. Lanfranchi, M. A. Pellinghelli, *J. Organomet. Chem.* **1994**, *481*, 173–178.
[441] W. L. F. Armarego, C. L. L. Chai, *Purification of laboratory chemicals*, 5th ed., Butterworth-Heinemann, Amsterdam and Boston, **2003**.
[442] G. R. Fulmer, A. J. M. Miller, N. H. Sherden, H. E. Gottlieb, A. Nudelman, B. M. Stoltz, J. E. Bercaw, K. I. Goldberg, *Organometallics* **2010**, *29*, 2176–2179.
[443] Agilent Technologies, *User Manual: Organic Acids Analysis Kit, PN 5063-6510*, https://www.agilent.com/cs/library/usermanuals/public/5968-9047E_print.pdf.pdf (accessed 01.10.2019).
[444] G. Sheldrick, *Acta Cryst. A* **2008**, *64*, 112–122.
[445] G. Sheldrick, *Acta Cryst. C* **2015**, *71*, 3–8.
[446] A. Spek, *Acta Cryst. C* **2015**, *71*, 9–18.
[447] D. Kratzert, I. Krossing, *J. Appl. Cryst.* **2018**, *51*, 928–934.
[448] S. Lounissi, G. Zampella, J.-F. Capon, L. De Gioia, F. Matoussi, S. Mahfoudhi, F. Y. Pétillon, P. Schollhammer, J. Talarmin, *Chem. Eur. J.* **2012**, *18*, 11123–11138.
[449] I.-S. H. Lee, E. H. Jeoung, M. M. Kreevoy, *J. Am. Chem. Soc.* **1997**, *119*, 2722–2728.
[450] Y.-L. Rao, H. Amarne, L. D. Chen, M. L. Brown, N. J. Mosey, S. Wang, *J. Am. Chem. Soc.*

2013, *135*, 3407–3410.

[451] A. G. Wright, T. Weissbach, S. Holdcroft, *Angew. Chem. Int. Ed.* **2016**, *55*, 4818–4821.

[452] T. Beissel, B. S. P. C. Della Vedova, K. Wieghardt, R. Boese, *Inorg. Chem.* **1990**, *29*, 1736–1741.

[453] J. H. Koek, S. W. Russell, L. van der Wolf, R. Hage, J. B. Warnaar, A. L. Spek, J. Kerschner, L. DelPizzo, *J. Chem. Soc., Dalton Trans.* **1996**, 353–362.

[454] Z. Han, L. Rong, J. Wu, L. Zhang, Z. Wang, K. Ding, *Angew. Chem. Int. Ed.* **2012**, *51*, 13041–13045.

[455] C.-T. Yang, Y. Fu, Y.-B. Huang, J. Yi, Q.-X. Guo, L. Liu, *Angew. Chem. Int. Ed.* **2009**, *48*, 7398–7401.

[456] J. Ebels, S. Spirk, R. Pietschnig, *A Facile Lab Synthesis of Red Selenium*, **2006**, doi: 10.3390/ecsoc-10-01431.

[457] P. J. Bailey, R. A. Coxall, C. M. Dick, S. Fabre, L. C. Henderson, C. Herber, S. T. Liddle, D. Loroño-González, A. Parkin, S. Parsons, *Chem. Eur. J.* **2003**, *9*, 4820–4828.

[458] A. Vacca, C. Nativi, M. Cacciarini, R. Pergoli, S. Roelens, *J. Am. Chem. Soc.* **2004**, *126*, 16456–16465.

[459] J. Vela, L. Zhu, C. J. Flaschenriem, W. W. Brennessel, R. J. Lachicotte, P. L. Holland, *Organometallics* **2007**, *26*, 3416–3423.

[460] G. L. Guillet, F. T. Sloane, D. M. Ermert, M. W. Calkins, M. K. Peprah, E. S. Knowles, E. Čižmár, K. A. Abboud, M. W. Meisel, L. J. Murray, *Chem. Commun.* **2013**, *49*, 6635–6637.

[461] L. J. Murray, W. W. Weare, J. Shearer, A. D. Mitchell, K. A. Abboud, *J. Am. Chem. Soc.* **2014**, *136*, 13502–13505.

[462] G. N. Di Francesco, A. Gaillard, I. Ghiviriga, K. A. Abboud, L. J. Murray, *Inorg. Chem.* **2014**, *53*, 4647–4654.

[463] B. J. Cook, G. N. Di Francesco, R. B. Ferreira, J. T. Lukens, K. E. Silberstein, B. C. Keegan, V. J. Catalano, K. M. Lancaster, J. Shearer, L. J. Murray, *Inorg. Chem.* **2018**, *57*, 11382–11392.

Appendix

4 Experimental Section

4.1 Materials and Methods

All reactions were conducted under an argon atmosphere, unless stated otherwise (standard Schlenk techniques). Air-sensitive compounds were weighed inside a glove box under an argon atmosphere. Filtrations under inert gas atmosphere were performed using PTFE cannulas fitted with *Whatman glass microfiber filters*.

Unless otherwise stated, all chemicals were commercially available, purchased from ABCR, Acros Organics, Alfa Aesar, ChemPur, Fisher Scientific, Sigma-Aldrich, and TCI and used without further purification. $^{13}C_5$-α-ketoisovaleric acid (sodium salt, 98% $^{13}C_5$) was obtained from Eurisotop. Carbon dioxide (4.8 grade) and oxygen (grade 5.0) were obtained from Linde. Molecular sieves were activated by heating under vacuum ($1 \cdot 10^{-3}$ mbar) at 150 °C overnight and heating under vacuum ($1 \cdot 10^{-3}$ mbar) to 650 °C prior to utilization. Anhydrous toluene, THF, MeCN, CH_2Cl_2, and hexane were obtained from an Inert Technologies solvent purification system (passing through a column of activated alumina), transferred onto activated molecular sieves (3 Å or 4 Å), degassed by bubbling argon through the solvent for a minimum of 30 min and stored under Ar. Anhydrous Et_2O, DMF, EtOH, and MeOH were obtained from an *Inert Technologies* solvent purification system (passing through a column of activated alumina), degassed by bubbling argon through the solvent for a minimum of 30 min and stored under Ar. Anhydrous DMSO, $CHCl_3$, and *N*-methylpyrrolidinone (NMP) were obtained from Acros Organics (Extra Dry over molecular sieves) or Sigma-Aldrich, transferred onto activated molecular sieves (3 Å or 4 Å), degassed by bubbling argon through the solvent for a minimum of 30 min and stored under Ar. Anhydrous benzene (Na/benzophenone), and triethylamine (CaH_2) were dried using common procedures,[441] distilled, degassed *via* a minimum of three freeze-pump-thaw cycles and stored over activated molecular sieves (3 Å). 1,2-Dichlorobenzene was dried over activated molecular sieves (3 Å) and degassed by argon bubbling. TEOA, H_2SO_4, and high-purity water were degassed by argon bubbling and stored under argon. Deuterated solvents were dried over CaH_2 ($CDCl_3$, CD_2Cl_2, CD_3CN, acetone-d_6), Na/benzophenone ketyl (C_6D_6, THF-d_8) or activated 3 Å molecular sieves (DMSO-d_6, pyridine-d_5), degassed by a minimum of three freeze-pump-thaw cycles and stored over activated molecular sieves (3 Å). D_2O was degassed by a stream of argon.

Column chromatography was conducted using either distilled or HPLC grade solvents and either Al_2O_3 (Brockmann activity I, neutral) or silica (Macherey-Nagel, Silica 60 M, 0.04-0.063 mm). TLC was performed using Merck TLC Silica gel 60 F_{254}, Macherey-Nagel Alugram Xtra SIL G/UV_{254}, TLC Aluminum oxide 60 F_{254} (Merck) plates or aluminum oxide on TLC-PET foils by Fluka Analytical. Detection of the fractions was achieved using fluorescence quenching (254 nm) or staining with iodine, phosphomolybdic acid (PMA), $KMnO_4$, vanillin/H_2SO_4, or *p*-anisaldehyde.

Photoreactions were conducted using Lumatec Superlite 400 Hg-lamps and the radiant flux was adjusted using a Laserpoint Plus power meter equipped with a Laserpoint continuous

wave thermopile detector (0.19 – 25 μm, 10 mW – 40 W, 25 mm aperture) prior to illumination.

Compounds [Cu(bcp)(xantphos)]PF_6 (**42**)[126] and *Knölker* complex (**43**)[143] were prepared according to literature procedures within the *Catalysis for Energy* group. [Fe_2(μ-bpdt)$(CO)_6$] (bpdt = 1,1'-biphenyl-2,2'-dithiolate),[270] [Fe_2(μ-Cl-bdt)$(CO)_6$] (Cl-bdt = 1,4-dichlorobenzene-2,3-dithiolate),[260] and two batches of [Fe_2(μ-bdt)$(CO)_6$] (bdt = benzene-1,2-dithiolate)[262] were prepared according to literature-known procedures by Dr. Andrea Mele (UBO Brest). POP-xantphos and [Cu(bcp)(POP-xantphos)]PF_6 (**144**) were prepared by Dr. Paola A. Forero-Cortés (LIKAT Rostock, University of St. Andrews, University of Basel) *via* reported procedures.[228] Ionic liquids were obtained from Iolitec and dried according to reported procedures by Dr. Paola A. Forero-Cortés except for [tbmp]NTf_2 and [bmpyrr]NTf_2 which were dried *in vacuo* at 60 °C for a minimum of 2 h (1×10^{-3} mbar).[228]

4.2 Analysis

NMR spectra were recorded on 300 MHz (Avance 300, Fourier 300) or 400 MHz (Avance 400) Bruker spectrometers by the analytical department (LIKAT Rostock) and are reported relative to TMS (^{1}H, ^{13}C) or external standards of $BF_3{\cdot}Et_2O$ (^{11}B), $CFCl_3$ (^{19}F) and 85% H_3PO_4 (^{31}P). Referencing of the ^{1}H and ^{13}C NMR spectra was performed using the solvent residual signal.[412,442] Abbreviations for signal multiplicities are s (singlet), d (doublet), t (triplet), q (quartet), quint (quintet), sext (sextet), hept (heptet) and br (broad). The amount of formate formed in the photocatalytic CO_2 reduction reactions was determined by ^{1}H NMR spectroscopy using benzene as internal standard. **FTIR** spectra were recorded on a Bruker Alpha P FTIR spectrometer (ATR, diamond). **UV/VIs** spectra were collected on an Analytik Jena Specord S600 diode array spectrometer.

Elemental analysis was conducted by the analytical department (LIKAT Rostock).

Mass spectra were measured on Agilent 1260/6130 Quadrupol (ESI, LC-MS), Waters Xevo G2-XS-Tof (ESI, HR-MS) and Thermo Fisher Scientific Finnigan Electron MAT 95-XP (EI, HR-MS) instruments by the analytical department (LIKAT Rostock). **HR-MS** measurements for the identification of isotopic compositions of oxalate as part of the investigations on the reactivity of α-ketocarboxylates with Cu and α-ketocarboxyl-ligated Cu complexes were conducted by Dr. Holm Frauendorf (Georg-August-Universität Göttingen) on an Agilent micrOTOF spectrometer.

Capillary electrophoresis was conducted on an Agilent 7100 CE system equipped with an Agilent bare fused silica (72 cm effective length, 75 μm ID) CE capillary using the Agilent organic acid buffer (pH 5.6).[443] Detection of the anions was achieved using UV/Vis detection (λ=350/80 nm, λ(ref.)=200/10 nm). Preconditioning: run buffer (4 min to 10 min); Injection: pressure injection (p=50 mbar, t=2 s); Run parameters: T=25 °C, V=–25 kV, I=100 μA, P=6.0 W, t=12 min (modification of a method developed by Agilent[443]). Calibration is described in section 4.15.1.

Gas chromatography was performed on either an Agilent Technologies 7890A (HP Plot Q / FID – hydrocarbons, Carboxen / TCD – Ar carrier gas), an Agilent Technologies 6890N (HP Plot Q / FID – hydrocarbons, Carboxen / TCD – He carrier gas), or an Agilent Technologies 6890N (Carboxen 1000 /TCD / Methanizer / FID – He carrier gas). Calibrations were compiled using defined gas mixtures obtained from Linde and Air liquide. Following gas concentrations were utilized for the calibration for analysis of photocatalytic reactions:
GC 1): H_2: 1000 ppm, 0.25%, 0.51%, 1.00%, 4.74%; CO: 78 ppm, 250 ppm, 993 ppm, 1.00%, 5.82%; CH_4: 1000 ppm, 1.00%, 4.98%, 10.10%; CO_2: 1000 ppm, 1.00%, 4.99%, 10.10%, 24.68%, 45.59%, 100%. **GC 2)**: H_2: 1000 ppm, 0.25%, 0.51%, 1.01%, 4.74%; CO: 78 ppm, 238 ppm, 993 ppm, 0.99%, 5.82%; CH_4: 243 ppm, 1000 ppm, 1.02%, 4.98%; CO_2: 1000 ppm, 1.00%, 4.99%, 10.10%, 24.68%, 45.49%, 99.98%. **GC 3)**: H_2: 1000 ppm, 0.25%, 0.50%, 1.00%, 4.74%; CO: 1 ppm, 10 ppm, 79 ppm, 238 ppm, 997 ppm, 1.00%, 5.82%; CH_4: 10 ppm, 81 ppm, 243 ppm, 1000 ppm, 1.00%, 4.98%; CO_2: 1 ppm, 8 ppm, 250 ppm, 1000 ppm, 1.00%, 4.99%, 10.10%, 24.68%, 50.00%, 100.00%.
The following calibration was utilized for analysis of the headspace of stoichiometric reactions with the aim of CO_2 reductive coupling:
H_2: 105 ppm, 262 ppm, 527 ppm, 997 ppm, 0.25%, 0.51%, 1.01%, 5.00%, 10.0%, 25.3%, 50.4%, 100%; CO: 78 ppm, 238 ppm, 993 ppm, 0.99%, 5.82%, 10.1%; CH_4: 81 ppm, 993 ppm, 1.02%, 5.05%, 9.89%; CO_2: 1.00%, 5.02%, 10.1%, 25.0%, 49.6%, 95.0%, 100%.
5 mL of the headspace were taken as sample using a gas-tight syringe (Hamilton) and were injected in the sample loop (V = 1 mL). The gas from the sample loop (1 mL) was then injected into the GC under isobaric conditions.
X-ray crystallographic analyses were performed by Dr. Anke Spannenberg (LIKAT Rostock). Diffraction data were collected on a Bruker Kappa APEX II DUO or a STOE IPDS II diffractometer. The structures were solved by direct methods and refined by full-matrix least-squares procedures on F^2 using the SHELXTL software package.[444,445] For compounds **152** and **169** PLATON/SQUEEZE[446] was applied to remove co-crystallized solvent molecules from the diffraction data. For **168** the disordered molecular structure was resolved with the help of DSR (Disordered Structure Refinement) implemented in ShelXle.[447] Crystallographic data for **151** (CCDC 1855538) and **152** (CCDC 1855539) can be obtained free of charge by the joint Cambridge Crystallographic Data Centre and Fachinformationszentrum Karlsruhe *via* www.ccdc.cam.ac.uk/structures.
Cyclic voltammetry was conducted by Dr. Andrea Mele (UBO Brest) using a PG-STAT 128 N Autolab or a μ-Autolab (type III) electrochemical analyzer operated with the GPES software and a three-electrode cell under Ar. $[NBu_4][PF_6]$ was prepared and purified as described previously.[448] A 0.3 cm diameter vitreous carbon disk as working electrode (polished with alumina before the measurement), a platinum wire as counter electrode and an Ag/Ag^+ reference electrode were utilized. Internal referencing by addition of Ferrocene at the end of the measurements was conducted (potentials are stated against Fc^+/Fc).

4.3 Photocatalytic CO_2 Reduction Conducted in Ionic Liquids

Note: Procedures and results presented within this section have been previously reported elsewhere and are only implemented for the sake of complete documentation.[228] Detailed synthetic procedures for the novel complex utilized herein and full characterization can be obtained free of charge in the supplementary material (DOI: 10.1039/d0gc01627f). Likewise, NMR spectra for analysis of the liquid phase and GC chromatograms of the reaction headspaces can be obtained free of charge in the original supporting information.

4.3.1 General Procedure for the Photocatalytic CO_2 Reduction Conducted in Ionic Liquids

A similar procedure for photocatalytic CO_2 reduction was previously developed in our group.[131]

To a three-necked, double-walled photoreactor equipped with a stirring bar, a Teflon-coated rubber septum and connected to a gas-inlet tube and a thermostat (Figure S 1) under CO_2 atmosphere (prepared by three vacuum-Ar and three vacuum-CO_2 cycles) was added BIH (150 mg), degassed TEOA (1.5 mL), a solution/suspension of the respective Cu complex in IL (5 mL) and a solution/suspension of Fe *Knölker* complex **43** in IL (1 mL). CO_2 was bubbled through the reaction mixture for 30 min. The reactor was sealed by replacing the gas-inlet tube and closing the connection valve to the septum. Illumination (400-700 nm, 1.50 W) through a plain borosilicate glass wall initiated the reaction that was stopped after the time indicated. After the reaction, a gas sample (5 mL) was taken through the septum and gas chromatographically analyzed (moles of CO/H_2 calculated using the van der Waals molar volumes as described in the general procedure for photocatalytic CO_2 reduction with [FeFe] mimics). Analysis of the liquid phase by NMR spectroscopy was conducted using benzene as internal standard. TONs were calculated using equation (1). Results given for the photocatalytic reactions in ionic liquid reported in the following section are generally results of single experiments.

$$\mathrm{TON(X)} = \frac{n(\mathrm{X})}{n(\text{Fe complex})} - N(\mathrm{X_{coordinated}}) \qquad (1)$$

with n(X)=moles of product X; n(Fe complex)=moles of Fe complex; $N(\mathrm{X_{coordinated}})$=number of CO coordinated to Fe (only for X = CO).

In situ formation of the photosensitizer [Cu(bcp)(xantphos)]PF_6 in IL was attempted using solutions/suspensions of [Cu(MeCN)$_4$]PF_6 in IL (0.62 mL), xantphos in IL (2.5 mL) and bathocuproine in IL (2.0 mL) instead of the preformed complex.

Note that all complexes or ligands were sonicated in the respective IL for 20 min before addition.

4.3.2 Results of the Photocatalytic CO_2 Reduction Conducted in Ionic Liquids

Table S 1: Photocatalytic CO_2 reduction in ionic liquid media - single experiment results.

Entry	PS	Solvent	TON (CO)	TON (H_2)	TON (HCO_2H)
1	**144**	NMP/TEOA (5:1, *v* : *v*)	485	30	10
2	**144**	NMP/TEOA (5:1, *v* : *v*)	524	15	10
3	**144**	[bmim][OTf]/TEOA (4:1, *v* : *v*)	157	165	6
4	**144**	[bmim][OTf]/TEOA (4:1, *v* : *v*)	185	177	6
5	**42**	[bmim][OTf]/TEOA (4:1, *v* : *v*)	60	124	11
6[a]	**42**	[tbmp]NTf2]/TEOA (4:1, *v* : *v*)	57	293	10
7[a]	**42**	[tbmp]NTf2]/TEOA (4:1, *v* : *v*)	63	256	8
8	**144**	[bmpyrr][$N(CN)_2$]/TEOA (4:1, *v* : *v*)	26	≤3	≤3
9	**144**	[bmpyrr][$N(CN)_2$]/TEOA (4:1, *v* : *v*)	31	≤3	n.d.
10	**42**	[bmpyrr][$N(CN)_2$]/TEOA (4:1, *v* : *v*)	65	≤3	≤3
11	**42**	[bmpyrr][$N(CN)_2$]/TEOA (4:1, *v* : *v*)	89	≤3	≤3
12[a]	**42**	[bmpyrr][NTf_2]/TEOA (4:1, *v* : *v*)	59	325	6
13[a]	**42**	[bmpyrr][NTf_2]/TEOA (4:1, *v* : *v*)	54	308	5
14[a]	**42**	[bmpyrr][NTf_2]/TEOA (4:1, *v* : *v*)	69	383	5
15[b]	**42**	[bmpyrr][$N(CN)_2$]/TEOA (4:1, *v* : *v*)	1	≤3	≤3
16[c]	**42**	[bmpyrr][$N(CN)_2$]/TEOA (4:1, *v* : *v*)	77	≤3	≤3
17[c]	**42**	[bmpyrr][$N(CN)_2$]/TEOA (4:1, *v* : *v*)	81	≤3	≤3

Reaction conditions: BIH (150 mg), Cu PS (5.0 μmol), and [Fe] (**43**) (1 μmol) in the solvent mixture indicated (7.5 mL) under CO_2 (1 atm) at 25 °C under 400-700 nm irradiation (1.50 W), 5 h. [a]Biphasic reaction system due to non-miscibility of TEOA and the IL. [b]Instead of preformed **42**, an *in situ* system consisting of xantphos (15 μmol), bathocuproine (5.1 μmol), and $[Cu(MeCN)_4]PF_6$ (5.0 μmol) was utilized. [c]Cu PS **42** (5.0 μmol) in [bmpyrr][$N(CN)_2$] (1.0 mL) was added after 5.5 h and illumination continued for another 17.5 h.

Table S 2: Photocatalytic CO_2 reduction in ionic liquid media - control experiments.

Entry	[Fe] [μmol]	[Cu] [μmol]	TON (CO)	TON (H_2)	TON (HCO_2H)
1	1	-	≤1	≤3	≤3
2	-	5	≤1	≤3	≤3
3	-	-	≤1	≤3	≤3
4[a]	-	-	≤1	≤3	≤3
5[b]	1	5	≤1	≤3	≤3
6[c]	1	5	≤1	≤3	≤3

Reaction conditions: BIH (150 mg), Cu PS (**144**) (5.0 μmol), and [Fe] (**43**) (1 μmol) in [bmpyrr][$N(CN)_2$] (6.0 mL) and TEOA (1.5 mL) under CO_2 (1 atm) at 25 °C with 400-700 nm (1.50 W) for 5 h. [a][bmim][OTf] (6.0 mL) utilized instead of [bmpyrr][$N(CN)_2$]. [b]Reaction without CO_2 (under Ar). [c]Reaction in the absence of light.

4.4 Photocatalytic CO_2 Reduction with [FeFe] Hydrogenase Mimics

Note: Procedures and results presented within this section have been previously reported elsewhere and are only implemented for the sake of complete documentation.[244] NMR spectra for analysis of the liquid phase and GC chromatograms of the reaction headspace for the catalysis reactions can be obtained free of charge in the supplementary material (DOI: 10.1002/cctc.201901686).

4.4.1 Synthesis of 1,3-dimethyl-2-phenylbenzo[*d*]imidazole (BIH)

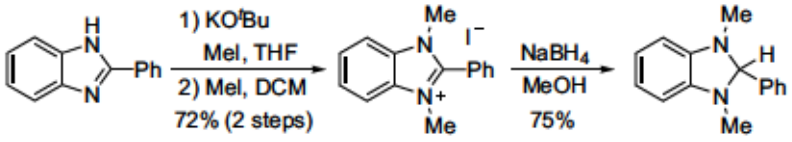

BIH was either prepared following a literature procedure[131,449] or utilizing a combination of three literature procedures for the individual steps[131,449–451] as reported previously.[244]

Methyl iodide (3.8 mL, 61 mmol, 1.18 equiv.) was added to 2-phenylbenzo[*d*]imidazole (10.0 g, 51.7 mmol, 1.00 equiv.) and KO^{t}Bu (6.1 g, 54.3 mmol, 1.05 equiv.) in THF in air. The flask was sealed and the reaction mixture stirred at r.t. for 25 h. The yellow suspension was concentrated under reduced pressure. DCM (240 mL) was then added and the mixture filtered to provide a yellow solution. The solid residue was extracted with additional DCM (20 mL) and all volatiles were evaporated under reduced pressure. The crude product (yellow oil) was directly converted in the next step without further purification.
Methyl iodide (9.0 mL, 15 mmol, 2.80 equiv.) was added to the yellow oil dissolved in DCM (60 mL). The flask was closed and the reaction mixture stirred at 29 °C for 24 h. The orange/red suspension was filtered using a cannula equipped with a glass microfiber filter and the solid residue was washed with Et_2O (2×50 mL, then 25 mL). Subsequent drying under reduced pressure yielded 1,3-dimethyl-2-phenylbenzo[*d*]imidazolium iodide (13.1 g, 37.4 mmol, 72% over two steps) as a beige to yellow solid.
^{1}H NMR (300 MHz, DMSO-d_6) δ = 8.14 (m, 2H), 7.93-7.87 (m, 2H), 7.86-7.72 (m, 5H), 3.90 (s, 6H) ppm.
The analytical data agrees with the data reported in the literature.[451]

$NaBH_4$ (5.21 g, 138 mmol, 3.68 equiv.) was added to a suspension of 1,3-dimethyl-2-phenylbenzo[*d*]imidazolium iodide (13.1 g, 37.4 mmol, 1.00 equiv.) in dry MeOH (150 mL) over 5 min at 0 °C. The suspension was allowed to warm to ambient temperature and stirring continued for 2 h. Volatiles were removed under reduced pressure and BIH (6.3 g, 28.2 mmol, 75%) was obtained after twofold recrystallization from EtOH/H_2O (2:1, *v*:*v*).
^{1}H NMR (300 MHz, DMSO-d_6) δ = 7.61-7.50 (m, 2H), 7.48-7.38 (m, 3H), 6.62 (m, 2H), 6.45 (m, 2H), 4.87 (s, 1H), 2.48 (s, 6H) ppm.
The analytical data is in accordance with the literature data.[449]

4.4.2 Synthesis of [Fe_2(μ-bdt)$(CO)_6$] (145)

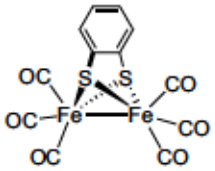

145 was prepared following a literature procedure.[262]

Benzene-1,2-dithiol (0.18 mL, 1.57 mmol, 1.00 equiv.) was added to a suspension of $Fe_3(CO)_{12}$ (878 mg, 1.57 mmol, 1.00 equiv.) in dry toluene (12 mL) and the reaction mixture heated to 125-130 °C for 1.5 h. Volatiles were removed *in vacuo*. Twofold column chromatography (SiO_2, pentane) yielded **145** (635 mg, 1.51 mmol, 96%) as red microcrystalline solid.

^{1}H NMR (300 MHz, C_6D_6) δ = 6.70-6.60 (m, 2H), 6.06-5.97 (m, 2H) ppm.

FTIR (ATR, diamond): $\tilde{\nu}$ = 3067, 2955, 2922, 2853, 2070, 2028, 2000, 1969, 1441, 1434, 1292, 1252, 1152, 1110, 1015, 978, 940, 869, 746, 616, 575, 550, 492, 439, 426 cm^{-1}.

Anal. Calcd. C 34.32, H 0.96, S 15.27. **Observed** C 33.97, H 0.6204, S 15.28.

Analytical data corresponded to that reported in the literature.[262]

4.4.3 Synthesis of [Fe_2(μ-bdt)(κ^2-xantphos)$(CO)_4$] (151)

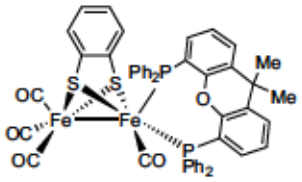

Synthesis of **151** has previously been reported.[244]

A light-red solution of [Fe_2(μ-bdt)$(CO)_6$] (16.1 mg, 38.2 µmol, 1.00 equiv.) and xantphos (22.0 mg, 38.0 µmol, 0.99 equiv.) dissolved in dry toluene (3.0 mL) was stirred and irradiated at 415 nm (1.00 W) at room temperature for 3 h resulting in a dark brown solution. Volatiles were removed *in vacuo* to provide a brown solid. Purification *via* column chromatography (Al_2O_3, neutral, Brockmann activity I, pentane/DCM, 7:1→5:1) and subsequent crystallization by slow diffusion of dry hexane (4.0 mL) into a DCM solution (1.6 mL) at 7 °C yielded **151** (23.1 mg, 24.5 µmol, 64%) as a brown solid. Crystals suitable for single crystal X-ray diffraction were grown *via* slow diffusion of dry hexane into a DCM solution of **151** at 7 °C.

^{1}H NMR (300 MHz, CD_2Cl_2): δ = 8.07-7.89 (m, 4H), 7.56 (d, J = 7.6 Hz, 2H), 7.38-7.27 (m, 6H), 7.07-6.98 (m, 4H), 6.93 (s, br, 2H), 6.87-6.78 (m, 2H), 6.78-6.69 (m, 4H), 6.56 (s, br, 2H), 6.04 (m, 4H), 2.01 (s, 3H), 1.70 (s, 3H) ppm.

^{31}P{^{1}H} NMR (122 MHz, CD_2Cl_2): δ = 58.9 (br) ppm.

^{13}C{^{1}H} NMR (75 MHz, CD_2Cl_2): δ = 220.2, 155.9 (d, J_{C-P} = 6.9 Hz), 151.5, 137.8 (d, J_{C-P} = 40.2 Hz), 136.4 (d, J_{C-P} = 11.2 Hz), 136.4 (d, J_{C-P} = 39.4 Hz), 134.9 (d, J_{C-P} = 3.2 Hz), 131.7 (br), 130.4, 130.0 (d, J_{C-P} = 2.1 Hz), 128.4 (d, J_{C-P} = 9.4 Hz), 128.3 (d, J_{C-P} = 2.0 Hz), 127.7 (d, J_{C-P} = 9.2 Hz), 127.1, 126.3, 124.7, 123.7 (d, J_{C-P} = 6.0 Hz), 37.0, 31.6, 23.0 ppm.

FTIR (ATR, diamond): $\tilde{\nu}$ =3356, 3054, 2960, 2922, 2851, 2021, 1971, 1947, 1883, 1656, 1631, 1586, 1572, 1480, 1466, 1432, 1402, 1362, 1260, 1229, 1186, 1152, 1085, 1024, 907, 878, 799, 736, 688, 615, 582, 557, 542, 505, 477 cm^{-1}.

Anal. Calcd. C 62.44, H 3.85, S 6.80. **Observed** C 62.72, H 3.584, S 7.083.

E_p(CH_2Cl_2-[NBu_4][PF_6] (0.2 M) under Ar at v = 0.2 V s^{-1}) = –2.07 V *vs.* Fc/Fc^+.
Note: ^{13}C NMR spectroscopic detection of the second CO signal and the signal corresponding to the 4/5-C of the xantphos scaffold was not achieved, presumably as a result of low intensity of these signals and C-P coupling.

4.4.4 Synthesis of [Fe_2(μ-bdt)(κ^2-bcp)(CO)$_4$] (152)

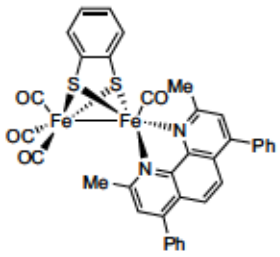

Synthesis of **152** has previously been reported.[244]

[Fe_2(μ-bdt)(CO)$_6$] (18.1 mg, 43.1 µmol, 1.00 equiv.) and bathocuproine (15.6 mg, 43.3 µmol, 1.00 equiv.) under Ar in dry toluene (3.0 mL) were sonicated for 10 min. The resulting bright red solution was stirred and illuminated at 415 nm (1.00 W) at r.t. for 3 h giving rise to a black solution. Volatiles were removed *in vacuo*. [Fe_2(μ-bdt)(κ^2-bcp)(CO)$_4$] (23.9 mg, 33.0 µmol, 76%) as dark brown/black crystalline solid was obtained *via* diffusion of dry hexane (6.0 mL) into a DCM solution (2.0 mL) of the solid residue at approx. 7 °C and subsequently at –30 °C. Suitable crystals for X-ray crystallographic analysis were obtained by liquid diffusion of dry hexane into a DCM solution of **152** at 7 °C.
^{1}H NMR (300 MHz, C_6D_6): δ = 7.35 (s, 2H), 7.19 (m, 10H), 7.12 (m, br, 2H), 6.70 (s, 2H), 6.26 (m, br, 2H), 3.00 (s, 6H) ppm.
^{13}C{^{1}H} NMR (75 MHz, C_6D_6): δ = 166.2, 153.3, 145.7, 137.2, 129.8, 128.9, 128.8, 126.8, 125.7, 125.5, 123.7, 123.3, 28.0 ppm.
FTIR (ATR, diamond): $\tilde{\nu}$ = 3054, 2955, 2920, 2851, 2008, 1948, 1929, 1886, 1619, 1601, 1560, 1484, 1437, 1400, 1353, 1284, 1262, 1229, 1179, 1157, 1101, 1076, 1028, 907, 885, 829, 749, 700, 626, 583, 560, 536, 509 cm^{-1}.
E_p(CH_2Cl_2-[NBu_4][PF_6] (0.2 M) under Ar at v = 0.2 V s^{-1}) = –1.87 V vs. Fc/Fc^+.
Note: Arguably due to overlapping with the solvent (C_6D_6) signal, one of the aromatic carbon signals was not observed in the ^{13}C NMR spectrum.

4.4.5 General Procedure for the Photocatalytic CO_2 Reduction with [FeFe] Hydrogenase Mimics

The procedure for photocatalytic CO_2 reduction was adapted from a procedure previously developed in our group.[131]

Photocatalytic CO_2 reduction was conducted in double-walled photoreactors (total volume 70-80 mL) equipped with a Teflon-coated magnetic stirring bar and connected to a gas-inlet tube and a teflon-coated rubber septum (Figure S 1). A thermostat connected to the reactor was utilized for maintaining constant temperature throughout the reaction time. The CO_2 atmosphere was prepared by three vacuum-argon cycles and three subsequent vacuum-CO_2 cycles. A solution of xantphos in NMP/TEOA (5 mL, 5:1, *v*:*v*), [$Cu(MeCN)_4$]PF_6 in NMP

(0.5 mL), bathocuproine in NMP/TEOA (2 mL, 5:1, *v*:*v*), BIH (120 mg) and NMP/TEOA (2 mL, 5:1, *v*:*v*) were added consecutively and the reaction mixture saturated with CO_2 *via* bubbling for 30 min. The gas-inlet tube was removed and the reactor sealed. A solution of the Fe complex in NMP/TEOA (0.5 mL, 5:1, *v*:*v*) was then added *via* the septum, the valve closed and the reaction started by illumination (wavelength and irradiation intensity as indicated) through a plain glass-wall. After the reaction, a gas sample (5 mL) was taken *via* the septum and analyzed by GC. Analysis of the liquid phase was performed by NMR spectroscopy in CD_2Cl_2 or DMSO-d_6 with benzene as internal standard. Van der Waals molar volumes for CO (24.44323 L/mol) and H_2 (24.48068 L/mol) at 101325 Pa and 25 °C were used to calculate the moles of product formed (using the total headspace in combination with the percentage of the respective gas determined by GC analysis).[131] CH_4 (1% in CO_2) was utilized as internal standard when indicated to ensure pressure variations within the reactor due to H_2 formation were not affecting this calculation method. CO, H_2 and HCO_2H TONs were calculated with respect to the catalyst amount and TON(CO) was corrected by the number of CO ligands of the utilized Fe complex (equation 1). All TON values stated in the tables are obtained from single experiments. In some reactions, CH_4 was detected as by-product with TONs below the accuracy achieved using the GC calibration ($TON(CH_4) \ll 31$).

In case of reactions with preformed photosensitizer [Cu(bcp)(xantphos)]PF_6 the general procedure for photocatalytic reactions was identical except for direct addition of the respective photosensitizer in NMP/TEOA (9.5 mL, 5:1, *v*:*v*) unless stated otherwise. Note that dissolving the ligands and metal complexes was facilitated by sonication of the mixture whenever necessary.

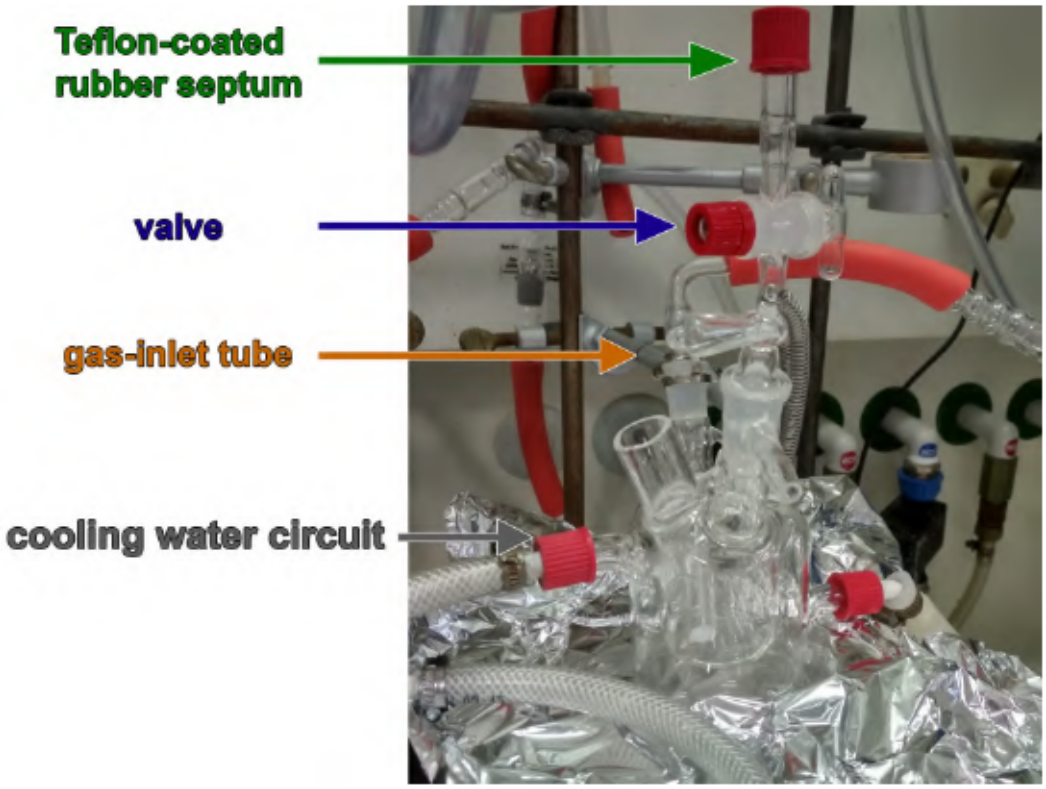

Figure S 1: Utilized reaction setup for photocatalytic CO_2 reduction.

4.4.6 Results of the Photocatalytic CO_2 Reduction with [FeFe] Hydrogenase Mimics

Table S 3: Direct comparison between preformed and *in situ* Cu PS **42**.

Entry	Photosensitizer	TON (CO)	TON (H_2)	TON (HCO_2H)	CO : H_2
1	preformed	75	476	238	0.16
2	preformed	86	623	233	0.14
3[a,b]	*in situ*	234	251	122	0.93
4[a,b]	*in situ*	246	239	86	1.0
5[a]	*in situ*	255	213	203	1.2
6[a]	*in situ*	234	192	161	1.3
7[a]	*in situ*	309	218	210	1.4
8[a]	*in situ*	287	256	159	1.1
9[a]	*in situ*	213	208	61	1.0

Reaction conditions: $[Fe_2(\mu\text{-bdt})(CO)_6]$ (0.1 µmol), photosensitizer (1 µmol), and BIH (120 mg) in NMP/TEOA (5:1, *v*:*v*, 10 mL) under CO_2 (1 atm) using 415 nm, 1.00 W, 25 °C, 3 h. [a]Prepared *in situ* starting from xantphos (3 µmol), bathocuproine (1 µmol), and $[Cu(MeCN)_4]PF_6$ (1 µmol). [b]CH_4 (1%) in CO_2 was utilized as internal standard to ensure no influence of pressure variations on the calculation method.

Table S 4: Influence of the composition of the *in situ* Cu PS.

Entry	[Cu]:N^N:P^P	TON (CO)	TON (H_2)	TON (HCO_2H)
1	1:1:3	234	251	122
2	1:1:3	246	239	86
3	1:1:3	255	213	203
4	1:1:3	234	192	161
5	1:1:3	309	218	210
6	1:1:3	287	256	159
7	1:1:3	213	208	61
8	1:10:3	167	282	454
9	1:10:3	33	$\leq$33	44
10	1:10:3	31	$\leq$33	54
11	1:10:3	18	42	34
12	1:10:3	16	40	31
13	1:1:10	259	491	667
14	1:1:10	217	165	67
15	1:1:10	195	165	79
16	1:1:10	351	307	375
17	1:1:10	328	293	410
18	1:1:6	328	359	132
19	1:1:6	363	385	171
20	1:3:3	329	298	190
21	1:3:3	312	342	299
22	1:3:6	222	153	78
23	1:3:6	287	184	118
24	1:2:5	409	227	218
25	1:2:5	334	242	263
26	1:2:5	295	216	150
27	1:2:5	270	184	113
28	1:2:5	350	264	248

Reaction conditions: $[Fe_2(\mu\text{-bdt})(CO)_6]$ (0.1 µmol), *in situ* Cu PS starting from xantphos (x µmol), bathocuproine (x µmol), and $[Cu(MeCN)_4]PF_6$ (x µmol), BIH (120 mg) in NMP/TEOA (5:1, *v*:*v*, 10 mL) under CO_2 (1 atm) using 415 nm, 1.00 W, 25 °C, 3 h. x corresponds directly to the number indicated in the [Cu]:N^N:P^P ratio.

Table S 5: Optimization of the illumination conditions.

Entry	λ [nm]	Radiant flux [W]	TON (CO)	TON (H_2)	TON (HCO_2H)
1	415	0.50	219	223	410
2	415	0.50	115	117	53
3	415	0.50	97	85	60
4	415	0.50	238	206	141
5	400-500	0.50	254	226	304
6	400-500	0.50	159	125	77
7	400-500	0.50	238	199	226
8	415	1.00	409	227	218
9	415	1.00	334	242	263

10	415	1.00	295	216	150
11	415	1.00	270	184	113
12	415	1.00	350	264	248
13	400-500	1.00	374	195	126
14	400-500	1.00	312	154	73
15	415	1.50	351	258	367
16	415	1.50	337	181	74
17	415	1.50	187	136	59
18	415	1.50	427	233	144
19	415	1.50	424	282	225
20	400-500	1.50	439	267	308
21	400-500	1.50	411	185	86
22	400-500	1.50	460	255	229

Reaction conditions: $[Fe_2(\mu\text{-bdt})(CO)_6]$ (0.1 μmol), *in situ* Cu PS starting from xantphos (5 μmol), bathocuproine (2 μmol), and $[Cu(MeCN)_4]PF_6$ (1 μmol), BIH (120 mg) in NMP/TEOA (5:1, *v*:*v*, 10 mL) under CO_2 (1 atm) at 25 °C using visible light (λ and radiant flux as indicated), 3 h .

Table S 6: Single experimental results for the photocatalytic CO_2 reduction with $[Fe_2(\mu\text{-bdt})(CO)_6]$.

Entry	TON (CO)	TON (H_2)	TON (HCO_2H)	CO:H_2	Date of the reaction
1	439	267	308	1.6	06.06.2018
2	411	185	86	2.2	11.06.2018
3	460	255	229	1.8	12.06.2018
4	51	81	197	0.63	20.12.2018
5	45	59	62	0.76	20.12.2018
6	226	129	233	1.8	08.01.2019
7	282	155	267	1.8	09.01.2019
8	439	226	411	1.9	09.01.2019
9	233	124	252	1.9	10.01.2019
10	53	46	248	1.2	10.01.2019
11	118	93	237	1.2	11.01.2019
12	104	89	470	1.3	11.01.2019
13	73	96	197	0.91	15.01.2019
14	83	91	222	0.76	15.01.2019
15	43	61	199	0.70	16.01.2019
16	59	66	224	0.89	16.01.2019
17	54	63	268	0.86	17.01.2019
18	10	≤33	178	0.71	18.01.2019
19	11	≤33	167	0.79	18.01.2019
20	66	72	230	0.92	19.01.2019
21	55	69	n.d.	0.79	19.01.2019
22	20	≤33	192	0.83	20.01.2019
23	21	≤33	187	0.72	20.01.2019
24[a]	32	49	236	0.65	21.01.2019
25[a]	39	54	182	0.72	21.01.2019
26	23	≤33	n.d.	0.77	23.01.2019
27	24	≤33	n.d.	0.73	23.01.2019

28	36	51	n.d.	0.71	24.01.2019
29	36	53	n.d.	0.68	24.01.2019
30	157	106	250	1.5	25.01.2019
31	176	105	231	1.7	25.01.2019
32	81	86	n.d.	0.94	26.01.2019
33	83	81	n.d.	1.0	26.01.2019
34	26	≤33	n.d.	0.87	01.02.2019
35	22	≤33	n.d.	0.96	01.02.2019
36	44	49	n.d.	0.90	06.02.2019
37	59	59	n.d.	1.0	06.02.2019
38	40	55	104	0.73	07.02.2019
39	41	57	105	0.72	07.02.2019
40	365	191	178	1.9	14.03.2019
41	388	195	167	2.0	14.03.2019
42	44	47	117	0.94	15.03.2019
43	46	47	138	0.98	15.03.2019
44	113	73	n.d.	1.5	18.03.2019
45	152	84	n.d.	1.8	18.03.2019
46	29	≤33	n.d.	0.88	22.03.2019
47	41	47	n.d.	0.87	22.03.2019
48	311	206	415	1.5	03.04.2019
49	408	174	155	2.3	03.04.2019
50	401	200	267	2.0	04.04.2019
51	448	202	273	2.2	04.04.2019
52	135	88	n.d.	1.5	16.04.2019
53	164	86	n.d.	1.9	16.04.2019
54	28	≤33	n.d.	1.1	17.04.2019
55	30	≤33	n.d.	1.2	17.04.2019
56	27	≤33	n.d.	9.0	23.04.2019
57	31	≤33	n.d.	7.8	23.04.2019
58	156	90	n.d.	1.7	30.04.2019
59	161	84	n.d.	1.9	30.04.2019

Reaction conditions: $[Fe_2(\mu\text{-bdt})(CO)_6]$ (0.1 µmol), *in situ* Cu PS starting from xantphos (5 µmol), bathocuproine (2 µmol), and $[Cu(MeCN)_4]PF_6$ (1 µmol), BIH (120 mg) in NMP/TEOA (5:1, *v*:*v*, 10 mL) under CO_2 (1 atm) at 25 °C under 400-500 nm, 1.50 W, 3 h. [a]One drop of H_2O was added to the reaction mixture. n.d. = not determined.

Table S 7: Influence of the catalyst loading on $[Fe_2(\mu\text{-bdt})(CO)_6]$-catalyzed CO_2 reduction.

Entry	*n*($[Fe_2(\mu\text{-bdt})(CO)_6]$) [µmol]	TON (CO)	TON (H_2)	TON (HCO_2H)
1	0.3	51	39	41
2	0.3	65	53	39
3	0.5	14	33	20
4	0.5	14	35	22
5	0.5	5	34	≤20
6	0.5	4	≤33	≤20
7	0.5	5	≤33	≤20
8	0.5	5	34	≤20

9	0.5	6	36	≤20
10	0.5	6	34	≤20

Reaction conditions: $[Fe_2(\mu\text{-bdt})(CO)_6]$ (x μmol), *in situ* Cu PS starting from xantphos (5 μmol), bathocuproine (2 μmol), and $[Cu(MeCN)_4]PF_6$ (1 μmol), BIH (120 mg) in NMP/TEOA (5:1, *v*:*v*, 10 mL) under CO_2 (1 atm) at 25 °C under 400-500 nm, 1.50 W, 3 h.

Table S 8: Photocatalytic CO_2 reduction - Reproducibility utilizing various [FeFe] complexes.

Entry	[Fe]	TON (CO)	TON (H_2)	TON (HCO_2H)
1	$[Fe_2(\mu\text{-Cl-bdt})(CO)_6]$	194	920	151
2	$[Fe_2(\mu\text{-Cl-bdt})(CO)_6]$	241	908	120
3	$[Fe_2(\mu\text{-Cl-bdt})(CO)_6]$	144	625	104
4	$[Fe_2(\mu\text{-Cl-bdt})(CO)_6]$	272	830	109
5	$[Fe_2(\mu\text{-bpdt})(CO)_6]$	375	98	30
6	$[Fe_2(\mu\text{-bpdt})(CO)_6]$	406	98	35
7	$[Fe_2(\mu\text{-bpdt})(CO)_6]$	115	44	65
8	$[Fe_2(\mu\text{-bpdt})(CO)_6]$	271	78	34
9	$[Fe_2(\mu\text{-bpdt})(CO)_6]$	292	127	57
10	$[Fe_2(\mu\text{-bpdt})(CO)_6]$	175	123	23
11	$[Fe_2(\mu\text{-bpdt})(CO)_6]$	99	45	58
12	$[Fe_2(\mu\text{-bpdt})(CO)_6]$	112	43	59
13	$[Fe_2(\mu\text{-bpdt})(CO)_6]$	270	76	53
14	$[Fe_2(\mu\text{-bpdt})(CO)_6]$	280	74	48
15[a]	$Fe_2(CO)_9$	36	106	33
16[a]	$Fe_2(CO)_9$	69	249	30
17[a]	$Fe_2(CO)_9$	14	199	44
18[a]	$Fe_2(CO)_9$	38	225	21

Reaction conditions: [Fe] (0.1 μmol), *in situ* Cu PS starting from xantphos (5 μmol), bathocuproine (2 μmol), and $[Cu(MeCN)_4]PF_6$ (1 μmol), BIH (120 mg) in NMP/TEOA (5:1, *v*:*v*, 10 mL) under CO_2 (1 atm) at 25 °C under 400-500 nm, 1.50 W, 3 h. [a]Solubility of $Fe_2(CO)_9$ in the solvent mixture appeared to be low.

Table S 9: Photocatalytic CO_2 reduction - Control experiments.

Entry	[Fe] [μmol]	[Cu] [μmol]	[bcp] [μmol]	[xantphos] [μmol]	[BIH] [mg]	TON (CO)	TON (H_2)	TON (HCO_2H)
1	-	1.0	1.0	3.0	120	≤1	≤33	22
2	-	1.0	1.0	3.0	120	≤1	≤33	≤20
3	0.1	-	-	-	120	≤1	≤33	≤20
4	0.1	-	-	-	120	≤1	≤33	≤20
5[a]	-	1.0	2.0	5.0	120	≤1	≤33	27
6[a]	-	1.0	2.0	5.0	120	≤1	≤33	26
7[a]	0.1	-	2.0	5.0	120	≤1	≤33	≤20
8	0.1	-	2.0	5.0	120	≤1	≤33	≤20
9	0.1	1.0	-	5.0	120	≤1	≤33	≤20
10	0.1	1.0	-	5.0	120	≤1	≤33	≤20
11	0.1	1.0	2.0	-	120	≤1	≤33	≤20
12	0.1	1.0	2.0	-	120	≤1	≤33	≤20
13	0.1	1.0	1.0	3.0	-	10	≤33	≤20

14	0.1	1.0	1.0	3.0	-	27	≤33	≤20
15	0.1	1.0	1.0	3.0	-	43	≤33	n.d.
16	0.1	1.0	1.0	3.0	-	37	≤33	n.d.
17[a]	0.1	1.0	2.0	5.0	-	81	41	n.d.
18[a]	0.1	1.0	2.0	5.0	-	83	38	n.d.
19[a,b]	0.1	1.0	2.0	5.0	120	19	≤33	n.d.
20[a,b]	0.1	1.0	2.0	5.0	120	17	≤33	n.d.
21[c]	0.1	1.0	1.0	3.0	120	≤1	≤33	≤20
22[c]	0.1	1.0	1.0	3.0	120	≤1	≤33	≤20
23[d]	0.1	1.0	1.0	3.0	120	≤1	≤33	≤20
24[d]	0.1	1.0	1.0	3.0	120	≤1	≤33	≤20
25[b]	0.1	1.0	1.0	3.0	120	11	≤33	≤20
26[b]	0.1	1.0	1.0	3.0	120	11	≤33	≤20
27[b]	0.1	1.0	1.0	3.0	120	11	≤33	n.d.
28[b]	0.1	1.0	1.0	3.0	120	13	≤33	n.d.

Reaction conditions: [Fe] (x μmol), *in situ* Cu PS starting from xantphos (x μmol), bathocuproine (x μmol), and $[Cu(MeCN)_4]PF_6$ (x μmol), BIH (x mg) in NMP/TEOA (5:1, *v*:*v*, 10 mL) under CO_2 (1 atm) at 25 °C under 415 nm, 1.00 W, 3 h. [a]Reaction performed with 400-500 nm (1.50 W). [b]Reaction performed without TEOA. [c]Without light. [d]Under Ar atmosphere. n.d. = not determined.

Table S 10: Application of novel [Fe] complexes **151** and **152** in combination with preformed Cu PS in the photocatalytic CO_2 reduction.

Entry	[Fe]	TON (CO)	TON (H_2)	TON (HCO_2H)
1	$[Fe_2(\mu\text{-bdt})(\kappa^2\text{-bcp})(CO)_4]$	58	380	76
2	$[Fe_2(\mu\text{-bdt})(\kappa^2\text{-bcp})(CO)_4]$	76	450	89
3	$[Fe_2(\mu\text{-bdt})(\kappa^2\text{-bcp})(CO)_4]$	44	367	80
4	$[Fe_2(\mu\text{-bdt})(\kappa^2\text{-bcp})(CO)_4]$	50	371	81
5	$[Fe_2(\mu\text{-bdt})(\kappa^2\text{-xantphos})(CO)_4]$	10	339	163
6	$[Fe_2(\mu\text{-bdt})(\kappa^2\text{-xantphos})(CO)_4]$	11	342	155

Reaction conditions: [Fe] (0.1 μmol), $[Cu(bcp)(xantphos)]PF_6$ (1 μmol), BIH (120 mg) in NMP/TEOA (5:1, *v*:*v*, 10 mL) under CO_2 (1 atm) at 25 °C under 415 nm, 1.00 W, 3 h.

Table S 11: Application of novel [Fe] complexes **151** and **152** in combination with *in situ* Cu PS in the photocatalytic CO_2 reduction.

Entry	[Fe]	TON (CO)	TON (H_2)	TON (HCO_2H)
1	$[Fe_2(\mu\text{-bdt})(\kappa^2\text{-bcp})(CO)_4]$	321	226	199
2	$[Fe_2(\mu\text{-bdt})(\kappa^2\text{-bcp})(CO)_4]$	363	235	194
3	$[Fe_2(\mu\text{-bdt})(\kappa^2\text{-xantphos})(CO)_4]$	95	92	42
4	$[Fe_2(\mu\text{-bdt})(\kappa^2\text{-xantphos})(CO)_4]$	130	105	49
5	$[Fe_2(\mu\text{-bdt})(\kappa^2\text{-xantphos})(CO)_4]$	60	89	66
6	$[Fe_2(\mu\text{-bdt})(\kappa^2\text{-xantphos})(CO)_4]$	98	101	38

Reaction conditions: [Fe] (0.1 μmol), *in situ* Cu PS starting from xantphos (3 μmol), bathocuproine (1 μmol), and $[Cu(MeCN)_4]PF_6$ (1 μmol), BIH (120 mg) in NMP/TEOA (5:1, *v*:*v*, 10 mL) under CO_2 (1 atm) at 25 °C under 415 nm, 1.00 W, 3 h.

4.5 Investigations on CO_2 Reductive Coupling with Disulfide-derived Cu Complexes

4.5.1 Synthesis of *N,N*-bis(pyridin-2-ylmethyl)-1-amino-2-propyl disulfide (154)

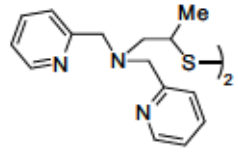

Disulfide **154** was prepared according to a slightly modified literature procedure.[227] It is worth mentioning that the aerial oxidation reported by Bouwman and co-workers[169] did not reach completion over the course of 18 h (Figure S 96).

To propylene sulfide (0.28 mL, 3.57 mmol, 1.00 equiv.) and di-(2-picolyl)amine (0.64 mL, 3.57 mmol, 1.00 equiv.) under Ar inside a pressure tube was added dry MeCN (5.0 mL). The tube was closed and the mixture heated to 90 °C for 20.5 h. The yellow solution was allowed to cool to r.t., subsequently added to a solution of iodine (459 mg, 1.81 mmol, 0.51 equiv) in degassed MeCN/H_2O (5 mL, 9:1 *v*:*v*) and stirred at r.t. for 135 min yielding a dark orange/brown solution. DCM (25 mL) was added and the reaction mixture poured into 1 M aqueous NaOH (15 mL). The layers were separated and the organic layer washed with saturated $Na_2S_2O_3$ solution (2×15 mL). The aqueous layer was extracted with DCM (20 mL), the combined organic layers were dried over $MgSO_4$ and volatiles evaporated under reduced pressure. Column chromatographic separation (Al_2O_3, neutral, DCM/MeOH 1:0→95:5) yielded **154** (586 mg) as a yellow/orange oil containing a mixture of (*R*, *R*), (*R*, *S*), and (*S*, *S*) isomers that was utilized without any further purification.

^{1}H NMR (300 MHz, CD_3CN): δ = 8.50-8.39 (m, 4H), 7.74-7.62 (m, 4H), 7.58-7.48 (m, 4H), 7.24-7.11 (m, 4H), 3.80-3.70 (m, 8H), 3.07-2.94 (m, 2H), 2.76-2.64 (m, 2H), 2.60-2.49 (m, 2H), 1.21-1.12 (m, 6H) ppm.

^{13}C{^{1}H} NMR (75 MHz, CD_3CN): δ = 160.4, 149.8, 137.3, 124.1, 123.0, 61.4, 61.0, 60.8, 45.3, 19.2, 19.1 ppm.

FTIR (ATR, neat): $\tilde{\nu}$ = 3051, 3008, 2959, 2921, 2861, 2819, 2726, 1588, 1568, 1472, 1432, 1365, 1302, 1246, 1221, 1148, 1124, 1091, 1075, 1046, 994, 979, 891, 870, 839, 756, 633, 615, 520, 501, 461 cm^{-1}.

MS (ESI): calculated *m*/*z* for $C_{30}H_{37}N_6S_2^+$ ($[M+H]^+$): 545.2521; found: 545.2527;
calculated *m*/*z* for $C_{30}H_{36}N_6S_2Na^+$ ($[M+Na]^+$): 567.2335; found: 567.2343.

Note: ^{1}H NMR spectra of **154** have previously been reported in CD_2Cl_2 (even though listed as CD_3CN)[169] and $CDCl_3$[227] and ^{13}C{^{1}H} NMR was reported in possibly CD_3CN[169] (not depicted in the literature).

4.5.2 Synthesis of 155

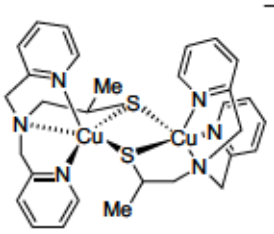

155 was prepared according to a literature procedure.[227]

To **154** (73.1 mg, 134 µmol, 1.00 equiv.) and $[Cu(MeCN)_4]PF_6$ (100 mg, 268 µmol, 2.00 equiv.) was added dry MeCN (6.5 mL). The dark green reaction mixture (Figure S 2) was stirred for 75 min and dry Et_2O (50 mL) was added causing precipitation of a dark green solid. Filtration *via* cannula, washing with dry Et_2O (5 mL) and drying *in vacuo* yielded **155** as dark green solid that was analyzed by NMR spectroscopy.

^{1}H NMR (300 MHz, CD_3CN): δ = 36.28 (br), 34.53 (br), 33.90 (br), 33.17 (br), 19.53 (br), 12.21 (s), 11.88 (s), 10.67 (br), 8.85 (br), 8.61 (br), 8.45 (dt, J = 31.8, 7.1 Hz), 8.20-7.72 (m), 7.67-7.54 (m), 7.42 (br), 7.26 (br), 4.46 (br), 3.92 (br), 3.43-2.44 (m), 1.63-0.93 (m) ppm.
Analytical data is in accordance with that reported in the literature.[227]

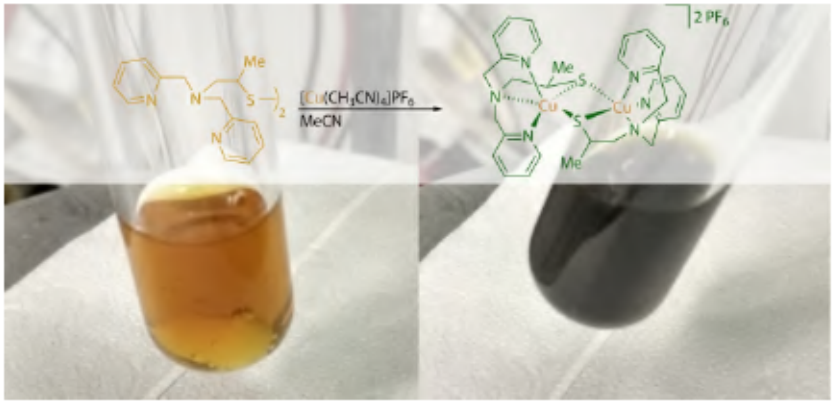

Figure S 2: Color change of the reaction mixture from orange/yellow to dark green upon addition of $[Cu(MeCN)_4]PF_6$ to a solution of the ligand in dry MeCN (in accordance with the literature[227]).

4.5.3 Reaction of 154 and $[Cu(MeCN)_4]PF_6$ with air

Exposure of **154** and $[Cu(MeCN)_4]PF_6$ to air was conducted according to a slightly modified literature procedure.[169]

To **154** (30.5 mg, 56 µmol, 1.00 equiv.) in dry MeCN (2.7 mL) under Ar was added $[Cu(MeCN)_4]PF_6$ (41.6 mg, 112 µmol, 1.99 equiv.) causing an instant color change from dark yellow to dark green. The mixture was stirred at r.t. for 5 min and subsequently poured into a vial in air and left to evaporate over 5 days. The resulting dark green/black solid was analyzed by NMR and FTIR spectroscopy (Figure S 246). Comparison with the NMR obtained from procedure 4.5.2 revealed the presence of a paramagnetic compound different from **155** (see Figure S 98).

^{1}H NMR (400 MHz, CD_3CN): δ = 11.74 (br), 10.88 (br), 10.40 (br), 9.26-6.74 (m, br), 2.35 (br), 1.48 (br) ppm.

FTIR (ATR, neat): $\tilde{\nu}$ = 3088, 2933, 1656, 1611, 1573, 1485, 1447, 1384, 1295, 1254, 1161,

1099, 1054, 1030, 993, 954, 828, 764, 739, 655, 599, 555, 485 cm^{-1}.
The solid product was subsequently subjected to NaOH treatment[193] to extract potentially formed CO_2 reduction products. 1 M NaOH (1.2 mL) and toluene (2.4 mL) were added to the dark green solid and the mixture stirred at r.t. for 23 h. Layers were separated, the organic layer extracted with water (3 mL) and the aqueous layer evaporated. The blue/green residue was extracted with DCM (4 mL) and subsequently dissolved/suspended in D_2O (0.6 mL) and analyzed by NMR spectroscopy (Figures S 99 & 100).
^{1}H NMR (400 MHz, D_2O): δ = 8.42 (s, HCO_2^-), 8.19 (br), 1.88 (s) ppm.
^{13}C{^{1}H} NMR (101 MHz, D_2O): δ = 181.6, 171.2 (HCO_2^-), 137.7, 23.4 ppm.

4.5.4 Protonation of 155 and Reaction with CO_2

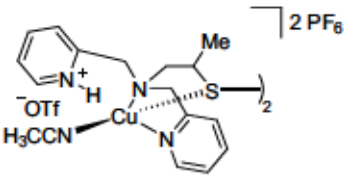

Protonation of **155** was conducted according to a modified literature procedure.[227]

154 (30.5 mg, 56.0 µmol, 1.00 equiv.) and $[Cu(MeCN)_4]PF_6$ (41.7 mg, 112 µmol, 2.00 equiv.) were dissolved in dry MeCN (2 mL) and stirred at r.t. for 30 min. A solution of HOTf (0.015 mL, 170 µmol, 3.03 equiv.) in dry MeCN (1.5 mL) was added to the dark green solution resulting in an immediate color change to light orange/yellow. The reaction mixture was stirred for 10 min. CO_2 was bubbled through the reaction mixture for 10 min without any noticeable change in color. Volatiles were removed *in vacuo* yielding a yellow solid that was analyzed by NMR spectroscopy.
^{1}H NMR (300 MHz, CD_3CN): δ = 13.82 (br, 3H), 8.84-8.69 (br, 4H), 8.60-8.43 (m, 4H), 8.10-7.83 (m, 8H), 4.39-4.07 (m, 8H), 3.06-2.51 (m, 8H), 1.32-1.04 (m, 8H) ppm.
Analytical data is in accordance with that reported for complex **156** as reported in the literature.[227] However, the signal at 13.82 ppm corresponding to the pyridinium protons has not been reported in the literature at room temperature and was only observed at –35 °C.[227] Also, note that due to broad impurities in the 3.1-2.5 and the 1.3-1.0 ppm region, a clear distinction between 6 and 8 protons is not possible. In the literature, the signal in the 3.1-2.5 ppm region had an integral of 6 while that in the 1.3-1.0 ppm range integrated to 8 protons.

4.6 Investigation of [Fe(tmtaa)] in the Reduction of CO_2

4.6.1 Synthesis of $FeBr_2(THF)_2$

$FeBr_2(THF)_2$ was prepared following a literature procedure.[38]

$FeBr_2$ (1.01 g, 4.70 mmol, 1.00 equiv.) and Fe powder (1.60 g, 28.7 mmol, 6.10 equiv.) were stirred in dry THF (110 mL) at r.t. for 14 d. Filtration (cannula) and removal of the volatiles *in vacuo* provided $FeBr_2(THF)_2$ (1.46 g, 4.08 mmol, 87%) as a beige solid.

4.6.2 Synthesis of [Ni(tmtaa)] (159)

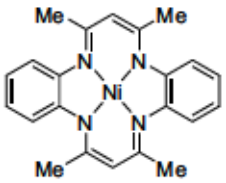

159 was prepared following a literature procedure.[286]

$Ni(OAc)_2 \cdot 4H_2O$ (5.15 g, 20.7 mmol, 1.00 equiv.), *o*-phenylenediamine (8.97 g, 82.9 mmol, 4.00 equiv.), and 2,4-pentanedione (8.31 g, 83.0 mmol, 4.01 equiv.) were suspended in ^{n}BuOH (125 mL) and heated to 135 °C for 3 h. The dark green reaction mixture was allowed to cool to r.t., MeOH (25 mL) was added and the mixture cooled to 0 °C for 15 min. Filtration, washing with cold MeOH (~20 mL) and drying *in vacuo* yielded **159** (6.34 g, 15.8 mmol, 76%) as purple microcrystalline solid.

^{1}H NMR (300 MHz, C_6D_6): δ = 6.54 (m, 8H), 4.66 (s, 2H), 1.75 (s, 12H) ppm.

The analytical data is in accordance with the literature data.[286]

4.6.3 Synthesis of H_2tmtaa·$(HCl)_2$ (160)

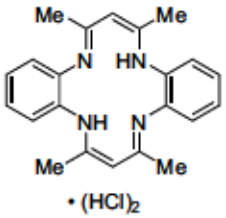

160 was prepared utilizing a modified literature procedure that did not require pressurized HCl gas.[286,287]

HCl gas generated by dropwise addition of conc. H_2SO_4 (70 mL, 1.31 mol, 122 equiv.) to previously dried NaCl (109 g, 1.86 mol, 174 equiv.) under Ar was passed through a suspension of [Ni(tmtaa)] (4.28 g, 10.7 mmol, 1.00 equiv.) in dry MeOH (80 mL) for 30 min. During this time, the color of the suspension changed from green to brown and a white solid precipitate formed. The mixture was allowed to cool to r.t. and was further cooled to 0 °C. The solid precipitate was filtered off and washed with cold, dry MeOH (10 mL, then 3×5 mL). The off-white solid was dried *in vacuo* to yield **160** (3.35 g, 8.03 mmol, 75% [assuming H_2tmtaa·$(HCl)_2$]).

^{1}H NMR (300 MHz, D_2O): δ = 7.45-7.18 (m, 8H), 4.69 (s, 2H), 2.58 (s, 12H) ppm.

The analytical data is in accordance with the literature.[286] However, reaction with NEt_3 yielded a green solid indicating the presence of residual $[NiCl_4]^{2-}$ which is not in accordance with the literature.[286] Presented yields are calculated for H_2tmtaa·$(HCl)_2$. However, subsequent anion exchange was mandatory for further preparation of H_2tmtaa and the derived Fe complex **118**.

4.6.4 Synthesis of H_2tmtaa·$(HPF_6)_2$ (161)

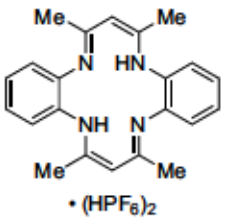

161 was prepared following a modified literature procedure.[287]

To a yellow solution of H_2tmtaa·$(HCl)_2$ (1.52 g, 3.64 mmol, 1.00 equiv.) in H_2O (20 mL) was added a solution of NH_4PF_6 (1.23 g, 7.56 mmol, 2.08 equiv.) in H_2O (2 mL) causing formation of a white precipitate. After stirring for 10 min at r.t., the solid was filtered off using a filter cannula and washed with H_2O (10 mL, then 4 mL). Drying *in vacuo* yielded H_2tmtaa·$(HPF_6)_2$ (1.96 g, 3.08 mmol, 85%) as a slightly yellow solid.

^{1}H NMR (300 MHz, DMSO-d_6): δ = 10.77 (s, 4H), 7.38 (m, 4H), 7.23 (m, 4H), 4.50 (s, 2H), 2.54 (s, 12H) ppm.

^{31}P{^{1}H} NMR (122 MHz, DMSO-d_6): δ = −144.2 (hept, J = 711 Hz) ppm.

^{13}C{^{1}H} NMR (75 MHz, DMSO-d_6): δ = 170.9, 132.8, 129.9, 128.6, 93.1, 21.2 ppm.

HR-MS (ESI): calculated *m*/*z* for $C_{22}H_{27}N_4^{2+}$ ([M–(2PF_6)]$^{2+}$): 173.1084; found: 173.1083.
calculated *m*/*z* for PF_6^- ([M–($C_{22}H_{26}N_4$)]$^-$): 144.9642; found: 144.9639.

FTIR (ATR, neat): $\tilde{\nu}$ = 3662, 3584, 3343, 3014, 2872, 1563, 1532, 1490, 1437, 1387, 1344, 1316, 1279, 1206, 1108, 1032, 974, 956, 901, 820, 759, 740, 599, 589, 554, 499, 472, 446 cm^{-1}.

The analytical data is in accordance with the literature.[287]

4.6.5 Synthesis of 4,11-Dihydro-5,7,12,14-tetramethyldibenzo[*b*,*i*][1,4,8,11]tetraazacyclotetradecine (H_2tmtaa) (162)

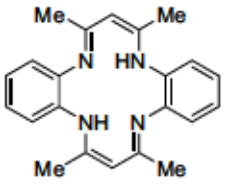

162 was prepared following a modified literature procedure.[287]

To **161** (505 mg, 793 µmol, 1.00 equiv.) in dry MeOH (2.0 mL) was added NEt_3 (0.22 mL, 1.58 mmol, 1.99 equiv.). The yellow suspension was stirred at r.t. for 1 h and subsequently filtered *via* cannula. The solid residue was dissolved in DCM (10 mL) and washed with sat. $NaHCO_3$ solution (2×8 mL) and H_2O (10 mL). The organic layer was dried over $MgSO_4$ and evaporated under reduced pressure yielding **162** (0.274 mg, 755 µmol, 95%) as a yellow solid that still contained traces of DCM.

^{1}H NMR (300 MHz, $CDCl_3$): δ = 12.58 (br, 2H), 6.99 (s, 8H), 4.88 (s, 2H), 2.13 (s, 12H) ppm.

^{13}C{^{1}H} NMR (75 MHz, $CDCl_3$): δ = 159.1, 138.7, 123.3, 123.1, 98.1, 21.1 ppm.

HR-MS (ESI): calculated *m*/*z* for $C_{22}H_{25}N_4^+$ ([M+H]$^+$): 345.2079; found: 345.2089.

FTIR (ATR, neat): $\tilde{\nu}$ = 3060, 3045, 3024, 2990, 2974, 2962, 2914, 2873, 2851, 2840, 1610, 1591, 1546, 1507, 1460, 1425, 1379, 1354, 1291, 1272, 1185, 1109, 1054, 1043, 1025, 1019, 1000, 937, 924, 821, 802, 790, 732, 684, 631, 603, 561, 531, 505, 475 cm^{-1}.

The analytical data is in accordance with the literature.[287]

4.6.6 Synthesis of [Fe(tmtaa)]·THF (118)

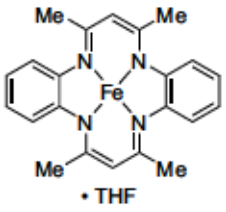

118 was prepared following a slightly modified literature procedure.[188] ^{n}BuLi (2.5 M in hexane, 0.73 mL, 1.82 mmol, 2.09 equiv.) was added to H_2tmtaa (301 mg, 873 µmol, 1.00 equiv.) in dry THF (4.5 mL). After stirring for 3 h at r.t., the deep red solution was added dropwise to a suspension of $FeBr_2(THF)_2$ (312 mg, 873 µmol, 1.00 equiv.) in dry THF (4.5 mL) at approx. –32 °C over 3 min. The reaction mixture was allowed to warm to r.t. and stirred for 15 h. The dark purple suspension was cooled to –40 °C and filtered *via* cannula. The dark purple solid residue was dried *in vacuo* to provide **118** (202 mg, 507 µmol, 58%).

^{1}H NMR (400 MHz, pyridine-d_5): δ = 6.51 (br, 4H), 6.27 (br, 4H), 3.90 (br, 2H), 3.66 (br, 4H), 1.71 (br, 12H), 1.62 (br, 4H) ppm.

The analytical data is in accordance with the literature data.[188]

4.6.7 General Procedure for the Preparation of $NaC_{10}H_8$

THF solutions of $NaC_{10}H_8$ were prepared following the general strategy reported in the literature.[285]

To freshly cut Na (excess) and $C_{10}H_8$ (1 equiv.) under Ar was added dry THF (0.10-0.14 M). The dark green reaction mixture was stirred overnight at r.t. and subsequently used without further purification.

4.6.8 General Procedure for Reduction of 118 with $NaC_{10}H_8$ and Subsequent CO_2 treatment

This procedure is a modified version of the protocol reported in the literature.[188]

To a suspension of **118** in dry THF (0.15-0.16 M) was added a solution of $NaC_{10}H_8$ (1.3-1.5 equiv.) in dry THF (1.0 mL). The resulting mixture was stirred at r.t. for 20-24 h and subsequently concentrated *in vacuo* to approx. 0.5 mL. Dry hexane (1-2 mL) was added and the resulting solid precipitate filtered off *via* cannula, in some cases washed with additional dry hexane (0.5 mL) and dried *in vacuo*. The remaining black solid was dissolved in dry toluene (0.02-0.03 M) and cooled to approx. –30 °C. CO_2 was bubbled though the reaction mixture for 10 min at this temperature, the Schlenk tube sealed under Ar overpressure (resulting in a CO_2/Ar mixture), allowed to warm to r.t. and stirred for 20-22 h yielding a dark purple suspension. All volatiles were removed *in vacuo* and the dark purple/black solid residue subjected to extraction according to the general procedure (4.6.11).

4.6.9 General Procedure for Reduction of 118 with Alkali Metals and Subsequent CO_2 Treatment in Toluene

This procedure is a modified version of the protocol reported in the literature.[188]

To **118** and the alkali metal under Ar was added dry THF (42-43 mM). The resulting mixture was stirred at r.t. for 19-24 h. In some cases, the resulting mixture was heated to 40-50 °C (see Table S 12). Volatiles were removed *in vacuo*, the resulting solid cooled to approx. –30 °C and the atmosphere exchanged for CO_2. Dry toluene (24-28 mM) was added and the reaction mixture allowed to warm to r.t., closed and stirred under constant CO_2 atmosphere from 22 to 73 h (see Table S 12) yielding a dark red/purple suspension. Volatiles were removed *in vacuo*. The remaining solid was subsequently extracted according to the general procedure (4.6.11).

4.6.10 General procedure for Reduction of 118 with Alkali Metals and Subsequent CO_2 Treatment *via* Freeze-pump-thaw

This procedure is based on a combination of modified literature protocols.[188,195]

To **118** and the alkali metal (1.2-1.4 equiv.) under Ar was added dry THF (34-46 mM). The resulting mixture was stirred at r.t. for 21-28 h. In case the CO_2 treatment was conducted in toluene, volatiles were removed *in vacuo* and dry toluene added to thus obtained solid residue (23 mM). The resulting mixture was frozen in liquid nitrogen and evacuated to 1×10^{-3} mbar. The frozen mixture was opened to a CO_2 atmosphere for ~1 s (caution: prolonged opening causes deposition of solid CO_2 that could shatter the flask upon thawing!). The nitrogen Dewar was removed and the mixture subsequently allowed to thaw in a water bath. After complete thawing, the mixture was opened to CO_2 for 30-60 s, closed under CO_2 atmosphere (1 atm) and stirred at r.t. for 18-22 h yielding a dark red/brown (for THF) or dark red/purple (toluene) suspension. Volatiles were removed *in vacuo*, the solid residue analyzed by FTIR spectroscopy and subjected to extraction according to the general procedure (4.6.11).

4.6.11 General Procedure for the Extraction of CO_2 Treatment Experiments with H_2O

Aqueous extraction was conducted *via* a modification of the reported protocol.[188]

Dry toluene and degassed H_2O (half the volume of toluene) were cautiously added to the solid residue of the CO_2 treatment reaction under Ar (8-15 mM final concentration based on initial amount of **118**) and the resulting mixture stirred overnight. Layers were separated using a syringe and the aqueous layer evaporated under reduced pressure. D_2O (0.6-0.8 mL) was added to the obtained residue, a part of the solution was utilized for analysis *via* capillary electrophoresis (0.02-0.2 mL) and the remaining solution analyzed by ^{1}H and ^{13}C NMR spectroscopy.

4.6.12 [Fe(tmtaa)] In the Reduction of CO_2 - Results

Table S 12: Results for the attempted CO_2 reduction utilizing [Fe(tmtaa)]·THF (**118**).

Entry	Proc.	[Fe] ([µmol])	Reductant ([µmol])	Solvent ([mL])	*t* [h]	FTIR $\tilde{\nu}$ [cm^{-1}]‡	^{13}C NMR δ [ppm] (HCO_3^{2-}/CO_3^{2-})	CE ($C_2O_4^{2-}$) [approx. yield]
1	4.6.8	80	$NaC_{10}H_8$ (107)	toluene (3.0)	10 min, 20	n.d.	163.1	<0.5%
2[a]	4.6.8	74	$NaC_{10}H_8$ (112)	toluene (4.0)	22	n.d.	164.7	<0.5%
3[b]	4.6.9	85	Na (1960)	toluene (3.0)	15 min, 24	n.d.	162.5	<0.5%
4[c]	4.6.9	64	Na (74)	toluene (2.6)	22	n.d.	164.9	<0.1%
5[d]	4.6.9	43	K (44)	toluene (1.8)	73	1912, 1654, 1648, 1638	163.1	<0.1%
6[e]	4.6.10	34	K (41)	toluene (1.5)	22	1911, 1654, 1648, 1638	162.4	<0.1%
7[f]	4.6.10	46	K (59)	toluene (2.0)	18	1911, 1653, 1648, 1636	164.0 [168.3]	<0.1%
8[g]	4.6.10	41	K (51)	THF (1.0)	20	1911	162.0	<0.1%
9[h]	4.6.10	35	K (49)	THF (1.0)	21	1911, 1652, 1635	168.3	<0.5%

Reactions were conducted according to the general procedure stated. Reaction times presented in the table are the times of CO_2 treatment or time of CO_2 bubbling and subsequent stirring (for reactions according to procedure 4.6.8). n.d. = not determined. ‡Characteristic vibrations are reported (IR spectra are presented in section 4.13.3). [a]Instead of CO_2 bubbling, the solid obtained from $NaC_{10}H_8$ treatment was directly set under CO_2 atmosphere at –31 °C and dry toluene was added. The reaction mixture was then stirred under constant CO_2 atmosphere. [b]The mixture was heated to 40 °C for 1.5 h after stirring for 24 h in the presence of Na and subsequently filtered *via cannula*. To the obtained solid after removal of all volatiles *in vacuo* was added dry toluene, the mixture cooled to –30 °C and CO_2 bubbled through for 10 min. The dry ice bath was removed and bubbling continued for another 5 min. The flask was sealed and the general procedure 4.6.9 followed for all further steps. [c]Heated to approx. 50 °C for 5 min after stirring with Na at r.t. for 19 h. [d]Heated to approx. 50 °C for 1 min after stirring with K at r.t. for 22 h. [e]Two freeze-pump-thaw cycles were performed. After 1.5 h under CO_2, a sample (0.1 mL) of the reaction mixture was taken under CO_2 overpressure. The solid residue after CO_2 treatment was analyzed by NMR spectroscopy in pyridine-d_5 indicating the presence of [Fe(tmtaa)]. [f]Headspace of the reaction (5 mL) was analyzed by GC prior to removal of the volatiles *in vacuo*. No gaseous CO_2 reduction products (CO, CH_4) have been detected. The pH of the NMR sample was adjusted by addition of 1 M NaOH (0.02 mL). The ^{13}C shift after pH adjustment is given in []. [g]The solid residue after CO_2 treatment was analyzed by NMR spectroscopy in pyridine-d_5 indicating the presence of presumably [Fe(tmtaa)]. [h]Two freeze-pump-thaw cycles were performed. After 30 min under CO_2, a sample (0.1 mL) of the reaction mixture was taken under CO_2 overpressure. The pH of the aqueous solution after extraction was adjusted with aqueous NaOH (1 M) prior to evaporation of the aqueous layer.

4.7 Investigation of 1,4,7-Tacn-derived Cu Complexes in CO_2 Reductive Coupling

4.7.1 Synthesis of $AgBPh_4$

$AgBPh_4$ was prepared following a literature procedure.[332]

A solution of $NaBPh_4$ (416 mg, 1.22 mmol, 1.00 equiv.) in H_2O (5 mL) was filtered (PTFE syringe filter) and added to a solution of $AgNO_3$ (207 mg, 1.22 mmol, 1.00 equiv.) in H_2O (5 mL). H_2O (10 mL) was added to the white suspension to facilitate stirring which was continued for 3 min. The solid precipitate was filtered off and washed with H_2O (5×3 mL). Drying *in vacuo* yielded $AgBPh_4$ (473 mg, 1.11 mmol, 91%) as an off-white solid.

4.7.2 Synthesis of 1,2-Bis(4-toluenesulfonyloxy)ethane (164)

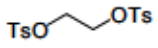

164 was prepared according to a modification of a literature procedure.[323]

To a solution of ethylene glycol (14.0 mL, 251 mmol, 1.00 equiv.) in triethylamine (160 mL) cooled with an ice bath was added *p*-toluenesulfonyl chloride (103 g, 539 mmol, 2.15 equiv.) in Et_2O (500 mL) over 2.5 h (the ice bath was removed after 90 min). After complete addition the colorless suspension was stirred for 19 h at r.t.. The white precipitate was filtered off and washed with Et_2O (100 mL), H_2O (~100 mL), MeOH (2×100 mL) and again Et_2O (100 mL). The white solid was dried under reduced pressure, suspended in EtOH (300 mL) and heated to 76 °C for 30 min. After cooling to r.t. the white solid was filtered off. Washing with cold EtOH (200 mL) and drying *in vacuo* yielded **164** as a white solid (75.5 g, 204 mmol, 81%).
^{1}H NMR (300 MHz, DMSO-d_6) δ = 7.72 (d, J = 8.3 Hz, 4H), 7.47 (d, J = 8.3 Hz, 4H), 4.17 (s, 4H), 2.42 (s, 6H) ppm.
The analytical data is in accordance with the literature data (NMR reported in $CDCl_3$).[325]

4.7.3 Synthesis of 1,4,7-Tris(4-toluenesulfonyl)-1,4,7-triazaheptane (165)

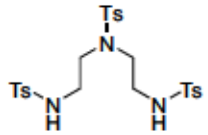

165 was prepared according to a modification of a literature procedure.[323]

To a solution of diethylenetriamine (17.5 mL, 161 mmol, 1.00 equiv.) and NaOH (20.0 g, 500 mmol, 3.10 equiv.) in H_2O (160 mL) cooled with an ice bath was added *p*-toluenesulfonyl chloride (100 g, 525 mmol, 3.25 equiv.) in Et_2O (500 mL) over four hours (the ice bath was removed after 15 min). The colorless suspension was stirred at r.t. for 18 h after complete addition. The white precipitate was filtered off and washed with H_2O (~150 mL) and MeOH (~100 mL). Thus obtained solid was suspended in EtOH (200 mL), heated to 76 °C for 30 min, allowed to cool to r.t. and filtered off. Compound **165** (74.8 g, 132 mmol, 81%) was obtained as a white solid after washing with cold EtOH (200 mL) and drying *in vacuo*.

^{1}H NMR (300 MHz, DMSO-d_6) δ = 7.74-7.61 (m, 6H), 7.54 (d, J = 8.3 Hz, 2H), 7.40 (d, J = 8.3 Hz, 4H), 7.37 (d, J = 8.3 Hz, 2H), 3.09-2.93 (m, 4H), 2.87-2.74 (m, 4H), 2.39 (s, 6H), 2.39 (s, 3H) ppm.
The analytical data is in accordance with the literature (NMR reported in acetone-d_6).[325]

4.7.4 Synthesis of 1,4,7-Tris(4-toluenesulfonyl)-1,4,7-triazacyclononane (166)

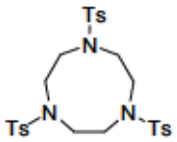

166 was prepared according to a modified literature procedure.[324]

To a suspension of **165** (25.2 g, 44.6 mmol, 1.00 equiv.) in dry EtOH (~150 mL) at 80 °C was added an EtOH solution of NaOEt, which was freshly prepared from dry EtOH (42 mL) and Na (2.10 g, 91.3 mmol, 2.05 equiv), over 15 min. The solution was stirred at 80 °C for 1 h. Volatiles were removed *in vacuo* yielding a colorless solid which was dissolved in dry DMF (~220 mL) and heated to 105 °C. A solution of **164** (16.5 g, 44.6 mmol, 1.00 equiv) in dry DMF (~220 mL) was added to the reaction mixture at this temperature over 2 h. After complete addition, heating of the reaction mixture to 110 °C was continued for 1 h after which the light yellow solution was allowed to cool to r.t. overnight. The reaction mixture was concentrated under reduced pressure until the formation of a precipitate was observed (at ~100 mL). The mixture was then poured into H_2O (450 mL) and the formed sticky precipitate was filtered off. $CHCl_3$ (120 mL) was added and the mixture sonicated for a few minutes. The two resulting layers were separated, the organic layer transferred into a round-bottom flask, carefully layered with EtOH (~250 mL) and stored at 5 °C for 5 d. The white solid was filtered off and washing with EtOH (~100 mL) followed by drying *in vacuo* provided **166** (16.8 g, 28.4 mmol, 64%).
^{1}H NMR (400 MHz, $CDCl_3$) δ = 7.70 (d, J = 8.3 Hz, 6H), 7.32 (d, J = 8.3 Hz, 6H), 3.42 (s, 12H), 2.43 (s, 9H) ppm.
The analytical data is in accordance with the literature.[325]

4.7.5 Synthesis of 1,4,7-Triallyl-1,4,7-triazacyclononane (127)

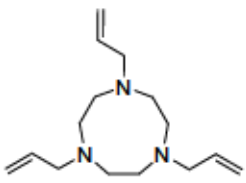

tacn·3HCl (**167**) was prepared utilizing an adapted literature procedure.[325]

To **166** (3.13 g, 5.28 mmol, 1.00 equiv.) under Ar was added conc. H_2SO_4 (7.0 mL, 131 mmol, 24.9 equiv.). The brownish solution was heated to 160 °C for 40 min and subsequently allowed to cool to r.t.. The black mixture was added dropwise into cold EtOH (26 mL). After complete addition, Et_2O (39 mL) was layered on top and the biphasic mixture stored at 5 °C for 2 d. The beige solid precipitate was filtered off, washed with Et_2O (~20 mL) and dissolved in H_2O (6 mL). Conc. HCl (3.4 mL) and EtOH (20 mL) were added causing the formation of an off-white solid. Filtration, washing with EtOH (20 mL), Et_2O (20 mL) and drying under reduced pressure gave **167** (1.37 g) as a crude product which still contained some SO_4^{2-}

and was utilized for the preparation of substituted 1,4,7-triazacyclononanes without further purification.

^{1}H NMR (300 MHz, D_2O) δ = 3.41 (s, 12H) ppm.

The analytical data is in accordance with the literature.[325]

127 was prepared using a slightly modified literature procedure.[326]

167 (1.37 g, 5.74 mmol, 1.00 equiv.) and powdered KOH (5.04 g, 89.8 mmol, 15.7 equiv.) were suspended in dry EtOH (7.5 mL) and stirred at r.t. for 3 h. Dry toluene (59 mL) was added and stirring continued for 24 h. The colorless suspension was filtered using a filter cannula equipped with a glass microfiber filter and volatiles were removed *in vacuo*. Powdered KOH (3.36 g, 59.9 mmol, 10.4 equiv.), dry toluene (72 mL) and allyl bromide (1.62 mL, 18.7 mmol, 3.26 equiv.) were added to the resulting sticky white to light-yellow solid and the mixture stirred at r.t. for 46 h. The light-yellow suspension was filtered and all volatiles were removed under reduced pressure. The oily residue was extracted with Et_2O (~175 mL) *via* filter cannula. Removal of the volatiles under reduced pressure yielded **127** (865 mg, 3.47 mmol, 60% over two steps) as a yellow oil.

^{1}H NMR (300 MHz, CD_3CN) δ = 5.87 (ddt, J = 17.3, 10.1, 6.4 Hz, 3H), 5.15 (ddt, J = 17.3, 2.2, 1.5 Hz, 3H), 5.06 (ddt, J = 10.2, 2.2, 1.2 Hz, 3H), 3.11 (dt, J = 6.4, 1.4 Hz, 6H), 2.70 (s, 12H) ppm.

^{13}C{^{1}H} NMR (101 MHz, CD_3CN): δ = 138.4, 116.8, 62.4, 56.2 ppm.

HR-MS (ESI): calculated *m/z* for $C_{15}H_{28}N_3^+$ ($[M+H]^+$): 250.2283; found: 250.2288.

FTIR (ATR, neat): $\tilde{\nu}$ = 3075, 3004, 2976, 2905, 2874, 2834, 2785, 1678, 1641, 1454, 1417, 1349, 1326, 1301, 1153, 1123, 1096, 1059, 1040, 992, 914, 868, 790, 775, 627, 561, 543 cm^{-1}.

Note: Purity of allyl bromide proved to be crucial for isolation of analytically pure **127** and subsequent column chromatographic purification was required in case non-distilled or non-freshly opened allyl bromide was utilized. Column chromatography (SiO_2, EtOAc/NEt_3 100:1 or DCM/NEt_3 30:1) can be conducted for further purification of **127**.

The analytical is in accordance with the literature (NMR reported in acetone-d_6).[326]

4.7.6 Synthesis of [Cu(127)I] (168)

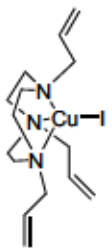

To CuI (16.0 mg, 84.0 μmol, 1.00 equiv.) under Ar was added a solution of **127** (21.0 mg, 84.2 μmol, 1.00 equiv.) in dry THF (3.0 mL). The reaction mixture was stirred at r.t. for 15 min yielding a colorless solution. Filtration *via* PTFE syringe filter and subsequent removal of the volatiles *in vacuo* yielded a light yellow solid. Slow diffusion of dry hexane (3.0 mL) into a solution of the crude product in dry THF (1.0 mL) at 5 °C provided **168** (18.1 mg, 41.2 μmol, 49%) as a crystalline solid. Crystals suitable for X-ray crystallographic analysis were grown by slow diffusion of dry hexane into a concentrated solution of **168** containing

$NaBPh_4$ in dry THF at 5 °C. Crystals with identical unit cell were obtained by slow diffusion of hexane into a solution of **168** in 1,2-dichlorobenzene at –32 °C in the absence of $NaBPh_4$.
^{1}H NMR (400 MHz, THF-d_8): δ = 6.67 (ddt, J = 17.1, 10.1, 6.9 Hz, 3H), 5.19 (ddt, J = 17.1, 2.2, 1.3 Hz, 3H), 5.13 (ddt, J = 10.1, 2.2, 1.1 Hz, 3H), 3.38 (dt, J = 6.9, 1.2 Hz, 6H), 2.77-2.57 (m, 12H) ppm.
^{13}C{^{1}H} NMR (101 MHz, THF-d_8): δ = 137.9, 118.7, 65.3, 53.8 ppm.
MS (ESI): calculated m/z for $C_{30}H_{54}Cu_2IN_6^+$ ([2M-I]$^+$): 751.2041; found: 751.
HR-MS (EI): calculated m/z for $C_{15}H_{27}CuN_3^+$ ([M-I]$^+$): 312.14955; found: 312.14958.
FTIR (ATR, neat): $\tilde{\nu}$ = 3071, 2998, 2973, 2912, 2877, 2822, 1640, 1486, 1452, 1419, 1389, 1369, 1353, 1330, 1319, 1295, 1249, 1171, 1148, 1115, 1095, 1083, 1034, 1021, 995, 985, 924, 888, 789, 769, 754, 685, 651, 583, 555, 498, 405 cm^{-1}.

4.7.7 Synthesis of [Cu(127)$(NO_3)_2$] (170)

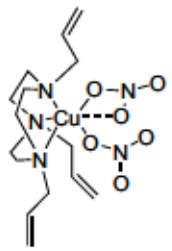

To a solution of $Cu(NO_3)_2{\cdot}3H_2O$ (66.6 mg, 276 μmol, 1.00 equiv.) in EtOH (0.3 mL) was added **127** (68.7 mg, 275 μmol, 1.00 equiv.) in EtOH (1.0 mL). The resulting blue suspension was stirred at r.t. for 8 h and subsequently filtered (filter cannula). The solid residue was washed with EtOH (0.5 mL) and dried under reduced pressure yielding **170** (60.1 mg, 137 μmol, 50%) as a blue solid. Crystals suitable for X-ray crystallographic analysis were obtained by slow evaporation from a solution of **170** in acetone.
FTIR (ATR, neat): $\tilde{\nu}$ = 3081, 3017, 2985, 2961, 2942, 2913, 2895, 2859, 1487, 1466, 1449, 1436, 1373, 1321, 1295, 1271, 1071, 1058, 1017, 1008, 988, 967, 929, 889, 805, 780, 752, 704, 688, 652, 562, 457, 439, 429 cm^{-1}.
Anal. Calcd. C 41.23, H 6.23, N 16.03. **Observed** C 41.21, H 6.289, N 15.96.

4.7.8 Synthesis of [Cu(127)(κ^2-C_2O_4)] (171)

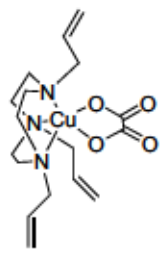

To $Cu(NO_3)_2{\cdot}3H_2O$ (32.1 mg, 133 μmol, 0.87 equiv.) in dry EtOH (0.5 mL) was added **127** (38.2 mg, 153 μmol, 1.00 equiv.) in dry EtOH (1.0 mL). The blue suspension was stirred at r.t. for 10 min and subsequently filtered *via* filter cannula. The blue solid residue was suspended in EtOH (1.0 mL). $Na_2C_2O_4$ (20.5 mg, 153 μmol, 1.00 equiv.) in H_2O (1.0 mL) was added and the dark blue solution stirred at r.t. for 1 h. Volatiles were removed *in vacuo* and the blue/white solid residue extracted with $MeNO_2$ (1.0+0.5 mL). The blue solid obtained after removal of all volatiles *in vacuo* was washed with THF (~5 mL), dissolved in $MeNO_2$ (~5 mL), and filtered. $MeNO_2$ was removed *in vacuo* and the blue solid recrystallized by cooling a solution in warm $MeNO_2$ (~0.4 mL) to –32 °C yielding **171** (3.8 mg, 9.5 μmol, 7%) as blue needles. Crystals suitable for X-ray crystallographic analysis were obtained by cooling a solution of **171** in warm $MeNO_2$ to –32 °C.
FTIR (ATR, neat): $\tilde{\nu}$ = 3512, 3438, 3082, 3019, 2996, 2975, 2925, 2908, 2860, 1711, 1668,

1650, 1558, 1502, 1457, 1439, 1421, 1376, 1347, 1339, 1326, 1284, 1252, 1241, 1150, 1106, 1083, 1061, 1017, 994, 968, 939, 886, 807, 779, 756, 687, 655, 590, 553, 534, 512, 475, 437, 415 cm^{-1}.

Anal. Calcd. C 50.92, H 6.79, N 10.48. **Observed** C 50.96, H 6.788, N 10.21.

4.7.9 Synthesis of [Cu(127)Cl_2] (173)

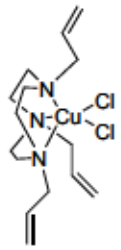

To $CuCl_2$ (22.9 mg, 170 µmol, 1.00 equiv.) was added **127** (42.6 mg, 171 µmol, 1.00 equiv.) in MeOH (1.5 mL). The resulting green solution was stirred at r.t. for 10 min. Volatiles were remove *in vacuo* yielding a green solid. Twofold recrystallization from hot $MeNO_2$ (0.8 mL, then 0.3 mL) yielded **173** (22.4 mg, 58.4 µmol, 34%) as green crystalline solid. Crystals suitable for X-ray crystallographic analysis were obtained by recrystallization from hot $MeNO_2$ using the complex obtained after column chromatographic separation ($MeNO_2$/MeOH/2 M NH_4Cl 1:2:7)[192] of the product obtained from the reaction of *in situ* formed **168** with $CsHCO_3$ (Table S 14, entry 1).

FTIR (ATR, neat): $\tilde{\nu}$ = 3064, 3004, 2970, 2920, 2900, 2846, 1640, 1559, 1493, 1453, 1432, 1422, 1396, 1370, 1360, 1350, 1335, 1325, 1309, 1285, 1249, 1169, 1149, 1134, 1086, 1062, 1031, 1015, 994, 970, 951, 930, 885, 859, 804, 776, 750, 715, 656, 603, 592, 559, 508, 476, 460, 436, 415 cm^{-1}.

Anal. Calcd. C 46.94, H 7.09, N 10.95. **Observed** C 47.00, H 7.211, N 10.75.

4.7.10 Synthesis of [(127)Cu(μ-C_2O_4)Cu(127)](BF_4)$_2$ (172)

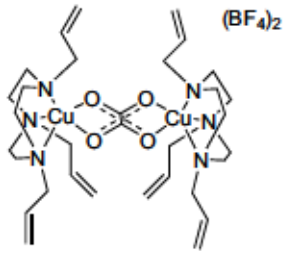

172 was prepared using a modified literature procedure for the synthesis of analogous [(tacn)Cu(μ-C_2O_4)Cu(tacn)](ClO_4)$_2$ complexes.[226]

To **127** (109 mg, 437 µmol, 1.00 equiv.) in MeOH/H_2O (4.6 mL, 1:1, *v*:*v*) was added a solution of Cu(BF_4)$_2$·6H_2O (151 mg, 438 µmol, 1.00 equiv.) in H_2O (2.3 mL). The blue solution was stirred at r.t. for 1.5 h and subsequently filtered *via* polyamide syringe filter. A solution of $Na_2C_2O_4$ (29.3 mg, 219 µmol, 0.50 equiv.) in H_2O (0.8 mL) was added and the dark blue solution left standing at ambient temperature for 11 d. Filtration *via* filter cannula, recrystallization from a minimum amount of hot $MeNO_2$ at 5 °C and drying *in vacuo* provided **172** (120 mg, 135 µmol, 62%) as blue solid. Crystals suitable for single crystal X-ray diffraction were obtained by slow evaporation of a MeOH solution of **172** at 5 °C.

FTIR (ATR, neat): $\tilde{\nu}$ = 3085, 2978, 2944, 2927, 2887, 2873, 2866, 1651, 1558, 1543, 1493, 1455, 1446, 1424, 1354, 1336, 1325, 1311, 1285, 1247, 1047, 1029, 1011, 987, 957, 938, 885, 858, 795, 778, 752, 708, 692, 678, 657, 558, 520, 479, 444, 437, 401 cm^{-1}.

Anal. Calcd. C 43.31, H 6.13, N 9.47. **Observed** C 43.37, H 6.163, N 9.428.

4.7.11 Synthesis of 1,4,7-Tribenzyl-1,4,7-triazacyclononane (174)

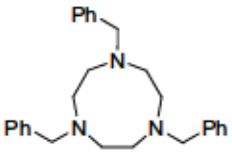

174 was synthesized using a modification of a literature procedure for the preparation of trisubstituted 1,4,7-triazacyclononanes.[326]

167 (1.00 g, 4.21 mmol, 1.00 equiv.) and powdered KOH (3.78 g, 67.3 mmol, 16.0 equiv.) were suspended in dry EtOH (5.5 mL) and stirred at r.t. for 135 min. Dry toluene (45 mL) was then added and stirring continued for another 21 h. The colorless suspension was filtered (cannula) and volatiles subsequently removed *in vacuo*. Powdered KOH (2.54 g, 45.2 mmol, 10.7 equiv.), dry toluene (55 mL) and benzyl bromide (1.60 mL, 13.5 mmol, 3.20 equiv.) were added and the mixture stirred for 56 h. The yellow suspension was filtered and volatiles evaporated under reduced pressure. The oily orange residue was extracted with Et_2O (3×40 mL) *via* filter cannula and the volatiles evaporated under reduced pressure. Column chromatographic separation (SiO_2, pentane/Et_2O/NEt_3 2:1:0 → 20:10:3) yielded **174** (1.02 g, 2.57 mmol, 61%) as a light-yellow oil.

^{1}H NMR (300 MHz, CD_3CN) δ = 7.35-7.18 (m, 15H), 3.58 (s, 6H), 2.75 (s, 12H) ppm.

^{13}C{^{1}H} NMR (75 MHz, CD_3CN): δ = 141.7, 130.0, 129.1, 127.7, 63.6„ 56.3 ppm.

HR-MS (ESI): calculated *m/z* for $C_{27}H_{34}N_3^+$ ($[M+H]^+$): 400.2753; found: 400.2748.

FTIR (ATR, neat): $\tilde{\nu}$ = 3083, 3060, 3025, 2923, 2903, 2871, 2788, 1600, 1584, 1493, 1451, 1354, 1322, 1299, 1270, 1204, 1136, 1096, 1072, 1058, 1046, 1027, 1004, 990, 907, 885, 788, 777, 752, 731, 697, 475 cm^{-1}.

A ^{1}H NMR spectrum in $CDCl_3$ had previously been reported in the literature.[452]

4.7.12 Synthesis of 1,4,7-Tri-1-propyl-1,4,7-triazacyclononane (175)

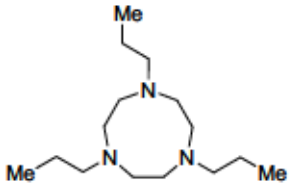

175 was synthesized using a modification of a literature procedure for the preparation of trisubstituted 1,4,7-triazacyclononanes.[326]

To **167** (620 mg, 2.60 mmol, 1.00 equiv.) and powdered KOH (1.49 g, 26.5 mmol, 10.2 equiv.) was added dry EtOH (4.0 mL) and the suspension stirred at r.t. for 2 h. Dry toluene (25 mL) was added and stirring continued for another 16 h. The colorless suspension was filtered (cannula) and volatiles were removed *in vacuo*. The white solid was suspended in dry toluene (30 mL) and powdered KOH (1.31 g, 23.3 mmol, 8.96 equiv.) was added followed by 1-bromopropane (0.77 mL, 8.48 mmol, 3.26 equiv.). The colorless suspension was stirred at r.t. for 2 d, filtered and volatiles were evaporated under reduced pressure. The residue was extracted with Et_2O (2×60 mL) *via* filter cannula and all volatiles evaporated under reduced pressure. The light-yellow oil was distilled *in vacuo* (1×10^{-3} mbar, 130 °C). Due to incomplete conversion, the resulting oil was dissolved in dry toluene (10 mL) powdered KOH (128 mg, 2.28 mmol, 0.88 equiv.) and 1-bromopropane (0.06 mL, 661 µmol, 0.25 equiv.) were added and the mixture stirred at r.t. for 82 h. Filtration, evaporation of the volatiles un-

der reduced pressure and subsequent extraction with Et_2O (40+20 mL) provided a colorless oil that still contained traces of mono- and disubstituted 1,4,7-triazacyclononane (detected by ^{1}H NMR spectroscopy). The oil was dissolved in dry toluene (5.0 mL), powdered KOH (370 mg, 6.59 mmol, 2.54 equiv.) and 1-bromopropane (0.11 mL, 1.21 mmol, 0.47 equiv.) were added and the mixture stirred at r.t. for 2 d. The mixture was filtered and volatiles evaporated under reduced pressure. Extraction of the residue with Et_2O (40 mL) and removal of volatiles under reduced pressure provided **175** (255 mg, 999 μmol, 38%) as a light-yellow oil.

^{1}H NMR (300 MHz, CD_3CN) δ = 2.68 (s, 12H), 2.40 (m, J = 7.3 Hz, 6H), 1.42 (sext, J = 7.3 Hz, 6H), 0.88 (t, J = 7.3 Hz, 9H) ppm.

^{13}C{^{1}H} NMR (75 MHz, CD_3CN): δ = 61.8, 57.1, 22.1, 12.3 ppm.

HR-MS (ESI): calculated *m/z* for $C_{15}H_{34}N_3^+$ ($[M+H]^+$): 256.2752; found: 256.2759.

FTIR (ATR, neat): $\tilde{\nu}$ = 2955, 2930, 2871, 2794, 2763, 1682, 1458, 1360, 1340, 1301, 1269, 1177, 1164, 1144, 1093, 1061, 1037, 1020, 993, 929, 915, 880, 799, 748, 714, 585, 561, 540 cm^{-1}.

Note: **175** had previously been prepared by alkylation of **tacn·3HBr** with $NaBH_4$ and propionic acid and a ^{1}H NMR spectrum in D_2O/DCl has also been reported.[453] Due to the associated risk of adding $NaBH_4$ at elevated temperature to essentially pure propionic acid, the procedure described herein offers a safer alternative.

4.7.13 Synthesis of [(^{H}PNP^{iPr})CuBr] (176)

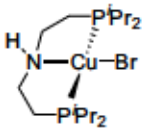

The synthesis of **176** was conducted using a modification of a literature procedure.[370]

To a suspension of [(Me_2S)CuBr] (120 mg, 581 μmol, 1.00 equiv.) in dry THF (10 mL) was added a THF solution of ^{H}PNP^{iPr} (10 wt%, 2.0 mL, 579 mmol, 1.00 equiv.) over 2 min. The reaction mixture was stirred at r.t. for 22 h yielding a colorless solution. Volatiles were removed *in vacuo*, the solid residue extracted with dry toluene (3×5 mL) and the extract concentrated to approx. 4 mL *in vacuo*. Additional dry toluene (4.5 mL) was added and the solution stored at 5 °C overnight and 13 d at –32 °C. The solid precipitate was filtered off *via* cannula at –35 °C and the solid residue extracted with dry THF (5 mL+0.5 mL). Volatiles were removed *in vacuo*, the solid redissolved in a minimum of dry THF, layered with dry hexane and stored at 5 °C for 1 month. Filtration and drying of the colorless crystalline solid provided **176** (155 mg, 346 μmol, 60%). Crystals suitable for X-ray crystallographic analysis were obtained by slow diffusion of dry hexane into a solution of **176** at 5 °C.

^{1}H NMR (300 MHz, C_6D_6): δ = 2.48 (m, 1H), 2.43-2.28 (m, 4H), 1.91-1.73 (m, 4H), 1.35-1.26 (m, 4H), 1.21-1.05 (m, 24H) ppm.

^{13}C{^{1}H} NMR (75 MHz, C_6D_6): δ = 45.3 (t, J = 4.0 Hz), 24.5 (t, J = 7.5 Hz), 24.2 (t, J = 6.9 Hz), 19.9 (t, J = 3.1 Hz), 19.7 (t, J = 3.1 Hz) ppm.

$^{31}P\{^1H\}$ NMR (121 MHz, C_6D_6): δ = 3.1 (br) ppm.
The analytical data is in accordance with the literature data.[370] The crystal structure of **176** reported herein is different from that reported earlier.[370]

4.7.14 Synthesis of [(^{H}PNP^{tBu})CuBr] (177)

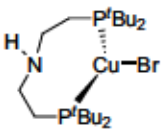

177 was prepared using a modification of a literature procedure for the preparation of **176**.[370]

To a suspension of [(Me_2S)CuBr] (205 mg, 995 µmol, 1.00 equiv.) in dry THF (20 mL) was added a THF solution of ^{H}PNP^{tBu} (10 wt%, 4.0 mL, 1.01 mmol, 1.01 equiv.) over 2 min. The reaction mixture was stirred at r.t. for 19 h and subsequently filtered *via* cannula. After removal of the volatiles *in vacuo*, the solid residue was dissolved in dry THF (21 mL), layered with dry hexane (26 mL) and stored at –32 °C for 6 d followed by storage at –78 °C for 1 d. Filtration *via* cannula and drying *in vacuo* provided **177** (342 mg, 677 µmol, 68%) as colorless crystalline solid. Crystals suitable for single crystal X-ray diffraction were obtained by slow diffusion of dry hexane into a concentrated solution of **177** in dry THF at –32 °C.
^{1}H NMR (300 MHz, C_6D_6): δ = 2.68-2.44 (m, 4H), 1.42-1.32 (m, 4H), 1.28 (d, J = 6.4 Hz, 18H), 1.25 (d, J = 6.4 Hz, 18H) ppm.
$^{13}C\{^1H\}$ NMR (75 MHz, C_6D_6): δ = 44.5 (t, J = 2.6 Hz), 33.6 (t, J = 5.9 Hz), 29.9 (t, J = 3.7 Hz), 19.3 (t, J = 4.2 Hz) ppm.
$^{31}P\{^1H\}$ NMR (121 MHz, C_6D_6): δ = 13.8 (br) ppm.
FTIR (ATR, neat): $\tilde{\nu}$ = 3271, 2979, 2957, 2938, 2894, 2861, 2820, 2796, 2698, 2643, 1469, 1389, 1364, 1357, 1221, 1177, 1132, 1047, 1032, 1019, 1008, 932, 921, 840, 811, 745, 683, 671, 607, 582, 548, 491, 471, 423, 404 cm^{-1}.
Anal. Calcd. C 47.57, H 8.98, N 2.77. **Observed** C 47.50, H 8.903, N 2.778.
Note: The NH proton was not visible in the ^{1}H NMR spectrum due to overlapping with the ^{t}Bu or methylene protons.

4.7.15 Synthesis of [(^{H}PNP^{Cy})CuBr] (178)

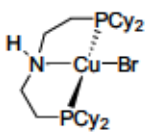

178 was prepared using a modification of a literature procedure for the preparation of **176**.[370]

^{H}PNP^{Cy} (135 mg, 289 µmol, 1.00 equiv.) and [(Me_2S)CuBr] (61.5 mg, 299 µmol, 1.04 equiv.) were suspended in dry THF (5 mL) and stirred at r.t. for 3 h. The reaction mixture was filtered and the solid residue extracted with dry THF (4 mL). Volatiles were removed *in vacuo* yielding a white solid which was dissolved in dry THF (8 mL) and layered with dry hexane (10 mL). Storage at –32 °C for 11 d yielded colorless needles that were filtered off *via* cannula and dried *in vacuo* yielding **178** (146 mg, 240 µmol, 83%). Crystals suitable for X-ray crystallographic analysis were obtained by slow diffusion of dry

hexane (10 mL) into a solution of **178** in dry THF (8 mL) at –32 °C.
^{1}H NMR (400 MHz, CD_2Cl_2): δ = 2.73 (m, 4H), 2.05 (br, 1H), 1.91 (t, J = 13.7 Hz, 8H), 1.84-1.62 (m, 20H), 1.51-1.33 (m, 8H), 1.33-1.19 (m, 12H) ppm.
^{13}C{^{1}H} NMR (101 MHz, CD_2Cl_2): δ = 45.7 (t, J = 3.7 Hz), 34.6 (t, J = 7.2 Hz), 30.3, 30.0, 28.0 (t, J = 5.5 Hz), 27.8 (t, J = 5.4 Hz), 26.8, 23.8 (t, J = 7.4 Hz) ppm.
^{31}P{^{1}H} NMR (162 MHz, CD_2Cl_2): δ = –5.1 (br) ppm.
FTIR (ATR, neat): $\tilde{\nu}$ = 3247, 3223, 2918, 2846, 1445, 1415, 1408, 1363, 1344, 1329, 1292, 1277, 1267, 1231, 1215 1193, 1175, 1102, 1071, 1044, 1003, 914, 886, 852, 821, 763, 744, 714, 658, 554, 459, 440, 426 cm^{-1}.
HR-MS (EI): calculated *m/z* for $C_{28}H_{53}BrCuNP_2^+$ ([M]$^+$): 607.21173; found: 607.21271.
Anal. Calcd. C 55.21, H 8.77, N 2.30. **Observed** C 55.07, H 8.634, N 2.028.

4.7.16 Synthesis of [((^{H}PNP^{Ph})CuBr)$_2$] (179)

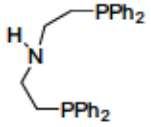

Deprotonation of ^{H}PNP^{Ph}·HCl was conducted following a modification of a literature procedure.[454]

^{H}PNP^{Ph}·HCl (260 mg, 544 μmol, 1.00 equiv.) was suspended in toluene (3.0 mL) and degassed 2.5 M aqueous NaOH (0.54 mL, 1.36 mmol, 2.50 equiv.) was added. The mixture was stirred at r.t. for 2.5 h, the aqueous layer removed *via* syringe and all volatiles removed *in vacuo*. The oily residue was extracted with dry toluene (3.0+1.5 mL). Removal of the volatiles *in vacuo* yielded ^{H}PNP^{Ph} (213 mg, 483 μmol, 89%) as a colorless oil that was utilized without further purification.
^{31}P{^{1}H} NMR (121 MHz, THF-d_8): δ = –20.3 ppm.

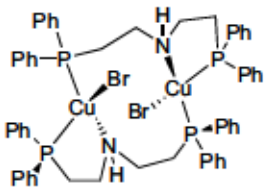

179 was prepared using a modification of a literature procedure for the preparation of **176**.[370]

To [(Me_2S)CuBr] (93.8 mg, 456 μmol, 1.00 equiv.) was added a solution of ^{H}PNP^{Ph} (209 mg, 473 μmol, 1.04 equiv.) in dry THF (6.0 mL). The reaction mixture was stirred at r.t. for 2 h, filtered (cannula) and volatiles were removed *in vacuo*. Dry toluene (15 mL) was added, the suspension filtered *via* cannula and the filtrate stored at –32 °C for 12 d. The formed colorless precipitate was filtered off (cannula) and dried *in vacuo* to provide **179** (183 mg, 313 μmol, 68%). Crystals suitable for X-ray crystallographic analysis were obtained by vapor diffusion of hexane into a solution of **179** in 1,2-dichlorobenzene over several months.
^{1}H NMR (400 MHz, CD_2Cl_2): δ = 7.56 (br, 8H), 7.37 (t, br, J = 7.2 Hz, 4H), 7.28 (m, br, J = 7.2 Hz, 8H), 2.82 (br, 5H), 2.33 (br, 4H) ppm.
^{13}C{^{1}H} NMR (101 MHz, CD_2Cl_2): δ = 134.1, 133.6 (t, J = 7.4 Hz), 130.2, 129.1 (t, J = 4.4 Hz), 44.6, 31.0 ppm.

$^{31}P\{^{1}H\}$ NMR (162 MHz, CD_2Cl_2): δ = –15.7 (br) ppm.
FTIR (ATR, neat): $\tilde{\nu}$ = 3439, 3176, 3069, 3047, 2921, 2851, 1585, 1571, 1481, 1458, 1433, 1408, 1378, 1332, 1307, 1276, 1212, 1184, 1157, 1137, 1095, 1025, 998, 956, 938, 910, 820, 735, 691, 506, 475, 468, 441, 414 cm^{-1}.
HR-MS (EI): calculated *m/z* for $C_{28}H_{29}BrCuNP_2^+$ ($[M]^+$): 583.02491; found: 583.02404.
Anal. Calcd. C 57.49, H 5.00, N 2.39. **Observed** C 57.59, H 5.045, N 2.205.
Note: ^{13}C-^{31}P coupling constants could not be determined for the signals at 134.1, 44.6, and 31.0 ppm due to low intensity of the signals as a result of the poor solubility of **179**.

4.7.17 Synthesis of 1,4,7-Triazacyclononane (180)

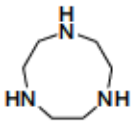

180 was prepared following a modified literature procedure.[325]

To **167** (600 mg, 2.51 mmol, 1.00 equiv.) in H_2O (1.3 mL) was added NaOH (294 mg, 7.35 mmol, 2.92 equiv.). $CHCl_3$ (20 mL) was added and the reaction mixture stirred at r.t. for 2 d. The layers were separated and the aqueous layer extracted with $CHCl_3$ (2×25 mL). The combined organic layers were dried over Na_2SO_4 and evaporated under reduced pressure at 30 °C to yield **180** (294 mg, 2.28 mmol, 90%) as a white solid.
^{1}H NMR (300 MHz, $CDCl_3$) δ = 2.78 (s, 12H), 2.27 (s, 3H) ppm.
The analytical data is in accordance with the literature data.[324]

4.7.18 Synthesis of 1,8-Bis((1,4-diallyl-1,4,7-triazonanyl)methyl)naphthalene (184)

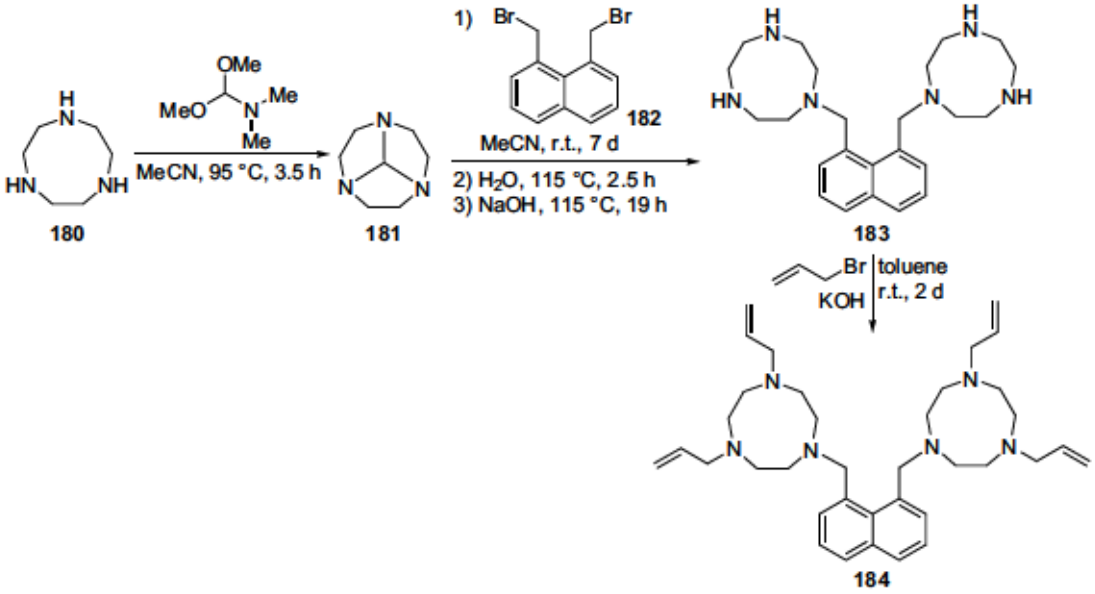

Preparation of tricyclic orthoamide **181** was conducted according to a literature procedure.[296]

To **180** (233 mg, 1.80 mmol, 1.00 equiv.) in dry MeCN (10 mL) was added 1,1-dimethoxydimethylamine (0.30 mL, 2.26 mmol, 1.25 equiv.) and the mixture heated to 95 °C for 3.5 h. The light-yellow solution was allowed to cool to r.t. and volatiles were removed *in vacuo* yielding crude 1,4,7-triazatricyclo[5.2.1.$0^{4,10}$]decane (**181**, 243 mg, 96%) as a yellow oil that was directly utilized in the next step without further purification.
^{1}H NMR (300 MHz, CD_3CN): δ = 4.74 (s, 1H), 2.96-2.82 (m, 6H), 2.80-2.67 (m, 6H) ppm.
^{13}C{^{1}H} NMR (75 MHz, CD_3CN): δ = 105.2, 52.7 ppm.
The analytical data is in accordance with the literature (albeit reported in $CDCl_3$).[296]

Formation of **183** was conducted by combining the literature procedure[297] with a procedure for the alkylation of **181**[296].

To **181** (243 mg, 1.74 mmol, 2.00 equiv.) and 1,8-bis(bromomethyl)naphthalene (273 mg, 869 μmol, 1.00 equiv.) was added dry MeCN (10 mL). The mixture was stirred at r.t. for 7 d giving rise to a beige suspension. The solid was filtered off using a filter cannula (equipped with a glass microfiber filter) and dried *in vacuo*. Degassed H_2O (14 mL) was added and the mixture heated to 115 °C for 2.5 h. NaOH (385 mg, 9.63 mmol, 11.1 equiv.) was added and the light-yellow solution heated to 115 °C for 19 h. The yellow/brown reaction mixture was allowed to cool to r.t. and subsequently extracted with $CHCl_3$ (3×15 mL). Drying of the organic layers over Na_2SO_4 and evaporation of the volatiles under reduced pressure gave crude 1,8-bis((1,4,7-triazonanyl)methyl)naphthalene (**183**, 224 mg, 544 μmol, 62%) as a an off-white foam that was utilized in the next step without further purification.
^{1}H NMR (300 MHz, DMSO-d_6: δ = 7.82 (dd, J = 8.2, 1.2 Hz, 2H), 7.58 (dd, J = 7.1, 1.1 Hz, 2H), 7.39 (dd, J = 8.0, 7.1 Hz, 2H), 4.41 (s, 4H), 2.65 (m, 12H), 2.28 (m, 12H) ppm.
^{13}C{^{1}H} NMR (75 MHz, DMSO-d_6): δ = 137.0, 135.9, 132.7, 130.8, 129.6, 125.1, 63.2, 54.2, 48.2, 47.8 ppm.
The analytical data is in accordance with the literature (albeit the NMR spectra were reported in $CDCl_3$).[297]

To crude **183** (224 mg, 544 μmol, 1.00 equiv.) was added powdered KOH (167 mg, 2.97 mmol, 5.47 equiv.) and dry toluene (10 mL). Allyl bromide (0.19 mL, 2.20 mmol, 4.04 equiv.) was added and the mixture stirred at r.t. for 2 d. The beige suspension was filtered and all volatiles evaporated under reduced pressure. The resulting beige sticky solid was extracted with Et_2O (60 mL) using a filter cannula. Column chromatography (SiO_2, DCM/NEt_3/MeOH 300:10:0→300:10:3) and subsequent extraction with benzene (3×2 mL) provided **184** as a yellow oil (68.7 mg, 120 μmol, 13% over 3 steps)
^{1}H NMR (300 MHz, C_6D_6): δ = 7.64 (dd, J = 8.1, 1.2 Hz, 2H), 7.49 (dd, J = 7.0, 1.2 Hz, 2H), 7.24 (dd, J = 8.1, 7.0 Hz, 2H), 5.84 (ddt, J = 16.5, 10.2, 6.3 Hz, 4H), 5.08-4.93 (m, 8H), 4.56 (s, 4H), 2.92 (d, J = 6.3 Hz, 8H), 2.88-2.78 (m, 8H), 2.62 (s, 8H), 2.60-2.49 (m, 8H) ppm.
^{13}C{^{1}H} NMR (75 MHz, C_6D_6): δ = 138.0, 137.8, 136.6, 133.5, 131.4, 129.7, 124.8, 116.3, 65.5, 62.1, 56.6, 56.0, 55.4 ppm.

HR-MS (ESI): calculated *m/z* for $C_{36}H_{55}N_6^+$ ([M+H]$^+$): 571.4488; found: 571.4489.
FTIR (ATR, neat): $\tilde{\nu}$ = 3072, 3039, 3003, 2972, 2917, 2871, 2832, 2793, 1663, 1642, 1608, 1508, 1454, 1438, 1417, 1351, 1301, 1261, 1123, 1090, 1032, 993, 916, 871, 841, 814, 778, 631, 499 cm^{-1}.

4.7.19 Synthesis of [Cu_2(184)I_2] (185)

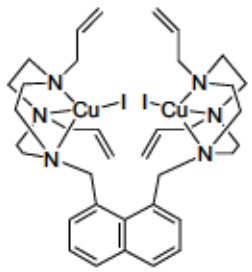

To CuI (28.2 mg, 148 µmol, 2.00 equiv.) was added **184** (42.2 mg, 73.9 µmol, 1.00 equiv.) in dry THF (3.0 mL). The resulting mixture was stirred at r.t. for 1 h, filtered *via* filter cannula and volatiles were removed *in vacuo* yielding a white to yellow solid. The solid was washed with dry THF (0.5 mL), subsequently dissolved in boiling, dry THF (3.5 mL) and left standing at r.t. yielding colorless to slightly yellow crystals. The mother liquor was filtered off *via* cannula and the crystalline solid extracted into boiling THF (2×2 mL) using a filter cannula. Addition of dry hexane (5.0 mL) to the THF extract caused the formation of a precipitate which was filtered off *via* cannula and dried *in vacuo* to give **185** (17.0 mg, 17.9 µmol, 24%) as a slightly yellow solid. Crystals suitable for X-ray crystallographic analysis were obtained by dissolving **185** in boiling, dry THF (5.0 mL) and allowing it to slowly cool to room temperature.
^{1}H NMR (400 MHz, CD_2Cl_2): δ = 8.34 (dd, *J* = 7.2, 0.9 Hz, 2H), 7.84 (dd, *J* = 8.2, 1.2 Hz, 2H), 7.48 (dd, *J* = 8.1, 7.2 Hz, 2H), 6.55-6.37 (m, 4H), 5.24-5.20 (m, 4H), 5.19 (s, br, 4H), 4.81 (s, 4H), 3.44-3.28 (m, 8H), 2.84-2.73 (m, 4H), 2.73-2.62 (m, 4H), 2.55-2.41 (m, 12H), 2.40-2.29 (m, 4H) ppm.
^{13}C{^{1}H} NMR (101 MHz, CD_2Cl_2): δ = 136.1, 135.8, 134.6, 134.2, 132.1, 130.7, 125.2, 119.6, 64.7, 63.7, 53.3, 53.1, 52.2 ppm.
MS (ESI): calculated *m/z* for $C_{36}H_{54}{}^{63}Cu^{65}CuI_2N_6^+$ ([M]$^+$): 952.1073; found: 952;
calculated *m/z* for $C_{36}H_{54}{}^{63}Cu^{65}CuIN_6^+$ ([M-I]$^+$): 823.2041; found: 823.
FTIR (ATR, neat): $\tilde{\nu}$ = 3053, 3038, 2997, 2978, 2906, 2875, 2846, 2824, 1687, 1640, 1603, 1578, 1481, 1453, 1420, 1367, 1335, 1296, 1262, 1166, 1147, 1097, 1068, 1029, 994, 923, 884, 840, 823, 809, 774, 749, 733, 704, 647, 611, 591, 555, 462, 435, 409 cm^{-1}.

4.7.20 General Procedure for the Removal of Potentially Formed CO_2 Reduction Products by NaOH Treatment

The general procedure for NaOH treatment with the aim of removal of potentially formed oxalate was adapted from a literature procedure.[193]

To the solid residue obtained after treatment of the respective Cu complex and the corresponding additives with CO_2 and subsequent removal of all volatiles *in vacuo* was added aqueous 1 M NaOH solution (excess, 11-16 equiv.) and toluene (twice the NaOH volume). The mixture was sonicated for ∼1 min and stirred overnight. If possible, layers were sep-

arated and the aqueous layer was evaporated under reduced pressure. In case no clear phase boundaries were visible, the entire reaction mixture was evaporated under reduced pressure. If stated, the resulting residue was extracted with DCM and air-dried afterwards. D_2O (0.6-0.8 mL) was added to the residue and a sample (0.02-0.10 mL) taken for analysis *via* capillary electrophoresis. The remaining sample was analyzed by ^1H and $^{13}C\{^1H\}$ NMR spectroscopy.

4.7.21 General Procedure for the Removal of Oxalate from [(127)Cu(μ-C_2O_4)Cu(127)]$(BF_4)_2$ (172) by NaOH Treatment

To **172** (21.3 mg, 24.0 μmol, 1.00 equiv.) was added 1 M aqueous NaOH (0.55 mL, 550 μmol, 11.5 equiv. based on Cu) and toluene (1.10 mL). The mixture was sonicated for ∼1 min and stirred at r.t. for 15 h. Layers were separated, the aqueous layer evaporated under reduced pressure and the resulting black/partially blue solid dried *in vacuo*. D_2O (0.60 mL) was added, a sample (0.04 mL) taken for capillary electrophoresis, and the mixture analyzed by ^1H and $^{13}C\{^1H\}$ NMR spectroscopy. Determination of the amount of oxalate by CE gave rise to an oxalate yield of 48% (average of two reactions) and defined the detection limit of oxalate by ^{13}C NMR spectroscopy (barely detectable for one of the two reactions). The yield assessed by this procedure was utilized as a factor (i.e. efficiency of the NaOH extraction) for calculation of oxalate yields by CE for reactions described within this section (4.7).

4.7.22 General Procedure A for Treatment of *In situ* Formed [Cu(NNN)]X with CO_2

To the Cu salt and any solid additives under a CO_2 atmosphere was added the *NNN* ligand in degassed MeOH (total volume as stated in section 4.7.28). The flask was sealed under a constant CO_2 atmosphere (1-1.5 atm) and stirred for the indicated time (see section 4.7.28). All volatiles were removed *in vacuo*, the obtained residue analyzed by FTIR spectroscopy and subsequently subjected to NaOH treatment according to the general procedure (4.7.20).

4.7.23 General Procedure B for Treatment of *In situ* Formed [Cu(NNN)]X with CO_2

To a suspension of the Cu salt and the solid additives in MeOH was added the *NNN* ligand in degassed MeOH (total volume as stated in the Tables in section 4.7.28). The resulting mixture was stirred at r.t. for 15 to 60 min and subsequently filtered *via* cannula fitted with a glass microfiber filter into another Schlenk flask that has been prepared under a CO_2 atmosphere. The flask was sealed under constant CO_2 atmosphere (1-1.5 atm) and stirred for the indicated time (see section 4.7.28). After the indicated reaction time, all volatiles were removed *in vacuo*. The resulting solid residue was analyzed by FTIR spectroscopy and where indicated subjected to removal of potentially formed oxalate *via* treatment with NaOH according to the general procedure for removal of oxalate (4.7.20).

4.7.24 General Procedure C for Treatment of *In situ* Formed [Cu(NNN)]X with CO_2

The procedure for CO_2 treatment by bubbling was adapted from the initial literature procedure.[192]

To a suspension of the Cu salt and the additives in degassed MeOH under Ar was added the *NNN* ligand in MeOH (total volume as stated in the Table S 13). The mixture was stirred at r.t. for 15 to 45 min after which CO_2 was bubbled through the suspension for the indicated time (see Table S 13) using a needle reaching into the suspension. After the reaction time, volatiles were removed *in vacuo* and the solid residue subjected to FTIR analysis and subsequent removal of potentially formed CO_2 reduction products according to the general procedure (4.7.20).

4.7.25 General Procedure D for Treatment of *In situ* Formed [Cu(NNN)]X with CO_2

To a suspension of the Cu salt and potential additives in degassed MeOH under Ar was added the *NNN* ligand in MeOH (total volume as stated in the Table S 13). The mixture was stirred at r.t. for 15 to 45 min after which CO_2 was bubbled through the suspension for the indicated time (see Table S 13) using a needle reaching into the suspension. The reaction mixture was sealed under an Ar overpressure after the CO_2 bubbling has been stopped and stirring was continued for the time stated. These two steps were repeated for the number of times stated in Table S 13. After the last CO_2 bubbling, volatiles were removed *in vacuo* and the solid residue subjected to FTIR analysis and subsequent removal of potentially formed CO_2 reduction products according to the general procedure (4.7.20).

4.7.26 General Procedure for the Treatment of *In situ* Formed [Cu(NNN)]X with $CsHCO_3$

Reactions with $CsHCO_3$ were performed *via* a modified literature protocol.[192]
To a suspension of the utilized Cu precursor and potential additives in degassed MeOH was added the *NNN* ligand (1.00 equiv.) in degassed MeOH (total volume as indicted in Table S 14) and the resulting mixture stirred at r.t. for 25 to 40 min. The reaction mixture was then transferred onto $CsHCO_3$ (1.05-2.05 equiv. based on the ligand), the flask sealed under Ar and stirred at r.t. for the indicated time (see Table S 14). Volatiles were removed *in vacuo*, the residue analyzed by FTIR spectroscopy and subsequently subjected to NaOH treatment for the removal of potentially formed CO_2 reduction products according to the general procedure (4.7.20).

4.7.27 General Procedure for Air Treatment of *In situ* Formed [Cu(NNN)]X

Air exposure was performed *via* a modified literature procedure.[192]
To a suspension of CuI and the additives in MeOH under Ar was added the *NNN* ligand in MeOH (total volume indicated in Table S 17). The resulting mixture was stirred at r.t. for 10 to 40 min after which it was transferred into a vial in air. Exhaled air was bubbled through the reaction mixture for ~15 s and the resulting suspension left to evaporate in air over the stated time period (see Table S 17). The obtained residue was analyzed by FTIR spectroscopy and subjected to NaOH treatment for the removal of potentially formed CO_2 reduction products according to the general procedure (4.7.20).

4.7.28 1,4,7-Tacn-ligated Cu Complexes in CO_2 Reduction - Results

Table S 13: Results for the attempted CO_2 reductive coupling by CO_2 bubbling utilizing *in situ* formed 1,4,7-tacn-ligated Cu complexes.

Entry	Proc.	[Cu] ([µmol])	Ligand ([µmol])	Additives ([µmol])	Solv. ([mL])	*t* [h]	FTIR $\tilde{\nu}$ [cm^{-1}]‡	^{13}C NMR δ [ppm] ($C_2O_4^{2-}$/HCO_2^-/CO_3^{2-})	CE ($C_2O_4^{2-}$) approx. yield [%]†
1[a]	C	CuI (502)	**127** (502)	$NaBPh_4$ (502)	MeOH (20)	11	1628	n.d.	n.d.
2[b,c]	D	CuI (393)	**127** (230)	$NaBPh_4$ (299)	MeOH (9.3)	2 + 2 + 2	1628	x/x/168.4	n.d.
3[b,d]	D	CuI (414)	**127** (242)	$NaBPh_4$ (316)	MeOH (9.8)	2.5 + 2 + 2.5 + 1.5 + 3 + 2.5	1628, 1617	x/x/168.4	<0.5 [<0.5]
4	C	CuI (120)	**127** (120)	$NaBPh_4$ (120)	MeOH (3.6)	12.5	1617	x/x/168.3	2 [1]
5[e]	D	CuI (120)	**127** (120)	$NaBPh_4$ (120)	MeOH (3.6)	1 + 1 + 3	1639, 1622, 1609	x/x/168.4	1 [1]
6[f]	D	CuI (110)	**127** (110)	$NaBPh_4$ (110)	MeOH (3.3)	2 + 2	1623	x/x/168.4	2 [1]
7[b,g]	D	CuI (391)	**127** (229)	$NaPF_6$ (344)	MeOH (9.3)	4 + 2	1642	x/171.2/168.4	<0.5 [<0.5]
8[b,h]	D	CuI (323)	**127** (189)	$NaBPh_4$ (246)	MeOH (7.6), THF (2.0)	4 + 2	1628	x/x/168.4	<0.5 [<0.5]

Reactions were conducted according to the general procedures C (4.7.24) and D (4.7.25) unless stated otherwise. n.d. = not determined; x = not observed. ‡Relevant vibrations in the 1700-1600 cm^{-1} region are reported (IR spectra are presented in section 4.13.4). †Note that approximate oxalate yields determined by CE are stated for signals coinciding with the signal of internal standard ($Na_2C_2O_4$) added to the samples after a first CE measurement and might be a result of other impurities as evident from blank experiments with e.g. dien (Table S 18, entry 10). Approximate oxalate yields stated in [] were calculated without taking into account the 48% efficiency of the NaOH treatment procedure assessed by procedure 4.7.21. [a]Reaction mixture was stirred under Ar for 2 h after complete bubbling and filtered in air. After FTIR analysis, unsuccessful recrystallization from $MeNO_2$ was attempted. [b]Residue after NaOH treatment was extracted with DCM. [c]The reaction mixture was filtered after 40 min under Ar prior to CO_2 bubbling. In between the CO_2 bubbling steps, the reaction mixture was stirred under Ar (19 h, 24 h) during which a decolorization from blue to slightly yellow was observed. The suspension was filtered after the first CO_2 bubbling step (after 13 h under Ar) and the solid residue analyzed by NMR spectroscopy (in D_2O and THF-d_8, respectively). Compound **169** crystallized from the THF-d_8 NMR solution. [d]Filtered after 45 min under Ar. Stirred under Ar (for 47 h, 14 h, 27 h, 44 h, 90 h) in between CO_2 bubbling steps (partial decolorization of the blue reaction mixture observable). Filtered after the first stirring under Ar (after 47 h). The slightly blue/white solid residue was analyzed by NMR spectroscopy in THF-d_8/D_2O (0.6/0.7 mL). Solvent entirely evaporated during the last CO_2 bubbling step. [e]The reaction mixture was stirred under Ar for (24 h, 21 h) in between CO_2 bubbling. A decolorization of the blue suspension was observed during the first stirring under Ar. No color change to blue was observed during the second CO_2 bubbling step. Samples of the reaction mixture (0.10 mL and 0.09 mL) were taken before and after the third CO_2 bubbling step and analyzed by UV/Vis spectroscopy (diluted with 1.4 mL and 1.5 mL MeOH, respectively). [f]The reaction mixture was stirred under Ar for 19 h in between CO_2 bubbling. A decolorization of the blue/green suspension was observed during stirring under Ar. The color changed again to blue/green during the second CO_2 bubbling step. Samples of the reaction mixture were taken prior to CO_2 bubbling (0.02 mL and 0.01 mL, diluted with 2.0 mL MeOH) and after CO_2 bubbling (0.10 mL and 0.09 mL, diluted with 1.9 mL MeOH) and analyzed by UV/Vis spectroscopy. [g]Filtered after 35 min under Ar. Stirred under Ar for 19 h in between CO_2 bubbling steps. During this time, the color of the solution remained blue/green. [h]Filtered after 35 min under Ar. Dry THF (2.0 mL) was added after filtration. Stirred for 48 h under Ar after CO_2 bubbling without decolorization of the blue solution.

Figure S 3: Repeatable color change upon CO_2 bubbling through a solution of CuI, **127**, and $NaBPh_4$ (1.7/1/1.3) in MeOH followed by stirring under Ar resulting in (partial) decolorization (Table S 13, entry 3).

Table S 14: Results for the attempted CO_2 reductive coupling utilizing **127**-ligated Cu complexes in combination with solid bicarbonates.

Entry	[Cu] ([μmol])	$MHCO_3$ ([μmol])	Additives ([μmol])	Solv. ([mL])	*t* [h]	FTIR $\tilde{\nu}$ [cm^{-1}]‡	^{13}C NMR δ [ppm] ($C_2O_4^{2-}$/HCO_2^-/CO_3^{2-})	CE ($C_2O_4^{2-}$) approx. yield [%]†
1[a]	CuI (210)	$CsHCO_3$ (271)	$NaBPh_4$ (210)	MeOH (29)	48	n.d.	n.d.	n.d.
2[b]	CuI (126)	$CsHCO_3$ (133)	$NaBPh_4$ (126)	MeOH (5.0)	16	1628, 1617	x/x/168.4	<1 [<0.5]
3[c]	CuI (120)	$CsHCO_3$ (126)	$NaBPh_4$ (120)	MeOH (4.0)	117	1628, 1617	x/x/168.4	<1 [<0.5]
4[d,e]	CuI (203)	$CsHCO_3$ (226)	$NaBPh_4$ (203)	MeOH (8.2), H_2O (0.5)	71	1629	x/171.3/168.4	n.d.
5[f]	CuI (150)	$CsHCO_3$ (300)	$NaPF_6$ (187)	MeOH (4.4)	168	1640	x/x/168.3	<0.5 [<0.5]
6[g]	CuI (126)	$CsHCO_3$ (134)	-	MeOH (5.0)	16.5	1661, 1644	x/x/168.3	11 [5][i]
7[d,h]	CuI (296)	$NaHCO_3$ (214)	$NaBPh_4$ (226)	MeOH (7.0)	210	1625	x/x/168.4	<1 [<0.5]
8[c]	$[Cu(MeCN)_4]PF_6$ (120)	$CsHCO_3$ (127)	-	MeOH (4.0)	118	1659	x/x/168.3	<0.5 [<0.5]
9[c]	$[Cu(MeCN)_4]PF_6$ (120)	$NaHCO_3$ (127)	-	MeOH (4.0)	118	1629	x/x/168.3	<1 [<0.5]

Reactions conducted following procedure 4.7.26 unless stated otherwise. n.d. = not determined; x = not observed. ‡Relevant vibrations in the 1700-1600 cm^{-1} region are reported (IR spectra are presented in section 4.13.4). †Note that approximate oxalate yields determined by CE are stated for signals coinciding with the signal of internal standard ($Na_2C_2O_4$) added to the samples after a first CE measurement and might be a result of other impurities as evident from blank experiments with e.g. dien (Table S 18, entry 10). Approximate oxalate yields stated in [] were calculated without taking into account the 48% efficiency of the NaOH treatment procedure assessed by procedure 4.7.21. [a]The mixture was filtered *via* cannula after the reaction time. Column chromatographic separation (SiO_2, MeOH/$MeNO_2$/2 M NH_4Cl 7:1:2), subsequent extraction of the green solid with $MeNO_2$ and recrystallization from hot $MeNO_2$ yielded [Cu(**127**)Cl_2] (**173**) as evidenced by X-ray crystallographic and elemental analysis. [b]The slightly blue mixture obtained after reaction was filtered *via* cannula and the solid obtained after removal of all volatiles *in vacuo* analyzed by FTIR and NMR (in CD_3OD) spectroscopy prior to NaOH treatment. [c]The headspace of the reaction (5 mL) was analyzed by GC prior to removal of all volatiles *in vacuo*. No gaseous CO_2 reduction products (CO, CH_4) have been detected. [d]The residue obtained after NaOH treatment was extracted with DCM. [e]$CsHCO_3$ in MeOH (4.2 mL) was added to CuI, $NaBPh_4$, and **127** in MeOH (4.0 mL). Degassed H_2O (0.5 mL) was added after 6.5 h. The mixture was filtered after the reaction time *via* cannula. [f]The mixture was filtered onto $CsHCO_3$ *via* cannula. [g]The solid obtained after removal of all volatiles *in vacuo* was analyzed by FTIR and NMR (in CD_3OD) spectroscopy prior to NaOH treatment. [h]**127** (0.59 equiv.) was utilized. The mixture was filtered onto $NaHCO_3$ *via* cannula. [i]Potential oxalate signal overlapping with another broad signal complicating integration (Figure S 357).

Table S 15: Results for the attempted CO_2 reductive coupling by CO_2 treatment of *in situ* formed Cu complexes: variation of parameters.

Entry	Proc.	[Cu] ([μmol])	Ligand ([μmol])	Additives ([μmol])	Solv. ([mL])	*t* [h]	FTIR $\tilde{\nu}$ [cm^{-1}]‡	^{13}C NMR δ [ppm] ($C_2O_4^{2-}$/HCO_2^-/CO_3^{2-})	CE ($C_2O_4^{2-}$) approx. yield [%]†
1[a]	A	CuI (120)	**127** (120)	$NaBPh_4$ (120)	MeOH (3.6)	24	1620	x/x/168.4	<1 [<0.5]
2[a]	A	CuI (120)	**127** (120)	$NaBPh_4$ (120)	MeOH (3.6)	118	1641	x/x/168.4	<0.5 [<0.5]
3[a]	A	CuI (120)	**127** (120)	$NaBPh_4$ (120)	MeOH (3.6), THF (0.4)	118	1641	x/x/168.4	<0.5 [<0.5]
4[b,c]	B	CuI (330)	**127** (194)	$NaBPh_4$ (252)	MeOH (9.0), THF (3.0)	354	1629	x/x/168.4	n.d.
5[a]	A	CuI (124)	**127** (125)	$NaBPh_4$ (125)	THF (3.8)	120	1641, 1621, 1609	x/x/x[h]	<0.5 [<0.5]
6[d]	A	CuI (141)	**127** (142)	$NaBPh_4$ (193)	THF (4.0)	644	1654, 1644, 1620, 1601	x/x/x[h]	1 [<0.5]
7	A	CuI (123)	**127** (124)	$NaBPh_4$ (124)	PhMe (5.0)	121	1638, 1620	x/x/168.3	<1 [<0.5]
8[a,e]	A	CuI (120)	**127** (120)	$NaBPh_4$ (120)	MeOH (3.6)	114	1643	x/x/168.4	3 [1]
9[f]	A	CuI (206)	**127** (121)	$NaBPh_4$ (158)	MeOH (4.9)	165	1641, 1628	x/171.2/168.4	<0.5 [<0.5]
10[g]	A	CuI (133)	**127** (133)	$NaBPh_4$ (135)	MeOH (5.0)	18	1635, 1622, 1608	x/x/168.4	<0.5 [<0.5]

Reaction conditions as described in the general procedures A (4.7.22) and B (4.7.23) unless stated otherwise. n.d. = not determined; x = not observed. ‡Relevant vibrations in the 1700-1600 cm^{-1} region are reported (IR spectra are presented in section 4.13.4). †Note that approximate oxalate yields determined by CE are stated for signals coinciding with the signal of internal standard ($Na_2C_2O_4$) added to the samples after a first CE measurement and might be a result of other impurities as evident from blank experiments with e.g. dien (Table S 18, entry 10). Approximate oxalate yields stated in [] were calculated without taking into account the 48% efficiency of the NaOH treatment procedure assessed by procedure 4.7.21. [a]The headspace of the reaction (5 mL) was analyzed by GC prior to removal of all volatiles *in vacuo*. No gaseous CO_2 reduction products (CO, CH_4) have been detected. [b]Residue after NaOH treatment extracted with DCM. [c]Conducted in a 250 mL Schlenk flask. Filtered after 30 min under Ar. CO_2 was bubbled through the solution for 30 min after which the reaction mixture was sealed under CO_2 atmosphere and stirred for 186 h. Dry THF (3 mL) was then added under CO_2 overpressure and stirring continued for 7 d. CO_2 was bubbled through the solution for 5.5 h prior to removal of volatiles *in vacuo*. [d]CO_2 was bubbled through the yellow solution for 26 min after stirring under CO_2 atmosphere for 27 d and prior to removal of all volatiles *in vacuo*. [e]Reaction conducted at 40 °C. [f]Reaction conducted at 35 °C. [g]Reaction illuminated at 400-700 nm (0.09 W) using a Lumatex Superlite (Hg lamp). [h]Broadened ^1H NMR possibly due to residual paramagnetic Cu^{2+}, hence ^{13}C NMR signals might not be observable due to residual paramagnetic species.

Table S 16: Results for the attempted CO_2 reductive coupling by CO_2 treatment of *in situ* formed Cu complexes in the presence of different additives.

Entry	[Cu] ([μmol])	Ligand ([μmol])	Additives ([μmol])	Solv. ([mL])	*t* [h]	FTIR $\tilde{\nu}$ [cm^{-1}]‡	^{13}C NMR δ [ppm] ($C_2O_4^{2-}$/HCO_2^-/CO_3^{2-})	CE ($C_2O_4^{2-}$) approx. yield [%]†
1[a]	CuI (120)	**127** (120)	KPF_6 (122)	MeOH (3.6)	119	1643	x/x/x[f]	<0.5 [<0.5]
2[b,c]	CuI (129)	**127** (129)	$AgBPh_4$ (129)	MeOH (5.0)	115	1665, 1641, 1611	x/171.2/168.5	2 [<1]
3[a]	$[Cu(MeCN)_4]PF_6$ (120)	**127** (120)	-	MeOH (3.6)	119	1639	x/x/x[f]	<1 [<0.5]
4	$[Cu(MeCN)_4]PF_6$ (123)	**127** (124)	-	MeOH (5.0)	166	1639	x/x/x[f]	<1 [<0.5]
5[b]	$[Cu(MeCN)_4]PF_6$ (127)	**127** (127)	$NaBPh_4$ (165)	MeOH (5.2)	119	1631	x/x/x	<1 [<0.5]
6[b]	$[Cu(MeCN)_4]PF_6$ (124)	**127** (125)	NaO_2CH (373)	MeOH (5.0)	114	1618	x/171.2/x	1 [<1]
7[b]	$[Cu(MeCN)_4]PF_6$ (123)	**127** (123)	$Mg(OTf)_2$ (247)	MeOH (5.0)	117	1649	x/x/168.5	<0.5 [<0.5]
8[b]	$[Cu(MeCN)_4]PF_6$ (130)	**127** (130)	$LiBF_4$ (160)	MeOH (5.2)	162	1638	x/x/x	<1 [<0.5]
9[b]	$[Cu(MeCN)_4]PF_6$ (124)	**127** (125)	$LiBF_4$ (277), NaO_2CH (373)	MeOH (5.0)	113	1624, 1598	x/171.2/x	<0.5 [<0.5]
10[b]	$[Cu(MeCN)_4]PF_6$ (123)	**127** (123)	Na_2SO_3 (304)	MeOH (5.0)	116	1637	x/x/168.3	n.d.[g]
11[d]	CuI (133)	**127** (133)	$NaBPh_4$ (134), $NaC_{10}H_8$ (137)	THF (5.0)	121	1579	x/x/168.4	4 [2]
12[d]	CuI (135)	**127** (135)	$NaBPh_4$ (135), $NaC_{10}H_8$ (137)	THF (5.0)	116	1579	x/x/x[f]	5 [2]
13[b,d]	CuI (129)	**127** (129)	$NaBPh_4$ (130), $NaC_{10}H_8$ (137)	THF (5.0)	118	1618, 1579	x/x/168.4	7 [3]
14[b,d]	CuI (124)	**127** (124)	$NaBPh_4$ (124), $NaC_{10}H_8$ (135)	THF (5.0)	23	1579	x/x/x	1 [<1]

15[e]	-	-	$NaC_{10}H_8$ (143)	THF (5.0)	116	1568	172.9/x/168.3	6 [3]
16[e]	-	-	$NaC_{10}H_8$ (142)	THF (5.0)	116	1568	x/x/168.3	7 [3]
17[b,e]	-	-	$NaC_{10}H_8$ (139)	THF (5.0)	24	1572	173.0/x/168.4	2 [1]

Reaction conditions as described in the general procedure A (4.7.22) unless stated otherwise. n.d. = not determined; x = not observed. [‡]Relevant vibrations in the 1700-1500 cm^{-1} region are reported (IR spectra are presented in section 4.13.4). [†]Note that approximate oxalate yields determined by CE are stated for signals coinciding with the signal of internal standard ($Na_2C_2O_4$) added to the samples after a first CE measurement and might be a result of other impurities as evident from blank experiments with e.g. dien (Table S 18, entry 10). Approximate oxalate yields stated in [] were calculated without taking into account the 48% efficiency of the NaOH treatment procedure assessed by procedure 4.7.21. [a]The headspace of the reaction (5 mL) was analyzed by GC prior to removal of all volatiles *in vacuo*. No gaseous CO_2 reduction products (CO, CH_4) have been detected. [b]Residue after NaOH treatment extracted with DCM. [c]To *in situ* prepared [Cu(**127**)I] in dry THF (2 mL) was added a suspension of $AgBPh_4$ in dry THF (8 mL). After stirring at r.t. under exclusion of light for 15 min, the suspension was filtered *via* cannula, volatiles removed *in vacuo* and the atmosphere exchanged for CO_2. Degassed MeOH (5 mL) was then added and general procedure 4.7.22 followed. Note that ^{13}C NMR signals depicted a poor signal-to-noise ratio. [d]Freshly prepared $NaC_{10}H_8$ in dry THF (1.0 mL) was added to CuI, $NaBPh_4$, and **127** in dry THF (4.0 mL) under CO_2 atmosphere. Additional ^{13}C NMR signals possibly indictating the presence of carboxylic acid derivatives at 182, 177 ppm were observed (not for entry 12). [e]Freshly prepared $NaC_{10}H_8$ in dry THF (1.0 mL) was added to dry THF (4.0 mL) under CO_2 atmosphere. Additional ^{13}C NMR signals possibly indictating the presence of carboxylic acid derivatives at 182, 177 ppm (entry 15-17) and with poor signal-to-noise ratio at 173 ppm (entry 15 and 17, see Figure S 123) were observed. [f]Broadened ^1H NMR possibly due to residual paramagnetic Cu^{2+}, hence ^{13}C NMR signals might not be observable due to residual paramagnetic species. [g]Due to the overlapping of the sulfite signal (assessed with a Na_2SO_3 solution) and a potential oxalate signal, oxalate identification/quantification was not possible by CE.

Table S 17: Treatment of *in situ* formed **127**-ligated Cu complexes with air.

Entry	[Cu] ([μmol])	127 ([μmol])	Additives ([μmol])	Solv. ([mL])	*t* [days]	FTIR $\tilde{\nu}$ [cm^{-1}][‡]	^{13}C NMR δ [ppm] ($C_2O_4^{2-}$/HCO_2^-/CO_3^{2-})	CE ($C_2O_4^{2-}$) approx. yield [%][†]
1	CuI (134)	134	$NaBPh_4$ (134)	MeOH (4.0)	41	1638, 1619	x/x/168.4	1 [<1]
2[a]	CuI (126)	126	$NaBPh_4$ (127)	MeOH (5.0)	7	1653, 1638, 1618	x/171.1/168.4	<1 [<0.5]
3[b]	CuI (123)	124	$NaBPh_4$ (124)	MeOH (1.0), EtOH (4.0)	1	1645	x/x/168.4	1 [<1]
4[c]	CuI (120)	121	$NaBPh_4$ (120)	MeOH (3.6)	3	1619	x/x/x	<0.5 [<0.5]
5[d]	CuI (126)	126	-	MeOH (5.0)	8	1654	x[e]/171.2/168.4	7 [4][f]

Reactions were conducted according to general procedure 4.7.27 unless stated otherwise. x = not observed. [‡]Relevant vibrations in the 1700-1600 cm^{-1} region are reported (IR spectra are presented in section 4.13.4). [†]Note that approximate oxalate yields determined by CE are stated for signals coinciding with the signal of internal standard ($Na_2C_2O_4$) added to the samples after a first CE measurement and might be a result of other impurities as evident from blank experiments with e.g. dien (Table S 18, entry 10). Approximate oxalate yields stated in [] were calculated without taking into account the 48% efficiency of the NaOH treatment procedure assessed by procedure 4.7.21. [a]After 7 d in air, the solid residue was extracted with hot $MeNO_2$ (1 mL) and the solution stored at 5 °C for 6 d causing formation of a green crystalline solid. The mother liquor was evaporated the solid residue as well as the crystalline solid were analyzed by FTIR spectroscopy and treated with NaOH according to procedure 4.7.20. [b]To CuI and $NaBPh_4$ in dry EtOH was added **127** in MeOH. [c]A sample (0.10 mL) of the colorless suspension obtained after 30 min under Ar was analyzed by UV/Vis spectroscopy (diluted to 1.7 mM in MeOH). The flask was then purged with O_2 using a balloon causing a rapid color change to green accompanied by precipitation of a green solid. The flask was sealed under O_2 atmosphere and stirred at r.t. for 90 min, after which a sample (0.10 mL) was taken and analyzed by UV/Vis spectroscopy (diluted to approx. 1.7 mM in MeOH). Stirring was continued for 3 d under O_2/Ar atmosphere. The headspace (5 mL) of the reaction was then analyzed by GC (traces of CO were detected - Figure S 335). [d]The residue obtained after NaOH treatment was extracted with DCM. [e]At 173.0 ppm, a signal might be observable (Figures S 122 & S 162). However, the poor signal-to-noise ratio precludes its assignment as a peak. [f]Broadening and apparent overlapping with another signal (Figure S 391) compromise its integration.

Table S 18: Results for the attempted CO_2 reductive coupling by CO_2 treatment of *in situ* formed Cu complexes with different ligands.

Entry	Proc.	[Cu] ([µmol])	Ligand ([µmol])	Additives ([µmol])	Solv. ([mL])	*t* [h]	FTIR $\tilde{\nu}$ [cm^{-1}]‡	^{13}C NMR δ [ppm] ($C_2O_4^{2-}$/HCO_2^-/CO_3^{2-})	CE ($C_2O_4^{2-}$) approx. yield [%]†
1[a]	A	CuI (123)	**174** (123)	$NaBPh_4$ (123)	MeOH (3.7)	120	1629	x/x/168.4	0.5 [<0.5]
2	B	CuI (154)	**174** (91)	$NaBPh_4$ (117)	MeOH (3.7)	238	1630	x/x/168.4	1 [<1]
3[a]	A	CuI (124)	**175** (124)	$NaBPh_4$ (124)	MeOH (3.8)	120	1656, 1633	x/x/168.4	<0.5 [<0.5]
4[b]	B	CuI (200)	**175** (117)	$NaBPh_4$ (153)	MeOH (4.9)	238	1654, 1630	x/171.1/168.4	<0.5 [<0.5]
5[a]	A	CuI (120)	**166** (120)	$NaBPh_4$ (120)	MeOH (5.5)	119	1629	x/x/168.4	3 [1][e]
6[a]	A	CuI (151)	**dpa** (151)	$NaBPh_4$ (150)	MeOH (4.6)	120	1619, 1600	x/x/x[d]	2 [1]
7[a]	A	CuI (184)	**dien** (184)	$NaBPh_4$ (184)	MeOH (5.5)	119	1648 (br), 1578	x/x/168.0[d]	28 [13][f]
8	A	CuI (189)	**dien** (189)	$NaBPh_4$ (189)	MeOH (5.6)	116	1647 (br), 1584	x/x/168.8	27 [13][f]
9	A	CuI (409)	**dien** (409)	$NaBPh_4$ (409)	MeOH (12.5)	119	1655 (br), 1576	x/x/168.4	10 [5][f]
10[c]	A	CuI (180)	**dien** (180)	$NaBPh_4$ (180)	MeOH (5.5)	120	1576	x/x/x	26 [12][f]
11[a]	A	**176** (115)	-	$NaBPh_4$ (115)	MeOH (3.5)	119	1579	x/x/x	<0.5 [<0.5]
12[a]	A	**177** (88)	-	$NaBPh_4$ (88)	MeOH (2.7)	118	1579	x/x/x	<1 [<0.5]
13[a]	A	**178** (66)	-	$NaBPh_4$ (66)	MeOH (2.0)	120	1579	x/x/x	<0.5 [<0.5]
14[a]	A	**179** (79)	-	$NaBPh_4$ (79)	MeOH (2.4)	120	1631, 1581	x/x/168.4	<0.5 [<0.5]
15[a]	A	CuI (63)	**184** (31)	$NaBPh_4$ (63)	MeOH (1.9)	118	1630	x/x/168.4	29 [14][g]
16[a]	A	CuI (53)	**184** (53)	$NaBPh_4$ (53)	MeOH (1.6)	114	1628, 1618	x/x/168.4	5 [2][g,h]

Reaction conditions as described in the general procedures A (4.7.22) and B (4.7.23) unless stated otherwise. x = not observed. ‡Relevant vibrations in the 1700-1500 cm^{-1} region are reported (IR spectra are presented in section 4.13.4). †Note that approximate oxalate yields determined by CE are stated for signals coinciding with the signal of internal standard ($Na_2C_2O_4$) added to the samples after a first CE measurement and might be a result of other impurities as evident from blank experiments with e.g. dien (Table S 18, entry 10). Approximate oxalate yields stated in [] were calculated without taking into account the 48% efficiency of the NaOH treatment procedure assessed by procedure 4.7.21. [a]The headspace of the reaction (5 mL) was analyzed by GC prior to removal of all volatiles *in vacuo*. No gaseous CO_2 reduction products (CO, CH_4) have been detected. [b]CO_2 was bubbled through the slightly yellow suspension for 3 h after 10 d under CO_2 atmosphere. The reaction mixture was then stirred for another 1.5 h under Ar atmosphere prior to removal of volatiles *in vacuo*. [c]Reaction conducted under an Ar atmosphere. [d]Broadened ^1H NMR possibly due to residual paramagnetic Cu^{2+}, hence ^{13}C NMR signals might not be observable due to residual paramagnetic species. [e]Integration hampered by disturbance of the baseline. [f]Note that blank experiments (Table S 18, entry 10) and variation of the scale (Table S 18, entry 9) preclude that this integral corresponds to oxalate and the presented yield is only depicted to highlight the complexity of oxalate detection by a single analytical method. [g]Approximate yield based on single experiment. Further experiments for confirmation of the yield required. [h]Overlapping with another signal (Figure S 407).

4.8 The Origin of Oxalate in CO_2 Reductive Coupling with Sodium Ascorbate and $[Cu_2(m\text{-xpt})_2X_2](PF_6)_2$

Note: Procedures and results presented within this section are reported elsewhere and are only implemented for the sake of complete documentation.[375]

4.8.1 Synthesis of $(Bu_4N)_2(C_2O_4)$

$(Bu_4N)_2(C_2O_4)$ was prepared according to a modified literature procedure.[455]

$Bu_4NOH{\cdot}30H_2O$ (1.91 g, 2.39 mmol, 2.00 equiv.) and $H_2C_2O_4$ (107 mg, 1.20 mmol, 1.00 equiv.) were dissolved in degassed H_2O (2.9 mL) and stirred at r.t. for 140 min. Volatiles were removed *in vacuo* and the remaining solid dried to provide $(Bu_4N)_2(C_2O_4)$ (quant.) as a white solid.

4.8.2 Synthesis of 1,3-Bis((4-(2-pyridyl)-1*H*-1,2,3-triazolyl)methyl)benzene (*m*-xpt)

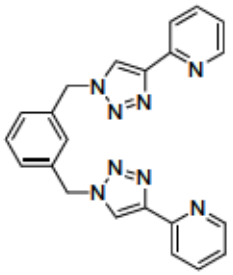

***m*-xpt** was prepared following the literature procedures with a few modifications in the purification.[376,377]

To 1,3-bis(bromomethyl)benzene (626 mg, 2.37 mmol, 1.00 equiv.) in DMF/H_2O (11.5 mL, 4:1, *v*:*v*) was added NaN_3 (323 mg, 4.97 mmol, 2.10 equiv.), Na_2CO_3 (251 mg, 2.37 mmol, 1.00 equiv.) $CuSO_4{\cdot}5H_2O$ (238 mg, 954 µmol, 0.40 equiv.), ascorbic acid (335 mg, 1.90 mmol, 0.80 equiv.) and 2-ethynylpyridine (0.48 mL, 4.75 mmol, 2.01 equiv.). The orange/brown suspension was stirred at r.t. for 22 h and subsequently poured into a solution of Na_2H_2EDTA (2.0 g, 5.4 mmol, 1.8 equiv.) in H_2O (100 mL) containing 28% aqueous NH_3 (5 mL). The mixture was extracted with $CHCl_3$ (2×80 mL, then 40 mL), dried over $MgSO_4$ and concentrated under reduced pressure (40 mbar, 55 °C). Cold Et_2O (100 mL) was added and the turbid solution stored at –32 °C for 5 d. The beige solid precipitate was filtered off and washed with Et_2O (15 mL). The solid was dissolved in $CHCl_3$ (40 mL) and filtered *via* filter cannula. Evaporation of the solvent under reduced pressure and subsequent column chromatographic purification (SiO_2, DCM/MeOH 20:1) provided ***m*-xpt** (777 mg, 1.97 mmol, 83%) as a beige solid.

^{1}H NMR (300 MHz, $CDCl_3$): δ = 8.53 (ddd, J = 4.9, 1.8, 0.9 Hz, 2H), 8.20 (ddd, J = 8.0, 1.1, 0.9 Hz, 2H), 8.17 (s, 2H), 7.80 (td, J = 7.8, 1.8 Hz, 2H), 7.42-7.27 (m, 4H), 7.26-7.20 (m, J = 7.6, 4.9, 1.2 Hz, 2H), 5.58 (s, 4H) ppm.

^{13}C{^{1}H} NMR (75 MHz, $CDCl_3$): δ = 149.9, 149.0, 137.6, 135.7, 130.3, 128.8, 128.0, 123.2, 122.5, 120.6, 54.1 ppm.

HR-MS (ESI): calculated *m*/*z* for $C_{22}H_{19}N_8^+$ ($[M+H]^+$): 395.1732; found: 395.1723; calculated *m*/*z* for $C_{22}H_{18}N_8Na^+$ ($[M+Na]^+$): 417.1546; found: 417.1541.

FTIR (ATR, neat): $\tilde{\nu}$ = 3131, 3108, 3089, 3046, 2994, 2953, 1593, 1569, 1546, 1474, 1461,

1437, 1415, 1348, 1339, 1303, 1247, 1227, 1203, 1171, 1147, 1083, 1043, 997, 978, 965, 940, 907, 895, 860, 843, 828, 784, 753, 735, 716, 706, 682, 662, 652, 621, 578, 544, 514, 478, 473, 445, 407 cm^{-1}.

Note: One aromatic signal was not observed in the ^{13}C NMR due to low signal intensity. In addition, assignment of the ^{1}H NMR signals based on the coupling constants characteristic for the pyridine moiety is not entirely in accordance with the assignment proposed in the literature.[377] Apart from that, analytical data is in accordance with that previously reported.[377]

4.8.3 Synthesis of $[Cu_2(m\text{-xpt})_2(NO_3)_2](NO_3)_2$ (197)

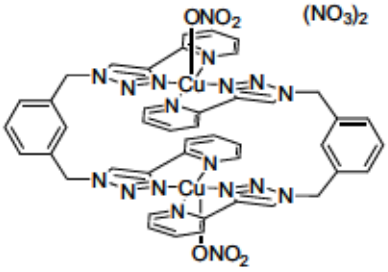

197 was prepared according to a literature procedure.[194]

To $Cu(NO_3)_2 \cdot 3H_2O$ (153 mg, 633 µmol, 1.00 equiv.) in MeCN (18 mL) was added a solution of *m*-xpt (250 mg, 633 µmol, 1.00 equiv.) in $CHCl_3$ (12.5 mL). The blue suspension was stirred at r.t. for 2 h. Filtration *via* filter cannula, washing of the solid with MeCN (10 mL) and $CHCl_3$ (15 mL) and drying under reduced pressure afforded **197** (368 mg, 316 µmol, quant.) as a light-blue solid.

FTIR (ATR, neat): $\tilde{\nu}$ = 3399, 3098, 1620, 1585, 1477, 1459, 1378, 1315, 1248, 1215 1161, 1123, 1096, 1062, 1041, 1026, 1000, 827, 786, 752, 715, 702, 684, 650, 597, 572, 510, 436 cm^{-1}.

4.8.4 Synthesis of $[Cu_2(m\text{-xpt})_2(NO_3)_2](PF_6)_2$ (135)

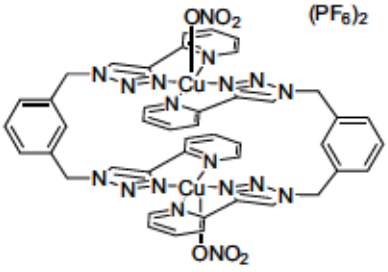

135 was prepared according to a slightly modified literature procedure.[194]

$[Cu_2(m\text{-xpt})_2(NO_3)_2](NO_3)_2$ (368 mg, 316 µmol, 1.00 equiv.) was dissolved in H_2O (46 mL) and NH_4PF_6 (343 mg, 2.10 mmol, 6.65 equiv.) dissolved in H_2O (5 mL) was added causing formation of a blue precipitate. The reaction mixture was stirred at r.t. for 14 min and subsequently filtered. The blue solid residue was washed with H_2O (20-30 mL) and Et_2O (10 mL). Drying under reduced pressure yielded **135** (348 mg, 262 µmol, 83%) as a blue solid.

HR-MS (ESI):

calculated *m*/*z* for $C_{44}H_{36}Cu_2N_{16}^{+}$ ($[M–2NO_2–2PF_6]^{2+}$): 457.0955; found: 457.0952.

FTIR (ATR, neat): $\tilde{\nu}$ = 3668, 3647, 3637, 3627, 3603, 3588, 3566, 3552, 3141, 3099, 3079, 3063, 3044, 1625, 1590, 1574, 1481, 1464, 1430, 1377, 1363, 1337, 1285, 1248, 1218, 1167, 1128, 1099, 1066, 1028, 1003, 904, 829, 784, 764, 744, 717, 703, 684, 651, 555, 511, 421, 417 cm^{-1}.

4.8.5 Synthesis of $[Cu_2(m\text{-xpt})_2Cl_2]Cl_2$ (198)

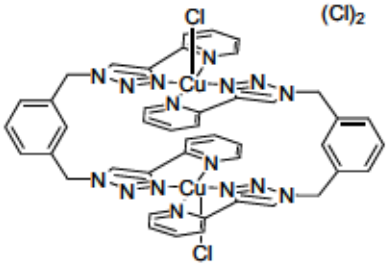

198 was prepared according to a literature procedure.[376]

To $CuCl_2$ (20.9 mg, 155 µmol, 1.01 equiv.) in MeCN (8.0 mL) was added a solution of *m*-xpt (60.8 mg, 154 µmol, 1.00 equiv.) in $CHCl_3$ (8.0 mL). The blue/green suspension was stirred at r.t. for 3 h. Filtration, washing of the solid with MeCN (2×10 mL) and $CHCl_3$ (2×10 mL) and drying *in vacuo* afforded **198** (69.5 mg, 65.7 µmol, 85%) as green solid.

MS (ESI):
calculated *m*/*z* for $C_{44}H_{36}Cu_2N_{16}^+$ ($[M–4Cl]^{2+}$): 457.0955; found: 457.
FTIR (ATR, neat): $\tilde{\nu}$ = 3354, 3097, 3034, 2987, 1615, 1577, 1455, 1349, 1325, 1277, 1248, 1213, 1162, 1116, 1092, 1059, 1029, 997, 906, 845, 787, 746, 712, 704, 683, 650, 607, 592, 551, 512, 425 cm^{-1}.

4.8.6 Synthesis of $[Cu_2(m\text{-xpt})_2Cl_2](PF_6)_2$ (136)

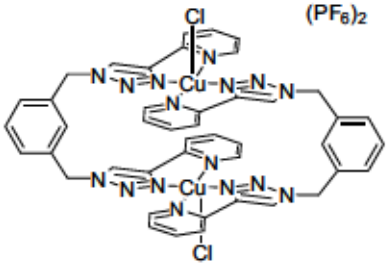

136 was prepared according to a slightly modified literature procedure.[194]

$[Cu_2(m\text{-xpt})_2Cl_2]Cl_2$ (237 mg, 224 µmol, 1.00 equiv.) was dissolved in H_2O (50 mL) and NH_4PF_6 (224 mg, 1.37 mmol, 6.11 equiv.) was added which caused formation of a blue/green precipitate. The reaction mixture was stirred at r.t. for 11 min and subsequently filtered. The solid residue was washed with H_2O (15 mL) and Et_2O (20 mL). Drying *in vacuo* yielded **136** (143 mg, 112 µmol, 50%) as blue solid.
HR-MS (ESI):
calculated *m*/*z* for $C_{44}H_{36}Cu_2N_{16}^+$ ($[M–2Cl–2PF_6]^{2+}$): 457.0955; found: 457.0946.
FTIR (ATR, neat): $\tilde{\nu}$ = 3651, 3632, 3589, 3581, 3568, 3552, 3141, 3123, 3077, 3065, 3057, 3037, 1620, 1586, 1476, 1460, 1431, 1282, 1248, 1216, 1163, 1126, 1097, 1063, 1025, 1002, 831, 781, 746, 715, 703, 684, 650, 556, 511, 419 cm^{-1}.

4.8.7 Synthesis of $[Cu_2(m\text{-xpt})_2](PF_6)_2$ (187)

187 was prepared according to a modification of a literature procedure.[194]

$[Cu_2(m\text{-xpt})_2(NO_3)_2](PF_6)_2$ (111 mg, 83.5 µmol, 1.00 equiv.) and sodium ascorbate (16.8 mg, 84.8 µmol, 1.02 equiv.) were dissolved in dry DMF (5.5 mL) and stirred at r.t. for 1 h. Dry Et_2O (22 mL) was slowly diffused into the yellow solution at –32 °C over 14 d. The yellow precipitate was filtered off *via* cannula, washed with dry Et_2O (4 mL) and dried *in vacuo* yielding **187** (94.9 mg, 63.8 µmol, 76% NMR yield) as yellow solid which still contained DMF.

^{1}H NMR (300 MHz, DMSO-d_6): δ = 9.18 (br, 4H), 8.45 (br, 4H), 8.11 (br, 8H), 7.48 (br, 10H), 7.33 (br, 2H), 5.78 (br, 8H) ppm.
^{31}P{^{1}H} NMR (122 MHz, DMSO-d_6): δ = −144.2 (hept, J = 711 Hz) ppm.
FTIR (ATR, neat): $\tilde{\nu}$ = 3141, 3099, 3016, 2958, 2930, 2864, 2808, 1661, 1607, 1569, 1491, 1472, 1449, 1411, 1388, 1360, 1343, 1320, 1256, 1237, 1205, 1158, 1090, 1055, 988, 832, 779, 743, 714, 704, 660, 638, 611, 574, 555, 512, 498, 442, 410 cm^{-1}.
Analytical data (^{1}H NMR) is in accordance with the literature, albeit the presence of DMF has not been described.[194]

4.8.8 Synthesis of [Cu$_2$(*m*-xpt)$_2$(μ-C$_2$O$_4$)](PF$_6$)$_2$ (137)

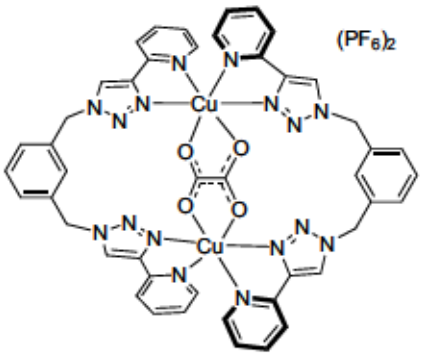

The synthesis of **137** *via* insertion of $C_2O_4^{2-}$ was performed according to a modification of the previously reported procedure.[194]

To **135** (161 mg, 119 µmol, 1.00 equiv.) and $(Bu_4N)_2C_2O_4$ (74.3 mg, 130 µmol, 1.09 equiv.) was added dry MeCN (16 mL) and the resulting blueish suspension stirred at r.t. for 6 h. The resulting green suspension was filtered in air, the mint green solid washed with MeCN (25 mL) and dried *in vacuo* to provide **137** (74.3 mg, 57.4 µmol, 47%).

FTIR (ATR, neat): $\tilde{\nu}$ = 3473, 3122, 2939, 1676, 1637, 1594, 1454, 1351, 1327, 1304, 1281, 1244, 1209, 1156, 1116, 1092, 1065, 1054, 1019, 995, 889, 875, 844, 826, 785, 765, 749, 717, 705, 682, 657, 644, 633, 606, 556, 512, 486, 446, 410 cm^{-1}.
The analytical data (IR) for **137** is in accordance with that reported in the literature.[194]

4.8.9 Removal of Oxalate from [Cu$_2$(*m*-xpt)$_2$(μ-C$_2$O$_4$)](PF$_6$)$_2$ (137)

Removal of oxalate *via* treatment with aqueous NaOH in the presence of toluene was adapted from a literature procedure.[193]

To complex **137** (29.3 mg, 22.6 µmol, 1.00 equiv.) prepared *via* insertion of $C_2O_4^{2-}$ into **135** (see 4.8.8) suspended in toluene (1 mL) was added 1 M aqueous NaOH (0.50 mL, 0.50 mmol, 22.0 equiv.). The suspension was stirred at r.t. for 16 h after which all volatiles were evaporated under reduced pressure at 50 °C yielding a brown/black solid residue. After extraction with DCM (1 mL), D_2O (0.6 mL) was added and the suspension analyzed by NMR spectroscopy. Addition of $Na_2C_2O_4$ after the first measurement proved the successful removal of oxalate from the complex *via* this method (Figure S 176).
^{13}C{^{1}H} NMR (101 MHz, D_2O): δ = 173.3 ppm ($Na_2C_2O_4$).

4.8.10 Reaction of *In situ* Formed $[Cu_2(m\text{-xpt})_2](PF_6)_2$ (187) with Air to Produce $[Cu_2(m\text{-xpt})_2(\mu\text{-}C_2O_4)](PF_6)_2$ (137)

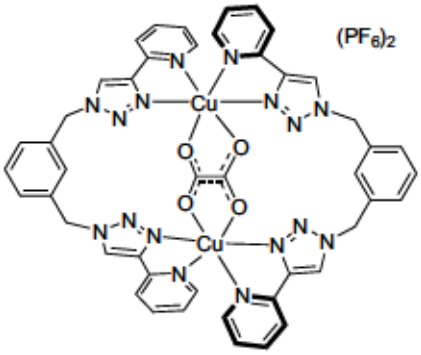

Formation of **137** in air was conducted according to a literature procedure.[194]

To **135** (49.8 mg, 37.5 µmol, 1.00 equiv.) and sodium ascorbate (11.2 mg, 56.5 µmol, 1.51 equiv.) under Ar was added dry DMF (5.0 mL). The mixture was stirred at r.t. for 2 h yielding a yellow solution which was poured into a crystallization dish and left to evaporate in air. The mixture was transferred into a smaller vial after 1 d and green octahedral crystals formed over the course of 2 weeks which were found to be **137**. Single crystal X-ray diffraction of these crystals revealed a unit cell identical to that reported in the literature.[194]

FTIR (ATR, neat): $\tilde{\nu}$ = 3150, 3128, 2925, 2850, 1668, 1638, 1610, 1573, 1455, 1382, 1355, 1330, 1304, 1282, 1248, 1211, 1152, 1115, 1090, 1067, 1056, 1017, 839, 820, 768, 748, 714, 654, 555, 508, 483 cm^{-1}.

Anal. Calcd. for $[Cu_2(m\text{-xpt})_2(\mu\text{-}C_2O_4)](PF_6)_2 \cdot$DMF C 43.05, H 3.17, N 17.42. **Observed** C 43.21, H 3.312, N 17.21.

An analogous reaction starting from **136** (51.0 mg, 39.9 µmol, 1.00 equiv.) and sodium ascorbate (12.4 mg, 62.6 µmol, 1.57 equiv.) in DMF (5.0 mL) resulted in the formation of **137** over 11 d in air, as evidenced by FTIR spectroscopy (Figure 316). In addition to green crystalline **137**, a blue solid was observed, as previously described.[194]

4.8.11 Removal of Oxalate from $[Cu_2(m\text{-xpt})_2(\mu\text{-}C_2O_4)](PF_6)_2$ (137)

Removal of oxalate *via* treatment with aqueous NaOH in the presence of toluene was adapted from a literature procedure.[193]

To complex **49** (55.1 mg) prepared *via* reaction of *in situ* formed **187** with air (see 4.8.10) suspended in toluene (2 mL) was added 1 M aqueous NaOH (1.0 mL, 1.00 mmol). The green suspension was stirred at r.t. for 17 h after which all volatiles were evaporated under reduced pressure yielding a blue/green solid residue. After extraction with DCM (2 mL), D_2O (0.7 mL) was added and the suspension analyzed by NMR spectroscopy. $Na_2C_2O_4$ and sodium formate as internal standards were added to the sample after the initial measurement (Figure S 177 & Figure S 178).

^{1}H NMR (300 MHz, D_2O): δ = 8.40 (s, NaO_2CH) ppm.

^{13}C{^{1}H} NMR (101 MHz, D_2O): δ = 173.2 ($Na_2C_2O_4$), 171.1 (NaO_2CH) ppm.

Note: Sodium formate is likely resulting from alkaline hydrolysis of co-crystallized DMF present in **137**.

4.8.12 *In situ* Generation of $[Cu_2(m\text{-xpt})_2](PF_6)_2$ (187), Subsequent Treatment with CO_2 and Air Yielding 137

To sodium ascorbate (10.8 mg, 54.5 μmol, 1.45 equiv.) and **135** (49.9 mg, 37.5 μmol, 1.00 equiv.) was added dry DMF (4.0 mL). The reaction mixture was stirred at r.t. for 1 h under an Ar atmosphere resulting in a yellow solution. The atmosphere was exchanged by flushing the flask with CO_2 for 2 min. After sealing the flask under a CO_2 overpressure, the mixture was stirred at r.t. for 6 d. No change in color was observed during this time (see Figure S 4).† Air (1 mL, followed by additional 12 mL after 7 d) was added to the yellow solution and stirring at r.t. continued for 11 d during which a color change to green was observed. Volatiles were removed *in vacuo* and the green solid residue dissolved in DMF. Slow evaporation of the DMF solution in air yielded a green crystalline solid which was analyzed by FTIR spectroscopy.

FTIR (ATR, neat): $\tilde{\nu}$ = 3150, 3131, 3098, 2926, 2886, 1668, 1638, 1611, 1574, 1542, 1491, 1474, 1456, 1382, 1355, 1331, 1305, 1283, 1249, 1212, 1153, 1116, 1091, 1067, 1057, 1018, 997, 977, 839, 819, 786, 773, 748, 714, 681, 654, 644, 607, 590, 555, 508, 483, 456, 441, 410 cm^{-1}.

†At this point, a sample (0.5 mL) was taken from the reaction mixture, transferred into a Teflon-coated screw cap septum-sealed UV/Vis cuvette and diluted with dry DMF (1.0 mL). Molten parafilm was utilized to cover the hole in the septum and the UV/Vis spectrum recorded. Air (4 mL) was then added to the UV/Vis cuvette and the resulting oxidation reaction UV/Vis spectroscopically followed over 189 h (Figure 38).

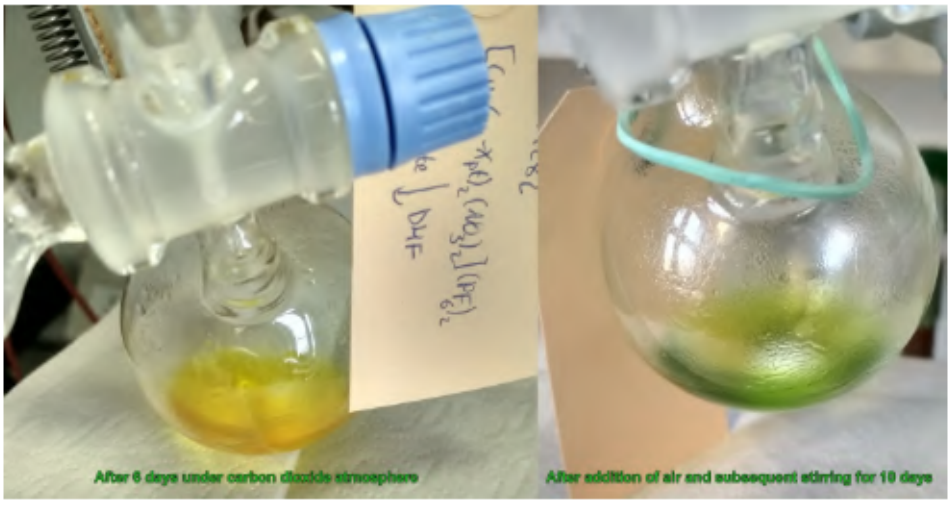

Figure S 4: *In situ* formed $[Cu_2(m\text{-xpt})_2](PF_6)_2$ in DMF after stirring under CO_2 for 6 d (left) and after addition of air (right).

4.8.13 *In situ* Generation of $[Cu_2(m\text{-xpt})_2](PF_6)_2$ (187), Treatment with O_2 Yielding 137 and Subsequent Removal of Oxalate

Dry DMF (11 mL) was added to **135** (110.2 mg, 82.9 μmol, 1.00 equiv.) and sodium ascorbate (25.1 mg, 127 μmol, 1.00 equiv.) under Ar. The reaction mixture was stirred at r.t. for 1.5 h yielding a yellow solution. The Ar atmosphere was exchanged for O_2 by bubbling a stream of O_2 through the solution (*via* balloon, see Figure S 5). The flask was sealed and stirred under O_2 atmosphere for 5 d at r.t. over which the color gradually changed to blue-green/green (Figure S 6). All volatiles were removed *in vacuo* and the remaining yellow/green solid analyzed by FTIR spectroscopy (Figure S 317) indicating the formation of **137**. Prolonged reaction time with O_2 (7 days) resulted in essentially identical product formation (see Figure S 317).

FTIR (ATR, neat): $\tilde{\nu}$ = 3150, 3130, 3070, 2932, 2856, 1799, 1668, 1640, 1611, 1573, 1498, 1473, 1455, 1384, 1356, 1330, 1305, 1282, 1247, 1211, 1152, 1114, 1091, 1067, 1056, 1018, 996, 895, 836, 820, 786, 774, 748, 714, 681, 660, 607, 589, 555, 508, 485, 410 cm^{-1}.

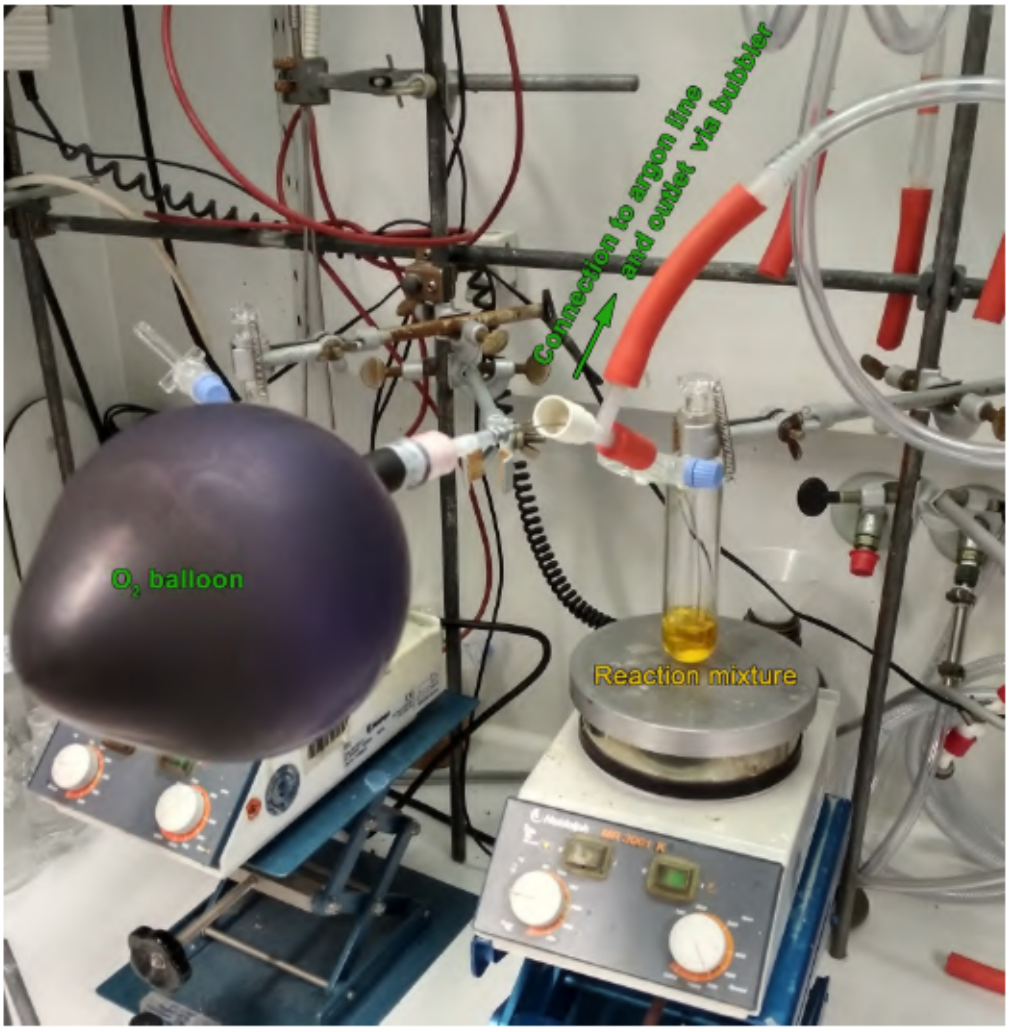

Figure S 5: Setup utilized for the treatment of *in situ* formed **137** with O_2 (balloon).

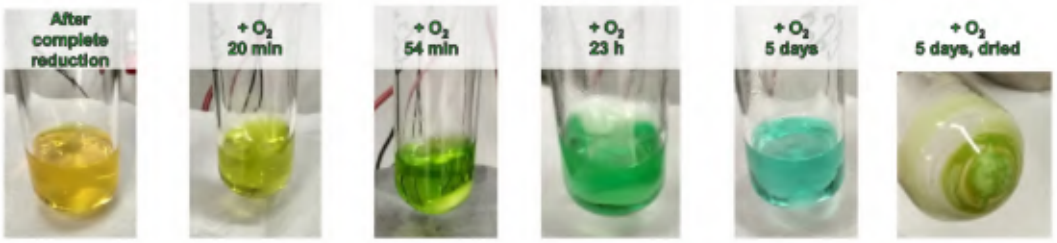

Figure S 6: Color change upon reaction of *in situ* formed **137** with O_2.

Dry toluene (3.6 mL) and degassed 1 M aqueous NaOH (1.8 mL, 1.80 mmol) were added to the yellow/green solid under Ar and the reaction mixture stirred at r.t. for 17 h resulting in a yellow suspension. Volatiles were removed *in vacuo* and the remaining solid residue extracted with dry DCM (4.0 mL). Degassed D_2O (1.0 mL) was added to the yellow solid residue and the yellow suspension analyzed by ^1H and ^{13}C NMR spectroscopy. Addition of $Na_2C_2O_4$ and sodium formate as internal standards further confirmed the presence of both salts (Figure S 179 & 180).

^1H NMR (300 MHz, D_2O): δ = 8.40 (s, NaO_2CH) ppm.

$^{13}C\{^1H\}$ NMR (75 MHz, D_2O): δ = 173.2 ($Na_2C_2O_4$), 171.1 (NaO_2CH) ppm.

Note: Sodium formate is likely resulting from alkaline hydrolysis of co-crystallized or residual DMF present in **137**.

4.9 CO_2 Reductive Coupling Based on Cu and α-Ketocarboxylates

4.9.1 Synthesis of Potassium Tris(3,5-di-*iso*-propylpyrazolato)borohydride (190)

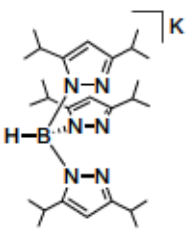

190 was prepared following a modified combination of literature procedures.[331,403]

KBH_4 (230 mg, 4.27 mmol, 1.00 equiv.) and 3,5-di-*iso*-propylpyrazole (2.07 g, 13.6 mmol, 3.18 equiv.) were heated to 200-250 °C for 24 h (heating was stopped every 2.5-5 h and the progress followed by NMR spectroscopy). The solid was extracted with dry DCM (4.0+2.0 mL) *via* filter cannula and volatiles were removed *in vacuo*. Unreacted 3,5-di-*iso*-propylpyrazole was sublimed off at 130-155 °C (1×10^{-3} mbar). **190** (582 mg, 0.99 mmol, 23% [71% purity by NMR]) was obtained as a white solid *via* twofold sublimation at 185-190 °C (1×10^{-3} mbar) and was utilized without further purification.

^{1}H NMR (300 MHz, THF-d_8): δ = 5.68 (s, 3H), 3.12 (sept, J = 6.9 Hz, 3H), 2.76 (sept, J = 6.9 Hz, 3H), 1.11 (d, J = 6.9 Hz, 18H), 0.96 (d, J = 6.9 Hz, 18H) ppm.

^{13}C{^{1}H} NMR (101 MHz, THF-d_8): δ = 157.5, 155.5, 96.4, 29.2, 27.1, 24.1, 23.8 ppm.

^{11}B{^{1}H} NMR (96 MHz, THF-d_8): δ = –6.1 ppm.

HR-MS (ESI): calculated *m/z* for $C_{27}H_{48}{}^{11}BN_6^+$ ([M–K+2H]$^+$): 467.4034; found: 467.4043.

FTIR (ATR, neat): $\tilde{\nu}$ = 3566, 3391, 3199, 3121, 2960, 2929, 2868, 2463, 1654, 1567, 1530, 1459, 1425, 1378, 1361, 1298, 1171, 1138, 1106, 1071, 1045, 1004, 958, 922, 897, 878, 784, 719, 659, 586, 508, 459 cm^{-1}.

Analytical data is in accordance with the literature[403] (NMR spectra in THF-d_8 have, to the best of our knowledge, not been reported).

4.9.2 Synthesis of [Cu(Tp^{iPr,iPr})Br] (191)

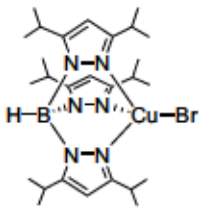

191 was prepared *via* a modified literature procedure.[331,404]

To KTp^{iPr,iPr} (36.0 mg, 71.3 μmol, 1.00 equiv.) and $CuBr_2$ (16.1 mg, 72.1 μmol, 1.01 equiv.) under Ar was added dry acetone (2.4 mL) and the mixture stirred at r.t. for 30 min. Volatiles were removed *in vacuo* to give a red/brown solid. The solid residue was extracted with hot, dry hexane (2 × 2.0 mL) *via* filter cannula and the resulting orange solution was left at r.t. resulting in the formation of dark red crystals of **191** (13.1 mg, 21.5 μmol, 30%) and some colorless crystals of **192**. Crystals of sufficient quality for X-ray crystallographic analysis of both compounds were obtained by crystallization from a hot hexane solution.

FTIR (ATR, neat) for **191** $\tilde{\nu}$ = 2963, 2928, 2867, 2547, 1533, 1470, 1428, 1396, 1381, 1362, 1301, 1168, 1134, 1107, 1050, 902, 841, 790, 751, 716, 649, 521, 463 cm^{-1}.

FTIR (ATR, neat) for **192** $\tilde{\nu}$ = 3188, 3138, 3106, 2960, 2929, 2869, 1562, 1468, 1379, 1360, 1333, 1307, 1256, 1179, 1139, 1107, 1053, 1021, 1006, 927, 878, 791, 722, 716, 690, 648, 518 cm^{-1}.

Note: Even though preparation of **191** has been described in the literature,[331,404] no analytical data apart from elemental analysis has previously been reported, to the best of our knowledge.

4.9.3 Synthesis of [Cu(Tp^{iPr,iPr})Cl] (193)

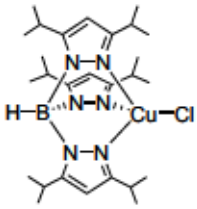

193 was prepared *via* a modified literature procedure.[404]

To KTp^{iPr,iPr} (43.3 mg, 85.8 μmol, 1.00 equiv.) and $CuCl_2$ (12.2 mg, 90.7 μmol, 1.06 equiv.) under Ar was added dry THF (3.0 mL) and the resulting mixture stirred at r.t. for 1 h yielding a deep red solution. Volatiles were removed *in vacuo* to give a red solid that was extracted with dry DCM (3.0 mL) using a syringe equipped with a PTFE syringe filter. Volatiles were again removed *in vacuo* and the red solid dissolved in dry hexane (6.0 mL) by sonification. The red/orange solution was stored at –32 °C overnight resulting in the formation of a red crystalline solid. The mother liquor was decanted at –30 °C using a syringe and the solid dried *in vacuo* to give **193** (15.0 mg, 26.6 μmol, 31%) as a red crystalline solid.
HR-MS (ESI): calculated *m/z* for $C_{27}H_{47}{}^{10}BClCuN_6^+$ ([M+H]$^+$): 563.2976; found: 563.3014; calculated *m/z* for $C_{27}H_{47}{}^{11}BClCuN_6^+$ ([M+H]$^+$): 564.2944; found: 564.2917.
FTIR (ATR, neat): $\tilde{\nu}$ = 2964, 2928, 2867, 2549, 1533, 1510, 1470, 1443, 1429, 1397, 1381, 1363, 1302, 1168, 1134, 1107, 1072, 1050, 925, 902, 881, 822, 790, 752, 717, 650, 585, 522, 511, 463 cm^{-1}.
The analytical data (B-H vibration) is in accordance with the literature.[404]

4.9.4 Synthesis of [Cu(Tp^{iPr,iPr})(O$_2$CC(O)CH(Me)$_2$)] (129)

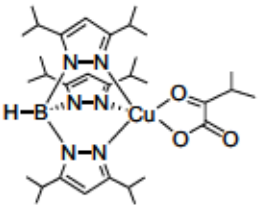

129 was prepared *via* a modification of the previously reported procedure.[193]

To sodium 3-methyl-2-oxobutyrate (6.0 mg, 43.5 μmol, 1.21 equiv.) in dry MeOH (0.4 mL) cooled to –20 to –30 °C was added a cold (–20 to –30 °C) solution of **193** (20.2 mg, 35.8 μmol, 1.00 equiv.) in dry DCM (1.0 mL). The cold bath was exchanged for an ice bath and stirring continued for another 10 min yielding a green solution. Volatiles were removed *in vacuo* at 0 °C. Dry DCM (0.4 mL) was added to the green solid and the mixture was filtered *via* syringe equipped with a syringe PTFE filter. Volatiles were removed *in vacuo* and the resulting green solid mostly dissolved in dry hexane (0.1 mL). Storage at –32 °C resulted in the formation of a green crystalline solid. The mother liquor was decanted *via* syringe at –20 to –30 °C. Drying *in vacuo* provided **129** (13.7 mg, 21.3 μmol, 59%) as a green crystalline solid.
HR-MS (ESI): calculated *m/z* for $C_{32}H_{54}{}^{11}BCuN_6O_3^+$ ([M+H]$^+$): 644.3646; found: 644.3645; calculated *m/z* for $C_{32}H_{53}{}^{11}BCuN_6O_3Na^+$ ([M+Na]$^+$): 666.3460; found: 666.3459.

FTIR (ATR, neat): $\tilde{\nu}$ = 3132, 2962, 2929, 2868, 2543, 1687, 1666, 1534, 1469, 1429, 1391, 1381, 1363, 1300, 1177, 1136, 1110, 1048, 1019, 957, 923, 900, 878, 822, 790, 759, 737, 715, 704, 653, 587, 545, 503 cm^{-1}.

4.9.5 Synthesis of [Cu(Tp^{iPr,iPr})($^{13}C_5$-$O_2CC(O)CH(Me)_2$)] (196)

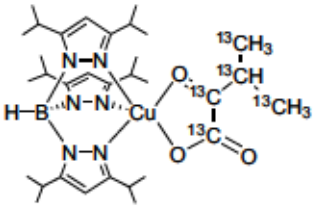

196 was prepared *via* a modification of the previously reported procedure for the synthesis of **129**.[193]

To **193** (29.5 mg, 52.3 μmol, 1.00 equiv.) and sodium $^{13}C_5$-3-methyl-2-oxobutyrate (9.4 mg, 65.7 μmol, 1.26 equiv.) cooled to –20 °C was added dry DCM (1.0 mL) followed by dry MeOH (0.4 mL). The mixture was then placed in an ice bath and stirring continued for 15 min yielding a green solution. Volatiles were removed *in vacuo* at 0 °C. Dry DCM (0.5 mL) was added to the green solid and the mixture was filtered *via* syringe equipped with a syringe PTFE filter. Volatiles were removed *in vacuo* and the resulting green solid mostly dissolved in dry hexane (0.4 mL). Storage at –32 °C resulted in the formation of a green microcrystalline solid. The mother liquor was decanted *via* syringe at –36 °C. Drying in vacuo provided **196** (28.7 mg, 44.2 μmol, 84%) as a green crystalline solid.

HR-MS (ESI):

calculated *m/z* for $^{13}C_5C_{27}H_{54}{}^{11}BCuN_6O_3{}^+$ ([M+H]$^+$): 649.3814; found: 649.3814;

calculated *m/z* for $^{13}C_5C_{27}H_{53}{}^{11}BCuN_6O_3Na^+$ ([M+Na]$^+$): 671.3628; found: 671.3631.

FTIR (ATR, neat): $\tilde{\nu}$ = 3123, 2964, 2930, 2869, 2550, 1644, 1625, 1533, 1470, 1428, 1389, 1381, 1363, 1301, 1286, 1267, 1179, 1136, 1108, 1088, 1050, 1031, 958, 922, 900, 879, 823, 802, 791, 758, 733, 716, 691, 653, 589, 545, 519, 491.

4.9.6 General Procedure for Treatment of Cu-α-ketocarboxylate Complexes with Air

The general procedure for air treatment was adapted from a literature procedure.[193]

The respective Cu α-ketocarboxylate complex (or the sodium α-ketocarboxylate and $Cu(BF_4)_2 \cdot 6\ H_2O$) was dissolved/suspended in the indicated volume of DCM in a vial in air (a small quantity of MeOH was added when a sodium α-ketocarboxylate was utilized and the suspension sonicated for approx. 1 min), layered with heptane (same volume as DCM) and left to evaporate in air over the time stated in Table S 19. After complete evaporation, the residue was analyzed by FTIR spectroscopy and subsequently subjected to removal of potential CO_2 reduction products by NaOH treatment according to the general procedure 4.7.20.

4.9.7 General Procedure for Treatment of Cu-α-ketocarboxylate Complexes with CO_2/O_2

The general procedure for CO_2/O_2 treatment was adapted from a literature procedure.[193]

The respective Cu complex was dissolved in dry toluene (volume indicated in Table S 20) in a 25 mL Schlenk tube under CO_2 atmosphere and stirred for 20-30 min. O_2 (12 mL) was then added *via* syringe, the flask sealed and the reaction mixture stirred under the CO_2/O_2 atmosphere for the time stated. Volatiles were removed *in vacuo* and the solid residue analyzed by FTIR spectroscopy. Subsequent extraction of the solid residue with NaOH was conducted according to the general procedure 4.7.20 in air.

4.9.8 General Procedure for Treatment of Sodium α-Ketoisovalerate with CO_2/O_2 for NMR Analysis

Sodium α-ketoisovalerate ($^{13}C_5$) and $Cu(BF_4)_2 \cdot 6\ H_2O$ were suspended in dry C_6D_6 or CD_2Cl_2 containing 10% CD_3OD to facilitate enhanced solubility under a CO_2 atmosphere in a 25 mL Schlenk tube and were sonicated for approx. 1 min. After stirring for 10-20 min, O_2 (12 mL) was added *via* syringe and the suspension stirred under the CO_2/O_2 atmosphere for the time stated. The solid was allowed to settle, the solution decanted and analyzed by NMR spectroscopy. After transferring the NMR solution back to the solid, all volatiles were removed *in vacuo*. The resulting solid residue was analyzed by FTIR spectroscopy and further subjected to NaOH treatment according to the general procedure 4.7.20 in air.

4.9.9 Cu-α-ketocarboxylate Complexes In CO_2 Reductive Coupling - Results

Table S 19: Results for the treatment of Cu-α-ketocarboxylate complexes with air for the potential reductive coupling of CO_2.

Entry	[Cu] ([μmol])	Additives ([μmol])	Solvent ([mL])	*t* [h]	FTIR $\tilde{\nu}$ [cm^{-1}]‡	^{13}C NMR δ [ppm] ($C_2O_4^{2-}$/HCO_2^-/CO_3^{2-})	CE ($C_2O_4^{2-}$) approx. yield [%]†
1[a]	**129** (19)	-	DCM/*n*heptane (0.5/0.5)	18	1654, 1602	x/x/x	3 [6]
2[b]	**196** (9.2)	-	DCM/*n*heptane (0.3/0.3)	18	1649, 1609, 1562	173.4/171.0/168.3	11 [21]
3[a,c,d]	$Cu(BF_4)_2(H_2O)_6$ (72)	**194** (72)	DCM/*n*heptane /MeOH (2/2/0.2)	90	1707, 1607	173.2/x/x	36 [73]
4[a,c]	$Cu(BF_4)_2(H_2O)_6$ (36)	**194** (36)	DCM/*n*heptane /MeOH (1/1/0.1)	63	1705, 1610	173.3/x/x	47 [94]
5[b,c]	$Cu(BF_4)_2(H_2O)_6$ (34)	**195** (34)	DCM/*n*heptane /MeOH (1/1/0.1)	65	1666, 1625, 1563	173.3/171.1/168.4	55 [110]
6[b,c]	$Cu(BF_4)_2(H_2O)_6$ (34)	**195** (34)	DCM/*n*heptane /MeOH (1/1/0.1)	40	1666, 1626, 1564	173.3/171.1/168.2	42 [84]
7[c]	-	**194** (37)	DCM/*n*heptane /MeOH (1/1/0.1)	42	1707, 1631	x/x/x	4 [8]
8[a,d]	$Cu(BF_4)_2(H_2O)_6$ (72)	Na pyruvate (73)	DCM/*n*heptane /MeOH (2/2/0.2)	16	1734, 1593	173.2/x/168.4	5 [11]

Reactions were conducted according to the general procedure 4.9.6 unless stated otherwise. x = not observed. ‡Characteristic vibrations are reported (IR spectra are presented in section 4.13.6). †Approximate oxalate yields stated were calculated without taking into account the efficiency of the NaOH treatment procedure. Yields stated are assuming a mononuclear mechanism. Corresponding yields for a potentially bimolecular formation of oxalate[193] are stated in []. [a]HR-MS (ESI) analysis of the residue after NaOH treatment revealed the presence of $^{12}C_2O_4^{2-}$ (see section 4.16.1). [b]HR-MS (ESI) analysis of the residue after NaOH treatment revealed the presence of $^{13}C_2O_4^{2-}$ while no mixed $^{12}C^{13}CO_4^{2-}$ was observed. [c]The solid starting materials were not entirely soluble. MeOH was added to facilitate higher solubility. [d]The solid residue after NaOH treatment was extracted with DCM prior to NMR/CE analysis.

Table S 20: Results for the treatment of Cu-α-ketocarboxylate complexes with CO_2/O_2 for the potential reductive coupling of CO_2.

Entry	[Cu] ([μmol])	Additives ([μmol])	Solvent ([mL])	*t* [h]	FTIR $\tilde{\nu}$ [cm^{-1}]‡	^{13}C NMR δ [ppm] ($C_2O_4^{2-}$/HCO_2^-/CO_3^{2-})	CE ($C_2O_4^{2-}$) approx. yield [%]†
1[a]	**129** (7.9)	-	toluene (0.5)	42	1659, 1600	x/x/x	3 [6]
2[b]	**196** (13)	-	toluene (0.8)	67	1642, 1613, 1561	173.4/x/168.3	1 [2]
3[b]	**196** (17)	-	toluene (1.1)	67	1640, 1613, 1555	173.4/x/168.4	1 [1]
4[c]	**$Cu(BF_4)_2(H_2O)_6$** (34)	**195** (34)	C_6D_6/CD_3OD (1.0/0.1)	93	1666, 1617, 1568	173.2/171.1/168.2	31 [62]
5[c]	**$Cu(BF_4)_2(H_2O)_6$** (34)	**195** (34)	CD_2Cl_2/CD_3OD (1.0/0.1)	93	1623, 1561	173.2/171.1/x	17 [34]

Reactions were conducted according to the general procedure 4.9.7 unless stated otherwise. x = not observed. ‡Characteristic vibrations are reported (IR spectra are presented in section 4.13.6). †Approximate oxalate yields stated were calculated without taking into account the efficiency of the NaOH treatment procedure. Yields stated are assuming a mononuclear mechanism. Corresponding yields for a bimolecular formation of oxalate[193] are stated in []. [a]HR-MS (ESI) analysis of the residue after NaOH treatment possibly indicates the presence of $^{12}C_2O_4^{2-}$ with poor signal-to-noise ratio (see section 4.16.1). [b]HR-MS (ESI) analysis of the residue after NaOH treatment revealed the presence of $^{13}C_2O_4^{2-}$ while no mixed $^{12}C^{13}CO_4^{2-}$ was observed. [c]Reactions were conducted according to general procedure 4.9.8. The solid starting materials were not entirely soluble, hence CD_3OD was added to facilitate higher solubility.

4.10 Investigation of Trinuclear Cu Complexes in the Reduction of CO_2

4.10.1 Synthesis of Red Selenium

Red selenium was prepared using a modified literature procedure.[456]

To H_2SO_4 (40 mL) under Ar at 145 °C was added powdered Se (530 mg, 6.71 mmol, 1.00 equiv.) and the reaction mixture stirred at 150 °C for 1 h. The dark-green reaction mixture was then slowly poured onto ice causing formation of a red solid. Filtration, washing with H_2O until the wash solution was pH neutral, washing with EtOH (10 mL) and Et_2O (10 mL) and subsequent drying *in vacuo* yielded red Se (422 mg, 5.35 mmol, 80%).

4.10.2 Synthesis of Benzyl Potassium

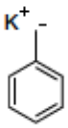

KBn was prepared according to a literature procedure.[457]

To KO^{t}Bu (439 mg, 3.91 mmol, 1.00 equiv.) in dry toluene (8.0 mL) at 0 °C was added ^{n}BuLi (2.5 M in hexane, 1.6 mL, 4.00 mmol, 1.02 equiv.). The orange suspension was allowed to warm to r.t. and stirred for 40 min. The orange solid was filtered off (cannula) and washed with dry toluene (2×4 mL) as well as dry hexane (1.6 mL). Drying *in vacuo* yielded KBn (463 mg, 3.56 mmol, 91%) as an orange solid.

4.10.3 Synthesis of 1,3,5-Tris(bromomethyl)-2,4,6-triethylbenzene (199)

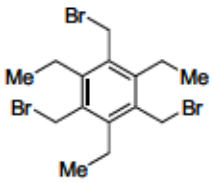

199 was prepared according to a literature procedure.[458]

To 1,3,5-triethylbenzene (4.0 mL, 21.3 mmol, 1.00 equiv.) and paraformaldehyde (6.77 g, 225 mmol, 10.6 equiv.) under Ar was added 40% HBr in AcOH (40 mL, 208 mmol, 9.77 equiv.). $ZnBr_2$ (8.16 g, 36.2 mmol, 1.70 equiv.) was added over 5 min at r.t. and the resulting brown suspension heated to 90 °C for 19 h. After cooling to r.t., the formed solid precipitate was filtered off and washed with H_2O (~200 mL). Drying under reduced pressure yielded **199** (8.00 g, 18.1 mmol, 85%) as a white solid.

^{1}H NMR (300 MHz, $CDCl_3$): δ = 4.58 (s, 6H), 2.94 (q, J = 7.6 Hz, 6H), 1.34 (t, J = 7.6 Hz, 9H) ppm.

The analytical data is in accordance with the literature data.[458]

4.10.4 Synthesis of 1,3,5-Tris(phthalimidomethyl)-2,4,6-triethylbenzene (200)

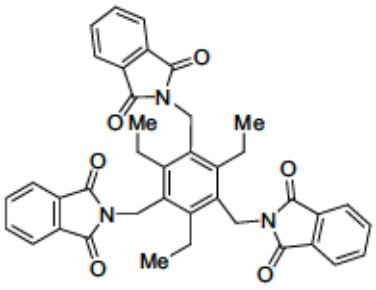

200 was prepared according to a modified literature procedure.[458]

To potassium phthalimide (6.75 g, 36.4 mmol, 4.02 equiv.) in dry DMSO (60 mL) was added **199** (4.00 g, 9.07 mmol, 1.00 equiv.) and the resulting suspension heated to 85 °C overnight. The yellow suspension was cooled to 0 °C, the solid precipitate filtered off and dissolved in DCM (80 mL). H_2O (80 mL) was added, the layers were separated and the aqueous layer extracted with DCM (80 mL). The combined organic layers were washed with H_2O (2×40 mL), dried over Na_2SO_4 and evaporated under reduced pressure. The mother liquor was poured into H_2O (150 mL), the formed white precipitate was filtered off and dissolved in DCM (80 mL). The organic layer was washed with H_2O (3×40 mL), dried over Na_2SO_4, evaporated under reduced pressure and combined with the previous extract. Column chromatographic purification (SiO_2, pentane/EtOAc 2:1→ EtOAc) yielded **200** (2.27 g, 3.56 mmol, 39%) as colorless to light-yellow solid.

^{1}H NMR (300 MHz, $CDCl_3$): δ = 7.85-7.77 (m, 6H), 7.72-7.64 (m, 6H), 4.94 (s, 6H), 3.10 (q, J = 7.6 Hz, 6H), 0.97 (t, J = 7.6 Hz, 9H) ppm.

The analytical data is in accordance with the literature data.[458]

4.10.5 Synthesis of 1,3,5-Tris(aminomethyl)-2,4,6-triethylbenzene (201)

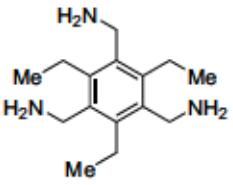

201 was prepared according to a literature procedure.[458]

To a suspension of **200** (2.06 g, 3.22 mmol, 1.00 equiv.) in dry EtOH/toluene (15 mL, 2:1 *v*:*v*) was added N_2H_4·1.5 H_2O (1.0 mL, 17.4 mmol, 5.42 equiv.). The reaction mixture was heated to 100 °C for 20 h resulting in a yellow suspension which was then allowed to cool to r.t.. The yellow solution was decanted, the colorless solid was dissolved in 40% aqueous KOH (75 mL) and extracted with $CHCl_3$ (3×100 mL). The organic layers were washed with H_2O (3×300 mL), dried over Na_2SO_4 and evaporated under reduced pressure to provide **201** (598 mg, 2.40 mmol, 74%) as a white solid.

^{1}H NMR (300 MHz, $CDCl_3$): δ = 3.88 (s, 6H), 2.83 (q, J = 7.5 Hz, 6H), 1.32 (br, 6H), 1.24 (t, J = 7.5 Hz, 9H) ppm.

^{13}C{^{1}H} NMR (75 MHz, $CDCl_3$): δ = 140.5, 137.6, 39.8, 22.7, 17.0 ppm.

The analytical data is in accordance with the literature data.[458]

4.10.6 Synthesis of 2,4-Pentanedione-2,2-(ethylene glycol) monoketal (202)

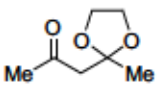

202 was prepared according to a literature procedure.[459]

To *p*-toluenesulfonic acid monohydrate (53.5 mg, 281 μmol, 0.1 mol%) was added benzene (46 mL), 2,4-pentanedione (24.0 mL, 233 mmol, 1.00 equiv.) and ethylene glycol (13.0 mL, 233 mmol, 1.00 equiv.). The mixture was heated to 95-115 °C in a Dean-Stark apparatus and the formed water regularly removed over 3 d. The resulting dark orange solution was concentrated under reduced pressure (10 mbar at 50 °C). Distillation under constant vacuum (5-6 mbar) at 55-90 °C (oil bath) yielded four fractions of **202** with different composition. The main fractions consisted of a 85:15 monoketal/diketal mixture (19.1 g of product mixture, 105 mmol monoketal [by NMR], 45% monoketal [by NMR]).

^{1}H NMR (300 MHz, C_6D_6): δ = 3.41 (s, 4H), 2.49 (quint, J = 0.5 Hz, 2H), 1.89 (t, J = 0.5 Hz, 3H), 1.36 (t, J = 0.5 Hz, 3H) ppm.

The analytical data is not entirely in accordance with the literature as the literature data has been reported as spectrum in C_6D_6, but appears to be recorded in $CDCl_3$.[459]

4.10.7 Synthesis of 142

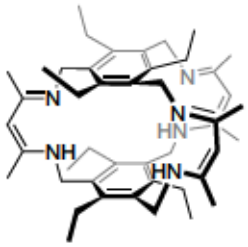

142 was prepared according to a literature procedure.[460]

To **201** (601 mg, 2.41 mmol, 1.00 equiv.) in dry MeOH (22 mL) was added **202** (559 mg, 3.64 mmol of monoketal [determined by ^{1}H NMR], 1.51 equiv.) and the yellow solution heated to 80 °C for 2 d. The suspension was cooled to 0 °C and filtered *via* cannula. The solid residue was washed with cold MeOH (0.5 mL). Drying *in vacuo* yielded **142** (465 mg, 673 μmol, 56%) as an off-white solid.

^{1}H NMR (300 MHz, $CDCl_3$): δ = 10.46 (br, 3H), 4.60 (s, 3H), 4.26 (s, 12H), 2.50 (q, J = 7.5 Hz, 12H), 2.02 (s, 18H), 1.07 (t, J = 7.5 Hz, 18H) ppm.

^{13}C{^{1}H} NMR (75 MHz, $CDCl_3$): δ = 159.9, 142.4, 133.3, 93.7, 45.2, 22.8, 20.2, 16.2 ppm.

HR-MS (ESI): calculated *m*/*z* for $C_{45}H_{67}N_6^+$ ($[M+H]^+$): 691.5427; found: 691.5432.

FTIR (ATR, neat): $\tilde{\nu}$ = 3049, 2964, 2920, 2914, 2899, 2872, 1617, 1546, 1484, 1431, 1365, 1327, 1272, 1232, 1104, 1090, 1073, 1055, 1025, 994, 937, 890, 875, 771, 721, 677, 654, 623, 608, 532, 522, 476, 428 cm^{-1}.

The analytical data is in accordance with the literature data.[460]

4.10.8 Synthesis of [Cu_3(142)] (203)

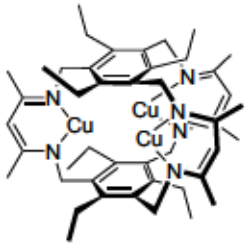

203 was prepared according to a literature procedure.[461]

To **142** (90.4 mg, 131 μmol, 1.00 equiv.) and KBn (57.9 mg, 445 μmol, 3.40 equiv.) under Ar was added dry THF (7.0 mL) and the reaction mixture stirred at r.t. for 15 min after which all volatiles were removed *in vacuo*. The atmosphere was exchanged to N_2 and the dark orange solid was dissolved in dry toluene (5.0 mL). $[CuOTf]_2 \cdot C_6H_6$ (101.1 mg, 201 μmol, 1.54 equiv.) dissolved in dry toluene (2.3 mL) was added and the resulting viscous red suspension was stirred at r.t. for 17 h. Filtration (cannula) of the reaction mixture and removal of all volatiles *in vacuo* yielded [Cu_3L] (58.2 mg, 66.2 μmol, 50%) as a red solid.

^{1}H NMR (300 MHz, C_6D_6): δ = 4.85 (s, 3H), 4.56 (s, 12H), 2.64 (q, J = 7.5 Hz, 12H), 2.08 (s, 18H), 1.16 (t, J = 7.5 Hz, 18H) ppm.

^{13}C{^{1}H} NMR (75 MHz, C_6D_6): δ = 164.9, 144.1, 138.0, 96.0, 49.4, 23.0, 22.7, 16.9 ppm.

Note: The absence of residual triflate was proven by no detectable signal in the ^{19}F{^{1}H} NMR. Furthermore, the reaction under N_2 atmosphere is reported to result in a dinitrogen-coordinated complex.[461] However, it is indicated that handling under vacuum results in removal of N_2 from the complex.[461] As only the synthesis has been conducted under N_2 atmosphere and all subsequent handling was performed under Ar after drying *in vacuo*, no N_2 incorporation is assumed for the complex described herein.

The analytical data is in accordance with the literature data.[461,462]

4.10.9 Synthesis of [Cu_3(142)(Se)] (139)

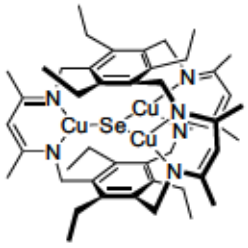

Synthesis of **139** according to a literature procedure[463] caused formation of significant amounts of free **142** due to unknown reasons. Thus, an alternative procedure for the synthesis of **139** is reported herein.

A solution of **203** (16.7 mg, 19.0 μmol, 1.00 equiv.) in dry THF (1.0 mL) was transferred onto red Se (2.2 mg, 27.9 μmol, 1.47 equiv.) and sonicated for 5 min. Volatiles were removed *in vacuo* and the brown solid residue extracted with dry hexane (2.0 mL) *via* syringe by filtration through a PTFE syringe filter. Volatiles were removed *in vacuo* to yield **139** (7.0 mg, 7.3 μmol, 38%) as a dark green solid that still contained minor quantities of **142** (and hexane) evident from ^{1}H NMR spectroscopy.

^{1}H NMR (400 MHz, C_6D_6): δ = 4.96 (s, 3H), 4.50 (s, 12H), 2.69 (q, J = 7.6 Hz, 12H), 2.06 (s, 18H), 1.13 (t, J = 7.6 Hz, 18H) ppm.

The analytical data is in accordance with the literature.[195]

4.10.10 General Procedure for CO_2 Reduction with 139 Utilizing KC_8 as Reducing Agent

This procedure is a modified version of the original literature protocol.[463]

A solution of **139** in dry THF was added to KC_8 (excess, 29-50 equiv.) in dry THF (final concentration 0.5-0.9 mM) under Ar. Three consecutive freeze-pump-thaw cycles were conducted with the reaction mixture. After the 3rd pump-step, the reaction mixture was opened to a CO_2 atmosphere for ~1 s while still being frozen in liquid N_2 (caution: prolonged opening causes deposition of solid CO_2 that could shatter the flask upon thawing!). The mixture was allowed to thaw in a water bath, opened to constant CO_2 pressure until at r.t. and closed. After stirring at r.t. overnight, the dark blue/purple solution was filtered off *via* Teflon cannula. The color of the solution changed from dark blue/purple to green during the filtration process. Volatiles were removed *in vacuo* and the resulting dark green solid analyzed by NMR spectroscopy.

The solid residue from the first filtration was extracted with dry MeOH (2×10 mL) and all volatiles removed *in vacuo*. Thus obtained solid residue was dissolved in D_2O (0.6 mL) and analyzed by capillary electrophoresis (0.03 mL or 0.2 mL) and NMR spectroscopy.

4.10.11 CO_2 Reduction with 139 and KC_8 - Results

Table S 21: Results for the CO_2 reduction with [Cu_3(**142**)Se] utilizing KC_8 as reducing agent.

Entry	[Cu] ([μmol])	KC_8 ([μmol])	Solvent ([mL])	*t* [h]	^{13}C NMR δ [ppm] ($C_2O_4^{2-}$/HCO_2^-/CO_3^{2-})	CE ($C_2O_4^{2-}$) approx. yield [%]†
1[a]	**139** (7)	362	THF (13.5)	17	x/171.0/168.3	7
2[a]	**139** (13)	385	THF (15)	17	x/171.0/168.3	2

Reactions were conducted according to the general procedure (4.10.10) unless stated otherwise. x = not observed. †Approximate oxalate yields stated were calculated without taking into account possible oxalate loss during the extraction procedure and might thus be lower than the true yield. [a]NMR spectroscopic analysis (in C_6D_6) of the solid residue obtained from the THF solution identified **142** and **139** as the main two species.

4.11 Single Crystal X-ray Diffraction

X-ray crystal structure analysis of compound **151**

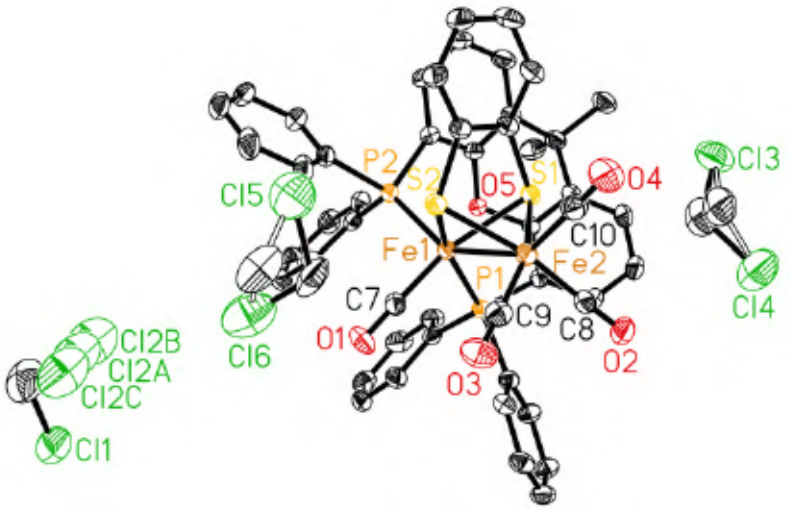

Figure S 7: Molecular structure of **151** (thermal ellipsoids are shown at 50% probability level and H atoms are omitted for clarity). The solvent molecules (CH_2Cl_2) are disordered (occupancies: Cl2A:Cl2B:Cl2C 0.5:0.3:0.2, C51A:C51B 0.6:0.4, C52A:C52B 0.3:0.2).

Table S 22: Crystal data and structure refinement for **151**.

Crystal description	Brown prism
Empirical formula	$C_{51.5}H_{41}Cl_5Fe_2O_5P_2S_2$
Formula weight	1154.85 g·mol^{-1}
Temperature	150(2) K
Wavelength	0.71073 Å
Crystal system	Monoclinic
Space group	$P2_1/n$
Unit cell dimensions	a = 14.7832(11) Å α = 90°
	b = 22.4173(16) Å β = 103.6673(13)°
	c = 15.6892(11) Å γ = 90°
Volume	5052.2(6) Å^3
Z	4
Density (calculated)	1.518 g·cm^{-3}
Absorption coefficient	1.032 mm^{-1}
F(000)	2356
Crystal size	0.30 × 0.28 × 0.21 mm
Θ range for data collection	1.684 to 27.999°
Index ranges	$-19 \leq h \leq 19$, $-29 \leq k \leq 29$, $-20 \leq l \leq 20$
Reflections collected	116535
Independent reflections	12187 [R_{int} = 0.0328]

Data / restraints / parameters	12187 / 44 / 636
Goodness-of-fit on F^2	1.041
Final R indices [I>2σ(I)]	R_1 = 0.0490, wR_2 = 0.1422
R indices (all data)	R_1 = 0.0591, wR_2 = 0.1555
Largest diff. peak/hole	1.726 and −1.314 e · Å^{-3}

Note that the highest peak in the difference Fourier map is located 1.38 Å from C51B and the deepest hole 0.6 Å from Cl1 (both located close to a disordered CH_2Cl_2).

X-ray crystal structure analysis of compound **152**

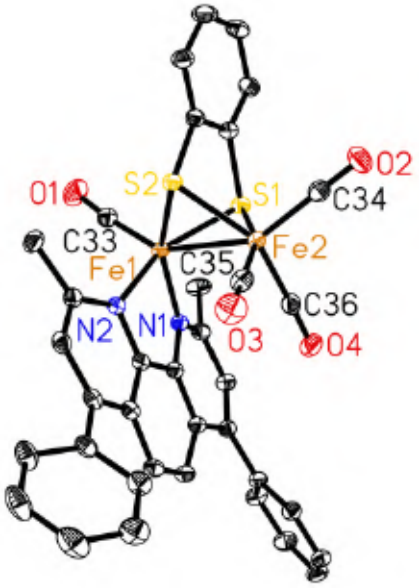

Figure S 8: Molecular structure of **152** (thermal ellipsoids are shown at 50% probability level and H atoms are omitted for clarity).

Table S 23: Crystal data and structure refinement for **152**.

Crystal description	Brown prism
Empirical formula	$C_{36}H_{24}Fe_2N_2O_4S_2$
Formula weight	724.39 g·mol^{-1}
Temperature	150(2) K
Wavelength	0.71073 Å
Crystal system	Triclinic
Space group	$P\bar{1}$
Unit cell dimensions	a = 10.5761(8) Å α = 98.1886(18)°
	b = 12.2528(9) Å β = 97.1056(18)°
	c = 14.1578(11) Å γ = 113.7770(17)°
Volume	1628.3(2) Å^3
Z	2
Density (calculated)	1.478 g·cm^{-3}

Absorption coefficient	1.062 mm^{-1}
F(000)	740
Crystal size	0.41 × 0.31 × 0.24 mm
Θ range for data collection	1.483 to 27.998°
Index ranges	$-13 \leq h \leq 13, -16 \leq k \leq 16, -18 \leq l \leq 18$
Reflections collected	73817
Independent reflections	7858 [R_{int} = 0.0250]
Data / restraints / parameters	7858 / 0 / 417
Goodness-of-fit on F^2	1.052
Final R indices [I>2σ(I)]	R_1 = 0.0251, wR_2 = 0.0646
R indices (all data)	R_1 = 0.0278, wR_2 = 0.0669
Largest diff. peak/hole	0.391 and –0.323 e · $Å^{-3}$

X-ray crystal structure analysis of compound **168**

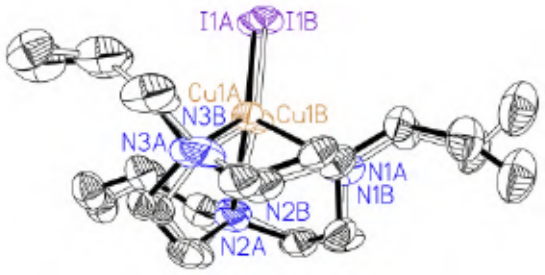

Figure S 9: Molecular structure of **168** (thermal ellipsoids are shown at 50% probability level, H atoms are omitted for clarity). **168** is disordered over two sites with occupancies of 0.531(6):0.469(6).

Table S 24: Crystal data and structure refinement for **168**.

Crystal description	Colorless needle
Empirical formula	$C_{15}H_{27}CuIN_3$
Formula weight	439.83 g·mol^{-1}
Temperature	150(2) K
Wavelength	1.54178 Å
Crystal system	Monoclinic
Space group	$P2_1/c$
Unit cell dimensions	a = 12.7569(4) Å α = 90°
	b = 16.9546(5) Å β = 100.087(2)°
	c = 8.6492(2) Å γ = 90°
Volume	1841.80(9) $Å^3$
Z	4
Density (calculated)	1.586 g·cm^{-3}
Absorption coefficient	14.780 mm^{-1}

F(000)	880
Crystal size	0.30 × 0.05 × 0.04 mm
Θ range for data collection	3.519 to 66.594°
Index ranges	$-15 \leq h \leq 14$, $-20 \leq k \leq 19$, $-10 \leq l \leq 10$
Reflections collected	14337
Independent reflections	3260 [R_{int} = 0.0387]
Data / restraints / parameters	3260 / 102 / 320
Goodness-of-fit on F^2	1.019
Final R indices [I>2σ(I)]	R_1 = 0.0258, wR_2 = 0.0643
R indices (all data)	R_1 = 0.0302, wR_2 = 0.0670
Largest diff. peak/hole	0.528 and –0.276 e · Å^{-3}

X-ray crystal structure analysis of compound **169**

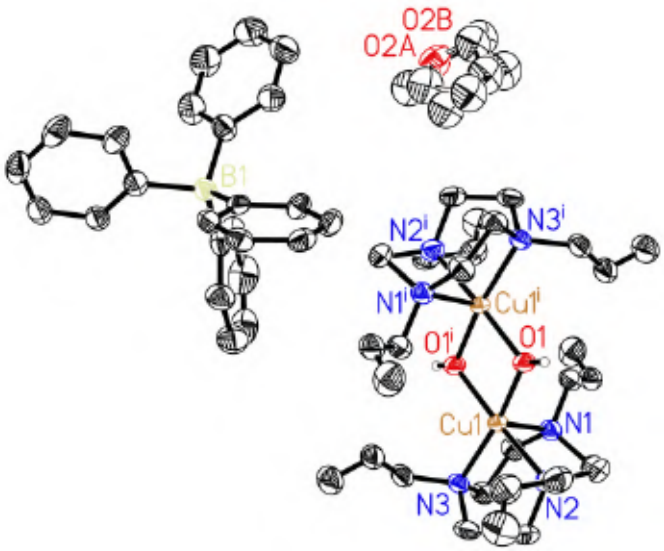

Figure S 10: Molecular structure of **169** (thermal ellipsoids are shown at 50% probability level and C-bound H atoms are omitted for clarity; symmetry code to generate equivalent atoms (i): –x+1, –y+1, –z+1). The solvent molecule (THF) is disordered over two sites with occupancies of 0.520(8):0.480(8).

Table S 25: Crystal data and structure refinement for **169**.

Crystal description	Blue prism
Empirical formula	$C_{86}H_{112}B_2Cu_2N_6O_4$
Formula weight	1442.51 g·mol^{-1}
Temperature	150(2) K
Wavelength	0.71073 Å
Crystal system	Monoclinic
Space group	$P2_1/n$
Unit cell dimensions	a = 17.7104(4) Å α = 90°

	b = 12.0392(4) Å β = 92.184(2)°
	c = 20.4805(4) Å γ = 90°
Volume	4363.7(2) Å^3
Z	2
Density (calculated)	1.098 g·cm^{-3}
Absorption coefficient	0.535 mm^{-1}
F(000)	1540
Crystal size	0.40 × 0.22 × 0.17 mm
Θ range for data collection	1.492 to 27.998°
Index ranges	$-23 \leq h \leq 23$, $-15 \leq k \leq 15$, $-27 \leq l \leq 27$
Reflections collected	73772
Independent reflections	10530 [R_{int} = 0.0542]
Data / restraints / parameters	10530 / 136 / 465
Goodness-of-fit on F^2	0.908
Final R indices [I>2σ(I)]	R_1 = 0.0475, wR_2 = 0.1245
R indices (all data)	R_1 = 0.0728, wR_2 = 0.1321
Largest diff. peak/hole	0.704 and –0.546 e · Å^{-3}

X-ray crystal structure analysis of compound **170**

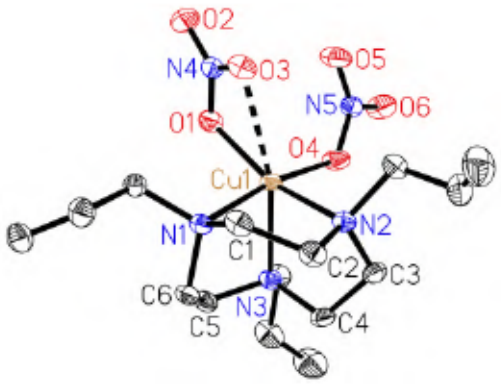

Figure S 11: Molecular structure of **170** (thermal ellipsoids are shown at 50% probability level and H atoms are omitted for clarity).

Table S 26: Crystal data and structure refinement for **170**.

Crystal description	Part of a blue needle
Empirical formula	$C_{15}H_{27}CuN_5O_6$
Formula weight	436.95 g·mol^{-1}
Temperature	150(2) K
Wavelength	0.71073 Å
Crystal system	Monoclinic
Space group	$P2_1/n$

Unit cell dimensions	a = 8.8043(4) Å α = 90°
	b = 19.7822(8) Å β = 90.7192(17)°
	c = 11.0839(5) Å γ = 90°
Volume	1930.31(15) Å^3
Z	4
Density (calculated)	1.504 g·cm^{-3}
Absorption coefficient	1.173 mm^{-1}
F(000)	916
Crystal size	0.21 × 0.14 × 0.12 mm
Θ range for data collection	2.059 to 27.993°
Index ranges	$-11 \leq h \leq 11$, $-26 \leq k \leq 26$, $-14 \leq l \leq 14$
Reflections collected	42129
Independent reflections	4664 [R_{int} = 0.0268]
Data / restraints / parameters	4664 / 0 / 244
Goodness-of-fit on F^2	1.019
Final R indices [I>2σ(I)]	R_1 = 0.0243, wR_2 = 0.0637
R indices (all data)	R_1 = 0.0288, wR_2 = 0.0665
Largest diff. peak/hole	0.353 and –0.186 e · Å^{-3}

X-ray crystal structure analysis of compound **171**

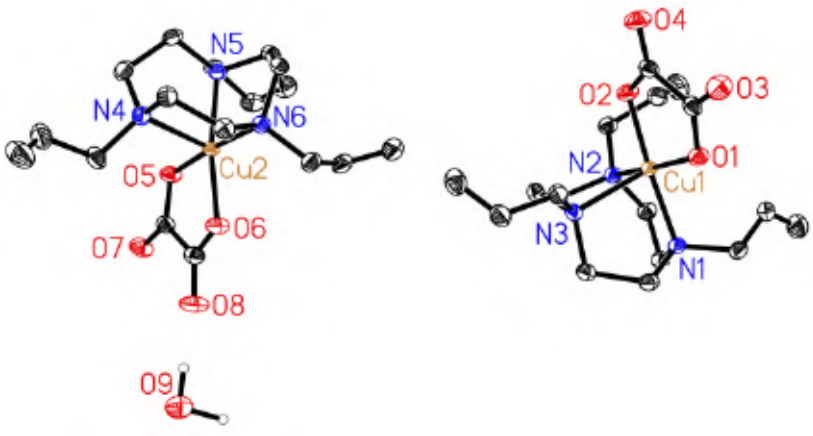

Figure S 12: Molecular structure of **171** (thermal ellipsoids are shown at 50% probability level and C-bound H atoms are omitted for clarity).

Table S 27: Crystal data and structure refinement for **171**.

Crystal description	Part of a blue plate
Empirical formula	$C_{17}H_{28}CuN_3O_{4.5}$
Formula weight	409.96 g·mol^{-1}
Temperature	150(2) K
Wavelength	1.54178 Å
Crystal system	Monoclinic
Space group	$P2_1/c$
Unit cell dimensions	a = 13.4227(7) Å α = 90°
	b = 15.7896(8) Å β = 94.6505(18)°
	c = 17.7903(9) Å γ = 90°
Volume	3758.0(3) Å^3
Z	8
Density (calculated)	1.449 g·cm^{-3}
Absorption coefficient	1.895 mm^{-1}
F(000)	1728
Crystal size	0.38 × 0.07 × 0.04 mm
Θ range for data collection	3.303 to 66.684°
Index ranges	$-15 \leq h \leq 15$, $-18 \leq k \leq 18$, $-21 \leq l \leq 21$
Reflections collected	45183
Independent reflections	6641 [R_{int} = 0.0363]
Data / restraints / parameters	6641 / 0 / 468
Goodness-of-fit on F^2	1.027
Final R indices [I>2σ(I)]	R_1 = 0.0281, wR_2 = 0.0753
R indices (all data)	R_1 = 0.0316, wR_2 = 0.0786
Largest diff. peak/hole	0.346 and –0.251 e · Å^{-3}

X-ray crystal structure analysis of compound **172**

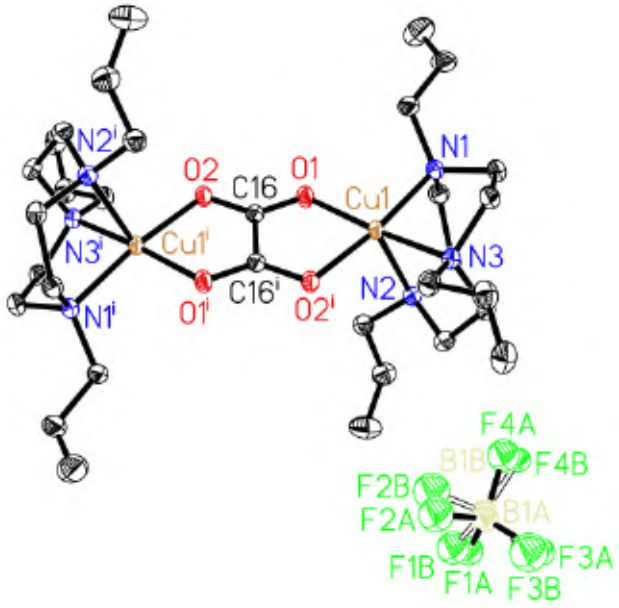

Figure S 13: Molecular structure of **172** (thermal ellipsoids are shown at 50% probability level and H atoms are omitted for clarity; symmetry code to generate equivalent atoms (i): –x, 1–y, 1–z). The BF_4 anion is disordered over two sites with occupancies of 0.66(2):0.34(2).

Table S 28: Crystal data and structure refinement for **172**.

Crystal description	Blue prism
Empirical formula	$C_{32}H_{54}B_2Cu_2F_8N_6O_4$
Formula weight	887.51 g·mol^{-1}
Temperature	150(2) K
Wavelength	0.71073 Å
Crystal system	Triclinic
Space group	$P\bar{1}$
Unit cell dimensions	a = 8.9959(3) Å α = 74.7062(12)°
	b = 9.6236(4) Å β = 77.7155(11)°
	c = 12.4608(4) Å γ = 70.1423(11)°
Volume	969.63(6) Å^3
Z	1
Density (calculated)	1.520 g·cm^{-3}
Absorption coefficient	1.179 mm^{-1}
F(000)	460
Crystal size	0.34 × 0.13 × 0.07 mm
Θ range for data collection	2.301 to 27.999°
Index ranges	$-11 \leq h \leq 11, -12 \leq k \leq 12, -16 \leq l \leq 16$
Reflections collected	36282
Independent reflections	4682 [R_{int} = 0.0273]

Data / restraints / parameters	4682 / 28 / 240
Goodness-of-fit on F^2	1.036
Final R indices [I>2σ(I)]	R_1 = 0.0376, wR_2 = 0.0919
R indices (all data)	R_1 = 0.0431, wR_2 = 0.0963
Largest diff. peak/hole	1.042 and –0.999 e · Å^{-3}

X-ray crystal structure analysis of compound **173**

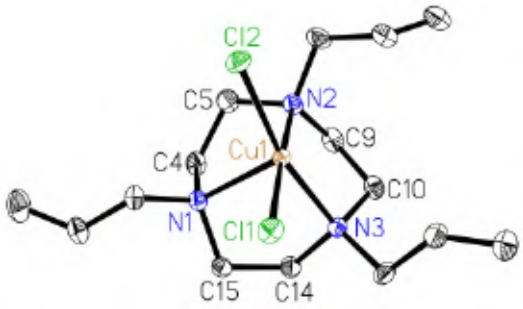

Figure S 14: Molecular structure of **173** (thermal ellipsoids are shown at 50% probability level and H atoms are omitted for clarity).

Table S 29: Crystal data and structure refinement for **173**.

Crystal description	Green prism
Empirical formula	$C_{15}H_{27}Cl_2CuN_5$
Formula weight	383.83 g·mol^{-1}
Temperature	150(2) K
Wavelength	0.71073 Å
Crystal system	Orthorhombic
Space group	$P2_12_12_1$
Unit cell dimensions	a = 8.3314(5) Å α = 90°
	b = 12.7118(7) Å β = 90°
	c = 16.5149(9) Å γ = 90°
Volume	1749.05(17) Å^3
Z	4
Density (calculated)	1.458 g·cm^{-3}
Absorption coefficient	1.552 mm^{-1}
F(000)	804
Crystal size	0.48 × 0.31 × 0.24 mm
Θ range for data collection	2.022 to 28.996°
Index ranges	$-11 \leq h \leq 11$, $-17 \leq k \leq 17$, $-22 \leq l \leq 16$
Reflections collected	22334
Independent reflections	4668 [R_{int} = 0.0225]
Data / restraints / parameters	4668 / 0 / 190

Goodness-of-fit on F^2	1.039
Final R indices [I>2σ(I)]	R_1 = 0.0189, wR_2 = 0.0488
R indices (all data)	R_1 = 0.0195, wR_2 = 0.0492
Largest diff. peak/hole	0.333 and –0.366 e · Å^{-3}

X-ray crystal structure analysis of compound **176**

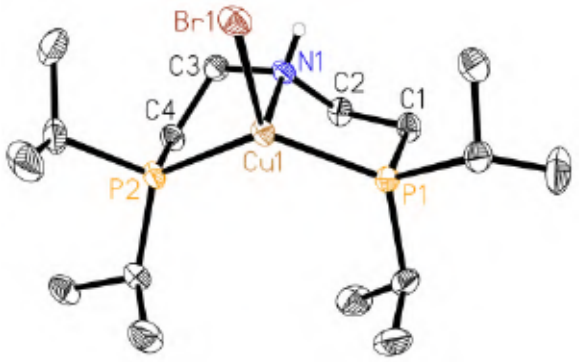

Figure S 15: Molecular structure of **176** (thermal ellipsoids are shown at 50% probability level and C-bound H atoms are omitted for clarity).

Table S 30: Crystal data and structure refinement for **176**.

Crystal description	Colorless prism
Empirical formula	$C_{16}H_{37}BrCuNP_2$
Formula weight	448.85 g·mol^{-1}
Temperature	150(2) K
Wavelength	0.71073 Å
Crystal system	Monoclinic
Space group	$P2_1/c$
Unit cell dimensions	a = 10.0743(10) Å α = 90°
	b = 13.7219(14) Å β = 102.1220(18)°
	c = 15.7700(16) Å γ = 90°
Volume	2131.4(4) Å^3
Z	4
Density (calculated)	1.399 g·cm^{-3}
Absorption coefficient	3.045 mm^{-1}
F(000)	936
Crystal size	0.35 × 0.29 × 0.21 mm
Θ range for data collection	1.987 to 27.996°
Index ranges	$-13 \leq h \leq 13$, $-18 \leq k \leq 18$, $-20 \leq l \leq 20$
Reflections collected	45576
Independent reflections	5145 [R_{int} = 0.0328]
Data / restraints / parameters	5145 / 0 / 202

Goodness-of-fit on F^2	1.036
Final R indices [I>2σ(I)]	R_1 = 0.0210, wR_2 = 0.0510
R indices (all data)	R_1 = 0.0257, wR_2 = 0.0528
Largest diff. peak/hole	0.434 and –0.285 e · Å^{-}3

X-ray crystal structure analysis of compound **177**

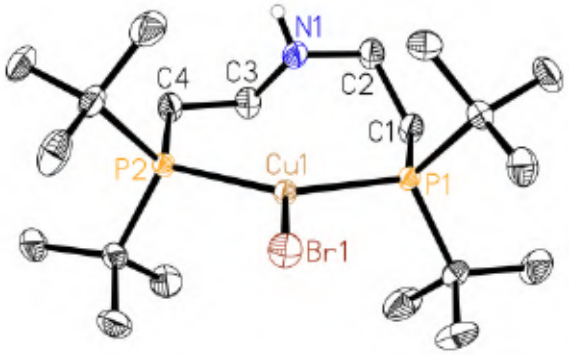

Figure S 16: Molecular structure of **177** (thermal ellipsoids are shown at 50% probability level and C-bound H atoms are omitted for clarity).

Table S 31: Crystal data and structure refinement for **177**.

Crystal description	Colorless plate
Empirical formula	$C_{20}H_{45}BrCuNP_2$
Formula weight	504.96 g·mol^{-1}
Temperature	150(2) K
Wavelength	0.71073 Å
Crystal system	Monoclinic
Space group	$P2_1/n$
Unit cell dimensions	a=8.5466(5) Å α= 90°
	b=21.4368(12) Å β=92.8766(9)°
	c=13.6316(7) Å γ=90°
Volume	2494.3(2) Å^3
Z	4
Density (calculated)	1.345 g·cm^{-}3
Absorption coefficient	2.610 mm^{-1}
F(000)	1064
Crystal size	0.34 × 0.28 × 0.08 mm
Θ range for data collection	1.772 to 28.000°
Index ranges	$-11 \leq h \leq 11$, $-28 \leq k \leq 28$, $-17 \leq l \leq 17$
Reflections collected	47961
Independent reflections	6022 [R_{int} = 0.0276]

Data / restraints / parameters	6022 / 0 / 242
Goodness-of-fit on F^2	1.026
Final R indices [I>2σ(I)]	R_1 = 0.0199, wR_2 = 0.0492
R indices (all data)	R_1 = 0.0243, wR_2 = 0.0516
Largest diff. peak/hole	0.462 and –0.220 e · Å^{-3}

X-ray crystal structure analysis of compound **178**

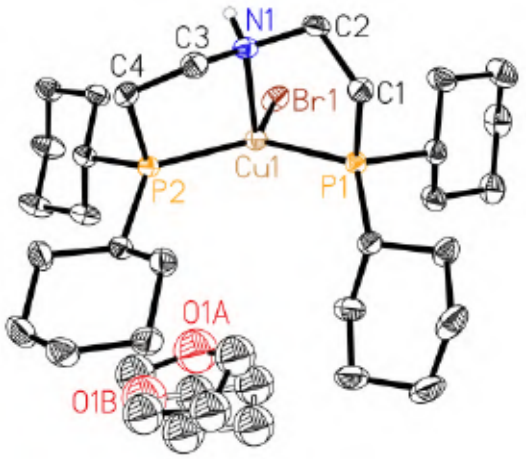

Figure S 17: Molecular structure of **178** (thermal ellipsoids are shown at 50% probability level and C-bound H atoms are omitted for clarity). The solvent molecule (THF) is disordered over two sites with occupancies of 0.7:0.3.

Table S 32: Crystal data and structure refinement for **178**.

Crystal description	Colorless needle
Empirical formula	$C_{32}H_{61}BrCuNOP_2$
Formula weight	681.20 g·mol^{-1}
Temperature	150(2) K
Wavelength	0.71073 Å
Crystal system	Triclinic
Space group	$P\bar{1}$
Unit cell dimensions	a = 9.2817(5) Å α = 71.8879(14)°
	b = 11.5019(7) Å β = 86.0092(14)°
	c = 17.4052(10) Å γ = 74.9191(14)°
Volume	1705.11(17) Å^3
Z	2
Density (calculated)	1.327 g·cm^{-3}
Absorption coefficient	1.930 mm^{-1}
F(000)	724
Crystal size	0.50 × 0.17 × 0.11 mm
Θ range for data collection	1.925 to 27.999°

Index ranges	$-12 \leq h \leq 12$, $-15 \leq k \leq 15$, $-22 \leq l \leq 22$
Reflections collected	89796
Independent reflections	8233 [R_{int} = 0.0297]
Data / restraints / parameters	8233 / 19 / 334
Goodness-of-fit on F^2	1.035
Final R indices [I>2σ(I)]	R_1 = 0.0325, wR_2 = 0.0855
R indices (all data)	R_1 = 0.0379, wR_2 = 0.0895
Largest diff. peak/hole	1.010 and −1.023 e · Å^{-3}

X-ray crystal structure analysis of compound **179**

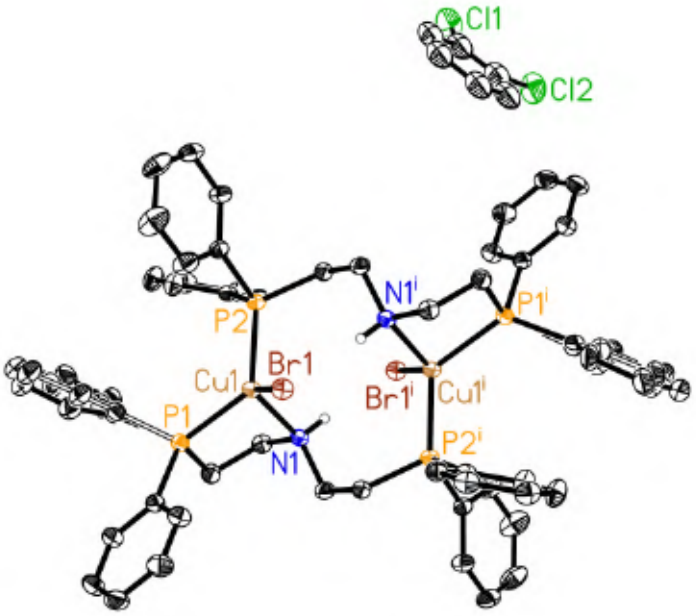

Figure S 18: Molecular structure of **179** (thermal ellipsoids are shown at 50% probability level and C-bound H atoms are omitted for clarity; symmetry code to generate equivalent atoms (i): –x+2, –y+2, –z+1). One of the P1-bound phenyl groups is disordered over two sites with occupancies of 0.50(2):0.50(2).

Table S 33: Crystal data and structure refinement for **179**.

Crystal description	Part of a colorless plate
Empirical formula	$C_{62}H_{62}Br_2Cl_2Cu_2N_2P_4$
Formula weight	1316.81 g·mol^{-1}
Temperature	150(2) K
Wavelength	0.71073 Å
Crystal system	Triclinic
Space group	$P\bar{1}$
Unit cell dimensions	a = 9.2467(3) Å α = 88.1421(14)°
	b = 9.9565(4) Å β = 77.2595(14)°

	c = 16.5489(6) Å γ = 78.5798(13)°
Volume	1456.54(9) Å^3
Z	1
Density (calculated)	1.501 g·cm^{-3}
Absorption coefficient	2.344 mm^{-1}
F(000)	670
Crystal size	0.29 × 0.15 × 0.11 mm
Θ range for data collection	2.087 to 27.999°
Index ranges	$-12 \leq h \leq 12$, $-13 \leq k \leq 13$, $-21 \leq l \leq 21$
Reflections collected	53285
Independent reflections	7023 [R_{int} = 0.0282]
Data / restraints / parameters	7023 / 181 / 362
Goodness-of-fit on F^2	1.030
Final R indices [I>2σ(I)]	R_1 = 0.0281, wR_2 = 0.0734
R indices (all data)	R_1 = 0.0338, wR_2 = 0.0771
Largest diff. peak/hole	0.913 and –0.518 e · Å^{-3}

X-ray crystal structure analysis of compound **185**

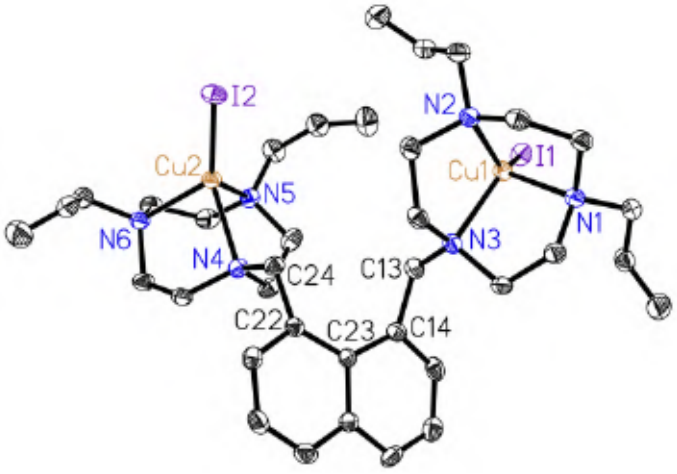

Figure S 19: Molecular structure of **185** (thermal ellipsoids are shown at 50% probability level and H atoms are omitted for clarity).

Table S 34: Crystal data and structure refinement for **185**.

Crystal description	Colorless plate
Empirical formula	$C_{36}H_{54}Cu_2I_2N_6$
Formula weight	951.73 g·mol^{-1}
Temperature	150(2) K
Wavelength	0.71073 Å
Crystal system	Triclinic
Space group	$P\bar{1}$

Unit cell dimensions	a = 12.5613(8) Å α = 113.3253(14)°
	b = 12.5988(8) Å β = 94.0461(16)°
	c = 14.7239(9) Å γ = 112.4090(14)°
Volume	1909.6(2) Å^3
Z	2
Density (calculated)	1.655 g·cm^{-3}
Absorption coefficient	2.763 mm^{-1}
F(000)	952
Crystal size	0.23 × 0.14 × 0.11 mm
Θ range for data collection	1.560 to 25.998°
Index ranges	$-15 \leq h \leq 15$, $-15 \leq k \leq 15$, $-18 \leq l \leq 18$
Reflections collected	63126
Independent reflections	7468 [R_{int} = 0.0298]
Data / restraints / parameters	7468 / 0 / 415
Goodness-of-fit on F^2	1.070
Final R indices [I>2σ(I)]	R_1 = 0.0273, wR_2 = 0.0716
R indices (all data)	R_1 = 0.0306, wR_2 = 0.0737
Largest diff. peak/hole	1.393 and –0.500 e · Å^{-3}

Note that the highest peak in the difference Fourier map is located 1.51 Å from I2 and the deepest hole 0.75 Å from I1.

X-ray crystal structure analysis of compound **191**

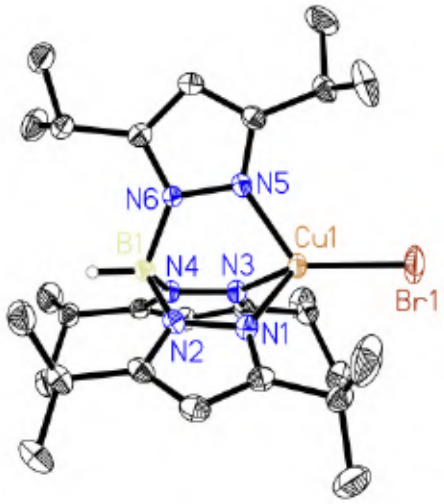

Figure S 20: Molecular structure of **191** (thermal ellipsoids are shown at 50% probability level and C-bound H atoms are omitted for clarity).

Table S 35: Crystal data and structure refinement for **191**.

Crystal description	Red prism
Empirical formula	$C_{27}H_{46}BBrCuN_6$
Formula weight	608.96 g·mol^{-1}
Temperature	150(2) K
Wavelength	0.71073 Å
Crystal system	Monoclinic
Space group	$P2_1/c$
Unit cell dimensions	a = 10.0419(8) Å α = 90°
	b = 16.3354(13) Å β = 101.9989(16)°
	c = 18.9924(14) Å γ = 90°
Volume	3047.4(4) Å^3
Z	4
Density (calculated)	1.327 g·cm^{-3}
Absorption coefficient	2.053 mm^{-1}
F(000)	1276
Crystal size	0.24 × 0.10 × 0.08 mm
Θ range for data collection	1.660 to 27.999°
Index ranges	$-13 \leq h \leq 13$, $-21 \leq k \leq 21$, $-24 \leq l \leq 25$
Reflections collected	55296
Independent reflections	7359 [R_{int} = 0.0568]
Data / restraints / parameters	7359 / 0 / 341
Goodness-of-fit on F^2	1.020
Final R indices [I>2σ(I)]	R_1 = 0.0394, wR_2 = 0.0841
R indices (all data)	R_1 = 0.0640, wR_2 = 0.0956
Largest diff. peak/hole	1.124 and –1.016 e · Å^{-3}

X-ray crystal structure analysis of compound **192**

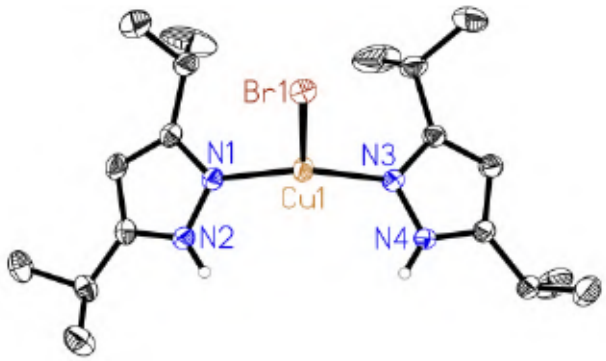

Figure S 21: Molecular structure of **192** (thermal ellipsoids are shown at 50% probability level and C-bound H atoms are omitted for clarity).

Table S 36: Crystal data and structure refinement for **192**.

Crystal description	Colorless prism
Empirical formula	$C_{18}H_{32}BrCuN_4$
Formula weight	447.92 g·mol^{-1}
Temperature	150(2) K
Wavelength	0.71073 Å
Crystal system	Triclinic
Space group	$P\bar{1}$
Unit cell dimensions	a = 9.5314(7) Å α = 75.6463(13)°
	b = 9.8578(8) Å β = 72.6924(13)°
	c = 12.5043(10) Å γ = 89.3814(13)°
Volume	1084.15(15) Å^3
Z	2
Density (calculated)	1.372 g·cm^{-3}
Absorption coefficient	2.857 mm^{-1}
F(000)	464
Crystal size	0.42 × 0.25 × 0.17 mm
Θ range for data collection	2.137 to 27.998°
Index ranges	$-12 \leq h \leq 12$, $-13 \leq k \leq 13$, $-16 \leq l \leq 16$
Reflections collected	43226
Independent reflections	5228 [R_{int} = 0.0217]
Data / restraints / parameters	5228 / 0 / 233
Goodness-of-fit on F^2	1.058
Final R indices [I>2σ(I)]	R_1 = 0.0210, wR_2 = 0.0528
R indices (all data)	R_1 = 0.0236, wR_2 = 0.0543
Largest diff. peak/hole	0.631 and –0.442 e · Å^{-3}

4.12 NMR Spectroscopic Analysis

4.12.1 NMR Spectra – Synthesized Compounds

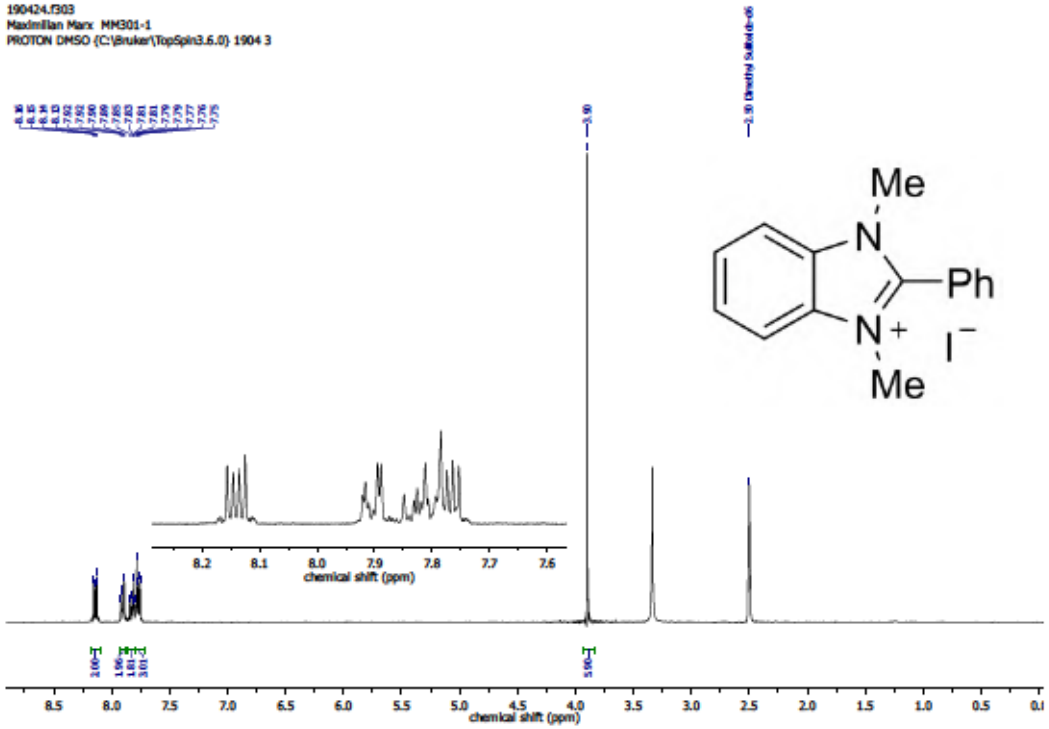

Figure S 22: ^{1}H NMR (300 MHz, DMSO-d_6) of 1,3-dimethyl-2-phenylbenzo[*d*]imidazolium iodide.

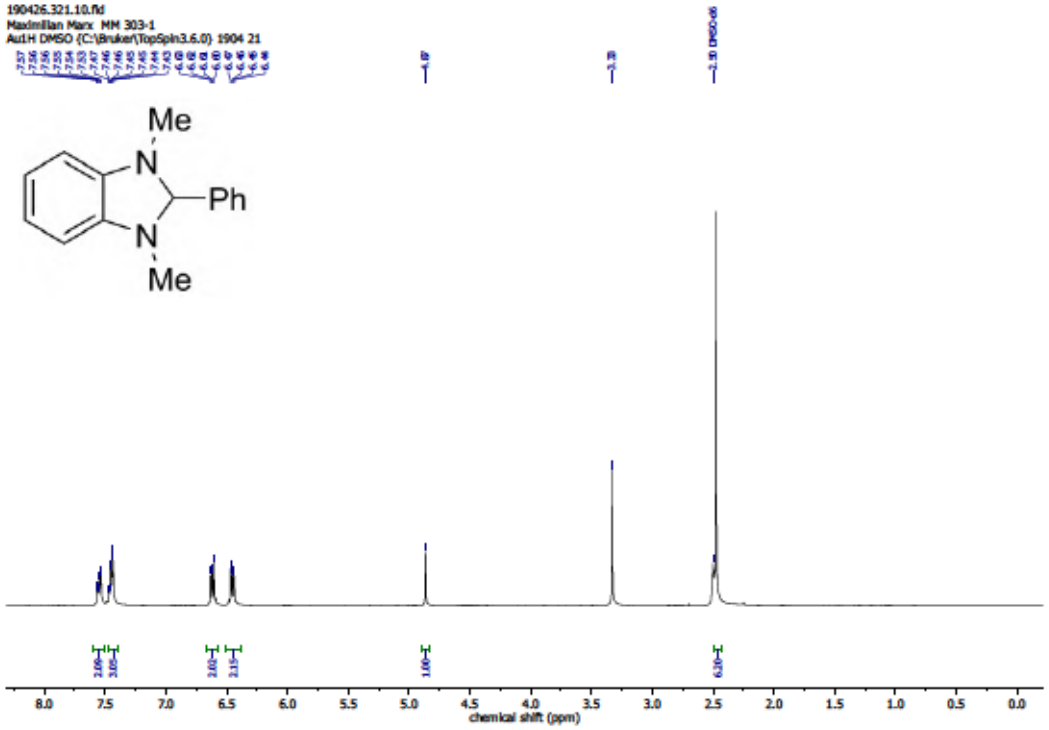

Figure S 23: ^{1}H NMR (300 MHz, DMSO-d_6) of **BIH**.

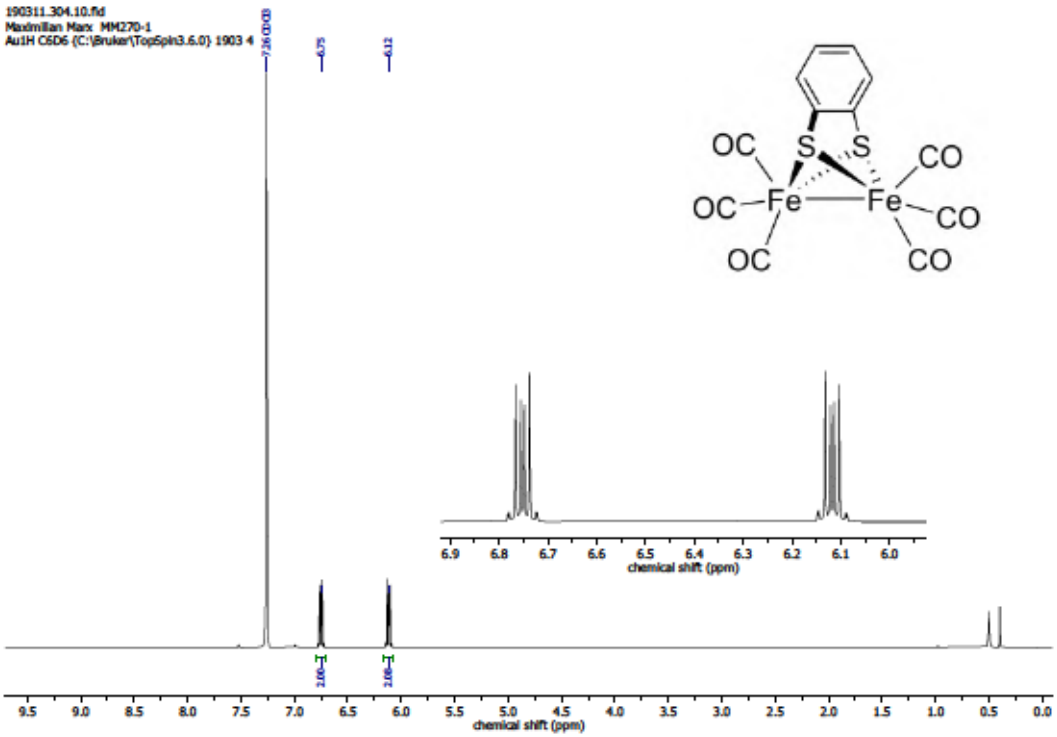

Figure S 24: ^{1}H NMR (300 MHz, C_6D_6) of **145**.

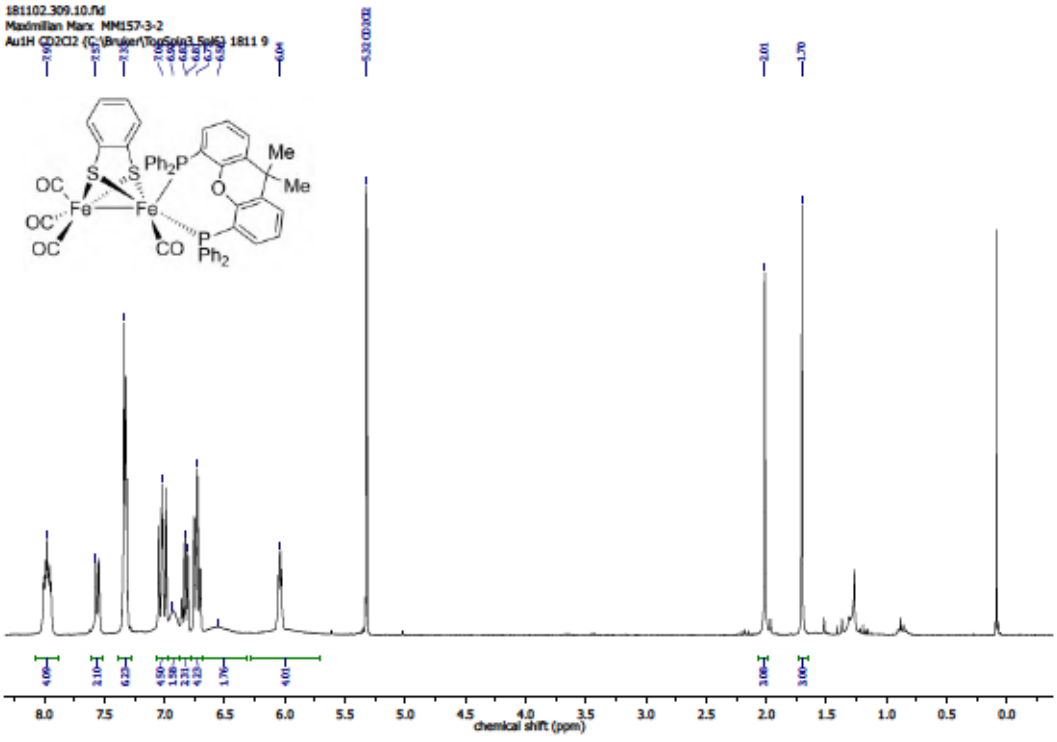

Figure S 25: ^{1}H NMR (300 MHz, CD_2Cl_2) of **151**.

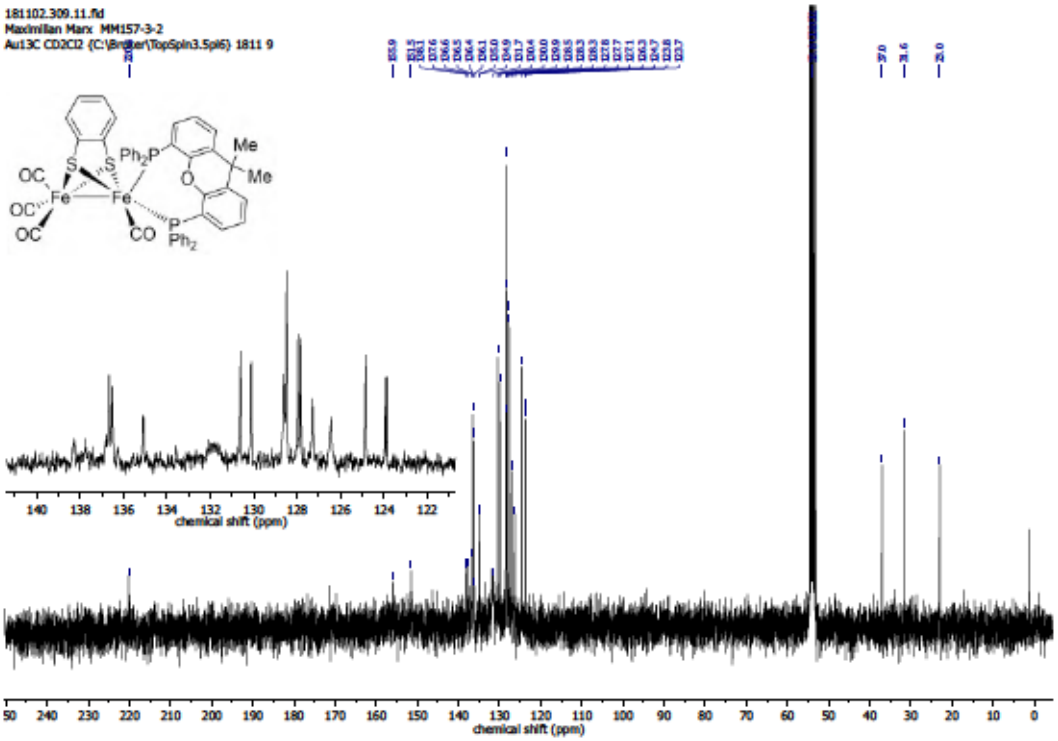

Figure S 26: $^{13}C\{^{1}H\}$ NMR (75 MHz, CD_2Cl_2) of **151**.

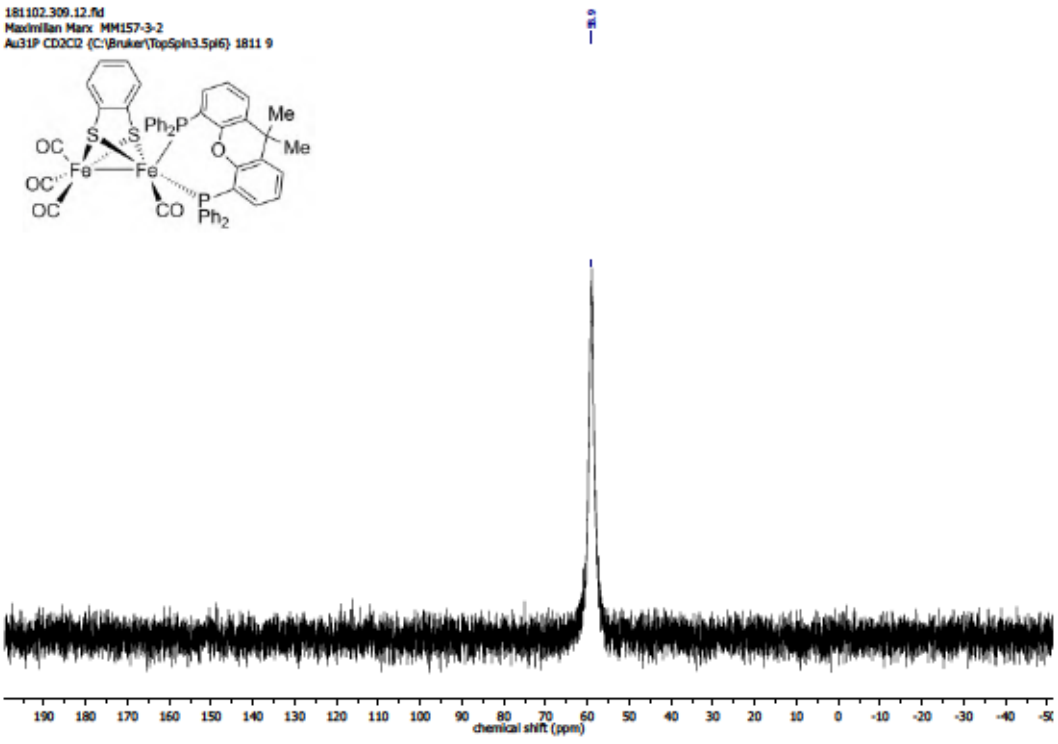

Figure S 27: $^{31}P\{^{1}H\}$ NMR (122 MHz, CD_2Cl_2) of **151**.

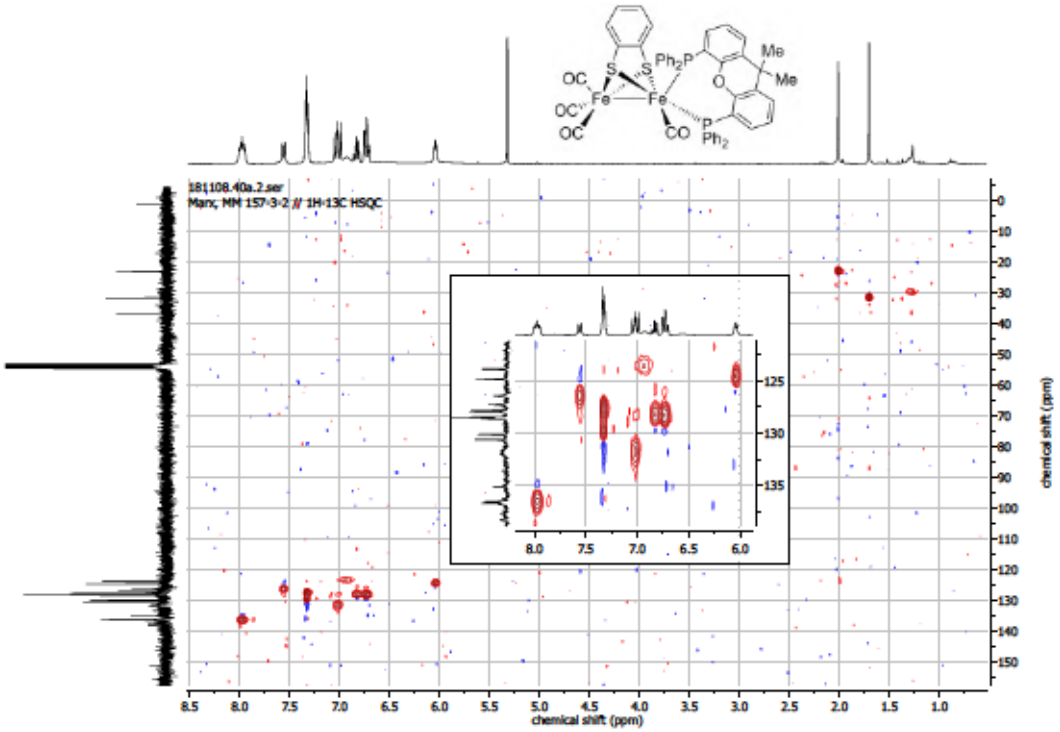

Figure S 28: (^{1}H,^{13}C) HSQC NMR (400 MHz, CD_2Cl_2) of **151**.

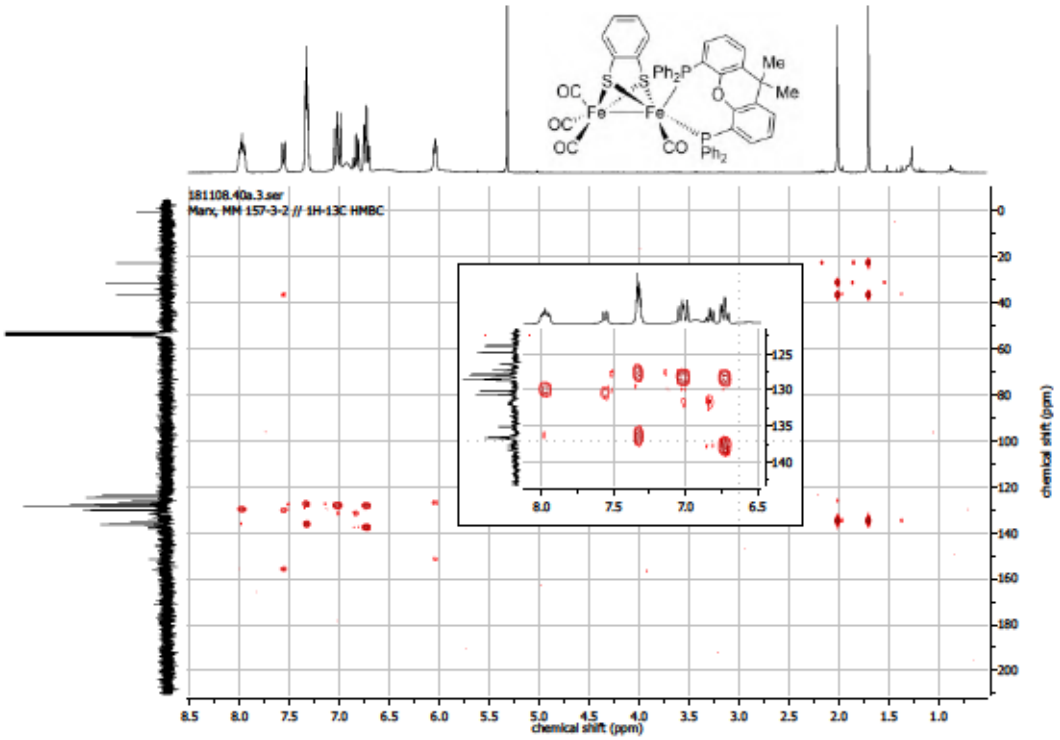

Figure S 29: (^{1}H,^{13}C) HMBC NMR (400 MHz, CD_2Cl_2) of **151**.

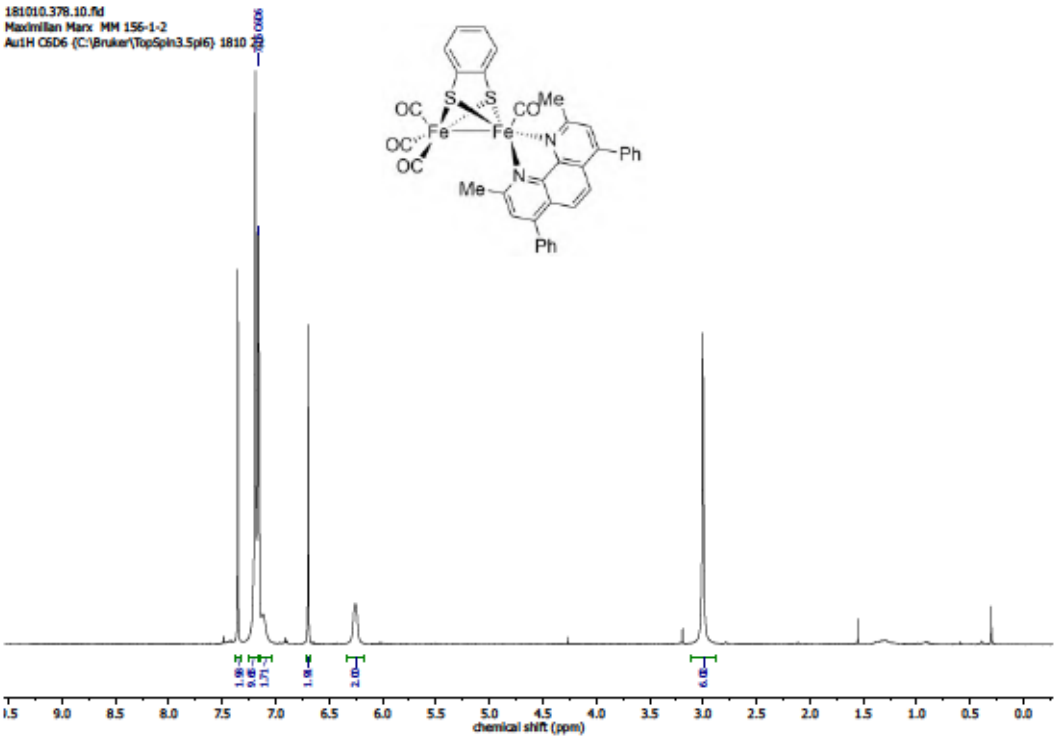

Figure S 30: ^{1}H NMR (300 MHz, C_6D_6) of **152**.

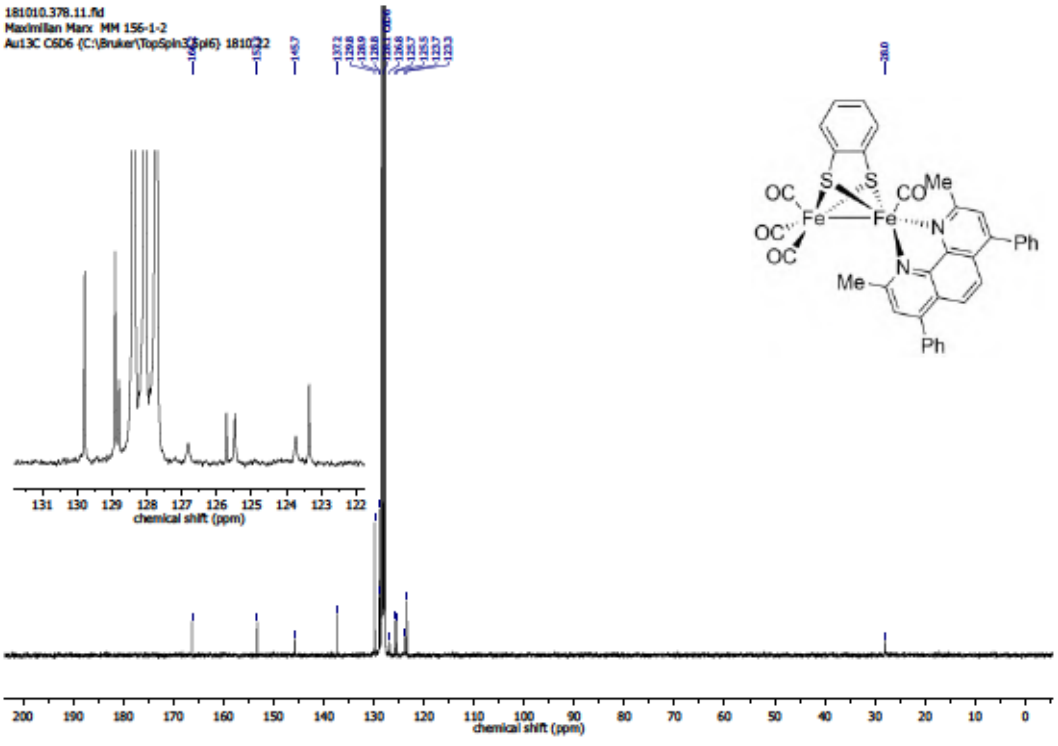

Figure S 31: $^{13}C\{^{1}H\}$ NMR (75 MHz, C_6D_6) of **152**.

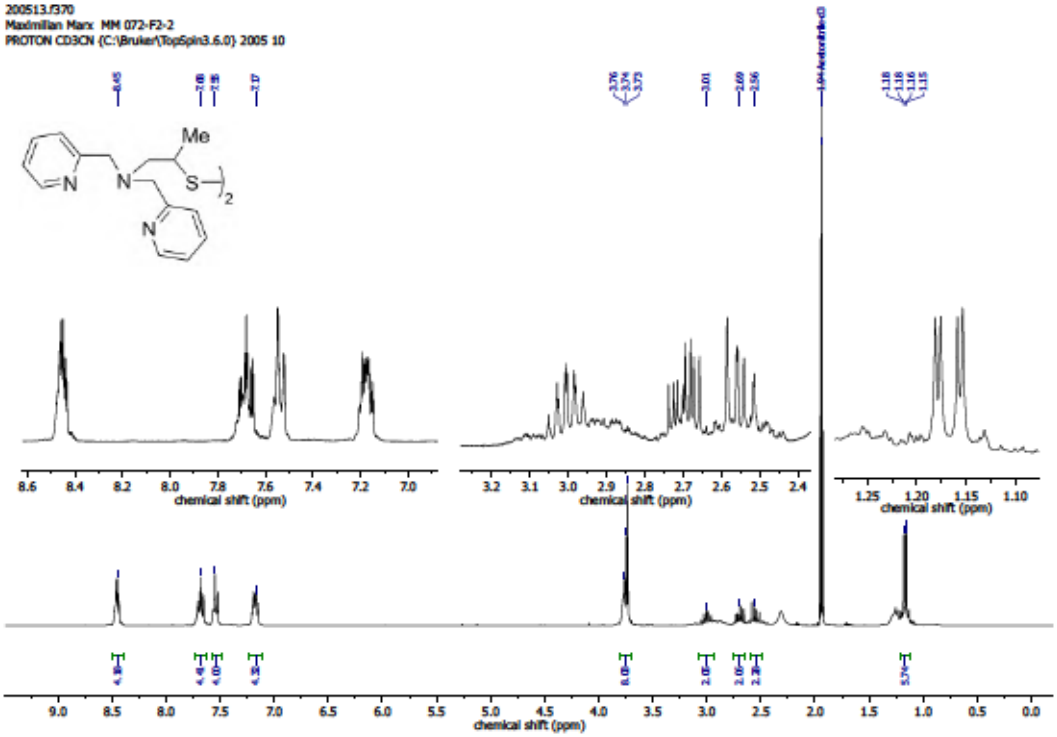

Figure S 32: ^{1}H NMR (300 MHz, CD_3CN) of **154**.

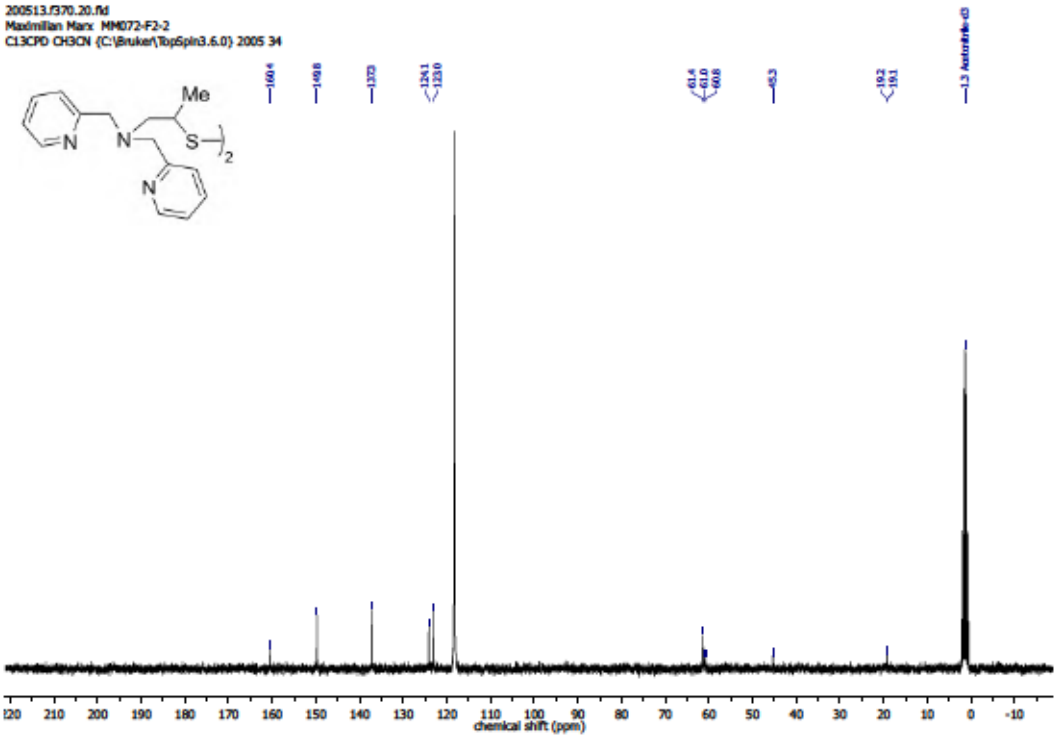

Figure S 33: $^{13}C\{^{1}H\}$ NMR (75 MHz, CD_3CN) of **154**.

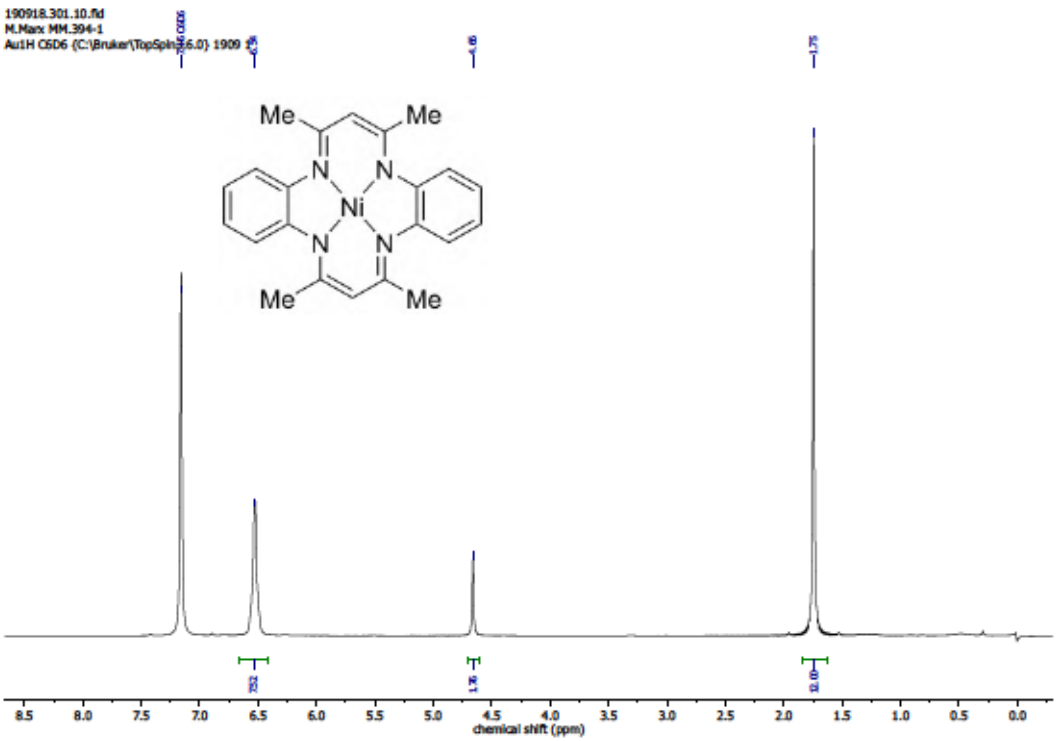

Figure S 34: ^{1}H NMR (300 MHz, C_6D_6) of **159**.

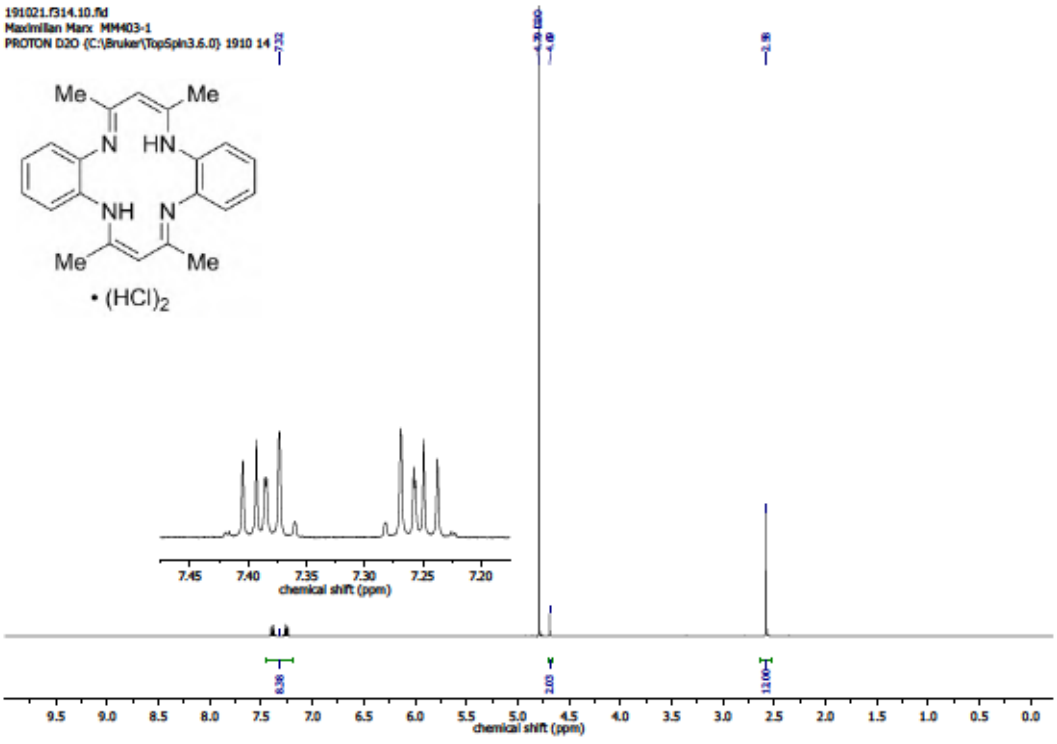

Figure S 35: ^{1}H NMR (300 MHz, D_2O) of **160**.

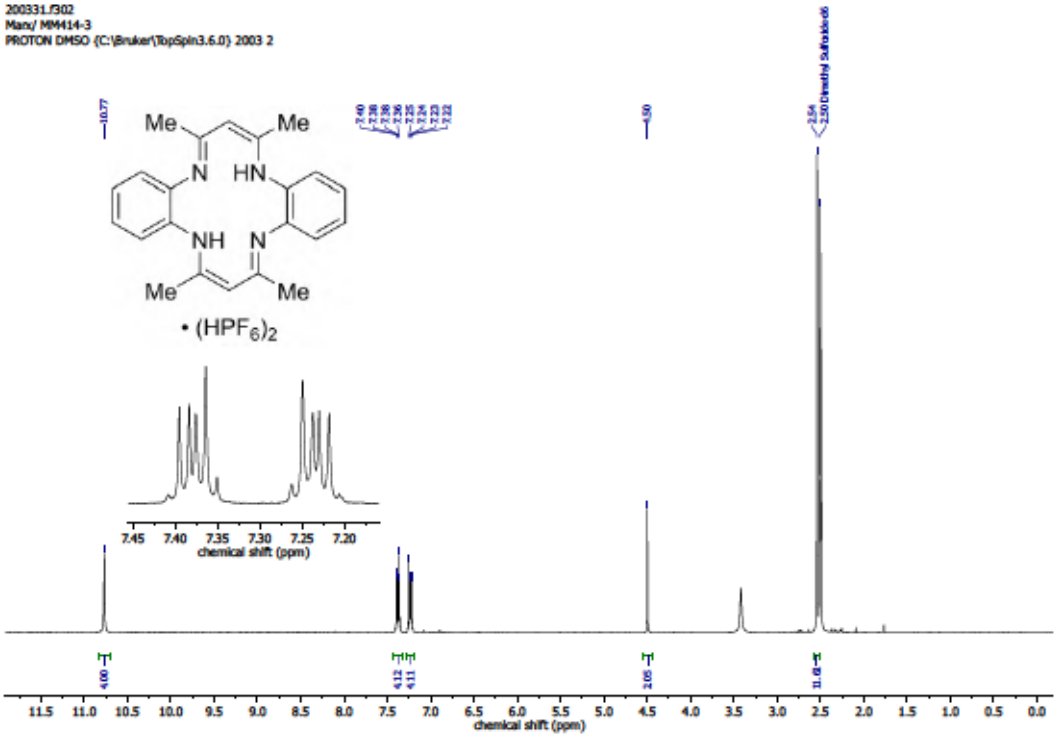

Figure S 36: ^{1}H NMR (300 MHz, DMSO-d_6) of **161**.

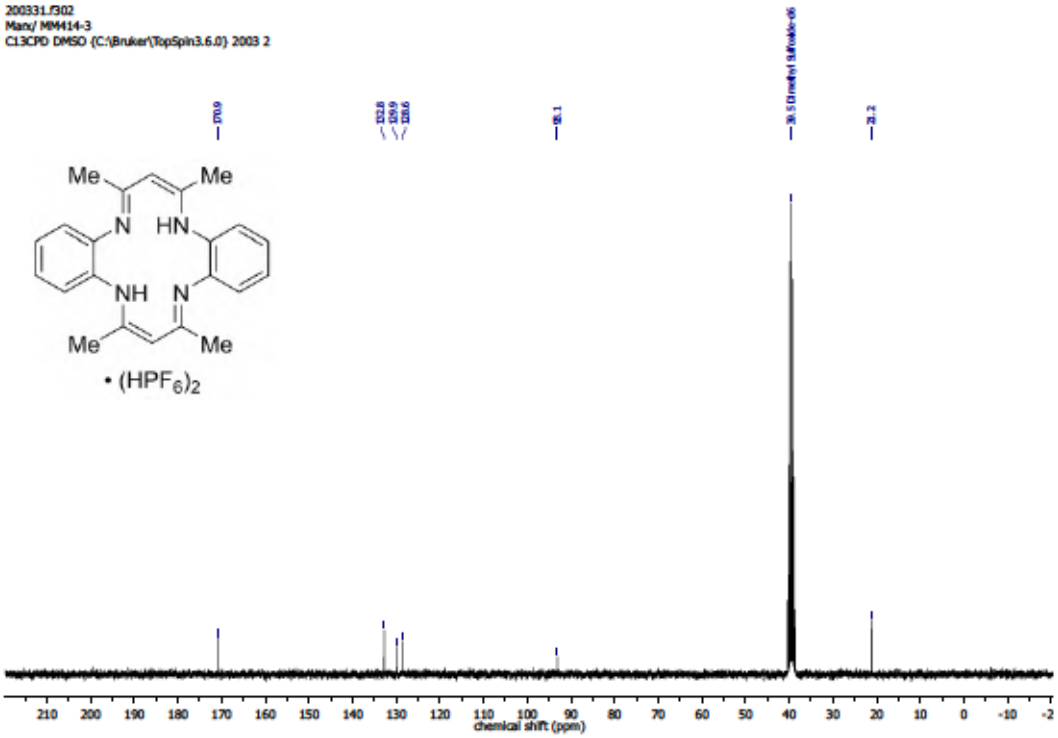

Figure S 37: ^{13}C{^{1}H} NMR (75 MHz, DMSO-d_6) of **161**.

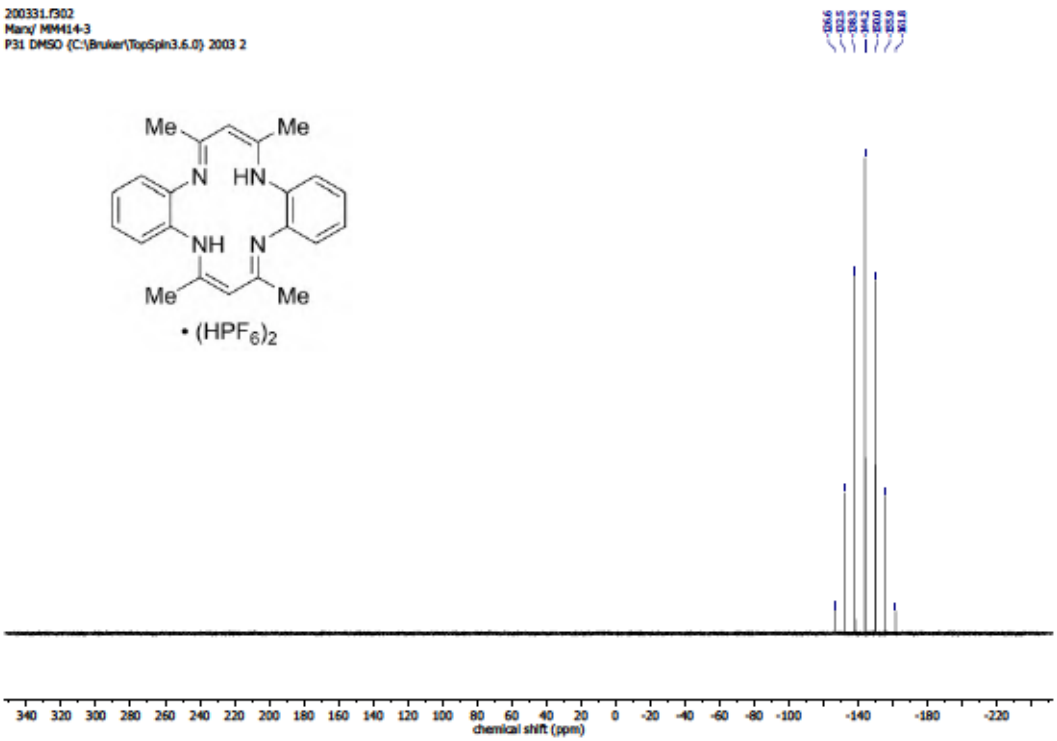

Figure S 38: $^{31}P\{^{1}H\}$ NMR (122 MHz, DMSO-d_6) of **161**.

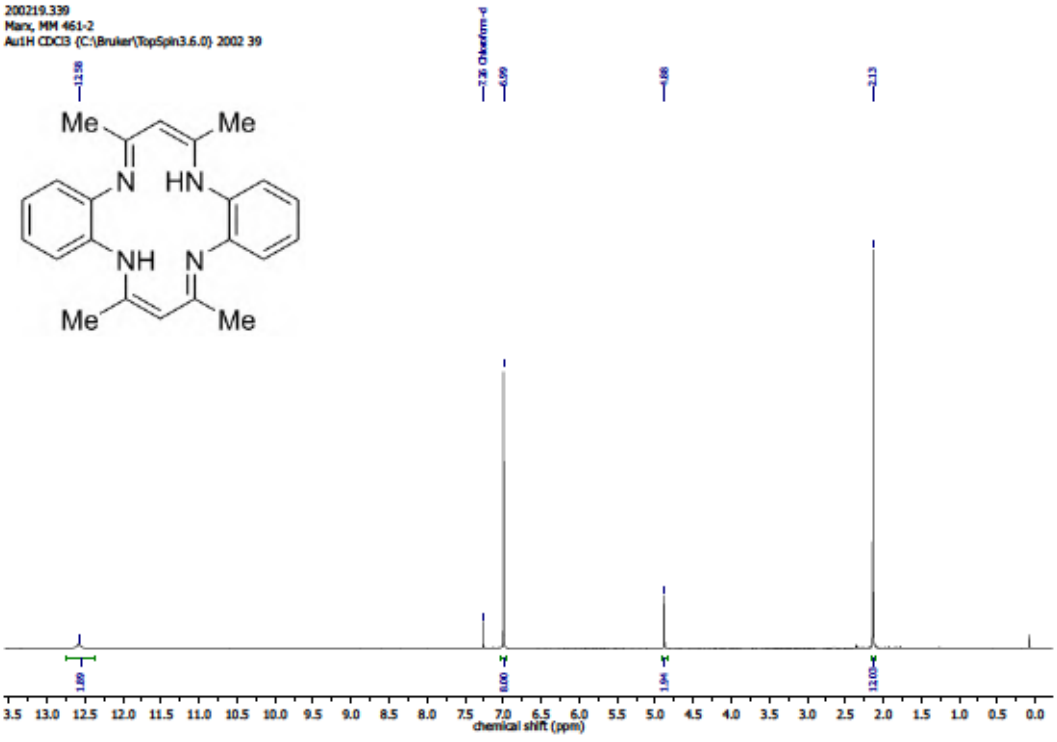

Figure S 39: ^{1}H NMR (300 MHz, $CDCl_3$) of **162**.

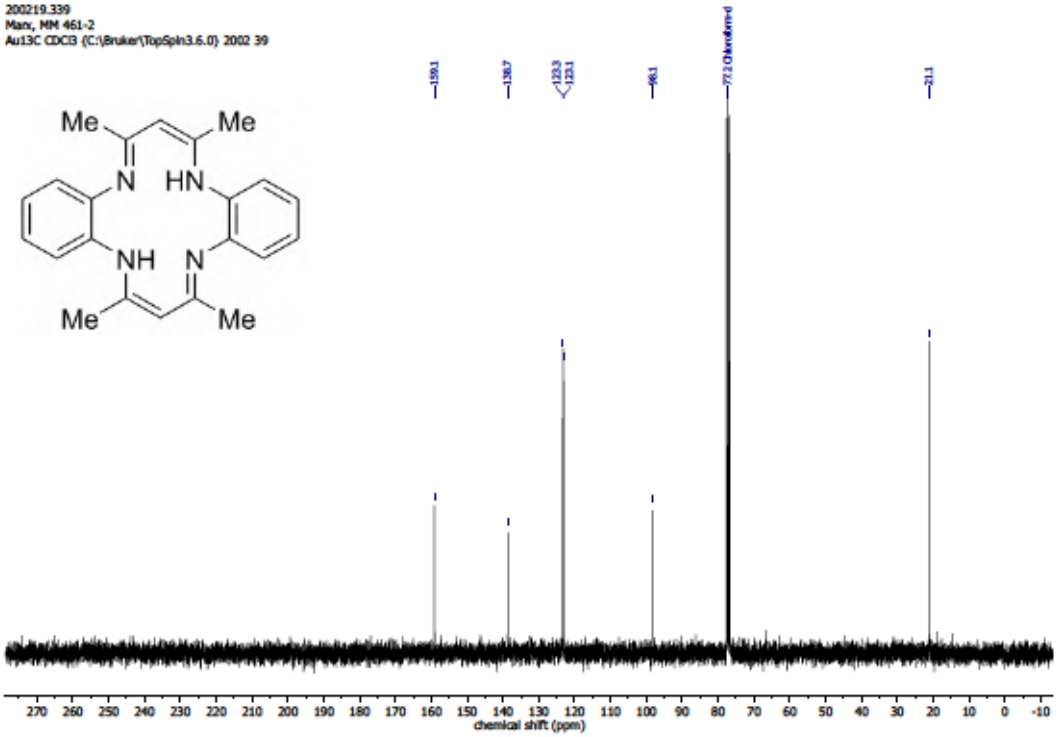

Figure S 40: $^{13}C\{^{1}H\}$ NMR (75 MHz, $CDCl_3$) of **162**.

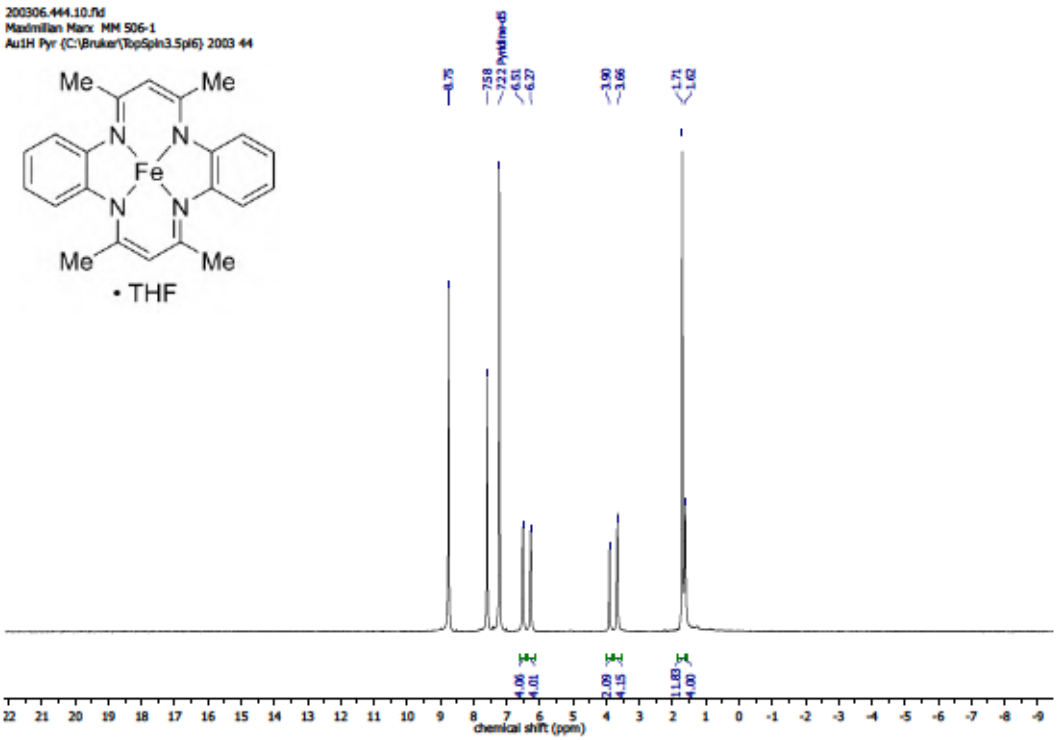

Figure S 41: ^{1}H NMR (400 MHz, pyridine-d_5) of **118**.

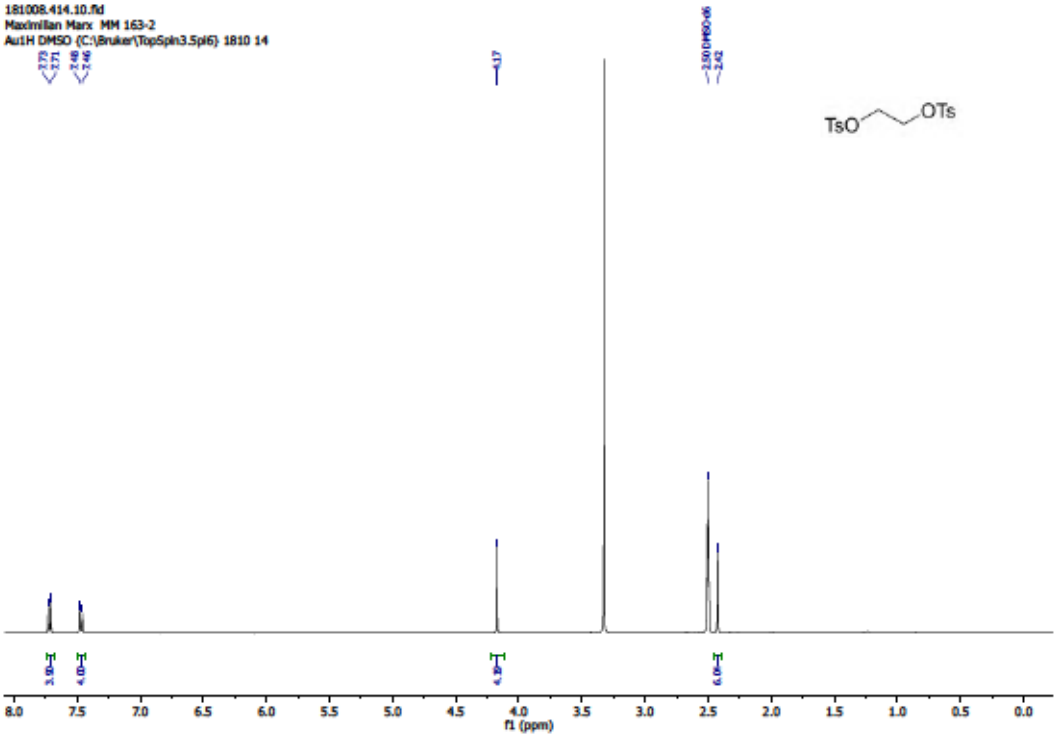

Figure S 42: ^{1}H NMR (400 MHz, DMSO-d_6) of **164**.

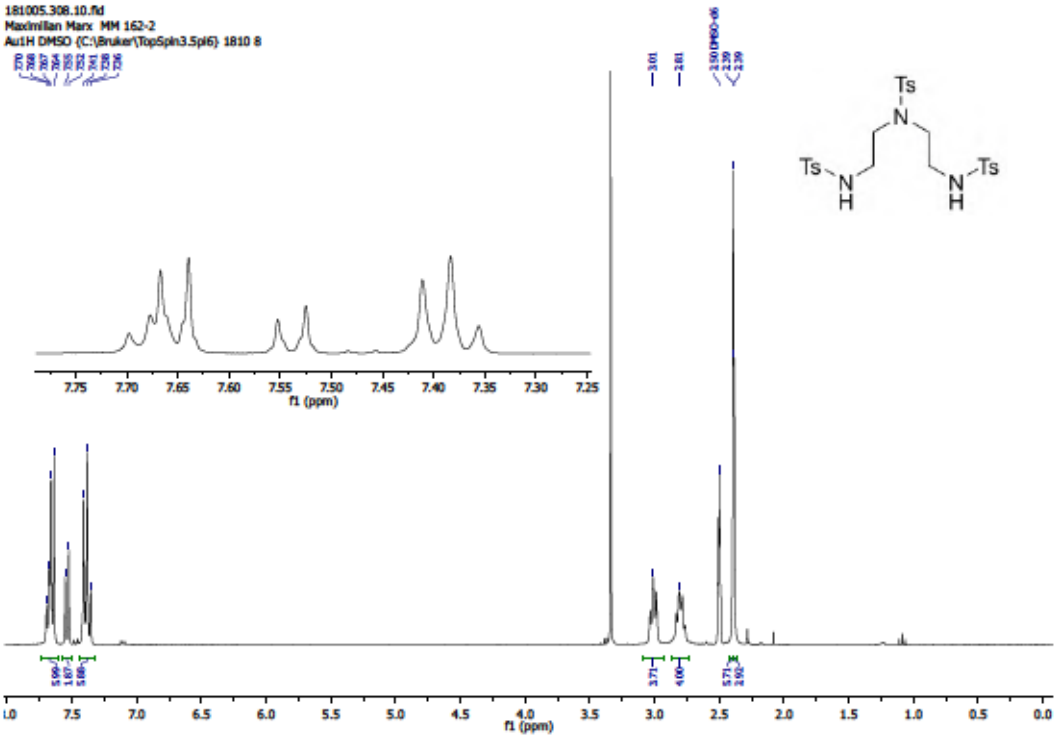

Figure S 43: ^{1}H NMR (300 MHz, DMSO-d_6) of **165**.

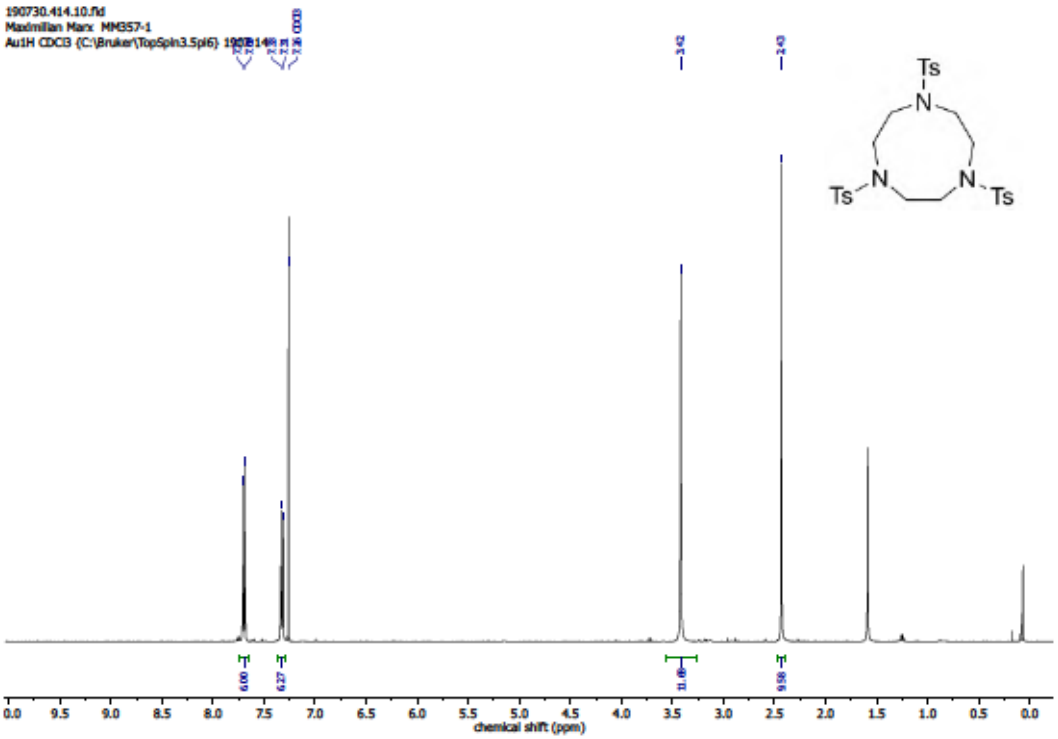

Figure S 44: ^{1}H NMR (400 MHz, $CDCl_3$) of **166**.

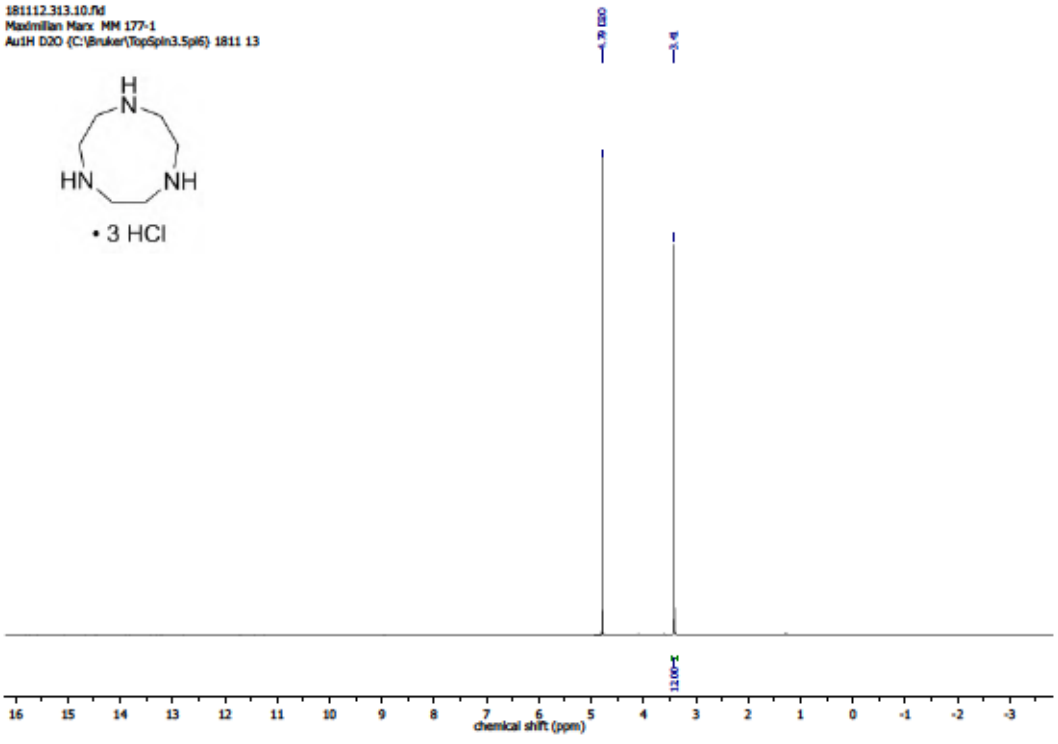

Figure S 45: ^{1}H NMR (300 MHz, D_2O) of tacn·3HCl **167**.

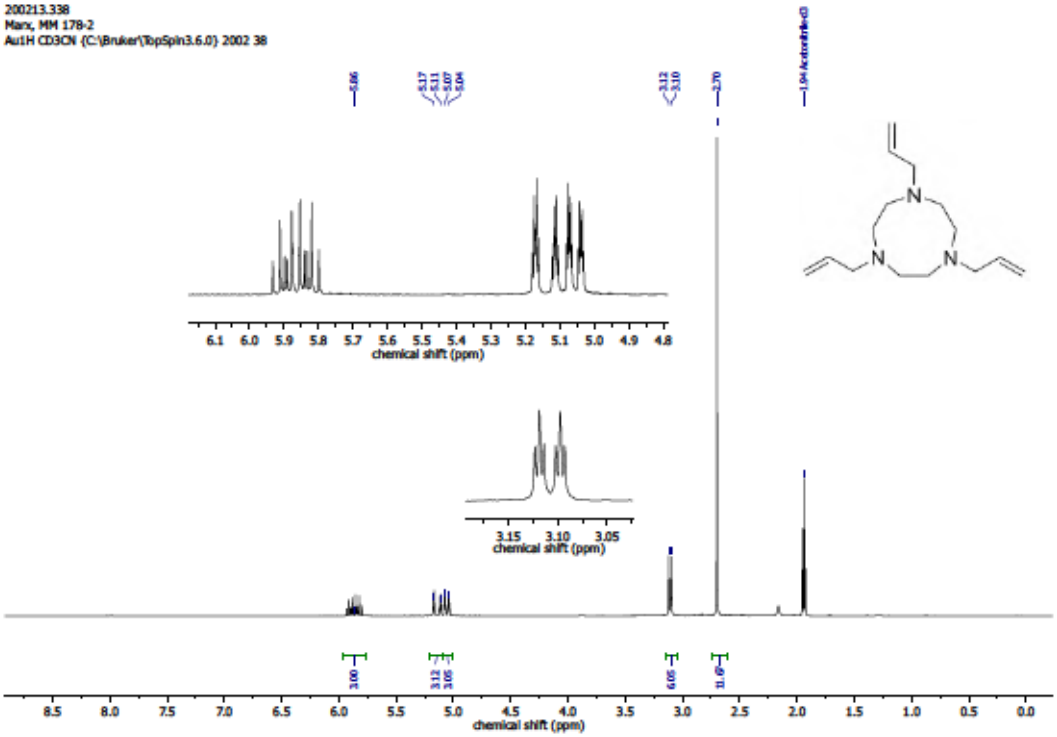

Figure S 46: ^{1}H NMR (300 MHz, CD_3CN) of **127**.

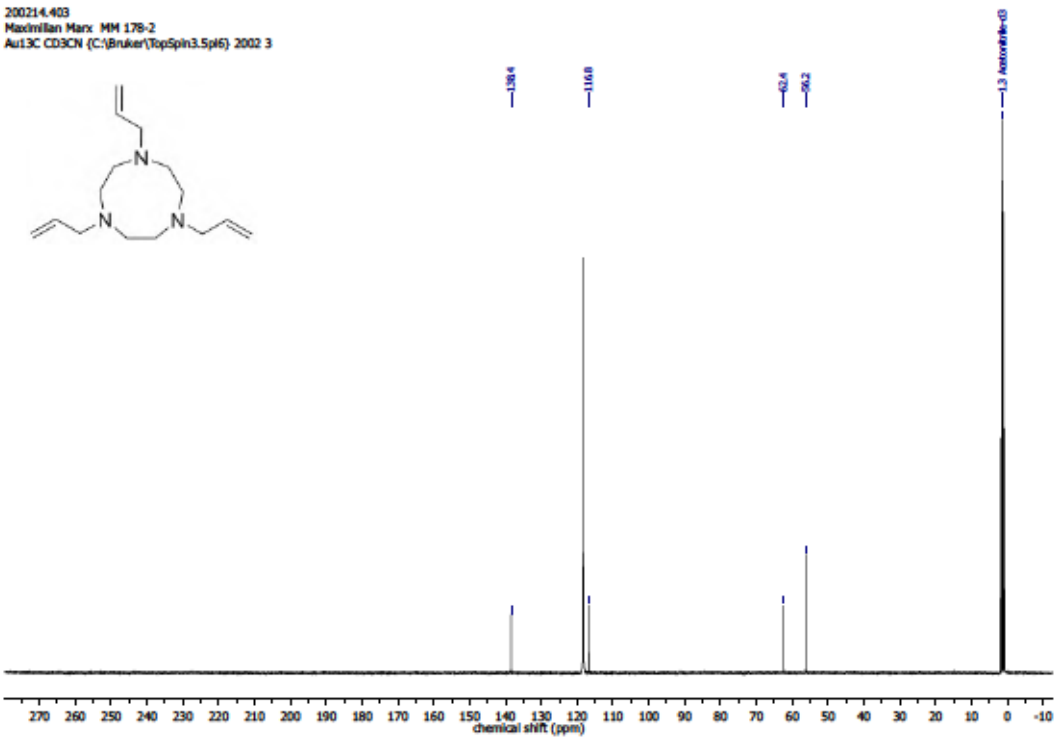

Figure S 47: $^{13}C\{^{1}H\}$ NMR (101 MHz, CD_3CN) of **127**.

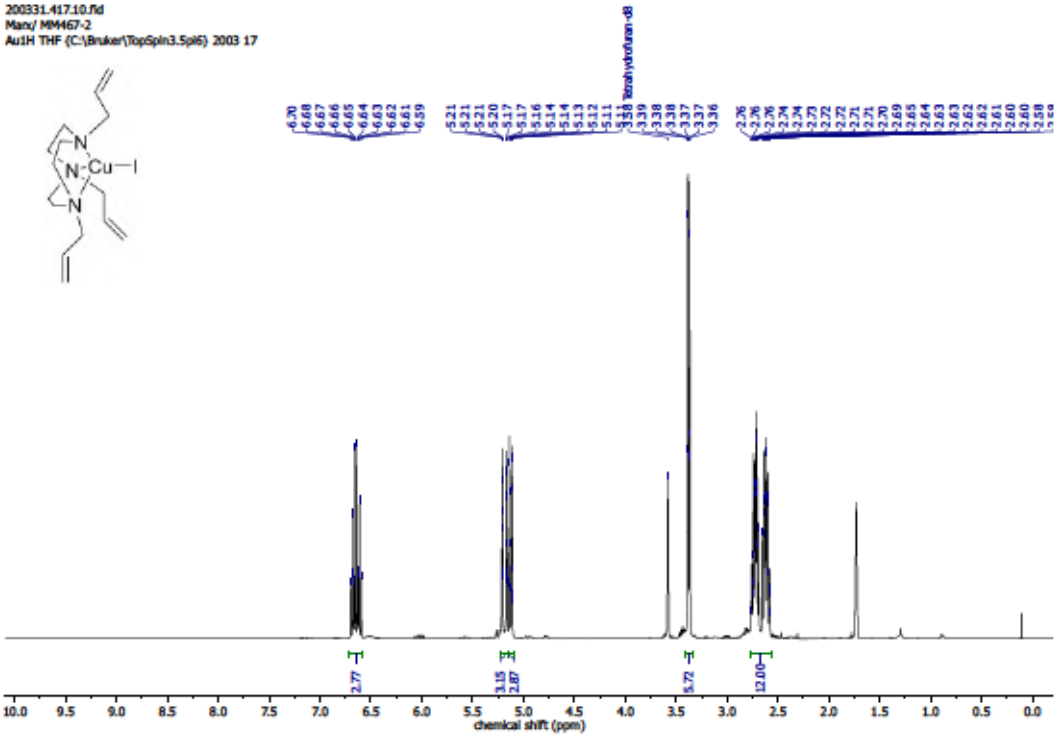

Figure S 48: ^{1}H NMR (400 MHz, THF-d_8) of **168**.

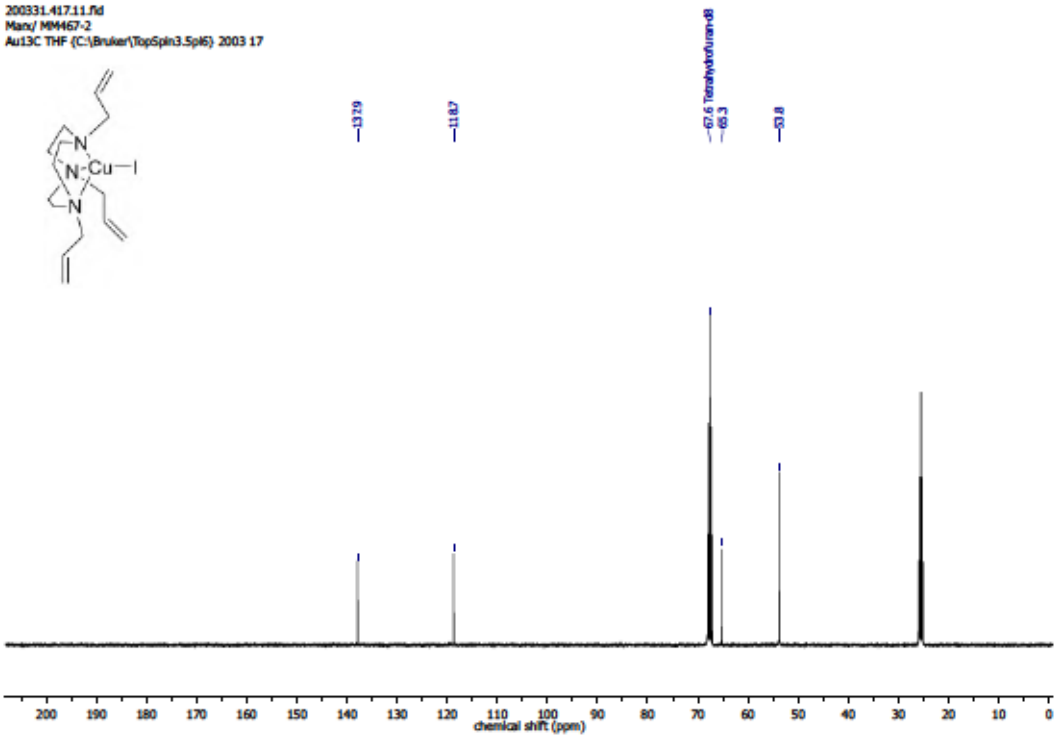

Figure S 49: ^{13}C{^{1}H} NMR (101 MHz, THF-d_8) of **168**.

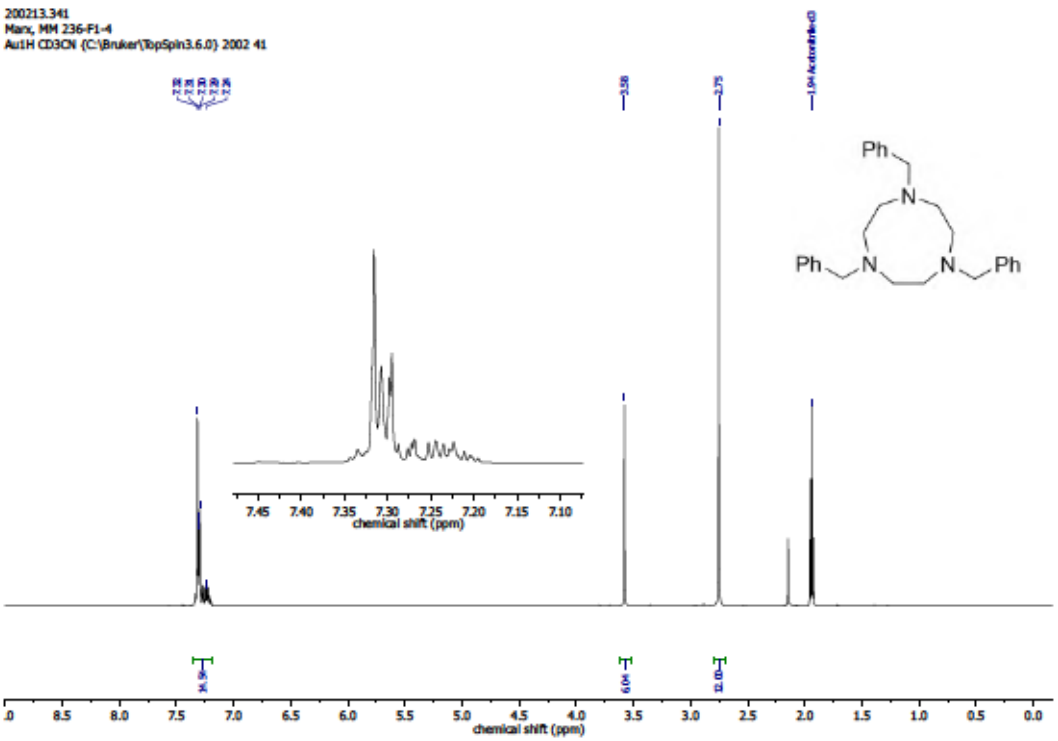

Figure S 50: ^{1}H NMR (300 MHz, CD_3CN) of **174**.

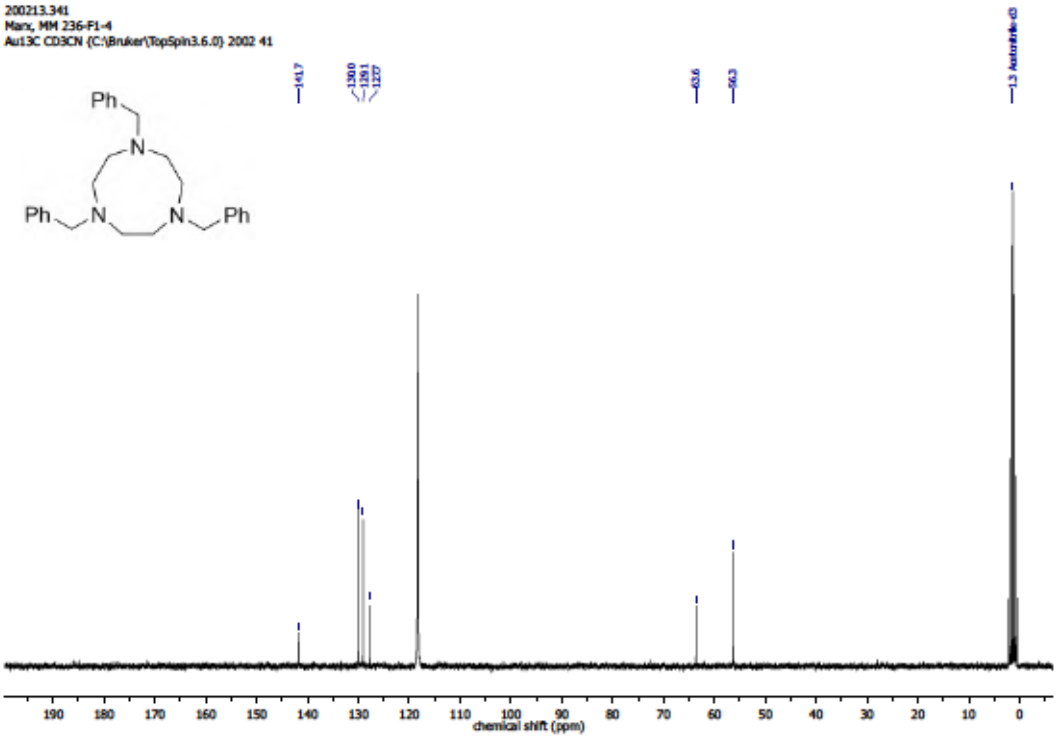

Figure S 51: $^{13}C\{^{1}H\}$ NMR (75 MHz, CD_3CN) of **174**.

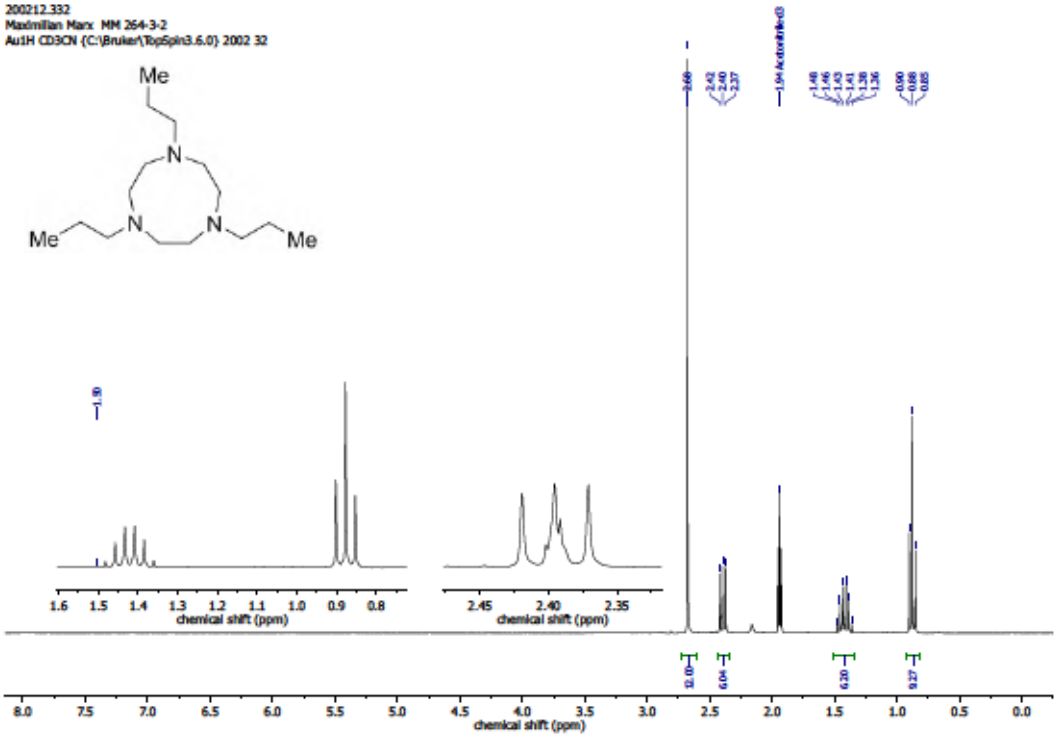

Figure S 52: ^{1}H NMR (300 MHz, CD_3CN) of **175**.

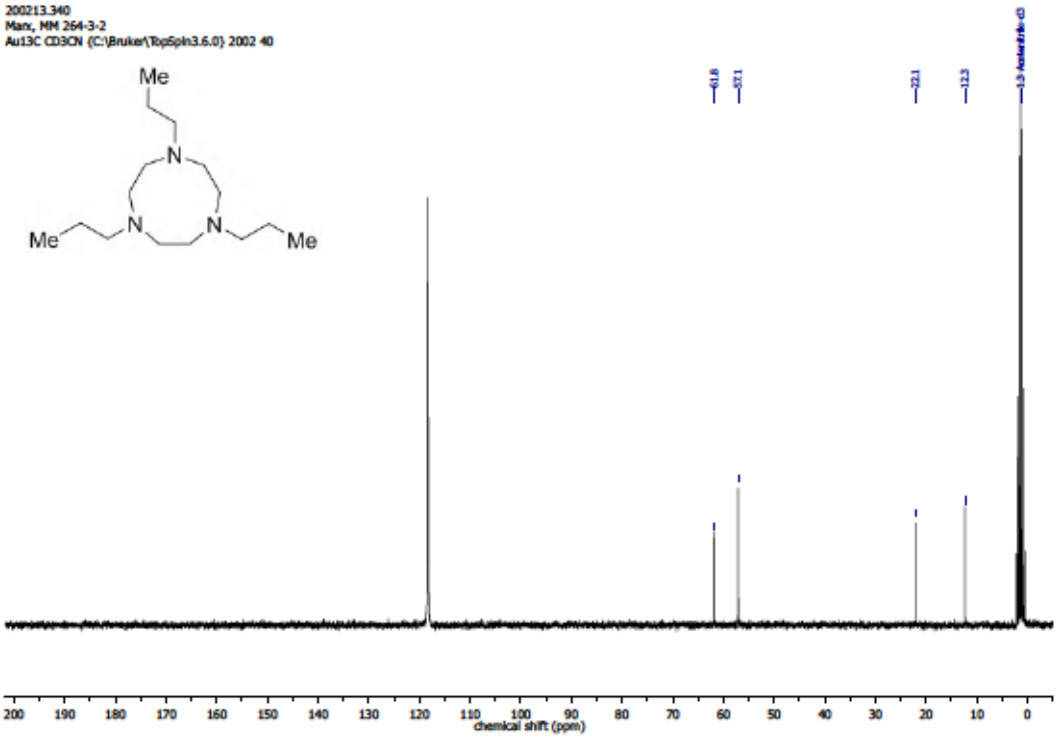

Figure S 53: $^{13}C\{^{1}H\}$ NMR (75 MHz, CD_3CN) of **175**.

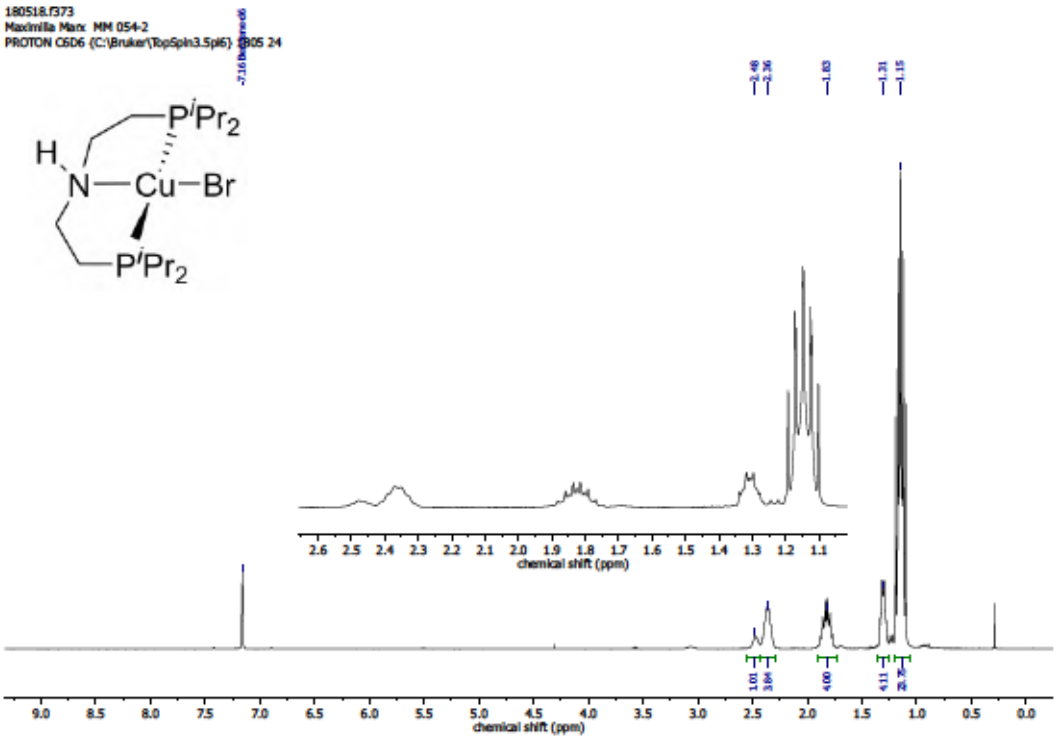

Figure S 54: ^{1}H NMR (300 MHz, C_6D_6) of **176**.

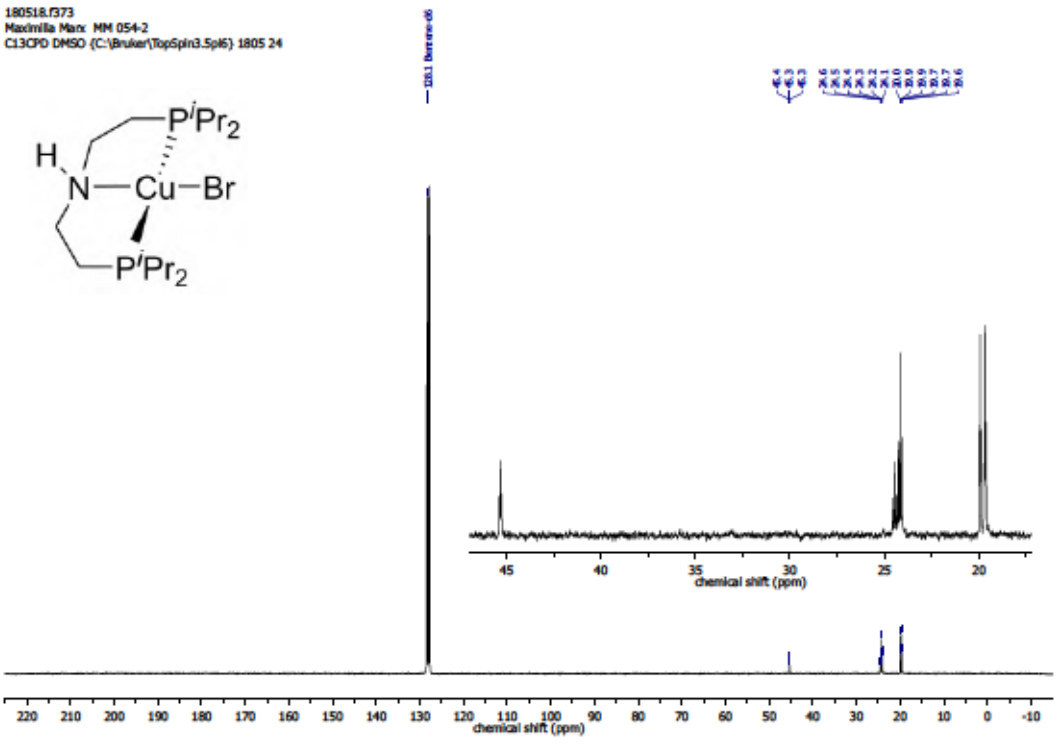

Figure S 55: $^{13}C\{^1H\}$ NMR (75 MHz, C_6D_6) of **176**.

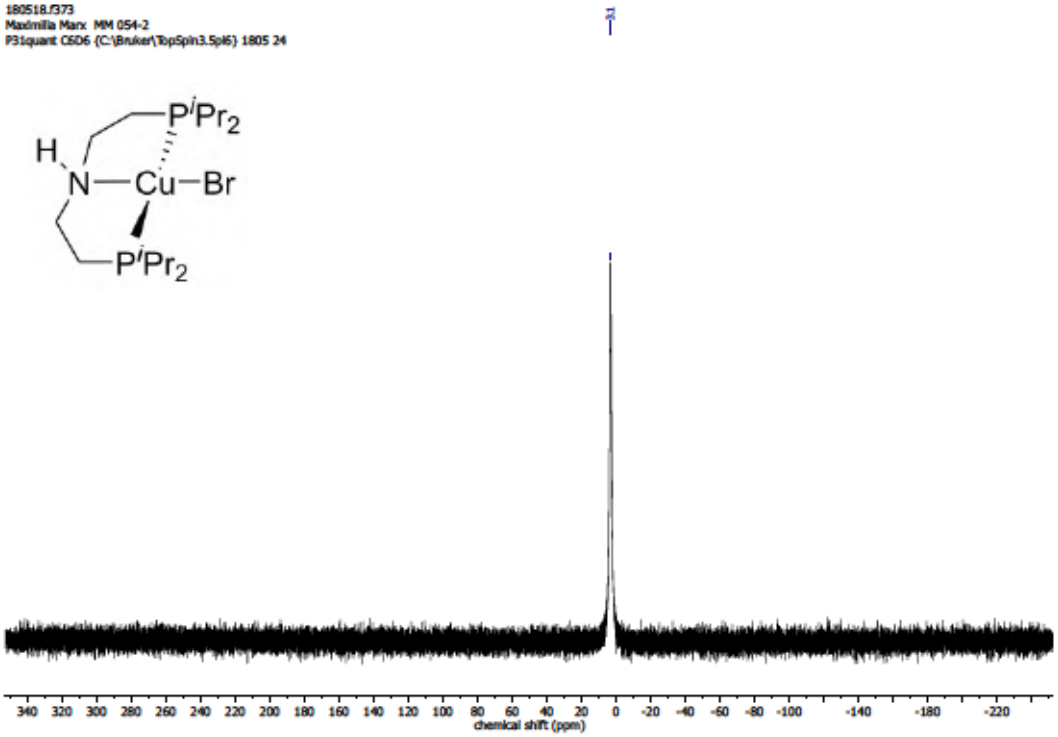

Figure S 56: $^{31}P\{^{1}H\}$ NMR (122 MHz, C_6D_6) of **176**.

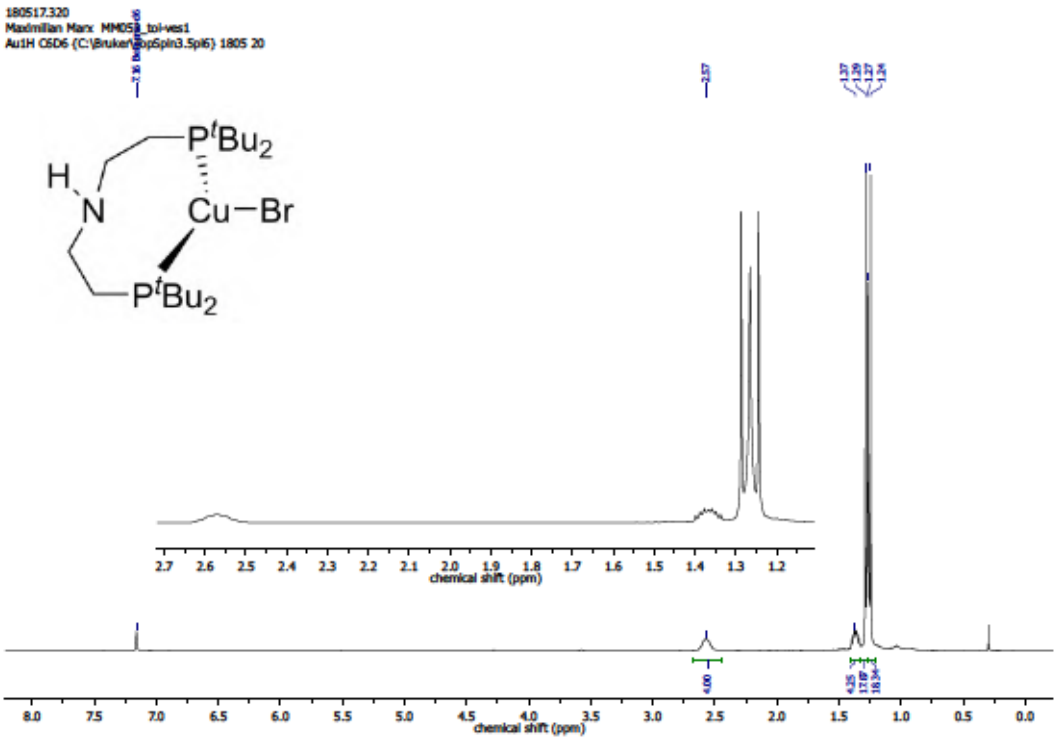

Figure S 57: ^{1}H NMR (300 MHz, C_6D_6) of **177**.

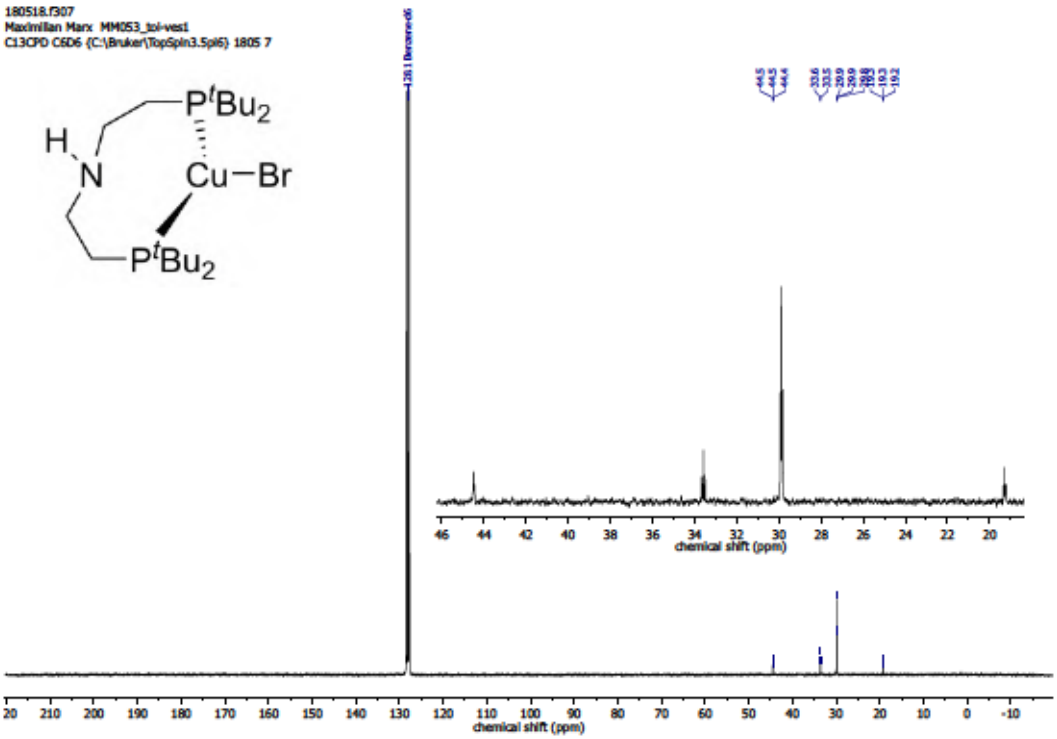

Figure S 58: $^{13}C\{^1H\}$ NMR (75 MHz, C_6D_6) of **177**.

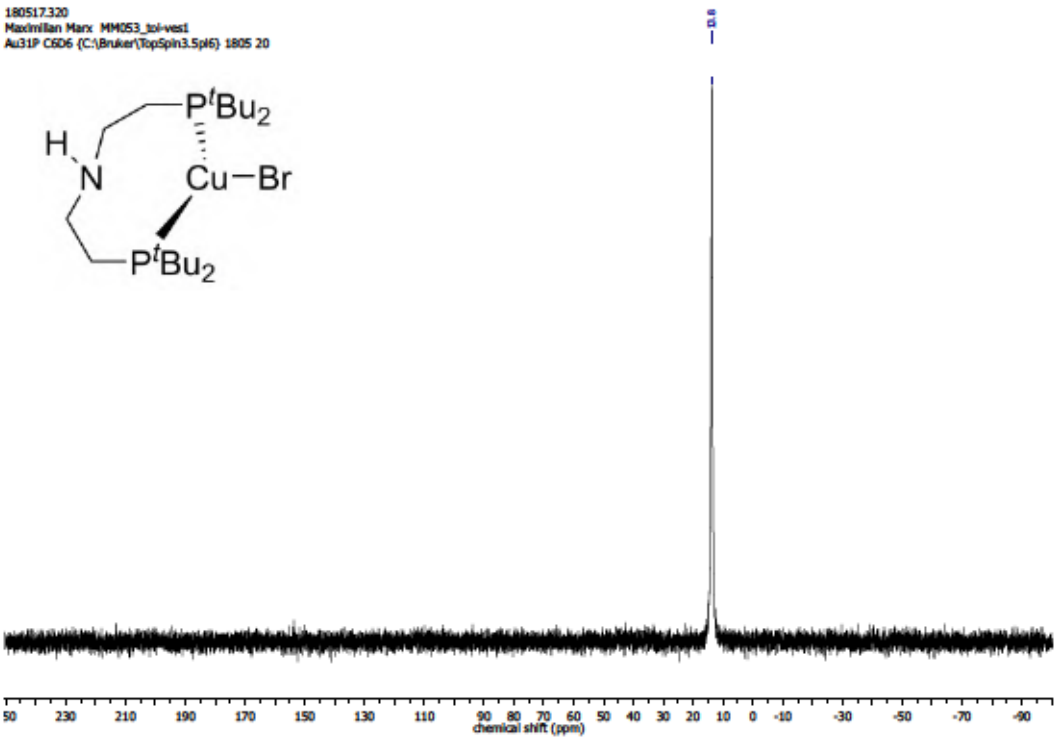

Figure S 59: $^{31}P\{^1H\}$ NMR (122 MHz, C_6D_6) of **177**.

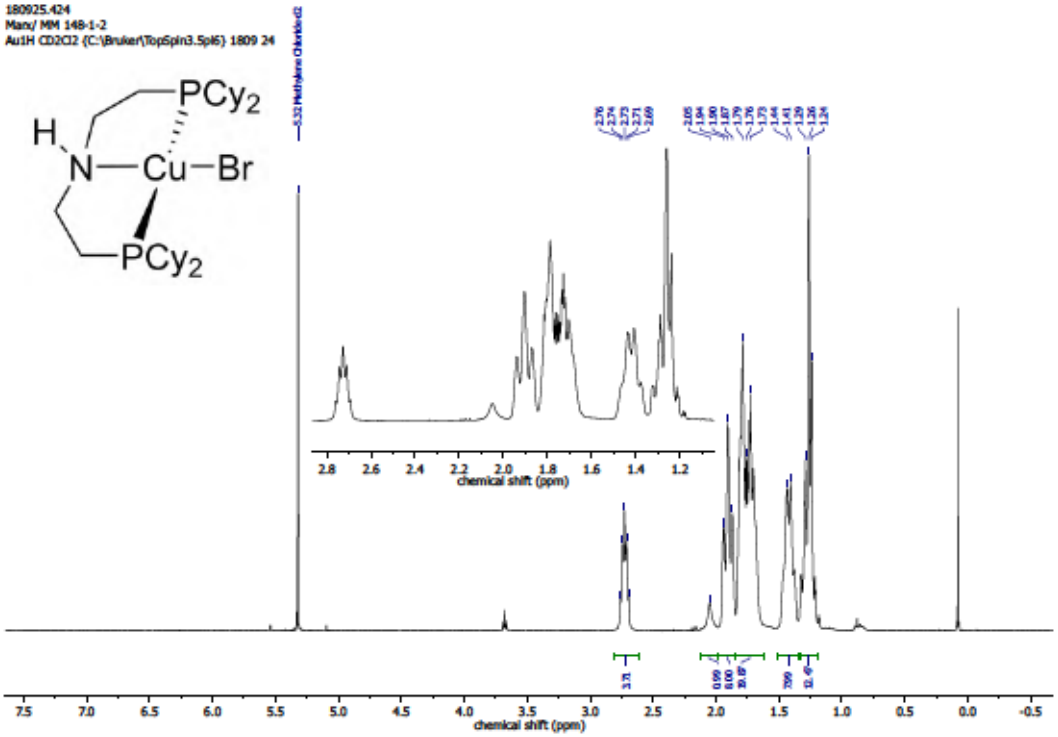

Figure S 60: ^{1}H NMR (400 MHz, CD_2Cl_2) of **178**.

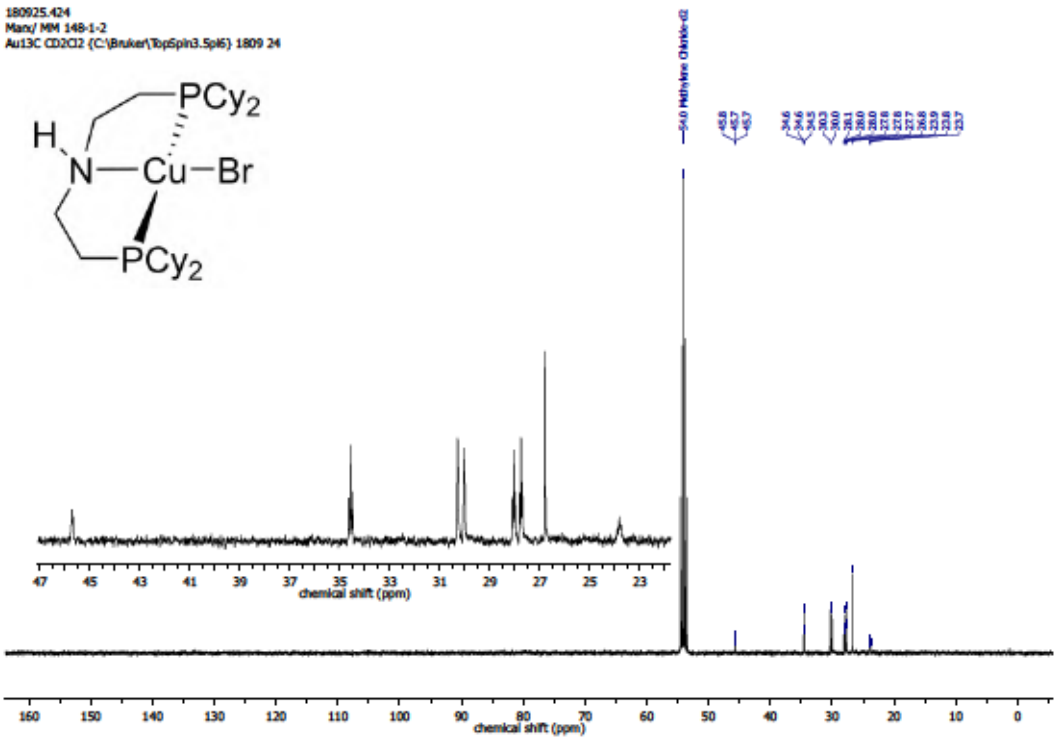

Figure S 61: ^{13}C{^{1}H} NMR (101 MHz, CD_2Cl_2) of **178**.

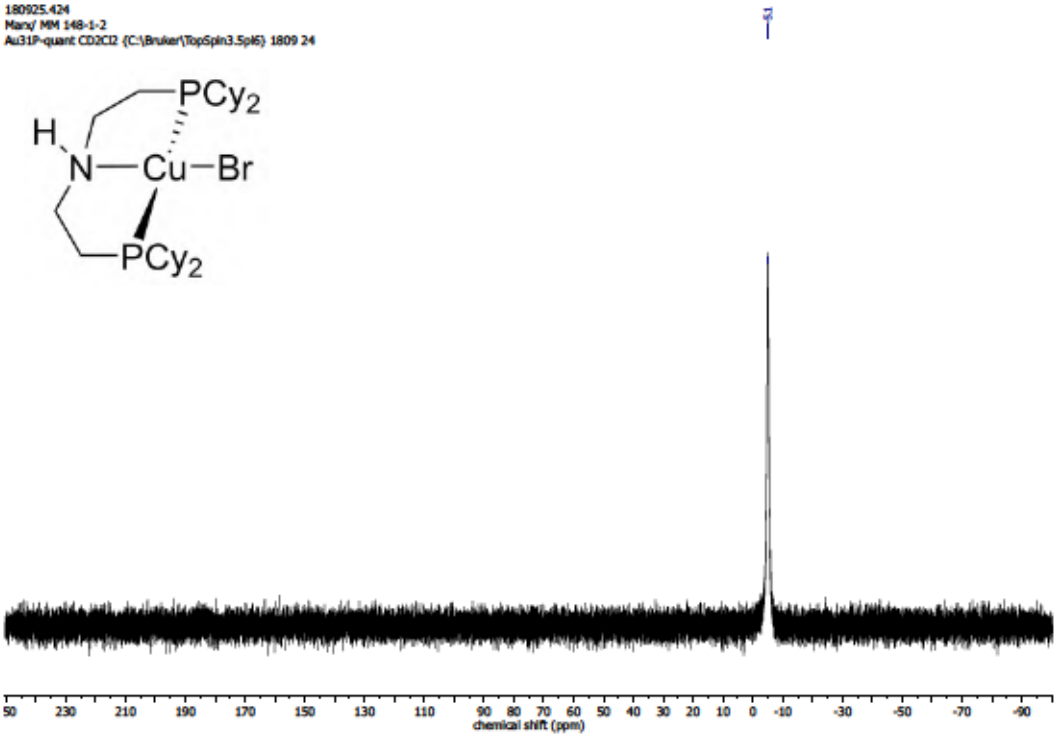

Figure S 62: $^{31}P\{^{1}H\}$ NMR (162 MHz, CD_2Cl_2) of **178**.

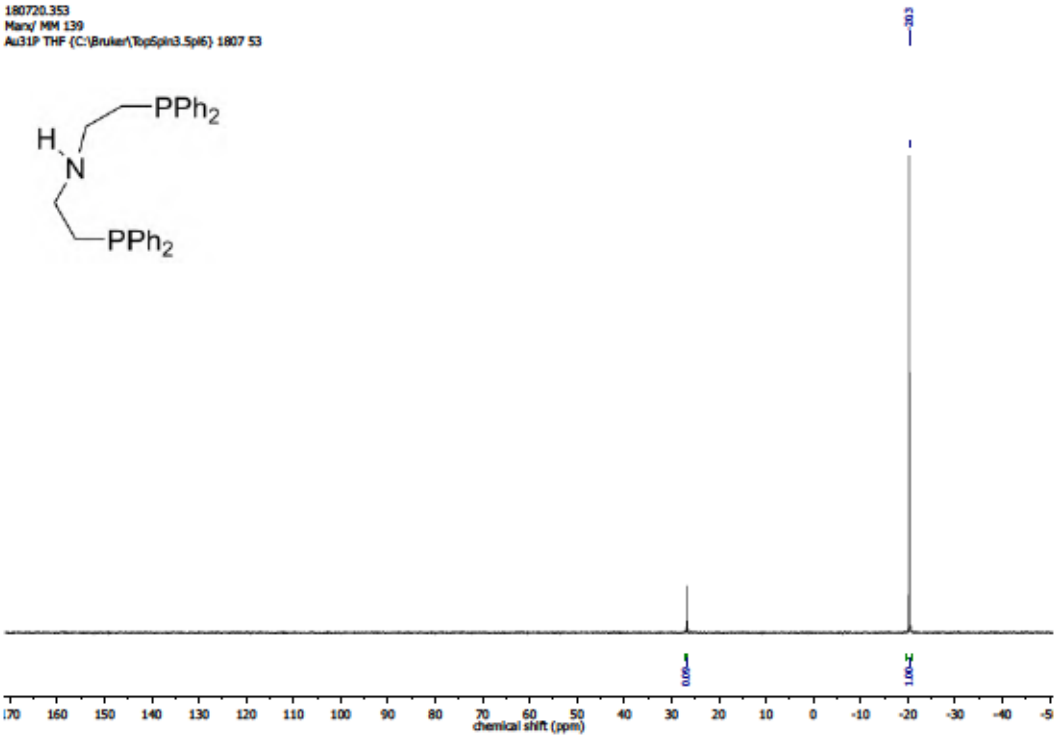

Figure S 63: $^{31}P\{^{1}H\}$ NMR (122 MHz, THF-d_8) of **HPNP^{Ph}**.

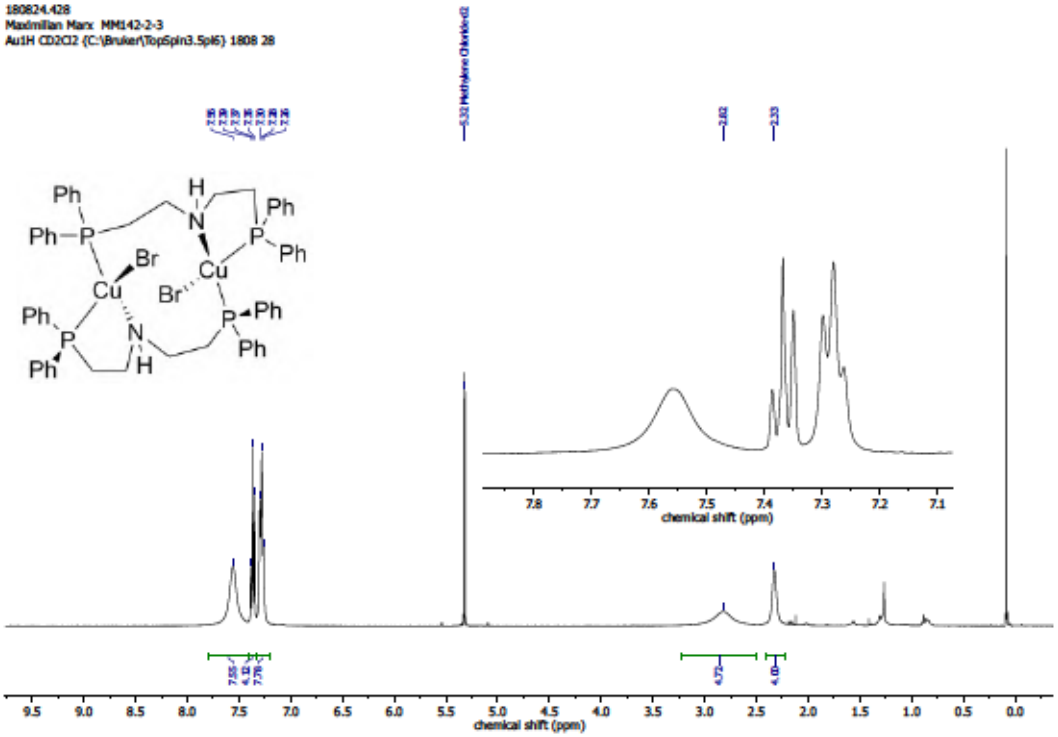

Figure S 64: ^{1}H NMR (400 MHz, CD_2Cl_2) of **179**.

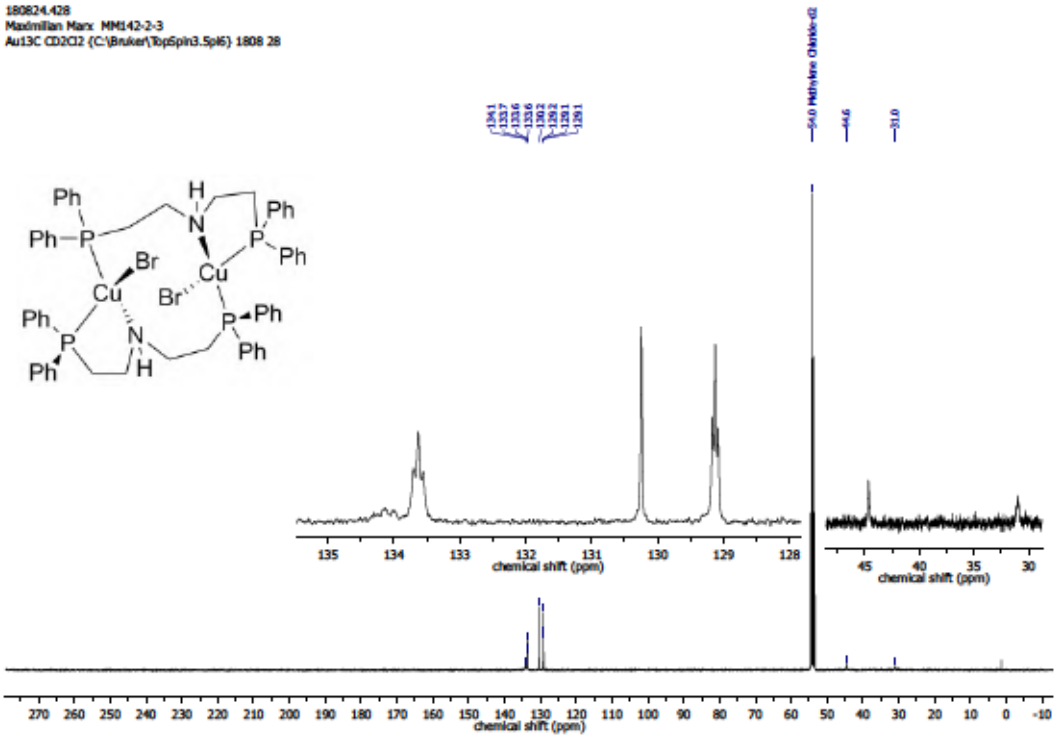

Figure S 65: ^{13}C{^{1}H} NMR (101 MHz, CD_2Cl_2) of **179**.

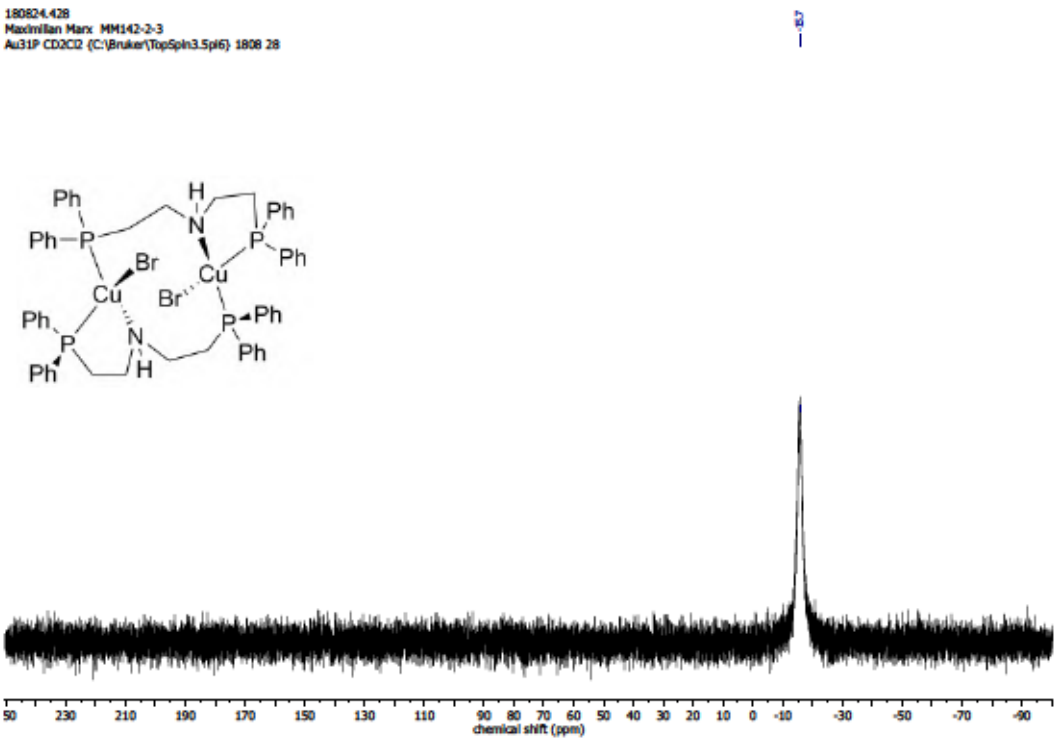

Figure S 66: $^{31}P\{^{1}H\}$ NMR (162 MHz, CD_2Cl_2) of **179**.

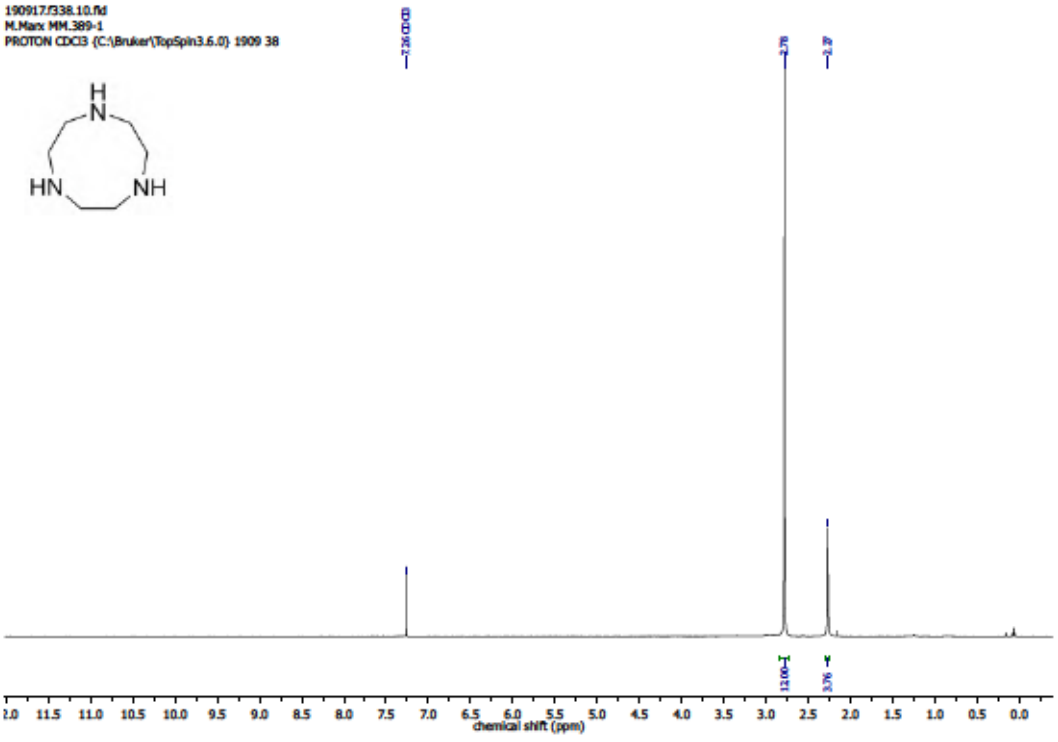

Figure S 67: ^{1}H NMR (300 MHz, $CDCl_3$) of **180**.

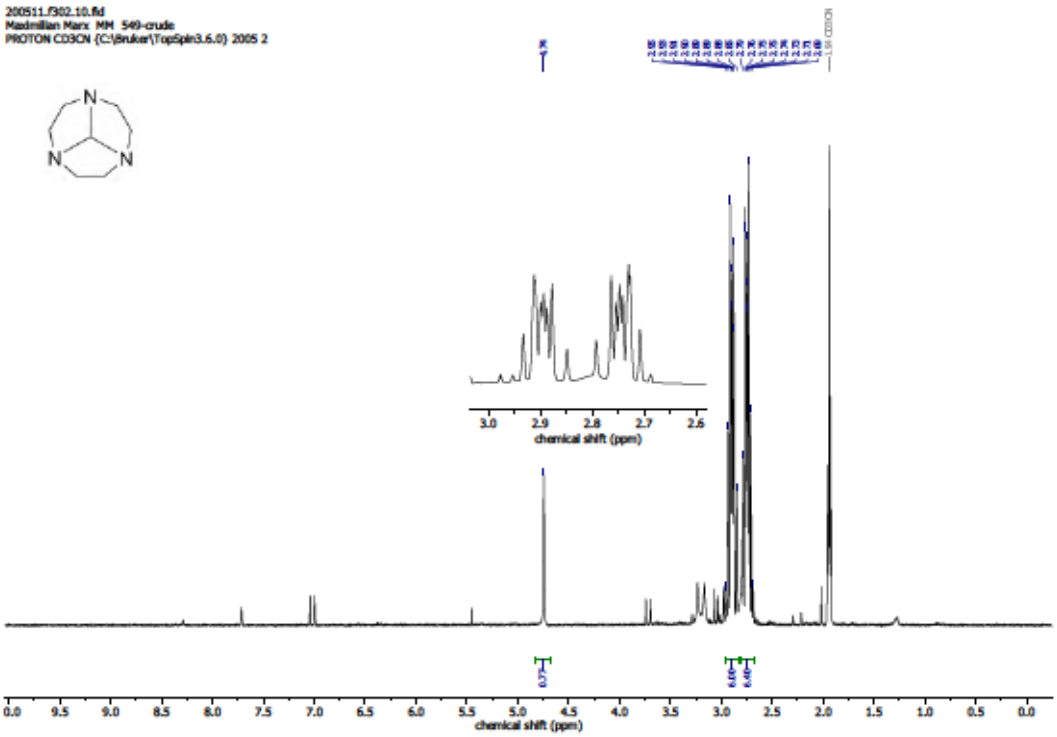

Figure S 68: ^{1}H NMR (300 MHz, CD_3CN) of **181**.

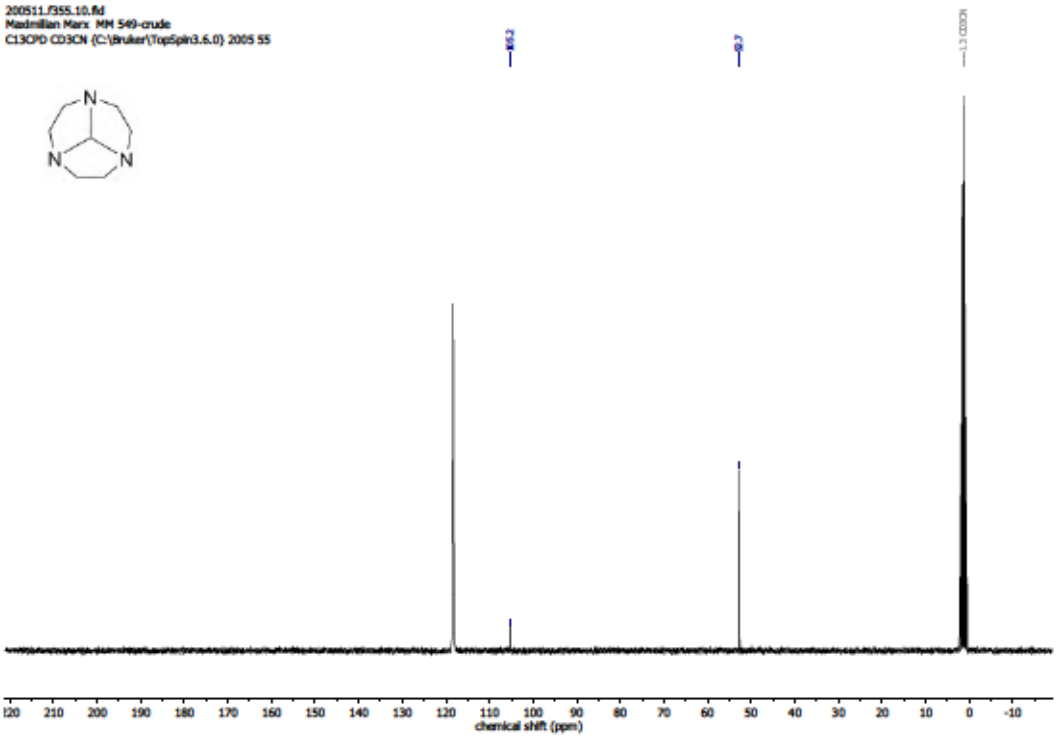

Figure S 69: $^{13}C\{^{1}H\}$ NMR (75 MHz, CD_3CN) of **181**.

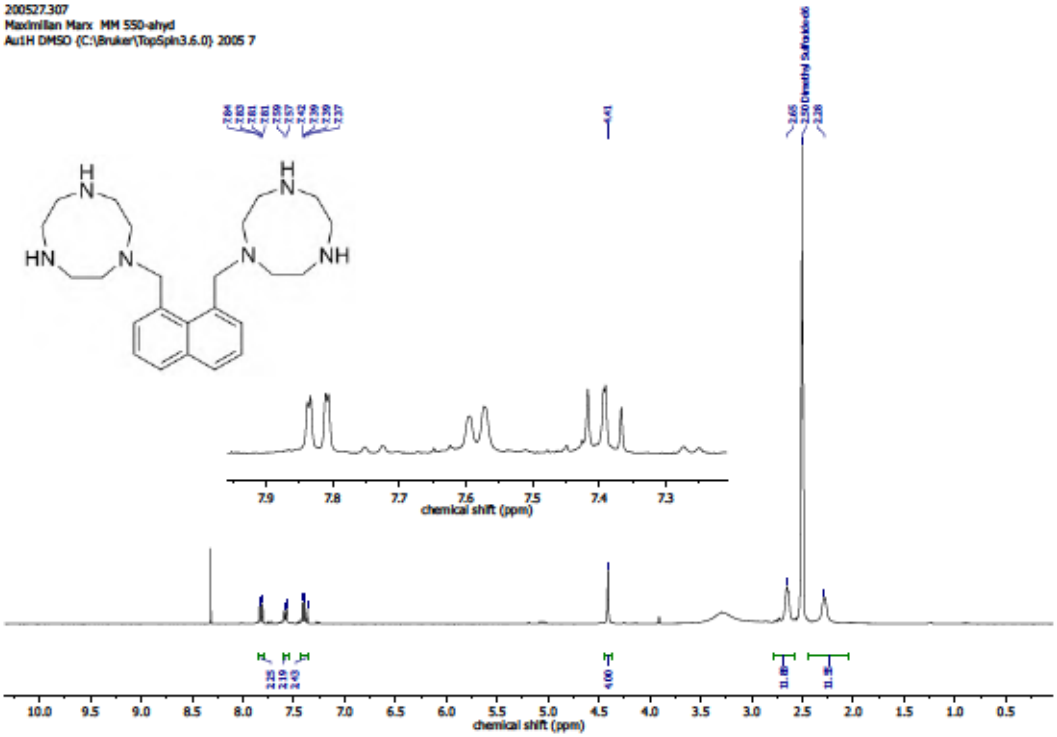

Figure S 70: ^{1}H NMR (300 MHz, DMSO-d_6) of **183**.

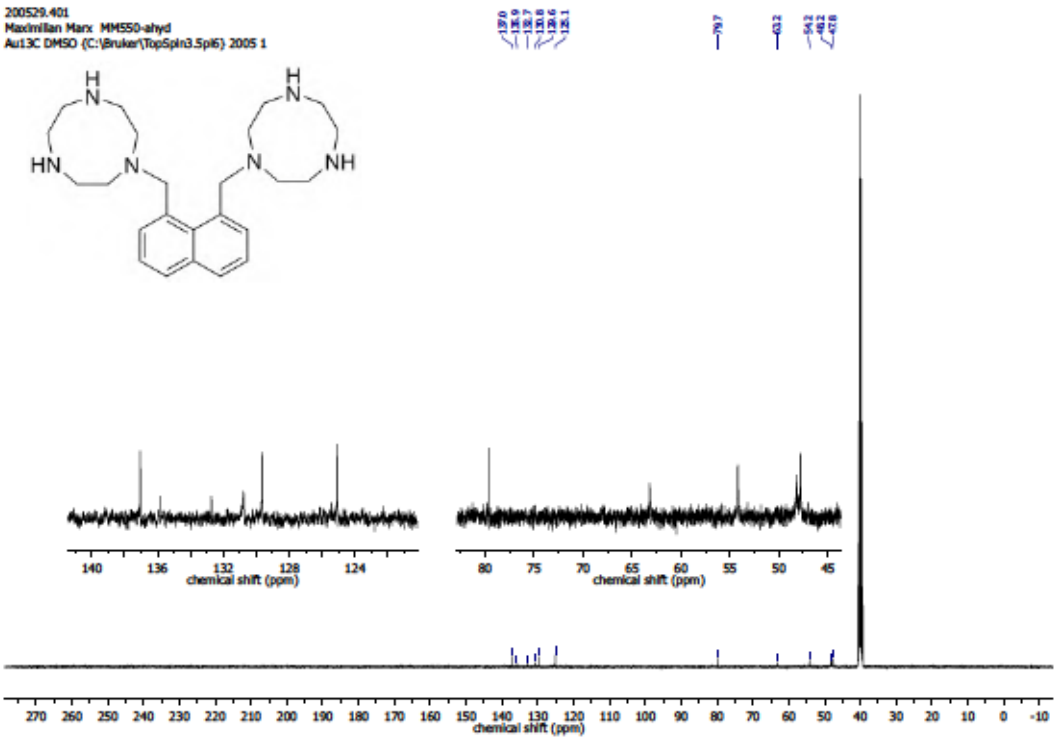

Figure S 71: ^{13}C{^{1}H} NMR (101 MHz, DMSO-d_6) of **183**.

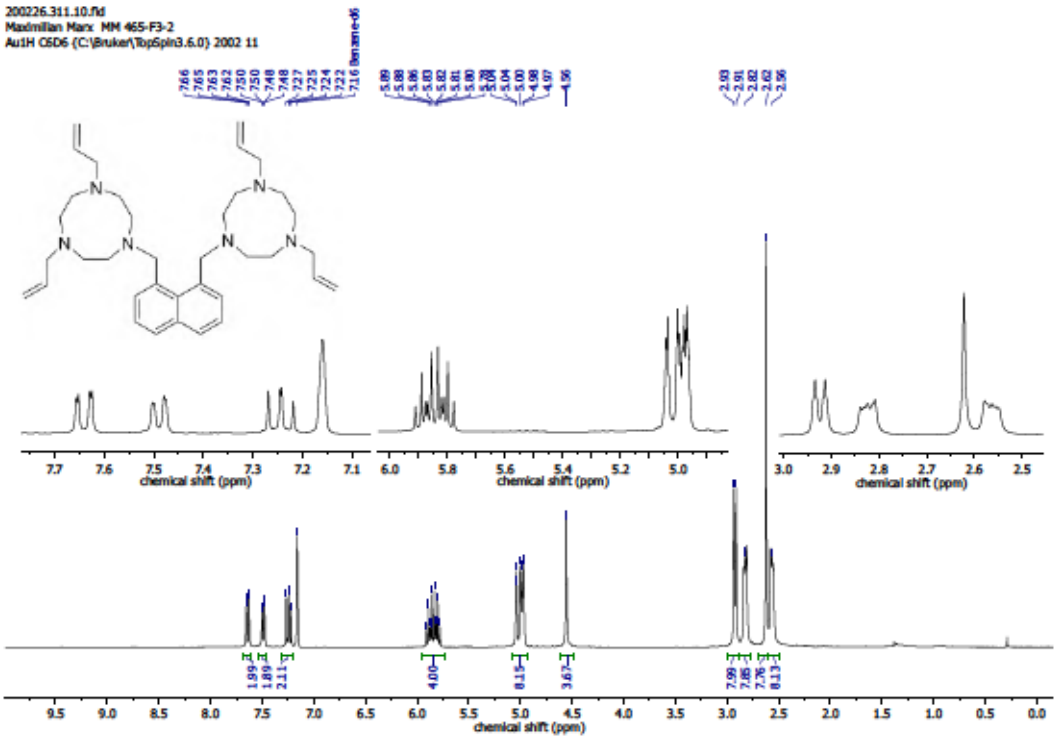

Figure S 72: ^{1}H NMR (300 MHz, C_6D_6) of **184**.

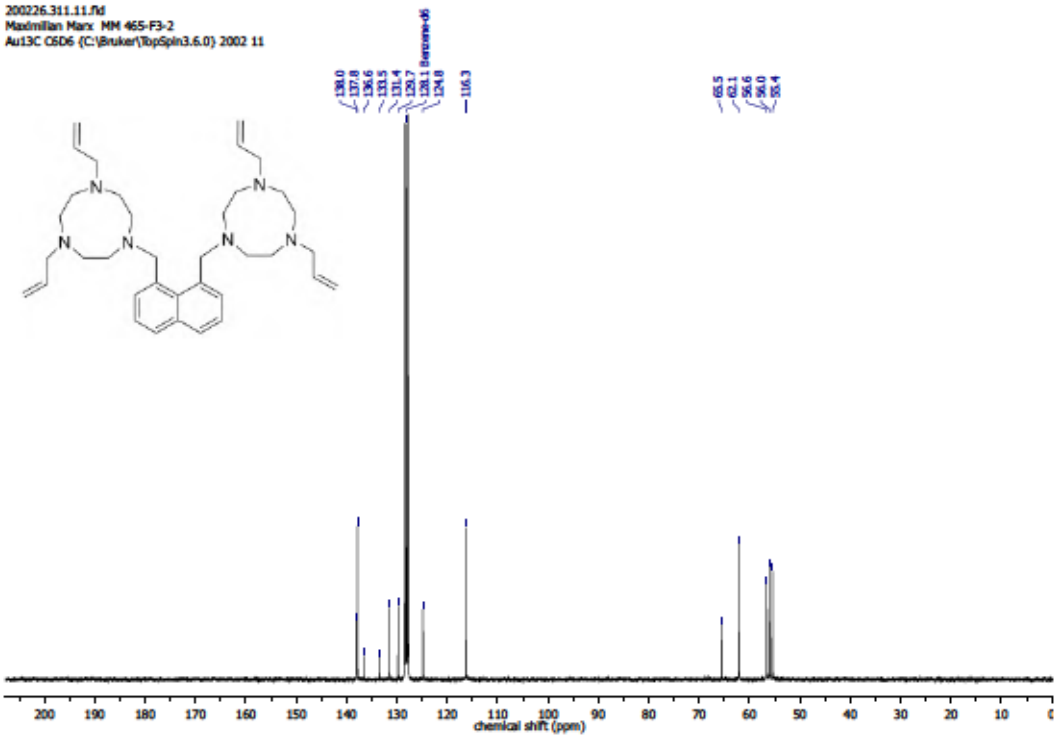

Figure S 73: $^{13}C\{^{1}H\}$ NMR (75 MHz, C_6D_6) of **184**.

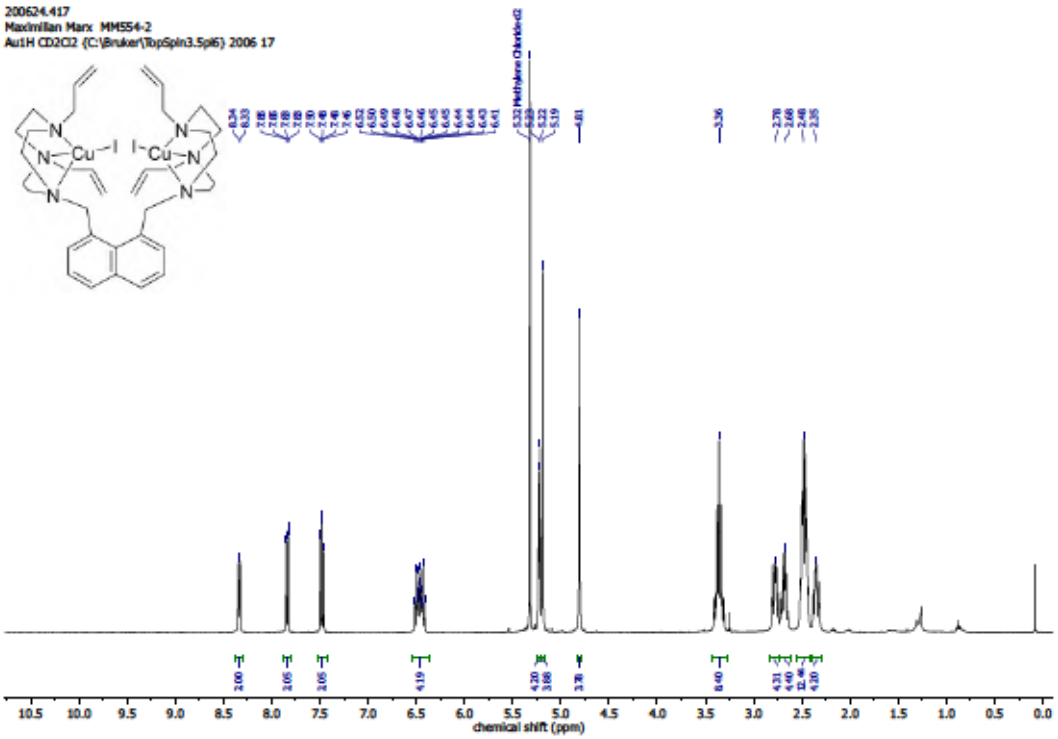

Figure S 74: ^{1}H NMR (400 MHz, CD_2Cl_2) of **185**.

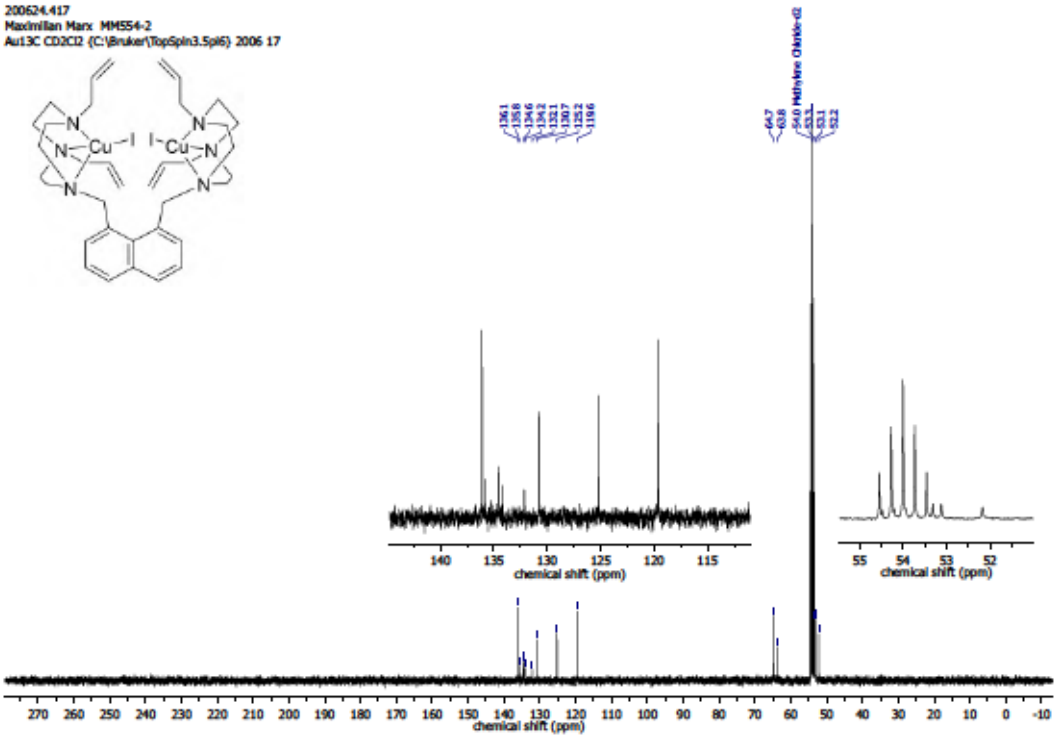

Figure S 75: ^{13}C{^{1}H} NMR (101 MHz, CD_2Cl_2) of **185**.

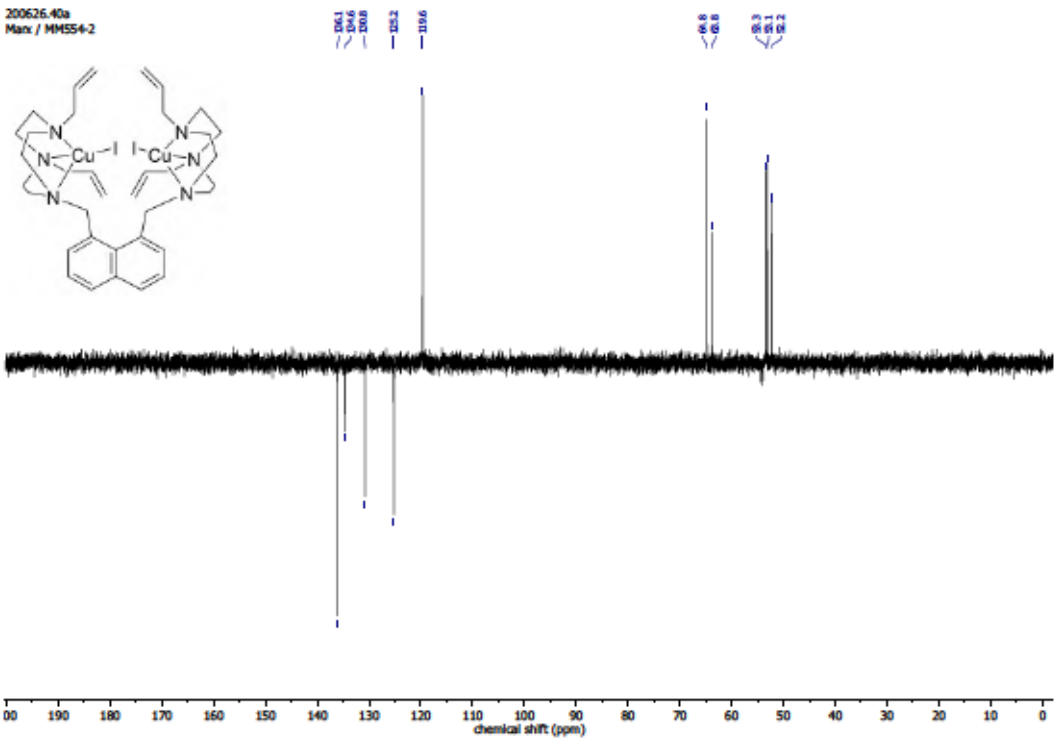

Figure S 76: $^{13}C\{^{1}H\}$ DEPT-135 (101 MHz, CD_2Cl_2) of **185**.

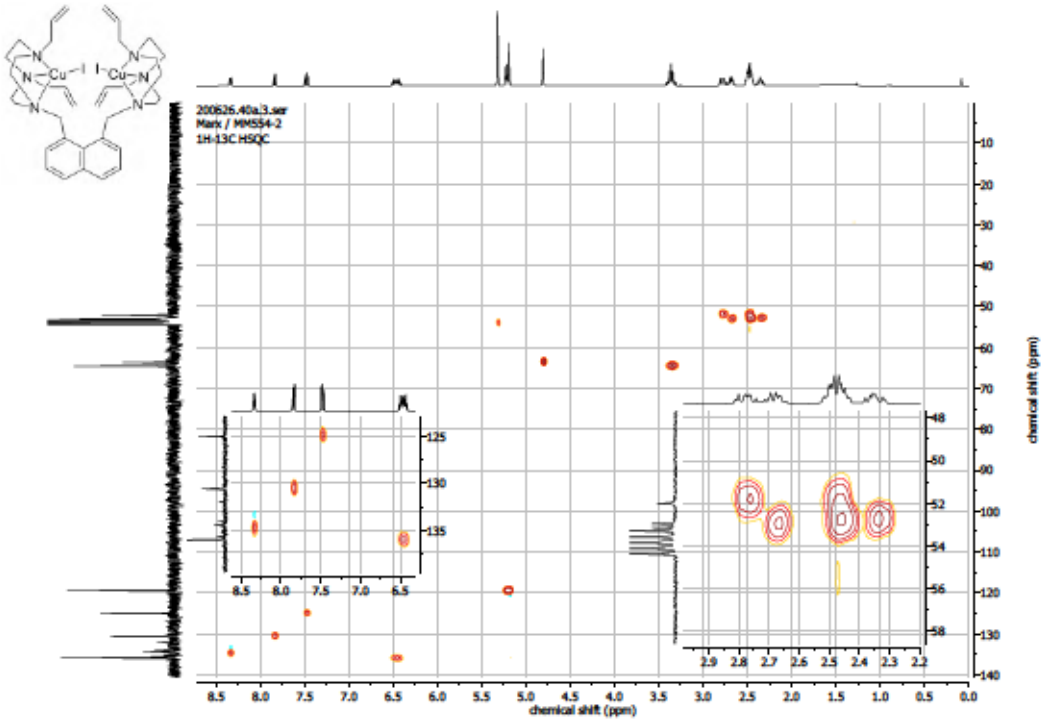

Figure S 77: (^{1}H,^{13}C) HSQC NMR (400 MHz, CD_2Cl_2) of **185**.

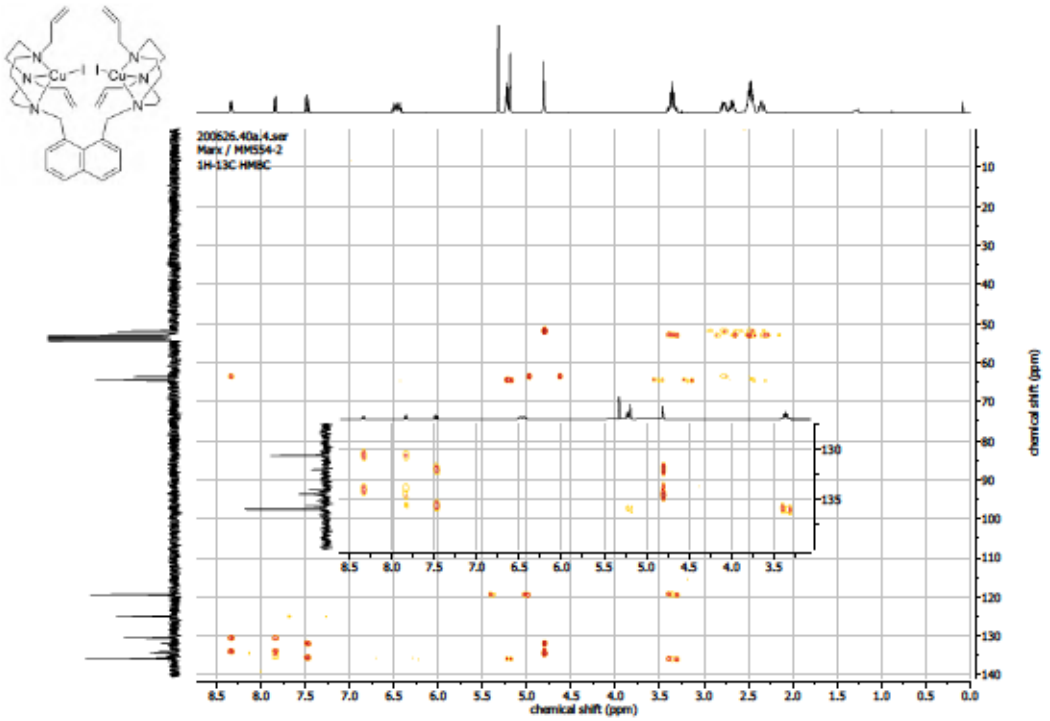

Figure S 78: (^{1}H,^{13}C) HMBC NMR (400 MHz, CD_2Cl_2) of **185**.

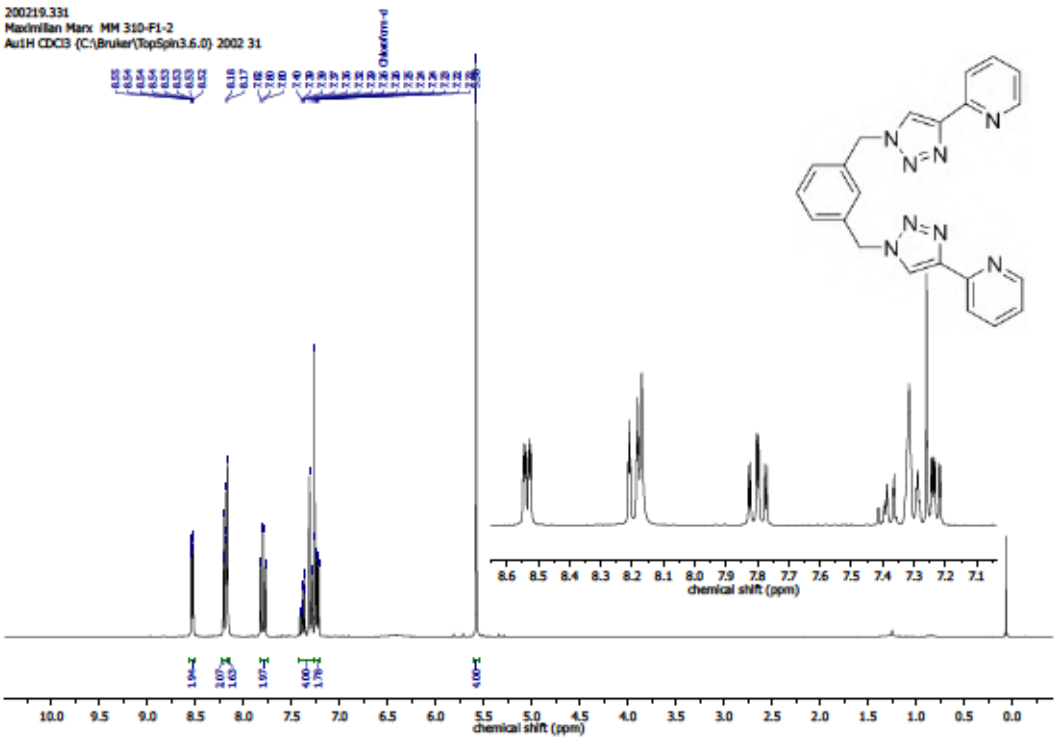

Figure S 79: ^{1}H NMR (300 MHz, $CDCl_3$) of ***m*-xpt**.

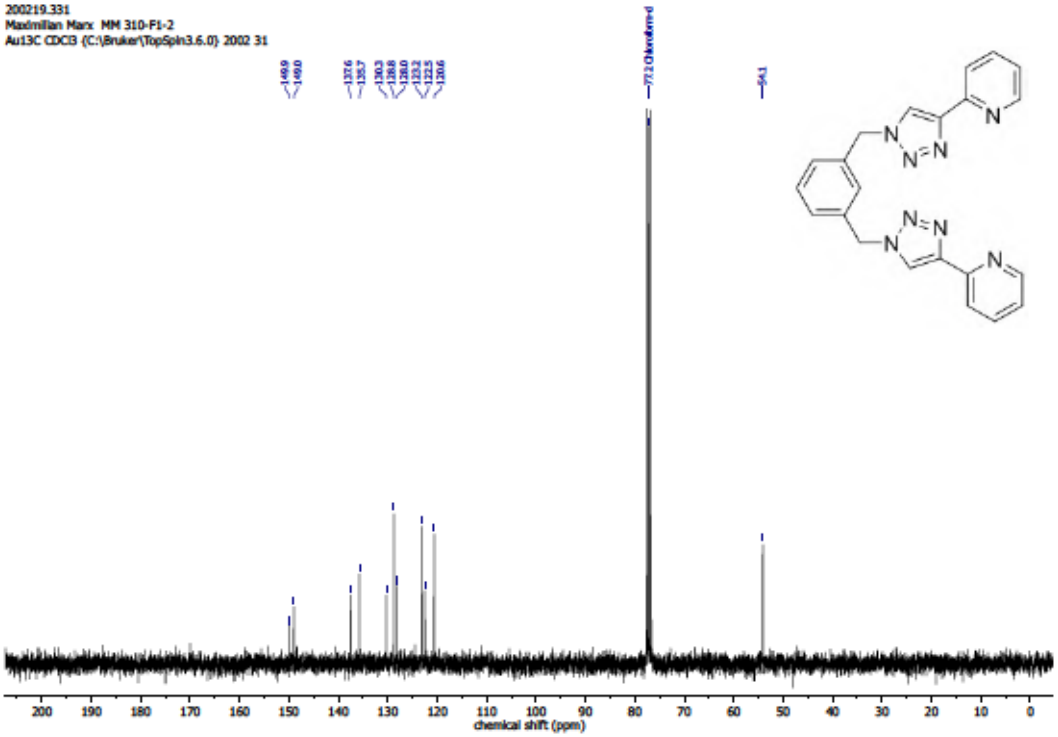

Figure S 80: $^{13}C\{^{1}H\}$ NMR (75 MHz, $CDCl_3$) of ***m*-xpt**.

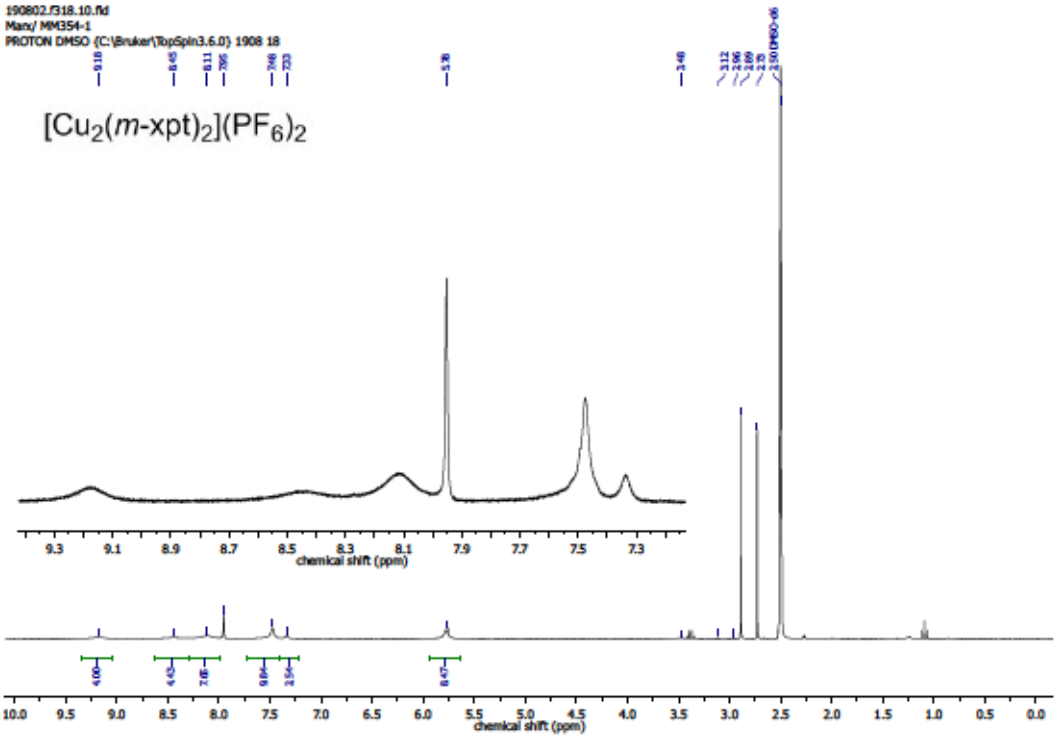

Figure S 81: ^{1}H NMR (300 MHz, DMSO-d_6) of **187**.

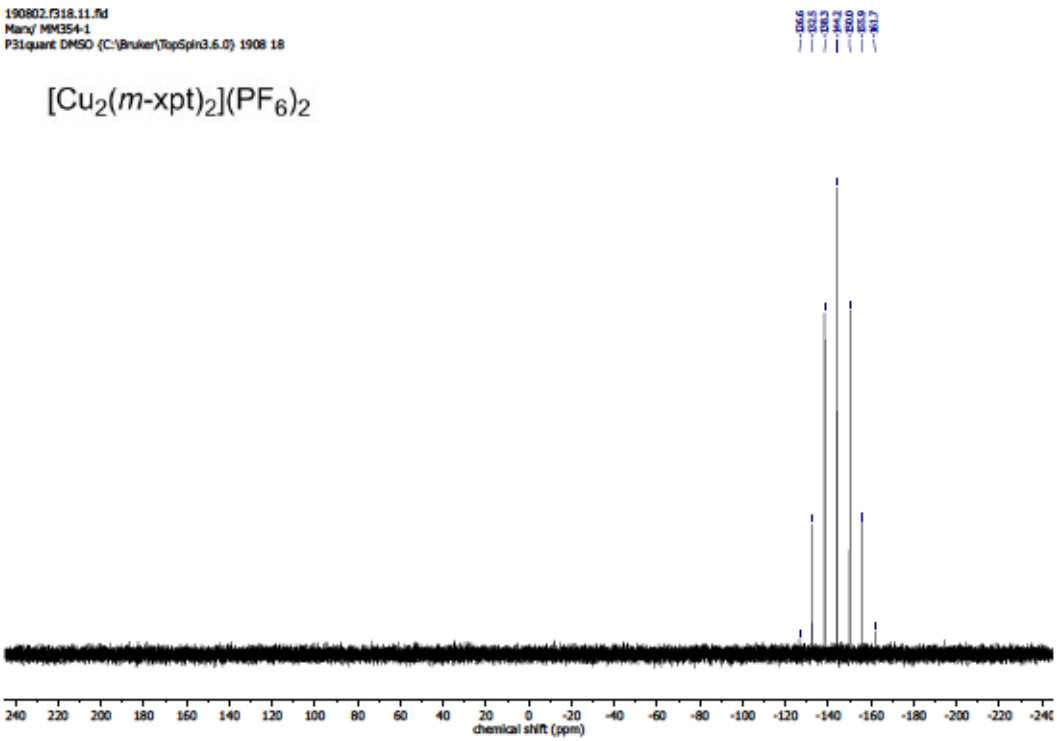

Figure S 82: $^{31}P\{^{1}H\}$ NMR (122 MHz, DMSO-d_6) of **187**.

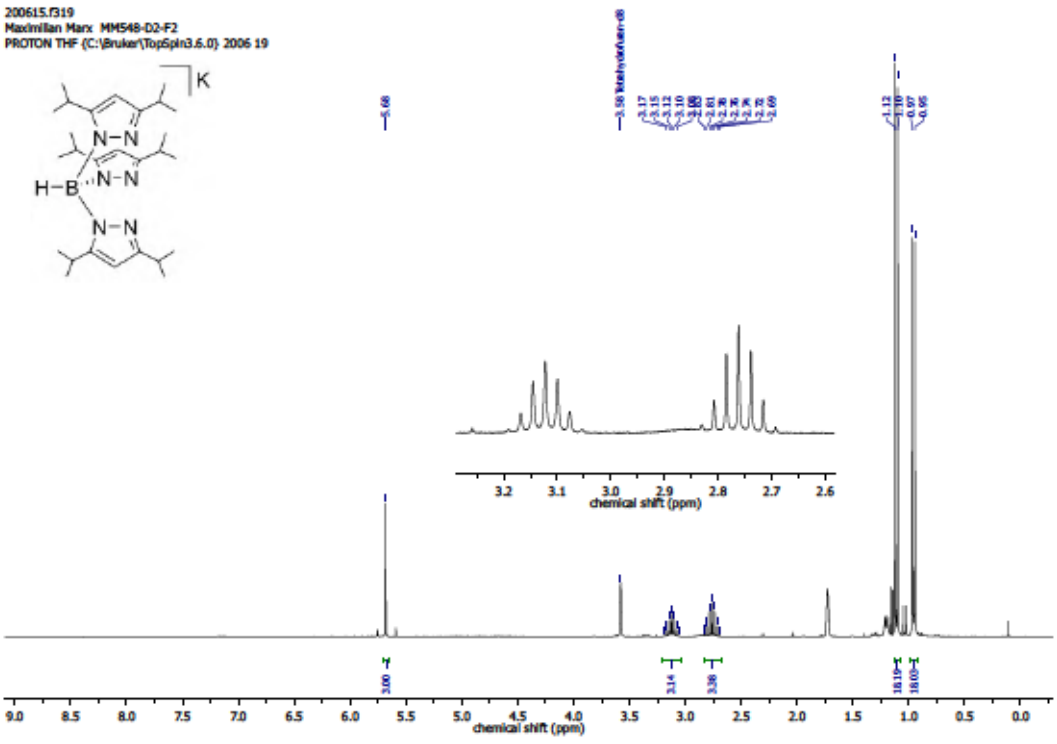

Figure S 83: ^{1}H NMR (300 MHz, THF-d_8) of **190**.

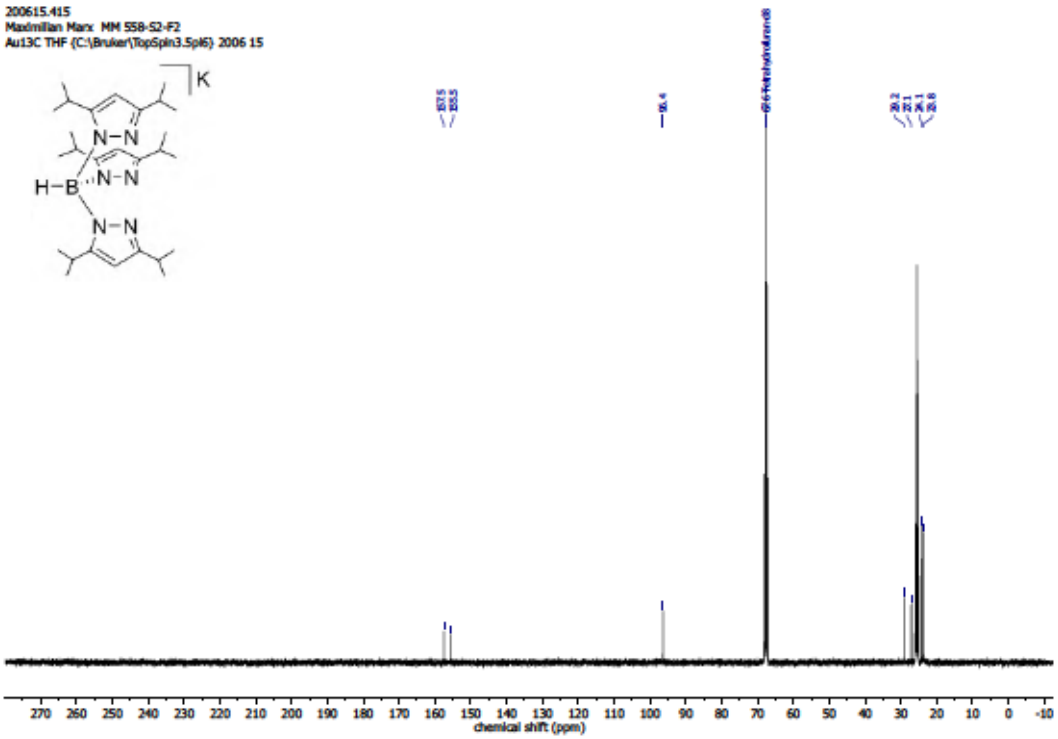

Figure S 84: $^{13}C\{^{1}H\}$ NMR (101 MHz, THF-d_8) of **190**.

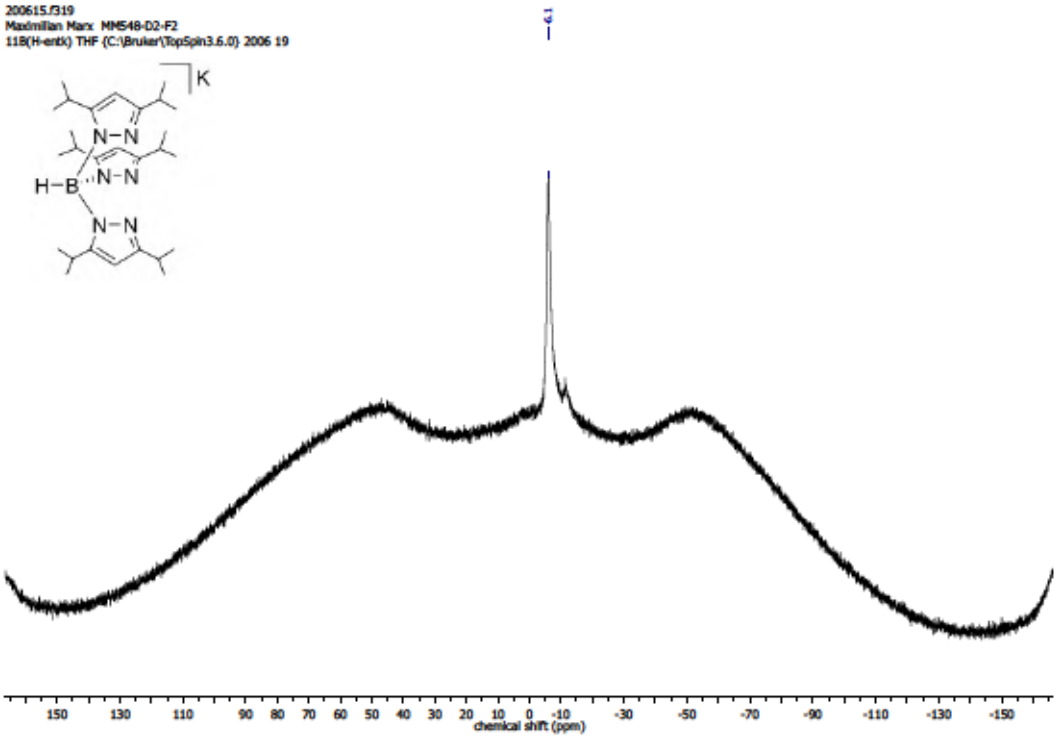

Figure S 85: $^{11}B\{^{1}H\}$ NMR (96 MHz, THF-d_8) of **190**.

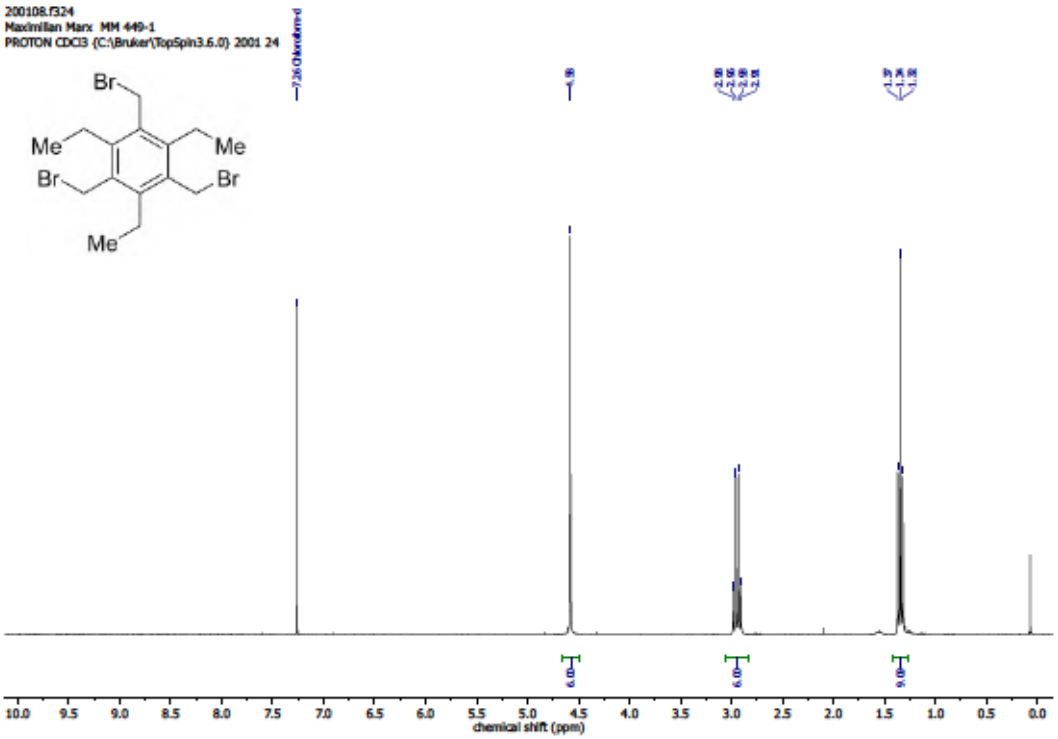

Figure S 86: ^{1}H NMR (300 MHz, $CDCl_3$) of **199**.

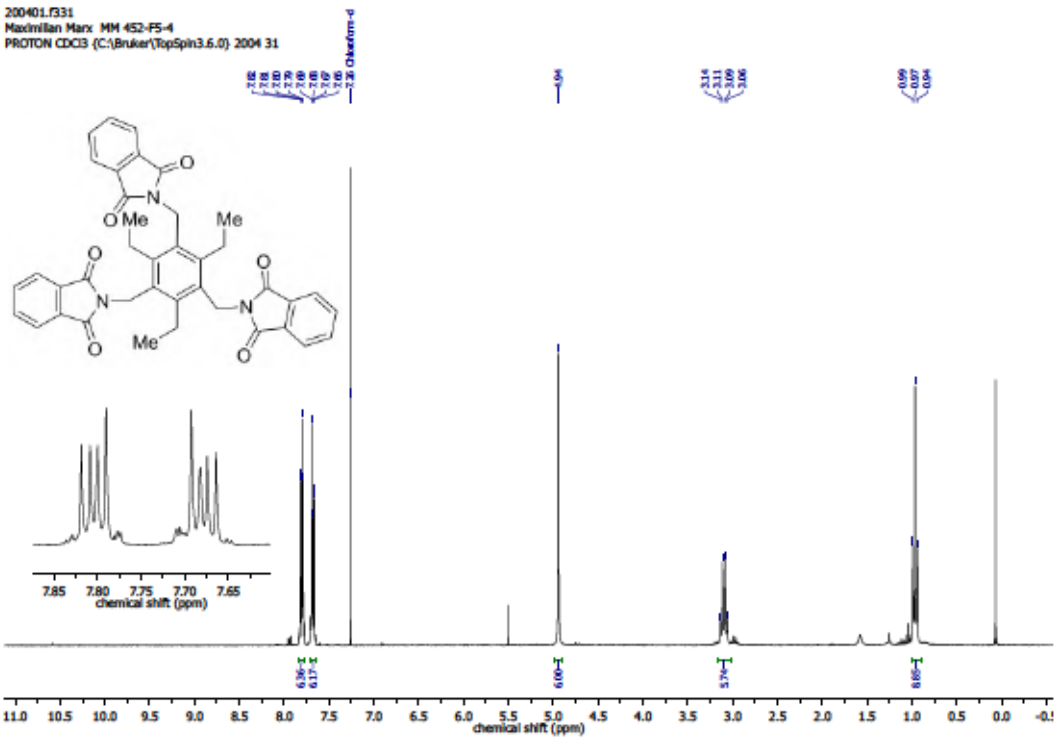

Figure S 87: ^{1}H NMR (300 MHz, $CDCl_3$) of **200**.

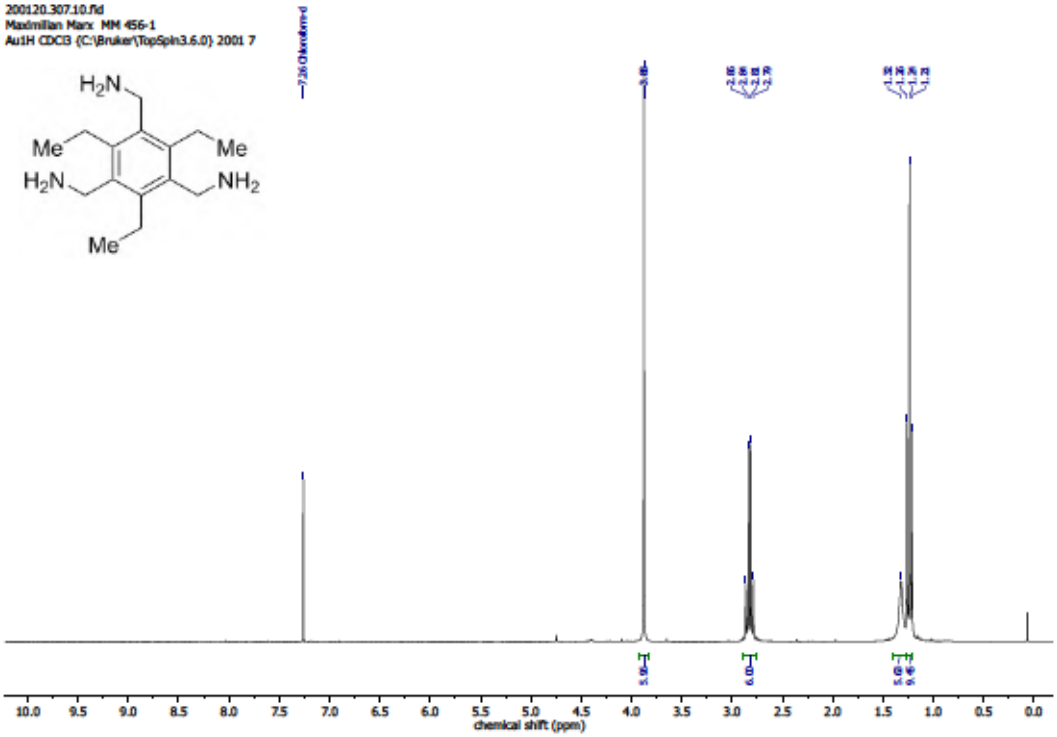

Figure S 88: ^{1}H NMR (300 MHz, $CDCl_3$) of **201**.

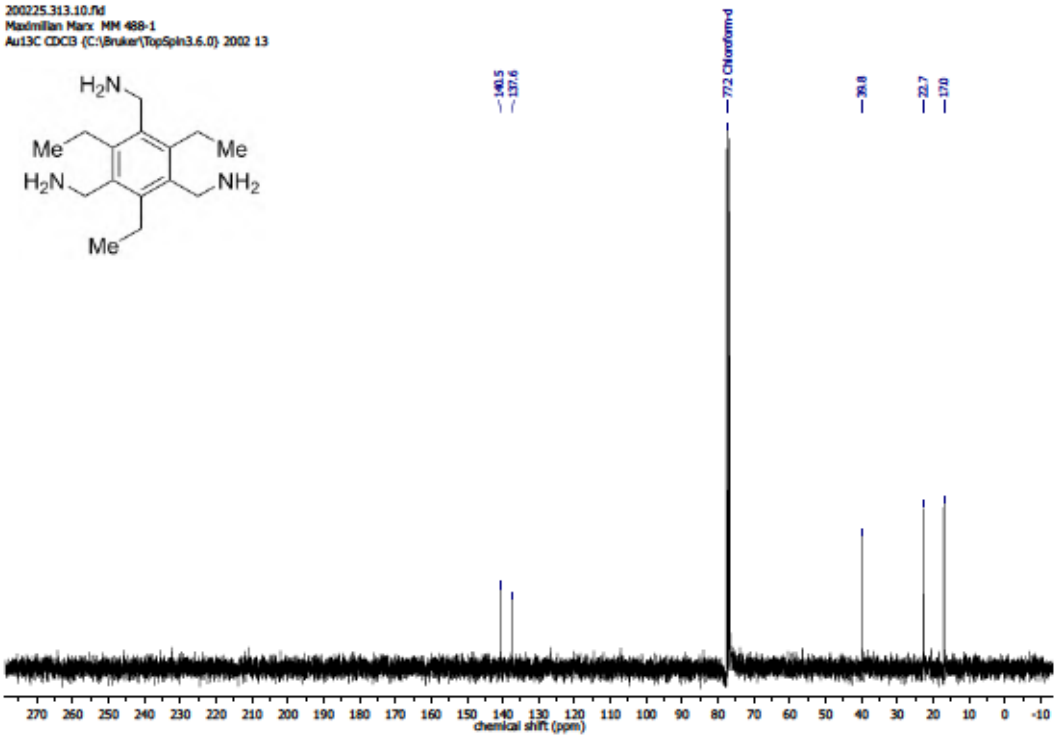

Figure S 89: ^{13}C{^{1}H} NMR (75 MHz, $CDCl_3$) of **201**.

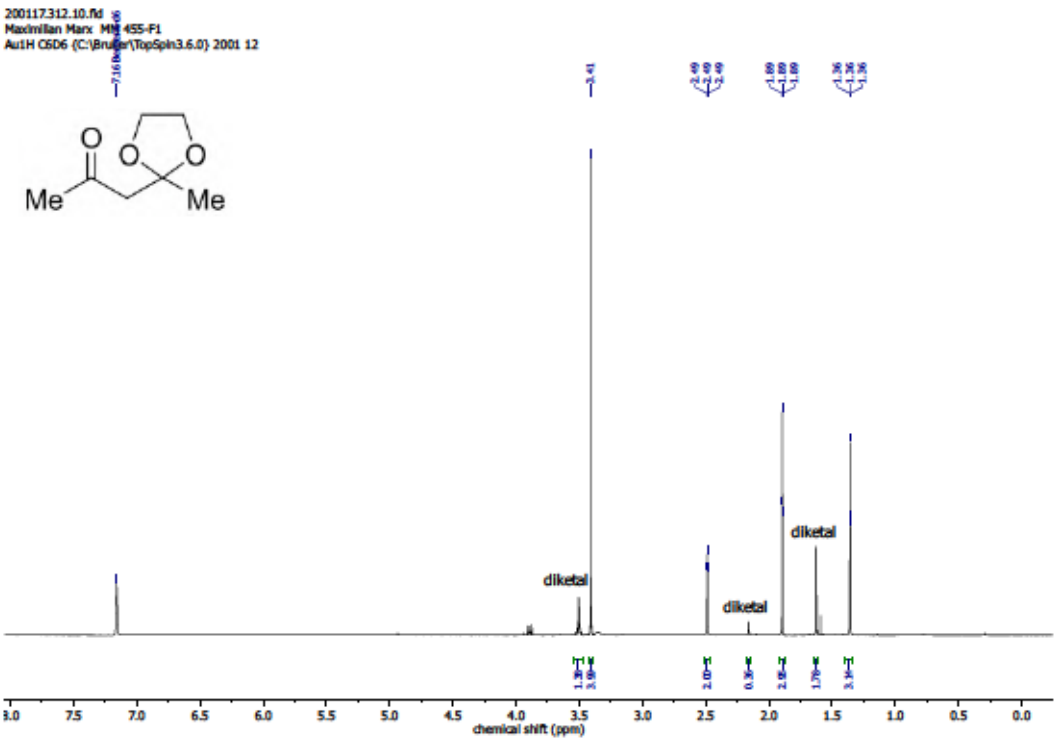

Figure S 90: ^{1}H NMR (300 MHz, C_6D_6) of **202**.

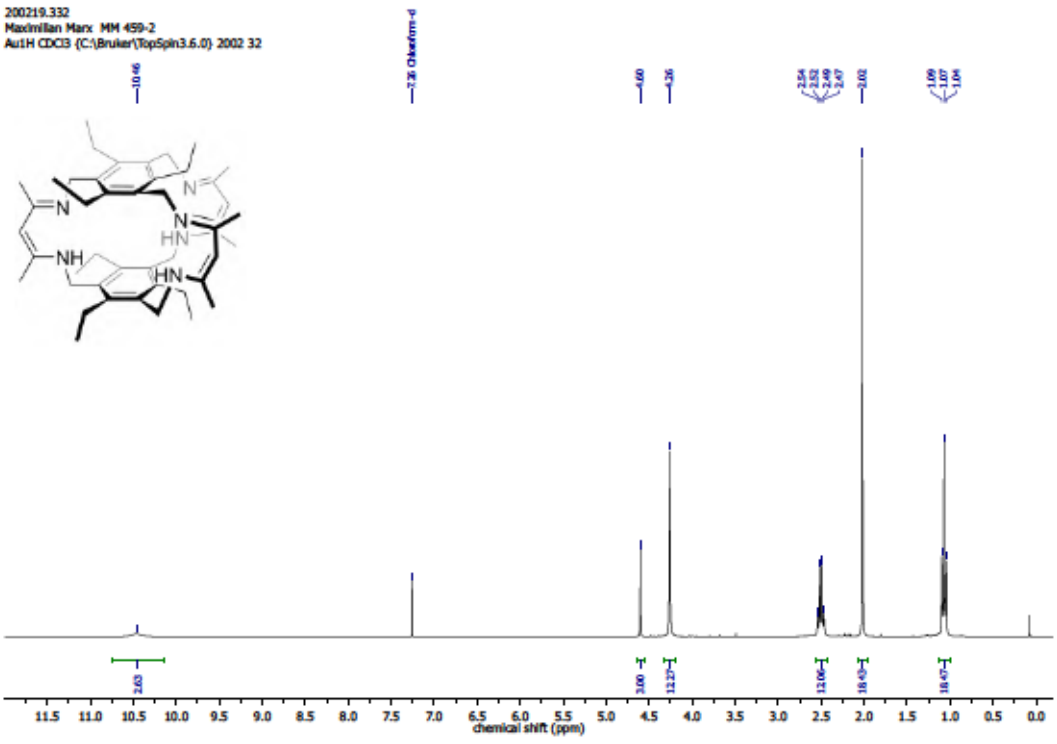

Figure S 91: ^{1}H NMR (300 MHz, $CDCl_3$) of **142**.

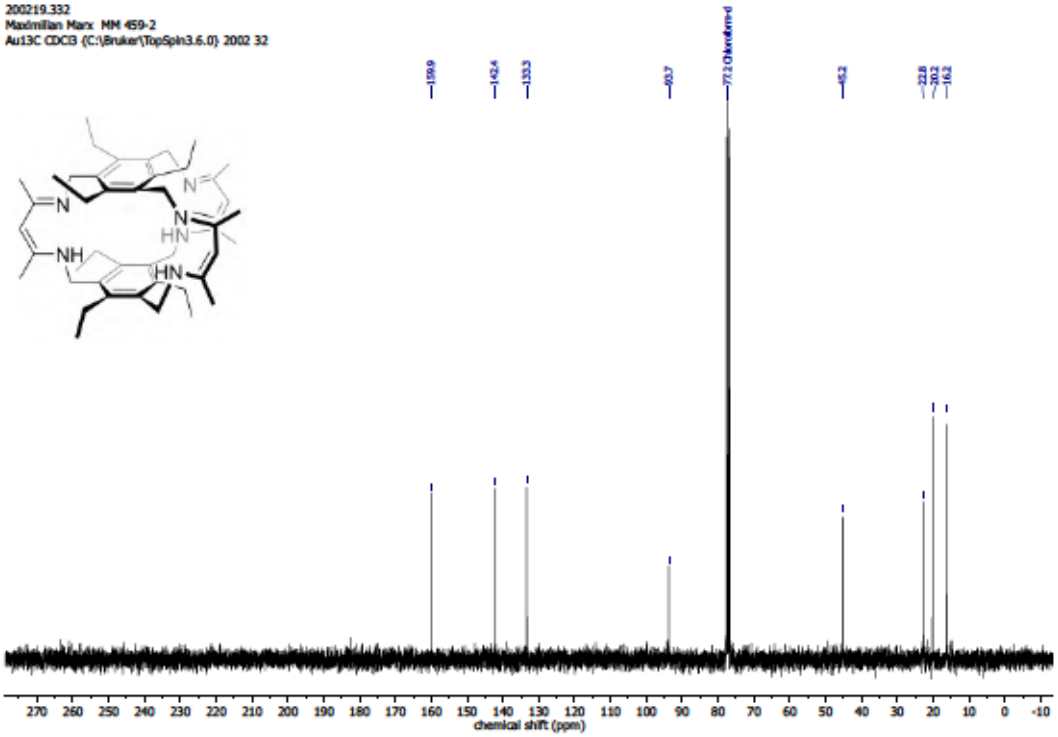

Figure S 92: $^{13}C\{^{1}H\}$ NMR (75 MHz, $CDCl_3$) of **142**.

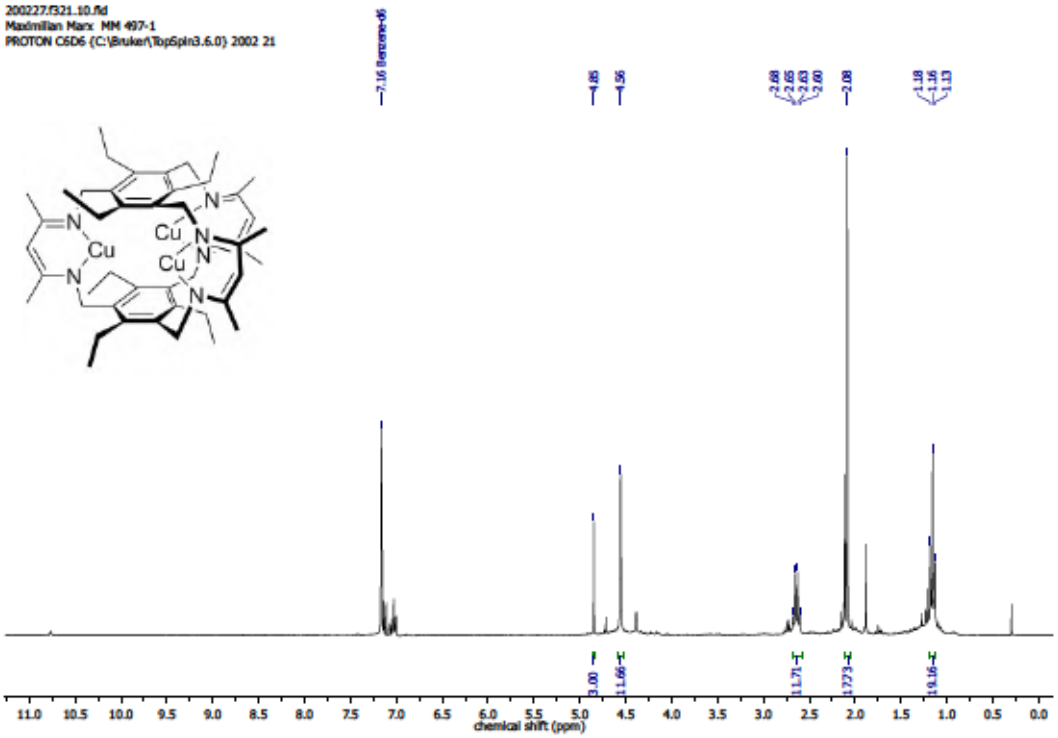

Figure S 93: ^{1}H NMR (300 MHz, C_6D_6) of **203**.

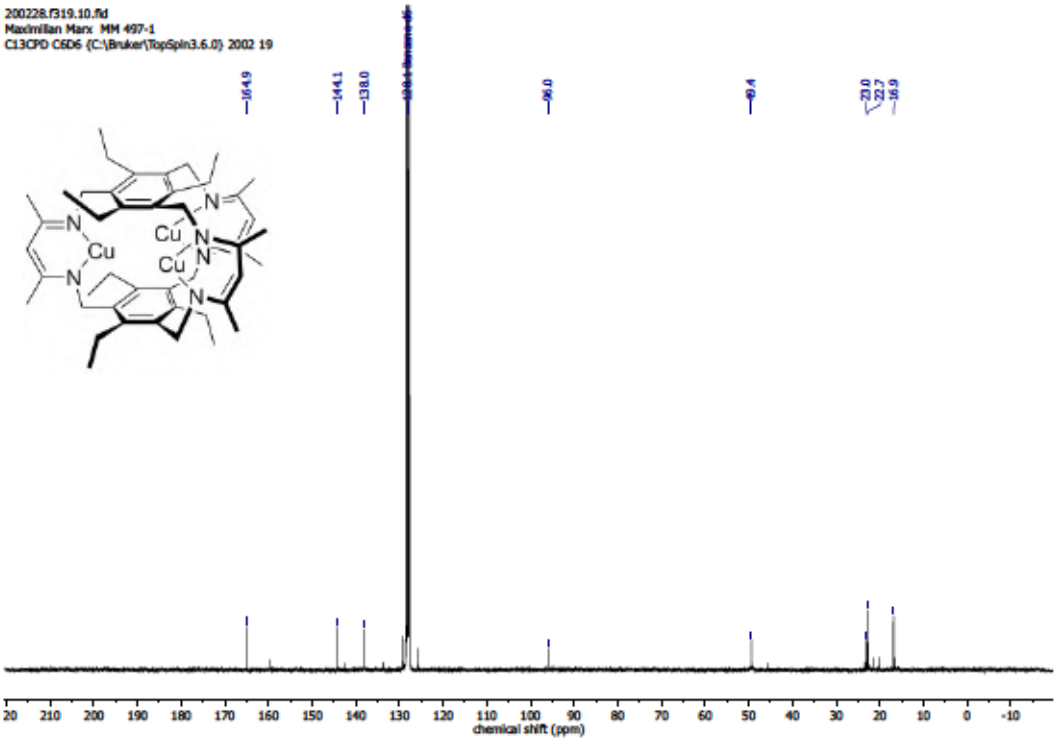

Figure S 94: $^{13}C\{^{1}H\}$ NMR (75 MHz, C_6D_6) of **203**.

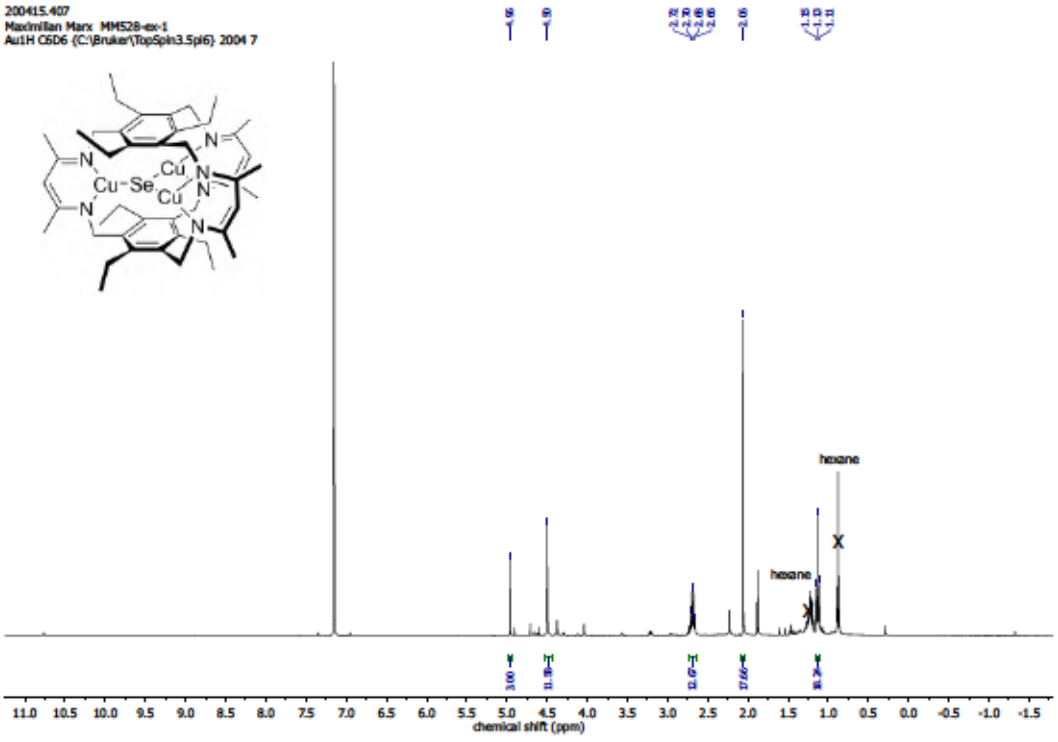

Figure S 95: ^{1}H NMR (400 MHz, C_6D_6) of **139**.

4.12.2 NMR Spectra – CO_2 Reductive Coupling with Disulfide-derived Cu Complexes

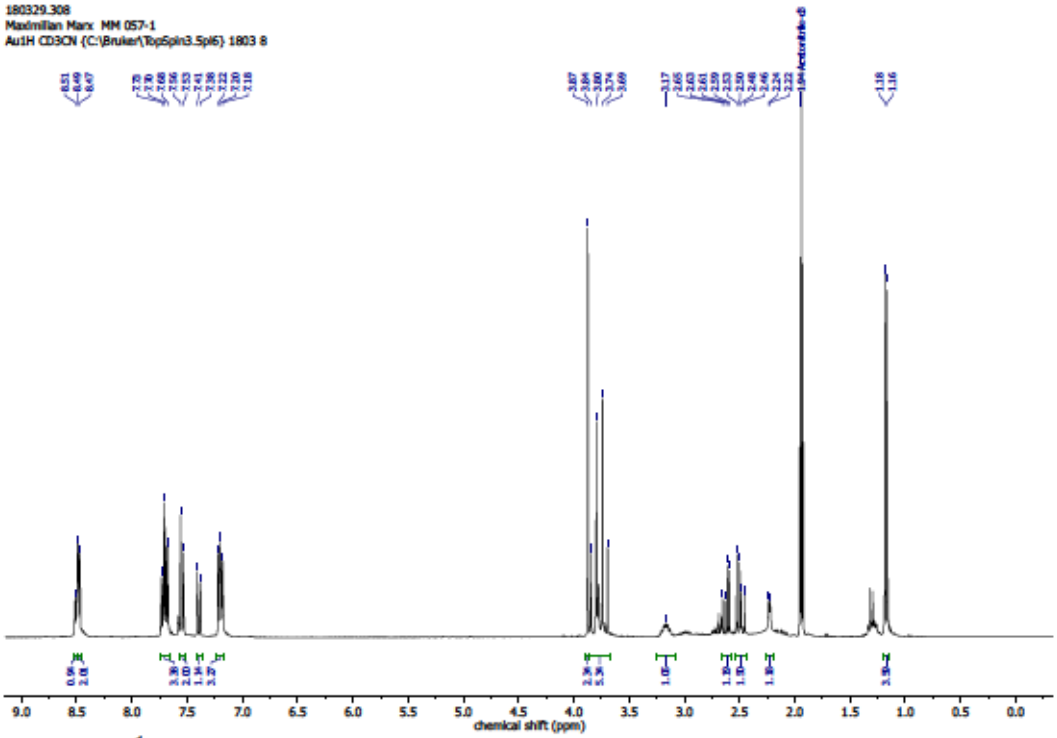

Figure S 96: ^{1}H NMR (300 MHz, CD_3CN) of the reaction of dipicolylamine and propylene sulfide in dry MeCN (13 h reflux) and subsequent aerial oxidation (18 h) according to a literature procedure.[169]

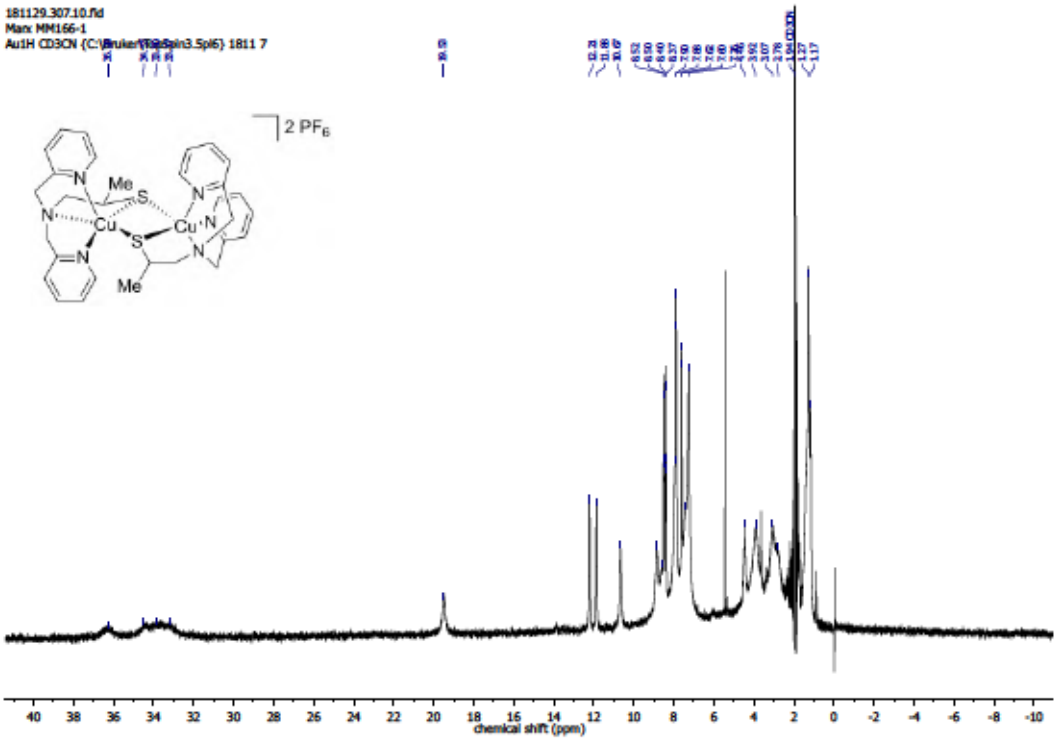

Figure S 97: ^{1}H NMR (300 MHz, CD_3CN) of **155**.

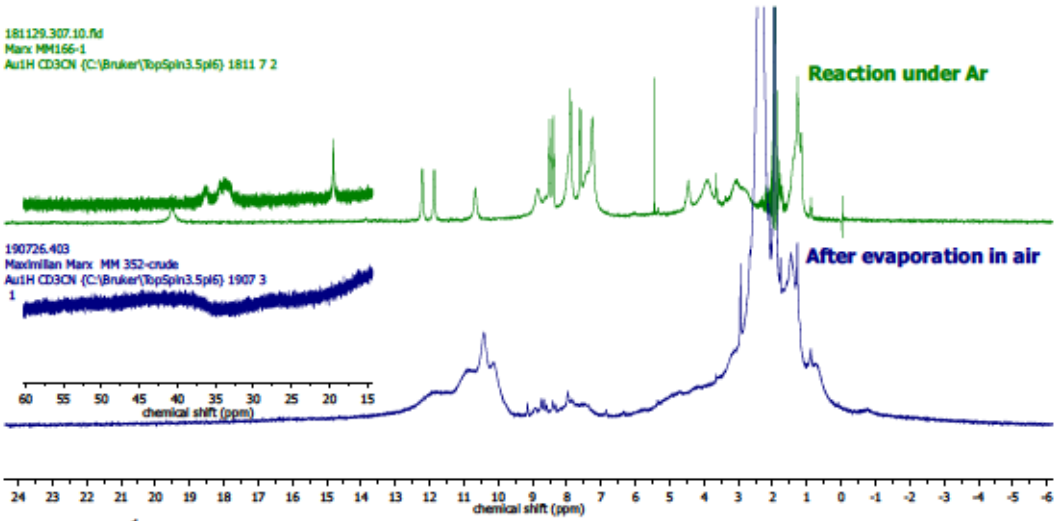

Figure S 98: ^{1}H NMR (CD_3CN) of **155** (green) and of the product obtained after evaporation of *in situ* formed **155** in air (blue) (see 4.5.3).

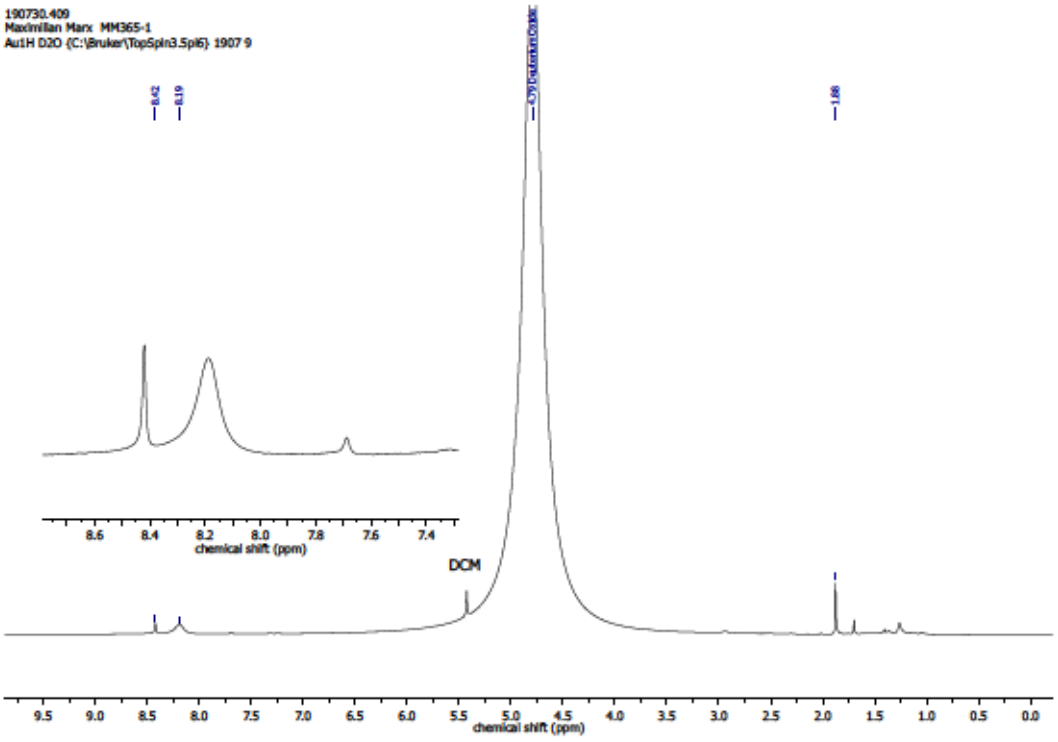

Figure S 99: ^{1}H NMR (400 MHz, D_2O) of of the product obtained after evaporation of *in situ* formed **155** in air and subsequent NaOH treatment.

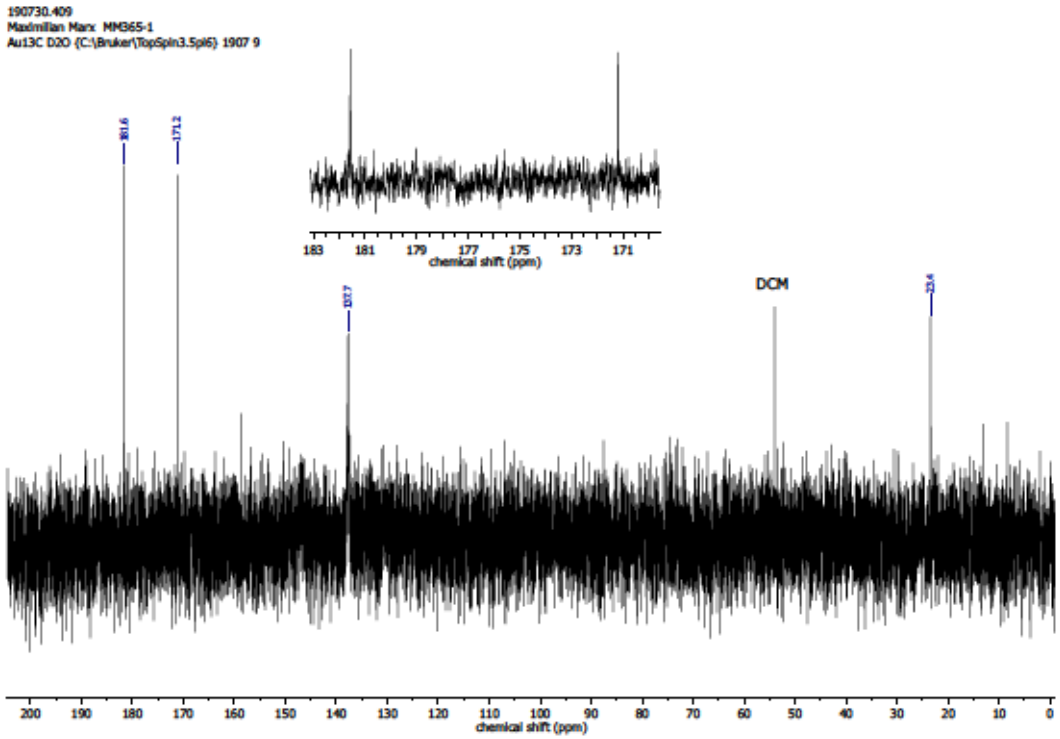

Figure S 100: $^{13}C\{^{1}H\}$ NMR (101 MHz, D_2O) of of the product obtained after evaporation of *in situ* formed **155** in air and subsequent NaOH treatment.

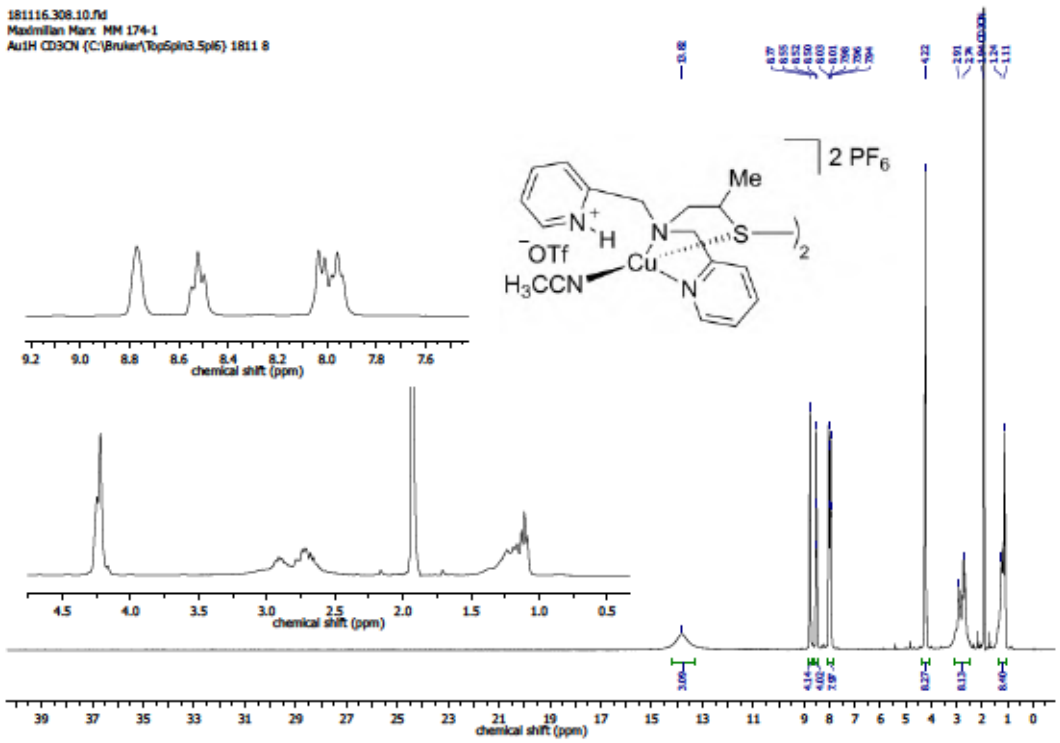

Figure S 101: ^{1}H NMR (300 MHz, CD_3CN) after protonation of **155** resulting in **156** and subsequent CO_2 treatment (see 4.5.4).

4.12.3 NMR Spectra – Reactions with [Fe(tmtaa)]

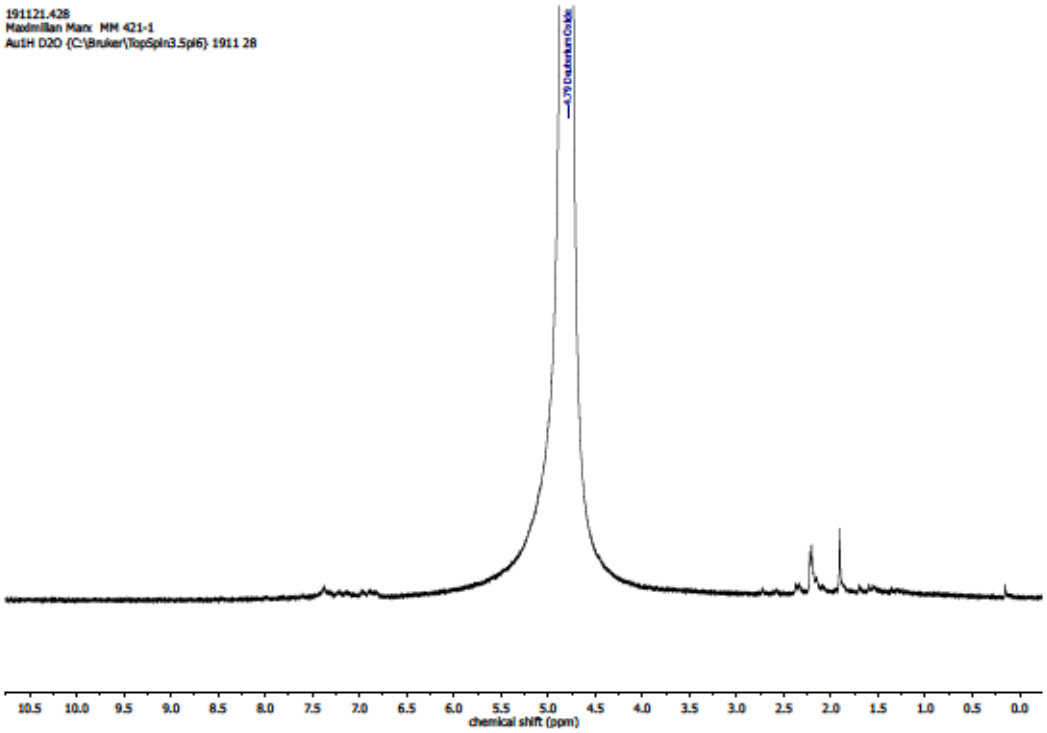

Figure S 102: ^{1}H NMR spectrum (400 MHz, D_2O) of the aqueous extract of the reaction of **118** with $NaC_{10}H_8$ and subsequent CO_2 treatment in toluene (Table S 12, entry 1).

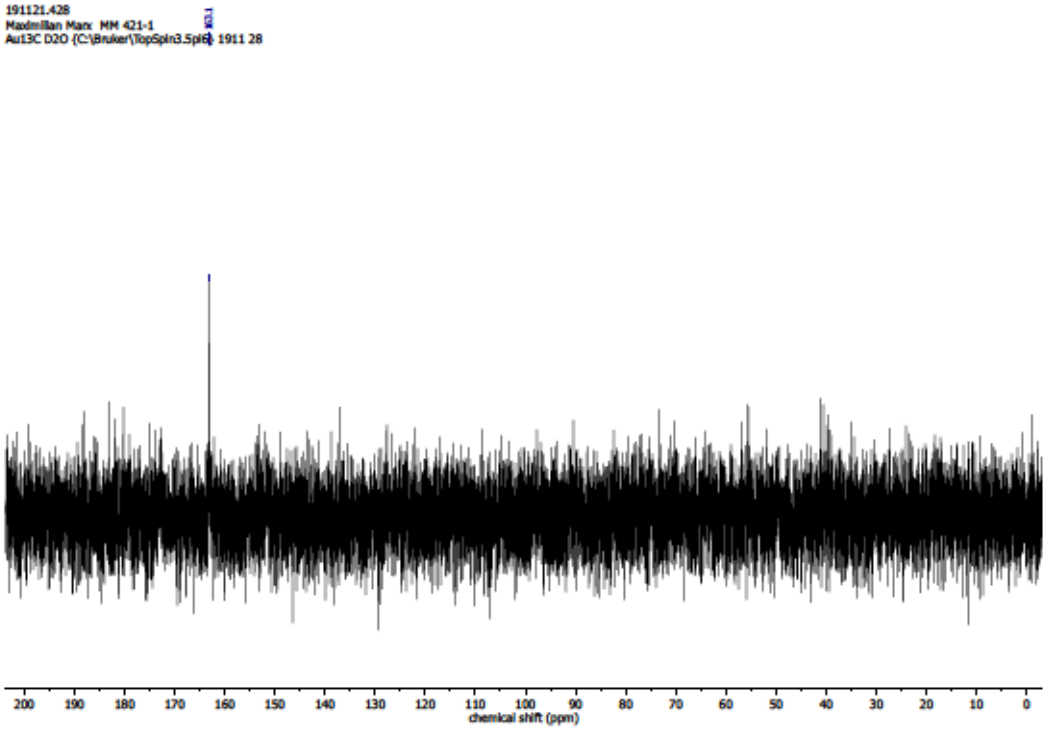

Figure S 103: $^{13}C\{^{1}H\}$ NMR spectrum (101 MHz, D_2O) of the aqueous extract of the reaction of **118** with $NaC_{10}H_8$ and subsequent CO_2 treatment in toluene (Table S 12, entry 1).

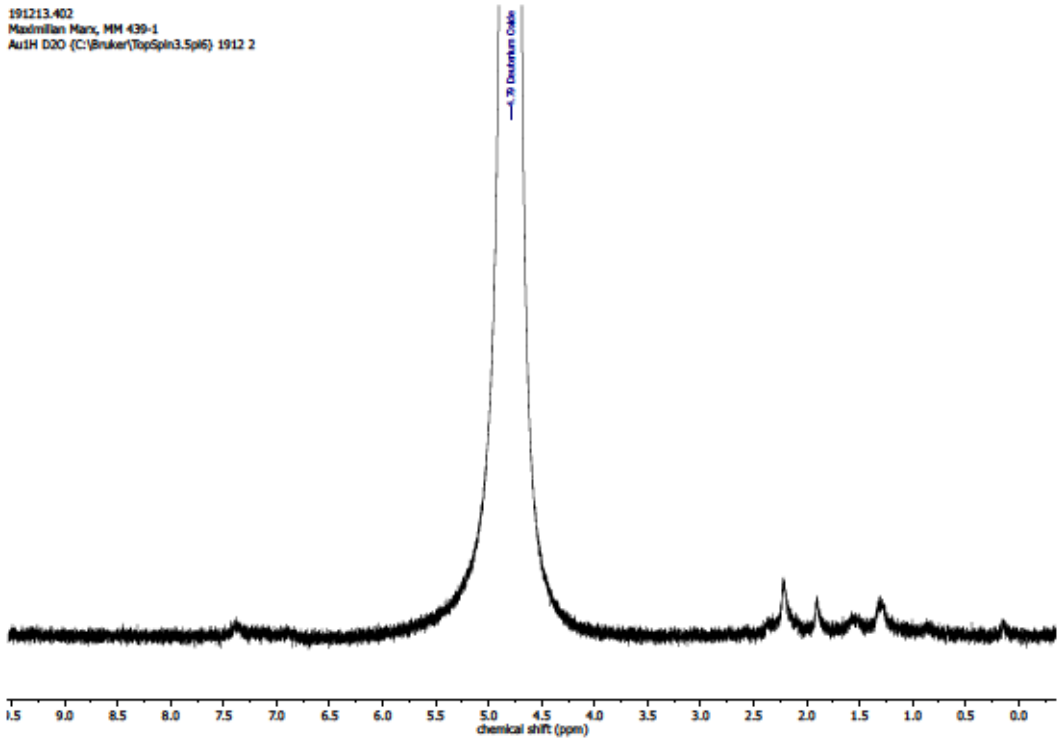

Figure S 104: ^{1}H NMR spectrum (400 MHz, D_2O) of the aqueous extract of the reaction of **118** with $NaC_{10}H_8$ and subsequent CO_2 treatment in toluene (Table S 12, entry 2).

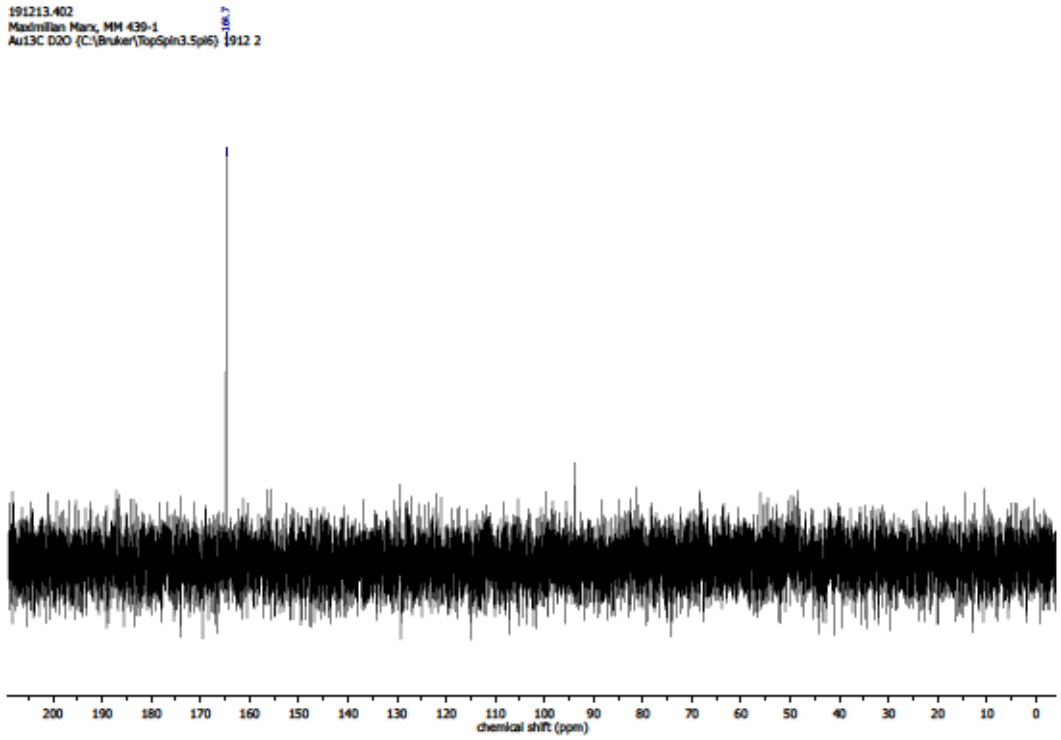

Figure S 105: $^{13}C\{^{1}H\}$ NMR spectrum (101 MHz, D_2O) of the aqueous extract of the reaction of **118** with $NaC_{10}H_8$ and subsequent CO_2 treatment in toluene (Table S 12, entry 2).

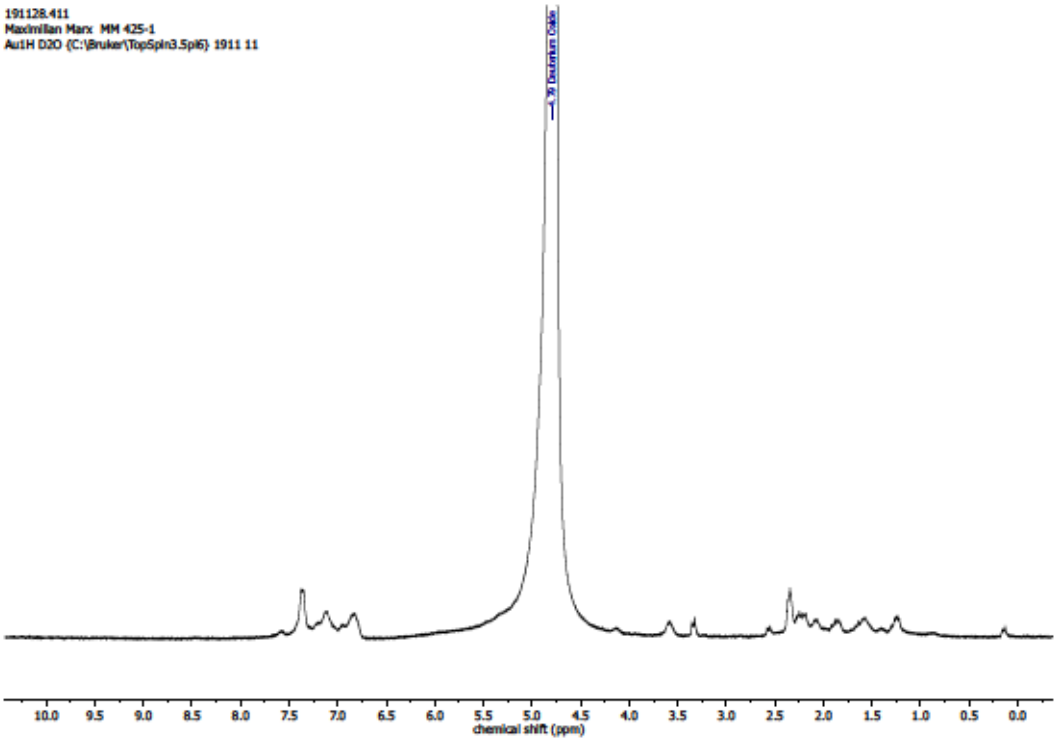

Figure S 106: ^{1}H NMR spectrum (400 MHz, D_2O) of the aqueous extract of the reaction of **118** with Na and subsequent CO_2 treatment in toluene (Table S 12, entry 3).

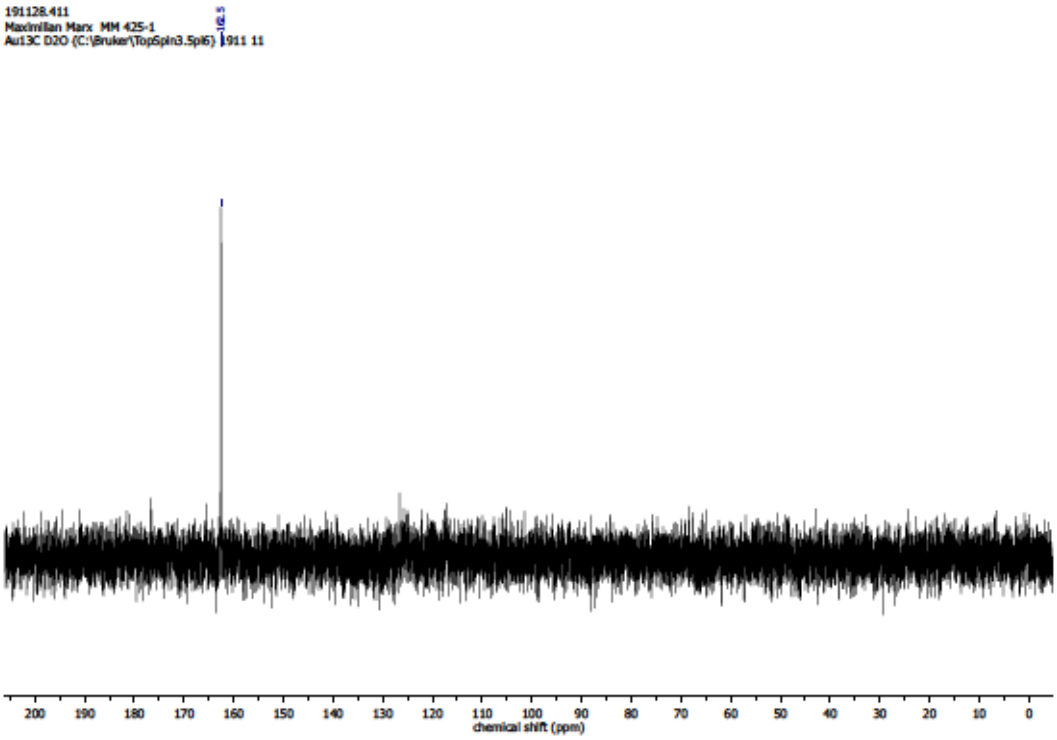

Figure S 107: $^{13}C\{^{1}H\}$ NMR spectrum (101 MHz, D_2O) of the aqueous extract of the reaction of **118** with Na and subsequent CO_2 treatment in toluene (Table S 12, entry 3).

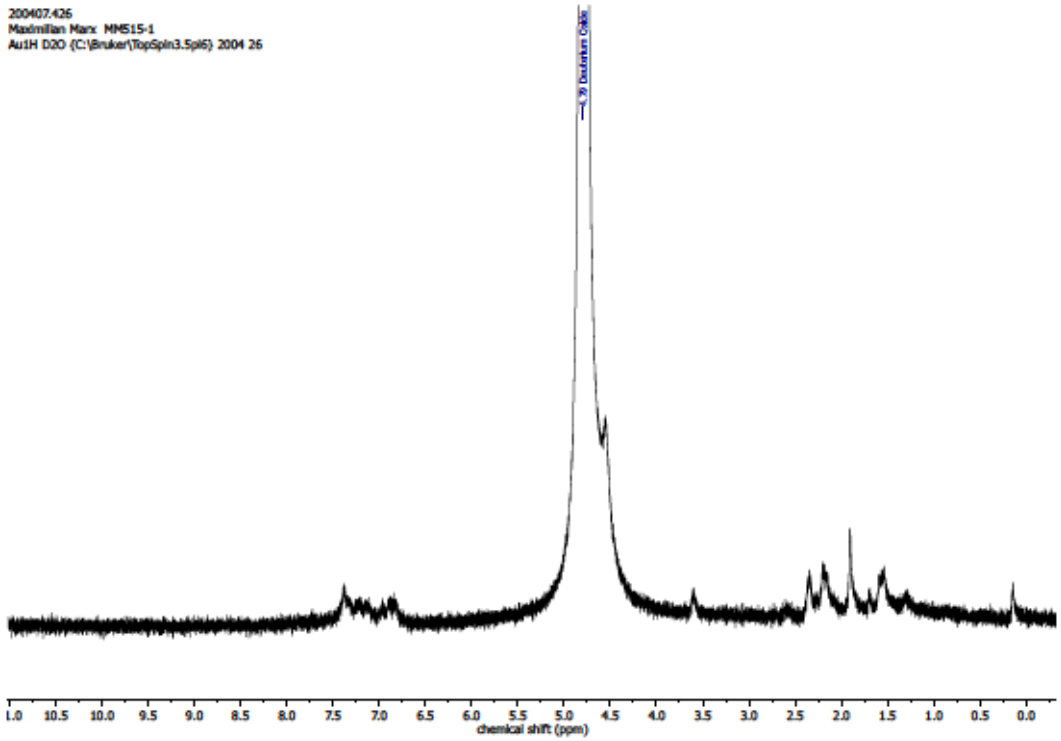

Figure S 108: ^{1}H NMR spectrum (400 MHz, D_2O) of the aqueous extract of the reaction of **118** with Na and subsequent CO_2 treatment in toluene (Table S 12, entry 4).

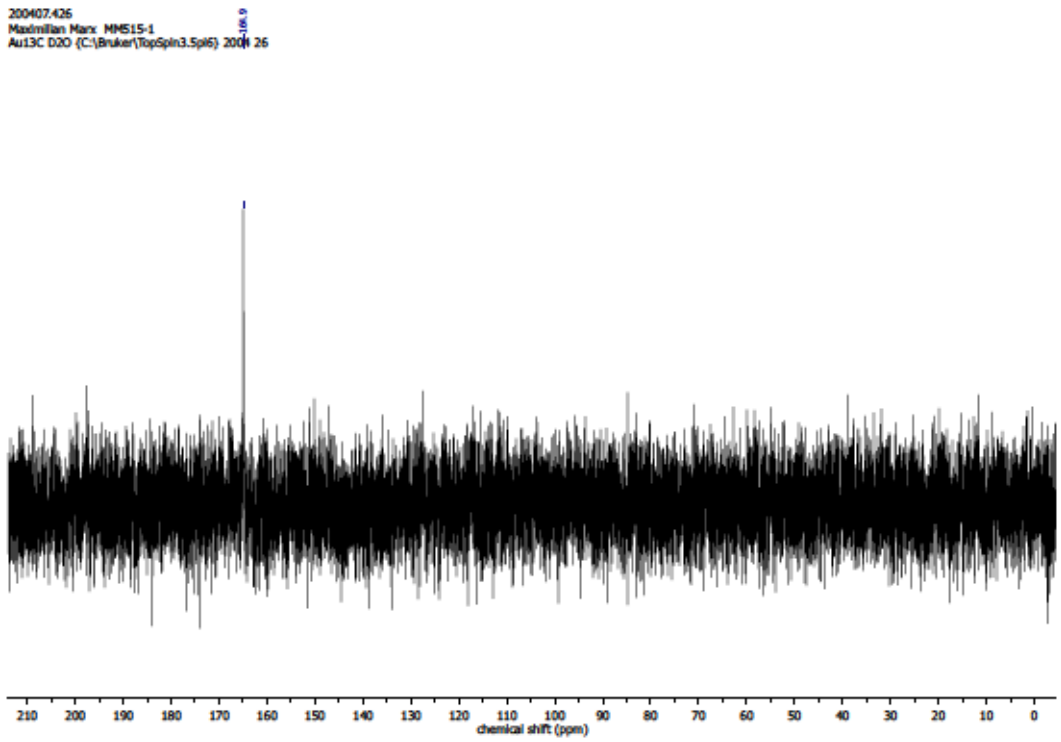

Figure S 109: $^{13}C\{^{1}H\}$ NMR spectrum (101 MHz, D_2O) of the aqueous extract of the reaction of **118** with Na and subsequent CO_2 treatment in toluene (Table S 12, entry 4).

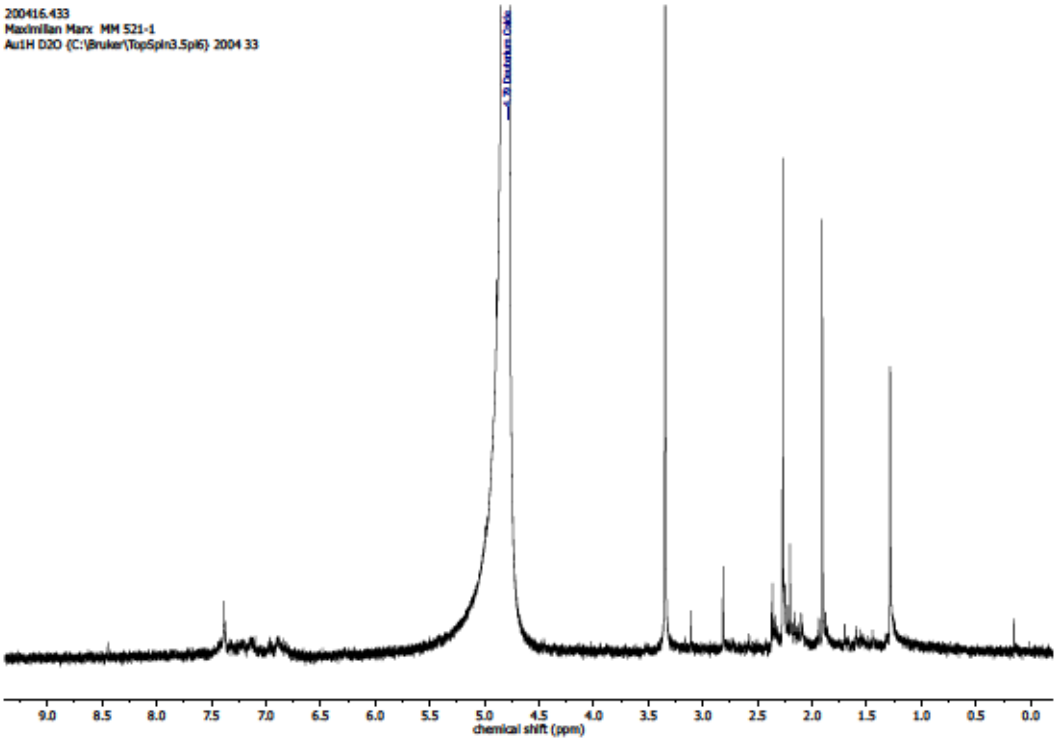

Figure S 110: ^{1}H NMR spectrum (400 MHz, D_2O) of the aqueous extract of the reaction of **118** with K and subsequent CO_2 treatment in toluene (Table S 12, entry 5).

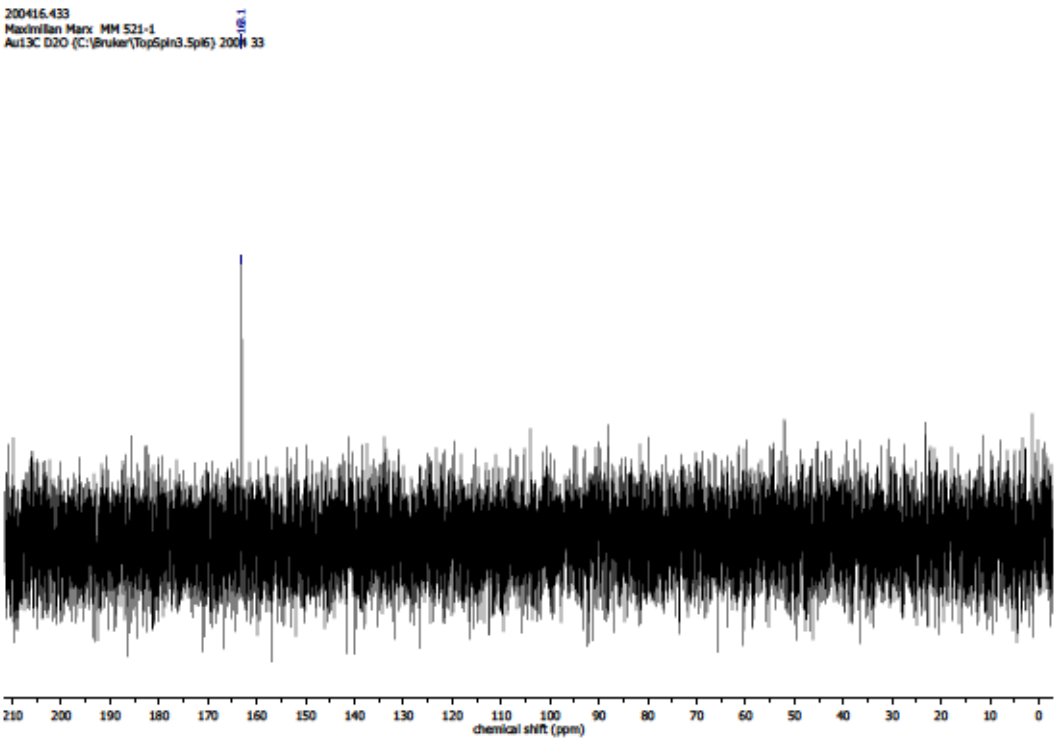

Figure S 111: $^{13}C\{^{1}H\}$ NMR spectrum (101 MHz, D_2O) of the aqueous extract of the reaction of **118** with K and subsequent CO_2 treatment in toluene (Table S 12, entry 5).

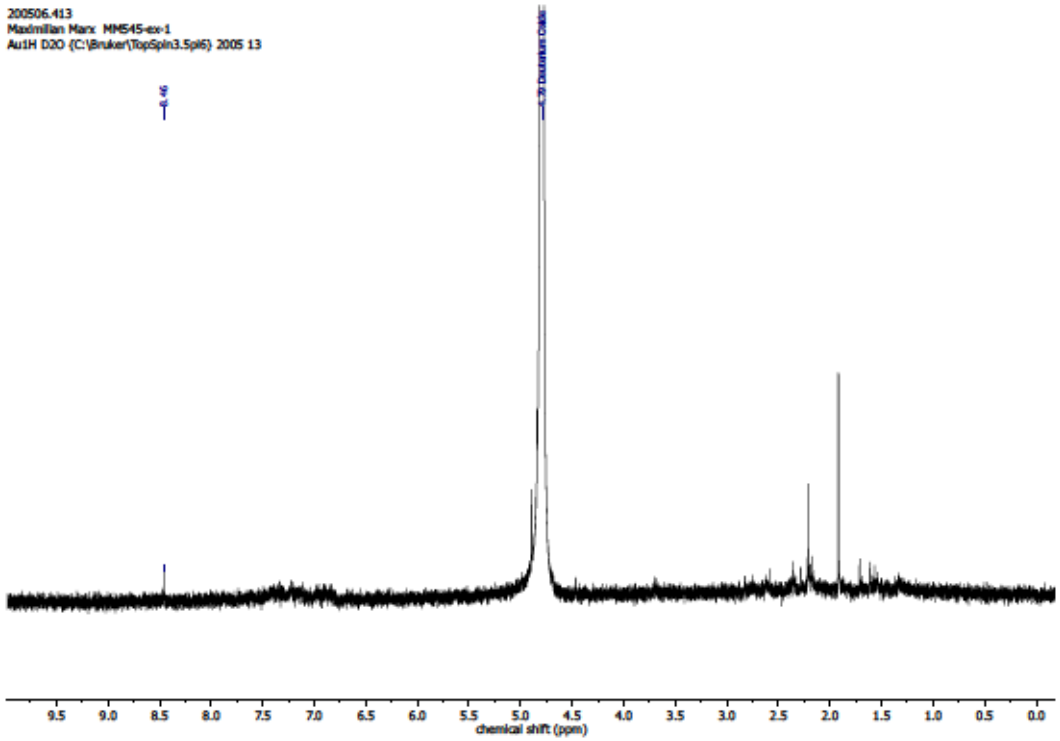

Figure S 112: ^{1}H NMR spectrum (400 MHz, D_2O) of the aqueous extract of the reaction of **118** with K and subsequent CO_2 treatment in toluene (Table S 12, entry 6).

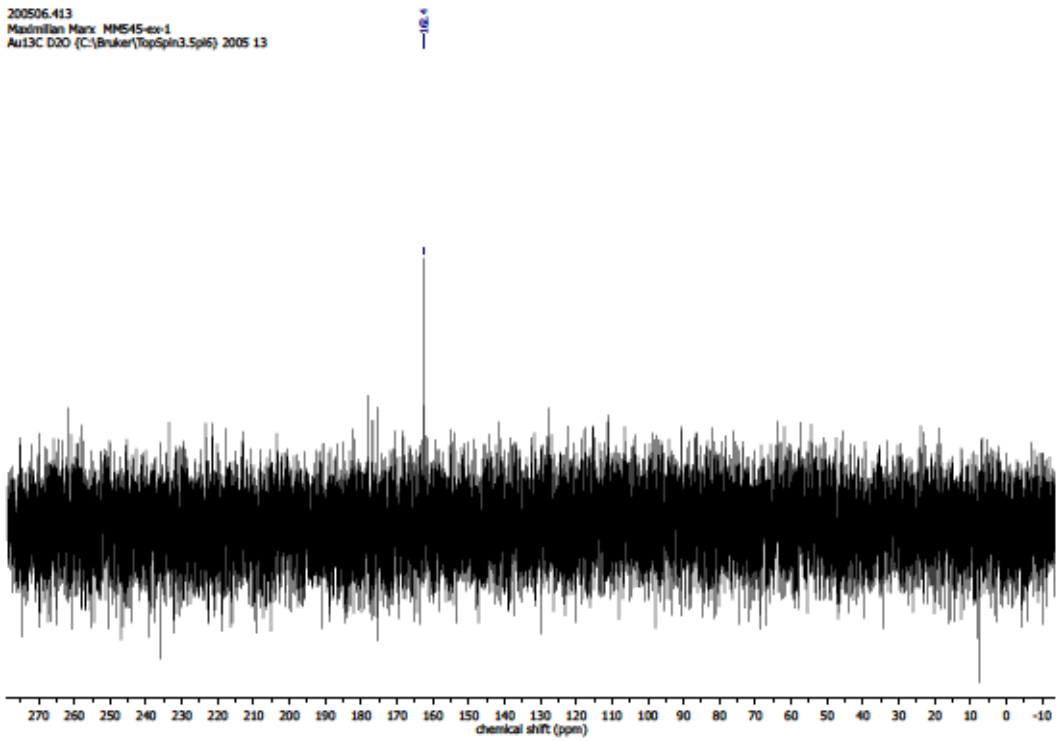

Figure S 113: $^{13}C\{^{1}H\}$ NMR spectrum (101 MHz, D_2O) of the aqueous extract of the reaction of **118** with K and subsequent CO_2 treatment in toluene (Table S 12, entry 6).

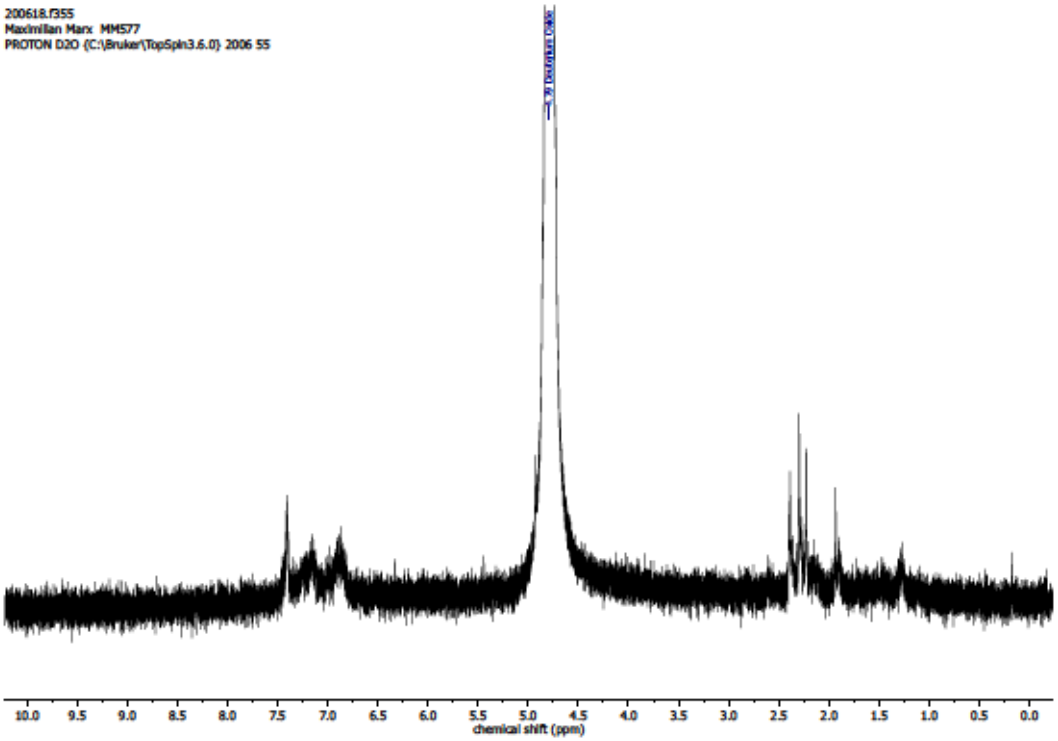

Figure S 114: ^{1}H NMR spectrum (300 MHz, D_2O) of the aqueous extract of the reaction of **118** with K and subsequent CO_2 treatment in toluene (Table S 12, entry 7).

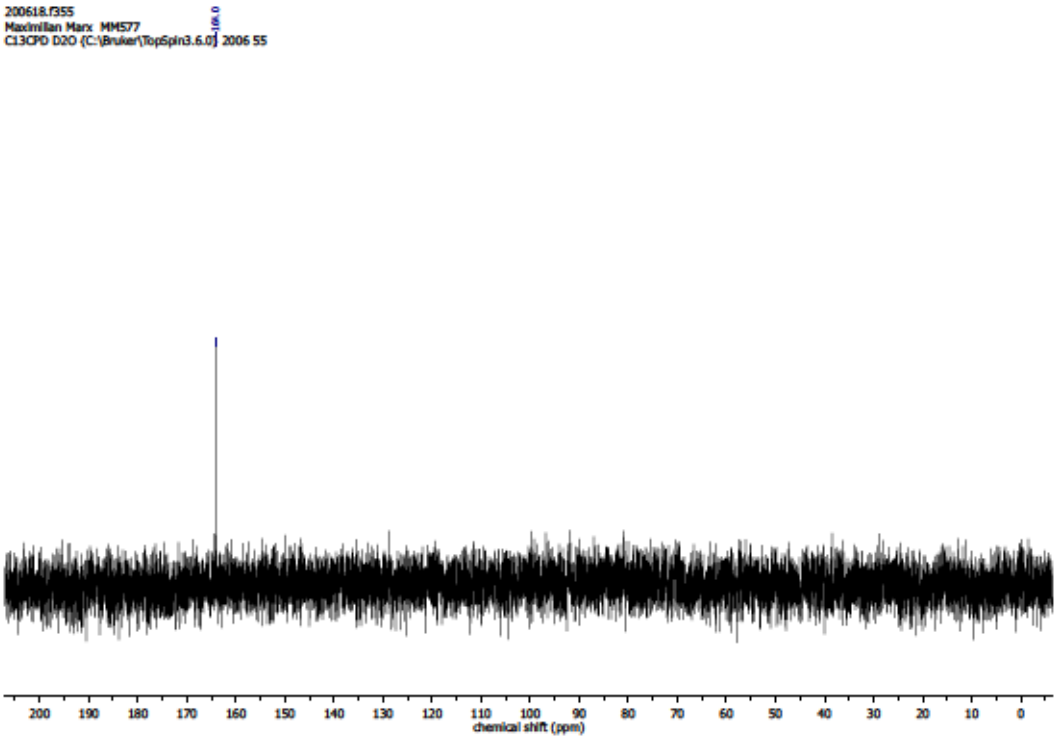

Figure S 115: $^{13}C\{^{1}H\}$ NMR spectrum (75 MHz, D_2O) of the aqueous extract of the reaction of **118** with K and subsequent CO_2 treatment in toluene (Table S 12, entry 7).

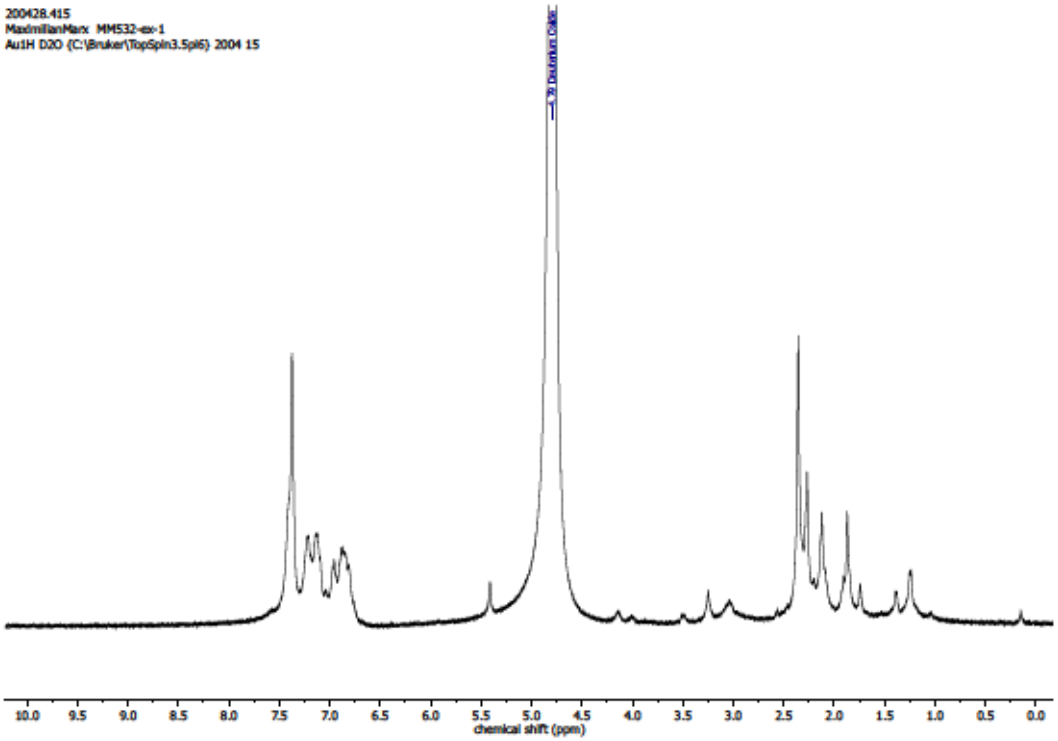

Figure S 116: ^{1}H NMR spectrum (400 MHz, D_2O) of the aqueous extract of the reaction of **118** with K and subsequent CO_2 treatment in THF (Table S 12, entry 8).

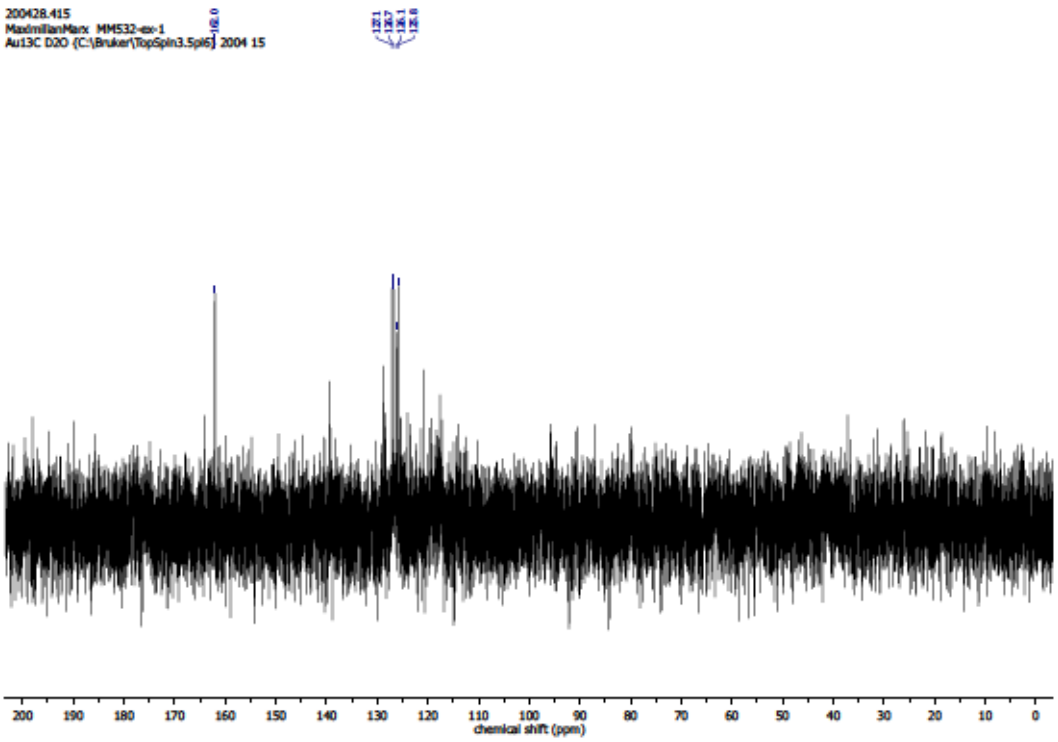

Figure S 117: $^{13}C\{^{1}H\}$ NMR spectrum (101 MHz, D_2O) of the aqueous extract of the reaction of **118** with K and subsequent CO_2 treatment in THF (Table S 12, entry 8).

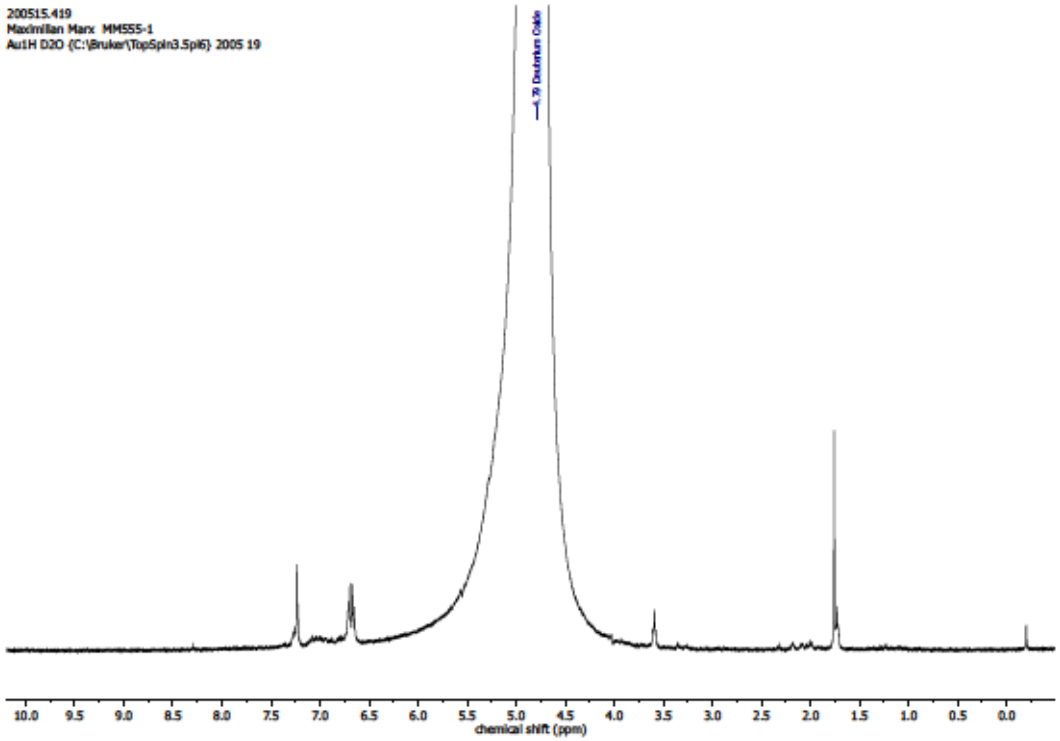

Figure S 118: ^{1}H NMR spectrum (400 MHz, D_2O) of the aqueous extract of the reaction of **118** with K and subsequent CO_2 treatment in THF (Table S 12, entry 9).

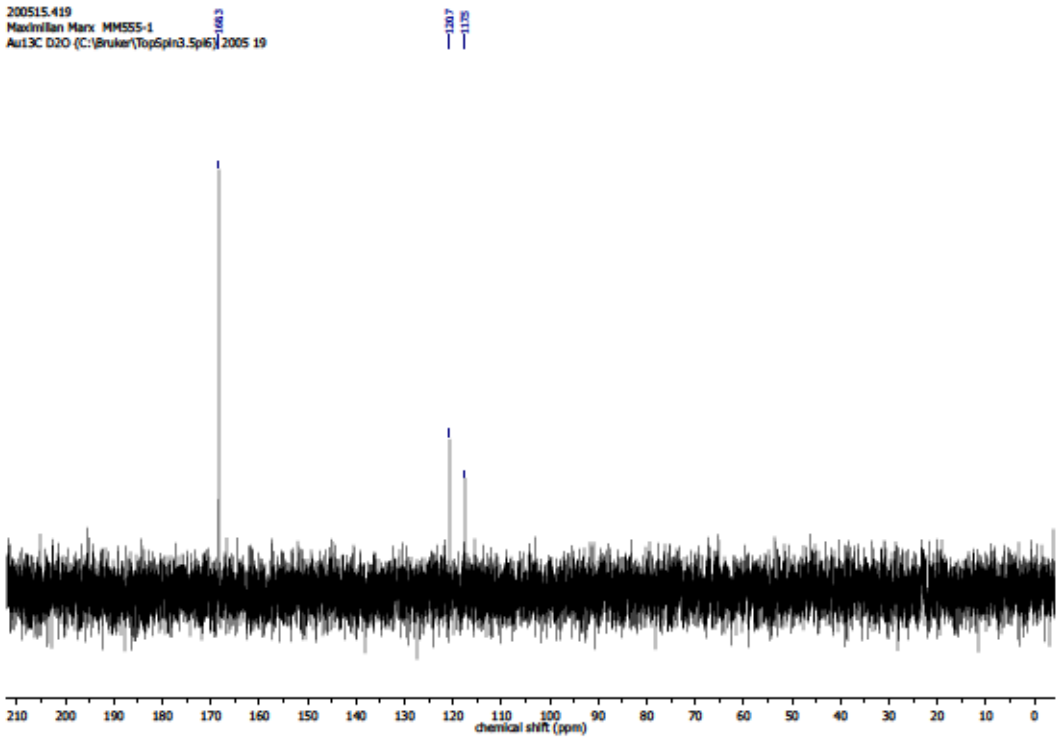

Figure S 119: $^{13}C\{^{1}H\}$ NMR spectrum (101 MHz, D_2O) of the aqueous extract of the reaction of **118** with K and subsequent CO_2 treatment in THF (Table S 12, entry 9).

4.12.4 NMR Spectra – Reactions of 1,4,7-Tacn-ligated Cu Complexes

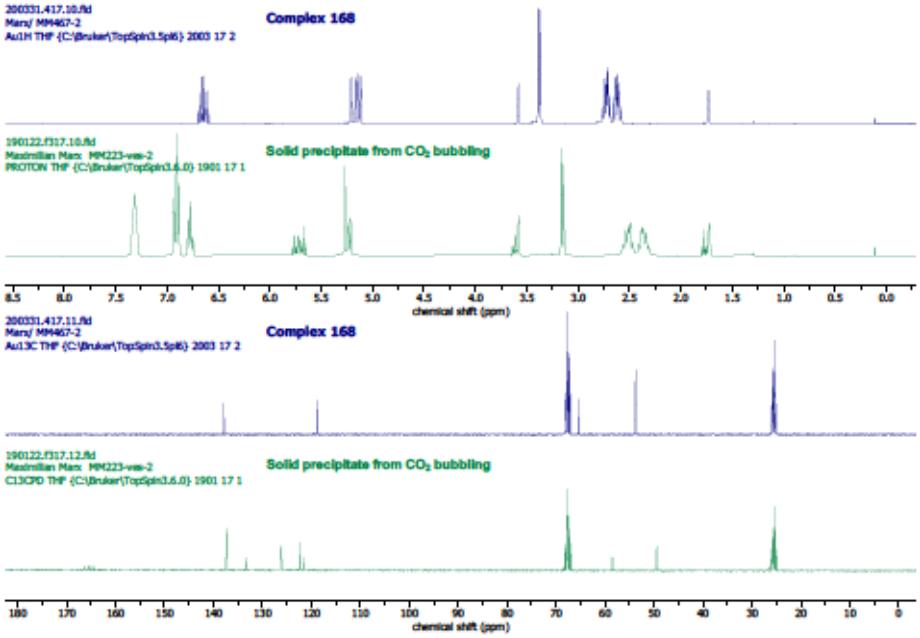

Figure S 120: ^{1}H NMR and ^{13}C NMR spectra (THF-d_8) of complex **168** (blue) and of the solid precipitate formed upon CO_2 bubbling through a MeOH solution of CuI, **127**, and $NaBPh_4$ (1.7/1/1.5 - Table S 13, entry 2).

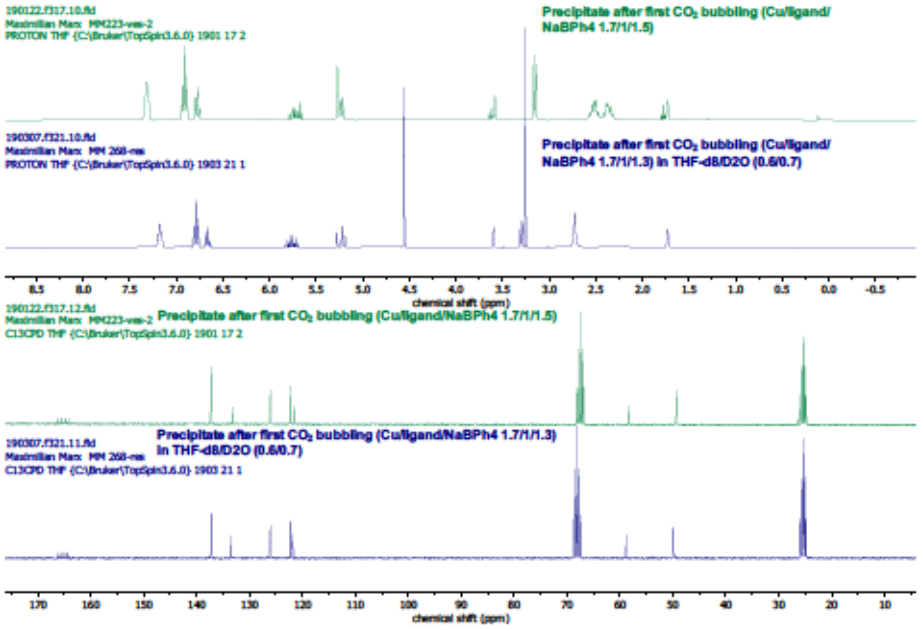

Figure S 121: ^{1}H (300 MHz, THF-d_8 or THF-d_8/D_2O) and ^{13}C (75 MHz, THF-d_8 or THF-d_8/D_2O) NMR spectra of the solid precipitate formed upon CO_2 bubbling through a solution of CuI, **127**, and $NaBPh_4$ in MeOH, isolated by filtration (Green: Table S 13, entry 2; blue: Table S 13, entry 3).

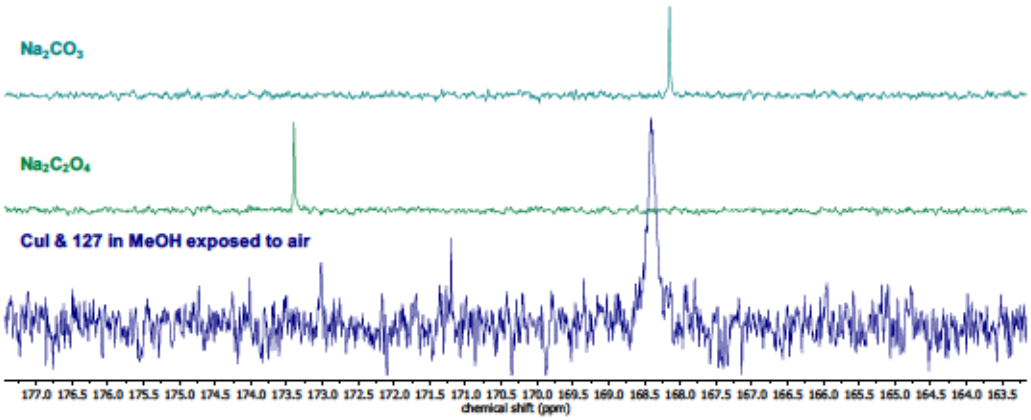

Figure S 122: $^{13}C\{^1H\}$ NMR spectra (D_2O) of the residue obtained after NaOH treatment of the product obtained by air exposure of CuI and **127** in MeOH (Table S 17, entry 5) and NMR spectra of Na_2CO_3 and $Na_2C_2O_4$ for direct comparison.

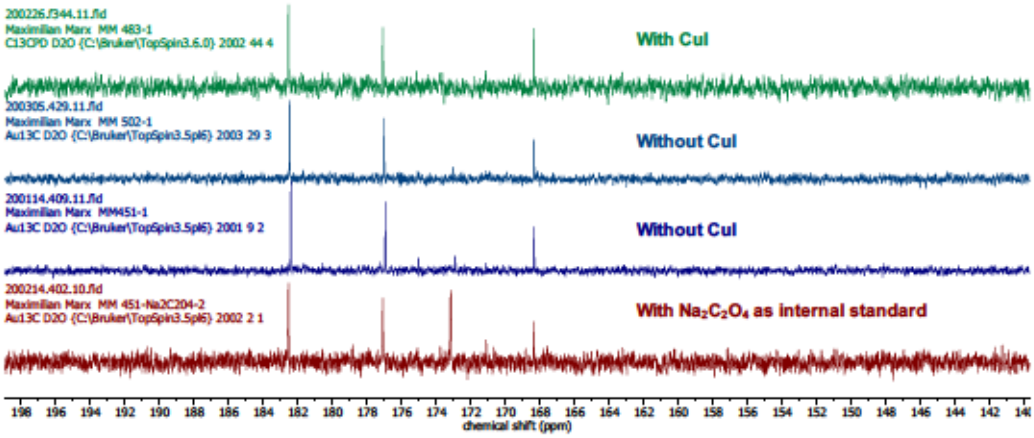

Figure S 123: $^{13}C\{^1H\}$ NMR spectra (D_2O) of the residue obtained after NaOH treatment of the reactions of CO_2 with $NaC_{10}H_8$ with CuI, **127** and $NaBPh_4$ (top, Table S 16, entry 13) and in their absence (Table S 16, entries 15 and 17). $Na_2C_2O_4$ was added as internal standard for direct comparison (bottom).

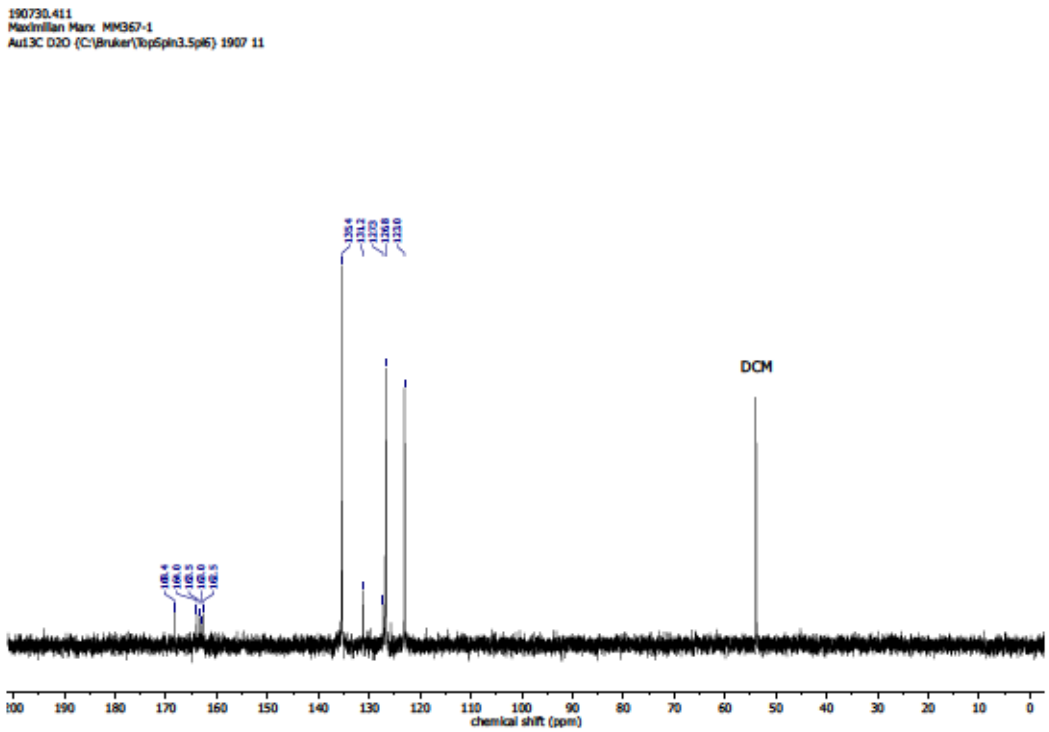

Figure S 124: $^{13}C\{^1H\}$ NMR spectrum (101 MHz, D_2O) of the NaOH extract of Table S 13, entry 2 – CO_2 treatment (bubbling) of **127**, CuI and $NaBPh_4$ in MeOH.

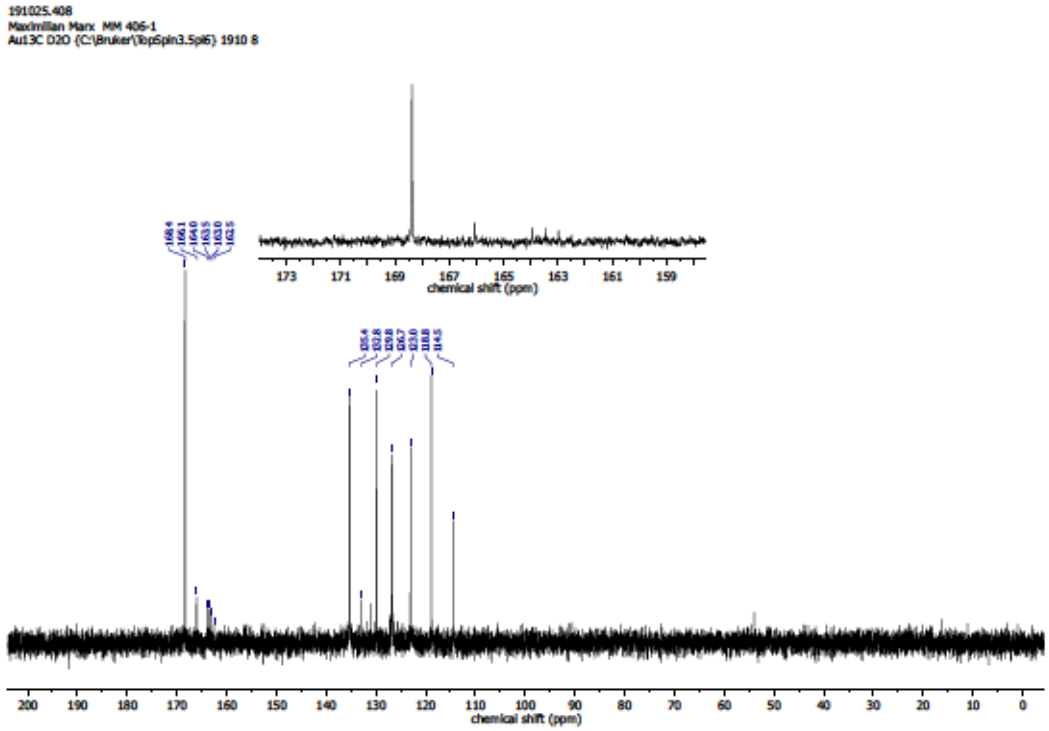

Figure S 125: $^{13}C\{^1H\}$ NMR spectrum (101 MHz, D_2O) of the NaOH extract of Table S 13, entry 3 – CO_2 treatment (bubbling) of **127**, CuI and $NaBPh_4$ in MeOH.

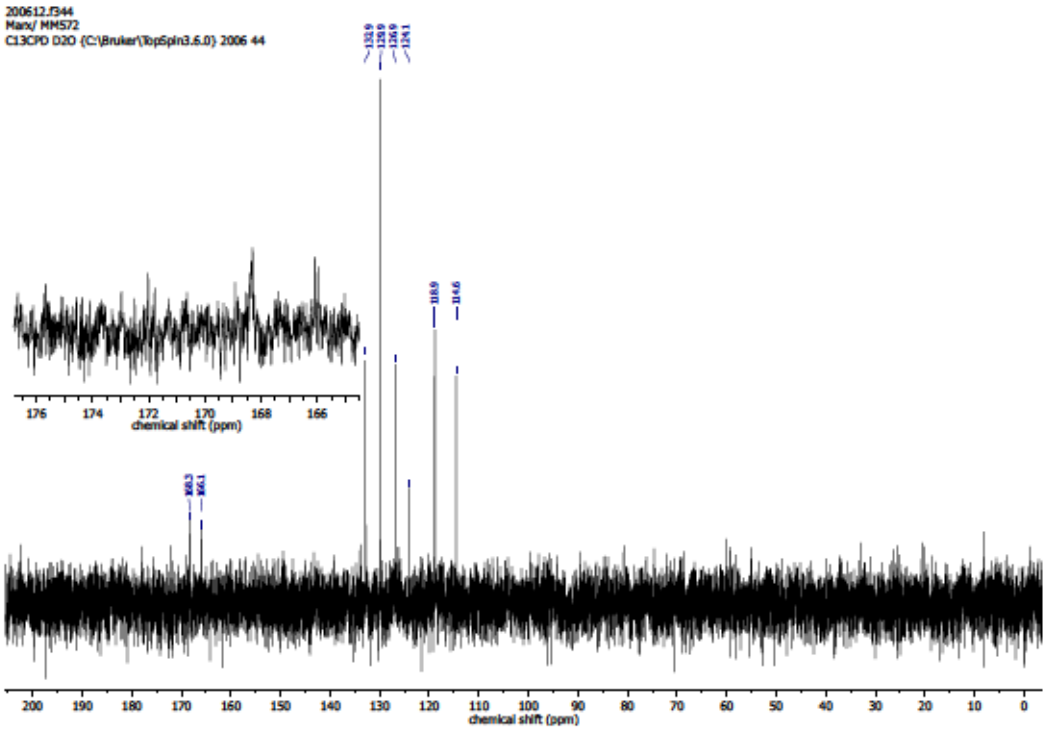

Figure S 126: $^{13}C\{^{1}H\}$ NMR spectrum (75 MHz, D_2O) of the NaOH extract of Table S 13, entry 4 – CO_2 treatment (bubbling) of **127**, CuI and $NaBPh_4$ in MeOH.

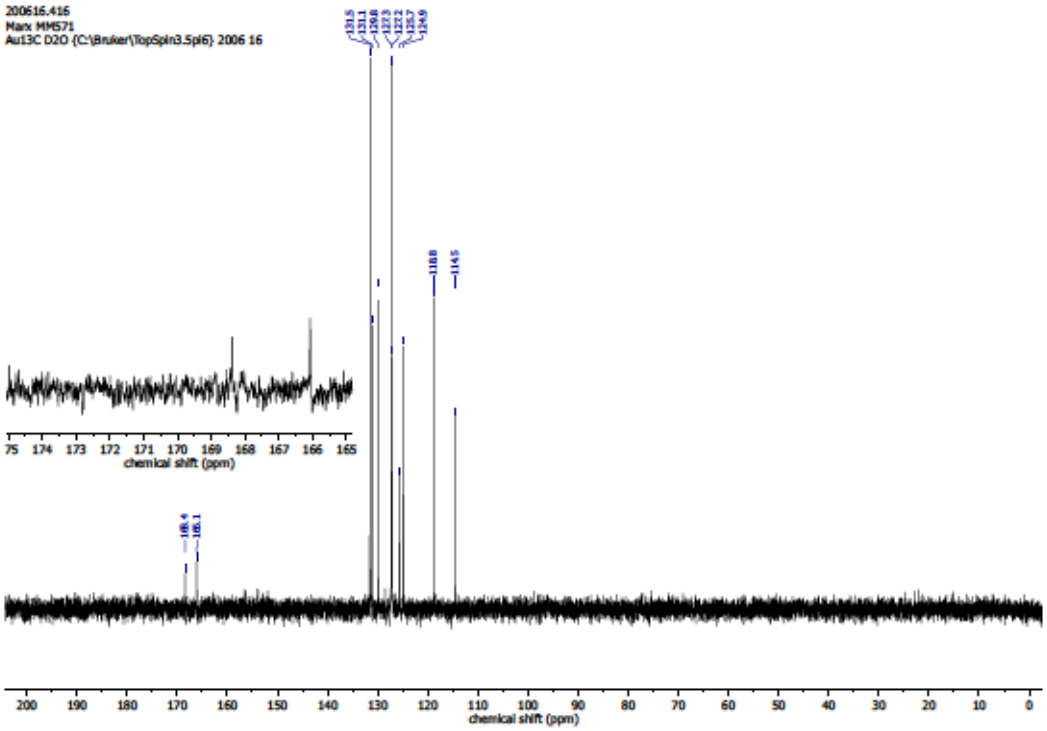

Figure S 127: $^{13}C\{^{1}H\}$ NMR spectrum (101 MHz, D_2O) of the NaOH extract of Table S 13, entry 5 – CO_2 treatment (bubbling) of **127**, CuI and $NaBPh_4$ in MeOH.

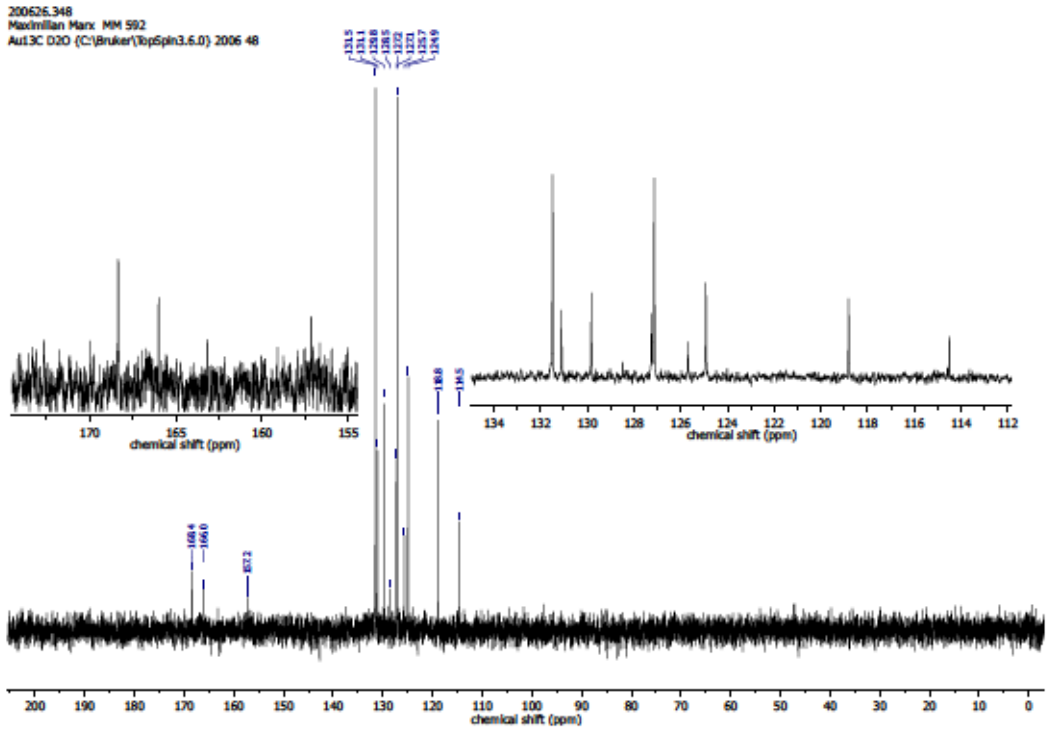

Figure S 128: $^{13}C\{^{1}H\}$ NMR spectrum (75 MHz, D_2O) of the NaOH extract of Table S 13, entry 6 – CO_2 treatment (bubbling) of **127**, CuI and $NaBPh_4$ in MeOH.

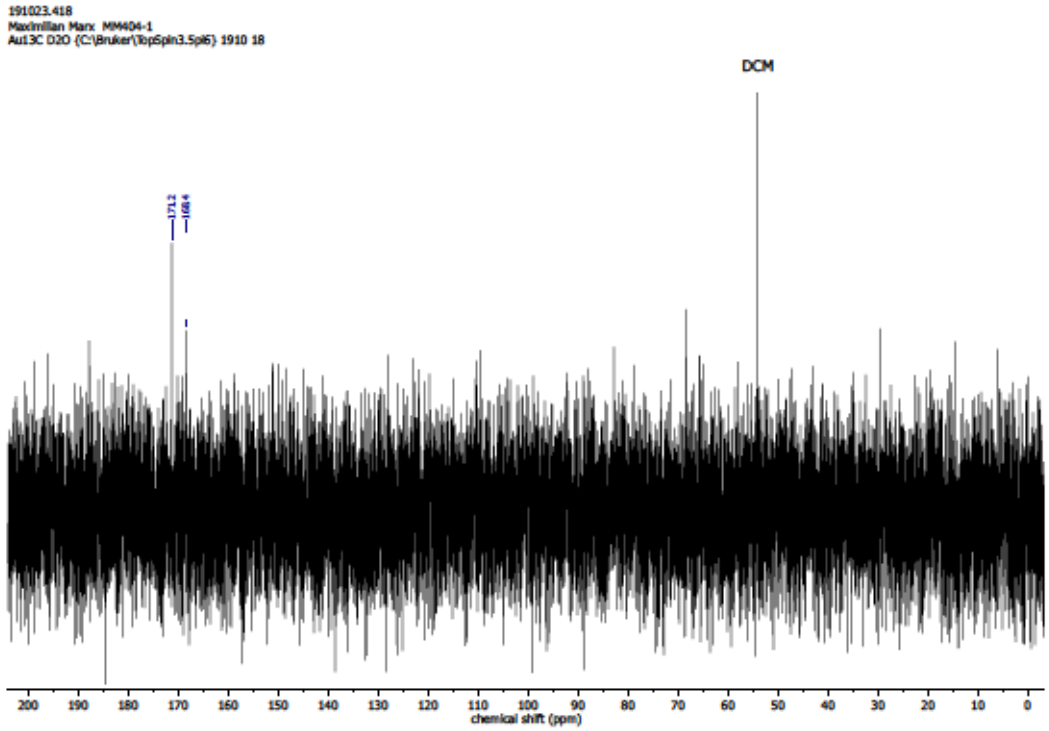

Figure S 129: $^{13}C\{^{1}H\}$ NMR spectrum (101 MHz, D_2O) of the NaOH extract of Table S 13, entry 7 – CO_2 treatment (bubbling) of **127**, CuI and $NaPF_6$ in MeOH.

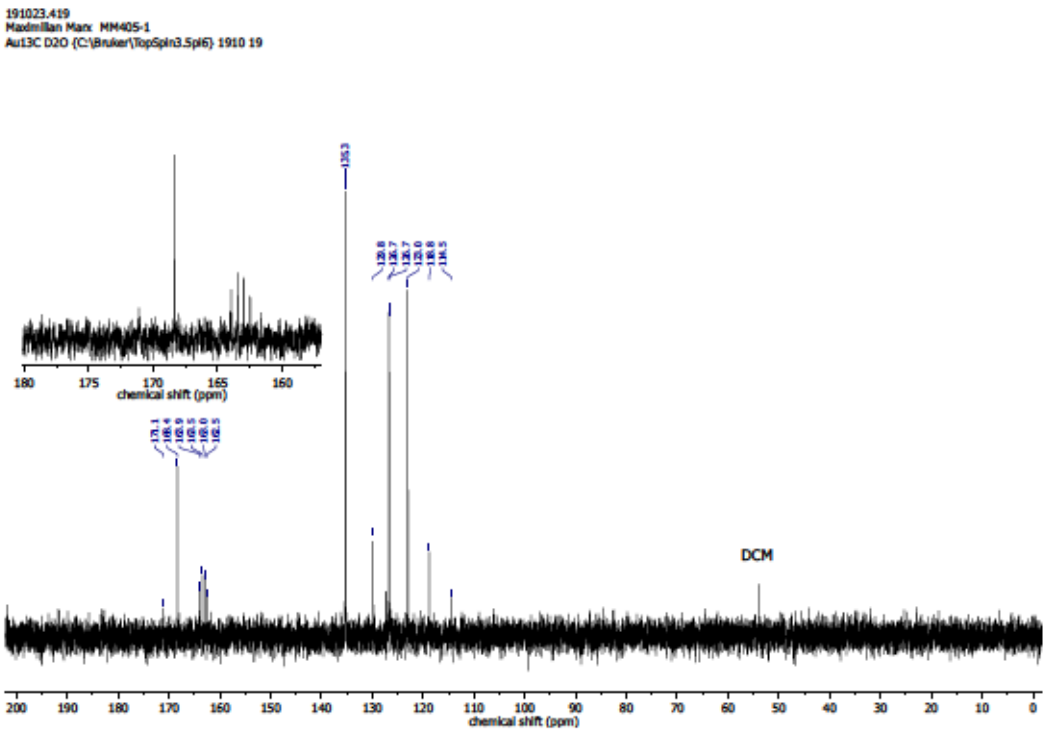

Figure S 130: $^{13}C\{^{1}H\}$ NMR spectrum (101 MHz, D_2O) of the NaOH extract of Table S 13, entry 8 – CO_2 treatment (bubbling) of **127**, CuI and $NaBPh_4$ in MeOH/THF.

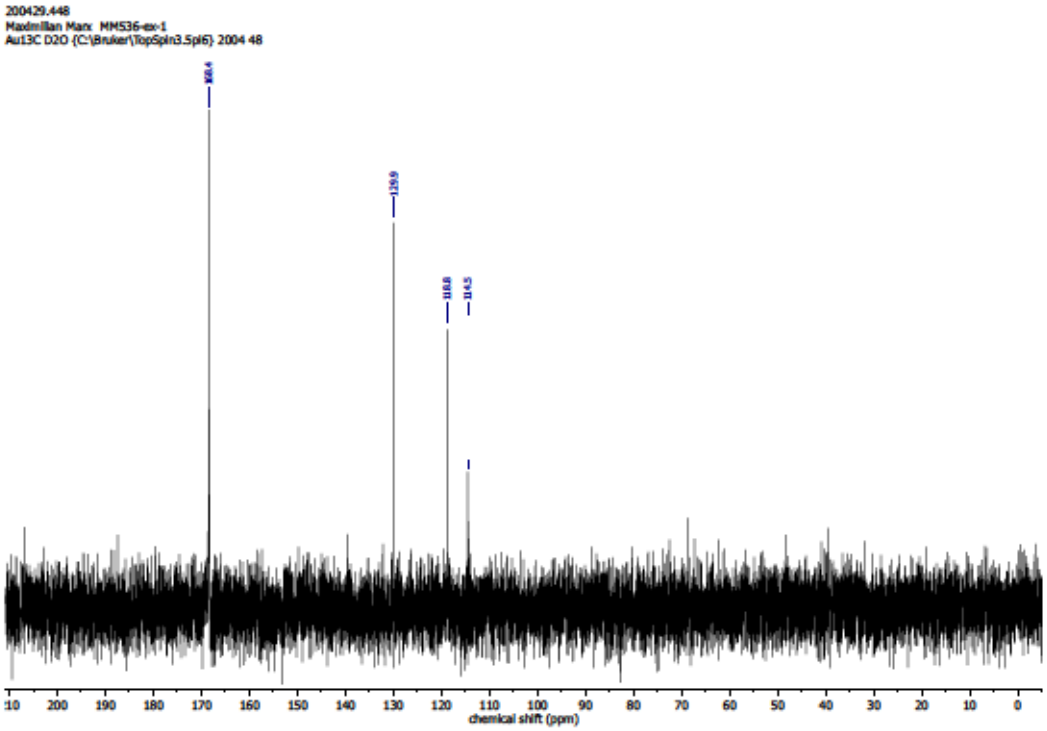

Figure S 131: $^{13}C\{^{1}H\}$ NMR spectrum (101 MHz, D_2O) of the NaOH extract of Table S 14, entry 2 – $CsHCO_3$ treatment of **127**, CuI and $NaBPh_4$ in MeOH.

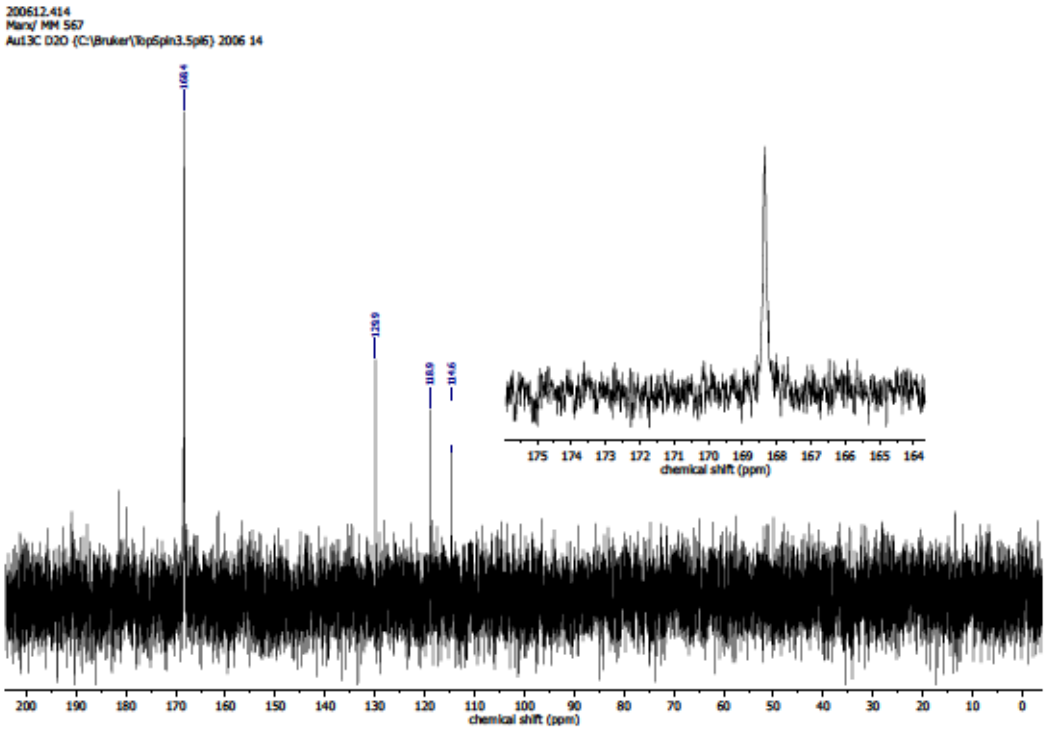

Figure S 132: $^{13}C\{^1H\}$ NMR spectrum (101 MHz, D_2O) of the NaOH extract of Table S 14, entry 3 – $CsHCO_3$ treatment of **127**, CuI and $NaBPh_4$ in MeOH.

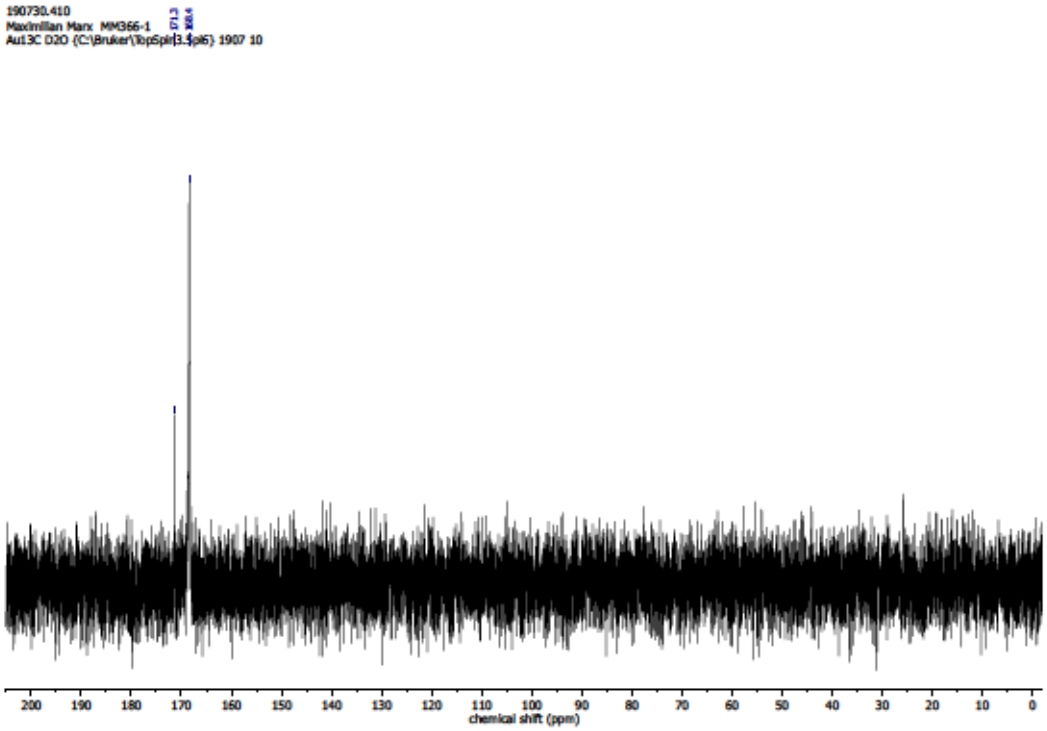

Figure S 133: $^{13}C\{^1H\}$ NMR spectrum (101 MHz, D_2O) of the NaOH extract of Table S 14, entry 4 – $CsHCO_3$ treatment of **127**, CuI and $NaBPh_4$ in $MeOH/H_2O$.

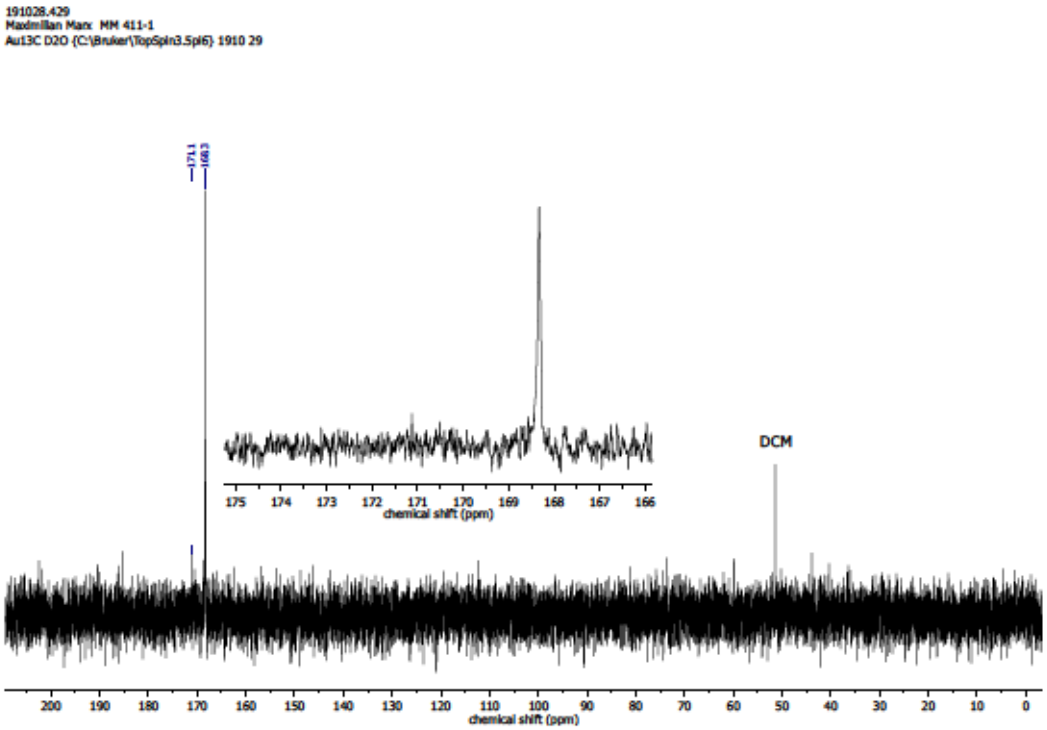

Figure S 134: $^{13}C\{^{1}H\}$ NMR spectrum (101 MHz, D_2O) of the NaOH extract of Table S 14, entry 5 – $CsHCO_3$ treatment of **127**, CuI and $NaPF_6$ in MeOH.

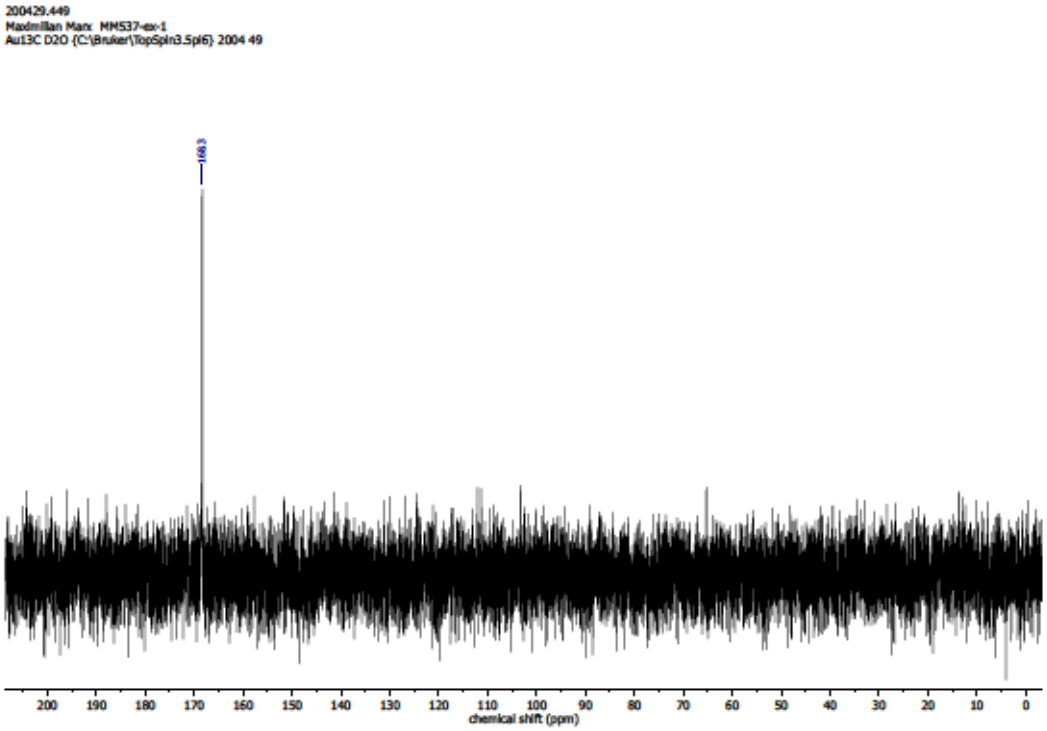

Figure S 135: $^{13}C\{^{1}H\}$ NMR spectrum (101 MHz, D_2O) of the NaOH extract of Table S 14, entry 6 – $CsHCO_3$ treatment of **127** and CuI in MeOH.

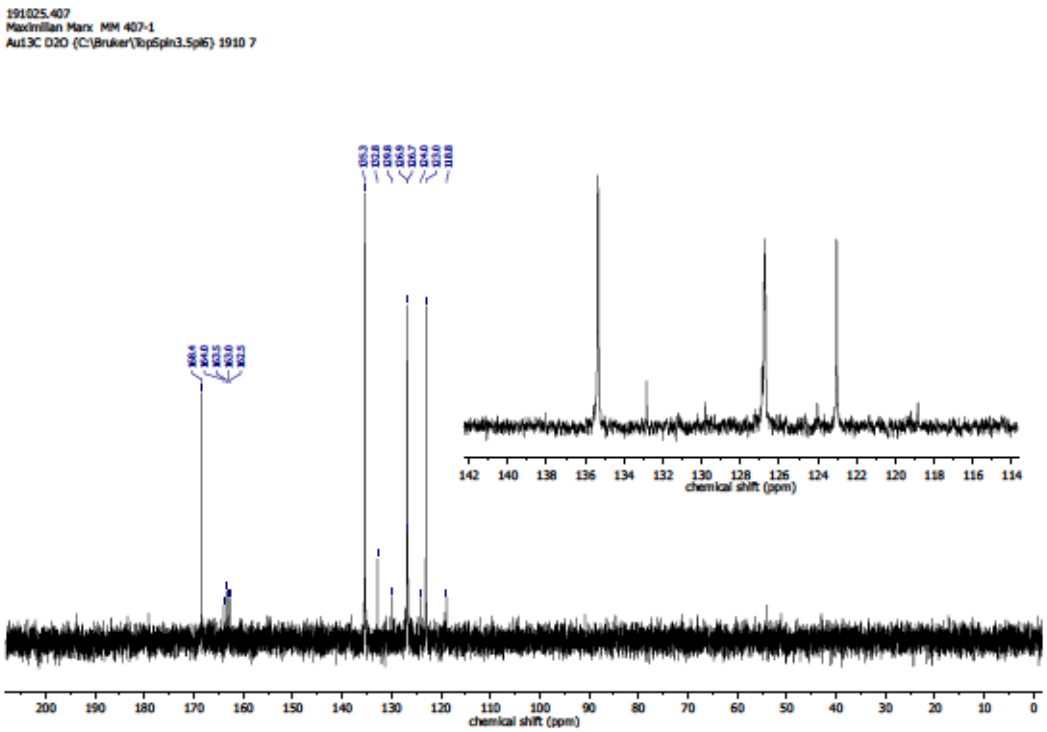

Figure S 136: $^{13}C\{^1H\}$ NMR spectrum (101 MHz, D_2O) the NaOH extract of Table S 14, entry 7 – $NaHCO_3$ treatment of **127**, CuI and $NaBPh_4$ in MeOH.

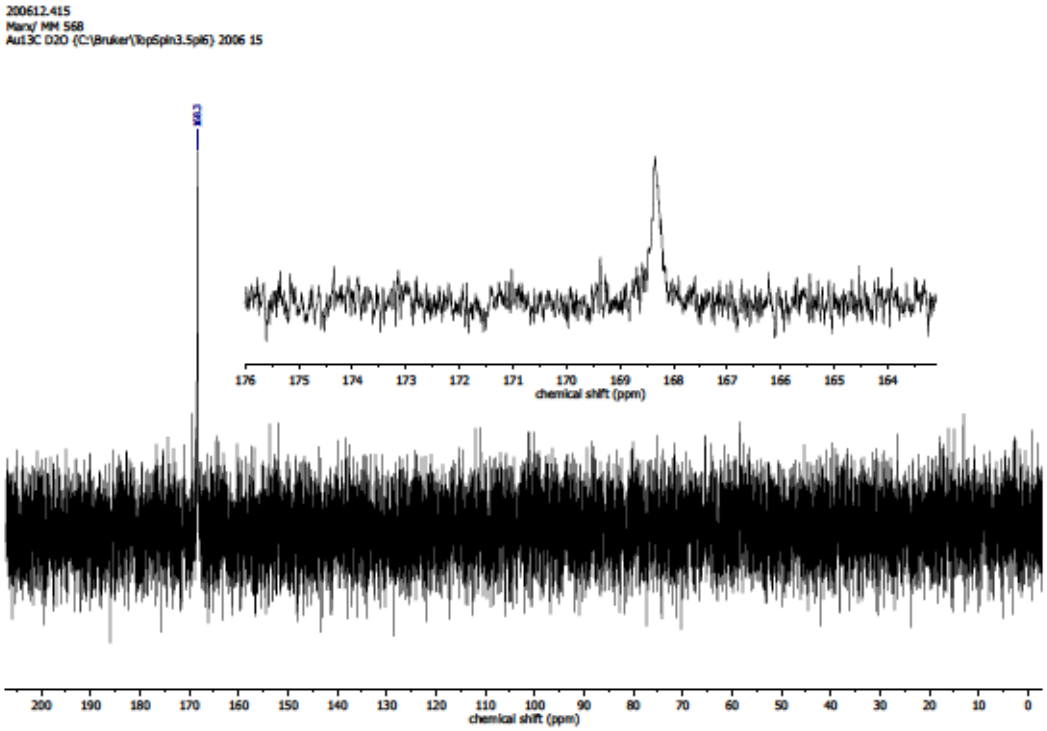

Figure S 137: $^{13}C\{^1H\}$ NMR spectrum (101 MHz, D_2O) the NaOH extract of Table S 14, entry 8 – $CsHCO_3$ treatment of **127** and $[Cu(MeCN)_4]PF_6$ in MeOH.

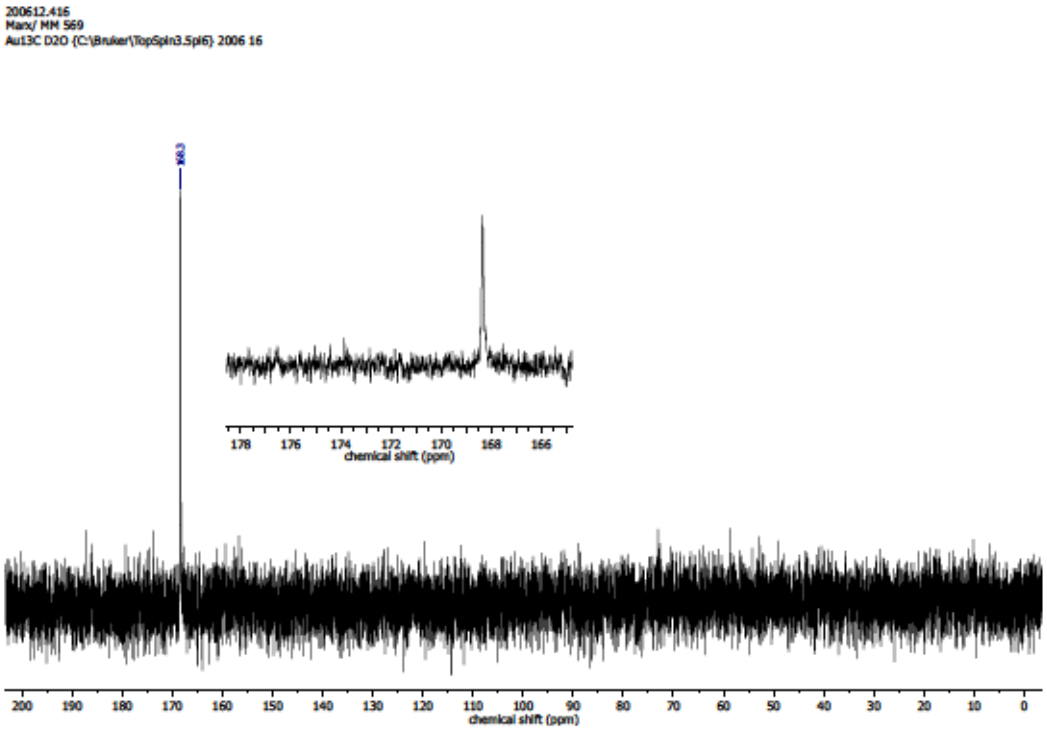

Figure S 138: $^{13}C\{^{1}H\}$ NMR spectrum (101 MHz, D_2O) of the NaOH extract of Table S 14, entry 9 – $NaHCO_3$ treatment of **127** and $[Cu(MeCN)_4]PF_6$ in MeOH.

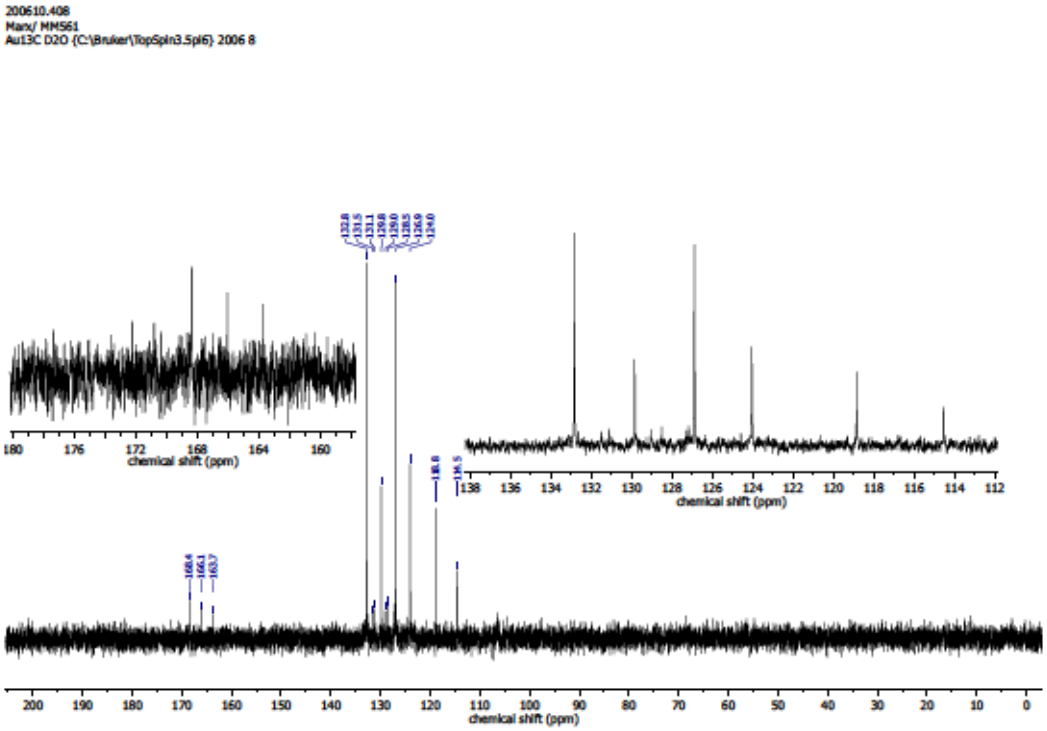

Figure S 139: $^{13}C\{^{1}H\}$ NMR spectrum (101 MHz, D_2O) of the NaOH extract of Table S 15, entry 1 – CO_2 treatment of **127**, CuI and $NaBPh_4$ in MeOH.

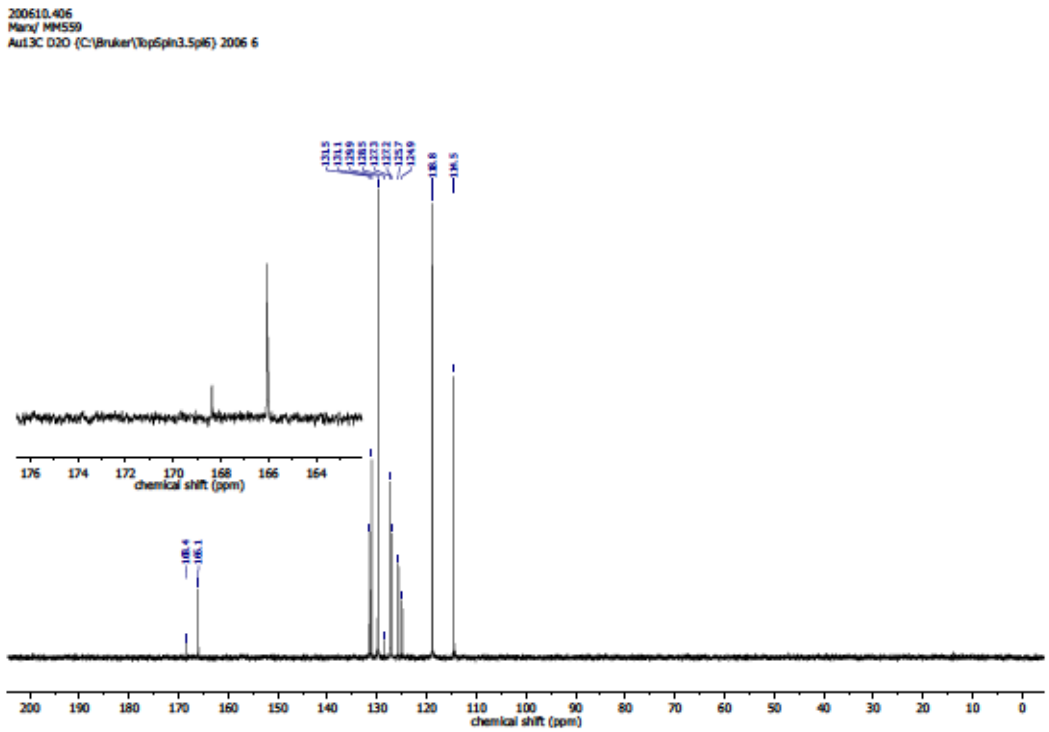

Figure S 140: $^{13}C\{^{1}H\}$ NMR spectrum (101 MHz, D_2O) of the NaOH extract of Table S 15, entry 2 – CO_2 treatment of **127**, CuI and $NaBPh_4$ in MeOH.

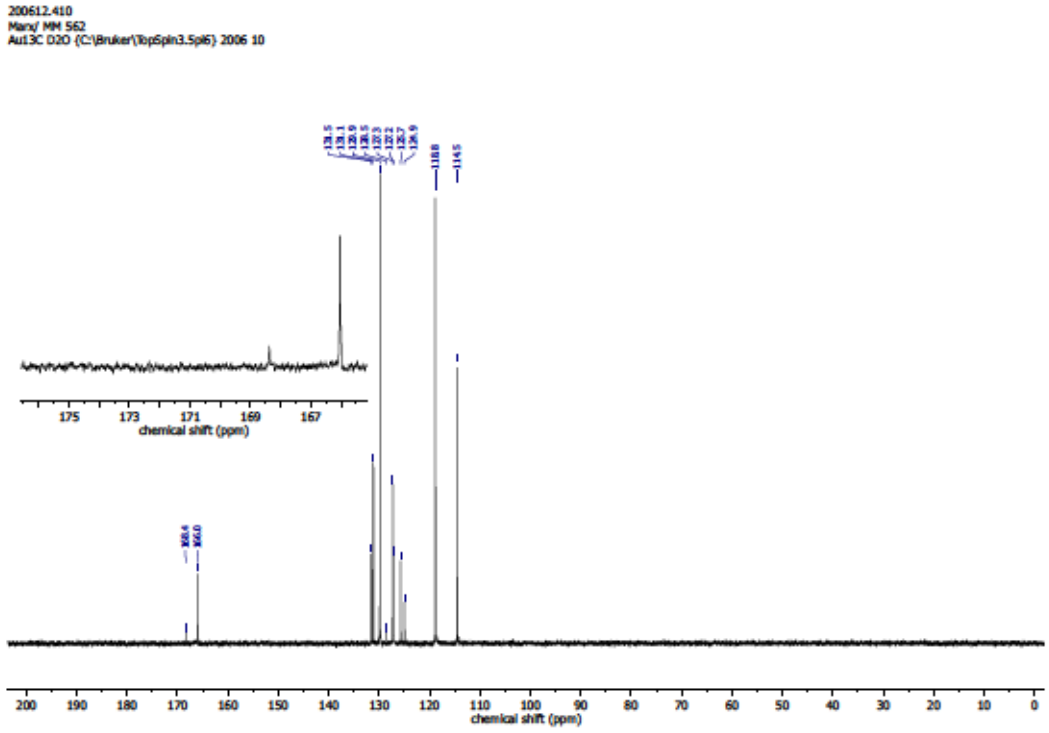

Figure S 141: $^{13}C\{^{1}H\}$ NMR spectrum (101 MHz, D_2O) of the NaOH extract of Table S 15, entry 3 – CO_2 treatment of **127**, CuI and $NaBPh_4$ in MeOH/THF.

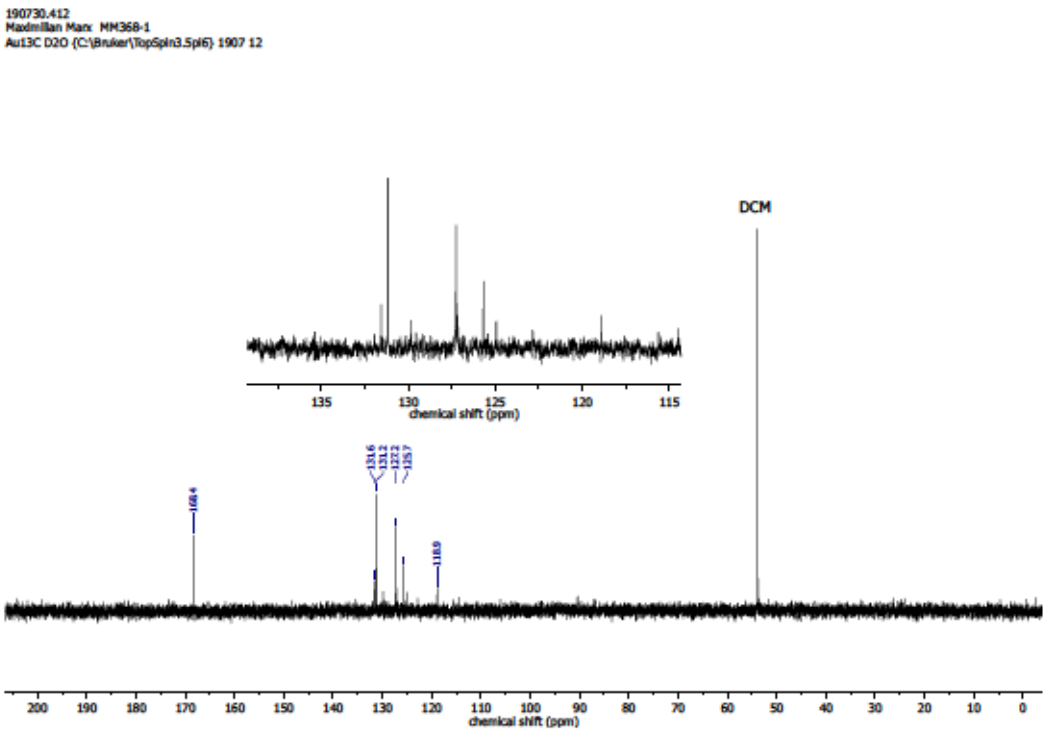

Figure S 142: $^{13}C\{^1H\}$ NMR spectrum (101 MHz, D_2O) of the NaOH extract of Table S 15, entry 4 – CO_2 treatment of **127**, CuI and $NaBPh_4$ in MeOH/THF.

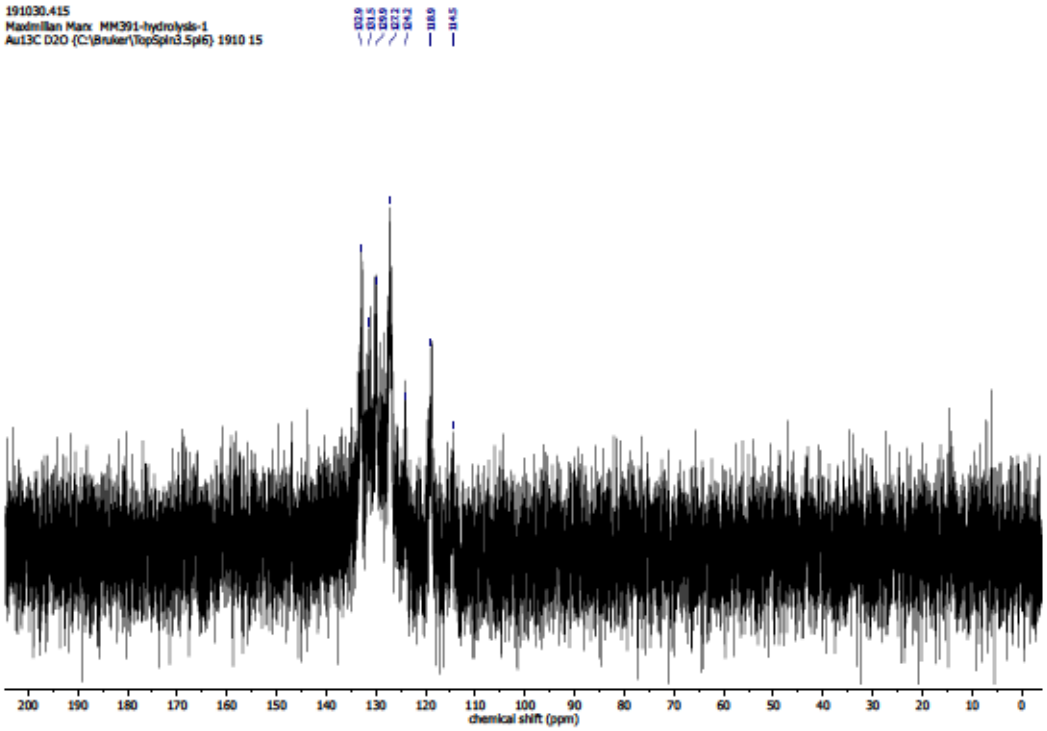

Figure S 143: $^{13}C\{^1H\}$ NMR spectrum (101 MHz, D_2O) of the NaOH extract of Table S 15, entry 6 – CO_2 treatment of **127**, CuI and $NaBPh_4$ in THF.

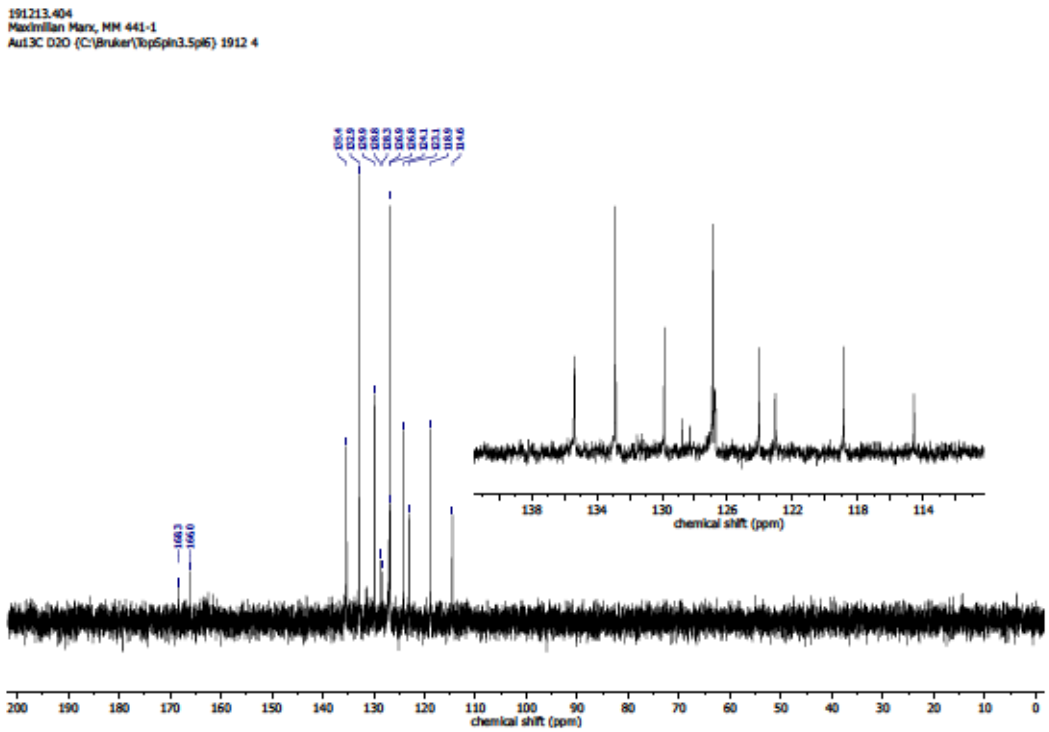

Figure S 144: $^{13}C\{^{1}H\}$ NMR spectrum (101 MHz, D_2O) of the NaOH extract of Table S 15, entry 7 – CO_2 treatment of **127**, CuI and $NaBPh_4$ in toluene.

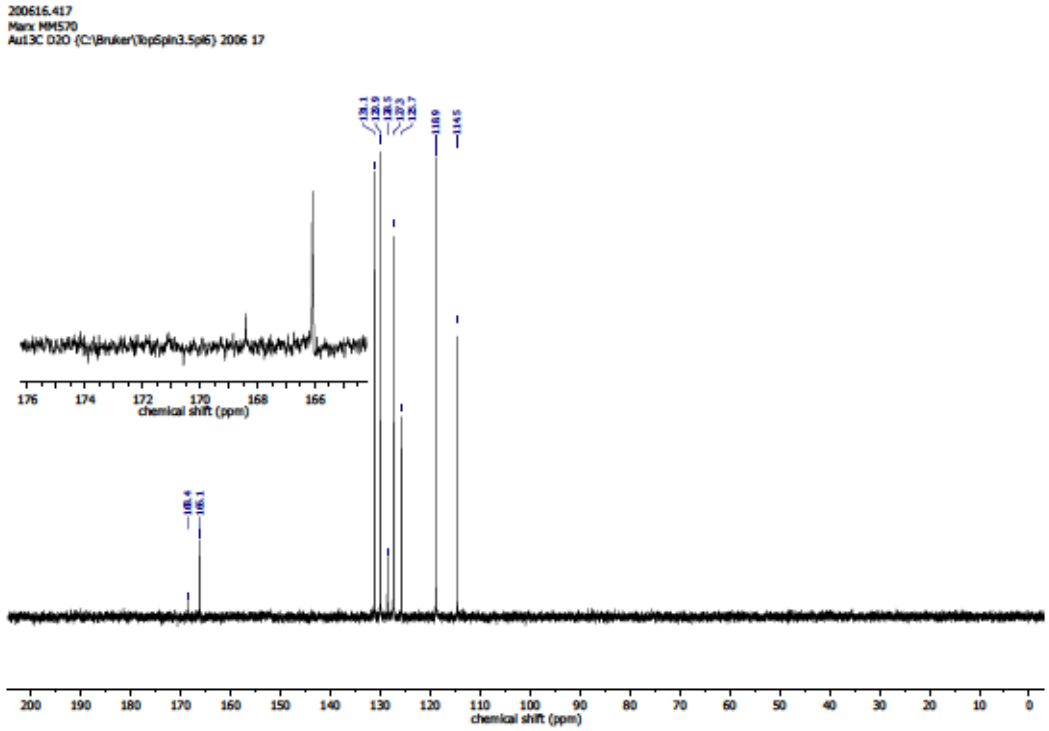

Figure S 145: $^{13}C\{^{1}H\}$ NMR spectrum (101 MHz, D_2O) of the NaOH extract of Table S 15, entry 8 – CO_2 treatment of **127**, CuI and $NaBPh_4$ in MeOH at 40 °C.

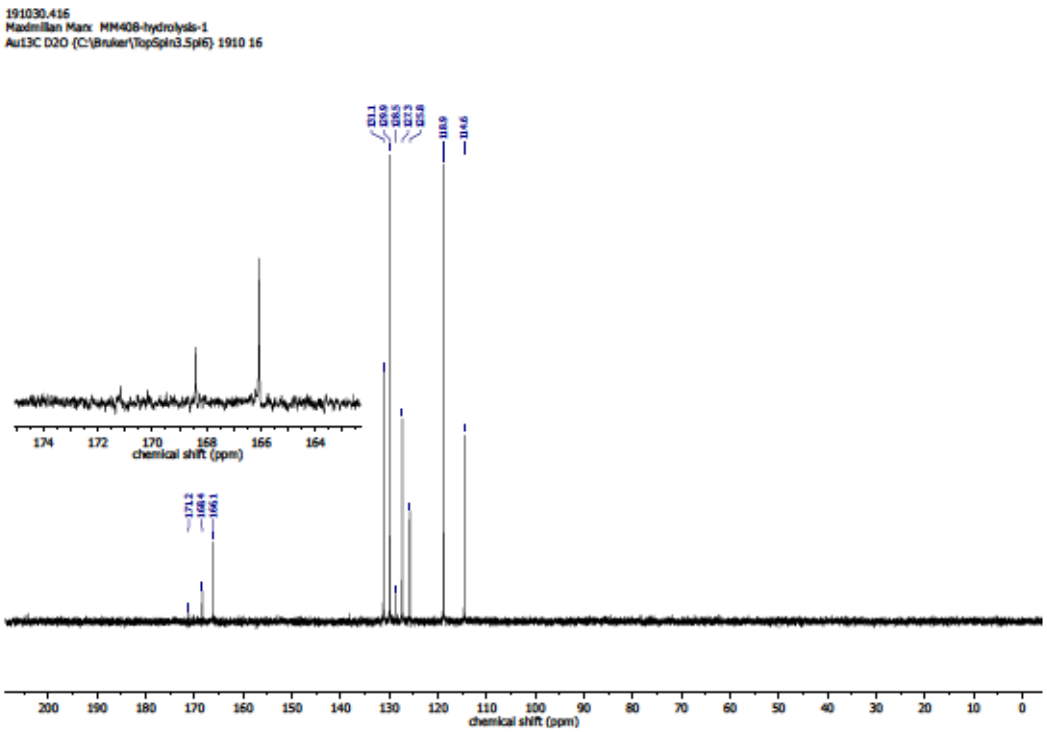

Figure S 146: $^{13}C\{^1H\}$ NMR spectrum (101 MHz, D_2O) of the NaOH extract of Table S 15, entry 9 – CO_2 treatment of **127**, CuI and $NaBPh_4$ in MeOH at 35 °C.

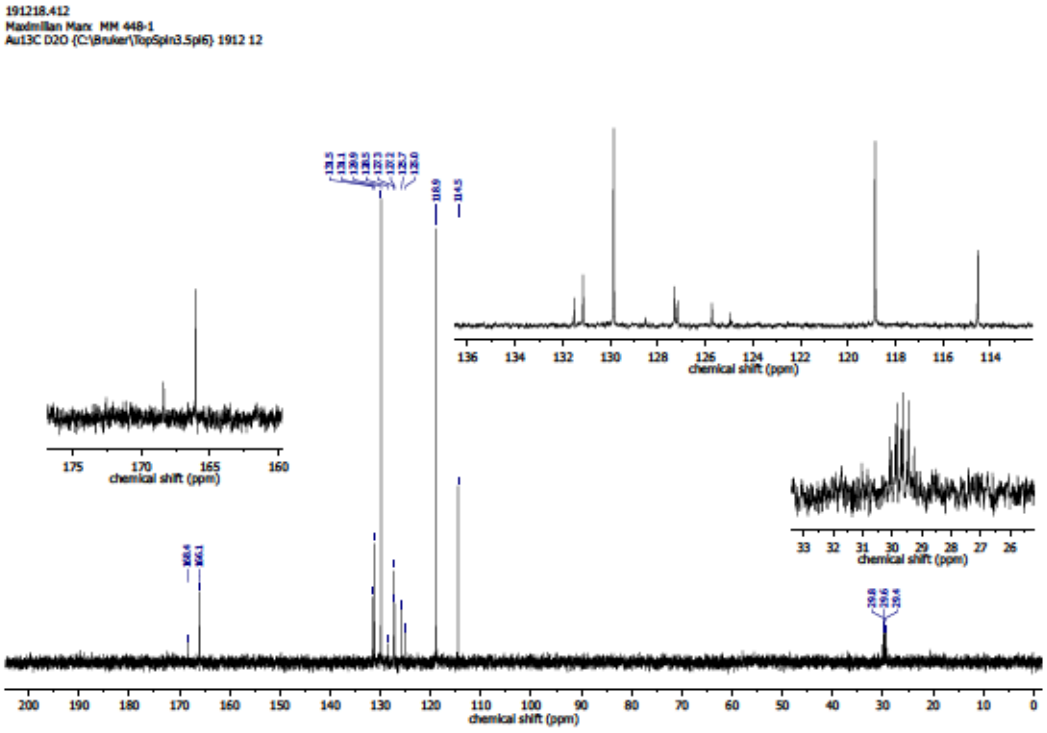

Figure S 147: $^{13}C\{^1H\}$ NMR spectrum (101 MHz, D_2O) of the NaOH extract of Table S 15, entry 10 – CO_2 treatment and illumination (400-700 nm, 0.09 W) of **127**, CuI and $NaBPh_4$ in MeOH.

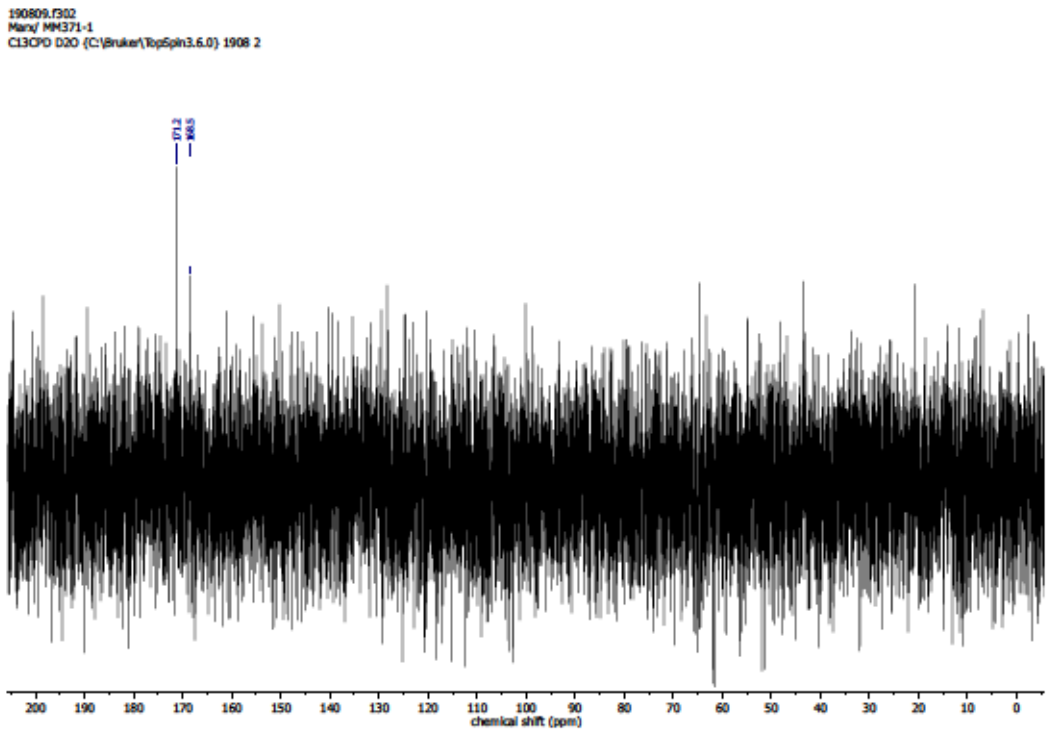

Figure S 148: $^{13}C\{^{1}H\}$ NMR spectrum (75 MHz, D_2O) of the NaOH extract of Table S 16, entry 2 – CO_2 treatment of **127**, CuI and $AgBPh_4$ in MeOH.

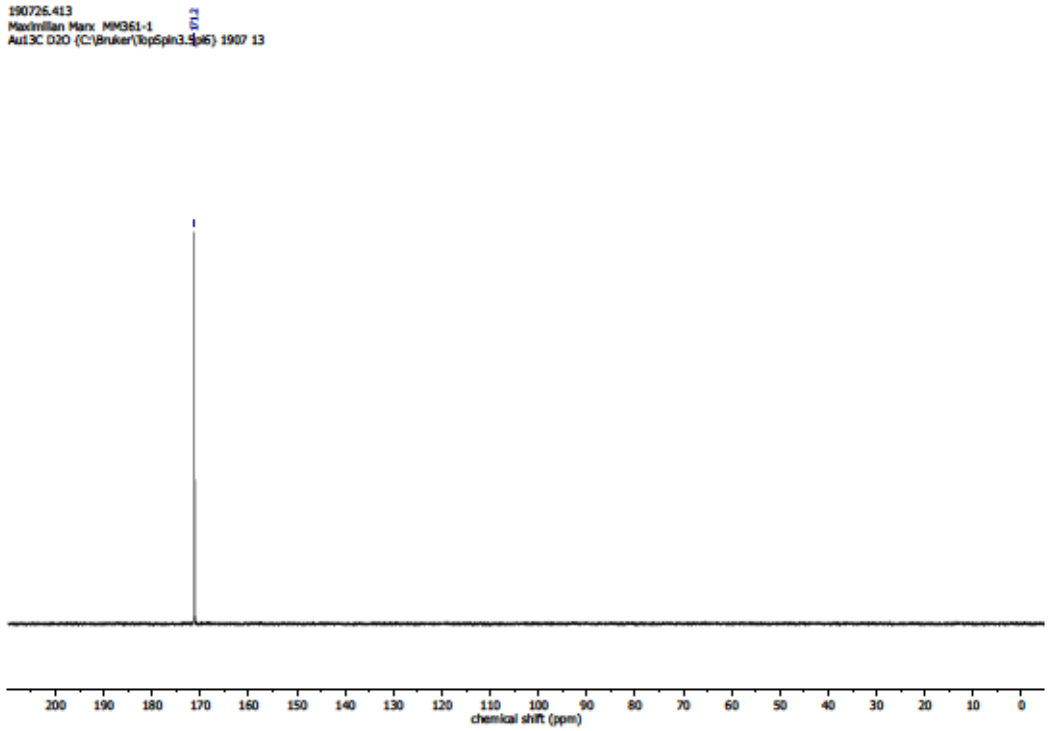

Figure S 149: $^{13}C\{^{1}H\}$ NMR spectrum (101 MHz, D_2O) of the NaOH extract of Table S 16, entry 6 – CO_2 treatment of **127**, $[Cu(MeCN)_4]PF_6$ and NaO_2CH in MeOH.

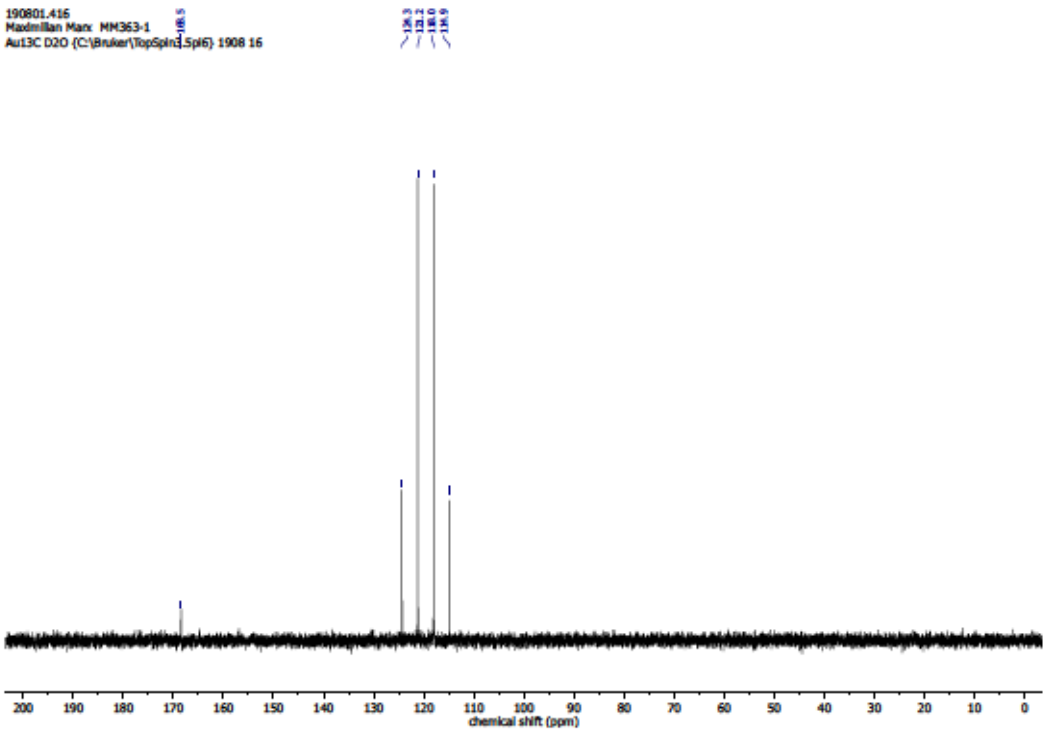

Figure S 150: $^{13}C\{^{1}H\}$ NMR spectrum (101 MHz, D_2O) of the NaOH extract of Table S 16, entry 7 – CO_2 treatment of **127**, $[Cu(MeCN)_4]PF_6$ and $Mg(OTf)_2$ in MeOH.

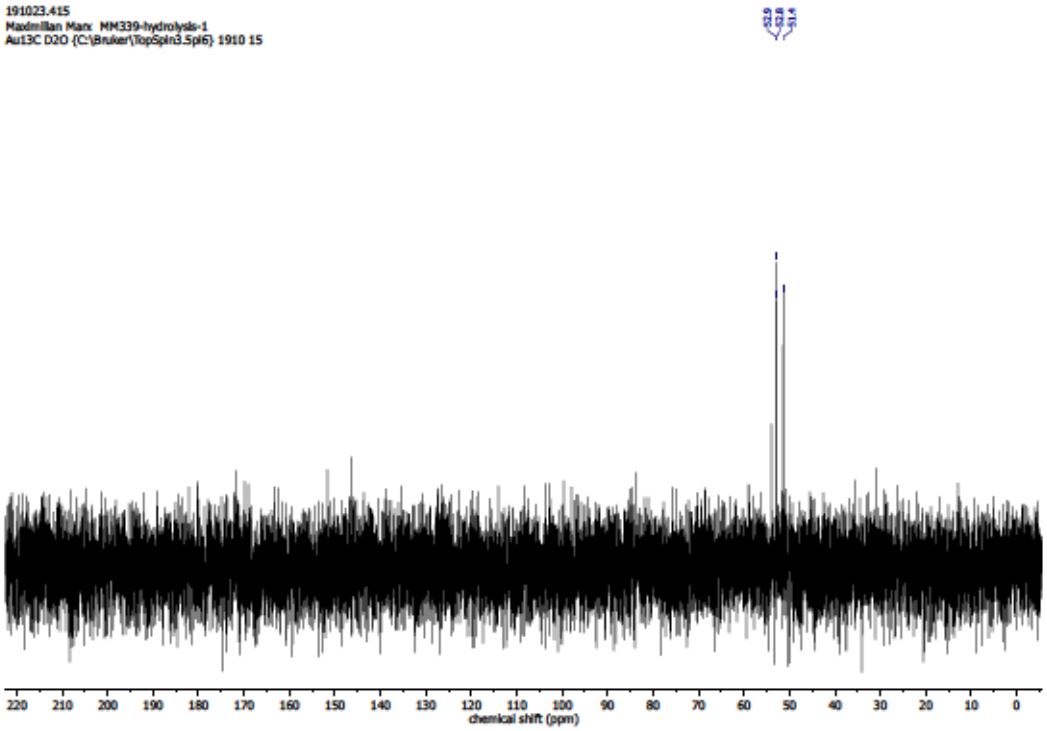

Figure S 151: $^{13}C\{^{1}H\}$ NMR spectrum (101 MHz, D_2O) of the NaOH extract of Table S 16, entry 8 – CO_2 treatment of **127**, $[Cu(MeCN)_4]PF_6$ and $LiBF_4$ in MeOH.

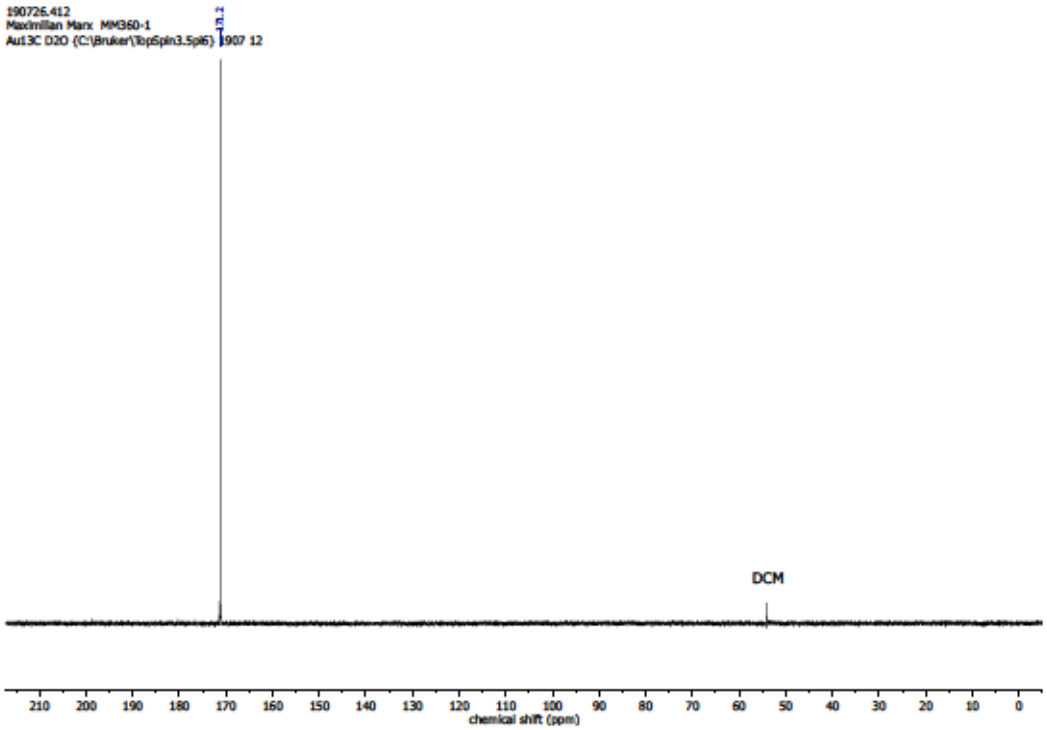

Figure S 152: $^{13}C\{^1H\}$ NMR spectrum (101 MHz, D_2O) of the NaOH extract of Table S 16, entry 9 – CO_2 treatment of **127**, $[Cu(MeCN)_4]PF_6$, $LiBF_4$ and NaO_2CH in MeOH.

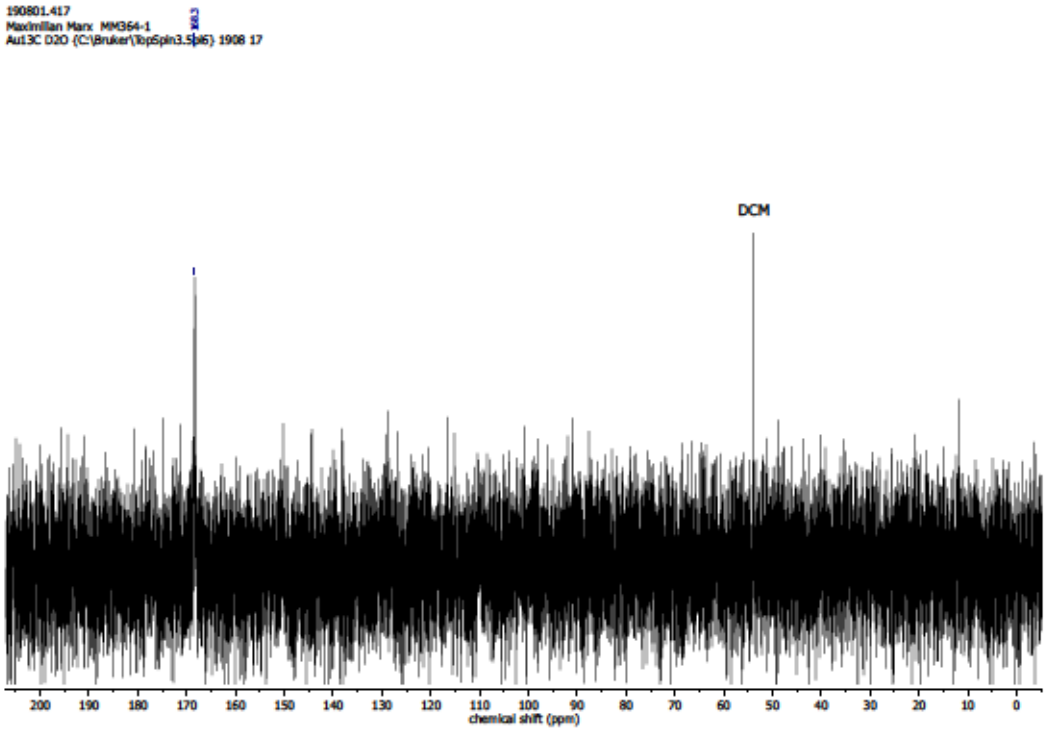

Figure S 153: $^{13}C\{^1H\}$ NMR spectrum (101 MHz, D_2O) of the NaOH extract of Table S 16, entry 10 – CO_2 treatment of **127**, $[Cu(MeCN)_4]PF_6$ and Na_2SO_3 in MeOH.

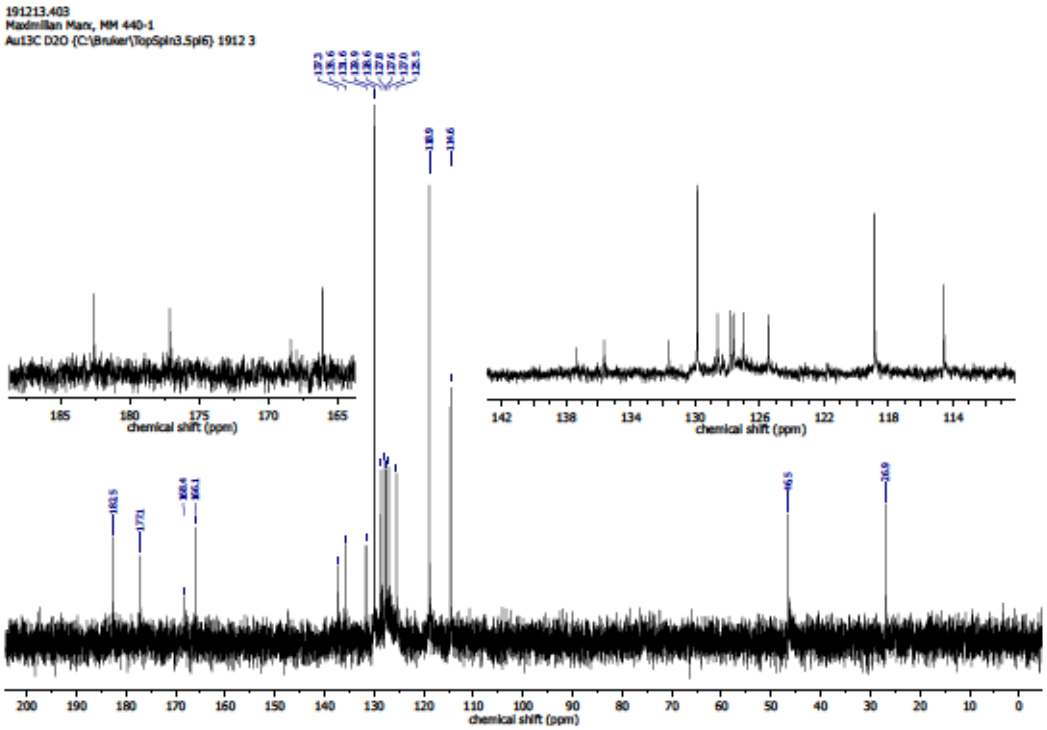

Figure S 154: $^{13}C\{^{1}H\}$ NMR spectrum (101 MHz, D_2O) of the NaOH extract of Table S 16, entry 11 – CO_2 treatment of **127**, CuI, $NaBPh_4$ and $NaC_{10}H_8$ in THF.

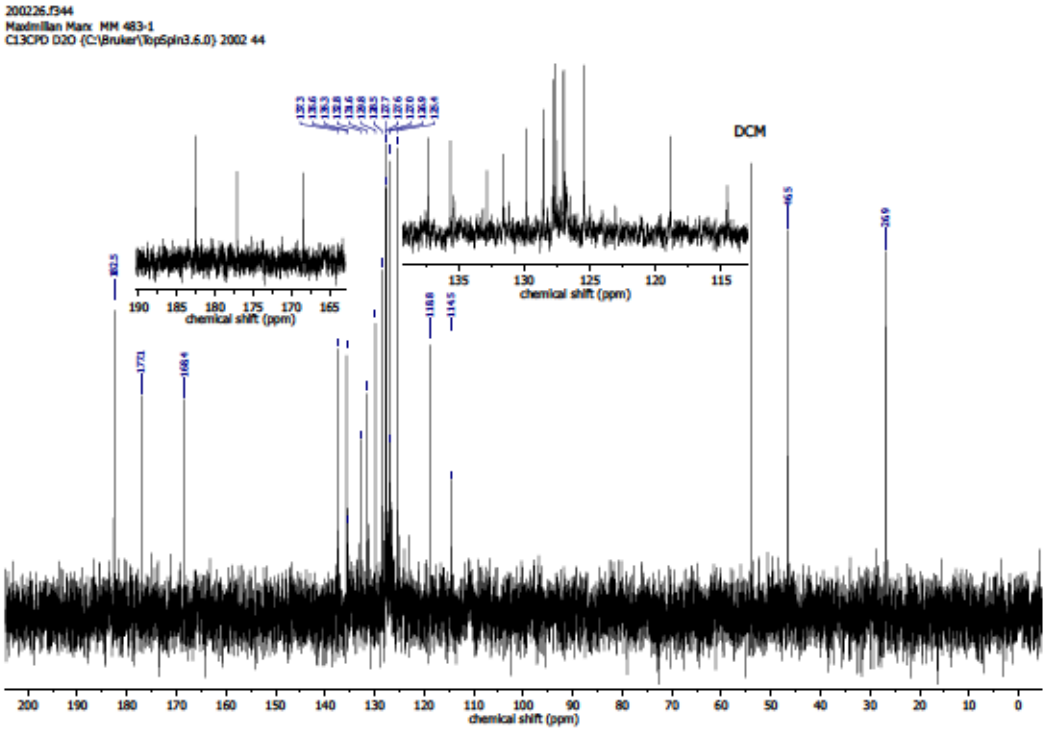

Figure S 155: $^{13}C\{^{1}H\}$ NMR spectrum (75 MHz, D_2O) of the NaOH extract of Table S 16, entry 13 – CO_2 treatment of **127**, CuI, $NaBPh_4$ and $NaC_{10}H_8$ in THF.

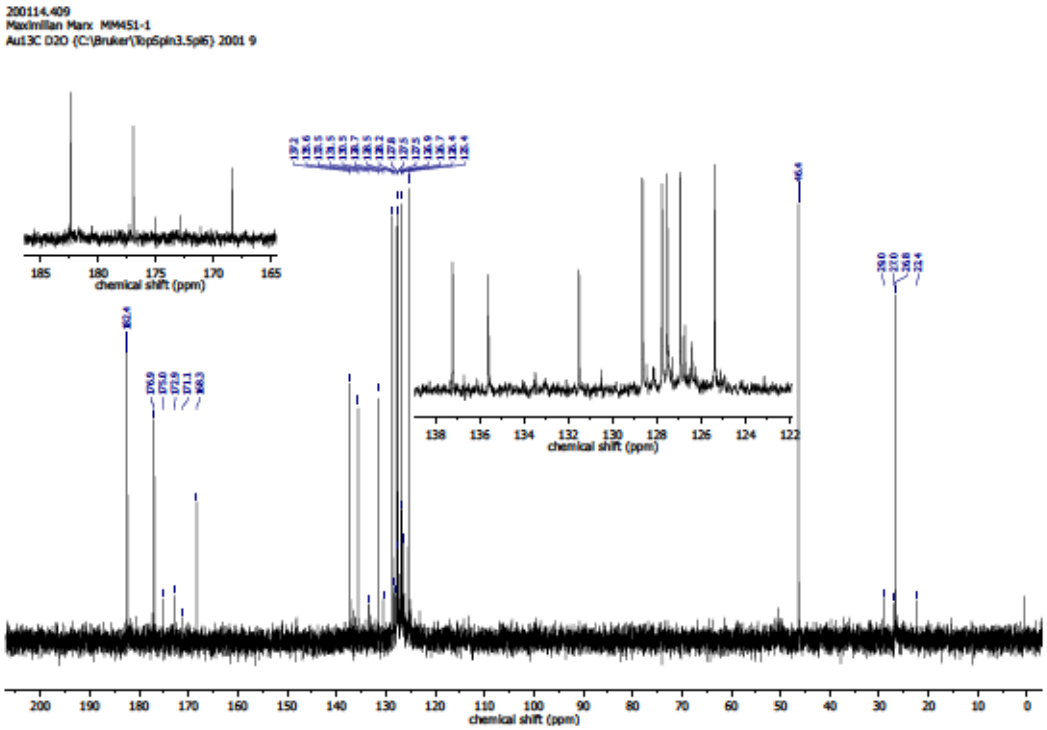

Figure S 156: $^{13}C\{^1H\}$ NMR spectrum (101 MHz, D_2O) of the NaOH extract of Table S 16, entry 15 – CO_2 treatment of $NaC_{10}H_8$ in THF.

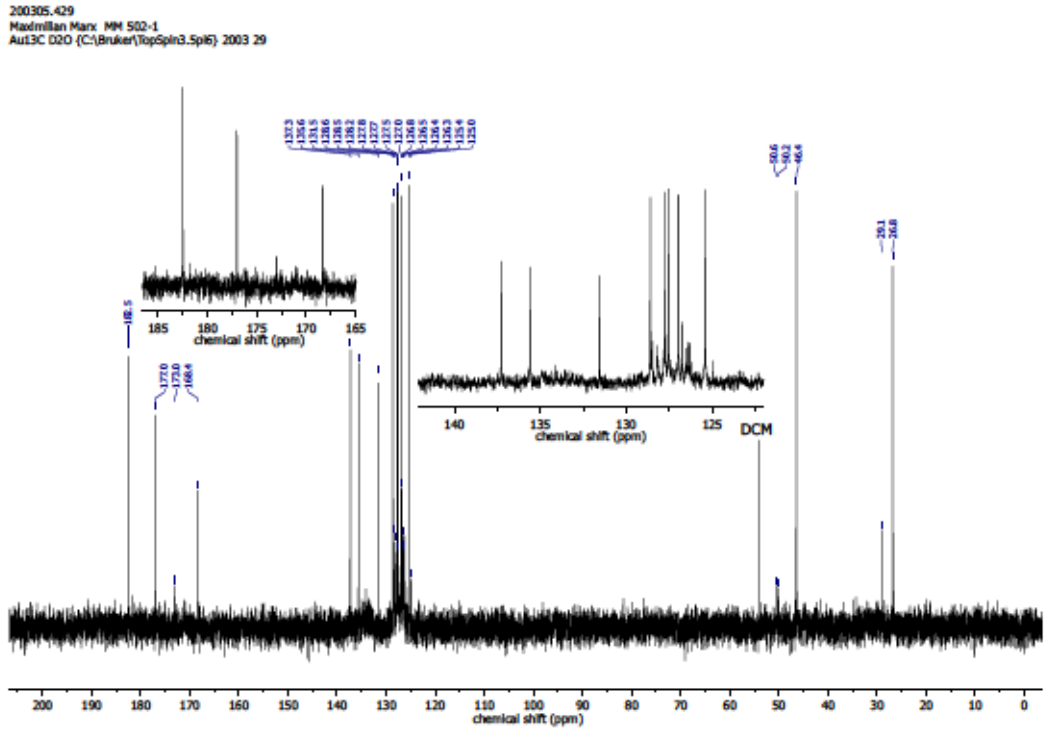

Figure S 157: $^{13}C\{^1H\}$ NMR spectrum (101 MHz, D_2O) of the NaOH extract of Table S 16, entry 17 – CO_2 treatment of $NaC_{10}H_8$ in THF.

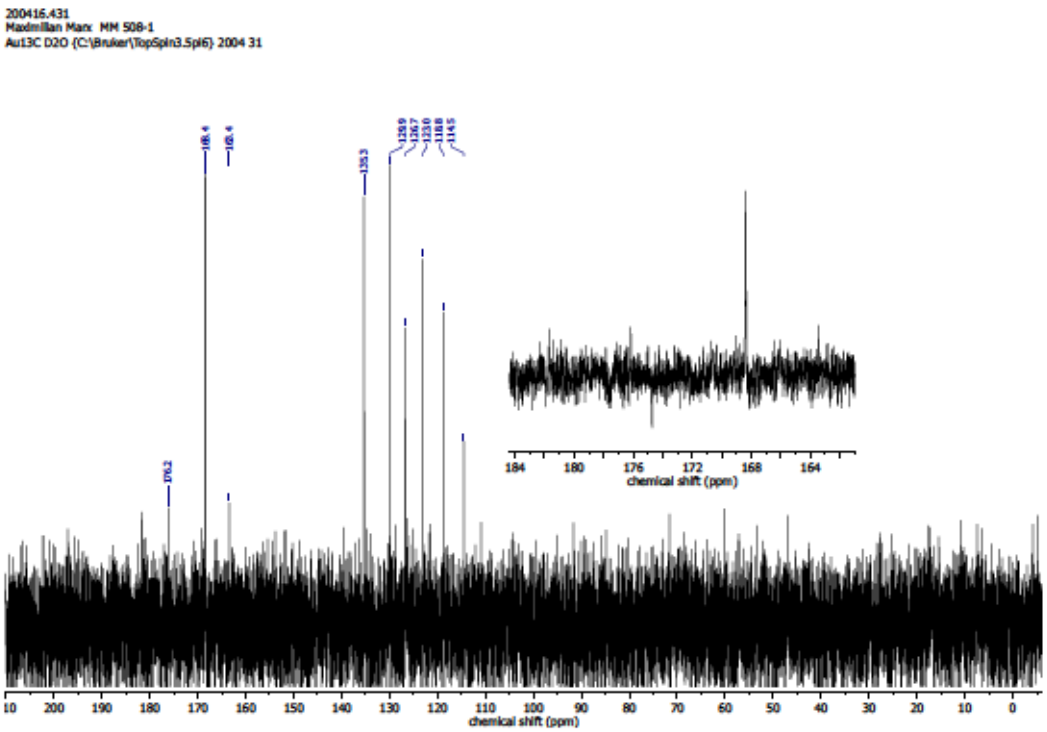

Figure S 158: $^{13}C\{^{1}H\}$ NMR spectrum (101 MHz, D_2O) of the NaOH extract of Table S 17, entry 1 – Air exposure of a solution of CuI, **127** and $NaBPh_4$ in MeOH.

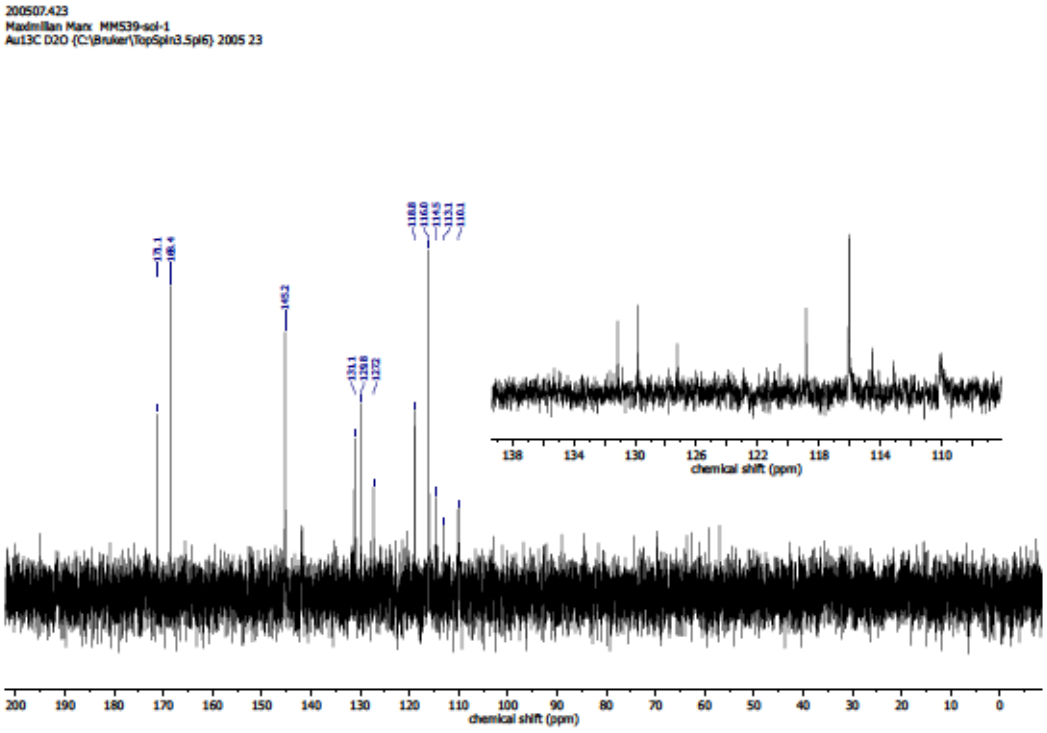

Figure S 159: $^{13}C\{^{1}H\}$ NMR spectrum (101 MHz, D_2O) of the NaOH extract of Table S 17, entry 2 – Air exposure of a solution of CuI, **127** and $NaBPh_4$ in MeOH.

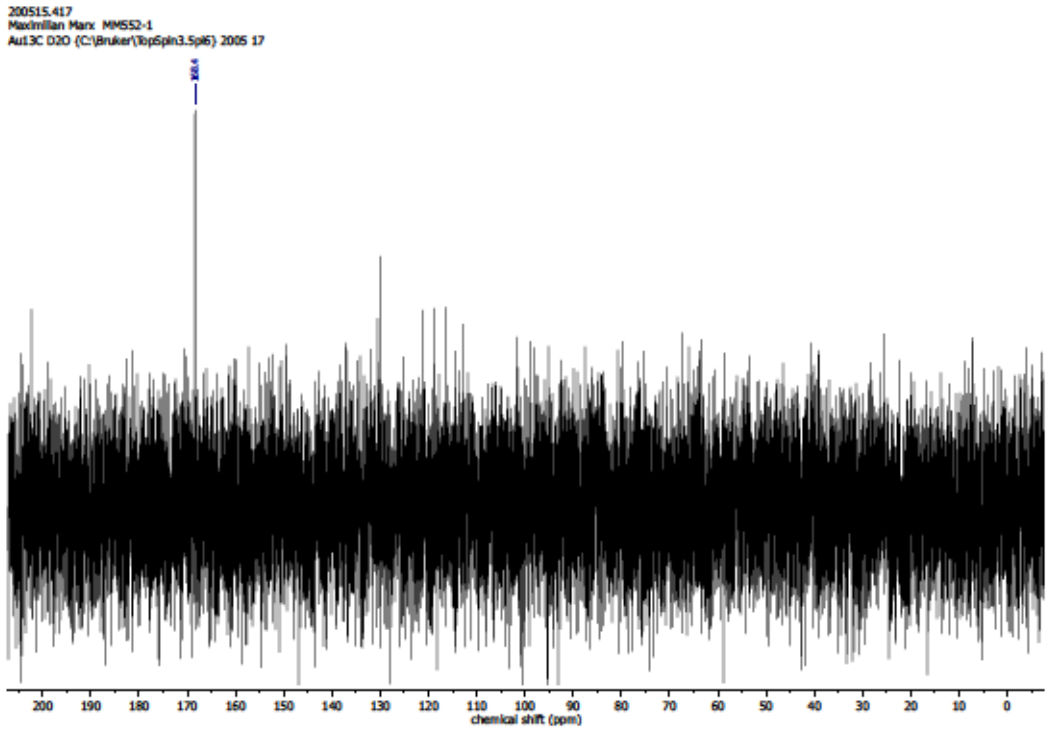

Figure S 160: $^{13}C\{^1H\}$ NMR spectrum (101 MHz, D_2O) of the NaOH extract of Table S 17, entry 3 – Air exposure of a solution of CuI, **127** and $NaBPh_4$ in MeOH/EtOH.

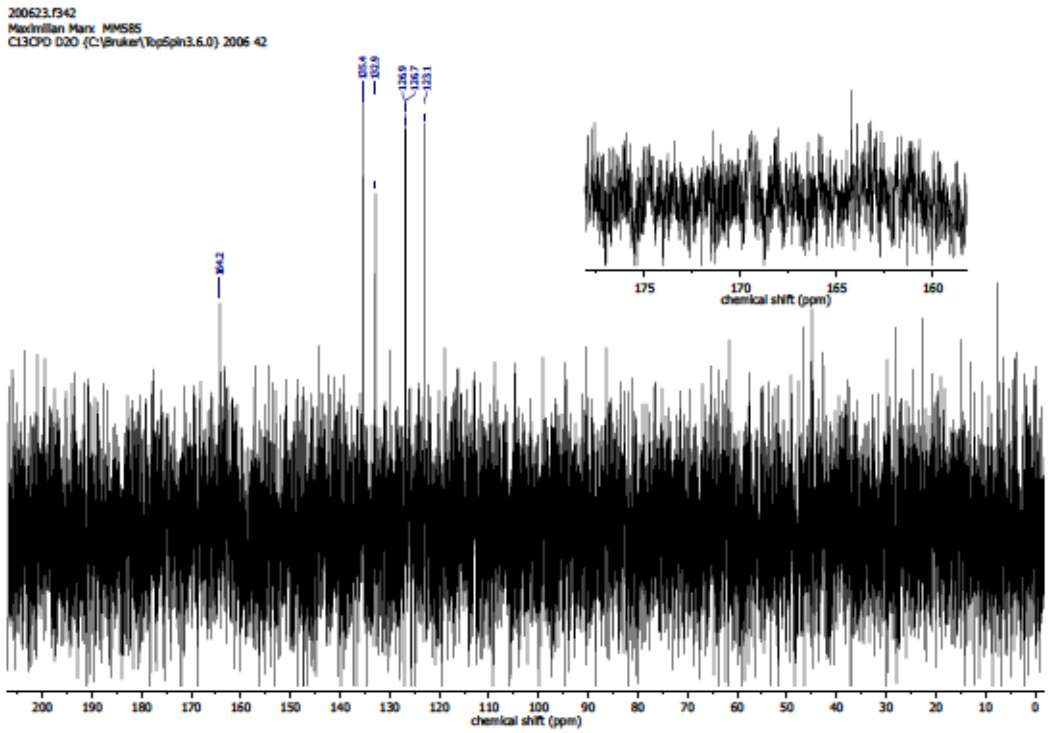

Figure S 161: $^{13}C\{^1H\}$ NMR spectrum (75 MHz, D_2O) of the NaOH extract of Table S 17, entry 4 – O_2 treatment of a solution of CuI, **127** and $NaBPh_4$ in MeOH.

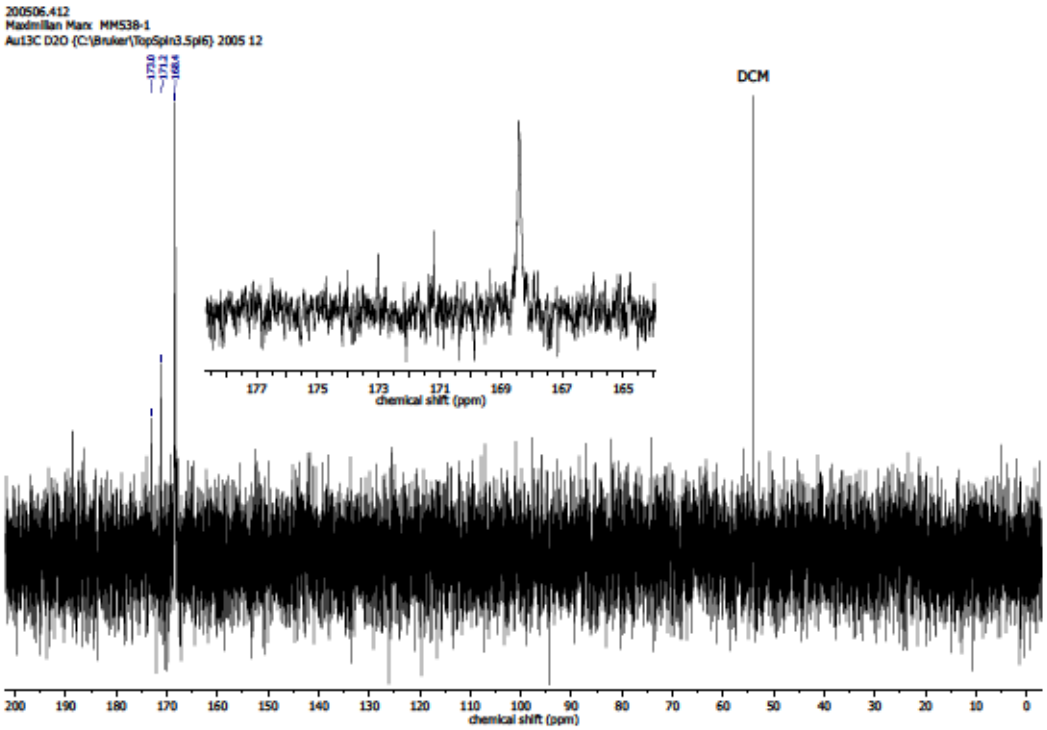

Figure S 162: $^{13}C\{^{1}H\}$ NMR spectrum (101 MHz, D_2O) of the NaOH extract of Table S 17, entry 5 – Air exposure of a solution of CuI and **127** in MeOH.

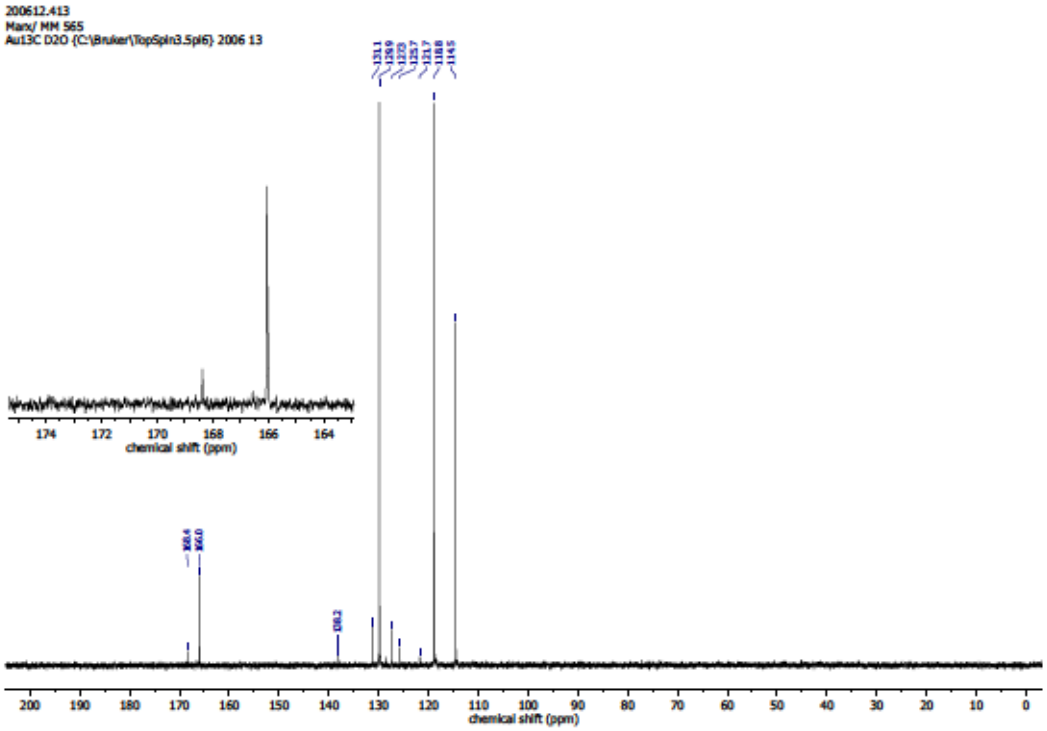

Figure S 163: $^{13}C\{^{1}H\}$ NMR spectrum (101 MHz, D_2O) of the NaOH extract of Table S 18, entry 1 – CO_2 treatment of **174**, CuI and $NaBPh_4$ in MeOH.

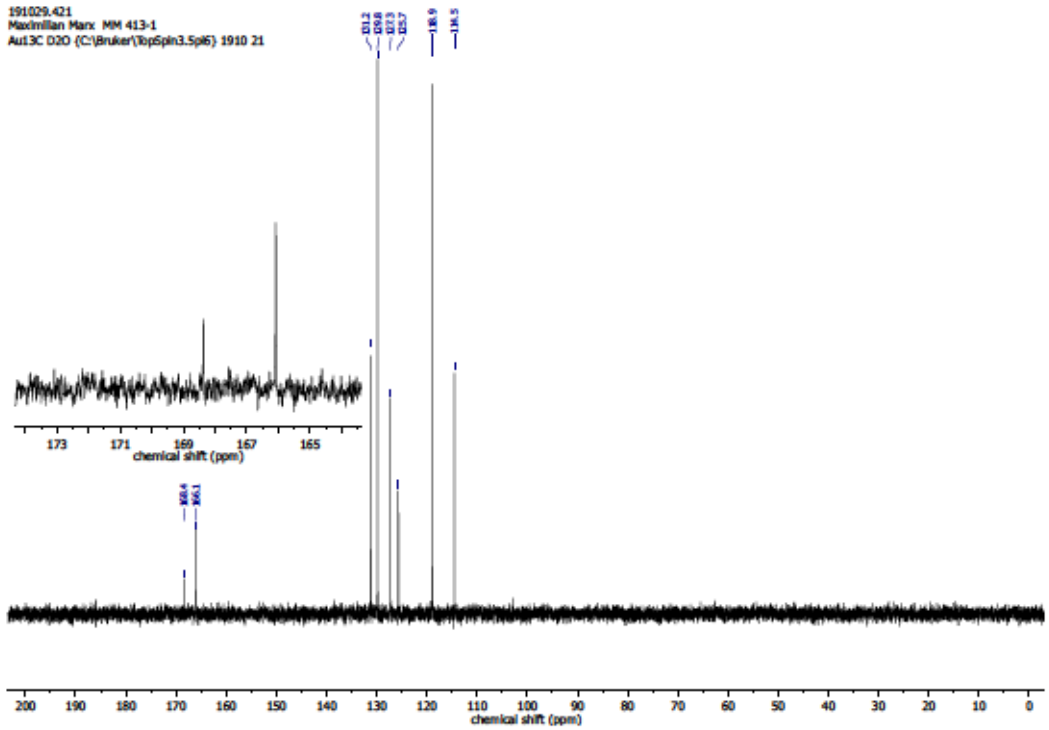

Figure S 164: $^{13}C\{^{1}H\}$ NMR spectrum (101 MHz, D_2O) of the NaOH extract of Table S 18, entry 2 – CO_2 treatment of **174**, CuI and $NaBPh_4$ in MeOH.

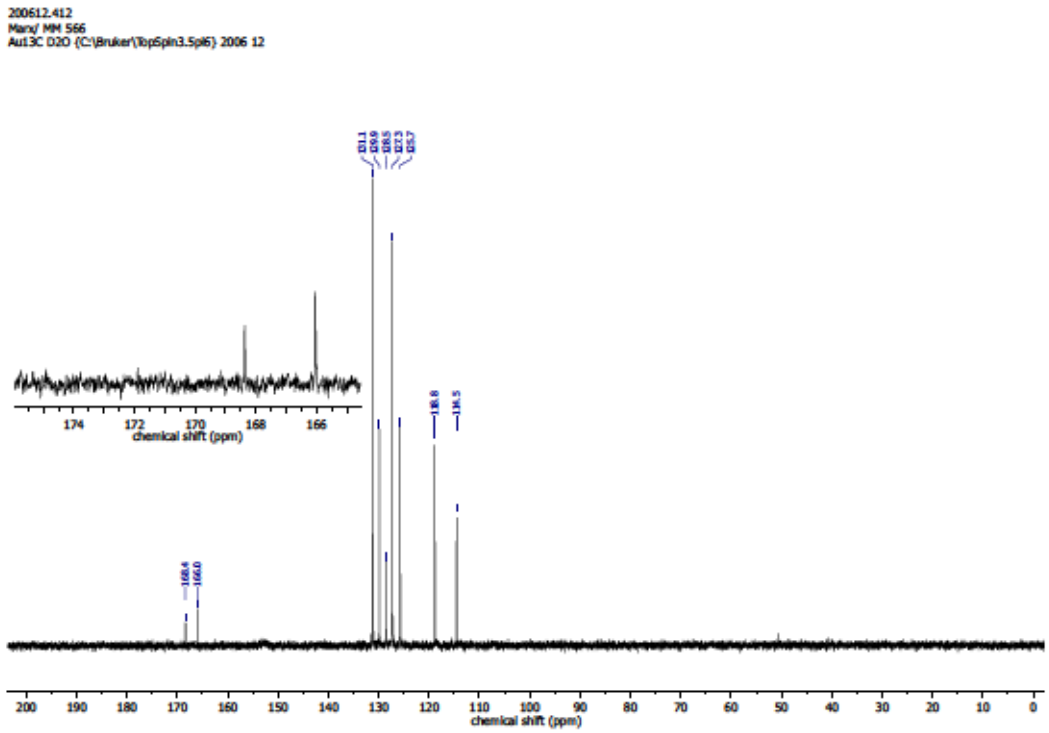

Figure S 165: $^{13}C\{^{1}H\}$ NMR spectrum (101 MHz, D_2O) of the NaOH extract of Table S 18, entry 3 – CO_2 treatment of **175**, CuI and $NaBPh_4$ in MeOH.

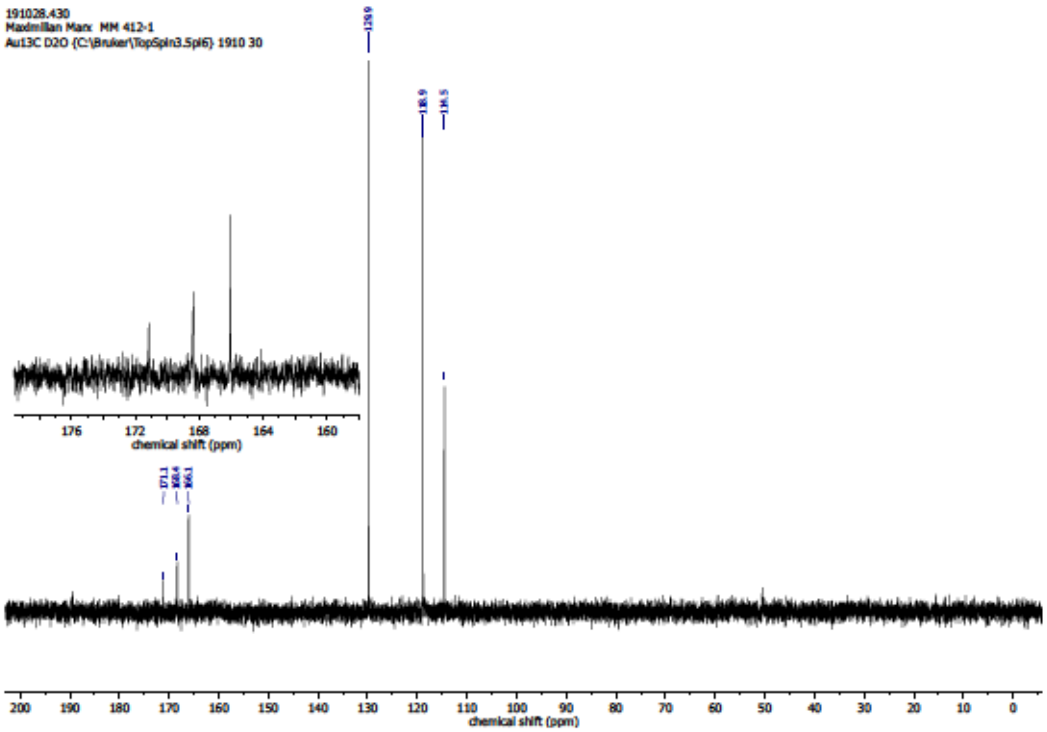

Figure S 166: $^{13}C\{^1H\}$ NMR spectrum (101 MHz, D_2O) of the NaOH extract of Table S 18, entry 4 – CO_2 treatment of **175**, CuI and $NaBPh_4$ in MeOH.

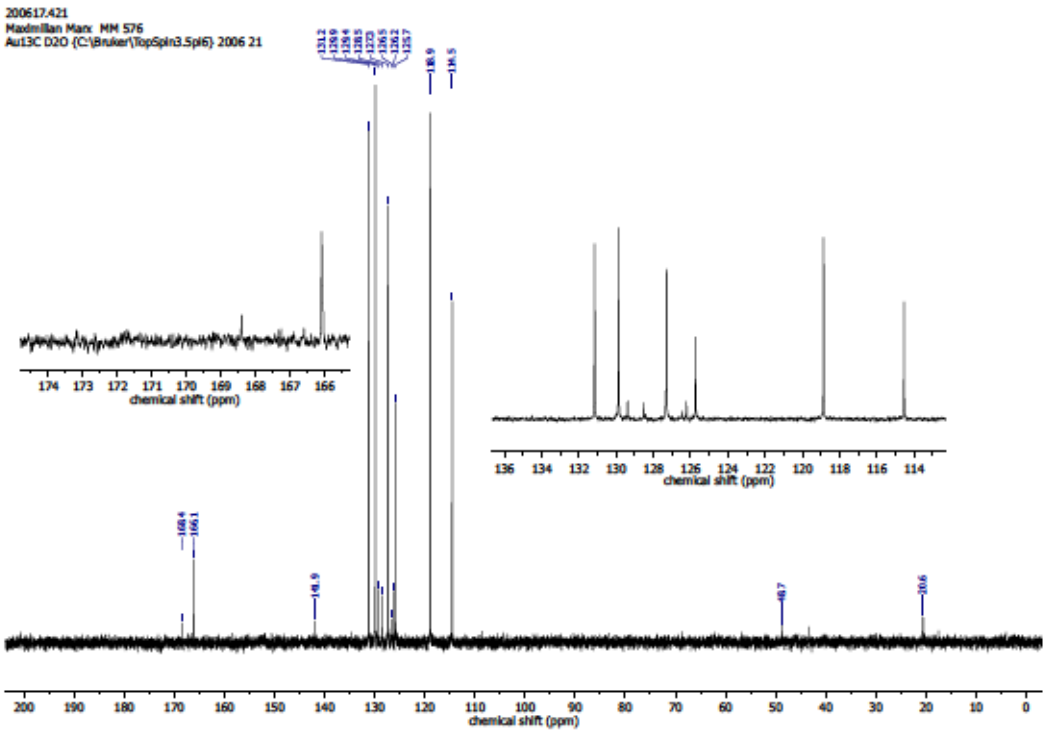

Figure S 167: $^{13}C\{^1H\}$ NMR spectrum (101 MHz, D_2O) of the NaOH extract of Table S 18, entry 5 – CO_2 treatment of **166**, CuI and $NaBPh_4$ in MeOH.

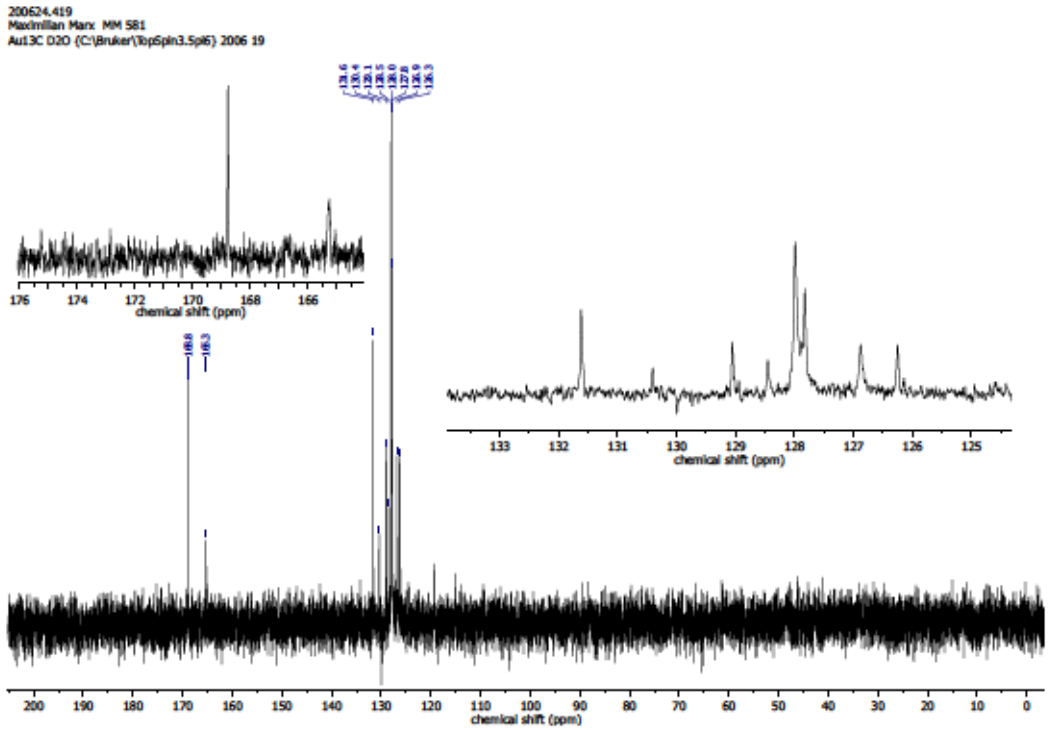

Figure S 168: $^{13}C\{^{1}H\}$ NMR spectrum (101 MHz, D_2O) of the NaOH extract of Table S 18, entry 8 – CO_2 treatment of **dien**, CuI and $NaBPh_4$ in MeOH.

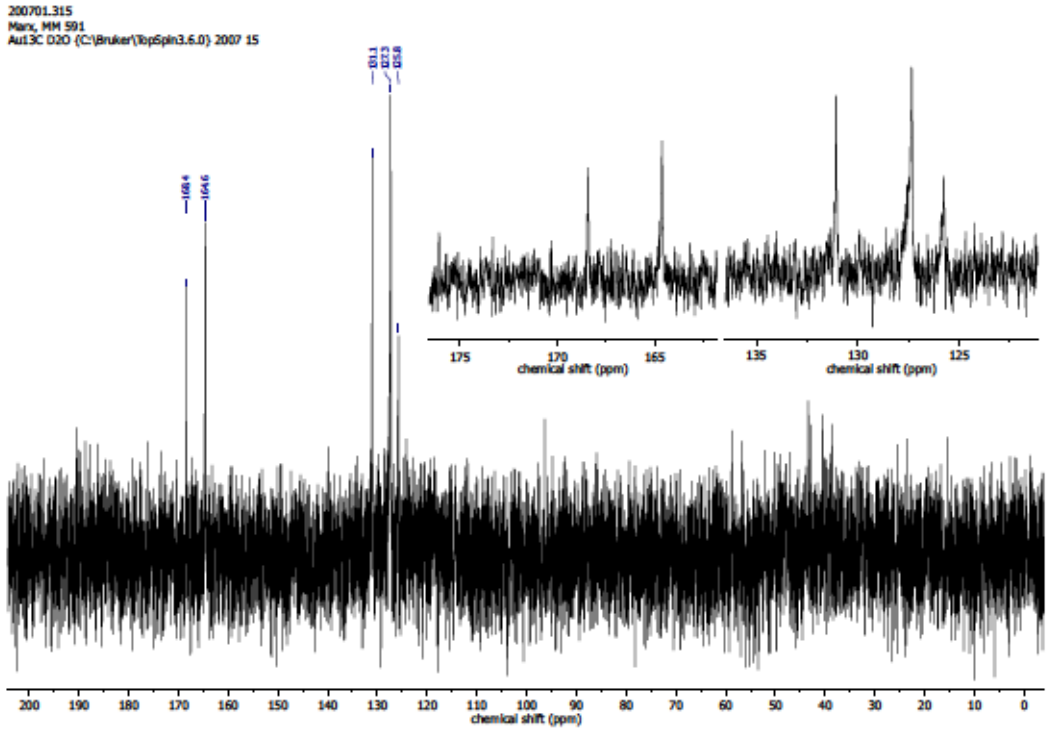

Figure S 169: $^{13}C\{^{1}H\}$ NMR spectrum (75 MHz, D_2O) of the NaOH extract of Table S 18, entry 9 – CO_2 treatment of **dien**, CuI and $NaBPh_4$ in MeOH.

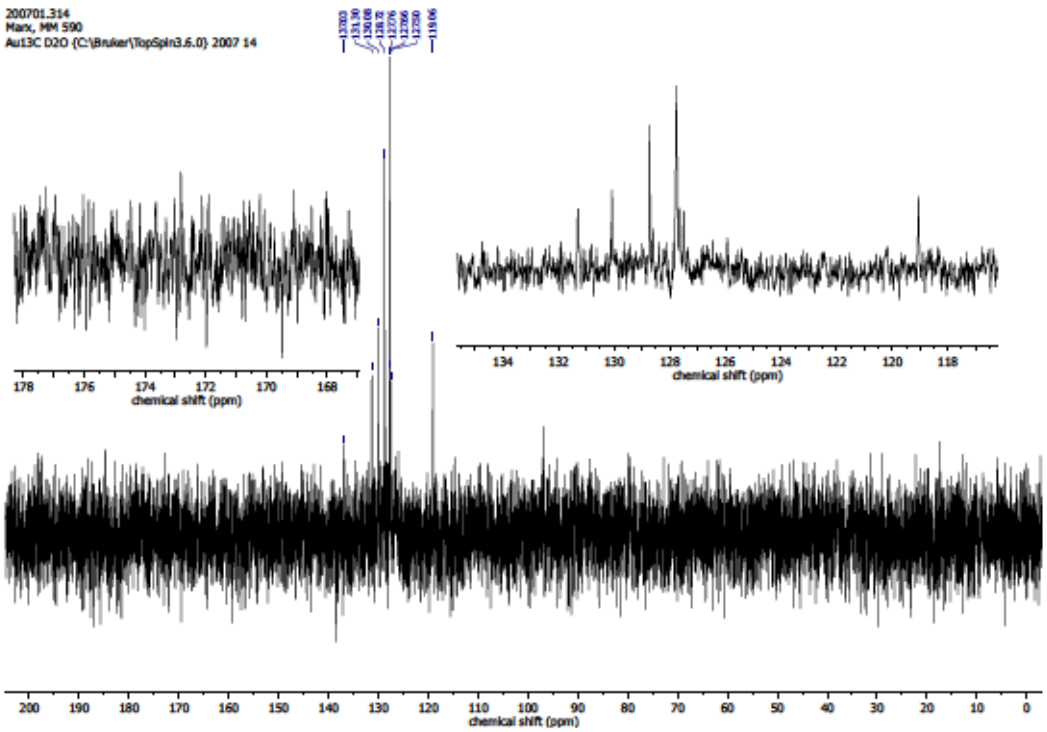

Figure S 170: $^{13}C\{^{1}H\}$ NMR spectrum (75 MHz, D_2O) of the NaOH extract of Table S 18, entry 10 – **dien**, CuI and $NaBPh_4$ in MeOH under Ar.

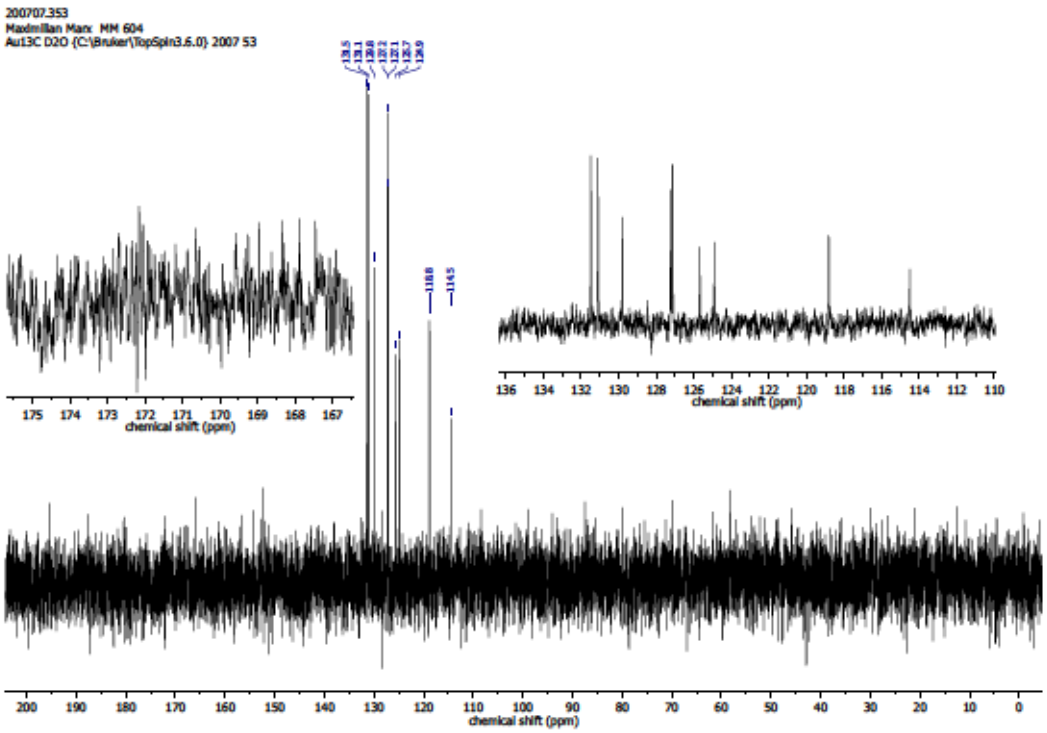

Figure S 171: $^{13}C\{^{1}H\}$ NMR spectrum (75 MHz, D_2O) of the NaOH extract of Table S 18, entry 11 – CO_2 treatment of **176** and $NaBPh_4$ in MeOH.

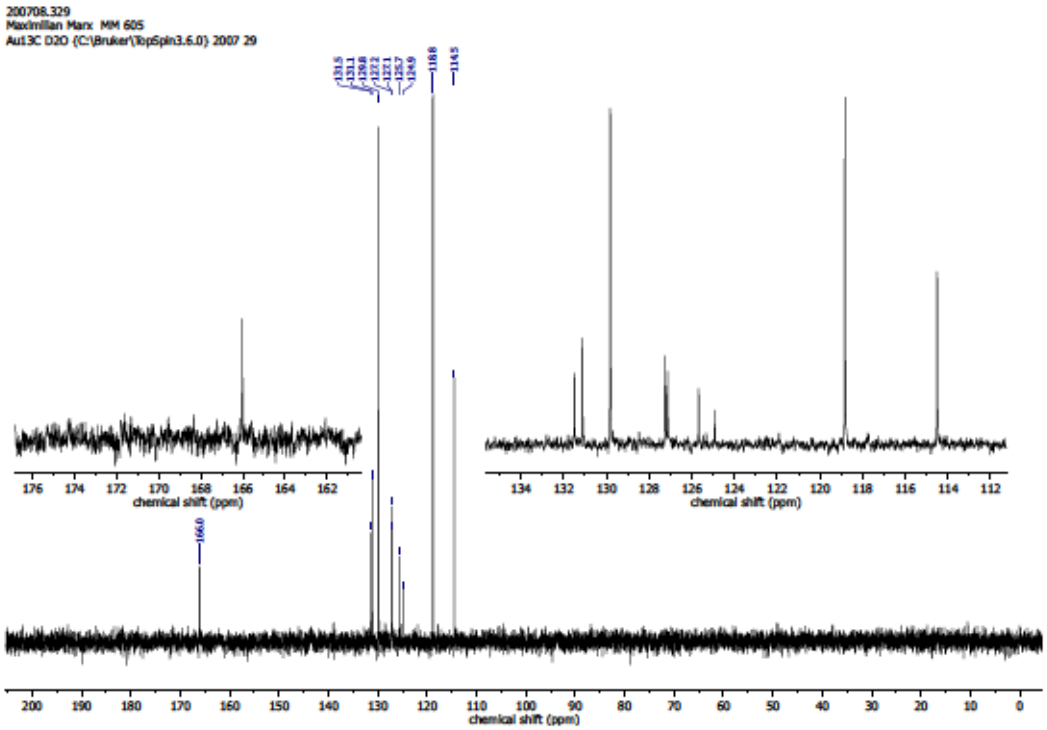

Figure S 172: $^{13}C\{^{1}H\}$ NMR spectrum (75 MHz, D_2O) of the NaOH extract of Table S 18, entry 13 – CO_2 treatment of **178** and $NaBPh_4$ in MeOH.

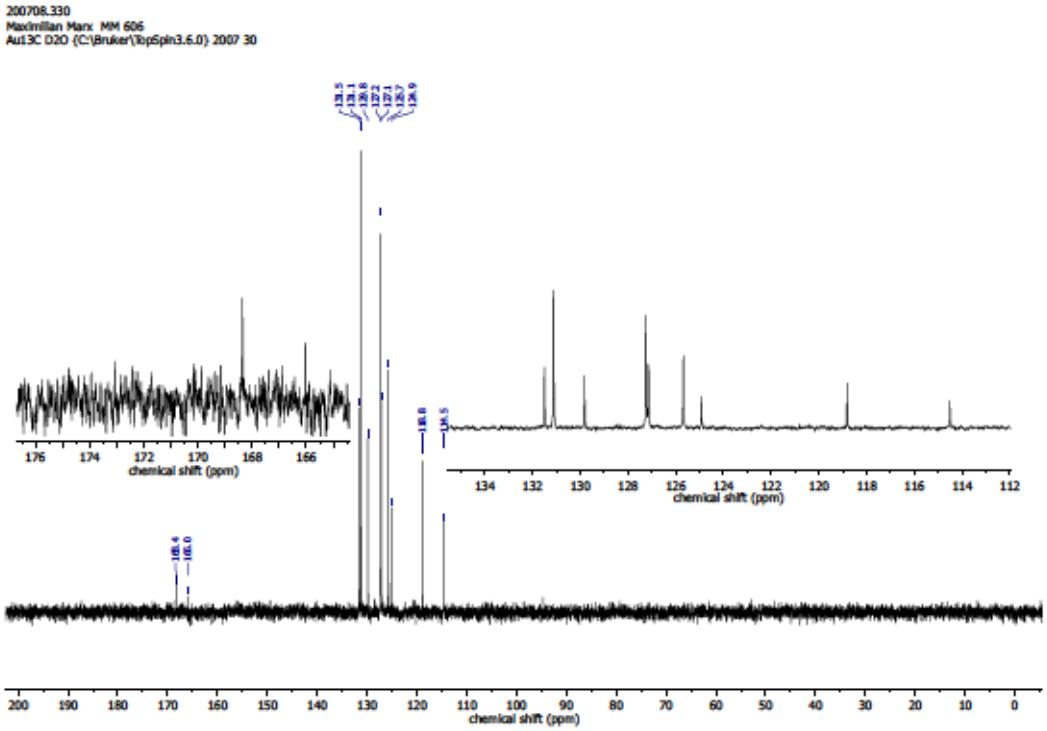

Figure S 173: $^{13}C\{^{1}H\}$ NMR spectrum (75 MHz, D_2O) of the NaOH extract of Table S 18, entry 14 – CO_2 treatment of **179** and $NaBPh_4$ in MeOH.

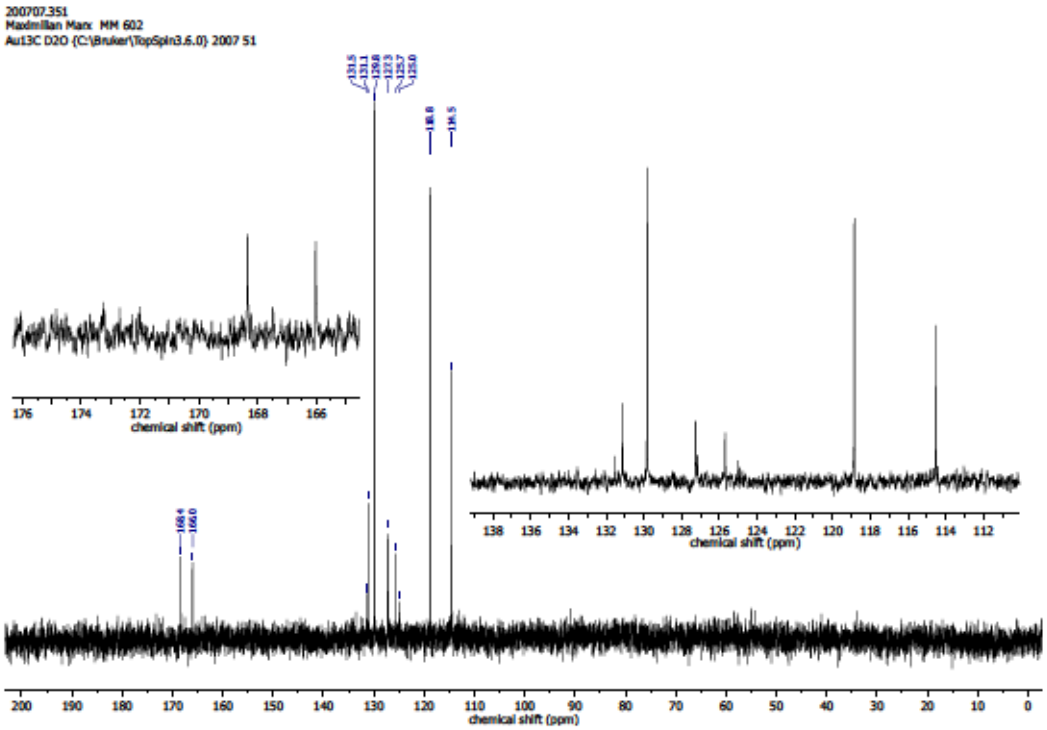

Figure S 174: $^{13}C\{^{1}H\}$ NMR spectrum (75 MHz, D_2O) of the NaOH extract of Table S 18, entry 15 – CO_2 treatment of **184**, CuI and $NaBPh_4$ in MeOH.

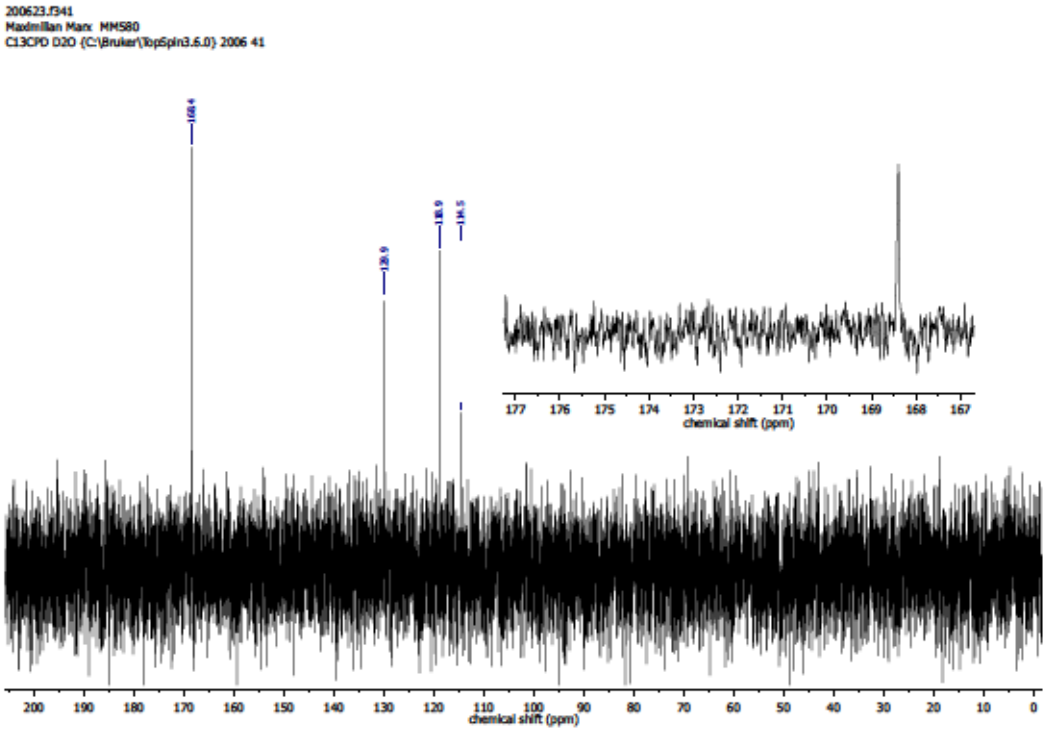

Figure S 175: $^{13}C\{^{1}H\}$ NMR spectrum (75 MHz, D_2O) of the NaOH extract of Table S 18, entry 16 – CO_2 treatment of **184**, CuI and $NaBPh_4$ in MeOH.

4.12.5 NMR Spectra – Reactions of $[Cu_2(m\text{-xpt})X_2](PF_6)_2$ complexes

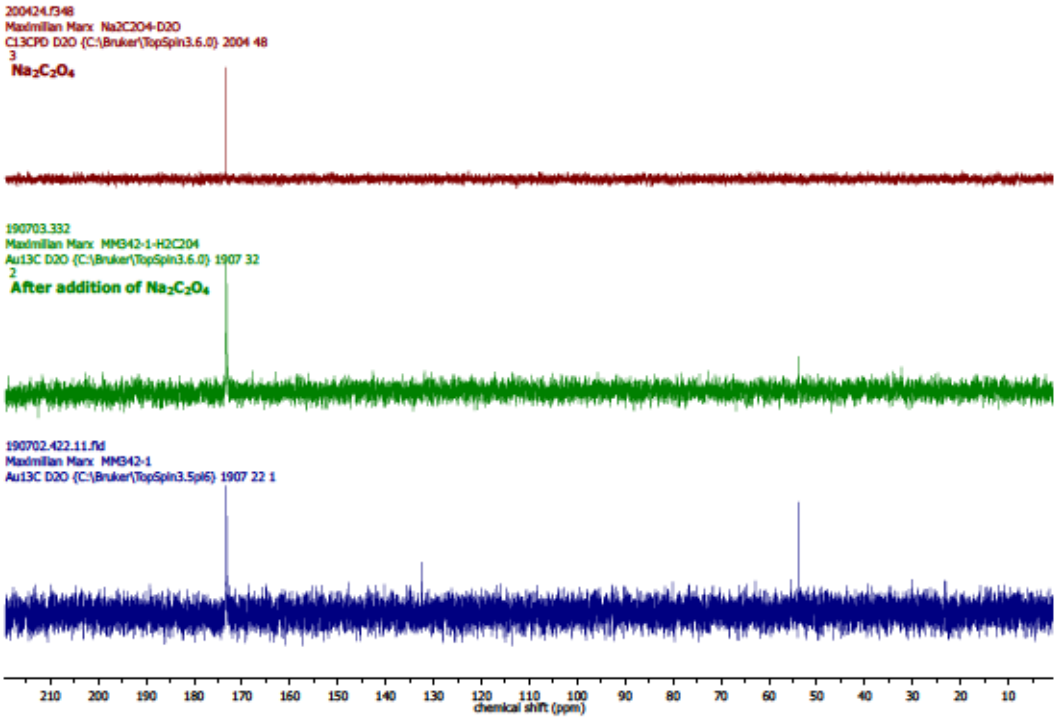

Figure S 176: $^{13}C\{^1H\}$ NMR (D_2O) of the residue obtained after NaOH treatment of **137** (prepared from $(Bu_4N)_2C_2O_4$) and comparison with $^{13}C\{^1H\}$ NMR spectra after addition of internal standard ($Na_2C_2O_4$).

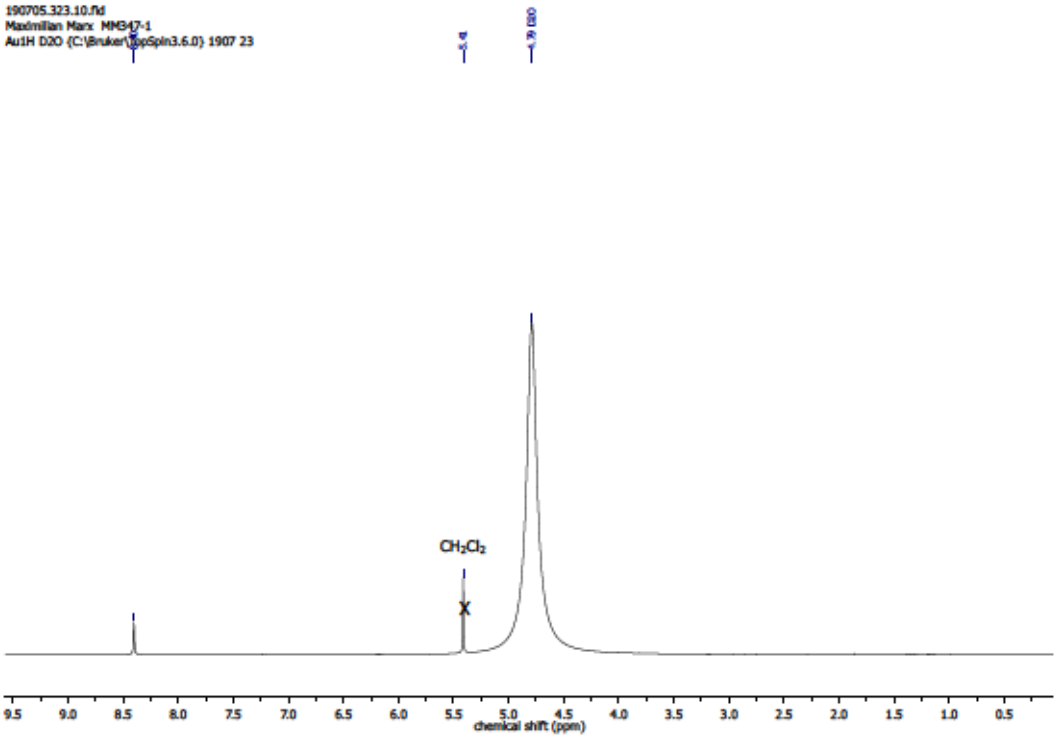

Figure S 177: ^1H NMR (300 MHz, D_2O) after NaOH treatment of the reaction of *in situ* formed **187** with air.

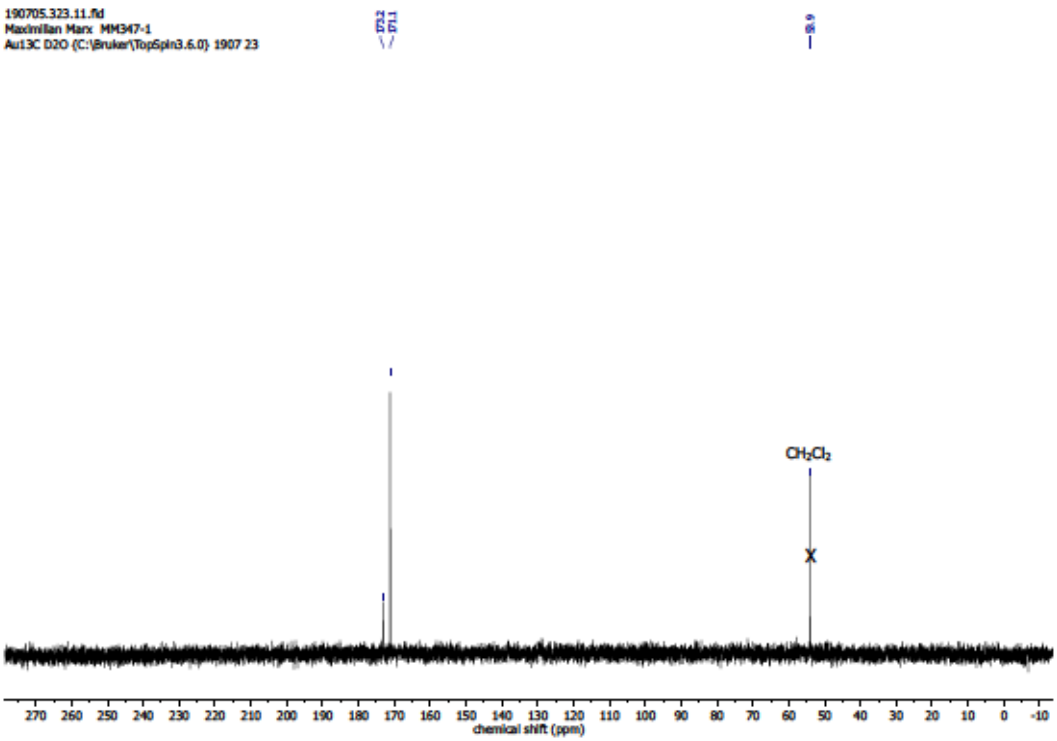

Figure S 178: $^{13}C\{^1H\}$ NMR (75 MHz, D_2O) after NaOH treatment of the reaction of *in situ* formed **187** with air.

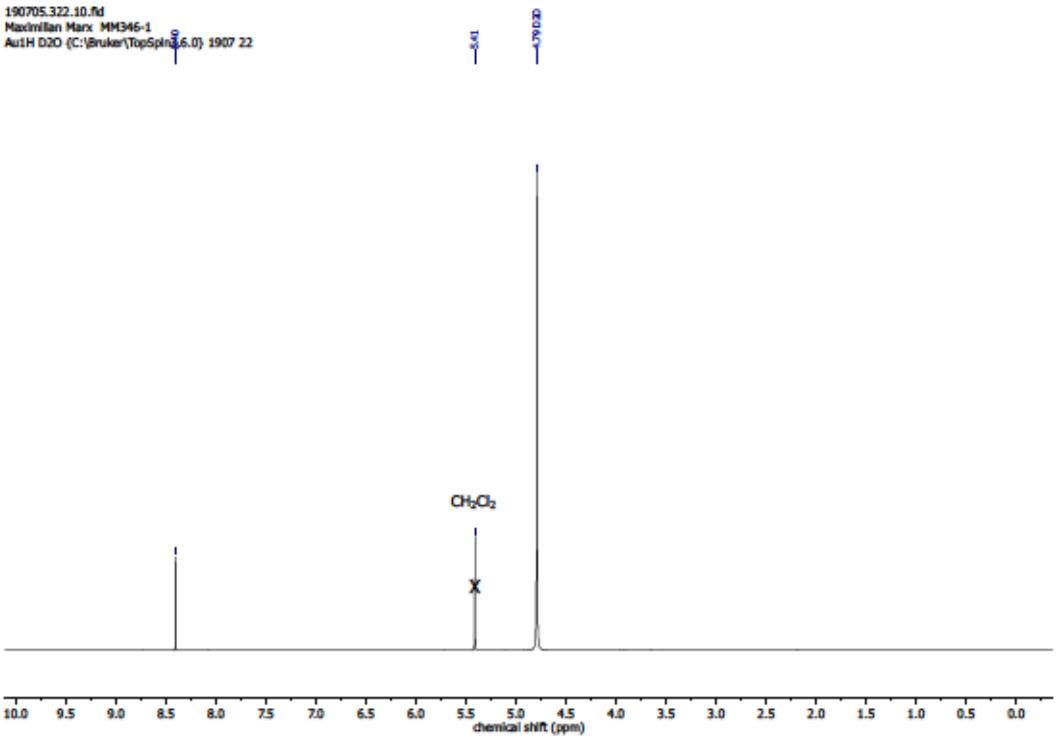

Figure S 179: ^1H NMR (300 MHz, D_2O) after NaOH treatment of the reaction of *in situ* formed **187** with O_2.

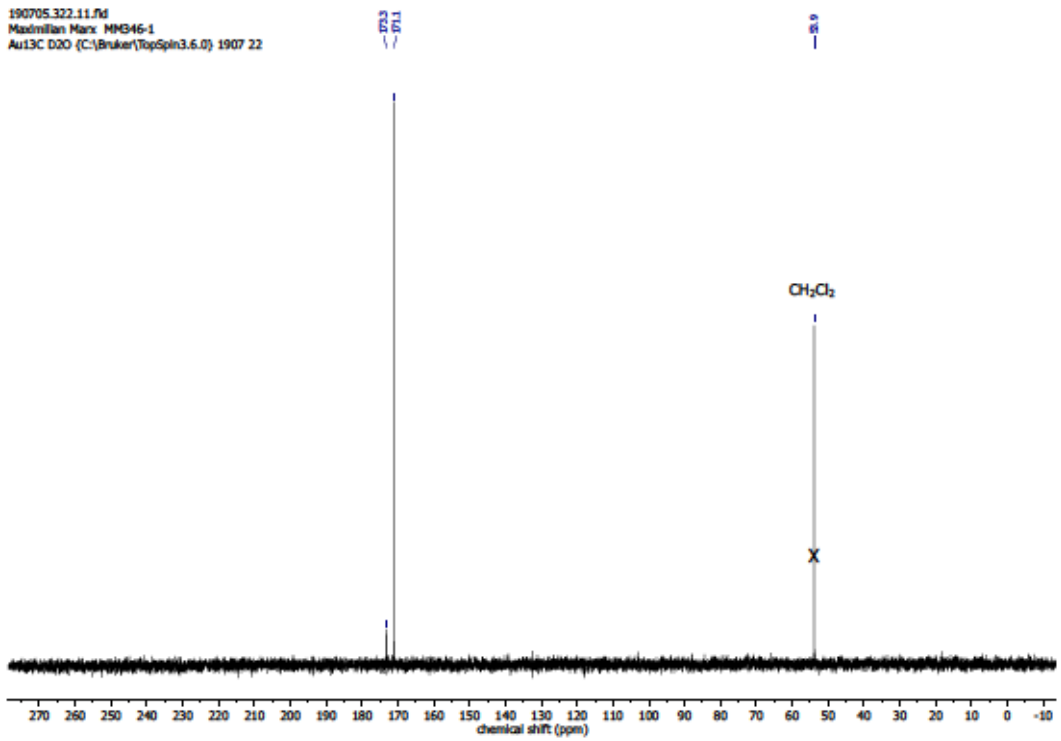

Figure S 180: $^{13}C\{^1H\}$ NMR (75 MHz, D_2O) after NaOH treatment of the reaction of *in situ* formed **187** with O_2.

4.12.6 NMR Spectra – Reactions of α-Ketocarboxylates

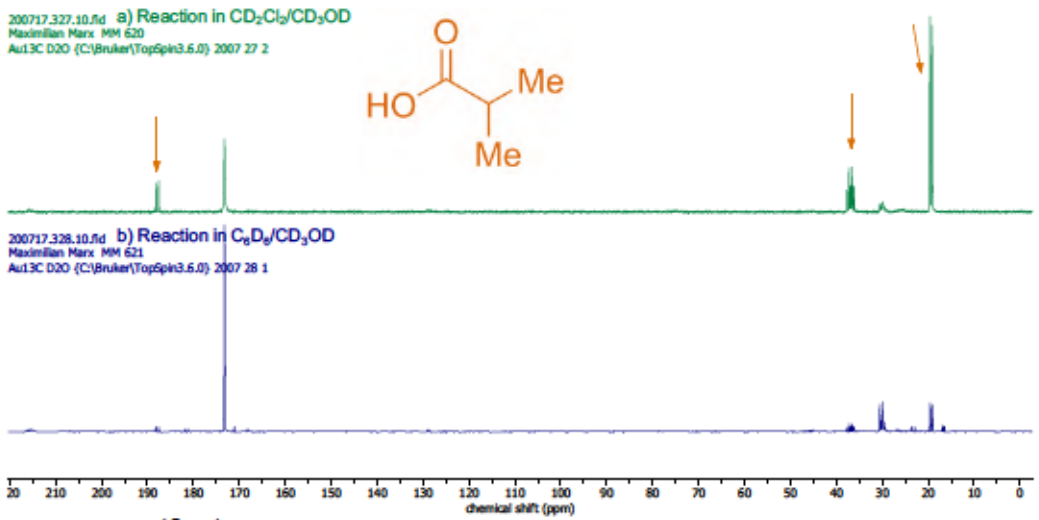

Figure S 181: $^{13}C\{^1H\}$ NMR spectra (75 MHz, D_2O) of the aqueous extract obtained after NaOH treatment of the residue from reaction of **195** and $Cu(BF_4)_2 \cdot 6H_2O$ with CO_2/O_2 in CD_2Cl_2/CD_3OD or C_6D_6/CD_3OD.

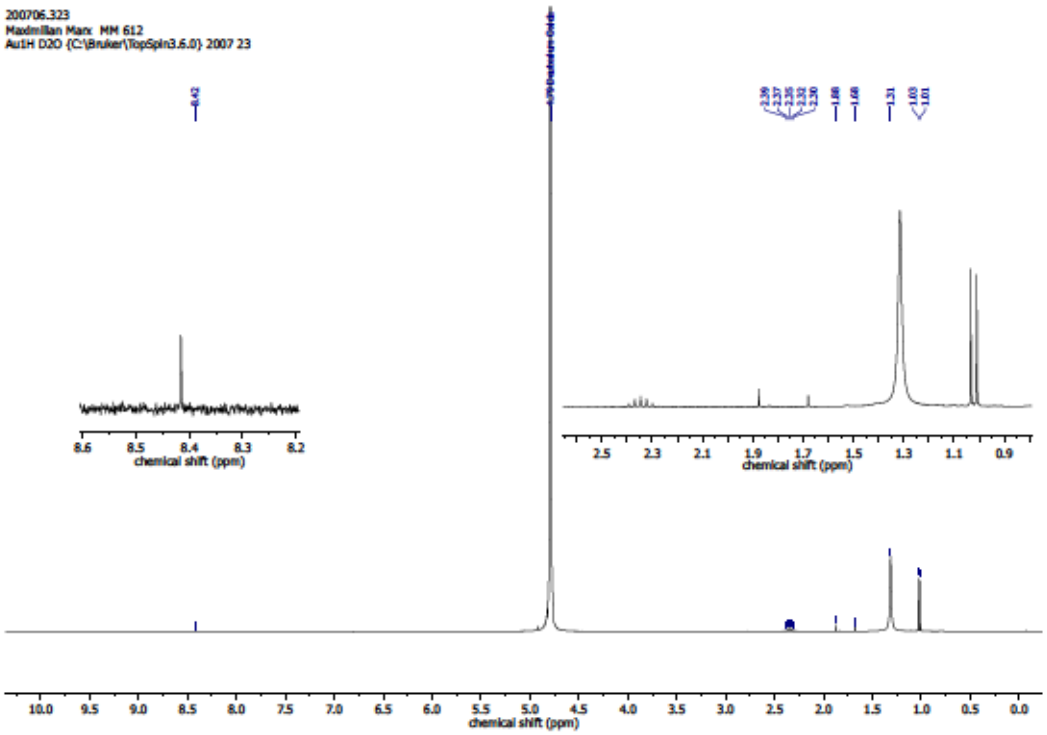

Figure S 182: ^1H NMR spectrum (300 MHz, D_2O) of the NaOH extract of Table S 19, entry 1 – air exposure of **129** in DCM/^{n}heptane.

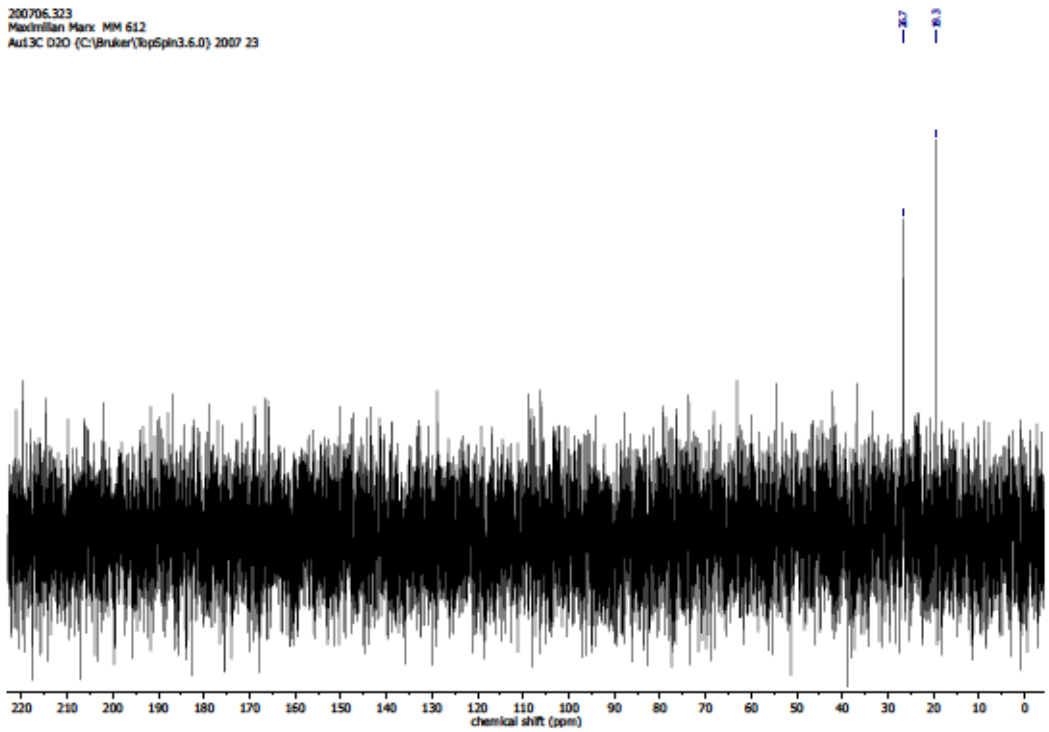

Figure S 183: $^{13}C\{^{1}H\}$ NMR spectrum (75 MHz, D_2O) of the NaOH extract of Table S 19, entry 1 – air exposure of **129** in DCM/^{n}heptane.

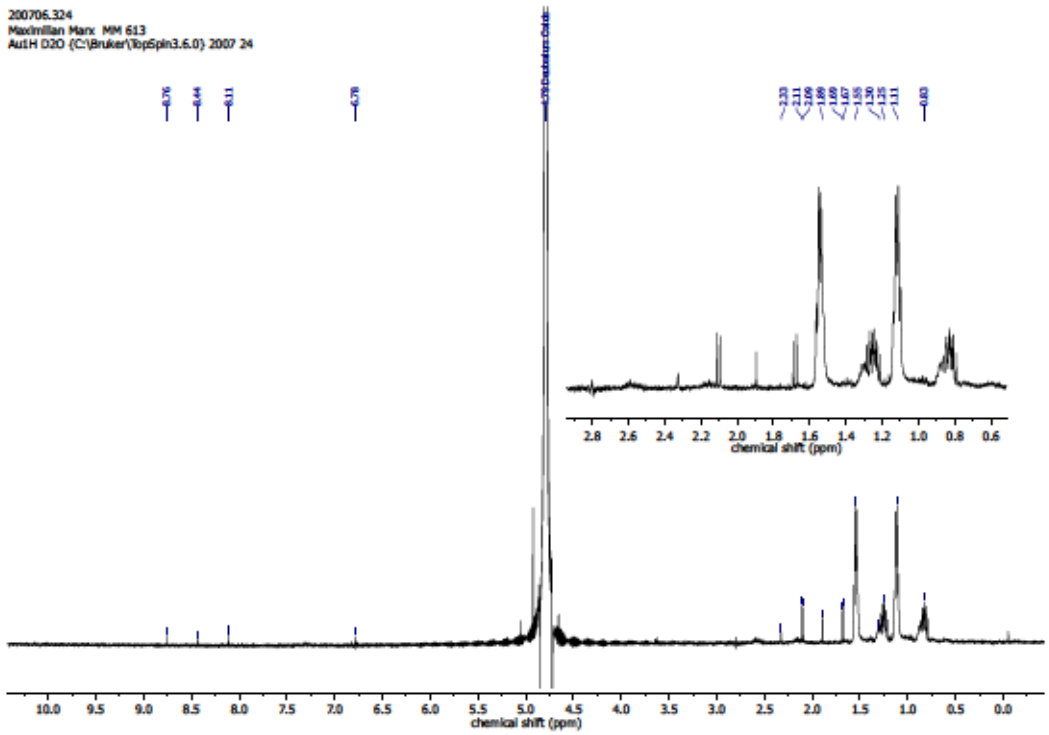

Figure S 184: ^{1}H NMR spectrum (300 MHz, D_2O) of the NaOH extract of Table S 19, entry 2 – air exposure of **196** in DCM/^{n}heptane.

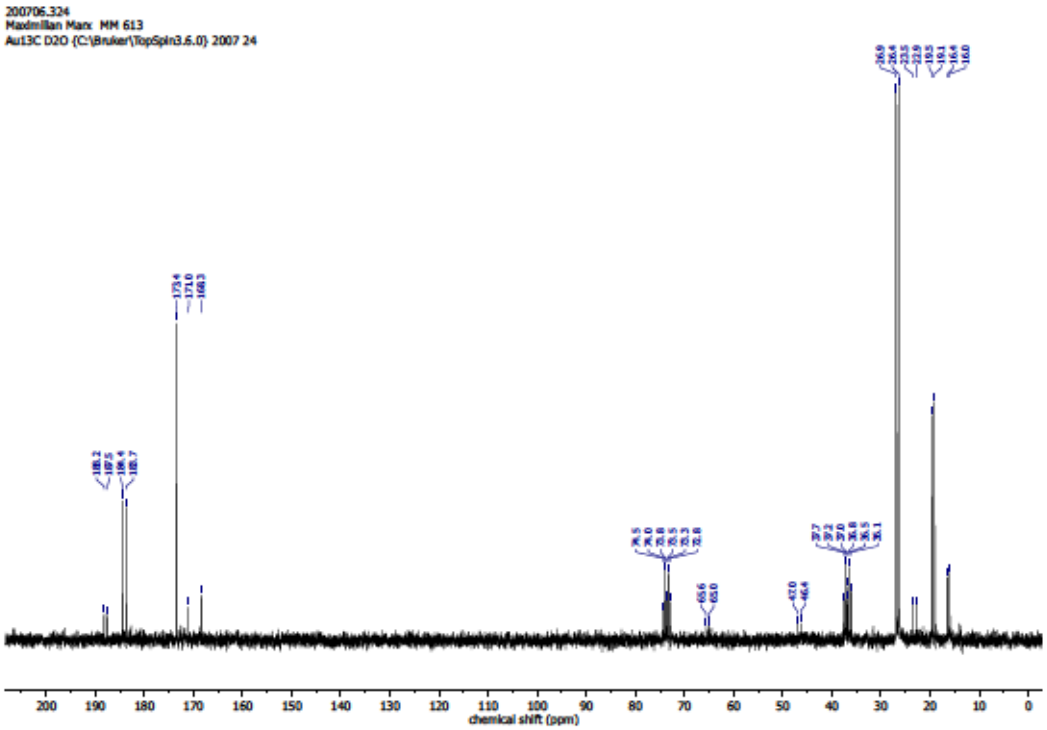

Figure S 185: $^{13}C\{^{1}H\}$ NMR spectrum (75 MHz, D_2O) of the NaOH extract of Table S 19, entry 2 – air exposure of **196** in DCM/^{n}heptane.

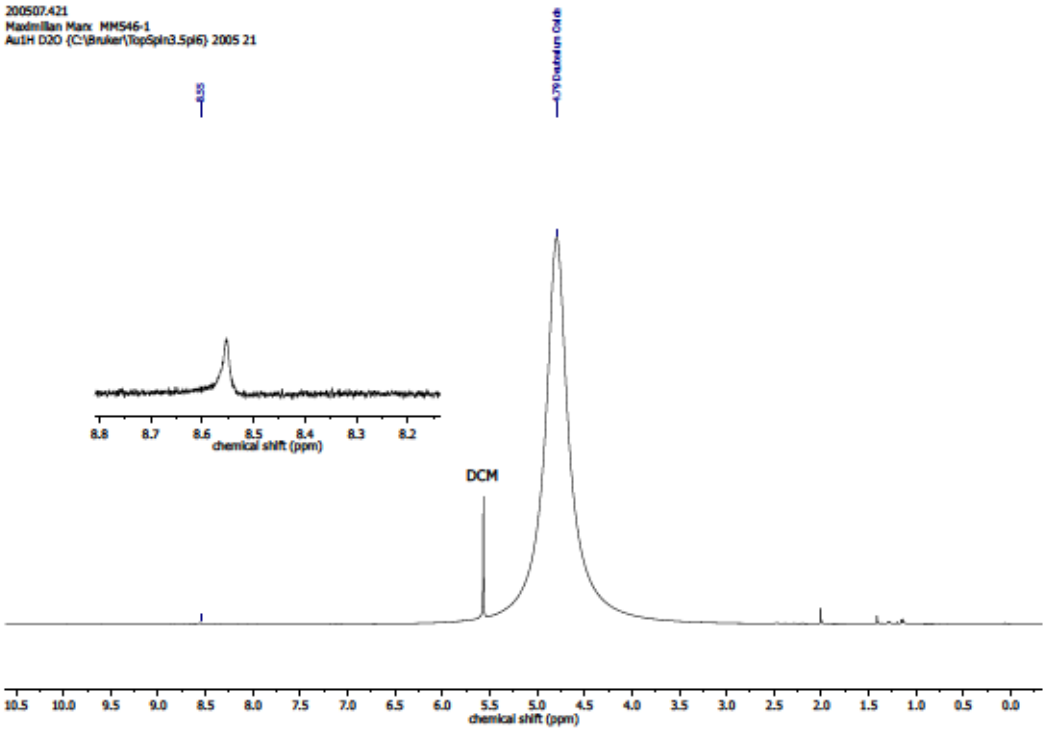

Figure S 186: ^{1}H NMR spectrum (400 MHz, D_2O) of the NaOH extract of Table S 19, entry 3 – air exposure of sodium 3-methyl-2-oxobuyrate and $Cu(BF_4)_2{\cdot}6H_2O$ in DCM/MeOH/^{n}heptane.

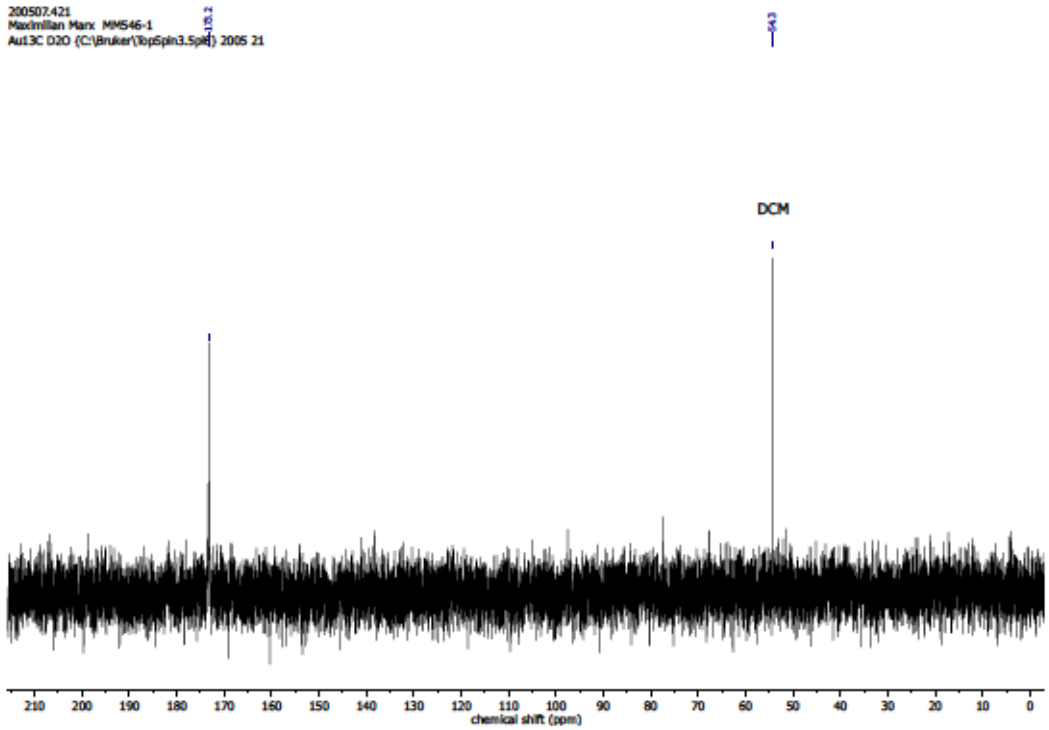

Figure S 187: $^{13}C\{^1H\}$ NMR spectrum (101 MHz, D_2O) of the NaOH extract of Table S 19, entry 3 – air exposure of sodium 3-methyl-2-oxobuyrate and $Cu(BF_4)_2{\cdot}6H_2O$ in DCM/MeOH/^{n}heptane.

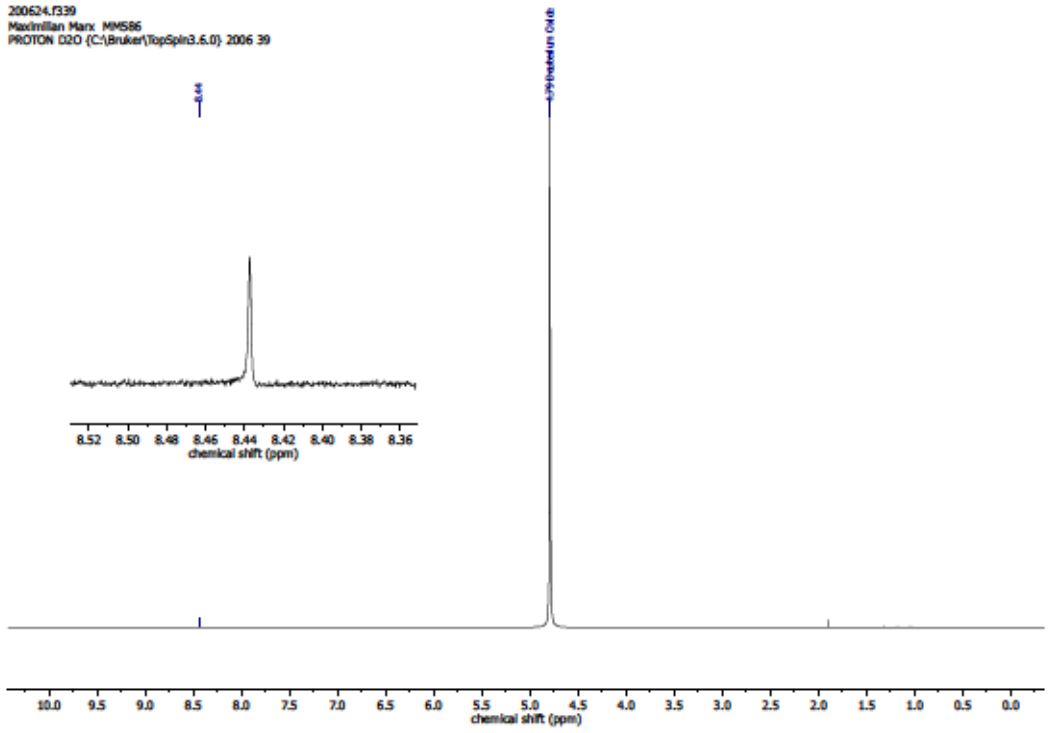

Figure S 188: ^1H NMR spectrum (300 MHz, D_2O) of the NaOH extract of Table S 19, entry 4 – air exposure of sodium 3-methyl-2-oxobuyrate and $Cu(BF_4)_2{\cdot}6H_2O$ in DCM/MeOH/^{n}heptane.

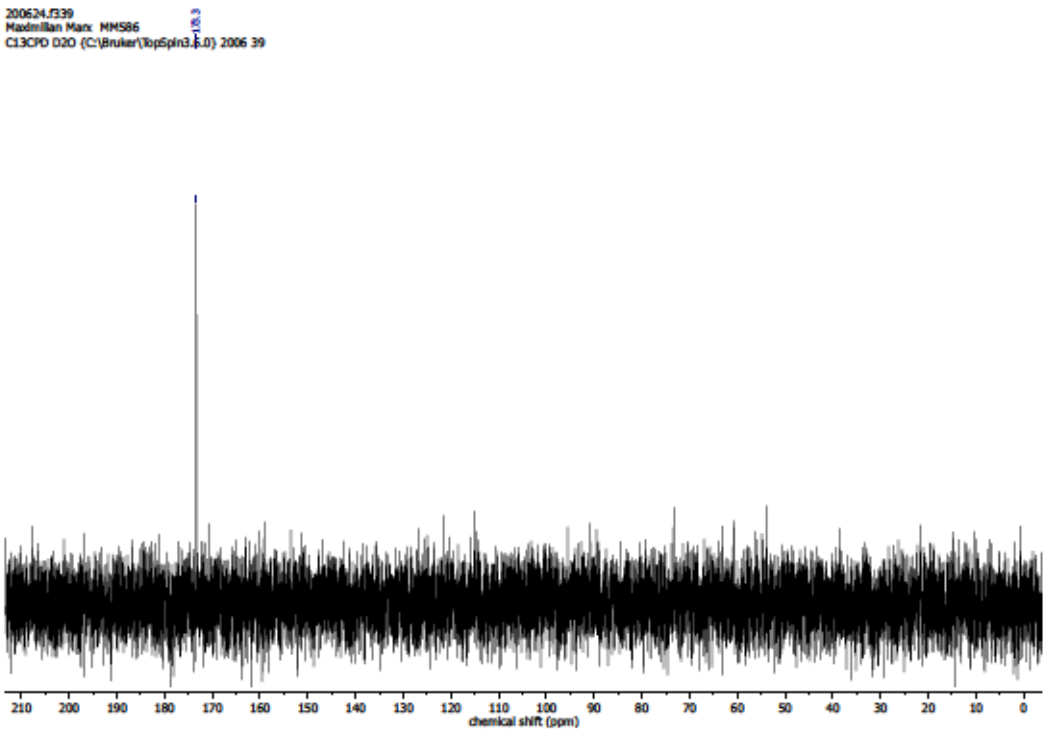

Figure S 189: $^{13}C\{^{1}H\}$ NMR spectrum (75 MHz, D_2O) of the NaOH extract of Table S 19, entry 4 – air exposure of sodium 3-methyl-2-oxobuyrate and $Cu(BF_4)_2{\cdot}6H_2O$ in DCM/MeOH/^{n}heptane.

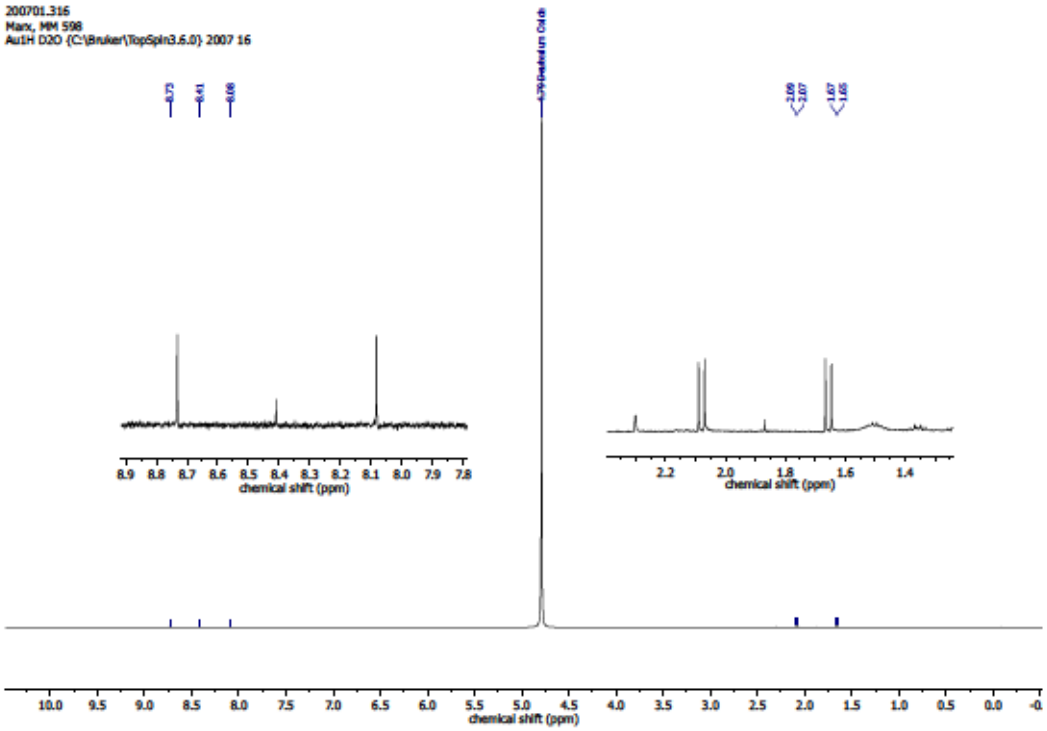

Figure S 190: ^{1}H NMR spectrum (300 MHz, D_2O) of the NaOH extract of Table S 19, entry 5 – air exposure of sodium $^{13}C_5$-3-methyl-2-oxobuyrate and $Cu(BF_4)_2{\cdot}6H_2O$ in DCM/MeOH/^{n}heptane.

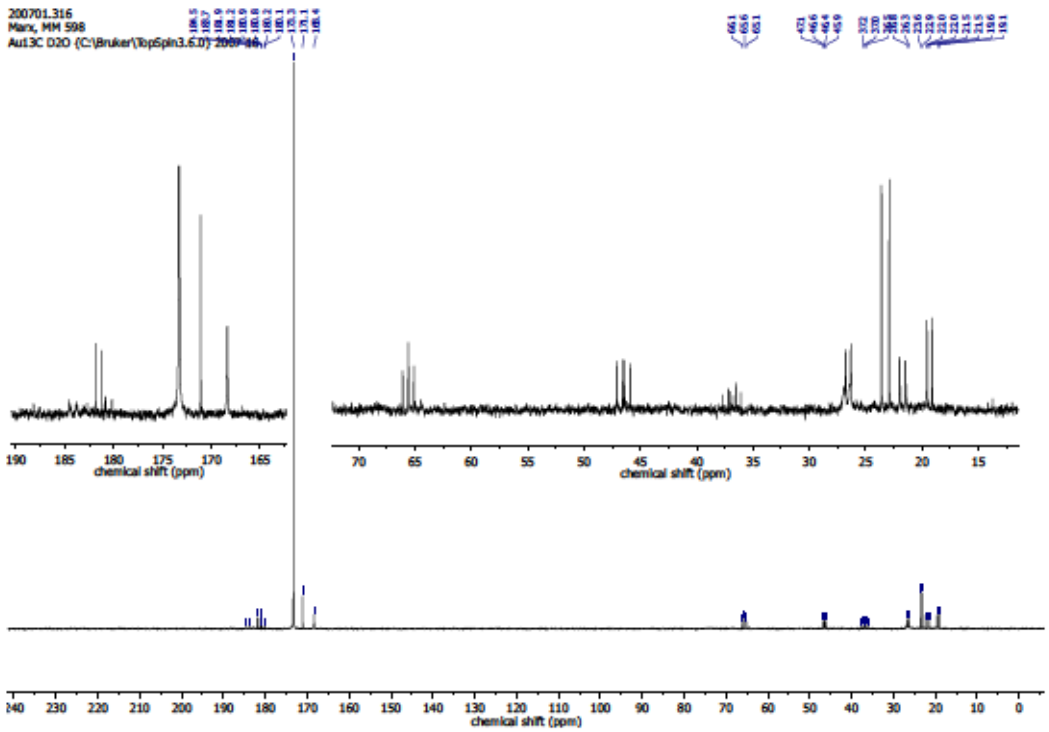

Figure S 191: $^{13}C\{^{1}H\}$ NMR spectrum (75 MHz, D_2O) of the NaOH extract of Table S 19, entry 5 – air exposure of sodium $^{13}C_5$-3-methyl-2-oxobuyrate and $Cu(BF_4)_2{\cdot}6H_2O$ in DCM/MeOH/^{n}heptane.

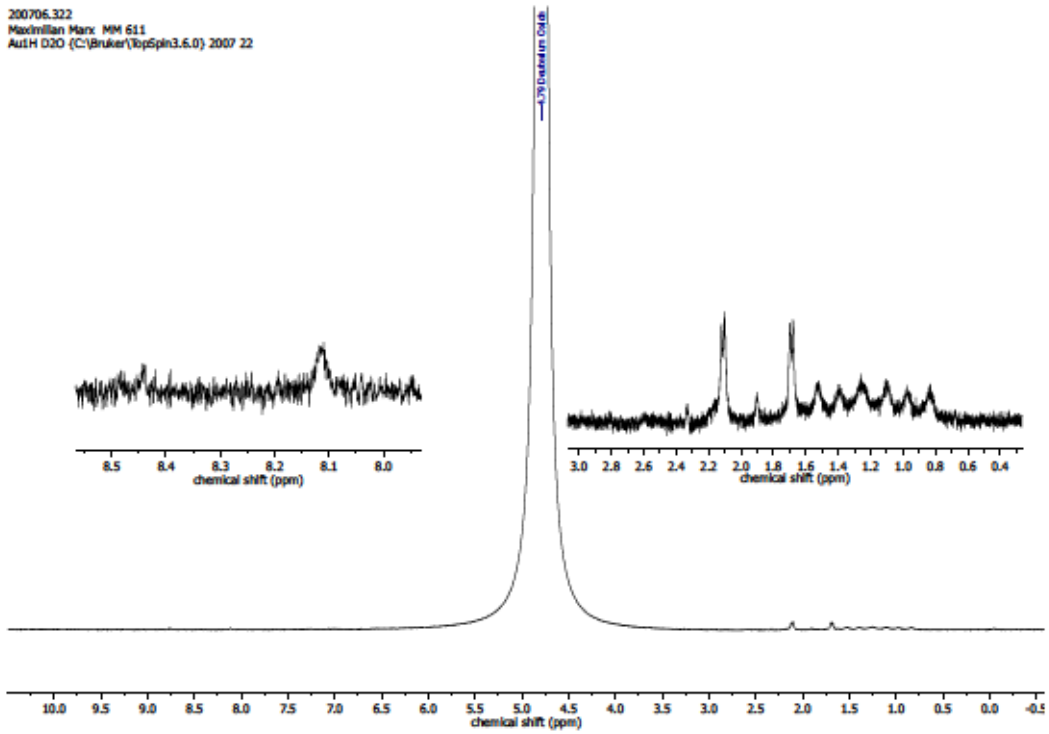

Figure S 192: ^{1}H NMR spectrum (300 MHz, D_2O) of the NaOH extract of Table S 19, entry 6 – air exposure of sodium $^{13}C_5$-3-methyl-2-oxobuyrate and $Cu(BF_4)_2{\cdot}6H_2O$ in DCM/MeOH/^{n}heptane.

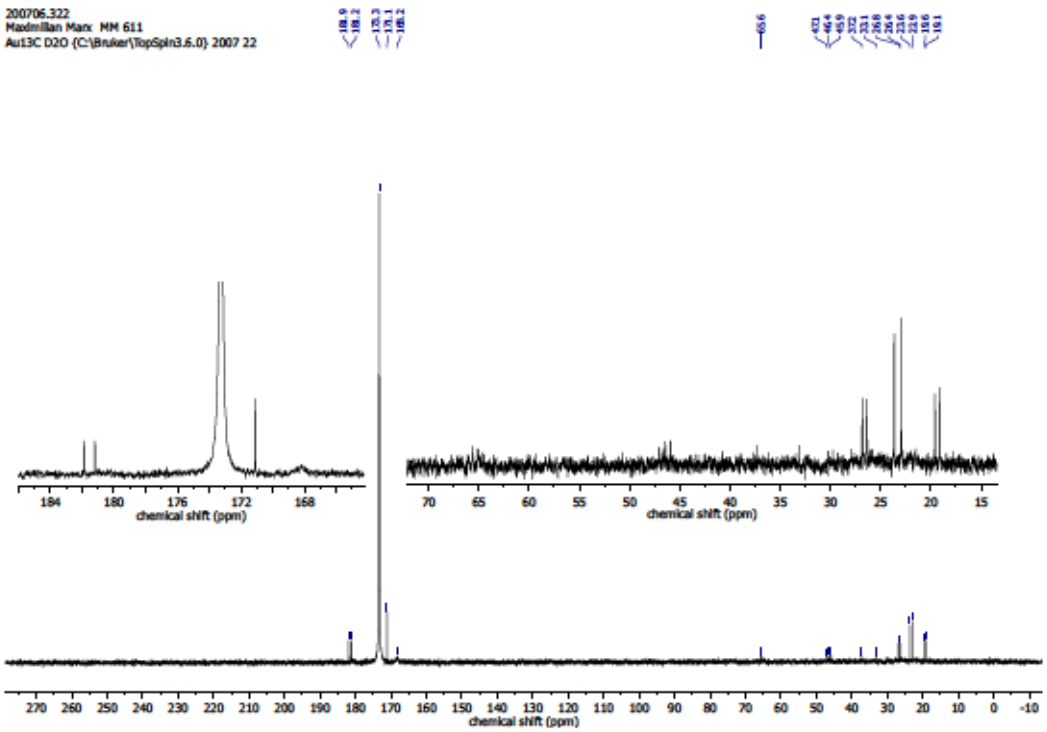

Figure S 193: $^{13}C\{^{1}H\}$ NMR spectrum (75 MHz, D_2O) of the NaOH extract of Table S 19, entry 6 – air exposure of sodium $^{13}C_5$-3-methyl-2-oxobuyrate and $Cu(BF_4)_2{\cdot}6H_2O$ in DCM/MeOH/^{n}heptane.

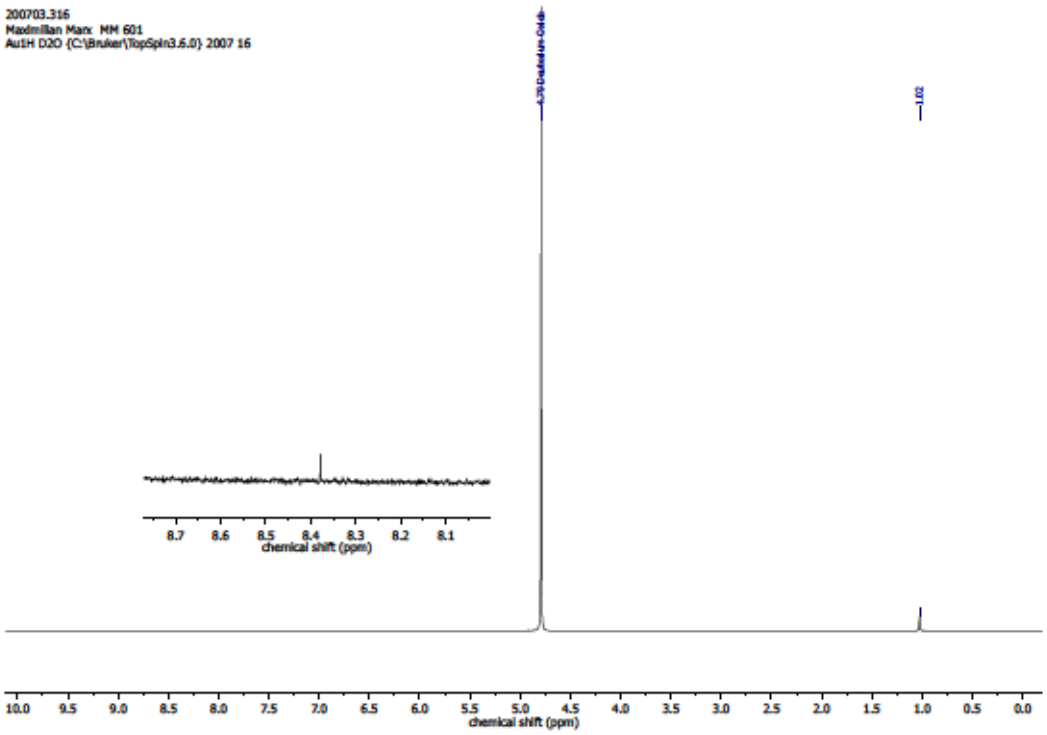

Figure S 194: ^{1}H NMR spectrum (300 MHz, D_2O) of the NaOH extract of Table S 19, entry 7 – air exposure of sodium 3-methyl-2-oxobuyrate in DCM/MeOH/^{n}heptane.

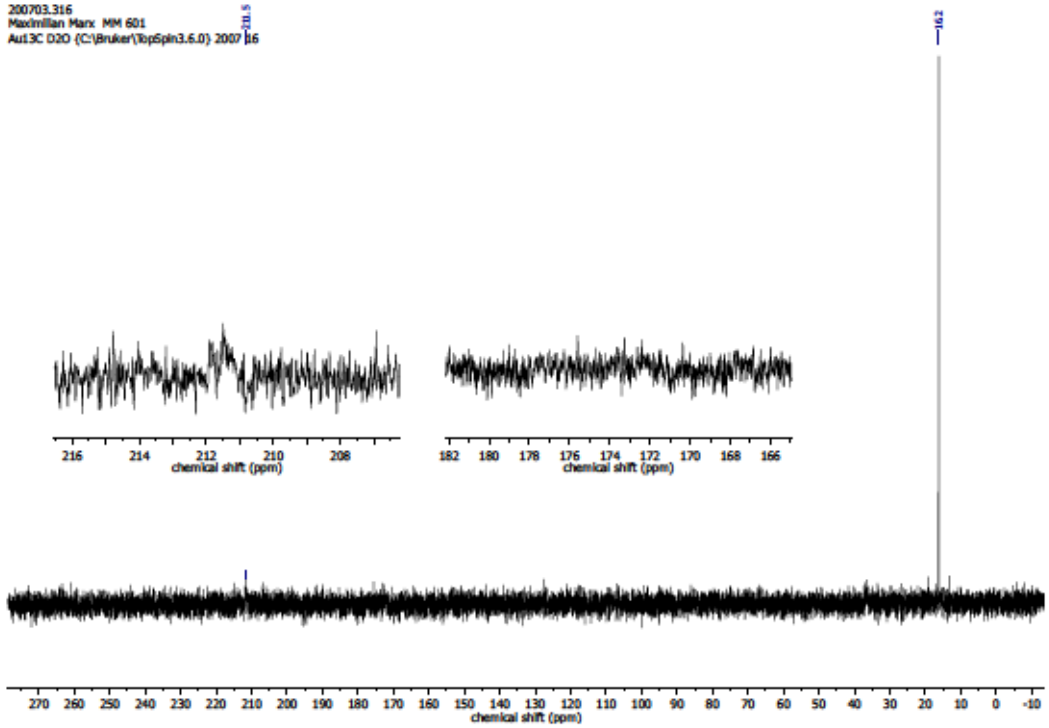

Figure S 195: $^{13}C\{^{1}H\}$ NMR spectrum (75 MHz, D_2O) of the NaOH extract of Table S 19, entry 7 – air exposure of sodium 3-methyl-2-oxobuyrate in DCM/MeOH/^{n}heptane.

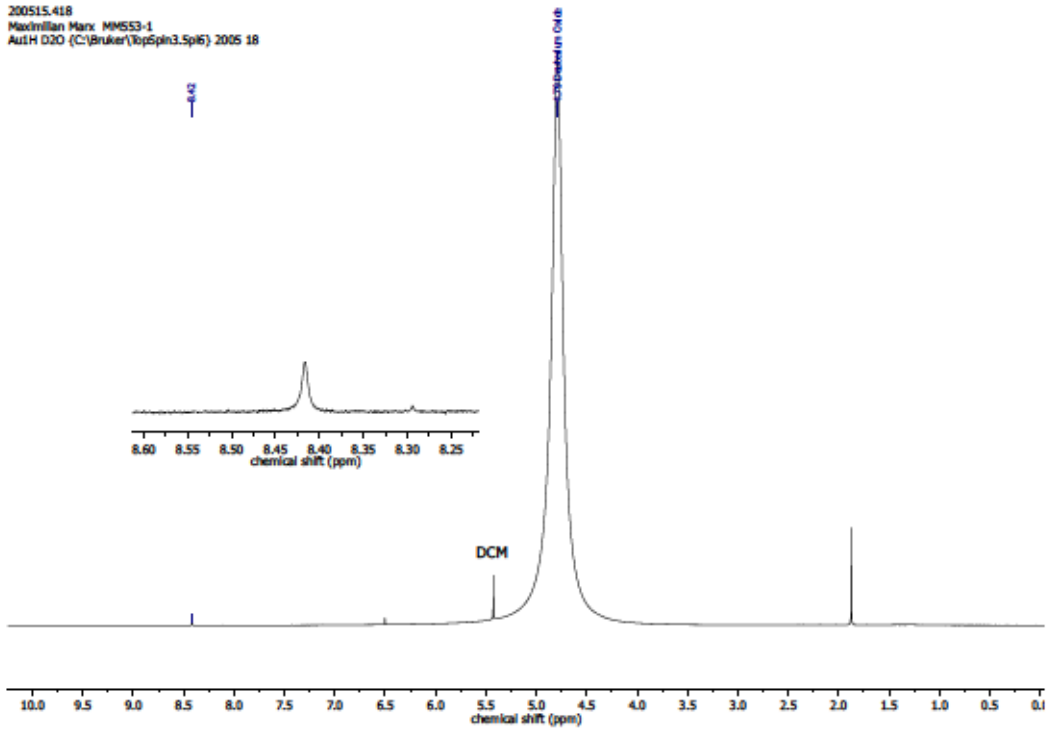

Figure S 196: ^{1}H NMR spectrum (400 MHz, D_2O) of the NaOH extract of Table S 19, entry 8 – air exposure of sodium pyruvate and $Cu(BF_4)_2{\cdot}6H_2O$ in DCM/MeOH/^{n}heptane.

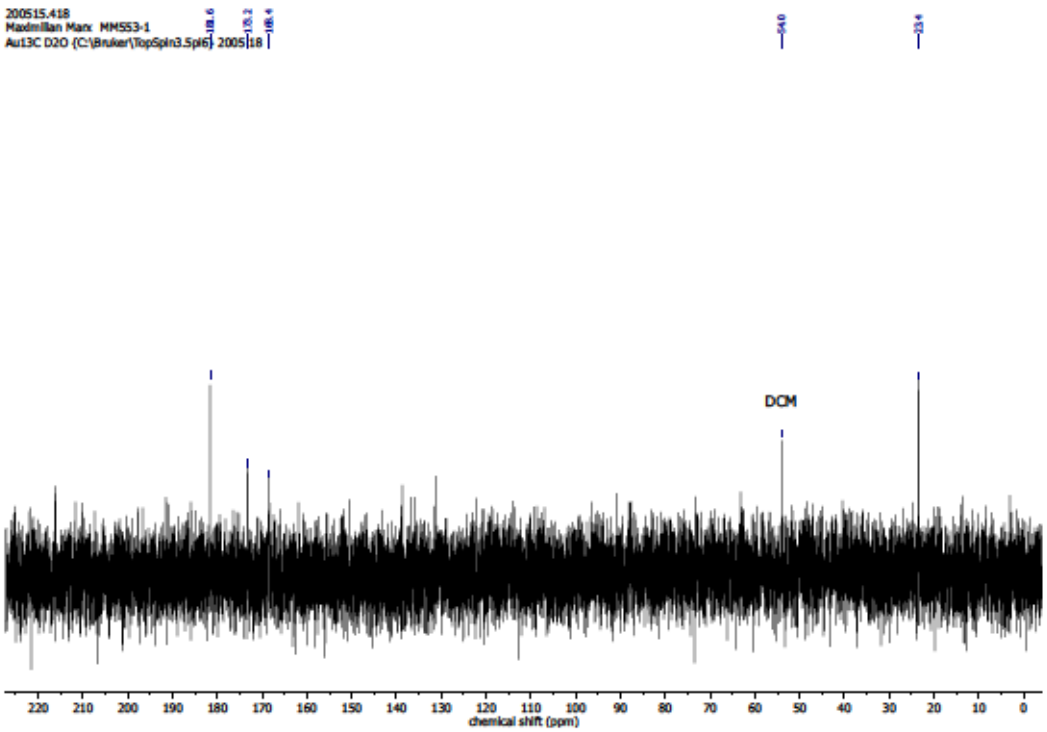

Figure S 197: $^{13}C\{^{1}H\}$ NMR spectrum (101 MHz, D_2O) of the NaOH extract of Table S 19, entry 8 – air exposure of sodium pyruvate and $Cu(BF_4)_2 \cdot 6H_2O$ in DCM/MeOH/^{n}heptane.

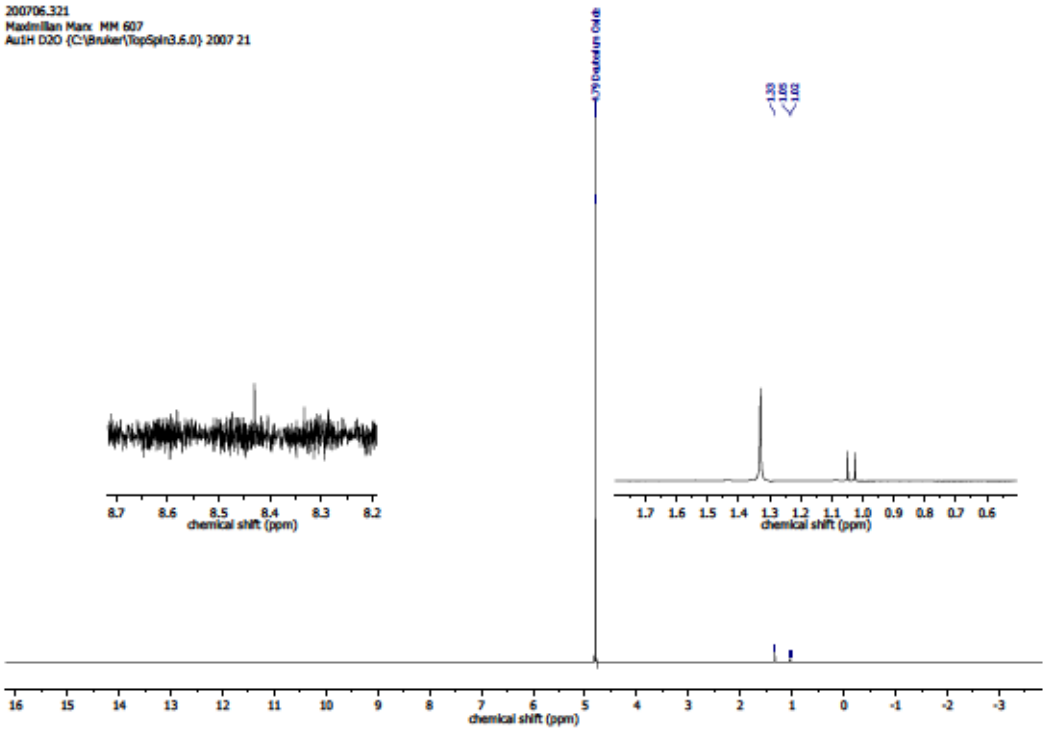

Figure S 198: ^{1}H NMR spectrum (300 MHz, D_2O) of the NaOH extract of Table S 20, entry 1 – reaction of **129** with CO_2/O_2 in toluene.

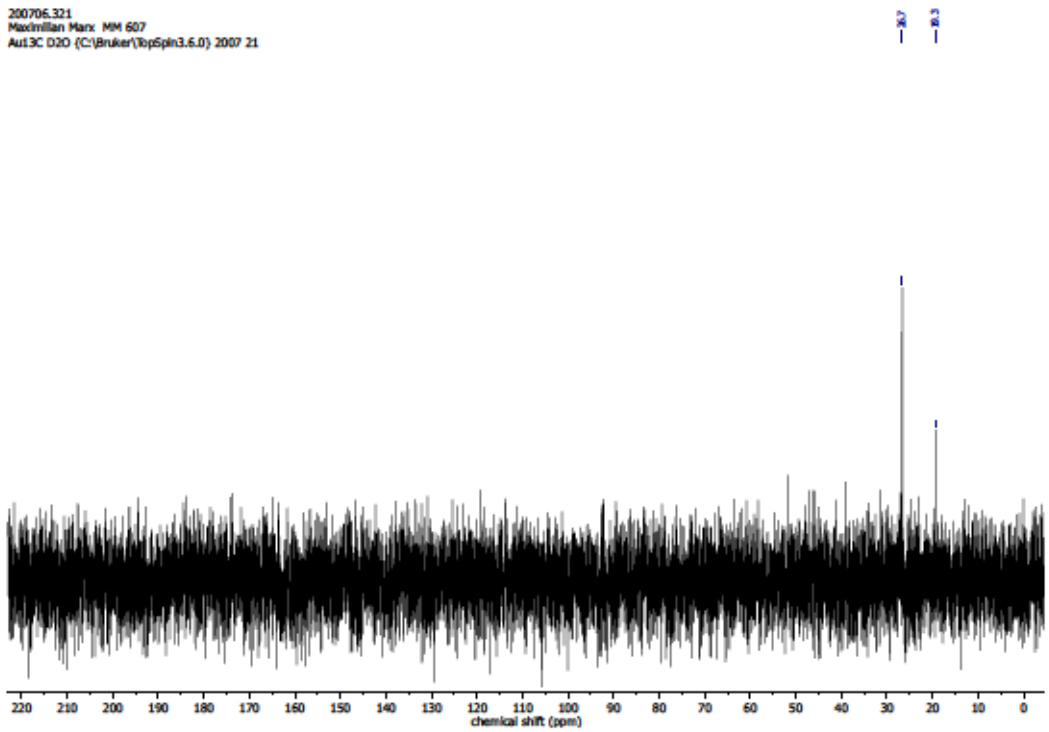

Figure S 199: $^{13}C\{^{1}H\}$ NMR spectrum (75 MHz, D_2O) of the NaOH extract of Table S 20, entry 1 – reaction of **129** with CO_2/O_2 in toluene.

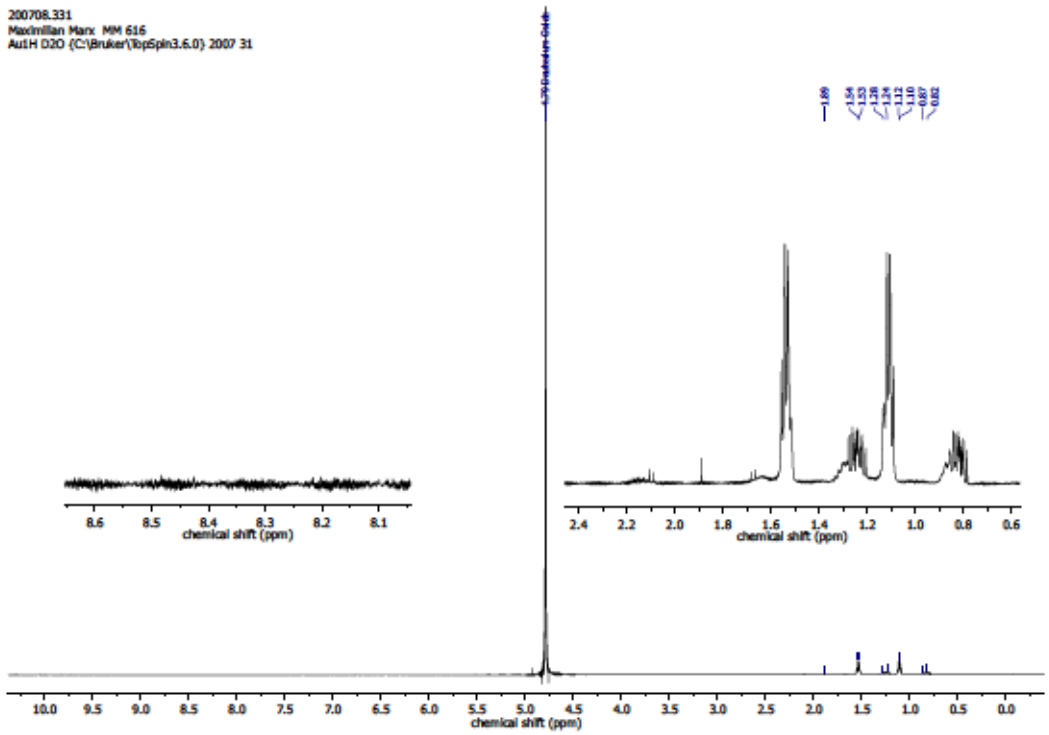

Figure S 200: ^{1}H NMR spectrum (300 MHz, D_2O) of the NaOH extract of Table S 20, entry 2 – reaction of **196** with CO_2/O_2 in toluene.

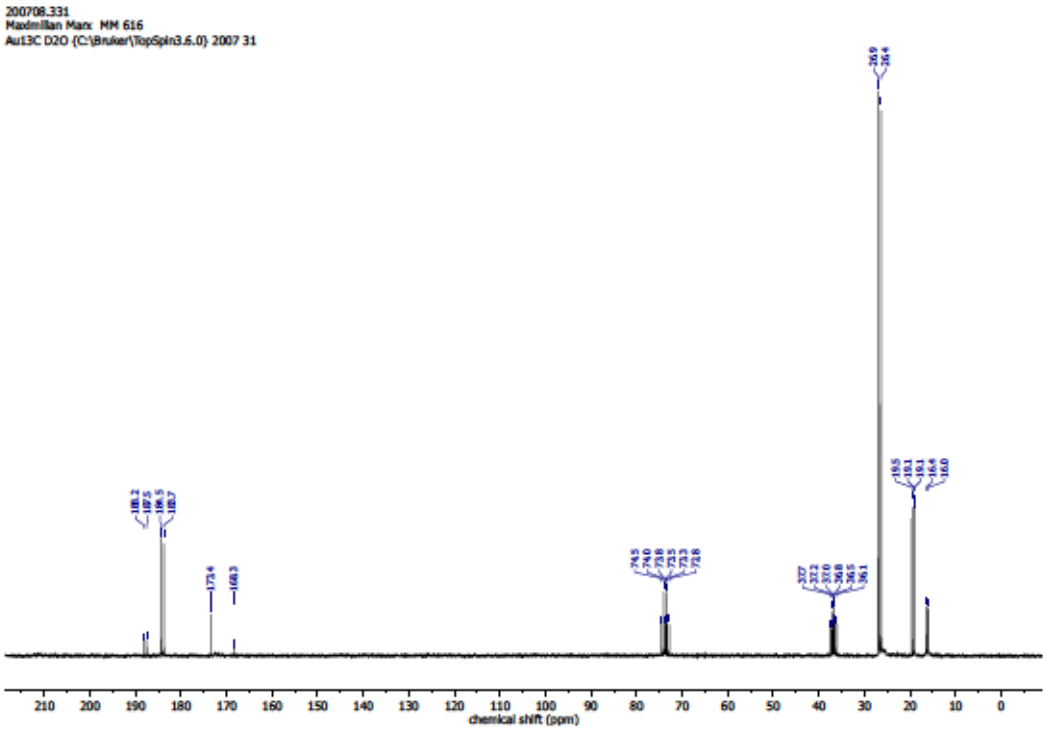

Figure S 201: $^{13}C\{^{1}H\}$ NMR spectrum (75 MHz, D_2O) of the NaOH extract of Table S 20, entry 2 – reaction of **196** with CO_2/O_2 in toluene.

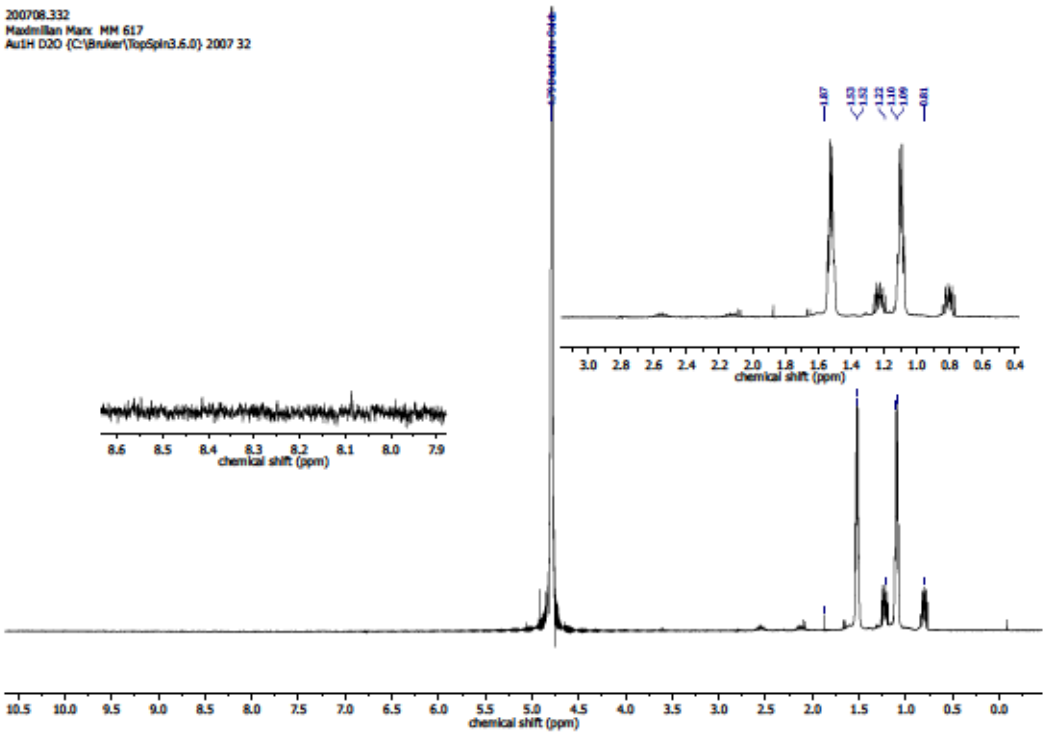

Figure S 202: ^{1}H NMR spectrum (300 MHz, D_2O) of the NaOH extract of Table S 20, entry 3 – reaction of **196** with CO_2/O_2 in toluene.

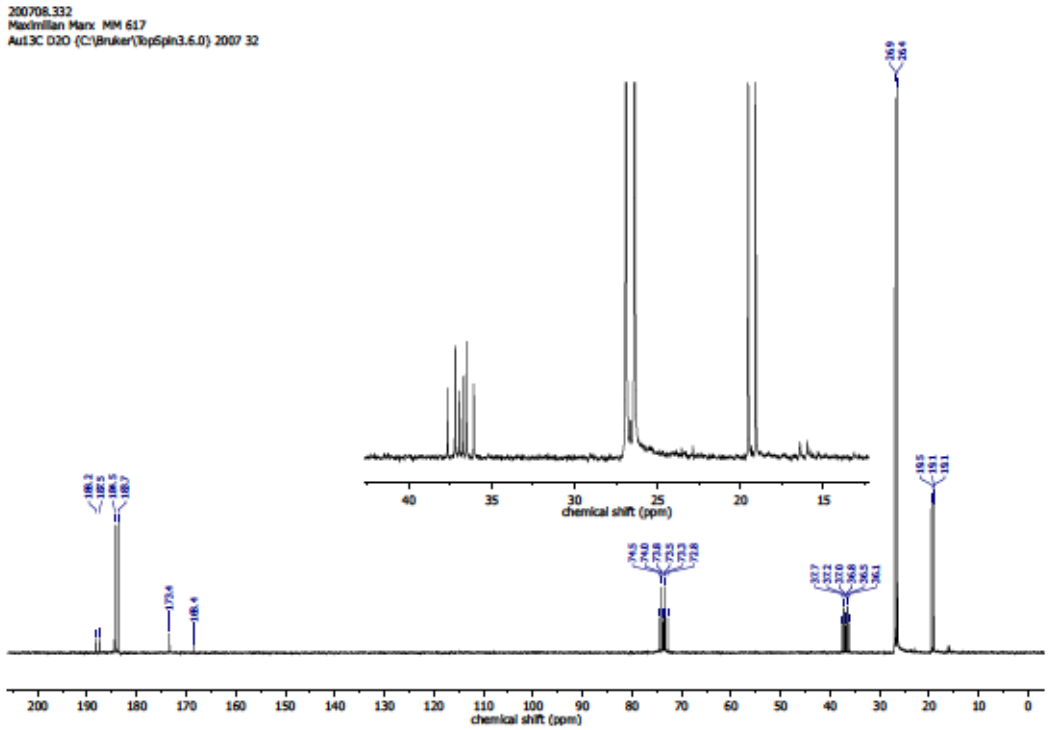

Figure S 203: $^{13}C\{^{1}H\}$ NMR spectrum (75 MHz, D_2O) of the NaOH extract of Table S 20, entry 3 – reaction of **196** with CO_2/O_2 in toluene.

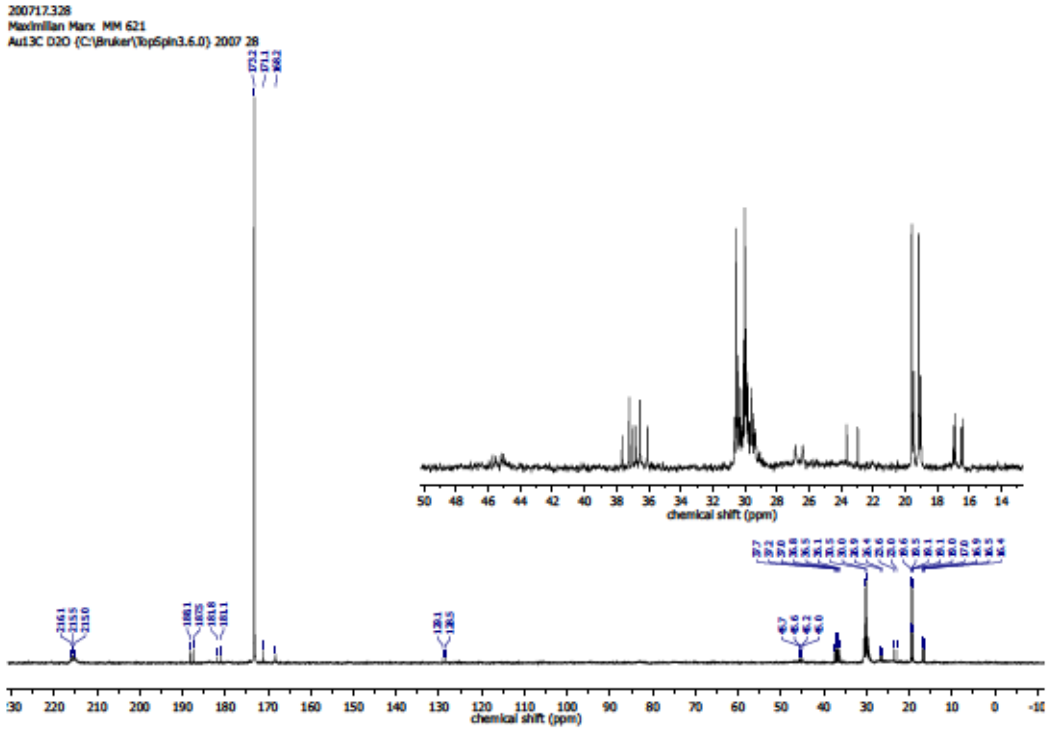

Figure S 204: $^{13}C\{^{1}H\}$ NMR spectrum (75 MHz, D_2O) of the NaOH extract of Table S 20, entry 4 – reaction of sodium $^{13}C_5$-3-methyl-2-oxobuyrate and $Cu(BF_4)_2{\cdot}6H_2O$ with CO_2/O_2 in C_6D_6/CD_3OD.

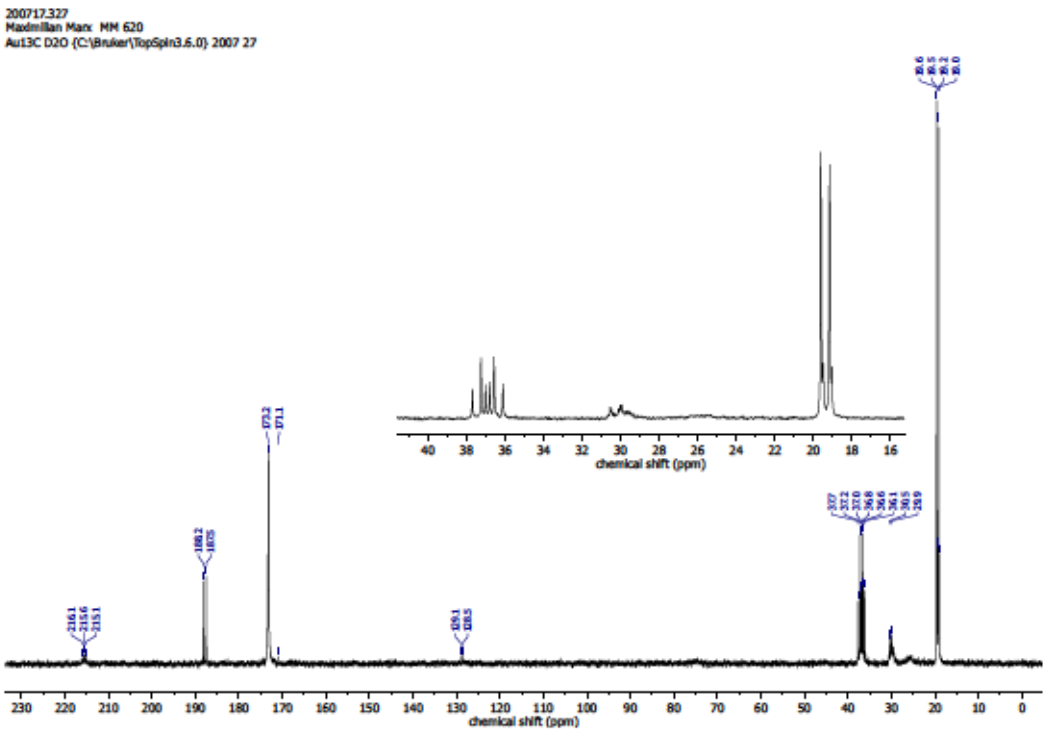

Figure S 205: $^{13}C\{^{1}H\}$ NMR spectrum (75 MHz, D_2O) of the NaOH extract of Table S 20, entry 5 – reaction of sodium $^{13}C_5$-3-methyl-2-oxobuyrate and $Cu(BF_4)_2{\cdot}6H_2O$ with CO_2/O_2 in CD_2Cl_2/CD_3OD.

4.12.7 NMR Spectra – Reactions of 139 with KC_8 and CO_2

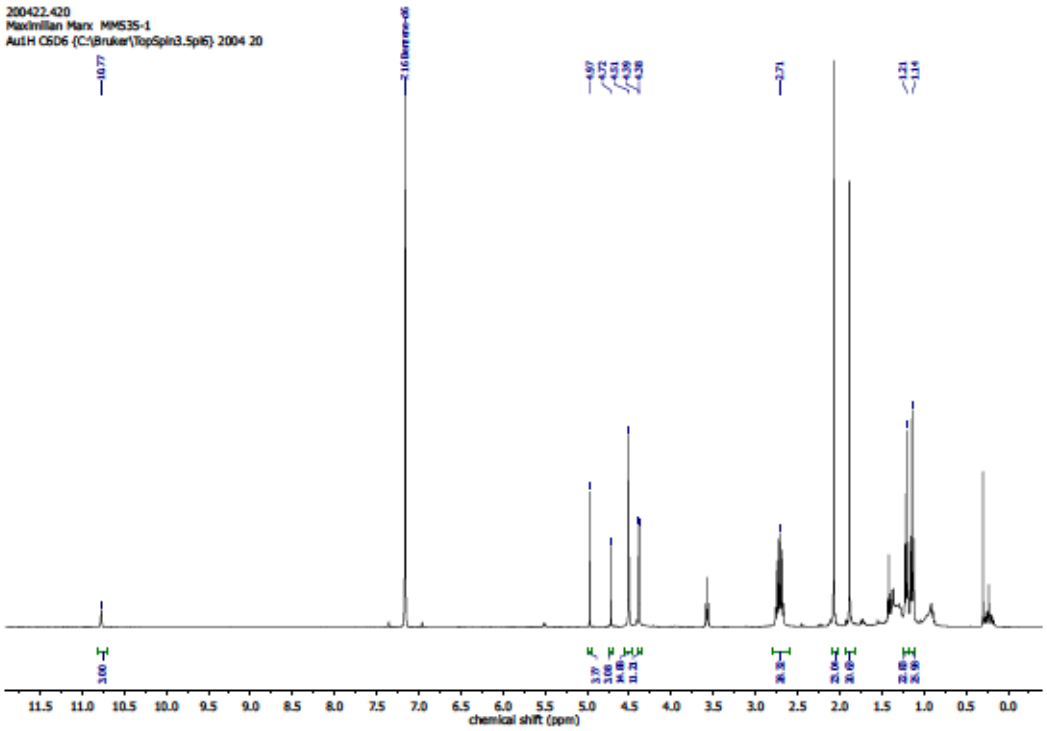

Figure S 206: ^{1}H NMR spectrum (400 MHz, C_6D_6) of the filtered THF solution of Table S 21, entry 1 – reaction of **139** and KC_8 with CO_2 in THF.

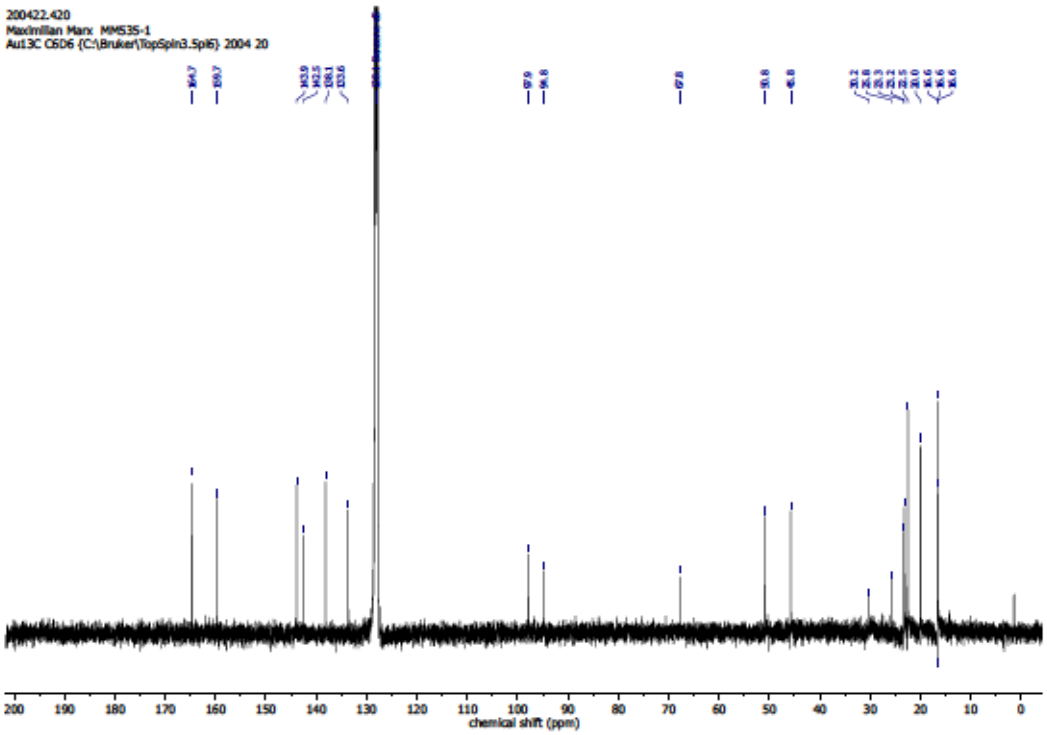

Figure S 207: $^{13}C\{^{1}H\}$ NMR spectrum (101 MHz, C_6D_6) of the filtered THF solution of Table S 21, entry 1 – reaction of **139** and KC_8 with CO_2 in THF.

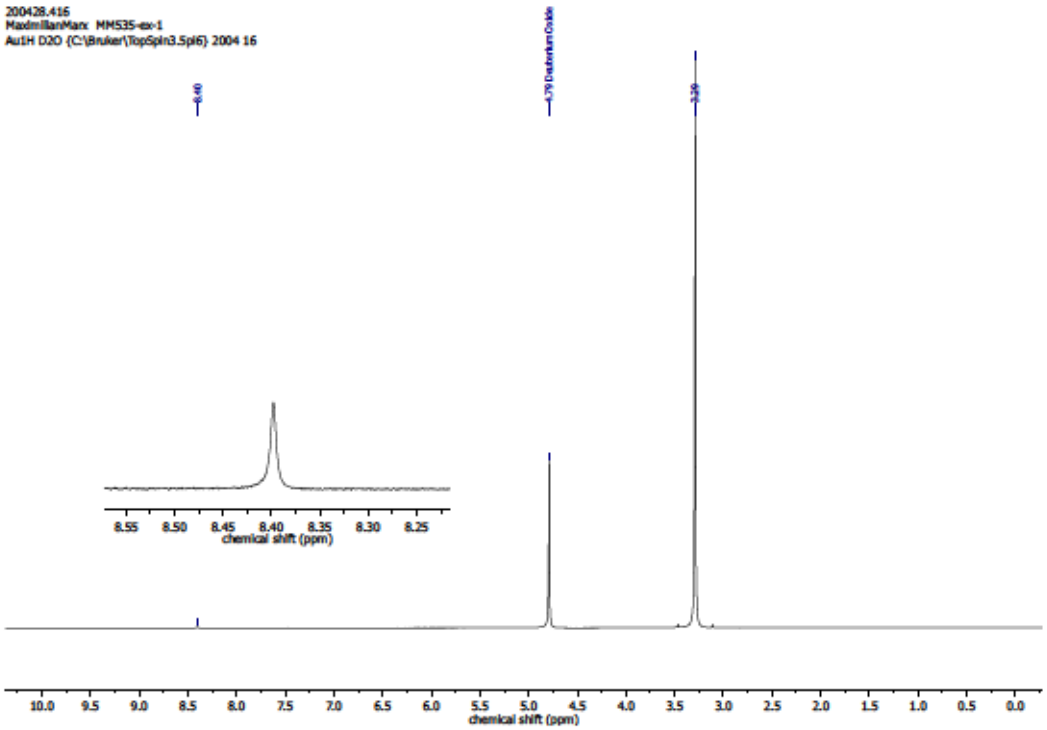

Figure S 208: ^{1}H NMR spectrum (400 MHz, D_2O) of the MeOH extract of Table S 21, entry 1 – reaction of **139** and KC_8 with CO_2 in THF.

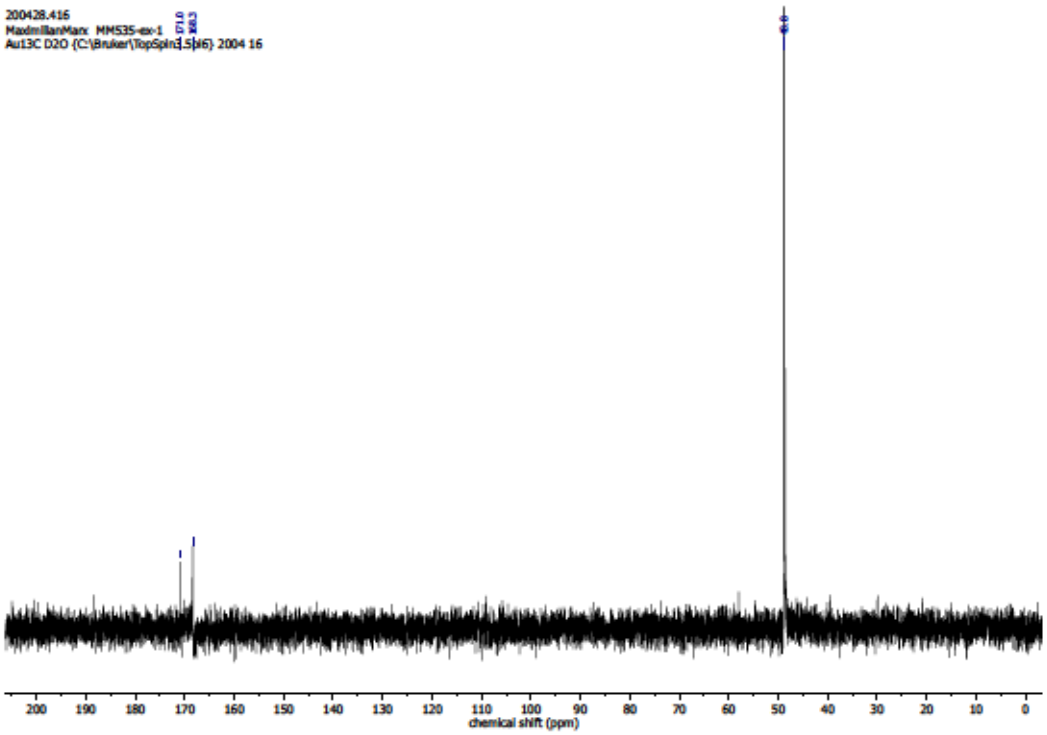

Figure S 209: $^{13}C\{^{1}H\}$ NMR spectrum (101 MHz, D_2O) of the MeOH extract of Table S 21, entry 1 – reaction of **139** and KC_8 with CO_2 in THF.

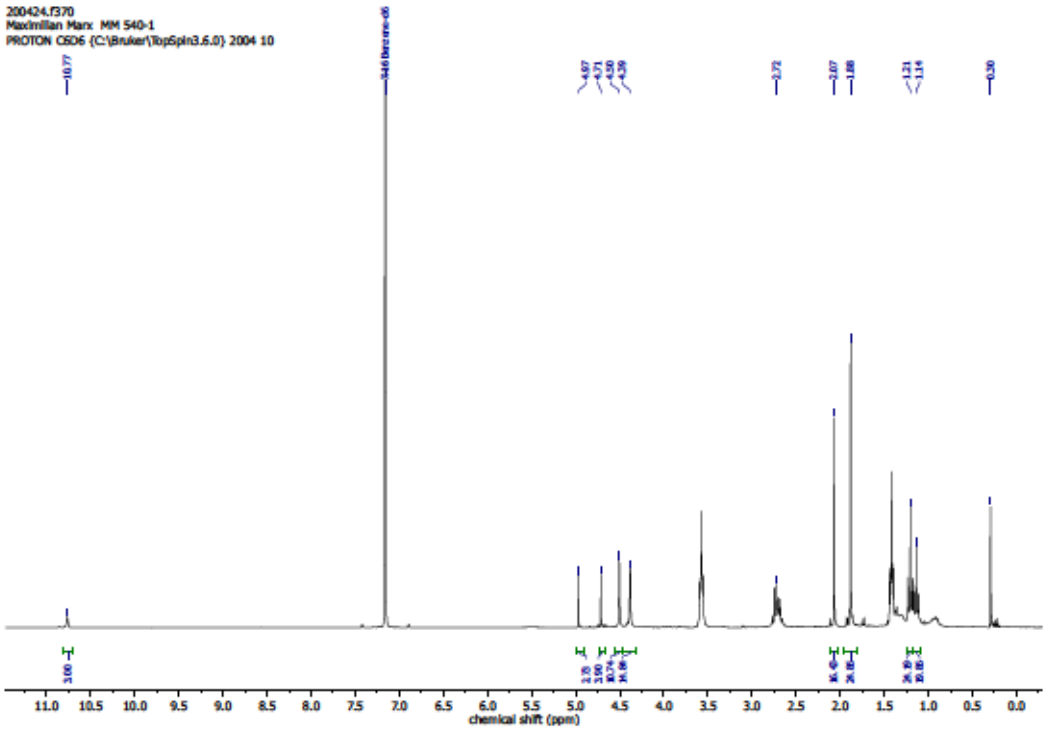

Figure S 210: ^{1}H NMR spectrum (300 MHz, C_6D_6) of the filtered THF solution of Table S 21, entry 2 – reaction of **139** and KC_8 with CO_2 in THF.

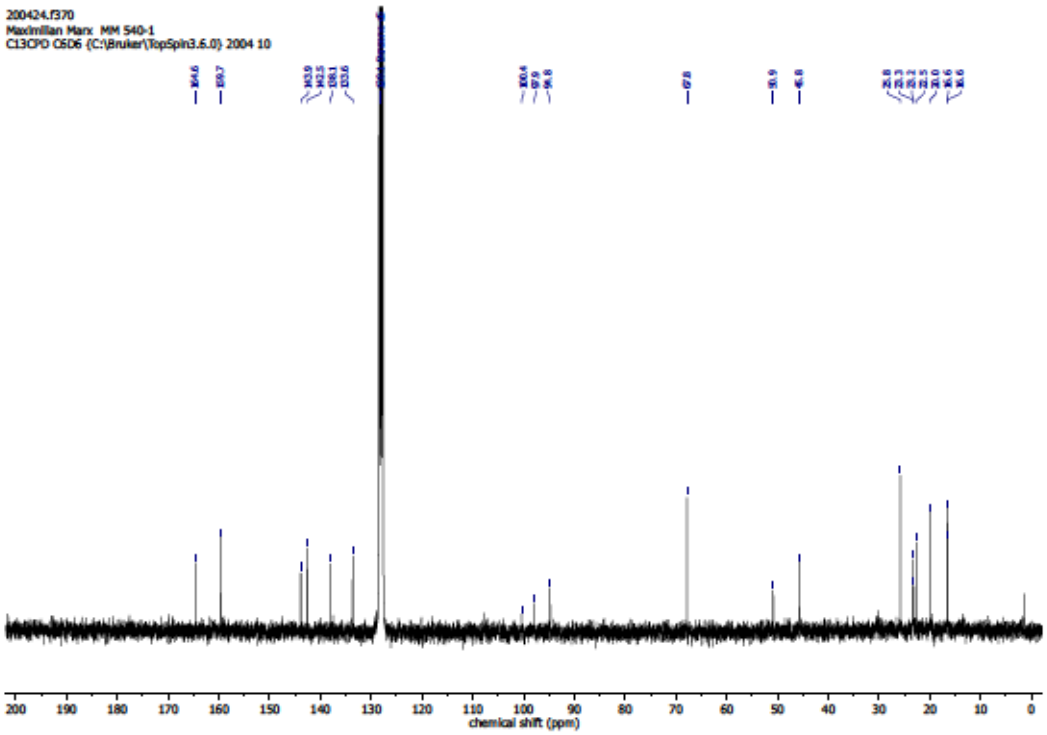

Figure S 211: $^{13}C\{^{1}H\}$ NMR spectrum (75 MHz, C_6D_6) of the filtered THF solution of Table S 21, entry 2 – reaction of **139** and KC_8 with CO_2 in THF.

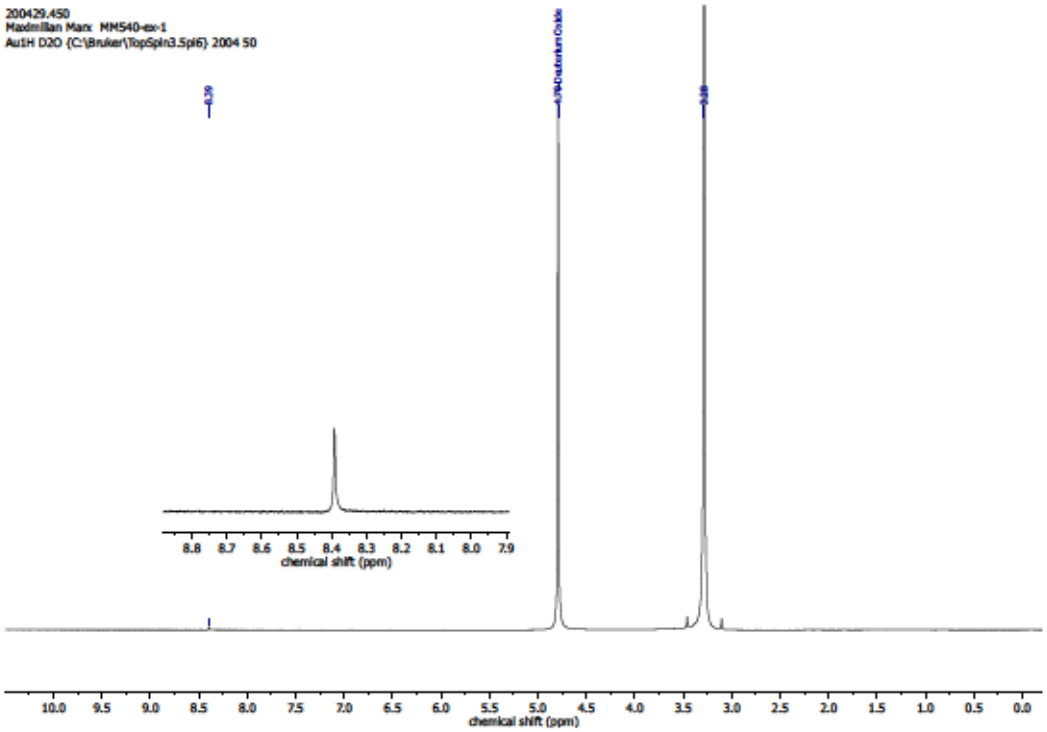

Figure S 212: ^{1}H NMR spectrum (400 MHz, D_2O) of the MeOH extract of Table S 21, entry 2 – reaction of **139** and KC_8 with CO_2 in THF.

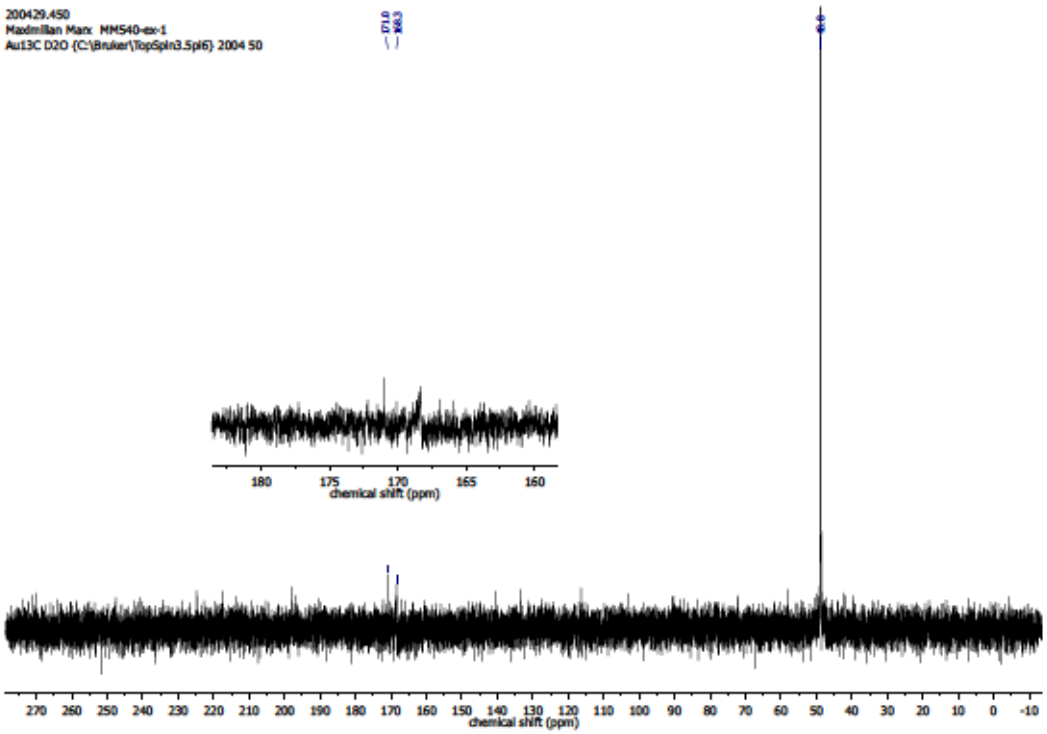

Figure S 213: $^{13}C\{^{1}H\}$ NMR spectrum (101 MHz, D_2O) of the MeOH extract of Table S 21, entry 2 – reaction of **139** and KC_8 with CO_2 in THF.

4.13 IR Spectroscopic Analysis

4.

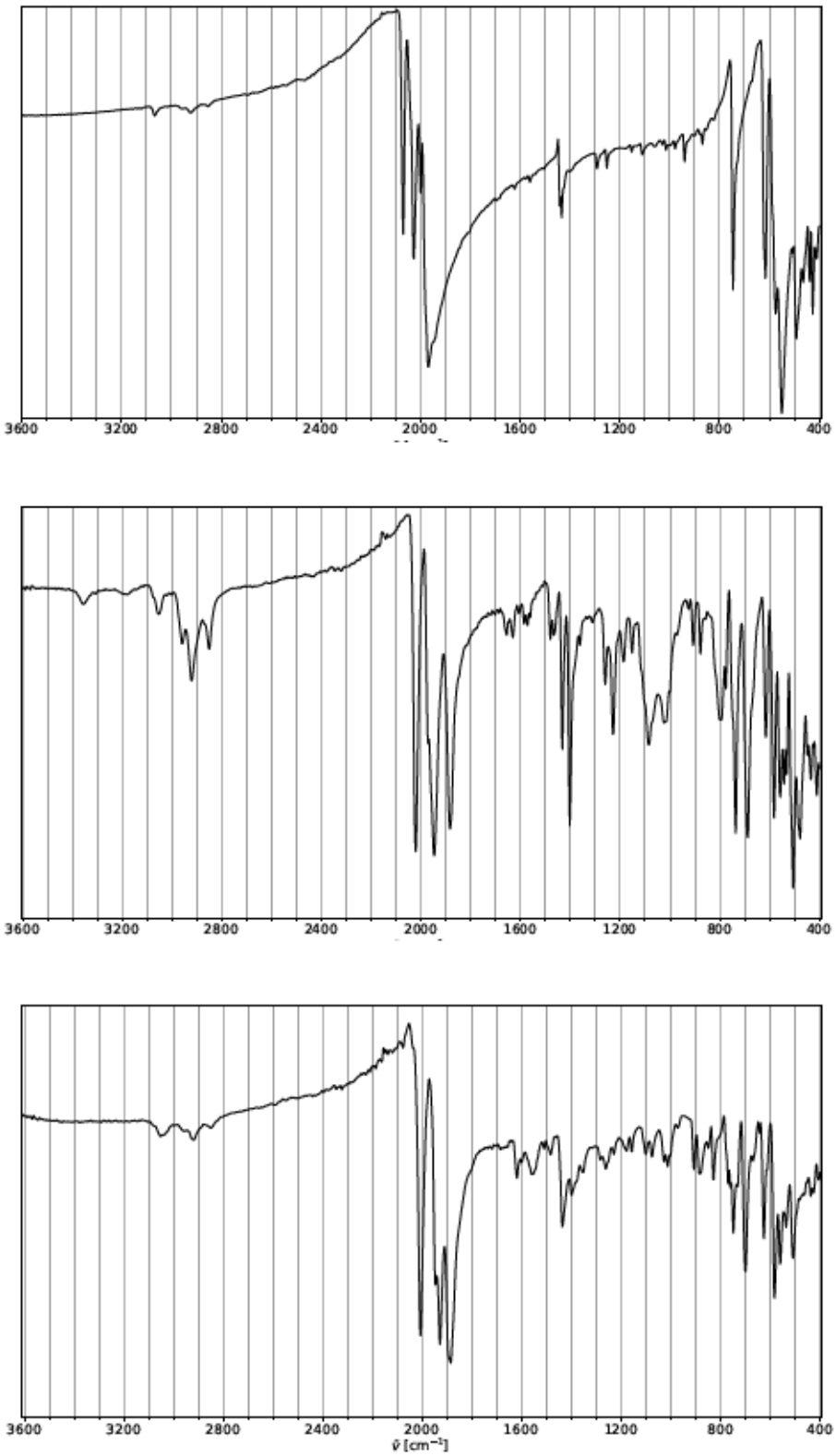

Figure S 216: FTIR (diamond ATR, neat) of **152**.

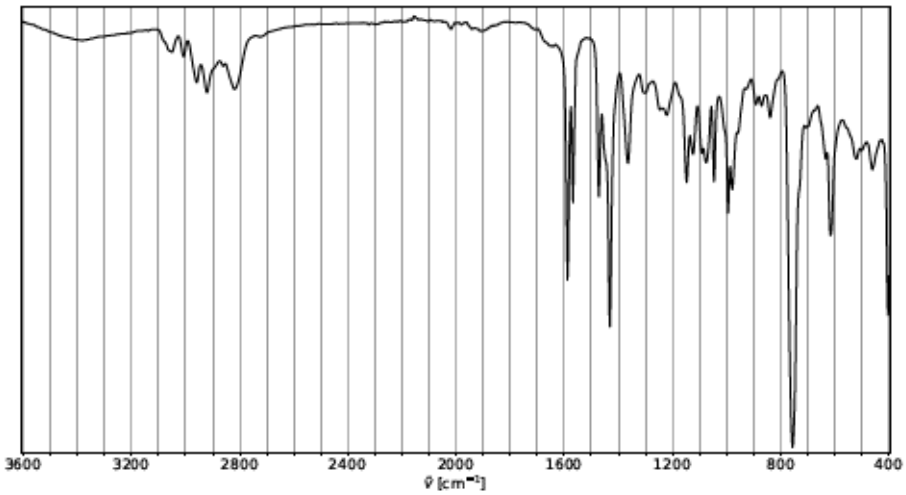

Figure S 217: FTIR (diamond ATR, neat) of **154**.

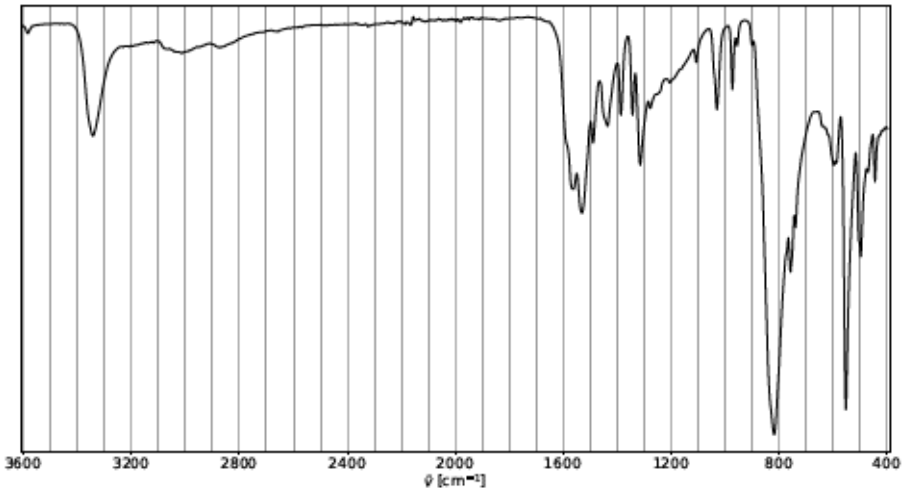

Figure S 218: FTIR (diamond ATR, neat) of **161**.

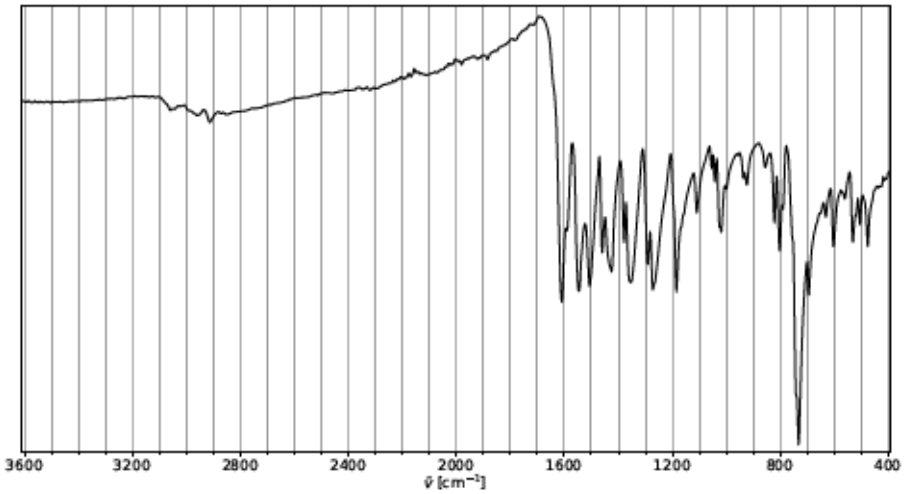

Figure S 219: FTIR (diamond ATR, neat) of **162**.

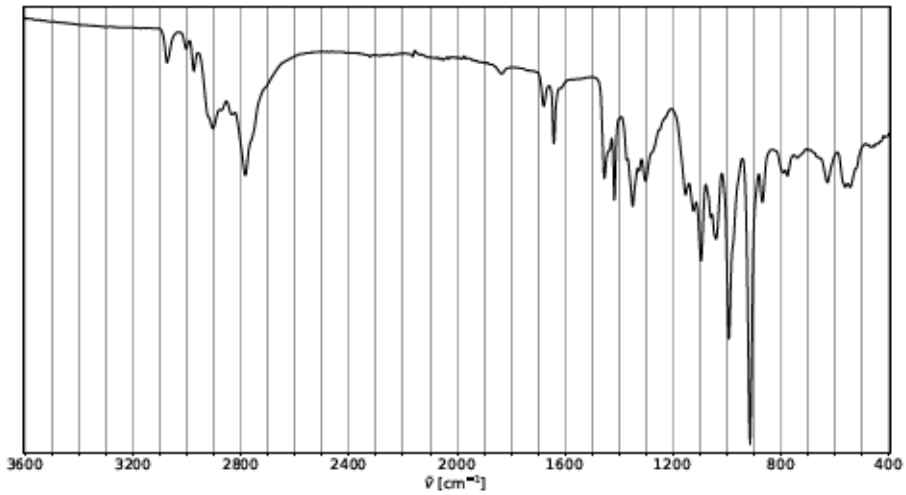

Figure S 220: FTIR (diamond ATR, neat) of **127**.

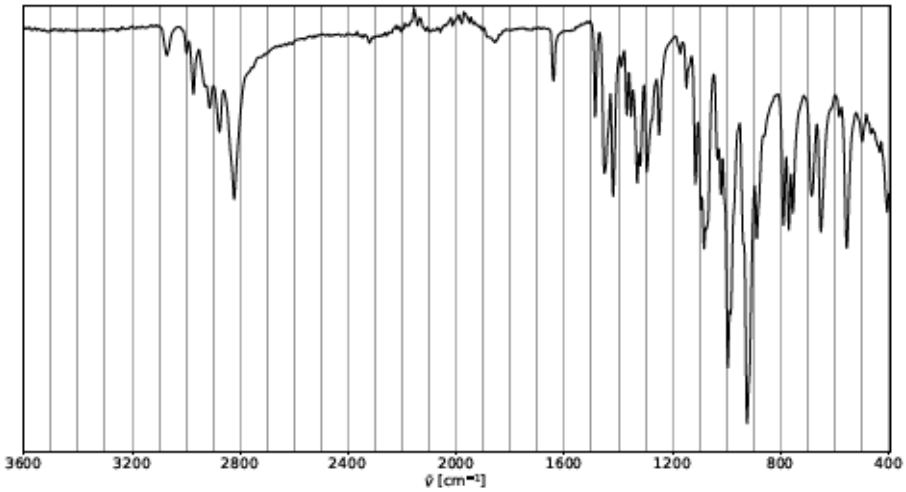

Figure S 221: FTIR (diamond ATR, neat) of **168**.

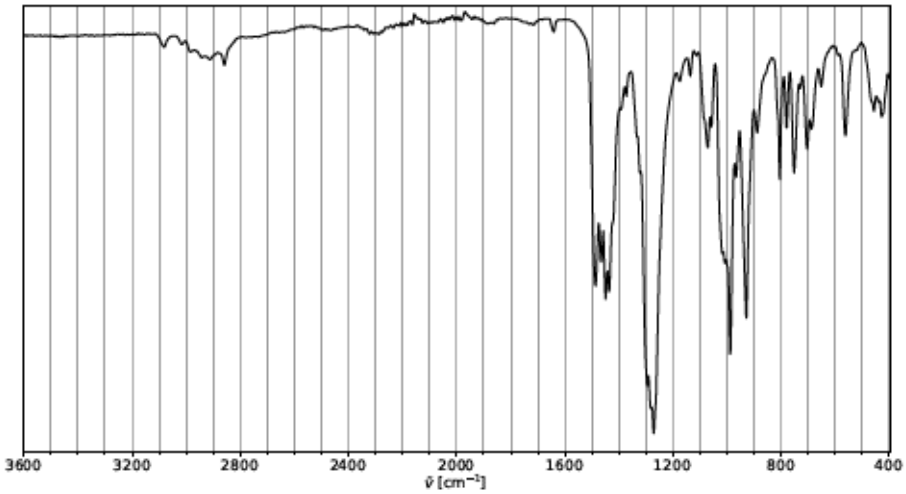

Figure S 222: FTIR (diamond ATR, neat) of **170**.

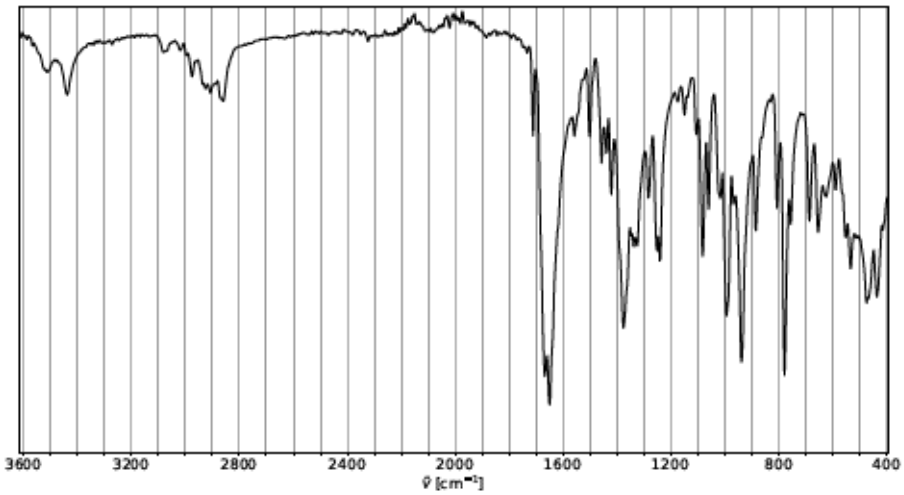

Figure S 223: FTIR (diamond ATR, neat) of **171**.

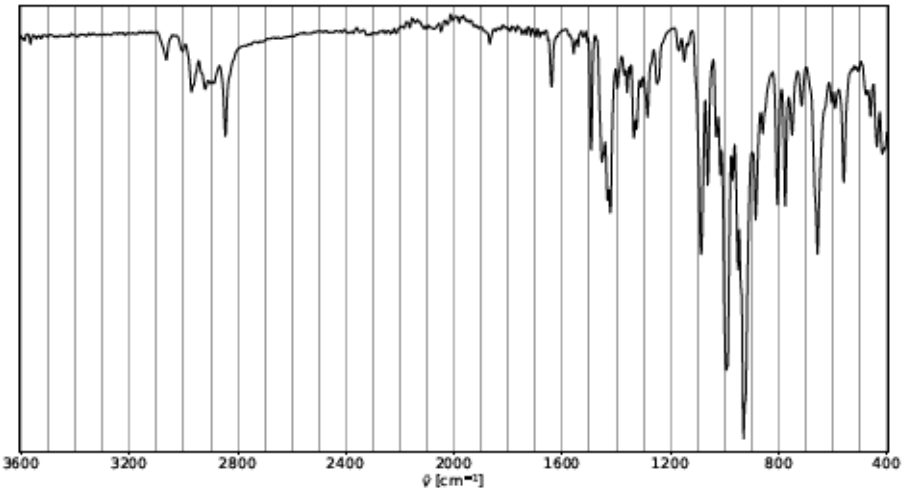

Figure S 224: FTIR (diamond ATR, neat) of **173**.

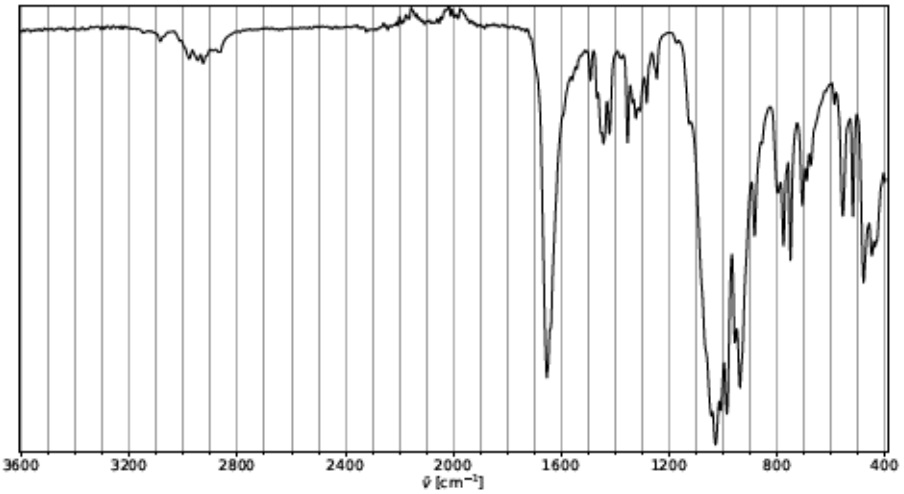

Figure S 225: FTIR (diamond ATR, neat) of **172**.

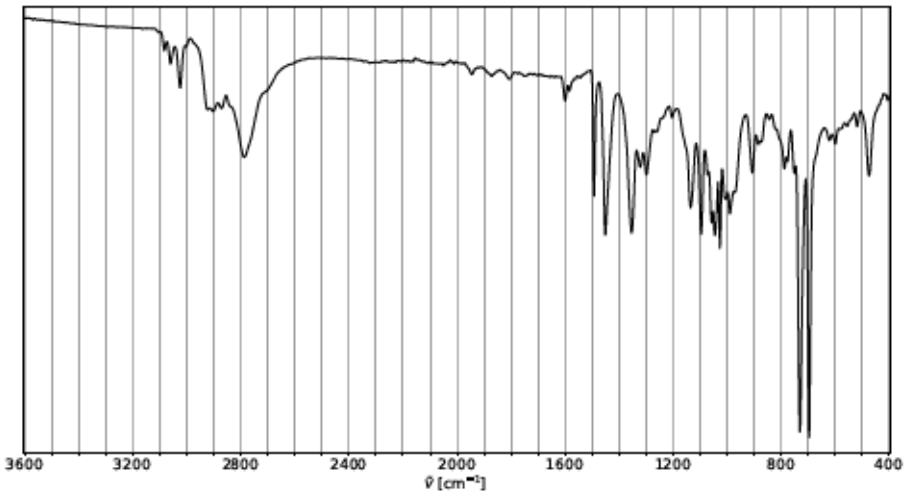

Figure S 226: FTIR (diamond ATR, neat) of **174**.

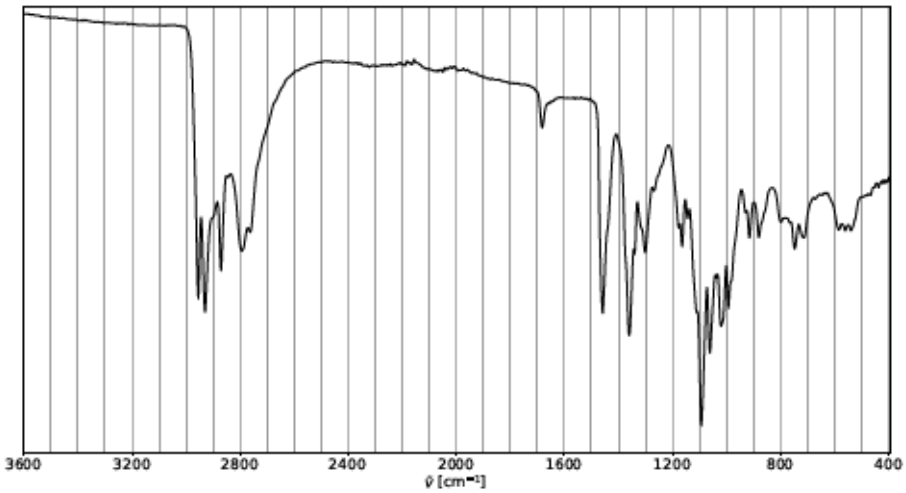

Figure S 227: FTIR (diamond ATR, neat) of **175**.

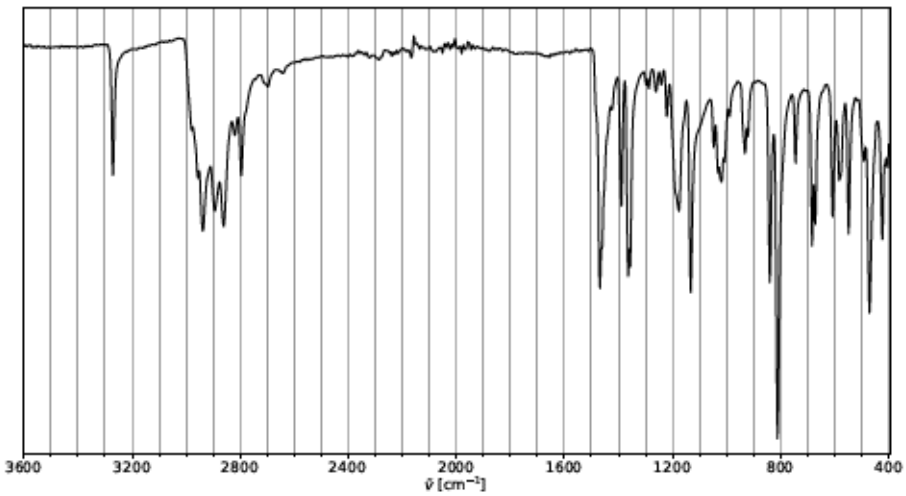

Figure S 228: FTIR (diamond ATR, neat) of **177**.

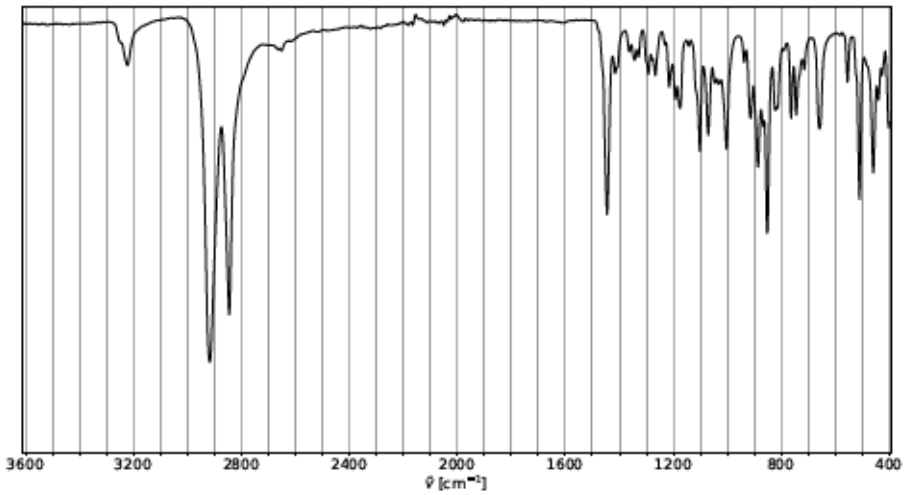

Figure S 229: FTIR (diamond ATR, neat) of **178**.

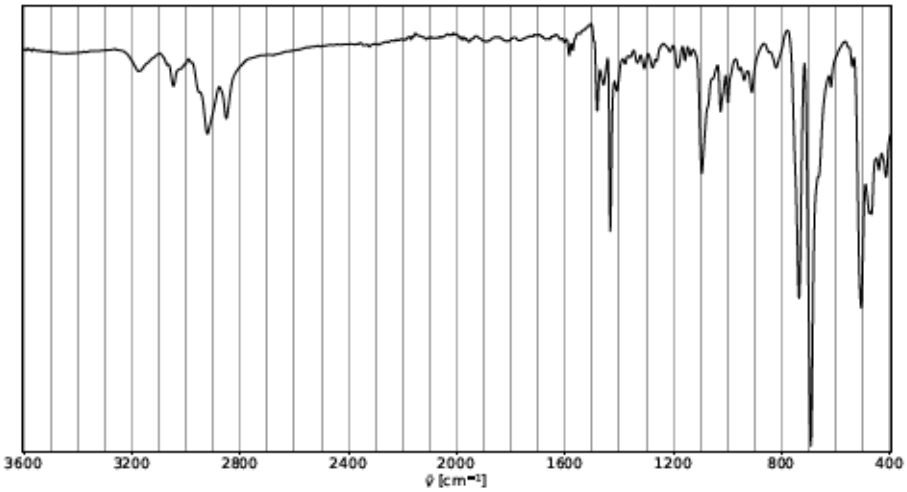

Figure S 230: FTIR (diamond ATR, neat) of **179**.

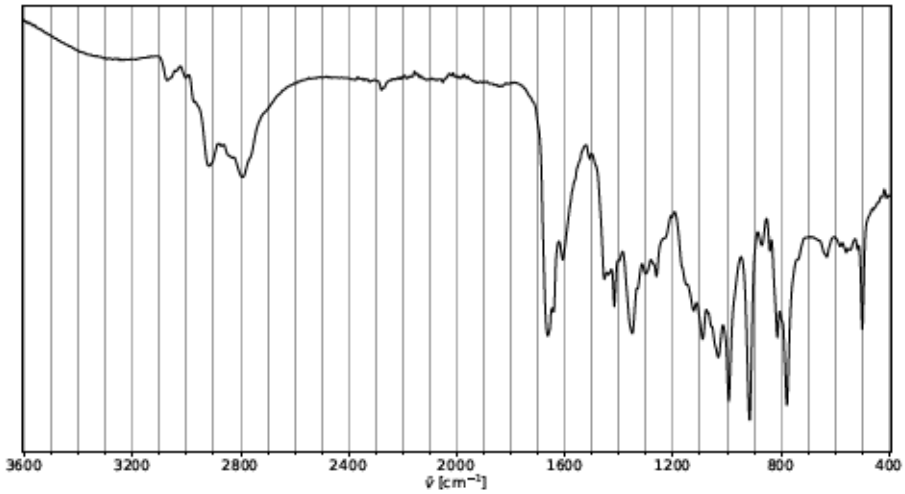

Figure S 231: FTIR (diamond ATR, neat) of **184**.

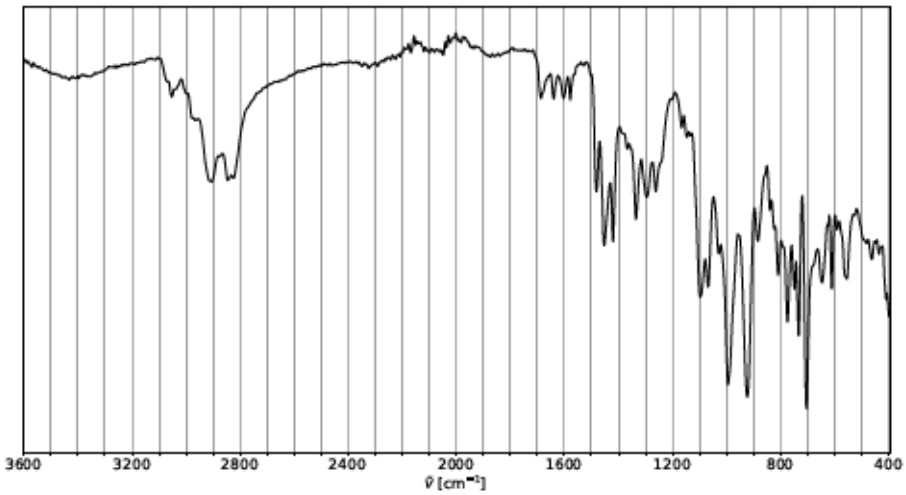

Figure S 232: FTIR (diamond ATR, neat) of **185**.

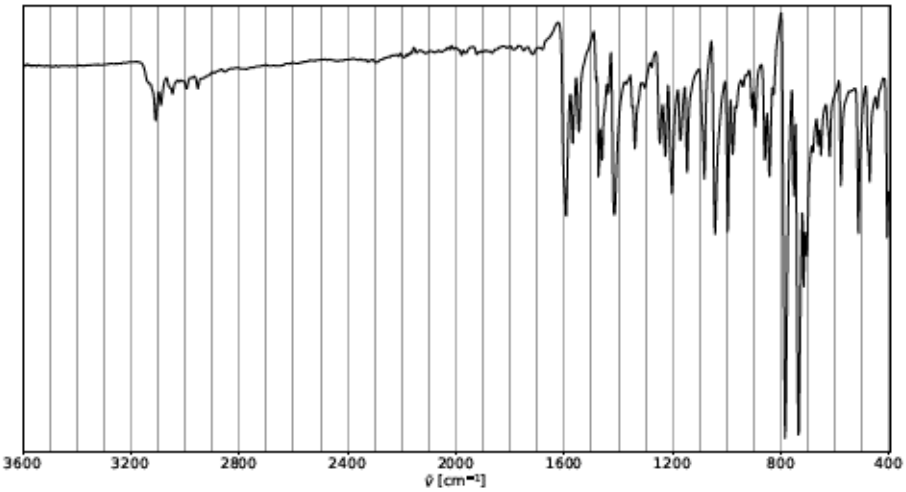

Figure S 233: FTIR (diamond ATR, neat) of ***m*-xpt**.

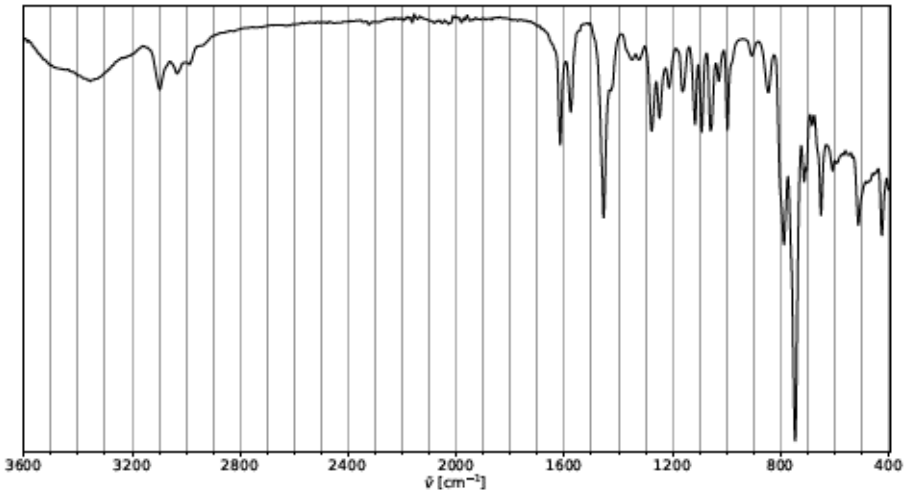

Figure S 234: FTIR (diamond ATR, neat) of **198**.

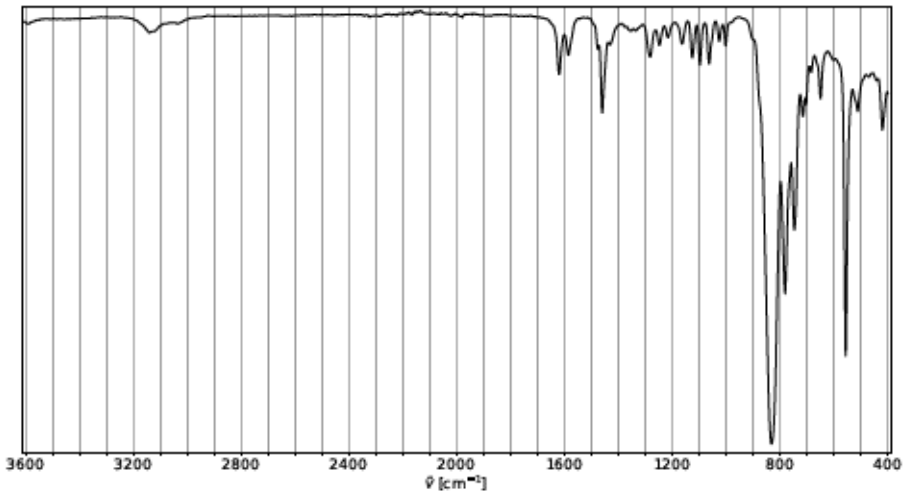

Figure S 235: FTIR (diamond ATR, neat) of **136**.

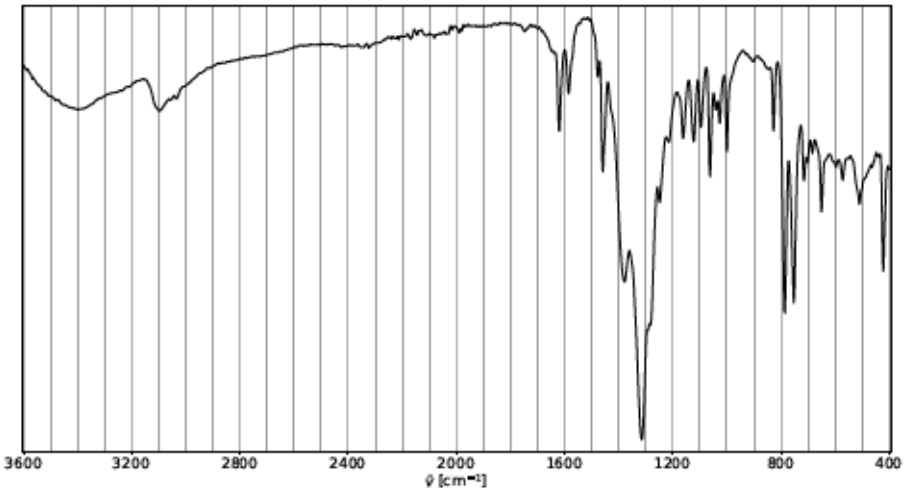

Figure S 236: FTIR (diamond ATR, neat) of **197**.

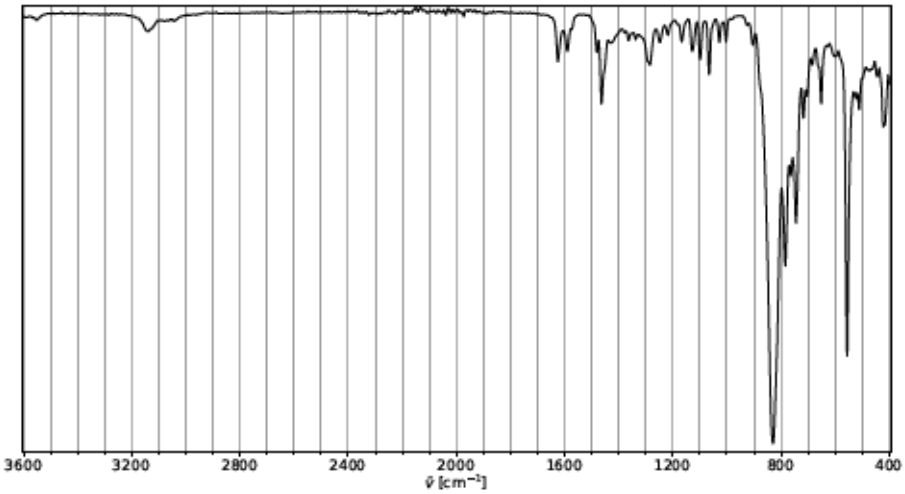

Figure S 237: FTIR (diamond ATR, neat) of **135**.

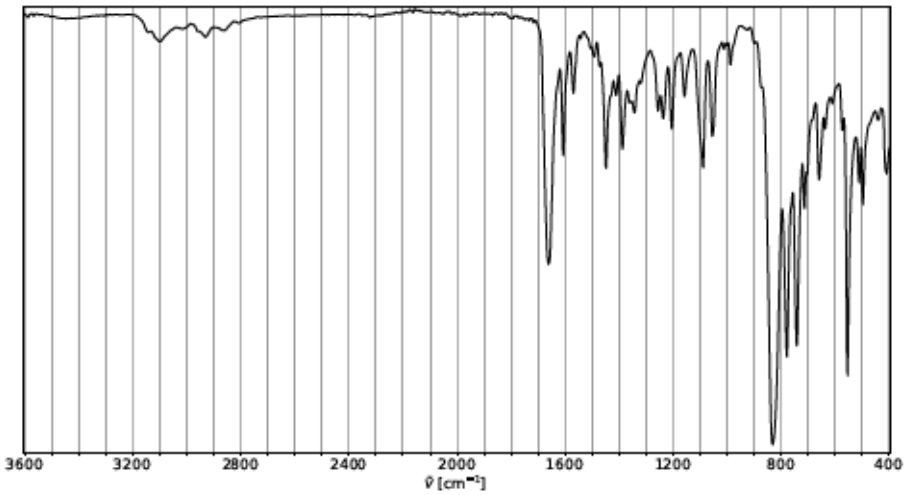

Figure S 238: FTIR (diamond ATR, neat) of **187**.

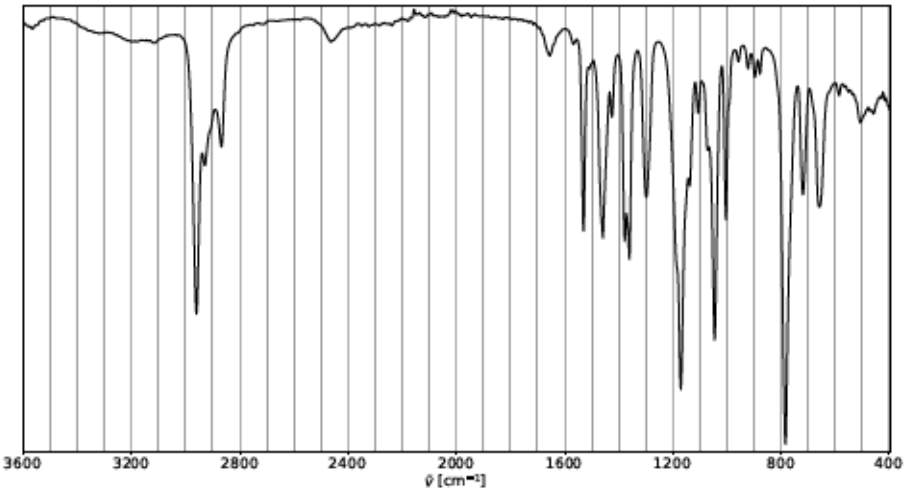

Figure S 239: FTIR (diamond ATR, neat) of **190**.

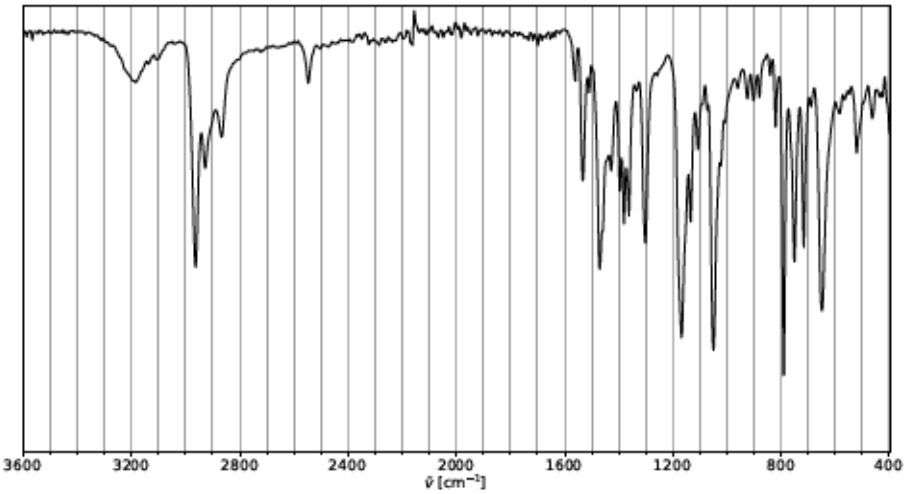

Figure S 240: FTIR (diamond ATR, neat) of **191**.

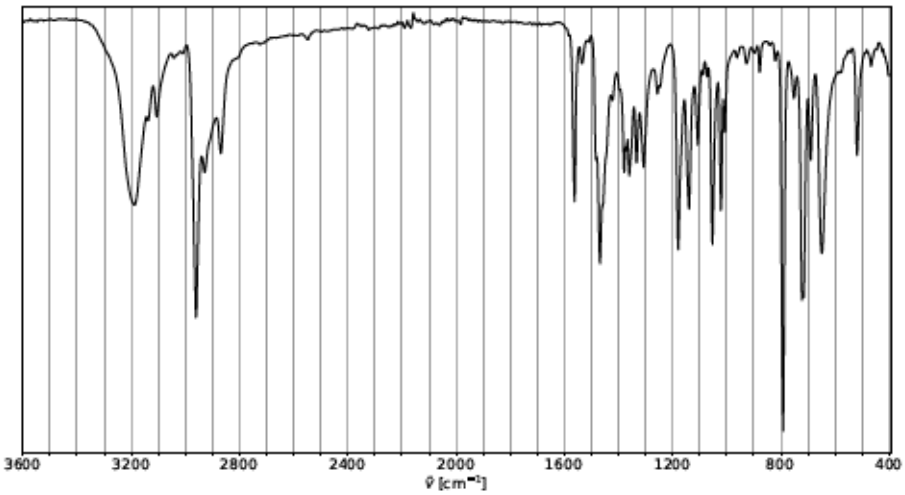

Figure S 241: FTIR (diamond ATR, neat) of **192**.

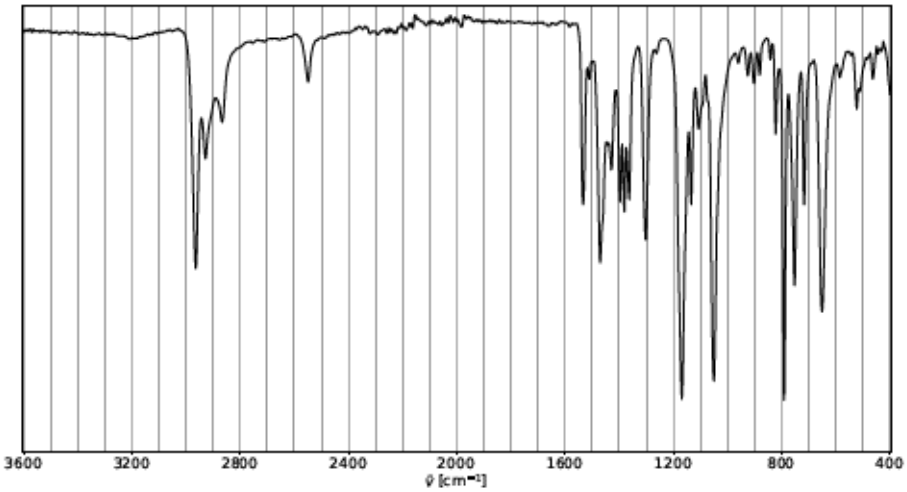

Figure S 242: FTIR (diamond ATR, neat) of **194**.

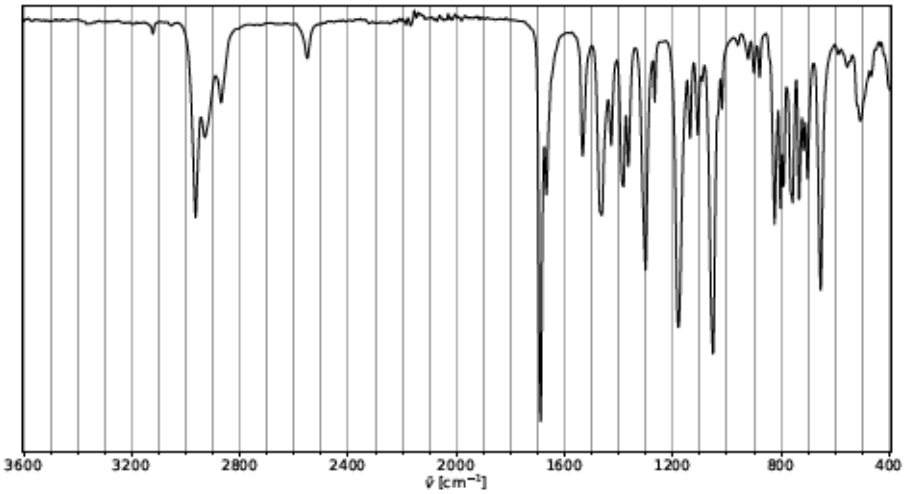

Figure S 243: FTIR (diamond ATR, neat) of **129**.

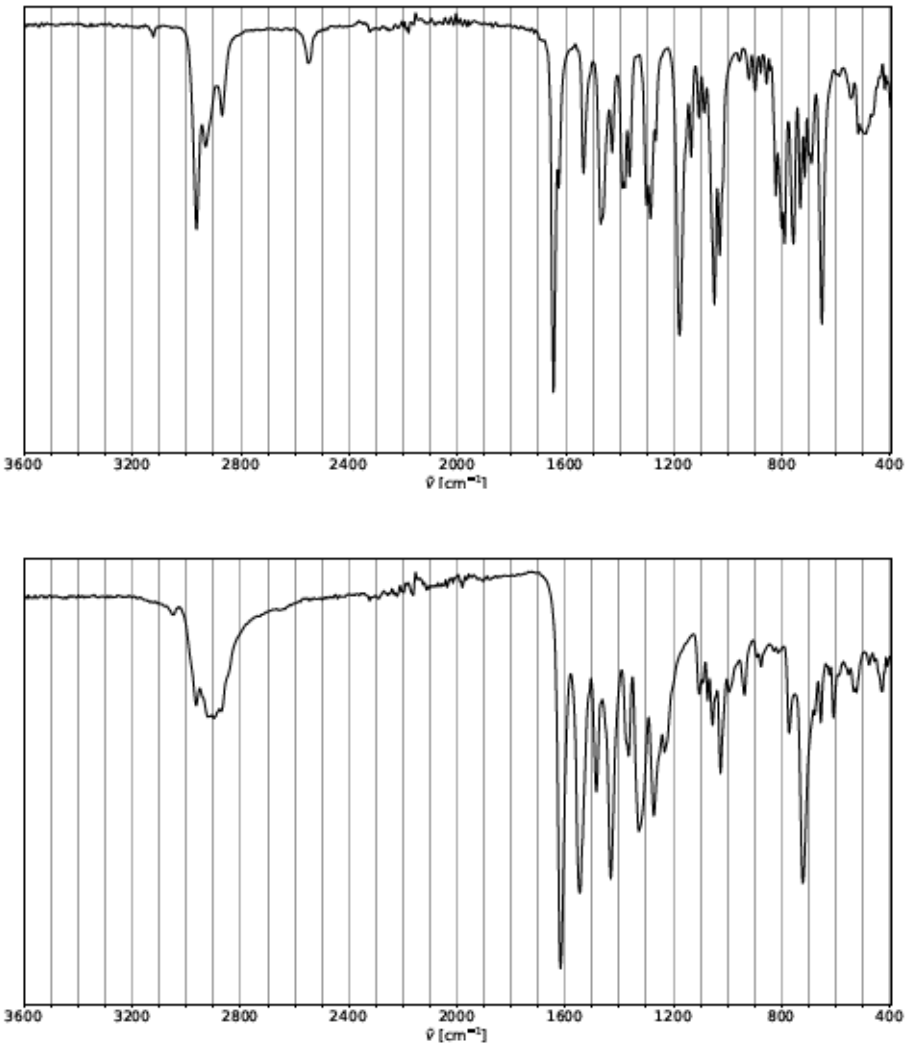

Figure S 245: FTIR (diamond ATR, neat) of **142**.

4. **es**

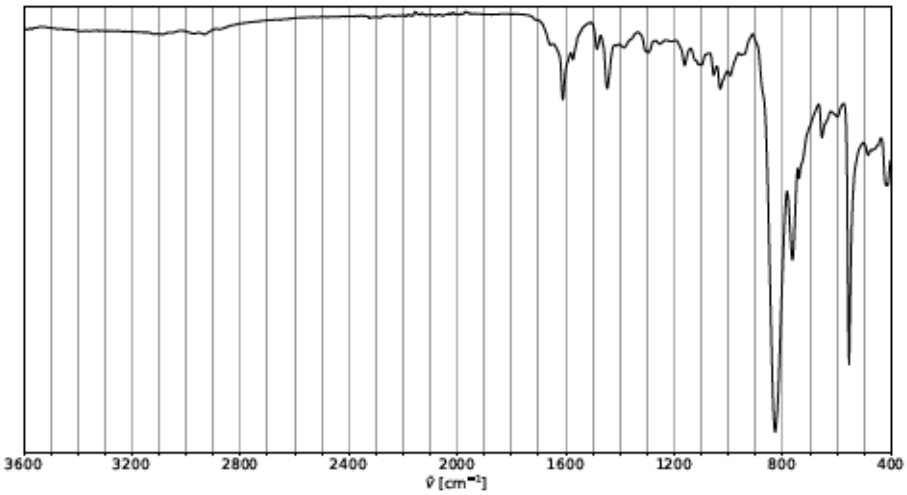

Figure S 246: FTIR (diamond ATR, neat) of of the product obtained after evaporation of *in situ* formed **155** in air (procedure 4.5.3).

4.

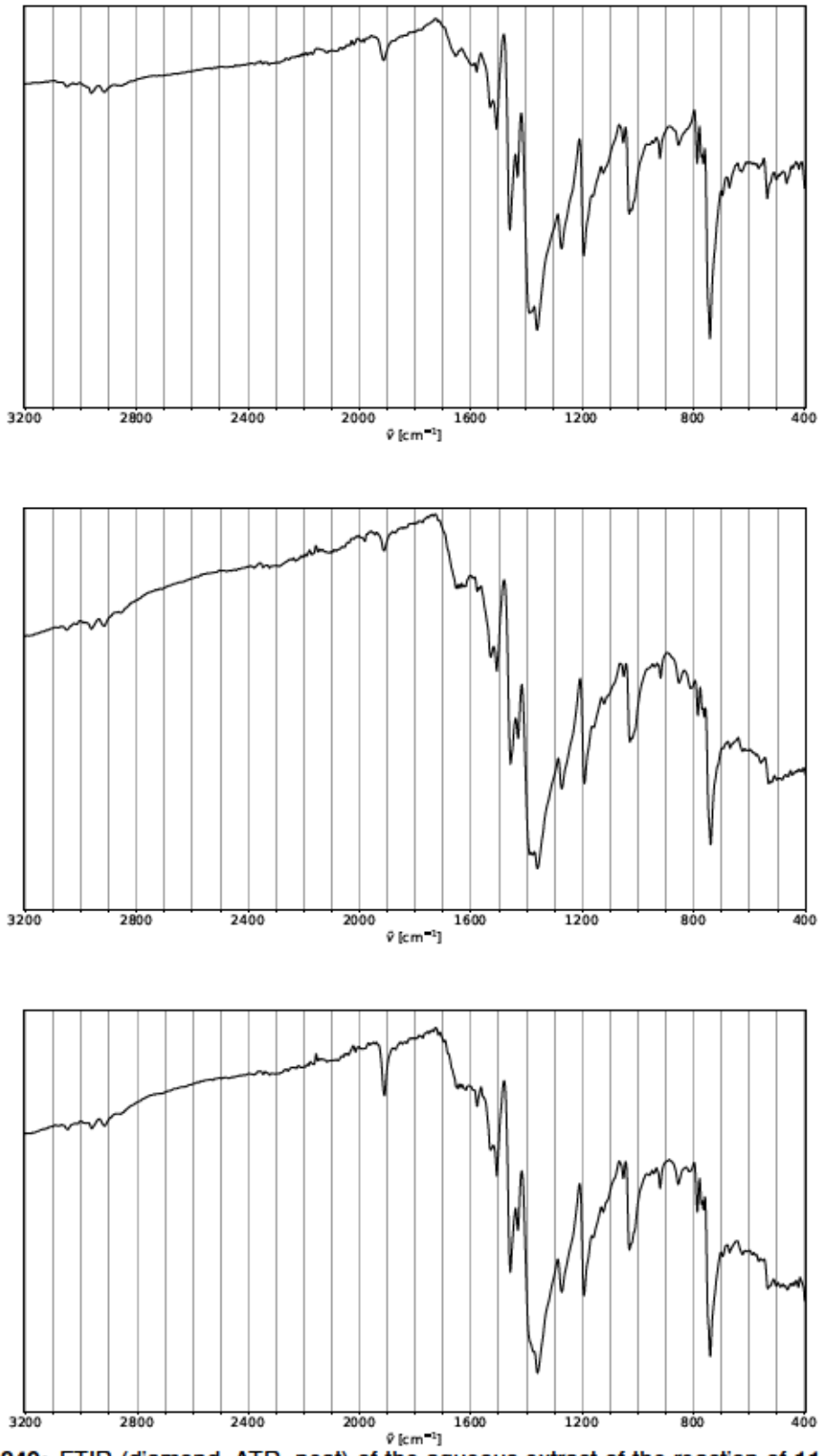

Figure S 249: FTIR (diamond, ATR, neat) of the aqueous extract of the reaction of **118** with K and subsequent CO_2 treatment in toluene (Table S 12, entry 7).

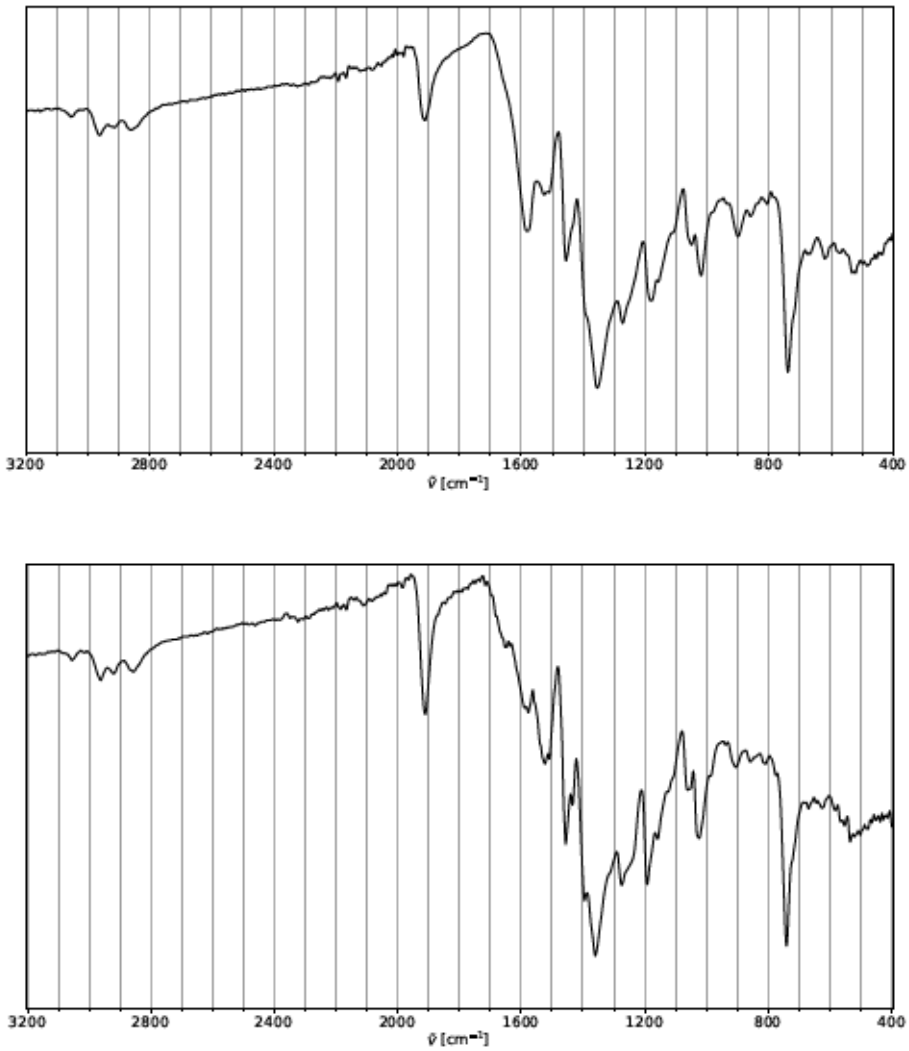

Figure S 251: FTIR (diamond, ATR, neat) of the reaction of **118** with K and subsequent CO_2 treatment in THF (Table S 12, entry 9).

4.1

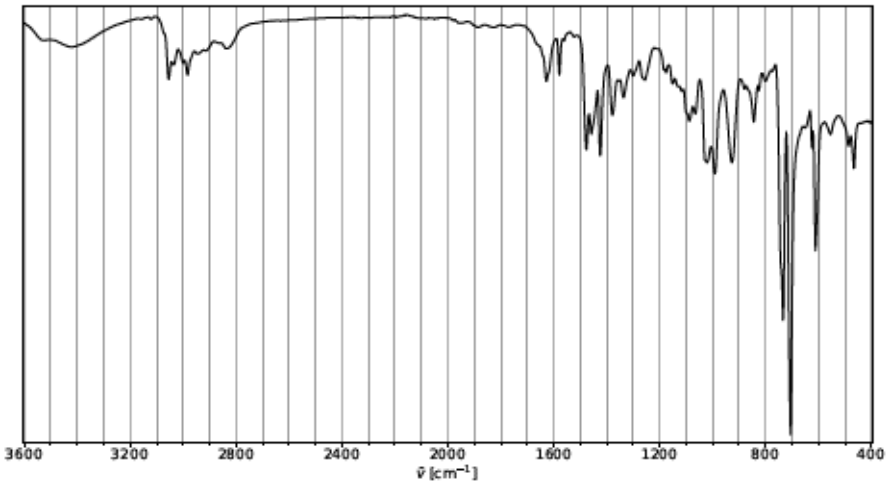

Figure S 252: FTIR (diamond, ATR, neat) of the product obtained by CO_2 treatment (bubbling) o

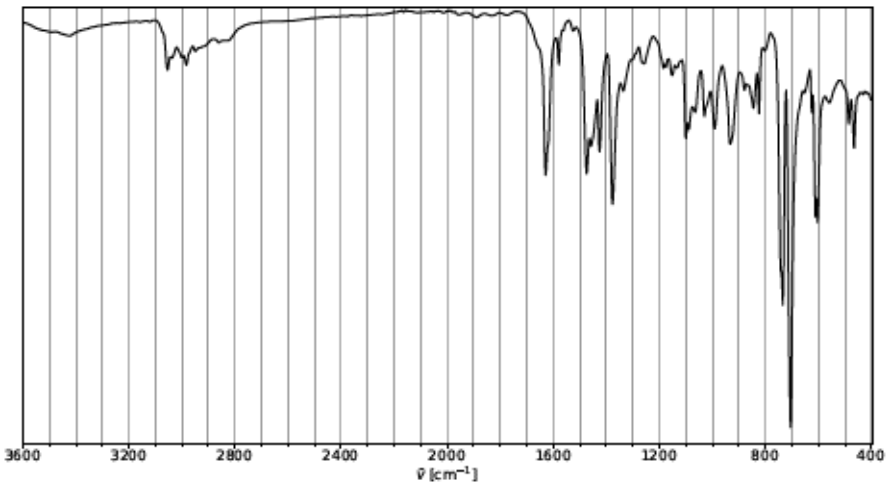

Figure S 253: FTIR (diamond, ATR, neat) of the product obtained by CO_2 treatment (bubbling) o

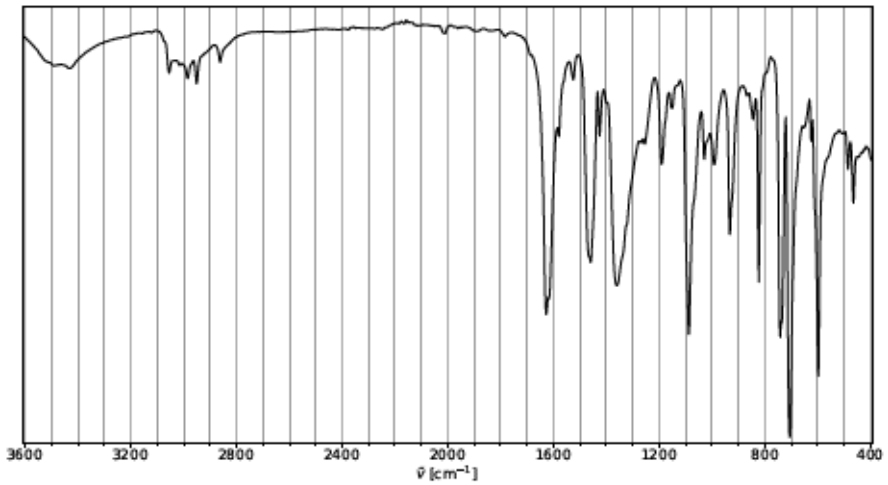

Figure S 254: FTIR (diamond, ATR, neat) of the product obtained by CO_2 treatment (bubbling) of **127**, CuI and $NaBPh_4$ in MeOH (Table S 13, entry 3).

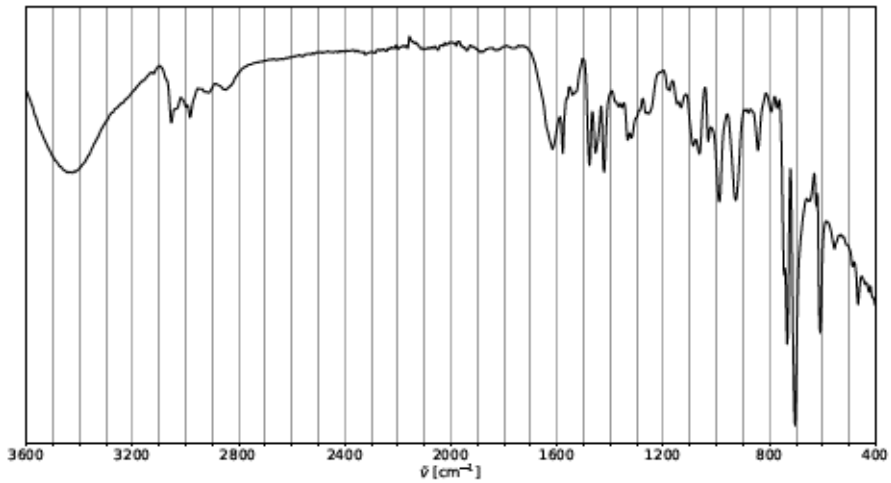

Figure S 255: FTIR (diamond, ATR, neat) of the product obtained by CO_2 treatment (bubbling) o

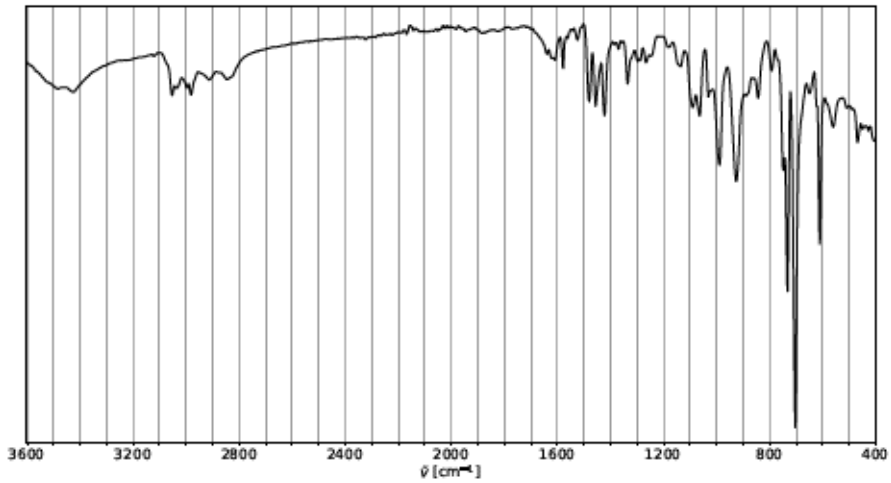

Figure S 256: FTIR (diamond, ATR, neat) of the product obtained by CO_2 treatment (bubbling) of **127**, CuI and $NaBPh_4$ in MeOH (Table S 13, entry 5).

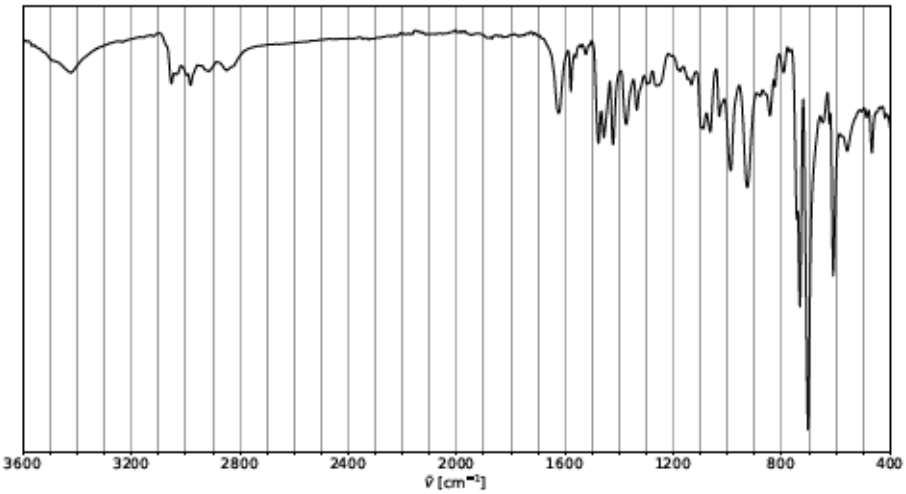

Figure S 257: FTIR (diamond, ATR, neat) of the product obtained by CO_2 treatment (bubbling) of **127**, CuI and $NaBPh_4$ in MeOH (Table S 13, entry 6).

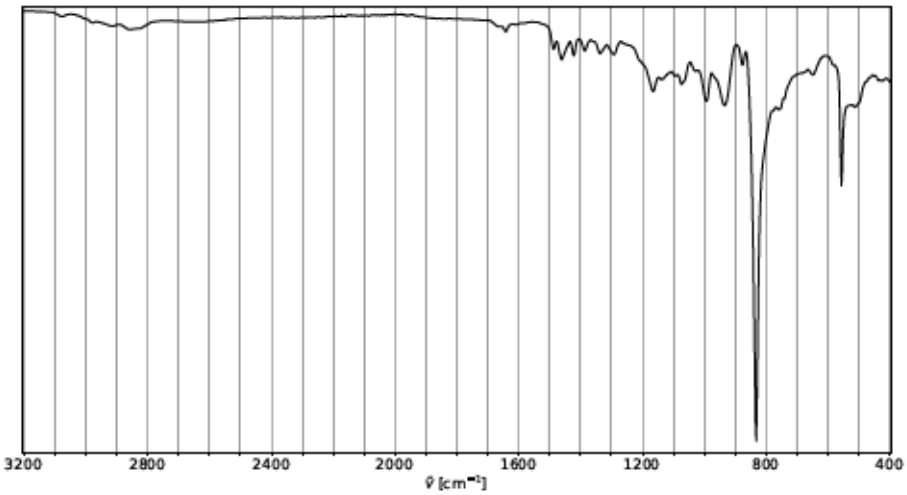

Figure S 258: FTIR (diamond, ATR, neat) of the product obtained by CO_2 treatment (bubbling)

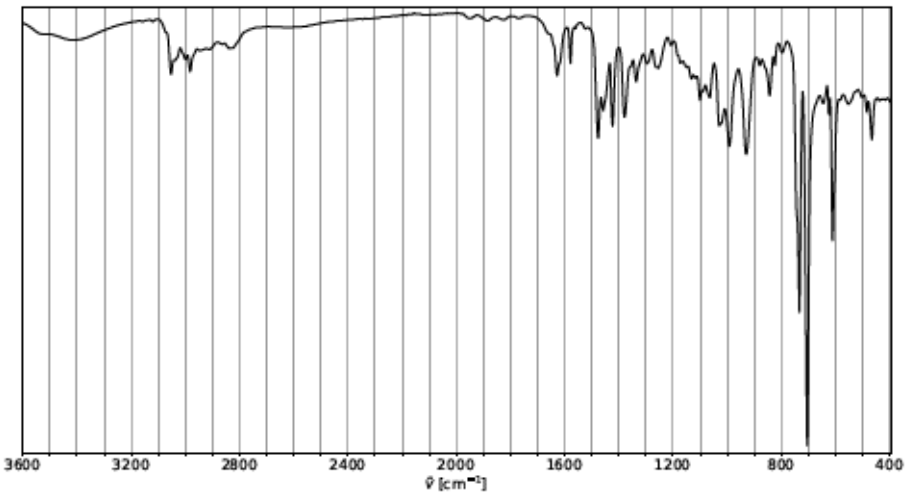

Figure S 259: FTIR (diamond, ATR, neat) of the product obtained by CO_2 treatment (bubbling)

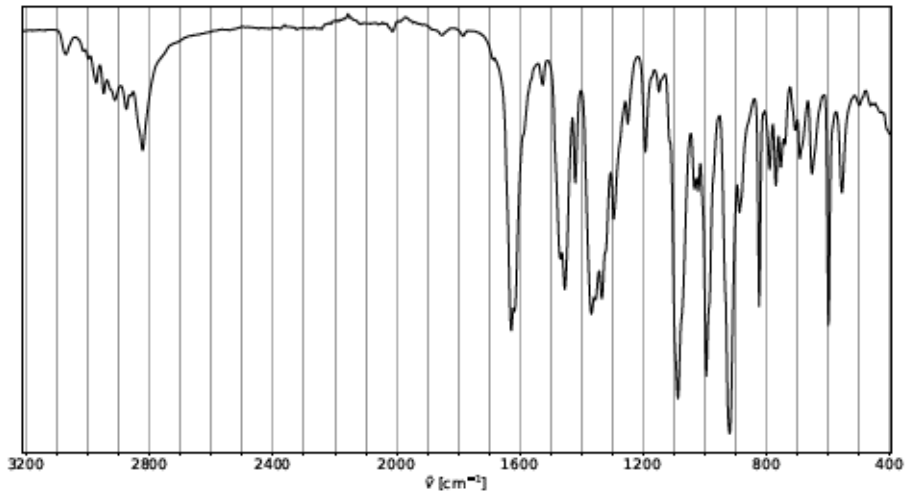

Figure S 260: FTIR (diamond, ATR, neat) of the product obtained by $CsHCO_3$ treatment of **127**, CuI and $NaBPh_4$ in MeOH (Table S 14, entry 2).

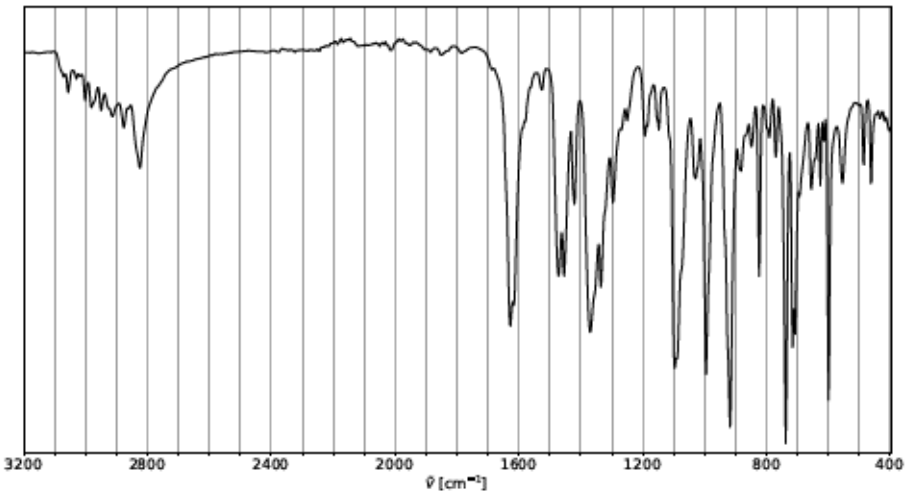

Figure S 261: FTIR (diamond, ATR, neat) of the product obtained $CsHCO_3$ treatment of **127**,

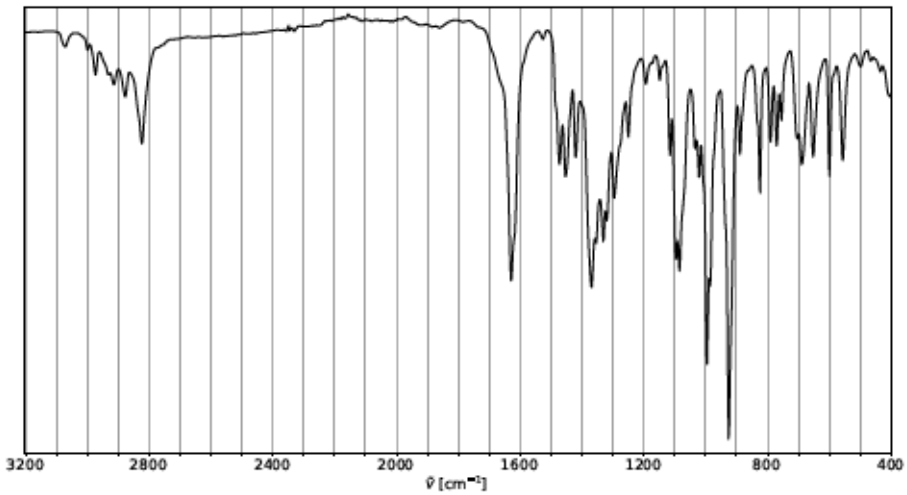

Figure S 262: FTIR (diamond, ATR, neat) of the product obtained by $CsHCO_3$ treatment of **127**,

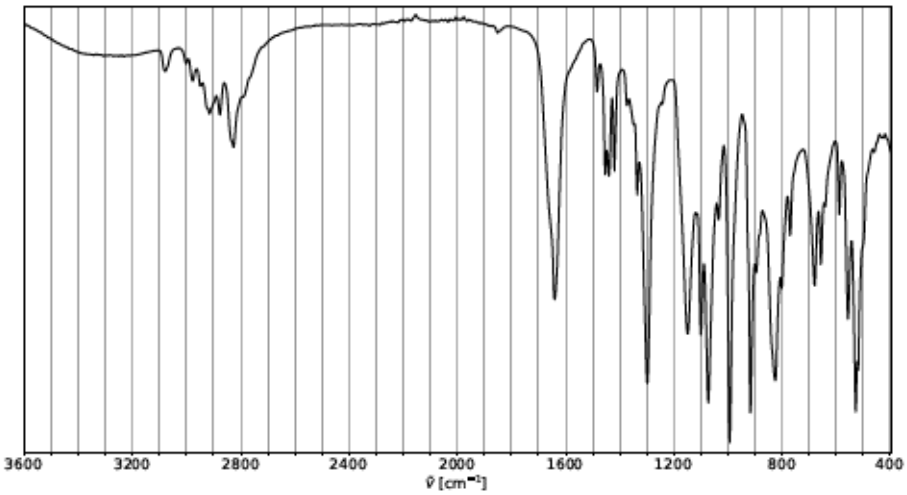

Figure S 263: FTIR (diamond, ATR, neat) of the product obtained by $CsHCO_3$ treatment of **127**, CuI and $NaPF_6$ in MeOH (Table S 14, entry 5).

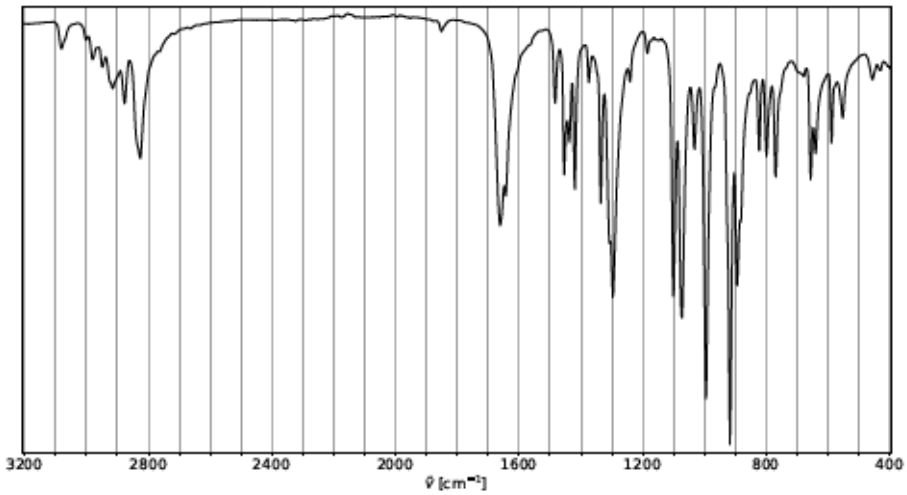

Figure S 264: FTIR (diamond, ATR, neat) of the product obtained by $CsHCO_3$ treatment of **127**

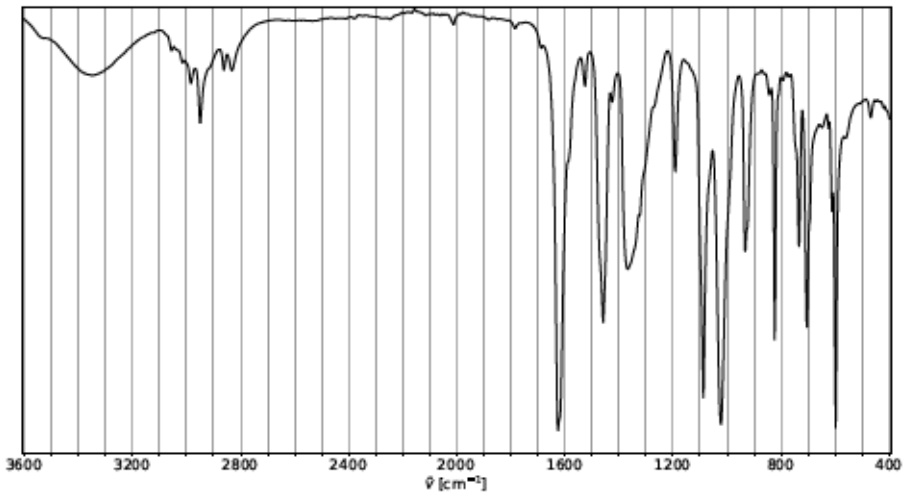

Figure S 265: FTIR (diamond, ATR, neat) of the product obtained $NaHCO_3$ treatment of **127**,

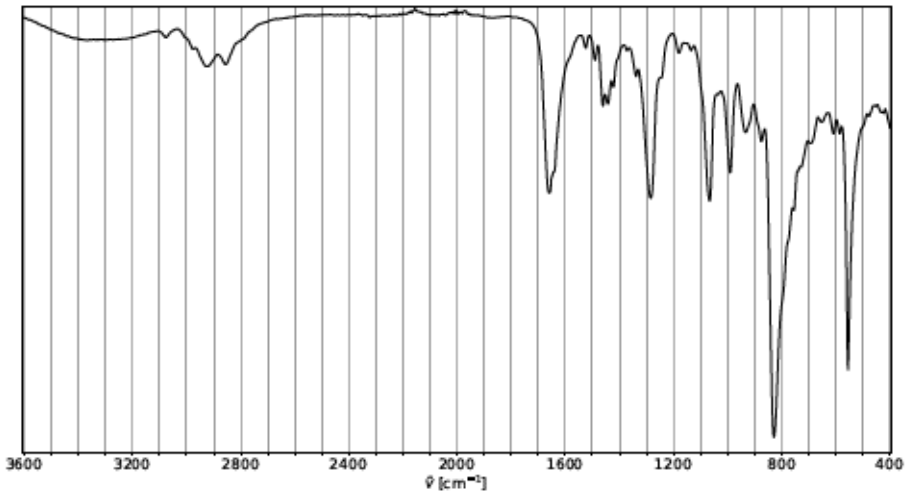

Figure S 266: FTIR (diamond, ATR, neat) of the product obtained by $CsHCO_3$ treatment of **127** and $[Cu(MeCN)_4]PF_6$ in MeOH (Table S 14, entry 8).

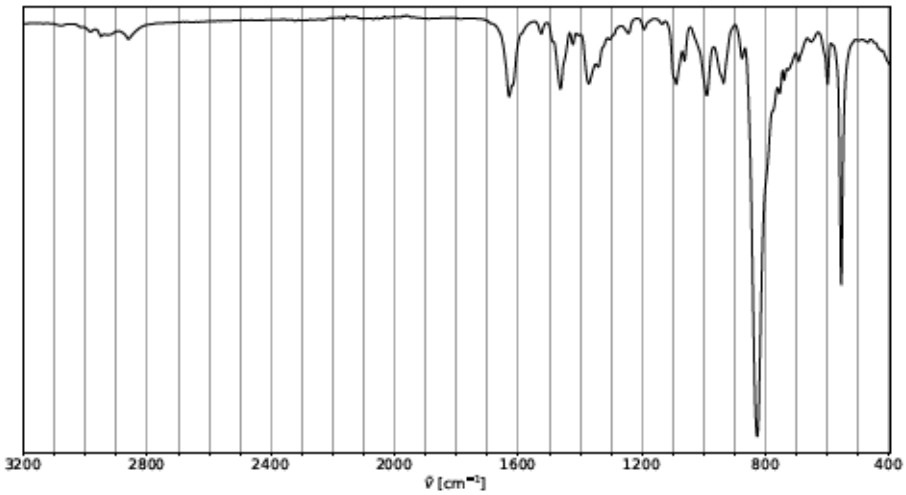

Figure S 267: FTIR (diamond, ATR, neat) of the product obtained by $NaHCO_3$ treatment of **127**

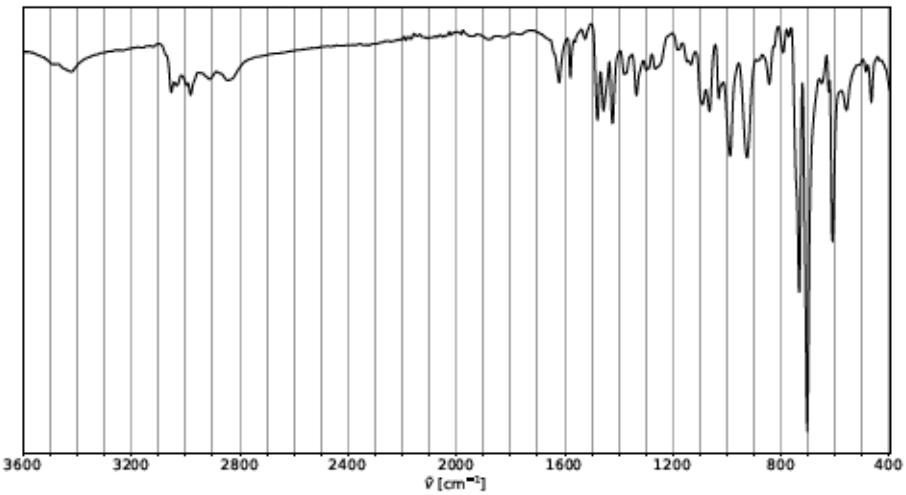

Figure S 268: FTIR (diamond, ATR, neat) of the product obtained by CO_2 treatment of **127**, CuI

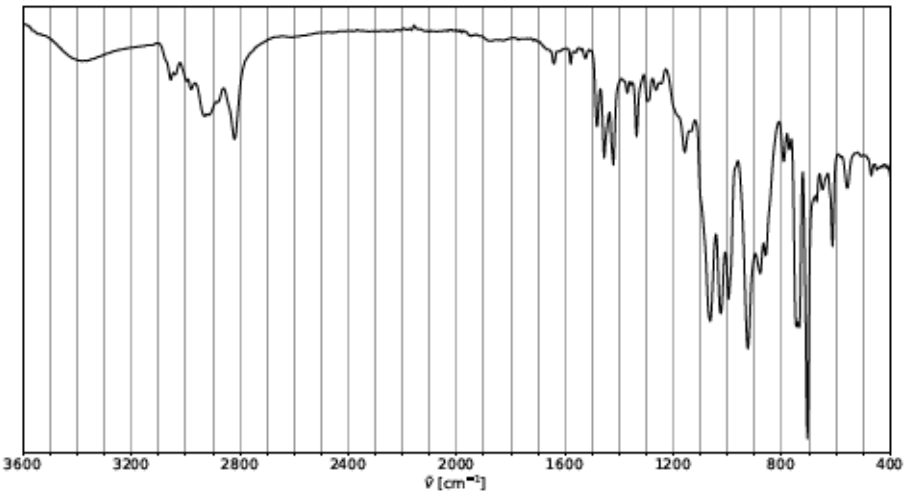

Figure S 269: FTIR (diamond, ATR, neat) of the product obtained by CO_2 treatment of **127**, CuI and $NaBPh_4$ in MeOH (Table S 15, entry 2).

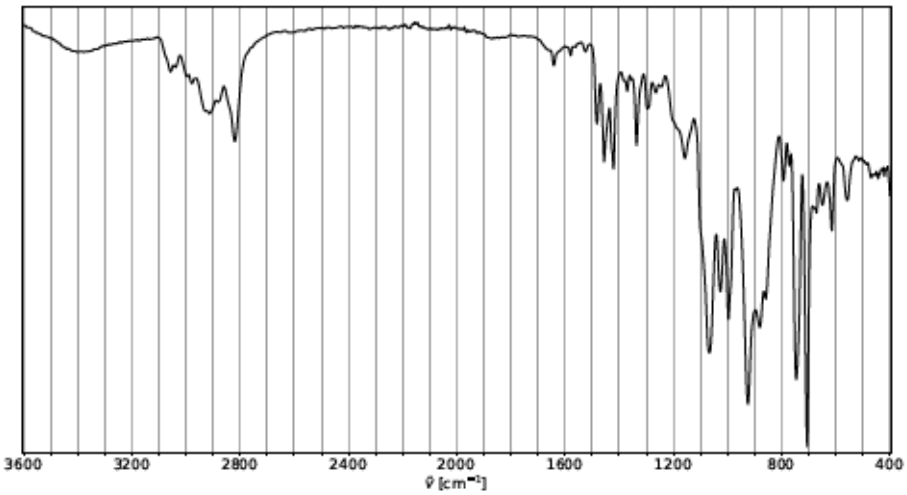

Figure S 270: FTIR (diamond, ATR, neat) of the product obtained by CO_2 treatment of **127**, CuI

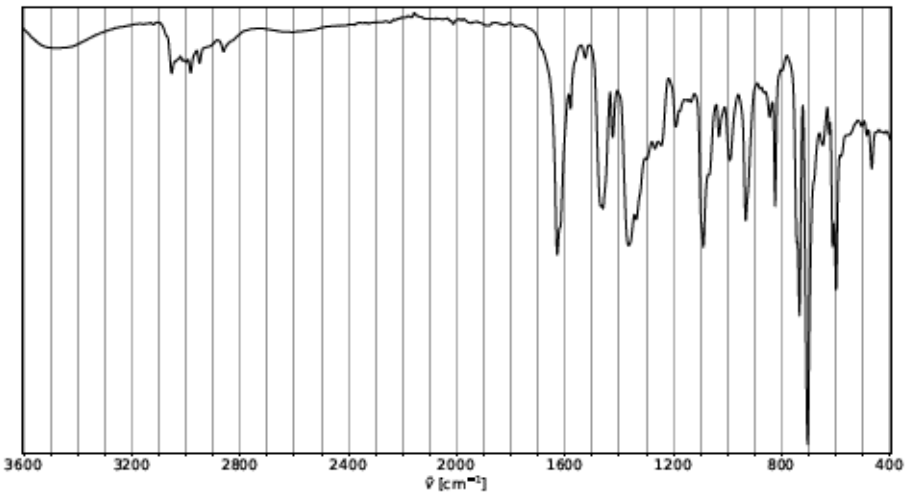

Figure S 271: FTIR (diamond, ATR, neat) of the product obtained by CO_2 treatment of **127**, CuI

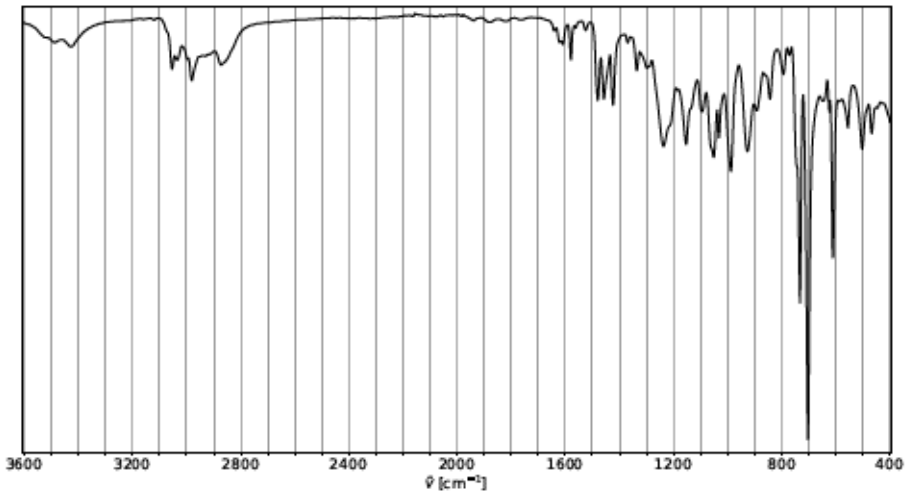

Figure S 272: FTIR (diamond, ATR, neat) of the product obtained by CO_2 treatment of **127**, CuI and $NaBPh_4$ in THF (Table S 15, entry 5).

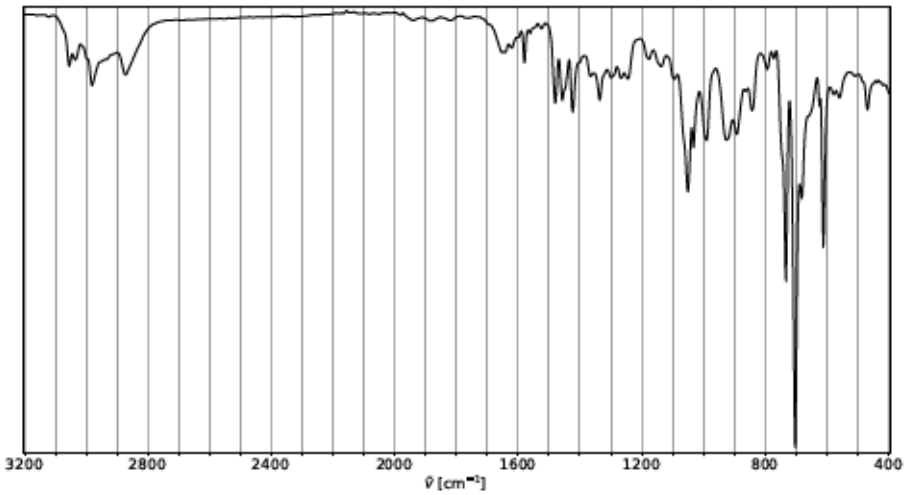

Figure S 273: FTIR (diamond, ATR, neat) of the product obtained by CO_2 treatment of **127**, CuI

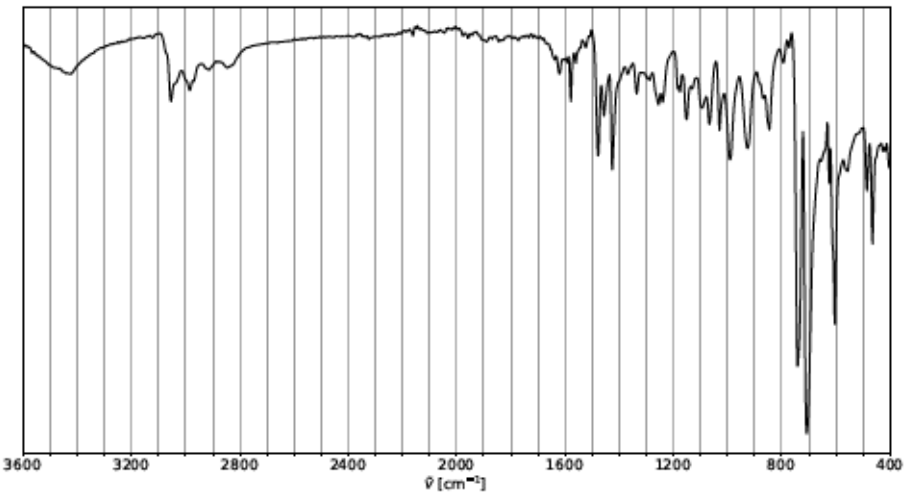

Figure S 274: FTIR (diamond, ATR, neat) of the product obtained by CO_2 treatment of **127**, CuI

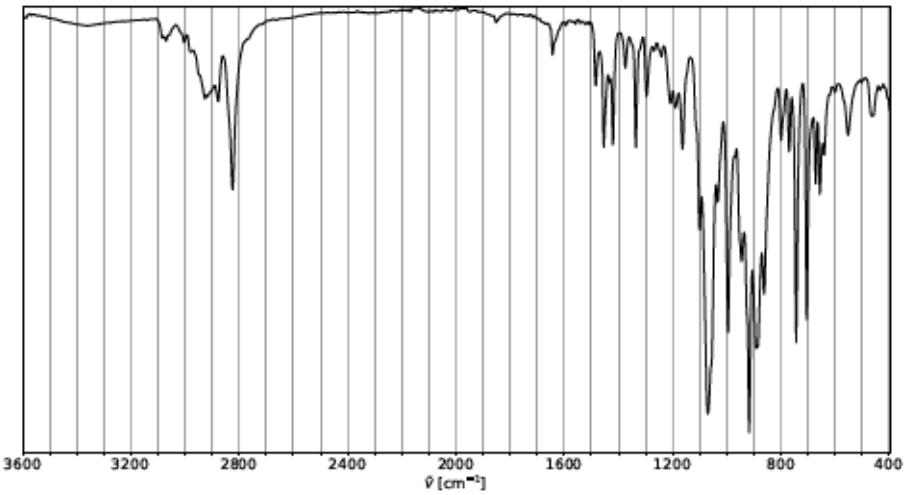

Figure S 275: FTIR (diamond, ATR, neat) of the product obtained by CO_2 treatment of **127**, CuI and $NaBPh_4$ in MeOH at 40 °C (Table S 15, entry 8).

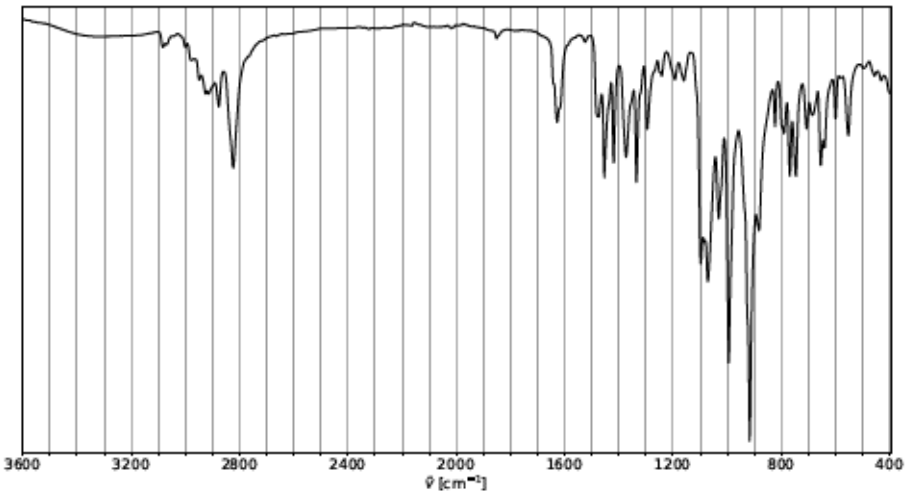

Figure S 276: FTIR (diamond, ATR, neat) of the product obtained by CO_2 treatment of **127**, CuI

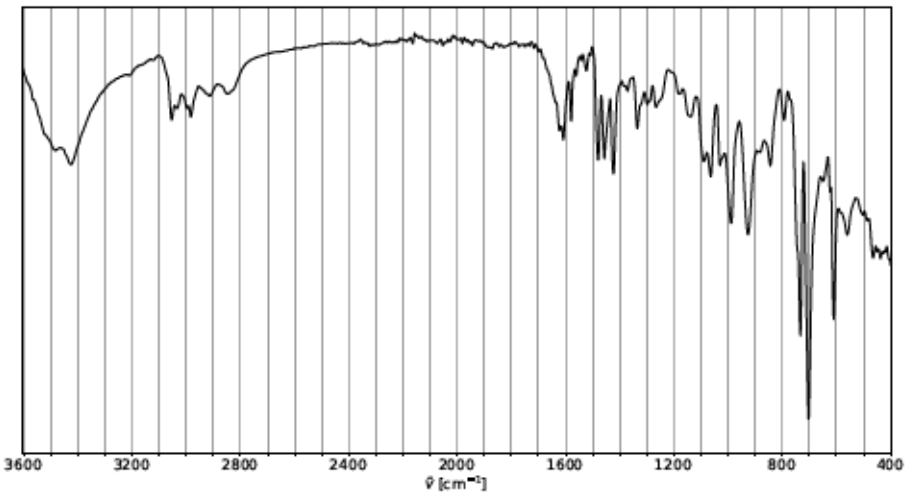

Figure S 277: FTIR (diamond, ATR, neat) of the product obtained by CO_2 treatment and illumi-

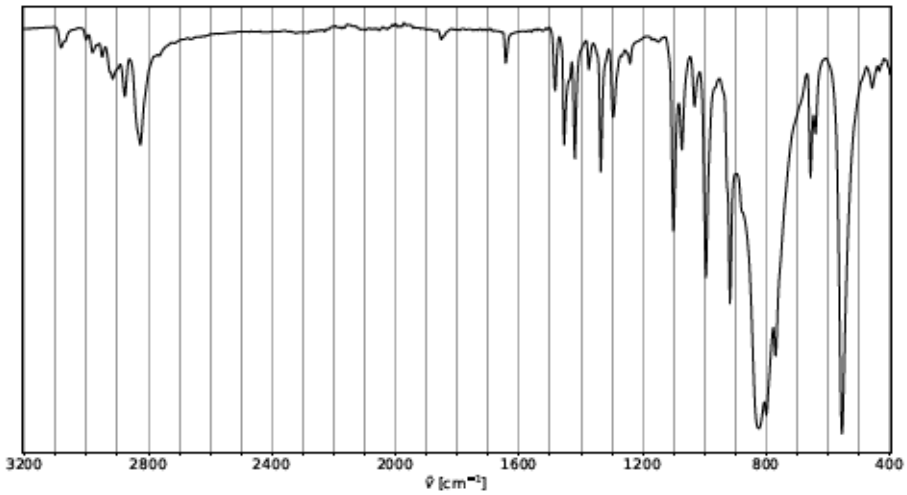

Figure S 278: FTIR (diamond, ATR, neat) of the product obtained by CO_2 treatment of **127**, CuI and KPF_6 in MeOH (Table S 16, entry 1).

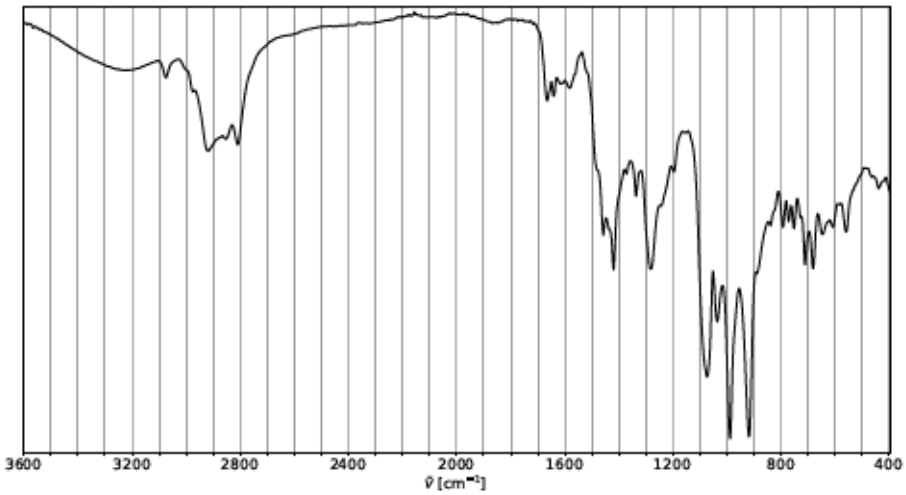

Figure S 279: FTIR (diamond, ATR, neat) of the product obtained by CO_2 treatment of **127**, CuI

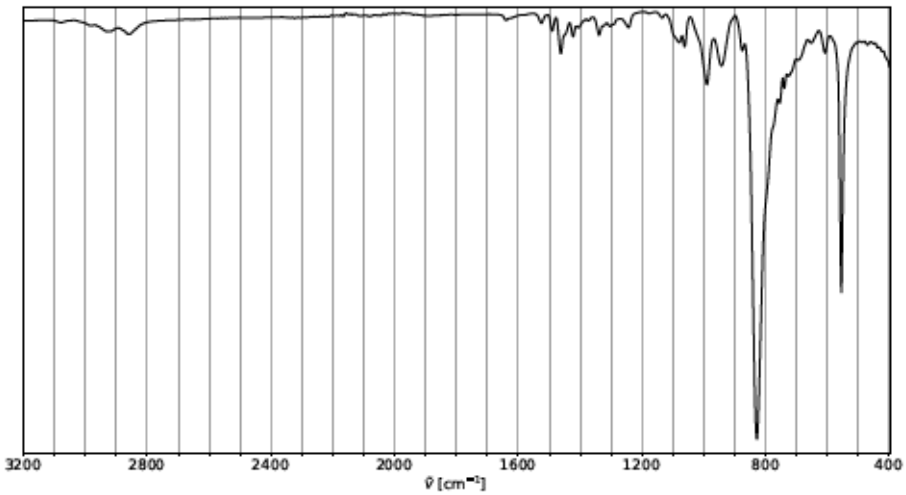

Figure S 280: FTIR (diamond, ATR, neat) of the product obtained by CO_2 treatment of **127** and

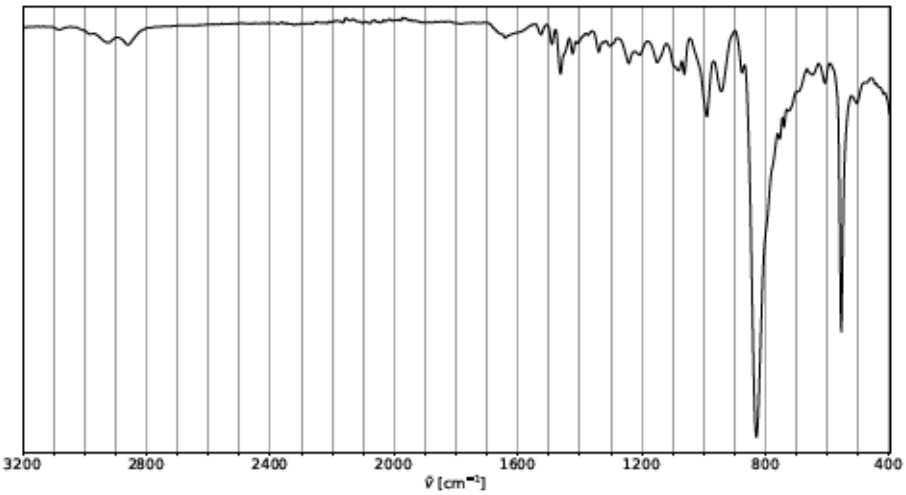

Figure S 281: FTIR (diamond, ATR, neat) of the product obtained by CO_2 treatment of **127** and $[Cu(MeCN)_4]PF_6$ in MeOH (Table S 16, entry 4).

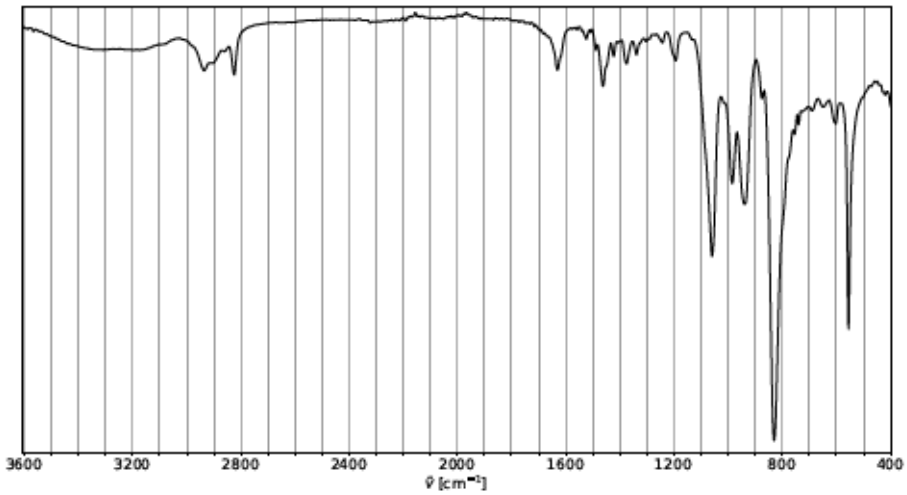

Figure S 282: FTIR (diamond, ATR, neat) of the product obtained by CO_2 treatment of **127**,

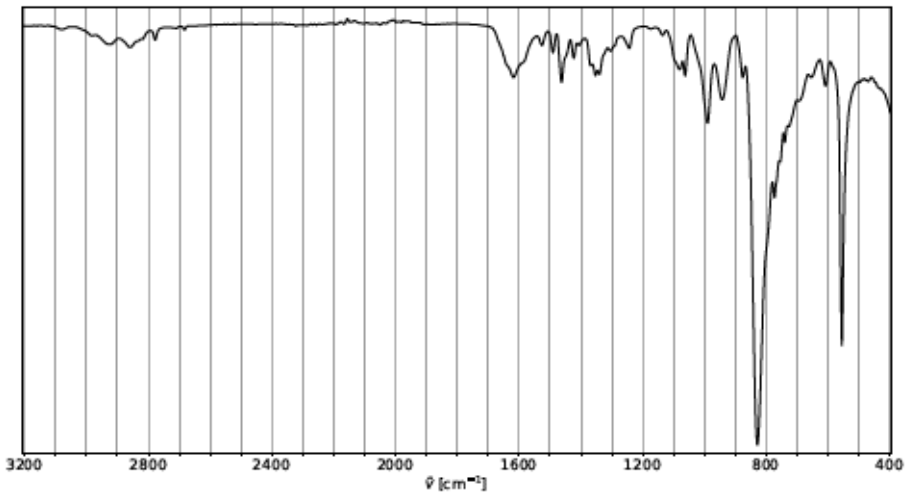

Figure S 283: FTIR (diamond, ATR, neat) of the product obtained by CO_2 treatment of **127**,

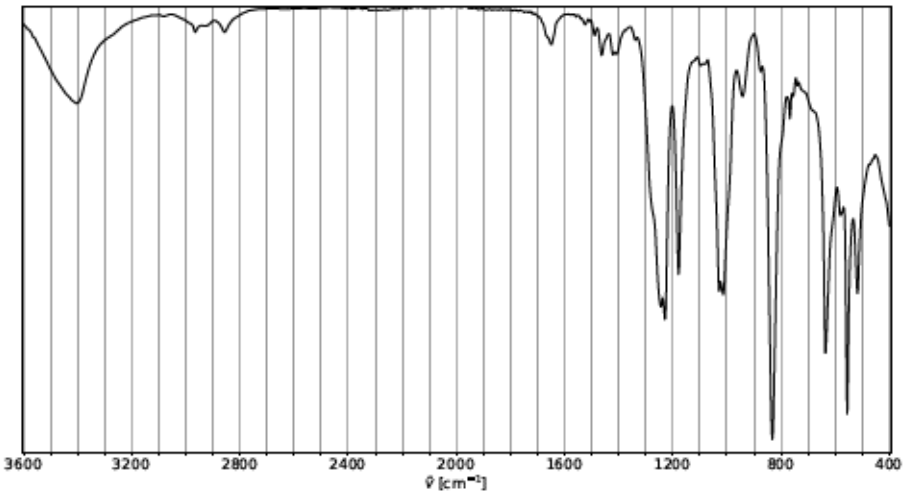

Figure S 284: FTIR (diamond, ATR, neat) of the product obtained by CO_2 treatment of **127**, $[Cu(MeCN)_4]PF_6$ and $Mg(OTf)_2$ in MeOH (Table S 16, entry 7).

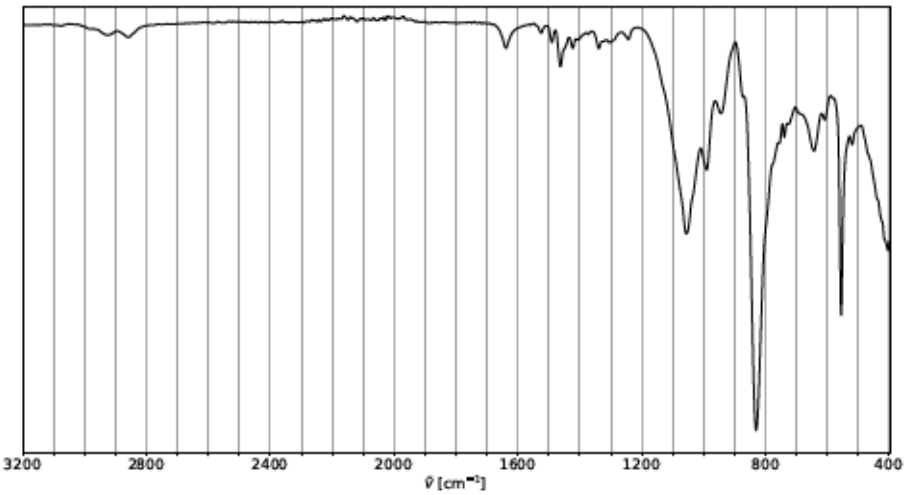

Figure S 285: FTIR (diamond, ATR, neat) of the product obtained by CO_2 treatment of **127**,

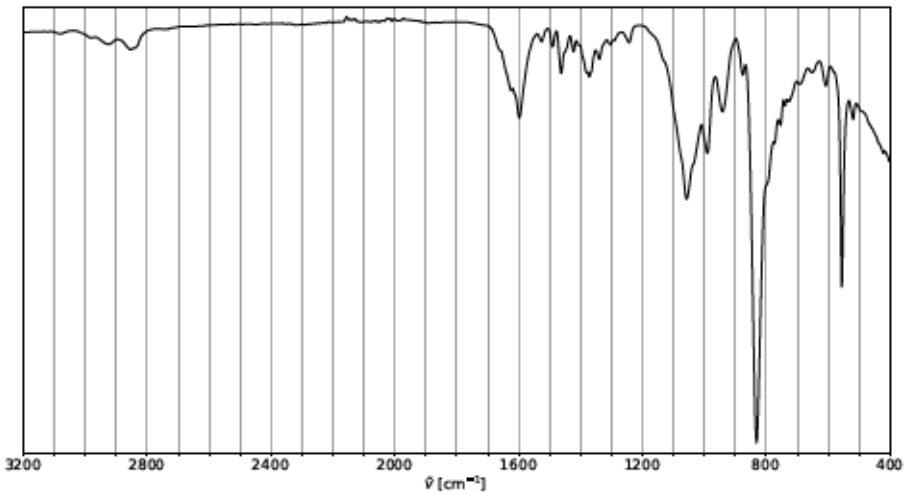

Figure S 286: FTIR (diamond, ATR, neat) of the product obtained by CO_2 treatment of **127**,

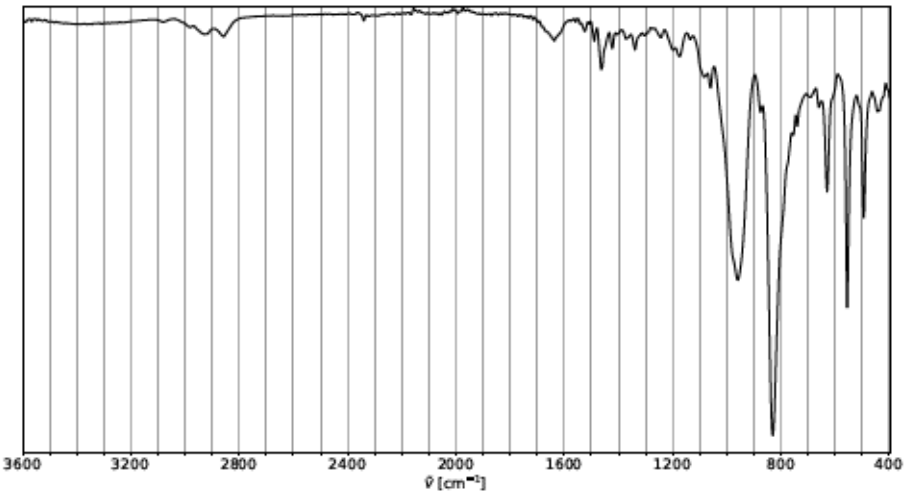

Figure S 287: FTIR (diamond, ATR, neat) of the product obtained by CO_2 treatment of **127**, $[Cu(MeCN)_4]PF_6$ and Na_2SO_3 in MeOH (Table S 16, entry 10).

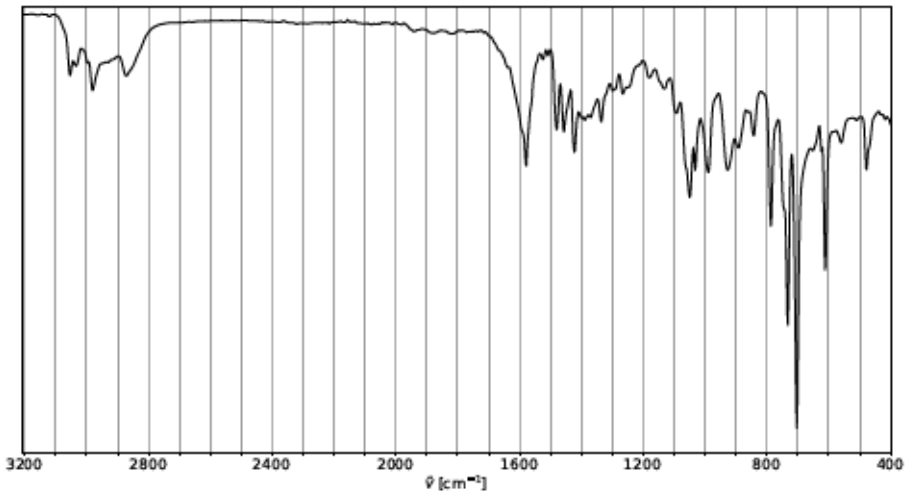

Figure S 288: FTIR (diamond, ATR, neat) of the product obtained by CO_2 treatment of **127**, CuI,

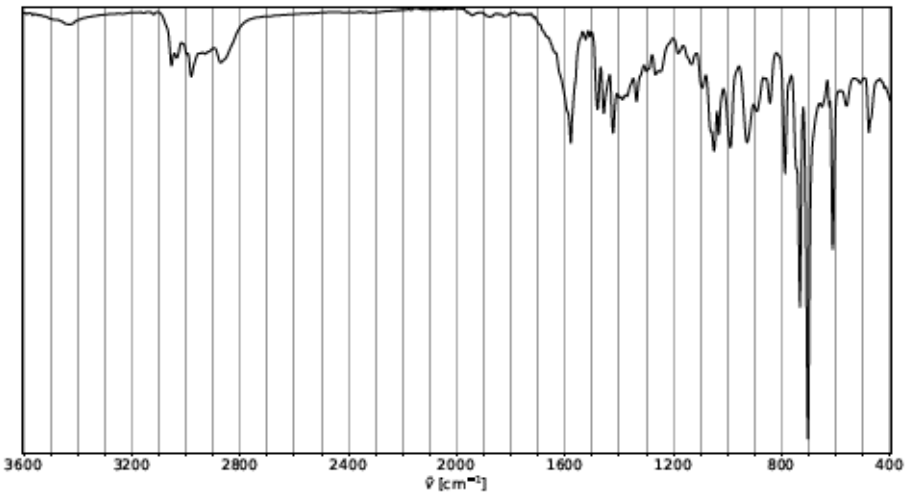

Figure S 289: FTIR (diamond, ATR, neat) of the product obtained by CO_2 treatment of **127**, CuI,

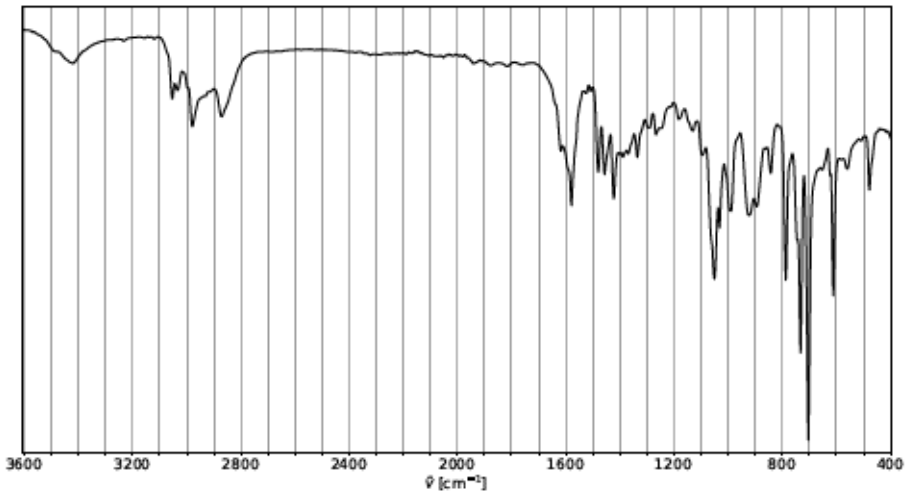

Figure S 290: FTIR (diamond, ATR, neat) of the product obtained by CO_2 treatment of **127**, CuI, $NaBPh_4$ and $NaC_{10}H_8$ in THF (Table S 16, entry 13).

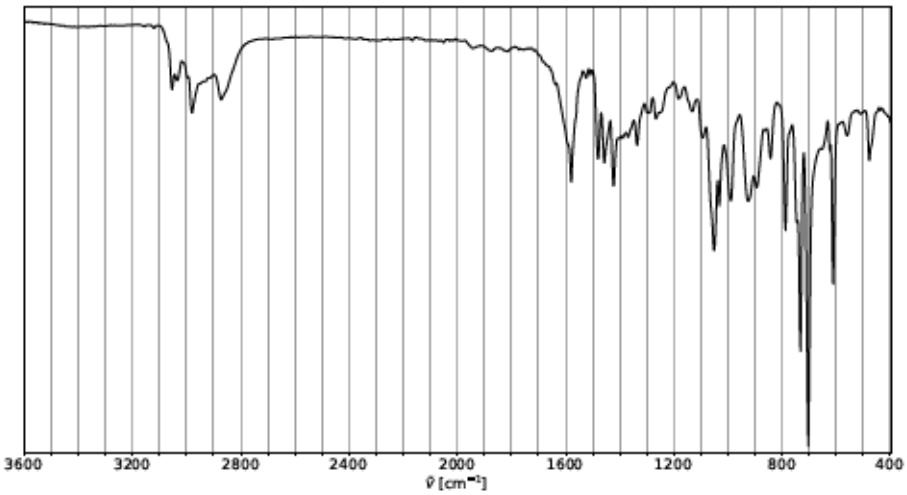

Figure S 291: FTIR (diamond, ATR, neat) of the product obtained by CO_2 treatment of **127**, CuI,

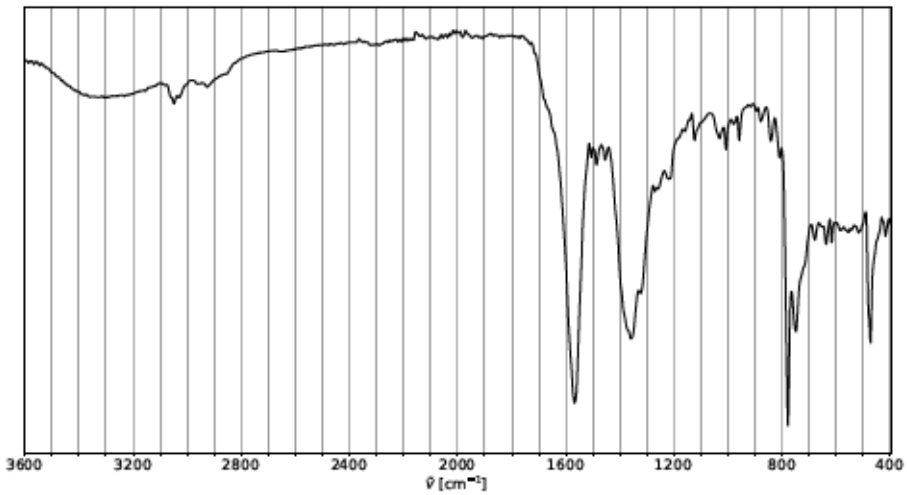

Figure S 292: FTIR (diamond, ATR, neat) of the product obtained by CO_2 treatment of $NaC_{10}H_8$

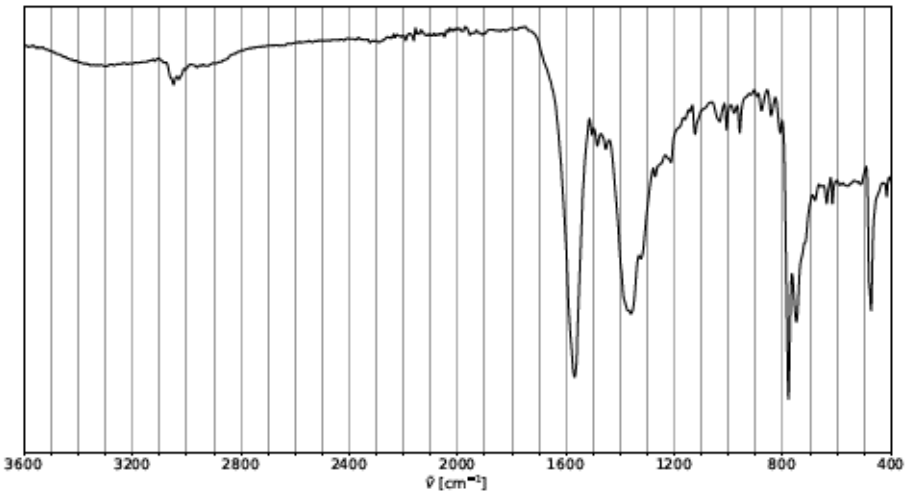

Figure S 293: FTIR (diamond, ATR, neat) of the product obtained by CO_2 treatment of $NaC_{10}H_8$ in THF (Table S 16, entry 16).

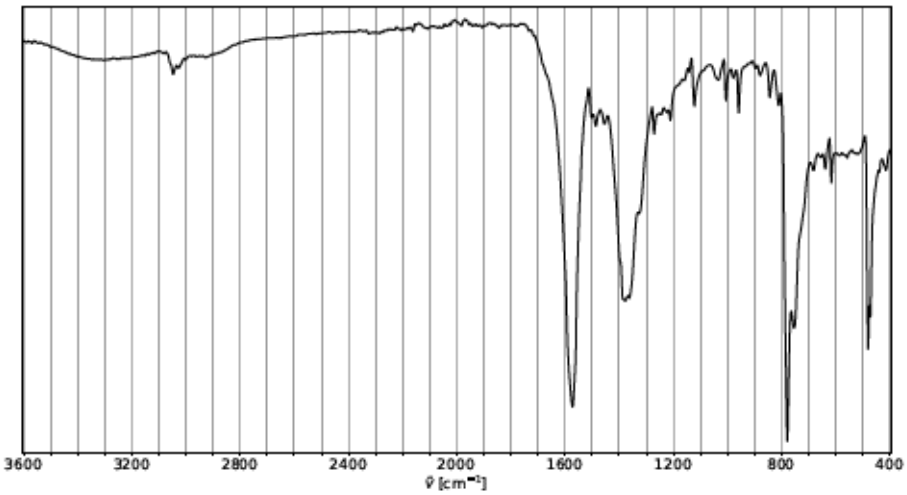

Figure S 294: FTIR (diamond, ATR, neat) of the product obtained by CO_2 treatment of $NaC_{10}H_8$

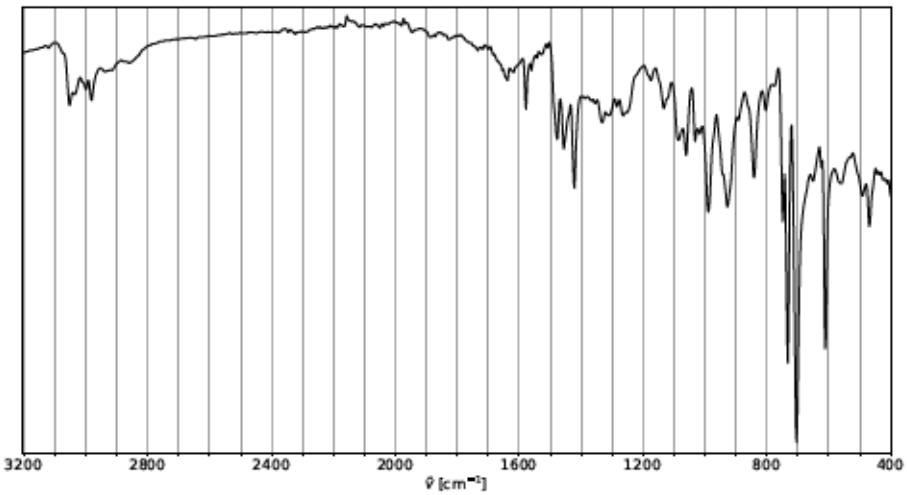

Figure S 295: FTIR (diamond, ATR, neat) of the product obtained by Air exposure of a solution

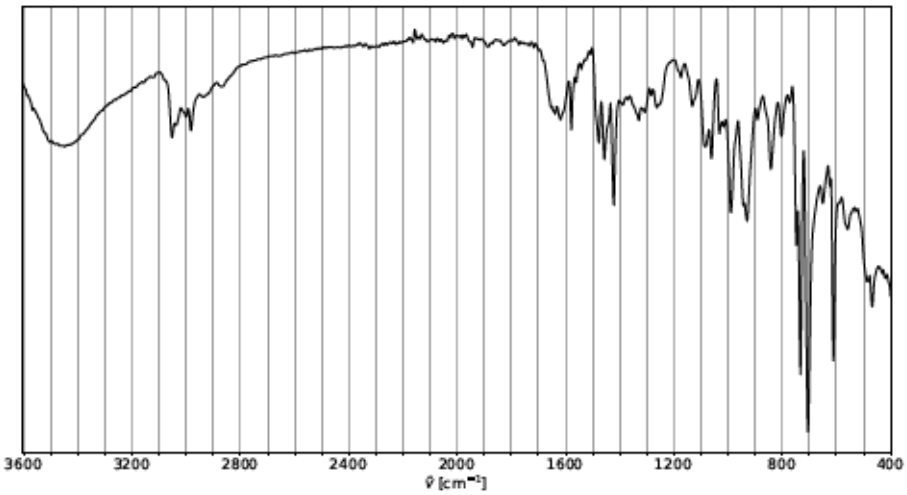

Figure S 296: FTIR (diamond, ATR, neat) of the product obtained by Air exposure of a solution of CuI, **127** and $NaBPh_4$ in MeOH (Table S 17, entry 2).

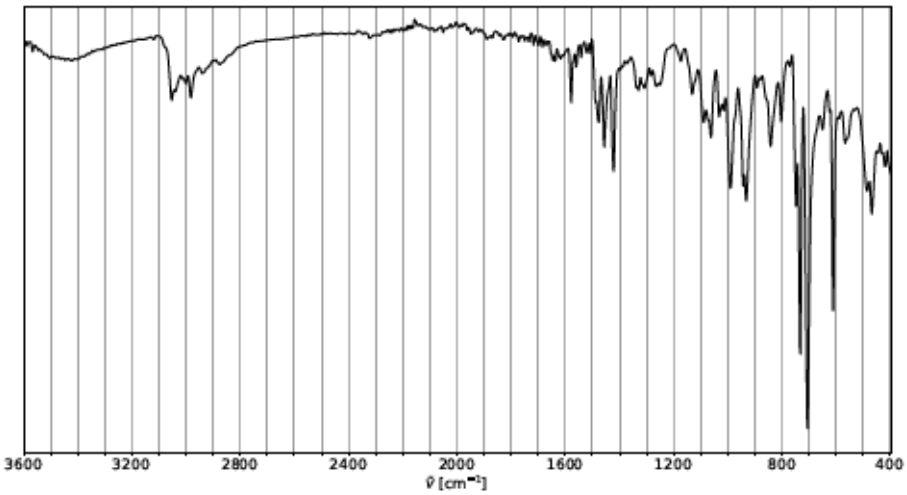

Figure S 297: FTIR (diamond, ATR, neat) of the product obtained by Air exposure of a solution

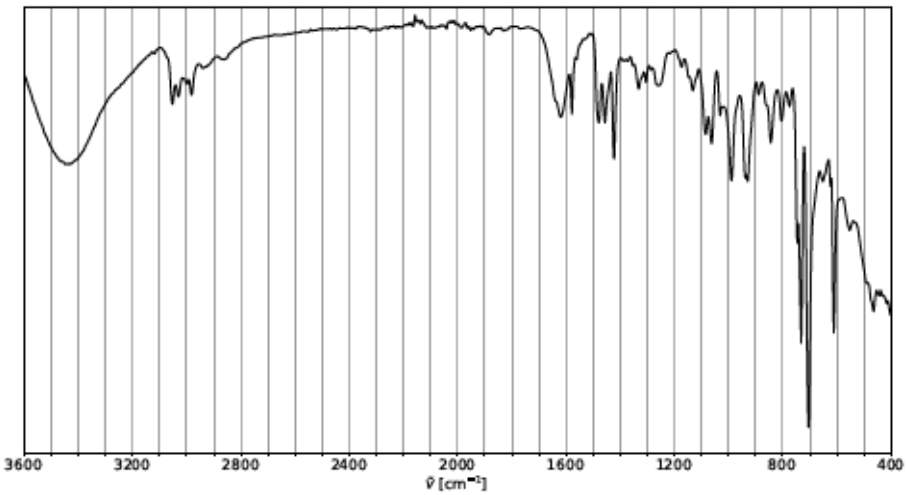

Figure S 298: FTIR (diamond, ATR, neat) of the product obtained by O_2 treatment of a solution

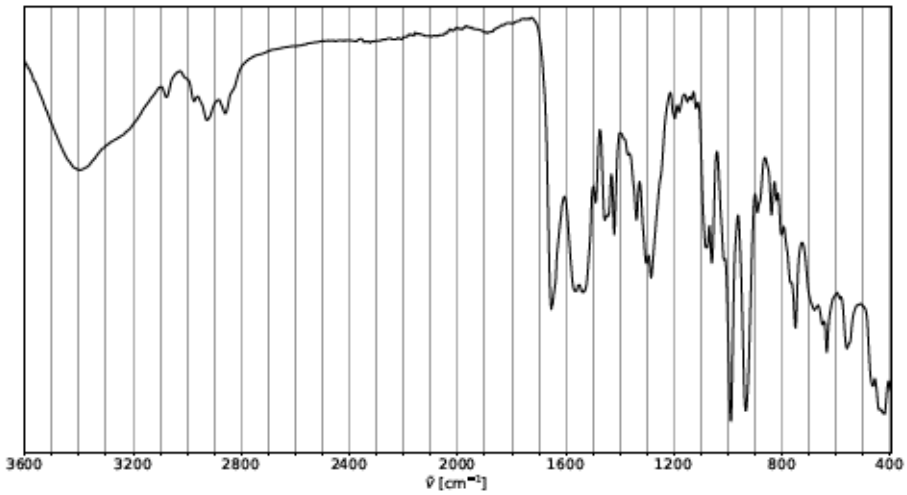

Figure S 299: FTIR (diamond, ATR, neat) of the product obtained by Air exposure of a solution of CuI and **127** in MeOH (Table S 17, entry 5).

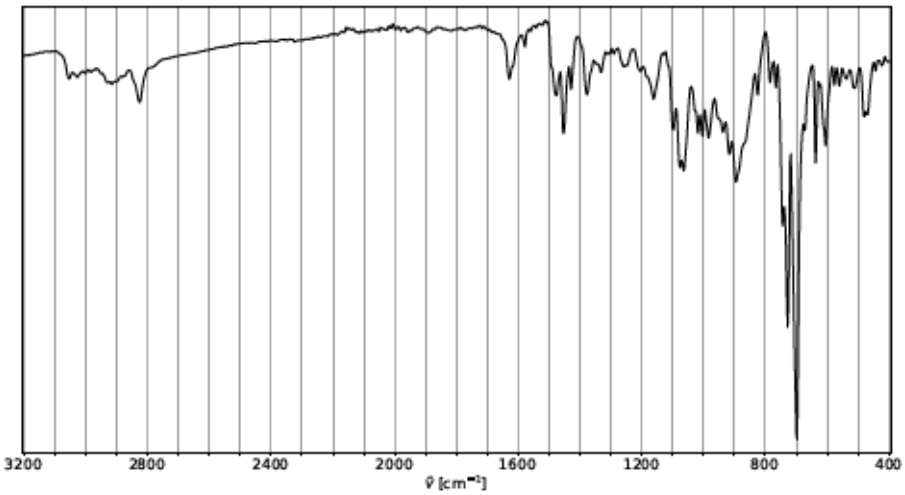

Figure S 300: FTIR (diamond, ATR, neat) of the product obtained by CO_2 treatment of **174**, CuI

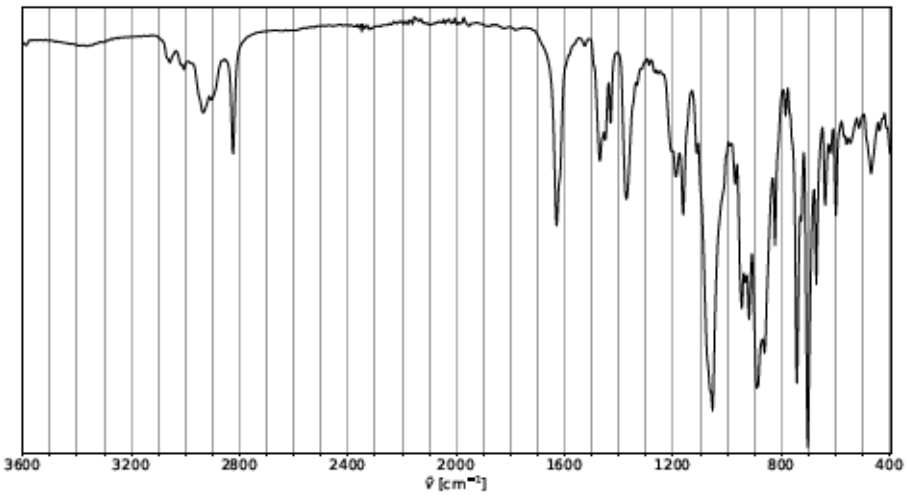

Figure S 301: FTIR (diamond, ATR, neat) of the product obtained by CO_2 treatment of **174**, CuI

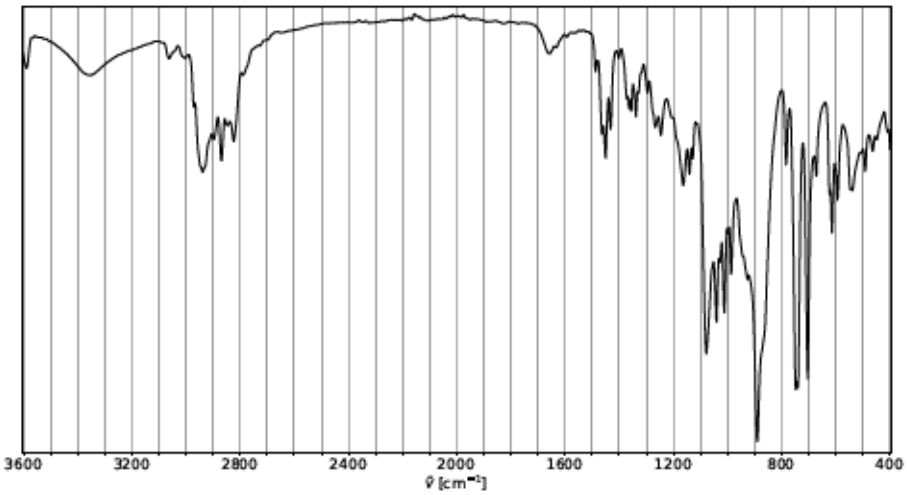

Figure S 302: FTIR (diamond, ATR, neat) of the product obtained by CO_2 treatment of **175**, CuI and $NaBPh_4$ in MeOH (Table S 18, entry 3).

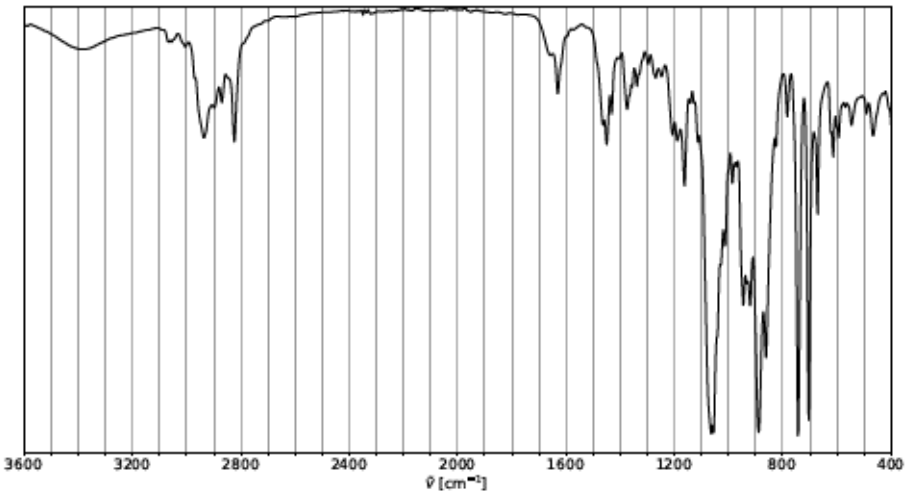

Figure S 303: FTIR (diamond, ATR, neat) of the product obtained by CO_2 treatment of **175**, CuI

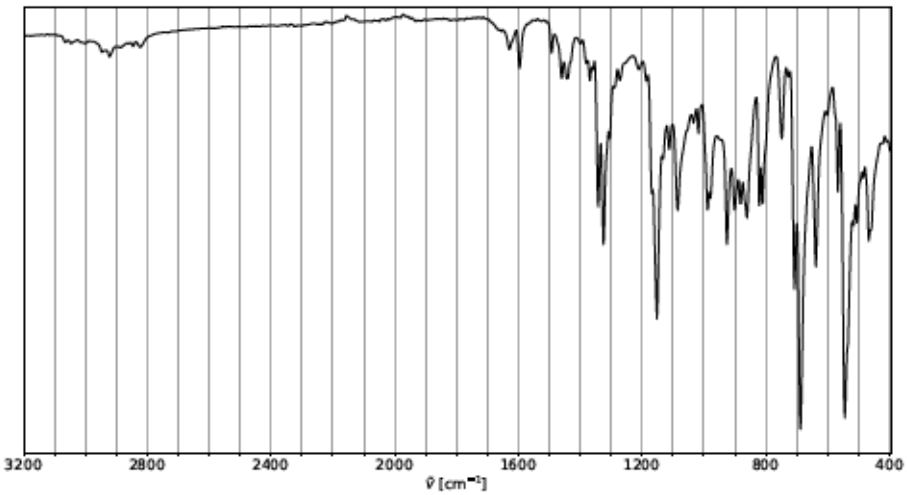

Figure S 304: FTIR (diamond, ATR, neat) of the product obtained by CO_2 treatment of **166**, CuI

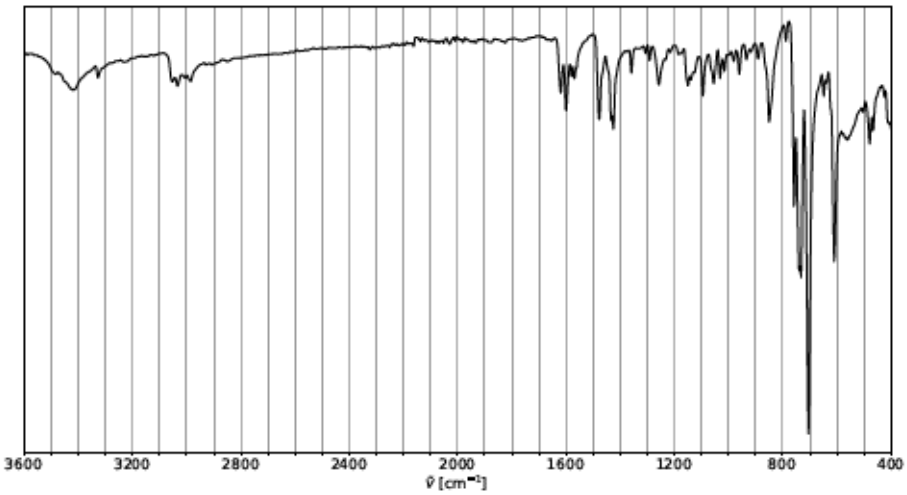

Figure S 305: FTIR (diamond, ATR, neat) of the product obtained by CO_2 treatment of **dpa**, CuI and $NaBPh_4$ in MeOH (Table S 18, entry 6).

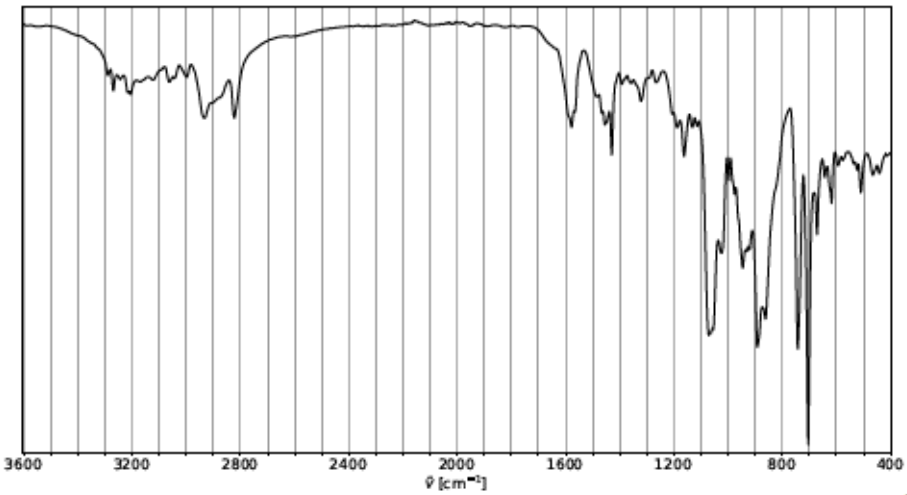

Figure S 306: FTIR (diamond, ATR, neat) of the product obtained by CO_2 treatment of **dien**, CuI

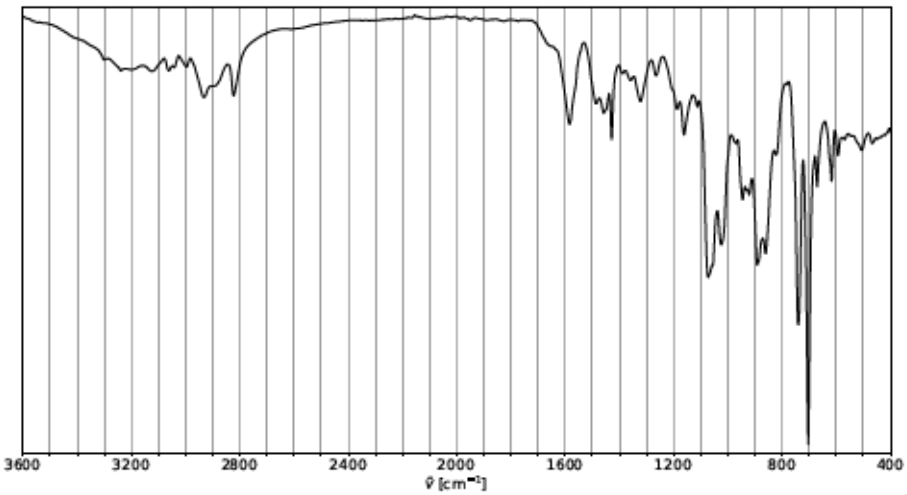

Figure S 307: FTIR (diamond, ATR, neat) of the product obtained by CO_2 treatment of **dien**, CuI

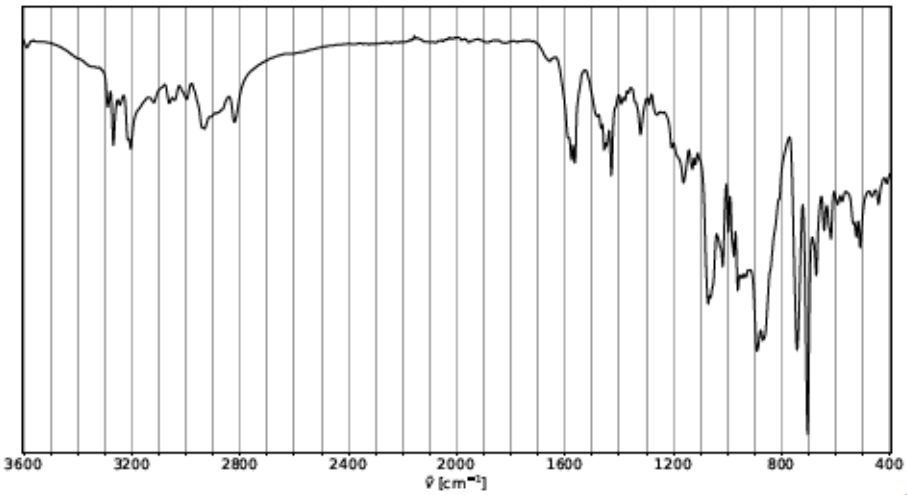

Figure S 308: FTIR (diamond, ATR, neat) of the product obtained by CO_2 treatment of **dien**, CuI and $NaBPh_4$ in MeOH (Table S 18, entry 9).

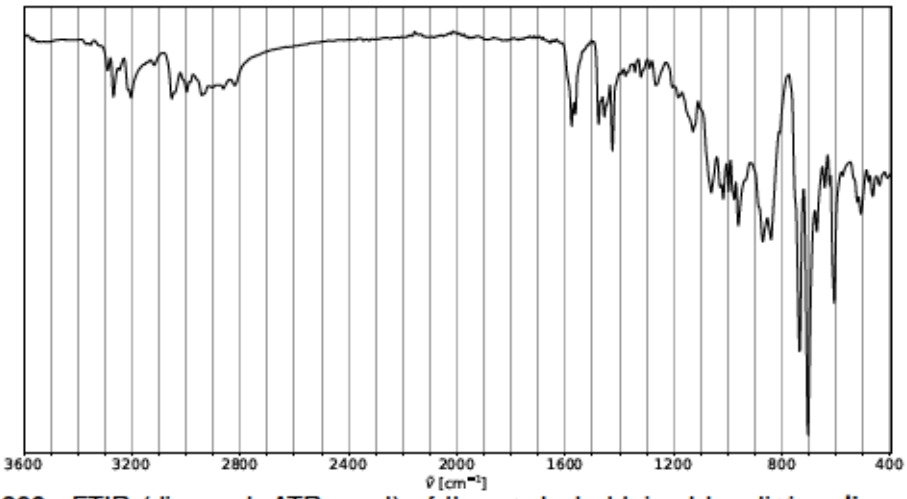

Figure S 309: FTIR (diamond, ATR, neat) of the product obtained by stirring **dien**, CuI and

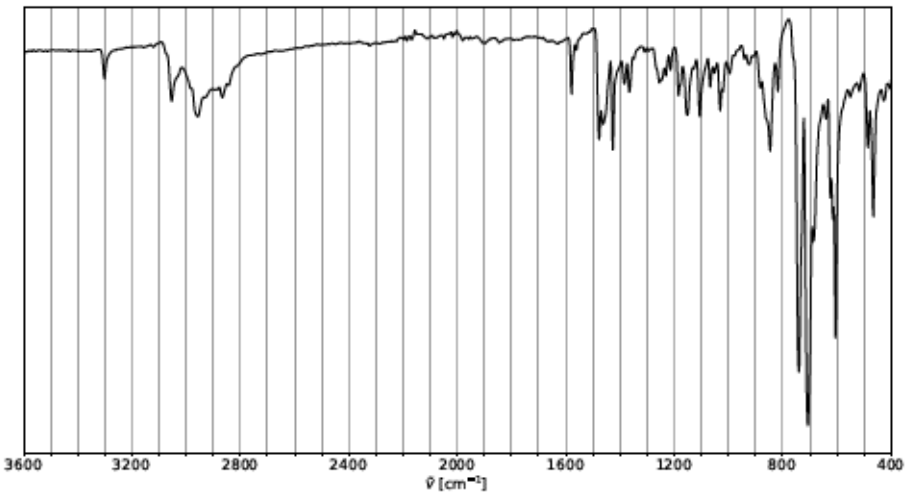

Figure S 310: FTIR (diamond, ATR, neat) of the product obtained by CO_2 treatment of **176** and

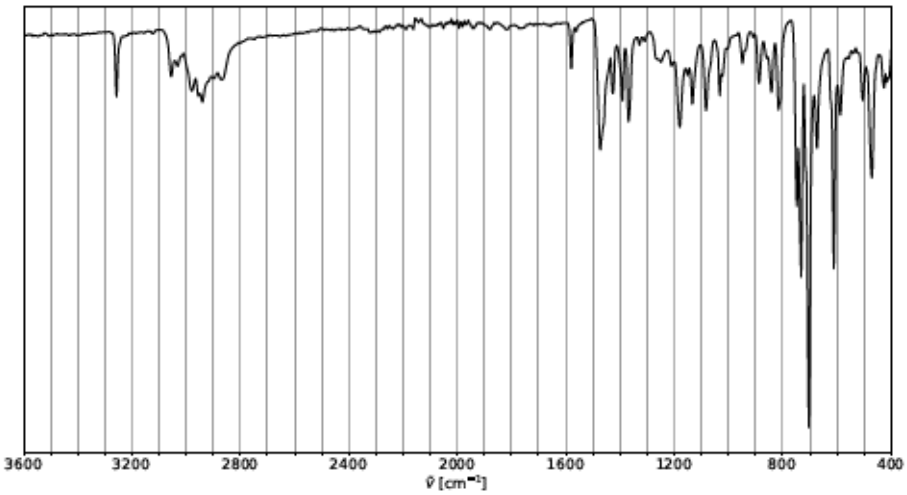

Figure S 311: FTIR (diamond, ATR, neat) of the product obtained by CO_2 treatment of **177** and $NaBPh_4$ in MeOH (Table S 18, entry 12).

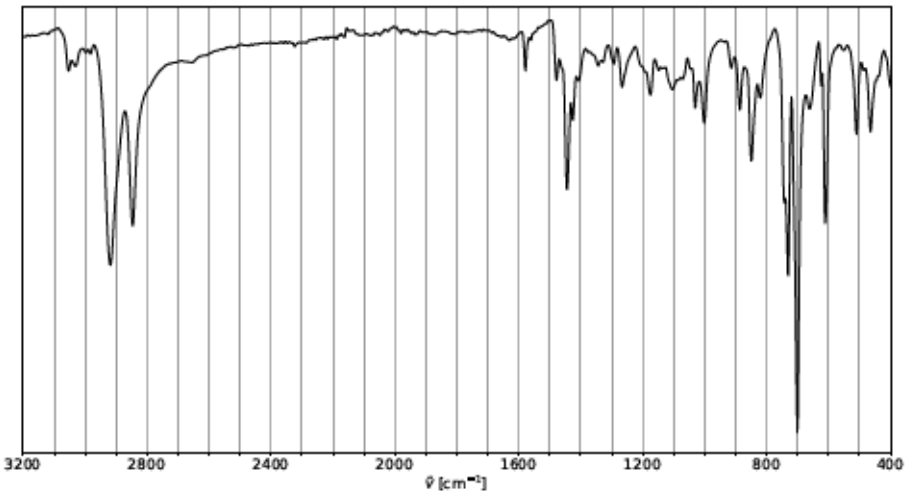

Figure S 312: FTIR (diamond, ATR, neat) of the product obtained by CO_2 treatment of **178** and

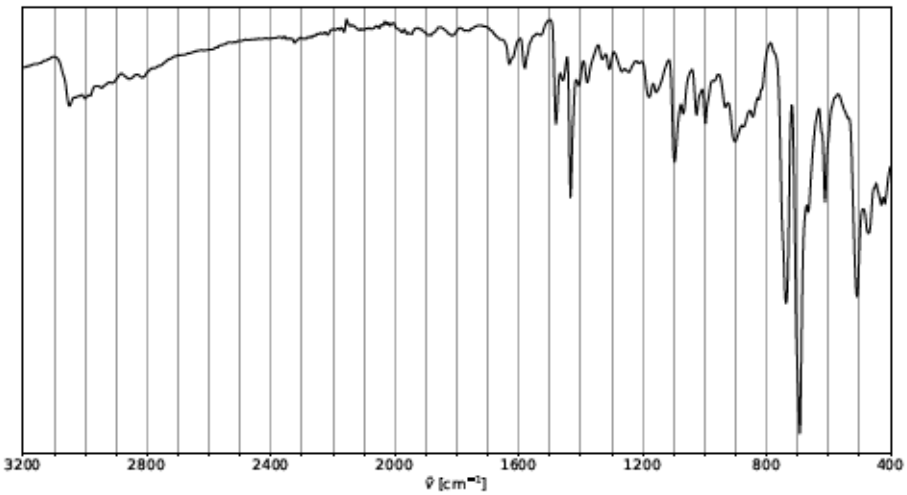

Figure S 313: FTIR (diamond, ATR, neat) of the product obtained by CO_2 treatment of **179** and

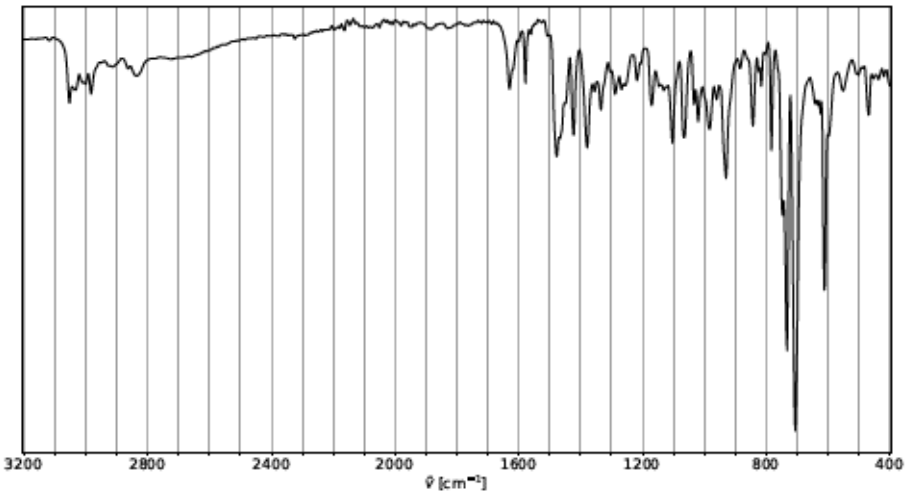

Figure S 314: FTIR (diamond, ATR, neat) of the product obtained by CO_2 treatment of **184**, CuI and $NaBPh_4$ in MeOH (Table S 18, entry 15).

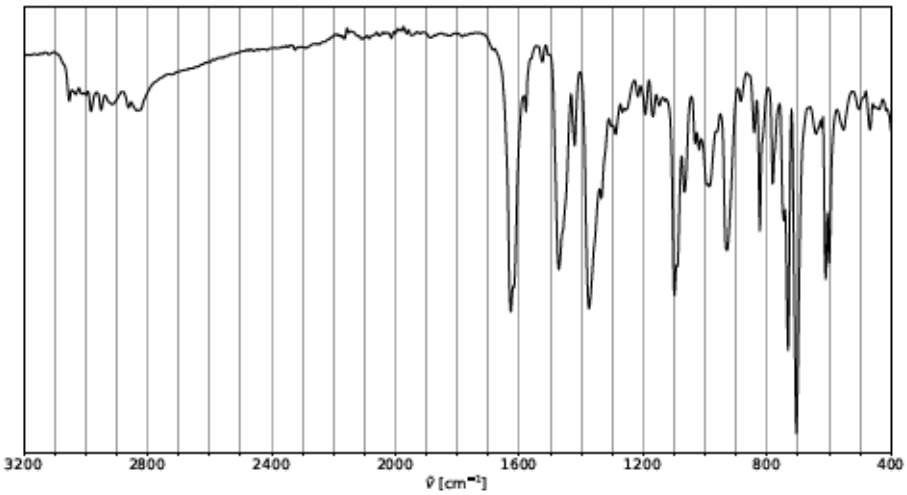

Figure S 315: FTIR (diamond, ATR, neat) of the product obtained by CO_2 treatment of **184**, CuI and $NaBPh_4$ in MeOH (Table S 18, entry 16).

4.

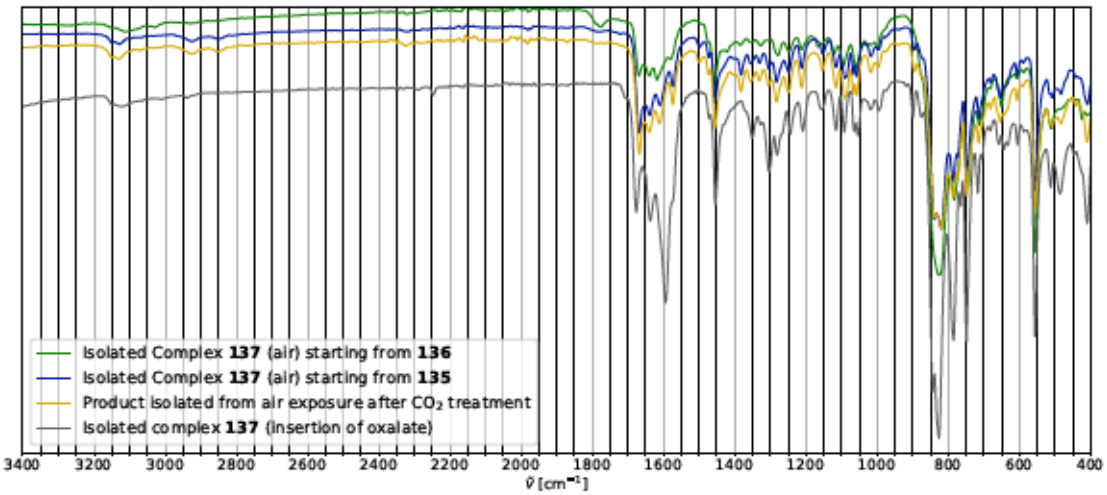

Figure S 316: FTIR (diamond ATR, neat) of **137** formed *via* reaction of *in situ* formed **187** with air starting from **136** or **135** compared to product isolated after CO_2 treatment and subsequent

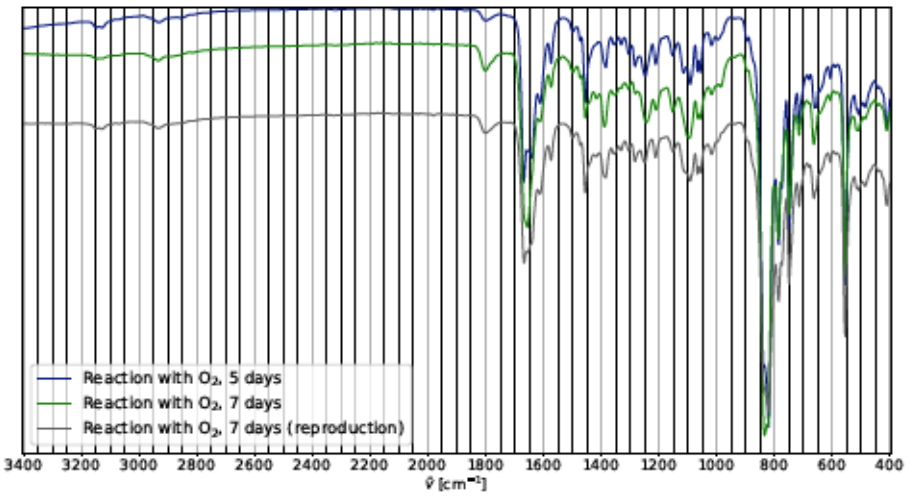

Figure S 317: FTIR (diamond ATR, neat) of **137** formed *via* reaction of *in situ* formed **187** with O_2 over 5 or 7 days.

4.13.6 FTIR Spectra – Reactions of α-Ketocarboxylates

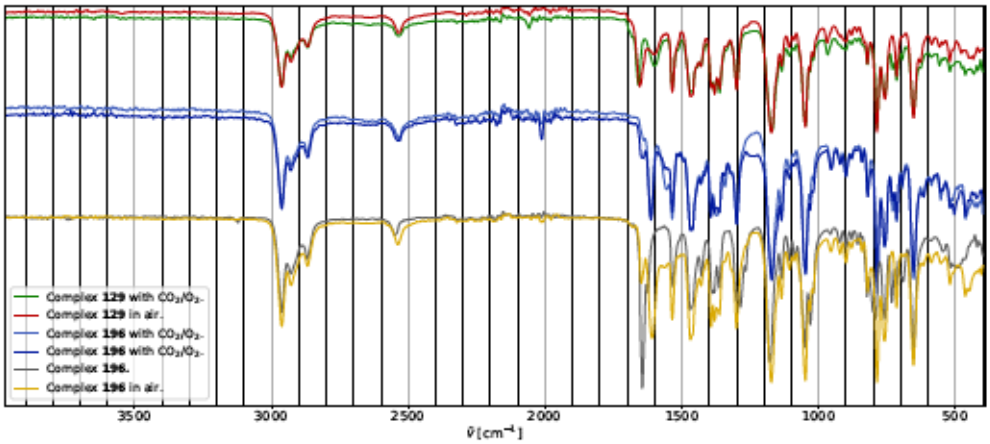

Figure S 318: FTIR spectra of the products obtained by CO_2/O_2 treatment of **129** and **196** in toluene, the products obtained from air exposure of these in CH_2Cl_2 and **196** for comparison.

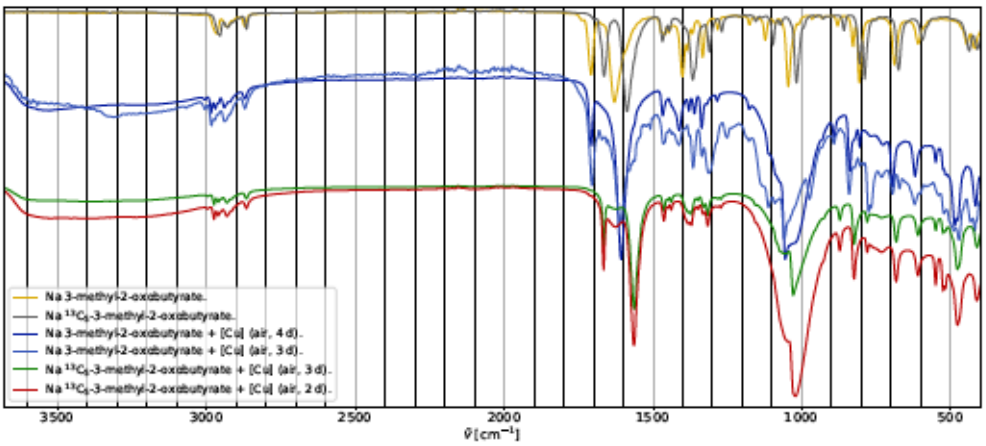

Figure S 319: FTIR spectra of the α-ketocarboxylates **194** and **195** and the products obtained by exposure of these in the presence of $Cu(BF_4)_2{\cdot}6H_2O$ in DCM/MeOH/heptane (1:0.1:1, *v*:*v*:*v*) to air.

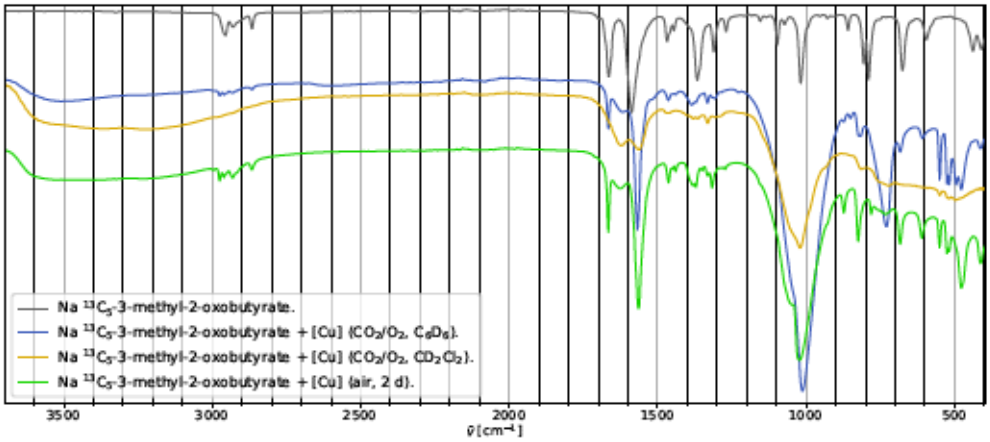

Figure S 320: FTIR spectra of **195** and the products obtained from its exposure to air or CO_2/O_2 in the presence of $Cu(BF_4)_2{\cdot}6H_2O$ in DCM/MeOH/heptane (air) or CD_2Cl_2/CD_3OD and C_6D_6/CD_3OD (CO_2/O_2).

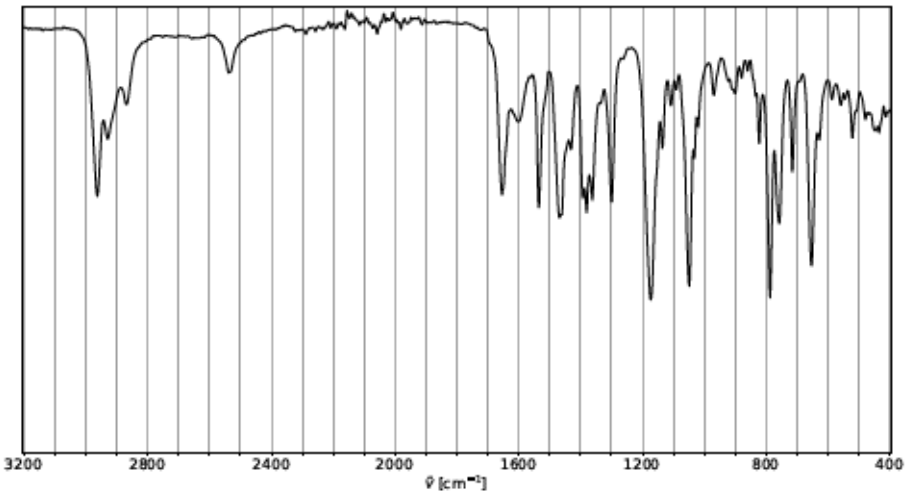

Figure S 321: FTIR (diamond, ATR, neat) of the product obtained by air exposure of **129** in

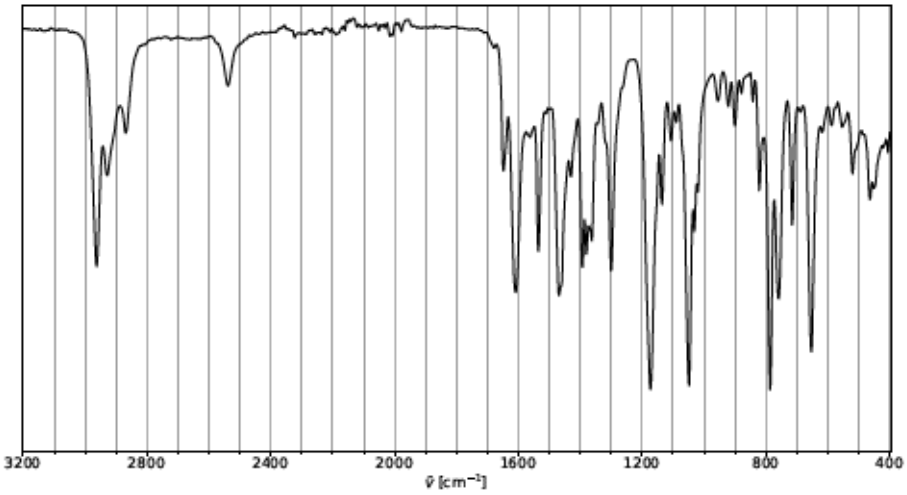

Figure S 322: FTIR (diamond, ATR, neat) of the product obtained by air exposure of **196** in

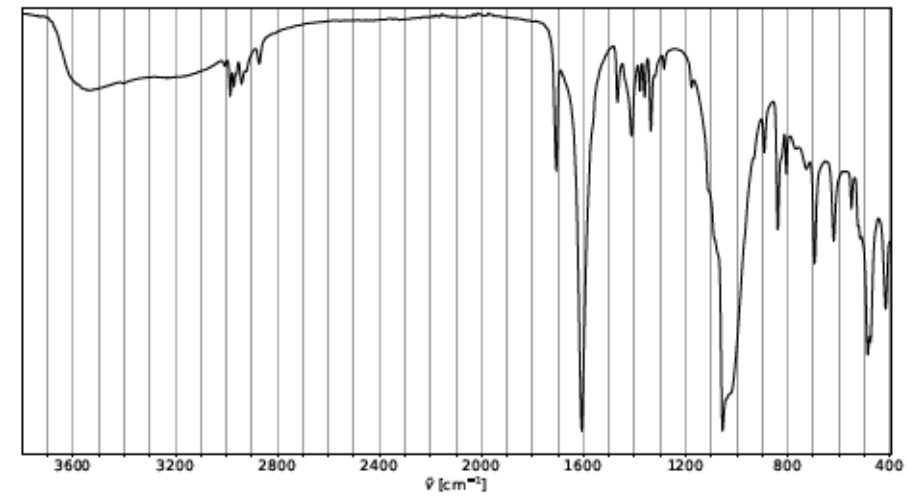

Figure S 323: FTIR (diamond, ATR, neat) of the product obtained by air exposure of sodium 3-methyl-2-oxobuyrate and $Cu(BF_4)_2{\cdot}6H_2O$ in DCM/MeOH/^{n}heptane (Table S 19, entry 3).

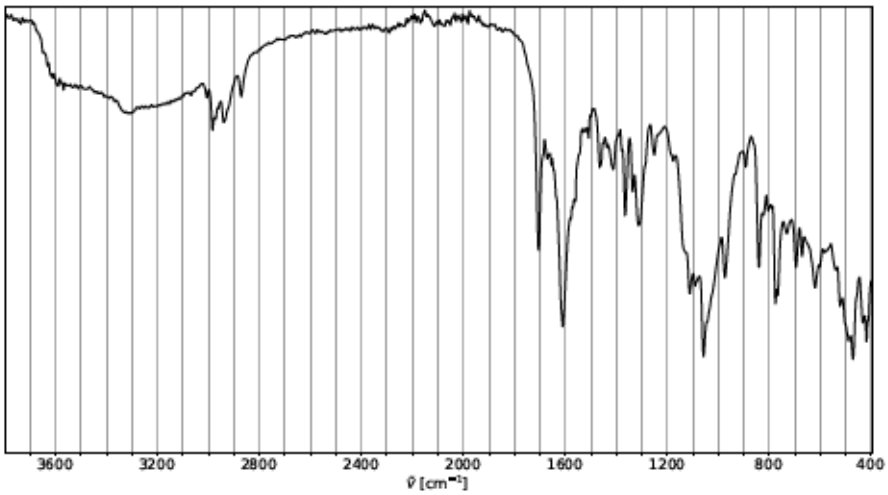

Figure S 324: FTIR (diamond, ATR, neat) of the product obtained by air exposure of sodium

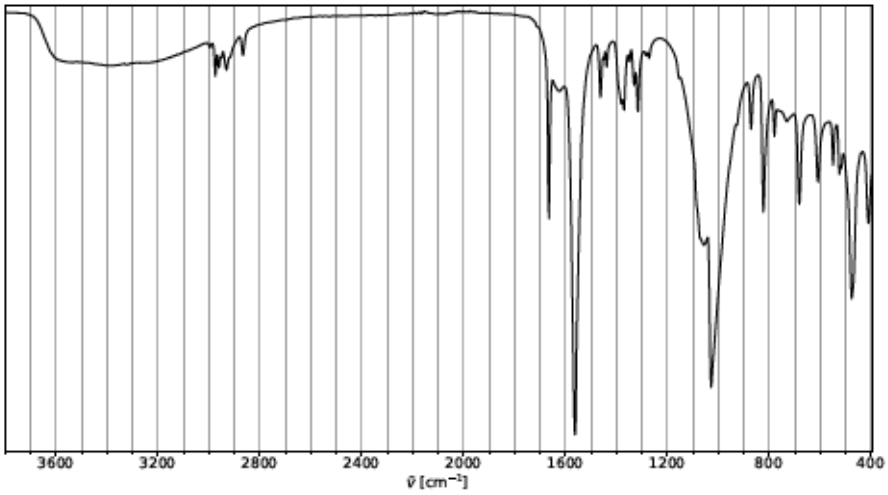

Figure S 325: FTIR (diamond, ATR, neat) of the product obtained by air exposure of sodium

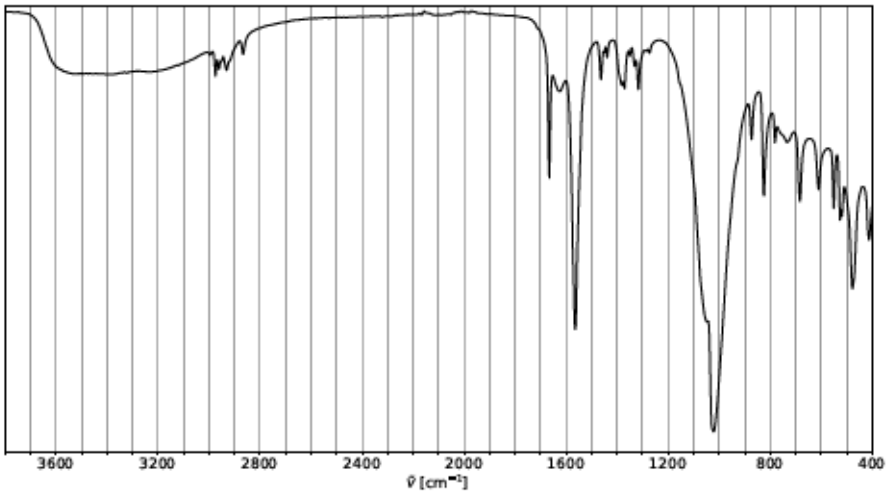

Figure S 326: FTIR (diamond, ATR, neat) of the product obtained by air exposure of sodium $^{13}C_5$-3-methyl-2-oxobuyrate and $Cu(BF_4)_2{\cdot}6H_2O$ in DCM/MeOH/^{n}heptane (Table S 19, entry 6).

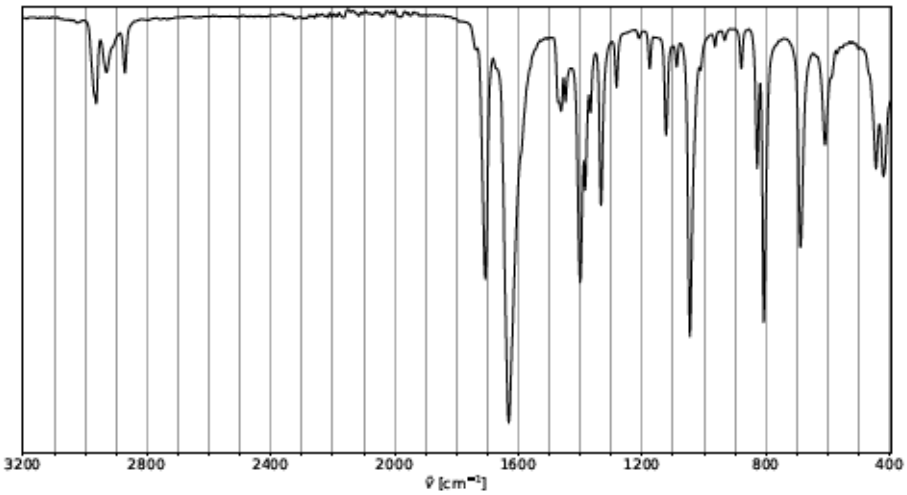

Figure S 327: FTIR (diamond, ATR, neat) of the product obtained by air exposure of sodium

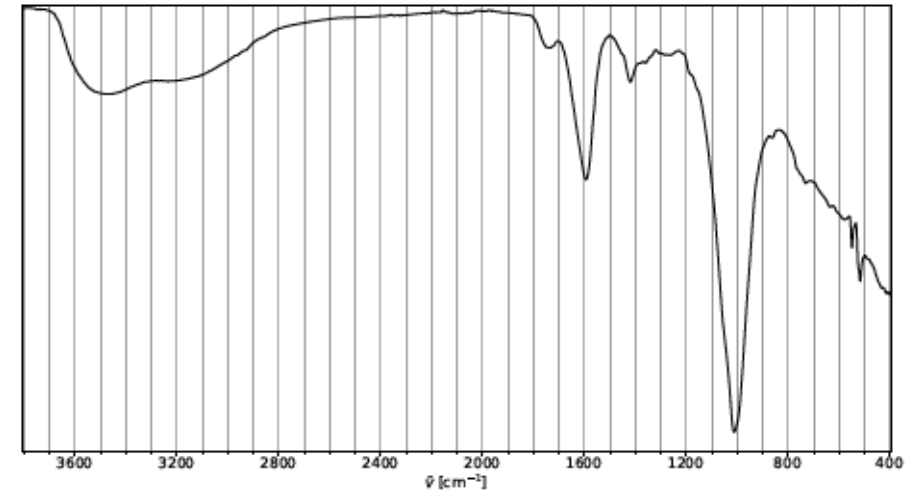

Figure S 328: FTIR (diamond, ATR, neat) of the product obtained by air exposure of sodium

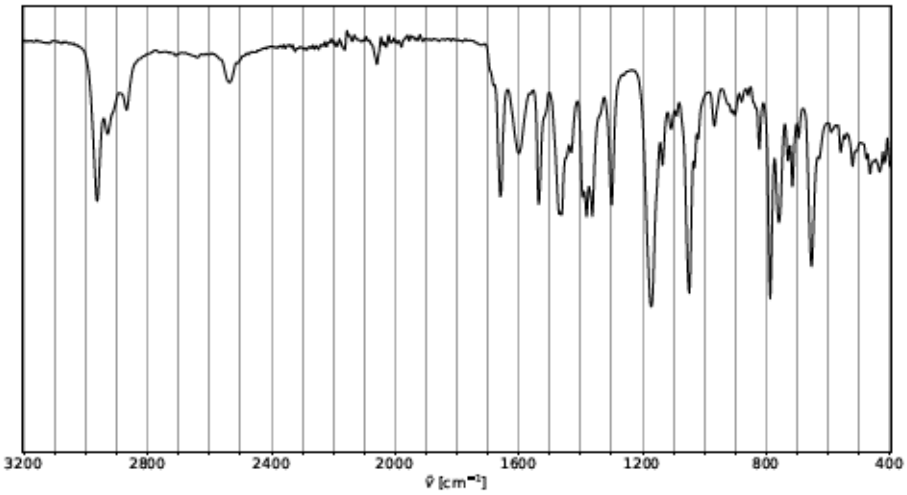

Figure S 329: FTIR (diamond, ATR, neat) of the product obtained by reaction of **129** with CO_2/O_2 in toluene (Table S 20, entry 1).

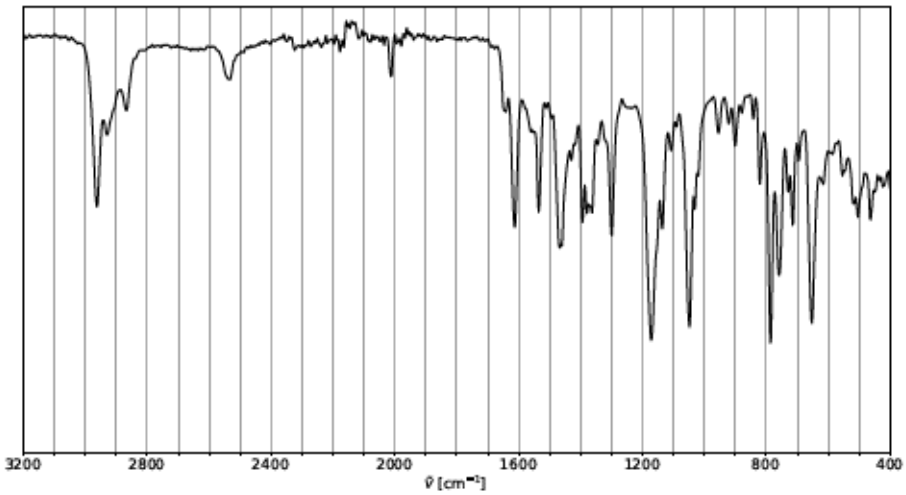

Figure S 330: FTIR (diamond, ATR, neat) of the product obtained by reaction of **196** with CO_2/O_2
i

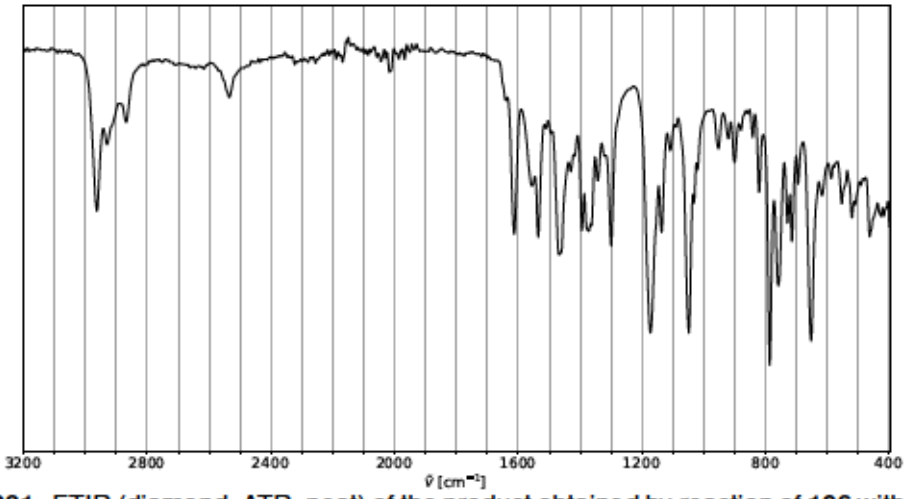

Figure S 331: FTIR (diamond, ATR, neat) of the product obtained by reaction of **196** with CO_2/O_2
i

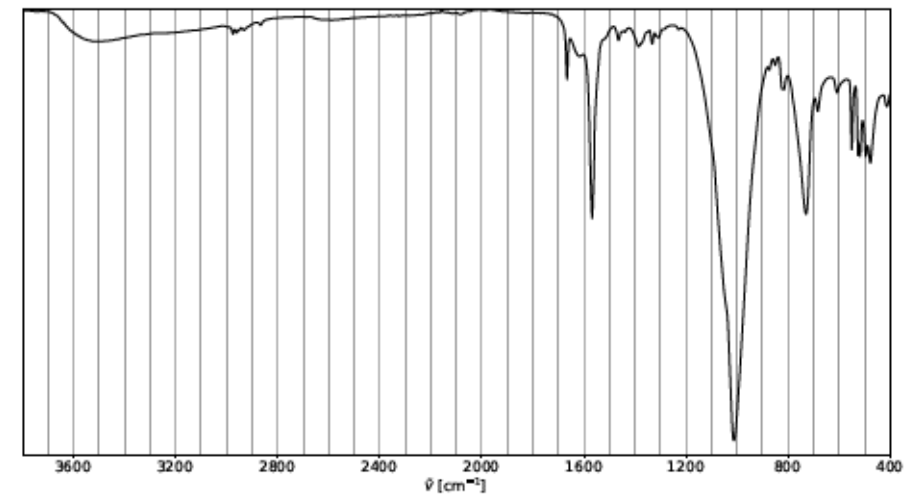

Figure S 332: FTIR (diamond, ATR, neat) of the product obtained by reaction of sodium $^{13}C_5$-3-methyl-2-oxobuyrate and $Cu(BF_4)_2{\cdot}6H_2O$ with CO_2/O_2 in C_6D_6/CD_3OD (Table S 20, entry 4).

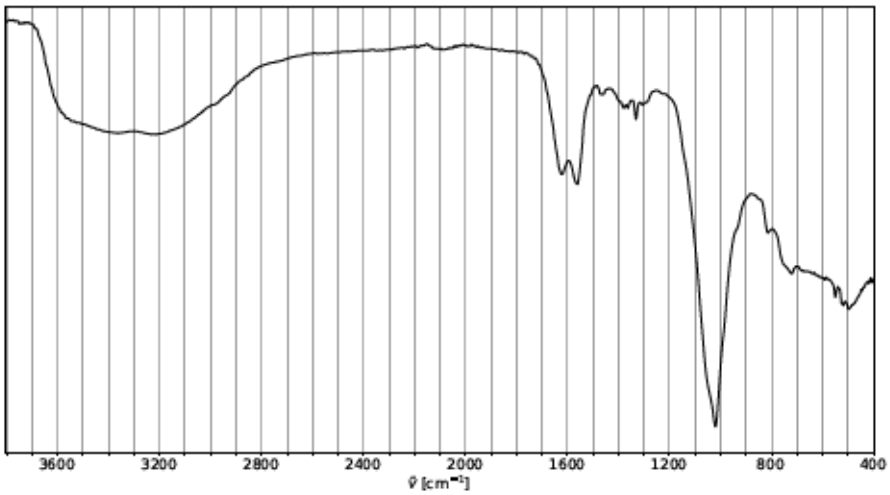

Figure S 333: FTIR (diamond, ATR, neat) of the product obtained by reaction of sodium $^{13}C_5$-3-methyl-2-oxobuyrate and $Cu(BF_4)_2{\cdot}6H_2O$ with CO_2/O_2 in CD_2Cl_2/CD_3OD (Table S 20, entry 5).

4.14 Gas Chromatography

4.14.1 GC Analysis – Reactions with [Fe(tmtaa)]

```
Data File C:\CHEM32\1\DATA\2020\2006\200617\SIG1004755.D
Sample Name: MM577

==========================================================================
Acq. Operator   : HD
Acq. Instrument : GC Lab 1.132                    Location :   -
Injection Date  : 6/17/2020 10:08:42 AM
                                                  Inj Volume : Manually
Acq. Method     : C:\CHEM32\1\METHODS\SAUERSTOFFMESSUNG.M
Last changed    : 6/16/2020 6:28:59 PM by HD
Analysis Method : C:\CHEM32\1\METHODS\SAUERSTOFF_CAL_0919.M
Last changed    : 6/16/2020 5:36:28 PM by EA
                  (modified after loading)
Sample Info     : headspace (5 mL)

Additional Info : Peak(s) manually integrated
```

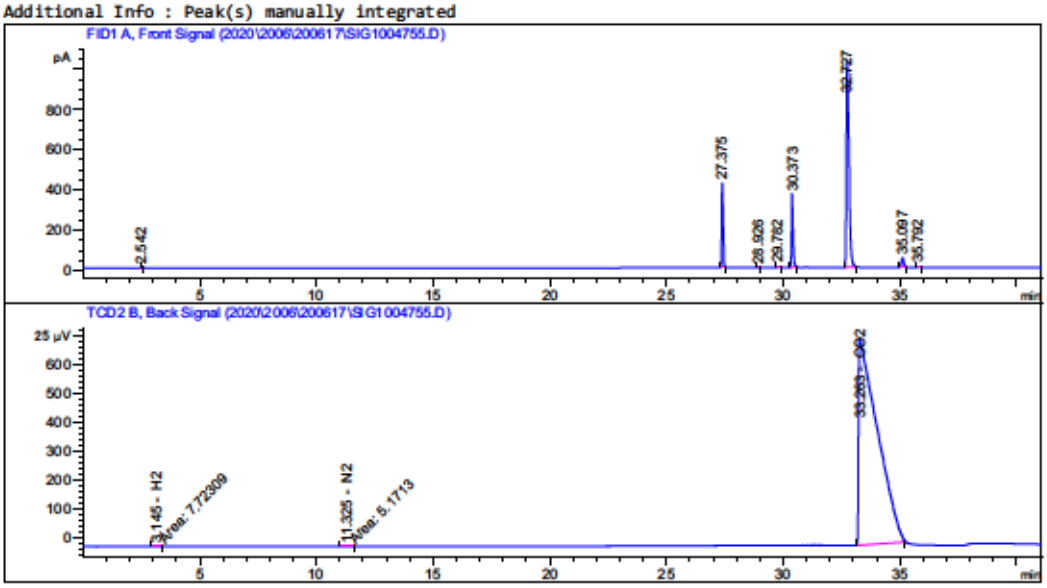


```
==========================================================================
                      External Standard Report
==========================================================================

Sorted By             :      Signal
Calib. Data Modified  :      6/16/2020 5:36:26 PM
Multiplier            :      1.0000
Dilution              :      1.0000
Use Multiplier & Dilution Factor with ISTDs

Signal 1: FID1 A, Front Signal


Signal 2: TCD2 B, Back Signal

RetTime  Type     Area      Amt/Area    Amount   Grp   Name
 [min]          [25 µV*s]              [% Vol.]
-------|------|----------|----------|----------|--|------------------
  3.145 MM        7.72309 3.80886e-4 2.94162e-3    H2
 10.703            -          -          -         O2

GC Lab 1.132 6/17/2020 11:46:31 AM EA                        Page   1 of 2
```

Figure S 334: GC analysis of the headspeace after CO_2 treatment of [Fe(tmtaa)(THF)] reduced with K in toluene (Table S 12, entry 7).

4.14.2 GC Analysis – Reactions of 1,4,7-Tacn-ligated Cu Complexes

```
Data File C:\CHEM32\1\DATA\2020\2006\200622\SIG1004767.D
Sample Name: MM585

================================================================
Acq. Operator   : MM
Acq. Instrument : GC Lab 1.132                  Location :   -
Injection Date  : 6/22/2020 11:08:06 AM
                                                Inj Volume : Manually
Acq. Method     : C:\CHEM32\1\METHODS\SAUERSTOFFMESSUNG.M
Last changed    : 6/22/2020 10:58:26 AM by MM
Analysis Method : C:\CHEM32\1\METHODS\SAUERSTOFF_CAL_0919.M
Last changed    : 6/22/2020 12:30:30 PM by EA
                  (modified after loading)
Sample Info     : headspace (5 mL)

Additional Info : Peak(s) manually integrated
```

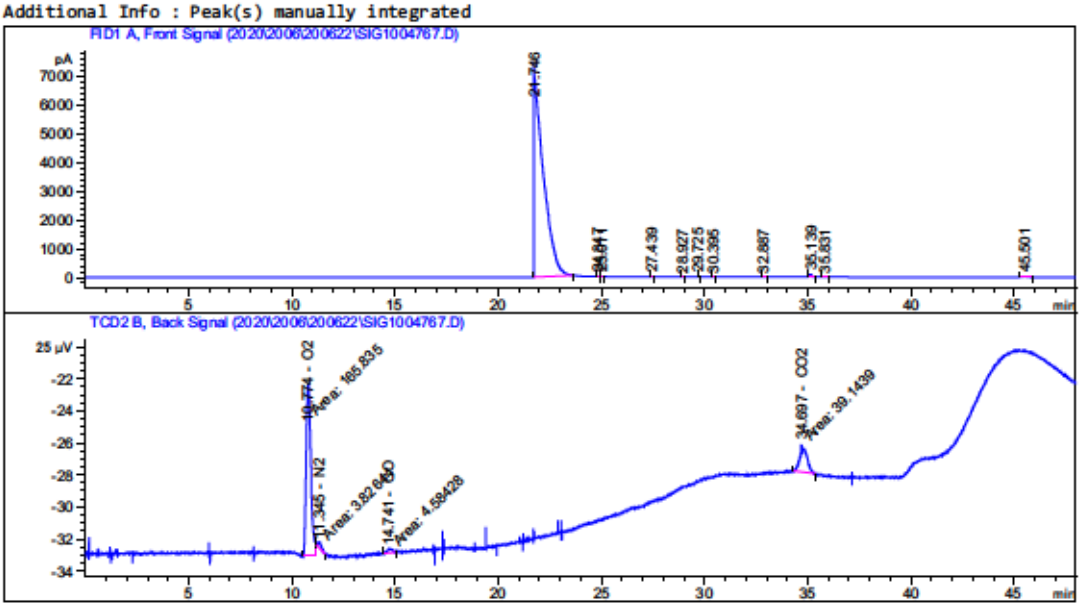


```
================================================================
                    External Standard Report
================================================================

Sorted By             :      Signal
Calib. Data Modified  :      6/22/2020 12:30:30 PM
Multiplier            :      1.0000
Dilution              :      1.0000
Use Multiplier & Dilution Factor with ISTDs

Signal 1: FID1 A, Front Signal


Signal 2: TCD2 B, Back Signal

RetTime  Type     Area      Amt/Area    Amount   Grp   Name
 [min]         [25 µV*s]              [% Vol.]
-------|------|----------|----------|----------|--|------------------
  4.112            -          -          -        H2
 10.774 MM      165.83492 2.00000e-2    3.31670    O2

GC Lab 1.132 6/22/2020 12:30:34 PM EA                    Page   1 of 2
```

Figure S 335: GC analysis of the headspeace after O_2 treatment of CuI, $NaBPh_4$, and **127** in MeOH (Table S 17, entry 4).

```
Data File C:\CHEM32\1\DATA\2020\2007\200704\SIG1004819.D
Sample Name: MM602

================================================================
Acq. Operator   : mm
Acq. Instrument : GC Lab 1.132                  Location :   -
Injection Date  : 7/6/2020 10:09:01 AM
                                                Inj Volume : Manually
Acq. Method     : C:\CHEM32\1\METHODS\SAUERSTOFFMESSUNG.M
Last changed    : 7/4/2020 7:17:01 PM by SR
Analysis Method : C:\CHEM32\1\METHODS\SAUERSTOFF_CAL_0919.M
Last changed    : 7/3/2020 6:05:29 PM by EA
                  (modified after loading)
Sample Info     : headspace (5 mL)

Additional Info : Peak(s) manually integrated
```

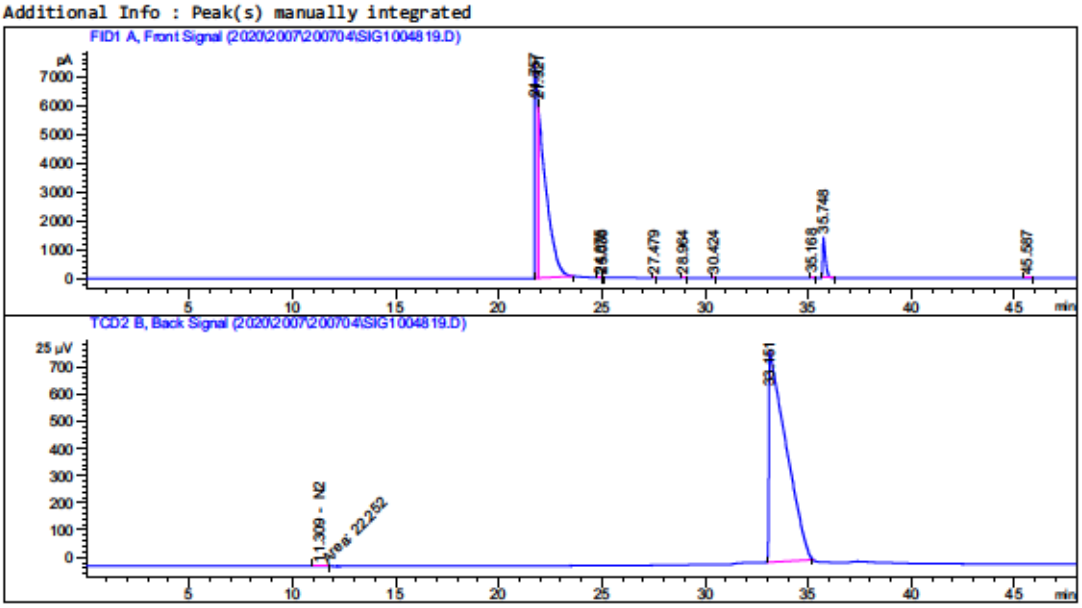


```
================================================================
                    External Standard Report
================================================================

Sorted By             :      Signal
Calib. Data Modified  :      7/3/2020 8:01:42 PM
Multiplier            :      1.0000
Dilution              :      1.0000
Use Multiplier & Dilution Factor with ISTDs

Signal 1: FID1 A, Front Signal


Signal 2: TCD2 B, Back Signal

RetTime  Type     Area      Amt/Area    Amount   Grp   Name
 [min]         [25 µV*s]              [% Vol.]
-------|------|----------|----------|----------|--|------------------
  3.300           -          -          -        H2
 10.703           -          -          -        O2

GC Lab 1.132 7/6/2020 3:01:17 PM EA                    Page   1 of 2
```

Figure S 336: GC analysis of the headspeace after O_2 treatment of CuI, $NaBPh_4$, and **184** in MeOH (Table S 18, entry 15).

4.15 Capillary Electrophoresis

4.15.1 CE Analysis - Calibration

Calibration for quantitative determination of oxalate was conducted with the help of $Na_2C_2O_4$ stock solutions. Concentrations, integrals and the derived concentration per integral are presented in Table S 37. Two calibration runs are further plotted in Figure S 337. Moles of oxalate in the sample were calculated using equation 2. Yields were calculated by dividing the obtained amount of oxalate by the moles of the respective substrate taking into account the stoichiometry of the reaction (mono- *vs.* binuclear).[XXVIII]

Table S 37: Calibration of the oxalate signal utilizing $Na_2C_2O_4$ solutions

Entry	$[Na_2C_2O_4]$ [M]	Integral (I)	$[Na_2C_2O_4]$/I [M]
1	$1.49 \cdot 10^{-5}$	1.353	$1.10 \cdot 10^{-5}$
2[a]	$1.49 \cdot 10^{-5}$	1.697	$0.88 \cdot 10^{-5}$
3	$1.52 \cdot 10^{-5}$	1.452	$1.05 \cdot 10^{-5}$
4	$1.79 \cdot 10^{-5}$	1.802	$0.99 \cdot 10^{-5}$
5	$3.73 \cdot 10^{-5}$	2.967	$1.26 \cdot 10^{-5}$
6[a]	$3.73 \cdot 10^{-5}$	3.132	$1.19 \cdot 10^{-5}$
7	$3.81 \cdot 10^{-5}$	2.741	$1.39 \cdot 10^{-5}$
8	$7.46 \cdot 10^{-5}$	6.565	$1.14 \cdot 10^{-5}$
9[a]	$7.46 \cdot 10^{-5}$	7.519	$0.99 \cdot 10^{-5}$
10	$7.61 \cdot 10^{-5}$	5.413	$1.41 \cdot 10^{-5}$
11	$3.73 \cdot 10^{-4}$	35.70	$1.05 \cdot 10^{-5}$
12[a]	$3.73 \cdot 10^{-4}$	34.72	$1.07 \cdot 10^{-5}$
13	$3.81 \cdot 10^{-4}$	26.88	$1.42 \cdot 10^{-5}$
	$\bar{x}([Na_2C_2O_4]/I)$[b] $\equiv \Gamma = (1.15 \pm 0.13) \cdot 10^{-5}$ mol L^{-1}		

Integrals are averages of two runs unless stated otherwise. [a]Integral determined by single CE analysis. [b]Arithmetic mean of three calibration series and the corresponding standard deviation.

$$n(C_2O_4^{2-}) = c_{tot}(C_2O_4^{2-}) \cdot V_{tot} = c_{CE}(C_2O_4^{2-}) \cdot \frac{V_{tot}}{V_{sample}} \cdot V_{CE}$$
$$= \Gamma \cdot I(C_2O_4^{2-}) \cdot \frac{V_{tot}}{V_{sample}} \cdot V_{CE} \quad (2)$$

With $n(C_2O_4^{2-})$ = total moles of oxalate formed, $c_{tot}(C_2O_4^{2-})$ = total concentration of oxalate in the sample, V_{tot} = total sample volume, $c_{CE}(C_2O_4^{2-})$ = concentration of oxalate in the CE sample, V_{sample} = volume of the sample taken for CE analysis, V_{CE} = total volume of the CE sample ($V_{sample} + V_{H_2O}$), $\Gamma = \bar{x}([Na_2C_2O_4]/I)$, $I(C_2O_4^{2-})$ = integral of the oxalate peak.

[XXVIII] Note that for reactions conducted with 1,4,7-triazacyclononanes (generally in section 4.7), the determined oxalate yield was divided by the efficiency of NaOH extraction (48%) assessed by procedure 4.7.21.

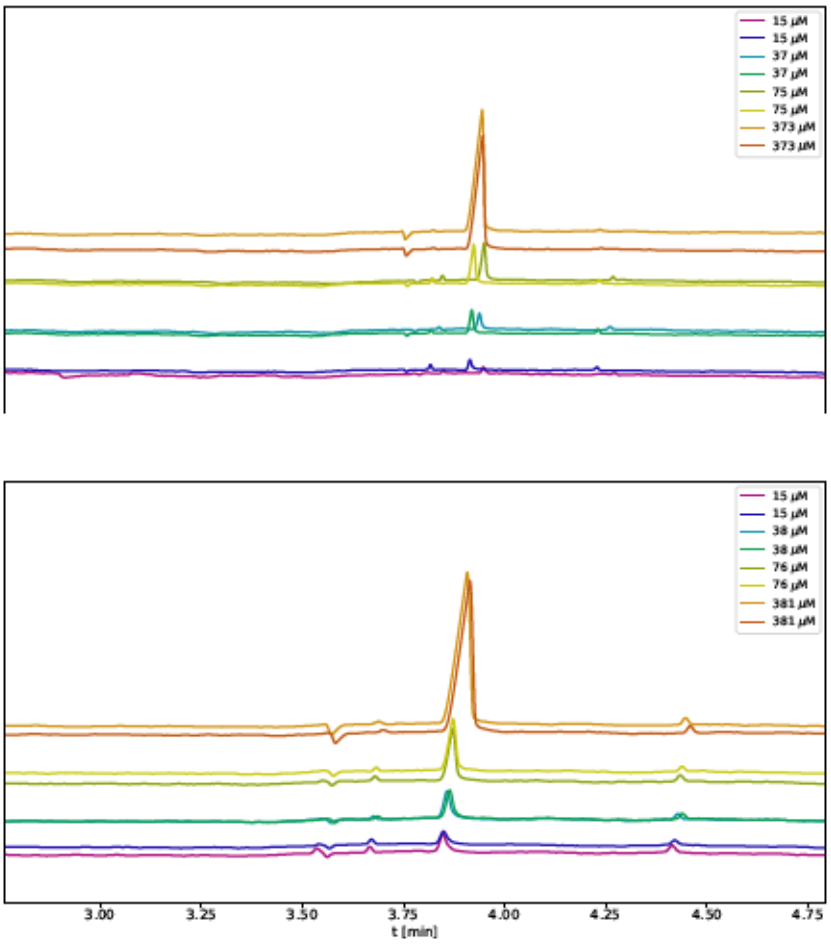

Figure S 337: Electropherograms for $Na_2C_2O_4$ solutions of known concentration for calibration of the CE.

4.15.2 CE Analysis – Reactions with [Fe(tmtaa)]

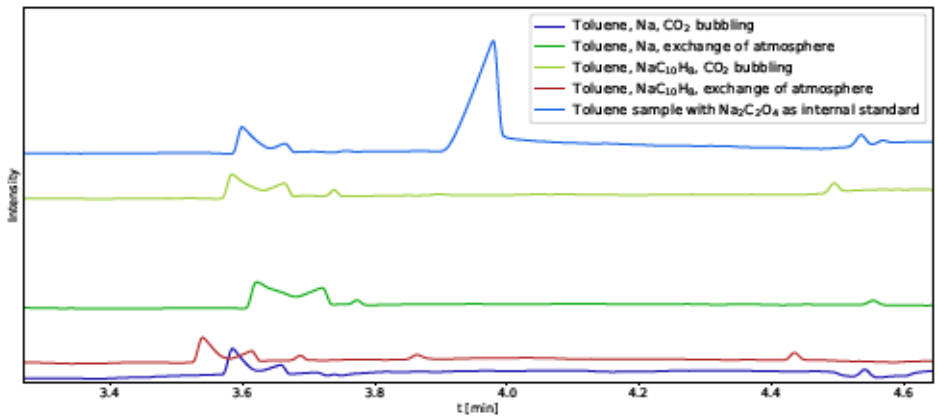

Figure S 338: Capillary electropherogram of the aqueous extract after CO_2 treatment of **118** treated with Na or $NaC_{10}H_8$ (Table S 12, entries 1-4), respectively.

```
Data File C:\Chem32\1\Data\1911\191121\191121-7_MM421-1.D
Sample Name: MM421-1

======================================================================
Acq. Operator   : SYSTEM
Sample Operator : SYSTEM
Acq. Instrument : CE                          Location :  23
Injection Date  : 21/11/2019 16:26:19
Acq. Method     : C:\Chem32\1\Methods\CE\Marx-Oxalate25C-Flush4mV12-191106.M
Last changed    : 12/11/2019 10:53:07 by SYSTEM
Analysis Method : C:\Chem32\1\Methods\CE\Spuel-extended-200227.M
Last changed    : 5/6/2020 16:37:44 by SYSTEM
                  (modified after loading)
Sample Info     : First run on 21.11.19
                  NMR solution of MM421-1 (0.02 mL) diluted with H2O (0.8 mL)

Additional Info : Peak(s) manually integrated
```

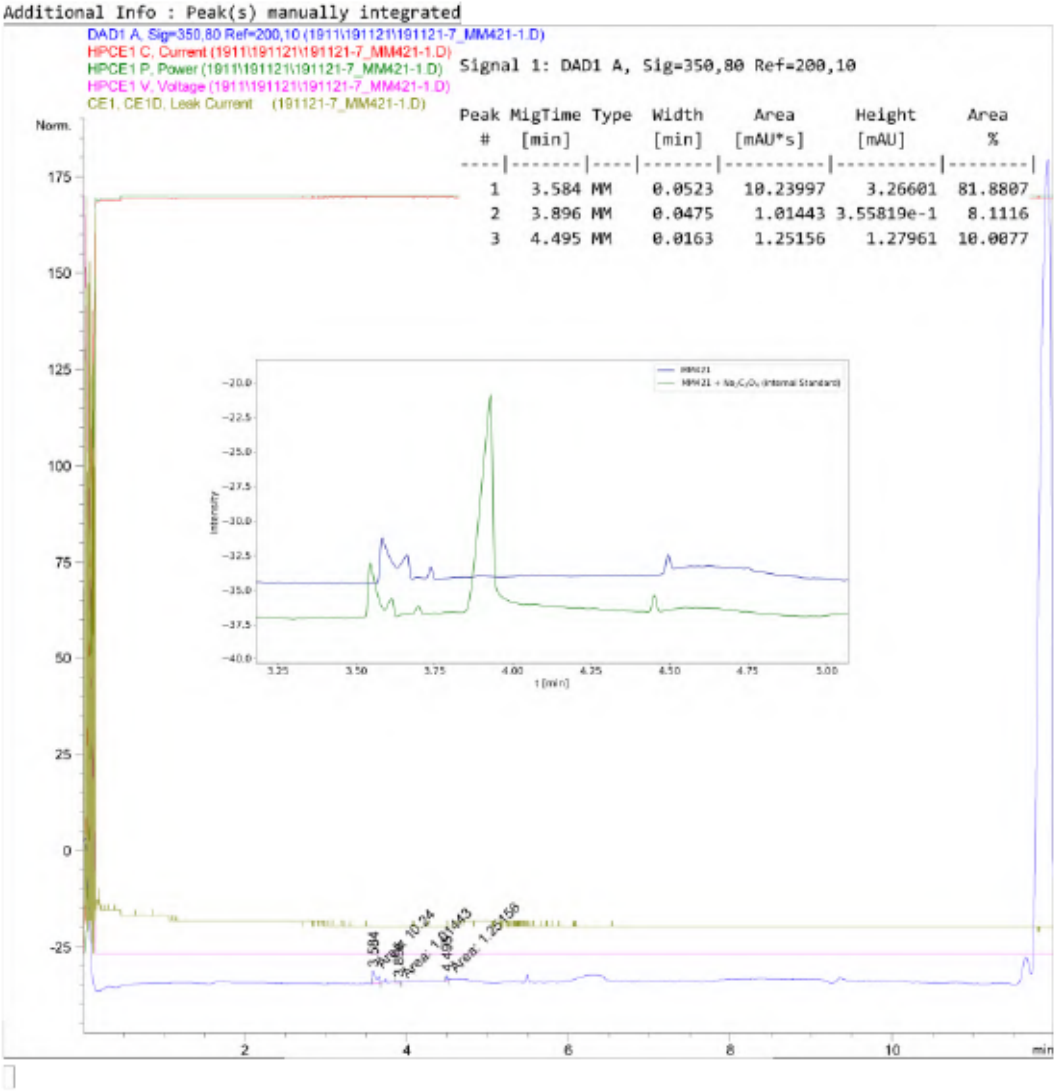


```
CE 5/6/2020 16:56:06 SYSTEM                                Page  1 of 2
```

Figure S 339: Condensed CE analysis of the aqueous extract of the reaction of **118** with $NaC_{10}H_8$ and subsequent CO_2 treatment in toluene (Table S 12, entry 1).

Data File C:\Chem32\1\Data\2002\200226\200226-1_MM439-2.D
Sample Name: MM439-2

Acq. Operator	: SYSTEM
Sample Operator	: SYSTEM
Acq. Instrument	: CE Location : 23
Injection Date	: 26/2/2020 15:52:08
Acq. Method	: C:\Chem32\1\Methods\CE\Marx-Oxalate25C-Flush10mV12-200114.M
Last changed	: 14/1/2020 13:19:47 by SYSTEM
Analysis Method	: C:\Chem32\1\Methods\CE\Spuel-extended-200227.M
Last changed	: 5/6/2020 16:37:44 by SYSTEM (modified after loading)
Sample Info	: NMR solution of MM439-2 (0.02 mL diluted with 0.6 mL H2O)
Additional Info	: Peak(s) manually integrated

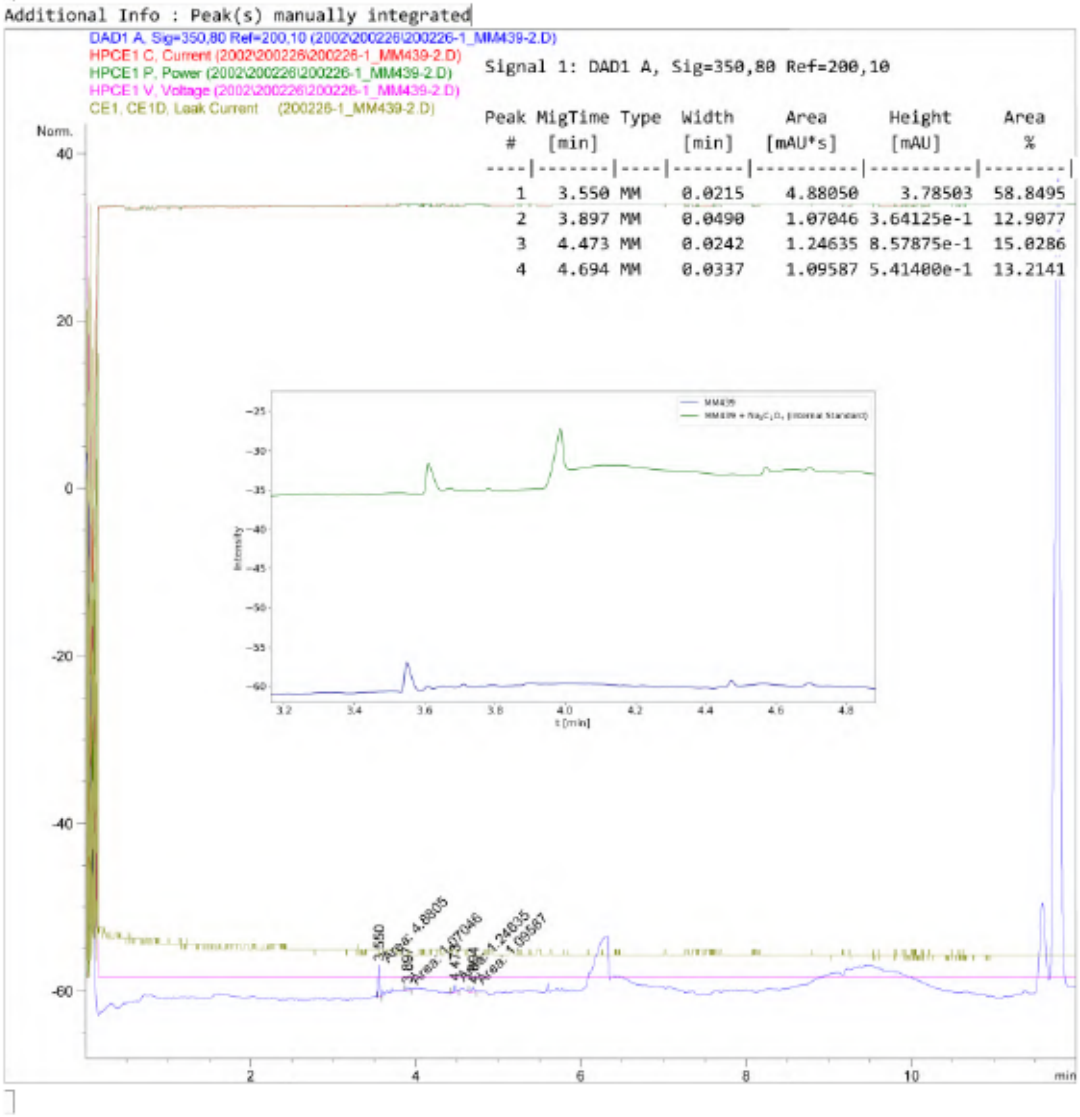

Signal 1: DAD1 A, Sig=350,80 Ref=200,10

Peak #	MigTime [min]	Type	Width [min]	Area [mAU*s]	Height [mAU]	Area %
1	3.550	MM	0.0215	4.88050	3.78503	58.8495
2	3.897	MM	0.0490	1.07046	3.64125e-1	12.9077
3	4.473	MM	0.0242	1.24635	8.57875e-1	15.0286
4	4.694	MM	0.0337	1.09587	5.41400e-1	13.2141

CE 5/6/2020 17:07:52 SYSTEM Page 1 of 2

Figure S 340: Condensed CE analysis of the aqueous extract of the reaction of **118** with $NaC_{10}H_8$ and subsequent CO_2 treatment in toluene (Table S 12, entry 2).

Data File C:\Chem32\1\Data\2001\200114\200114-1_MM425-1.D
Sample Name: MM425-1

Acq. Operator	: SYSTEM		
Sample Operator	: SYSTEM		
Acq. Instrument	: CE	Location :	20
Injection Date	: 14/1/2020 13:32:01		
Acq. Method	: C:\CHEM32\1\METHODS\CE\Marx-Oxalate25C-Flush10mV12-200114.M		
Last changed	: 14/1/2020 13:19:47 by SYSTEM		
Analysis Method	: C:\Chem32\1\Methods\CE\Spuel-extended-200227.M		
Last changed	: 5/6/2020 16:37:44 by SYSTEM (modified after loading)		
Sample Info	: First run, 10 min flush NMR sample of MM425-1 (0.02 mL diluted with 0.6 mL H2O)		
Additional Info	: Peak(s) manually integrated		

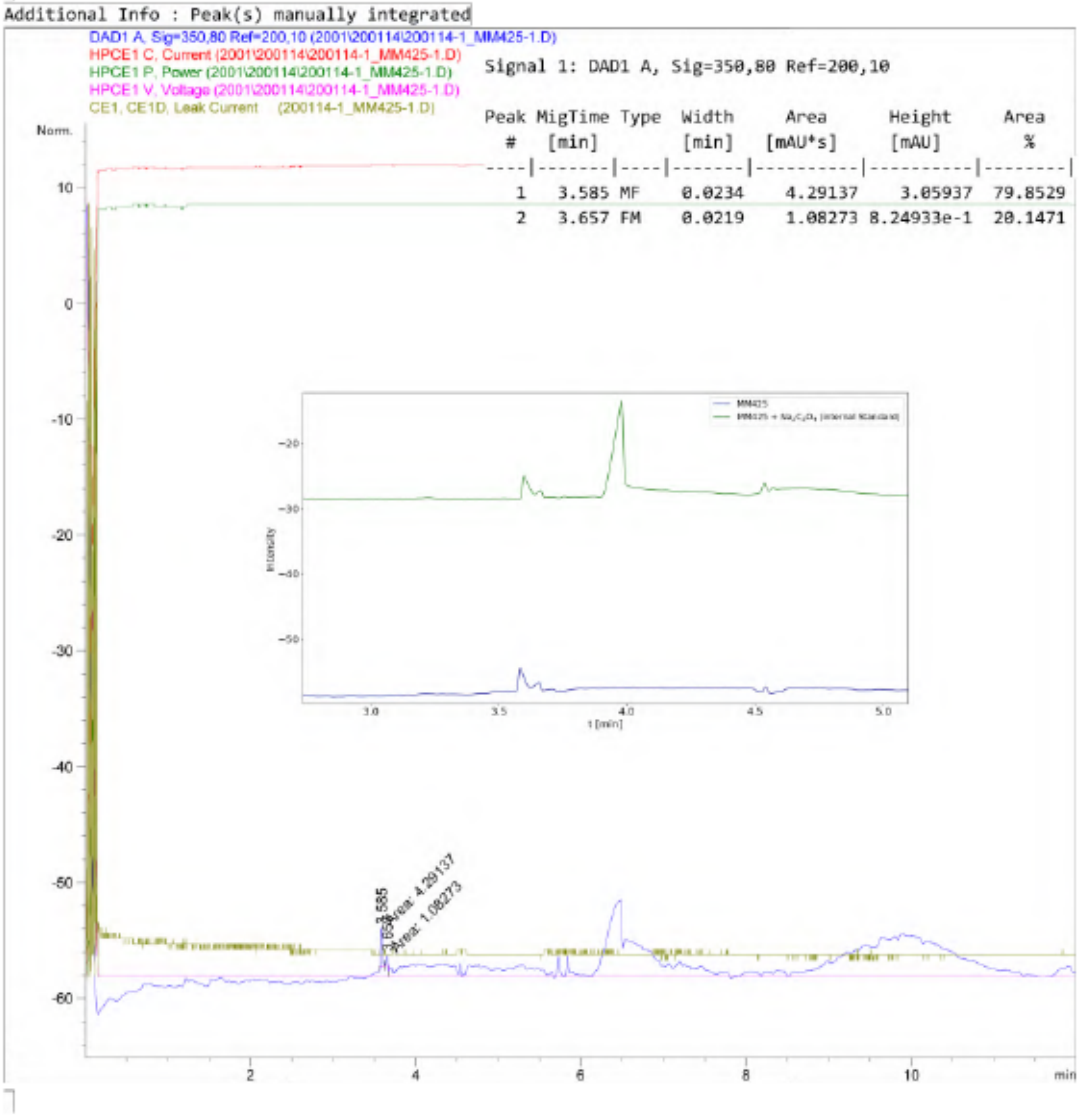

CE 5/6/2020 17:04:42 SYSTEM Page 1 of 2

Figure S 341: Condensed CE analysis of the aqueous extract of the reaction of **118** with Na and subsequent CO_2 treatment in toluene (Table S 12, entry 3).

Data File C:\Chem32\1\Data\2006\200602\200602-1_MM515-1.D
Sample Name: MM515-1

Acq. Operator	: SYSTEM	
Sample Operator	: SYSTEM	
Acq. Instrument	: CE	Location : 25
Injection Date	: 2/6/2020 16:11:30	
Acq. Method	: C:\Chem32\1\Methods\CE\Marx-Oxalate25C-Flush10mV12-200114.M	
Last changed	: 14/1/2020 13:19:47 by SYSTEM	
Analysis Method	: C:\Chem32\1\Methods\CE\Spuel-extended-200227.M	
Last changed	: 2/6/2020 18:47:32 by SYSTEM (modified after loading)	
Sample Info	: NMR solution of MM515-1 (0.2 mL) diluted with H2O (0.4 ml)	
Additional Info	: Peak(s) manually integrated	

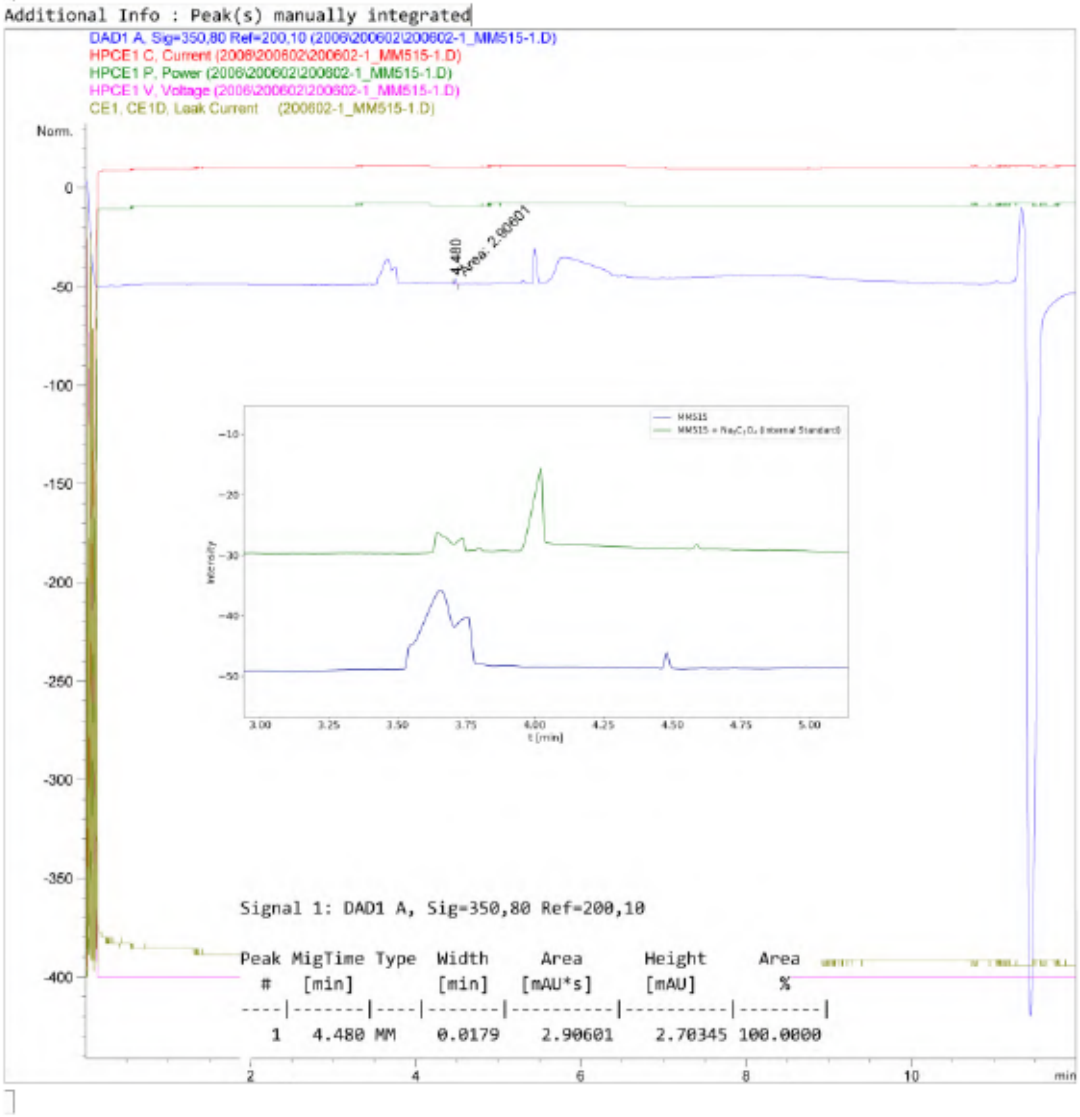

CE 2/6/2020 20:11:33 SYSTEM Page 1 of 2

Figure S 342: Condensed CE analysis of the aqueous extract of the reaction of **118** with Na and subsequent CO_2 treatment in toluene (Table S 12, entry 4).

Data File C:\Chem32\1\Data\2006\200602\200602-2_MM521-1.D
Sample Name: MM521-1

Acq. Operator	: SYSTEM
Sample Operator	: SYSTEM
Acq. Instrument	: CE Location : 26
Injection Date	: 2/6/2020 16:35:01
Acq. Method	: C:\Chem32\1\Methods\CE\Marx-Oxalate25C-Flush10mV12-200114.M
Last changed	: 14/1/2020 13:19:47 by SYSTEM
Analysis Method	: C:\Chem32\1\Methods\CE\Spuel-extended-200227.M
Last changed	: 2/6/2020 18:47:32 by SYSTEM (modified after loading)
Sample Info	: NMR solution of MM521-1 (0.2 mL) diluted with H2O (0.4 ml)
Additional Info	: Peak(s) manually integrated

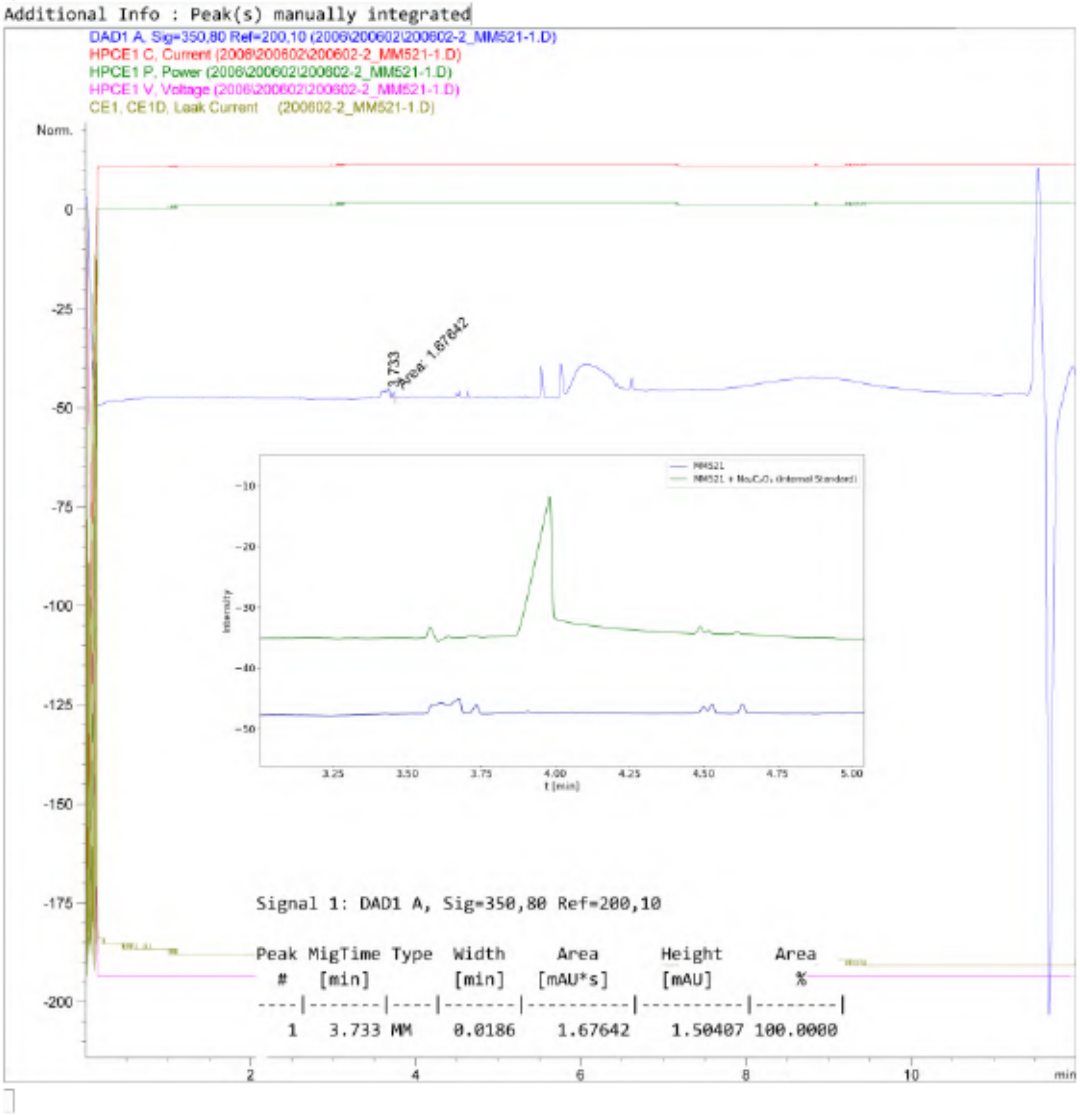

CE 2/6/2020 20:11:54 SYSTEM Page 1 of 2

Figure S 343: Condensed CE analysis of the aqueous extract of the reaction of **118** with K and subsequent CO_2 treatment in toluene (Table S 12, entry 5).

Data File C:\Chem32\1\Data\2006\200602\200602-4_MM545-1.D
Sample Name: MM545-1

Acq. Operator	: SYSTEM
Sample Operator	: SYSTEM
Acq. Instrument	: CE Location : 30
Injection Date	: 2/6/2020 17:22:06
Acq. Method	: C:\Chem32\1\Methods\CE\Marx-Oxalate25C-Flush10mV12-200114.M
Last changed	: 14/1/2020 13:19:47 by SYSTEM
Analysis Method	: C:\Chem32\1\Methods\CE\Spuel-extended-200227.M
Last changed	: 5/6/2020 16:37:44 by SYSTEM (modified after loading)
Sample Info	: NMR solution of MM545-1 (0.2 mL) diluted with H2O (0.4 ml)
Additional Info	: Peak(s) manually integrated

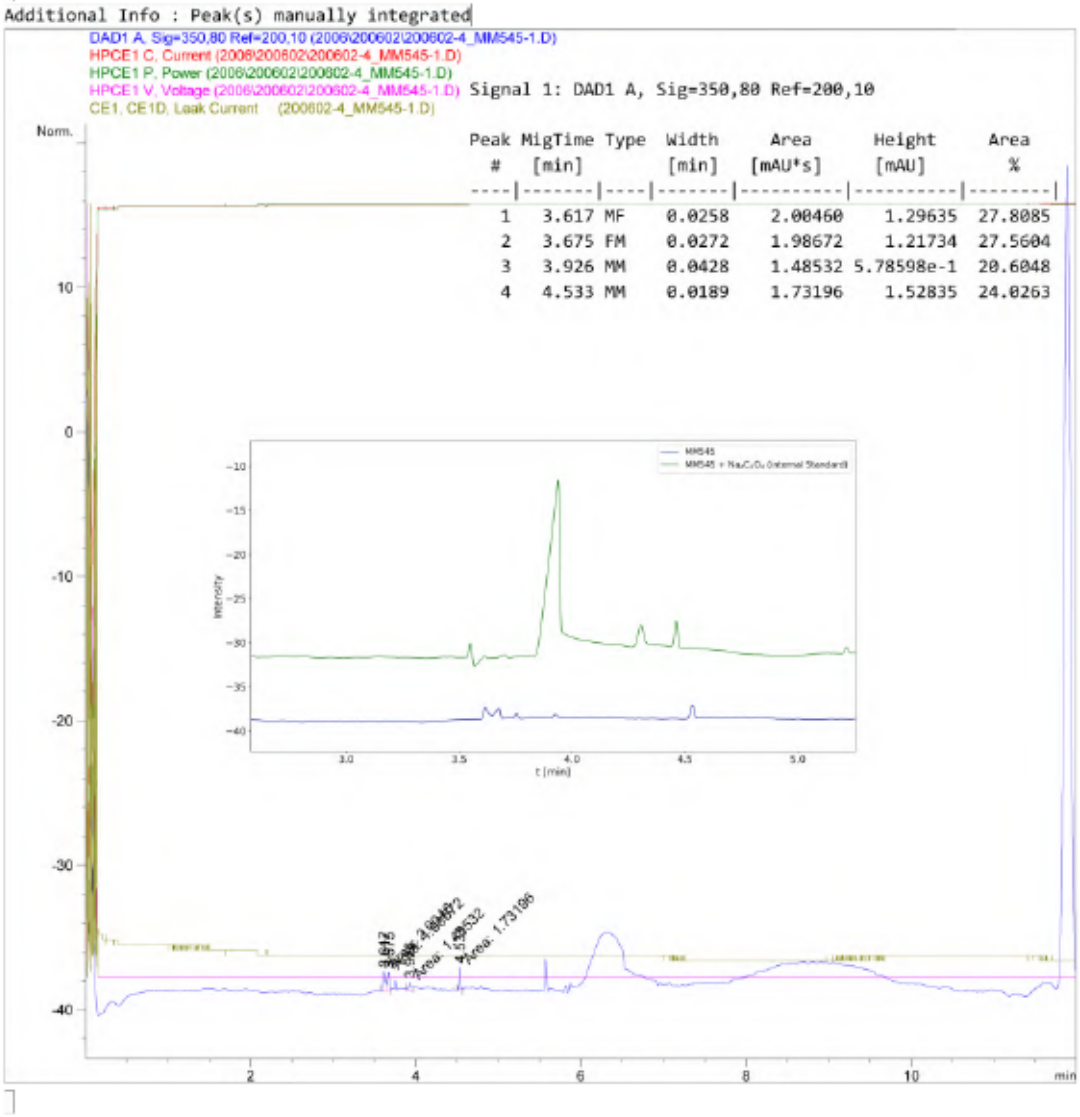

CE 5/6/2020 17:39:09 SYSTEM Page 1 of 2

Figure S 344: Condensed CE analysis of the aqueous extract of the reaction of **118** with K and subsequent CO_2 treatment in toluene (Table S 12, entry 6).

Data File C:\Chem32\1\Data\2006\200619\200619-1_MM577.D
Sample Name: MM577

Acq. Operator	: SYSTEM		
Sample Operator	: SYSTEM		
Acq. Instrument	: CE	Location :	15
Injection Date	: 19/6/2020 12:12:40		
Acq. Method	: C:\Chem32\1\Methods\CE\Marx-Oxalate25C-Flush10mV12-200114.M		
Last changed	: 14/1/2020 13:19:47 by SYSTEM		
Analysis Method	: C:\Chem32\1\Methods\CE\SwitchOff-200227.M		
Last changed	: 19/6/2020 14:38:54 by SYSTEM (modified after loading)		
Sample Info	: NMR solution of MM577 (0.20 mL) diluted with H2O (0.4 ml)		
Additional Info	: Peak(s) manually integrated		

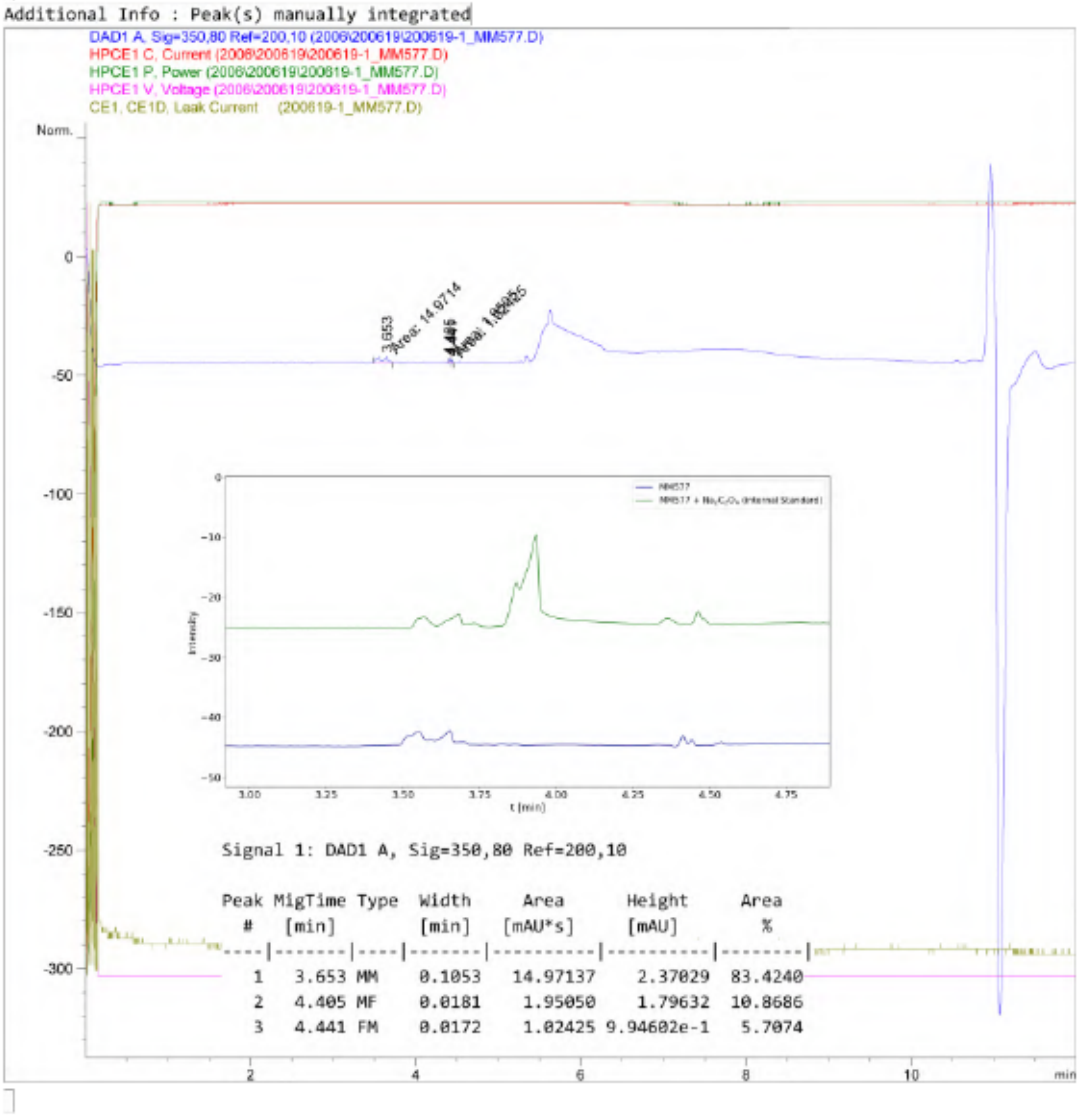

Signal 1: DAD1 A, Sig=350,80 Ref=200,10

Peak #	MigTime [min]	Type	Width [min]	Area [mAU*s]	Height [mAU]	Area %
1	3.653	MM	0.1053	14.97137	2.37029	83.4240
2	4.405	MF	0.0181	1.95050	1.79632	10.8686
3	4.441	FM	0.0172	1.02425	9.94602e-1	5.7074

Figure S 345: Condensed CE analysis of the aqueous extract of the reaction of **118** with K and subsequent CO_2 treatment in toluene (Table S 12, entry 7).

Data File C:\Chem32\1\Data\2006\200602\200602-3_MM532-1.D
Sample Name: MM532-1

Acq. Operator	: SYSTEM		
Sample Operator	: SYSTEM		
Acq. Instrument	: CE	Location :	28
Injection Date	: 2/6/2020 16:58:36		
Acq. Method	: C:\Chem32\1\Methods\CE\Marx-Oxalate25C-Flush10mV12-200114.M		
Last changed	: 14/1/2020 13:19:47 by SYSTEM		
Analysis Method	: C:\Chem32\1\Methods\CE\Spuel-extended-200227.M		
Last changed	: 2/6/2020 18:47:32 by SYSTEM (modified after loading)		
Sample Info	: NMR solution of MM532-1 (0.2 mL) diluted with H2O (0.4 ml)		
Additional Info	: Peak(s) manually integrated		

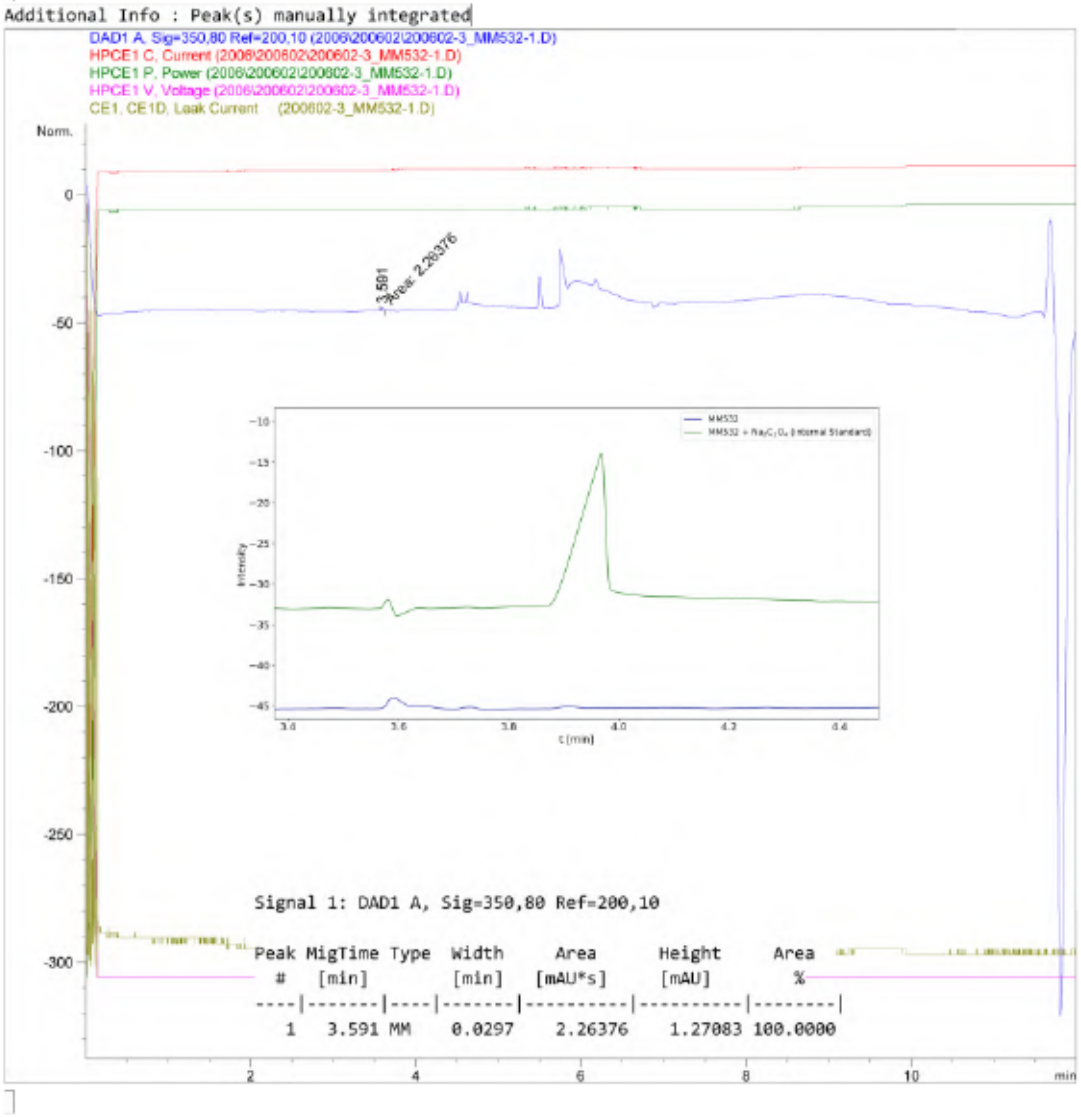

Signal 1: DAD1 A, Sig=350,80 Ref=200,10

Peak #	MigTime [min]	Type	Width [min]	Area [mAU*s]	Height [mAU]	Area %
1	3.591	MM	0.0297	2.26376	1.27083	100.0000

Figure S 346: Condensed CE analysis of the aqueous extract of the reaction of **118** with K and subsequent CO_2 treatment in THF (Table S 12, entry 8).

Data File C:\Chem32\1\Data\2005\200527\200527-4_MM555-1.D
Sample Name: MM555-1

Acq. Operator	: SYSTEM
Sample Operator	: SYSTEM
Acq. Instrument	: CE Location : 20
Injection Date	: 27/5/2020 14:32:34
Acq. Method	: C:\Chem32\1\Methods\CE\Marx-Oxalate25C-Flush10mV23-V13-200428.M
Last changed	: 28/4/2020 15:34:00 by SYSTEM
Analysis Method	: C:\Chem32\1\Methods\CE\Spuel-extended-200227.M
Last changed	: 27/5/2020 14:08:30 by SYSTEM (modified after loading)
Sample Info	: NMR solution of MM555-1 (0.03 mL diluted with 0.6 mL H2O)
Additional Info	: Peak(s) manually integrated

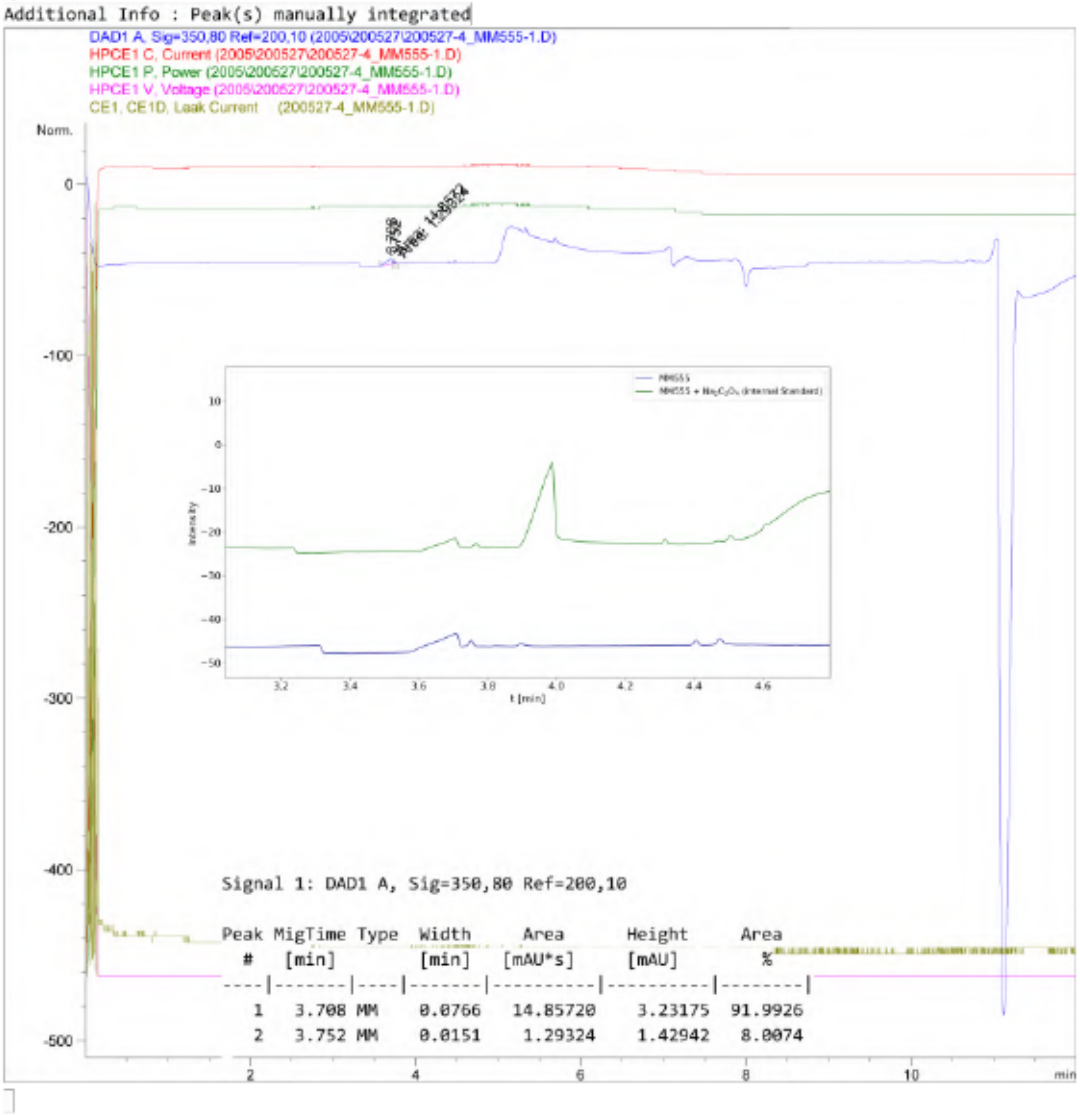

Signal 1: DAD1 A, Sig=350,80 Ref=200,10

Peak #	MigTime [min]	Type	Width [min]	Area [mAU*s]	Height [mAU]	Area %
1	3.708	MM	0.0766	14.85720	3.23175	91.9926
2	3.752	MM	0.0151	1.29324	1.42942	8.0074

CE 27/5/2020 17:18:59 SYSTEM Page 1 of 2

Figure S 347: Condensed CE analysis of the aqueous extract of the reaction of **118** with K and subsequent CO_2 treatment in THF (Table S 12, entry 9).

4.15.3 CE analysis – Reactions of 1,4,7-Tacn-ligated Cu Complexes

Data File C:\Chem32\1\Data\1911\191112\191112-5_MM406-1.D
Sample Name: MM406-1

```
==========================================================================
Acq. Operator   : SYSTEM
Sample Operator : SYSTEM
Acq. Instrument : CE                                Location :   23
Injection Date  : 12/11/2019 12:49:01
Acq. Method     : C:\Chem32\1\Methods\CE\Marx-Oxalate25C-Flush4mV12-191106.M
Last changed    : 12/11/2019 10:53:07 by SYSTEM
Analysis Method : C:\Chem32\1\Methods\CE\Spuel-extended.M
Last changed    : 21/11/2019 14:20:04 by SYSTEM
                  (modified after loading)
Sample Info     : NMR solution of MM406-1 (0.02 mL diluted with 0.8 mL H2O)
                  5 min flush, first run on 12.11.19

Additional Info : Peak(s) manually integrated
```

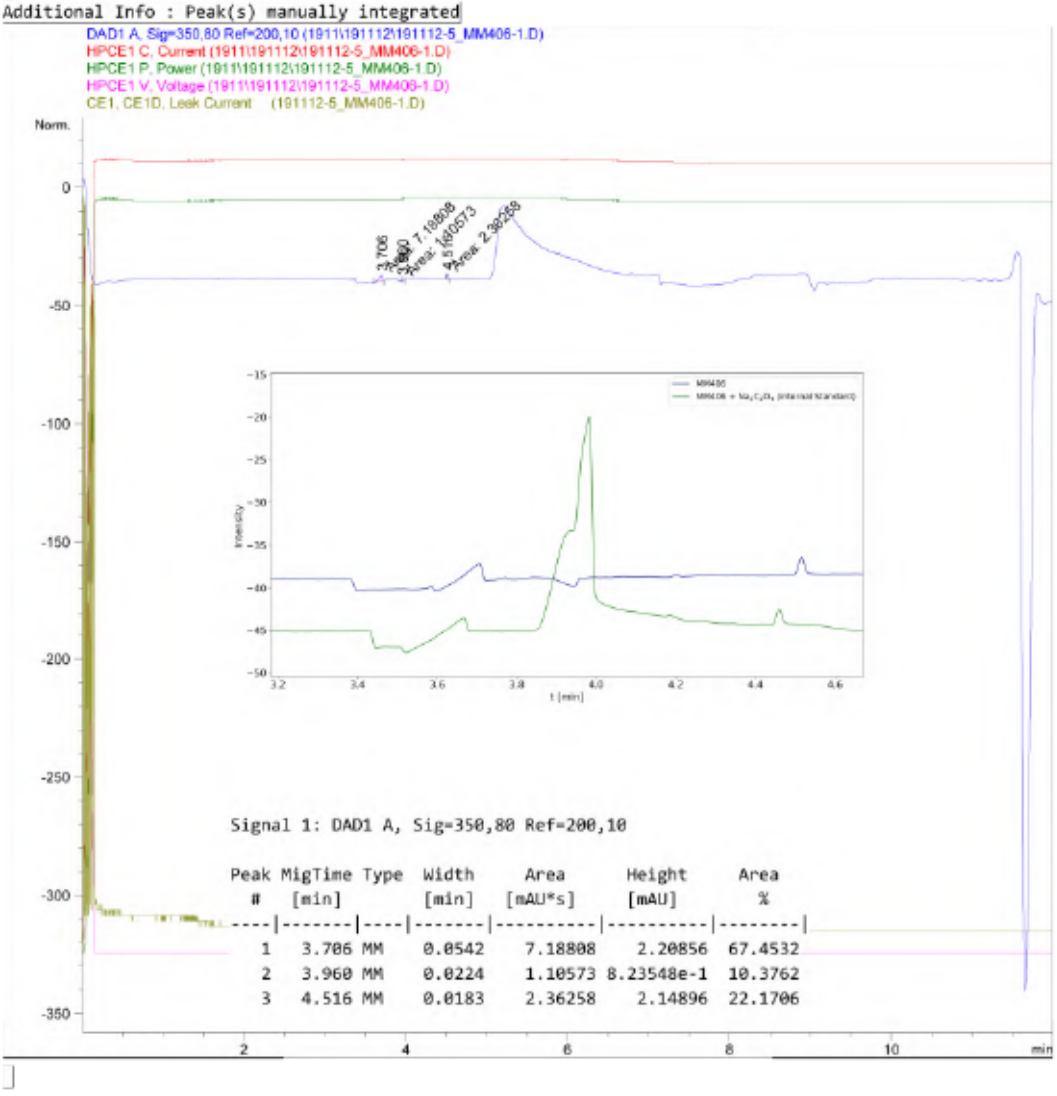

Signal 1: DAD1 A, Sig=350,80 Ref=200,10

Peak #	MigTime [min]	Type	Width [min]	Area [mAU*s]	Height [mAU]	Area %
1	3.706	MM	0.0542	7.18808	2.20856	67.4532
2	3.960	MM	0.0224	1.10573	8.23548e-1	10.3762
3	4.516	MM	0.0183	2.36258	2.14896	22.1706

CE 21/11/2019 19:06:05 SYSTEM Page 1 of 2

Figure S 348: Condensed CE analysis for the NaOH extract of Table S 13, entry 3 – CO_2 treatment (bubbling) of **127**, CuI and $NaBPh_4$ in MeOH.

```
Data File C:\Chem32\1\Data\2006\200616\200616-10_MM572.D
Sample Name: MM572

======================================================================
Acq. Operator   : SYSTEM
Sample Operator : SYSTEM
Acq. Instrument : CE                              Location :  39
Injection Date  : 16/6/2020 16:51:22
Acq. Method     : C:\Chem32\1\Methods\CE\Marx-Oxalate25C-Flush10mV12-200114.M
Last changed    : 14/1/2020 13:19:47 by SYSTEM
Analysis Method : C:\Chem32\1\Methods\CE\Spuel-extended-200227.M
Last changed    : 16/6/2020 14:26:33 by SYSTEM
                  (modified after loading)
Sample Info     : NMR solution of MM572 (0.04 mL) diluted w. H2O (0.6 ml)

Additional Info : Peak(s) manually integrated
```

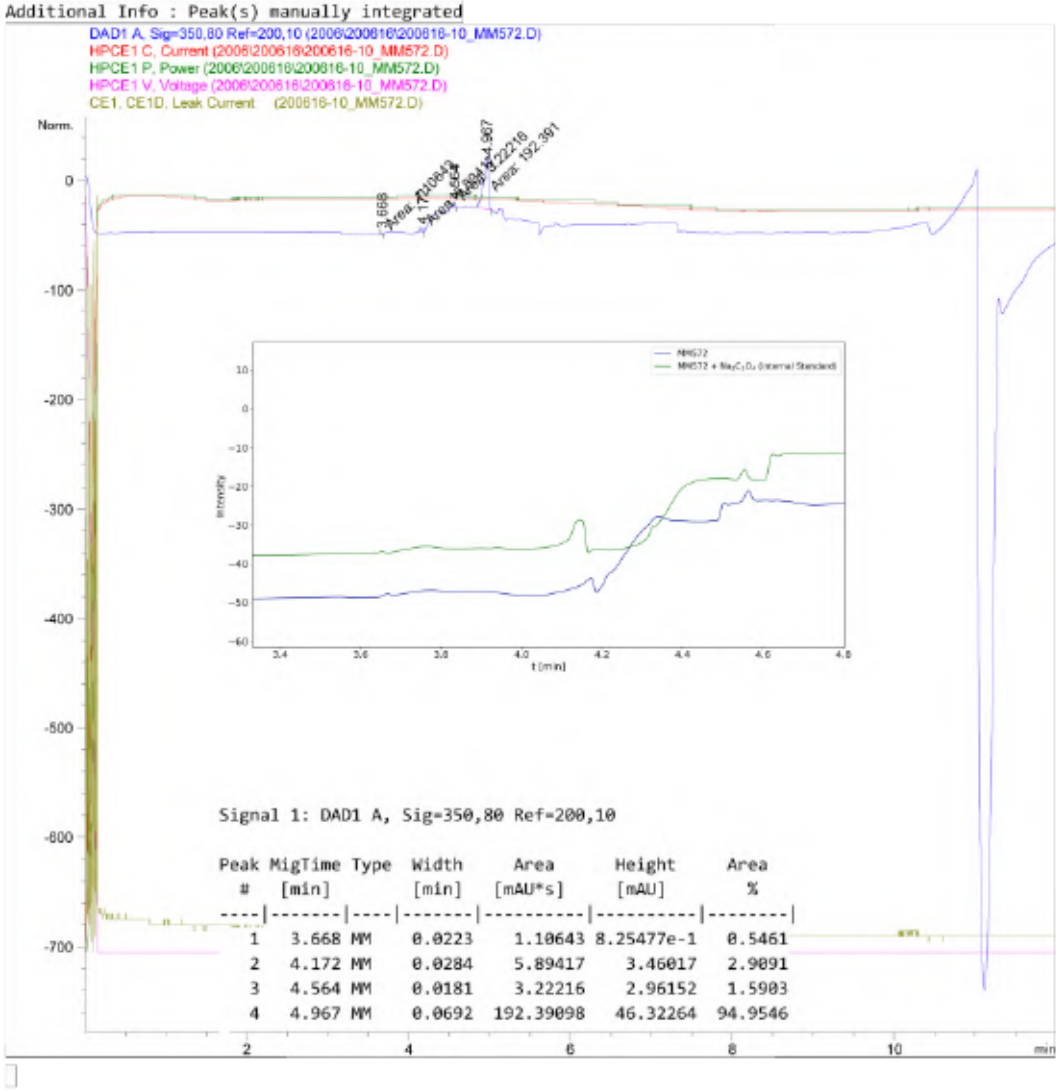

Signal 1: DAD1 A, Sig=350,80 Ref=200,10

Peak #	MigTime [min]	Type	Width [min]	Area [mAU*s]	Height [mAU]	Area %
1	3.668	MM	0.0223	1.10643	8.25477e-1	0.5461
2	4.172	MM	0.0284	5.89417	3.46017	2.9091
3	4.564	MM	0.0181	3.22216	2.96152	1.5903
4	4.967	MM	0.0692	192.39098	46.32264	94.9546

```
CE 16/6/2020 19:48:46 SYSTEM                              Page  1 of 2
```

Figure S 349: Condensed CE analysis for the NaOH extract of Table S 13, entry 4 – CO_2 treatment (bubbling) of **127**, CuI and $NaBPh_4$ in MeOH.

Data File C:\Chem32\1\Data\2006\200616\200616-8_MM571.D
Sample Name: MM571

```
==================================================================
Acq. Operator   : SYSTEM
Sample Operator : SYSTEM
Acq. Instrument : CE                          Location :   38
Injection Date  : 16/6/2020 15:47:21
Acq. Method     : C:\Chem32\1\Methods\CE\Marx-Oxalate25C-Flush10mV23-V13-200428.M
Last changed    : 28/4/2020 15:34:00 by SYSTEM
Analysis Method : C:\Chem32\1\Methods\CE\Spuel-extended-200227.M
Last changed    : 16/6/2020 14:26:33 by SYSTEM
                  (modified after loading)
Sample Info     : NMR solution of MM571 (0.04 mL) diluted w. H2O (0.6 ml)

Additional Info : Peak(s) manually integrated
```

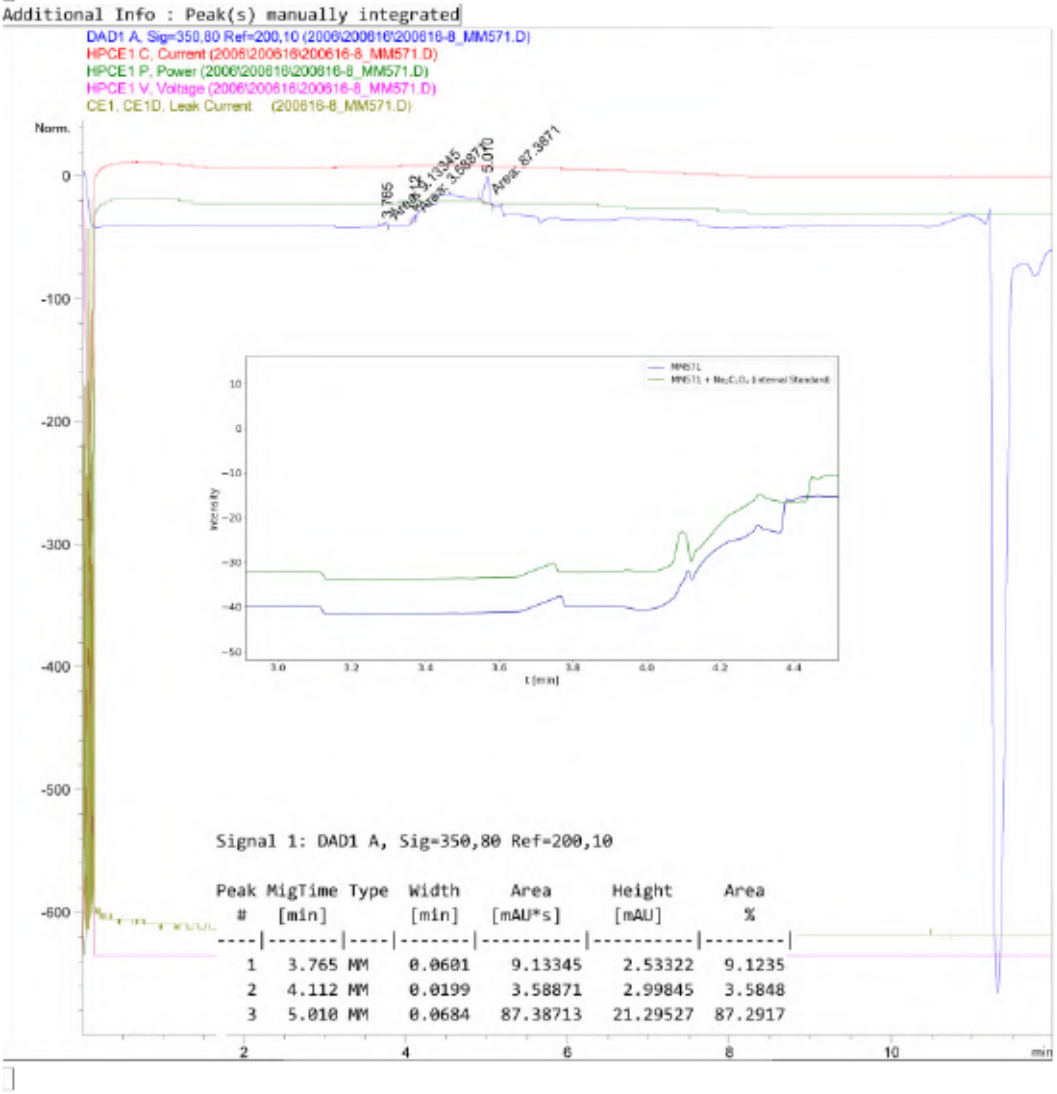

Signal 1: DAD1 A, Sig=350,80 Ref=200,10

Peak #	MigTime [min]	Type	Width [min]	Area [mAU*s]	Height [mAU]	Area %
1	3.765	MM	0.0601	9.13345	2.53322	9.1235
2	4.112	MM	0.0199	3.58871	2.99845	3.5848
3	5.010	MM	0.0684	87.38713	21.29527	87.2917

CE 16/6/2020 18:43:43 SYSTEM Page 1 of 2

Figure S 350: Condensed CE analysis for the NaOH extract of Table S 13, entry 5 – CO_2 treatment (bubbling) of **127**, CuI and $NaBPh_4$ in MeOH.

Data File C:\Chem32\1\Data\2006\200626\200626-1_MM592.D
Sample Name: MM592

Acq. Operator	: SYSTEM
Sample Operator	: SYSTEM
Acq. Instrument	: CE Location : 33
Injection Date	: 26/6/2020 10:53:04
Acq. Method	: C:\Chem32\1\Methods\CE\Marx-Oxalate25C-Flush10mV12-200114.M
Last changed	: 14/1/2020 13:19:47 by SYSTEM
Analysis Method	: C:\Chem32\1\Methods\CE\SwitchOff-200227.M
Last changed	: 26/6/2020 11:11:38 by SYSTEM (modified after loading)
Sample Info	: NMR sample of MM592 (0.04 mL) diluted with H2O (0.6 ml)
Additional Info	: Peak(s) manually integrated

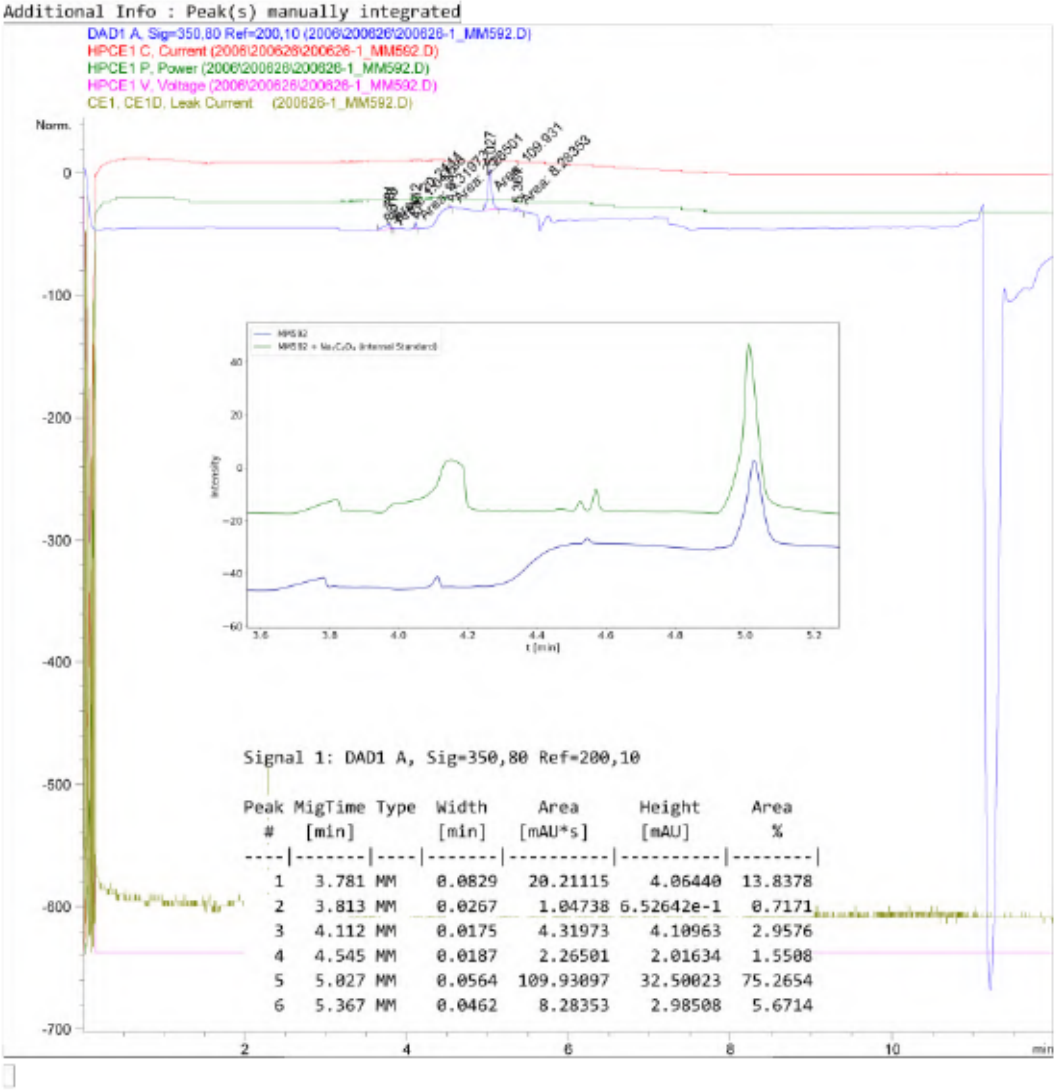

Signal 1: DAD1 A, Sig=350,80 Ref=200,10

Peak #	MigTime [min]	Type	Width [min]	Area [mAU*s]	Height [mAU]	Area %
1	3.781	MM	0.0829	20.21115	4.06440	13.8378
2	3.813	MM	0.0267	1.04738	6.52642e-1	0.7171
3	4.112	MM	0.0175	4.31973	4.10963	2.9576
4	4.545	MM	0.0187	2.26501	2.01634	1.5508
5	5.027	MM	0.0564	109.93097	32.50023	75.2654
6	5.367	MM	0.0462	8.28353	2.98508	5.6714

CE 26/6/2020 12:29:05 SYSTEM Page 1 of 2

Figure S 351: Condensed CE analysis for the NaOH extract of Table S 13, entry 6 – CO_2 treatment (bubbling) of **127**, CuI and $NaBPh_4$ in MeOH.

Data File C:\Chem32\1\Data\1911\191112\191112-3_MM404-1.D
Sample Name: MM404-1

```
==================================================================
Acq. Operator    : SYSTEM
Sample Operator  : SYSTEM
Acq. Instrument  : CE                          Location :   21
Injection Date   : 12/11/2019 11:59:33
Acq. Method      : C:\Chem32\1\Methods\CE\Marx-Oxalate25C-Flush4mV12-191106.M
Last changed     : 12/11/2019 11:24:12 by SYSTEM
Analysis Method  : C:\Chem32\1\Methods\CE\Marx-Oxalate25C-Flush10mV23-V13-200428.M
Last changed     : 27/8/2020 16:36:34 by SYSTEM
                   (modified after loading)
Method Info      : 02.10.2019 Methode geändert auf Agilent Organic Acids Kit

Sample Info      : NMR solution of MM404-1 (0.02 mL diluted with 0.8 mL H2O)
                   5 min flush, first run on 12.11.19

Additional Info : Peak(s) manually integrated
```

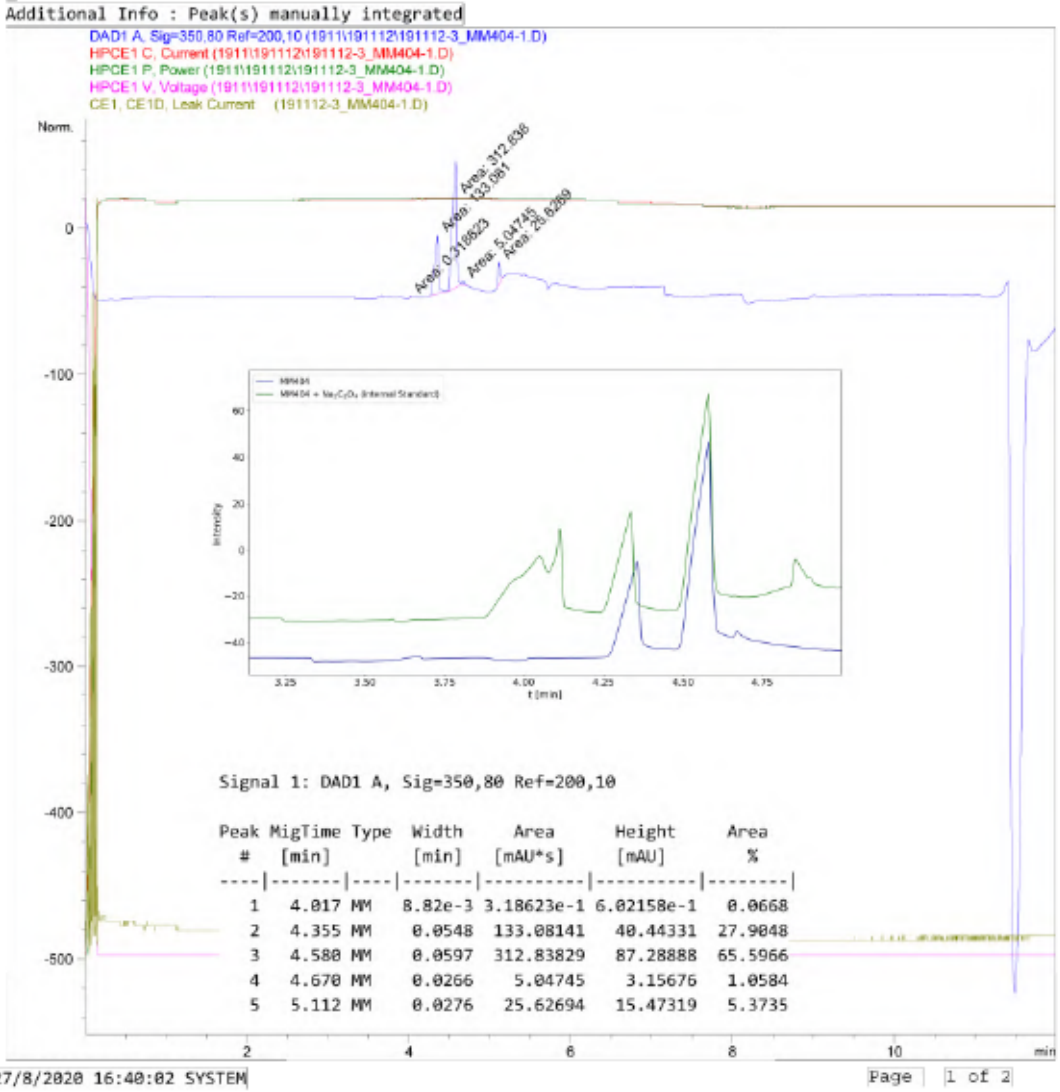

Peak #	MigTime [min]	Type	Width [min]	Area [mAU*s]	Height [mAU]	Area %
1	4.017	MM	8.82e-3	3.18623e-1	6.02158e-1	0.0668
2	4.355	MM	0.0548	133.08141	40.44331	27.9048
3	4.588	MM	0.0597	312.83829	87.28888	65.5966
4	4.670	MM	0.0266	5.04745	3.15676	1.0584
5	5.112	MM	0.0276	25.62694	15.47319	5.3735

CE 27/8/2020 16:40:02 SYSTEM Page 1 of 2

Figure S 352: Condensed CE analysis for the NaOH extract of Table S 13, entry 7 – CO_2 treatment (bubbling) of **127**, CuI and $NaPF_6$ in MeOH.

Data File C:\Chem32\1\Data\1911\191112\191112-4_MM405-1.D
Sample Name: MM405-1

```
======================================================================
Acq. Operator   : SYSTEM
Sample Operator : SYSTEM
Acq. Instrument : CE                          Location :   22
Injection Date  : 12/11/2019 12:25:32
Acq. Method     : C:\Chem32\1\Methods\CE\Marx-Oxalate25C-Flush4mV12-191106.M
Last changed    : 12/11/2019 10:53:07 by SYSTEM
Analysis Method : C:\Chem32\1\Methods\CE\Marx-Oxalate25C-Flush10mV23-V13-200428.M
Last changed    : 27/8/2020 16:36:34 by SYSTEM
                  (modified after loading)
Method Info     : 02.10.2019 Methode geändert auf Agilent Organic Acids Kit

Sample Info     : NMR solution of MM405-1 (0.02 mL diluted with 0.8 mL H2O)
                  5 min flush, first run on 12.11.19

Additional Info : Peak(s) manually integrated
```

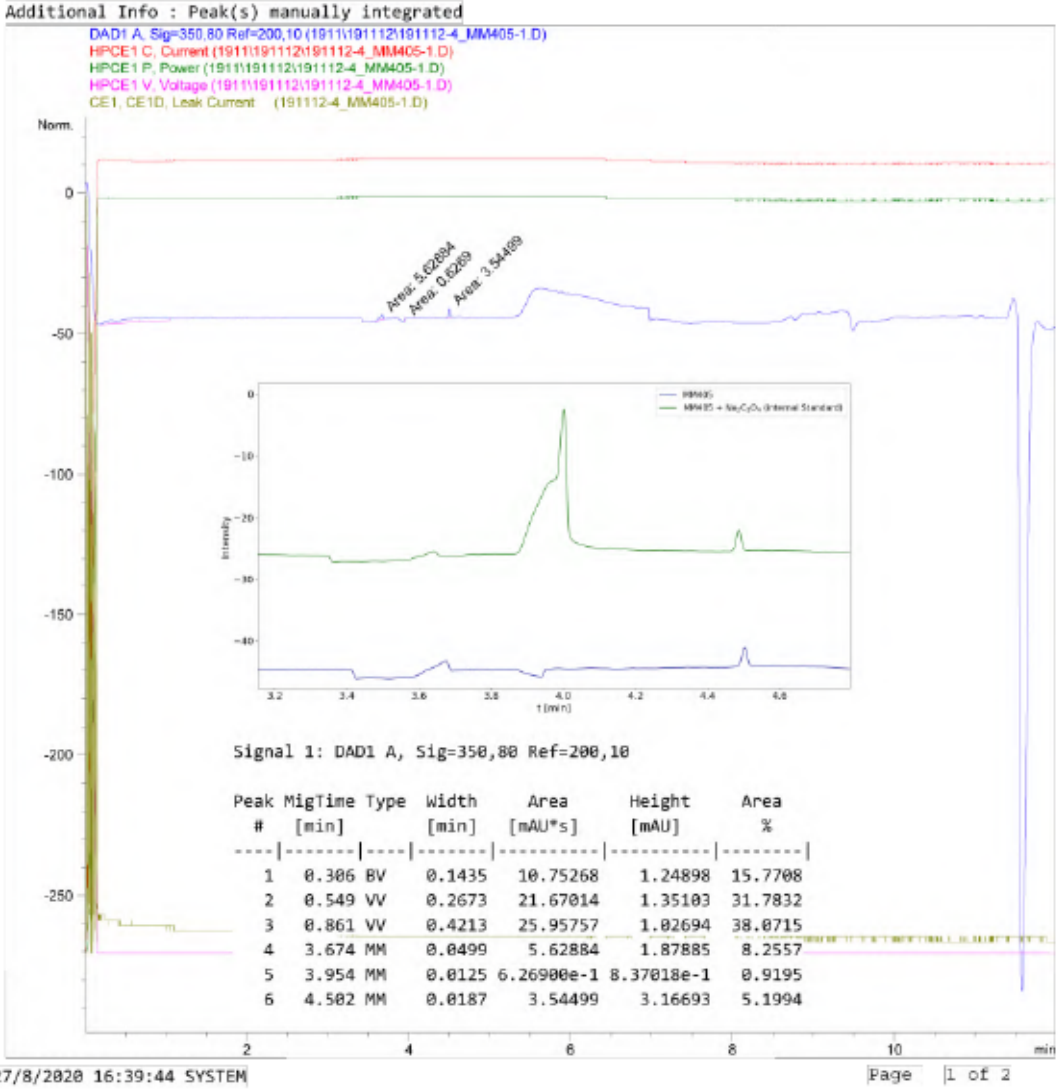

Signal 1: DAD1 A, Sig=350,80 Ref=200,10

Peak #	MigTime [min]	Type	Width [min]	Area [mAU*s]	Height [mAU]	Area %
1	0.306	BV	0.1435	10.75268	1.24898	15.7708
2	0.549	VV	0.2673	21.67014	1.35103	31.7832
3	0.861	VV	0.4213	25.95757	1.02694	38.0715
4	3.674	MM	0.0499	5.62884	1.87885	8.2557
5	3.954	MM	0.0125	6.26900e-1	8.37018e-1	0.9195
6	4.582	MM	0.0187	3.54499	3.16693	5.1994

CE 27/8/2020 16:39:44 SYSTEM Page 1 of 2

Figure S 353: Condensed CE analysis for the NaOH extract of Table S 13, entry 8 – CO_2 treatment (bubbling) of **127**, CuI and $NaBPh_4$ in MeOH/THF.

Data File C:\Chem32\1\Data\2004\200428\200428-3_MM536-1.D
Sample Name: MM536-1

```
=====================================================================
Acq. Operator   : SYSTEM
Sample Operator : SYSTEM
Acq. Instrument : CE                              Location :   37
Injection Date  : 28/4/2020 13:17:48
Acq. Method     : C:\Chem32\1\Methods\CE\Marx-Oxalate25C-Flush10mV12-200114.M
Last changed    : 14/1/2020 13:19:47 by SYSTEM
Analysis Method : C:\Chem32\1\Methods\CE\Spuel-extended-200227.M
Last changed    : 5/6/2020 16:37:44 by SYSTEM
                  (modified after loading)
Sample Info     : NMR sample of MM536-1 (0.03 mL diluted with 0.6 mL H2O)

Additional Info : Peak(s) manually integrated
```

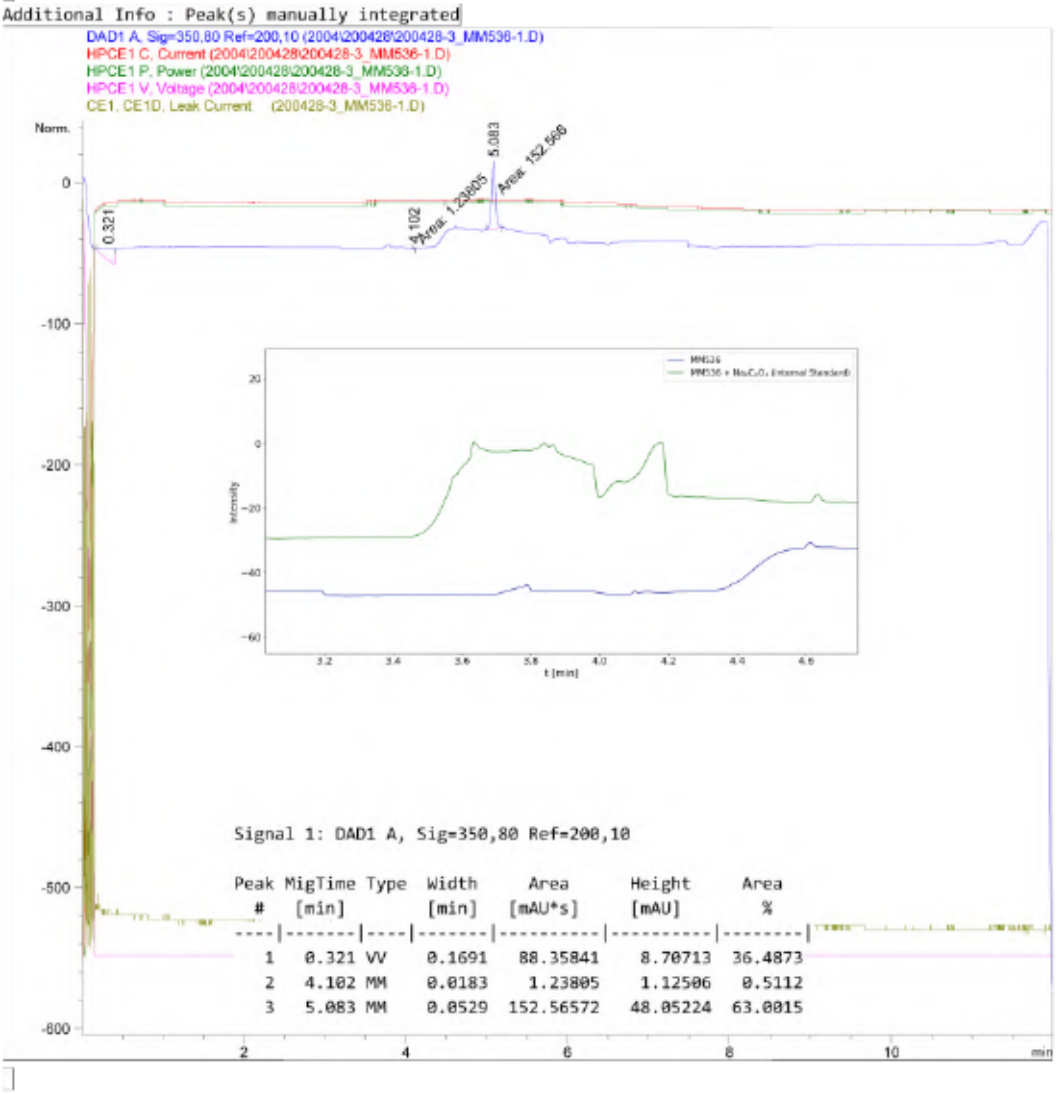

Signal 1: DAD1 A, Sig=350,80 Ref=200,10

Peak #	MigTime [min]	Type	Width [min]	Area [mAU*s]	Height [mAU]	Area %
1	0.321	VV	0.1691	88.35841	8.70713	36.4873
2	4.102	MM	0.0183	1.23805	1.12506	0.5112
3	5.083	MM	0.0529	152.56572	48.05224	63.0015

CE 5/6/2020 17:22:50 SYSTEM Page 1 of 2

Figure S 354: Condensed CE analysis for the NaOH extract of Table S 14, entry 2 – $CsHCO_3$ treatment of **127**, CuI and $NaBPh_4$ in MeOH.

Data File C:\Chem32\1\Data\2006\200610\200610-3_MM567.D
Sample Name: MM567

Acq. Operator	: SYSTEM
Sample Operator	: SYSTEM
Acq. Instrument	: CE Location : 27
Injection Date	: 10/6/2020 14:54:13
Acq. Method	: C:\Chem32\1\Methods\CE\Marx-Oxalate25C-Flush10mV12-200114.M
Last changed	: 14/1/2020 13:19:47 by SYSTEM
Analysis Method	: C:\Chem32\1\Methods\CE\Spuel-extended-200227.M
Last changed	: 10/6/2020 15:17:04 by SYSTEM (modified after loading)
Sample Info	: NMR solution of MM567 (0.04 mL) diluted with H2O (0.6 mL)
Additional Info	: Peak(s) manually integrated

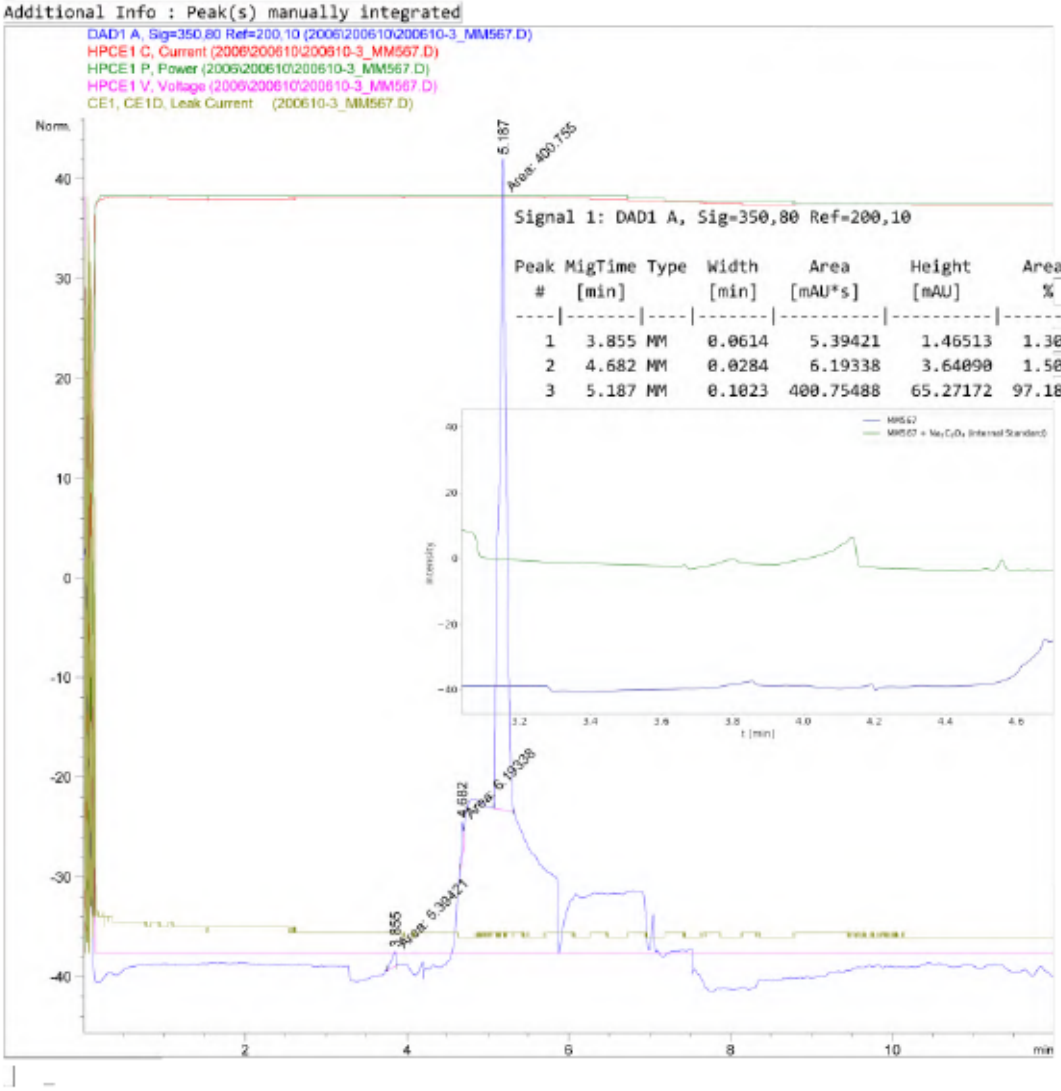

Signal 1: DAD1 A, Sig=350,80 Ref=200,10

Peak #	MigTime [min]	Type	Width [min]	Area [mAU*s]	Height [mAU]	Area %
1	3.855	MM	0.0614	5.39421	1.46513	1.3082
2	4.682	MM	0.0284	6.19338	3.64090	1.5020
3	5.187	MM	0.1023	400.75488	65.27172	97.1898

CE 10/6/2020 19:17:21 SYSTEM Page 1 of 2

Figure S 355: Condensed CE analysis for the NaOH extract of Table S 14, entry 3 – $CsHCO_3$ treatment of **127**, CuI and $NaBPh_4$ in MeOH.

Data File C:\Chem32\1\Data\1911\191112\191112-8_MM411-1.D
Sample Name: MM411-1

```
==================================================================
Acq. Operator   : SYSTEM
Sample Operator : SYSTEM
Acq. Instrument : CE                          Location :   26
Injection Date  : 12/11/2019 13:53:53
Acq. Method     : C:\Chem32\1\Methods\CE\Marx-Oxalate25C-Flush4mV34-191108.M
Last changed    : 8/11/2019 15:48:42 by SYSTEM
Analysis Method : C:\Chem32\1\Methods\CE\Marx-Oxalate25C-Flush10mV23-V13-200428.M
Last changed    : 27/8/2020 16:36:34 by SYSTEM
                  (modified after loading)
Method Info     : 02.10.2019 Methode geändert auf Agilent Organic Acids Kit

Sample Info     : NMR solution of MM411-1 (0.02 mL diluted with 0.8 mL H2O)
                  5 min flush, first run on 12.11.19

Additional Info : Peak(s) manually integrated
```

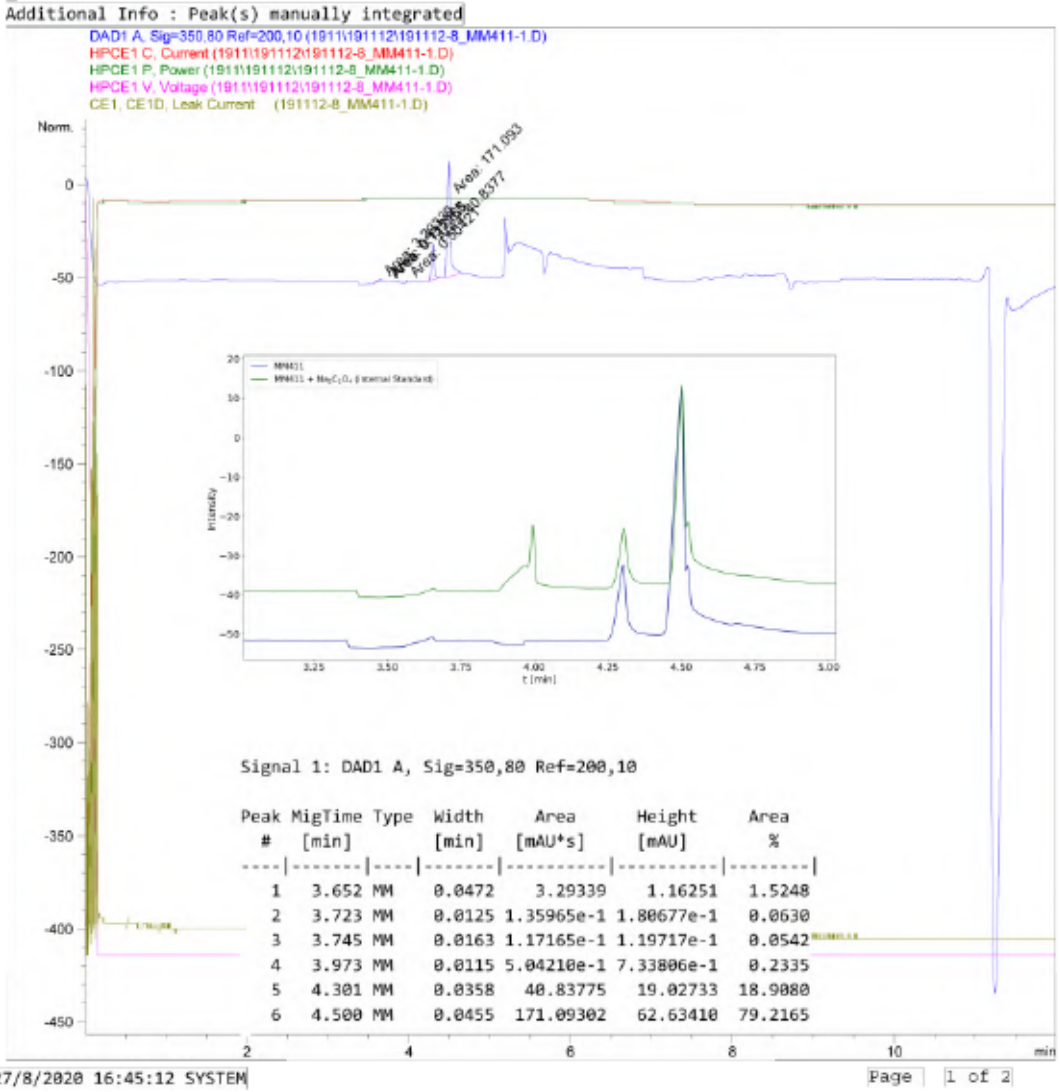

Signal 1: DAD1 A, Sig=350,80 Ref=200,10

Peak #	MigTime [min]	Type	Width [min]	Area [mAU*s]	Height [mAU]	Area %
1	3.652	MM	0.0472	3.29339	1.16251	1.5248
2	3.723	MM	0.0125	1.35965e-1	1.80677e-1	0.0630
3	3.745	MM	0.0163	1.17165e-1	1.19717e-1	0.0542
4	3.973	MM	0.0115	5.04210e-1	7.33806e-1	0.2335
5	4.301	MM	0.0358	40.83775	19.02733	18.9080
6	4.500	MM	0.0455	171.09302	62.63410	79.2165

CE 27/8/2020 16:45:12 SYSTEM Page 1 of 2

Figure S 356: Condensed CE analysis for the NaOH extract of Table S 14, entry 5 – $CsHCO_3$ treatment of **127**, CuI and $NaPF_6$ in MeOH.

```
Data File C:\Chem32\1\Data\2004\200428\200428-4_MM537-1.D
Sample Name: MM537-1

======================================================================
Acq. Operator   : SYSTEM
Sample Operator : SYSTEM
Acq. Instrument : CE                              Location :   38
Injection Date  : 28/4/2020 13:41:18
Acq. Method     : C:\Chem32\1\Methods\CE\Marx-Oxalate25C-Flush10mV12-200114.M
Last changed    : 14/1/2020 13:19:47 by SYSTEM
Analysis Method : C:\Chem32\1\Methods\CE\Spuel-extended-200227.M
Last changed    : 5/6/2020 16:37:44 by SYSTEM
                  (modified after loading)
Sample Info     : NMR sample of MM537-1 (0.03 mL diluted with 0.6 mL H2O)

Additional Info : Peak(s) manually integrated
```

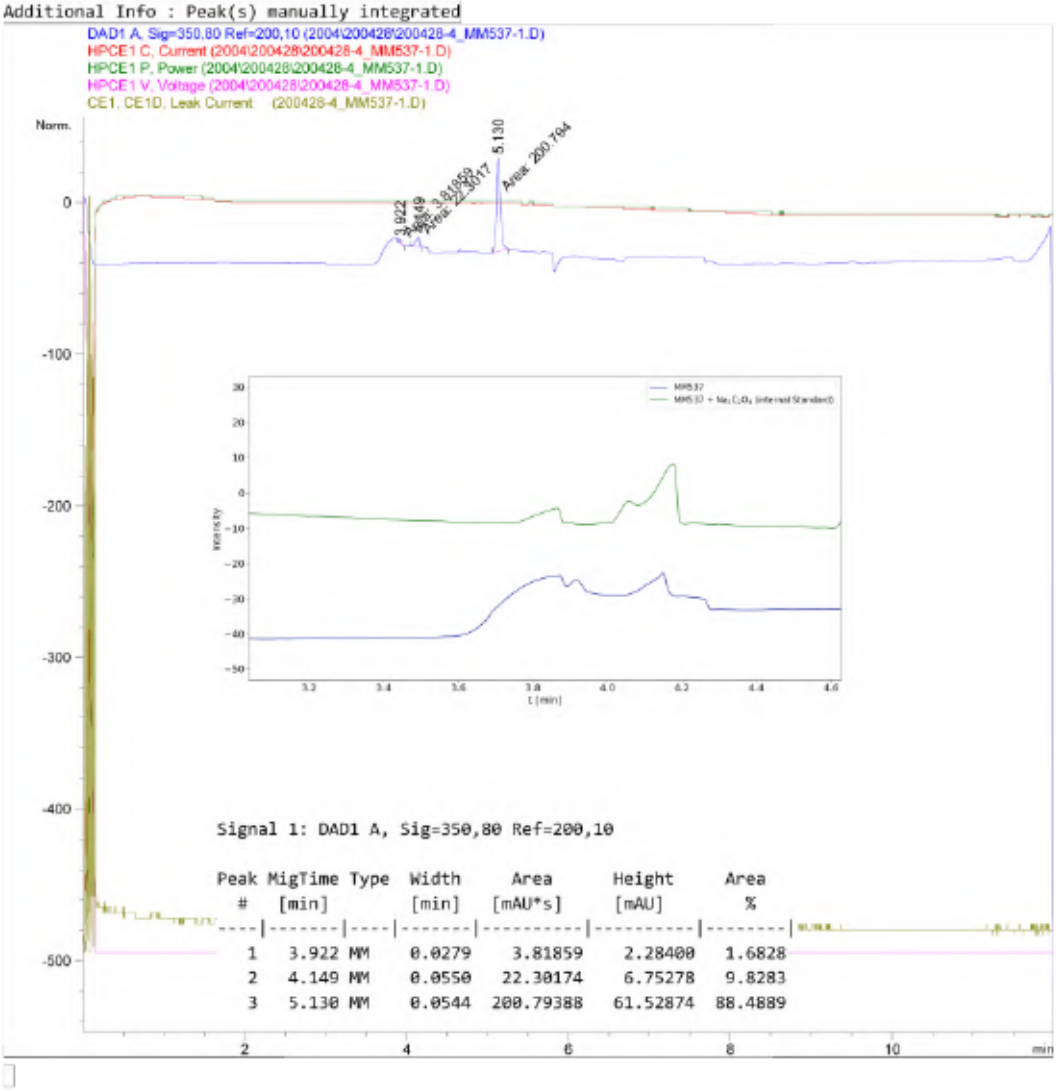


```
Signal 1: DAD1 A, Sig=350,80 Ref=200,10

Peak MigTime Type  Width     Area      Height    Area
  #   [min]       [min]   [mAU*s]     [mAU]      %
----|-------|----|-------|----------|----------|--------|
   1   3.922 MM   0.0279    3.81859    2.28400   1.6828
   2   4.149 MM   0.0550   22.30174    6.75278   9.8283
   3   5.130 MM   0.0544  200.79388   61.52874  88.4889
```

```
CE 5/6/2020 17:23:04 SYSTEM                              Page   1 of 2
```

Figure S 357: Condensed CE analysis for the NaOH extract of Table S 14, entry 6 – $CsHCO_3$ treatment of **127** and CuI in MeOH.

```
Data File C:\Chem32\1\Data\1911\191112\191112-6_MM407-1.D
Sample Name: MM407-1

======================================================================
Acq. Operator   : SYSTEM
Sample Operator : SYSTEM
Acq. Instrument : CE                              Location :   24
Injection Date  : 12/11/2019 13:12:31
Acq. Method     : C:\Chem32\1\Methods\CE\Marx-Oxalate25C-Flush4mV12-191106.M
Last changed    : 12/11/2019 10:53:07 by SYSTEM
Analysis Method : C:\Chem32\1\Methods\CE\Spuel-extended.M
Last changed    : 21/11/2019 14:20:04 by SYSTEM
                  (modified after loading)
Sample Info     : NMR solution of MM407-1 (0.02 mL diluted with 0.8 mL H2O)
                  5 min flush, first run on 12.11.19

Additional Info : Peak(s) manually integrated
```

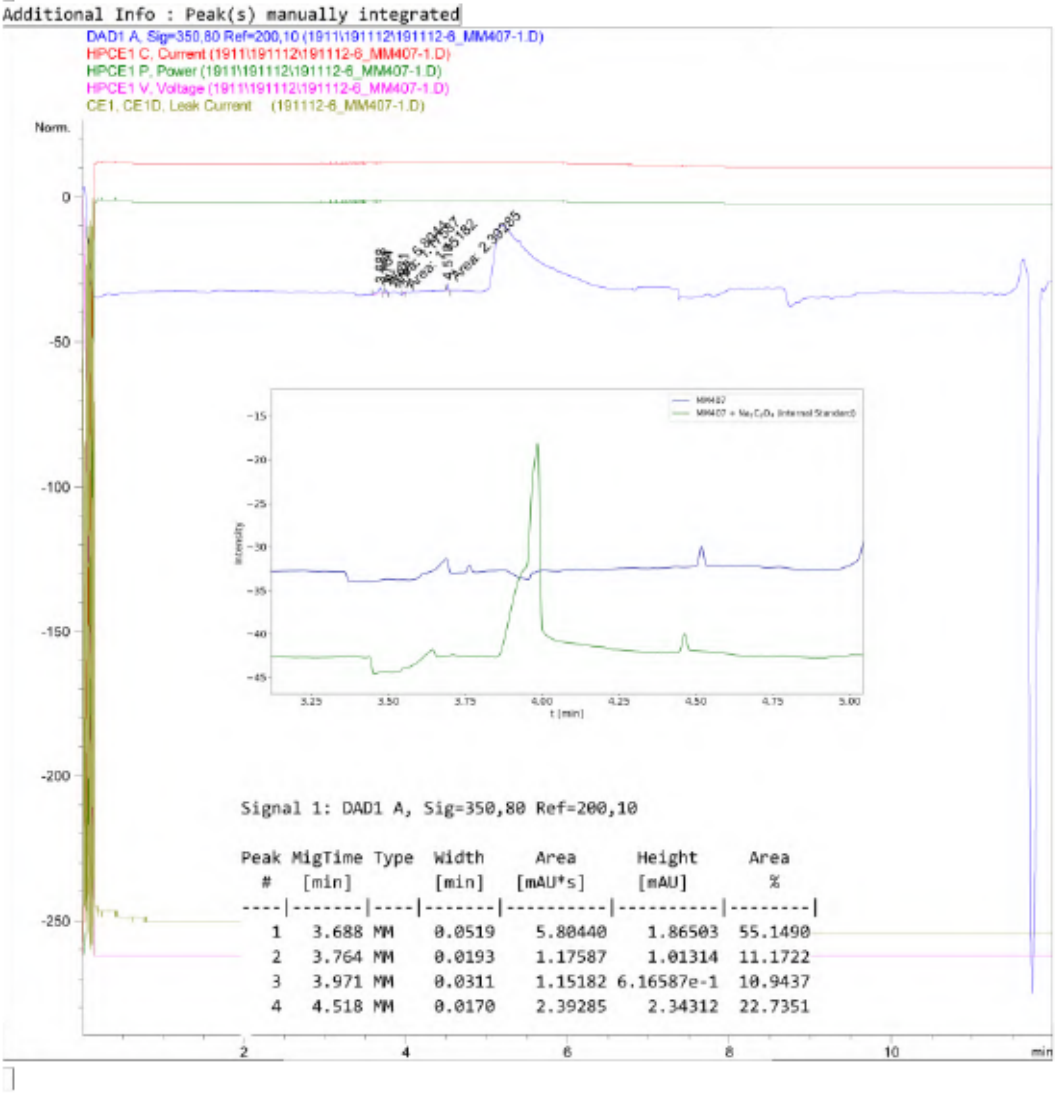


```
Signal 1: DAD1 A, Sig=350,80 Ref=200,10

Peak MigTime Type  Width     Area      Height     Area
  #   [min]       [min]   [mAU*s]     [mAU]       %
----|-------|----|-------|----------|----------|--------|
   1   3.688 MM    0.0519    5.80440    1.86503  55.1490
   2   3.764 MM    0.0193    1.17587    1.01314  11.1722
   3   3.971 MM    0.0311    1.15182 6.16587e-1  10.9437
   4   4.518 MM    0.0170    2.39285    2.34312  22.7351
```

```
CE 21/11/2019 19:05:50 SYSTEM                              Page  1 of 2
```

Figure S 358: Condensed CE analysis for the NaOH extract of Table S 14, entry 7 – $NaHCO_3$ treatment of **127**, CuI and $NaBPh_4$ in MeOH.

```
Data File C:\Chem32\1\Data\2006\200610\200610-4_MM568.D
Sample Name: MM568

======================================================================
Acq. Operator   : SYSTEM
Sample Operator : SYSTEM
Acq. Instrument : CE                          Location :   28
Injection Date  : 10/6/2020 15:17:42
Acq. Method     : C:\Chem32\1\Methods\CE\Marx-Oxalate25C-Flush10mV12-200114.M
Last changed    : 14/1/2020 13:19:47 by SYSTEM
Analysis Method : C:\Chem32\1\Methods\CE\Spuel-extended-200227.M
Last changed    : 10/6/2020 15:17:04 by SYSTEM
                  (modified after loading)
Sample Info     : NMR solution of MM568 (0.04 mL) diluted with H2O (0.6 mL)

Additional Info : Peak(s) manually integrated
```

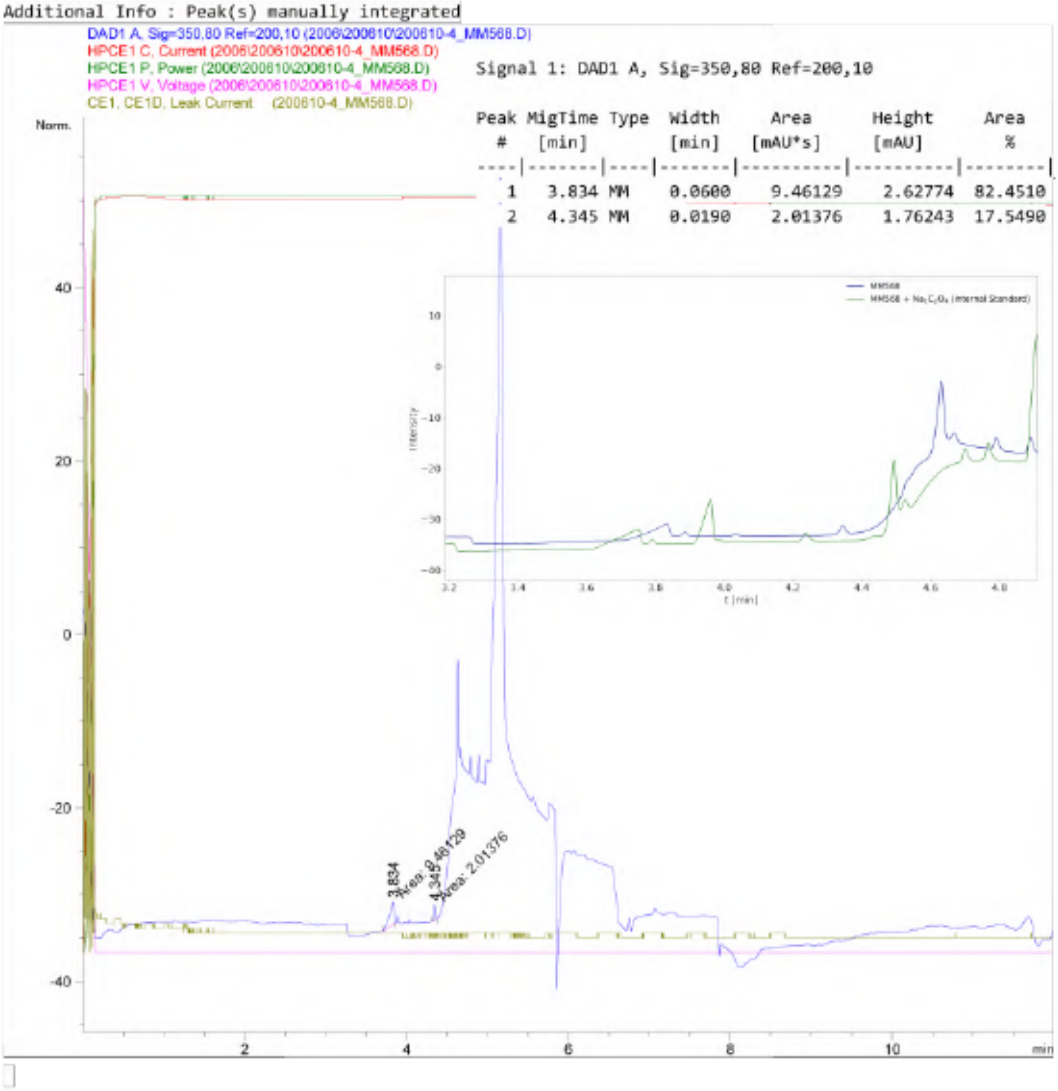


```
CE 10/6/2020 19:17:34 SYSTEM                              Page   1 of 2
```

Figure S 359: Condensed CE analysis for the NaOH extract of Table S 14, entry 8 – $CsHCO_3$ treatment of **127** and $[Cu(MeCN)_4]PF_6$ in MeOH.

Data File C:\Chem32\1\Data\2006\200610\200610-5_MM569.D
Sample Name: MM569

Acq. Operator	: SYSTEM
Sample Operator	: SYSTEM
Acq. Instrument	: CE Location : 29
Injection Date	: 10/6/2020 15:41:12
Acq. Method	: C:\Chem32\1\Methods\CE\Marx-Oxalate25C-Flush10mV12-200114.M
Last changed	: 14/1/2020 13:19:47 by SYSTEM
Analysis Method	: C:\Chem32\1\Methods\CE\Spuel-extended-200227.M
Last changed	: 10/6/2020 15:17:04 by SYSTEM (modified after loading)
Sample Info	: NMR solution of MM569 (0.04 mL) diluted with H2O (0.6 mL)
Additional Info	: Peak(s) manually integrated

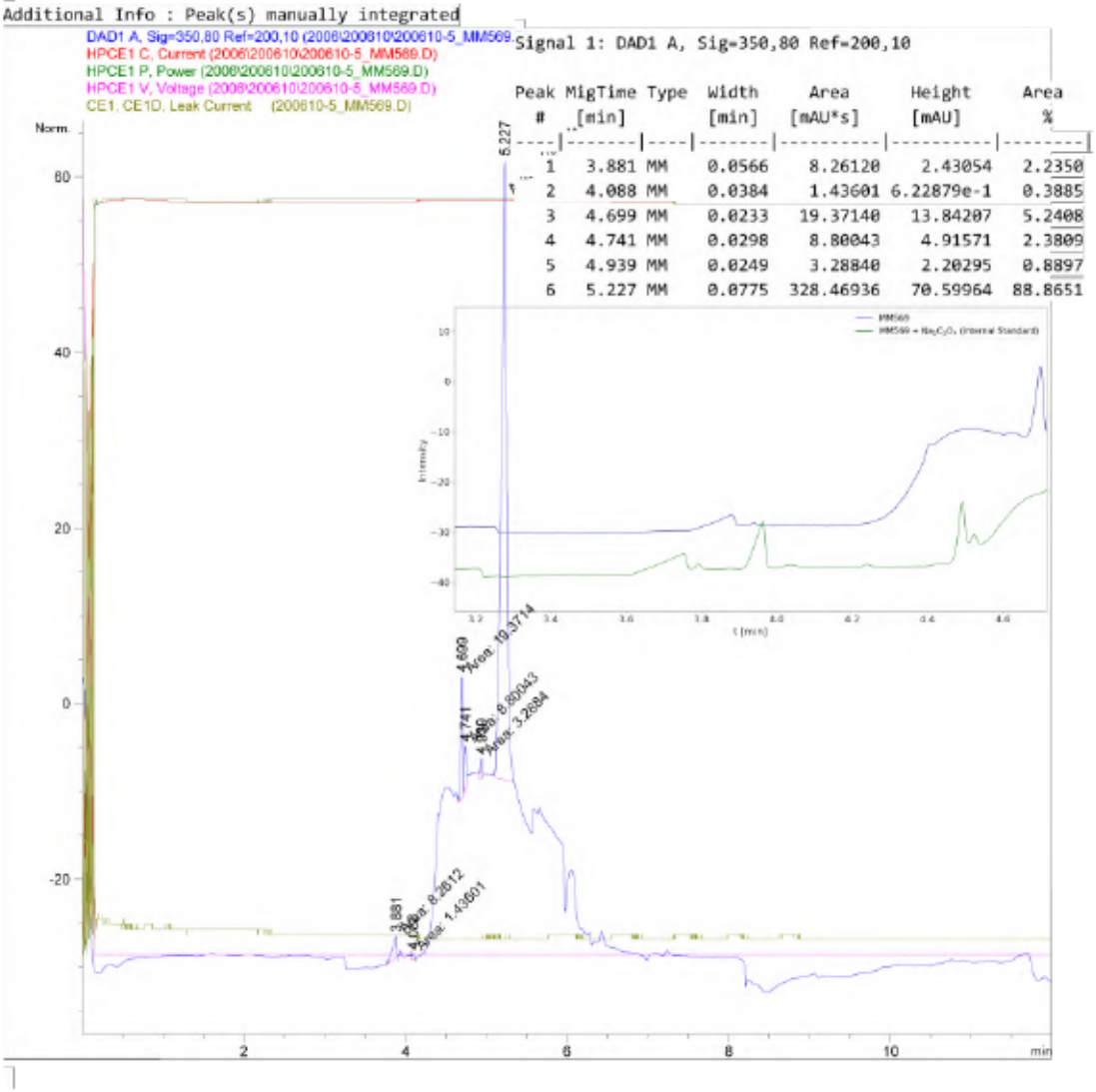

Signal 1: DAD1 A, Sig=350,80 Ref=200,10

Peak #	MigTime [min]	Type	Width [min]	Area [mAU*s]	Height [mAU]	Area %
1	3.881	MM	0.0566	8.26120	2.43054	2.2350
2	4.088	MM	0.0384	1.43601	6.22879e-1	0.3885
3	4.699	MM	0.0233	19.37140	13.84207	5.2408
4	4.741	MM	0.0298	8.80043	4.91571	2.3809
5	4.939	MM	0.0249	3.28840	2.20295	0.8897
6	5.227	MM	0.0775	328.46936	70.59964	88.8651

CE 10/6/2020 19:17:47 SYSTEM Page 1 of 2

Figure S 360: Condensed CE analysis for the NaOH extract of Table S 14, entry 9 – $NaHCO_3$ treatment of **127** and $[Cu(MeCN)_4]PF_6$ in MeOH.

```
Data File C:\Chem32\1\Data\2006\200609\200609-3_MM561.D
Sample Name: MM561

======================================================================
Acq. Operator   : SYSTEM
Sample Operator : SYSTEM
Acq. Instrument : CE                          Location :  27
Injection Date  : 9/6/2020 14:42:57
Acq. Method     : C:\Chem32\1\Methods\CE\Marx-Oxalate25C-Flush10mV12-200114.M
Last changed    : 14/1/2020 13:19:47 by SYSTEM
Analysis Method : C:\Chem32\1\Methods\CE\Spuel-extended-200227.M
Last changed    : 9/6/2020 15:45:25 by SYSTEM
                  (modified after loading)
Sample Info     : NMR solution of MM561 (0.04 mL) diluted with H2O (0.6 ml)

Additional Info : Peak(s) manually integrated
```

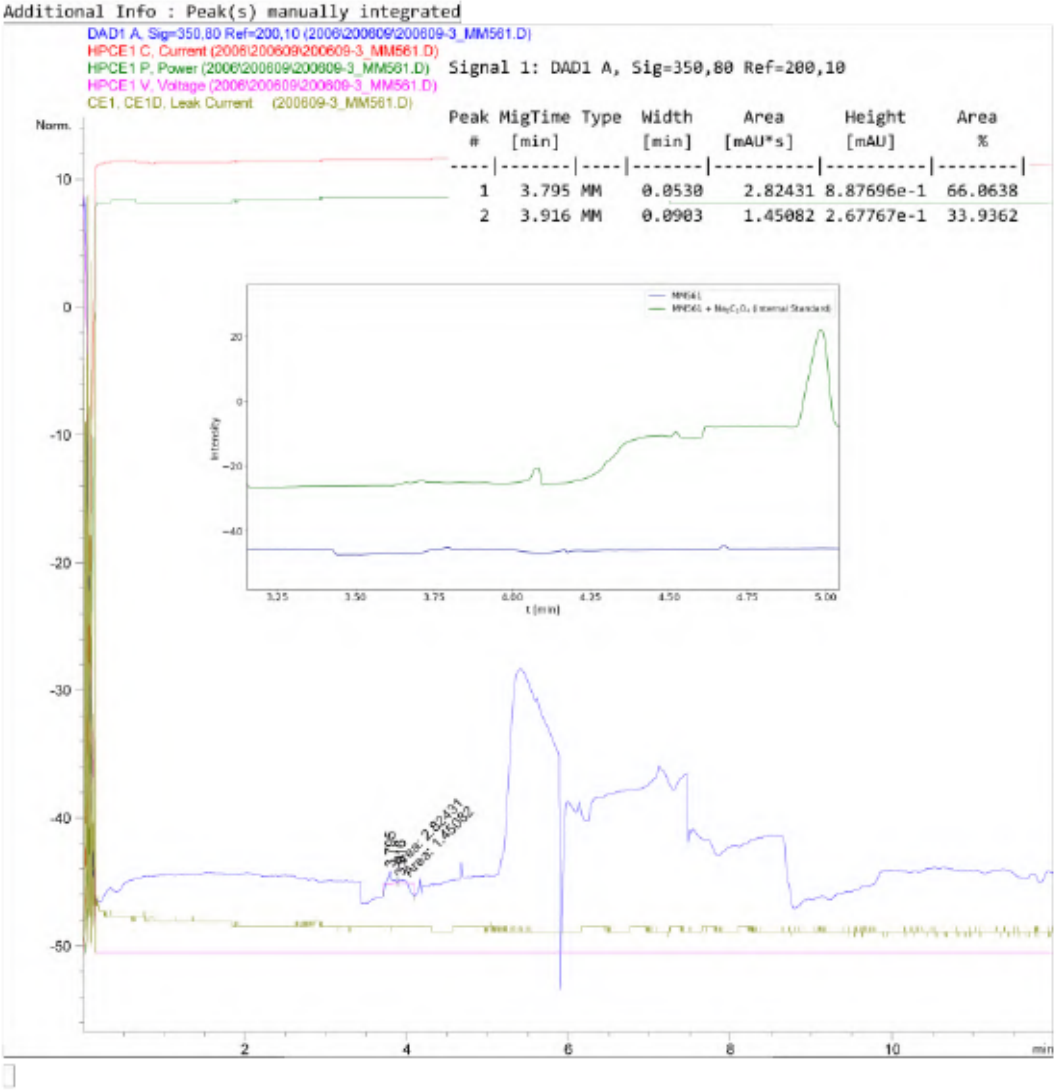


```
CE 9/6/2020 18:44:29 SYSTEM                                  Page  1 of 2
```

Figure S 361: Condensed CE analysis for the NaOH extract of Table S 15, entry 1 – CO_2 treatment of **127**, CuI and $NaBPh_4$ in MeOH.

Data File C:\Chem32\1\Data\2006\200609\200609-1_MM559.D
Sample Name: MM559

```
==================================================================
Acq. Operator   : SYSTEM
Sample Operator : SYSTEM
Acq. Instrument : CE                          Location :   25
Injection Date  : 9/6/2020 13:55:52
Acq. Method     : C:\Chem32\1\Methods\CE\Marx-Oxalate25C-Flush10mV12-200114.M
Last changed    : 14/1/2020 13:19:47 by SYSTEM
Analysis Method : C:\Chem32\1\Methods\CE\Spuel-extended-200227.M
Last changed    : 9/6/2020 15:45:25 by SYSTEM
                  (modified after loading)
Sample Info     : NMR solution of MM559 (0.04 mL) diluted with H2O (0.6 ml)

Additional Info : Peak(s) manually integrated
```

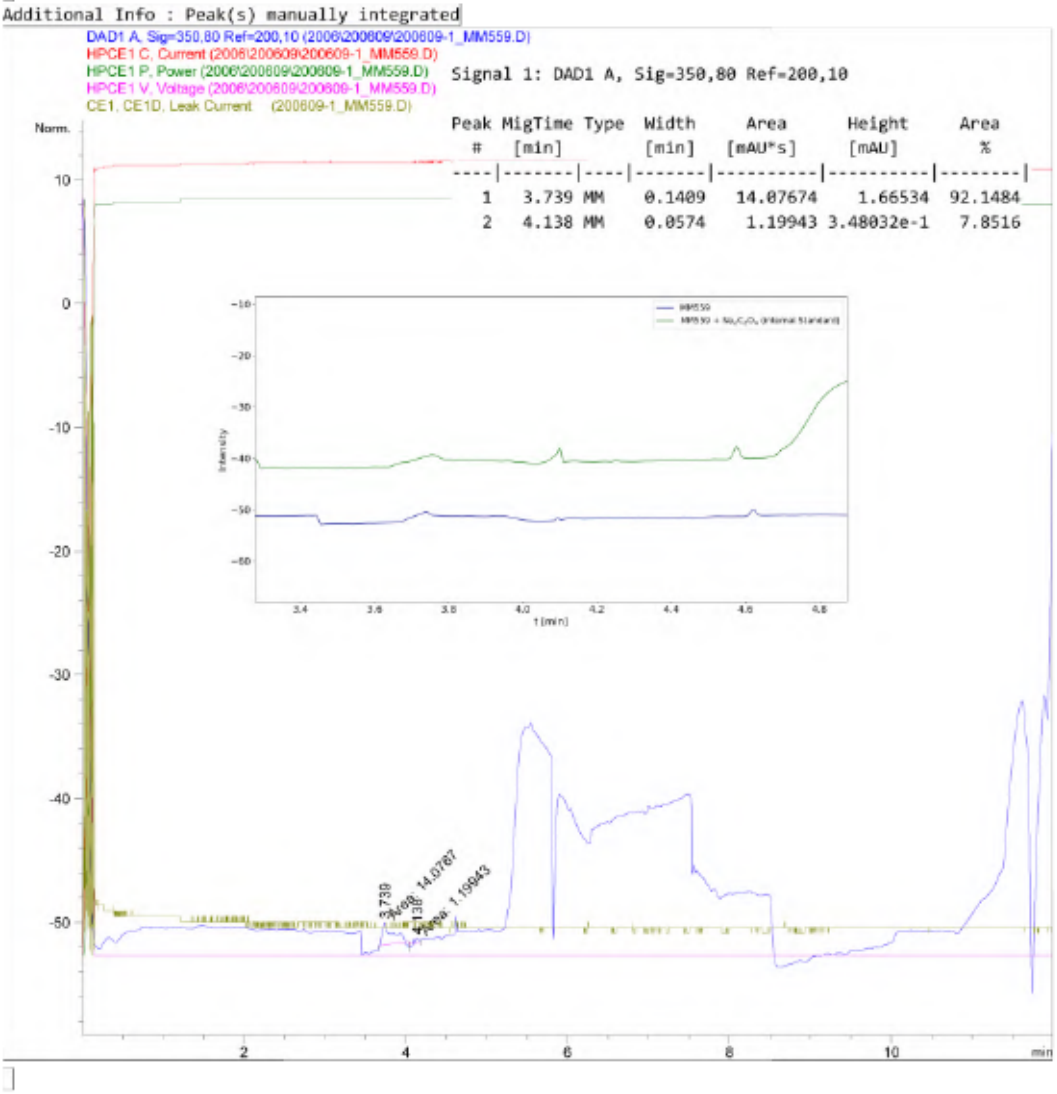

CE 9/6/2020 18:45:06 SYSTEM Page 1 of 2

Figure S 362: Condensed CE analysis for the NaOH extract of Table S 15, entry 2 – CO_2 treatment of **127**, CuI and $NaBPh_4$ in MeOH.

```
Data File C:\Chem32\1\Data\2006\200609\200609-4_MM562.D
Sample Name: MM562

=====================================================================
Acq. Operator   : SYSTEM
Sample Operator : SYSTEM
Acq. Instrument : CE                          Location :   28
Injection Date  : 9/6/2020 15:06:27
Acq. Method     : C:\Chem32\1\Methods\CE\Marx-Oxalate25C-Flush10mV12-200114.M
Last changed    : 14/1/2020 13:19:47 by SYSTEM
Analysis Method : C:\Chem32\1\Methods\CE\Spuel-extended-200227.M
Last changed    : 9/6/2020 15:45:25 by SYSTEM
                  (modified after loading)
Sample Info     : NMR solution of MM562 (0.04 mL) diluted with H2O (0.6 ml)

Additional Info : Peak(s) manually integrated
```

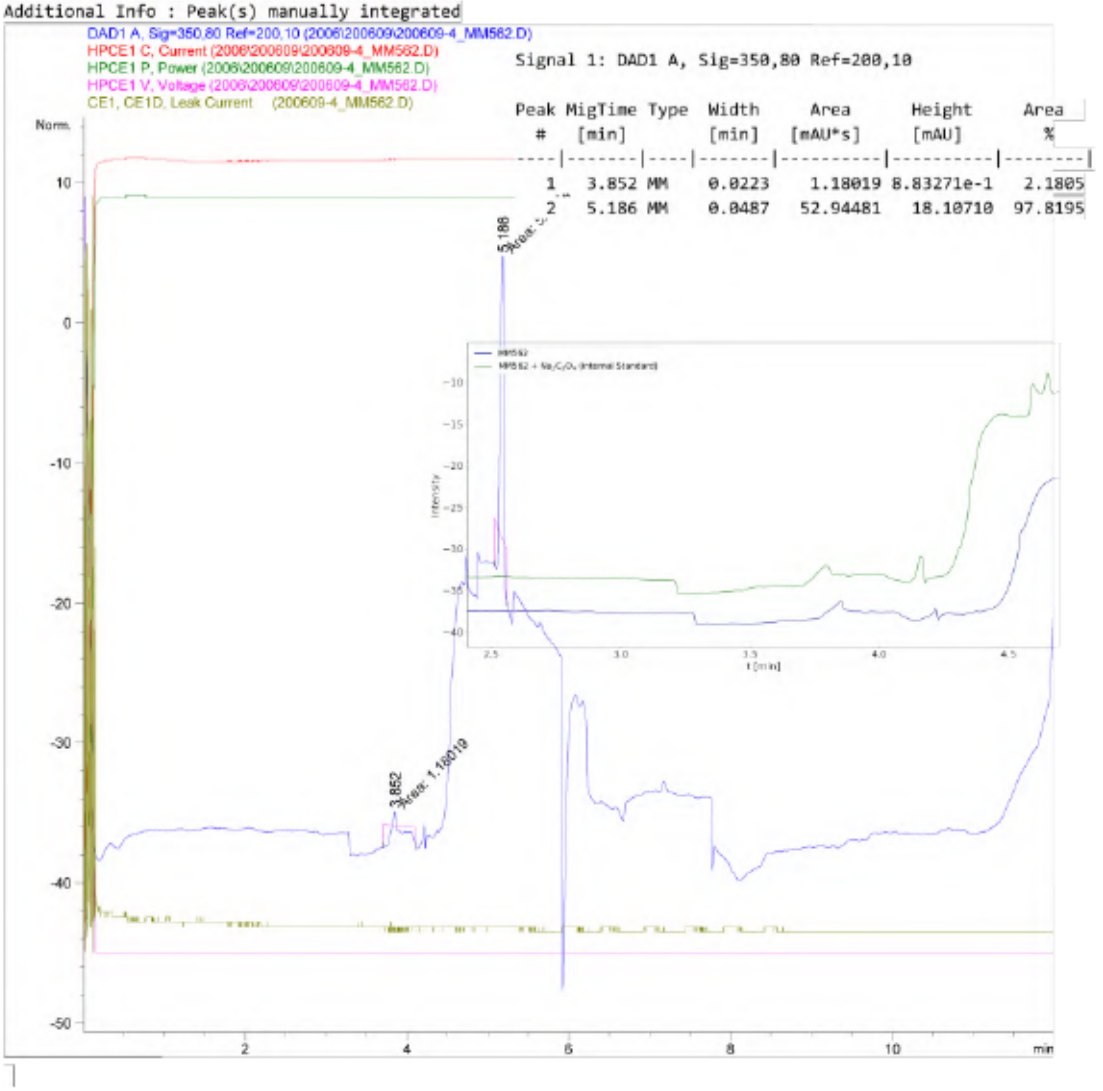

Figure S 363: Condensed CE analysis for the NaOH extract of Table S 15, entry 3 – CO_2 treatment of **127**, CuI and $NaBPh_4$ in MeOH/THF.

Data File C:\Chem32\1\Data\2006\200617\200617-1_MM573.D
Sample Name: MM573

```
====================================================================
Acq. Operator   : SYSTEM
Sample Operator : SYSTEM
Acq. Instrument : CE                              Location :   15
Injection Date  : 17/6/2020 14:54:04
Acq. Method     : C:\Chem32\1\Methods\CE\Marx-Oxalate25C-Flush10mV12-200114.M
Last changed    : 14/1/2020 13:19:47 by SYSTEM
Analysis Method : C:\Chem32\1\Methods\CE\Spuel-extended-200227.M
Last changed    : 17/6/2020 16:48:17 by SYSTEM
                  (modified after loading)
Sample Info     : NMR solution of MM573 (0.04 ml) diluted with H2O (0.6 ml)

Additional Info : Peak(s) manually integrated
```

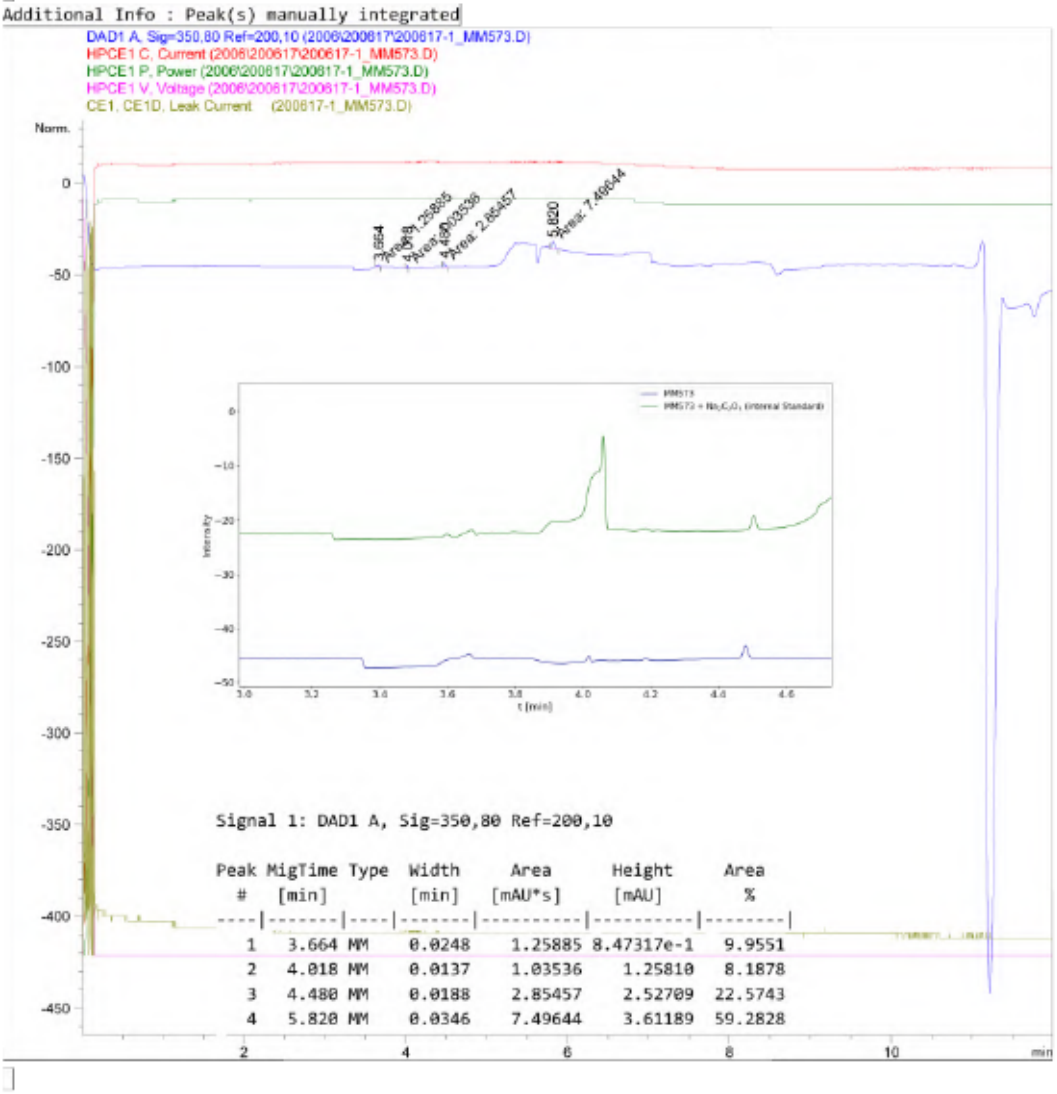

Signal 1: DAD1 A, Sig=350,80 Ref=200,10

Peak #	MigTime [min]	Type	Width [min]	Area [mAU*s]	Height [mAU]	Area %
1	3.664	MM	0.0248	1.25885	8.47317e-1	9.9551
2	4.018	MM	0.0137	1.03536	1.25810	8.1878
3	4.480	MM	0.0188	2.85457	2.52709	22.5743
4	5.820	MM	0.0346	7.49644	3.61189	59.2828

CE 17/6/2020 17:10:11 SYSTEM Page 1 of 2

Figure S 364: Condensed CE analysis for the NaOH extract of Table S 15, entry 5 – CO_2 treatment of **127**, CuI and $NaBPh_4$ in THF.

```
Data File C:\Chem32\1\Data\1911\191112\191112-2_MM391-1.D
Sample Name: MM391-1

======================================================================
Acq. Operator   : SYSTEM
Sample Operator : SYSTEM
Acq. Instrument : CE                          Location :  20
Injection Date  : 12/11/2019 11:31:41
Acq. Method     : C:\Chem32\1\Methods\CE\Marx-Oxalate25C-Flush4mV12-191106.M
Last changed    : 12/11/2019 11:24:12 by SYSTEM
                  (modified after loading)
Analysis Method : C:\Chem32\1\Methods\CE\Marx-Oxalate25C-Flush10mV23-V13-200428.M
Last changed    : 27/8/2020 16:36:34 by SYSTEM
                  (modified after loading)
Method Info     : 02.10.2019 Methode geändert auf Agilent Organic Acids Kit

Sample Info     : NMR solution of MM391-1 (0.02 mL diluted with 0.8 mL H2O)
                  5 min flush, first run on 12.11.19

Additional Info : Peak(s) manually integrated
```

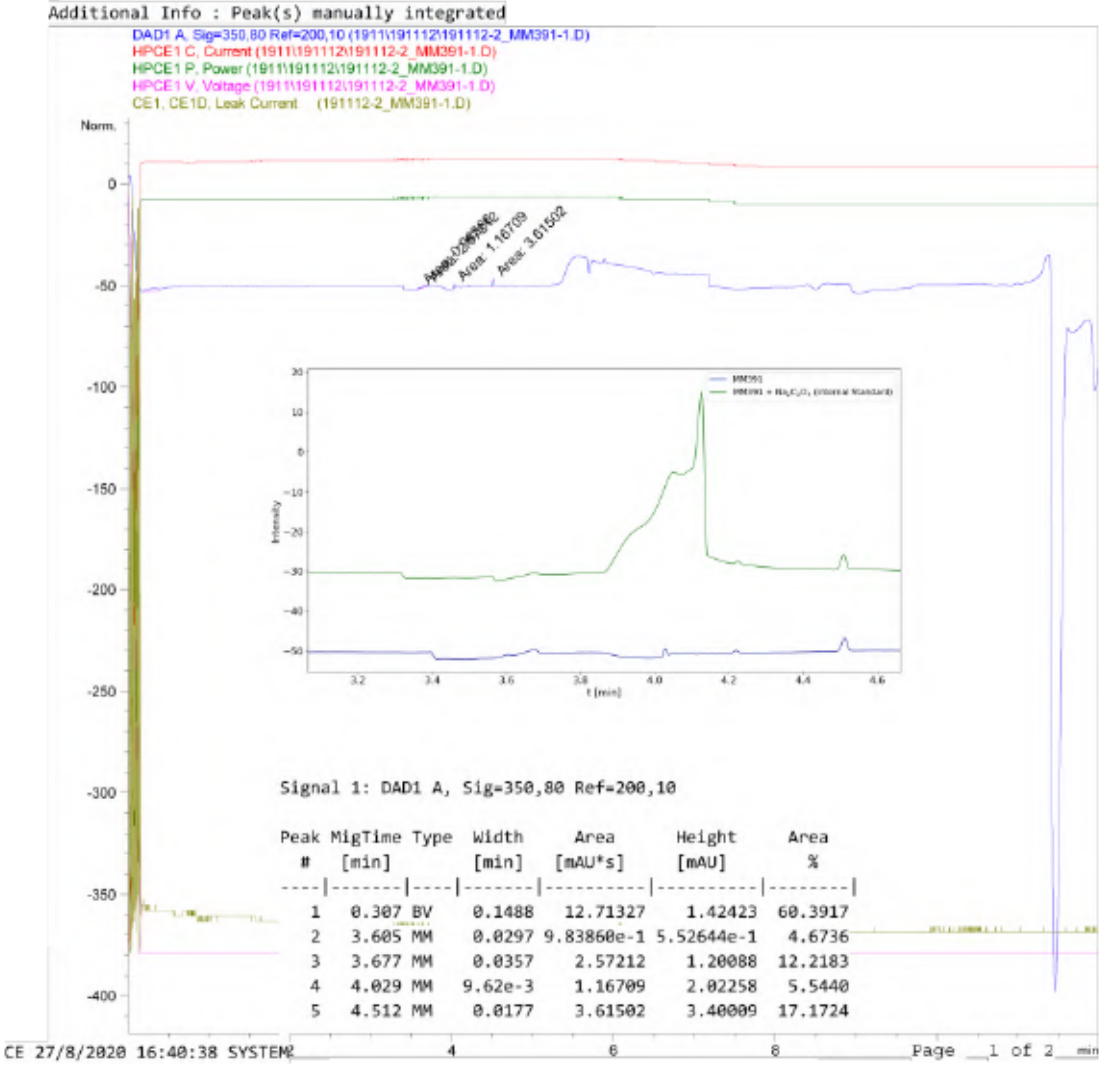

Figure S 365: Condensed CE analysis for the NaOH extract of Table S 15, entry 6 – CO_2 treatment of **127**, CuI and $NaBPh_4$ in THF.

```
Data File C:\Chem32\1\Data\1912\191217\191217-3_MM441-1.D
Sample Name: MM441-1

======================================================================
Acq. Operator   : SYSTEM
Sample Operator : SYSTEM
Acq. Instrument : CE                              Location :   22
Injection Date  : 17/12/2019 14:12:38
Acq. Method     : C:\CHEM32\1\METHODS\CE\Marx-Oxalate25C-Flush5mV12-191106.M
Last changed    : 17/12/2019 13:47:38 by SYSTEM
Analysis Method : C:\Chem32\1\Methods\CE\Spuel-extended.M
Last changed    : 17/12/2019 13:46:25 by SYSTEM
                  (modified after loading)
Sample Info     : NMR sample of MM441-1 (0.02 mL diluted with 0.6 mL H2O)
                  Sample prepared on 17.12.19

Additional Info : Peak(s) manually integrated
```

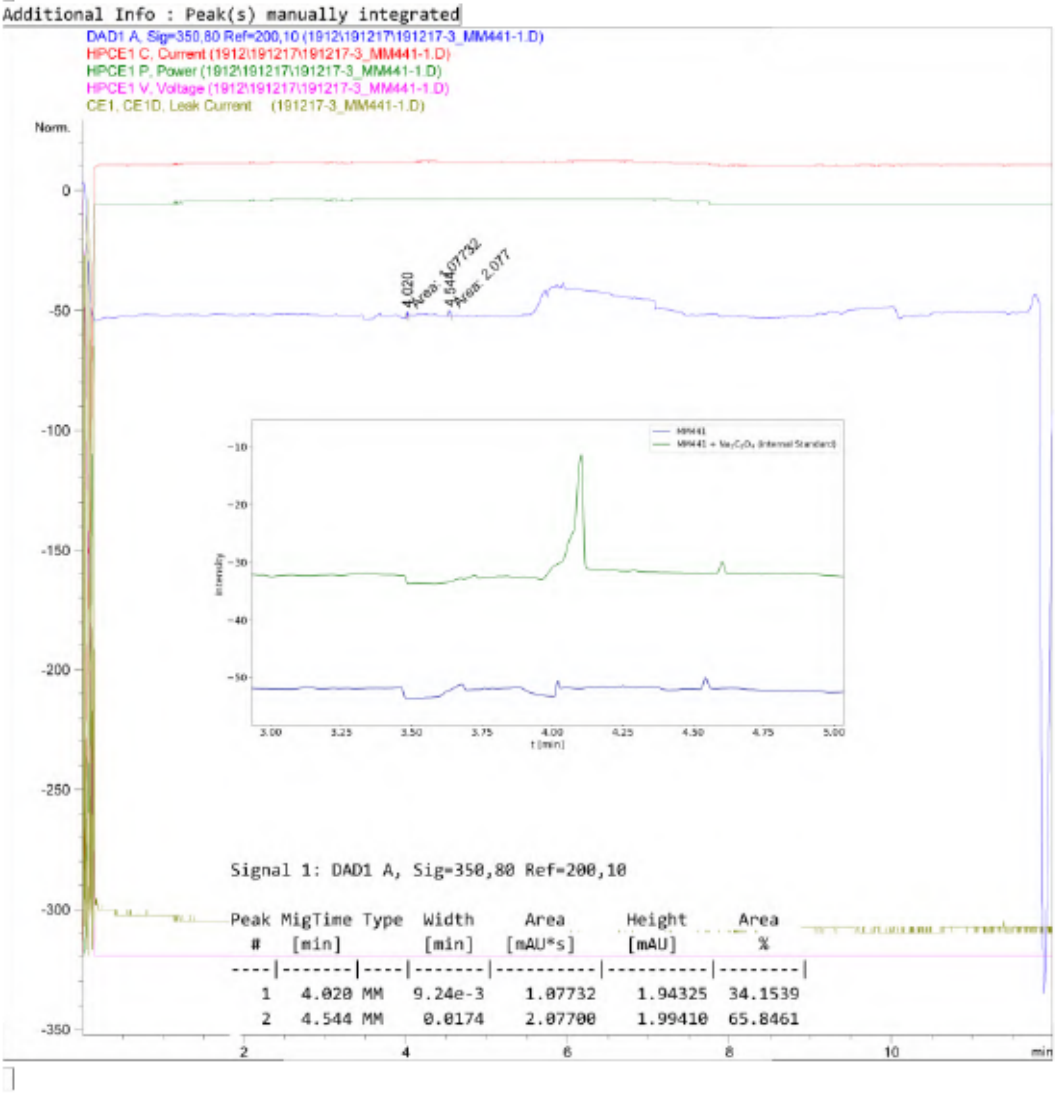


```
Signal 1: DAD1 A, Sig=350,80 Ref=200,10

Peak MigTime Type  Width     Area      Height    Area
  #   [min]       [min]   [mAU*s]     [mAU]      %
----|-------|----|-------|----------|----------|--------|
   1   4.020 MM   9.24e-3   1.07732   1.94325  34.1539
   2   4.544 MM    0.0174   2.07700   1.99410  65.8461

CE 17/12/2019 17:03:46 SYSTEM                          Page  1 of 2
```

Figure S 366: Condensed CE analysis for the NaOH extract of Table S 15, entry 7 – CO_2 treatment of **127**, CuI and $NaBPh_4$ in toluene.

```
Data File C:\Chem32\1\Data\2006\200616\200616-7_MM570.D
Sample Name: MM570

======================================================================
Acq. Operator   : SYSTEM
Sample Operator : SYSTEM
Acq. Instrument : CE                          Location :   37
Injection Date  : 16/6/2020 15:23:51
Acq. Method     : C:\Chem32\1\Methods\CE\Marx-Oxalate25C-Flush10mV23-V13-200428.M
Last changed    : 28/4/2020 15:34:00 by SYSTEM
Analysis Method : C:\Chem32\1\Methods\CE\Spuel-extended-200227.M
Last changed    : 17/6/2020 16:48:17 by SYSTEM
                  (modified after loading)
Sample Info     : NMR solution of MM570 (0.04 mL) diluted w. H2O (0.6 ml)

Additional Info : Peak(s) manually integrated
```

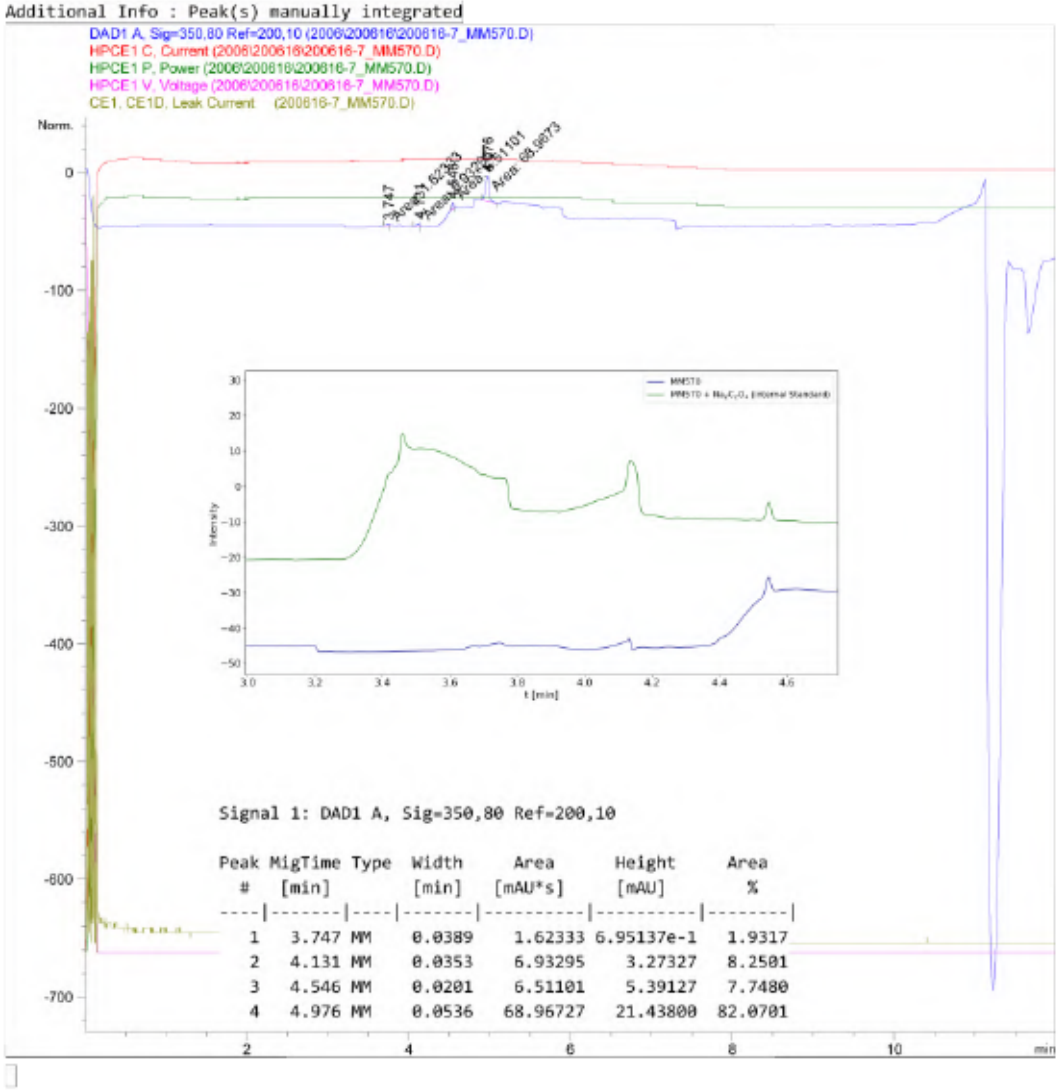


```
Signal 1: DAD1 A, Sig=350,80 Ref=200,10

Peak MigTime Type  Width     Area      Height     Area
  #   [min]       [min]   [mAU*s]     [mAU]       %
----|-------|----|-------|----------|----------|--------|
   1   3.747 MM    0.0389    1.62333 6.95137e-1   1.9317
   2   4.131 MM    0.0353    6.93295    3.27327   8.2501
   3   4.546 MM    0.0201    6.51101    5.39127   7.7480
   4   4.976 MM    0.0536   68.96727   21.43800  82.0701
```


Figure S 367: Condensed CE analysis for the NaOH extract of Table S 15, entry 8 – CO_2 treatment of **127**, CuI and $NaBPh_4$ in MeOH at 40 °C.

```
Data File C:\Chem32\1\Data\1911\191112\191112-7_MM408-1.D
Sample Name: MM408-1

======================================================================
Acq. Operator   : SYSTEM
Sample Operator : SYSTEM
Acq. Instrument : CE                          Location :   25
Injection Date  : 12/11/2019 13:35:23
Acq. Method     : C:\Chem32\1\Methods\CE\Marx-Oxalate25C-Flush4mV34-191108.M
Last changed    : 12/11/2019 13:28:14 by SYSTEM
                  (modified after loading)
Analysis Method : C:\Chem32\1\Methods\CE\Marx-Oxalate25C-Flush10mV23-V13-200428.M
Last changed    : 27/8/2020 16:36:34 by SYSTEM
                  (modified after loading)
Method Info     : 02.10.2019 Methode geändert auf Agilent Organic Acids Kit

Sample Info     : NMR solution of MM408-1 (0.02 mL diluted with 0.8 mL H2O)
                  5 min flush, first run on 12.11.19

Additional Info : Peak(s) manually integrated
```

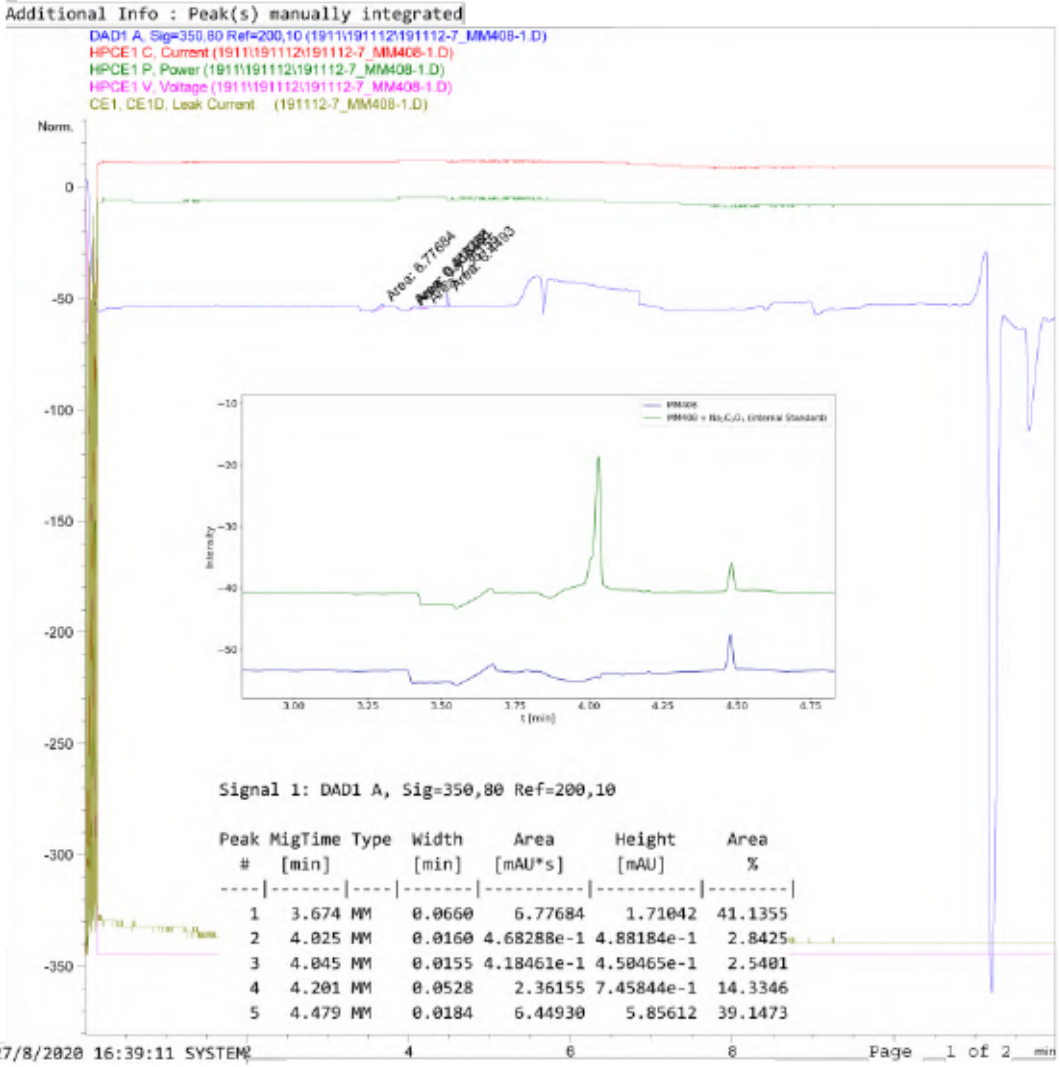

Signal 1: DAD1 A, Sig=350,80 Ref=200,10

Peak #	MigTime [min]	Type	Width [min]	Area [mAU*s]	Height [mAU]	Area %
1	3.674	MM	0.0660	6.77684	1.71042	41.1355
2	4.025	MM	0.0160	4.68288e-1	4.88184e-1	2.8425
3	4.045	MM	0.0155	4.18461e-1	4.50465e-1	2.5401
4	4.201	MM	0.0528	2.36155	7.45844e-1	14.3346
5	4.479	MM	0.0184	6.44930	5.85612	39.1473

Figure S 368: Condensed CE analysis for the NaOH extract of Table S 15, entry 9 – CO_2 treatment of **127**, CuI and $NaBPh_4$ in MeOH at 35 °C.

Data File C:\Chem32\1\Data\1912\191217\191217-8_MM448-1.D
Sample Name: MM448-1

```
=====================================================================
Acq. Operator   : SYSTEM
Sample Operator : SYSTEM
Acq. Instrument : CE                              Location :   23
Injection Date  : 18/12/2019 10:30:03
Acq. Method     : C:\Chem32\1\Methods\CE\Marx-Oxalate25C-Flush4mV12-191106.M
Last changed    : 12/11/2019 10:53:07 by SYSTEM
Analysis Method : C:\Chem32\1\Methods\CE\Spuel-extended.M
Last changed    : 18/12/2019 11:13:37 by SYSTEM
                  (modified after loading)
Sample Info     : NMR sample of MM448-1 (0.02 mL of NMR solution diluted with 0.6 mL H2O)
                  First run 18.12.19

Additional Info : Peak(s) manually integrated
```

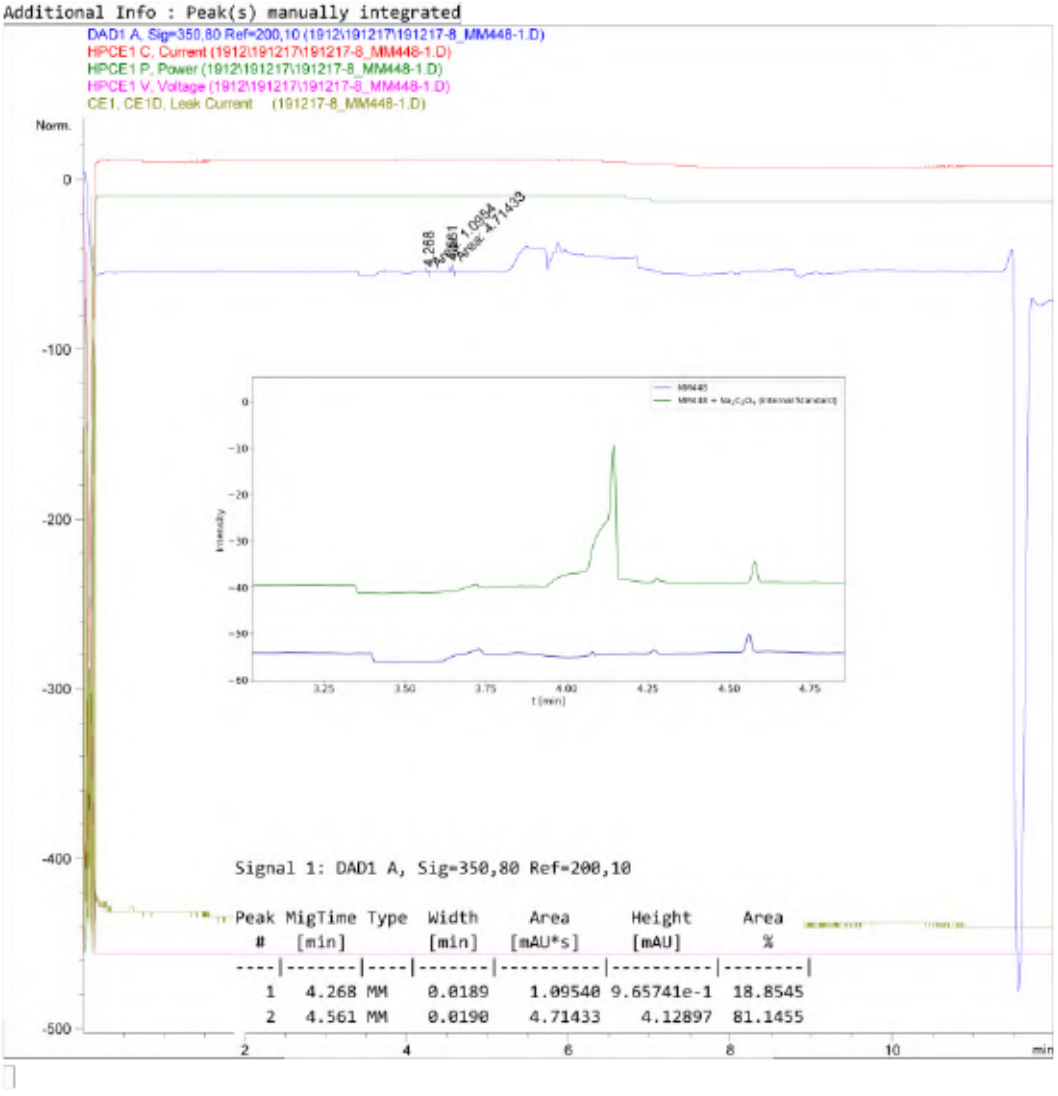

CE 18/12/2019 13:30:23 SYSTEM Page 1 of 2

Figure S 369: Condensed CE analysis for the NaOH extract of Table S 15, entry 10 – CO_2 treatment and illumination (400-700 nm, 0.09 W) of **127**, CuI and $NaBPh_4$ in MeOH.

```
Data File C:\Chem32\1\Data\2006\200609\200609-2_MM560.D
Sample Name: MM560

======================================================================
Acq. Operator   : SYSTEM
Sample Operator : SYSTEM
Acq. Instrument : CE                          Location :   26
Injection Date  : 9/6/2020 14:19:23
Acq. Method     : C:\Chem32\1\Methods\CE\Marx-Oxalate25C-Flush10mV12-200114.M
Last changed    : 14/1/2020 13:19:47 by SYSTEM
Analysis Method : C:\Chem32\1\Methods\CE\Spuel-extended-200227.M
Last changed    : 9/6/2020 15:45:25 by SYSTEM
                  (modified after loading)
Sample Info     : NMR solution of MM560 (0.04 mL) diluted with H2O (0.6 ml)

Additional Info : Peak(s) manually integrated
```

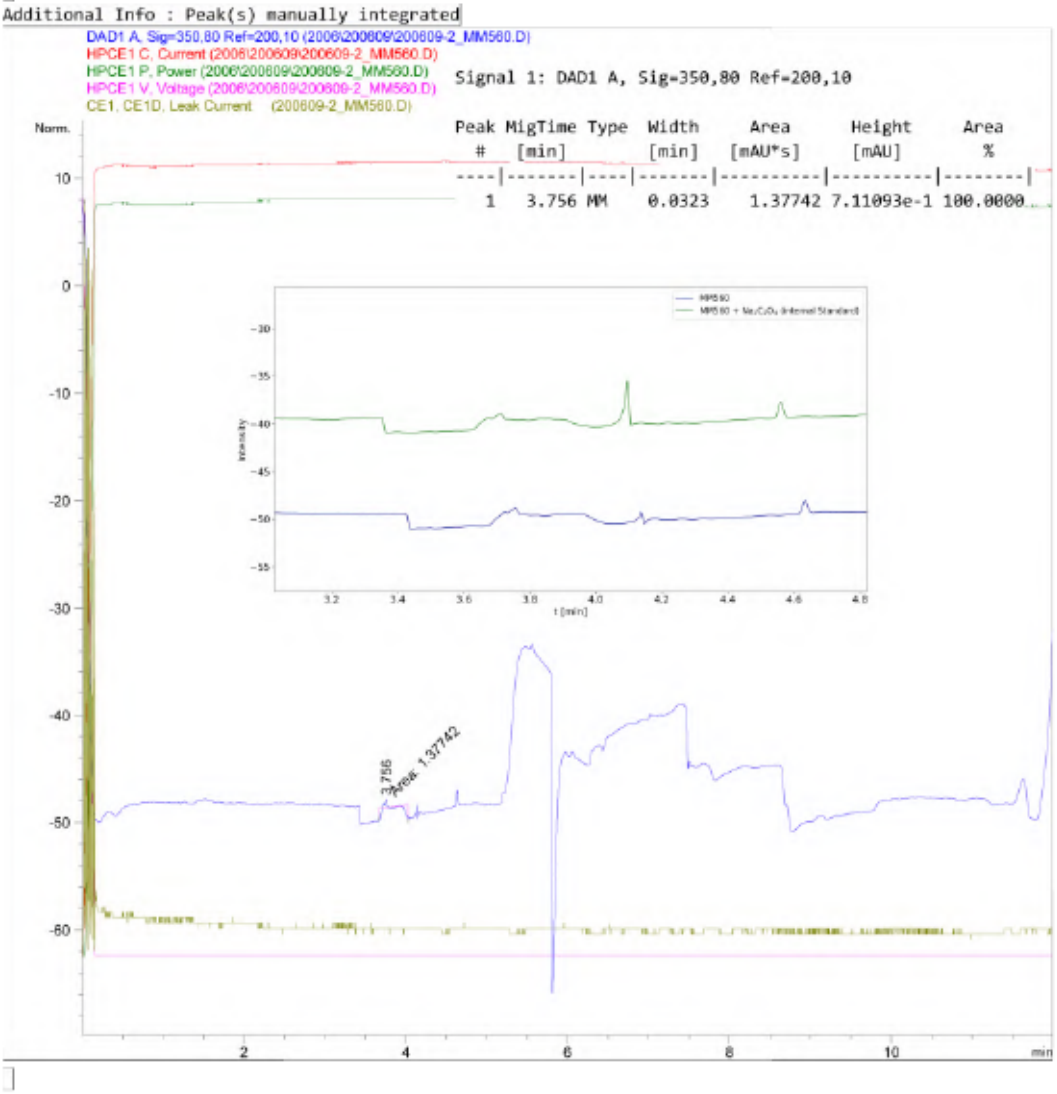


```
CE 9/6/2020 18:44:54 SYSTEM                                Page  1 of 2
```

Figure S 370: Condensed CE analysis for the NaOH extract of Table S 16, entry 1 – CO_2 treatment of **127**, CuI and KPF_6 in MeOH.

Data File C:\Chem32\1\Data\1911\191108\191108-13_MM371-1.D
Sample Name: MM371-1

```
==================================================================
Acq. Operator   : SYSTEM
Sample Operator : SYSTEM
Acq. Instrument : CE                          Location :   26
Injection Date  : 8/11/2019 14:39:22
Acq. Method     : C:\CHEM32\1\METHODS\CE\Marx-Oxalate25C-Flush4mV34-191108.M
Last changed    : 8/11/2019 13:40:25 by SYSTEM
Analysis Method : C:\Chem32\1\Methods\CE\Marx-Oxalate25C-Flush10mV23-V13-200428.M
Last changed    : 27/8/2020 16:36:34 by SYSTEM
                  (modified after loading)
Method Info     : 02.10.2019 Methode geändert auf Agilent Organic Acids Kit

Sample Info     : NMR solution of MM371-1 (0.02 mL diluted with 0.8 mL H2O)
                  5 min flush, 25 °C

Additional Info : Peak(s) manually integrated
```

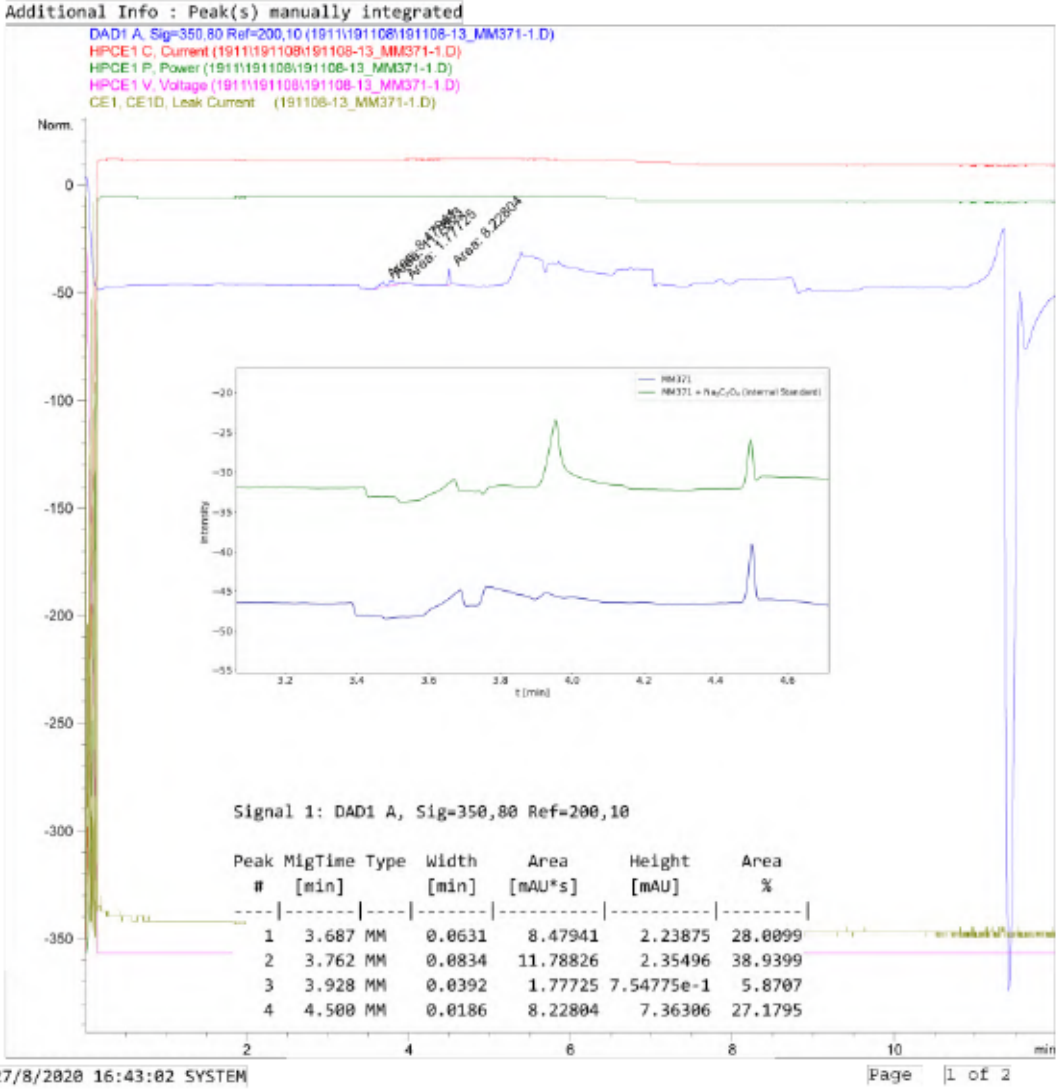

CE 27/8/2020 16:43:02 SYSTEM Page 1 of 2

Figure S 371: Condensed CE analysis for the NaOH extract of Table S 16, entry 2 – CO_2 treatment of **127**, CuI and $AgBPh_4$ in MeOH.

Data File C:\Chem32\1\Data\2006\200622\200622-1_MM563.D
Sample Name: MM563

```
==================================================================
Acq. Operator   : SYSTEM
Sample Operator : SYSTEM
Acq. Instrument : CE                              Location :   21
Injection Date  : 22/6/2020 11:50:32
Acq. Method     : C:\Chem32\1\Methods\CE\Marx-Oxalate25C-Flush10mV12-200114.M
Last changed    : 14/1/2020 13:19:47 by SYSTEM
Analysis Method : C:\Chem32\1\Methods\CE\SwitchOff-200227.M
Last changed    : 22/6/2020 17:11:11 by SYSTEM
                  (modified after loading)
Sample Info     : NMR solution of MM563 (0.04 mL) diluted with H2O (0.6 mL)

Additional Info : Peak(s) manually integrated
```

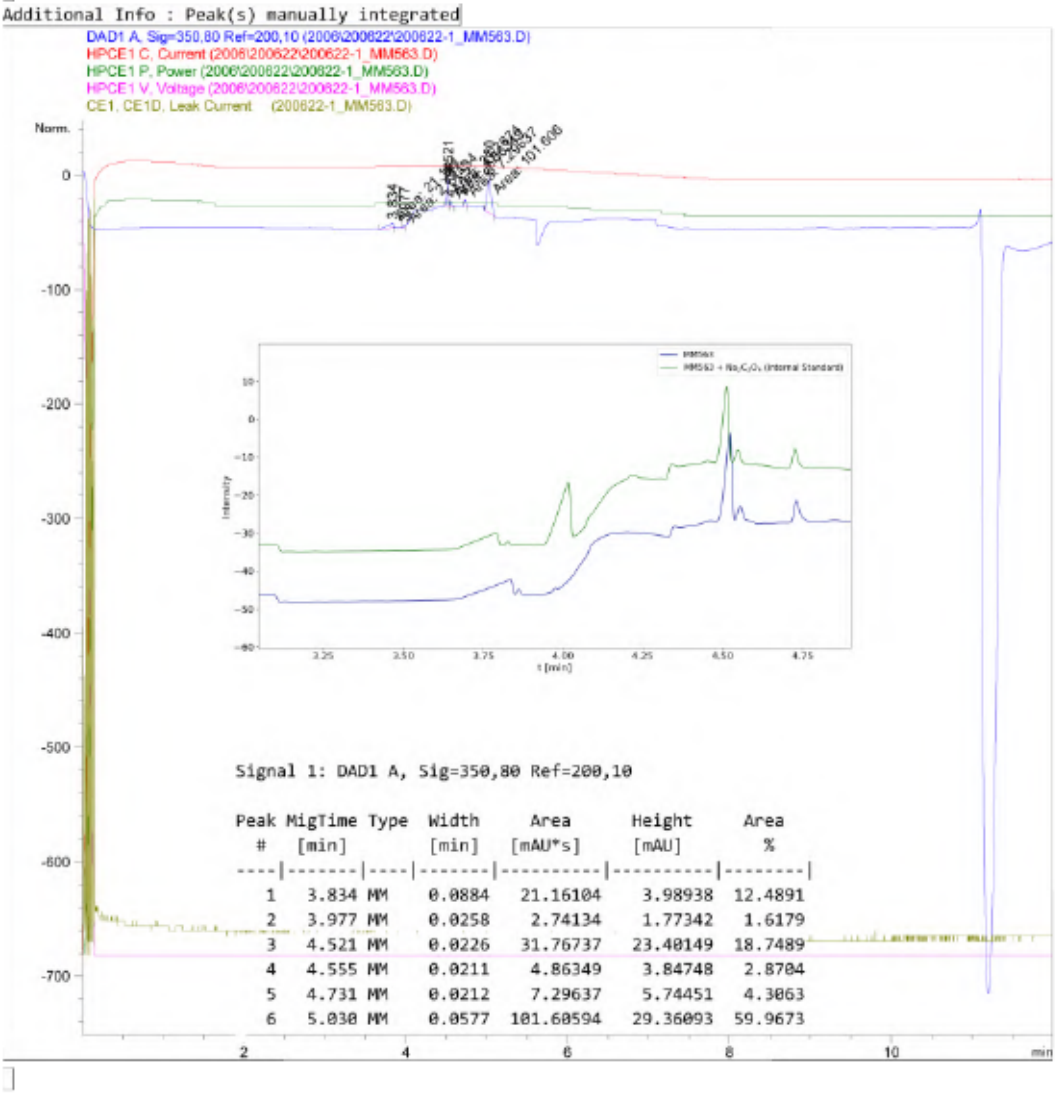

Signal 1: DAD1 A, Sig=350,80 Ref=200,10

Peak #	MigTime [min]	Type	Width [min]	Area [mAU*s]	Height [mAU]	Area %
1	3.834	MM	0.0884	21.16104	3.98938	12.4891
2	3.977	MM	0.0258	2.74134	1.77342	1.6179
3	4.521	MM	0.0226	31.76737	23.40149	18.7489
4	4.555	MM	0.0211	4.86349	3.84748	2.8704
5	4.731	MM	0.0212	7.29637	5.74451	4.3063
6	5.038	MM	0.0577	101.60594	29.36093	59.9673

CE 22/6/2020 17:11:15 SYSTEM Page 1 of 2

Figure S 372: Condensed CE analysis for the NaOH extract of Table S 16, entry 3 – CO_2 treatment of **127** and $[Cu(MeCN)_4]PF_6$ in MeOH.

Data File C:\Chem32\1\Data\1911\191121\191121-3_MM316-1.D
Sample Name: MM316-1

```
======================================================================
Acq. Operator   : SYSTEM
Sample Operator : SYSTEM
Acq. Instrument : CE                          Location :  21
Injection Date  : 21/11/2019 14:52:27
Acq. Method     : C:\Chem32\1\Methods\CE\Marx-Oxalate25C-Flush4mV12-191106.M
Last changed    : 12/11/2019 10:53:07 by SYSTEM
Analysis Method : C:\Chem32\1\Methods\CE\Marx-Oxalate25C-Flush10mV23-V13-200428.M
Last changed    : 27/8/2020 16:36:34 by SYSTEM
                  (modified after loading)
Method Info     : 02.10.2019 Methode geändert auf Agilent Organic Acids Kit

Sample Info     : First run on 21.11.19
                  NMR solution of MM316-1 (0.02 mL) diluted with H2O (0.8 mL)

Additional Info : Peak(s) manually integrated
```

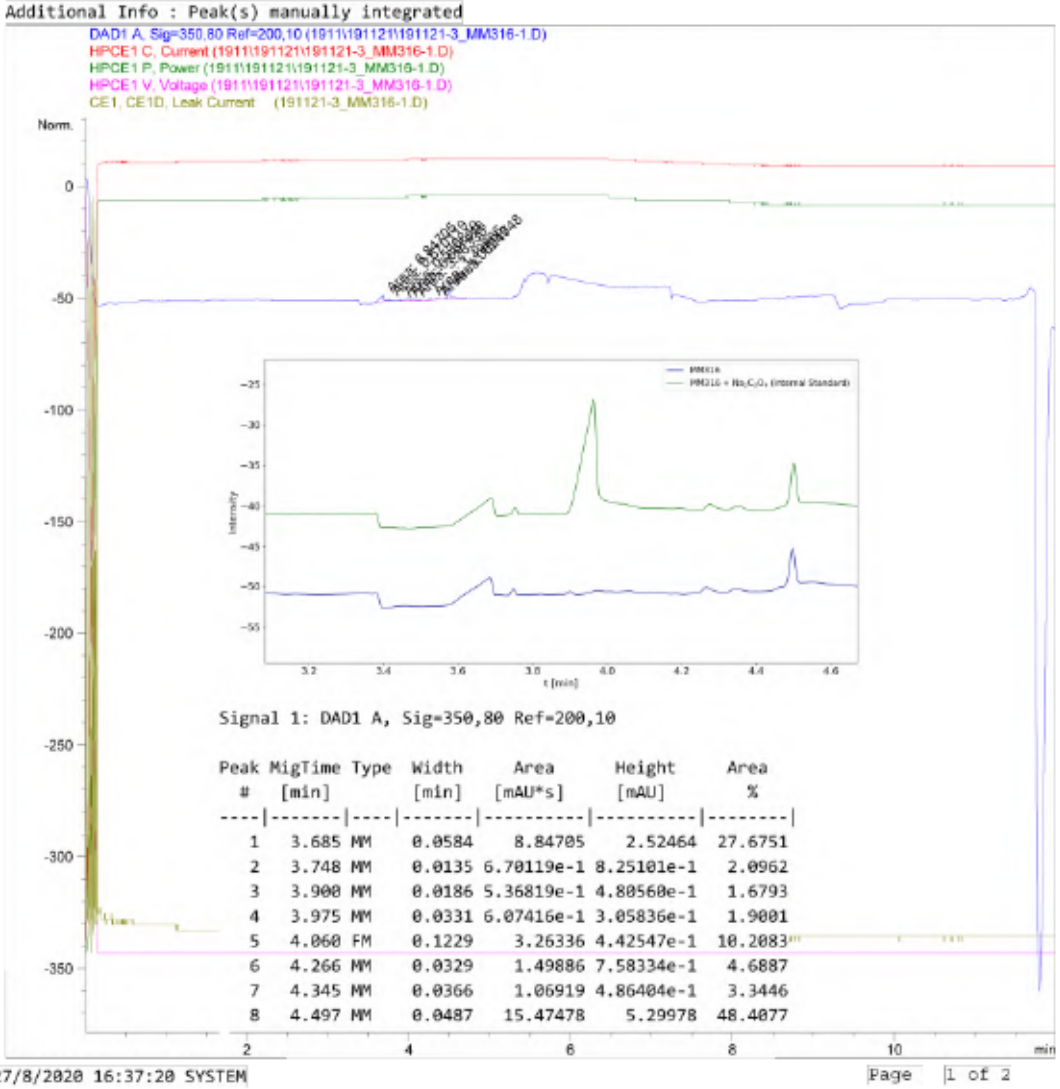

Signal 1: DAD1 A, Sig=350,80 Ref=200,10

Peak #	MigTime [min]	Type	Width [min]	Area [mAU*s]	Height [mAU]	Area %
1	3.685	MM	0.0584	8.84705	2.52464	27.6751
2	3.748	MM	0.0135	6.70119e-1	8.25101e-1	2.0962
3	3.900	MM	0.0186	5.36819e-1	4.80560e-1	1.6793
4	3.975	MM	0.0331	6.07416e-1	3.05836e-1	1.9001
5	4.060	FM	0.1229	3.26336	4.42547e-1	10.2083
6	4.266	MM	0.0329	1.49886	7.58334e-1	4.6887
7	4.345	MM	0.0366	1.06919	4.86404e-1	3.3446
8	4.497	MM	0.0487	15.47478	5.29978	48.4077

CE 27/8/2020 16:37:20 SYSTEM Page 1 of 2

Figure S 373: Condensed CE analysis for the NaOH extract of Table S 16, entry 4 – CO_2 treatment of **127** and $[Cu(MeCN)_4]PF_6$ in MeOH.

Data File C:\Chem32\1\Data\1911\191108\191108-14_MM372-1.D
Sample Name: MM372-1

```
==================================================================
Acq. Operator   : SYSTEM
Sample Operator : SYSTEM
Acq. Instrument : CE                          Location :   27
Injection Date  : 8/11/2019 15:02:40
Acq. Method     : C:\CHEM32\1\METHODS\CE\Marx-Oxalate25C-Flush4mV34-191108.M
Last changed    : 8/11/2019 13:40:25 by SYSTEM
Analysis Method : C:\Chem32\1\Methods\CE\Marx-Oxalate25C-Flush10mV23-V13-200428.M
Last changed    : 27/8/2020 16:36:34 by SYSTEM
                  (modified after loading)
Method Info     : 02.10.2019 Methode geändert auf Agilent Organic Acids Kit

Sample Info     : NMR solution of MM372-1 (0.02 mL diluted with 0.8 mL H2O)
                  5 min flush, 25 °C

Additional Info : Peak(s) manually integrated
```

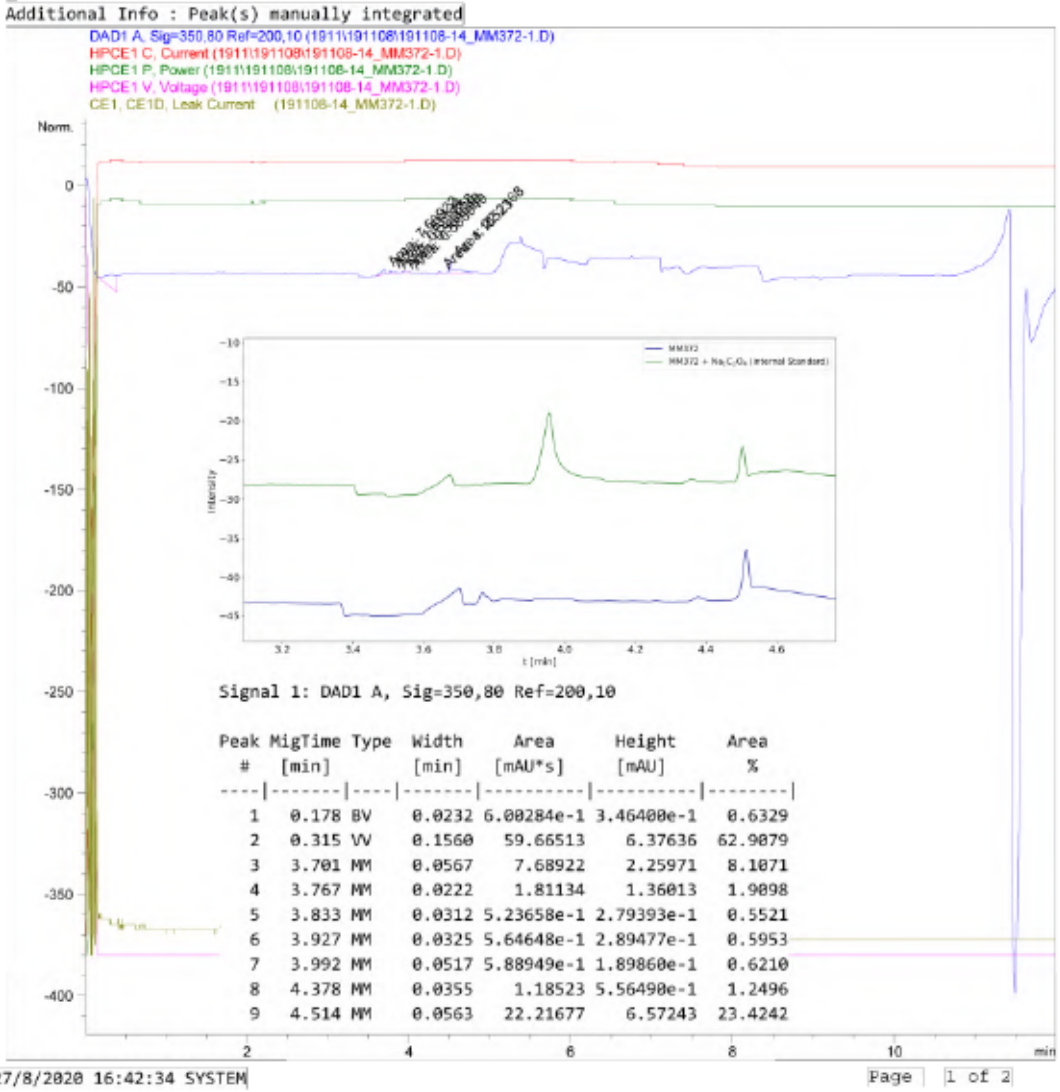

Signal 1: DAD1 A, Sig=350,80 Ref=200,10

Peak #	MigTime [min]	Type	Width [min]	Area [mAU*s]	Height [mAU]	Area %
1	0.178	BV	0.0232	6.00284e-1	3.46400e-1	0.6329
2	0.315	VV	0.1560	59.66513	6.37636	62.9079
3	3.701	MM	0.0567	7.68922	2.25971	8.1071
4	3.767	MM	0.0222	1.81134	1.36013	1.9098
5	3.833	MM	0.0312	5.23658e-1	2.79393e-1	0.5521
6	3.927	MM	0.0325	5.64648e-1	2.89477e-1	0.5953
7	3.992	MM	0.0517	5.88949e-1	1.89860e-1	0.6210
8	4.378	MM	0.0355	1.18523	5.56490e-1	1.2496
9	4.514	MM	0.0563	22.21677	6.57243	23.4242

CE 27/8/2020 16:42:34 SYSTEM Page 1 of 2

Figure S 374: Condensed CE analysis for the NaOH extract of Table S 16, entry 5 – CO_2 treatment of **127**, $[Cu(MeCN)_4]PF_6$ and $NaBPh_4$ in MeOH.

Data File C:\Chem32\1\Data\1911\191108\191108-8_MM361-1.D
Sample Name: MM361-1

Acq. Operator	: SYSTEM	
Sample Operator	: SYSTEM	
Acq. Instrument	: CE	Location : 23
Injection Date	: 8/11/2019 13:23:11	
Acq. Method	: C:\Chem32\1\Methods\CE\Marx-Oxalate25C-Flush4mV12-191106.M	
Last changed	: 8/11/2019 11:05:47 by SYSTEM	
Analysis Method	: C:\Chem32\1\Methods\CE\Spuel-extended-200227.M	
Last changed	: 5/6/2020 16:37:44 by SYSTEM (modified after loading)	
Sample Info	: NMR solution of MM361-1 (0.02 mL diluted with 0.8 mL H2O) 5 min flush, 25 °C	

Additional Info : Peak(s) manually integrated

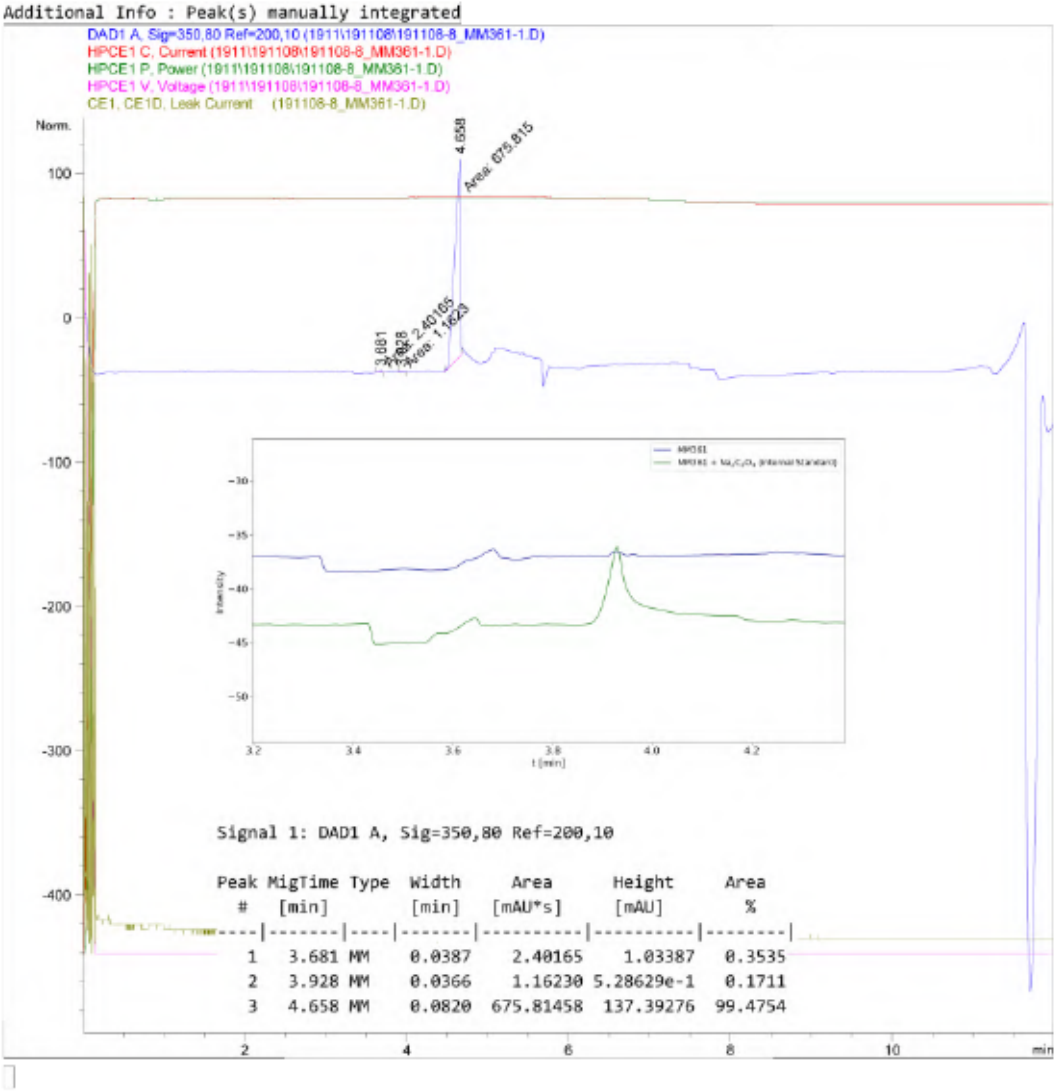

Signal 1: DAD1 A, Sig=350,80 Ref=200,10

Peak #	MigTime [min]	Type	Width [min]	Area [mAU*s]	Height [mAU]	Area %
1	3.681	MM	0.0387	2.40165	1.03387	0.3535
2	3.928	MM	0.0366	1.16230	5.28629e-1	0.1711
3	4.658	MM	0.0820	675.81458	137.39276	99.4754

CE 5/6/2020 16:44:20 SYSTEM Page 1 of 2

Figure S 375: Condensed CE analysis for the NaOH extract of Table S 16, entry 6 – CO_2 treatment of **127**, $[Cu(MeCN)_4]PF_6$ and NaO_2CH in MeOH.

Data File C:\Chem32\1\Data\1911\191108\191108-9_MM363-1.D
Sample Name: MM363-1

```
=====================================================================
Acq. Operator   : SYSTEM
Sample Operator : SYSTEM
Acq. Instrument : CE                              Location :   24
Injection Date  : 8/11/2019 13:52:47
Acq. Method     : C:\CHEM32\1\METHODS\CE\Marx-Oxalate25C-Flush4mV34-191108.M
Last changed    : 8/11/2019 13:40:25 by SYSTEM
Analysis Method : C:\Chem32\1\Methods\CE\Spuel-extended-200227.M
Last changed    : 5/6/2020 16:37:44 by SYSTEM
                  (modified after loading)
Sample Info     : NMR solution of MM363-1 (0.02 mL diluted with 0.8 mL H2O)
                  5 min flush, 25 °C

Additional Info : Peak(s) manually integrated
```

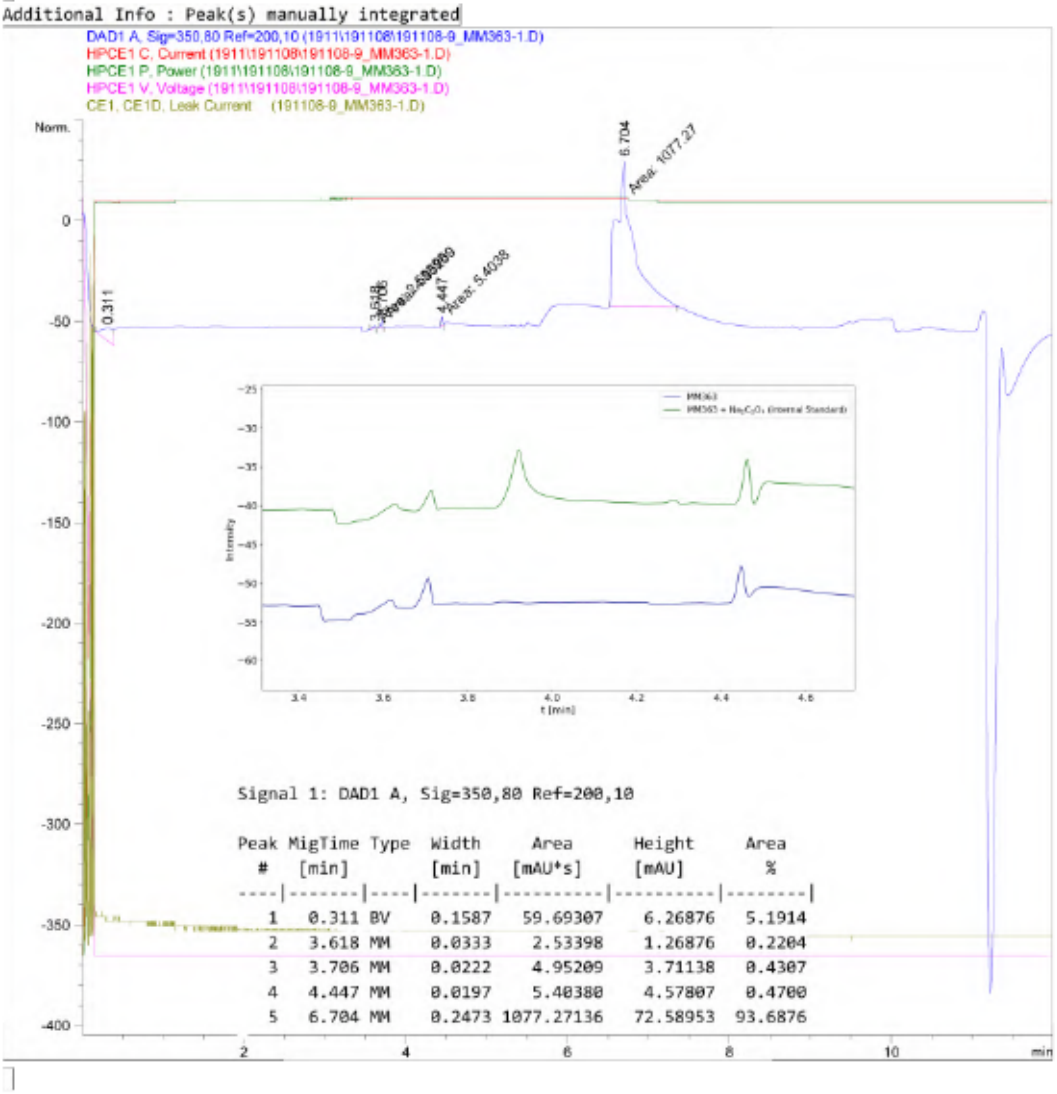

Signal 1: DAD1 A, Sig=350,80 Ref=200,10

Peak #	MigTime [min]	Type	Width [min]	Area [mAU*s]	Height [mAU]	Area %
1	0.311	BV	0.1587	59.69307	6.26876	5.1914
2	3.618	MM	0.0333	2.53398	1.26876	0.2204
3	3.706	MM	0.0222	4.95209	3.71138	0.4307
4	4.447	MM	0.0197	5.48380	4.57807	0.4700
5	6.704	MM	0.2473	1077.27136	72.58953	93.6876

CE 5/6/2020 16:50:47 SYSTEM Page 1 of 2

Figure S 376: Condensed CE analysis for the NaOH extract of Table S 16, entry 7 – CO_2 treatment of **127**, $[Cu(MeCN)_4]PF_6$ and $Mg(OTf)_2$ in MeOH.

```
Data File C:\Chem32\1\Data\1911\191108\191108-6_MM339-1.D
Sample Name: MM339-1

======================================================================
Acq. Operator   : SYSTEM
Sample Operator : SYSTEM
Acq. Instrument : CE                              Location :   21
Injection Date  : 8/11/2019 12:33:46
Acq. Method     : C:\Chem32\1\Methods\CE\Marx-Oxalate25C-Flush4mV12-191106.M
Last changed    : 8/11/2019 11:05:47 by SYSTEM
Analysis Method : C:\Chem32\1\Methods\CE\Spuel-extended-200227.M
Last changed    : 5/6/2020 16:37:44 by SYSTEM
                  (modified after loading)
Sample Info     : NMR solution of MM339-1 (0.02 mL diluted with 0.8 mL H2O)
                  5 min flush, 25 °C

Additional Info : Peak(s) manually integrated
```

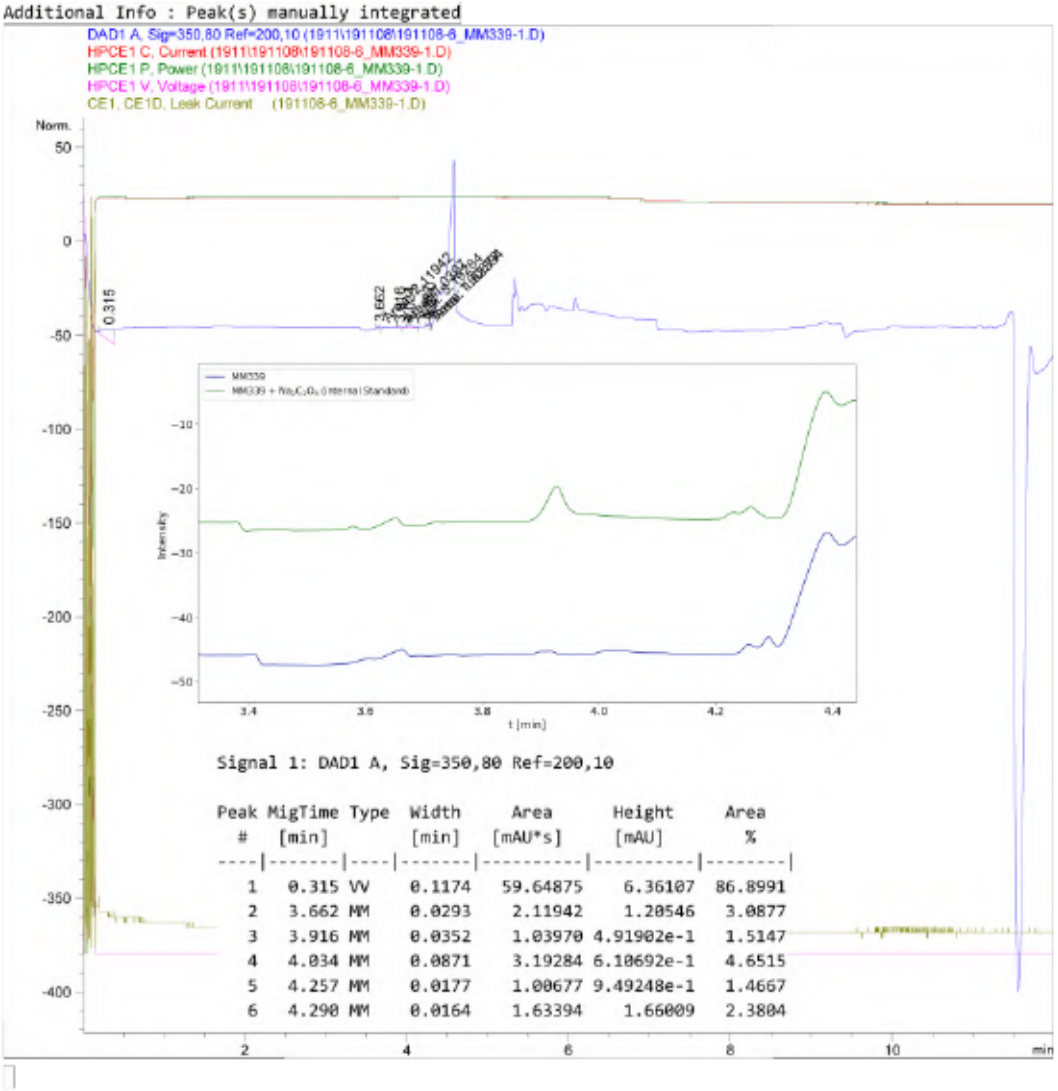


```
Signal 1: DAD1 A, Sig=350,80 Ref=200,10

Peak MigTime Type  Width     Area      Height     Area
  #   [min]       [min]   [mAU*s]     [mAU]       %
----|-------|----|-------|----------|----------|--------|
   1   0.315 VV    0.1174   59.64875    6.36107  86.8991
   2   3.662 MM    0.0293    2.11942    1.20546   3.0877
   3   3.916 MM    0.0352    1.03970 4.91902e-1   1.5147
   4   4.034 MM    0.0871    3.19284 6.10692e-1   4.6515
   5   4.257 MM    0.0177    1.00677 9.49248e-1   1.4667
   6   4.290 MM    0.0164    1.63394    1.66009   2.3804
```


Figure S 377: Condensed CE analysis for the NaOH extract of Table S 16, entry 8 – CO_2 treatment of **127**, $[Cu(MeCN)_4]PF_6$ and $LiBF_4$ in MeOH.

Data File C:\Chem32\1\Data\1911\191108\191108-7_MM360-1.D
Sample Name: MM360-1

```
==================================================================
Acq. Operator   : SYSTEM
Sample Operator : SYSTEM
Acq. Instrument : CE                          Location :   22
Injection Date  : 8/11/2019 12:57:03
Acq. Method     : C:\Chem32\1\Methods\CE\Marx-Oxalate25C-Flush4mV12-191106.M
Last changed    : 8/11/2019 11:05:47 by SYSTEM
Analysis Method : C:\Chem32\1\Methods\CE\Spuel-extended-200227.M
Last changed    : 5/6/2020 16:37:44 by SYSTEM
                  (modified after loading)
Sample Info     : NMR solution of MM360-1 (0.02 mL diluted with 0.8 mL H2O)
                  5 min flush, 25 °C

Additional Info : Peak(s) manually integrated
```

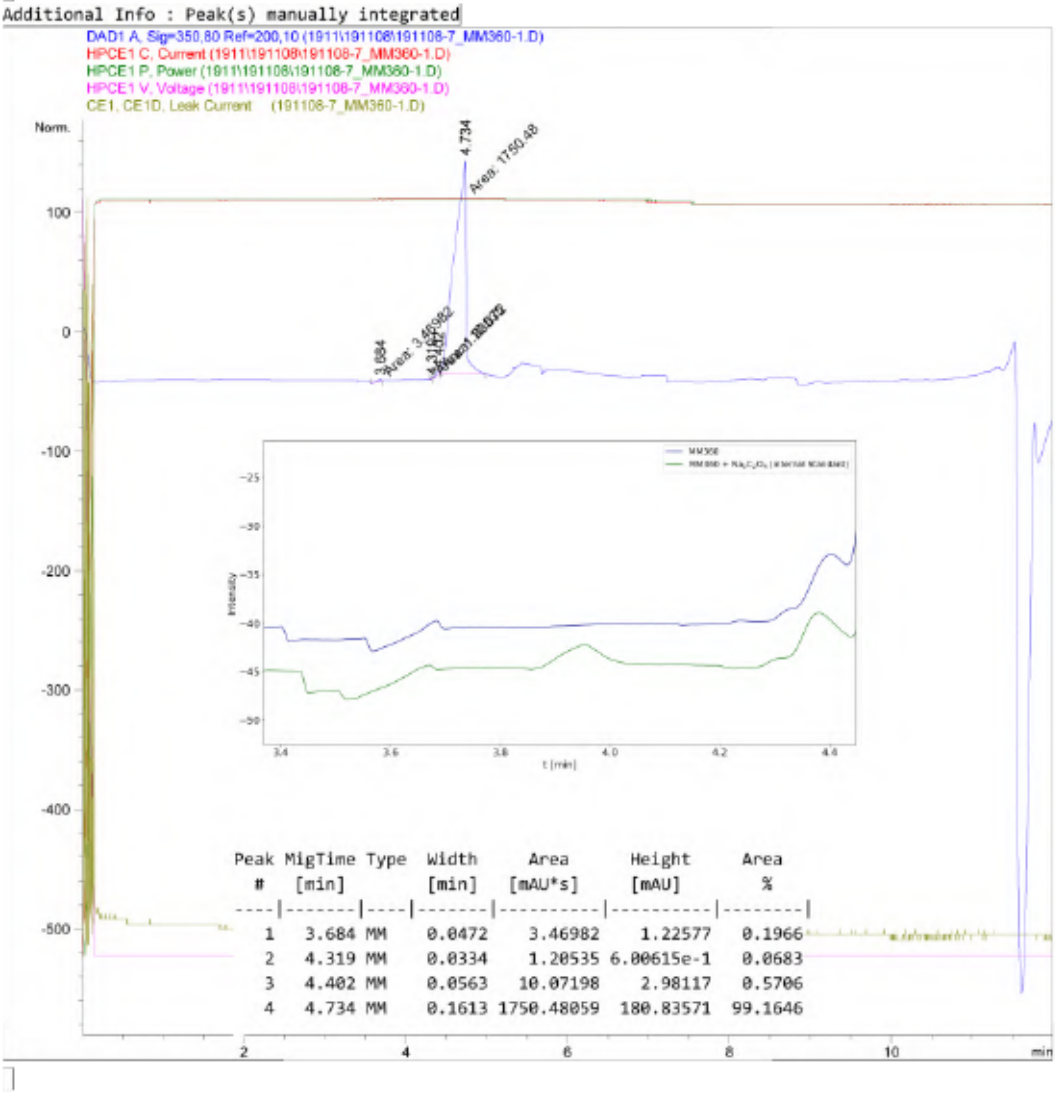

Peak #	MigTime [min]	Type	Width [min]	Area [mAU*s]	Height [mAU]	Area %
1	3.684	MM	0.0472	3.46982	1.22577	0.1966
2	4.319	MM	0.0334	1.20535	6.00615e-1	0.0683
3	4.402	MM	0.0563	10.07198	2.98117	0.5706
4	4.734	MM	0.1613	1750.48059	180.83571	99.1646

CE 5/6/2020 16:43:09 SYSTEM Page 1 of 2

Figure S 378: Condensed CE analysis for the NaOH extract of Table S 16, entry 9 – CO_2 treatment of **127**, $[Cu(MeCN)_4]PF_6$, $LiBF_4$ and NaO_2CH in MeOH.

Data File C:\Chem32\1\Data\1911\191108\191108-10_MM364-1.D
Sample Name: MM364-1

Acq. Operator	: SYSTEM	
Sample Operator	: SYSTEM	
Acq. Instrument	: CE	Location : 25
Injection Date	: 8/11/2019 14:16:05	
Acq. Method	: C:\CHEM32\1\METHODS\CE\Marx-Oxalate25C-Flush4mV34-191108.M	
Last changed	: 8/11/2019 13:40:25 by SYSTEM	
Analysis Method	: C:\Chem32\1\Methods\CE\Spuel-extended-200227.M	
Last changed	: 5/6/2020 16:37:44 by SYSTEM (modified after loading)	
Sample Info	: NMR solution of MM364-1 (0.02 mL diluted with 0.8 mL H2O) 5 min flush, 25 °C	
Additional Info	: Peak(s) manually integrated	

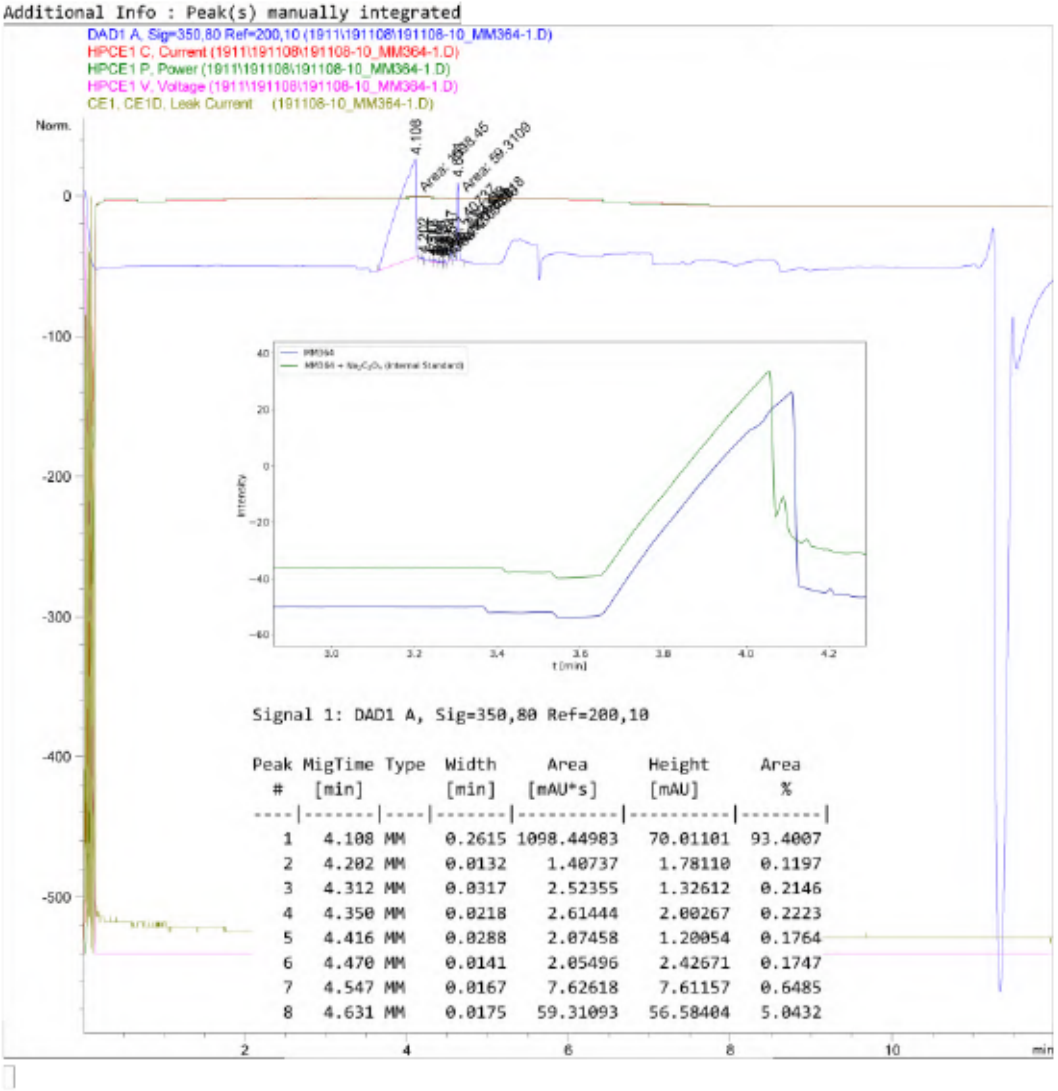

Signal 1: DAD1 A, Sig=350,80 Ref=200,10

Peak #	MigTime [min]	Type	Width [min]	Area [mAU*s]	Height [mAU]	Area %
1	4.108	MM	0.2615	1098.44983	70.01101	93.4007
2	4.202	MM	0.0132	1.40737	1.78110	0.1197
3	4.312	MM	0.0317	2.52355	1.32612	0.2146
4	4.350	MM	0.0218	2.61444	2.00267	0.2223
5	4.416	MM	0.0288	2.07458	1.20054	0.1764
6	4.470	MM	0.0141	2.05496	2.42671	0.1747
7	4.547	MM	0.0167	7.62618	7.61157	0.6485
8	4.631	MM	0.0175	59.31093	56.58404	5.0432

CE 5/6/2020 16:51:13 SYSTEM Page 1 of 2

Figure S 379: Condensed CE analysis for the NaOH extract of Table S 16, entry 10 – CO_2 treatment of **127**, $[Cu(MeCN)_4]PF_6$ and Na_2SO_3 in MeOH.

```
Data File C:\Chem32\1\Data\1912\191217\191217-2_MM440-1.D
Sample Name: MM440-1

======================================================================
Acq. Operator   : SYSTEM
Sample Operator : SYSTEM
Acq. Instrument : CE                              Location :   21
Injection Date  : 17/12/2019 13:54:06
Acq. Method     : C:\CHEM32\1\METHODS\CE\Marx-Oxalate25C-Flush5mV12-191106.M
Last changed    : 17/12/2019 13:47:38 by SYSTEM
Analysis Method : C:\Chem32\1\Methods\CE\Spuel-extended.M
Last changed    : 17/12/2019 13:46:25 by SYSTEM
                  (modified after loading)
Sample Info     : NMR sample of MM440-1 (0.02 mL diluted with 0.6 mL H2O)
                  Sample prepared on 17.12.19

Additional Info : Peak(s) manually integrated
```

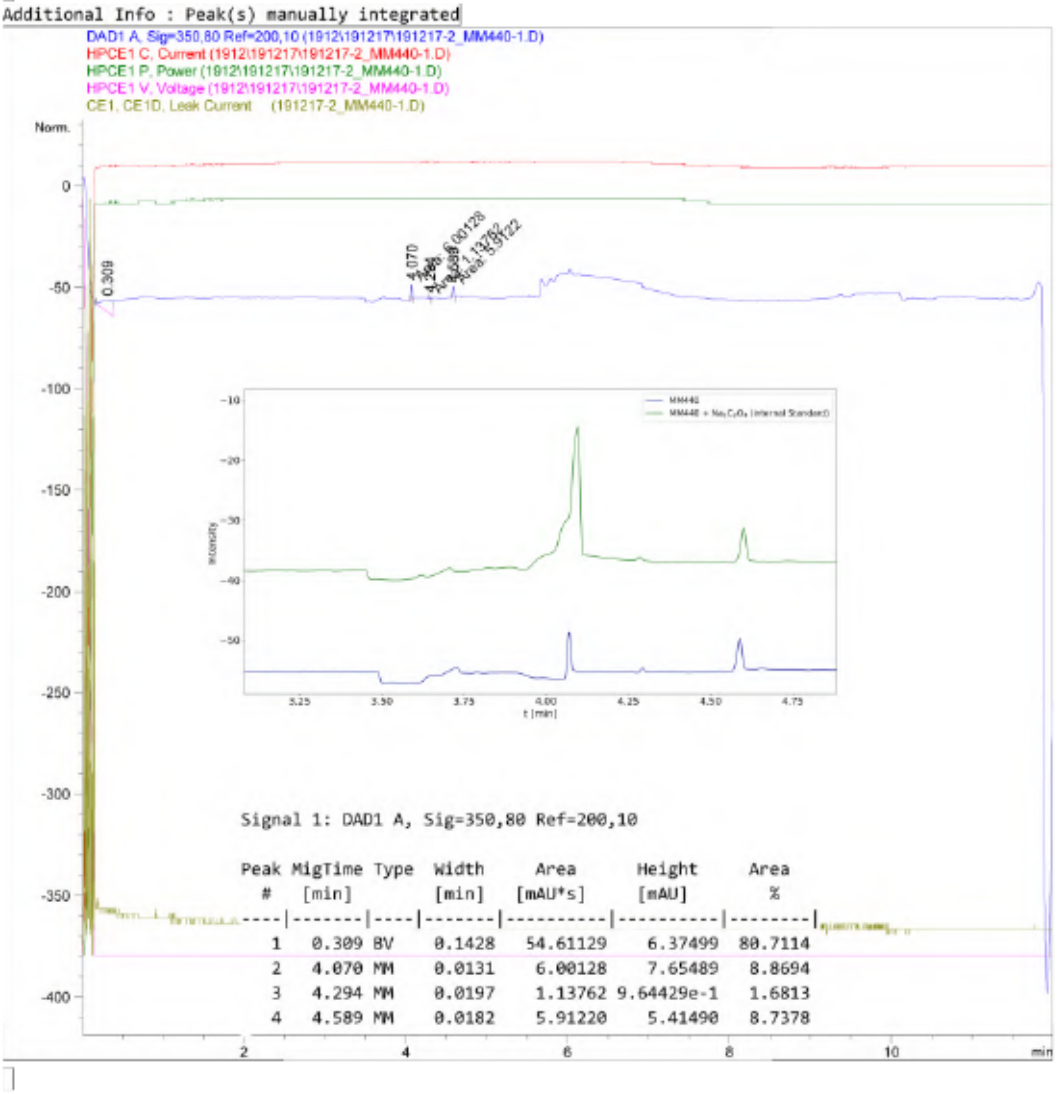


```
Signal 1: DAD1 A, Sig=350,80 Ref=200,10

Peak MigTime Type  Width     Area      Height     Area
  #   [min]       [min]   [mAU*s]     [mAU]       %
----|-------|----|-------|----------|----------|--------|
   1   0.309 BV    0.1428   54.61129    6.37499  80.7114
   2   4.070 MM    0.0131    6.00128    7.65489   8.8694
   3   4.294 MM    0.0197    1.13762 9.64429e-1   1.6813
   4   4.589 MM    0.0182    5.91220    5.41490   8.7378
```

```
CE 17/12/2019 17:03:33 SYSTEM                              Page  1 of 2
```

Figure S 380: Condensed CE analysis for the NaOH extract of Table S 16, entry 11 – CO_2 treatment of **127**, CuI, $NaBPh_4$ and $NaC_{10}H_8$ in THF.

Data File C:\Chem32\1\Data\2001\200114\200114-3_MM450-1.D
Sample Name: MM450-1

Acq. Operator	: SYSTEM	
Sample Operator	: SYSTEM	
Acq. Instrument	: CE	Location : 22
Injection Date	: 14/1/2020 14:19:03	
Acq. Method	: C:\CHEM32\1\METHODS\CE\Marx-Oxalate25C-Flush10mV12-200114.M	
Last changed	: 14/1/2020 13:19:47 by SYSTEM	
Analysis Method	: C:\Chem32\1\Methods\CE\Spuel-extended-200227.M	
Last changed	: 5/6/2020 16:37:44 by SYSTEM (modified after loading)	
Sample Info	: First run, 10 min flush NMR sample of MM450-1 (0.02 mL diluted with 0.6 mL H2O)	

Additional Info : Peak(s) manually integrated

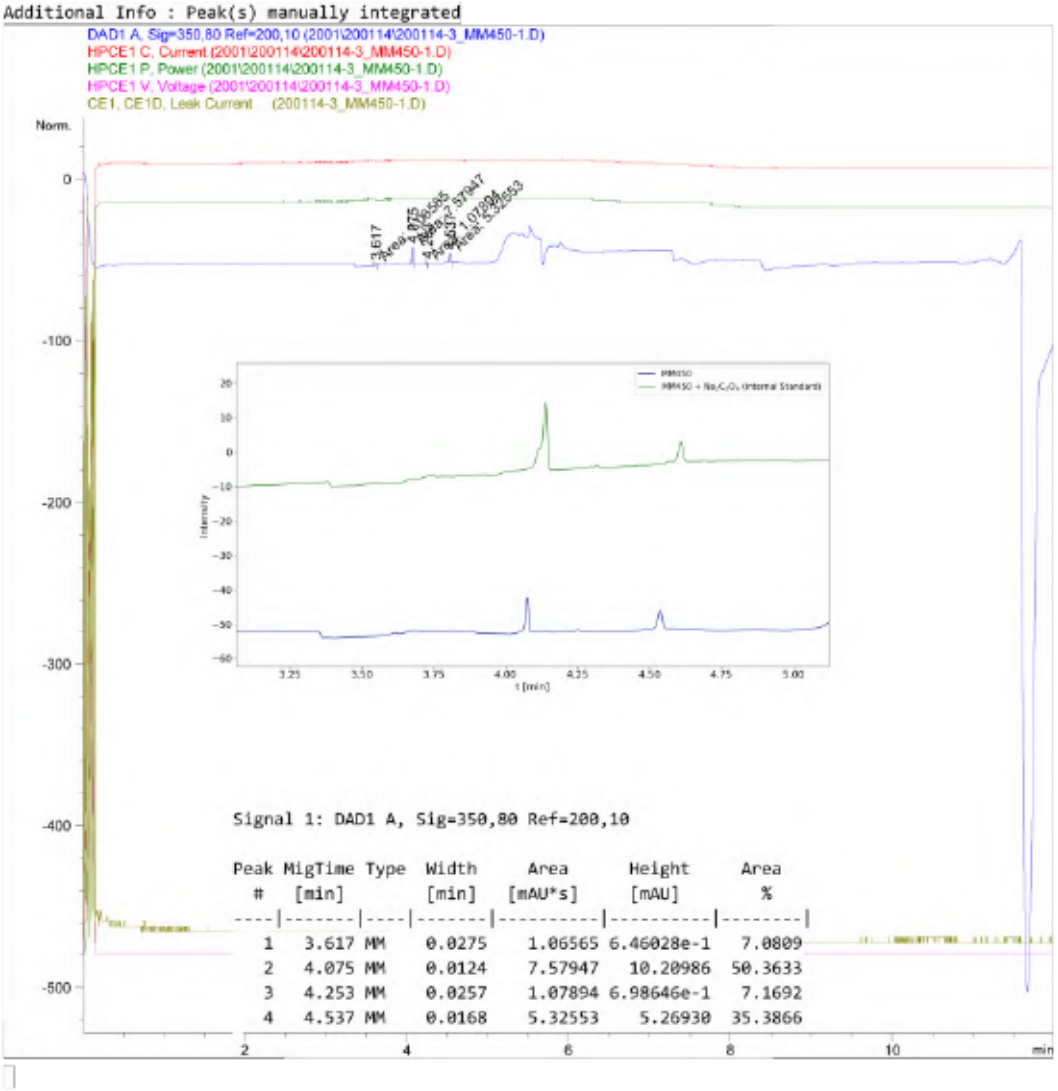

Signal 1: DAD1 A, Sig=350,80 Ref=200,10

Peak #	MigTime [min]	Type	Width [min]	Area [mAU*s]	Height [mAU]	Area %
1	3.617	MM	0.0275	1.06565	6.46028e-1	7.0809
2	4.075	MM	0.0124	7.57947	10.20986	50.3633
3	4.253	MM	0.0257	1.07894	6.98646e-1	7.1692
4	4.537	MM	0.0168	5.32553	5.26930	35.3866

CE 5/6/2020 17:05:20 SYSTEM Page 1 of 2

Figure S 381: Condensed CE analysis for the NaOH extract of Table S 16, entry 12 – CO_2 treatment of **127**, CuI, $NaBPh_4$ and $NaC_{10}H_8$ in THF.

```
Data File C:\Chem32\1\Data\2002\200226\200226-2_MM483-1.D
Sample Name: MM483-1

======================================================================
Acq. Operator   : SYSTEM
Sample Operator : SYSTEM
Acq. Instrument : CE                              Location :   24
Injection Date  : 26/2/2020 16:17:57
Acq. Method     : C:\Chem32\1\Methods\CE\Marx-Oxalate25C-Flush10mV12-200114.M
Last changed    : 14/1/2020 13:19:47 by SYSTEM
Analysis Method : C:\Chem32\1\Methods\CE\Spuel-extended.M
Last changed    : 28/2/2020 14:21:34 by SYSTEM
                  (modified after loading)
Sample Info     : NMR solution of MM483-1 (0.02 mL diluted with 0.6 mL H2O)

Additional Info : Peak(s) manually integrated
```

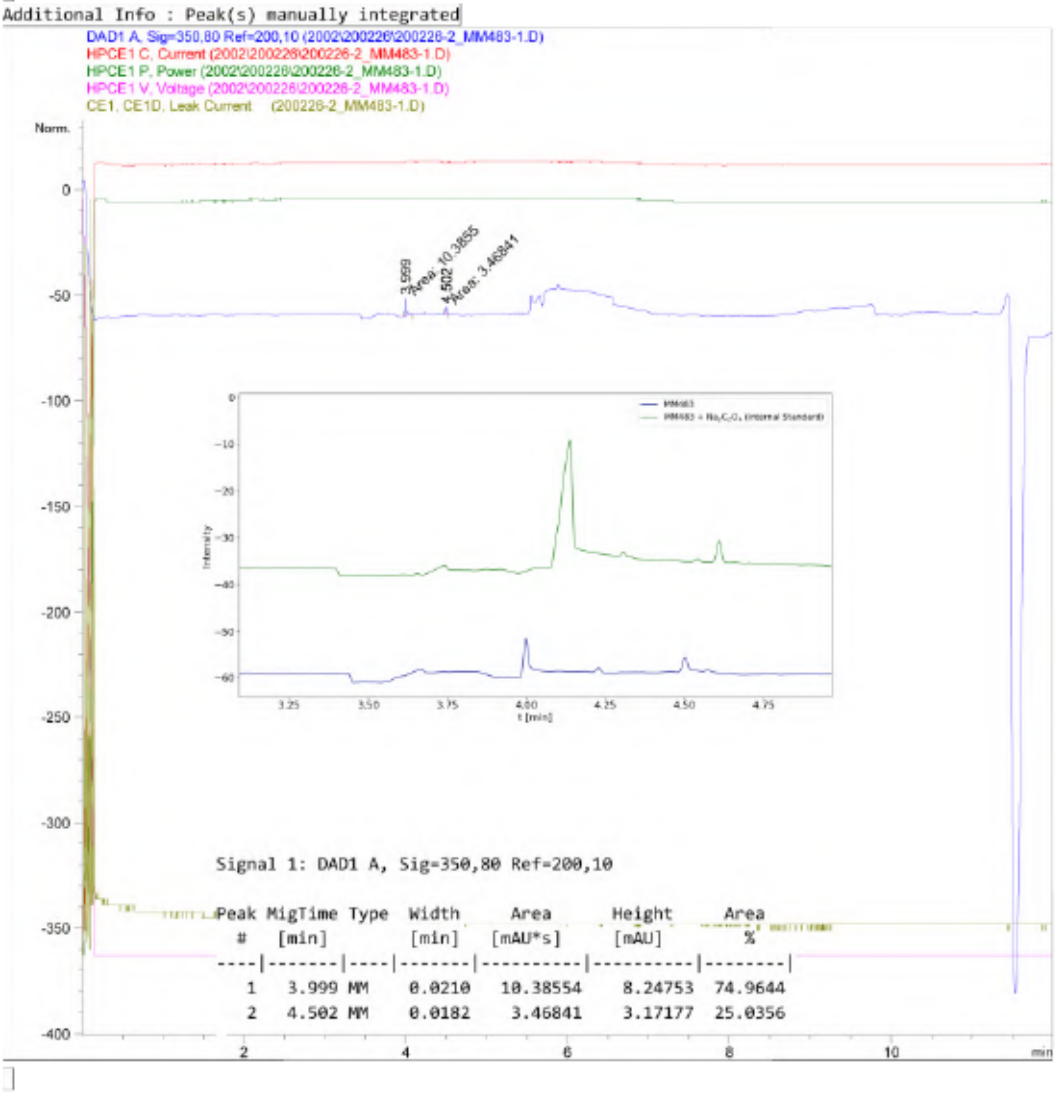


```
Signal 1: DAD1 A, Sig=350,80 Ref=200,10

Peak MigTime Type  Width     Area      Height    Area
  #   [min]       [min]   [mAU*s]     [mAU]      %
----|-------|----|-------|----------|----------|--------|
  1   3.999 MM    0.0210   10.38554    8.24753  74.9644
  2   4.502 MM    0.0182    3.46841    3.17177  25.0356
```

```
CE 28/2/2020 14:26:45 SYSTEM                              Page  1 of 2
```

Figure S 382: Condensed CE analysis for the NaOH extract of Table S 16, entry 13 – CO_2 treatment of **127**, CuI, $NaBPh_4$ and $NaC_{10}H_8$ in THF.

```
Data File C:\Chem32\1\Data\2004\200407\200407-2_MM501-1.D
Sample Name: MM501-1

======================================================================
Acq. Operator   : SYSTEM
Sample Operator : SYSTEM
Acq. Instrument : CE                              Location :   25
Injection Date  : 7/4/2020 14:10:30
Acq. Method     : C:\Chem32\1\Methods\CE\Marx-Oxalate25C-Flush10mV12-200114.M
Last changed    : 14/1/2020 13:19:47 by SYSTEM
Analysis Method : C:\Chem32\1\Methods\CE\DEF_CE.M
Last changed    : 7/4/2020 13:52:33 by SYSTEM
                  (modified after loading)
Sample Info     : NMR sample of MM501 (0.03 mL diluted with 0.6 mL H2O)
                  First run on 07.04.20 (sample from 05.03.20)

Additional Info : Peak(s) manually integrated
```

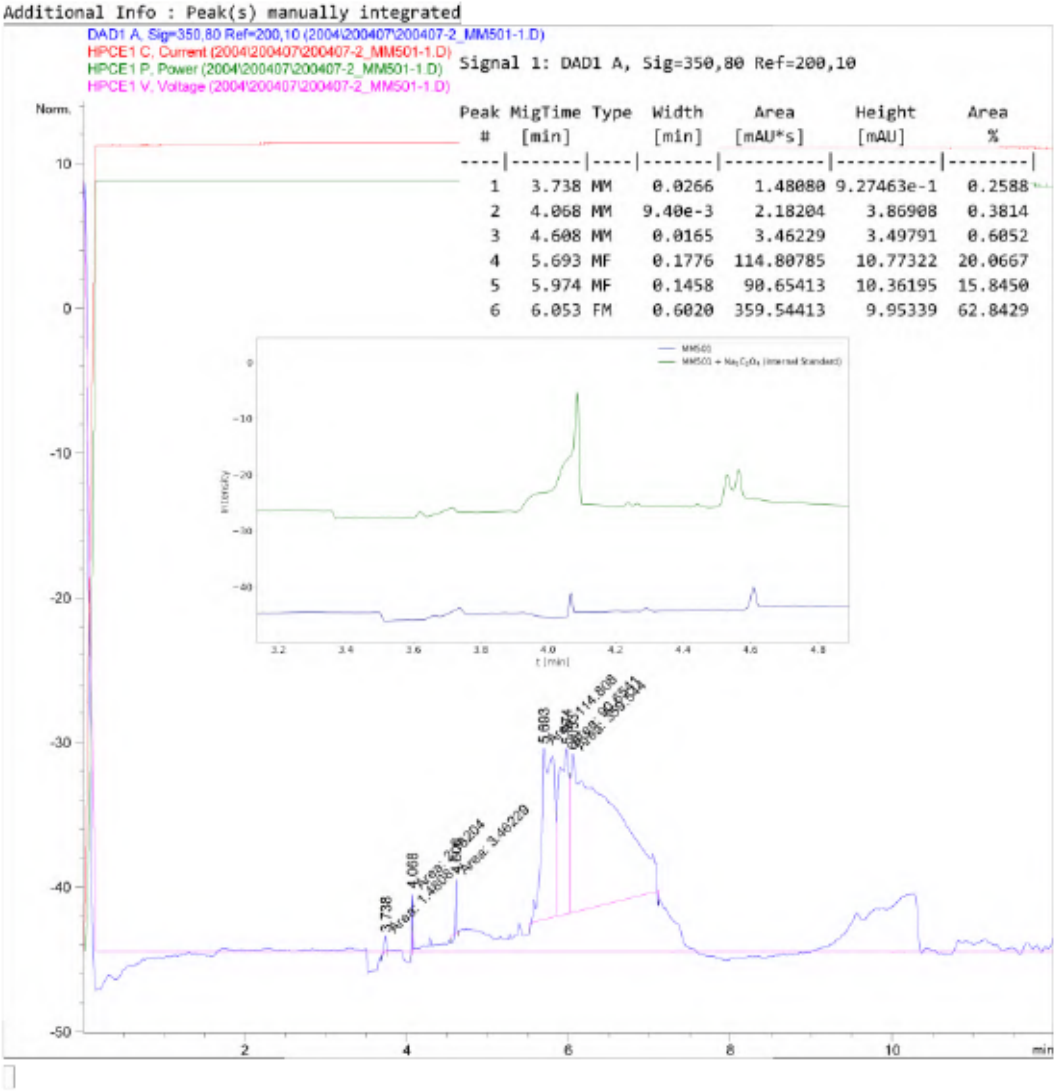

Peak #	MigTime [min]	Type	Width [min]	Area [mAU*s]	Height [mAU]	Area %
1	3.738	MM	0.0266	1.48080	9.27463e-1	0.2588
2	4.068	MM	9.40e-3	2.18204	3.86908	0.3814
3	4.608	MM	0.0165	3.46229	3.49791	0.6052
4	5.693	MF	0.1776	114.80785	10.77322	20.0667
5	5.974	MF	0.1458	90.65413	10.36195	15.8450
6	6.053	FM	0.6020	359.54413	9.95339	62.8429

```
CE 7/4/2020 19:55:33 SYSTEM                                Page   1 of 2
```

Figure S 383: Condensed CE analysis for the NaOH extract of Table S 16, entry 14 – CO_2 treatment of **127**, CuI, $NaBPh_4$ and $NaC_{10}H_8$ in THF.

Data File C:\Chem32\1\Data\2001\200114\200114-2_MM451-1.D
Sample Name: MM451-1

```
====================================================================
Acq. Operator    : SYSTEM
Sample Operator  : SYSTEM
Acq. Instrument  : CE                              Location :   21
Injection Date   : 14/1/2020 13:55:33
Acq. Method      : C:\CHEM32\1\METHODS\CE\Marx-Oxalate25C-Flush10mV12-200114.M
Last changed     : 14/1/2020 13:19:47 by SYSTEM
Analysis Method  : C:\Chem32\1\Methods\CE\Spuel-extended-200227.M
Last changed     : 5/6/2020 16:37:44 by SYSTEM
                   (modified after loading)
Sample Info      : First run, 10 min flush
                   NMR sample of MM451-1 (0.02 mL diluted with 0.6 mL H2O)

Additional Info : Peak(s) manually integrated
```

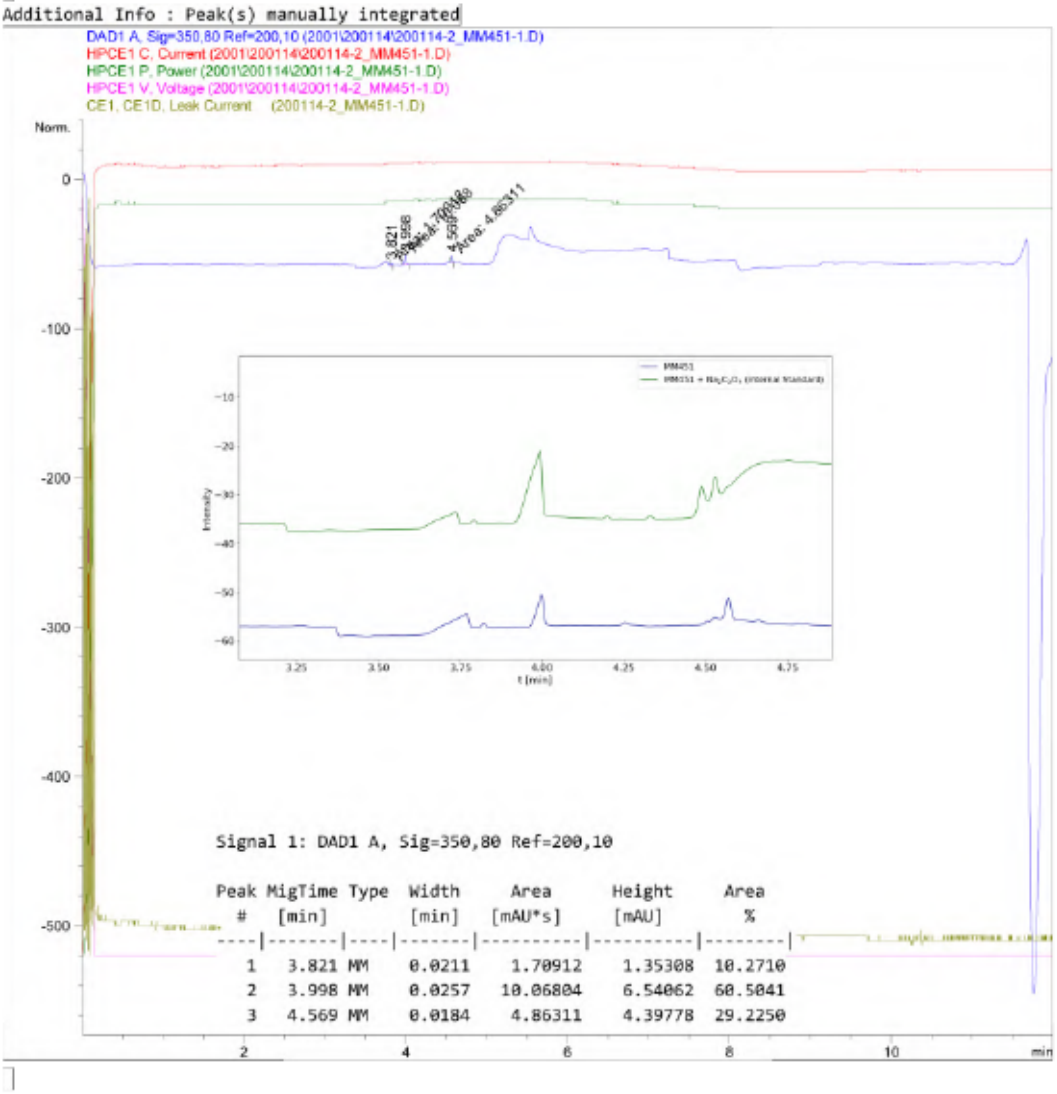

Signal 1: DAD1 A, Sig=350,80 Ref=200,10

Peak #	MigTime [min]	Type	Width [min]	Area [mAU*s]	Height [mAU]	Area %
1	3.821	MM	0.0211	1.70912	1.35308	10.2710
2	3.998	MM	0.0257	10.06804	6.54062	60.5041
3	4.569	MM	0.0184	4.86311	4.39778	29.2250

CE 5/6/2020 17:05:02 SYSTEM Page 1 of 2

Figure S 384: Condensed CE analysis for the NaOH extract of Table S 16, entry 15 – CO_2 treatment of $NaC_{10}H_8$ in THF.

Data File C:\Chem32\1\Data\2002\200226\200226-3_MM484-1.D
Sample Name: MM484-1

```
=====================================================================
Acq. Operator   : SYSTEM
Sample Operator : SYSTEM
Acq. Instrument : CE                              Location :   25
Injection Date  : 26/2/2020 16:41:26
Acq. Method     : C:\Chem32\1\Methods\CE\Marx-Oxalate25C-Flush10mV12-200114.M
Last changed    : 14/1/2020 13:19:47 by SYSTEM
Analysis Method : C:\Chem32\1\Methods\CE\Spuel-extended.M
Last changed    : 28/2/2020 14:21:34 by SYSTEM
                  (modified after loading)
Sample Info     : NMR solution of MM484-1 (0.02 mL diluted with 0.6 mL H2O)

Additional Info : Peak(s) manually integrated
```

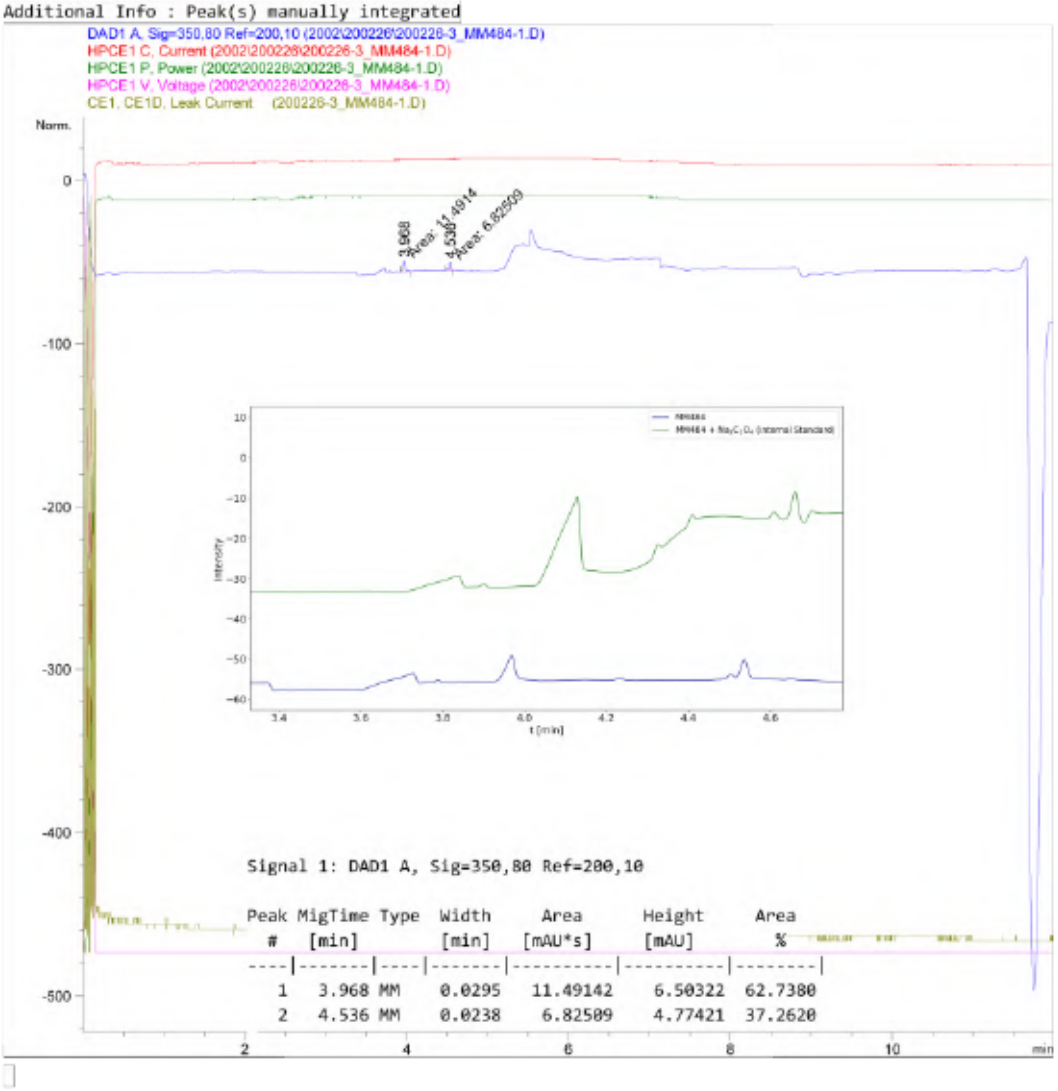

Peak #	MigTime [min]	Type	Width [min]	Area [mAU*s]	Height [mAU]	Area %
1	3.968	MM	0.0295	11.49142	6.50322	62.7380
2	4.536	MM	0.0238	6.82509	4.77421	37.2620

CE 28/2/2020 14:26:18 SYSTEM Page 1 of 2

Figure S 385: Condensed CE analysis for the NaOH extract of Table S 16, entry 16 – CO_2 treatment of $NaC_{10}H_8$ in THF.

```
Data File C:\Chem32\1\Data\2004\200407\200407-3_MM502-1.D
Sample Name: MM502-1

======================================================================
Acq. Operator   : SYSTEM
Sample Operator : SYSTEM
Acq. Instrument : CE                              Location :   26
Injection Date  : 7/4/2020 14:33:59
Acq. Method     : C:\Chem32\1\Methods\CE\Marx-Oxalate25C-Flush10mV12-200114.M
Last changed    : 14/1/2020 13:19:47 by SYSTEM
Analysis Method : C:\Chem32\1\Methods\CE\DEF_CE.M
Last changed    : 7/4/2020 13:52:33 by SYSTEM
                  (modified after loading)
Sample Info     : NMR sample of MM502 (0.03 mL diluted with 0.6 mL H2O)
                  First run on 07.04.20 (sample from 05.03.20)

Additional Info : Peak(s) manually integrated
```

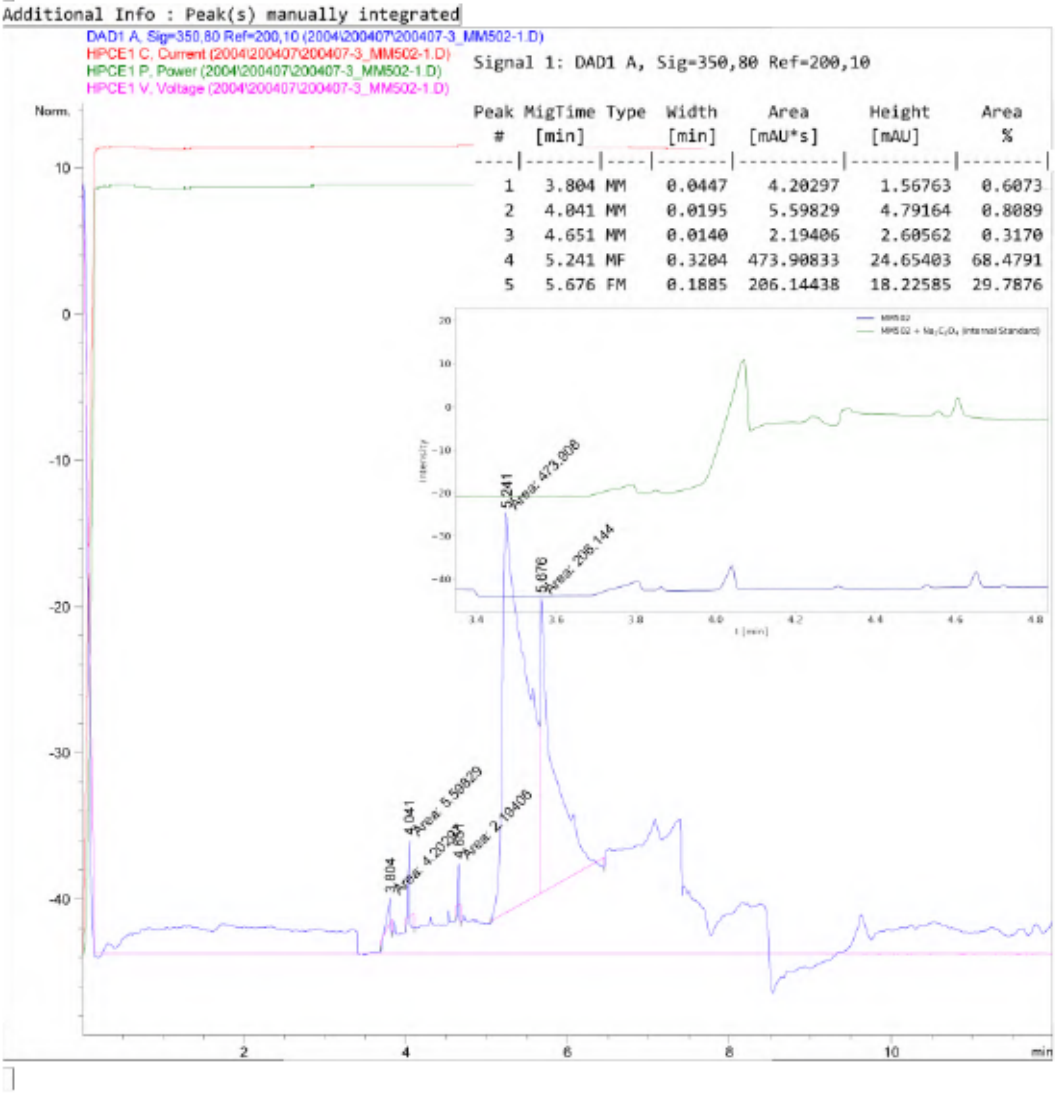

Peak #	MigTime [min]	Type	Width [min]	Area [mAU*s]	Height [mAU]	Area %
1	3.804	MM	0.0447	4.20297	1.56763	0.6073
2	4.041	MM	0.0195	5.59829	4.79164	0.8089
3	4.651	MM	0.0140	2.19406	2.60562	0.3170
4	5.241	MF	0.3204	473.90833	24.65403	68.4791
5	5.676	FM	0.1885	206.14438	18.22585	29.7876

```
CE 7/4/2020 19:55:48 SYSTEM                              Page  1 of 2
```

Figure S 386: Condensed CE analysis for the NaOH extract of Table S 16, entry 17 – CO_2 treatment of $NaC_{10}H_8$ in THF.

Data File C:\Chem32\1\Data\2004\200416\200416-2_MM508-1.D
Sample Name: MM508-1

```
=====================================================================
Acq. Operator   : SYSTEM
Sample Operator : SYSTEM
Acq. Instrument : CE                              Location :   31
Injection Date  : 16/4/2020 13:28:05
Acq. Method     : C:\Chem32\1\Methods\CE\Marx-Oxalate25C-Flush10mV12-200114.M
Last changed    : 14/1/2020 13:19:47 by SYSTEM
Analysis Method : C:\Chem32\1\Methods\CE\Spuel-extended-200227.M
Last changed    : 5/6/2020 16:37:44 by SYSTEM
                  (modified after loading)
Sample Info     : NMR sample of MM508-1 (0.03 mL diluted with 0.6 ml H2O)

Additional Info : Peak(s) manually integrated
```

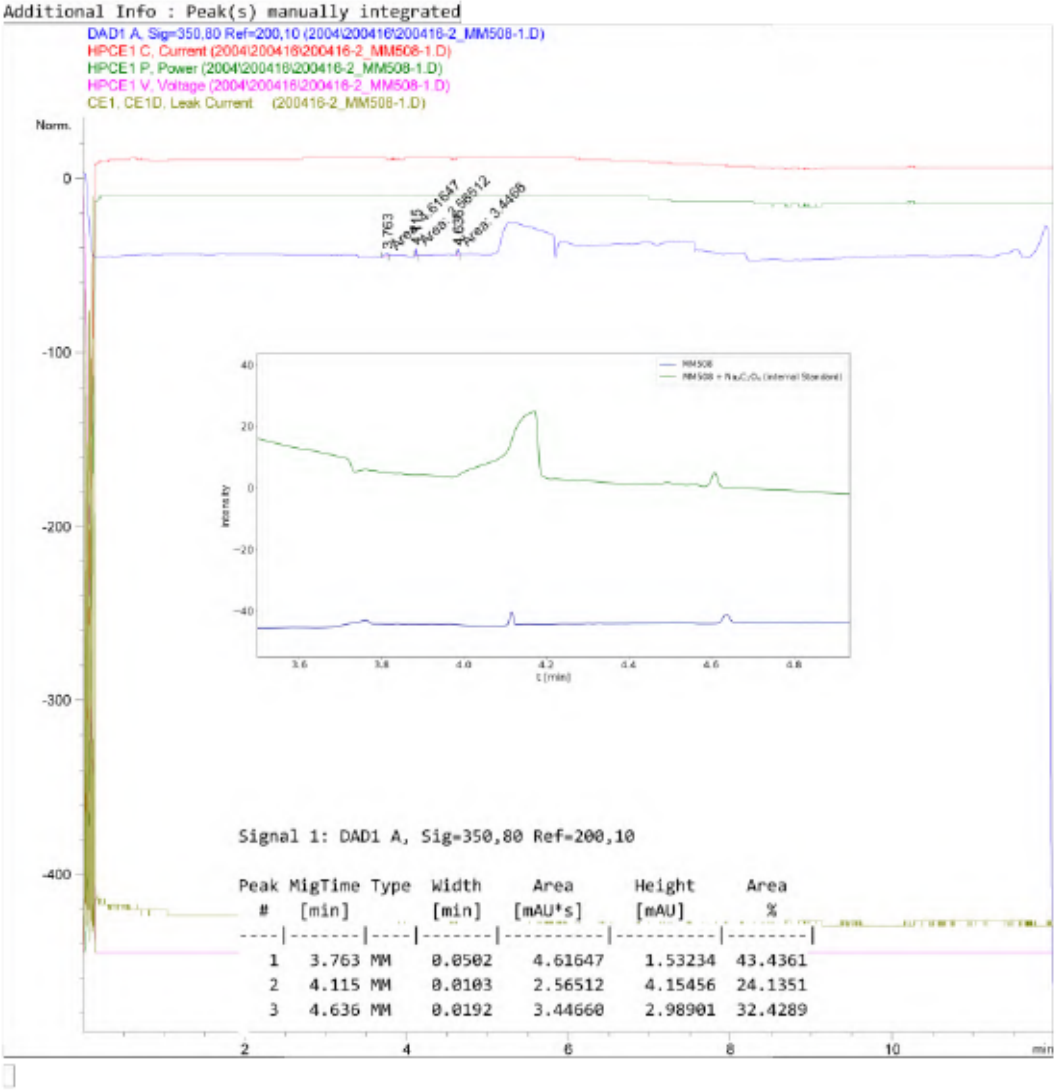

Signal 1: DAD1 A, Sig=350,80 Ref=200,10

Peak #	MigTime [min]	Type	Width [min]	Area [mAU*s]	Height [mAU]	Area %
1	3.763	MM	0.0502	4.61647	1.53234	43.4361
2	4.115	MM	0.0103	2.56512	4.15456	24.1351
3	4.636	MM	0.0192	3.44660	2.98901	32.4289

CE 5/6/2020 17:15:31 SYSTEM Page 1 of 2

Figure S 387: Condensed CE analysis for the NaOH extract of Table S 17, entry 1 – Air exposure of a solution of CuI, **127** and $NaBPh_4$ in MeOH.

```
Data File C:\Chem32\1\Data\2005\200506\200506-4_MM539-sol-1.D
Sample Name: MM539-sol-1

======================================================================
Acq. Operator   : SYSTEM
Sample Operator : SYSTEM
Acq. Instrument : CE                              Location :   23
Injection Date  : 6/5/2020 14:26:09
Acq. Method     : C:\Chem32\1\Methods\CE\Marx-Oxalate25C-Flush10mV12-200114.M
Last changed    : 14/1/2020 13:19:47 by SYSTEM
Analysis Method : C:\Chem32\1\Methods\CE\Spuel-extended-200227.M
Last changed    : 5/6/2020 16:37:44 by SYSTEM
                  (modified after loading)
Sample Info     : NMR sample of MM539-sol-1 (0.03 mL diluted with 0.6 mL H2O)

Additional Info : Peak(s) manually integrated
```

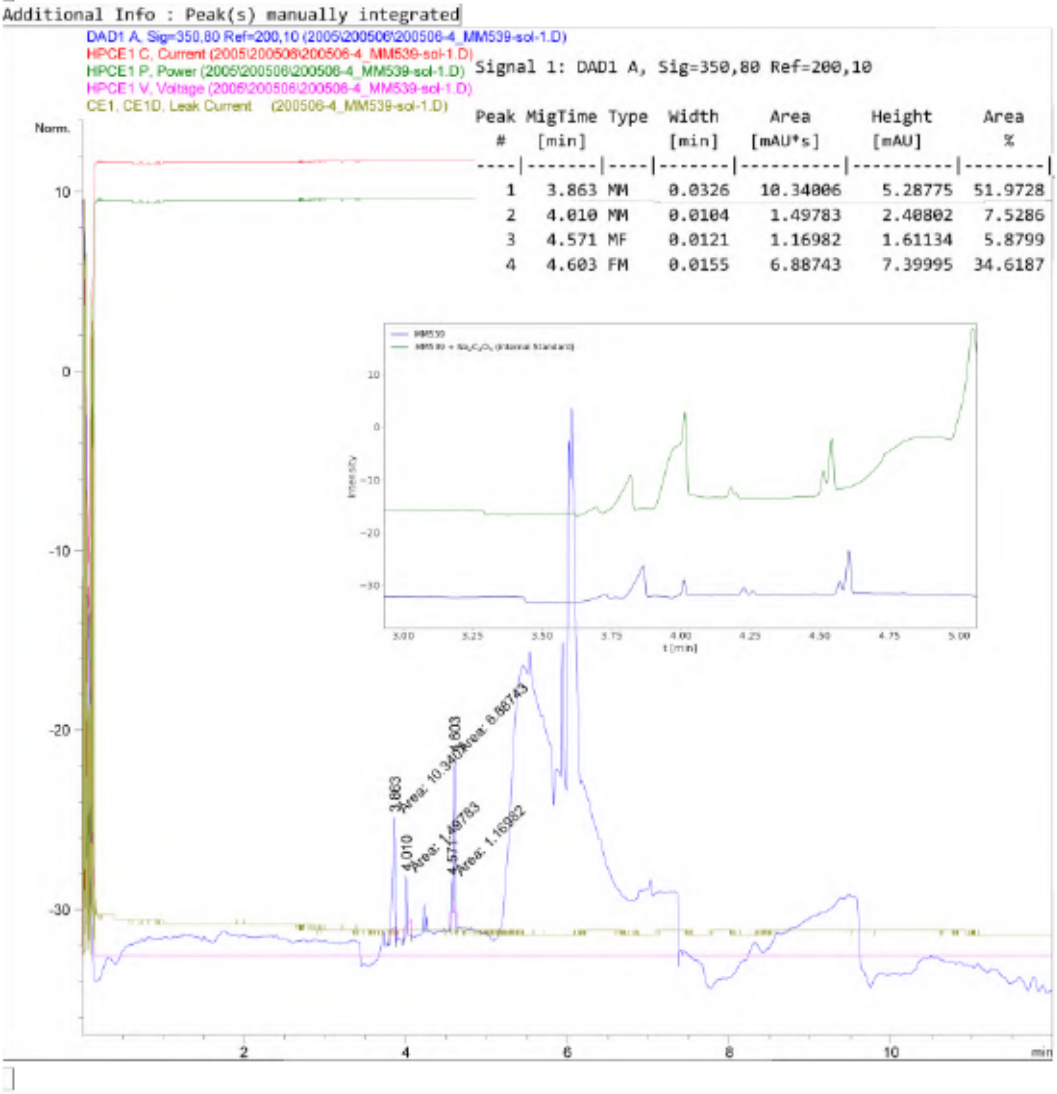

Signal 1: DAD1 A, Sig=350,80 Ref=200,10

Peak #	MigTime [min]	Type	Width [min]	Area [mAU*s]	Height [mAU]	Area %
1	3.863	MM	0.0326	10.34006	5.28775	51.9728
2	4.010	MM	0.0104	1.49783	2.40802	7.5286
3	4.571	MF	0.0121	1.16982	1.61134	5.8799
4	4.603	FM	0.0155	6.88743	7.39995	34.6187

```
CE 5/6/2020 17:31:29 SYSTEM                                Page   1 of 2
```

Figure S 388: Condensed CE analysis for the NaOH extract of Table S 17, entry 2 – Air exposure of a solution of CuI, **127** and $NaBPh_4$ in MeOH.

Data File C:\Chem32\1\Data\2005\200527\200527-5_MM552-1.D
Sample Name: MM552-1

```
==================================================================
Acq. Operator   : SYSTEM
Sample Operator : SYSTEM
Acq. Instrument : CE                              Location :   21
Injection Date  : 27/5/2020 14:56:04
Acq. Method     : C:\Chem32\1\Methods\CE\Marx-Oxalate25C-Flush10mV23-V13-200428.M
Last changed    : 28/4/2020 15:34:00 by SYSTEM
Analysis Method : C:\Chem32\1\Methods\CE\Spuel-extended-200227.M
Last changed    : 27/5/2020 14:08:30 by SYSTEM
                  (modified after loading)
Sample Info     : NMR solution of MM552-1 (0.03 mL diluted with 0.6 mL H2O)

Additional Info : Peak(s) manually integrated
```

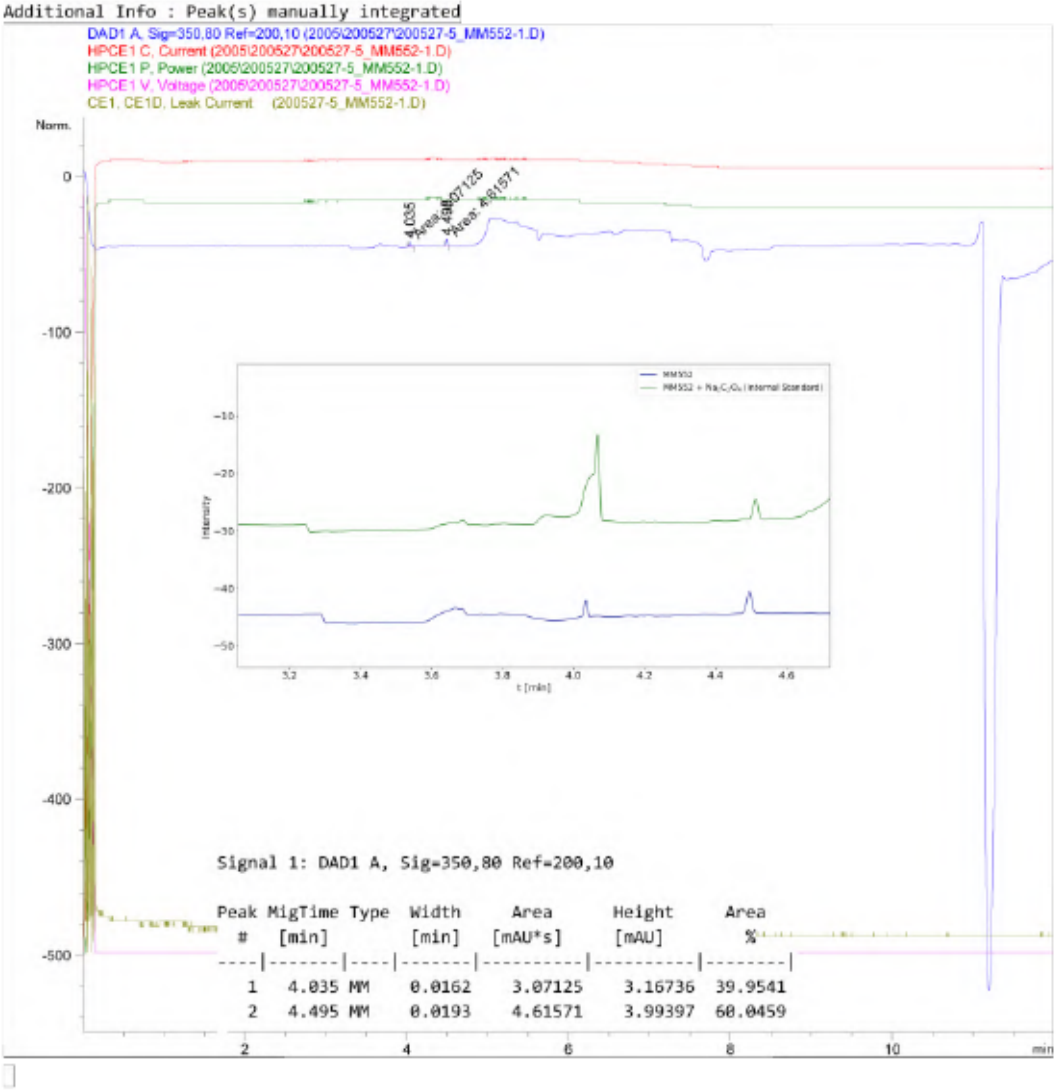

Signal 1: DAD1 A, Sig=350,80 Ref=200,10

Peak #	MigTime [min]	Type	Width [min]	Area [mAU*s]	Height [mAU]	Area %
1	4.035	MM	0.0162	3.07125	3.16736	39.9541
2	4.495	MM	0.0193	4.61571	3.99397	60.0459

Figure S 389: Condensed CE analysis for the NaOH extract of Table S 17, entry 3 – Air exposure of a solution of CuI, **127** and $NaBPh_4$ in MeOH/EtOH.

Data File C:\Chem32\1\Data\2006\200623\200623-2_MM585.D
Sample Name: MM585

```
=====================================================================
Acq. Operator   : SYSTEM
Sample Operator : SYSTEM
Acq. Instrument : CE                              Location :   29
Injection Date  : 23/6/2020 13:02:00
Acq. Method     : C:\Chem32\1\Methods\CE\Marx-Oxalate25C-Flush10mV12-200114.M
Last changed    : 14/1/2020 13:19:47 by SYSTEM
Analysis Method : C:\Chem32\1\Methods\CE\SwitchOff-200227.M
Last changed    : 23/6/2020 13:21:11 by SYSTEM
                  (modified after loading)
Sample Info     : NMR solution of MM585 (0.04 ml) diluted with H2O (0.6 ml)

Additional Info : Peak(s) manually integrated
```

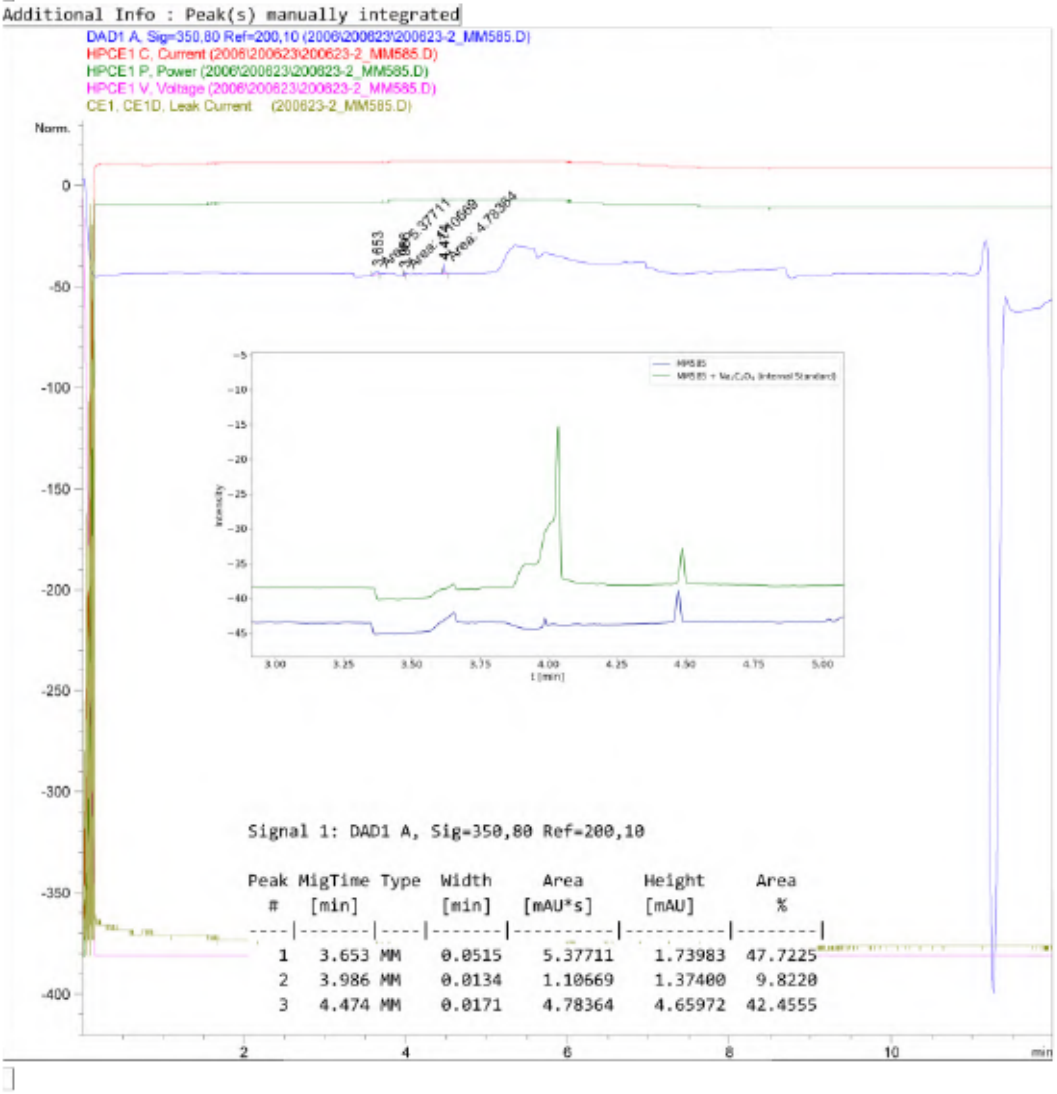

Signal 1: DAD1 A, Sig=350,80 Ref=200,10

Peak #	MigTime [min]	Type	Width [min]	Area [mAU*s]	Height [mAU]	Area %
1	3.653	MM	0.0515	5.37711	1.73983	47.7225
2	3.986	MM	0.0134	1.10669	1.37400	9.8220
3	4.474	MM	0.0171	4.78364	4.65972	42.4555

CE 23/6/2020 14:58:11 SYSTEM Page 1 of 2

Figure S 390: Condensed CE analysis for the NaOH extract of Table S 17, entry 4 – O_2 treatment of a solution of CuI, **127** and $NaBPh_4$ in MeOH.

Data File C:\Chem32\1\Data\2005\200506\200506-2_MM538-1.D
Sample Name: MM538-1

Acq. Operator	: SYSTEM		
Sample Operator	: SYSTEM		
Acq. Instrument	: CE	Location :	21
Injection Date	: 6/5/2020 13:39:08		
Acq. Method	: C:\Chem32\1\Methods\CE\Marx-Oxalate25C-Flush10mV12-200114.M		
Last changed	: 14/1/2020 13:19:47 by SYSTEM		
Analysis Method	: C:\Chem32\1\Methods\CE\Spuel-extended-200227.M		
Last changed	: 5/6/2020 16:37:44 by SYSTEM (modified after loading)		
Sample Info	: NMR sample of MM538-1 (0.03 mL diluted with 0.6 mL H2O)		
Additional Info	: Peak(s) manually integrated		

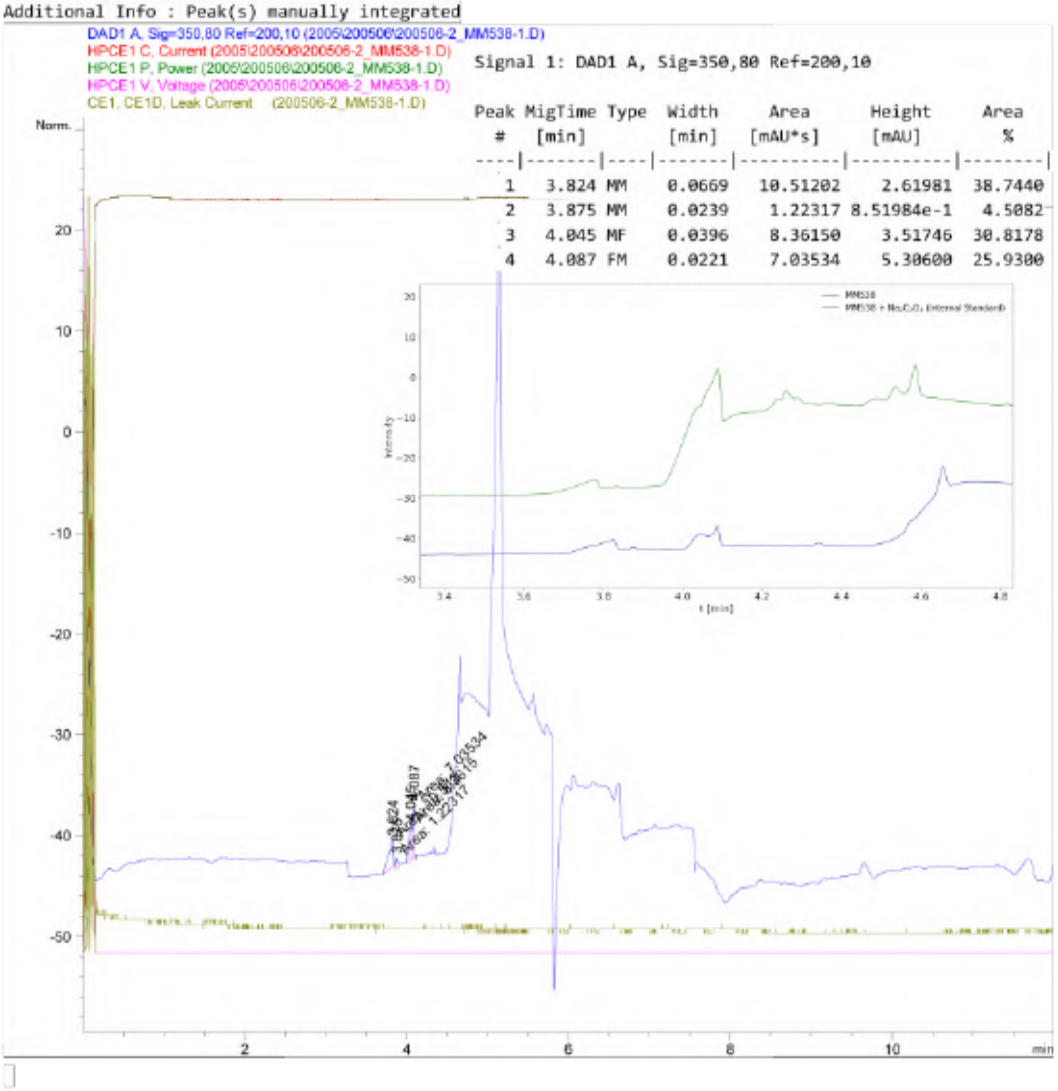

Signal 1: DAD1 A, Sig=350,80 Ref=200,10

Peak #	MigTime [min]	Type	Width [min]	Area [mAU*s]	Height [mAU]	Area %
1	3.824	MM	0.0669	10.51202	2.61981	38.7440
2	3.875	MM	0.0239	1.22317	8.51984e-1	4.5082
3	4.045	MF	0.0396	8.36150	3.51746	30.8178
4	4.087	FM	0.0221	7.03534	5.30600	25.9300

CE 5/6/2020 17:30:47 SYSTEM Page 1 of 2

Figure S 391: Condensed CE analysis for the NaOH extract of Table S 17, entry 5 – Air exposure of a solution of CuI and **127** in MeOH.

Data File C:\Chem32\1\Data\2006\200610\200610-1_MM565.D
Sample Name: MM565

```
==================================================================
Acq. Operator   : SYSTEM
Sample Operator : SYSTEM
Acq. Instrument : CE                              Location :   25
Injection Date  : 10/6/2020 14:07:12
Acq. Method     : C:\Chem32\1\Methods\CE\Marx-Oxalate25C-Flush10mV12-200114.M
Last changed    : 14/1/2020 13:19:47 by SYSTEM
Analysis Method : C:\Chem32\1\Methods\CE\Spuel-extended-200227.M
Last changed    : 10/6/2020 15:17:04 by SYSTEM
                  (modified after loading)
Sample Info     : NMR solution of MM565 (0.04 mL) diluted with H2O (0.6 mL)

Additional Info : Peak(s) manually integrated
```

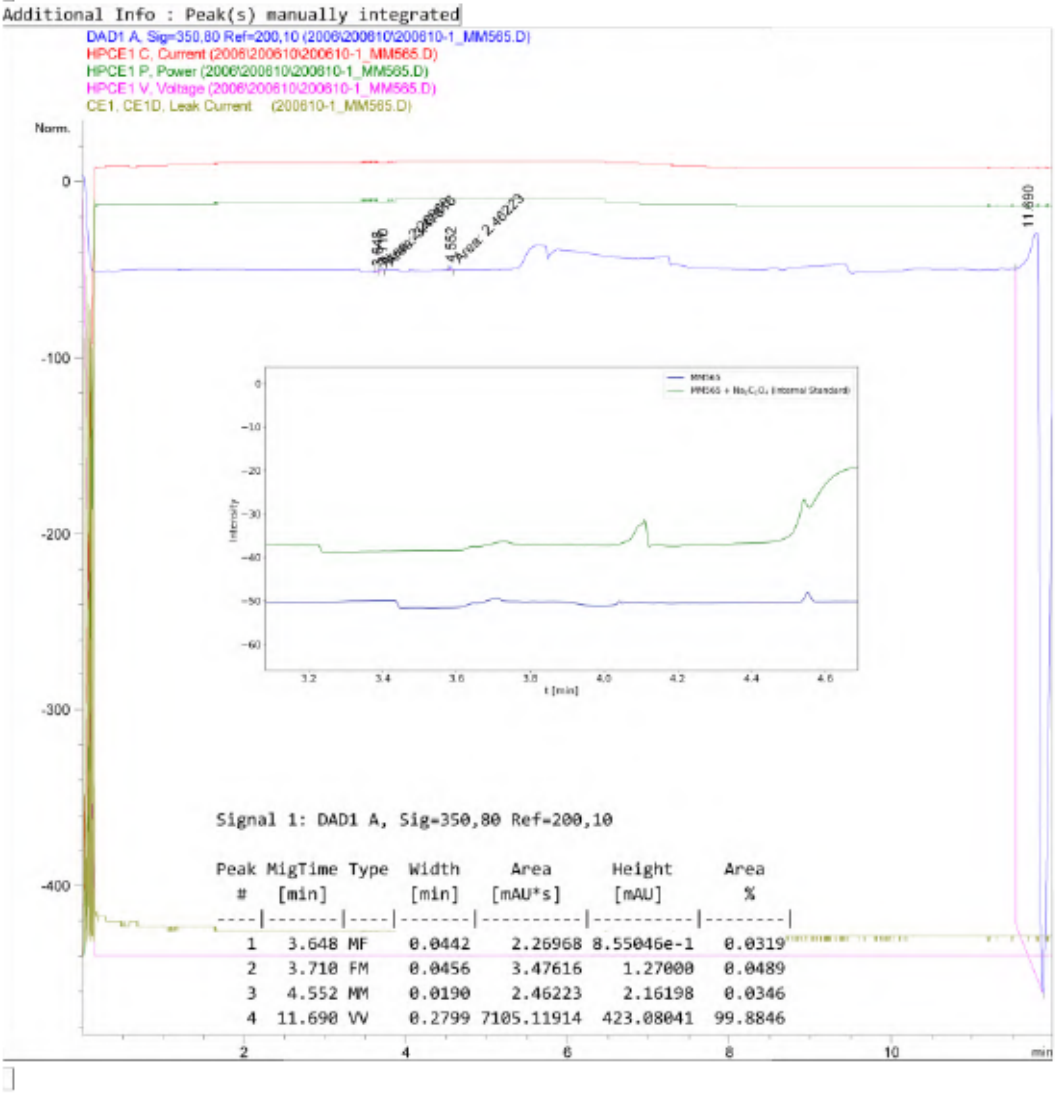

Signal 1: DAD1 A, Sig=350,80 Ref=200,10

Peak #	MigTime [min]	Type	Width [min]	Area [mAU*s]	Height [mAU]	Area %
1	3.648	MF	0.0442	2.26968	8.55046e-1	0.0319
2	3.710	FM	0.0456	3.47616	1.27000	0.0489
3	4.552	MM	0.0190	2.46223	2.16198	0.0346
4	11.690	VV	0.2799	7105.11914	423.08041	99.8846

CE 10/6/2020 19:16:50 SYSTEM Page 1 of 2

Figure S 392: Condensed CE analysis for the NaOH extract of Table S 18, entry 1 – CO_2 treatment of **174**, CuI and $NaBPh_4$ in MeOH.

Data File C:\Chem32\1\Data\1911\191112\191112-10_MM413-1.D
Sample Name: MM413-1

```
======================================================================
Acq. Operator   : SYSTEM
Sample Operator : SYSTEM
Acq. Instrument : CE                          Location :   28
Injection Date  : 12/11/2019 14:31:39
Acq. Method     : C:\Chem32\1\Methods\CE\Marx-Oxalate25C-Flush4mV34-191108.M
Last changed    : 8/11/2019 15:48:42 by SYSTEM
Analysis Method : C:\Chem32\1\Methods\CE\Marx-Oxalate25C-Flush10mV23-V13-200428.M
Last changed    : 27/8/2020 16:36:34 by SYSTEM
                  (modified after loading)
Method Info     : 02.10.2019 Methode geändert auf Agilent Organic Acids Kit

Sample Info     : NMR solution of MM413-1 (0.02 mL diluted with 0.8 mL H2O)
                  5 min flush, first run on 12.11.19

Additional Info : Peak(s) manually integrated
```

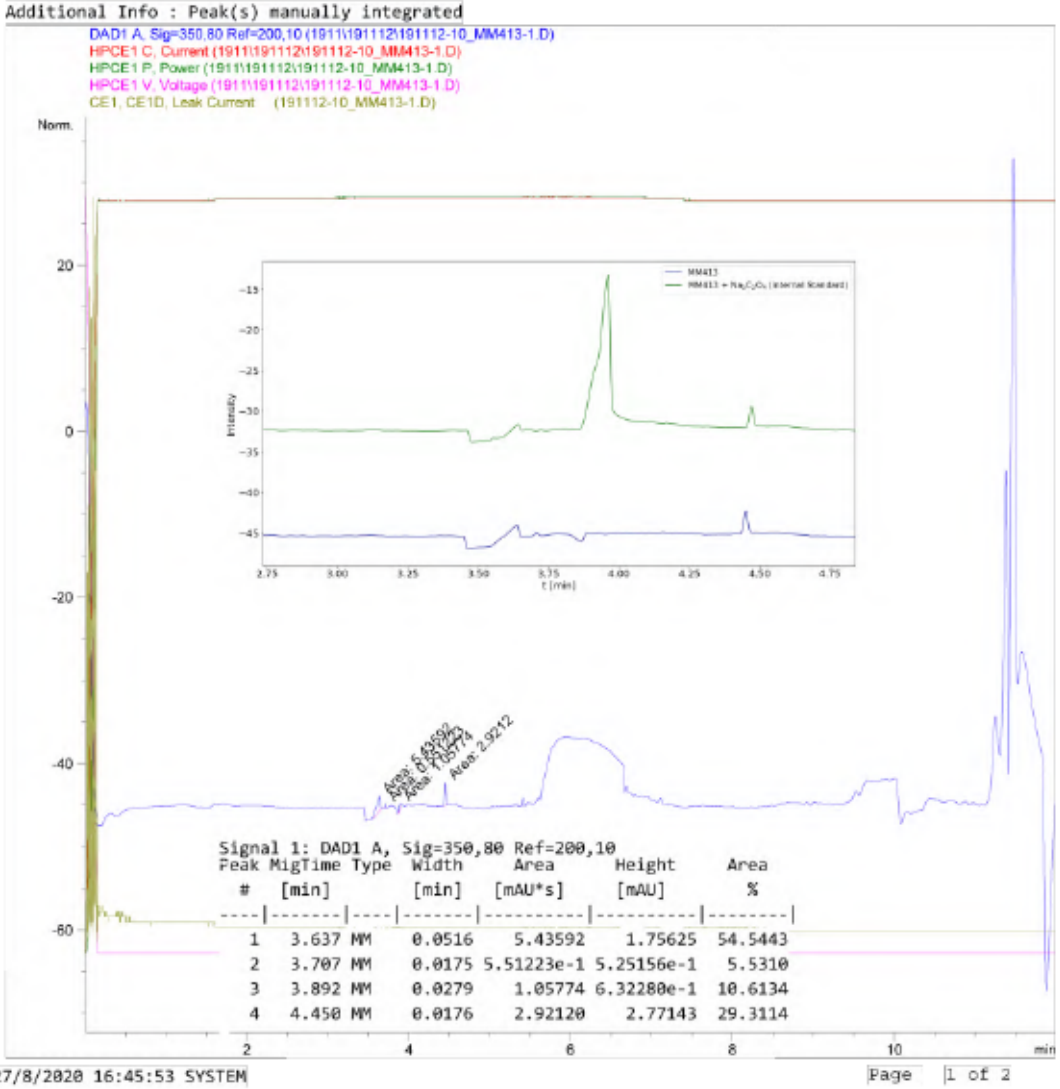

Signal 1: DAD1 A, Sig=350,80 Ref=200,10

Peak #	MigTime [min]	Type	Width [min]	Area [mAU*s]	Height [mAU]	Area %
1	3.637	MM	0.0516	5.43592	1.75625	54.5443
2	3.707	MM	0.0175	5.51223e-1	5.25156e-1	5.5310
3	3.892	MM	0.0279	1.05774	6.32280e-1	10.6134
4	4.450	MM	0.0176	2.92120	2.77143	29.3114

CE 27/8/2020 16:45:53 SYSTEM Page 1 of 2

Figure S 393: Condensed CE analysis for the NaOH extract of Table S 18, entry 2 – CO_2 treatment of **174**, CuI and $NaBPh_4$ in MeOH.

```
Data File C:\Chem32\1\Data\2006\200610\200610-2_MM566.D
Sample Name: MM566

======================================================================
Acq. Operator   : SYSTEM
Sample Operator : SYSTEM
Acq. Instrument : CE                              Location :   26
Injection Date  : 10/6/2020 14:30:44
Acq. Method     : C:\Chem32\1\Methods\CE\Marx-Oxalate25C-Flush10mV12-200114.M
Last changed    : 14/1/2020 13:19:47 by SYSTEM
Analysis Method : C:\Chem32\1\Methods\CE\Spuel-extended-200227.M
Last changed    : 10/6/2020 15:17:04 by SYSTEM
                  (modified after loading)
Sample Info     : NMR solution of MM566 (0.04 mL) diluted with H2O (0.6 mL)

Additional Info : Peak(s) manually integrated
```

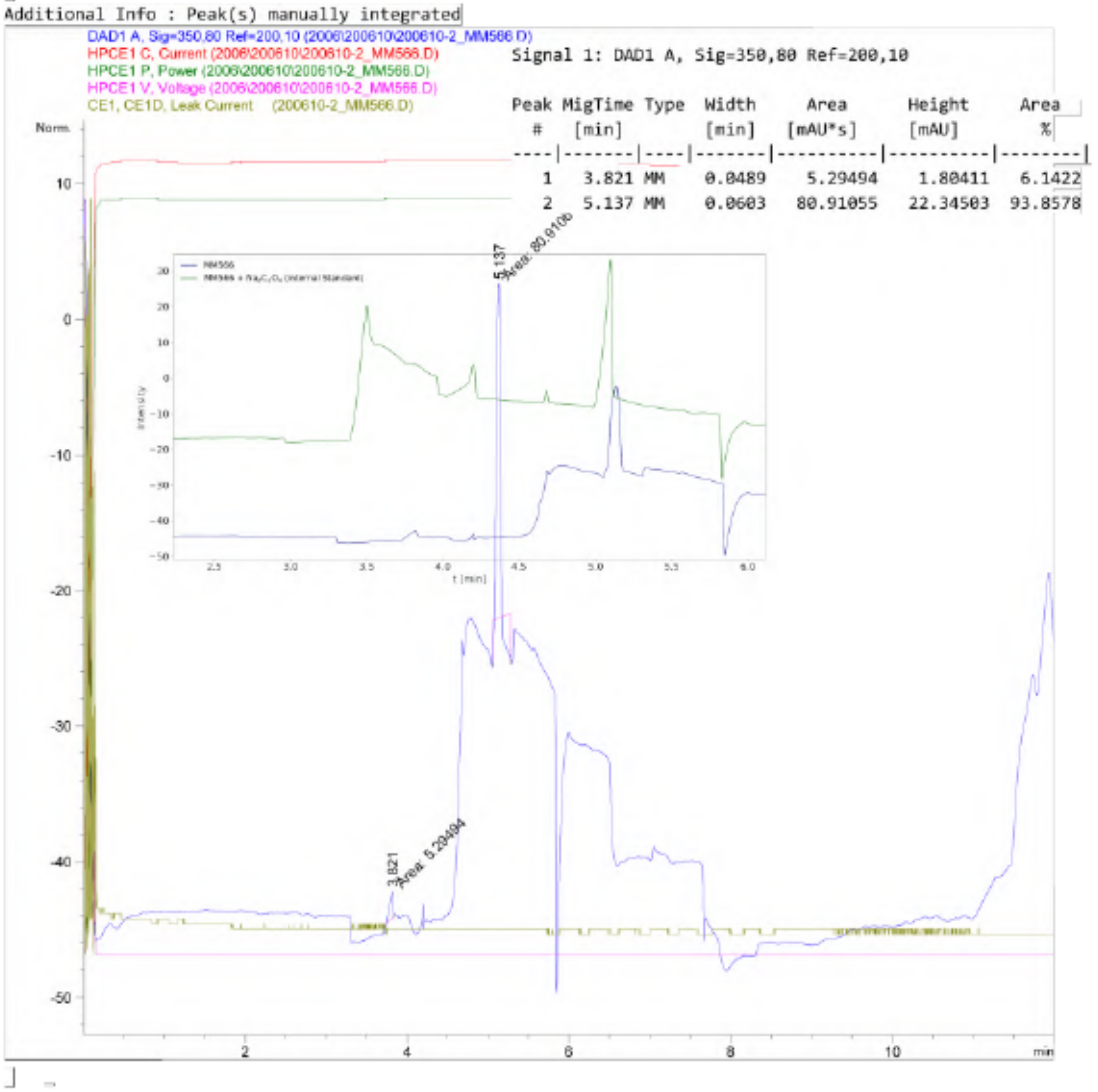


```
Signal 1: DAD1 A, Sig=350,80 Ref=200,10

Peak MigTime Type  Width     Area      Height     Area
  #   [min]      [min]   [mAU*s]     [mAU]       %
----|-------|----|-------|----------|----------|--------|
   1  3.821 MM   0.0489    5.29494    1.80411   6.1422
   2  5.137 MM   0.0603   80.91055   22.34503  93.8578
```

```
CE 10/6/2020 19:17:08 SYSTEM                              Page   1 of 2
```

Figure S 394: Condensed CE analysis for the NaOH extract of Table S 18, entry 3 – CO_2 treatment of **175**, CuI and $NaBPh_4$ in MeOH.

Data File C:\Chem32\1\Data\1911\191112\191112-9_MM412-1.D
Sample Name: MM412-1

```
==================================================================
Acq. Operator   : SYSTEM
Sample Operator : SYSTEM
Acq. Instrument : CE                          Location :   27
Injection Date  : 12/11/2019 14:13:08
Acq. Method     : C:\Chem32\1\Methods\CE\Marx-Oxalate25C-Flush4mV34-191108.M
Last changed    : 8/11/2019 15:48:42 by SYSTEM
Analysis Method : C:\Chem32\1\Methods\CE\Marx-Oxalate25C-Flush10mV23-V13-200428.M
Last changed    : 27/8/2020 16:36:34 by SYSTEM
                  (modified after loading)
Method Info     : 02.10.2019 Methode geändert auf Agilent Organic Acids Kit

Sample Info     : NMR solution of MM412-1 (0.02 mL diluted with 0.8 mL H2O)
                  5 min flush, first run on 12.11.19

Additional Info : Peak(s) manually integrated
```

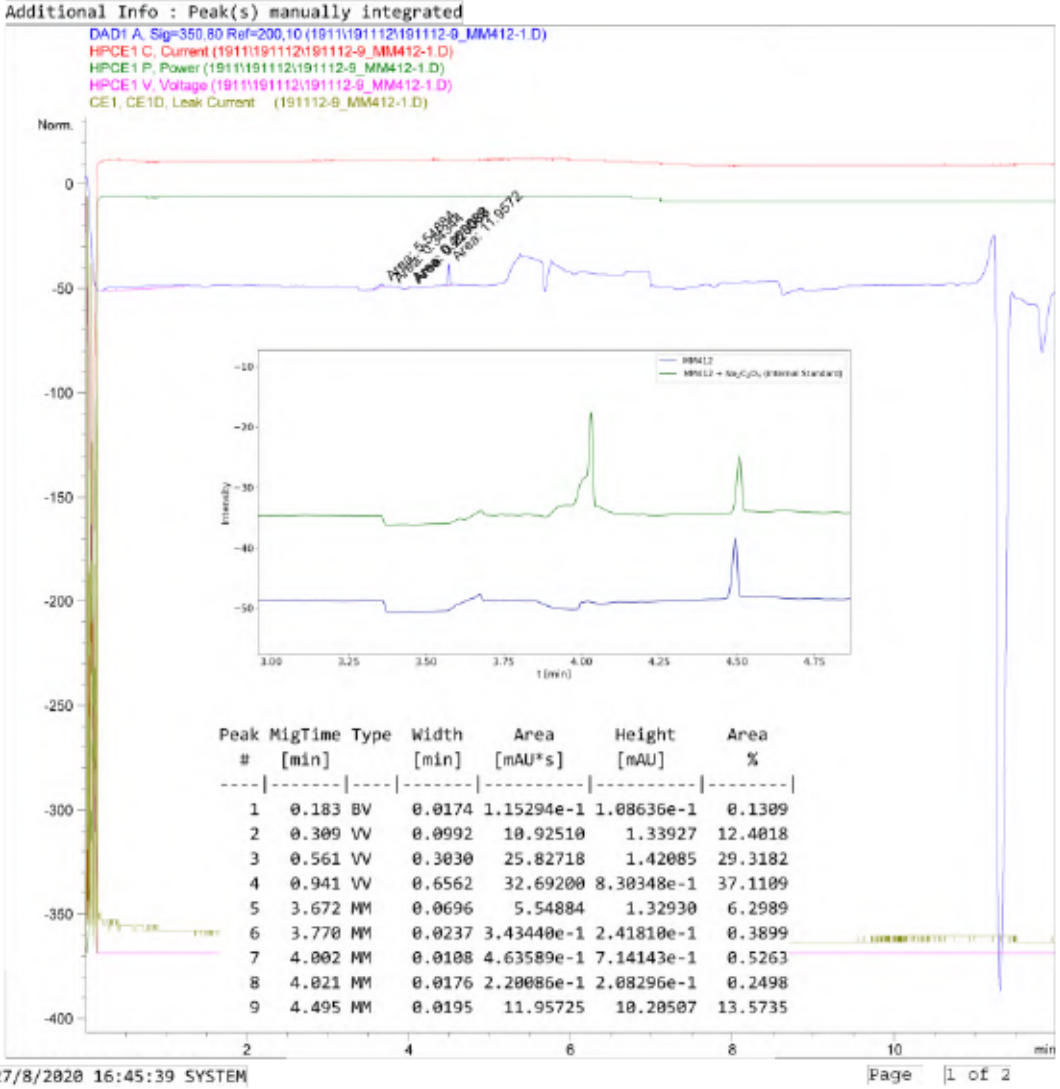

Peak #	MigTime [min]	Type	Width [min]	Area [mAU*s]	Height [mAU]	Area %
1	0.183	BV	0.0174	1.15294e-1	1.08636e-1	0.1309
2	0.309	VV	0.0992	10.92510	1.33927	12.4018
3	0.561	VV	0.3030	25.82718	1.42085	29.3182
4	0.941	VV	0.6562	32.69200	8.30348e-1	37.1109
5	3.672	MM	0.0696	5.54884	1.32930	6.2989
6	3.770	MM	0.0237	3.43440e-1	2.41810e-1	0.3899
7	4.002	MM	0.0108	4.63589e-1	7.14143e-1	0.5263
8	4.021	MM	0.0176	2.20086e-1	2.08296e-1	0.2498
9	4.495	MM	0.0195	11.95725	10.20507	13.5735

CE 27/8/2020 16:45:39 SYSTEM Page 1 of 2

Figure S 395: Condensed CE analysis for the NaOH extract of Table S 18, entry 4 – CO_2 treatment of **175**, CuI and $NaBPh_4$ in MeOH.

Data File C:\Chem32\1\Data\2006\200617\200617-5_MM576.D
Sample Name: MM576

```
==================================================================
Acq. Operator   : SYSTEM
Sample Operator : SYSTEM
Acq. Instrument : CE                          Location :   18
Injection Date  : 17/6/2020 17:01:08
Acq. Method     : C:\Chem32\1\Methods\CE\Marx-Oxalate25C-Flush10mV23-V13-200428.M
Last changed    : 28/4/2020 15:34:00 by SYSTEM
Analysis Method : C:\Chem32\1\Methods\CE\Spuel-extended-200227.M
Last changed    : 17/6/2020 16:48:17 by SYSTEM
                  (modified after loading)
Sample Info     : NMR solution of MM576 (0.04 ml) diluted with H2O (0.6 ml)

Additional Info : Peak(s) manually integrated
```

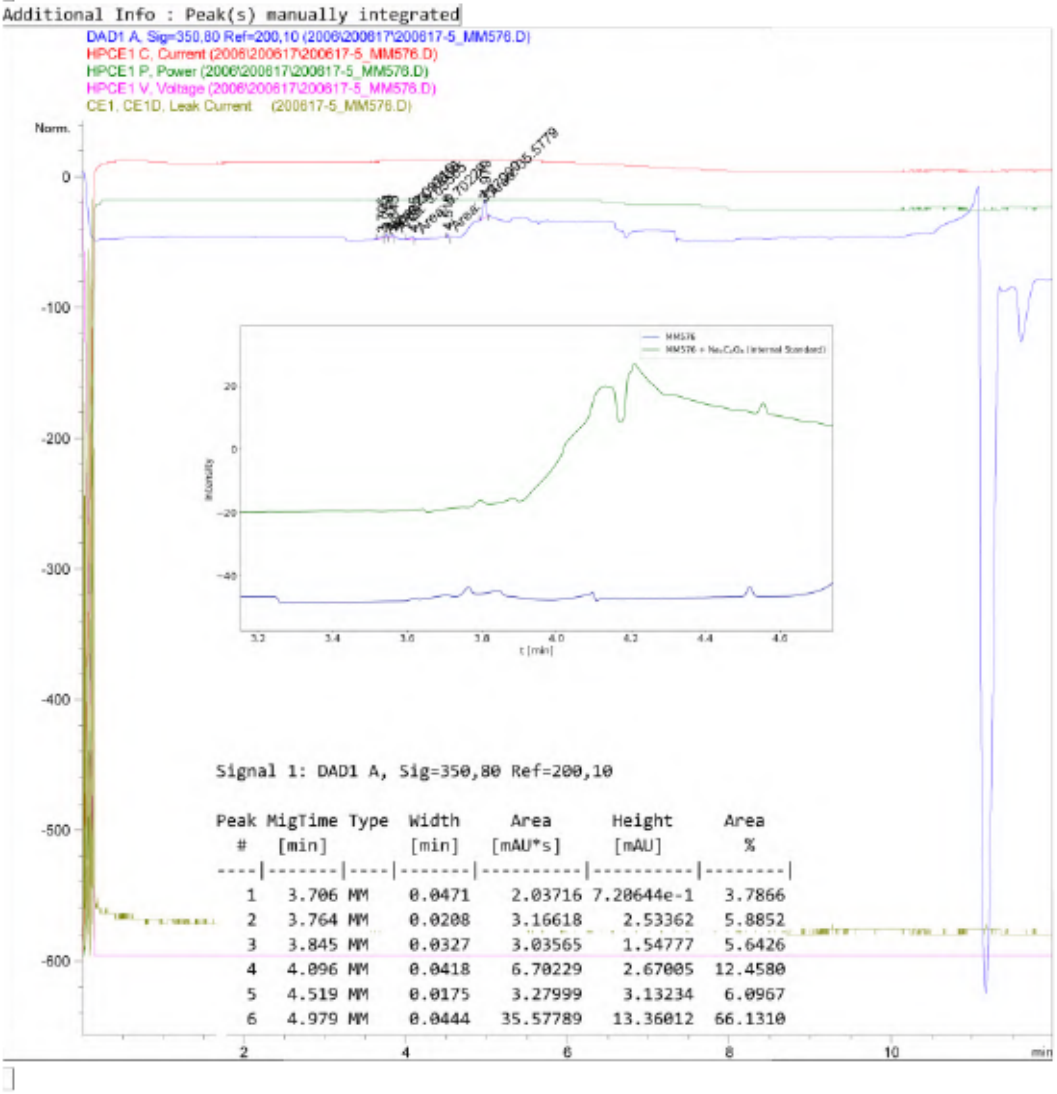

Signal 1: DAD1 A, Sig=350,80 Ref=200,10

Peak #	MigTime [min]	Type	Width [min]	Area [mAU*s]	Height [mAU]	Area %
1	3.706	MM	0.0471	2.03716	7.20644e-1	3.7866
2	3.764	MM	0.0208	3.16618	2.53362	5.8852
3	3.845	MM	0.0327	3.03565	1.54777	5.6426
4	4.096	MM	0.0418	6.70229	2.67005	12.4580
5	4.519	MM	0.0175	3.27999	3.13234	6.0967
6	4.979	MM	0.0444	35.57789	13.36012	66.1310

CE 17/6/2020 17:14:51 SYSTEM Page 1 of 2

Figure S 396: Condensed CE analysis for the NaOH extract of Table S 18, entry 5 – CO_2 treatment of **166**, CuI and $NaBPh_4$ in MeOH.

Data File C:\Chem32\1\Data\2006\200617\200617-2_MM574.D
Sample Name: MM574

```
==================================================================
Acq. Operator   : SYSTEM
Sample Operator : SYSTEM
Acq. Instrument : CE                          Location :   16
Injection Date  : 17/6/2020 15:17:34
Acq. Method     : C:\Chem32\1\Methods\CE\Marx-Oxalate25C-Flush10mV12-200114.M
Last changed    : 14/1/2020 13:19:47 by SYSTEM
Analysis Method : C:\Chem32\1\Methods\CE\Spuel-extended-200227.M
Last changed    : 17/6/2020 16:48:17 by SYSTEM
                  (modified after loading)
Sample Info     : NMR solution of MM574 (0.04 ml) diluted with H2O (0.6 ml)

Additional Info : Peak(s) manually integrated
```

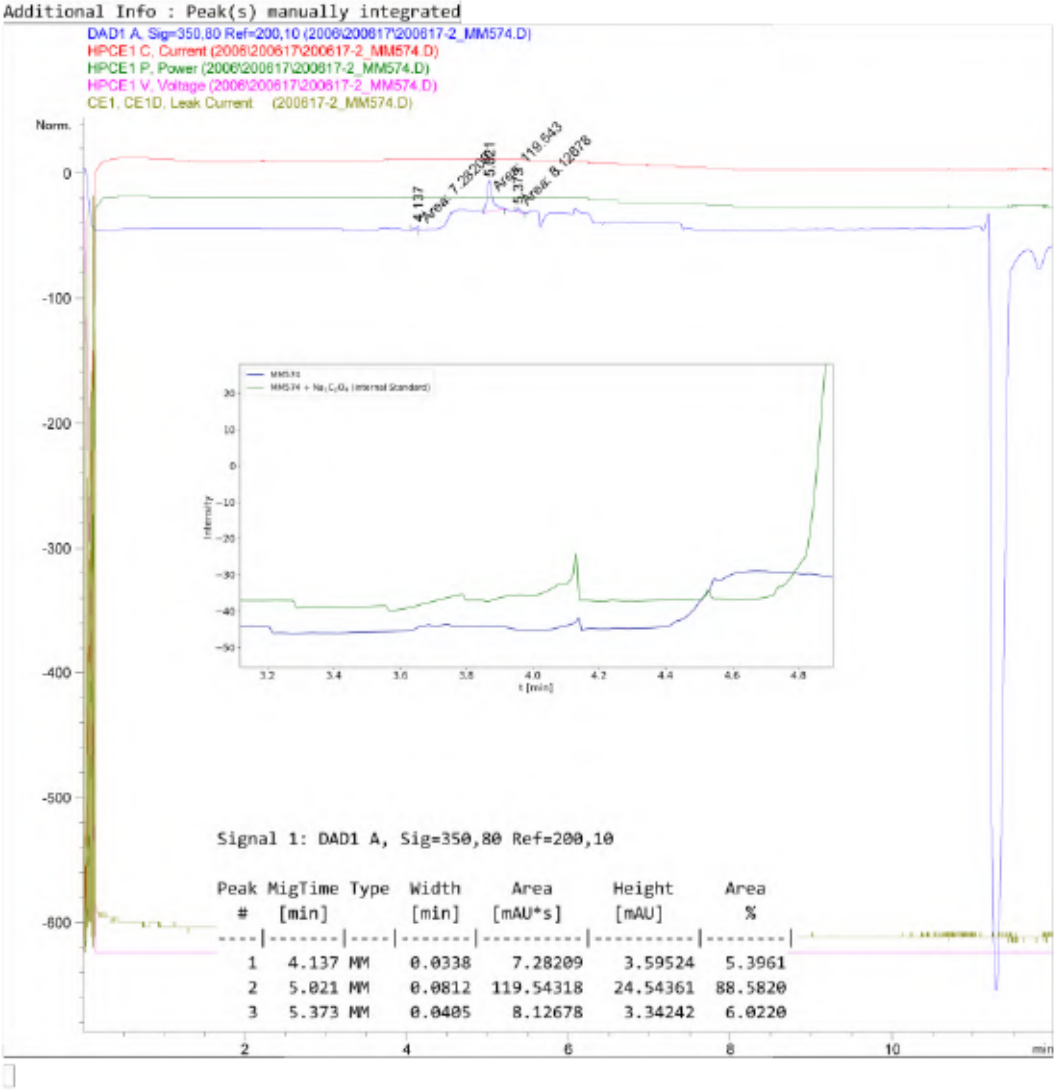

CE 17/6/2020 17:10:27 SYSTEM Page 1 of 2

Figure S 397: Condensed CE analysis for the NaOH extract of Table S 18, entry 6 – CO_2 treatment of **dpa**, CuI and $NaBPh_4$ in MeOH.

Data File C:\Chem32\1\Data\2006\200617\200617-6_MM575.D
Sample Name: MM575

```
====================================================================
Acq. Operator   : SYSTEM
Sample Operator : SYSTEM
Acq. Instrument : CE                              Location :   17
Injection Date  : 17/6/2020 17:24:36
Acq. Method     : C:\Chem32\1\Methods\CE\Marx-Oxalate25C-Flush10mV23-V13-200428.M
Last changed    : 28/4/2020 15:34:00 by SYSTEM
Analysis Method : C:\Chem32\1\Methods\CE\Spuel-extended-200227.M
Last changed    : 17/6/2020 16:48:17 by SYSTEM
                  (modified after loading)
Sample Info     : NMR solution of MM575 (0.04 ml) diluted with H2O (0.6 ml)

Additional Info : Peak(s) manually integrated
```

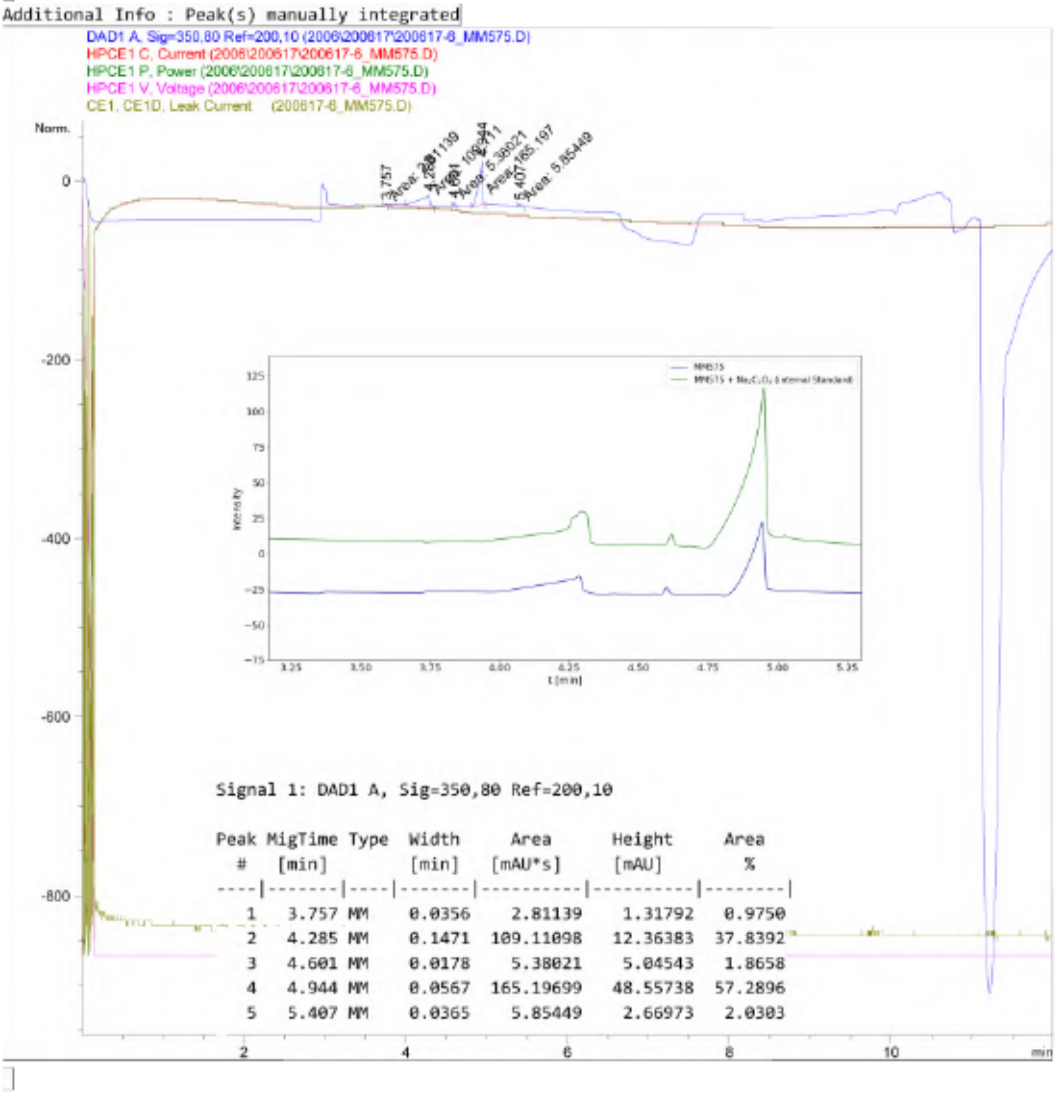

Signal 1: DAD1 A, Sig=350,80 Ref=200,10

Peak #	MigTime [min]	Type	Width [min]	Area [mAU*s]	Height [mAU]	Area %
1	3.757	MM	0.0356	2.81139	1.31792	0.9750
2	4.285	MM	0.1471	109.11098	12.36383	37.8392
3	4.601	MM	0.0178	5.38021	5.04543	1.8658
4	4.944	MM	0.0567	165.19699	48.55738	57.2896
5	5.407	MM	0.0365	5.85449	2.66973	2.0303

CE 17/6/2020 17:58:17 SYSTEM Page 1 of 2

Figure S 398: Condensed CE analysis for the NaOH extract of Table S 18, entry 7 – CO_2 treatment of **dien**, CuI and $NaBPh_4$ in MeOH.

Data File C:\Chem32\1\Data\2006\200626\200626-2_MM581.D
Sample Name: MM581

Acq. Operator	: SYSTEM
Sample Operator	: SYSTEM
Acq. Instrument	: CE Location : 32
Injection Date	: 26/6/2020 11:16:40
Acq. Method	: C:\Chem32\1\Methods\CE\Marx-Oxalate25C-Flush10mV12-200114.M
Last changed	: 14/1/2020 13:19:47 by SYSTEM
Analysis Method	: C:\Chem32\1\Methods\CE\SwitchOff-200227.M
Last changed	: 26/6/2020 11:11:38 by SYSTEM (modified after loading)
Sample Info	: NMR sample of MM581 (0.04 mL) diluted with H2O (0.6 ml)
Additional Info	: Peak(s) manually integrated

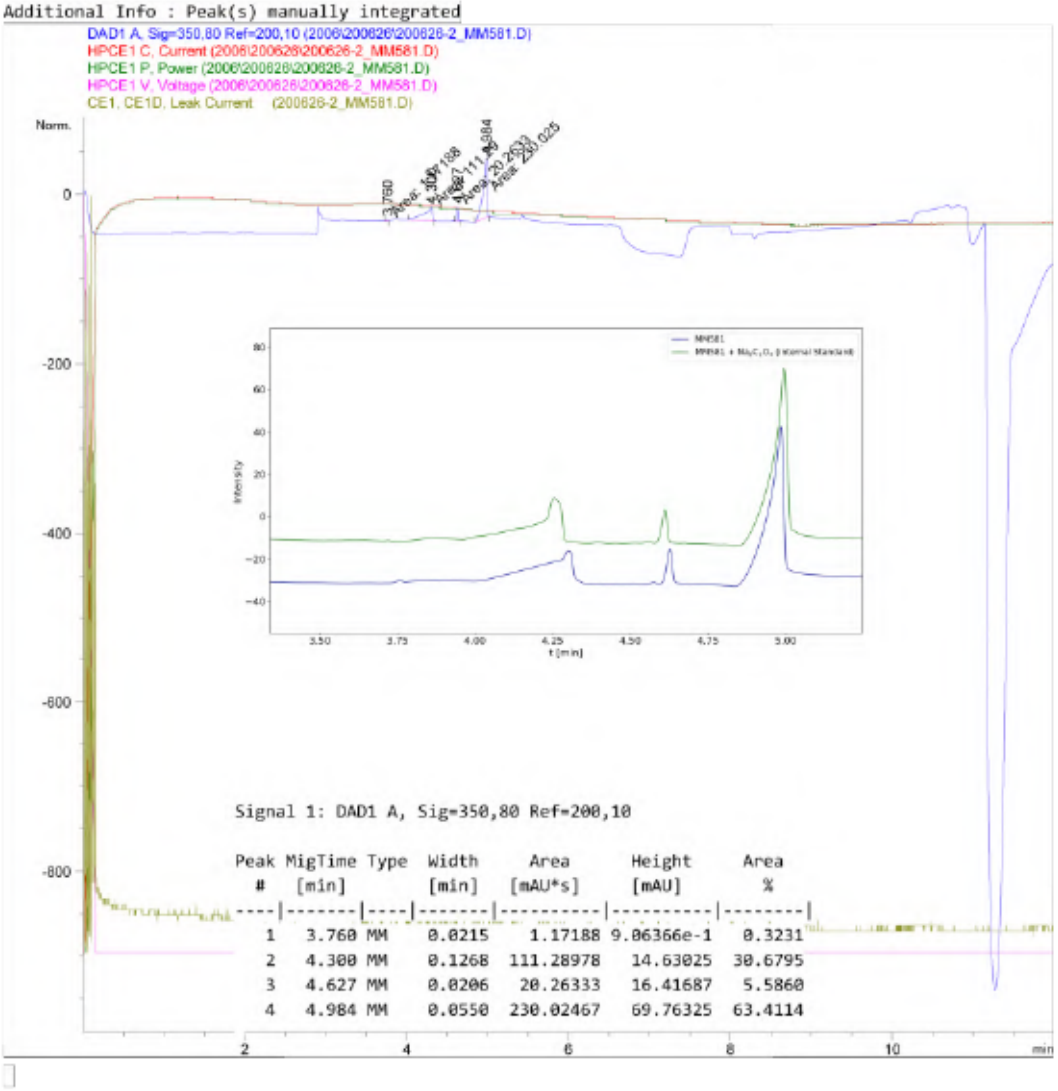

Signal 1: DAD1 A, Sig=350,80 Ref=200,10

Peak #	MigTime [min]	Type	Width [min]	Area [mAU*s]	Height [mAU]	Area %
1	3.760	MM	0.0215	1.17188	9.06366e-1	0.3231
2	4.300	MM	0.1268	111.28978	14.63025	30.6795
3	4.627	MM	0.0206	20.26333	16.41687	5.5860
4	4.984	MM	0.0550	230.02467	69.76325	63.4114

CE 26/6/2020 12:28:42 SYSTEM Page 1 of 2

Figure S 399: Condensed CE analysis for the NaOH extract of Table S 18, entry 8 – CO_2 treatment of **dien**, CuI and $NaBPh_4$ in MeOH.

Data File C:\Chem32\1\Data\2007\200701\200701-3_MM591.D
Sample Name: MM591

```
==================================================================
Acq. Operator   : SYSTEM
Sample Operator : SYSTEM
Acq. Instrument : CE                              Location :   36
Injection Date  : 1/7/2020 10:24:46
Acq. Method     : C:\Chem32\1\Methods\CE\Marx-Oxalate25C-Flush10mV12-200114.M
Last changed    : 14/1/2020 13:19:47 by SYSTEM
Analysis Method : C:\Chem32\1\Methods\CE\SwitchOff-200227.M
Last changed    : 1/7/2020 09:49:37 by SYSTEM
                  (modified after loading)
Sample Info     : NMR solution of MM591 (0.04 mL) diluted with H2O (0.6 ml)

Additional Info : Peak(s) manually integrated
```

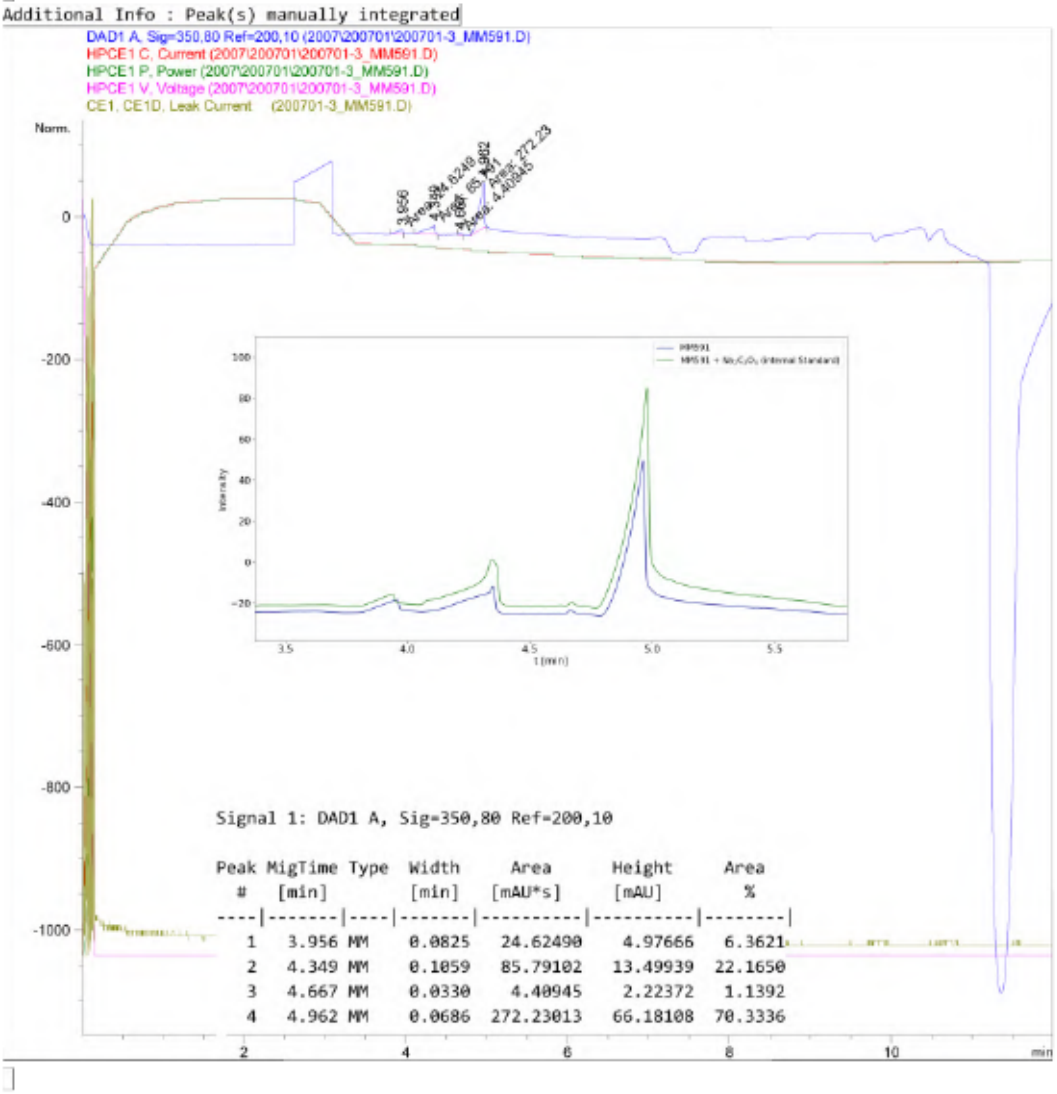

Signal 1: DAD1 A, Sig=350,80 Ref=200,10

Peak #	MigTime [min]	Type	Width [min]	Area [mAU*s]	Height [mAU]	Area %
1	3.956	MM	0.0825	24.62490	4.97666	6.3621
2	4.349	MM	0.1059	85.79102	13.49939	22.1650
3	4.667	MM	0.0330	4.40945	2.22372	1.1392
4	4.962	MM	0.0686	272.23013	66.18108	70.3336

CE 1/7/2020 14:16:35 SYSTEM Page 1 of 2

Figure S 400: Condensed CE analysis for the NaOH extract of Table S 18, entry 9 – CO_2 treatment of **dien**, CuI and $NaBPh_4$ in MeOH.

```
Data File C:\Chem32\1\Data\2007\200701\200701-2_MM590.D
Sample Name: MM590

======================================================================
Acq. Operator   : SYSTEM
Sample Operator : SYSTEM
Acq. Instrument : CE                          Location :  35
Injection Date  : 1/7/2020 10:01:16
Acq. Method     : C:\Chem32\1\Methods\CE\Marx-Oxalate25C-Flush10mV12-200114.M
Last changed    : 14/1/2020 13:19:47 by SYSTEM
Analysis Method : C:\Chem32\1\Methods\CE\SwitchOff-200227.M
Last changed    : 1/7/2020 09:49:37 by SYSTEM
                  (modified after loading)
Sample Info     : NMR solution of MM590 (0.04 mL) diluted with H2O (0.6 ml)

Additional Info : Peak(s) manually integrated
```

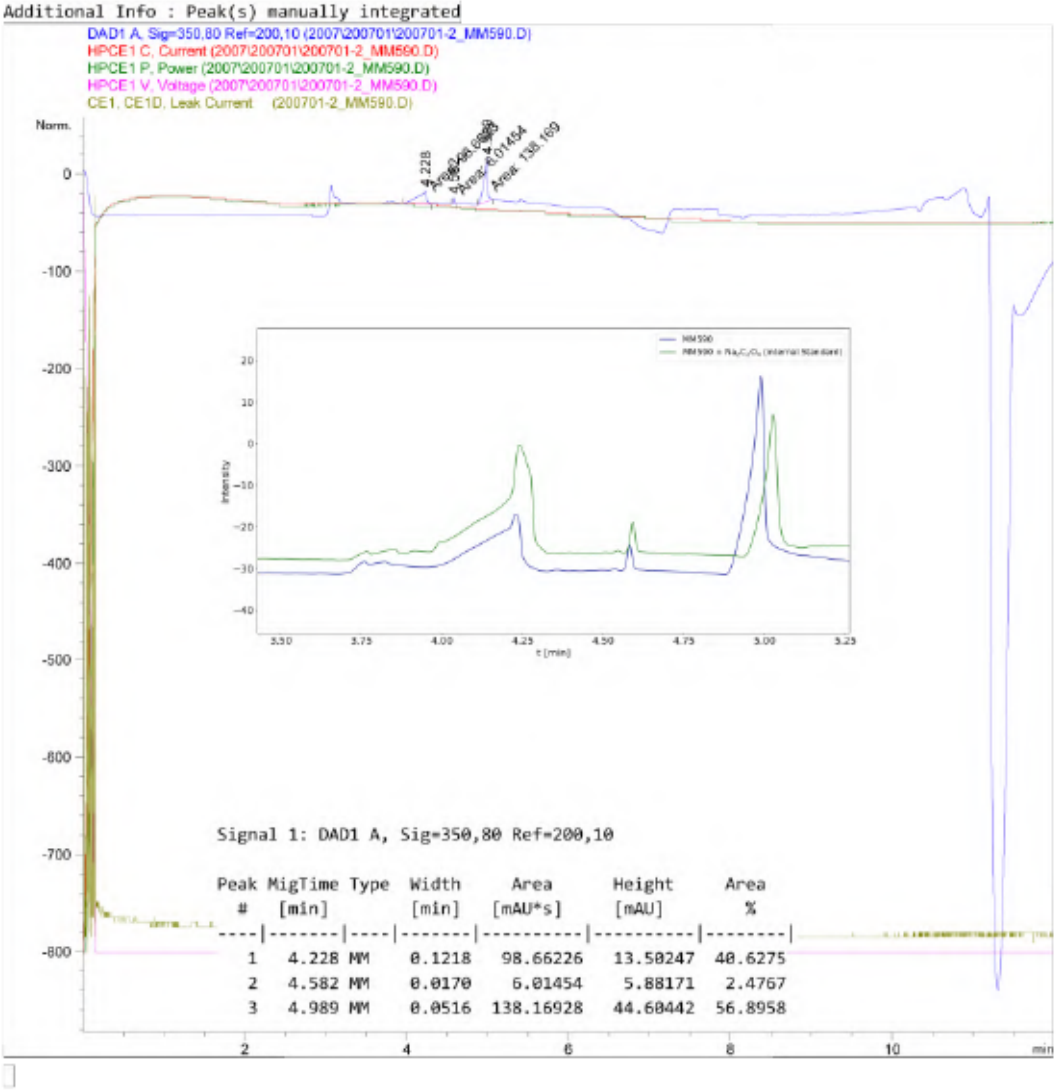


```
Signal 1: DAD1 A, Sig=350,80 Ref=200,10

Peak MigTime Type  Width     Area      Height     Area
  #   [min]       [min]   [mAU*s]     [mAU]       %
----|-------|----|-------|----------|----------|--------|
   1   4.228 MM    0.1218   98.66226   13.50247  40.6275
   2   4.582 MM    0.0170    6.01454    5.88171   2.4767
   3   4.989 MM    0.0516  138.16928   44.60442  56.8958
```

```
CE 1/7/2020 14:16:21 SYSTEM                                Page  1 of 2
```

Figure S 401: Condensed CE analysis for the NaOH extract of Table S 18, entry 10 – **dien**, CuI and $NaBPh_4$ in MeOH under Ar.

```
Data File C:\Chem32\1\Data\2007\200707\200707-3_MM604.D
Sample Name: MM604

======================================================================
Acq. Operator   : SYSTEM
Sample Operator : SYSTEM
Acq. Instrument : CE                              Location :   22
Injection Date  : 7/7/2020 13:39:07
Acq. Method     : C:\Chem32\1\Methods\CE\Marx-Oxalate25C-Flush10mV12-200114.M
Last changed    : 14/1/2020 13:19:47 by SYSTEM
Analysis Method : C:\Chem32\1\Methods\CE\SwitchOff-200227.M
Last changed    : 7/7/2020 17:20:34 by SYSTEM
                  (modified after loading)
Sample Info     : NMR solution of MM604 (0.04 mL) diluted with H2O (0.6 mL)

Additional Info : Peak(s) manually integrated
```

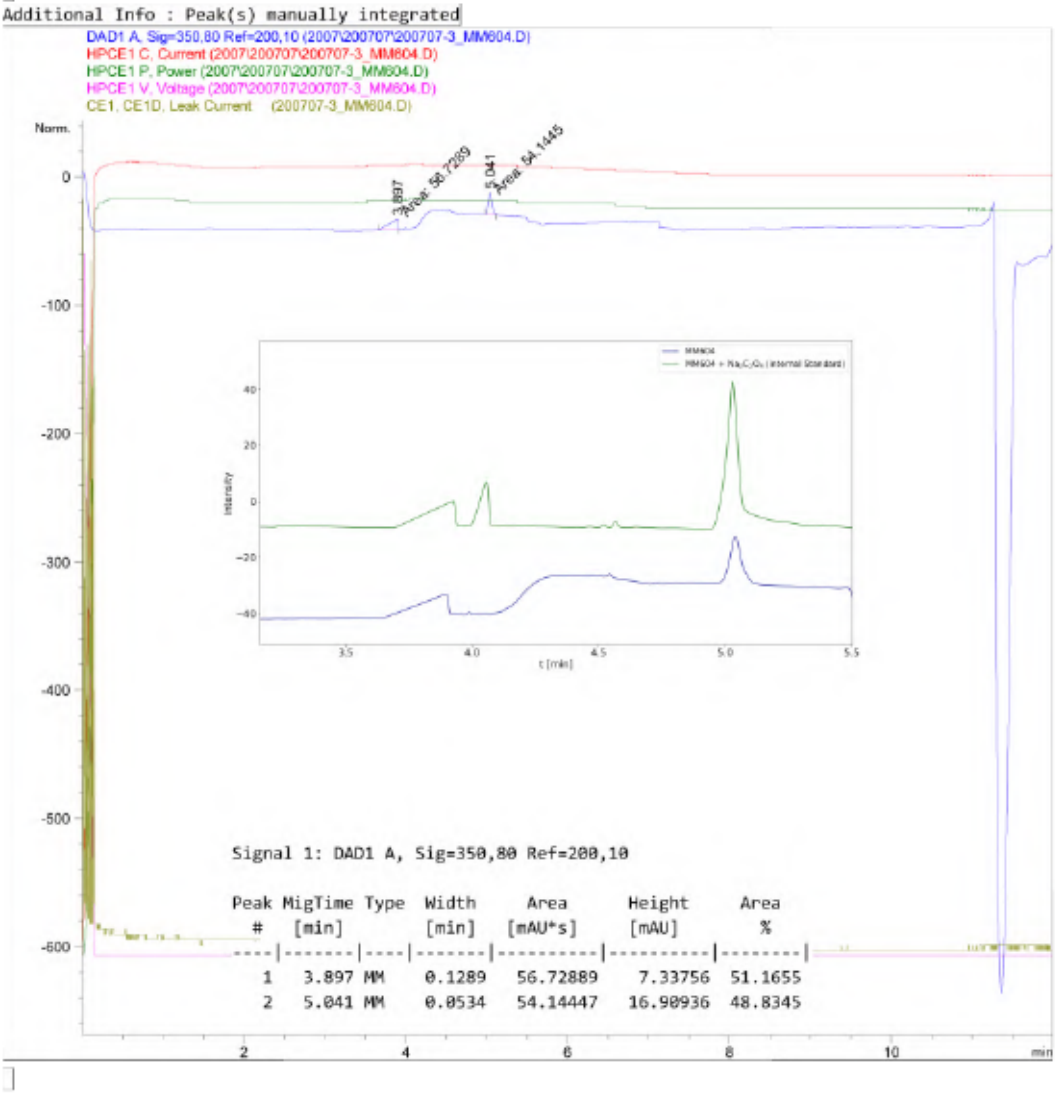


```
Signal 1: DAD1 A, Sig=350,80 Ref=200,10

Peak MigTime Type  Width     Area      Height    Area
  #   [min]       [min]   [mAU*s]     [mAU]      %
----|-------|----|-------|----------|----------|--------|
   1   3.897 MM    0.1289   56.72889   7.33756  51.1655
   2   5.041 MM    0.0534   54.14447  16.90936  48.8345
```

```
CE 7/7/2020 19:48:27 SYSTEM                              Page  1 of 2
```

Figure S 402: Condensed CE analysis for the NaOH extract of Table S 18, entry 11 – CO_2 treatment of **176** and $NaBPh_4$ in MeOH.

Data File C:\Chem32\1\Data\2007\200707\200707-2_MM603.D
Sample Name: MM603

```
==================================================================
Acq. Operator   : SYSTEM
Sample Operator : SYSTEM
Acq. Instrument : CE                              Location :   21
Injection Date  : 7/7/2020 13:15:38
Acq. Method     : C:\Chem32\1\Methods\CE\Marx-Oxalate25C-Flush10mV12-200114.M
Last changed    : 14/1/2020 13:19:47 by SYSTEM
Analysis Method : C:\Chem32\1\Methods\CE\SwitchOff-200227.M
Last changed    : 7/7/2020 17:20:34 by SYSTEM
                  (modified after loading)
Sample Info     : NMR solution of MM603 (0.04 mL) diluted with H2O (0.6 mL)

Additional Info : Peak(s) manually integrated
```

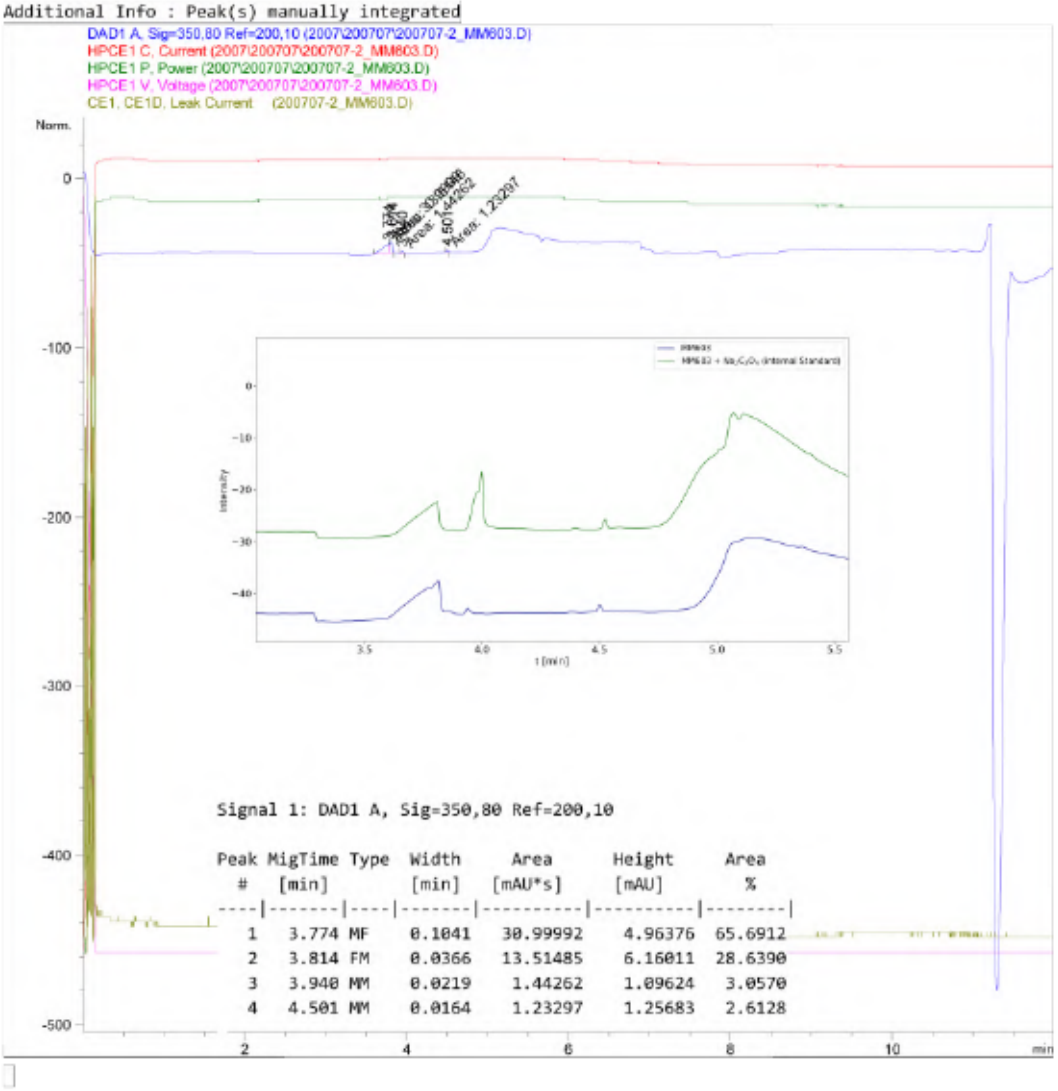

Signal 1: DAD1 A, Sig=350,80 Ref=200,10

Peak #	MigTime [min]	Type	Width [min]	Area [mAU*s]	Height [mAU]	Area %
1	3.774	MF	0.1041	30.99992	4.96376	65.6912
2	3.814	FM	0.0366	13.51485	6.16011	28.6390
3	3.940	MM	0.0219	1.44262	1.09624	3.0570
4	4.501	MM	0.0164	1.23297	1.25683	2.6128

CE 7/7/2020 19:48:40 SYSTEM Page 1 of 2

Figure S 403: Condensed CE analysis for the NaOH extract of Table S 18, entry 12 – CO_2 treatment of **177** and $NaBPh_4$ in MeOH.

Data File C:\Chem32\1\Data\2007\200707\200707-4_MM605.D
Sample Name: MM605

```
======================================================================
Acq. Operator   : SYSTEM
Sample Operator : SYSTEM
Acq. Instrument : CE                              Location :   23
Injection Date  : 7/7/2020 14:02:37
Acq. Method     : C:\Chem32\1\Methods\CE\Marx-Oxalate25C-Flush10mV12-200114.M
Last changed    : 14/1/2020 13:19:47 by SYSTEM
Analysis Method : C:\Chem32\1\Methods\CE\SwitchOff-200227.M
Last changed    : 7/7/2020 17:20:34 by SYSTEM
                  (modified after loading)
Sample Info     : NMR solution of MM605 (0.04 mL) diluted with H2O (0.6 mL)

Additional Info : Peak(s) manually integrated
```

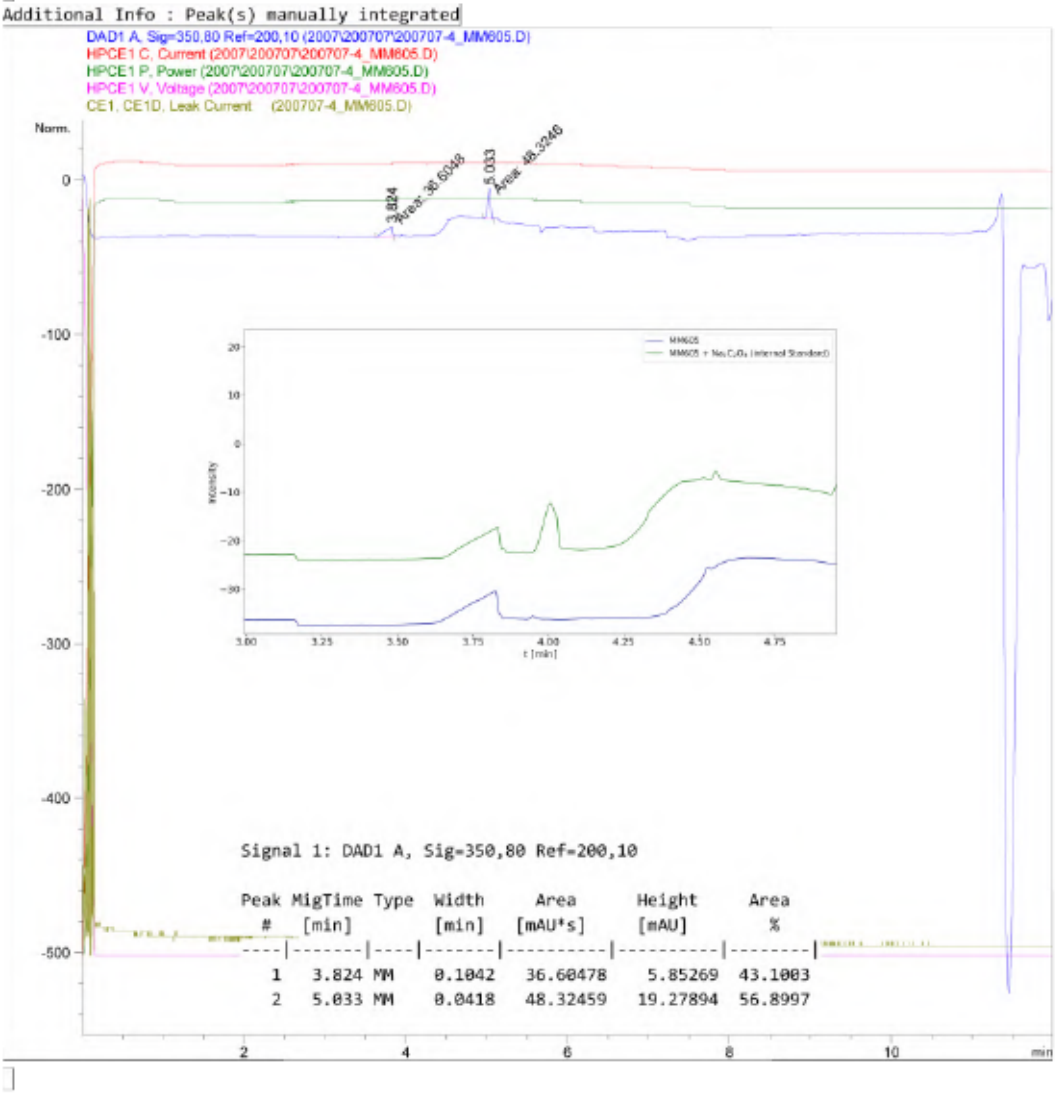

Signal 1: DAD1 A, Sig=350,80 Ref=200,10

Peak #	MigTime [min]	Type	Width [min]	Area [mAU*s]	Height [mAU]	Area %
1	3.824	MM	0.1042	36.60478	5.85269	43.1083
2	5.033	MM	0.0418	48.32459	19.27894	56.8997

CE 7/7/2020 19:48:09 SYSTEM Page 1 of 2

Figure S 404: Condensed CE analysis for the NaOH extract of Table S 18, entry 13 – CO_2 treatment of **178** and $NaBPh_4$ in MeOH.

Data File C:\Chem32\1\Data\2007\200707\200707-6_MM606.D
Sample Name: MM606

Acq. Operator	: SYSTEM
Sample Operator	: SYSTEM
Acq. Instrument	: CE Location : 24
Injection Date	: 7/7/2020 15:08:00
Acq. Method	: C:\Chem32\1\Methods\CE\Marx-Oxalate25C-Flush10mV23-V13-200428.M
Last changed	: 28/4/2020 15:34:00 by SYSTEM
Analysis Method	: C:\Chem32\1\Methods\CE\SwitchOff-200227.M
Last changed	: 7/7/2020 17:20:34 by SYSTEM (modified after loading)
Sample Info	: NMR solution of MM606 (0.04 mL) diluted with H2O (0.6 mL)
Additional Info	: Peak(s) manually integrated

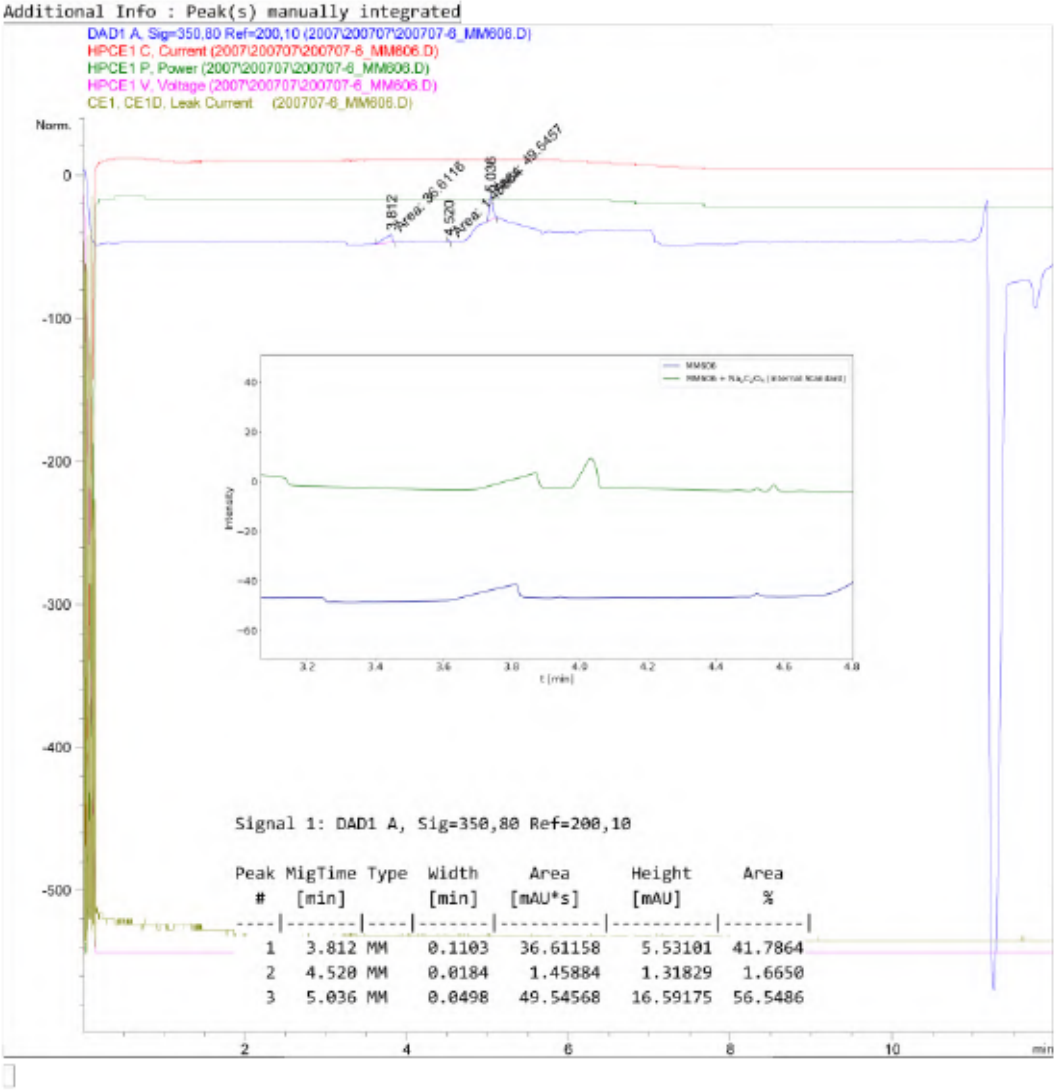

Signal 1: DAD1 A, Sig=350,80 Ref=200,10

Peak #	MigTime [min]	Type	Width [min]	Area [mAU*s]	Height [mAU]	Area %
1	3.812	MM	0.1103	36.61158	5.53101	41.7864
2	4.520	MM	0.0184	1.45884	1.31829	1.6650
3	5.036	MM	0.0498	49.54568	16.59175	56.5486

CE 7/7/2020 19:47:19 SYSTEM Page 1 of 2

Figure S 405: Condensed CE analysis for the NaOH extract of Table S 18, entry 14 – CO_2 treatment of **179** and $NaBPh_4$ in MeOH.

Data File C:\Chem32\1\Data\2007\200707\200707-1_MM602.D
Sample Name: MM602

```
======================================================================
Acq. Operator   : SYSTEM
Sample Operator : SYSTEM
Acq. Instrument : CE                              Location :   20
Injection Date  : 7/7/2020 12:52:05
Acq. Method     : C:\Chem32\1\Methods\CE\Marx-Oxalate25C-Flush10mV12-200114.M
Last changed    : 14/1/2020 13:19:47 by SYSTEM
Analysis Method : C:\Chem32\1\Methods\CE\SwitchOff-200227.M
Last changed    : 7/7/2020 17:20:34 by SYSTEM
                  (modified after loading)
Sample Info     : NMR solution of MM602 (0.10 mL) diluted with H2O (0.5 mL)

Additional Info : Peak(s) manually integrated
```

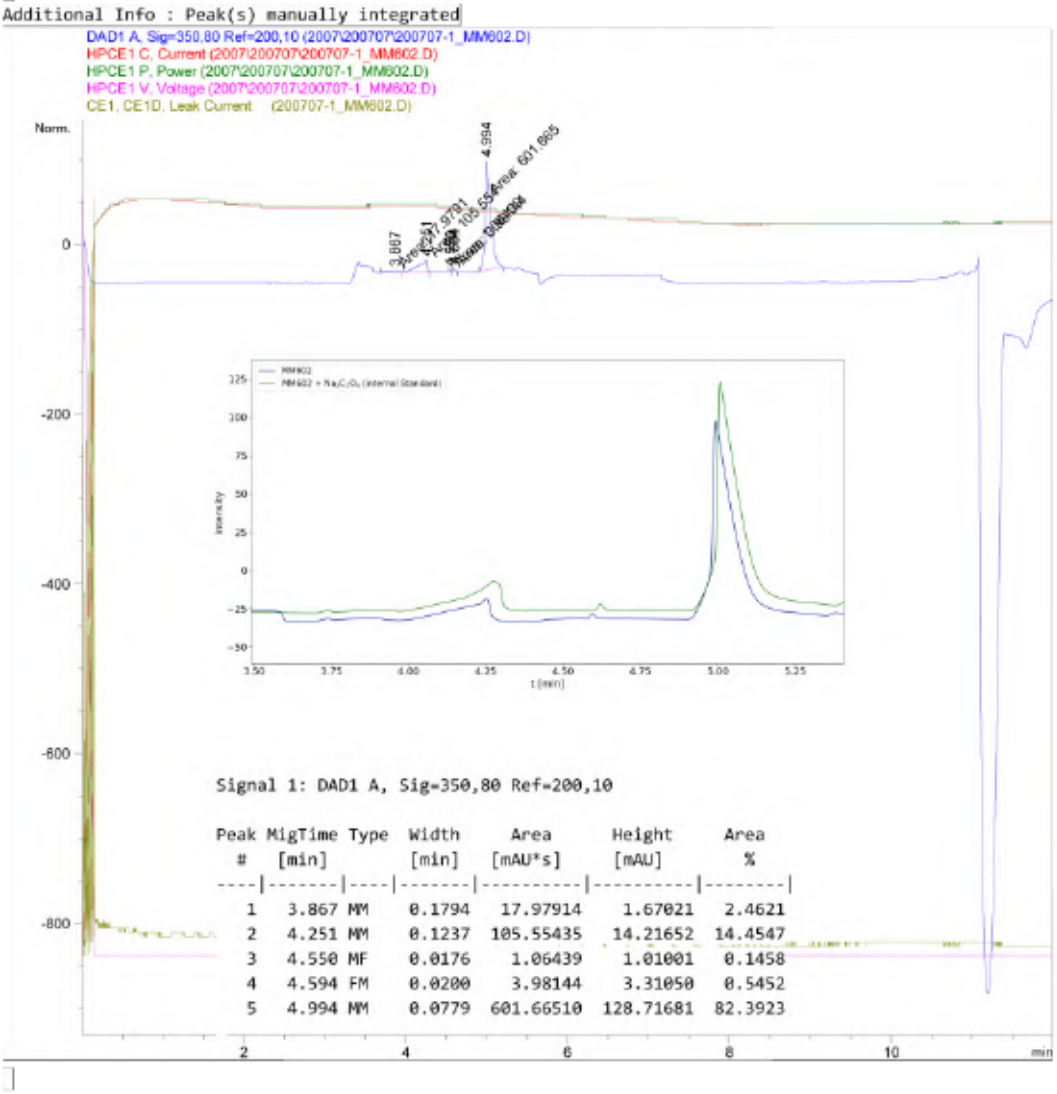

Signal 1: DAD1 A, Sig=350,80 Ref=200,10

Peak #	MigTime [min]	Type	Width [min]	Area [mAU*s]	Height [mAU]	Area %
1	3.867	MM	0.1794	17.97914	1.67021	2.4621
2	4.251	MM	0.1237	105.55435	14.21652	14.4547
3	4.550	MF	0.0176	1.06439	1.01001	0.1458
4	4.594	FM	0.0200	3.98144	3.31050	0.5452
5	4.994	MM	0.0779	601.66510	128.71681	82.3923

CE 7/7/2020 19:48:54 SYSTEM Page 1 of 2

Figure S 406: Condensed CE analysis for the NaOH extract of Table S 18, entry 15 – CO_2 treatment of **184**, CuI and $NaBPh_4$ in MeOH.

Data File C:\Chem32\1\Data\2006\200623\200623-1_MM580.D
Sample Name: MM580

```
=====================================================================
Acq. Operator   : SYSTEM
Sample Operator : SYSTEM
Acq. Instrument : CE                              Location :   28
Injection Date  : 23/6/2020 12:38:29
Acq. Method     : C:\Chem32\1\Methods\CE\Marx-Oxalate25C-Flush10mV12-200114.M
Last changed    : 14/1/2020 13:19:47 by SYSTEM
Analysis Method : C:\Chem32\1\Methods\CE\SwitchOff-200227.M
Last changed    : 23/6/2020 13:21:11 by SYSTEM
                  (modified after loading)
Sample Info     : NMR solution of MM580 (0.10 ml) diluted with H2O (0.5 ml)

Additional Info : Peak(s) manually integrated
```

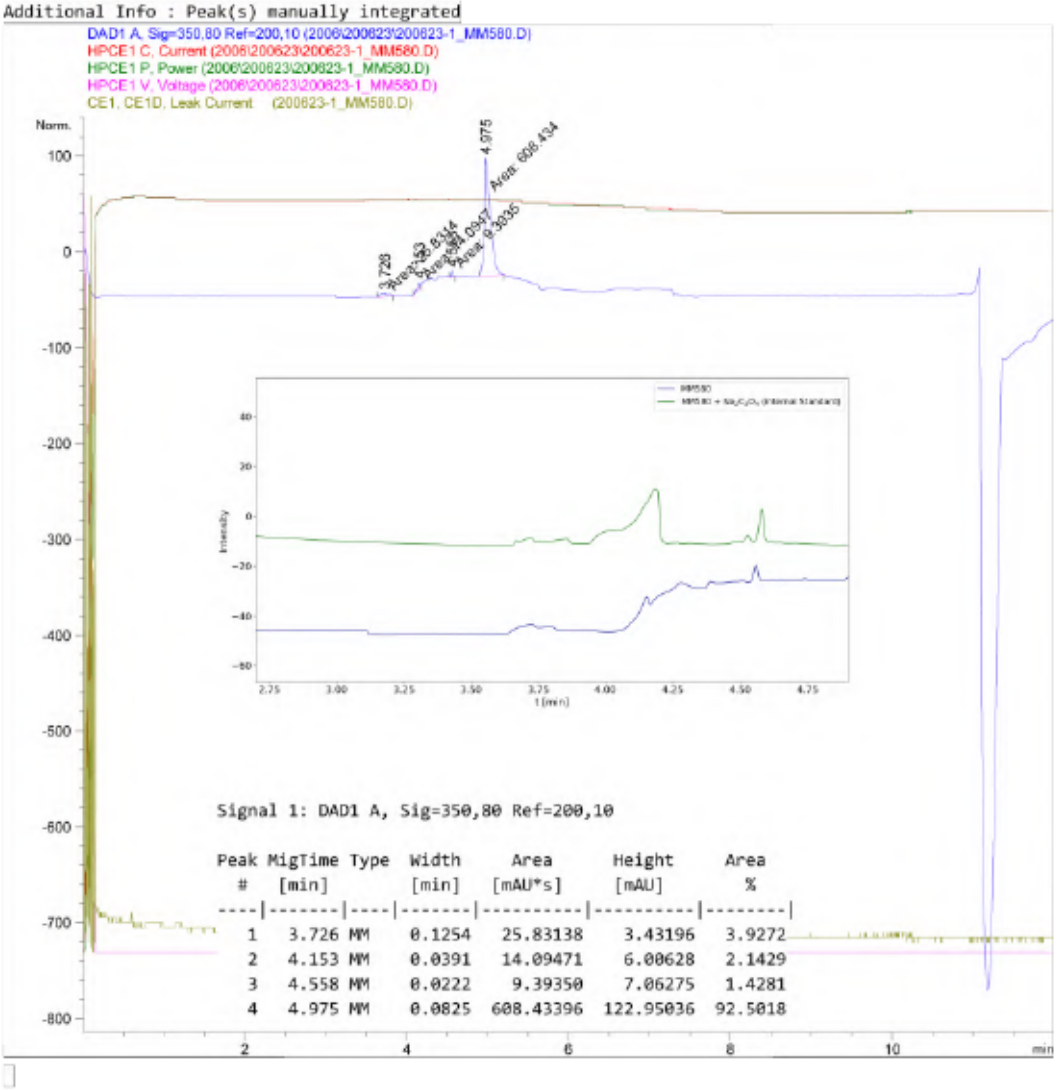

Signal 1: DAD1 A, Sig=350,80 Ref=200,10

Peak #	MigTime [min]	Type	Width [min]	Area [mAU*s]	Height [mAU]	Area %
1	3.726	MM	0.1254	25.83138	3.43196	3.9272
2	4.153	MM	0.0391	14.09471	6.00628	2.1429
3	4.558	MM	0.0222	9.39350	7.06275	1.4281
4	4.975	MM	0.0825	608.43396	122.95036	92.5018

CE 23/6/2020 14:57:41 SYSTEM Page 1 of 2

Figure S 407: Condensed CE analysis for the NaOH extract of Table S 18, entry 16 – CO_2 treatment of **184**, CuI and $NaBPh_4$ in MeOH.

4.15.4 CE analysis – Reactions of α-Ketocarboxylates

```
Data File C:\Chem32\1\Data\2007\200706\200706-3_MM612.D
Sample Name: MM612

=====================================================================
Acq. Operator   : SYSTEM
Sample Operator : SYSTEM
Acq. Instrument : CE                                Location :  17
Injection Date  : 6/7/2020 14:45:38
Acq. Method     : C:\Chem32\1\Methods\CE\Marx-Oxalate25C-Flush10mV12-200114.M
Last changed    : 14/1/2020 13:19:47 by SYSTEM
Analysis Method : C:\Chem32\1\Methods\CE\SwitchOff-200227.M
Last changed    : 6/7/2020 14:33:42 by SYSTEM
                  (modified after loading)
Sample Info     : NMR solution of MM612 (0.06 mL) diluted with H2O (0.6 ml)

Additional Info : Peak(s) manually integrated
```

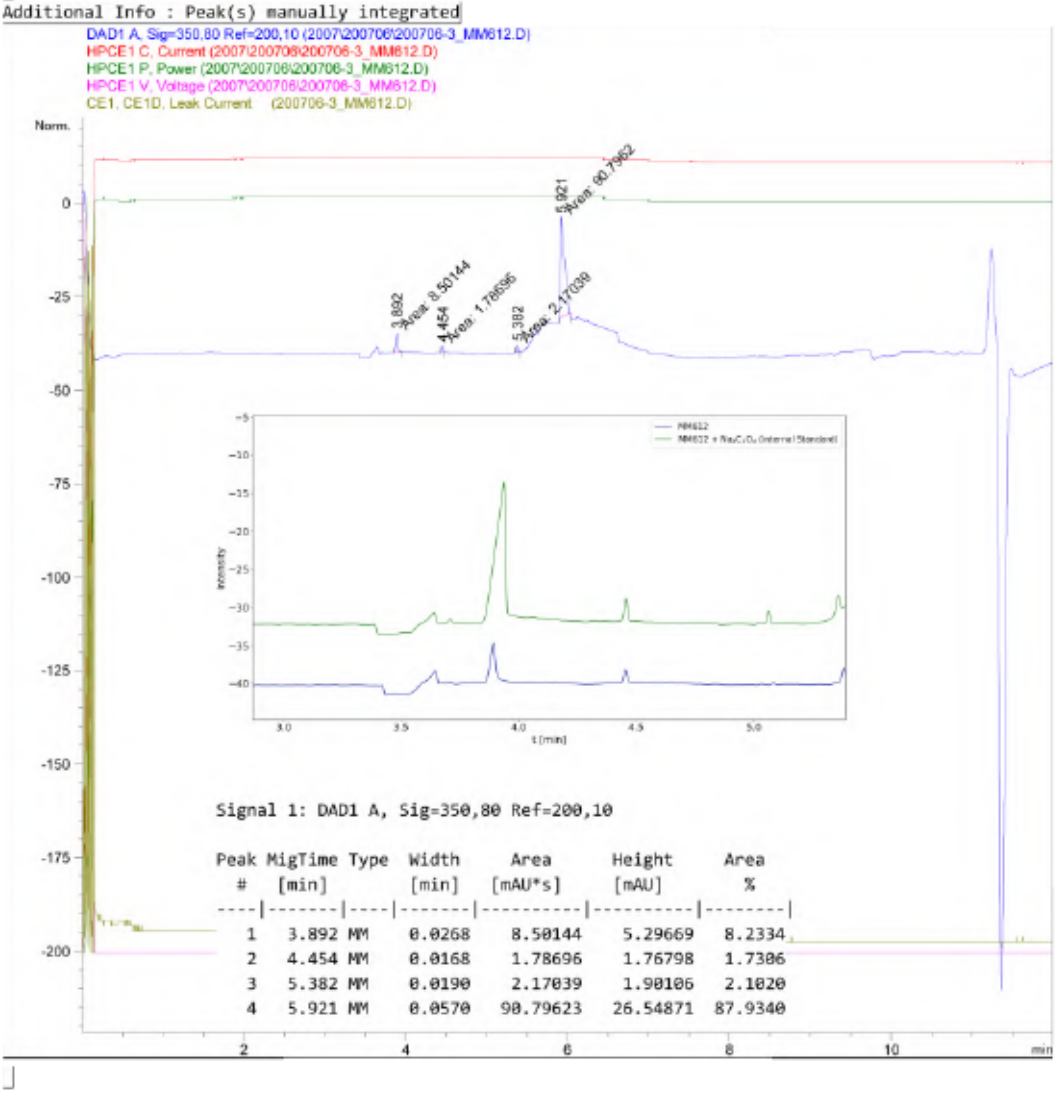


```
Signal 1: DAD1 A, Sig=350,80 Ref=200,10

Peak MigTime Type  Width     Area      Height     Area
  #   [min]       [min]   [mAU*s]     [mAU]       %
----|-------|----|-------|----------|----------|--------|
   1   3.892 MM    0.0268    8.50144    5.29669   8.2334
   2   4.454 MM    0.0168    1.78696    1.76798   1.7306
   3   5.382 MM    0.0190    2.17039    1.90106   2.1020
   4   5.921 MM    0.0570   90.79623   26.54871  87.9340
```

```
CE 6/7/2020 15:38:27 SYSTEM                                Page  1 of 2
```

Figure S 408: Condensed CE analysis for the NaOH extract of Table S 19, entry 1 – air exposure of **129** in DCM/^{n}heptane.

```
Data File C:\Chem32\1\Data\2007\200706\200706-1_MM613.D
Sample Name: MM613

=====================================================================
Acq. Operator   : SYSTEM
Sample Operator : SYSTEM
Acq. Instrument : CE                          Location :  15
Injection Date  : 6/7/2020 13:40:54
Acq. Method     : C:\Chem32\1\Methods\CE\Marx-Oxalate25C-Flush10mV12-200114.M
Last changed    : 14/1/2020 13:19:47 by SYSTEM
Analysis Method : C:\Chem32\1\Methods\CE\SwitchOff-200227.M
Last changed    : 6/7/2020 14:33:42 by SYSTEM
                  (modified after loading)
Sample Info     : NMR solution of MM613 (0.06 mL) diluted with H2O (0.6 ml)

Additional Info : Peak(s) manually integrated
```

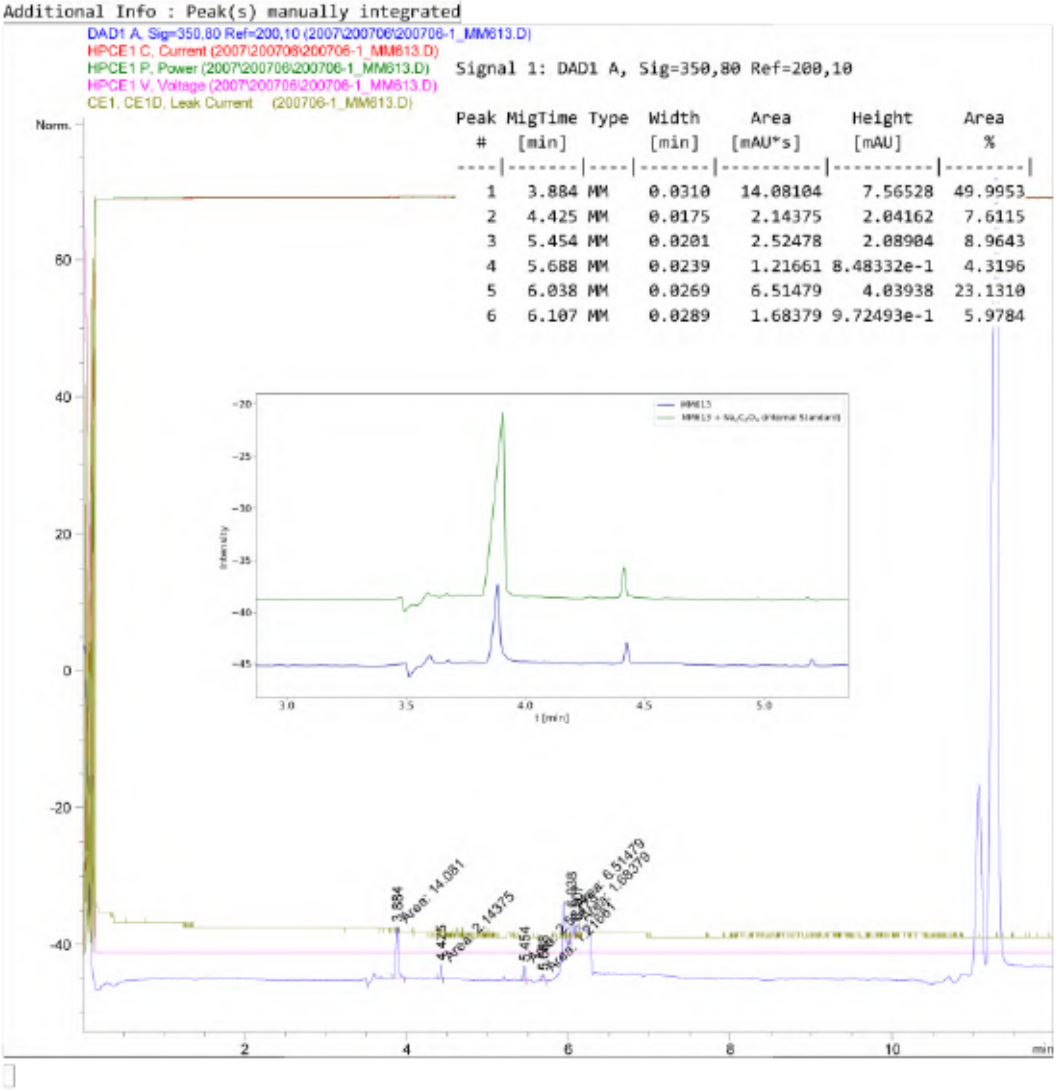


```
Signal 1: DAD1 A, Sig=350,80 Ref=200,10

Peak MigTime Type  Width     Area      Height     Area
  #   [min]       [min]   [mAU*s]     [mAU]       %
----|-------|----|-------|----------|----------|--------|
   1   3.884 MM    0.0310   14.08104   7.56528  49.9953
   2   4.425 MM    0.0175    2.14375   2.04162   7.6115
   3   5.454 MM    0.0201    2.52478   2.08904   8.9643
   4   5.688 MM    0.0239    1.21661 8.48332e-1   4.3196
   5   6.038 MM    0.0269    6.51479   4.03938  23.1310
   6   6.107 MM    0.0289    1.68379 9.72493e-1   5.9784
```


Figure S 409: Condensed CE analysis for the NaOH extract of Table S 19, entry 2 – air exposure of **196** in DCM/^{n}heptane.

```
Data File C:\Chem32\1\Data\2005\200506\200506-5_MM546-1.D
Sample Name: MM546-1

======================================================================
Acq. Operator   : SYSTEM
Sample Operator : SYSTEM
Acq. Instrument : CE                              Location :   24
Injection Date  : 6/5/2020 14:53:27
Acq. Method     : C:\Chem32\1\Methods\CE\Marx-Oxalate25C-Flush10mV23-V13-200428.M
Last changed    : 28/4/2020 15:34:00 by SYSTEM
Analysis Method : C:\Chem32\1\Methods\CE\Spuel-extended-200227.M
Last changed    : 5/6/2020 16:37:44 by SYSTEM
                  (modified after loading)
Sample Info     : NMR sample of MM5461-1 (0.03 mL diluted with 0.6 mL H2O)

Additional Info : Peak(s) manually integrated
```

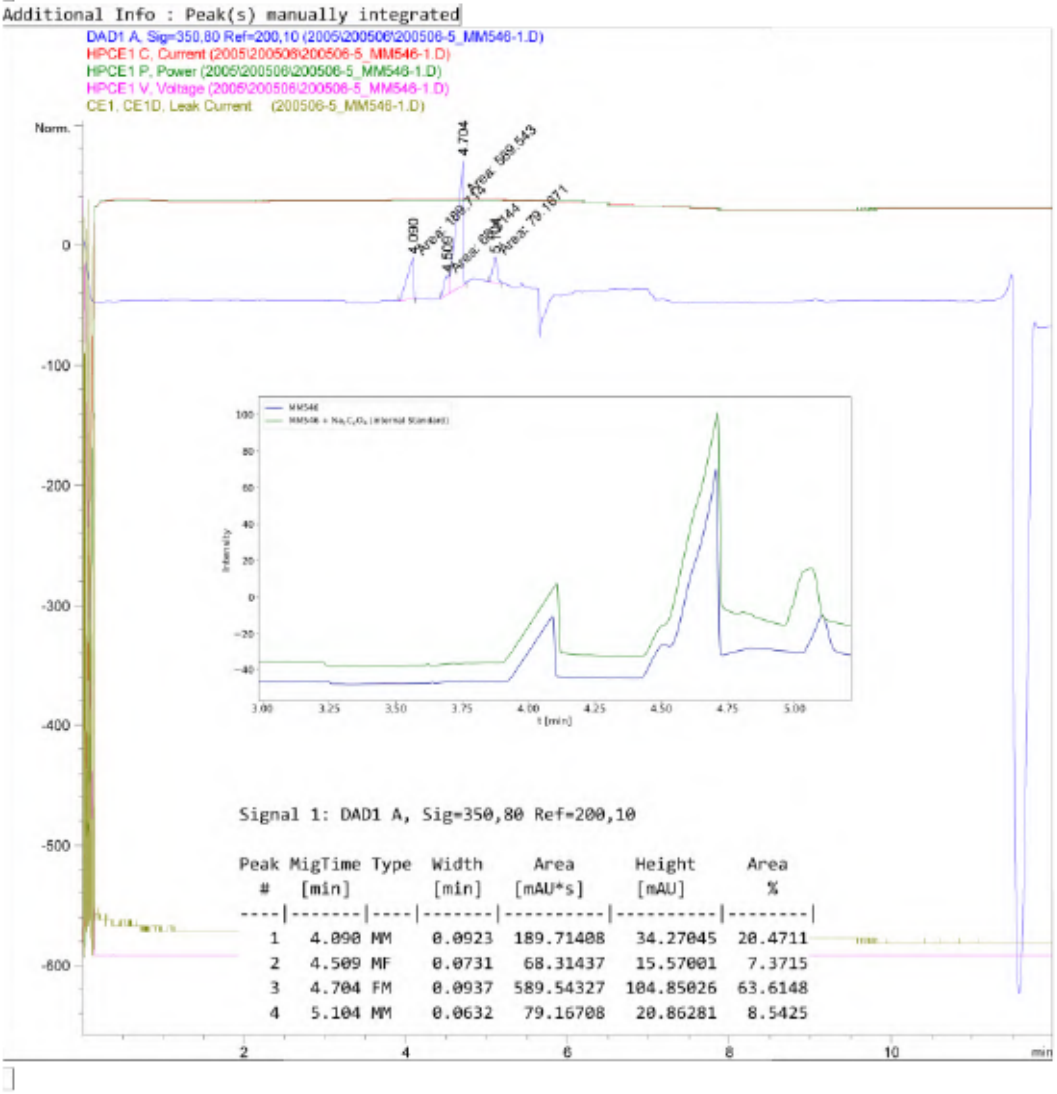


```
Signal 1: DAD1 A, Sig=350,80 Ref=200,10

Peak MigTime Type  Width     Area      Height     Area
  #   [min]       [min]   [mAU*s]     [mAU]       %
----|-------|----|-------|----------|----------|--------|
   1   4.090 MM    0.0923  189.71408   34.27045  20.4711
   2   4.509 MF    0.0731   68.31437   15.57001   7.3715
   3   4.704 FM    0.0937  589.54327  104.85026  63.6148
   4   5.104 MM    0.0632   79.16708   20.86281   8.5425
```

```
CE 5/6/2020 17:32:12 SYSTEM                                Page   1 of 2
```

Figure S 410: Condensed CE analysis for the NaOH extract of Table S 19, entry 3 – air exposure of sodium 3-methyl-2-oxobuyrate and $Cu(BF_4)_2{\cdot}6H_2O$ in DCM/MeOH/^{n}heptane.

Data File C:\Chem32\1\Data\2006\200623\200623-4_MM586.D
Sample Name: MM586

```
==================================================================
Acq. Operator   : SYSTEM
Sample Operator : SYSTEM
Acq. Instrument : CE                          Location :   30
Injection Date  : 23/6/2020 14:03:07
Acq. Method     : C:\Chem32\1\Methods\CE\Marx-Oxalate25C-Flush10mV12-200114.M
Last changed    : 14/1/2020 13:19:47 by SYSTEM
Analysis Method : C:\Chem32\1\Methods\CE\SwitchOff-200227.M
Last changed    : 23/6/2020 13:21:11 by SYSTEM
                  (modified after loading)
Sample Info     : NMR solution of MM586 (0.04 ml) diluted with H2O (0.6 ml)

Additional Info : Peak(s) manually integrated
```

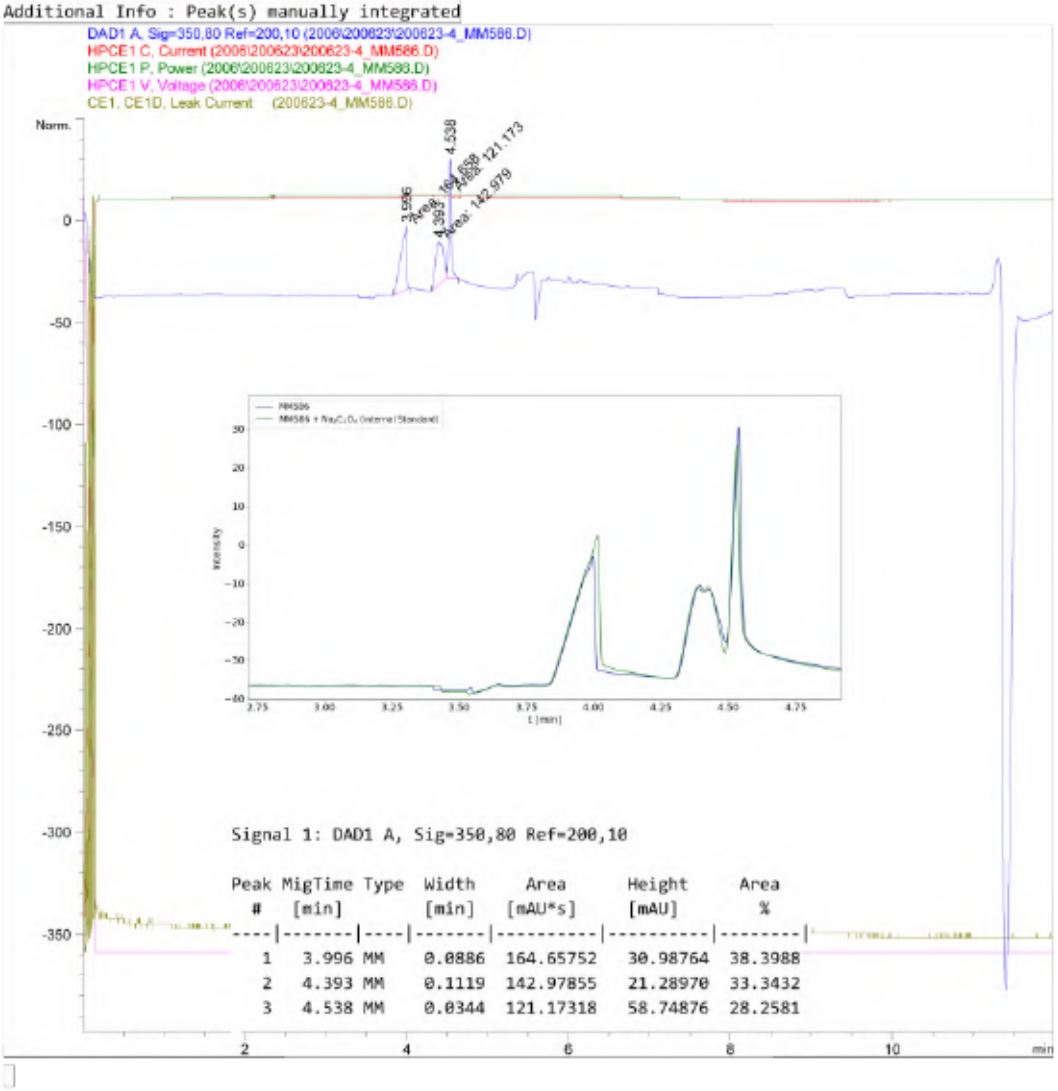

CE 23/6/2020 14:58:23 SYSTEM Page 1 of 2

Figure S 411: Condensed CE analysis for the NaOH extract of Table S 19, entry 4 – air exposure of sodium 3-methyl-2-oxobuyrate and $Cu(BF_4)_2 \cdot 6H_2O$ in DCM/MeOH/^{n}heptane.

Data File C:\Chem32\1\Data\2007\200701\200701-4_MM598.D
Sample Name: MM598

```
==================================================================
Acq. Operator   : SYSTEM
Sample Operator : SYSTEM
Acq. Instrument : CE                              Location :   37
Injection Date  : 1/7/2020 10:48:15
Acq. Method     : C:\Chem32\1\Methods\CE\Marx-Oxalate25C-Flush10mV12-200114.M
Last changed    : 14/1/2020 13:19:47 by SYSTEM
Analysis Method : C:\Chem32\1\Methods\CE\SwitchOff-200227.M
Last changed    : 1/7/2020 09:49:37 by SYSTEM
                  (modified after loading)
Sample Info     : NMR solution of MM598 (0.04 mL) diluted with H2O (0.6 ml)

Additional Info : Peak(s) manually integrated
```

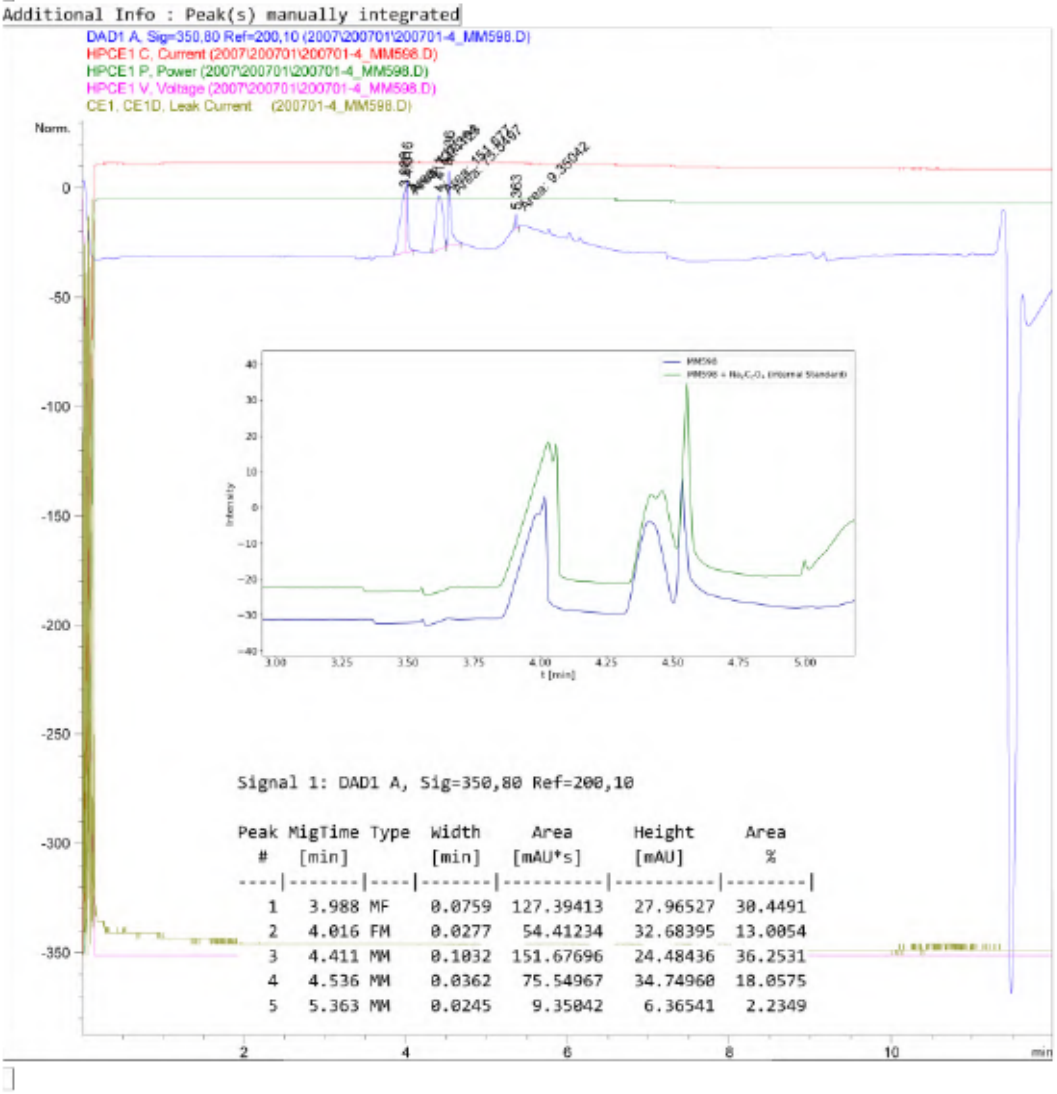

Signal 1: DAD1 A, Sig=350,80 Ref=200,10

Peak #	MigTime [min]	Type	Width [min]	Area [mAU*s]	Height [mAU]	Area %
1	3.988	MF	0.0759	127.39413	27.96527	30.4491
2	4.016	FM	0.0277	54.41234	32.68395	13.0054
3	4.411	MM	0.1032	151.67696	24.48436	36.2531
4	4.536	MM	0.0362	75.54967	34.74960	18.0575
5	5.363	MM	0.0245	9.35042	6.36541	2.2349

CE 1/7/2020 14:16:50 SYSTEM Page 1 of 2

Figure S 412: Condensed CE analysis for the NaOH extract of Table S 19, entry 5 – air exposure of sodium $^{13}C_5$-3-methyl-2-oxobuyrate and $Cu(BF_4)_2{\cdot}6H_2O$ in DCM/MeOH/^{n}heptane.

Data File C:\Chem32\1\Data\2007\200706\200706-4_MM611.D
Sample Name: MM611

```
Acq. Operator   : SYSTEM
Sample Operator : SYSTEM
Acq. Instrument : CE                              Location :  18
Injection Date  : 6/7/2020 15:09:06
Acq. Method     : C:\Chem32\1\Methods\CE\Marx-Oxalate25C-Flush10mV12-200114.M
Last changed    : 14/1/2020 13:19:47 by SYSTEM
Analysis Method : C:\Chem32\1\Methods\CE\SwitchOff-200227.M
Last changed    : 6/7/2020 14:33:42 by SYSTEM
                  (modified after loading)
Sample Info     : NMR solution of MM611 (0.04 mL) diluted with H2O (0.6 ml)

Additional Info : Peak(s) manually integrated
```

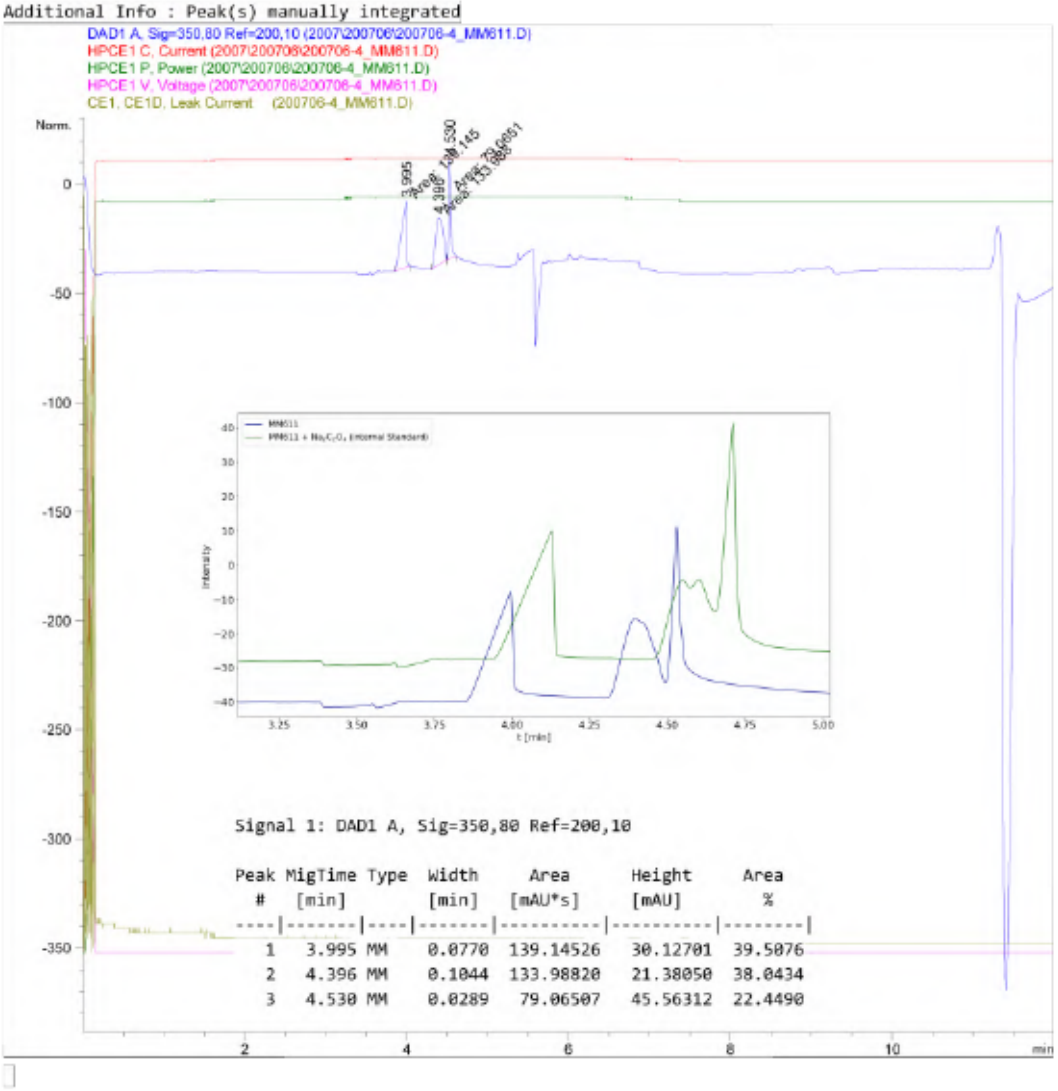

Signal 1: DAD1 A, Sig=350,80 Ref=200,10

Peak #	MigTime [min]	Type	Width [min]	Area [mAU*s]	Height [mAU]	Area %
1	3.995	MM	0.0770	139.14526	30.12701	39.5076
2	4.396	MM	0.1044	133.98820	21.38050	38.0434
3	4.530	MM	0.0289	79.06507	45.56312	22.4490

CE 6/7/2020 15:38:09 SYSTEM Page 1 of 2

Figure S 413: Condensed CE analysis for the NaOH extract of Table S 19, entry 6 – air exposure of sodium $^{13}C_5$-3-methyl-2-oxobuyrate and $Cu(BF_4)_2{\cdot}6H_2O$ in DCM/MeOH/^{n}heptane.

Data File C:\Chem32\1\Data\2007\200703\200703-1_MM601.D
Sample Name: MM601

```
==========================================================================
Acq. Operator   : SYSTEM
Sample Operator : SYSTEM
Acq. Instrument : CE                              Location :   15
Injection Date  : 3/7/2020 11:28:08
Acq. Method     : C:\Chem32\1\Methods\CE\Marx-Oxalate25C-Flush10mV12-200114.M
Last changed    : 14/1/2020 13:19:47 by SYSTEM
Analysis Method : C:\Chem32\1\Methods\CE\SwitchOff-200227.M
Last changed    : 3/7/2020 11:54:18 by SYSTEM
                  (modified after loading)
Sample Info     : NMR sample of MM601 (0.04 mL) diluted with H2O (0.6 mL)

Additional Info : Peak(s) manually integrated
```

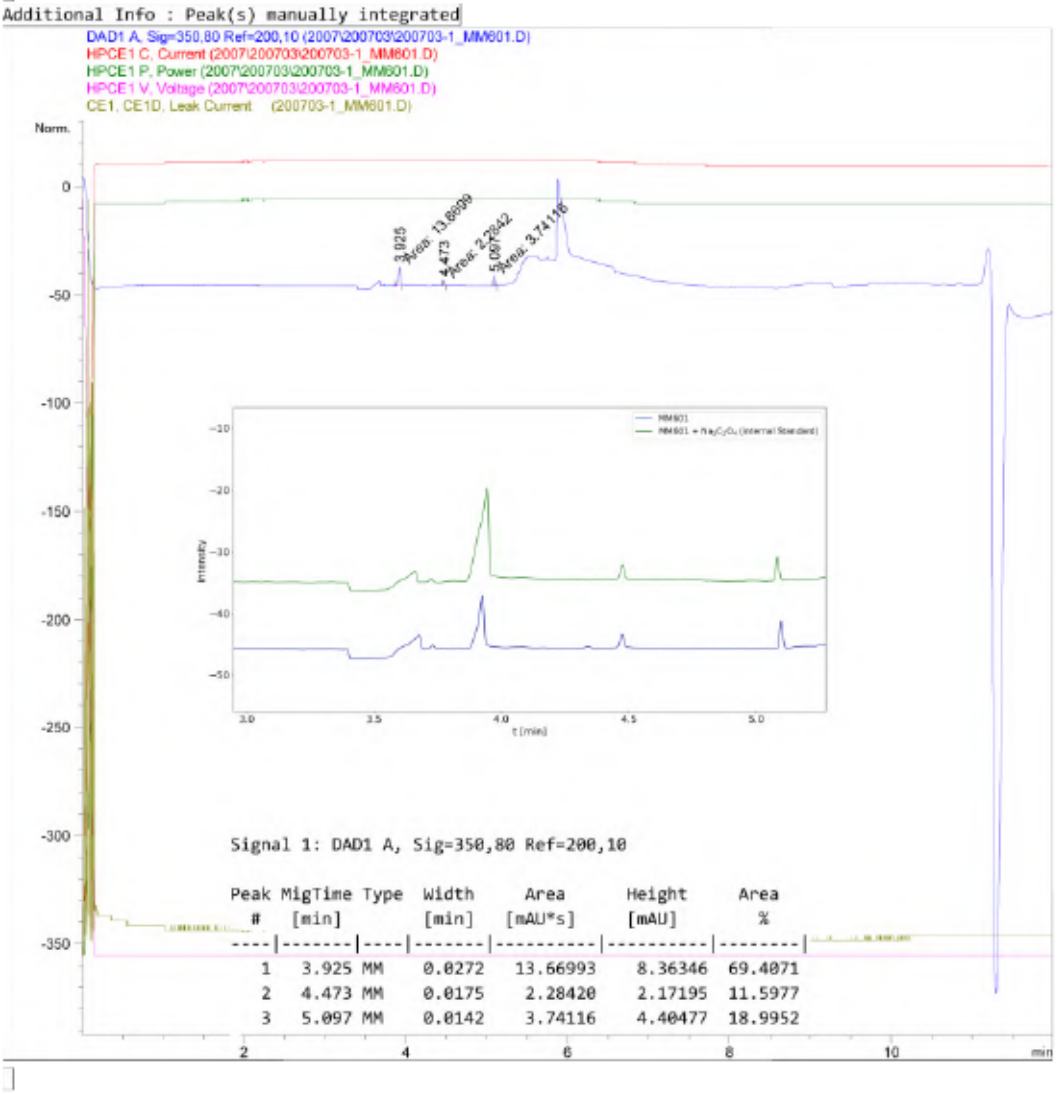

Signal 1: DAD1 A, Sig=350,80 Ref=200,10

Peak #	MigTime [min]	Type	Width [min]	Area [mAU*s]	Height [mAU]	Area %
1	3.925	MM	0.0272	13.66993	8.36346	69.4071
2	4.473	MM	0.0175	2.28420	2.17195	11.5977
3	5.097	MM	0.0142	3.74116	4.40477	18.9952

CE 3/7/2020 17:09:16 SYSTEM Page 1 of 2

Figure S 414: Condensed CE analysis for the NaOH extract of Table S 19, entry 7 – air exposure of sodium 3-methyl-2-oxobuyrate in DCM/MeOH/^{n}heptane.

Data File C:\Chem32\1\Data\2005\200527\200527-6_MM553-1.D
Sample Name: MM553-1

```
==================================================================
Acq. Operator   : SYSTEM
Sample Operator : SYSTEM
Acq. Instrument : CE                          Location :   22
Injection Date  : 27/5/2020 15:19:32
Acq. Method     : C:\Chem32\1\Methods\CE\Marx-Oxalate25C-Flush10mV23-V13-200428.M
Last changed    : 28/4/2020 15:34:00 by SYSTEM
Analysis Method : C:\Chem32\1\Methods\CE\Spuel-extended-200227.M
Last changed    : 27/5/2020 14:08:30 by SYSTEM
                  (modified after loading)
Sample Info     : NMR solution of MM553-1 (0.03 mL diluted with 0.6 mL H2O)

Additional Info : Peak(s) manually integrated
```

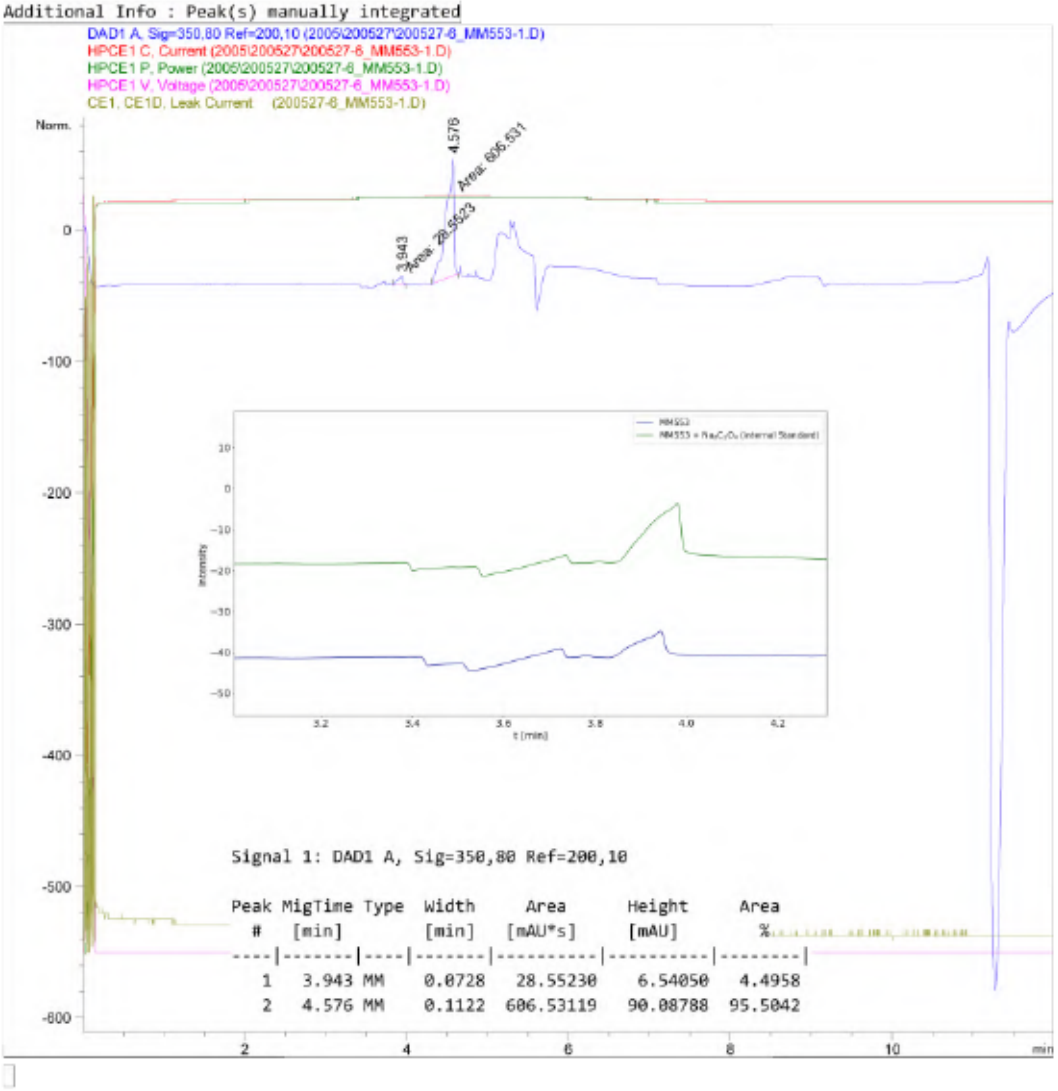

Signal 1: DAD1 A, Sig=350,80 Ref=200,10

Peak #	MigTime [min]	Type	Width [min]	Area [mAU*s]	Height [mAU]	Area %
1	3.943	MM	0.0728	28.55230	6.54050	4.4958
2	4.576	MM	0.1122	606.53119	90.08788	95.5042

CE 27/5/2020 17:19:34 SYSTEM Page 1 of 2

Figure S 415: Condensed CE analysis for the NaOH extract of Table S 19, entry 8 – air exposure of sodium pyruvate and $Cu(BF_4)_2{\cdot}6H_2O$ in DCM/MeOH/^{n}heptane.

```
Data File C:\Chem32\1\Data\2007\200706\200706-2_MM607.D
Sample Name: MM607

======================================================================
Acq. Operator   : SYSTEM
Sample Operator : SYSTEM
Acq. Instrument : CE                          Location :   16
Injection Date  : 6/7/2020 14:04:27
Acq. Method     : C:\Chem32\1\Methods\CE\Marx-Oxalate25C-Flush10mV12-200114.M
Last changed    : 14/1/2020 13:19:47 by SYSTEM
Analysis Method : C:\Chem32\1\Methods\CE\SwitchOff-200227.M
Last changed    : 6/7/2020 14:33:42 by SYSTEM
                  (modified after loading)
Sample Info     : NMR solution of MM607 (0.06 mL) diluted with H2O (0.6 ml)

Additional Info : Peak(s) manually integrated
```

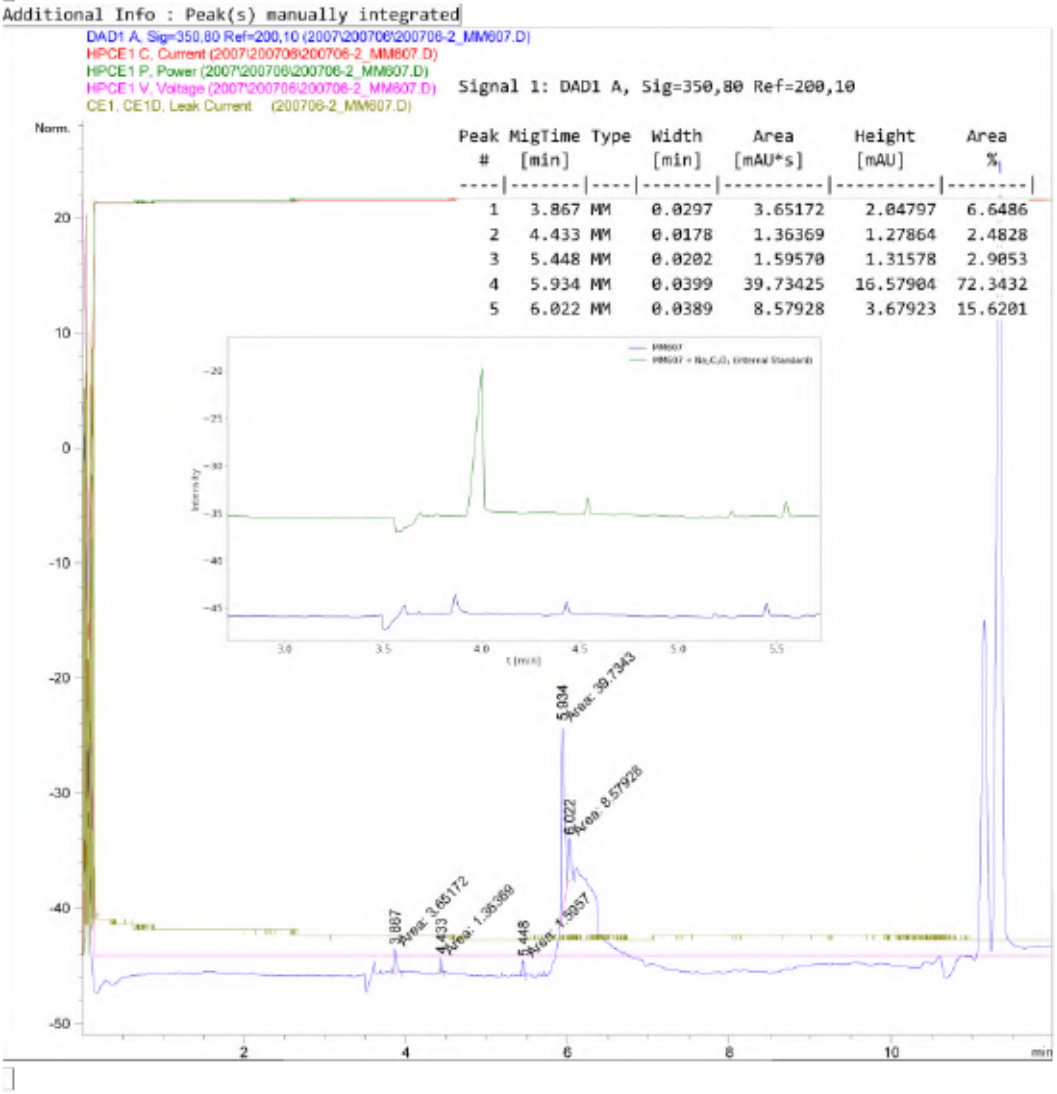


```
CE 6/7/2020 14:38:30 SYSTEM                              Page   1 of 2
```

Figure S 416: Condensed CE analysis for the NaOH extract of Table S 20, entry 1 – reaction of **129** with CO_2/O_2 in toluene.

```
Data File C:\Chem32\1\Data\2007\200707\200707-8_MM616.D
Sample Name: MM616

======================================================================
Acq. Operator   : SYSTEM
Sample Operator : SYSTEM
Acq. Instrument : CE                              Location :   25
Injection Date  : 7/7/2020 16:00:20
Acq. Method     : C:\Chem32\1\Methods\CE\Marx-Oxalate25C-Flush10mV23-V13-200428.M
Last changed    : 28/4/2020 15:34:00 by SYSTEM
Analysis Method : C:\Chem32\1\Methods\CE\SwitchOff-200227.M
Last changed    : 7/7/2020 17:20:34 by SYSTEM
                  (modified after loading)
Sample Info     : NMR solution of MM616 (0.06 mL) diluted with H2O (0.6 mL)

Additional Info : Peak(s) manually integrated
```

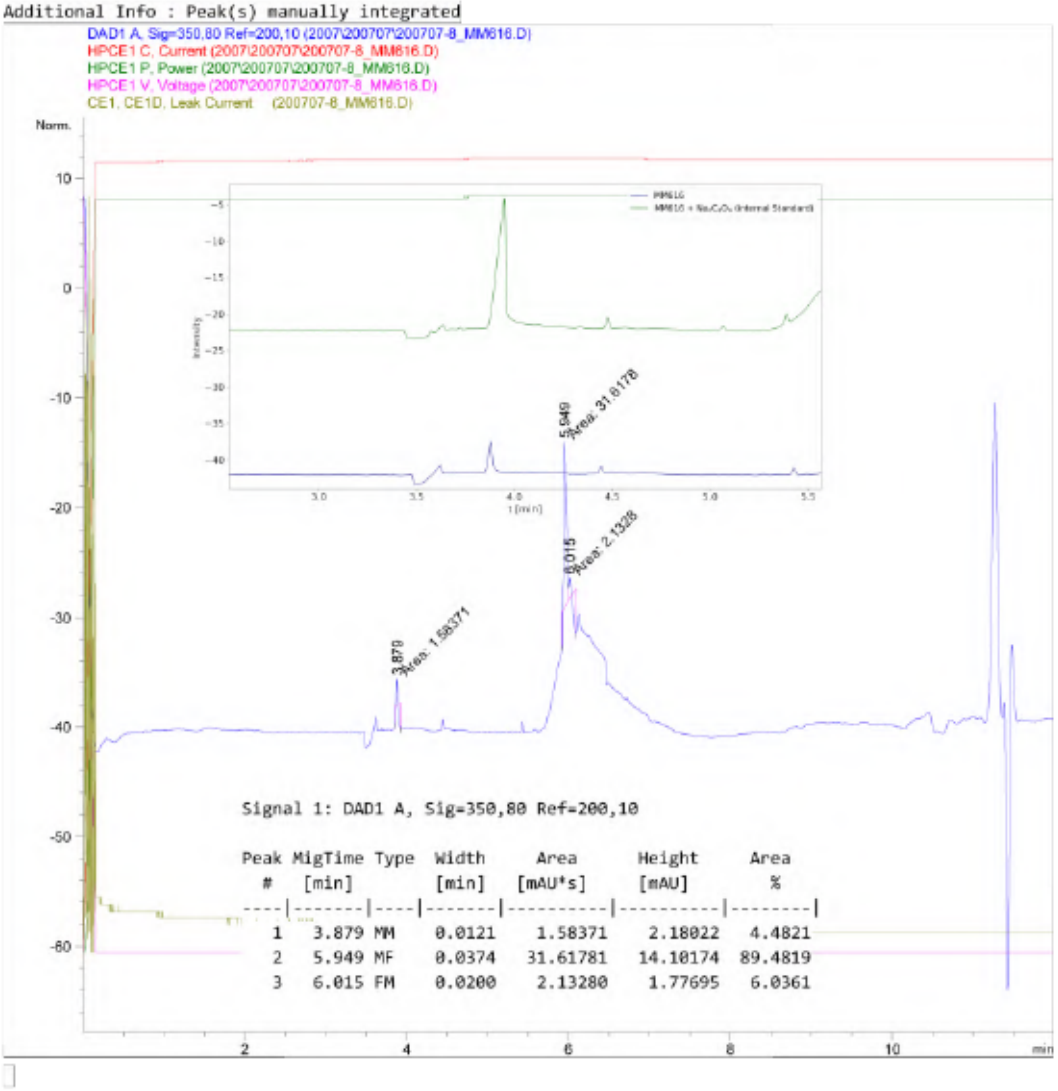


```
CE 7/7/2020 19:45:31 SYSTEM                                  Page   1 of 2
```

Figure S 417: Condensed CE analysis for the NaOH extract of Table S 20, entry 2 – reaction of **196** with CO_2/O_2 in toluene.

Data File C:\Chem32\1\Data\2007\200707\200707-7_MM616.D
Sample Name: MM616

Acq. Operator	: SYSTEM
Sample Operator	: SYSTEM
Acq. Instrument	: CE Location : 26
Injection Date	: 7/7/2020 15:35:16
Acq. Method	: C:\Chem32\1\Methods\CE\Marx-Oxalate25C-Flush10mV23-V13-200428.M
Last changed	: 28/4/2020 15:34:00 by SYSTEM
Analysis Method	: C:\Chem32\1\Methods\CE\SwitchOff-200227.M
Last changed	: 7/7/2020 17:20:34 by SYSTEM (modified after loading)
Sample Info	: NMR solution of MM616 (0.06 mL) diluted with H2O (0.6 mL)
Additional Info	: Peak(s) manually integrated

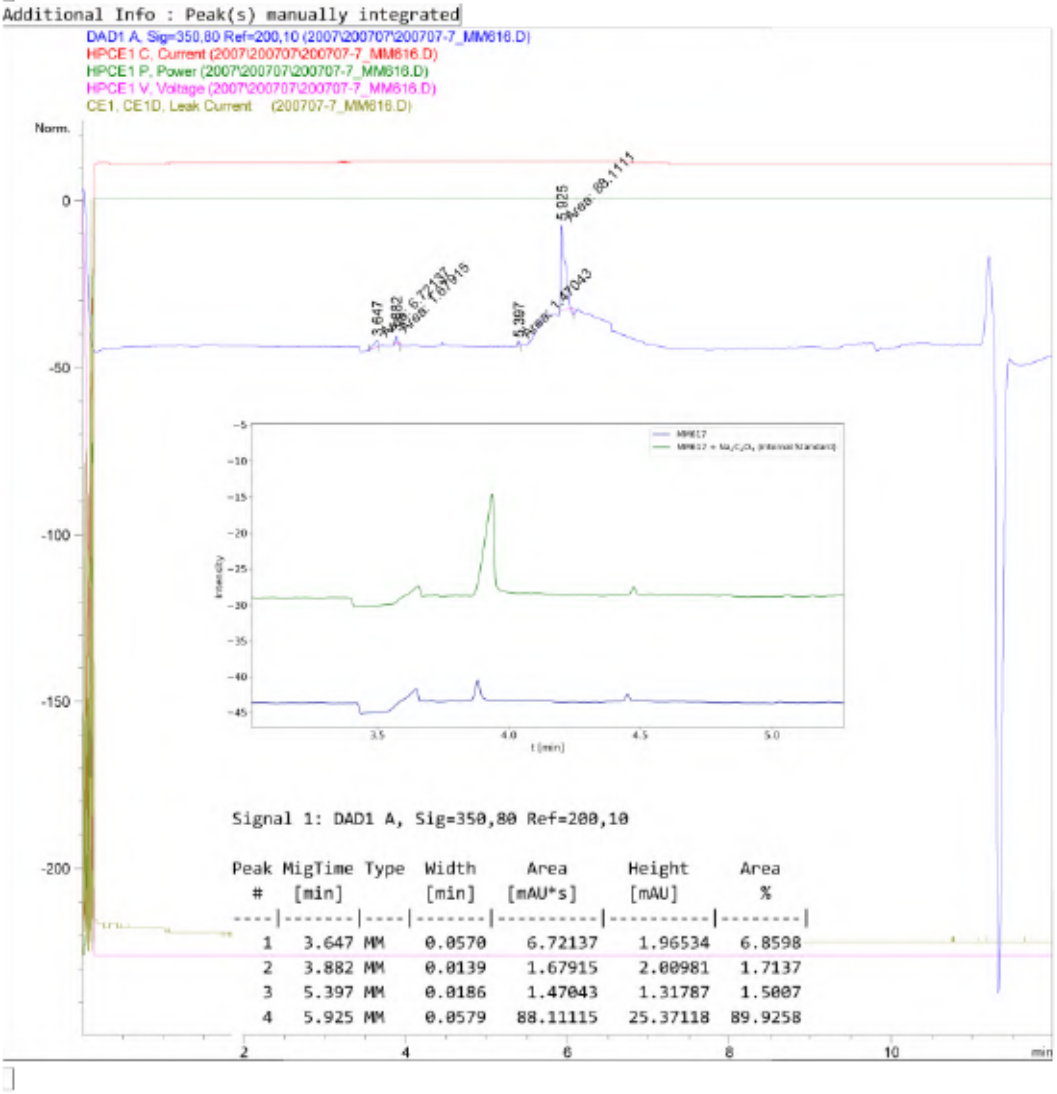

Signal 1: DAD1 A, Sig=350,80 Ref=200,10

Peak #	MigTime [min]	Type	Width [min]	Area [mAU*s]	Height [mAU]	Area %
1	3.647	MM	0.0570	6.72137	1.96534	6.8598
2	3.882	MM	0.0139	1.67915	2.00981	1.7137
3	5.397	MM	0.0186	1.47043	1.31787	1.5007
4	5.925	MM	0.0579	88.11115	25.37118	89.9258

CE 7/7/2020 19:47:39 SYSTEM Page 1 of 2

Figure S 418: Condensed CE analysis for the NaOH extract of Table S 20, entry 3 – reaction of **196** with CO_2/O_2 in toluene.

```
Data File C:\Chem32\1\Data\2007\200717\200717-2_MM621.D
Sample Name: MM621

======================================================================
Acq. Operator   : SYSTEM
Sample Operator : SYSTEM
Acq. Instrument : CE                          Location :  16
Injection Date  : 17/7/2020 14:11:44
Acq. Method     : C:\Chem32\1\Methods\CE\Marx-Oxalate25C-Flush10mV12-200114.M
Last changed    : 14/1/2020 13:19:47 by SYSTEM
Analysis Method : C:\Chem32\1\Methods\CE\SwitchOff-200227.M
Last changed    : 17/7/2020 14:34:24 by SYSTEM
                  (modified after loading)
Sample Info     : NMR solution of MM621 (0.10 mL) diluted with H2O (0.5 mL)

Additional Info : Peak(s) manually integrated
```

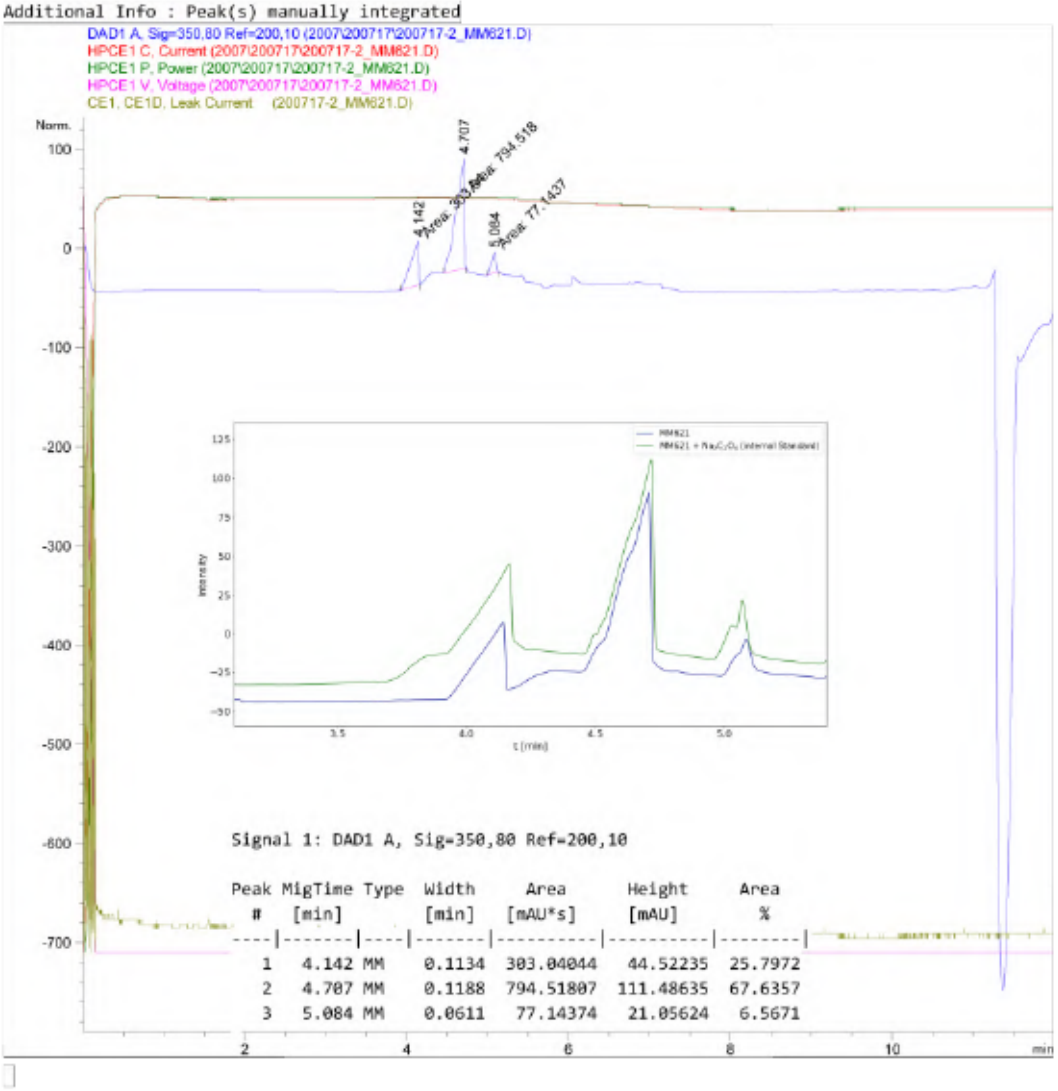

Peak #	MigTime [min]	Type	Width [min]	Area [mAU*s]	Height [mAU]	Area %
1	4.142	MM	0.1134	303.04044	44.52235	25.7972
2	4.707	MM	0.1188	794.51807	111.48635	67.6357
3	5.084	MM	0.0611	77.14374	21.05624	6.5671

```
CE 17/7/2020 16:19:07 SYSTEM                                Page  1 of 2
```

Figure S 419: Condensed CE analysis for the NaOH extract of Table S 20, entry 4 – reaction of sodium $^{13}C_5$-3-methyl-2-oxobuyrate and $Cu(BF_4)_2{\cdot}6H_2O$ with CO_2/O_2 in C_6D_6/CD_3OD.

Data File C:\Chem32\1\Data\2007\200717\200717-1_MM620.D
Sample Name: MM620

```
=====================================================================
Acq. Operator   : SYSTEM
Sample Operator : SYSTEM
Acq. Instrument : CE                              Location :   15
Injection Date  : 17/7/2020 13:48:15
Acq. Method     : C:\Chem32\1\Methods\CE\Marx-Oxalate25C-Flush10mV12-200114.M
Last changed    : 14/1/2020 13:19:47 by SYSTEM
Analysis Method : C:\Chem32\1\Methods\CE\SwitchOff-200227.M
Last changed    : 17/7/2020 14:34:24 by SYSTEM
                  (modified after loading)
Sample Info     : NMR solution of MM620 (0.10 mL) diluted with H2O (0.5 mL)

Additional Info : Peak(s) manually integrated
```

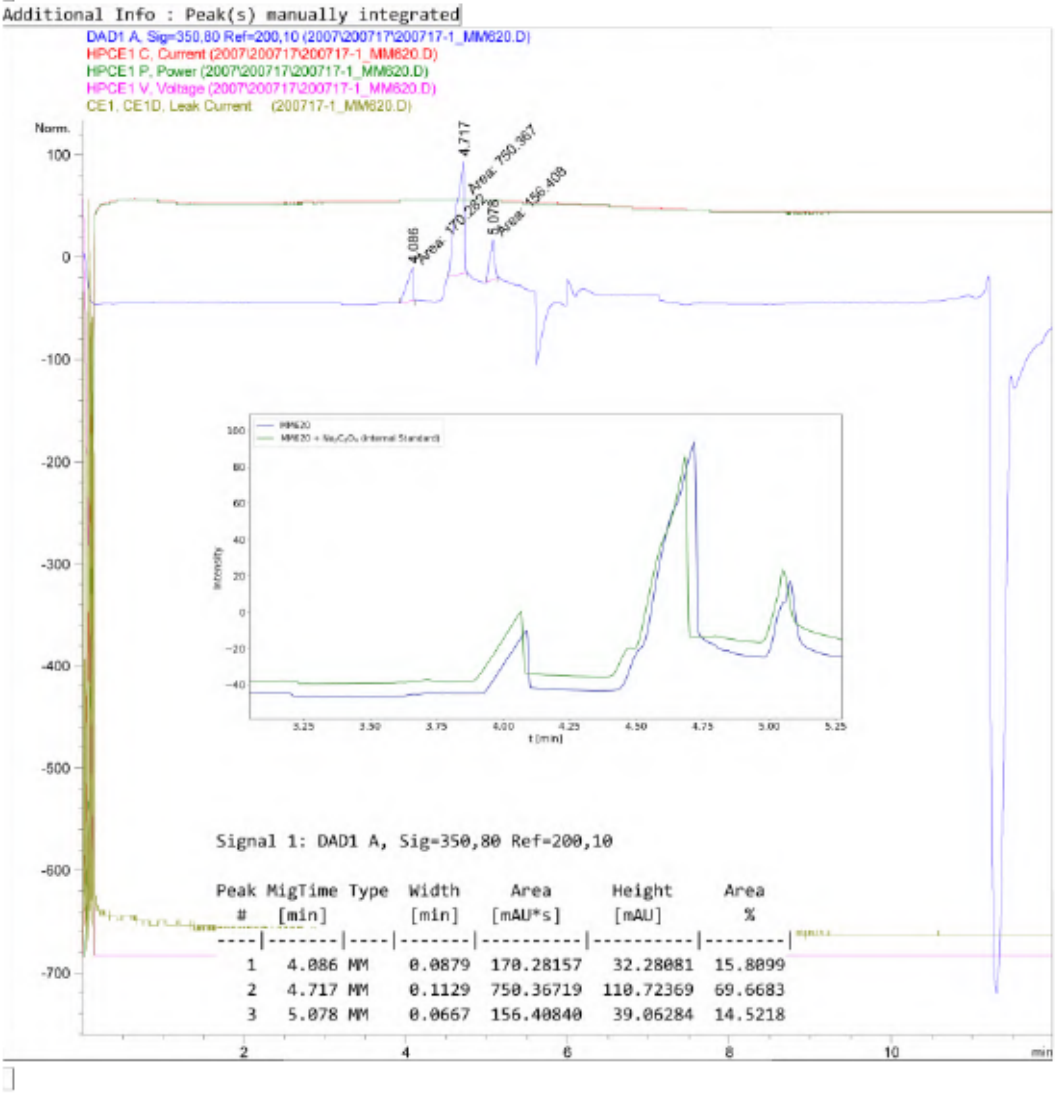

Signal 1: DAD1 A, Sig=350,80 Ref=200,10

Peak #	MigTime [min]	Type	Width [min]	Area [mAU*s]	Height [mAU]	Area %
1	4.086	MM	0.0879	170.28157	32.28081	15.8099
2	4.717	MM	0.1129	750.36719	110.72369	69.6683
3	5.078	MM	0.0667	156.40840	39.06284	14.5218

CE 17/7/2020 16:18:52 SYSTEM Page 1 of 2

Figure S 420: Condensed CE analysis for the NaOH extract of Table S 20, entry 5 – reaction of sodium $^{13}C_5$-3-methyl-2-oxobuyrate and $Cu(BF_4)_2{\cdot}6H_2O$ with CO_2/O_2 in CD_2Cl_2/CD_3OD.

4.15.5 CE Analysis – Reactions of 139 with KC_8 and CO_2

Data File C:\Chem32\1\Data\2006\200602\200602-7_MM535-1.D
Sample Name: MM535-1

Acq. Operator	: SYSTEM
Sample Operator	: SYSTEM
Acq. Instrument	: CE Location : 29
Injection Date	: 2/6/2020 18:33:44
Acq. Method	: C:\Chem32\1\Methods\CE\Marx-Oxalate25C-Flush10mV23-V13-200428.M
Last changed	: 28/4/2020 15:34:00 by SYSTEM
Analysis Method	: C:\Chem32\1\Methods\CE\Spuel-extended-200227.M
Last changed	: 5/6/2020 16:37:44 by SYSTEM
	(modified after loading)
Sample Info	: NMR solution of MM535-1 (0.2 mL) diluted with H2O (0.4 ml)

Additional Info : Peak(s) manually integrated

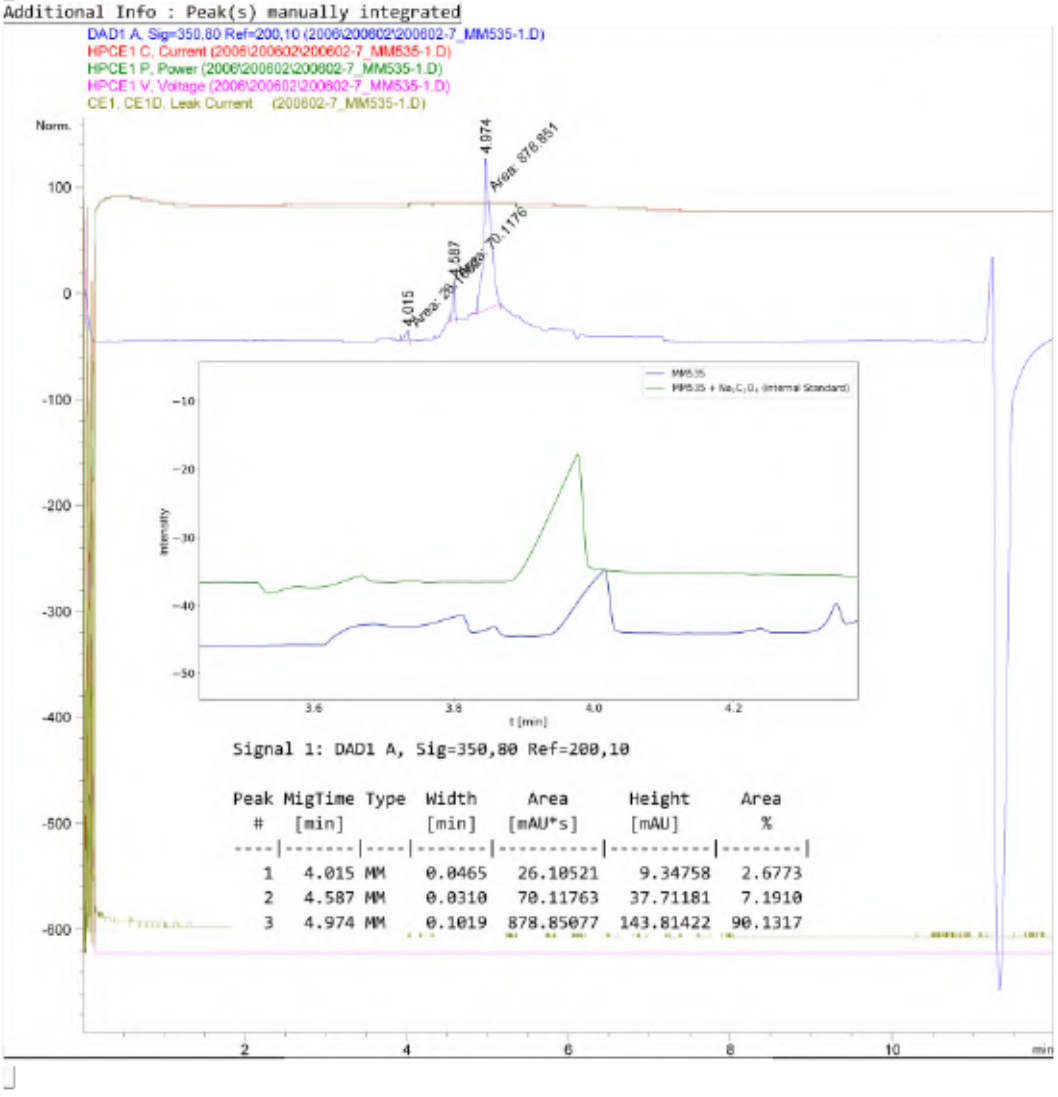

Signal 1: DAD1 A, Sig=350,80 Ref=200,10

Peak #	MigTime [min]	Type	Width [min]	Area [mAU*s]	Height [mAU]	Area %
1	4.015	MM	0.0465	26.10521	9.34758	2.6773
2	4.587	MM	0.0310	70.11763	37.71181	7.1910
3	4.974	MM	0.1019	878.85077	143.81422	90.1317

CE 5/6/2020 17:40:11 SYSTEM Page 1 of 2

Figure S 421: Condensed CE analysis for the MeOH extract of Table S 21, entry 1 – reaction of **139** and KC_8 with CO_2 in THF.

```
Data File C:\Chem32\1\Data\2004\200428\200428-5_MM540-1.D
Sample Name: MM540-1

======================================================================
Acq. Operator   : SYSTEM
Sample Operator : SYSTEM
Acq. Instrument : CE                          Location :  39
Injection Date  : 28/4/2020 14:04:48
Acq. Method     : C:\Chem32\1\Methods\CE\Marx-Oxalate25C-Flush10mV12-200114.M
Last changed    : 14/1/2020 13:19:47 by SYSTEM
Analysis Method : C:\Chem32\1\Methods\CE\Spuel-extended-200227.M
Last changed    : 5/6/2020 16:37:44 by SYSTEM
                  (modified after loading)
Sample Info     : NMR sample of MM540-1 (0.03 mL diluted with 0.6 mL H2O)

Additional Info : Peak(s) manually integrated
```

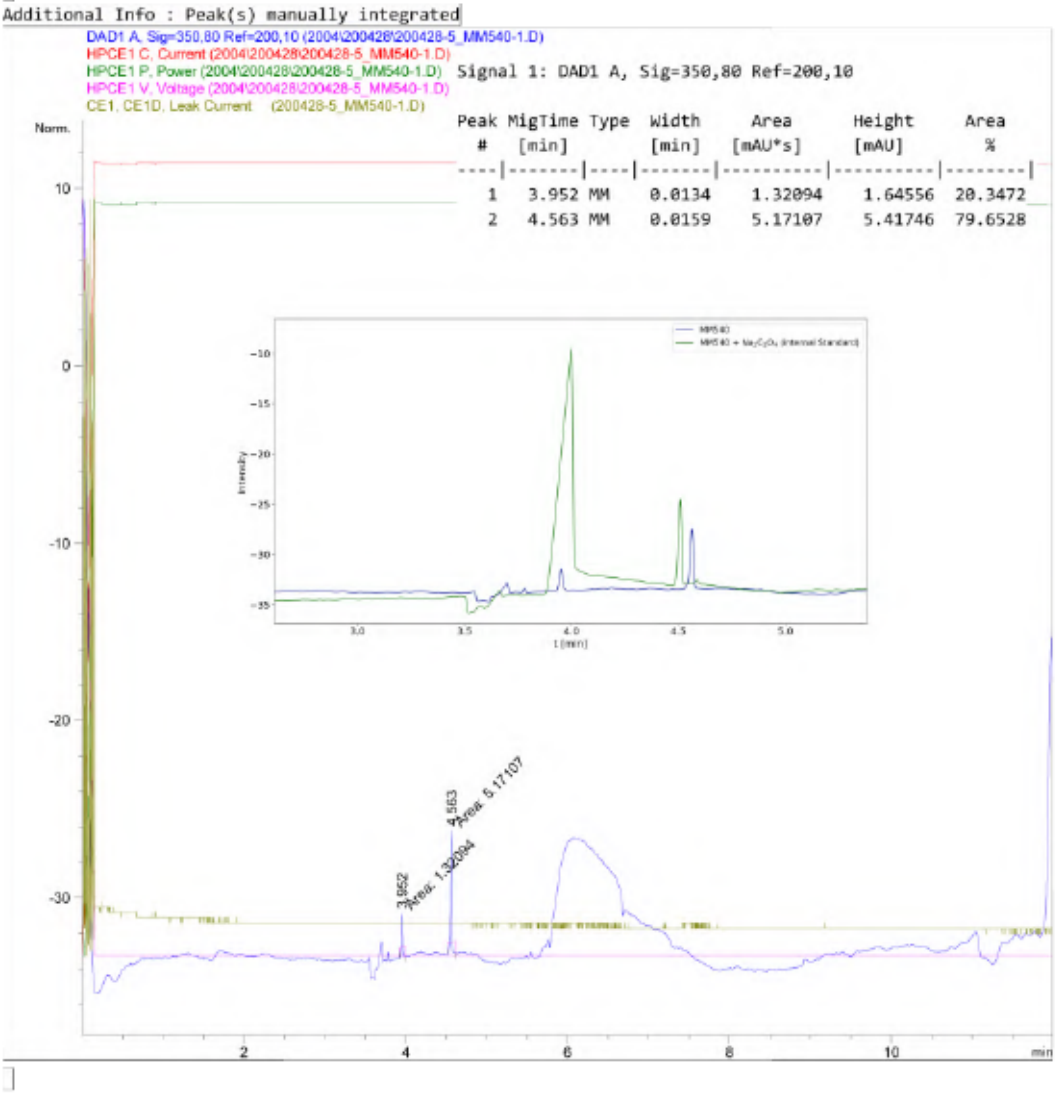


```
CE 5/6/2020 17:23:24 SYSTEM                                Page  1 of 2
```

Figure S 422: Condensed CE analysis for the MeOH extract of Table S 21, entry 2 – reaction of **139** and KC_8 with CO_2 in THF.

4.16 Mass Spectrometry

4.16.1 HR-MS Analysis – Reactions of α-Ketocarboxylates

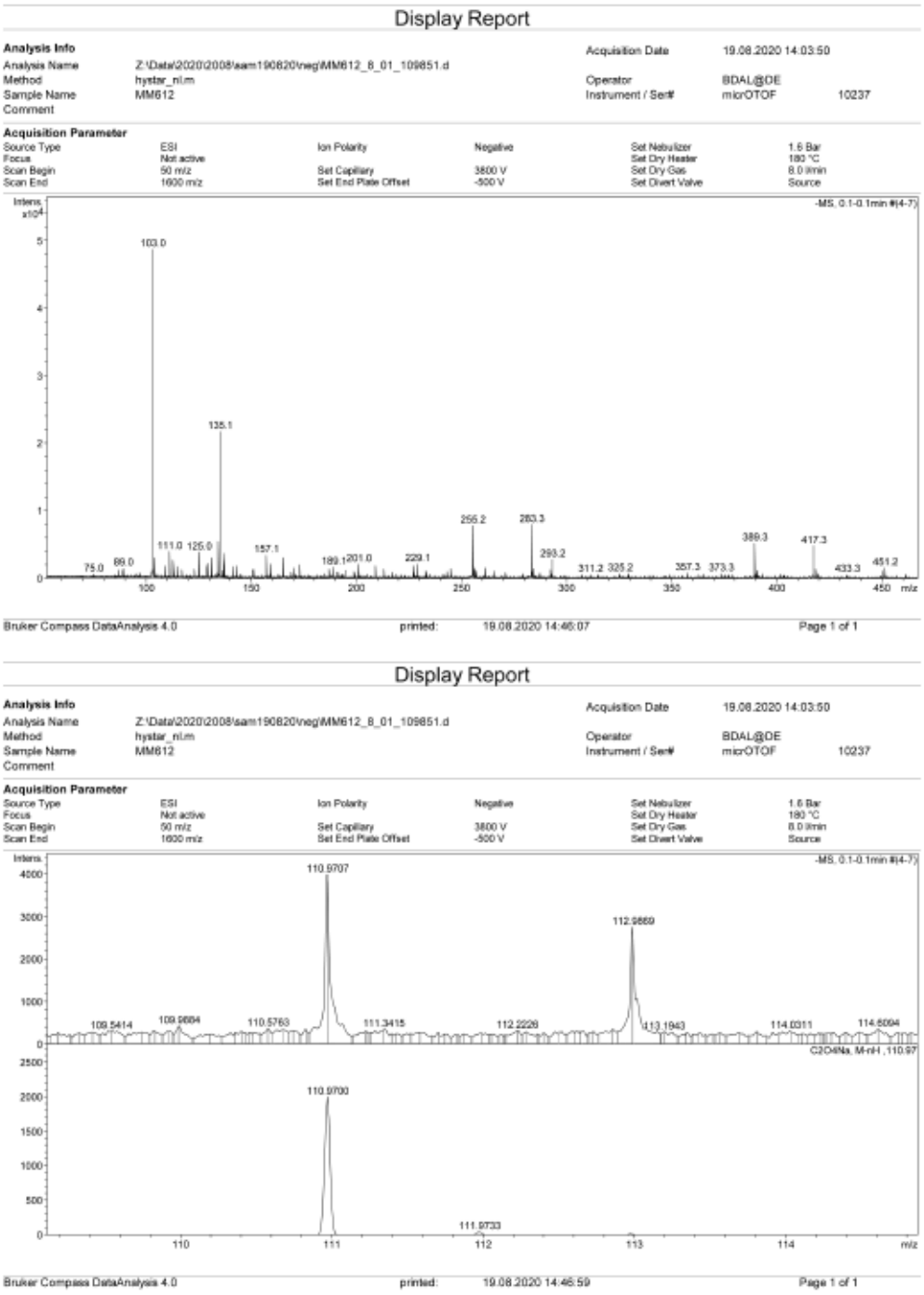

Figure S 423: HR-MS (ESI) analysis of the NaOH extract of Table S 19, entry 1 – air exposure of **129** in DCM/^{n}heptane.

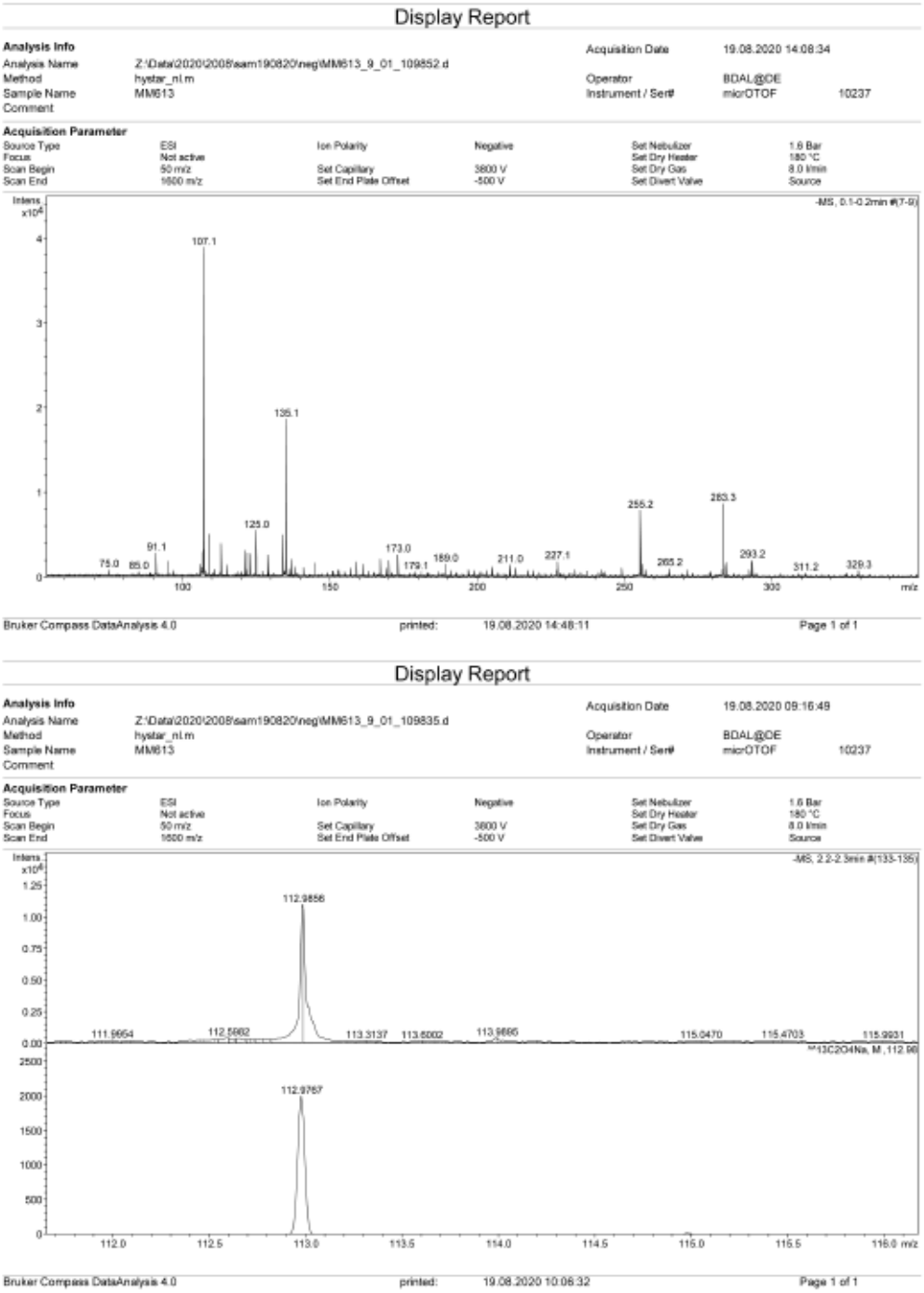

Figure S 424: HR-MS (ESI) analysis (part 1) of the NaOH extract of Table S 19, entry 2 – air exposure of **196** in DCM/^{n}heptane.

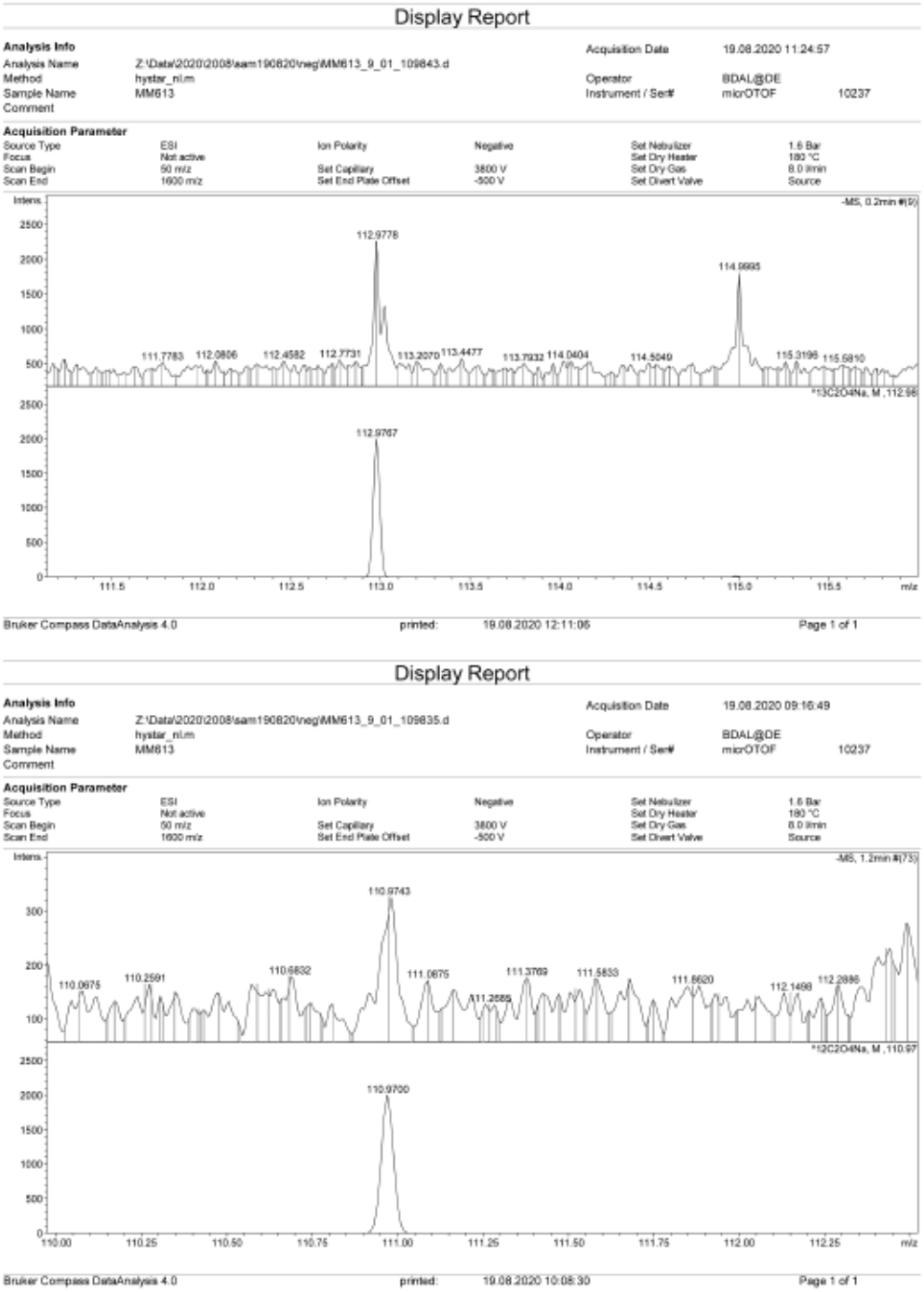

Figure S 425: HR-MS (ESI) analysis (part 2) of the NaOH extract of Table S 19, entry 2 – air exposure of **196** in DCM/^{n}heptane.

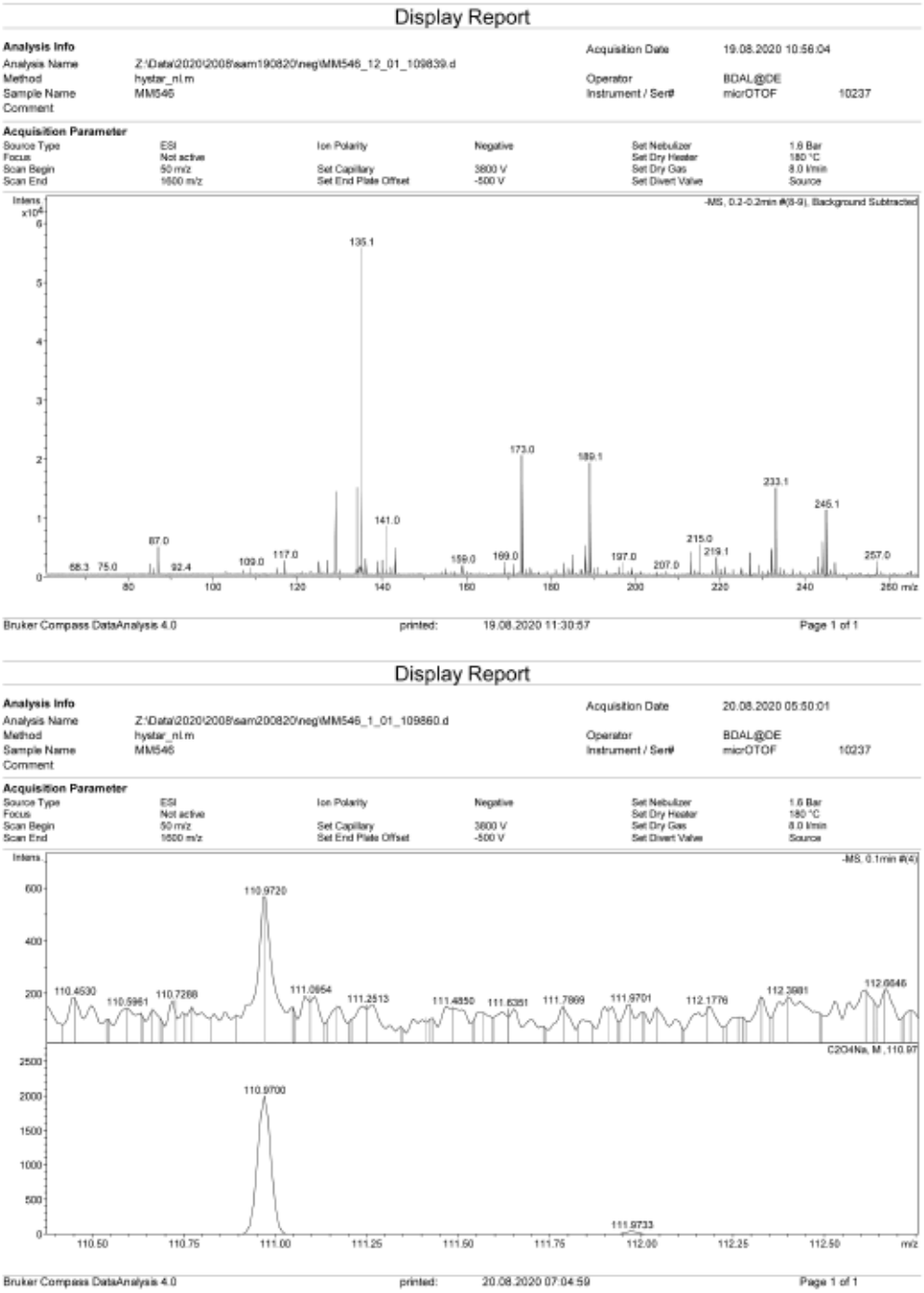

Figure S 426: HR-MS (ESI) analysis of the NaOH extract of Table S 19, entry 3 – air exposure of sodium 3-methyl-2-oxobuyrate and $Cu(BF_4)_2{\cdot}6H_2O$ in DCM/MeOH/^{n}heptane.

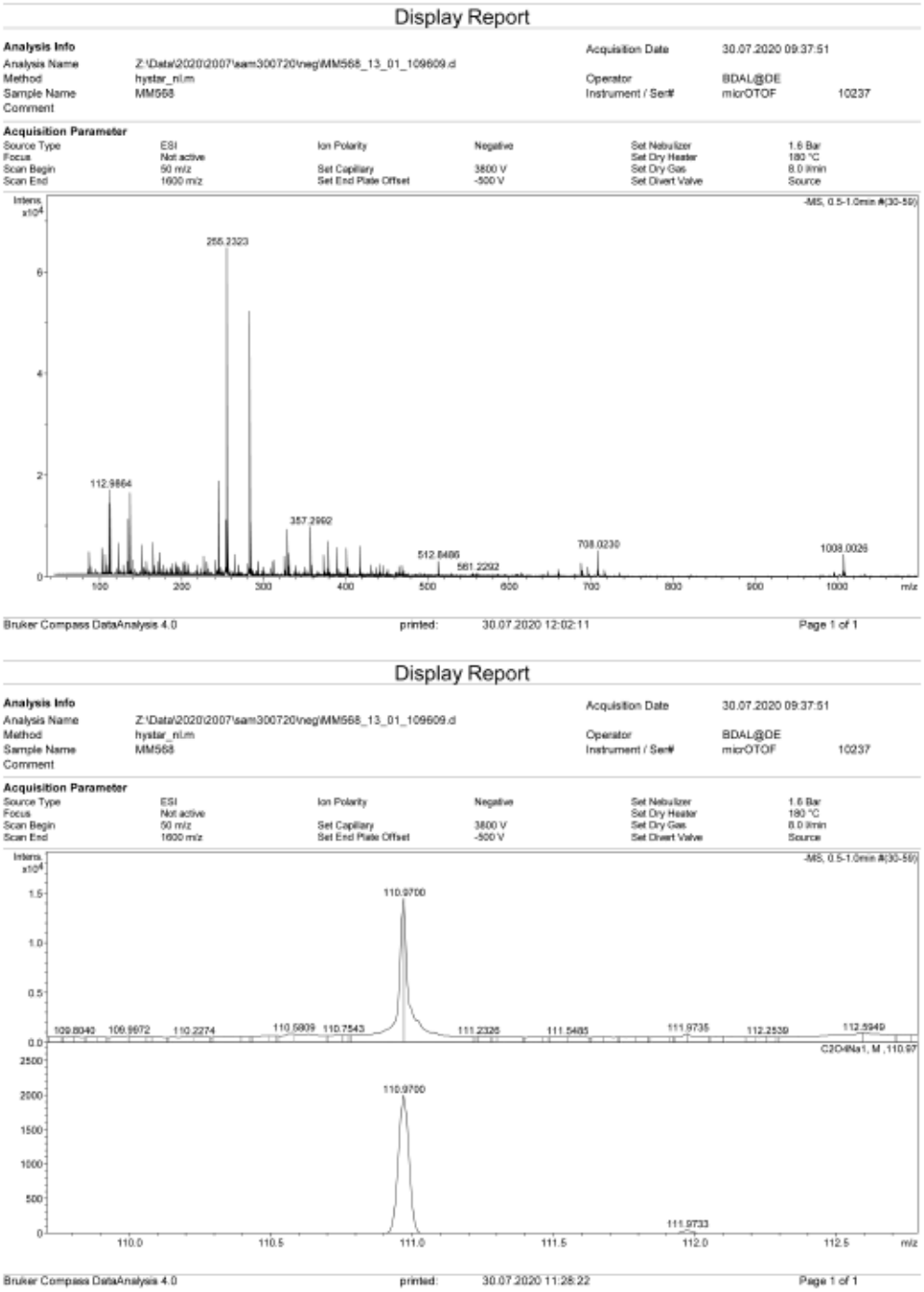

Figure S 427: HR-MS (ESI) analysis of the NaOH extract of Table S 19, entry 4 – air exposure of sodium 3-methyl-2-oxobuyrate and $Cu(BF_4)_2 \cdot 6H_2O$ in DCM/MeOH/^{n}heptane.

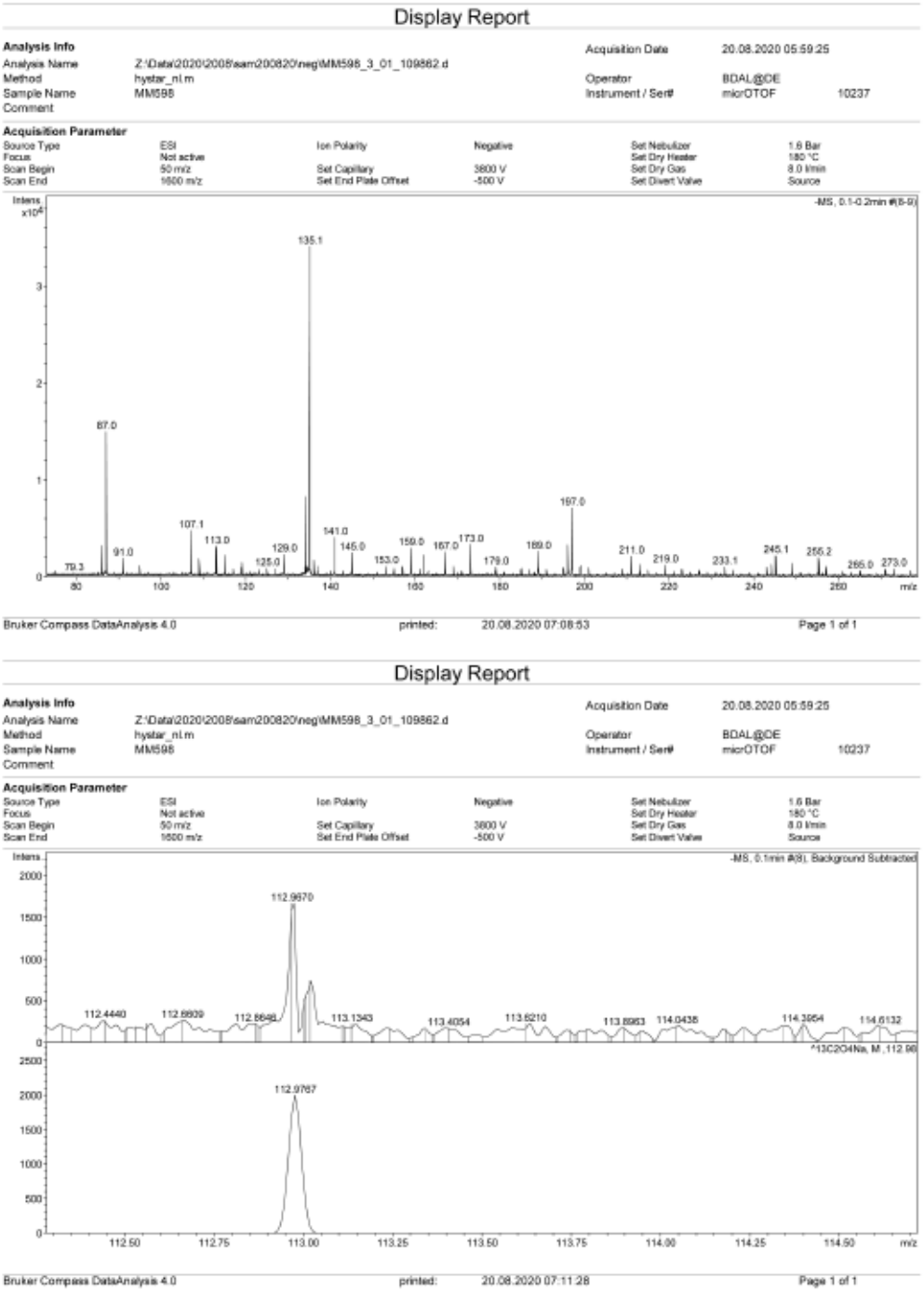

Figure S 428: HR-MS (ESI) analysis of the NaOH extract of Table S 19, entry 5 – air exposure of sodium $^{13}C_5$-3-methyl-2-oxobuyrate and $Cu(BF_4)_2{\cdot}6H_2O$ in DCM/MeOH/^{n}heptane.

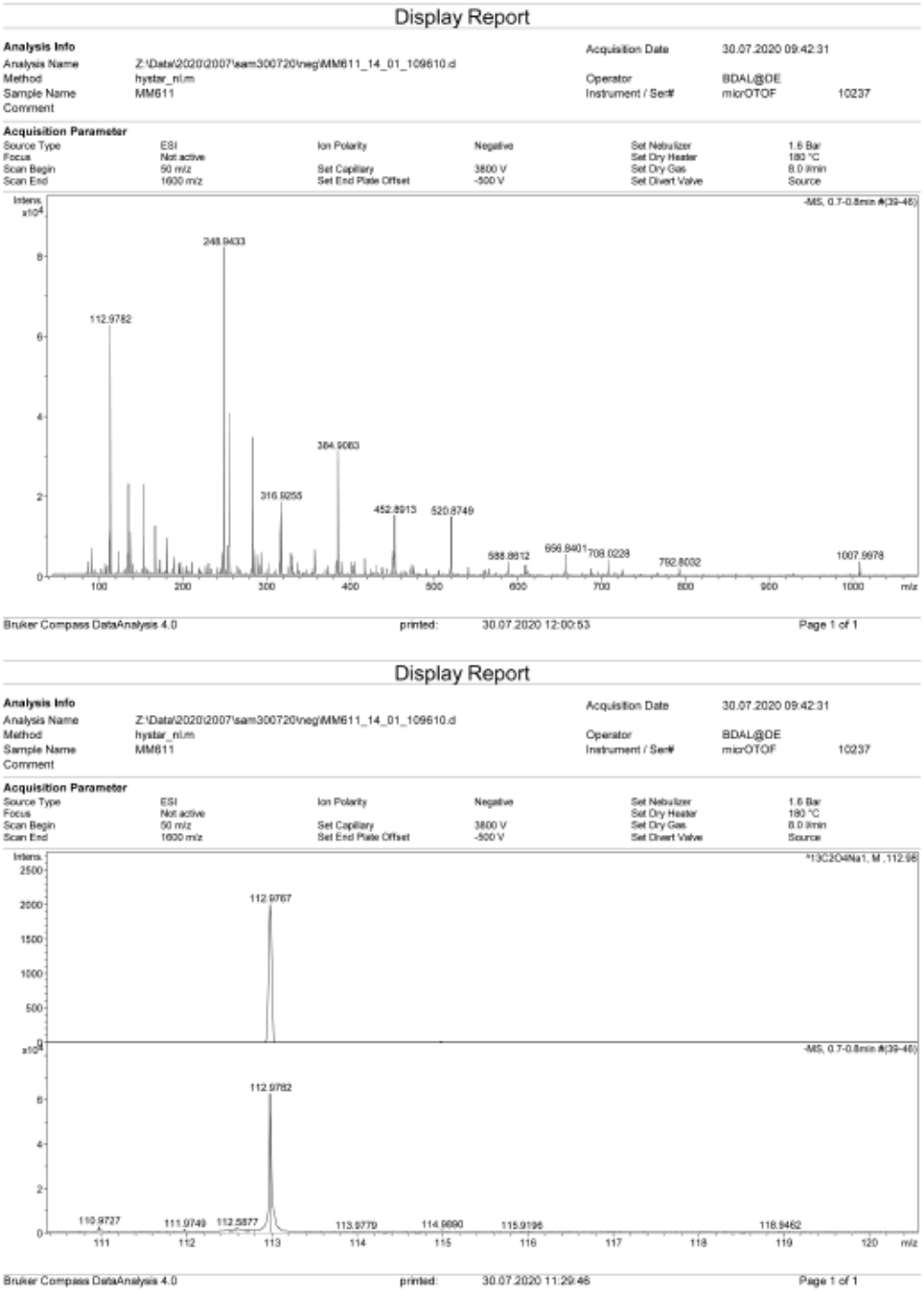

Figure S 429: HR-MS (ESI) analysis of the NaOH extract of Table S 19, entry 6 – air exposure of sodium $^{13}C_5$-3-methyl-2-oxobuyrate and $Cu(BF_4)_2{\cdot}6H_2O$ in DCM/MeOH/^{n}heptane.

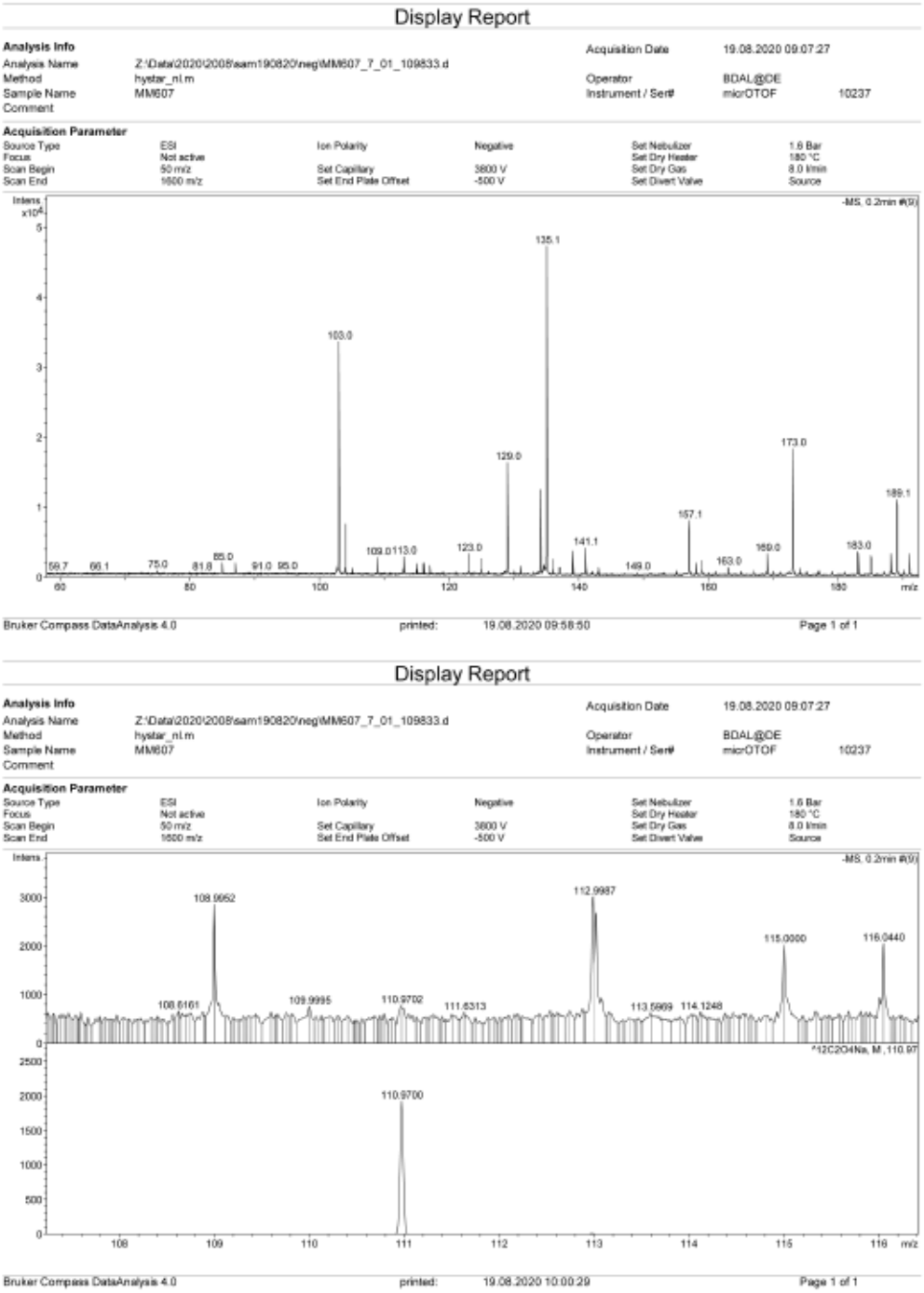

Figure S 430: HR-MS (ESI) analysis of the NaOH extract of Table S 20, entry 1 – reaction of **129** with CO_2/O_2 in toluene.

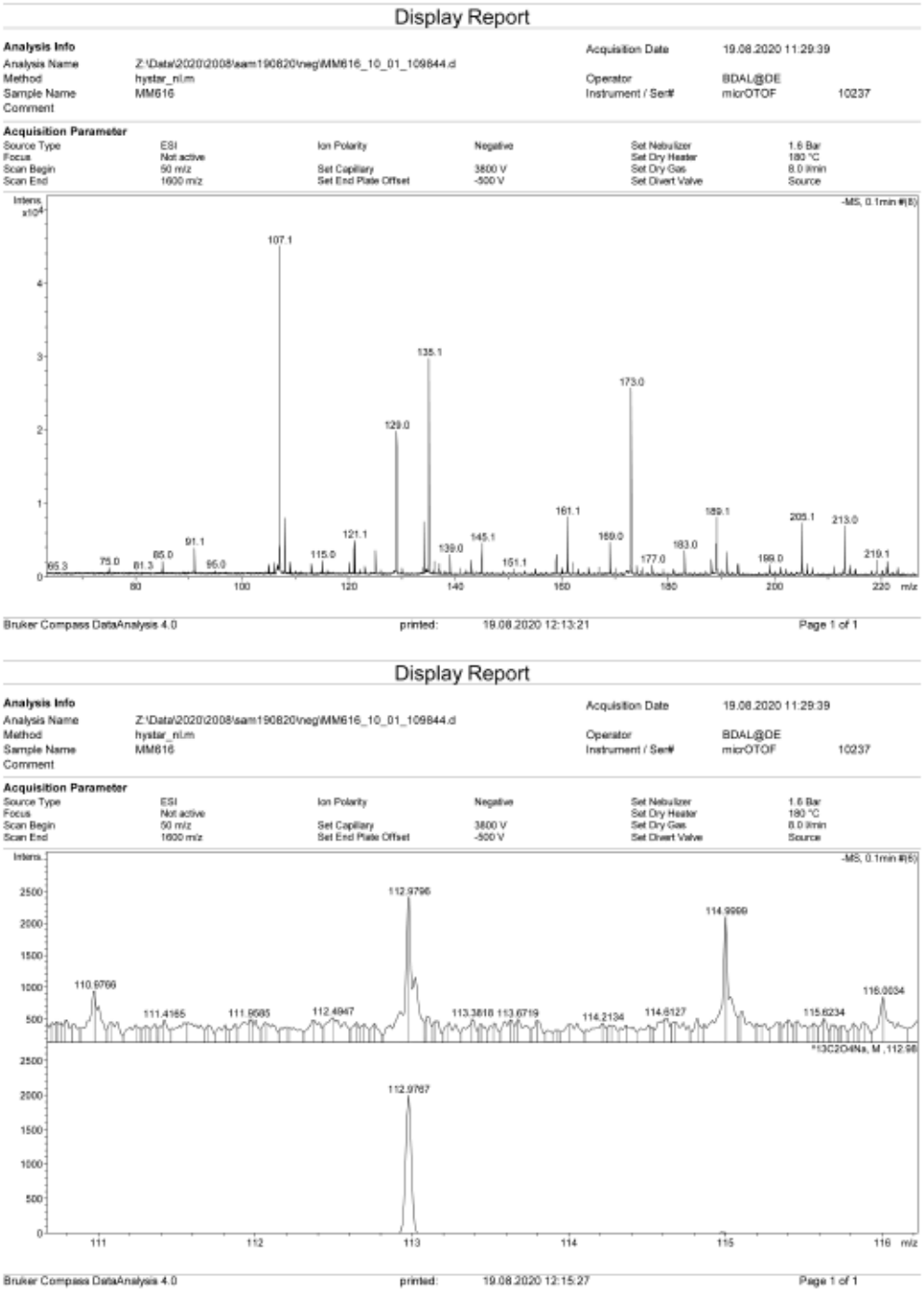

Figure S 431: HR-MS (ESI) analysis of the NaOH extract of Table S 20, entry 2 – reaction of **196** with CO_2/O_2 in toluene.

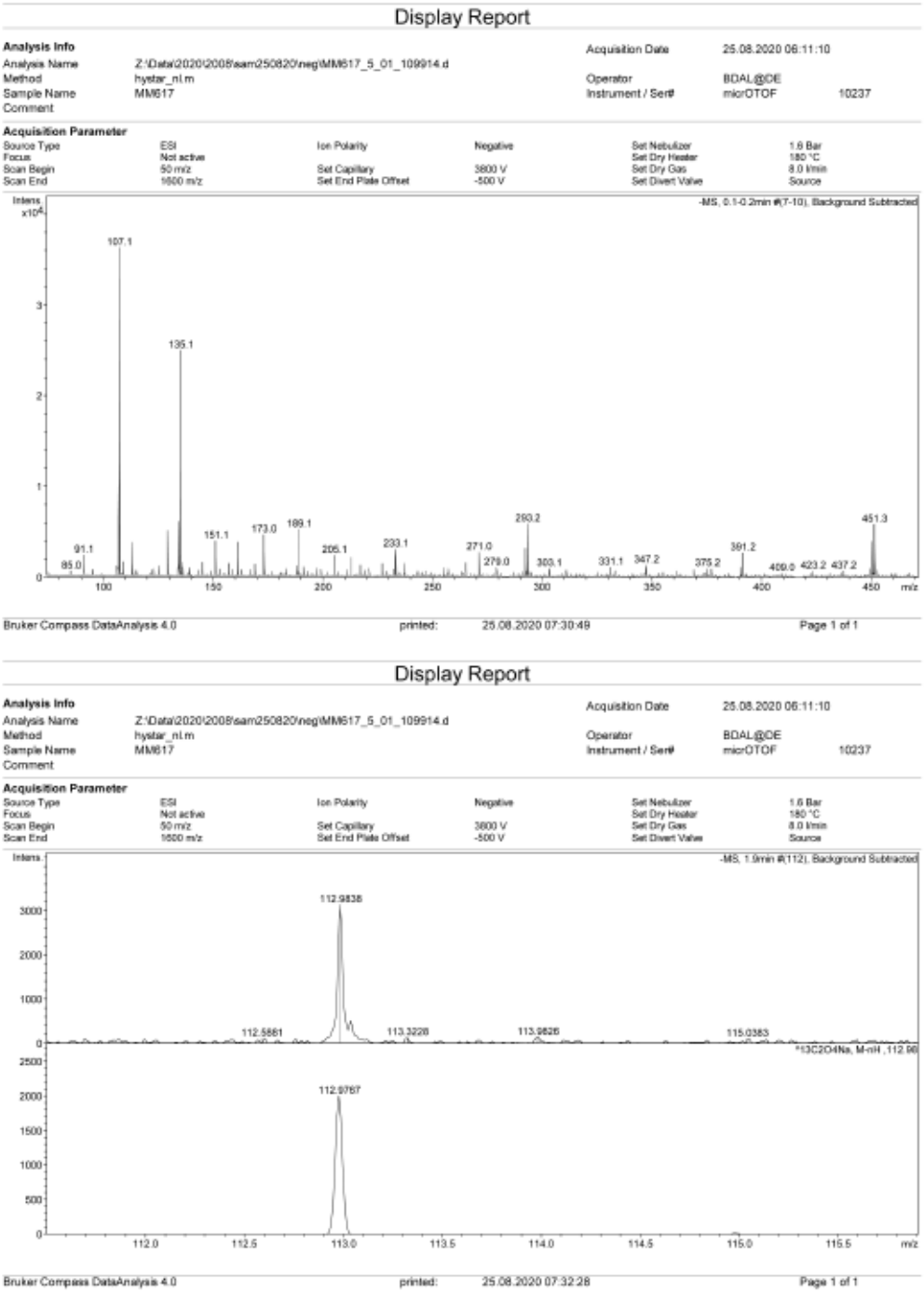

Figure S 432: HR-MS (ESI) analysis of the NaOH extract of Table S 20, entry 3 – reaction of **196** with CO_2/O_2 in toluene.

4.17 UV/Vis Spectroscopy

4.17.1 UV/Vis Spectroscopic Analysis of 1,4,7-Tacn-ligated Cu Complexes

UV/Vis samples were prepared under Ar and transferred into a cuvette sealed with a Teflon-coated rubber septum. Air exposure of the same samples for the indicated time was conducted after the initial measurement under Ar. UV/Vis spectra presented within this section and in Figure 33 were baseline corrected by subtraction of the UV/Vis spectrum of the utilized solvent (MeOH).

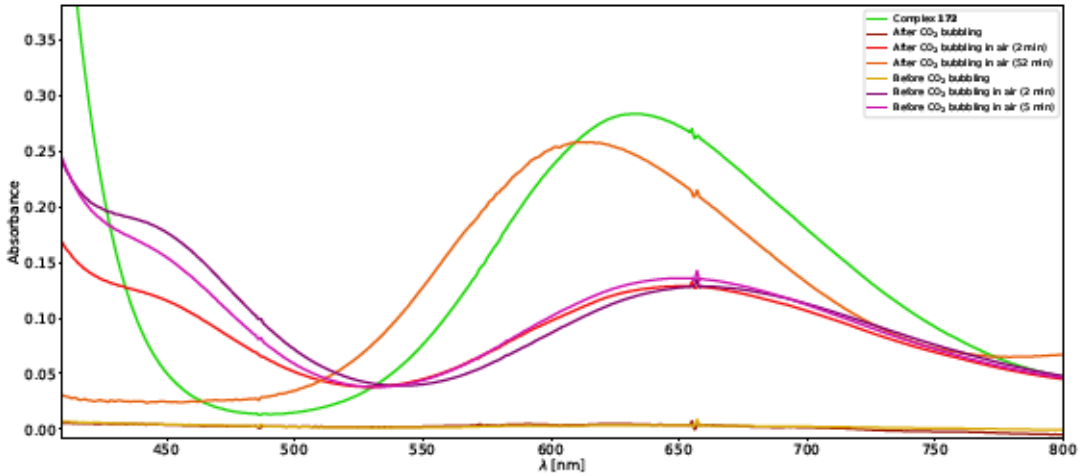

Figure S 433: UV/Vis spectra (450-800 nm) of **172** (1.7 mM in MeOH) and a solution of **127**, CuI and $NaBPh_4$ in MeOH (Table S 13, entry 5) before CO_2 bubbling (2.3 mM) and after 3 h of CO_2 bubbling (ca. 2.1 mM - evaporation of the solvent during the bubbling procedure prohibits a precise statement of the concentration) and the same samples exposed to air for the indicated tir

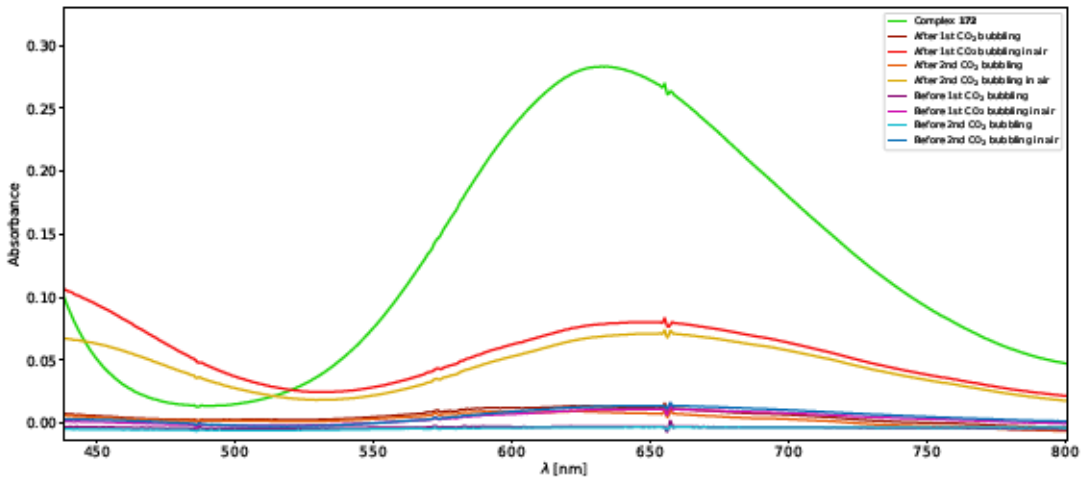

Figure S 434: UV/Vis spectra (450-800 nm) of **172** (1.7 mM in MeOH) and a solution of **127**, CuI and $NaBPh_4$ in MeOH (Table S 13, entry 6) before CO_2 bubbling (0.3 mM) and after 2 h of CO_2 bubbling (ca. 1.7 mM - evaporation of the solvent during the bubbling procedure prohibits a precise statement of the concentration) and the same reaction mixture after stirring under Ar for 19 h (ca. 0.2 mM in MeOH) and after 2nd 2 h CO_2 bubbling (ca. 1.5 mM in MeOH). The same UV/Vis samples were exposed to air for the indicated time and recorded again for comparison.

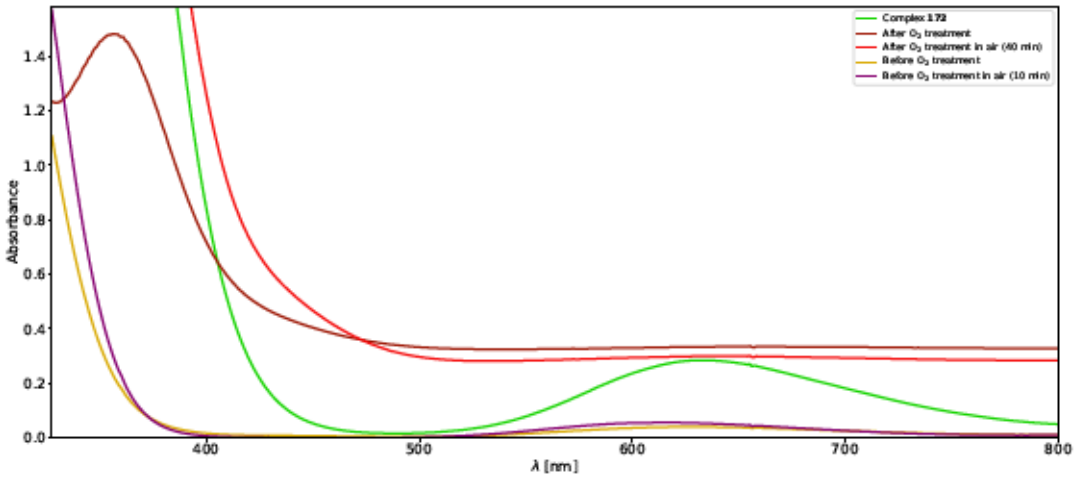

Figure S 435: UV/Vis spectra (350-800 nm) of **172** (1.7 mM in MeOH) and a solution of **127**, CuI and $NaBPh_4$ in MeOH (Table S 17, entry 4) before O_2 treatment (1.7 mM) and after 1.5 h under O_2 atmosphere (ca. 1.7 mM). The same UV/Vis samples were exposed to air for the indicated time and recorded again for comparison.